PLANTS AND MICROBIAL COMMUNITIES: DIVERSITY, PATHOGENS AND BIOLOGICAL CONTROL

EDITED BY: Yong Wang, Amin Uddin Mridha and Jia Liu

PUBLISHED IN: Frontiers in Microbiology

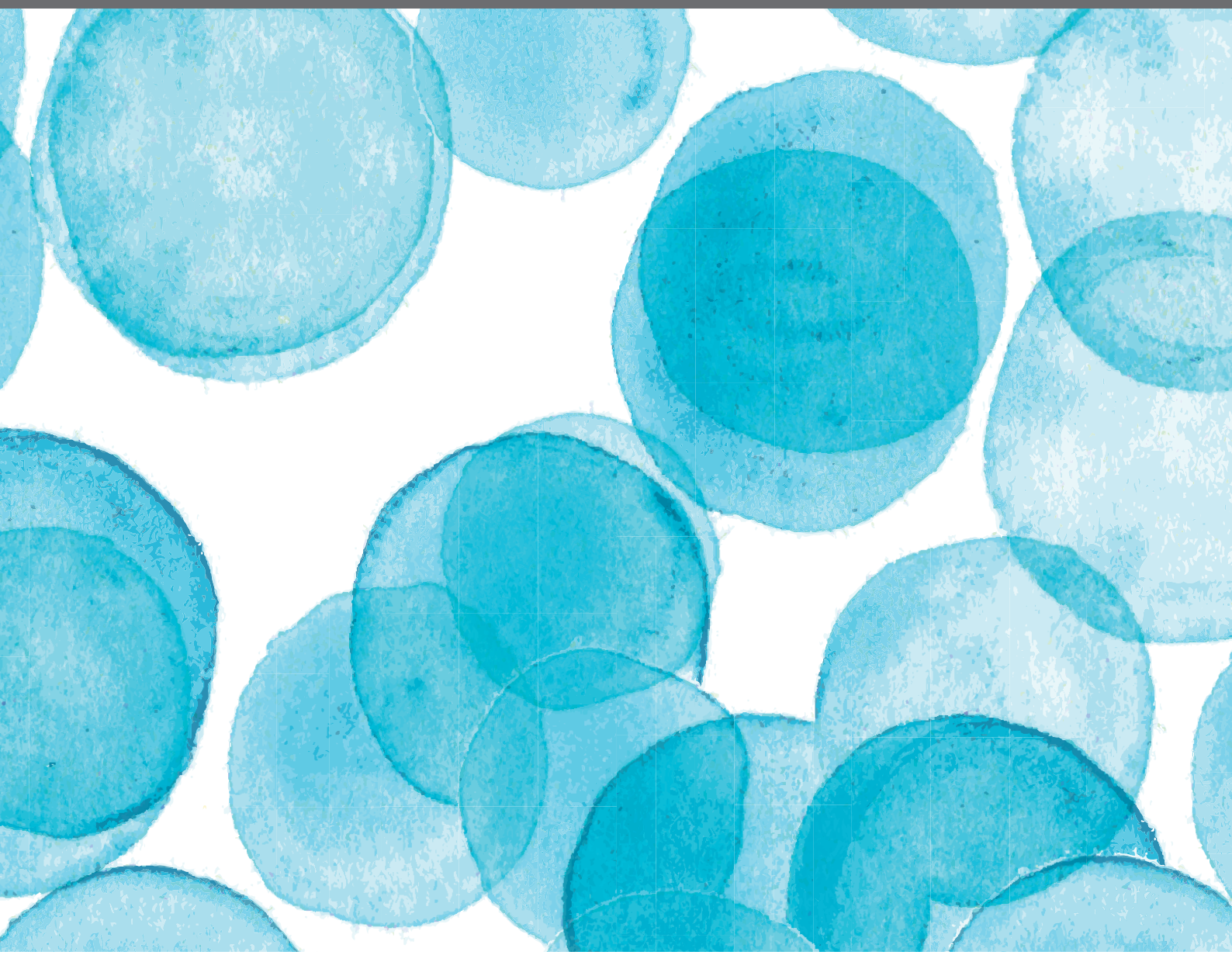

frontiers Research Topics

frontiers

ISSN 1664-8714
ISBN 978-2-88976-136-4
DOI 10.3389/978-2-88976-136-4

About Frontiers

Frontiers is more than just an open-access publisher of scholarly articles: it is a pioneering approach to the world of academia, radically improving the way scholarly research is managed. The grand vision of Frontiers is a world where all people have an equal opportunity to seek, share and generate knowledge. Frontiers provides immediate and permanent online open access to all its publications, but this alone is not enough to realize our grand goals.

Frontiers Journal Series

The Frontiers Journal Series is a multi-tier and interdisciplinary set of open-access, online journals, promising a paradigm shift from the current review, selection and dissemination processes in academic publishing. All Frontiers journals are driven by researchers for researchers; therefore, they constitute a service to the scholarly community. At the same time, the Frontiers Journal Series operates on a revolutionary invention, the tiered publishing system, initially addressing specific communities of scholars, and gradually climbing up to broader public understanding, thus serving the interests of the lay society, too.

Dedication to Quality

Each Frontiers article is a landmark of the highest quality, thanks to genuinely collaborative interactions between authors and review editors, who include some of the world's best academicians. Research must be certified by peers before entering a stream of knowledge that may eventually reach the public - and shape society; therefore, Frontiers only applies the most rigorous and unbiased reviews.
Frontiers revolutionizes research publishing by freely delivering the most outstanding research, evaluated with no bias from both the academic and social point of view. By applying the most advanced information technologies, Frontiers is catapulting scholarly publishing into a new generation.

What are Frontiers Research Topics?

Frontiers Research Topics are very popular trademarks of the Frontiers Journals Series: they are collections of at least ten articles, all centered on a particular subject. With their unique mix of varied contributions from Original Research to Review Articles, Frontiers Research Topics unify the most influential researchers, the latest key findings and historical advances in a hot research area! Find out more on how to host your own Frontiers Research Topic or contribute to one as an author by contacting the Frontiers Editorial Office: frontiersin.org/about/contact

PLANTS AND MICROBIAL COMMUNITIES: DIVERSITY, PATHOGENS AND BIOLOGICAL CONTROL

Topic Editors:
Yong Wang, Guizhou University, China
Amin Uddin Mridha, University of Chittagong, Bangladesh
Jia Liu, Chongqing University of Arts and Sciences, China

Citation: Wang, Y., Mridha, A. U., Liu, J., eds. (2022). Plants and Microbial Communities: Diversity, Pathogens and Biological Control. Lausanne: Frontiers Media SA. doi: 10.3389/978-2-88976-136-4

Table of Contents

frontiers in Microbiology

ORIGINAL RESEARCH
published: 22 October 2020
doi: 10.3389/fmicb.2020.590944

Analyzing Ash Leaf-Colonizing Fungal Communities for Their Biological Control of *Hymenoscyphus fraxineus*

*Regina Becker[1], Kristina Ulrich[2], Undine Behrendt[1], Michael Kube[3] and Andreas Ulrich[1]**

[1] *Microbial Biogeochemistry, Research Area Landscape Functioning, Leibniz Centre for Agricultural Landscape Research (ZALF), Müncheberg, Germany,* [2] *Institute of Forest Genetics, Johann Heinrich von Thünen Institute, Waldsieversdorf, Germany,* [3] *Integrative Infection Biology Crops-Livestock, University of Hohenheim, Stuttgart, Germany*

The invasive ascomycete *Hymenoscyphus fraxineus* has been threatening *Fraxinus excelsior* populations throughout Europe for over two decades. Since the infection and first colonization by the pathogen occurs in leaves, leaf-colonizing microorganisms have been discussed as a barrier and as possible biocontrol agents against the disease. To identify fungal groups with health-supporting potential, we compared the fungal microbiota of compound leaves from susceptible and tolerant ash trees in four ash stands with high *H. fraxineus* exposure. The fungal communities were analyzed both culture-independently by ITS2 amplicon sequencing and by the taxonomic classification of 1,704 isolates using matrix-assisted laser desorption/ionization time of flight mass spectrometry (MALDI-TOF MS) or sequencing of the entire ITS region. The fungal community structure did not show significant differences depending on the health status. However, for several OTUs and a MALDI group, a significantly higher abundance was found in tolerant ash trees. Thus, the yeast *Papiliotrema flavescens* was significantly increased and accounted for 12.3% of the mycobiome of tolerant ashes (OTU0003), and it had also a distinctly higher abundance among the isolates. The filamentous ascomycete *Sarocladium strictum* was increased 24-fold among the isolates of tolerant trees, but its abundance was comparably low. An *in vitro* screening for the growth inhibition of the pathogen *via* cocultivation resulted in 28 yeast-like isolates and 79 filamentous fungi with antagonistic activity. A statistical cocultivation test on two *H. fraxineus* strains confirmed six of the yeast-like isolates that suppressed *H. fraxineus* significantly, from 39–50%, two of them through a fungicidal effect. The highest inhibition rates among the yeasts were found for three isolates belonging to *Aureobasidium pullulans* and *P. flavescens*. The cocultivation test of the filamentous isolates revealed higher effects compared to the yeasts. Four isolates showed significant inhibition of both *H. fraxineus* strains with a rate of 72–100%, and five further isolates inhibited only one *H. fraxineus* strain significantly. The most effective isolates were members of the genus *Cladosporium*. During the next step, *in planta* tests will be necessary to verify the efficacy of the antagonistic isolates and to assess their suitability as biocontrol agents.

Keywords: ash dieback, antagonism, *Fraxinus excelsior*, mycobiome, cocultivation, phyllosphere

OPEN ACCESS

Edited by:
Yong Wang,
Guizhou University, China

Reviewed by:
Qian Guoliang,
Nanjing Agricultural University, China
Jia Liu,
Chongqing University of Arts and Sciences, China

***Correspondence:**
Andreas Ulrich
aulrich@zalf.de

Specialty section:
This article was submitted to Microbe and Virus Interactions with Plants, a section of the journal Frontiers in Microbiology

Received: *03 August 2020*
Accepted: *02 October 2020*
Published: *22 October 2020*

Citation:
Becker R, Ulrich K, Behrendt U, Kube M and Ulrich A (2020) Analyzing Ash Leaf-Colonizing Fungal Communities for Their Biological Control of Hymenoscyphus fraxineus. Front. Microbiol. 11:590944. doi: 10.3389/fmicb.2020.590944

INTRODUCTION

In recent decades, ash dieback has spread from north-eastern Poland to all over Europe, and it threatens the future of the common ash (*Fraxinus excelsior*) because of its associated severe damage and high mortality rates (Kowalski and Holdenrieder, 2009; Timmermann et al., 2011; McKinney et al., 2014; Skovsgaard et al., 2017). This disease is caused by the invasive ascomycete *Hymenoscyphus fraxineus* (Kowalski, 2006; Queloz et al., 2011; Baral et al., 2014). The fungus was introduced from East Asia, where it lives in asymptomatic association with the Manchurian ash (*Fraxinus mandshurica*) (Zhao et al., 2013; Gross et al., 2014; Han et al., 2014; Cleary et al., 2016). *H. fraxineus* infections come from airborne ascospores that germinate on leaves and penetrate the cuticula and the epidermis. Starting from the infected leaves, the pathogen is able to colonize the petioles and subsequently the twigs and shoots. This leads to blockages of the xylem vessels as well as lesions of the cambium and finally the crown starts dying back (Gross et al., 2014). Infection and colonization by the pathogen can be prevented or reduced by genetically mediated defense mechanisms. Thus, several ash species, such as *F. mandshurica* and *Fraxinus ornus*, the native flowering ash, tolerate this pathogen based on weak susceptibility (Gross et al., 2014; Kirisits and Schwanda, 2015; Drenkhan et al., 2017). A hereditary resilience seems to also be present within the common ash, which is reflected in the occurrence of individual healthy-looking trees in infested stands (Stener, 2013; Lobo et al., 2014; Wohlmuth et al., 2018). Resistance is considered as a polygenic trait, the specific function of which is still poorly understood (Wohlmuth et al., 2018; Stocks et al., 2019). However, it is assumed that the resilience of the host is significantly influenced by its microbiome (Berg et al., 2017; Compant et al., 2019; Liu et al., 2020). Bacteria and fungi that colonize the surface and the endosphere of the plant can suppress invaders directly by resource competition, parasitism and antibiosis or indirectly by activating the plant's own defense system (Latz et al., 2018; Fadiji and Babalola, 2020). In addition, some endophytic microorganisms are able to promote plant growth and development, resulting in an increased resilience in response to stress and pathogens (Glick, 2012; Hossain et al., 2017). These different mechanisms, which can occur simultaneously, are activated in interaction with the plant's metabolism and the environmental conditions (Berg and Smalla, 2009; Berg et al., 2015).

To assess the role of fungal endophytes in ash dieback tolerance, the structure of leaf- and twig-associated fungal communities of tolerant and diseased ashes was investigated over a series of studies (Cross et al., 2017; Hanackova et al., 2017a; Schlegel et al., 2018; Kosawang et al., 2019). Different approaches showed significant variations in the community structure depending on the plant location, season and plant genotype. In particular, the composition of twig-associated fungal communities differed significantly between ash species, i.e., *Fraxinus angustifolia*, *Fraxinus latifolia, F. mandshurica*, and *F. ornus* but also between genotypes of *F. excelsior*. However, a direct and distinctive relation to ash dieback susceptibility could not be detected (Kosawang et al., 2019; Griffiths et al., 2020). Griffiths et al. (2020) observed that higher *H. fraxineus* infection levels were associated with higher fungal diversity and the presence of specific fungal genera.

The complex interactions between the resistance, plant genotype and associated microorganisms make it challenging to identify specific microbial groups with disease-suppressing potential. It is assumed that health-supporting taxa should primarily be present in tolerant hosts (Schulz et al., 2019). However, only a few species have been identified so far, which are clearly associated with *H. fraxineus* tolerance. Cleary et al. (2016) analyzed the phyllosphere fungal communities of the dieback-tolerant ash *F. mandshurica* and identified *Mycosphaerella* as the dominant fungal genus in these trees. *Mycosphaerella* was found in all the *F. mandshurica* samples collected in eastern Russia and was limited to this ash species. A study on the leaf petioles of common ashes showed increased frequencies of *Aureobasidium pullulans* in healthy trees, while in diseased trees, *Alternaria* and *Cytospora* species were also frequently represented (Davydenko et al., 2013). Other investigations focused on the *in vitro* testing of ash leaf endophytes for antagonism against *H. fraxineus*. A row of fungal isolates obtained from tolerant ash species as well as *F. excelsior* indicated antagonistic activity in cocultivation with the pathogen (Hanackova et al., 2017a; Kosawang et al., 2018; Halecker et al., 2020). However, cocultivation experiments also showed that both partners, *H. fraxineus* and the endophytic isolate, are often inhibited by mutual antagonisms (Schulz et al., 2015; Halecker et al., 2020). Therefore, comprehensive tests are required to identify effective antagonistic candidates whose colonization and activities are not or only weakly suppressed by *H. fraxineus.*

In this study, we combined a high-throughput sequencing approach and cultivation methods to analyze the fungal communities of susceptible and tolerant common ashes. The comparative analyses were aimed at detecting the fungal groups that are specific to tolerant trees and might therefore be involved in disease suppression. In parallel, the isolates were subjected to an extensive screening for *H. fraxineus* growth inhibition. Based on the primary screening, the best isolates were evaluated in a statistical cocultivation test for their antagonism against the pathogen.

MATERIALS AND METHODS

Study Site and Sampling

Compound ash leaf material was obtained by sampling of ash trees from four forest districts in Northeast Germany in July of 2017. Observations taken during long-term monitoring projects revealed a very low occurrence of single trees with low susceptibility in stands that were severely affected by *H. fraxineus* (Sündermann and Jütte, 2014). In each of the districts (A–D), four pairs of adjacent trees consisting of an affected (K) and a tolerant (P) tree were chosen for sampling. Details of the sampling campaign and sample preparation are described in

Ulrich et al. (2020). Accordingly, the same leaf samples were used in this study to analyze the fungal community.

Amplicon Sequencing and Analysis of the ITS2 Region

For high comparability among analyses, the total DNA used to investigate of the bacterial community (Ulrich et al., 2020) was also applied to study the fungal community. For this purpose, the ITS2 region was chosen because it has a lower length variability compared to the ITS1 region combined with higher genetic diversity. It also reduces the pitfalls caused by introns in the flanking rDNA of the ITS1 region of some species (Tedersoo et al., 2015). The ITS2 region was amplified with the primers fITS7 (5′-GTGARTCATCGAATCTTTG-3′) (Ihrmark et al., 2012) and ITS4 (5′-TCCTCCGCTTATTGATATGC-3′) (White et al., 1990), preventing the amplification of the host plant DNA. PCR amplification was conducted as described by Ihrmark et al. (2012). The primers were extended with a heterogeneity spacer and a barcode sequence. The amplicons were checked with gel electrophoresis, purified with an MSB Spin PCRapace kit (Invitek, Essen, Germany) and mixed to equimolar DNA concentrations. The library preparation and Illumina MiSeq 300-bp paired-end sequencing were performed at LGC Genomics Berlin.

The raw sequence data were analyzed with Mothur v. 1.39.1 (Schloss et al., 2009; RRID:SCR_011947) in accordance with the MiSeq SOP (Kozich et al., 2013). In addition, the ITS2 region was extracted with ITSx 1.1.2 (Bengtsson-Palme et al., 2013) by removing the flanking 5.8S and 28S rRNA gene fragments. Chimeras were removed using the Uchime algorithm. For phylogenetic identification, the sequences were compared to the dynamic UNITE database (version 8.2) using a confidence threshold of 80%. The operational taxonomic units (OTUs) were generated with the VSEARCH algorithm without using a multiple sequence alignment (Edgar, 2010) at a similarity of 97%. Singletons were discarded as suggested in the UPARSE pipeline (Edgar, 2013). The phylogenetic assignment of the OTUs was checked manually using BLAST searches of the UNITE database as well as the NCBI taxonomy browser. All the samples were subsampled to the minimum number of sequences among all the samples. The paired sequence reads were deposited in the public Sequence Read Archive (SRA, RRID: SCR_004891) repository under the accession number PRJNA611938.

Statistical analyses were performed using the phyloseq, vegan and ape packages in R 3.6.0, as well as MicrobiomeAnalyst (Chong et al., 2020; RRID:SCR_015022). The alpha diversity indices Chao 1, Shannon, and Simpson were calculated. Significant differences between the fungal communities were tested using an Analysis of Similarity (ANOSIM). The phylogenetic composition of the ash microbiome was visualized with a Krona chart (Ondov et al., 2011). The differential abundance at different taxonomic levels was analyzed with the metagenomeSeq tool using a false discovery rate (FDR) for multiple test correction (Paulson et al., 2013). An indicator species analysis was performed with PC-Ord v. 7.02 (McCune and Mefford, 2015) by applying the procedure by Dufrêne and Legendre (1997).

Cultivation of Fungal Epi/Endophytes

Ground material of compound ash leaves were serially diluted in 0.8% NaCl, plated on PDA (Merck, Darmstadt) and incubated for seven to ten days at room temperature. To determine the population densities, colony forming units (CFU) were counted and expressed as CFU per gram of fresh weight. Approximately 50 isolates per sample were randomly selected for analysis. From the filamentous fungi, the mycelium was subcultivated on PDA and pure cultures were scraped from the Petri dishes using a sterile scalpel and transferred to agar slants (PDA) for storage and further processing. Yeast-like fungi were purified by streak plate method and stored as cryo-cultures (−80°C) in nutrient broth containing 40% glycerol until analysis.

Dereplication and Classification of Fungal Isolates

Matrix-assisted laser desorption/ionization time of flight mass spectrometry (MALDI-TOF MS) was applied as a reliable method for the dereplication and classification of yeasts in environmental analyses (Chudejova et al., 2017; Huschek and Witzel, 2019). Prior to this measurement, the yeast-like isolates were freshly inoculated on CASO agar (Fluka, Buchs, Switzerland) and cultivated for 24 h at 25°C. Mass spectra were obtained based on the whole-cell measurement protocol as described by Ulrich et al. (2020). The analysis was performed on a microflex^{TM} LT/SH MALDI-TOF mass spectrometer (Bruker Daltonics, Bremen, Germany) using Flex Control 3.4 software. Isolates showing spectra with a score value >2.3 (highly probable species identification) were considered as identified by the Bruker database. Isolates with a lower score were compared with each other and grouped on the basis of a score value >2.3.

Representative strains of the unidentified groups were taxonomically classified by sequencing of the complete fungal ITS rRNA region. Total DNA was extracted from single colonies by resuspending in 20 µl of 25 mM NaOH/0.25% SDS followed by incubation for 15 min at 95°C. The amplification was performed using the universal primer pair ITS1F (Gardes and Bruns, 1993) and ITS4 (White et al., 1990). PCRs were performed using PCR Master Mix 2× (Thermo Fisher Scientific, Darmstadt, Germany) containing 0.2 µM of each primer. The thermal cycling conditions were as follows: an initial denaturation step of 95°C for 5 min; 10 cycles of 95°C for 30 s, 60°C for 30 s with a touchdown of −1°C by cycle and 72°C for 1 min, 30 cycles of 95°C for 30 s, 50°C for 30 s and 72°C for 1 min. The PCR products were checked on a 1% agarose gel and the fragments of approximately 600–700 bp were sequenced using the primer ITS1F. The fungal isolates were taxonomically assigned using the UNITE fungal ITS database version 8.0 (Kõljalg et al., 2013) and the species names were approved by the NCBI taxonomy browser. After supplementing the MALDI BiotyperTM database with the spectra of the reference strains, a reliable taxonomic identification of all the fungal isolates was achieved. All the MALDI groups were assigned at the species level.

For the classification of filamentous fungi, small pieces of mycelia (ca. 0.5 cm^2) were scraped from agar cultures using a sterile scalpel. To extract the DNA, a modified CTAB protocol was used according to Doyle (1990). In brief, for the first lysis step, the mycelium was frozen at −80°C in 2 ml tubes containing 8–10 ceramic beads (1.4 mm; Omni International, Kennesaw, United States) and subsequently ground for 25 s with a speed of 7.45 m/s using the Bead Ruptor 24 (Omni International). After the addition of 750 µL of CTAB buffer and sample incubation of the samples for 30 min at 65°C, the procedure followed the regular protocol. Filamentous fungal isolates were identified by sequencing the entire ITS region of ribosomal DNA as described above and assigned at the species level as well.

A community analysis of culturable fungi was performed by combining all the isolates classified by either MALDI-TOF MS or direct sequencing. The B2P sample was removed from the analysis as an outlier due to the small number of only seven isolates. For the statistical analysis, the number of isolates per sample was normalized using the CSS method (Paulson et al., 2013). Significant differences in the community composition between tolerant and susceptible trees were tested at all taxonomic levels using the MetagenomeSeq tool (MicrobiomeAnalyst, $P_{FDR} < 0.05$).

In vitro Screening and Statistical Test for Antagonistic Activity Against *H. fraxineus*

All the fungal isolates were screened for antagonistic activity against *H. fraxineus* P3. To simulate the conditions of their natural habitat, cultivation was performed on PDA medium enriched with ash shoot extract (30 g ash leaves/L PDA) at 22°C (Hanackova et al., 2017a). Due to its slow growth, *H. fraxineus* P3 was incubated for 5 to 6 days before the isolates for testing were struck out. Depending on the growth type of the isolates (yeasts or filamentous fungi), two different approaches were used:

The antagonistic potential of yeast-like fungi was estimated using an assay according to Pane and Zaccardelli (2015). An agar plug (ø 5 mm) containing fresh *H. fraxineus* mycelium was placed in the center of the Petri dish (ø 8 cm), whereas four different yeast counterparts were spread around the four edges of the plate. Plates, solely carrying *H. fraxineus* served as control. The colony radius (r) of *H. fraxineus* was measured after seven and 14 days until the control reached the edge of the plate. The inhibitory effect was estimated using the formula percent growth inhibition = $100 \times [(r_{control} - r_{cocultivation})/r_{control}]$. Isolates with inhibition rates >30% were chosen for a subsequent statistical test including three replicates and two *H. fraxineus* strains (P3, HF23). In this approach, only one isolate per plate was spread out along the edges of the plate, and the inhibition rates were calculated by measuring the diameter of the *H. fraxineus* mycelium.

The filamentous fungi were tested in dual cultures with agar plugs (ø 5 mm) of the fungal isolates and *H. fraxineus* mycelium at a distance of 4 cm. The test included a self-inhibition control by pairing two *H. fraxineus* colonies of the same strain and a negative control by pairing *H. fraxineus* with an agar plug without mycelium. Similar to Hanackova et al. (2017a), the growth of *H. fraxineus* was measured as the colony radius on a connective line between the two colonies as well as on a line measuring 45° up and down from this line after seven and 14 days of dual culture. The inhibition of *H. fraxineus* was estimated after averaging the three measured values and using the formula mentioned above. Isolates that indicated higher inhibition rates compared to the self-inhibition were evaluated again in a statistical test, as outlined above.

In addition, the statistical tests on the yeasts and filamentous fungi were ultimately used to evaluate the vitality of the residual *H. fraxineus* mycelium after confrontation with the fungal isolates. For this purpose, agar plugs with the remaining *H. fraxineus* mycelium (P3, HF23) were picked from the three replicates and incubated separately on PDA with ash shoot extract. The growth of the mycelium was assessed after 2 weeks in comparison to the untreated control.

To verify the pathogenicity of the *H. fraxineus* isolates P3 and HF23, 2-year-old ash seedlings were inoculated with either isolate using an approach modified according to Przybyl (2003). The typical symptoms of ash dieback (Gross et al., 2014) were monitored over the course of 8 weeks, and the virulence of both isolates was confirmed.

RESULTS

Fungal Community Structure of Susceptible and Tolerant Ashes

ITS2-Based Community Profiling

The mycobiomes of 16 tolerant and 16 susceptible trees were studied by amplicon sequencing of the ITS2 rRNA region. Although only visibly healthy leaves and petioles were sampled from both the tolerant and the diseased trees, an extremely high proportion of *H. fraxineus* (86%) was found in the fungal community of one sample (C2K). Due to this contamination, this sample was excluded from further analysis. All the other samples contained a low proportion of the pathogen *H. fraxineus* with an average of 0.03% of the fungal community. In total, the sequences could be assigned to 1012 operational taxonomic units (OTUs) with an average of 210 OTUs per sample. For the statistical analyses, the sequences were rarefied to 10,707 reads per sample.

The comparison of fungal communities from tolerant and susceptible trees showed no significant differences in the genetic diversity (e.g., with a mean Shannon index of 2.72 ± 0.23 vs. 2.65 ± 0.44). An analysis of the composition of the mycobiome revealed small but significant differences in grouping by sample location (forest districts) and health status (ANOSIM $R = 0.1898$, $P < 0.001$). **Figure 1** displays the differences in the fungal community structure. The second axis indicated some deviations between tolerant and susceptible ashes for forest districts A and C. However, the pairwise comparisons of the health status did not show significant differences for any of the districts.

In total, 61% of the sequences were assigned to the phylum *Ascomycota* and 38% to the phylum *Basidiomycota*, and only 0.46% of the fungal sequences could not be classified (**Figure 2**).

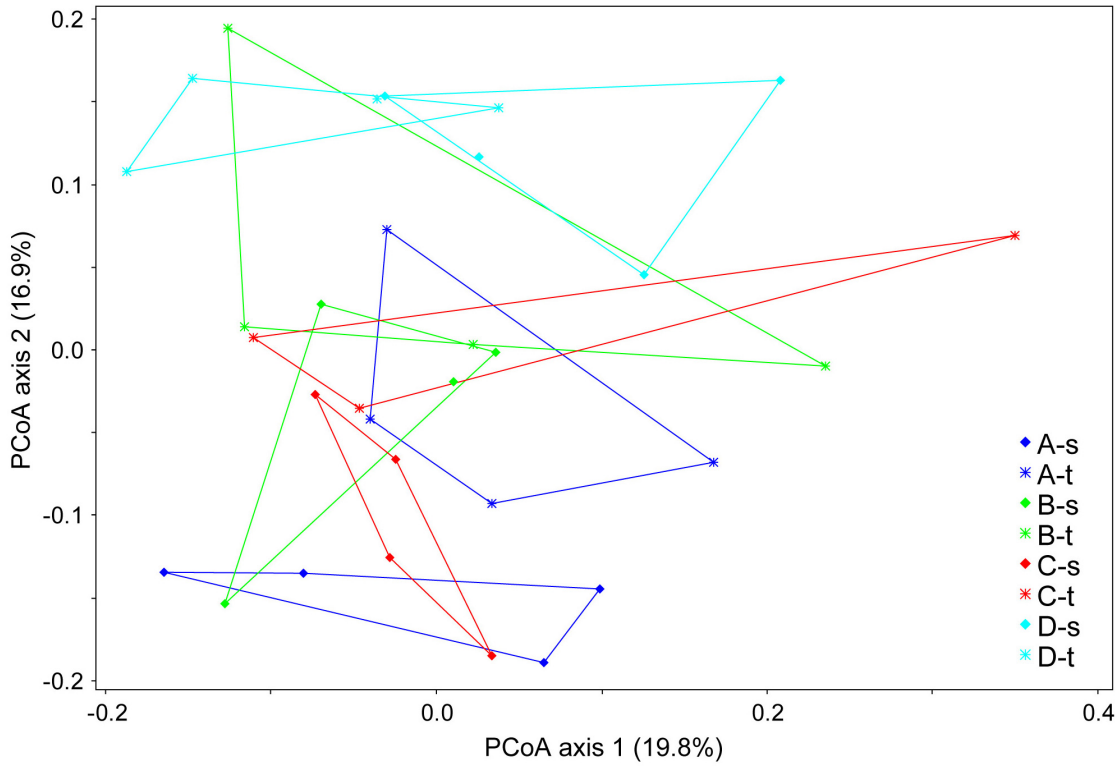

FIGURE 1 | Community clustering of the mycobiome of tolerant **(t)** and susceptible **(s)** ashes from the four forest districts **(A–D)**. A principle coordinate analysis (PCoA) was applied based on a Bray-Curtis distance matrix.

At the class level, *Dothideomycetes* dominated the fungal community with 54%, followed by *Tremellomycetes* with 28%. At the species level, *A. pullulans* showed the highest abundance with 32%, followed by *Cladosporium* spp. (11%), *Papiliotrema flavescens* (10%) and *Vishniacozyma carnescens* (9%). Thus, four species represented more than 60% of the fungal community.

When comparing the mycobiome at the species level, only the yeast *P. flavescens* was significantly increased in tolerant trees (approximately 2-fold). At the OTU level, the differential abundance analysis revealed 18 OTUs with a proportion of more than 0.02% that were significantly increased in tolerant trees (**Figure 3**). Remarkably, a group identified as *P. flavescens* (OTU0003) accounted for 12.3% of the fungal community in tolerant ashes. Additional OTUs with higher amounts in tolerant plants (e.g., OTU0014, 0026, and 0036) belonged to *Microstroma*, uncl. *Dothidiomycetes* and *Neosetophoma*. However, the abundances of these taxa were comparably low.

An indicator species analysis at the OTU level revealed four groups for the tolerant ash trees. It again concerns *P. flavescens* (OTU0003), but *Microstroma album* (OTU0014), *Vishniacozyma dimennae* (OTU0139) and *Exobasidium* spp. (OTU0141) could also be proven ($p < 0.05$).

Culturable Fungal Communities

In addition to the marker gene analysis, the culturable leaf-associated fungal community was compared between tolerant and susceptible ash trees. The population densities of the fungi ranged between 1×10^4 and 4×10^5 CFU/g fresh weight with no significant differences depending on the health status. Previous studies showed that the leaf fungal density is very changeable with yeasts ranging between 10 and 10^{10} and filamentous fungi between 10^2 and 10^8 CFU/g (Thompson et al., 1993; Inacio et al., 2002). In total, 931 filamentous isolates were classified *via* ITS rRNA sequencing and 773 yeast-like isolates *via* MALDI-TOF MS. The 1,704 isolates were grouped at the species level into 49 phylotypes belonging to 42 genera.

The majority of fungal isolates was assigned to the phylum *Ascomycota* (72%) followed by *Basidiomycota* with 28%. At the class level, *Dothideomycetes* (63%), and *Tremellomycetes* (28%) dominated the community. At the species level, a clear dominance of the saprophytic yeasts *A. pullulans* (50.5%), *P. flavescens* (14.1%), and *V. carnescens* (9%) was observed. The most abundant species *A. pullulans*, which is known for its switch between yeast-like and filamentous growth mode, accounted for 28% of the yeasts and 69% of the filamentous fungi. Thus, the filamentous fungi were clearly dominated by *A. pullulans*, whereas *P. flavescens* was the predominant yeast (31%).

When comparing trees with different health statuses, *P. flavescens* occurred in higher abundance in tolerant trees (**Figure 4**). However, this difference could not be statistically ensured. *Sarocladium strictum* isolates made up a lower

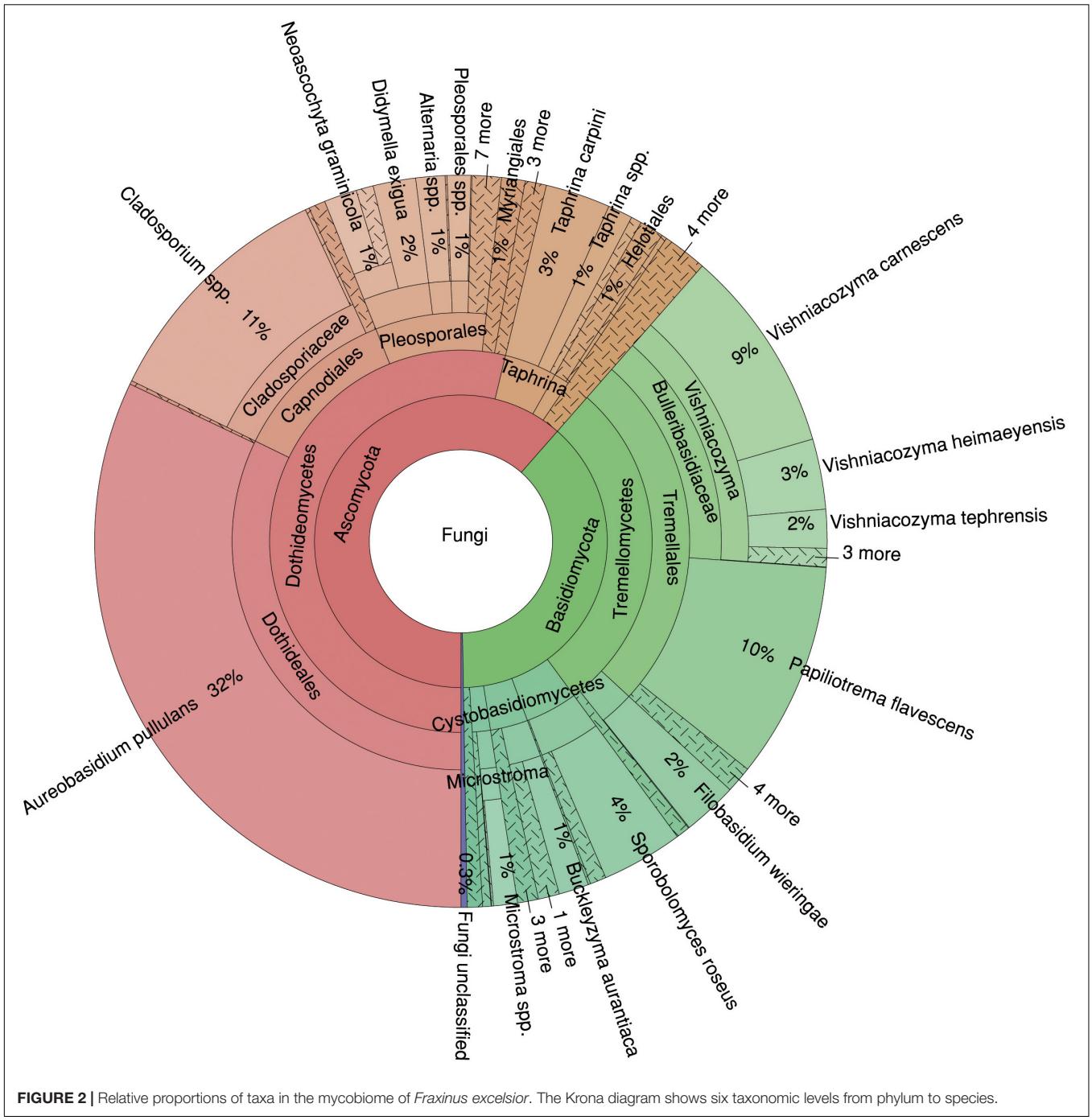

FIGURE 2 | Relative proportions of taxa in the mycobiome of *Fraxinus excelsior*. The Krona diagram shows six taxonomic levels from phylum to species.

proportion but showed a significant difference with a 24-fold increase in tolerant trees.

In vitro Antagonistic Activity of Fungal Isolates

Yeast-Like Fungi

To detect potential antagonists, the yeast isolates were screened for growth inhibition of *H. fraxineus* P3. Overall, the screening revealed a high proportion of isolates with slight inhibitory effects. One-fifth of the isolates inhibited *H. fraxineus* by 31–50%. The potential antagonists were obtained in a comparable ratio from susceptible and tolerant trees. They were dominated by *A. pullulans* (56%), followed by the *Basidiomycota* members *P. flavescens* (23%) and *Vishniacozyma* spp. (13%). Other taxa such as *Metschnikowia* sp., *Cystobasidium pinicola* and *Kwoniella newhampshirensis* were represented in frequencies between 5% and less than 1%. The highest inhibition rates were achieved by *A. pullulans* isolates with 37% on average, while the mean inhibition of the other taxa was slightly lower with 32–34%.

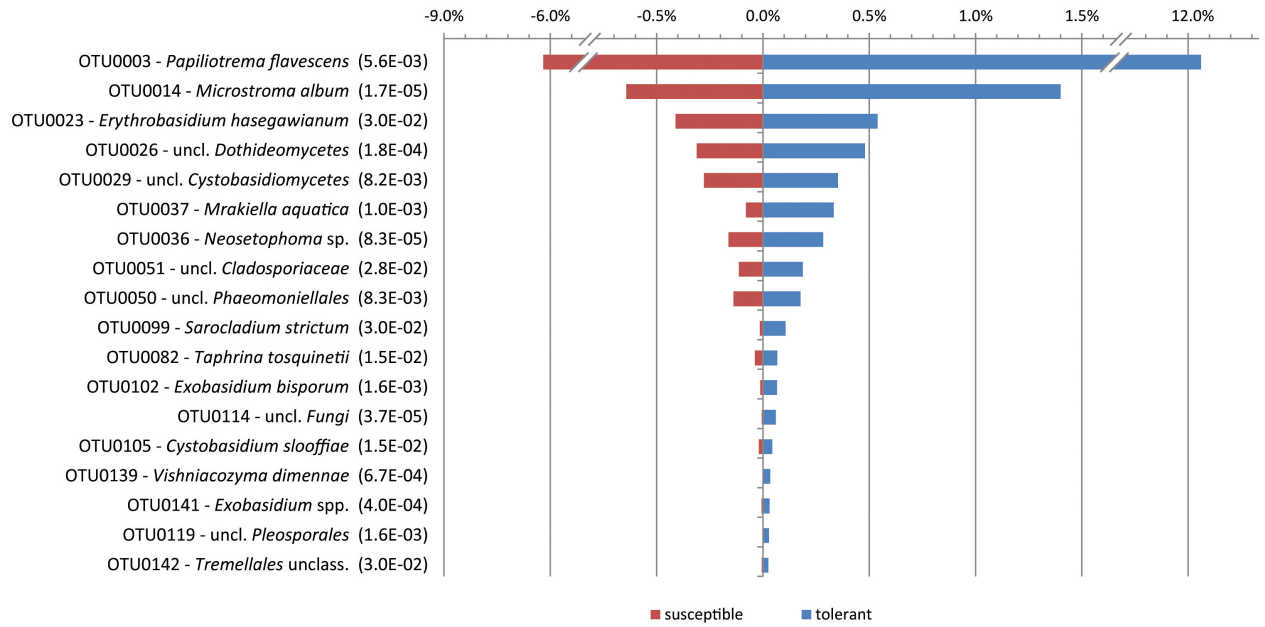

FIGURE 3 | Significantly increased OTUs in tolerant ashes. The OTUs are sorted according to their relative abundance (>0.02), and the level of significance (FDR) is given in brackets.

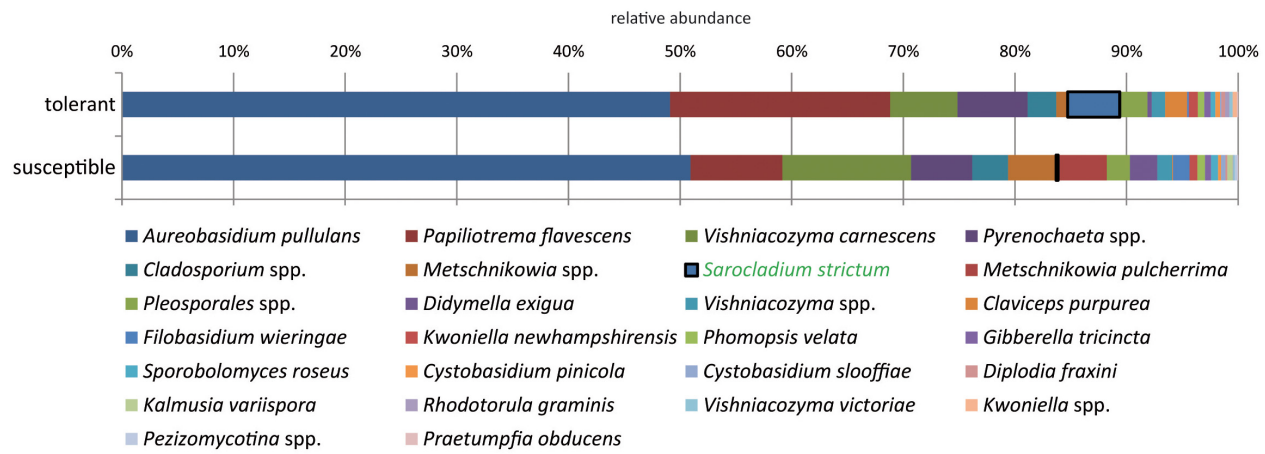

FIGURE 4 | Comparison of the culturable fungal community from tolerant and susceptible ashes at the species level. The species significantly increased in resistant trees is highlighted.

Based on the primary screening, 28 isolates with an inhibition rate above 30% were subjected to the statistical test on antagonism against two *H. fraxineus* isolates. The isolates were derived from all the locations and from both susceptible and tolerant trees. An overview on the antagonistic potential of the yeasts is given in **Table 1**. In total, six of the 28 isolates significantly inhibited the growth of *H. fraxineus* HF23 at 39–50%. The *H. fraxineus* strain P3 was inhibited by these yeasts over a similar range, but this finding could not be statistically ensured. After cocultivation, the vitality of the remaining *H. fraxineus* mycelium was also examined. Ten out of the 28 isolates were able to completely kill *H. fraxineus* P3, whereas the vitality of HF23 was only slightly injured. Remarkably, four of the nine isolates of *P. flavescens,* a species that was found to have increased in tolerant trees, were able to devitalize *H. fraxineus* P3. When summarizing all the antagonistic features, the best isolates were A3P046, A3K040, and A3P071. D3K042 and C4K010 showed a strong fungistatic effect during the cocultivation test indicated by the ability of the pathogen to regrow. The antagonistic activity is exemplarily shown for isolates A3K040 and A3P071 in **Figure 5**. In addition to the growth inhibition, a lightening of the mycelium was visible, indicating an ongoing lysis that started approximately

TABLE 1 | Antagonistic activity of yeast-like epi/endophytic fungi as assessed by the growth inhibition of *H. fraxineus* and the vitality of the remaining pathogen mycelium.

Isolate	Taxonomic assignment	Growth inhibition rate in dual culture (%)[a]		Vitality of mycelium (% of untreated control)	
		P3	HF23	P3	HF23
A3K052	*Aureobasidium pullulans*	39.2	37.3	54.9	92.2
A3P046	*Aureobasidium pullulans*	41.0	45.7*	0.0	89.3
A4K061	*Aureobasidium pullulans*	41.0	35.8	61.1	84.0
A2P099	*Aureobasidium pullulans*	40.7	36.7	0.0	85.5
C1P011	*Aureobasidium pullulans*	32.5	37.5	0.0	85.3
A3K040	*Aureobasidium pullulans*	34.6	39.2*	0.0	89.5
A1K043	*Aureobasidium pullulans*	41.3	39.8*	71.8	88.8
C4K081	*Aureobasidium pullulans*	37.5	40.0*	35.7	68.1
D1P037	*Aureobasidium pullulans*	44.9	37.8	100.0	87.0
B4P060	*Aureobasidium pullulans*	38.3	37.0	95.3	76.8
D3P009b	*Cystobasidium pinicola*	16.7	32.9	102.0	115.4
B3K004	*Metschnikowia pulcherrima*	37.3	34.1	87.0	84.9
C3P008	*Metschnikowia* sp.	25.9	35.8	0.0[b]	73.6
A3P071	*Papiliotrema flavescens*	25.9	38.3	0.0	93.3
A4P066	*Papiliotrema flavescens*	23.5	30.3	0.0	87.8
B3P048	*Papiliotrema flavescens*	27.2	25.3	0.0	100.0
A2P025	*Papiliotrema flavescens*	25.6	35.0	0.0	91.9
C2P072	*Papiliotrema flavescens*	23.5	33.3	100.0	66.7
C2K025	*Papiliotrema flavescens*	25.9	35.8	100.0	87.5
D4K115	*Papiliotrema flavescens*	25.0	37.8	94.0	97.2
C4K058	*Papiliotrema flavescens*	25.7	31.3	92.3	76.0
C1P081	*Papiliotrema flavescens*	25.9	37.8	81.9	94.5
D3K042	*Papiliotrema flavescens*	33.3	50.0*	93.8	82.1
A3P017	*Vishniacozyma carnescens*	27.5	32.1	85.3	75.0
C2K045	*Vishniacozyma carnescens*	25.9	29.6	96.9	104.3
C4K010	*Vishniacozyma carnescens*	30.8	47.5*	79.6	76.9
C4K012	*Vishniacozyma* sp.	28.6	35.4	0.0[b]	98.6
B3P084	*Vishniacozyma* sp.	32.1	29.3	58.7	89.7

[a] *Growth inhibition was tested on the H. fraxineus isolates P3 and HF23. *Significantly increased in comparison to the control M. pulcherrima (B3K065), which did not show antagonistic activity in dual cultures (growth inhibition rates: 28.4 and 15.8). The test was performed by Kruskal-Wallis one-way analysis of variance on ranks followed by pairwise comparisons with Dunn's method ($P < 0.05$).* [b] *Detection of the antagonistic isolate inside the recovered H. fraxineus mycelium or instead of the mycelium.*

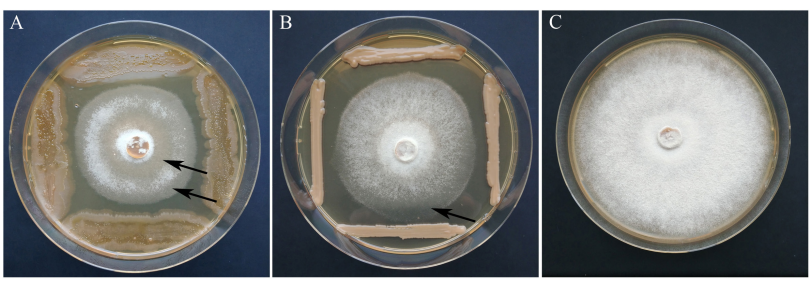

FIGURE 5 | Growth inhibition of *H. fraxineus* P3 after cocultivation with *A. pullulans* A3K040 **(A)** and *P. flavescens* A3P071 **(B)** in comparison to the control **(C)**. The clearing of the *H. fraxineus* mycelium which indicates an ongoing lysis of the pathogen is marked by arrows.

10 days after cocultivation. This effect was differently pronounced in both isolates.

Filamentous Fungi

Due to the high proportion of *A. pullulans* among the filamentous fungi, more than half of the fungi tested here belonged to this species. To avoid testing clones of the same strain, only a selection of *A. pullulans* strains was tested per sample. Accordingly, the screening of filamentous fungi included 695 isolates. As a result, 79 isolates (11.4% of the total isolates) inhibited the pathogen growth by at least 43%, i.e., higher than the mean self-inhibition rate of *H. fraxineus* P3. The highest values were determined for

the *Cladosporium* isolates C1K002 and A3K053 with inhibition rates of 70 and 60%. The positively screened isolates obtained in comparable proportions from tolerant and susceptible trees represented members of *Aureobasidium* (40%), *Pyrenochaeta* (16%), *Cladosporium* (10%), *Gibberella* (10%), and *Pleosporales* (8%) as well as *Diplodia, Didymella, Sarocladium*, and *Phomopsis* with lower occurrence. The inhibition rates per group varied between 41 and 55%.

Most likely due to the different test procedures, the filamentous isolates inhibited *H. fraxineus* P3 by 48%, whereas the mean inhibition rate of yeast-like isolates was 37%. Otherwise, not only the procedure but also the morphological status of the fungal isolate could be of importance for the antagonistic properties of fungi.

Out of the 79 antagonistic isolates, 37 were derived from different samples and taxonomic groups. To exclude clones from the subsequent statistical test, only these isolates were selected. As shown in **Table 2**, four isolates suppressed either *H. fraxineus* strain significantly with inhibition rates from 72 to 100%. The inhibitory effects were distinctly above the level of self-inhibition for *H. fraxineus*. Five further isolates inhibited one of the *H. fraxineus* strains significantly with rates between 57 and 93%.

The most effective isolates C1K002 and D1K008, which inhibited the pathogen almost completely, were members of the genus *Cladosporium*. Both isolates showed a rapid growth by strong sporulation and were already able to suppress the *H. fraxineus* strains during the first week of cocultivation. Accordingly, the growth of *H. fraxineus* was affected even in its initial phase. After 14 days, no or very few mycelia from *H. fraxineus* had grown (**Figure 6** and **Table 2**). A third *Cladosporium* isolate (A3K053) showed an almost comparable antagonistic activity, with inhibition rates of 72 to 76%. Additionally, B2K028 and D1K016 were able to kill the pathogen more or less completely. This killing was achieved by the ingrowing of the antagonistic fungus into the *H. fraxineus* colony. Consequently, the antagonistic isolate was predominantly detected in the re-cultivation approach. The fourth isolate with clear significant effects, C4K037, was identified as *Gibberella tricincta.* Like other strains of this species, this isolate also tended to invade the *H. fraxineus* colony, which partly led to its occurrence in the re-cultivated mycelium of the pathogen (**Table 2**). In general, fungicidal effects that became visible during the re-cultivation approach have been observed within several taxonomic groups. These effects particularly concern isolates of fast-growing species: for example, *Diplodia fraxini*, *Cladosporium* sp., *Phomopsis velata,* and to a lesser extent, *A. pullulans*, and *S. strictum*.

DISCUSSION

To identify fungal taxa associated with tolerance to *H. fraxineus*, we analyzed the fungal communities of ash leaves by ITS2 amplicon sequencing and culturing. Leaf-colonizing fungi are considered as a barrier to invaders such as *H. fraxineus* that spread starting from leaf infections (Cross et al., 2017; Hanackova et al., 2017b). The indigenous fungi fight against the invading pathogen directly by resource and space competition, partly supported by antibiosis, parasitism or indirectly by the induction of plant resistance (Busby et al., 2016; Jia et al., 2020).

Our study was based on the assumption that both epi- and endophytic fungi interact with the pathogen in a similar way. During and directly after the invasion and penetration of epidermal tissue, the pathogenic fungus is in contact with both habitats, the phyllosphere and endosphere of the ash leaves. Aside from that, several indigenous microorganisms can switch between the two habitats (Hardoim et al., 2015; van Overbeek and Saikkonen, 2016). Accordingly, both habitats were sampled in a combined approach.

Culture-independent as well as culturing approaches showed a strong presence of saprophytic yeasts, especially within the phyllosphere communities (Slavikova et al., 2007; Davydenko et al., 2013; Hanackova et al., 2017a; Kemler et al., 2017). Yeasts thrive on plant exudates, whereas plants can benefit from the secondary metabolites produced by yeast, e.g., auxins, chelates, and glycolipids (Fonseca and Inacio, 2006; Kemler et al., 2017). In addition, several yeasts possess antifungal activities based on resource competition, antibiosis, biofilm formation or the production of volatile organic compounds (Liu et al., 2013; Freimoser et al., 2019). Therefore, an intensive colonization of leaves with yeasts can contribute to higher plant fitness and pathogen resistance. While yeasts are very common in the phyllosphere, the endophytic community is dominated by filamentous fungi (Prior et al., 2017). In our study, the fungal

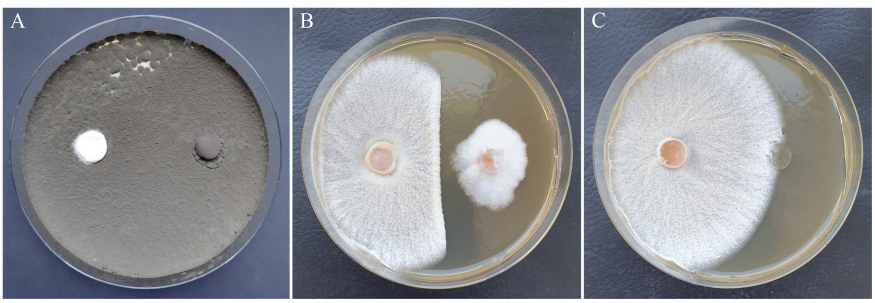

FIGURE 6 | Growth inhibition of *H. fraxineus* HF23 after cocultivation with *Cladosporium* sp. C1K002 **(A)** and *Sarocladium strictum* D3P026-P **(B)** in comparison to the *H. fraxineus* control **(C)**. Left plate side: *H. fraxineus*, right plate side: agar plug with antagonist **(A, B)** or without mycelium **(C)**.

TABLE 2 | Antagonistic activity of filamentous epi/endophytic fungi as assessed by the growth inhibition of *H. fraxineus* and a vitality test of the remaining pathogen mycelium.

Isolate	Taxonomic assignment	Growth inhibition rate in dual culture (%)[a]		Vitality of mycelium (% of untreated control)[a]	
		P3	HF23	P3	HF23
A1P017	*Aureobasidium pullulans*	43.8	42.5	90.8	42.3[b]
A3K056	*Aureobasidium pullulans*	43.8	48.3	90.8	80.8[b]
A1K012	*Aureobasidium pullulans*	43.8	41.4	89.5	70.5[b]
A3P027	*Aureobasidium pullulans*	41.9	42.5	90.8	102.6
A4P023	*Aureobasidium pullulans*	44.8	52.9	76.3[b]	93.8[b]
B1K008	*Aureobasidium pullulans*	42.9	52.9	76.3	102.6
B3P001	*Aureobasidium pullulans*	44.8	46.0	90.8	32.1[b]
B4P025	*Aureobasidium pullulans*	45.7	42.5	88.2	56.3
C1P010	*Aureobasidium pullulans*	43.8	20.9	90.0	94.8
C3K025	*Aureobasidium pullulans*	41.9	34.8	90.0	3.4[b]
C1K002	*Cladosporium* sp.	100.0*	100.0*	0.0*	0.0
D1K008	*Cladosporium* sp.	87.2*	100.0*	20.0[b]	0.0
A3K053	*Cladosporium* sp.	75.8*	71.6*	36.8[b]	0.0[b]
D1K021	*Cladosporium* sp.	42.8	74.7	60.0[b]	0.0[b]
C2K082	*Cladosporium* sp.	44.8	93.3*	86.0[b]	0.0
B4K021	*Didymella exigua*	44.8	42.8	90.0[b]	86.2[b]
D1K016	*Diplodia fraxini*	49.7	59.6	0.0*,[b]	8.6[b]
C4P019	*Gibberella tricincta*	72.1*	71.2	80.0	86.2[b]
C4K037	*Gibberella tricincta*	75.6*	86.4*	76.0[b]	95.0
B2K028	*Phomopsis velata*	55.6	52.9	0.0*,[b]	0.0[b]
B4K006a	*Phomopsis velata*	36.9	27.6	92.0[b]	94.8[b]
B4K006b	*Phomopsis velata*	46.7	39.4	50.0[b]	17.2[b]
B1P004	*Phomopsis velata*	51.7	16.5	0.0*,[b]	85.7[b]
B2K017	*Pleosporales* spp.	59.6	57.8	86.6	100.0
B2K022	*Pleosporales* spp.	66.7*	54.9	81.6[b]	100.0
B1P005	*Pleosporales* spp.	45.4	54.5	86.0	89.3
C2K088	*Pleosporales* spp.	22.4	−3.8	88.0	76.9
A4K021	*Pyrenochaeta* spp.	44.7	26.6	78.3	100.0
A4P009	*Pyrenochaeta* spp.	67.5*	31.4	80.3	95.0
B1K010	*Pyrenochaeta* spp.	57.5*	51.0	78.9	95.0
A1K007	*Pyrenochaeta spp.*	52.1	28.1	80.6	91.3
B4P008	*Pyrenochaeta spp.*	51.1	26.6	81.2	87.5
B3P007	*Pyrenochaeta spp.*	50.0	28.1	83.6	100.0
C3P017	*Pyrenochaeta spp.*	40.8	7.6	88.0	83.9
C2K078	*Pyrenochaeta spp.*	38.2	7.6	88.0	90.3
D3P026-P	*Sarocladium strictum*	46.2	40.0	55.1	107.7
C2P015	*Sarocladium strictum*	33.7	42.4	80.0	53.6[b]
Self-inhibition	*H. fraxineus*	49.3	43.6	92.4	97.2

[a]*Growth inhibition was tested on the H. fraxineus isolates P3 and HF23. *Significantly increased in comparison to control Didymella unclass. (B4K020), which did not show antagonistic activity in dual cultures (growth inhibition rates: 20.4 and 19.8). The test was performed by Kruskal-Wallis one-way analysis of variance on ranks followed by pairwise comparisons with Dunn's method ($P < 0.05$).* [b]*Detection of the antagonistic isolate inside the re-cultivated H. fraxineus mycelium.*

community was clearly dominated by the yeast-like fungus *A. pullulans*. This species is a very abundant colonizer of plant surfaces but was also often isolated as an endophyte from trees (Albrectsen et al., 2010; Martin-Garcia et al., 2012), including common ash (Slavikova et al., 2007; Davydenko et al., 2013; Hanackova et al., 2017a). As a pleiomorphic fungus, it is known to switch between yeast and mycelial forms in response to its environmental conditions (Ramos and García Acha, 1975; Campbell et al., 2004). Among the next-most abundant fungi, *P. flavescens* and *V. carnescens* belong to yeasts, while *Pyrenochaeta* spp. and *Cladosporium* spp. have filamentous growth habits.

The fungal communities of tolerant and susceptible *F. excelsior* trees showed a similar genetic diversity and community structure. Nevertheless, the differential abundance analysis and the indicator species analysis revealed several OTUs as well as an isolate group with significant relations to the health status of the trees. In addition to the predominant *P. flavescens*

OTU0003, several less abundant OTUs and the isolate group *S. strictum* could be detected. Strains from the genus *Papiliotrema* are known for their protective effect against fungal disease-related pre- and postharvest losses of different crops. Especially isolates of *P. flavescens* (formerly *Cryptococcus flavescens*) are widely used as biocontrol agents against head blight on cereals caused by *Fusarium graminearum* (Dunlap and Schisler, 2010; McSpadden Gardener et al., 2014; Schisler et al., 2014). Similarly, the postharvest infestation of different fruits with common pathogens such as *Botrytis cinerea*, *Alternaria alternata*, and *Penicillium expansum* were shown to be reduced effectively by *P. flavescens* and *P. laurentii* strains (Qin and Tian, 2004; Zhang et al., 2007; Kheireddine et al., 2018). Various *Sarocladium* strains are discussed as potential antagonists due to the formation of antifungal substances such as antibiotics and hydrolytic enzymes (Wicklow et al., 2005; Guimarães et al., 2017). In addition, *S. strictum* has been shown to have disease-reducing effects through mycoparasitism, e.g., on *Botrytis cinerea* and *Helminthosporium solani* (Rivera et al., 2007; Choi et al., 2008). However, the use of *S. strictum* as a biocontrol agent might be limited due to the putative human pathogenic potential of this species (Schell and Perfect, 1996; Sharma et al., 2013). Consequently, the comprehensive analysis by applying a marker gene study and a culturing approach resulted in two distinct fungal groups which are specific to tolerant ash trees and might be associated with the ability of the trees to resist the pathogen.

As a result of the cocultivation test on antagonism, several yeast isolates were found to possess an antagonistic capacity by a direct growth reduction of *H. fraxineus* (of up to 50%) and/or an ongoing mycelium lysis, resulting in the complete killing of one of the pathogen strains. Cell-lytic effects from the secretion of exoenzymes have been described for several antagonistic yeasts (Bar-Shimon et al., 2004; Zhang et al., 2011, 2012). The lysis of fungal cell walls usually involves various synergistically acting enzymes, including glucanases, chitinases and proteases (Salazar and Asenjo, 2007). In particular, numerous strains of *A. pullulans* harbor a broad spectrum of lytic enzymes. This enzymatic activity as well as the production of other antimicrobial compounds make *A. pullulans* a versatile biocontrol agent (Federici, 1982; Prasongsuk et al., 2018). Similar to *P. flavescens*, *A. pullulans* but also *Metschnikowia* and *Vishniacozyma* strains can effectively mitigate pre- and postharvest infections (Mari et al., 2012; Gramisci et al., 2018; Pawlikowska et al., 2019).

Compared to the yeasts, the filamentous fungi usually showed stronger antagonistic effects, even if the differences of the applied tests were taken into account. Three *Cladosporium isolates* (C1K002, D1K008, and A3K053) suppressed both *H. fraxineus* strains significantly with inhibition rates of 72–100%. The strong effects were also indicated by a clear reduction in the pathogen vitality. Fungicidal effects were also observed for *Diplodia fraxini* D1K016 and *Phomopsis velata* B2K028. All these isolates were representatives of fast-growing species that affected and displaced the pathogen in dual culture by strong sporulation or by overgrowing. Hanackova et al. (2017a) tested a number of endophytic fungi of common ashes in a similar approach and found comparable high inhibition rates. The best results were also achieved for fast-growing species, e.g., *Botrytis cinerea* and *Phoma macrostoma*. However, *Diplodia fraxini,* species of *Phomopsis* (syn. *Diaporthe*) and *Botrytis cinerea* are also known as plant pathogens (Elena et al., 2018; Hua et al., 2018; Sessa et al., 2018). Moreover, a promising antagonist (*Hypoxylon rubiginosum*) was also found through the detection of the antifungal metabolite phomopsidin, although the *in vitro* inhibitory effect was less pronounced (Halecker et al., 2020). Remarkably, studying endophytic fungi from dieback-tolerant ash species including *F. mandshurica* and *F. ornus* resulted in somewhat lower antagonistic activity against *H. fraxineus,* with inhibition rates of 40–64% (Kosawang et al., 2018).

Three of the isolates with the highest antagonistic activity were members of the genus *Cladosporium*. This genus was found to be the second-most abundant taxon among the leaf fungal communities of the dieback-tolerant Manchurian ash (Cleary et al., 2016). Furthermore, *Cladosporium* is closely related to the genus *Mycosphaerella* (Braun et al., 2003), which represented the predominant fungal group of the Manchurian ash (Cleary et al., 2016). Both genera include numerous widespread species varying in their ecological roles, including plant pathogens, mutualistic endophytes, saprophytes or hyperparasites on other fungi (Crous, 2009; Bensch et al., 2012). The ability of *Cladosporium* species to parasitize other fungi, in particular those causing rust diseases of agricultural and forestry crops (i.e., *Puccinia* sp.) has been demonstrated for decades in numerous studies (Tsuneda and Hiratsuka, 1979; Moricca et al., 2005; Zhan et al., 2014; Torres et al., 2017). One *Cladosporium* species (*C. delicatulum*) was also found to be a mycoparasite on *Taphrina pruni*, the plum gall pathogen of *Prunus* species (Amanelah Baharvandi and Zafari, 2015). Thus, recent data indicate that *Cladosporium* species have potential in plant diseases management. However, further studies are needed to clarify the biology of the antagonism. Since some *Cladosporium* strains can also be pathogenic to vertebrate hosts, including humans (Sandoval-Denis et al., 2016), the biosafety of the respective strains must be guaranteed on a case-specific basis (Torres et al., 2017).

The two *H. fraxineus* strains used in the dual culture experiment showed a different sensitivity to a range of antagonists. The *H. fraxineus* strain P3 was more damaged by some yeast isolates, while HF23 showed a higher sensitivity to individual filamentous fungi, including isolates of *Cladosporium*. *H. fraxineus* is known for its intrinsic diversity, which was indicated by the differing growth rates, enzymatic activity and virulence of various isolates (Junker, 2013; Junker et al., 2017). Against the background that the ash dieback invasion of Europe started with only two strains, a further increase in genetic diversity can be expected (McMullan et al., 2018). Accordingly, subsequent *in planta* tests of antagonistic activity should be performed with infected petioles representing the natural *H. fraxineus* populations from a typical ash forest. It remains unclear to what extent our results from the *in vitro* studies can be confirmed using this approach. Another critical aspect of *in vitro* testing is the lack of interactions of the antagonists with the plant holobiont. The complex plant-microbiota interaction can lead to both a reduction and an enhancement of the desired effect (Knudsen et al., 1997; Schulz et al., 2015; Latz et al., 2018).

In conclusion, the comparative analysis of the leaf-inhabiting fungi from susceptible and tolerant ashes revealed a high similarity in the community structure. Only a few fungal groups primarily belonging to *P. flavescens* and *S. strictum*, showed a distinctly higher abundance in tolerant ashes. These specific groups are suggested to improve pathogen tolerance, which could be mediated by competition, by inducing a systemic resistance or just by altering the microbial community structure (Pieterse et al., 2014; Romera et al., 2019). Additionally, *in vitro* tests of antagonism against *H. fraxineus* indicated clear inhibitory effects of various yeasts and particularly of several fast growing filamentous fungi. Both, the yeasts with the relatively mild inhibitory effects and the filamentous species with stronger activities, particularly *Cladosporium* sp. C1K002 and D1K008, could be involved in disease suppression. Based on these results, for the next step, *in planta* tests are necessary to evaluate these promising groups and isolates with respect to their efficacy and stability in inhibiting *H. fraxineus*. In this context, possible shifts in the microbial community should be studied and might be correlated with the plant health as well.

DATA AVAILABILITY STATEMENT

The datasets presented in this study can be found in online repositories. The names of the repository/repositories and accession number(s) can be found below: https://www.ncbi.nlm.nih.gov/genbank/, PRJNA611938.

AUTHOR CONTRIBUTIONS

RB and KU performed the experiments, analyzed the data, and prepared the manuscript. UB performed the MALDI-TOF MS analysis. KU, MK, and AU conducted the microbiome analysis. All authors listed here substantially contributed to and approved the manuscript. AU and MK supervised the entire study.

FUNDING

This study was supported by Grant 22006116 from the Fachagentur Nachwachsende Rohstoffe (FNR), Germany.

ACKNOWLEDGMENTS

We thank our colleagues from the forest district of Lendershagen, as well as Ben Bubner, Volker Schneck and Falk Schäfer for monitoring the ash plots and for their assistance with the sampling campaign. We are grateful to Ulrike Klauß and Heidrun Mattauch for providing excellent technical assistance.

REFERENCES

Albrectsen, B. R., Bjorken, L., Varad, A., Hagner, A., Wedin, M., Karlsson, J., et al. (2010). Endophytic fungi in European aspen (*Populus tremula*) leaves-diversity, detection, and a suggested correlation with herbivory resistance. *Fungal Divers.* 41, 17–28. doi: 10.1007/s13225-009-0011-y

Amanelah Baharvandi, H., and Zafari, D. (2015). Identification of *Cladosporium delicatulum* as a mycoparasite of *Taphrina pruni*. *Arch. Phytopathol.* 48, 688–697. doi: 10.1080/03235408.2015.1099886

Baral, H.-O., Queloz, V., and Hosoya, T. (2014). *Hymenoscyphus fraxineus*, the correct scientific name for the fungus causing ash dieback in Europe. *IMA Fungus* 5, 79–80. doi: 10.5598/imafungus.2014.05.01.09

Bar-Shimon, M., Yehuda, H., Cohen, L., Weiss, B., Kobeshnikov, A., Daus, A., et al. (2004). Characterization of extracellular lytic enzymes produced by the yeast biocontrol agent *Candida oleophila*. *Curr. Genet.* 45, 140–148. doi: 10.1007/s00294-003-0471-7

Bengtsson-Palme, J., Ryberg, M., Hartmann, M., Branco, S., Wang, Z., Godhe, A., et al. (2013). Improved software detection and extraction of ITS1 and ITS2 from ribosomal ITS sequences of fungi and other eukaryotes for analysis of environmental sequencing data. *Methods Ecol. Evol.* 4, 914–919. doi: 10.1111/2041-210x.12073

Bensch, K., Braun, U., Groenewald, J. Z., and Crous, P. W. (2012). The genus *Cladosporium*. *Stud. Mycol.* 72, 1–379. doi: 10.3114/sim0003

Berg, G., Koberl, M., Rybakova, D., Muller, H., Grosch, R., and Smalla, K. (2017). Plant microbial diversity is suggested as the key to future biocontrol and health trends. *FEMS Microbiol. Ecol.* 93:fix050. doi: 10.1093/femsec/fix050

Berg, G., Rybakova, D., Grube, M., and Köberl, M. (2015). The plant microbiome explored: implications for experimental botany. *J. Exp. Bot.* 67, 995–1002. doi: 10.1093/jxb/erv466

Berg, G., and Smalla, K. (2009). Plant species and soil type cooperatively shape the structure and function of microbial communities in the rhizosphere. *FEMS Microbiol. Ecol.* 68, 1–13.

Braun, U., Crous, P., Dugan, F., Groenewald, J. Z., and Hoog, S. (2003). Phylogeny and taxonomy of *Cladosporium*-like hyphomycetes, including *Davidiella* gen. nov., the teleomorph of *Cladosporium* s. str. *Mycol. Prog.* 2, 3–18. doi: 10.1007/s11557-006-0039-2

Busby, P. E., Ridout, M., and Newcombe, G. (2016). Fungal endophytes: modifiers of plant disease. *Plant Mol. Biol.* 90, 645–655. doi: 10.1007/s11103-015-0412-0

Campbell, B., Siddique, A.-B., McDougall, B., and Seviour, R. (2004). Which morphological forms of the fungus *Aureobasidium pullulans* are responsible for pullulan production? *FEMS Microbiol. Lett.* 232, 225–228. doi: 10.1016/S0378-1097(04)00076-X

Choi, G., Kim, J.-C., Jang, K., Cho, K., and Kim, H. (2008). Mycoparasitism of *Acremonium strictum* BCP on *Botrytis cinerea*, the gray mold pathogen. *J. Microbiol. Biotechnol.* 18, 167–170.

Chong, J., Liu, P., Zhou, G., and Xia, J. (2020). Using microbiomeanalyst for comprehensive statistical, functional, and meta-analysis of microbiome data. *Nat. Protoc.* 15, 799–821. doi: 10.1038/s41596-019-0264-1

Chudejova, K., Bohac, M., Skalova, A., Rotova, V., Papagiannitsis, C. C., Hanzlickova, J., et al. (2017). Validation of a novel automatic deposition of bacteria and yeasts on MALDI target for MALDI-TOF MS-based identification using MALDI Colonyst robot. *PLoS One* 12:e0190038. doi: 10.1371/journal.pone.0190038

Cleary, M., Nguyen, D., Marciulyniene, D., Berlin, A., Vasaitis, R., and Stenlid, J. (2016). Friend or foe? Biological and ecological traits of the European ash dieback pathogen *Hymenoscyphus fraxineus* in its native environment. *Sci. Rep.* 6:21895. doi: 10.1038/srep21895

Compant, S., Samad, A., Faist, H., and Sessitsch, A. (2019). A review on the plant microbiome: ecology, functions, and emerging trends in microbial application. *J. Adv. Res.* 19, 29–37. doi: 10.1016/j.jare.2019.03.004

Cross, H., Sønstebø, J. H., Nagy, N. E., Timmermann, V., Solheim, H., Børja, I., et al. (2017). Fungal diversity and seasonal succession in ash leaves infected by the invasive ascomycete *Hymenoscyphus fraxineus*. *New Phytol.* 213, 1405–1417. doi: 10.1111/nph.14204

Crous, P. (2009). Taxonomy and phylogeny of the genus *Mycosphaerella* and its anamorphs. *Fungal Divers.* 38, 1–24.

Davydenko, K., Vasaitis, R., Stenlid, J., and Menkis, A. (2013). Fungi in foliage and shoots of *Fraxinus excelsior* in eastern Ukraine: a first report on *Hymenoscyphus pseudoalbidus*. *Forest Pathol.* 43, 462–467. doi: 10.1111/efp.12055

Doyle, J. J. (1990). Isolation of plant DNA from fresh tissue. *Focus* 12, 13–15.

Drenkhan, R., Solheim, H., Bogacheva, A., Riit, T., Adamson, K., Drenkhan, T., et al. (2017). *Hymenoscyphus fraxineus* is a leaf pathogen of local *Fraxinus* species in the Russian far east. *Plant Pathol.* 66, 490–500. doi: 10.1111/ppa.12588

Dufrêne, M., and Legendre, P. (1997). Species assemblages and indicator species: the need for a flexible asymmetrical approach. *Ecol. Monogr.* 67, 345–366.

Dunlap, C. A., and Schisler, D. A. (2010). Fluidized-bed drying and storage stability of *Cryptococcus flavescens* OH 182.9, a biocontrol agent of Fusarium head blight. *Biocontrol Sci. Technol.* 20, 465–474. doi: 10.1080/09583150903572377

Edgar, R. C. (2010). Search and clustering orders of magnitude faster than BLAST. *Bioinformatics* 26, 2460–2461. doi: 10.1093/bioinformatics/btq461

Edgar, R. C. (2013). UPARSE: highly accurate OTU sequences from microbial amplicon reads. *Nat. Methods* 10, 996–998. doi: 10.1038/nmeth.2604

Elena, G., León, M., Abad-Campos, P., Armengol, J., Mateu-Andrés, I., and Güemes-Heras, J. (2018). First report of *Diplodia fraxini* causing dieback of *Fraxinus angustifolia* in Spain. *Plant Dis.* 102, 2645–2645. doi: 10.1094/pdis-05-18-0792-pdn

Fadiji, A. E., and Babalola, O. O. (2020). Elucidating mechanisms of endophytes used in plant protection and other bioactivities with multifunctional prospects. *Front. Bioeng. Biotechnol.* 8:467. doi: 10.3389/fbioe.2020.00467

Federici, F. (1982). Extracellular enzymatic activities in *Aureobasidium pullulans*. *Mycologia* 74, 738–743. doi: 10.2307/3792859

Fonseca, A., and Inacio, J. P. (2006). "Phylloplane yeasts," in *Biodiversity and Ecophysiology of Yeasts*, eds G. Peter and C. Rosa (Berlin: Springer), 263–301.

Freimoser, F. M., Rueda-Mejia, M. P., Tilocca, B., and Migheli, Q. (2019). Biocontrol yeasts: mechanisms and applications. *World J. Microbiol. Biotechnol.* 35:154. doi: 10.1007/s11274-019-2728-4

Gardes, M., and Bruns, T. D. (1993). ITS primers with enhanced specificity for *Basidiomycetes* – application to the identification of mycorrhizae and rusts. *Mol. Ecol.* 2, 113–118. doi: 10.1111/j.1365-294X.1993.tb00005.x

Glick, B. R. (2012). Plant growth-promoting bacteria: mechanisms and applications. *Scientifica* 2012:15. doi: 10.6064/2012/963401

Gramisci, B. R., Lutz, M. C., Lopes, C. A., and Sangorrín, M. P. (2018). Enhancing the efficacy of yeast biocontrol agents against postharvest pathogens through nutrient profiling and the use of other additives. *Biol. Control* 121, 151–158. doi: 10.1016/j.biocontrol.2018.03.001

Griffiths, S. M., Galambao, M., Rowntree, J., Goodhead, I., Hall, J., O'Brien, D., et al. (2020). Complex associations between cross−kingdom microbial endophytes and host genotype in ash dieback disease dynamics. *J. Ecol.* 108, 291–309. doi: 10.1111/1365-2745.13302

Gross, A., Holdenrieder, O., Pautasso, M., Queloz, V., and Sieber, T. N. (2014). *Hymenoscyphus pseudoalbidus*, the causal agent of European ash dieback. *Mol. Plant Pathol.* 15, 5–21. doi: 10.1111/mpp.12073

Guimarães, R. A., da Silva, Lobo, V. L., Côrtes, M. V. C. B., Corsi de Filippi, M. C., and Prabhu, A. S. (2017). Characterization of *Sarocladium oryzae* and its reduction potential of rice leaf blast. *Pesq. Agropec. Trop. Goiânia* 47, 41–52.

Halecker, S., Wennrich, J.-P., Rodrigo, S., Andrée, N., Rabsch, L., Baschien, C., et al. (2020). Fungal endophytes for biocontrol of ash dieback: the antagonistic potential of *Hypoxylon rubiginosum*. *Fungal Ecol.* 45:100918. doi: 10.1016/j.funeco.2020.100918

Han, J.-G., Shrestha, B., Hosoya, T., Lee, K.-H., Sung, G.-H., and Shin, H.-D. (2014). First report of the ash dieback pathogen *Hymenoscyphus fraxineus* in Korea. *Mycobiology* 42, 391–396. doi: 10.5941/MYCO.2014.42.4.391

Hanackova, Z., Havrdova, L., Cerny, K., Zahradnik, D., and Koukol, O. (2017a). Fungal endophytes in ash shoots – diversity and inhibition of *Hymenoscyphus fraxineus*. *Balt. For.* 23, 89–106.

Hanackova, Z., Koukol, O., Cmokova, A., Zahradnik, D., and Havrdova, L. (2017b). Direct evidence of *Hymenoscyphus fraxineus* infection pathway through the petiole-shoot junction. *Forest Pathol.* 47:12370. doi: 10.1111/efp.12370

Hardoim, P. R., van Overbeek, L. S., Berg, G., Pirttilä, A. M., Compant, S., Campisano, A., et al. (2015). The hidden world within plants: ecological and evolutionary considerations for defining functioning of microbial endophytes. *Microbiol. Mol. Biol. Rev.* 79, 293–320. doi: 10.1128/mmbr.00050-14

Hossain, M. M., Sultana, F., and Islam, S. (2017). "Plant growth-promoting fungi (PGPF): phytostimulation and induced systemic resistance," in *Plant-Microbe Interactions in Agro-Ecological Perspectives*, eds D. Singh, H. Singh, and R. Prabha (Singapore: Springer).

Hua, L., Yong, C., Zhanquan, Z., Boqiang, L., Guozheng, Q., and Shiping, T. (2018). Pathogenic mechanisms and control strategies of *Botrytis cinerea* causing post-harvest decay in fruits and vegetables. *Food Qual. Saf.* 2, 111–119. doi: 10.1093/fqsafe/fyy016

Huschek, D., and Witzel, K. (2019). Rapid dereplication of microbial isolates using matrix-assisted laser desorption ionization time-of-flight mass spectrometry: a mini-review. *J. Adv. Res.* 19, 99–104. doi: 10.1016/j.jare.2019.03.007

Ihrmark, K., Bödeker, I. T. M., Cruz-Martinez, K., Friberg, H., Kubartova, A., Schenck, J., et al. (2012). New primers to amplify the fungal ITS2 region – evaluation by 454-sequencing of artificial and natural communities. *FEMS Microbiol. Ecol.* 82, 666–677.

Inacio, J., Pereira, P., de Carvalho, M., Fonseca, A., Amaral-Collaco, M. T., and Spencer-Martins, I. (2002). Estimation and diversity of phylloplane mycobiota on selected plants in a Mediterranean-type ecosystem in Portugal. *Microb. Ecol.* 44, 344–353. doi: 10.1007/s00248-002-2022-z

Jia, Q., Qu, J., Mu, H., Sun, H., and Wu, C. (2020). Foliar endophytic fungi: diversity in species and functions in forest ecosystems. *Symbiosis* 80, 103–132. doi: 10.1007/s13199-019-00663-x

Junker, C. (2013). *Pathogenese und Ansätze zur Kontrolle von Hymenoscyphus Pseudoalbidus – Erreger der Eschentriebsterbens: Variabilität von Virulenz, Morphologie, Biochemie und Sekundärstoffwechsel*. Ph.D. thesis, Technische Universität Braunschweig, Brunswick.

Junker, C., de Vries, J., Eickhorst, C., and Schulz, B. (2017). Each isolate of *Hymenoscyphus fraxineus* is unique as shown by exoenzyme and growth rate profiles. *Balt. For.* 23, 25–40.

Kemler, M., Witfeld, F., Begerow, D., and Yurkov, A. (2017). "Phylloplane yeasts in temperate climates," in *Yeasts in Natural Ecosystems: Diversity*, eds P. Buzzini, M.-A. Lachance, and A. Yurkov (Cham: Springer International Publishing), 171–197.

Kheireddine, A., Essghaier, B., Hedi, A., Dhieb, C., and Sadfi-Zouaoui, N. (2018). New epiphytic yeasts able to reduce grey mold disease on apples. *Plant Prot. Sci.* 54, 248–257. doi: 10.17221/103/2017-pps

Kirisits, T., and Schwanda, K. (2015). First definite report of natural infection of *Fraxinus ornus* by *Hymenoscyphus fraxineus*. *Forest Pathol.* 45, 430–432.

Knudsen, I. M. B., Hockenhull, J., Jensen, D. F., Gerhardson, B., Hökeberg, M., Tahvonen, R., et al. (1997). Selection of biological control agents for controlling soil and seed-borne diseases in the field. *Eur. J. Plant Pathol.* 103, 775–784. doi: 10.1023/A:1008662313042

Kõljalg, U., Nilsson, R. H., Abarenkov, K., Tedersoo, L., Taylor, A. F. S., Bahram, M., et al. (2013). Towards a unified paradigm for sequence-based identification of fungi. *Mol. Ecol.* 22, 5271–5277. doi: 10.1111/mec.12481

Kosawang, C., Amby, D. B., Bussaban, B., McKinney, L. V., Xu, J., Kjaer, E. D., et al. (2018). Fungal communities associated with species of *Fraxinus* tolerant to ash dieback, and their potential for biological control. *Fungal Biol.* 122, 110–120. doi: 10.1016/j.funbio.2017.11.002

Kosawang, C., Sorensen, H., Kjaer, E. D., Dilokpimol, A., McKinney, L. V., Collinge, D. B., et al. (2019). Defining the twig fungal communities of *Fraxinus* species and *Fraxinus excelsior* genotypes with differences in susceptibility to ash dieback. *Fungal Ecol.* 42:100859. doi: 10.1016/j.funeco.2019.08.003

Kowalski, T. (2006). *Chalara fraxinea* sp nov associated with dieback of ash (*Fraxinus excelsior*) in Poland. *Forest Pathol.* 36, 264–270. doi: 10.1111/j.1439-0329.2006.00453.x

Kowalski, T., and Holdenrieder, O. (2009). Pathogenicity of *Chalara fraxinea*. *Forest Pathol.* 39, 1–7. doi: 10.1111/j.1439-0329.2008.00565.x

Kozich, J. J., Westcott, S. L., Baxter, N. T., Highlander, S. K., and Schloss, P. D. (2013). Development of a dual-index sequencing strategy and curation pipeline for analyzing amplicon sequence data on the MiSeq Illumina sequencing platform. *Appl. Environ. Microbiol.* 79, 5112–5120. doi: 10.1128/Aem.01043-13

Latz, M. A. C., Jensen, B., Collinge, D. B., and Jorgensen, H. J. L. (2018). Endophytic fungi as biocontrol agents: elucidating mechanisms in disease suppression. *Plant Ecol. Divers.* 11, 555–567. doi: 10.1080/17550874.2018.1534146

Liu, H., Brettell, L. E., Qiu, Z., and Singh, B. K. (2020). Microbiome-mediated stress resistance in plants. *Trends Plant Sci.* 25, 733–743. doi: 10.1016/j.tplants.2020.03.014

Liu, J., Sui, Y., Wisniewski, M., Droby, S., and Liu, Y. (2013). Review: utilization of antagonistic yeasts to manage postharvest fungal diseases of fruit. *Int. J. Food Microbiol.* 167, 153–160. doi: 10.1016/j.ijfoodmicro.2013.09.004

Lobo, A., Hansen, J. K., McKinney, L. V., Nielsen, L. R., and Kjær, E. D. (2014). Genetic variation in dieback resistance: growth and survival of *Fraxinus excelsior* under the influence of *Hymenoscyphus pseudoalbidus*. *Scand. J. For. Res.* 29, 519–526. doi: 10.1080/02827581.2014.950603

Mari, M., Martini, C., Spadoni, A., Rouissi, W., and Bertolini, P. (2012). Biocontrol of apple postharvest decay by *Aureobasidium pullulans*. *Postharvest Biol. Technol.* 73, 56–62. doi: 10.1016/j.postharvbio.2012.05.014

Martin-Garcia, J., Muller, M. M., and Diez, J. J. (2012). ITS-based comparison of endophytic mycota in twigs of native *Populus nigra* and cultivated *P.* x *euramericana* (cv. I-214) stands in Northern Spain. *Ann. For. Sci.* 69, 49–57. doi: 10.1007/s13595-011-0129-4

McCune, B., and Mefford, M. J. (2015). *PC-ORD. Multivariate Analysis of Ecological Data*, 7.0 Edn. Gleneden Beach, OR: MjM Software.

McKinney, L. V., Nielsen, L. R., Collinge, D. B., Thomsen, I. M., Hansen, J. K., and Kjaer, E. D. (2014). The ash dieback crisis: genetic variation in resistance can prove a long-term solution. *Plant Pathol.* 63, 485–499. doi: 10.1111/ppa.12196

McMullan, M., Rafiqi, M., Kaithakottil, G., Clavijo, B. J., Bilham, L., Orton, E., et al. (2018). The ash dieback invasion of Europe was founded by two genetically divergent individuals. *Nat. Ecol. Evol.* 2, 1000–1008. doi: 10.1038/s41559-018-0548-9

McSpadden Gardener, B. B., Anderson Paul, P., Boehm, M. J., Rong, X., and Schisler, D. (2014). *Methods for using Crytococcus flavescens Strains for Biological Control of Fusarium Head Blight*. *Papers in Plant Pathology – Patent Application Publication* US Google Patent No. 2014/0271560A1.

Moricca, S., Ragazzi, A., and Assante, G. (2005). "Biocontrol of rust fungi by *Cladosporium tenuissimum*," in *Rust Diseases of Willow and Poplar*, eds M. H. Pei and A. R. McCracken (Wallingford: CAB International), 213–219.

Ondov, B. D., Bergman, N. H., and Phillippy, A. M. (2011). Interactive metagenomic visualization in a Web browser. *BMC Bioinformatics* 12:385. doi: 10.1186/1471-2105-12-385

Pane, C., and Zaccardelli, M. (2015). Evaluation of *Bacillus* strains isolated from solanaceous phylloplane for biocontrol of Alternaria early blight of tomato. *Biol. Control* 84, 11–18. doi: 10.1016/j.biocontrol.2015.01.005

Paulson, J. N., Stine, O. C., Bravo, H. C., and Pop, M. (2013). Differential abundance analysis for microbial marker-gene surveys. *Nat. Methods* 10, 1200–1205. doi: 10.1038/Nmeth.2658

Pawlikowska, E., James, S. A., Breierova, E., Antolak, H., and Kregiel, D. (2019). Biocontrol capability of local *Metschnikowia* sp. isolates. *Anton. Leeuw. Int. J. G.* 112, 1425–1445. doi: 10.1007/s10482-019-01272-w

Pieterse, C. M. J., Zamioudis, C., Berendsen, R. L., Weller, D. M., Wees, S. C. M. V., and Bakker, P. A. H. M. (2014). Induced systemic resistance by beneficial microbes. *Annu. Rev. Phytopathol.* 52, 347–375. doi: 10.1146/annurev-phyto-082712-102340

Prasongsuk, S., Lotrakul, P., Ali, I., Bankeeree, W., and Punnapayak, H. (2018). The current status of *Aureobasidium pullulans* in biotechnology. *Folia Microbiol.* 63, 129–140. doi: 10.1007/s12223-017-0561-4

Prior, R., Feige, A., and Begerow, D. (2017). Antagonistic activity of the phyllosphere fungal community. *Sydowia* 69, 183–198. doi: 10.12905/0380.sydowia69-2017-0483

Przybyl, K. (2003). Effect of *Pseudomonas* spp. on inoculation of young plants of *Fraxinus excelsior* stem with *Diplodia mutila*. *Dendrobiology* 50, 29–32.

Qin, G., and Tian, S. (2004). Biocontrol of postharvest diseases of jujube fruit by *Cryptococcus laurentii* combined with a low dosage of fungicides under different storage conditions. *Plant Dis.* 88, 497–501. doi: 10.1094/PDIS.2004.88.5.497

Queloz, V., Grunig, C., Berndt, R., Kowalski, T., Sieber, T., and Holdenrieder, O. (2011). Cryptic speciation in *Hymenoscyphus albidus*. *Forest Pathol.* 41, 133–142. doi: 10.1111/j.1439-0329.2010.00645.x

Ramos, S., and García Acha, I. (1975). A vegetative cycle of *Pullularia pullulans*. *Trans. Br. Mycol. Soc.* 64, 129–135, IN8–IN9. doi: 10.1016/S0007-1536(75)80083-0

Rivera, V., Freeman, T., Gudmestad, N., and Secor, G. (2007). Mycoparasitism of *Helminthosporium solani* by *Acremonium strictum*. *Phytopathology* 97, 1331–1337. doi: 10.1094/PHYTO-97-10-1331

Romera, F. J., Garcia, M. J., Lucena, C., Martinez-Medina, A., Aparicio, M. A., Ramos, J., et al. (2019). Induced systemic resistance (ISR) and Fe deficiency responses in dicot plants. *Front. Plant Sci.* 10:287. doi: 10.3389/fpls.2019.00287

Salazar, O., and Asenjo, J. A. (2007). Enzymatic lysis of microbial cells. *Biotechnol. Lett.* 29, 985–994. doi: 10.1007/s10529-007-9345-2

Sandoval-Denis, M., Gene, J., Sutton, D. A., Wiederhold, N. P., Cano-Lira, J. F., and Guarro, J. (2016). New species of *Cladosporium* associated with human and animal infections. *Persoonia* 36, 281–298. doi: 10.3767/003158516X691951

Schell, W. A., and Perfect, J. R. (1996). Fatal, disseminated *Acremonium strictum* infection in a neutropenic host. *J. Clin. Microbiol.* 34, 1333–1336.

Schisler, D. A., Core, A. B., Boehm, M. J., Horst, L., Krause, C., Dunlap, C. A., et al. (2014). Population dynamics of the *Fusarium* head blight biocontrol agent *Cryptococcus flavescens* OH 182.9 on wheat anthers and heads. *Biol. Control* 70, 17–27. doi: 10.1016/j.biocontrol.2013.11.011

Schlegel, M., Queloz, V., and Sieber, T. N. (2018). The endophytic mycobiome of european ash and sycamore maple leaves – geographic patterns, host specificity and influence of ash dieback. *Front. Microbiol.* 9:2345. doi: 10.3389/fmicb.2018.02345

Schloss, P. D., Westcott, S. L., Ryabin, T., Hall, J. R., Hartmann, M., Hollister, E. B., et al. (2009). Introducing mothur: open-source, platform-independent, community-supported software for describing and comparing microbial communities. *Appl. Environ. Microbiol.* 75, 7537–7541. doi: 10.1128/Aem.01541-09

Schulz, B., Haas, S., Junker, C., Andree, N., and Schobert, M. (2015). Fungal endophytes are involved in multiple balanced antagonisms. *Curr. Sci.* 109, 39–45.

Schulz, B., Rabsch, L., and Junker, C. (2019). "Chemical warfare in the plant microbiome leads to a balance of antagonisms and a healthy plant," in *Seed Endophytes: Biology and Biotechnology*, eds S. K. Verma and J. F. J. White (Berlin: Springer).

Sessa, L., Abreo, E., Bettucci, L., and Lupo, S. (2018). Diversity and virulence of *Diaporthe* species associated with wood disease symptoms in deciduous fruit trees in Uruguay. *Phytopathol. Mediterr.* 56, 431–444.

Sharma, A., Hazarika, N. K., Barua, P., Shivaprakash, M. R., and Chakrabarti, A. (2013). *Acremonium strictum*: report of a rare emerging agent of cutaneous hyalohyphomycosis with review of literatures. *Mycopathologia* 176, 435–441. doi: 10.1007/s11046-013-9709-1

Skovsgaard, J. P., Wilhelm, G. J., Thomsen, I. M., Metzler, B., Kirisits, T., Havrdova, L., et al. (2017). Silvicultural strategies for *Fraxinus excelsior* in response to dieback caused by *Hymenoscyphus fraxineus*. *Forestry* 90, 455–472. doi: 10.1093/forestry/cpx012

Slavikova, E., Vadkertiova, R., and Vranova, D. (2007). Yeasts colonizing the leaf surfaces. *J. Basic Microbiol.* 47, 344–350. doi: 10.1002/jobm.200710310

Stener, L.-G. (2013). Clonal differences in susceptibility to the dieback of *Fraxinus excelsior* in southern Sweden. *Scand. J. Forest Res.* 28, 205–216. doi: 10.1080/02827581.2012.735699

Stocks, J. J., Metheringham, C. L., Plumb, W. J., Lee, S. J., Kelly, L. J., Nichols, R. A., et al. (2019). Genomic basis of European ash tree resistance to ash dieback fungus. *Nat. Ecol. Evol.* 3, 1686–1696. doi: 10.1038/s41559-019-1036-6

Sündermann, J., and Jütte, K. (2014). Eschentriebsterben – Forst- und holzwirtschaftliche Strategien zum Umgang mit dem neuartigen Eschentriebsterben; Teilvorhaben 1: Nachhaltige Eschenholzproduktion sowie Erprobung effizienter und bodenschonender Holzernteverfahren auf sensiblen Nassstandorten. Schlussbericht FNR-Verbundvorhaben No. 22007410. Available online at: https://www.fnr.de/index.php?id=11150&fkz=22007410 (accessed August 3, 2020).

Tedersoo, L., Anslan, S., Bahram, M., Polme, S., Riit, T., Liiv, I., et al. (2015). Shotgun metagenomes and multiple primer pair-barcode combinations of amplicons reveal biases in metabarcoding analyses of fungi. *Mycokeys* 10, 1–43. doi: 10.3897/mycokeys.10.4852

Thompson, I. P., Bailey, M. J., Fenlon, J. S., Fermor, T. R., Lilley, A. K., Lynch, J. M., et al. (1993). Quantitative and qualitative seasonal changes in the microbial community from the phyllosphere of sugar beet (*Beta vulgaris*). *Plant Soil* 150, 177–191. doi: 10.1007/BF00013015

Timmermann, V., Børja, I., Hietala, A., Kirisits, T., and Solheim, H. (2011). Ash dieback: pathogen spread and diurnal patterns of ascospore dispersal, with special emphasis on Norway. *EPPO Bull.* 41, 14–20. doi: 10.1111/j.1365-2338.2010.02429.x

Torres, D. E., Rojas-Martínez, R. I., Zavaleta-Mejía, E., Guevara-Fefer, P., Márquez-Guzmán, G. J., and Pérez-Martínez, C. (2017). *Cladosporium cladosporioides* and *Cladosporium pseudocladosporioides* as potential new fungal antagonists of

Puccinia horiana Henn., the causal agent of chrysanthemum white rust. *PLoS One* 12:e0170782. doi: 10.1371/journal.pone.0170782

Tsuneda, A., and Hiratsuka, Y. (1979). Mode of parasitism of a mycoparasite, *Cladosporium gallicola*, on western gall rust, *Endocronartium harknessii*. *Can. J. Plant Pathol.* 1, 31–36. doi: 10.1080/07060667909501480

Ulrich, K., Becker, R., Behrendt, U., Kube, M., and Ulrich, A. (2020). A comparative analysis of ash leaf-colonizing bacterial communities identifies putative antagonists of *Hymenoscyphus fraxineus*. *Front. Microbiol.* 11:966. doi: 10.3389/fmicb.2020.00966

van Overbeek, L. S., and Saikkonen, K. (2016). Impact of bacterial–fungal interactions on the colonization of the endosphere. *Trends Plant Sci.* 21, 230–242. doi: 10.1016/j.tplants.2016.01.003

White, T. J., Burns, T., Lee, S., and Taylor, J. (1990). "Amplification and direct sequencing of fungal ribosomal genes for phylogenetics," in *PCR Protocols. A Guide to Methods and Applications*, eds M. A. Innis, D. H. Gelfand, J. J. Sninsky, and T. J. White (San Diego, CA: Academic Press), 315–322.

Wicklow, D. T., Roth, S., Deyrup, S. T., and Gloer, J. B. (2005). A protective endophyte of maize: *Acremonium zeae* antibiotics inhibitory to *Aspergillus flavus* and *Fusarium verticillioides*. *Mycol. Res.* 109, 610–618. doi: 10.1017/S0953756205002820

Wohlmuth, A., Essl, F., and Heinze, B. (2018). Genetic analysis of inherited reduced susceptibility of *Fraxinus excelsior* L. seedlings in Austria to ash dieback. *Forestry* 91, 514–525. doi: 10.1093/forestry/cpy012

Zhan, G., Tian, Y., Wang, F., Chen, X., Guo, J., Jiao, M., et al. (2014). A novel fungal hyperparasite of *Puccinia striiformis* f. sp. *tritici*, the causal agent of wheat stripe rust. *PLoS One* 9:e111484. doi: 10.1371/journal.pone.0111484

Zhang, D., Spadaro, D., Valente, S., Garibaldi, A., and Gullino, M. L. (2011). Cloning, characterization and expression of an exo-1,3-ß-glucanase gene from the antagonistic yeast, *Pichia guilliermondii* strain M8 against grey mold on apples. *Biol. Control* 59, 284–293.

Zhang, D., Spadaro, D., Valente, S., Garibaldi, A., and Gullino, M. L. (2012). Cloning, characterization, expression and antifungal activity of an alkaline serine protease of *Aureobasidium pullulans* PL5 involved in the biological control of postharvest pathogens. *Int. J. Food Microbiol.* 153, 453–464. doi: 10.1016/j.ijfoodmicro.2011.12.016

Zhang, H., Zheng, X., and Yu, T. (2007). Biology control of postharvest diseases of peach with *Cryptococcus laurentii*. *Food Control* 18, 287–291. doi: 10.1016/j.foodcont.2005.10.007

Zhao, Y.-J., Hosoya, T., Baral, H.-O., Hosaka, K., and Kakishima, M. (2013). *Hymenoscyphus pseudoalbidus*, the correct name for *Lambertella albida* reported from Japan. *Mycotaxon* 122, 25–41. doi: 10.5248/122.25

Conflict of Interest: The authors declare that the research was conducted in the absence of any commercial or financial relationships that could be construed as a potential conflict of interest.

frontiers in Microbiology

ORIGINAL RESEARCH
published: 07 December 2020
doi: 10.3389/fmicb.2020.597545

Pdel, Encoding a Low-Affinity cAMP Phosphodiesterase, Regulates Conidiation and Pathogenesis in *Alternaria alternata* Tangerine Pathotype

*Weiwei Lv, Xiangwen Kong, Changyong Zhou and Kezhi Tang**

Citrus Research Institute, Southwest University, Chongqing, China

Based on intracellular second messenger cAMP, the cyclic AMP-protein kinase A (cAMP-PKA) pathway transforms extracellular stimuli to activate effectors and downstream signaling components, mediating physiological processes in filamentous fungi. The concentration of intracellular cAMP was regulated by adenylate cyclase biosynthesis and cAMP phosphodiesterase (PDEs) hydrolysis, which mediate signal transduction and termination. In this study, we used a gene deletion and complementary strategy to characterize the functions of *AaPdel* and *AaPdeh* genes, which encoded low-affinity PDEs (Pdel) and high-affinity PDEs (Pdeh), respectively, in *Alternaria alternata*. *AaPdel*, but not *AaPdeh*, was found to be a key regulator in conidiation and pathogenesis in *A. alternata*. Δ*AaPdel* showed defects in conidiation, producing approximately 65% reduced conidiation and forming lowly pigmented aberrant structures. In response to osmotic stress, Δ*AaPdel* was more sensitive to non-ionic osmotic stress than ionic osmotic stress. Moreover, *AaPdel* deletion mutants had defects in vegetative growth and hyphal growth. Further analyses showed that the high chitin content of Δ*AaPdel* might account for the sensitivity to Congo red. Based on the attenuated pathogenicity and lowly pigmented aberrant structures, the laccase activity analysis found that both *AaPdel* and *AaPdeh* were involved in laccase activity regulation. Our data further support the PKA-mediated cAMP signaling pathway, as we have found that *AaPdel* was involved in intracellular cAMP levels in *A. alternata*.

Keywords: *Alternaria alternata* tangerine pathotype, cAMP phosphodiesterase, conidiation, cell wall integrity, osmotic stress, pathogenicity

OPEN ACCESS

Edited by:
Jia Liu,
Chongqing University of Arts and Sciences, China

Reviewed by:
Bo Zhu,
Shanghai Jiao Tong University, China
Giorgio Maresi,
Fondazione Edmund Mach, Italy

****Correspondence:***
Kezhi Tang
tangkezhi@cric.cn

Specialty section:
This article was submitted to Microbe and Virus Interactions with Plants, a section of the journal Frontiers in Microbiology

Received: *21 August 2020*
Accepted: *16 November 2020*
Published: *07 December 2020*

Citation:
Lv W, Kong X, Zhou C and Tang K (2020) Pdel, Encoding a Low-Affinity cAMP Phosphodiesterase, Regulates Conidiation and Pathogenesis in Alternaria alternata Tangerine Pathotype. Front. Microbiol. 11:597545. doi: 10.3389/fmicb.2020.597545

INTRODUCTION

Seven pathotypes of *Alternaria alternata* have been identified in tangerine, Japanese pear, strawberry, apple, tomato, rough lemon, and tobacco (Hatta et al., 2002; Thomma, 2003). Alternaria brown spot disease (ABS) caused by the tangerine pathotype of *A. alternata* reduces quality and yield of tangerine production in China (Lee et al., 2015). Under the optimum condition of 28°C and high humidity, the *A. alternata* infected both leaves, twigs, and fruits, forming necrosis, and spread extensively (Solel and Kimchi, 1998). Infected leaves act as the primary infection source, and

conidia are derived from the lesions of infected leaves (Wang et al., 2018). As a necrotrophic fungus, the tangerine pathotype of *A. alternata* produced the host selective toxin *A. citri* toxin (ACT) to kill and colonize the host cells (Tsuge et al., 2013; Ma et al., 2019). In the infection process, the ACT toxin spreads along the veins of the leaves, forming irregular "v"-shaped or like-round lesions. By causing electrolyte leakage, tangerine and its hybrids are susceptible to the ACT toxin (Otani et al., 1995; Ito et al., 2004).

In filamentous fungi, cells respond to external stimuli through cell-surface receptors and complex signal transduction pathways. The cyclic AMP-protein kinase A (cAMP-PKA) pathway is one of the major studied pathways mediating physiological processes in filamentous fungi (Zhu et al., 2017). Based on the cAMP, intracellular second messenger, extracellular stimuli could be transformed to activate effectors and stimulate downstream signaling components (Calvo et al., 2002). The cAMP-PKA pathway consists of G protein-coupled receptors (GPCRs), heterotrimeric G proteins, adenylate cyclase (AC), cAMP, and protein kinase A (PKA) (Houslay et al., 2007). The concentration of intracellular cAMP was regulated by adenylate cyclase biosynthesis and cAMP phosphodiesterase (PDEs) hydrolysis, which mediated signal transduction and termination (Jin et al., 1992). Two identified GTP-binding proteins, Ras1 and Ras2, regulate cAMP production by activating adenylate cyclase (Ramanujam and Naqvi, 2010). And PDEs were directly acting on active site, mediating cAMP hydrolysis to 5′-AMP (Conti and Beavo, 2007; Wilson et al., 2010). PDEs play an important role in the cAMP-PKA pathway, but their specific functions in *A. alternata* remain poorly understood.

In *Saccharomyces cerevisiae*, cAMP levels are modulated by two cAMP phosphodiesterase, low-affinity phosphodiesterase Pdel, and high-affinity phosphodiesterase Pde2. There is no obvious homology between Pde1 and Pde2. Simultaneously knockouting of *Pde1* and *Pde2* doubled the cAMP concentration, increased sensitivity to heat shock, and growth defects in non-fermentable carbon sources (Londesborough and Suoranta, 1983; Uno et al., 1983). *Pde2* regulates cAMP level induced by glucose stimulation, while there is no significant difference of cAMP level between the *Pde1* deletion mutant and the wild-type strain (Hu et al., 2010). *Pde1* does not regulate the cAMP level directly, but mediates a PKA negative feedback loop (Wera et al., 1997; Ma et al., 1999; Zhao et al., 2007; Caza and Kronstad, 2019).

In plant-microbe interactions, the fungus *Magnaporthe oryzae PdeH* (*Pde2*) has a dominant role in conidiation, pathogenicity, and intracellular cAMP level regulation. Compared with the wild-type strain, simultaneous knockout of *PdeH* and *PdeL* resulted in a 10-fold increase in cAMP level and completed disappearance of pathogenicity, whereas *PdeL* (*Pde1*) had no obvious function in *M. oryzae* (Zhang et al., 2011). The expression of GFP protein shows that PdeH localizes predominantly to the cytoplasm, while PdeL locates to the nucleus. *PdeH*-involved cAMP signaling is crucial for signal transduction and pathogenicity in *M. oryzae* (Ramanujam and Naqvi, 2010). In *Candida albicans*, the *PDE2* deletion mutant exhibits reduced invasion and virulence. In the simultaneous knockout of *CaPDE2* and *CaPDE1*, pathogenicity is abolished completely, indicating that *Pde1* contributes to virulence as a secondary role (Wilson et al., 2010). In phytopathogenic fungus *Botrytis cinerea*, the Δ*bcpde2* exhibits a significant reduction in vegetative growth, spore formation, germination, and pathogenicity, but the Δ*bcpde1* displays a similar phenotype to the wild-type strain (Harren et al., 2013). In *Fusarium graminearum*, inactivation of *PDE2* but not *PDE1* results in activating PKA activities and increases DON production (Jiang et al., 2016).

In *A. alternata*, the cAMP-PKA pathway remains poorly understood, and no regulated genes have been identified. In this study, characterization of PDEs in *A. alternata* have been conducted. We have identified high and low-affinity cAMP phosphodiesterase in *A. alternata* and through targeted gene deletion, analyzed the gene function in vegetative growth, conidiation, stress response, cell wall integrity (CWI), intracellular cAMP level, laccase activity, and pathogenicity.

MATERIALS AND METHODS

Strains and Growth Condition

The *A. alternata* Z7 was used as a wild-type strain in this study (Wang et al., 2016). And the fungal strains defective of *AaPdel*, coding low-affinity cAMP phosphodiesterase, and *AaPdeh*, coding high-affinity cAMP phosphodiesterase, were used as deletion mutants (Δ*AaPdel* and Δ*AaPdeh*). For activating strains and determining characteristics of colonies, all strains were cultured on potato dextrose agar (PDA) plates for 4–8 days at 28°C. After targeted gene deletion, the resulting transformants were selected on TB3 medium (yeast extract 3 g, casamino acids 3 g, sucrose 200 g, and agar 7.5 g per liter of purified water) containing hygromycin (Kong et al., 2018). On the vegetative growth analyses, the wild type and deletion mutants were cultured on minimal medium (KCl 0.5 g, $NaNO_3$ 2 g, KH_2PO_4 1 g, $MgSO_4{\cdot}7H_2O$ 0.5 g, $FeSO_4$ 0.01 g, sucrose 10 g, trace elements 200 μL and agar 20 g per liter of purified water) and complete medium (per liter of minimal medium supplied with yeast extract 1 g, casein hydrolysate 1 g, and peptone 2 g), respectively (Tang et al., 2020).

Targeted Gene Deletion and Complementation Analysis

Gene replacement through the hygromycin-resistance cassette released from pCX62 was used to generate the deletion mutants (Dong et al., 2015). The upper fragment of the target gene (S1) and hygromycin B gene (H1) were amplified and fused together by two-step overlapping PCR. And the lower fragment of the target gene (S2) and hygromycin B gene (H2) were fused to another fragment. The two resulting fragments with a hygromycin-resistance cassette were introduced into the protoplasts of the wild type by the polyethylene glycol (PEG)-mediated knockout technique (Rehman et al., 2016). To confirm the correct gene replacement, the resulting transformants resistant to hygromycin (TB3 medium with 250 mg/ml hygromycin), were identified by PCR assay and southern blot analysis.

Conidiation

The conidia of strains were harvested by blending with distilled water and scraping the colonies grown on V8 medium at 28°C for 8 days (Timmer et al., 1998). After filtering into two layers of sterile gauze, conidia were quantified by hemocytometer (QIUJING, China) and microscope (OLYMPUS, Japan). The conidia germinating rate and conidia diameter were assessed by microscopic examination of 200 conidia each for at least three repetitions. The statistical significance on conidiation of wild type, deletion mutants and complementary strains, was determined by one-way ANOVA and Duncan's new multiple range test ($P < 0.05$).

Nucleic Acid Manipulation

The homology of the targeted gene and protein sequences were searched in the Blast program and resources at NCBI[1] . Analyses of protein subcellular localization were predicted by WoLF PSORT[2]. Fungal genomic DNA and total RNA extraction were extracted from the mycelia grown in PDB medium for 36 h at 28°C. Fungal genomic DNA extraction was carried out using CTAB as previously described, and total RNA extraction was performed using Trizol (Invitrogen). Plasmid DNA was purified using the Plasmid DNA Miniprep Kit (Qiagen).

Vegetable Growth and Stress Treatment

Four kinds of growth medium [PDA, V8, minimal medium (MM), and complete medium (CM)] were configured to determine the involvement of vegetative growth between deletion mutants and wild-type strain. To analyse the involvement of *AaPdel* and *AaPdeh* in cell wall integrity and osmotic stress response, 3 days activated strains were inoculated on PDA amended with different chemicals. The same concentration of osmotic-stress inducer, 1M sorbitol, 1M NaCl, 1M KCl, or 1M sucrose was added to the PDA plate, respectively. And SDS or Congo red (CR) inducing medium was configured to analyse the cell wall integrity of strains. The diameter of colonies were measured in two perpendicular directions after 5 days of incubation at 28°C, and each treatment was replicated for at least three times. And the growth rates were presented as the mean ± SD of at least three repeats. Statistical significance of growth rates of mutants and wild type was determined by one-way ANOVA and Duncan's new multiple range test (MRT) ($P < 0.05$).

Quantification of Intracellular cAMP

Mycelia, grown in PDB medium for 36 h at 28°C and freeze-dried for 1.5 h, were quickly ground in liquid nitrogen and mixed with 200 μL of 6% trichloroacetic acid (TCA). Intracellular cAMP extraction was in accordance with the method described previously (Liu et al., 2007), and cAMP levels were measured using the AlphaScreen Assay Kit (PerkinElmer, Waltham, MA) according to the supplier's instruction.

[1]https://www.ncbi.nlm.nih.gov

[2]https://www.genscript.com/psort/wolf_psort.html

Pathogenicity Assay

In the pathogenicity assay, the 10 days conidia harvested from V8 medium were diluted to a concentration of 1.0×10^5 conidia ml^{-1}. At least 20 leaves of tangerine (*Citrus reticulata* Blanco) with nearly identified size and maturity, were inoculated with 20 μL conidial suspension of wild type, deletion mutants, and complementary mutants (Solel and Kimchi, 1998). Distilled water was inoculated on the leaves as a positive control. The phenotype was recorded at 3–5 dpi (days post inoculation), with three repetitions in each treatment. According to Perina et al. (2019) the average scale levels based on the percentage of lesion area were quantified.

Laccase Activity Assay

Laccase activity was quantified as described previously (Mtibaa et al., 2018). Based on the oxidation of ABTS, the activated strains of wild type, Δ*AaPdel*, Δ*AaPdeh*, and complementary mutants were inoculated on the ABTS medium at 28°C. The morphology of these colonies was observed and photographed at 6 dpi. For the enzyme solution preparation, mycelial plugs of activated strains were cultured in 50 mL PDB liquid medium for 36 h. After filtration, mycelial pellets were harvested and mixed with 1 mL Tris-HCl. And the supernatant collected by centrifuge (10,000 rpm, 10 min) was the enzyme solution. Laccase activity was determined by 0.5 mM ABTS oxidation mixing in 0.1 M NaAc-HAc buffer, pH 4.0 at 28°C and measured the spectrophotometer absorbance at 420 nm. The resulted laccase activity was defined as the units U mL^{-1}, with 1 U being the amount of enzyme oxidizing 1 μmol of ABTS per min (Irfan et al., 2018).

Statistical Analysis

Data was presented as the mean ± SD of at least three independent experiments. Statistical significance was analyzed by one-way ANOVA and Duncan's new multiple range test (MRT). Different letters represent significant differences at $P < 0.05$.

RESULTS

AaPdel, but Not *AaPdeh*, Is Involved in Mycelial Growth and Hyphal Growth

Through blasting *S. cerevisiae* Pde1 and Pde2 in the proteome of *A. alternata*, the corresponding OWY42401.1 and OWY42000.1 were identified by high protein homology, and named AaPdel and AaPdeh, respectively. The sequence alignment demonstrated that the AaPdel protein exhibited 18.50–52.59% similarity with *S. cerevisiae* ScPde1, *M. oryzae* MoPdel, *C. albicans* CaPdel, and the AaPdeh protein exhibited 30.26–69.59% similarity with *S. cerevisiae* ScPde2, *M. oryzae* MoPdeh, *C. albicans* CaPde2, and *Botrytis cinerea* Bcpde2. The phylogenetic tree of two identified proteins were shown in **Figures 1C,D**, respectively. The identified *AaPdel* gene encodes a 1,100-amino-acid polypeptide, and the identified *AaPdeh* gene encodes a 961-amino-acid polypeptide. As demonstrated in **Figure 1A**, the split-marker approach was used to generate deletion mutants. To confirm the correct

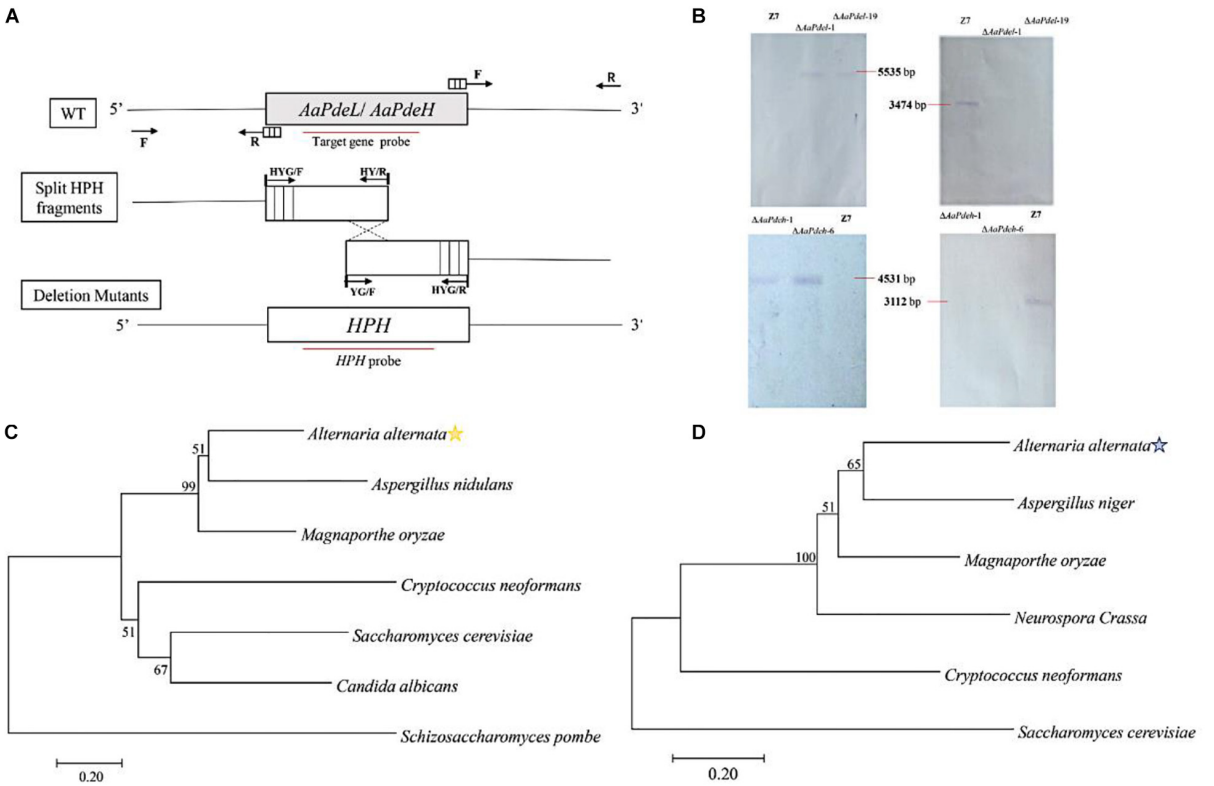

FIGURE 1 | Constructionprotect and verification of the *AaPdel* and *AaPdeh* deletion and complementary mutants of *Alternaria alternata*. **(A)** Schematic of gene knockout. Targeted disruption of *AaPdel* and *AaPdeh* in *A. alternata* using split-marker gene replacement strategy. Through a homologous integration, overlapping DNA fragments of hygromycin-resistance gene cassette (*HPH*) were used for gene replacement. Arrows represented to primer binding sites, and the red line delineates the probe used for Southern blot analysis. **(B)** Southern blot analysis for the wild-type strain and deletion mutants. **(C)** The phylogenetic tree constructed based on the neighbor-joining method with 1,000 bootstrap replicates by MEGA7.0 program. Figures represent the occurrence percentage, and the value less than 50 was not shown. Phylogenetic tree generated based on the amino acid of AaPdel homologous. **(D)** Phylogenetic tree generated based on the amino acid of AaPdeh homologous.

gene replacement, the resulting transformants were selected based on the resistance to hygromycin (TB3 medium containing 250 mg/ml hygromycin). And *AaPdel* transformants were verified by three primer pairs of PLP1F/H855R, H856F/PLP2R, and PLF/PLR. *AaPdeh* transformants were identified through PHP1F/H855R, H856F/PHP2R, and PHF/PHR (**Supplementary Figure 1**). Southern blot analysis was used for further analysis of the deletion mutants. Genomic DNA of *AaPdel* and *AaPdeh* transformants were respectively, digested with *Hin*dIII, *BgI* II, *Xho*I, and *Sal*I. A 5,535-bp fragment in the deletion mutants of *AaPdel* and a 4,531-bp fragment in the deletion mutants of *AaPdeh* were probed with *HPH* gene. And when probed with homologous target genes, respectively, 3,474 and 3,112-bp fragments were only found in the wild type, indicating correct replacement of the target genes (**Figure 1B**).

The wild type, z7; deletion mutants, Δ*AaPdel*-1, Δ*AaPdel*-19, Δ*AaPdeh*-1, and Δ*AaPdeh*-6; and complement strains, *AaPdel-cp* and *AaPdeh-cp*, were inoculated on four vegetative mediums of PDA, V8, CM, and MM, respectively. The colony morphology and diameter were assessed after growing for 6 days and measured in two orthogonal directions. The Δ*AaPdel* displayed similar vegetative growth defects on the PDA, MM, CM, and V8 media (**Figure 2A**). On the CM medium with sufficient nutrient elements, the growth rates of Δ*AaPdel* were decreased by 14%, significantly lower than the corresponding WT. On the MM covering the basic nutrient elements of fungal growth, the percentage growth rates of Δ*AaPdel* were decreased by 7.5%. The Δ*AaPdel* reduced growth on regular PDA medium by 6.6–7.8% compared with the wild type (**Figure 2B**). By light microscope observation, the wild type exhibited abundant and thick hyphal branch, while the hyphal growth of *AaPdel* deletion mutants was sparse (**Figure 2C**). However, the fungal strains defective of *AaPdeh*, coding high-affinity cAMP phosphodiesterase, exhibited no obvious growth defects in radical growth and colony morphology, which were in line with the wild type. The above results indicate that the *AaPdel* gene is involved in the mycelial growth of *A. alternata* while *AaPdeh* has a limited contribution.

AaPdel Contributes to Conidia Formation and Morphology

To analyze potential gene functions in conidiation, the conidial suspension of wild type, deletion mutants, and supplementary strains were counted on a hemocytometer and photographed

under a microscope at 40 times magnification. On the V8 medium, the Δ*AaPdel* formed colony with 10% reduced-growth-rate and produced approximately 65% reduced conidiation compared to the wild type (**Figure 3A**). The sporulation of the wild type Z7 was about 12.38×10^5, while the sporulation of the *AaPdel* mutant was about 4×10^5 (**Figure 3C**). Over 200 spore diameters of each strain were measured, and the spore morphology was observed under a microscope. The conidia of

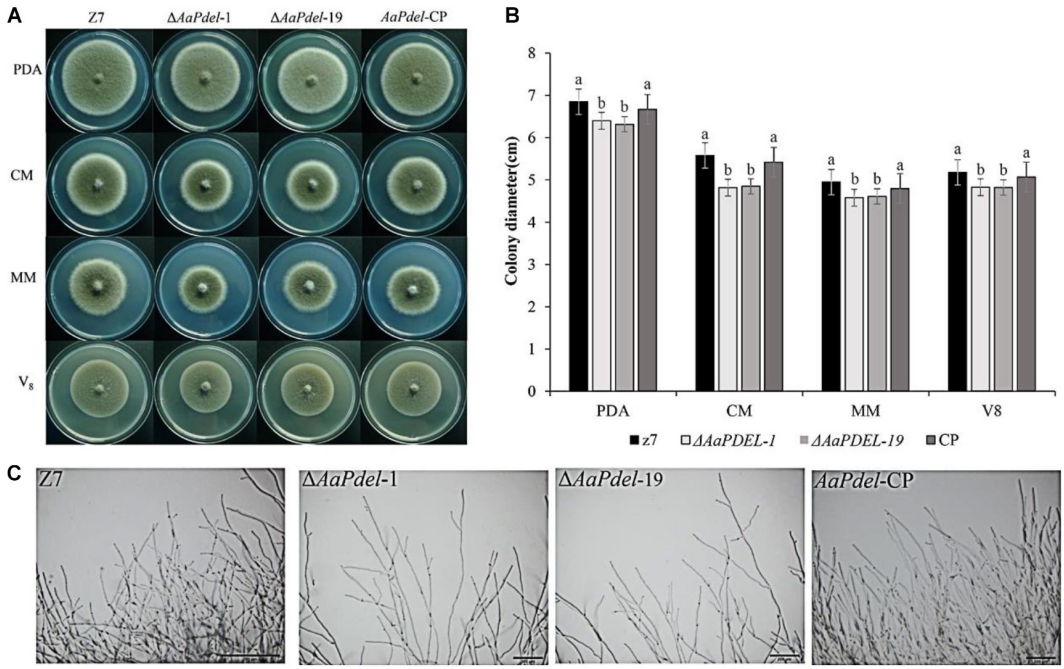

FIGURE 2 | The deletion of *AaPdel* had significant effects on vegetative growth. **(A)** The phenotype of the wild-type strain, Z7; the deletion mutants, Δ*AaPdel*-1 and Δ*AaPdel*-19; and the complemented strain of Δ*AaPdel*, *AaPdel*-CP. All strains were inoculated on potato dextrose agar (PDA), minimal medium (MM), complete medium (CM), and V8 medium for 5 days at 28°C. **(B)** Statistical analyses of colony diameter. Colony diameter was presented as the mean ± SD of at least three independent experiments. Different letters on a graph denoted statistical significance at $P = 0.05$. **(C)** Hyphal morphology of wild type (Z7), *AaPdel* deletion mutants (Δ*AaPdel*-1 and Δ*AaPdel*-19) and complemented (*AaPdel*-CP) strains.

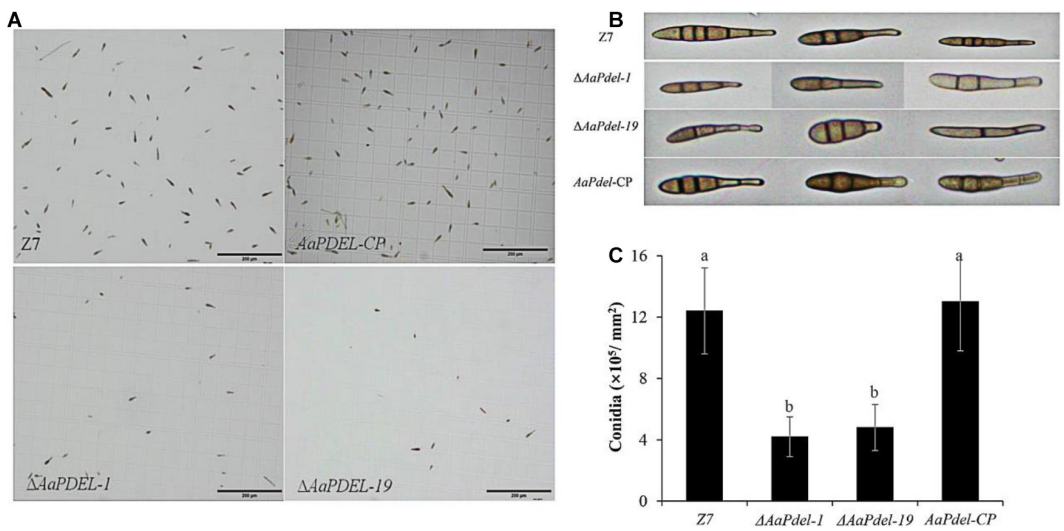

FIGURE 3 | The Δ*AaPdel* of *Alternaria alternata* exhibited a significant reduction in conidia formation. **(A)** Light microscopy images of conidial suspension produced on V8 medium. **(B)** Conidia morphology of *A. alternata* strains examined by light microscopy. Δ*AaPdel* formed lowly pigmented aberrant structures. **(C)** Statistical analyses of conidia production. Statistical significance was analyzed by one-way ANOVA and Duncan's new multiple range test (MRT). Different letters represent significant differences at $P < 0.05$.

Δ*AaPdel* had varied morphologies, forming lowly pigmented aberrant structures. The conidia of Δ*AaPdel* were light gray, while the wild type and the complementary strain produced typical dark brown conidia (**Figure 3B**). However, through statistical analysis, *AaPdel* was not involved in conidia diameter and germination rate. There was no significant difference between Δ*AaPdeh* and wild type in terms of conidia production, germination rate, and morphology (**Supplementary Figure 2**). In summary, the *AaPdel* gene is involved in regulating the conidia production and pigment synthesis of conidia in *A. alternata.*

AaPdel Plays a Role in Intracellular cAMP Level Regulation

Two cAMP phosphodiesterase-encoding genes were analyzed in the regulation of the intracellular cAMP level. Compared with the wild type, Δ*AaPdel* led to decreased accumulation of cAMP level, while the loss of *AaPdeh* led to the similar accumulation of cAMP level with the wild type. The trend was further confirmed by the complementation assay (**Figure 4**). The intracellular cAMP level of *AaPdel*-CP and *AaPdeh*-CP was consistent with the wild-type strain. *AaPdel* plays a role in intracellular cAMP level regulation.

AaPdel Is Involved in Response to Osmotic Stress and Oxidative Stress

To analyze the defects in response to the osmotic stress on the mutants, the activated strains were inoculated on PDA medium amended with 1 M sorbitol, 1 M NaCl, 1M KCl, or 1 M sucrose. Compared with the growth of the PDA medium with no stress factor present, the growth of all tested strains was restrained to the osmotic stress. The Δ*AaPdel*-1 and Δ*AaPdel*-19 mutants were hypersensitive to the osmotic stress inducers. The Δ*AaPdel* exhibited greater sensitivity to the non-ionic osmotic stress (sorbitol and sucrose) than the ionic osmotic stress (NaCl and KCl) (**Figure 5A**). Among these, the growth rate of Δ*AaPdel*-1 in sorbitol or sucrose were decreased by 10.58 and 10.11%, respectively, compared with the wild-type strain. Whereas with the ionic osmotic stress, the inhibitory effect of Δ*AaPdel*, Δ*AaPdeh* was similar compared with the wild type (**Table 1**). Online analysis of protein subcellular localization revealed that AaPdel protein was mainly located on the plasma membrane. According to the data, this different phenotype might be caused by the same concentrate Na^+ and K^+ treatment (**Figure 5B**).

In order to analyse the defects in response to the oxidative stress, the activated strains were inoculated on PDA medium added with oxidative stress factors (20 mM H_2O_2 or 3 mM VK_3) after 5 days cultured at 28°C. The Δ*AaPdel* was hypersensitive to the oxidative stress inducers (**Figure 5A**). Δ*AaPdel*-1 had 23.24 and 66.67% inhibition rate, respectively, on PDA supplemented with H_2O_2 or VK_3. The details of inhibition rate were presented in **Table 1**. However, under osmotic and oxidative stresses, the inhibition rates of Δ*AaPdeh-1* and Δ*AaPdeh-6* were similar to the wild type (**Supplementary Figure 3**).

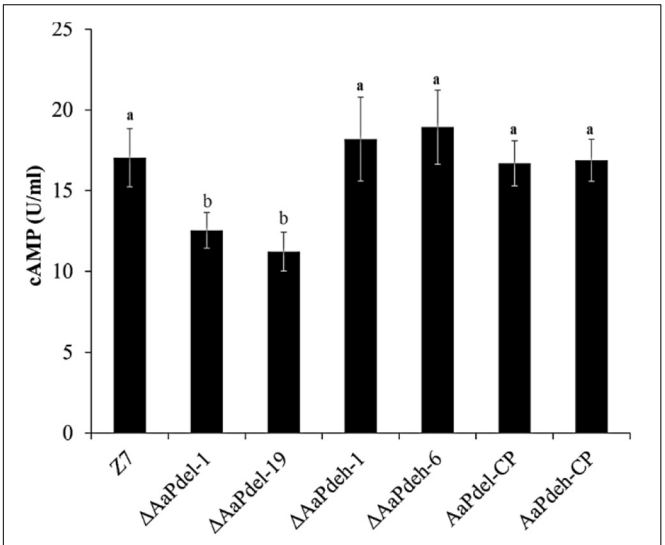

FIGURE 4 | Intracellular cAMP quantification of Δ*AaPdel* and Δ*AaPdeh* during the hyphal stage in *Alternaria alternata*. Bar graphs depicted the levels of intracellular cAMP in the mycelia of Δ*AaPdeh*, Δ*AaPdel*, wild type, and complemented strain, which were cultured in liquid PDB for 48 h. Bars represented standard error. Different letters mark significant differences at $P < 0.05$.

AaPdel Played a Role in the Maintenance of Cell Wall Integrity

Cell wall stress tolerance assays were performed by inoculating WT and mutant strains onto PDA medium supplemented with either 0.02% SDS or 100 μg/ml of CR. By serving PDA as control, the growth of strains was restrained to both SDS and CR. And the *AaPdel* mutants were hypersensitive to the cell wall stress reagents (**Figure 5C**). Compared with the wild type, the inhibition rate of the *AaPdel* mutants was significantly increased in 0.02% SDS (**Table 1**). Chitin, the major component of the cell wall in *A. alternata*, was further quantified in deletion mutants and the wild-type strain. The chitin content of Δ*AaPdel* was higher than that of the wild type and complemented strain, indicating *AaPdel* was involved in cell wall integrity and architecture (**Figure 5D**). However, the Δ*AaPdeh-1* and Δ*AaPdeh-6* were not more sensitive to the cell wall stress reagents. These stresses disturb cell wall biosynthesis in *A. alternata*, activating the CWI pathway. The CWI of the *AaPdel* mutant was affected, indicating that *AaPdel* is involved in the maintenance of CWI.

AaPdel Is Required for Pathogenicity

The pathogenicity was assessed by inoculating the leaves of tangerine with conidial suspension at a concentration of 1.0×10^5 conidia ml^{-1}. At 3 dpi, there were obvious lesions on the part of the leaves infected by wild type and complementary strains, but only mild lesions were observed on the leaves inoculated with Δ*AaPdel-1* and Δ*AaPdel*-19. At 5 dpi, Δ*AaPdel*-1 and Δ*AaPdel*-19 conidial suspensions incited small necrotic lesions in the leave (**Figure 6**). According to Perina et al. (2019), the average scale levels quantified the disease severity of deletion mutants and Z7 were 4 and 6, respectively. It showed nearly

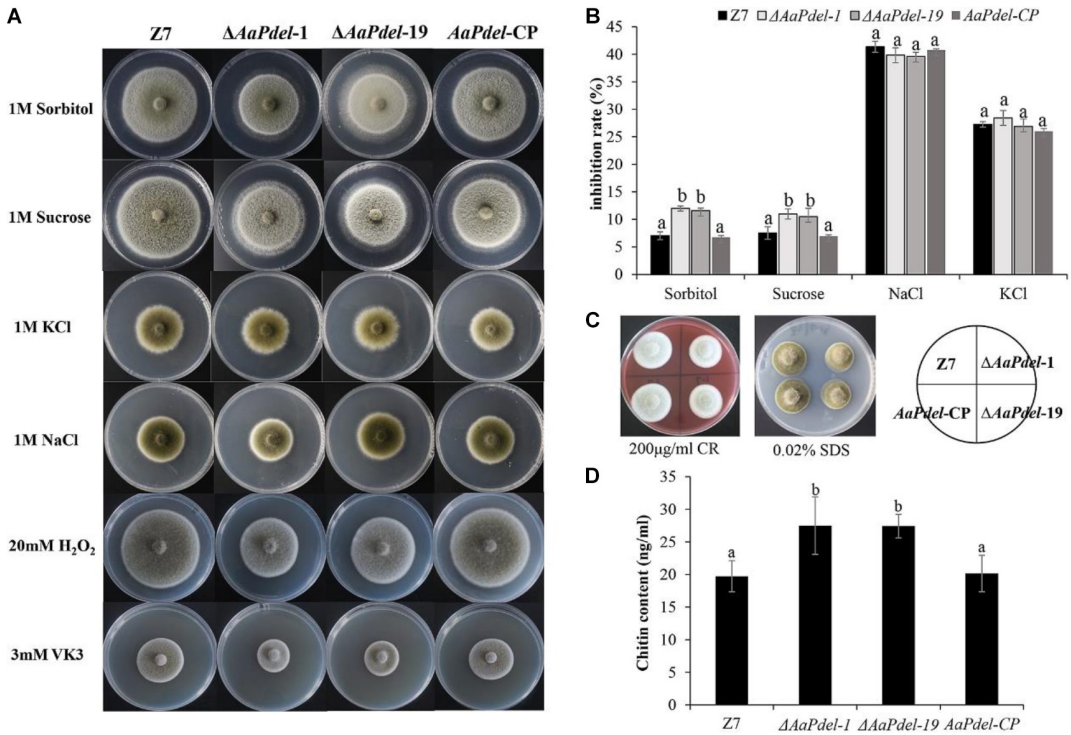

FIGURE 5 | Effect of osmotic stress, oxidative stress and cell wall stress. **(A)** The phenotype of the wild-type strain (Z7); the deletion mutants (Δ*AaPdel*-1 *and* Δ*AaPdel*-19); and the complemented strain of Δ*AaPdel* (*AaPdel*-CP) inoculated on PDA medium amended with osmotic stress and oxidative stress. **(B)** Statistical analyses of inhibition rate on the osmotic stress. Results were presented as the mean ± SD of at least three independent experiments. Statistical significance was analyzed by one-way ANOVA and Duncan's new multiple range test (MRT). Different letters mark significant differences at $P < 0.05$. **(C)** The phenotype of the strains inoculated on PDA medium with cell wall stress factors of sodium dodecyl sulfate (SDS) and Congo red (CR). **(D)** Quantitative analysis of cell wall chitin levels in wild-type strain, *AaPdel* deletion mutants, and complemented strains. Bars represented standard error. Different letters represent statistically significant differences (Duncan's new multiple range test, $p < 0.05$).

TABLE 1 | Inhibition rate of osmotic, oxidative stress and cell wall integrity assay in the wild type Z7, Δ*AaPdel*, *AaPdel*-CP in *Alternaria alternata*.

Strain	Inhibition rate (%)							
	Sorbitol 1M	Sucrose 1M	NaCl 1M	KCl 1M	Congo Red 200 μg/ml	SDS 0.02%	H_2O_2 20 mM	VK_3 3 mM
Z7	7.03 ± 0.71^A	7.52 ± 0.46^A	41.36 ± 0.32^A	27.25 ± 0.45^A	45.75 ± 3.37^A	7.54 ± 0.61^A	12.65 ± 3.17^A	49.56 ± 5.22^A
Δ*AaPdel*-1	11.98 ± 1.15^B	10.98 ± 0.92^B	39.84 ± 0.25^A	28.43 ± 1.51^A	53.75 ± 2.32^B	15.63 ± 1.25^B	23.24 ± 5.86^B	66.67 ± 7.29^B
Δ*AaPdel*-19	11.61 ± 0.98^B	10.50 ± 1.35^B	39.58 ± 0.25^A	26.91 ± 0.80^A	54.49 ± 4.51^B	13.55 ± 0.95^B	21.24 ± 3.57^B	56.08 ± 2.80^B
AaPdel-CP	6.75 ± 0.51^A	6.95 ± 0.35^A	40.75 ± 0.50^A	26.00 ± 1.35^A	44.98 ± 2.65^A	7.50 ± 0.51^A	11.55 ± 2.11^A	52.26 ± 3.80^A

Different letters represent statistically significant differences (Duncan's new multiple range test, $p < 0.05$).

75% reduced lesion area compared with WT. And *Pdel*-CP strain complemented the attenuated pathogenicity of Δ*AaPdel*. In contrast, the necrotic lesions induced by Δ*AaPdeh*-1 and Δ*AaPdeh*-6 were as serious as the wild type in pathogenicity (**Supplementary Figure 4**). Taken together, *AaPdel*, coding low-affinity cAMP phosphodiesterase, was involved in regulating the pathogenicity of *A. alternata*.

AaPdel and *AaPdeh* Regulate Laccase Activity

Laccase is a copper-containing oxidase mainly involved in the catalysis of lignin degradation, pigment synthesis, and fungal pathogenicity. To determine the involvement of PDEs in laccase activity, we used a specific substrate, 2,2′-azino-di-3-ethylbenzthiazoline-6-sulfonate (ABTS). The oxidized dark purple stain can be observed at the colonies of both the Δ*AaPdel,*Δ*AaPdeh* mutants and the wild-type strain (**Figure 7A**). To further demonstrate the laccase activity difference between *AaPdel* and *AaPdeh* mutants, the crude enzyme solution was extracted and analyzed by spectrophotometer at 420 nm for 5 min. The statistical analyses showed that the laccase activity of both Δ*AaPdel* and Δ*AaPdeh* mutants were significantly lower than that of the wild type, and Δ*AaPdel* had a stronger inhibitory effect on laccase (**Figure 7B**). The above results indicate that both *AaPdel* and *AaPdeh* are

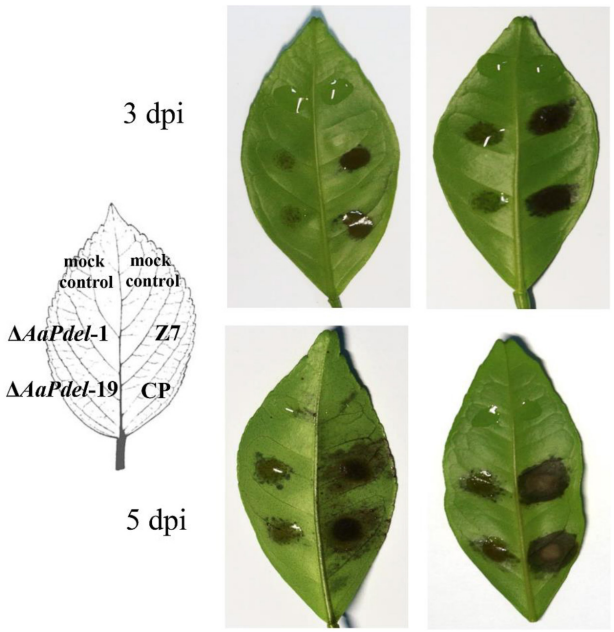

FIGURE 6 | Mutation of *AaPdel* affected *Alternaria alternata* pathogenicity. Necrotic lesions of *A. alternata* on detached tangerine leaves induced by 20 μL conidial suspension (10^5 conidia per mL) of wild type Z7, Δ*AaPdel* mutants, and the complemented strain, respectively. The mock controls were treated with distilled water only. Necrotic lesions were observed and photographed 3 and 5 dpi, respectively.

involved in regulating laccase activity, and *AaPdel* plays a primary role in this pathway.

DISCUSSION

In fungi and yeast, cAMP signaling cascade regulate a large amount of cellular and biological processes. Since the discovery of cAMP-PKA pathway, PDEs have been characterized as important phosphodiesterase for cAMP level regulation in plant pathogens, including the budding yeast (*S. cerevisiae*) and filamentous fungi (*F. graminearum*, *M. oryzae*, *C. albicans,* and so on). Two PDEs, low-affinity phosphodiesterase Pdel (Pde1) and high-affinity phosphodiesterase Pdeh (Pde2), are involved in cAMP level regulation (Bahn et al., 2003). *Pdeh* is widespread in fungi and mammals, while *Pdel* is only found in fungi. In this study, the biological functions of the *AaPdel* and *AaPdeh* in *A. alternata* were preliminarily explored through gene replacement strategy, and it was found that *AaPdel* but not *AaPdeh* played a dominant role in biological processes of *A. alternata*, which differed from previously reported findings. Our data further support the PKA-mediated cAMP signaling pathway by showing that the regulator is involved in intracellular cAMP level.

In filamentous fungi, identified *PDEL* gene functions are mainly concentrated on conidiation, as in *F. graminearum* and *Setosphaeria turcica*. Our result was similar to those described above. The conidia production of the *AaPdel* deletion mutant was 65% lower than that of the wild type and complemented strain of Δ*AaPdel*. Also, the color of the Δ*AaPdel* conidia was relatively lighter. In *M. oryzae* and *Aspergillus flavus*, the *PdeH* deletion mutant also exhibited defects in vegetative growth and conidiation (Yang et al., 2017). In *S. turcica*, the deletion of the *StH-PDE* gene resulted in a loss of conidiation ability. Whereas the absence of *AaPdeh* did not result in the defects of conidia production, diameter, germination rate, and vegetative growth. The Δ*AaPdel* had growth defects on four vegetative growth media, and formed colonies with short, dense aerial hyphae. The growth defects of Δ*AaPdel* were extremely severe on the CM medium with sufficient nutrient elements. Comparing the utilization of basic nutrient elements, *AaPdel* might be involved in the utilization of certain nutrient elements. The *AaPdel* gene plays an important role in regulating conidiation and hypha growth.

The same concentration of osmotic stressors (sorbitol, sucrose, NaCl, and KCl) were used to analyze defects in stress response (Hanin et al., 2016). Δ*AaPdel* was more sensitive to non-ionic osmotic stress (sorbitol and sucrose) than ionic osmotic stress (NaCl and KCl). Among the analyzed osmotic stressors, sorbitol (a sugar alcohol), had the most significant inhibitory effect on the *AaPdel* deletion mutant. Whereas in the ionic osmotic stress, the inhibitory effect was the same when comparing the Δ*AaPdel*, Δ*AaPdeh*, and wild-type strain. According to the data, this phenotypic difference might be caused by the same concentration Na^+ and K^+ treatment. Analyses of protein subcellular localization revealed that the AaPdel protein mainly located on the plasma membrane. Hence, it can be hypothesized that *AaPdel* is involved in sodium-potassium pump regulation on the plasma membrane.

As the first barrier, the fungal cell wall and plasma membrane were of great significance to maintain the structural integrity and against external stresses. The fungal cell wall and plasma membrane are indispensable for maintaining the shape of the cell, and are also involved in signal transmission. In this study, Δ*AaPdel* was more sensitive to cell wall inhibitors CR and SDS, while Δ*AaPdeh* growth was similar to the wild type. SDS acts as a cell wall inhibitor by reducing the stability of the membrane to reveal the defect of the cell wall. CR inhibits binding to major components of the fungal cell wall, chitin and β-1,4-glucan (Gong et al., 2020). On the one hand, *AaPdel* appeared to be the sensor for signaling in response to the cell wall antagonist CR, which interferes with cell wall assembly by binding to chitin. Further analyses showed that the high chitin content of Δ*AaPdel* might account for the sensitivity to CR. However, the Δ*AaPdeh*-1 and Δ*AaPdeh*-6 were not more sensitive to cell wall stress reagents. Maintenance of cell wall integrity relies on the CWI pathway, a conserved cascade pathway, triggered by transmembrane sensors in response to extracellular stresses in fungus. These stresses disturb cell wall biosynthesis in *A. alternata*, activating the CWI pathway. The CWI of the *AaPdel* mutant was affected, indicating that *AaPdel* was involved in the maintenance of CWI.

Laccase is a copper-containing oxidase mainly involved in the catalysis of lignin degradation, pigment synthesis, and fungal pathogenicity (Mtibaa et al., 2018). The phenotype of lighter conidia color and attenuated pathogenicity led us to analyze the laccase activity. To determine the involvement of PDEs,

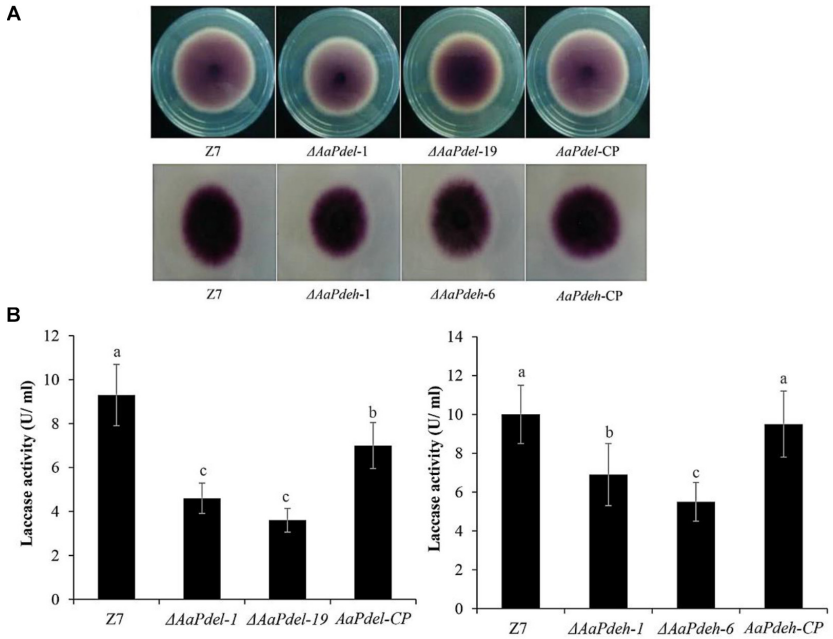

FIGURE 7 | The laccases activity assays of Δ*AaPdel* and Δ*AaPdeh* of *Alternaria alternata*. **(A)** Laccase activity was tested on PDA medium with 0.03% ABTS culture at 28°C. Discoloration was observed and photographed 6 dpi. **(B)** Statistical analyses of laccase activity, which was determined by the ABTS oxidizing test. Statistical significance was analyzed by one-way ANOVA and Duncan's new multiple range test (MRT). Different letters mark significant differences at $P < 0.05$.

the laccase activity of the Δ*AaPdel*, Δ*AaPdeh*, wild type, and complemented strain were tested and compared. We found that the wild type and complemented strain produced laccase, forming a dark purple hole on the ABTS medium, whereas the laccase activity of both Δ*AaPdel* and Δ*AaPdeh* was significantly lower than that of wild type and complemented strain. Consistent with our results, previous studies have demonstrated that the *MoPdeh* and *MoPdel* genes regulate intracellular laccase activity, and *MoPdel* plays a regulatory role in *M. oryzae*.

Research addressing gene functions in fungi has mainly focused on pathogens and those genes involved in pathogenicity or virulence. Among the studied PDEs, some genes encoding high-affinity phosphodiesterase affect pathogenicity. In *S. turcica*, the *StH-PDE* gene regulates secondary metabolism, melanin synthesis, and pathogenicity. The gene encoding high-affinity phosphodiesterase in *T. serrata* is involved in the regulation of mycelial growth and pathogenicity. *MoPdeH* (*Pde2*) has a dominant role in conidiation, pathogenicity, and intracellular cAMP level regulation, whereas *MoPdel* (Pde1) had no obvious function in *M. oryzae*. In this research, the finding was contrary to previous studies. In *A. alternata*, the Δ*AaPdel* mutant induced much smaller lesions than that of the wild type, whereas the Δ*AaPdeh* mutant induced lesions as drastic as those in the wild-type strain. Chitin is one of the fungal PAMPs, and the high content in Δ*AaPdel* may triggered rapid and strong plant parttern-triggered immunity. Above all, the attenuated pathogenicity of Δ*AaPdel* was probably caused by defects in the utilization of certain nutrient elements, osmotic stress response, plasma membrane, low laccase activity, high chitin content in the cell wall, and PKA-mediated cAMP signaling pathway.

PDEs target specific intracellular sites or signal transduction complexes and localize not only in the cytoplasm, but also in membrane, nucleus, and cytoskeleton locations (Houslay et al., 1998). Hu et al. (2010) reported that, like its low-affinity counterpart, the high-affinity phosphodiesterase may also play an important role in PKA negative feedback loop through the Pde2 localization assays. The localization of Pde2-GFP was affected by the carbon sources available and the cAMP-dependent PKA in the yeast *S. cerevisiae*. Pde2 is concentrated in the nucleus of cells grown on glucose, while it is distributed in the nucleus and cytoplasm of cells grown on some non-fermentable carbon sources. And PKA positively regulates the nuclear accumulation of Pde2. Elevated PKA activity increased the nuclear concentration of Pde2. Whereas in PKA attenuated strains, Pde2 is unable to concentrate in the nucleus of cells grown on glucose. Ramanujam and Naqvi (2010) reported the location of PdeH-GFP and PdeL-GFP during asexual and pathogenic development in *M. oryzae*. Although PdeH-GFP was cytoplasmic, it was dynamically associated with the plasma membrane and vesicle compartment, and the PdeL-GFP was predominantly localized in the nucleus. In *Aspergillus flavus*, PdeL-GFP shows a strong fluorescent signal in the nucleus of the hyphae, and PdeH-GFP is likely to be localized to punctate structures in the cytosol, rather than the nucleus. The localization of PDEs is complicated and dynamic. And limited to the resolution of the microscope, the reported location of the PDEs haven't been directly localized to the organelle. In this study, we use online software to analyze the gene sequence. Online analysis of protein subcellular localization revealed that the AaPdel protein was predominantly located on the plasma membrane

and the AaPdeh protein was located in the nucleus. From the perspective of protein subcellular localization, the AaPdeh protein was parallel to MoPdeL and AfPdeL, both in the nucleus. While AaPdel protein was similar to MoPdeH and AfPdeH. Further analysis of the signal peptides and transit peptides in AaPdel protein, revealed that the AaPdel protein was localized to the secretory pathway. We also investigate whether the two cAMP phosphodiesterase-encoding genes directly contribute to the intracellular cAMP level. Compared with the wild type, Δ*AaPdel* led to decreased accumulation of cAMP level, while the loss of *AaPdeh* led to the similar accumulation of cAMP level with the wild type. *AaPdel* regulated the intracellular cAMP level. This inverse trend of gene function in *A. alternata* was in accordance with the protein location difference between many fungi. We speculate that although PDEs homology has been identified in many filamentous fungi, their functions are not consistent, and there was no clear association between the conserved domain and physiological function. The inconsistent gene function may due to different protein location. It indicated that PKA-mediated cAMP signaling pathway was complicated in *A. alternata,* and needed further analysis.

In this study, the *AaPdel* and *AaPdeh* genes were identified to encode low-affinity PDEs (Pdel) and high-affinity PDEs (Pdeh) in *A. alternata*. We used a gene deletion and complementation strategy to characterize the gene function of *AaPdel* and *AaPdeh.* In *A. alternata*, *AaPdel* regulated intracellular cAMP levels during the hyphal stage. Deletion of *AaPdel*, but not *AaPdeh*, was found to play a role in conidiation and pathogenicity in *A. alternata*. Δ*AaPdel* showed a defect in conidiation, producing approximately 65% reduced conidiation and forming lowly pigmented aberrant structures. Upon exposure to osmotic stressors, Δ*AaPdel* had growth defects in response to osmotic stress, which was more sensitive to non-ionic osmotic stress than ionic osmotic stress. This different phenotype might be caused by the same concentrate Na^+ and K^+ treatment. Moreover, *AaPdel* deletion mutants had defects in vegetative growth, hyphal growth and pathogencity. Further analyses showed that the high chitin content of Δ*AaPdel* might account for the sensitivity to CR. Based on the attenuated pathogenicity and lowly pigmented aberrant structures, the laccase activity analyses found that both *AaPdel* and *AaPdeh* were involved in laccase activity regulation. Our data further support the PKA-mediated cAMP signaling pathway, as we have found the regulators of *AaPdel* is involved in intracellular cAMP levels in *A. alternata.* The inconsistent gene function may due to different protein location. In *A. alternata*, cAMP-PKA pathway played important roles in signal transduction, but the function of the genes involved in this pathway required further study.

DATA AVAILABILITY STATEMENT

The original contributions presented in the study are included in the article/**Supplementary Material**, further inquiries can be directed to the corresponding author/s.

AUTHOR CONTRIBUTIONS

KT, XK, and WL conceived and designed the experiments. CZ contributed to reagents, materials, and analysis tools. WL and XK performed the experiments. WL, KT, and CZ analyzed the data and wrote the manuscript. All authors read and approved the final manuscript.

FUNDING

This research was funded by the earmarked fund for China Agricultural Research System (No. CARS-27) and the Chongqing Program for Science and Technology Development (No. cstc2012gg-yyjsx0001).

SUPPLEMENTARY MATERIAL

The Supplementary Material for this article can be found online at: https://www.frontiersin.org/articles/10.3389/fmicb.2020.597545/full#supplementary-material

Supplementary Figure 1 | PCR results of Δ*AaPdel* transformants were verified by three primer pairs of PLP1F/H855R, H856F/PLP2R, and PLF/PLR. *AaPdeh* transformants were identified through PHP1F/H855R, H856F/PHP2R, and PHF/PHR.

Supplementary Figure 2 | The conidia of *AaPdeh* deletion mutants exhibit similar phenotype with wild-type strain. **(A)** The conidia morphology examined by light microscopy. **(B)** Statistical analysis of conidia production. The quantity of conidia was quantified after cultured on the V8 medium in dark for 8 days. Bars indicate standard errors of at least three repetitions.

Supplementary Figure 3 | The sensitivity of the *AaPdeh* mutants to osmotic stress. Z7, Δ*AaPdeh*-1, Δ*AaPdeh*-6, and *AaPdeh*-CP strains were inoculated on PDA amended with osmotic stressors, NaCl, KCl, sorbitol or sucrose, respectively.

Supplementary Figure 4 | Similar necrotic lesions induced by Δ*AaPdeh* strain and wild type Z7 on detached tangerine leaves. The conidial suspension at 1.0 × 105 conidia/ml of *Alternaria alternata* wild type Z7, Δ*AaPdeh* and the complemented strains were inoculated on leaves, respectively. The purified water was used as mock control.

REFERENCES

Bahn, Y. S., Staab, J., and Sundstrom, P. (2003). Increased high-affinity phosphodiesterase *PDE2* gene expression in germ tubes counteracts CAP1-dependent synthesis of cyclic AMP, limits hypha production and promotes virulence of *Candida albicans*. *Mol. Microbiol.* 50, 391–409. doi: 10.1046/j.1365-2958.2003.03692.x

Calvo, A. M., Wilson, R. A., Bok, J. W., and Keller, N. P. (2002). Relationship between secondary metabolism and fungal development. *Microbiol. Mol. Biol. Rev.* 66, 447–459. doi: 10.1128/mmbr.66.3.447-459.2002

Caza, M., and Kronstad, J. W. (2019). The cAMP/protein kinase a pathway regulates virulence and adaptation to host conditions in *Cryptococcus neoformans*. *Front. Cell. Infect. Microbiol.* 9:212. doi: 10.3389/fcimb.2019.00212

Conti, M., and Beavo, J. (2007). Biochemistry and physiology of cyclic nucleotide phosphocliesterases: essential components in cyclic nucleotide signaling. *Annu. Rev. Biochem.* 76, 481–511. doi: 10.1146/annurev.biochem.76.060305.150444

Dong, Y. H., Li, Y., Zhao, M. M., Jing, M. F., Liu, X. Y., Liu, M. X., et al. (2015). Global genome and transcriptome analyses of *Magnaporthe oryzae* epidemic isolate 98-06 uncover novel effectors and pathogenicity-related genes, revealing gene gain and lose dynamics in genome evolution. *PLoS Pathog.* 11:e1004801. doi: 10.1371/journal.ppat.1004801

Gong, B.-Q., Wang, F.-Z., and Li, J.-F. (2020). Hide-and-seek: chitin-triggered plant immunity and fungal counterstrategies. *Trends Plant Sci.* 25, 805–816. doi: 10.1016/j.tplants.2020.03.006

Hanin, M., Ebel, C., Ngom, M., Laplaze, L., and Masmoudi, K. (2016). New insights on plant salt tolerance mechanisms and their potential use for breeding. *Front. Plant Sci.* 7:1787. doi: 10.3389/fpls.2016.01787

Harren, K., Brandhoff, B., Knodler, M., and Tudzynski, B. (2013). The high-Affinity phosphodiesterase *BcPde2* has impact on growth, differentiation and virulence of the phytopathogenic ascomycete *Botrytis cinerea*. *PLoS One* 8:e0078525. doi: 10.1371/journal.pone.0078525

Hatta, R., Ito, K., Hosaki, Y., Tanaka, T., Tanaka, A., Yamamoto, M., et al. (2002). A conditionally dispensable chromosome controls host-specific pathogenicity in the fungal plant pathogen *Alternaria alternata*. *Genetics* 161, 59–70.

Houslay, M. D., Baillie, G. S., and Maurice, D. H. (2007). cAMP-specific phosphodiesterase-4 enzymes in the cardiovascular system - A molecular toolbox for generating compartmentalized cAMP signaling. *Circ. Res.* 100, 950–966. doi: 10.1161/01.res.0000261934.56938.38

Houslay, M. D., Sullivan, M., and Bolger, G. B. (1998). The multienzyme PDE4 cyclic adenosine monophosphate-specific phosphodiesterase family: intracellular targeting, regulation, and selective inhibition by compounds exerting antiinflammatory and antidepressant actions. *Adv. Pharmacol.* 44, 225–342. doi: 10.1016/s1054-3589(08)60128-3

Hu, Y., Liu, E. K., Bai, X. J., and Zhang, A. L. (2010). The localization and concentration of the PDE2-encoded high-affnity cAMP phosphodiesterase is regulated by cAMP-dependent protein kinase A in the yeast *Saccharomyces cerevisiae*. *FEMS Yeast Res.* 10, 177–187. doi: 10.1111/j.1567-1364.2009.00598.x

Irfan, M., Mehmood, S., Irshad, M., and Anwar, Z. (2018). Optimized production, purification and molecular characterization of fungal laccase through *Alternaria alternata*. *Turk. J. Biochem. Turk. Biyokimya. Dergisi.* 43, 613–622. doi: 10.1515/tjb-2017-0239

Ito, K., Tanaka, T., Hatta, R., Yamamoto, M., Akimitsu, K., and Tsuge, T. (2004). Dissection of the host range of the fungal plant pathogen *Alternaria alternata* by modification of secondary metabolism. *Mol. Microbiol.* 52, 399–411. doi: 10.1111/j.1365-2958.2004.04004.x

Jiang, C., Zhang, C. K., Wu, C. L., Sun, P. P., Hou, R., Liu, H. Q., et al. (2016). TRI6 and TRI10 play different roles in the regulation of deoxynivalenol (DON) production by cAMP signalling in *Fusarium graminearum*. *Environ. Microbiol.* 18, 3689–3701. doi: 10.1111/1462-2920.13279

Jin, S. L. C., Swinnen, J. V., and Conti, M. (1992). Characterization of the structure of a low Km, rolipram-sensitive cAMP phosphodiesterase-mapping of the catalytic domain. *J. Biol. Chem.* 267, 18929–18939.

Kong, X. W., Tang, F. Y., Lv, W. W., Zhang, Q., and Tang, K. Z. (2018). Optimization of protoplast preparation and regeneration conditions of *Alternaria alternata*. *J. Plant Prot.* 45, 1431e1432.

Lee, H. B., Patriarca, A., and Magan, N. (2015). *Alternaria* in food: ecophysiology, mycotoxin production and toxicology. *Mycobiology* 43, 93–106. doi: 10.5941/myco.2015.43.2.93

Liu, H., Suresh, A., Willard, F. S., Siderovski, D. P., Lu, S., and Naqvi, N. I. (2007). *Rgs1* regulates multiple G alpha subunits in *Magnaporthe* pathogenesis, asexual growth and thigmotropism. *EMBO J.* 26, 690–700. doi: 10.1038/sj.emboj.7601536

Londesborough, J., and Suoranta, K. (1983). The zinc-containing high Km cyclic-nucleotide phosphodiesterase of bakers-yeast. *J. Biol. Chem.* 258, 2966–2972.

Ma, H. J., Zhang, B., Gai, Y. P., Sun, X. P., Chung, K. R., and Li, H. Y. (2019). Cell-wall-degrading enzymes required for virulence in the host selective toxin-producing necrotroph *Alternaria alternata* of citrus. *Front. Microbiol.* 10:2514. doi: 10.3389/fmicb.2019.02514

Ma, P. S., Wera, S., Van Dijck, P., and Thevelein, J. M. (1999). The PDE1-encoded low-affinity phosphodiesterase in the yeast *Saccharomyces cerevisiae* has a specific function in controlling agonist-induced cAMP signaling. *Mol. Biol. Cell* 10, 91–104. doi: 10.1091/mbc.10.1.91

Mtibaa, R., Barriuso, J., de Eugenio, L., Aranda, E., Belbahri, L., Nasri, M., et al. (2018). Purification and characterization of a fungal laccase from the ascomycete *Thielavia* sp. and its role in the decolorization of a recalcitrant dye. *Int. J. Biol. Macromol.* 120(Pt B), 1744–1751. doi: 10.1016/j.ijbiomac.2018.09.175

Otani, H., Kohmoto, K., and Kodama, M. (1995). *Alternaria* toxins and their effects on host plants. *Can. J. Bot. Rev. Can. Bot.* 73, S453–S458. doi: 10.1139/b95-282

Perina, F. J., Belan, L. L., Moreira, S. I., Nery, E. M., Alves, E., and Pozza, E. A. (2019). Diagrammatic scale for assessment of alternaria brown spot severity on tangerine leaves. *J. Plant Pathol.* 101, 981–990. doi: 10.1007/s42161-019-00306-6

Ramanujam, R., and Naqvi, N. I. (2010). PdeH, a high-affinity cAMP phosphodiesterase, is a key regulator of asexual and pathogenic differentiation in *Magnaporthe oryzae*. *PLoS Pathog.* 6:e1000897. doi: 10.1371/journal.ppat.1000897

Rehman, L., Su, X. F., Guo, H. M., Qi, X. L., and Cheng, H. M. (2016). Protoplast transformation as a potential platform for exploring gene function in *Verticillium dahliae*. *BMC Biotechnol.* 16:9. doi: 10.1186/s12896-016-0287-4

Solel, Z., and Kimchi, M. (1998). Histopathology of infection of Minneola tangelo by *Alternaria alternata* pv. citri and the effect of host and environmental factors on lesion development. *J. Phytopathol.* 146, 557–561. doi: 10.1111/j.1439-0434.1998.tb04754.x

Tang, K., Lv, W., Zhang, Q., and Zhou, C. (2020). Coding the alpha-subunit of SNF1 kinase, *Snf1* is required for the conidiogenesis and pathogenicity of the *Alternaria alternata* tangerine pathotype. *Fungal Biol.* 124, 562–570. doi: 10.1016/j.funbio.2020.02.008

Thomma, B. (2003). *Alternaria* spp.: from general saprophyte to specific parasite. *Mol. Plant Pathol.* 4, 225–236. doi: 10.1046/j.1364-3703.2003.00173.x

Timmer, L. W., Solel, Z., Gottwald, T. R., Ibanez, A. M., and Zitko, S. E. (1998). Environmental factors affecting production, release, and field populations of conidia of *Alternaria alternata*, the cause of brown spot of citrus. *Phytopathology* 88, 1218–1223. doi: 10.1094/phyto.1998.88.11.1218

Tsuge, T., Harimoto, Y., Akimitsu, K., Ohtani, K., Kodama, M., Akagi, Y., et al. (2013). Host-selective toxins produced by the plant pathogenic fungus *Alternaria alternata*. *FEMS Microbiol. Rev.* 37, 44–66. doi: 10.1111/j.1574-6976.2012.00350.x

Uno, I., Matsumoto, K., and Ishikawa, T. (1983). Characterization of a cyclic-nucleotide phosphodiesterase-deficient mutant in yeast. *J. Biol. Chem.* 258, 3539–3542.

Wang, M., Sun, X., Yu, D., Xu, J., Chung, K., and Li, H. (2016). Genomic and transcriptomic analyses of the tangerine pathotype of *Alternaria alternata* in response to oxidative stress. *Sci. Rep.* 6:32437. doi: 10.1038/srep32437

Wang, M., Yang, X., Ruan, R., Fu, H., and Li, H. (2018). *Csn5* is required for the conidiogenesis and pathogenesis of the *Alternaria alternata* tangerine pathotype. *Front. Microbiol.* 9:508. doi: 10.3389/fmicb.2018.00508

Wera, S., Ma, P. S., and Thevelein, J. M. (1997). Glucose exerts opposite effects on mRNA versus protein and activity levels of Pde1, the low-affinity cAMP phosphodiesterase from budding yeast, *Saccharomyces cerevisiae*. *FEBS Lett.* 420, 147–150. doi: 10.1016/s0014-5793(97)01508-1

Wilson, D., Fiori, A., Brucker, K. D., Dijck, P. V., and Stateva, L. (2010). *Candida albicans* Pde1p and Gpa2p comprise a regulatory module mediating agonist-induced cAMP signalling and environmental adaptation. *Fungal Genet. Biol.* 47, 742–752. doi: 10.1016/j.fgb.2010.06.006

Yang, K., Liu, Y., Liang, L., Li, Z., Qin, Q., Nie, X., et al. (2017). The high-affinity phosphodiesterase PdeH regulates development and aflatoxin biosynthesis in *Aspergillus flavus*. *Fungal Genet. Biol.* 101, 7–19. doi: 10.1016/j.fgb.2017.02.004

Zhang, H., Liu, K., Zhang, X., Tang, W., Wang, J., Guo, M., et al. (2011). Two phosphodiesterase genes, *PDEL* and *PDEH*, regulate development and pathogenicity by modulating intracellular cyclic AMP levels in *Magnaporthe oryzae*. *PLoS One* 6:e17241. doi: 10.1371/journal.pone.0017241

Zhao, X., Mehrabi, R., and Xu, J.-R. (2007). Mitogen-activated protein kinase pathways and fungal pathogenesis. *Eukaryot. Cell* 6, 1701–1714. doi: 10.1128/ec.00216-07

Zhu, W. J., Zhou, M., Xiong, Z. Y., Peng, F., and Wei, W. (2017). The cAMP-PKA signaling pathway regulates pathogenicity, hyphal growth, appressorial formation, conidiation, and stress tolerance in *Colletotrichum higginsianu*. *Front. Microbiol.* 8:1416. doi: 10.3389/fmicb.2017.01416

Conflict of Interest: The authors declare that the research was conducted in the absence of any commercial or financial relationships that could be construed as a potential conflict of interest.

frontiers in Microbiology

ORIGINAL RESEARCH
published: 10 December 2020
doi: 10.3389/fmicb.2020.605152

Isolation of *Burkholderia* sp. HQB-1, A Promising Biocontrol Bacteria to Protect Banana Against Fusarium Wilt Through Phenazine-1-Carboxylic Acid Secretion

Zhizhou Xu[1,2], Mingyuan Wang[1], Jinpeng Du[1], Ting Huang[1], Jianfu Liu[1], Tao Dong[3] and Yinglong Chen[4]**

[1] Research Center of Horticultural Science and Engineering, Huaqiao University, Xiamen, China, [2] College of Plant Protection, Nanjing Agricultural University, Nanjing, China, [3] Institute of Fruit Tree Research, Guangdong Academy of Agricultural Sciences, Guangzhou, China, [4] UWA Institute of Agriculture, UWA School of Agriculture and Environment, The University of Western Australia, Perth, WA, Australia

OPEN ACCESS

Edited by:
Yong Wang,
Guizhou University, China

Reviewed by:
Orlando Borras-Hidalgo,
Qilu University of Technology, China
Sonia Rippa,
University of Technology Compiegne, France

***Correspondence:**
Mingyuan Wang
w_mingyuan@163.com
Yinglong Chen
yinglong.chen@uwa.edu.au

Specialty section:
This article was submitted to Microbe and Virus Interactions with Plants, a section of the journal Frontiers in Microbiology

Received: 11 September 2020
Accepted: 18 November 2020
Published: 10 December 2020

Citation:
Xu Z, Wang M, Du J, Huang T, Liu J, Dong T and Chen Y (2020) Isolation of Burkholderia sp. HQB-1, A Promising Biocontrol Bacteria to Protect Banana Against Fusarium Wilt Through Phenazine-1-Carboxylic Acid Secretion. Front. Microbiol. 11:605152. doi: 10.3389/fmicb.2020.605152

Fusarium wilt is a devastating soil-borne fungal disease caused by *Fusarium oxysporum* f.sp. *cubense* (Foc). In recent years, some antifungal bacteria have been applied for the prevention and biocontrol of pathogenic fungi. In our study, a bacterial strain HQB-1, isolated from banana rhizosphere soil, was cultured for investigation. It showed broad-spectrum antifungal activities against representative phytopathogenic fungi including *Fusarium oxysporum*, *Colletotrichum gloeosporioides*, *Botrytis cinerea*, and *Curvularia fallax*. The strain HQB-1 was identified as *Burkholderia* sp. by morphological, physiological, and biochemical examinations, confirmed by 16S rRNA gene sequence analysis. Among the metabolites produced by the strain, we identified an antifungal compound which was identified phenazine-1-carboxylic acid (PCA) ($C_{13}H_8N_2O_2$) through ultraviolet, liquid chromatography quadrupole-time of flight mass spectrometer, and nuclear magnetic response. Furthermore, PCA exhibited the lowest minimum inhibitory concentration (MIC) against *F. oxysporum* (1.56 μg/ml) and yielded the highest MIC against *C. gloeosporioides*. Pot experiments showed that application of 5 μg/ml or more of PCA efficiently controlled banana wilt and promoted the growth of banana plants. These results suggested that *Burkholderia* sp. HQB-1, as an important microbial resource of PCA, could be a promising biological agent against wilt diseases and promoting banana growth.

Keywords: antifungal activity, *Burkholderia*, banana *Fusarium* wilt, LC-Q-TOF-MS, phenazine-1-carboxylic acid

INTRODUCTION

Banana (*Musa* spp.), is one of the most important fruit crops, widely cultivated in tropical and subtropical areas, providing staple food for over 400 million people (Dale et al., 2017). With the increase in exportation, banana becomes an important source for foreign exchange in China (Wang B. et al., 2013). However, in recent years, Fusarium wilt, also known as Panama disease, has

become one of the most destructive soil-borne diseases threatening banana production worldwide (Davis et al., 1996; Ploetz, 2005; Fourie et al., 2011). Fusarium wilt is caused by *Fusarium oxysporum* f. sp. *cubense* (Foc) with the Tropical Race 4 (Foc TR4) causing the most severe damage among the four races of this pathogen. It has been demonstrated that the pathogen Foc TR4 can infect banana roots, penetrate into the root xylem, spread into the rhizome and pseudostem xylem within several days after infection (Warman and Aitken, 2018), and eventually cause the occlusion of vascular bundle and the blocking of water and nutrients transportation (Li et al., 2017). Once Foc TR4 was introduced to or detected in banana orchard, it is quite difficult to eradicate. Because the chlamydospores of Foc TR4 can survive for a long period of time in soil (Viljoen, 2002), it is becoming one of the most crucial limiting factors in banana production (O'Donnell et al., 1998; Lin et al., 2009). Therefore, it is necessary and imperative to efficiently control the occurrence and spread of Foc TR4 in banana.

Traditionally, chemical pesticide is considered to be a simple and direct approach to control Fusarium wilt (Fuchs et al., 1999; Getha et al., 2005). However, chemical residues not only provided unsatisfactory control levels but also lead to severe environmental pollutions and induce the development of resistant strains (Kanini et al., 2013). Though resistant breeding cultivars have been studied and widely used for a long time, polyploidy, low reproductive fertility and complete sterility of banana are the main reasons for the limited success of the breeding program (Shepherd, 1987). Crop rotation slowly reduces pathogen density in the soil but its effectiveness is restricted once the disease outbreak occurred (Chellemi et al., 2016). Recently, biological control, especially the application of biocontrol microorganisms, has been widely studied due to its advantage as an economically and environmentally friendly method (Leeman et al., 1996). However, the available microorganisms for biocontrol of plant diseases may also lead to inconsistent performance and poor activity in the soil environment (Saravanan et al., 2003). Thus, the isolation and screening of highly efficient and broad-spectrum antagonistic microorganisms are the key for the development of biocontrol agents. New bioformulation technologies like nanotechnologies, formulation of microbial consortia and/or their metabolites need to be developed to improve their efficacy and deepen the knowledge of biocontrol microorganisms (Bubici et al., 2019).

The genus *Burkholderia* has become increasingly important during the past several decades because of its capability in producing abundant secondary metabolites with antimicrobial, insecticidal, herbicidal, or growth-promotion traits (Jeong et al., 2003; Singh et al., 2013; Kunakom and Eustáquio, 2019). Several *Burkholderia* strains like *B. vietnamiensis*, *B. ambifaria*, and *B. pyrrocinia* have been reported to be potential and efficient biological control agents (Mahenthiralingam et al., 2008). In fact, the key mechanism for the antagonistic effects of *Burkholderia* against plant pathogens is the production of antimicrobial secondary metabolites (Schmidt et al., 2010; Eberl and Vandamme, 2016). Among them, cepacin, phenazine, and pyrrolnitrin have been shown to play roles as antibiotics in controlling plant diseases (Parker et al., 1984; Cartwright et al., 1995; Xu et al., 2013). Siderophores produced by *Burkholderia* not only exhibit survival competition with pathogens but also promote the growth of the plant (Jiang et al., 2008). However, a large number of new natural compounds produced by *Burkholderia* is still unknown, and the isolation, purification, and identification of these bio-functional natural products, especially as antimicrobials, need to be further investigated.

In this study, we screened and isolated a broad-spectrum antagonistic bacterial strain HQB-1 from the rhizosphere soil of banana plants. The taxonomic status of HQB-1 was determined as *Burkholderia* sp. according to the 16S rRNA gene sequence analysis combined with morphological, physiological, and biochemical characteristics. Moreover, the antifungal component phenazine-1-carboxylic acid (PCA) produced by *Burkholderia* sp. HQB-1 was separated and identified by column chromatography, ultraviolet (UV), liquid chromatography quadrupole-time of flight mass spectrometer (LC-Q-TOF-MS), and nuclear magnetic response (NMR). The bio-controlling effect of PCA was further investigated via pot experiments. The aim of this study was to analyze the antifungal metabolites from potential beneficial microbial resources and to identify the main efficient compound that could be used to prevent Fusarium wilt in banana.

MATERIALS AND METHODS

Soil Sample Collection, Isolation of Fusarium Wilt Antagonistic Bacteria and Antifungal Activity

Twelve rhizosphere soil samples including clay and silt loam and were collected from healthy plants found in a pathogen-infested banana orchard, which has been planted banana for 15 years, at Changtai County, Zhangzhou City, Fujian Province, China (24.65°N, 117.72°E) as described by Chen et al. (2013). The plants were gently removed from the farmland, the loose soil was removed by shaking, and the soil attached to the roots was collected by a brush. The soil samples were placed into clean, dry, and sterile polythene bags, transported to the laboratory, and stored at 4°C until further analysis.

The samples were suspended in 0.85% of NaCl and spread on Luria-Bertani (LB) agar. After incubation at 30°C for 2 days, bacterial colonies with different morphological characteristics were selected and re-streaked on fresh LB agar until the homogeneous colonies appeared. Fifty-six isolated strains were further sub-cultured in LB broth on a rotary shaker. For long-term storage of bacterial strains, 50% (v/v) glycerol solution was added to the liquid culture for freezing at −80°C.

Several important phytopathogenic fungi were chosen and used in the present study, included *Fusarium oxysporum* f. sp. *cubense* Tropical Race 4 (Foc TR4, ATCC 76255), *Colletotrichum gloeosporioides* (ATCC 16330), *Botrytis cinerea* (ATCC 11542), and *Curvularia fallax* (ATCC 38579). These strains were provided by the Institute of Tropical Bioscience and Biotechnology, China Academy of Tropical Agricultural Sciences, Haikou, China. The antifungal activity of isolated

strains was determined according to Reyes-Chilpa et al. (1997) and Chen et al. (2018) with slight modifications. Briefly, a fungal plug ($\Phi = 6$ mm) was inoculated in the center of a plate filled with potato dextrose agar (PDA) medium; Each isolated bacterium was seeded with a sterile stick at a distance of 2.5 cm from the fungi. A fungal disk in the center of a plate without seeding isolated bacterium was served as a control. After incubation at 28°C for 5 days, the inhibition zone was recorded by measuring the distance between the edge of the fungal mycelium and the bacterial colony. The percentage inhibition of mycelial radial growth was calculated by the following formula:

Percent mycelial inhibition $= \frac{A-B}{A} \times 100$, where A is the mean colony diameter for the control, and B is the mean colony for the treatment (Nimaichand et al., 2015).

Morphology, Physiological, and Biochemical Tests of Antagonistic Bacteria

The morphological, physiological, and biochemical characteristics tests of the strain HQB-1 were further analyzed including: Gram-staining, temperature and pH range for growth, presence of pigment, catalase activity, oxidative or fermentative reaction, nitrate reduction, hydrolysis of casein, starch, Tween 80 and gelatin, activity of urease and pyruvate deaminase, tolerance to sodium chloride, production of indole, reaction of H_2S, Methyl Red-staining, and Voges-Proskauer tests. All these characteristics were then compared with the standard description of Bergey's Manual of Determinative Bacteriology (Buchanan and Gibbons, 1984).

To obtain scanning electron microscope (SEM) image of HQB-1, a 1 cm^2 transverse section of the bacterial strain on LB agar plate was obtained and fixed in 2.5% glutaraldehyde buffer at 4°C for 3 h. Then the bacterial cells were washed by phosphate-buffered saline (PBS) for three times and fixed in 1% osmic acid at 25°C for 5 h. After washing, the cells were dehydrated with 50, 70, 95, and 100% ethanol, respectively, for critical point drying and platinum-coating using an ion-sputter coater. The morphology of the specimen was observed at an opening voltage of 5 kV using a field-emission scanning electron microscopy (S-4800IIESEM, Hitachi, Japan).

16S rRNA Gene Sequencing and Phylogenetic Analysis

The strain HQB-1 was cultured in LB broth at 28°C in an orbital shaker for 12 h. The genomic DNA of the strain was extracted using the bacterial genomic DNA extraction kit (Takara, Beijing, China). The 16S rRNA sequences were amplified by PCR with the universal primers 27F (5′-GAGAGTTTGATCCTGGCTCAG-3′) and 1492R (5′-CTACGGCTACCTTGTTACGA-3′) (Gupta et al., 2014). The PCR conditions were as follows: initial denaturation at 94°C for 5 min, 30 cycles of 94°C for 45 s, 58°C for 60 s, and 72°C for 90 s, and a final extension at 72°C for 10 min. The PCR products were purified by Quick Gel Extraction Kit (TransGen Biotech, Beijing, China) and sequenced by Sangon Biotech (Shanghai, China). The 16S rRNA gene sequence was submitted to the GenBank database. The sequences were analyzed by a global alignment algorithm implemented in the EzBioCloud database[1] (Kim et al., 2012; Yoon et al., 2017) and blasted with the sequences of known species in NCBI database[2]. After multiple alignments of sequences via CLUSTAL_X (Thompson et al., 1997), the phylogenetic analysis was performed using the neighbor-joining method (Saitou and Nei, 1987) with MEGA version 6.0 (Tamura et al., 2007).

Fermentation of HQB-1 and Separation of Antifungal Components

Forty liters of LB broth with HQB-1 were grown in a 200 L fermentation tank.at 30°C for 4 days. At the end of fermentation, the cultural broth with HQB-1 was centrifuged at 10,000 × *g* for 20 min, and an equal volume of ethyl acetate (EA) was added into the cultural supernatant. This procedure was repeated three times. The EA layers were combined and the solvent was evaporated under vacuum at 40°C using a rotary evaporator for obtaining the final crude extract with approximately 36 g. The crude EA extract was then subjected to macroporous resin (XAD-16, Amberlite, United States) column chromatography and eluted with different (30, 60, and 100%) aqueous MeOH to yield three fractions (Fractions 1–3). The fractions were tested in plates for their antifungal activity, where a Foc TR4 mycelial plug (6 mm in diameter) was inoculated into 10 ml potato dextrose broth (PDB) per dish with 25 μg/ml of each fraction or DMSO (0.1% in sterile water, negative control). The most active fraction (Fraction 3) with visible inhibition was then passed through a silica gel (200 meshes) column (Sigma-Aldrich, Shanghai, China) and eluted with different ratios of methanol and chloroform (subfractions 1–3 were eluted with methanol and chloroform at the ratio of 1:3, 1:6, and 1:9, respectively).

Purification and Chemical Analysis of the Main Antifungal Component

The subfractions were also tested in the bioassays as described above, and the most active fraction was subjected to the analysis of the UV absorption spectrum (Shimadzu UV-2450, Japan). Liquid chromatographic separation was conducted in a reverse-phased C18 analytical column (Zorbax RRHD Eclipse Plus, 2.1 × 50 mm, 1.8 μm, Agilent, United States). A syringe pump delivering 5 μl was adjusted by the direct loop injection method (Hu et al., 2005). The mobile phase A was water with 0.1% acetic acid (v/v) and the mobile phase B was methanol. The chromatographic separation was held at the initial mobile phase composition (5% methanol) constant for 0.1 min, followed by a linear gradient to 95% methanol for 6 min, then decreased to 5% in 6–8 min, and followed by a one min post-run time after each analysis. All samples were performed on high performance liquid chromatography (HPLC) using a solvent containing 30% mobile phase A and 70% mobile phase B for 2 min, operated at a flow rate of 0.4 ml/min and the UV absorption at 365 nm. The HPLC-separated samples were then analyzed by quadrupole-time of flight mass spectrometer (TOF-MS) (Agilent1290-6545, United States). Electrospray ionization

[1] http://eztaxon-e.ezbiocloud.net/

[2] https://blast.ncbi.nlm.nih.gov/Blast.cgi

(ESI) was operated in negative ionization mode with other parameters used as following: capillary voltage was 4.0 kV; the temperature of dry gas (N_2) was 200°C; the flow rate of dry gas was 9 L/h at 35 psig spray pressure; the temperature of sheath was 350°C; the flow rate of sheath was 10 L/h, and the ion scanning range was m/z 100∼1100. The collision energy was set at 10∼40 eV for the MS/MS analysis. The mass data of the molecular ions were processed through the Mass Hunter Qualitative Analysis (version B.07.00) software.

Meanwhile, the bioactive subfraction was solved in deuterated chloroform ($CDCl_3$, $\delta = 77.0$ ppm) at the concentration of 10 mg/ml for the ^{1}H-NMR and ^{13}C-NMR experiments with a 5 mm probe by a Bruker spectrometer (500 MHz/Advance III, Advance Digital, Bruker, Germany). The spectra were obtained at 30°C using tetramethylsilane (TMS) as the internal standard. The NMR spectra were analyzed by MestReNova (version 6.1.1-6384) software.

Determination of the Minimum Inhibitory Concentration (MIC) of PCA

A standardized 96-well microdilution broth assay (Wedge and Kuhajek, 1998) was used to evaluate the antifungal activity of the pure compound from *Burkholderia* sp. HQB-1.

The MICs of phenazine-1-carboxylic acid (PCA) from the cultural broth of the strain HQB-1 against the fungal pathogens including *F. oxysporum*, *C. gloeosporioides*, *B. cinerea,* and *C. fallax*. Different concentrations of PCA (50.0, 25.0, 12.5, 6.25, 3.13, 1.56, 0.78, 0.39 and 0.20 μg/ml) were prepared by using 2-fold serial dilutions for minimum inhibitory concentration (MIC) test. The lowest concentration of PCA that inhibited fungal growth was recorded as the MIC. The concentration of the inoculated fungal pathogens was 1×10^6 CFU/ml. Carbendazim was used as a positive control and 0.1% DMSO as a negative control. The 96-well plates were covered with a plastic lid and incubated at 25°C for 72 h. The absorbance was measured at 620 nm by a microplate photometer (BioTek, BioTek Instrument Co., United States). Mean absorbance and standard errors were used to evaluate fungal growth after 72 h incubation (Wang X. et al., 2013).

Biological Assays

Biological assays were carried out in July–September 2019 at the greenhouse in Huaqiao University, Xiamen. Pathogen suspensions were prepared as follows: a 6 mm diameters agar disk containing 7-day-old pathogen was added to a flask containing PDB. The flask was incubated at 28°C, 170 rpm for 7 days, and then the suspension was filtered through four layers of sterilized gauze. The conidial suspension was determined using a biological microscope (Nikon, Japan) and adjusted with distilled water to give a final concentration of 1.0×10^6 CFU/ml for further use.

The soil used in this study was a mixture of peat and perlite (2:1, v/v) and sterilized at 120°C for 2 h. Three to four true leaves old banana (*Musa acuminata* L.) AAA group, cv. *Cavendish* seedlings (Shishengyuan Biological Technology Co., Ltd., Gaozhou, China) were transplanted in plastic pots (8 cm × 8 cm, with one plant standing in one cup) with 80 g soil for pot experiment. The fungal pathogen *F. oxysporum* Tropical Race 4 with a concentration of 1.0×10^6 CFU/ml was inoculated into the potting substrates 5 days before PCA treatments. Six treatment group were conducted as follows: (1) CK1 (negative control, non-inoculated Foc TR4 and application of 0.1% DMSO); (2) CK2 (positive control, inoculated Foc TR4 and application with sterile water); (3) PCA 1 μg/ml; (4) PCA 5 μg/ml; (5) PCA 25 μg/ml; (6) PCA 50 μg/ml. Each PCA treatment group was watered weekly with 5 ml PCA at the concentration of 1, 5, 25, or 50 μg/ml mixed in sterile water. Seven plants were included for each treatment, and the experiment was repeated three times. The banana seedlings were placed on a greenhouse bench with natural light for 60 days and watered regularly.

The physiological indexes of banana seedlings treated for 60 days were determined, including root length, plant height, stem diameter, leaf width and dry weight. The disease symptoms on each plant were recorded and rated in five classes from 0 to 4 according to Mak et al. (2004). The disease index (DI) was calculated as DI (%) = Σ (Class × Number of plants in that class)/(4 × Total number of assessed plants) × 100. Biocontrol efficiency (BE) was calculated using the following formula: BE (%) = (DI in sterile water controlled - DI in treatments)/DI in sterile water controlled × 100.

Statistical Analysis

Statistical analysis was performed using SPSS 19. The difference among treatments was determined based on one-way analysis of variance (ANOVA), and means were subjected to Duncan's multiple range test with significance set at $P < 0.05$.

FIGURE 1 | Antagonistic activity of the strain HQB-1 against *Fusarium oxysporum* Tropical Race 4 (Foc TR4). The co-cultivation HQB-1 and Foc TR4 grown on PDA medium at 28°C for 5 days.

TABLE 1 | Antifungal activities of strain HQB-1 against various pathogens.

Pathogenic fungi (strain#)	Mycelial inhibition (%)	Antifungal activity
Fusarium oxysporum (ATCC 76255)	56.7 ± 0.64a	++++
Colletotrichum gloeosporioides (ATCC 16330)	36.7 ± 1.15b	+++
Botrytis cinerea (ATCC 11542)	52.4 ± 0.83a	++++
Curvularia fallax (ATCC *38579)*	52.2 ± 0.68c	++++

Data are means ± SD (n = 3). Data of mycelial inhibition followed by different letters are significantly different at p < 0.05 level according to Duncan's multiple range test. The result of antifungal activity was expressed as the distance between the fungal pathogen and the area of antagonist growth after 5 days. - no inhibition zone; + (very weak), 0–5 mm; + + (weak), 5–10 mm; +++ (moderate), 10–15 mm; ++++ (strong), 15–20 mm; +++++ (very strong), >20 mm.

RESULTS

Isolation of the Strain HQB-1

A total of 11 bacterial isolates with 33.3 to 56.7% antagonistic effect was isolated from the soil samples in banana orchard. Among them, the isolate HQB-1 showed a more significant and stronger antagonistic activity against Foc TR4 on the plate (**Figure 1**) and exhibited a broad-spectrum antifungal activity against other plant pathogens. The growth inhibition of *F. oxysporum*, *C. gloeosporioides, B. cinerea,* and *C. fallax* was 56.7, 36.7, 52.4, and 52.2% respectively, after 5-day cultivation with HQB-1 (**Table 1**).

Morphological, Physiological, and Biochemical Identification of the Strain HQB-1

The strain HQB-1 was slightly yellow, shining, and smooth in colony appearance on the nutrient agar (NA) plate. The biochemical tests indicated that it is a gram-negative and rod-shaped bacterium. The shape of the strain HQB-1 was straight rod, and the size was (1.2–2.5) μm × (0.5–1.0) μm (**Figure 2**) under scanning electron microscope (SEM). The tests of catalase, methyl red, oxidative or fermentative acid production from carbohydrates, liquefaction of gelatin, phenylalanine deaminase and indole were positive; and the Voges-Proskauer tests, tests for the presence of pigment, hydrolysis of starch, urease, Tween 80, H_2S production, and creatine were negative. Besides, the strain HQB-1 can grow at a temperature range of 18–39°C.

16S rRNA Gene Sequencing and Phylogenetic Analysis of the Strain HQB-1

The 16S rRNA gene sequence (1471 bp) was submitted to GenBank with accession number MK612762. The sequence exhibited 99.7% similarity with *Burkholderia stagnalis* LMG

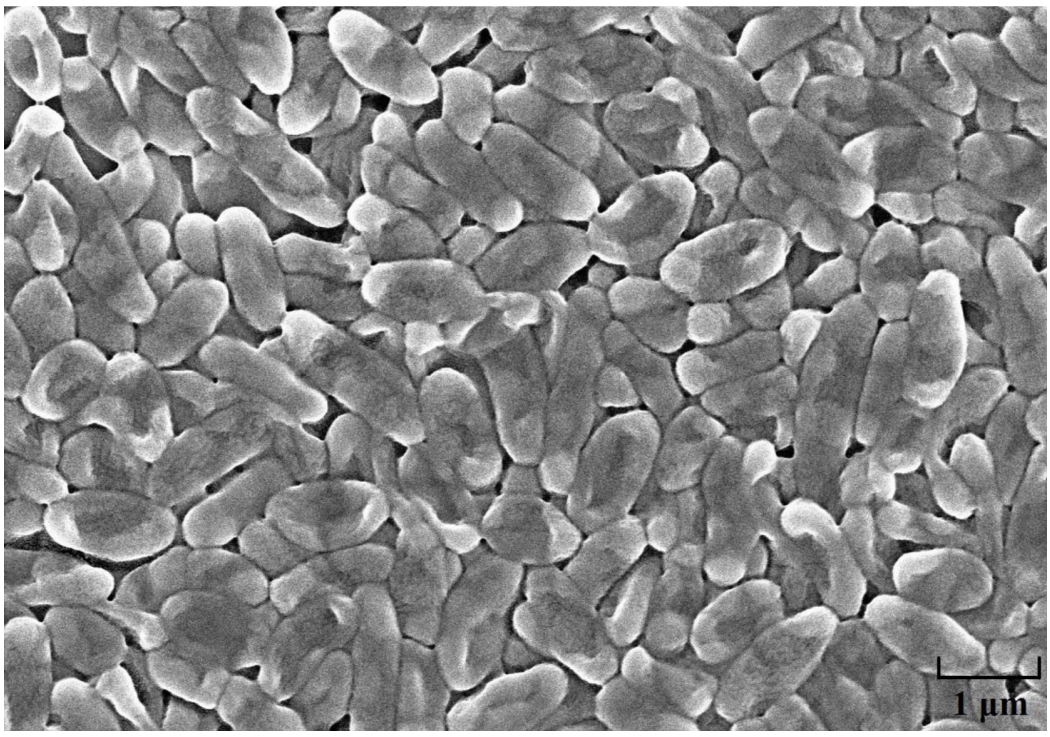

FIGURE 2 | Scanning electron microscope image of HQB-1. Morphological characters of *Burkholderia* sp. HQB-1 viewed using SEM. Scale bar means 1 μm in the image.

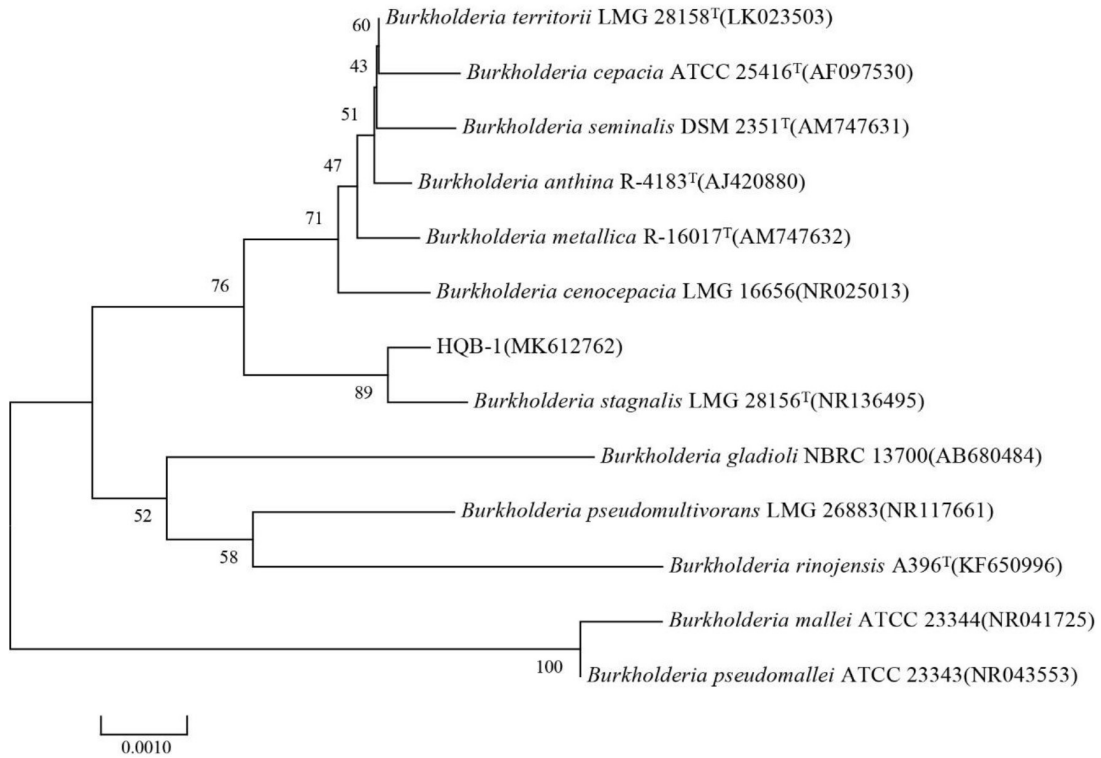

FIGURE 3 | Phylogenetic tree of the strain HQB-1 based on 16S rRNA gene sequence analysis. The bootstrap values (%) presented at the branches were calculated from 1,000 replications. The numbers in parentheses are the GenBank accession numbers. The scale bar 0.001 represents 2 nucleotide substitutions per 1,000 nucleotides. T means type strain.

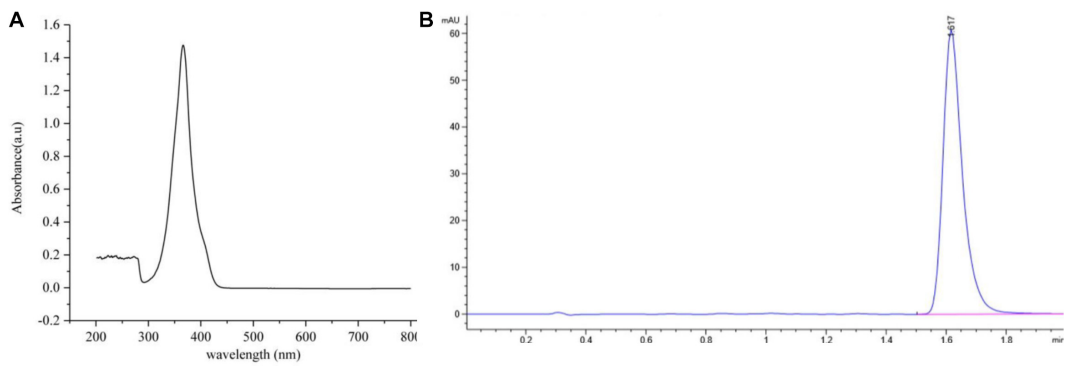

FIGURE 4 | The ultraviolet and HPLC data of the main active antifungal component produced by *Burkholderia* sp. HQB-1. **(A)** The UV absorption of the main active subfraction at a wavelength of 0-800 nm, the peak means the maximum absorption at the wavelength of 365 nm; **(B)** Chromatogram of the main active component conducted in C18 column with detection at 365 nm. The flow rate was set at 0.4 ml·min^{-1} and the presence of a single peak at 1.617 min indicated that the high purity compound. Absorbance × Retention Time.

28156^T (NR136495) by comparison against the EzBioCloud database and the BLASTn database in GenBank. After multiple alignments of sequences via CLUSTAL_X, a phylogenetic tree based on the neighbor-joining method using MEGA version 6.0 software demonstrated that HQB-1 fell into the cluster comprised of *Burkholderia* species (**Figure 3**). Therefore, based on morphological, physiological, and biochemical characteristics as well as the 16S rRNA gene sequence analysis, the strain HQB-1 is supposed to be affiliated to the genus *Burkholderia*.

Separation and Purification of the Main Active Antifungal Component

Antifungal activity assays showed that the most active antifungal compound was eluted with 100% MeOH by macroporous

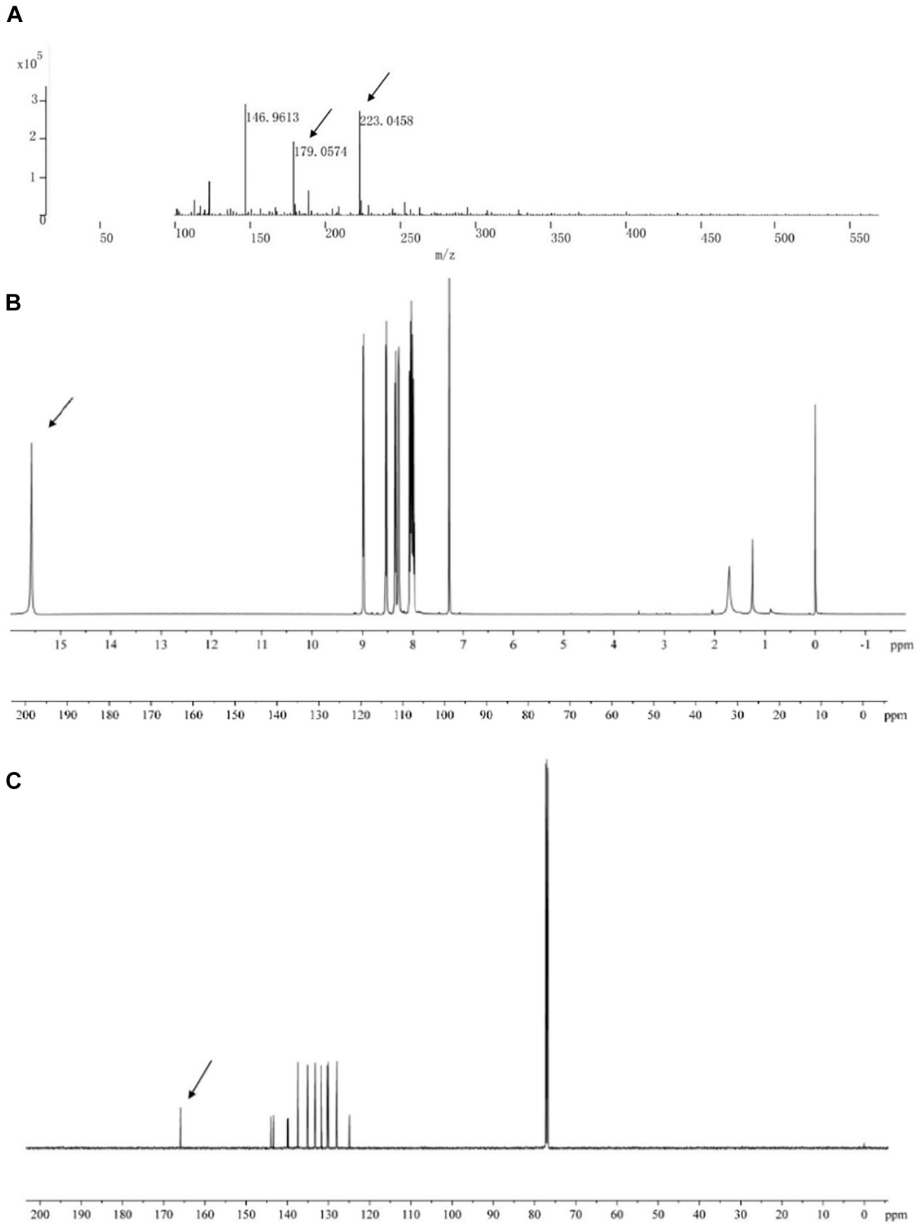

FIGURE 5 | Chemical analysis of the main active antifungal component produced by *Burkholderia* sp. HQB-1. **(A)** liquid chromatography quadrupole-time of flight mass spectrometer (LC-Q-TOF-MS). The ion peaks pointed by the arrows indicate the presence of carbon and proton MS data of m/z 179.0574 and m/z 223.0458, respectively. **(B,C)** ^{1}H-NMR and ^{13}C-NMR spectrum. The spectral data (δ in ppm, J in Hz) were measured at 30°C with CD_3Cl as the solvent. The tetramethylsilane (TMS) was used as internal standard.

resin column (Fraction 3) (**Supplementary Figure 1**). The subfraction with the strongest antifungal activity eluted in methanol and chloroform (1:9, v/v) was discovered using silica gel column chromatography (**Supplementary Table 1**). The solvent was slowly evaporated at room temperature to obtain greenish-yellow crystals. The chemical analysis of this active compound was performed by using UV and HPLC. The UV spectrum data (**Figure 4A**) showed a strong absorption and a broad peak at 365 nm, which indicated the presence of a phenazine moiety in the molecule. Then the active compound was subjected to HPLC with a C18 column, and a single peak with a retention time of 1.617 min under the 365 nm was detected (**Figure 4B**).

Structure Identification of the Main Active Antifungal Component

The main active antifungal component was then subjected to Q-TOF-MS and NMR. The MS spectra showed a molecular ion peak at m/z 223.0458 and the molecular formula as $C_{13}H_8N_2O_2$

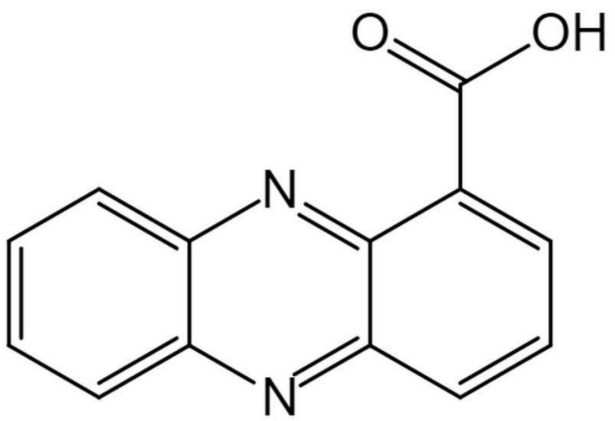

FIGURE 6 | Chemical structure of (phenazine-1-carboxylic acid) PCA isolated produced by *Burkholderia* sp. HQB-1.

was deduced (**Figure 5A**). The theoretical MS (Q-TOF) value of $C_{13}H_8N_2O_2$ ($[M\text{-}H]^-$) was calculated for mass 223.0513 and in this study mass 223.0512 was found. The MS/MS spectra of the component displayed a fragment ion peak at m/z 179.0574, which may be due to the loss of COOH. The major fragment ion at m/z 179 was close to the relative molecular mass of a phenazine ring.

The structure of the active compound was further identified by ^{1}H-NMR and ^{13}C-NMR spectroscopy. There were eight and thirteen well-resolved signals available in the ^{1}H-NMR and ^{13}C-NMR spectrum, respectively. Seven peaks in the 7.30–9.00 ppm region were assumed to be aromatic protons and the peak at 15.58 ppm was assigned to the carboxylic acid proton (**Figure 5B**). In the ^{13}C-NMR spectrum, twelve peaks in 124.91–144.07 ppm were assigned to be aromatic carbons, which indicated a symmetrical structure for the molecule. The peak at 165.93 ppm clearly indicated the presence of carbonyl carbon (**Figure 5C**). Meanwhile, the NMR spectra were compared with Scifinder[3] and SDBS information database[4], which indicated the target molecule as phenazine-1-carboxylic acid (PCA) ($C_{13}H_8N_2O_2$) (**Figure 6**).

MIC of PCA

According to the 96-well microtiter assay, the MIC values of purified PCA against *F. oxysporum*, *C. gloeosporioides*, *B. cinerea,* and *C. fallax* were 1.56, 6.13, 1.56, and 3.13, respectively (**Table 2**), which were lower than carbendazim treatments used as positive control. The lowest MIC of PCA was 1.56 μg/ml against *F. oxysporum* and *B. cinerea*. Whereas, the highest MIC of PCA was 6.13 μg/ml against *C. gloeosporioides*. The negative control (0.1% DMSO treated) had no inhibitory effect on the tested pathogenic fungi.

Effect of the Active Antifungal Component in Pot Experiments

The disease incidence measured for various treatments with different PCA concentrations (1, 5, and 25 μg/ml) were 40.8 ± 1.55, 19.1 ± 2.08, and 14.29% ± 1.84, respectively (**Table 3**). Meanwhile, the biocontrol efficiency was 51.2 ± 1.68, 77.2 ± 1.75, and 82.9% ± 1.43 respectively. PCA treatment at the concentration of 50 μg/ml completely inhibited Fusarium wilt in banana plants demonstrating strong antifungal activity against *F. oxysporum in vivo* (**Figure 7**). Furthermore, PCA treatments significantly promoted the growth of banana plants including root length, plant height, stem girth, leaf width, and dry weight compared with the control (**Table 4**). When the concentration of PCA reached more than 5 μg/ml, there was no significant difference in root length of banana plants between treatments. However, when the concentration of PCA reached more than 25 μg/ml, the difference in the growth of plant height was insignificant compared with DMSO treatment.

DISCUSSION

Soil-borne plant diseases, especially Fusarium wilt, cause a significant decline of the production in banana field (Ploetz, 2005). Biological control is considered to be a novel and efficient way to prevent and inhibit banana Fusarium wilt. The screening of antagonistic bacteria from soil microorganisms in fields with banana Fusarium wilt is of great practical significance in controlling this disease (Duan et al., 2020). In the soil bacteria community of healthy banana plants, the *Burkholderia* may be one of the most abundant genera that contribute to suppressing Fusarium wilt (Shen et al., 2014). It was well demonstrated that most of the *Burkholderia* sp. strains isolated from the rhizosphere of healthy plants have been used for controlling such plant disease and promoting the growth of the plant (Parke and Gurian-Sherman, 2001; Compant et al., 2008; Gu et al., 2009). In our study, the *Burkholderia* sp. strain HQB-1 was isolated and screened from

[3]http://scifinder.cas.org

[4]https://sdbs.db.aist.go.jp/

TABLE 2 | Values of minimum inhibitory concentration (MIC) of (phenazine-1-carboxylic acid) PCA against pathogenic fungi.

Pathogenic fungi	MIC of PCA (μg/ml)	MIC of carbendazim (μg/ml)	MIC of DMSO (μg/ml)
Fusarium oxysporum(ATCC 76255)	≥1.56	≥3.13	–
Colletotrichum gloeosporioides (ATCC 16330)	≥6.13	≥12.5	–
Botrytis cinerea (ATCC 11542)	≥1.56	≥6.25	–
Curvularia fallax (ATCC 38579)	≥3.13	≥6.25	–

–, no inhibitory effect.

TABLE 3 | The biocontrol effects of (phenazine-1-carboxylic acid (PCA) against banana Fusarium wilt.

PCA (μg/ml)	1	5	25	50	CK1	CK2
DI/%	40.8 ± 1.55b	19.1 ± 1.08bc	14.3 ± 1.84d	0e	15.7 ± 1.52ab	100a
BE/%	51.2 ± 1.68cd	77.2 ± 1.75c	82.9 ± 1.43b	100a	–	–

DI, disease index; BE, Biocontrol efficiency. CK1, negative control, non-inoculated Foc TR4 and application of 0.1% DMSO; CK2, positive control, inoculated Foc TR4 and application with sterile water. –, not detected. Data in the table are means ± SD (n = 7). For each parameter, mean data followed by different letters are significantly different at the P < 0.05 level by the least significant difference (LSD) test.

FIGURE 7 | Biocontrol by treatments with different concentrations of phenazine-1-carboxylic acid (PCA) on banana plants. Plants were grown for 60 days and watered weekly using water mixed with 5 ml of PCA at different concentrations. From left to right: banana plants were treated by 50, 25, 5, and 1 μg/ml PCA, respectively; CK1, negative control, non-inoculated Foc TR4 and application of 0.1% DMSO; CK2, positive control, inoculated Foc TR4 and application with sterile water. Scale bar means 5 cm in the image.

TABLE 4 | Effects of different concentrations of (phenazine-1-carboxylic acid) PCA treatments on the growth of banana plants.

Plant items	PCA (μg/ml)				CK1	CK2
	1.00	5.00	25.00	50.00		
Root length (cm)	2.62 ± 0.02d	3.87 ± 0.30c	3.91 ± 0.34b	4.47 ± 0.26a	3.53 ± 0.22bc	0.83 ± 0.35e
Plant height (cm)	10.13 ± 1.32c	12.47 ± 1.55ab	12.53 ± 0.85ab	13.90 ± 0.36a	12.57 ± 0.25ab	8.33 ± 1.10cd
Stem diameter (cm)	1.10 ± 0.10bcd	1.30 ± 0.10abc	1.47 ± 0.15a	1.37 ± 0.06a	1.33 ± 0.12ab	0.87 ± 0.23d
Leaf width (cm)	2.20 ± 0.61ab	2.57 ± 0.32ab	2.90 ± 0.46a	2.57 ± 0.60ab	2.45 ± 0.05ab	1.40 ± 0.30c
Dry weight (g)	1.00 ± 0.29d	1.42 ± 0.16c	1.87 ± 0.22a	1.55 ± 0.38ab	1.36 ± 0.11bcd	0.52 ± 0.15e

CK1, negative control, non-inoculated Foc TR4 and application of 0.1% DMSO; CK2, positive control, inoculated Foc TR4 and application with sterile water. Data in the table are means ± SD (n = 7). For each parameter, mean data followed by different letters are significantly different at the P < 0.05 level by the least significant difference (LSD) test.

banana rhizosphere soil. It exhibited an excellent antagonistic effect (56.7 ± 0.64%) against *F. oxysporum* and a broad-spectrum antifungal activity, which indicated that *Burkholderia* sp. HQB-1 has the potential to be a promising candidate against banana Fusarium wilt.

The genus *Burkholderia* was used as a biological agent against phytopathogenic fungi mainly due to its production of plentiful metabolites with antimicrobial activity (Hu and Young, 1998). In this study, to identify the potential antagonistic mechanisms of *Burkholderia* sp. HQB-1, we investigated the effect of the secondary metabolites secreted by this strain on inhibiting the mycelial growth of Foc TR4. The HQB-1 cultural broth was filtered through the 0.22 μm microfiltration membranes for salting-out and dialysis, whereas, the antimicrobial tests indicated that neither the proteins nor the enzymes in the HQB-1 metabolites possessed antifungal activity. The siderophore produced by the strain HQB-1 was determined by the chrome azurol S (CAS) method (Bultreys et al., 2001), but the quantitative tests showed that HQB-1 was not high-yield in siderophore (data not shown). However, the crude HQB-1 ethyl acetate extract possessed antifungal activity against *F. oxysporum*, which suggested that the secondary metabolites secreted from HQB-1 might contain antimicrobials. A greenish-yellow crystal was further purified by column macroporous resin and silica gel column chromatography, which exhibited a strong antifungal activity against Foc TR4 mycelial plug in

plates. The antifungal component showed a strong absorbance peak at 365 nm (**Figure 4A**) with UV spectral analysis, which indicated that the antifungal component might be a molecule bearing phenazine moiety (Hu et al., 2005). Furthermore, the ^{1}H-NMR spectrum (**Figure 5B**) revealed the presence of 8 aromatic protons and an ABCD pattern in the aromatic ring, the characteristics of which are typically found in phenazine derivatives. The ^{13}C-NMR spectrum (**Figure 5C**) revealed the presence 13 aromatic carbons that indicated a highly symmetrical structure for the target molecule (Gurusiddaiah et al., 1986). Both of the peaks at 15.58 ppm in ^{1}H-NMR and at 165.93 ppm in the ^{13}C-NMR spectrum demonstrated the presence of a carboxyl. Additionally, by compared with the NMR spectrum data in the SDBS information database, the chemical structure of the antifungal component was confirmed as phenazine-1-carboxylic acid (PCA) (**Figure 6**; Abraham et al., 2015).

Gurusiddaiah et al. (1986) found that the MIC values of PCA isolated from *Pseudomonas fluorescens* strain 2-79 against *F. oxysporum* was 25–30 μg/ml using the agar dilution method. PCA at 3.12 μg/ml reduced the mycelial growth of *B. cinerea* by 50%, and inhibited the formation of exopolysaccharide (Simionato et al., 2017). Zheng et al. (2019) reported that the MIC value of crude extracts of *Streptomyces* sp. FJAT-31547 against *F. oxysporum* was 6.250 μg/ml. In this study, the MIC values of PCA against plant pathogenic fungi were 1.563–6.13 μg/ml according to the results from 96-well microtiter assay (**Table 2**). The lowest MIC was 1.56 μg/ml against *F. oxysporum*, which indicated that PCA was more efficient than carbendazim. Thus, we proposed that PCA produced by *Burkholderia* sp. HQB-1 might be a key factor for the bacterial broad-spectrum antifungal activity against plant phytopathogenic fungi.

Phenazine-1-carboxylic acid has been reported to play an important role in inhibiting *F. oxysporum* in diverse crops such as chickpea, tomato, and wheat (Anjaiah et al., 1998; Chin-A-Woeng et al., 1998; Pastor et al., 2016). It seemed to be a more contributor to biocontrol *Fusarium oxysporum* than pyrrolnitrin in *Pseudomonas fluorescens* (Upadhyay and Srivastava, 2011). PCA is the main active component of the newly registered green biopesticide "Shenqinmycin," and its broad-spectrum inhibition of plant fungal pathogens of has been applied (Jin et al., 2015). The Shenqinmycin suspension with a concentration as low as 1% can prevent rice sheath blight, pepper blight, and cucumber seedling damping-off (Xu, 2013). However, the biocontrol effect of PCA against banana Fusarium wilt has not been well studied. In the present study, we investigated not only the antifungal activity of the PCA produced by HQB-1 against several phytopathogenic fungi was effective both *in vitro* and *in vivo*. Most of the banana plants in the current study could be efficiently protected from *F. oxysporum* infection, thus preventing Fusarium wilt, by 5 μg/ml PCA (BE, 77.2 ± 1.75%). Treatment with PCA at 500 μg/ml could protect most of the pepper plants from *Phytophthora* infection, and it also showed significant protective effect against anthracnose development on cucumber leaves (Lee et al., 2003). However, the mechanism of the antifungal effect of PCA remains unclear. Previous research reported that phenazine compounds are involved in inhibiting RNA synthesis and DNA binding (Morrison and Marley, 1976; Palchykovska et al., 2008), thereby interfering with redox balance and inducing the generation of reactive oxygen species (ROS) which eventually causes fungi death (Morales et al., 2010). Moreover, the phenazines may also have important physiological functions within phenazine-producing bacteria themselves. For example, it has been reported that the phenazine derivative pyocyanin leads to decreased levels of NADH in *Pseudomonas aeruginosa* grown under anoxic condition (Xu et al., 2013). We also found that proper concentrations (5–25 μg/ml) of PCA could increase the height and biomass, especially the root length of the banana plants compare with CK2 group (**Table 4**). This indicated the potential of PCA in facilitating water uptake, nutrient mobilization and growth promotion in banana plants. Thus, we propose that PCA might be critical for the broad-spectrum antifungal activity of *Burkholderia* sp. HQB-1 and it possesses a strong biocontrol effect on banana plants. The study of the antagonistic mechanism of PCA against *F. oxysporum* in banana and its practical application needs to be further investigation.

DATA AVAILABILITY STATEMENT

The raw data supporting the conclusions of this article will be made available by the authors, without undue reservation, to any qualified researcher.

AUTHOR CONTRIBUTIONS

ZX and MW conceived the study and prepared the manuscript. ZX, JD, and TH performed the experiments and analyzed the data. MW, JL, TD, and YC supervised and provided the suggestion of the research work. YC helped to revise the manuscript. All authors have read and approved the manuscript before submission.

FUNDING

This project was funded by the Promotion Program for Young and Middle-aged Teacher in Science and Technology Research of Huaqiao University (ZQN-YX507), the Special Project on Education and Research of Fujian Province (2017N5009), and the Subsidized Project for Postgraduates' Innovative Fund in Scientific Research of Huaqiao University (17013087004).

ACKNOWLEDGMENTS

We greatly thank Dr. Dengbo Zhou of the Institute of Tropical Bioscience and Biotechnology, China Academy of

Tropical Agricultural Sciences, Haikou, China for providing the phytopathogens. Additionally, we thank colleagues of the Instrumental Analysis Center of Huaqiao University for their support and providing access to the facilities needed for the chemical analysis of the microbial metabolites.

SUPPLEMENTARY MATERIAL

The Supplementary Material for this article can be found online at: https://www.frontiersin.org/articles/10.3389/fmicb.2020.605152/full#supplementary-material

REFERENCES

Abraham, A., Philip, S., Jacob, M. K., Narayanan, S. P., Jacob, C. K., and Kochupurackal, J. (2015). Phenazine-1-carboxylic acid mediated anti-oomycete activity of the endophytic *Alcaligenes* sp. eil-2 against *Phytophthora meadii*. *Microbiol. Res.* 170, 229–234. doi: 10.1016/j.micres.2014.06.002

Anjaiah, V., Koedam, N., Nowak-Thompson, B., Loper, J. E., Höfte, M., Tambong, J. T., et al. (1998). Involvement of phenazines and anthranilate in the antagonism of *Pseudomonas aeruginosa* PNA1 and Tn5 derivatives toward *Fusarium* spp. and *Pythium* spp. *Mol. Plant Microbe Interact.* 11, 847–854. doi: 10.1094/MPMI.1998.11.9.847

Bubici, G., Kaushal, M., Prigigallo, M. I., Gómez-Lama Cabanás, C., and Mercado-Blanco, J. (2019). Biological control agents against Fusarium wilt of banana. *Front. Microbiol.* 10:616. doi: 10.3389/fmicb.2019.00616

Buchanan, R. E., and Gibbons, N. E. (1984). *Bergey's Manual of Determinative Bacteriology*, 8th Edn. Baltimore, MD: Williams & Wilkins Co.

Bultreys, A., Gheysen, I., Maraite, H., and de Hoffmann, E. (2001). Characterization of fluorescent and non-fluorescent peptide siderophores produced by *Pseudomonas syringae* strains and their potential use in strain identification. *Appl. Environ. Microb.* 67, 1718–1727. doi: 10.1128/AEM.67.4.1718-1727.2001

Cartwright, D. K., Chilton, W. S., and Benson, D. M. (1995). Pyrrolnitrin and phenazine production by *Pseudomonas cepacia*, strain 5.5B, a biocontrol agent of *Rhizoctonia solani*. *Appl. Microbiol. Biotechnol.* 43, 211–216. doi: 10.1007/BF00172814

Chellemi, D. O., Gamliel, A., Katan, J., and Subbarao, K. V. (2016). Development and deployment of systems-based approaches for the management of soilborne plant pathogens. *Phytopathology* 106, 216–225. doi: 10.1094/PHYTO-09-15-0204-RVW

Chen, B., Zhang, X. Y., Huang, X., Liu, X. Y., Zhou, D. B., Tan, X., et al. (2013). Diversity analysis of soil fungi in *Fusarium* wilt of banana disease area. *Jiangsu Agric. Sci.* 41, 354–357.

Chen, Y., Zhou, D., Qi, D., Gao, Z., Xie, J., and Luo, Y. (2018). Growth promotion and disease suppression ability of a *Streptomyces* sp. CB-75 from banana rhizosphere soil. *Front. Microbiol.* 8:2704. doi: 10.3389/fmicb.2017.02704

Chin-A-Woeng, T. F. C., Bloemberg, G. V., van der Bij, A. J., van der Drift, K. M. G. M., Schripsema, J., Kroon, B., et al. (1998). Biocontrol by Phenazine-1-carboxamide-Producing *Pseudomonas chlororaphis* PCL1391 of tomato root rot caused by *Fusarium oxysporum* f. sp. *radicis-lycopersici*. *Mol. Plant Microbe Interact.* 11, 1069–1077. doi: 10.1094/MPMI.1998.11.11.1069

Compant, S., Nowak, J., Coenye, T., Clément, C., and Ait Barka, E. (2008). Diversity and occurrence of *Burkholderia* spp. in the natural environment. *FEMS Microbiol. Rev.* 32, 607–626. doi: 10.1111/j.1574-6976.2008.00113.x

Dale, J., James, A., Paul, J., Khanna, H., Smith, M., Peraza-Echeverria, S., et al. (2017). Transgenic cavendish bananas with resistance to Fusarium wilt tropical race 4. *Nat. Commun.* 8:1496. doi: 10.1038/s41467-017-01670-6

Davis, R. D., Moore, N. Y., and Kochman, J. K. (1996). Characterisation of a population of *Fusarium oxysporum* f. sp. *vasinfectum* causing wilt of cotton in Australia. *Aust. J. Agric. Res.* 47, 1143–1156. doi: 10.1071/AR9961143

Duan, Y., Chen, J., He, W., Chen, J., Pang, Z., Hu, H., et al. (2020). Fermentation optimization and disease suppression ability of a *Streptomyces* ma. *FS-4* from banana rhizosphere soil. *BMC Microbiol.* 20:24. doi: 10.1186/s12866-019-1688-z

Eberl, L., and Vandamme, P. (2016). Members of the genus *Burkholderia*: good and bad guys. *F1000res.* 5:1007. doi: 10.12688/f1000research.8221.1

Fourie, G., Steenkamp, E. T., Ploetz, R. C., Gordon, T. R., and Viljoen, A. (2011). Current status of the taxonomic position of *Fusarium oxysporum formae specialis cubense* within the *Fusarium oxysporum* complex. *Infect. Genet. Evol.* 11, 533–542. doi: 10.1016/j.meegid.2011.01.012

Fuchs, J. G., Moënne-Loccoz, Y., and Défago, G. (1999). Ability of nonpathogenic *Fusarium oxysporum* Fo47 to protect tomato against Fusarium wilt. *Biol. Control* 14, 105–110. doi: 10.1006/bcon.1998.0664

Getha, K., Vikineswary, S., Wong, W. H., Seki, T., Ward, A., and Goodfellow, M. (2005). Evaluation of *Streptomyces* sp. strain g10 for suppression of *Fusarium* wilt and rhizosphere colonization in pot-grown banana plantlets. *J. Ind. Microbiol. Biotechnol.* 32, 24–32. doi: 10.1007/s10295-004-0199-5

Gu, G. Y., Wang, N., Noel, C., Leif, S., and Lu, E. S. (2009). Ambr1 is a key transcriptional regulator for production of antifungal activity of *Burkholderia contaminans* strain MS14. *FEMS Microbiol. Lett.* 1, 54–60. doi: 10.1111/j.1574-6968.2009.01653.x

Gupta, V. K., Shivasharanappa, N., Kumar, V., and Kumar, A. (2014). Diagnostic evaluation of serological assays and different gene based PCR for detection of *Brucella melitensis* in goat. *Small Rumin. Res.* 117, 94–102. doi: 10.1016/j.smallrumres.2013.11.022

Gurusiddaiah, S., Weller, D. M., Sarkar, A., and Cook, R. J. (1986). Characterization of an antibiotic produced by a strain of *Pseudomonas fluorescens* inhibitory to *Gaeumannomyces graminis* var. *tritici* and *Pythium* spp. *Antimicrob. Agents Chemother.* 29, 488–495. doi: 10.1128/AAC.29.3.488

Hu, F. P., and Young, J. M. (1998). Biocidal activity in plant pathogenic *Acidovorax*, *Burkholderia*, *Herbaspirillum*, *Ralstonia* and *Xanthomonas* spp. *J. Appl. Microbiol.* 84, 263–271. doi: 10.1046/j.1365-2672.1998.00340.x

Hu, H. B., Yu, Q. X., Feng, C., Xue, H. Z., and Hur, B. K. (2005). Isolation and characterization of a new fluorescent *Pseudomonas* strain that produces both phenazine 1-carboxylic acid and pyoluteorin. *J. Microbiol. Biotechnol.* 15, 86–90.

Jeong, Y., Kim, J., Kim, S., Kang, Y., Nagamatsu, T., and Hwang, I. (2003). Toxoflavin produced by *Burkholderia glumae* causing rice grain rot is responsible for inducing bacterial wilt in many field crops. *Plant Dis.* 87, 890–895. doi: 10.1094/PDIS.2003.87.8.890

Jiang, C., Sheng, X., Qian, M., and Wang, Q. (2008). Isolation and characterization of a heavy metal-resistant *Burkholderia* sp. from heavy metal-contaminated paddy field soil and its potential in promoting plant growth and heavy metal accumulation in metal-polluted soil. *Chemosphere* 72, 157–164. doi: 10.1016/j.chemosphere.2008.02.006

Jin, K., Zhou, L., Jiang, H., Sun, S., Fang, Y., Liu, J., et al. (2015). Engineering the central biosynthetic and secondary metabolic pathways of *Pseudomonas aeruginosa* strain PA1201 to improve phenazine-1-carboxylic acid production. *Metab. Eng.* 32, 30–38. doi: 10.1016/j.ymben.2015.09.003

Kanini, G. S., Katsifas, E. A., Savvides, A. L., and Karagouni, A. D. (2013). Streptomyces rochei ACTA1551, an indigenous Greek isolate studied as a potential biocontrol agent against *Fusarium oxysporum* f. sp. *lycopersici*. *BioMed Res. Int.* 12:387230. doi: 10.1155/2013/387230

Kim, O. S., Cho, Y. J., Lee, K., Yoon, S. H., Kim, M., Na, H., et al. (2012). Introducing EzTaxon-e: a prokaryotic 16S rRNA gene sequence database with phylotypes that represent uncultured species. *Int. J. Syst. Evol. Microbiol.* 62, 716–721. doi: 10.1099/ijs.0.038075-0

Kunakom, S., and Eustáquio, A. S. (2019). *Burkholderia* as a source of natural products. *J. Nat. Prod.* 82, 2018–2037. doi: 10.1021/acs.jnatprod.8b01068

Lee, J. Y., Moon, S. S., and Hwang, B. K. (2003). Isolation and in vitro and in vivo activity against *Phytophthora capsici* and *Colletotrichum orbiculare* of phenazine-1-carboxylic acid from *Pseudomonas aeruginosa* strain GC-B26. *Pest Manag. Sci.* 59, 872–882. doi: 10.1002/ps.688

Leeman, M., den Ouden, F. M., Dirkx, F. P. M., Steijl, H., Bakker, P. A. H. M., and Schippers, B. (1996). Iron availability affects induction of systemic resistance to Fusarium wilt of radish by *Pseudomonas fluorescens*. *Phytopathology* 86, 149–155. doi: 10.1094/Phyto-86-149

Li, C., Yang, J., Li, W., Sun, J., and Peng, M. (2017). Direct root penetration and rhizome vascular colonization by *Fusarium oxysporum* f. sp. *cubense* are the key steps in the successful infection of Brazil Cavendish. *Plant Dis.* 101, 2073–2078. doi: 10.1094/PDIS-04-17-0467-RE

Lin, Y., Chang, J., Liu, E., Chao, C., Huang, J., and Chang, P. L. (2009). Development of a molecular marker for specific detection of *Fusarium*

oxysporum f. sp. *cubense* race 4. *Eur. J. Plant Pathol.* 123, 353–365. doi: 10.1007/s10658-008-9372-4

Mahenthiralingam, E., Baldwin, A., and Dowson, C. G. (2008). *Burkholderia cepacia* complex bacteria: opportunistic pathogens with important natural biology. *J. Appl. Microbiol.* 104, 1539–1551. doi: 10.1111/j.1365-2672.2007.03706.x

Mak, C., Mohamed, A. A., Liew, K. W., and Ho, Y. W. (2004). "Early screening technique for Fusarium wilt resistance in banana micropropagated plants," in *Banana Improvement: Cellular, Molecular, Biology, and Induced Mutations*, eds S. M. Jain and R. Swennen (Enfield, NH: Science Publishers, Inc), 219–227.

Morales, D. K., Jacobs, N. J., Rajamani, S., Krishnamurthy, M., Cubillos-Ruiz, J. R., and Hogan, D. A. (2010). Antifungal mechanisms by which a novel *Pseudomonas aeruginosa* phenazine toxin kills *Candida albicans* in biofilms. *Mol. Microbiol.* 78, 1379–1392. doi: 10.1111/j.1365-2958.2010.07414.x

Morrison, N. E., and Marley, G. M. (1976). The mode of action of clofazimine DNA binding studies. *Int. J. Lepr. Other. Mycobact. Dis.* 44, 133–134.

Nimaichand, S., Devi, A. M., Tamreihao, K., Ningthoujam, D. S., and Li, W. J. (2015). Actinobacterial diversity in limestonedeposit sites in Hundung, Manipur (India) and their antimicrobial activities. *Front. Microbiol.* 6:413. doi: 10.3389/fmicb.2015.00413

O'Donnell, K., Kistler, H. C., Cigelnik, E., and Ploetz, R. C. (1998). Multiple evolutionary origins of the fungus causing Panama disease of banana: concordant evidence from nuclear and mitochondrial gene genealogies. *P. Natl. Acad. Sci. U.S.A.* 95, 2044–2049. doi: 10.1073/pnas.95.5.2044

Palchykovska, L. G., Alexeeva, I. V., Kostina, V. G., Platonov, M. O., and Shved, A. D. (2008). New amides of phenazine-1-carboxylic acid: antimicrobial activity and structure-activity relationship. *Ukr. Biokhim. Zh.* 3, 140–147.

Parke, J. L., and Gurian-Sherman, D. (2001). Diversity of the *Burkholderia Cepacia* complex and implications for risk assessment of biological control strains. *Annu. Rev. Phytopathol.* 39, 225–258. doi: 10.1146/annurev.phyto.39.1.225

Parker, W. L., Rathnum, M. L., Seiner, V., Trejo, W. H., Principe, P. A., and Sykes, R. B. (1984). Cepacin A and cepacin B, two new antibiotics produced by *Pseudomonas cepacia*. *J. Antibiot.* 37, 431–440. doi: 10.7164/antibiotics.37.431

Pastor, N., Masciarelli, O., Fischer, S., Luna, V., and Rovera, M. (2016). Potential of *Pseudomonas putida* PCI2 for the protection of tomato plants against fungal pathogens. *Curr. Microbiol.* 73, 346–353. doi: 10.1007/s00284-016-1068-y

Ploetz, R. C. (2005). Fusarium-induced diseases of tropical, perennial crops. *Phytopathology* 96, 648–652. doi: 10.1094/PHYTO-96-0648

Reyes-Chilpa, R., Jimenez-Estrada, M., and Estrada-Muniz, E. (1997). Antifungal Xanthones from *Calophyllum brasiliensis* heartwood. *J. Chem. Ecol.* 23, 1901–1911. doi: 10.1023/B:JOEC.0000006459.88330.61

Saitou, N., and Nei, M. (1987). The neighbor-joining method: a new method for reconstructing phylogenetic trees. *Mol. Biol. Evol.* 4, 406–425. doi: 10.1093/oxfordjournals.molbev.a040454

Saravanan, T., Muthusamy, M., and Marimuthu, T. (2003). Development of integrated approach to manage the fusarial wilt of banana. *Crop Prot.* 9, 1117–1123. doi: 10.1016/S0261-2194(03)00146-7

Schmidt, S., Blom, J. F., Pernthaler, J., Berg, G., and Eberl, L. (2010). Production of the antifungal compound pyrrolnitrin is quorum sensing-regulated in members of the *Burkholderia cepacia* complex. *Environ. Microbiol.* 11, 1422–1437. doi: 10.1111/j.1462-2920.2009.01870.x

Shen, Z. Z., Wang, D. S., Ruan, Y. Z., Xue, C., Zhang, J., Li, R., et al. (2014). Deep 16S rRNA pyrosequencing reveals a bacterial community associated with banana Fusarium wilt disease suppression induced by bio-organic fertilizer application. *PLoS One* 9:e98420. doi: 10.1371/journal.pone.0098420

Shepherd, K. (1987). Banana breeding—past and present. *Acta Hortic.* 196, 37–43. doi: 10.17660/ActaHortic.1987.196.3

Simionato, A. S., Navarro, M. O. P., de Jesus, M. L. A., Barazetti, A. R., da Silva, C. S., Simões, G. C., et al. (2017). The effect of phenazine-1-carboxylic acid on mycelial growth of *Botrytis cinerea* produced by *Pseudomonas aeruginosa* LV strain. *Front. Microbiol.* 8:1102. doi: 10.3389/fmicb.2017.01102

Singh, A., Goel, Y., Rai, A. K., and Banerjee, U. C. (2013). Lipase catalyzed kinetic resolution for the production of (S)-3-[5-(4-fluoro-phenyl)-5-hydroxy-pentanoyl]-4-phenyl-oxazolidin-2-one: an intermediate for the synthesis of ezetimibe. *J. Mol. Catal. B Enzym.* 85-86, 99–104. doi: 10.1016/j.molcatb.2012.08.014

Tamura, K., Dudley, J., Nei, M., and Kumar, S. (2007). MEGA4: molecular evolutionary genetics analysis (MEGA) software version 4.0. *Mol. Biol. Evol.* 24, 1596–1599. doi: 10.1093/molbev/msm092

Thompson, J. D., Gibson, T. J., Plewniak, F., Jeanmougin, F., and Higgins, D. G. (1997). The CLUSTAL_X windows interface: flexible strategies for multiple sequence alignment aided by quality analysis tools. *Nucleic Acids Res.* 25, 4876–4882. doi: 10.1093/nar/25.24.4876

Upadhyay, A., and Srivastava, S. (2011). Phenazine-1-carboxylic acid is a more important contributor to biocontrol *Fusarium oxysporum* than pyrrolnitrin in *Pseudomonas fluorescens* strain Psd. *Microbiol. Res.* 4, 323–335. doi: 10.1016/j.micres.2010.06.001

Viljoen, A. (2002). The status of Fusarium wilt (Panama disease) of banana in South Africa. *S. Afr. J. Sci.* 98, 341–344.

Wang, B., Yuan, J., Zhang, J., Shen, Z., Zhang, M., Li, R., et al. (2013). Effects of novel bioorganic fertilizer produced by *Bacillus amyloliquefaciens* W19 on antagonism of Fusarium wilt of banana. *Biol. Fertil. Soils* 49, 435–446. doi: 10.1007/s00374-012-0739-5

Wang, X., Radwan, M. M., Taráwneh, A. H., Gao, J., Wedge, D. E., Rosa, L. H., et al. (2013). Antifungal activity against plant pathogens of metabolites from the endophytic fungus *Cladosporium cladosporioides*. *J. Agric. Food Chem.* 61, 4551–4555. doi: 10.1021/jf400212y

Warman, N. M., and Aitken, E. A. B. (2018). The movement of *Fusarium oxysporum* f. sp. *cubense* (Sub-Tropical Race 4) in susceptible cultivars of banana. *Front. Plant Sci.* 9:1748. doi: 10.3389/fpls.2018.01748

Wedge, D. E., and Kuhajek, J. M. (1998). A microbioassay for fungicide discovery. SAAS Bull. *Biochem. Biotechnol.* 11, 1–7.

Xu, N., Ahuja, E. G., Janning, P., Mavrodi, D. V., Thomashow, L. S., and Blankenfeldt, W. (2013). Trapped intermediates in crystals of the FMN-dependent oxidase PhzG provide insight into the final steps of phenazine biosynthesis. *Acta Crystallogr. D* 69, 1403–1413. doi: 10.1107/S0907444913008354

Xu, Y. (2013). "Genomic features and regulation of phenazine biosynthesis in the rhizosphere strain *Pseudomonas aeruginosa* M18," in *Microbial Phenazines*, eds S. Chincholkar and L. Thomashow (Berlin: Springer), 177–198. doi: 10.1007/978-3-642-40573-0_9

Yoon, S., Ha, S., Kwon, S., Lim, J., Kim, Y., Seo, H., et al. (2017). Introducing EzBioCloud: a taxonomically united database of 16S rRNA gene sequences and whole-genome assemblies. *Int. J. Syst. Evol. Microbiol.* 67, 1613–1617. doi: 10.1099/ijsem.0.001755

Zheng, X., Wang, J., Chen, Z., Zhang, H., Wang, Z., Zhu, Y., et al. (2019). A *Streptomyces* sp. strain: isolation, identification, and potential as a biocontrol agent against soilborne diseases of tomato plants. *Biol. Control.* 136:104004. doi: 10.1016/j.biocontrol.2019.104004

Conflict of Interest: The authors declare that the research was conducted in the absence of any commercial or financial relationships that could be construed as a potential conflict of interest.

frontiers in Microbiology

ORIGINAL RESEARCH
published: 07 January 2021
doi: 10.3389/fmicb.2020.614620

Biocontrol Potential of Grapevine Endophytic and Rhizospheric Fungi Against Trunk Pathogens

*Isidora Silva-Valderrama[1], Diana Toapanta[1], Maria de los Angeles Miccono[1,2], Mauricio Lolas[3], Gonzalo A. Díaz[3], Dario Cantu[2] and Alvaro Castro[1]**

[1] UC Davis Chile Life Sciences Innovation Center, Santiago, Chile, [2] Department of Viticulture and Enology, University of California, Davis, Davis, CA, United States, [3] Laboratorio de Patología Frutal, Facultad de Ciencias Agrarias, Universidad de Talca, Talca, Chile

Grapevine Trunk Diseases (GTDs) are a major challenge to the grape industry worldwide. GTDs are responsible for considerable loss of quality, production, and vineyard longevity. Seventy-five percent of Chilean vineyards are estimated to be affected by GTDs. GTDs are complex diseases caused by several fungi species, including members of the Botryosphaeriaceae family and *Phaeomoniella chlamydospora,* considered some of the most important causal agents for these diseases in Chile. In this study, we isolated 169 endophytic and 209 rhizospheric fungi from grapevines grown under organic and conventional farming in Chile. Multiple isolates of *Chaetomium* sp., *Cladosporium* sp., *Clonostachys rosea, Epicoccum nigrum, Purpureocillium lilacinum,* and *Trichoderma* sp. were evaluated for their potential of biocontrol activity against *Diplodia seriata*, *Neofusicoccum parvum,* and *Pa. chlamydospora.* Tests of antagonism were carried out using two dual-culture-plate methods with multiple media types, including agar containing grapevine wood extract to simulate *in planta* nutrient conditions. Significant pathogen growth inhibition was observed by all isolates tested. *Clonostachys rosea* showed 98.2% inhibition of all pathogens in the presence of grapevine wood extract. We observed 100% pathogen growth inhibition when autoclaved lignified grapevine shoots were pre-inoculated with either *C. rosea* strains or *Trichoderma* sp. Overall, these results show that *C. rosea* strains isolated from grapevines are promising biocontrol agents against GTDs.

Keywords: biological control, fungal antagonism, co-culture experiments, grapevine trunk diseases, fungal endophyte

OPEN ACCESS

Edited by:
Alan John Lander Phillips, Universidade de Lisboa, Portugal

Reviewed by:
Asha Janadaree Dissanayake, University of Electronic Science and Technology of China, China
Kathrin Blumenstein, University of Göttingen, Germany

***Correspondence:**
Alvaro Castro
alvcastro@ucdavis.edu

Specialty section:
This article was submitted to Microbe and Virus Interactions with Plants, a section of the journal Frontiers in Microbiology

Received: *06 October 2020*
Accepted: *01 December 2020*
Published: *07 January 2021*

Citation:
Silva-Valderrama I, Toapanta D, Miccono MA, Lolas M, Díaz GA, Cantu D and Castro A (2021) Biocontrol Potential of Grapevine Endophytic and Rhizospheric Fungi Against Trunk Pathogens. Front. Microbiol. 11:614620. doi: 10.3389/fmicb.2020.614620

INTRODUCTION

Grapevine trunk diseases (GTDs) are a major challenge to viticulture worldwide because they compromise the productivity and longevity of grapevines (*Vitis vinifera* L.) and increase production costs (Munkvold et al., 1994; Bertsch et al., 2013; Kaplan et al., 2016; Gramaje et al., 2018). GTDs are one of the main phytosanitary problems of the grape industry also in Chile (Auger et al., 2004; Díaz et al., 2011b). Chile is the first and fourth largest grape and wine exporter globally, respectively (Felzensztein, 2014; Pizarro, 2018; USDA Foreign Agricultural Center, 2019). In 2013, about 22% of the commercial vineyards in Chile showed symptoms of GTDs (Díaz et al., 2013; Latorre, 2018).

GTDs are a group of diseases affecting the grapevine trunk and internal tissue (Mugnai, 2011), resulting in foliar symptoms, cankers, and dieback of the plant (Gramaje et al., 2018). These diseases are caused by a wide range of fungi (Trouillas et al., 2010; Gramaje and Armengol, 2011; Úrbez-Torres, 2011; Augusti-Brisach and Armengol, 2013; Lombard et al., 2014; Gramaje et al., 2018) that often infect established grapevines through wounds produced during winter pruning (Rolshausen et al., 2010). GTDs can also spread during plant propagation (Aroca et al., 2010; Gramaje and Armengol, 2011), with infections found in dormant wood cuttings and young grafted plants (Waite and Morton, 2007; Gramaje and Armengol, 2011; Billones-Baaijens et al., 2013). In Chile, as in other viticulture areas, the most common microorganisms isolated from arms and trunks of grapevines with symptoms of GTDs are ascomycetous fungi and include *Phaeomoniella* (Pa.) *chlamydospora, Diplodia seriata* De Not., and *Neofusicoccum parvum* (Auger et al., 2004; Díaz et al., 2011a; Besoain et al., 2013; Díaz and Latorre, 2013; Díaz and Latorre, 2014).

Currently, there are no curative treatments against GTDs besides surgical removal of the infected organs (Surico et al., 2006; Wagschal et al., 2008; Gramaje et al., 2018; Mondello et al., 2018; Sosnowski and Mundy, 2018). GTDs are managed mostly by practices that aim to prevent infections (Gramaje et al., 2018; Mondello et al., 2018). Widely adopted preventive practices include late pruning (Petzoldt, 1981; Munkvold et al., 1994), double-pruning (Weber et al., 2007), and the application of protectants on fresh pruning wounds (Sosnowski and Mundy, 2019) as benomyl and tebuconazole (Bester et al., 2007), inorganic compounds as boric acid (Rolshausen and Gubler, 2005), or natural antifungal compounds as organic extracts (Mondello et al., 2018). Manual applications of these formulations as paints are effective, but costly and time-consuming, while spray applications are difficult due to the small surface and orientation of pruning wounds (Rolshausen et al., 2010; Wightwick et al., 2010; Bertsch et al., 2013). In addition, no genetic resistance against GTDs has been found in the grapevine germplasm (Surico et al., 2006; Wagschal et al., 2008).

Biocontrol of GTDs using microorganisms is a promising alternative. For example, *Trichoderma* spp. are effective as a protectant of pruning wounds (John et al., 2004; Halleen et al., 2010; Mondello et al., 2018). The goal of our work was to identify microorganisms with biocontrol potential among the natural microbial inhabitants of grapevines. Endophytes are microorganisms that inhabit and colonize the internal plant tissue without causing visible damage or illness in the host (Petrini, 1991; Hirsch and Braun, 1992; Stone et al., 2000; Schulz and Boyle, 2005). These microorganisms are known to mediate plant-environment as well as plant-pathogen interactions (White et al., 1997; Zabalgogeazcoa, 2008). The contribution of different epiphytes and endophyte species to plant defenses has been widely documented (Azevedo et al., 2000; Arnold et al., 2003; Pieterse et al., 2014). Plant defense induction and antibiotic substance production that inhibits the growth of pathogens and pests (Mousa and Raizada, 2013), by endophytic fungi (Arnold et al., 2001; Kaul et al., 2012), bacteria (Hardoim et al., 2008), viruses (Lehtonen et al., 2006), and insects (Azevedo et al., 2000) have been reported. The rationale behind focusing on endophytes in the search of effective biocontrol agents against GTDs was two-fold (Wicaksono et al., 2017). First, grapevine endophytes survive naturally inside this plant; therefore, these isolates, once applied, should have better chances to successfully colonize the internal tissue of the grapevine than biocontrol agents selected from other biological systems (Hardoim et al., 2008, 2015; López-Fernández et al., 2016). Second, endophytes share the same niche with plant pathogens; thus, in addition to plant-defense induction and antibiosis, they could also compete for space and nutrients with GTD pathogens (Zabalgogeazcoa, 2008; Aroca, 2013; Bacon and White, 2016).

Here we report the isolation and identification of endophytic and rhizospheric fungi from grapevines grown in commercial and non-commercial vineyards in Chile. From this collection, we selected antagonist candidates and evaluated them for growth inhibition activity against the main GTD fungal species found in Chile, in co-culture, and in planta assays, providing also a general inside of the mechanisms used for this. All of the above-mentioned, with the aim of finding potential biocontrol agents to control GTDs.

MATERIALS AND METHODS

Sample Origin and Plant Material

Samples of grapevine (*Vitis vinifera* L.) cv. Cabernet Sauvignon and Chardonnay were collected from four commercial vineyards located in the central valleys in Chile under either organic or, conventional farming systems in May 2017 (**Table 1**). Samples of cv. País were collected in September 2017 from a vineyard where diseases are not managed, located in the Codpa Valley, Chile (**Table 1**). All plants sampled presented no symptoms of GTDs.

Isolation of Endophytic Fungi

The isolation of endophytic fungi was performed following the methodology described in Pancher et al. (2012). Briefly, shoots (50 cm long) and roots were cut into 10-cm-long fragments. Fragments were surface disinfected by rounds of 2 min serial

TABLE 1 | Sample locations.

Vineyard	Variety	Location	Disease control	Planting year
Site 1	Chardonnay	−35°26′26.8764″S, −071°50′01.8600″W	conventional	
	Cabernet Sauvignon	−35°26′26.8764″S, −071°50′01.8600″W	conventional	
Site 2	Chardonnay	−34°42′53.3736″S, −071°02′20.5008″W	organic	2011
	Cabernet Sauvignon	−34°42′53.3736″S, −071°02′20.5008″W	organic	2009
Site 3		−33°44′592476″S, −070°56′18.6972″W	conventional	
Site 4	Cabernet Sauvignon	−33°44′592476″S, −070°56′18.6972″W	organic	2000
Site 5	País	−18°28′42.6″S, −070°05′16.2″W	none	1850

immersions in 90% ethanol, then 2% sodium hypochlorite solution, and 70% ethanol, followed by double-rinsing in sterile distilled water under laminar airflow. Absence of microbial growth on surface-sterilized shoots was confirmed by plating the distilled water from the last wash step on potato dextrose agar (PDA; BD-Difco) in Petri dishes, that were then incubated for 2 weeks at 25°C. After disinfection, fragments were further cut into 2.5 mm pieces. Each section was placed on Petri dishes (90-mm diameter), placing the vascular bundle toward the growing media, containing: (i) PDA (39 g L^{-1}; BD-Difco), (ii) malt extract agar (MEA, 33.6 g L^{-1}; BD-Difco), and (iii) plain agar (AA, 20 g L^{-1}; Difco), each one with antibiotics (streptomycin, 0.05 g L^{-1}, and chloramphenicol, 0.05 g L^{-1}). All Petri dishes were incubated at 25°C for 7 to 10 days under 12 h of light and 12 of darkness. Different colonies were tentatively identified based in morphology (Barnett and Hunter, 1955). Pure cultures were obtained from hyphal tip transfer to PDA media and maintained at 5°C.

Isolation of Rhizospheric Fungi

For each plant, 1.5 g of soil in direct contact with roots was carefully collected. In a laminar flow bench, 13.5 ml of sterile distilled water was added, before vigorous agitation for 20 min in a horizontal position. After 5 min of decantation, serial dilutions of the supernatant were made. 10^{-3} and 10^{-4} dilutions were used to inoculate PDA, MEA, and AA. To all media streptomycin, 0.05 g L^{-1} and chloramphenicol, 0.05 g L^{-1} were added. Plates were incubated for 7 to 14 days at 25°C.

Taxonomic Characterization of the Fungal Isolates

DNA extraction from cultivable isolated fungi (n = 387 isolates) was performed as described in Morales-Cruz et al. (2015), with the following modifications. Mycelium from 7 to 21 days old fungal cultures were frozen with 3 mm metal beads in tubes at −80°C. Tubes were shaken vigorously with a vortex for 5 min at maximum speed. Disrupted mycelium were resuspended in 200 μL of nuclease-free sterile-distilled water and then homogenized in a vortex for 15 s. Mycelium was incubated at 100°C for 10 min, followed by a centrifugation step at 14500 rpm for 2 min. An aliquot of 10 μL of the supernatant was used for the PCR runs. A 1:20 or 1:50 dilution was made in case of PCR inhibition occurred. ITS sequences were PCR amplified using ITS1 (TCCGTAGGTGAACCTGCGG) and ITS4 (TCCTCCGCTTATTGATATGC) primers (White et al., 1990). A 25 μL PCR reaction was carried out using 2.5 μL 1X Thermopol reaction buffer, 0.5 μL of 10 mM dNTPs, 0.5 μL of 10 μM ITS forward and reverse primers, 0.125 μL (1.25U/50 μL) Taq DNA polymerase (Promega, United States) and 10 μL of sample supernatant as a template. PCR reaction was performed with an initial denaturing step at 95°C for 2 min, and 35 cycles of 95°C for 30 s, 52°C for 30 s (White et al., 1990), and 72°C for 1 min, followed by a final extension phase at 72°C for 5 min. The PCR product was purified and sequenced at Macrogen Inc., South Korea. Amplicon sequencing analysis was carried out with Geneious (R11.1). Taxonomic identities were determined with BLASTN using the UNITE database 7.2 (Nilsson et al., 2019).

Pathogenic Fungal Strains and Control Antagonists Origin

Isolates of *Phaeomoniella chlamydospora* (#11 A), *Diplodia seriata* (N°117 Molina), *Neofussicoccum parvum* (N°156 Lolol) and the endophytic antagonist *Trichoderma* sp. (Altair 607 QR6 PB 6.0) were obtained from the Phytopathology Lab of Universidad de Talca. These isolates were obtained in 2017 from *V. vinifera* L. trunks as part of another project. Also, MAMULL (*Trichoderma gamsii* Volqui strain, *Bionectria ochroleuca* Mitique strain, *Hypocrea virens* Ñire strain, BioInsumos Nativa, Chile), TIFI (Giteniberica de Abonos, Spain), Tebuconazole 430 SC (SOLCHEM, concentrated suspension, Chile) were used as positive controls.

Test of Fungal Antagonism

Initial assessment of antagonistic properties was conducted against *D. seriata* as pathogen. Further evaluations on selected antagonists were carried out using *D. seriata, N. parvum*, and *P. chlamydospora*. Agar disks from a 7-day old actively growing colony were used. Co-culture assays were performed placing a 5 mm agar disk on one side of the Petri dish with PDA (39 g L^{-1}; Difco) or PA (200 g L^{-1} grapevine propagation material, 20 g L^{-1} agar) and on the opposite side a 5 mm agar disk containing the antagonist strain. Plates were incubated at 25°C for 7–28 days in darkness (Badalyan et al., 2002) using a randomized complete block design. Registered bioproducts MAMULL and TIFI were used as antagonistic controls. Pathogen growth area was evaluated at 7, 14, 21, and 28 days post-co-culture (Schindelin et al., 2012). Inhibition percentage was calculated using the pathogen growth area when was cultured alone (C) or in interaction with the antagonist (T) according to the formula I = [(C-T)/C) * 100] (Thampi and Suseela, 2017).

An in planta assay was also performed. Annual shoots were used for the experimental set-up to verify the antagonistic

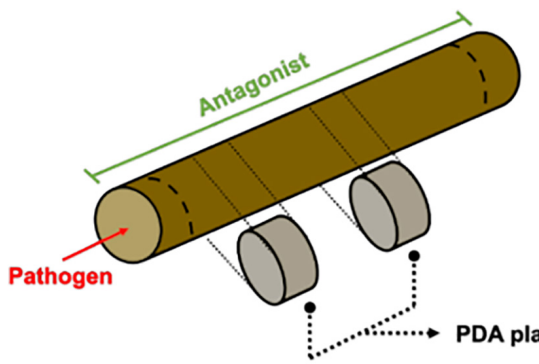

FIGURE 1 | Annual shoots essay diagram. Shortly, shoots were inoculated with a spore suspension of the antagonist. Twenty-four hours later, the pathogen was inoculated on one side of the shoot and incubated in a humid chamber. After seven days, small pieces were taken and cultured in PDA plates.

potential shown in plate co-culture. Several preliminary evaluations were carried out in order to test variability caused by autoclave sterilization of pruning material, humid-chamber moist maintenance, type of inoculum and time needed for the pathogen to grow through the wood piece. Even though tissue was dead, the overall shoot matrix structure was conserved after autoclave sterilization (data not shown). Internode portions of dormant cuttings were cut in 4.5 cm length pieces and then used fresh or autoclaved for 25 min at 121 °C. Agar mycelium plugs were evaluated as inoculum. In 2 days, pruning material in contact with the pathogen and/or antagonist plugs were covered in the mycelium. As the inoculum type was too different from a field inoculum, a spore suspension solution was used to inoculate the wood pieces. Mycelium/spore mix suspension

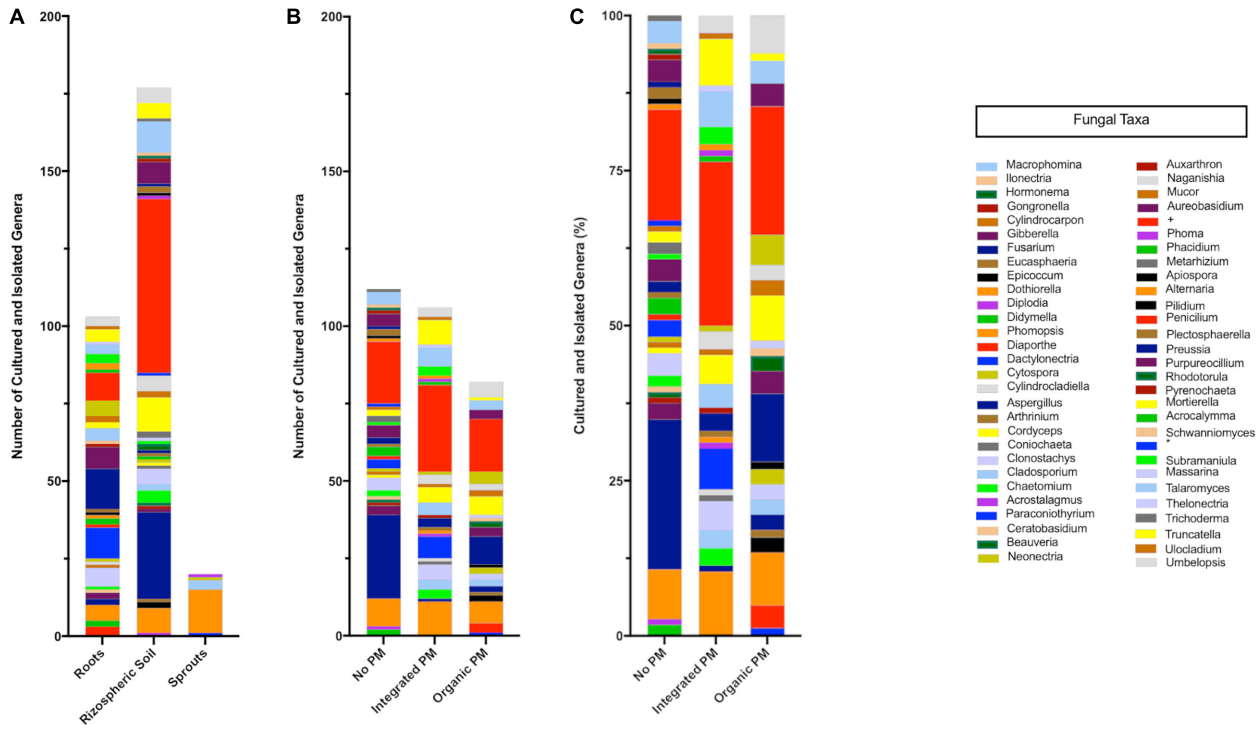

FIGURE 2 | Taxonomic composition of the isolated fungi. Values are separated according to the source **(A)** and phytosanitary regime (pest management program, PM) **(B,C)**. Cultured-isolates identified only to family level Nectriaceae (+) and class level Dothideomycetes (*) are also shown.

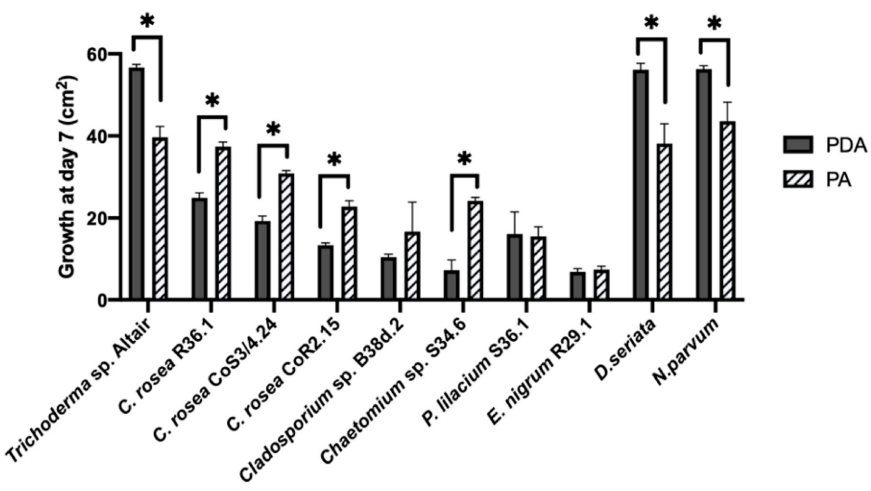

FIGURE 3 | Comparison of the growth area of antagonists and pathogens in two media. Growth was measured after 7 days in PDA (potato dextrose agar) and PA (plant agar). Bars with asterisk are significantly different from the control (Paired *T* test, $P < 0.001$). Error bars represent the standard error of the mean, $n = 5$.

of the pathogens *D. seriata* and *N. parvum* were prepared by flooding 30 days old plant agar culture (PA; 200 g L^{-1} grapevine dormant cutting, 20 g L^{-1} agar) with sterile distilled water. In the case of the antagonists *Clonostachys rosea* (isolates CoS3/4.24, CoR2.15 and R31.6) a spore suspension adjusted to 1×10^7 conidia mL^{-1} was used. Antagonist inoculation was carried out adding 40 μL of antagonist fresh spore suspension until it reached the woody stem cut end by capillarity. Tebuconazole (60 mL/100 L fields recommended doses; SOLCHEM, Chile) or sterile distilled water was applied in the same manner as controls. This experiment was carried out 5 times. Woody stem cuts were incubated in individual humid chambers for 24 h (**Figure 1**). Then, 10 μL of fresh pathogen mycelium/spore mix suspension was inoculated on the same side where the antagonist was inoculated previously and immediately placed in a horizontal position, preventing suspension diffusion. Incubation was carried out in humid chambers for 3–7 days. Afterward, the surface of the woody stem was disinfected by rubbing with 70% ethanol. With a hot sterile scalp, the bark and 0.5 cm of the woody stem ends were removed. Small pieces located at 1 and 2.5 cm from the inoculation point were collected and cultured in individual PDA plates at 25°C for 7 days. To evaluate the pathogen mycelium and spore suspension viability, 10 μL of the solution was inoculated in one side of the wooden piece as described above and immediately processed to obtain 3 mm pieces at 1 and 2.5 cm from the pathogen inoculation point. Every piece was cultured in PDA at 25°C for 7 days. The presence of the pathogen on PDA was evaluated under a light microscope.

Test of Antagonist Mechanism

To characterize the mechanism of antagonism, the same experimental setup of co-culture was carried out on water agar (AA, 20 g L^{-1}; Difco) with a microscope sterile slide covered by a thin layer of the same agar in its surface. Using a light microscope (MOTIC BA410), the sample was screened for loops of the antagonist hyphae around *N. parvum* and *D. seriata*, indicating mycoparasitism. This experiment was carried out 3 times. To determine antibiosis as the type of antagonist mechanism used, isolated fungi *E. nigrum* R39.1, *C. rosea* CoS3/4.4, and *Cladosporium* sp. B38d.2 were cultured in PDA plates (39 g L^{-1}; Difco) over cellophane paper for 7 days. Cellophane paper with the fungal colony was then removed from the plate and a mycelium plug of *D. seriata* or *N. parvum* was placed in the center. Plates were incubated for 7 days at 25°C and pathogen growth was evaluated. This experiment was carried out three times.

Statistical Analysis

Statistical analysis was conducted with GraphPad PRISM 8 (8.1.1 version, 2019).

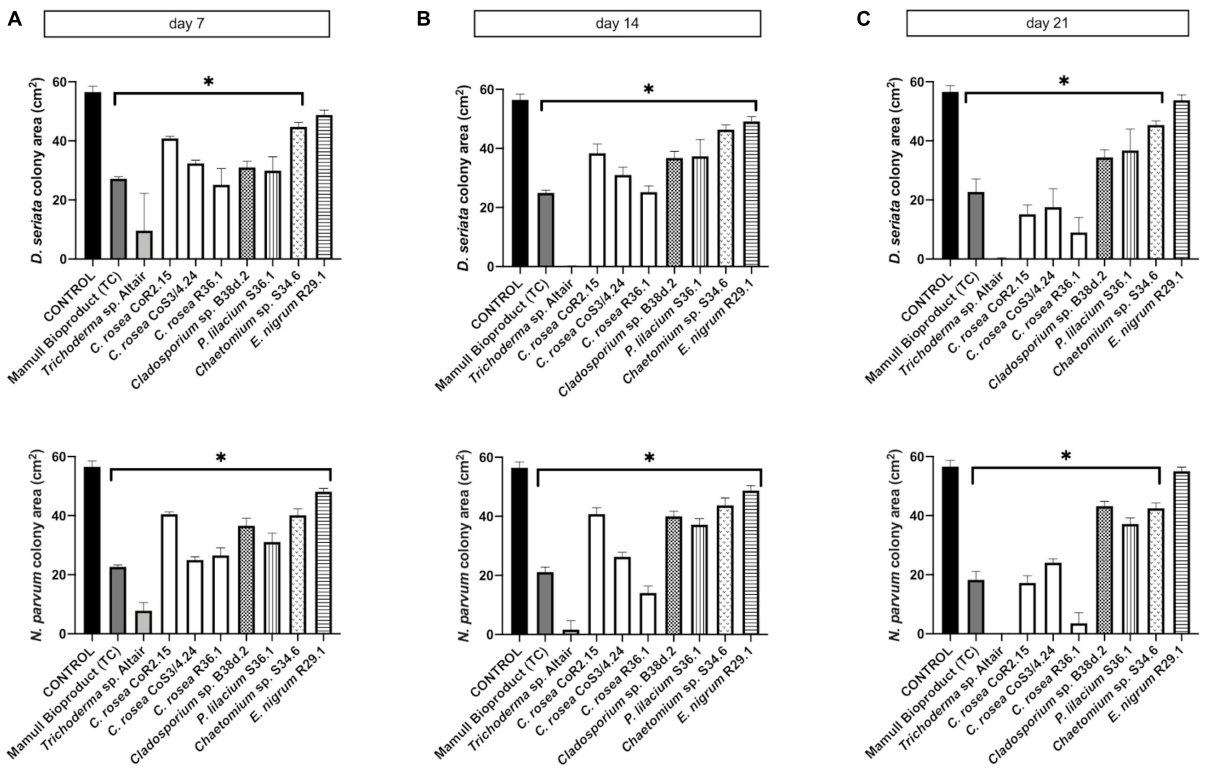

FIGURE 4 | Colony area measured after **(A)** 7, **(B)** 14, and **(C)** 21 days of inoculation of *D. seriata* (upper graphics) and *N. parvum* (bottom graphics), when growing alone (control) or in co-culture with the antagonists in PDA. Bars with asterisk are significantly different to the control (Tukey's test, $P < 0.001$). Error bars represent the standard error of the mean, $n = 5$.

RESULTS

Isolation and Identification of Endophytic and Rhizospheric Fungi

A total of 102 vineyard samples were collected to isolate endophytic and rhizospheric fungi associated with grapevines in Chile. Endophytic fungi were isolated from woody shoots, sprouts, and roots, while the rhizosphere ones were obtained from the soil in direct contact with the roots. Of these 102 samples, ninety were obtained from commercial vineyards in the central valleys of Chile and twelve from a vineyard in the Codpa Valley that has not been managed for disease protection for over 150 years. From these samples, a total of 221 and 166 morphologically different fungi were isolated from the commercial vineyards and the non-commercial Codpa Valley plants, respectively. Fungi were characterized taxonomically using ITS1 and ITS4 sequences. All fungal sequences were at least 98% identical to the best BLASTn hit in the UNITE database. We could assign taxonomy to a total of 300 isolates. The ITS sequence was discriminant at the species level for 227 isolates. The remaining were assigned to the corresponding genus or family. A total of 58 genera were represented, 37 and 38 among rhizospheric and endophytic fungi, respectively. As expected, below ground samples (rhizosphere and roots) were more diverse (56 genera) than sprouts and woody stems (5 genera) (**Figure 2**).

Effect of Fungal Antagonists on the Growth of GTD Fungi in Co-culture

To identify potential biocontrol agents for further characterization, we screened all isolates for antagonistic activity against *D. seriata* (**Supplementary Table 1**), a ubiquitous GTD pathogen. Based on the results of this initial screen, a total of eight isolates were selected for further characterization: *Trichoderma* sp. Altair, *Epicoccum nigrum* R29.1, three isolates of *Clonostachys rosea* (R 31.6, CoR2.15 and CoS3/4.24), *Cladosporium* sp. B38d.2, *Chaetomium* sp. S34.6 and *Purpureocillium lilacinum* S36.1 (**Supplementary Figure 1**). Previous reports described the antagonistic ability of the isolated genera against other phytopathogens (Cota et al., 2009; de Lima Fávaro et al., 2012; Solano Castillo et al., 2014; Hung et al., 2015; Costadone and Gubler, 2016; Del Frari et al., 2019).

To assess the antagonistic ability of the ten selected isolates, we co-cultured each one of them with *D. seriata* and *N. parvum*, two of the main fungi causing GTDs in Chile. Co-cultures were carried out on two different types of growth media: the commonly used potato dextrose agar (PDA) and a substrate made of agar and ground woody grapevine tissue aka, grapevine plant agar

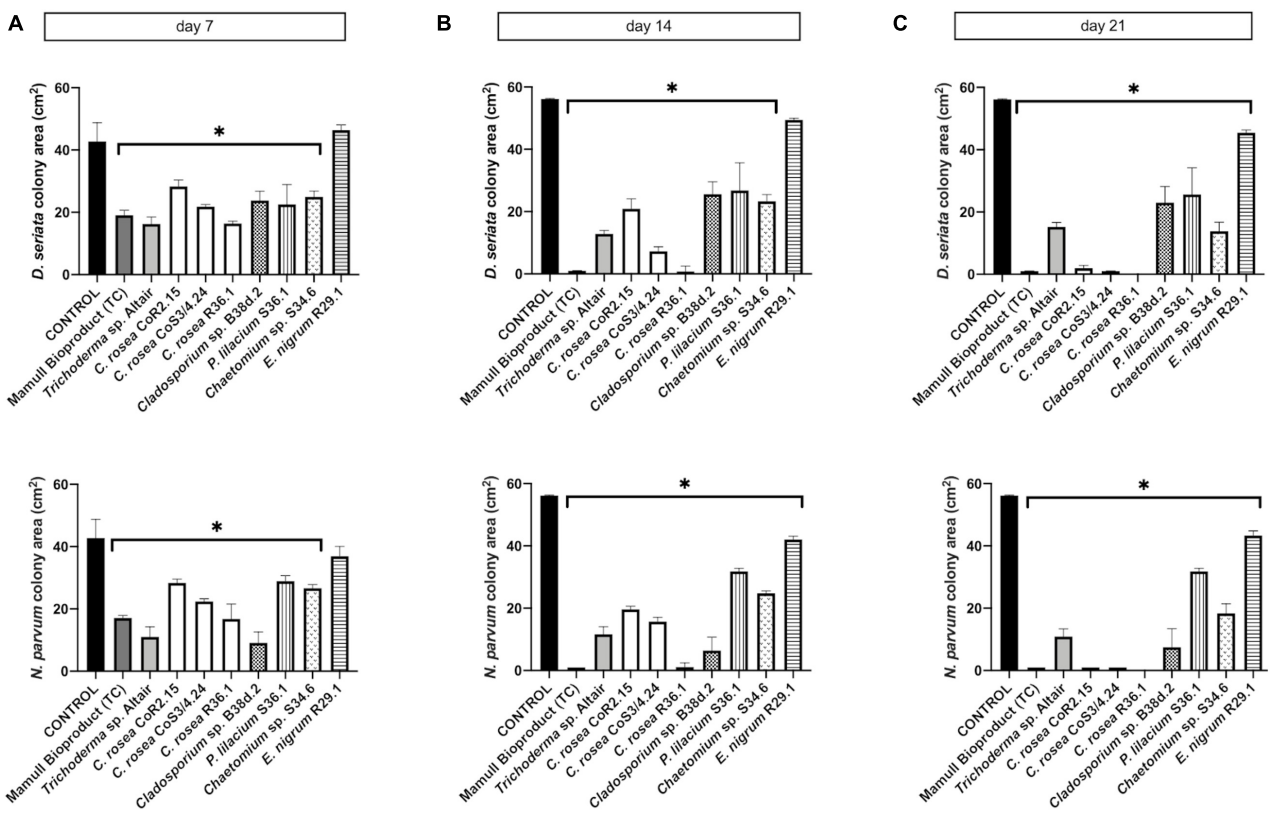

FIGURE 5 | Colony area measured after **(A)** 7, **(B)** 14, and **(C)** 21 days of inoculation of *D. seriata* (top row) and *N. parvum* (bottom row), when growing alone (control) or in co-culture with the antagonists in PA. Bars with asterisk are significantly different to the control (Tukey's test, $P < 0.001$). Error bars represent the standard error of the mean, $n = 5$.

(PA)] that simulates in planta nutrient composition (Massonnet et al., 2017). Isolates displayed a wide range of growth rates, which often differed between PDA and PA (**Figure 3**). Interestingly, most endophytes, including all *C. rosea* isolates, grew faster on PA than PDA. Different growth rates reflected the patterns of inhibition of *D. seriata* and *N. parvum* (**Figures 4**, **5**). The *Trichoderma* Altair isolate grew faster than the rest on PDA and reached its maximum inhibitory effect on both pathogens as early as day 7 in PDA. Growth inhibition only occurred upon physical contact between colonies of *Trichoderma* sp. and the pathogens. The faster growth on PA of the endophytes *Clonostachys, Chaetomium, Epicoccum,* and *Cladosporium* was associated with greater pathogen inhibition rates on this substrate compared to PDA, especially for the *Clonostachys* isolates. In PA, *C. rosea* overgrew the pathogen colony at least 7 days earlier than in PDA. All *C. rosea* strains inhibited over 98% pathogen growth in PA at day 21 (**Figure 5**). *Chaetomium* sp. S34.6 isolate inhibited pathogen growth by slowly growing in the plate until colony contact. By day 21 *Chaetomium* sp. S34.6 inhibited *D. seriata* and *N. parvum* growth by 59.1% and 86.75%, respectively, about two-fold the pathogen growth inhibition showed in PDA. Both species completely overgrew both pathogen colonies around 28 days. The antagonistic effect of *C. rosea* R36.1 and CoS3/4.24 occurred upon direct contact between colonies, which overgrew the pathogen colony within 21 days of growth. Instead, pathogen growth inhibition of *C. rosea* CoR2.15, *Purpureocillium lilacinum* S36.1, and *E. nigrum* R29.1 happened without evident physical contact between colonies. In PDA, *E. nigrum* produced a wide 0.8 to 1.2 cm orange-colored halo that was partially colonized only by *N. parvum* after 21 days of growth. The slow and limited growth of *Neofusicoccum parvum* was also visible in the halo produced by *Purpureocillium. Cladosporium* sp. B38d.2 showed an interesting difference in antagonist activity against *N. parvum* in PA, reaching its higher inhibition rate (**Figure 5**). When cultured with this pathogen, *Cladosporium* strongly sporulated, covering the entire plate, and stopped *N. parvum* early growth.

On PA, *C. rosea* inhibited *P. chlamydospora* almost completely (99.9%). Interestingly, *C. rosea* growth first paused without evident contact between colonies (**Figure 6**) at day 7, but later, by 14 days, it overgrew completely the pathogen colony. Overgrowth was also observed with *Trichoderma* sp. Altair in PDA.

Characterization of the Mechanisms of Antagonism

The antagonistic activity of endophytic biocontrol agents can depend on the competition for nutrients and induced resistance in the plant, and/or direct interaction with the release of pathogen inhibitory compounds or mycoparasitism (White et al., 1997; Arnold et al., 2001; Köhl et al., 2015). During co-culture, isolates of *C. rosea* showed pathogen inhibition both before and after direct contact between colonies, suggesting that

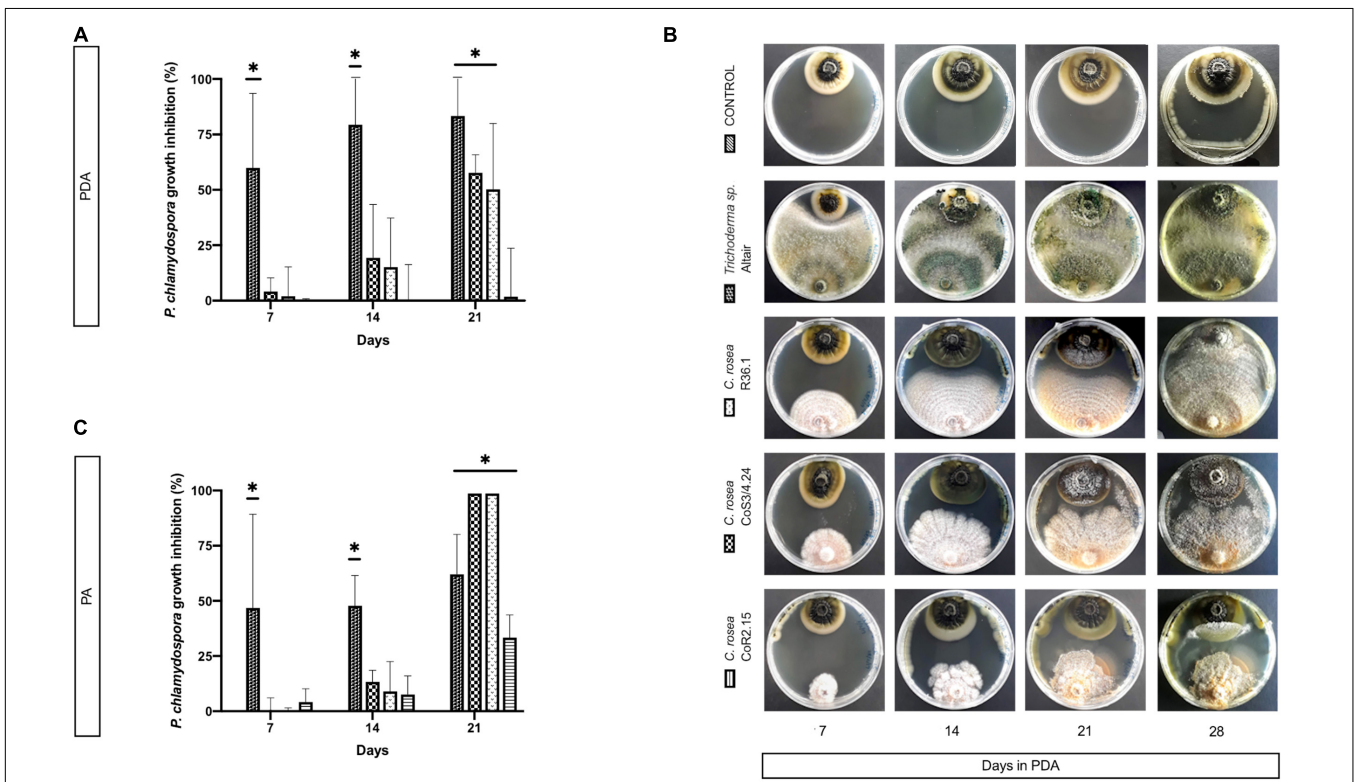

FIGURE 6 | Colony area measured at day 7, 14, and 21 post-inoculation of the pathogen *P. chlamydospora* when cultured alone or with the antagonists: *C. rosea* CoR2.15, CoS3/4.24, R36.1 or *Trichoderma* sp. Altair. Growth area was evaluated in potato dextrose agar, PDA, **(A)** and **(B)** and in grapevine plant agar, PA, **(C)**. Bars with asterisk are significantly different to the control (Tukey's test, $P < 0.001$). Error bars represent the standard error of the mean, $n = 5$.

both mechanisms could underlie its antagonistic properties. To evaluate the mode of action of *C. rosea* and *Trichoderma* sp. Altair, we studied under a light microscope the mycelium in the zone of interspecific interaction. For *C. rosea* CoS3/4.24 and R36.1, hyphal coiling, a sign of mycoparasitism, was consistently observed in all co-cultures with *N. parvum* and *D. seriata* (**Figure 7**). Hyphal coiling was only occasionally found in *Trichoderma* sp. Altair.

When *C. rosea* rhizosphere strain CoS3/4.24 was co-cultured with *D. seriata* or *N. parvum*, pathogen growth terminated before direct contact with *C. rosea* in correspondence of the halo surrounding the antagonist. In this case, the inhibitory activity of *C. rosea* may depend on a secreted antibiotic compound. This was also observed when *Cladosporium* sp. B38d.2 was used as antagonist. To test the inhibitory activity of the C. rosea secretome, we inoculated *C. rosea* on a sterilized cellophane membrane overlaid on PDA and incubated for seven days. The cellophane membrane was shown to be permeable to metabolites secreted by fungi (Dennis and Webster, 1971; Chambers, 1993; Sharmini et al., 2004; Rodriguez et al., 2011). After removing the cellophane membrane together with the *C. rosea* mycelium, we inoculated the plates with pathogens and measured their growth in comparison with normal PDA. Pathogen growth was significantly reduced on plates previously incubated with *C. rosea*, likely due to the secreted metabolites that permeated through the cellophane membrane (**Figure 8**). The inhibition caused by the secreted metabolites of *C. rosea* CoS3/4.24 led to a 47.2% and 50.1% reduction in growth of *D. seriata* and *N. parvum*, respectively. In the case of Cladosporium sp., 34.26% and 42.46% inhibition was observed against *N. parvum*

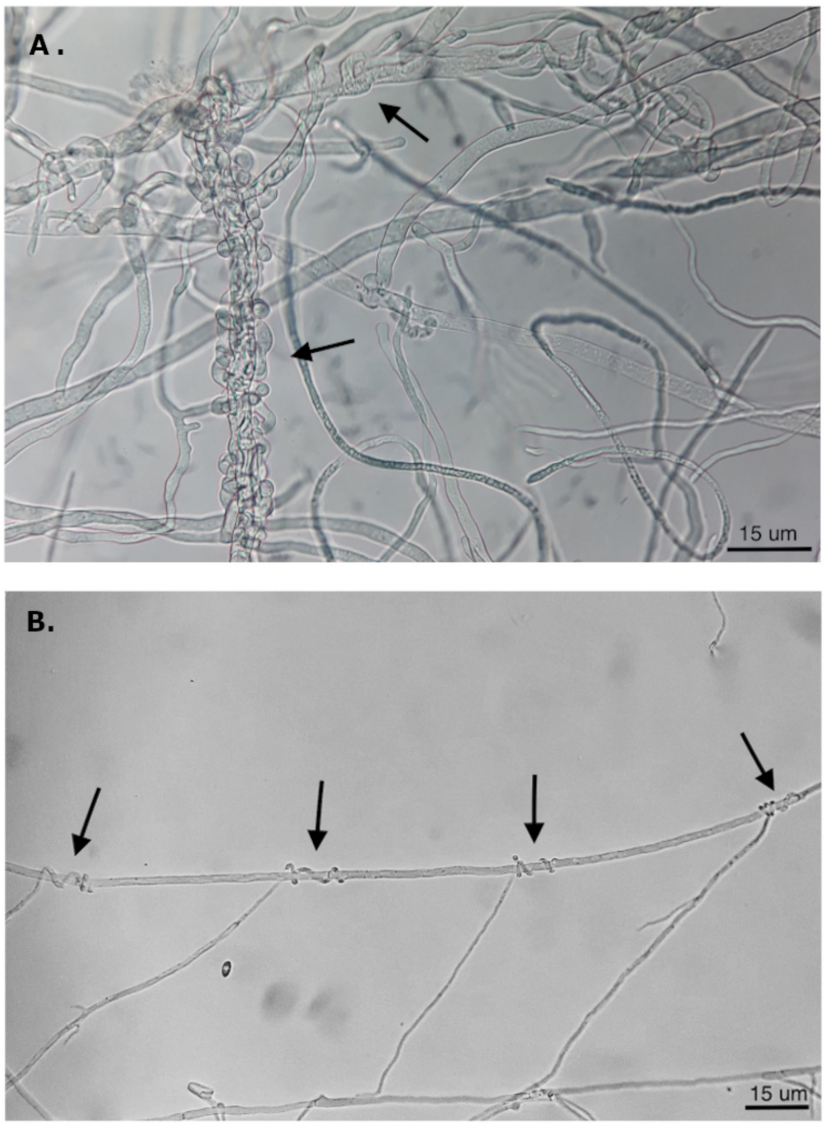

FIGURE 7 | Hyphal coiling of **(A)** *Trichoderma* Altair against *D. seriata* and **(B)** *C. rosea* CoS3/4.24 around hyphae of *N. parvum* (magnification 400X).

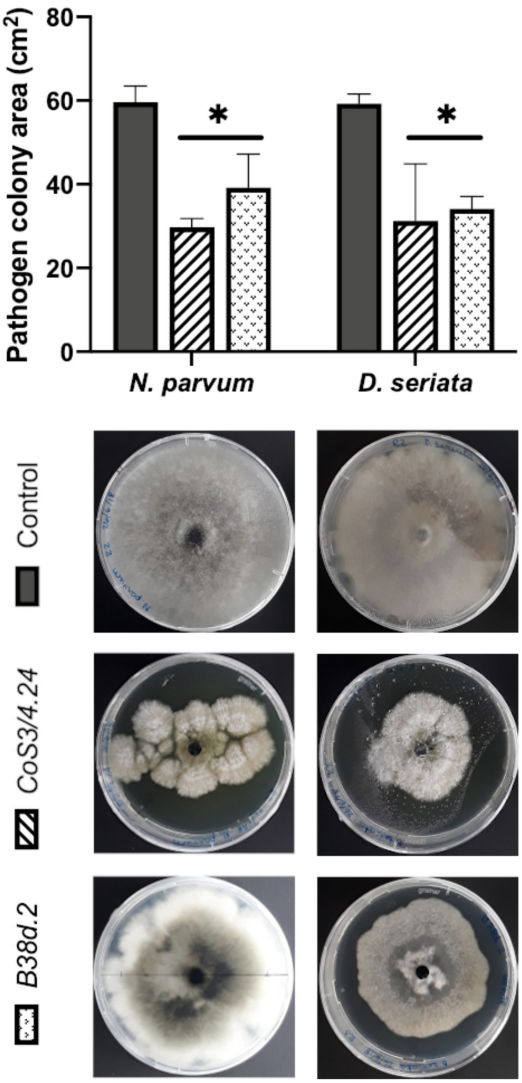

FIGURE 8 | Pathogen growth over secondary metabolites produced by antagonists *C. rosea* CoS3/4.24, *Cladosporium* sp. B38d.2 in PDA. Bars with asterisk are significantly different to the control (Tukey's test, $P < 0.001$). Error bars represent the standard error of the mean, $n = 5$.

and *D. seriata*, respectively. Changes in the pathogen colony morphology were also observed, especially when in contact with *C. rosea* CoS3/4.24 isolate secondary metabolites. *N. parvum* colony turned into several flat independent colonies with undulate margins, while *D. seriata* grew as one colony with irregular shape.

Effect of Fungal Antagonists on the Growth of GTD Fungi in One-Year old Grapevine Woody Shoots

As both growth and inhibition rates of GTD pathogens were significantly different in media containing grapevine annual shoot extract (plant agar, PA), we extended the testing of antagonism by using one-year-old lignified shoots (aka canes) as a substrate for co-cultures. We tested both sterile (autoclaved) and non-sterile canes. After 7 days, *C. rosea*, *N. parvum*, and *D. seriata* colonized completely the internal tissue of 4.5 cm-long autoclaved canes. The antagonists *C. rosea* strains were recovered in all pathogen co-inoculated samples after 7 days (**Figure 9**). No pathogen growth was observed at 0.5 cm from the pathogen inoculation point when treated with the antagonists. Interestingly, under the same conditions, Tebuconazole, a commercial synthetic fungicide, did not reduce *D. seriata* nor *N. parvum* growth.

We also performed the co-culture experiments on canes that were not subjected to autoclaving. Pathogens colonized the entire cane in 7 days in absence of any antagonist. In less than 0.1% and 10% of the co-culture assays, *N. parvum* and *D. seriata* were recovered from plant tissue previously inoculated with *C. rosea* isolates, respectively. In the case of CoS3/4.24 isolate, *N. parvum* and *D. seriata* growth inhibition was observed in 80% and 100% of the assays, respectively. In summary, the antagonistic potential of the *C. rosea* isolates shown in agar plate was confirmed in grapevine propagation material.

DISCUSSION

We isolated fungi from asymptomatic grapevines to find potential biocontrol agents against GTDs. As they share the same host with pathogens, these fungi may provide longer-lasting protection of grapevine tissues than biocontrol agents identified on other plant species (Zabalgogeazcoa, 2008; Latz et al., 2018). Three hundred eighty-seven different fungi and yeast were isolated and identified from multiple grapevine tissues and pest management systems. The observed diversity was limited to culturable fungi, since no cultivation-independent identification tools were applied. Taxa were determined solely based on the ITS sequence. Further validation using other informative sites, such as nu-SU-0817-59 and nu-SU-1196-39 (Borneman and Hartin, 2000) or TEF-1a (Ichi-Ishi and Inoue, 2005), would provide additional resolution for some of the isolates we were not able to characterize at the species level. As expected, rhizospheric soil showed to hold more fungal diversity than roots, and sprouts showed less cultivable diversity than any other sample. This was in agreement with previous studies using amplicon sequencing (Tan et al., 2017).

As the focus of this work was to find microorganisms able to colonize the grapevine persistently, we conducted this search during late Winter, at the beginning of the cold and wet season, when potentially beneficial microorganisms may compete with pathogens for the colonization of the host through pruning wounds (Arnold et al., 2003; Rolshausen et al., 2010; Travadon et al., 2016). Even if we could collect more samples from commercial vineyards than from the 150 year-old vines in the Codpa valley, the number of fungal taxa isolated from Codpa was higher than in commercial vineyards. The greater diversity found in Codpa might be due to the older age of the vines as well as the lack of pathogen control practices throughout the life of the vineyard, even if other cultural management practices as fertilization with animal manure have been done over generations.

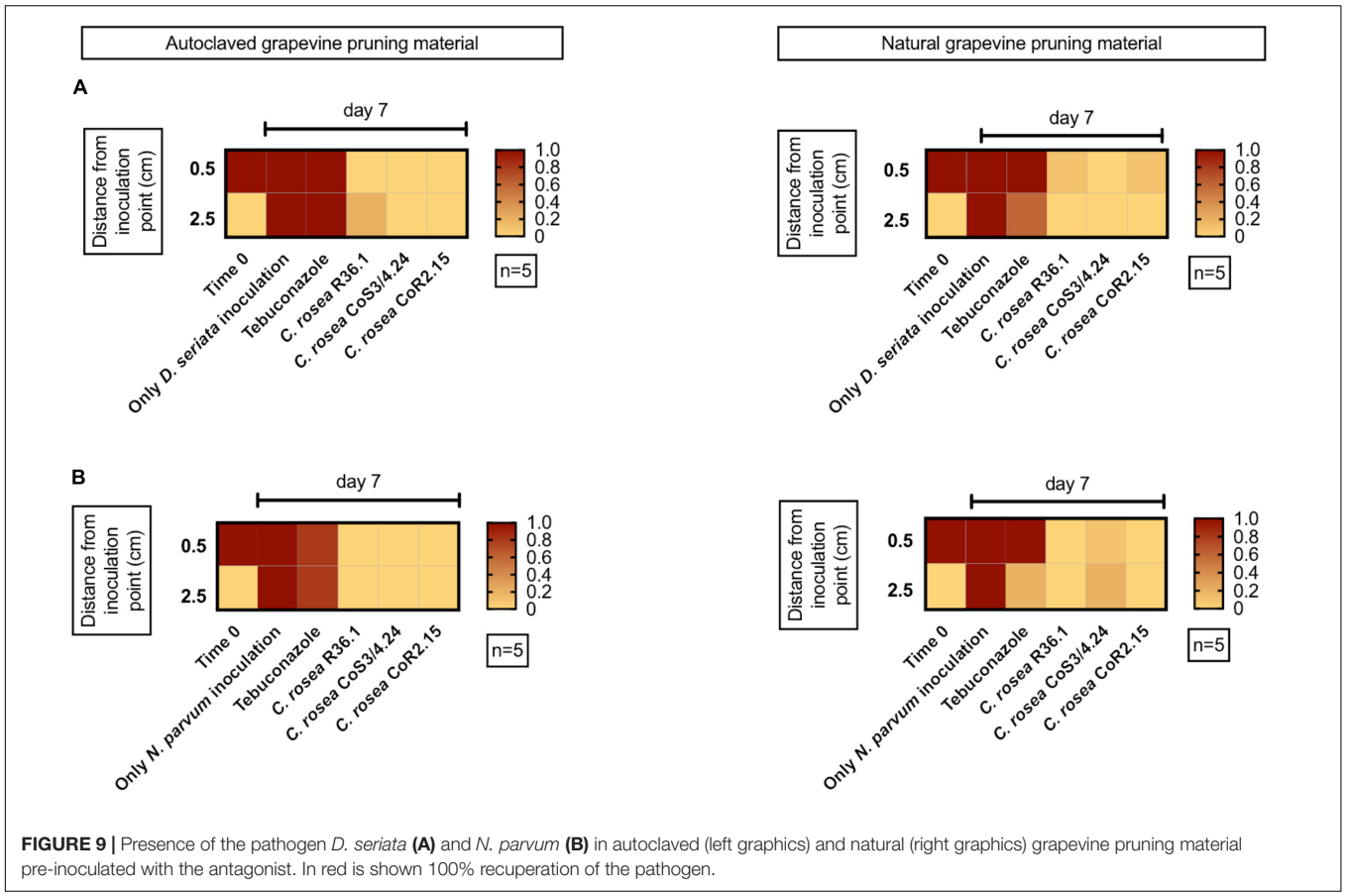

FIGURE 9 | Presence of the pathogen *D. seriata* **(A)** and *N. parvum* **(B)** in autoclaved (left graphics) and natural (right graphics) grapevine pruning material pre-inoculated with the antagonist. In red is shown 100% recuperation of the pathogen.

All fungi we isolated, characterized, and tested, with the exception of ***Epicoccum nigrum*** showed a significant growth inhibition of ***N. parvum*** and ***D. seriata*** in co-cultures on both PDA and PA. The ***Trichoderma*** Altair isolate and all ***C. rosea*** strains completely overgrew both pathogens by day 21. This was also observed against the pathogen ***P. chlamydospora*** in PA. However, variable biocontrol efficacy was observed between different isolates of the same species, as reported in Inch and Gilbert (2007). For example, the rhizosphere isolate ***C. rosea*** CoS3/4.24 grew faster on media and overgrew the pathogen earlier than the other ***C. rosea*** isolates. In contrast, the endophytic isolates of ***C. rosea*** showed better inhibition of ***N. parvum*** in grapevine woodie shoots. The endophytic isolate of ***Cladosporium*** also displayed antagonism in co-culture, in particular against ***N. parvum*** on PA. Its inhibitory activity seemed to be due to the high sporulation rate and not to the rapid growth of the mycelium observed in others (Schöneberg et al., 2015). ***Cladosporium*** sp. produces a great amount of black, hydrophobic spores, and a small mycelium underneath the dense spore mass. On PA as well as PDA, ***Chaetomium*** sp. showed a significant reduction of growth of ***N. parvum*** and ***D. seriata***, although weaker than that of ***Trichoderma***. The antagonistic activity of ***Chaetomium*** may be due to a slow mycoparasitism. Hyphae of ***Chaetomium*** has been described to penetrate and coil around pathogen hyphae at day 30 of co-culture (Hung et al., 2015). Strains of ***Chaetomium*** have also shown antagonist activity against different pathogens as ***Phytophthora nicotianae*** (Hung et al., 2015), ***Rhizoctonia solani*** (Gao et al., 2005) and ***Fusarium oxysporum*** (Huu Phong et al., 2016) among others. Some strains presented antibiosis as an antagonist strategy, but mycoparasitism has been also described for this genus (Hung et al., 2015).

Clonostachys rosea showed limited antagonism at early stages of co-culture on artificial media and completely inhibited pathogen growth only after 21 days. Importantly, *C. rosea* was particularly effective against pathogen colonization of autoclaved woodie shoots. Fungal growth dynamics and therefore, the interaction between colonies are likely influenced by the type of media (Schöneberg et al., 2015), in particular when nutrient-rich media are compared with substrates poor in nutrients, such as PA and woodie tissue. It is worth noting that different isolates displayed different antagonistic activities depending on the substrate. For example, *C. rosea* isolates R36.1 and CoR2.15 showed higher pathogen inhibition than CoS3/4.24 on woodie shoots that were not autoclaved. Interestingly, R36.1 and CoR2.15 were endophytic, while CoS3/4.24 was isolated from the rhizosphere. Although we did not find the same pattern when autoclaved tissue was used, the different behavior of endophytic and rhizospheric isolates supports the overall strategy to search for potential biocontrol agents among the natural inhabitants of grapevines.

Generally recognized control mechanisms for fungal biocontrol agents are (1) competition for nutrients and space, (2) induced resistance in the plant, both consisting in an indirect interaction with the pathogen, (3) inhibition through antibiosis, and (4) mycoparasitism (Latz et al., 2018; Köhl et al., 2019). The formation of short loops of the antagonist's hyphae around hyphae from another fungal species also called hyphal coiling (Barnett and Lilly, 1962; Assante et al., 2004; Gao et al., 2005). The coiling establishes an intimate contact with the parasitized hypha, penetrating the hypha and delivering antibiotic compounds and cell-wall degrading enzymes (Barnett and Lilly, 1962). This type of mycoparasitism has been commonly found in the genus *Trichoderma* (Howell, 2003; Benítez et al., 2004) and reported in *C. rosea* (Barnett and Lilly, 1962; Morandi et al., 2001). The Trichoderma sp. Altair isolate produced hyphal coils and also the *C. rosea* strains we tested. In all cases, we found a strong correlation between coiling and antagonism suggesting that mycoparasitism plays an important role in the interaction with the pathogens. In the case of *C. rosea* CoS3/4.24, a yellowish halo around the antagonist colony was present. Antibiosis was previously described for this species (Iqbal et al., 2017), but not all strains of the species show antibiotic production (Moraga-Suazo et al., 2016). Further studies should be performed with the *C. rosea* isolates to dissect the role of secondary metabolite production in pathogen growth inhibition and endophytic establishment in the grapevine as this might have important applications in agro-industrial areas (Karlsson et al., 2015). Direct interaction with the pathogen mode of action, as mycoparasitism and antibiosis, are highly desirable mechanisms for further production of commercial biocontrol agents, as they expose lower risks of human, plant and environmental toxicity (Köhl et al., 2019).

DATA AVAILABILITY STATEMENT

The datasets presented in this study can be found in online repositories. The names of the repository/repositories and accession number(s) can be found below: https://www.ncbi.nlm.nih.gov/genbank/, MN686237; https://www.ncbi.nlm.nih.gov/genbank/, MW077134; https://www.ncbi.nlm.nih.gov/genbank/, MW076517; https://www.ncbi.nlm.nih.gov/genbank/, MW130886; and https://www.ncbi.nlm.nih.gov/genbank/, MW130890.

AUTHOR CONTRIBUTIONS

IS-V was in charge of performing all experiments, developing and testing innovative evaluations, and writing the manuscript draft. DT gave strong support doing the experiments. MM gave guidance in the early steps of paper writing. ML and GD provided the pathogen fungi and *Trichoderma* sp. Altair isolates for evaluations, and some advice in project development and paper writing. DC gave invaluable and robust advice in paper writing. He also edited the manuscript a significant number of times. AC was in charge of the R&D department and the laboratory. He provided the first idea and gave guidance in every part of the project, generating the contacts for the development of this project. All authors contributed to the article and approved the submitted version.

ACKNOWLEDGMENTS

We would like to thank the VSPT group for let us collect samples from their vineyards and supporting this project. We would also like to thank Patricio Muñoz for providing samples of old grapevines from the Codpa valley. This research was funded by the Chilean Economic Development Agency (CORFO; Project 13CEI2-21852), VSPT Wine Group, and Universidad de Talca.

SUPPLEMENTARY MATERIAL

The Supplementary Material for this article can be found online at: https://www.frontiersin.org/articles/10.3389/fmicb.2020.614620/full#supplementary-material

REFERENCES

Arnold, A. E., Maynard, Z., and Gilbert, G. S. (2001). Fungal endophytes in dicotyledonous neotropical trees: patterns of abundance and diversity. *Mycol. Res.* 105, 1502–1507. doi: 10.1017/S0953756201004956

Arnold, A. E., Mejía, L. C., Kyllo, D., Rojas, E. I., Maynard, Z., Robbins, N., et al. (2003). Fungal endophytes limit pathogen damage in a tropical tree. *Proc. Natl. Acad. Sci. U.S.A.* 100, 15649–15654. doi: 10.1073/pnas.2533483100

Aroca, A., Gramaje, D., Armengol, J., García-Jiménez, J., and Raposo, R. (2010). Evaluation of the grapevine nursery propagation process as a source of *Phaeoacremonium* Spp. and *Phaeomoniella chlamydospora* and occurrence of trunk disease pathogens in rootstock mother vines in Spain. *Eur. J. Plant Pathol.* 126, 165–174. doi: 10.1007/s10658-009-9530-3

Aroca, R. (2013). *Symbiotic Endophytes*. Berlin: Springer-Verlag.

Assante, G., Maffi, D., Saracchi, M., Farena, G., Moricca, S., and Ragazzi, A. (2004). Histological studies on the *Mycoparasitism* of *Cladosporium tenuissimum* on *Urediniospores* of *Uromyees appendiculatus*. *Mycol. Res.* 108, 170–182. doi: 10.1017/S0953756203008852

Auger, J., Esterio, M., Pérez, I., Gubler, W. D., and Eskalen, A. (2004). First report of *Phaeomoniella chlamydospora* on *Vitis vinifera* and French American Hybrids in Chile. *Plant Dis.* 88, 1285–1285. doi: 10.1094/PDIS.2004.88.11.1285C

Augusti-Brisach, C., and Armengol, J. (2013). Black-foot disease of grapevine: an update on taxonomy, epidemiology and management strategies. *Phytopathol. Mediterra.* 52, 245–261. doi: 10.14601/Phytopathol_Mediterr-12662

Azevedo, J. L., Maccheroni, W., Odair Pereira, J., and Luiz De Araújo, W. (2000). Endophytic microorganisms: a review on insect control and recent advances on tropical plants. *EJB Electron. J. Biotechnol.* 3:717.

Bacon, C. W., and White, J. F. (2016). Functions, mechanisms and regulation of endophytic and epiphytic microbial communities of plants. *Symbiosis* 68, 87–98. doi: 10.1007/s13199-015-0350-2

Badalyan, S. M., Innocenti, G., and Garibyan, N. G. (2002). Antagonistic activity of xylotrophic mushrooms against. *Phytopathol. Mediterra.* 41, 220–225.

Barnett, H. L., and Hunter, B. B. (1955). Illustrated genera of imperfect fungi. *Trans. Br. Mycol. Soc.* 55, 113–116. doi: 10.1016/s0007-1536(55)80058-7

Barnett, H. L., and Lilly, V. G. (1962). A destructive Mycoparasyte, *Gliocladium roseum*. *Mycol. Soc. Am.* 54, 72–77. doi: 10.2307/3756600

Benítez, T., Rincón, A. M., Limón, M. C., and Codón, A. C. (2004). Biocontrol mechanisms of *Trichoderma* strains. *Int. Microbiol.* 7, 249–260.

Bertsch, C., Ramírez-Suero, M., Magnin-Robert, M., Larignon, P., Chong, J., Abou-Mansour, E., et al. (2013). Grapevine trunk diseases: complex and still poorly understood. *Plant Pathol.* 62, 243–265. doi: 10.1111/j.1365-3059.2012.02674.x

Besoain, X., Torres, C., Díaz, G. A., and Latorre, B. A. (2013). First report of *Neofusicoccum australe* associated with *Botryosphaeria* canker of grapevine in chile. *Plant Dis.* 97, 143–143. doi: 10.1094/pdis-07-12-0652-pdn

Bester, W., Crous, P. W., and Fourie, P. H. (2007). Evaluation of fungicides as potential grapevine pruning wound protectants against *Botryosphaeria* species. *Aust. Plant Pathol.* 36, 73–77. doi: 10.1071/AP06086

Billones-Baaijens, R., Jones, E. E., Ridgway, H. J., and Jaspers, M. V. (2013). Virulence affected by assay parameters during grapevine pathogenicity studies with *Botryosphaeriaceae* nursery isolates. *Plant Pathol.* 62, 1214–1225. doi: 10.1111/ppa.12051

Borneman, J., and Hartin, R. J. (2000). PCR primers that amplify fungal RRNA genes from environmental samples. *Appl. Environ. Microbiol.* 66, 4356–4360. doi: 10.1128/AEM.66.10.4356-4360.2000

Chambers, S. M. (1993). *Phytophthora Root Rot of Chestnut*. Doctorate thesis, University of Adelaide, Adelaide.

Costadone, L., and Gubler, W. D. (2016). *Biocontrol of Major Grapevine Diseases: Leading Research*, eds F. Mathieu, and S. Compant (Boston, MA: CABI).

Cota, L. V., Maffia, L. A., Mizubuti, E. S. G., and Macedo, P. E. F. (2009). Biological control by *Clonostachys rosea* as a key component in the integrated management of strawberry gray mold. *Biol. Control* 50, 222–230. doi: 10.1016/j.biocontrol.2009.04.017

de Lima Fávaro, L. C., de Souza Sebastianes, F. L., and Araújo, W. L. (2012). *Epicoccum nigrum* P16, a sugarcane endophyte, produces antifungal compounds and induces root growth. *PLoS One* 7:e36826. doi: 10.1371/journal.pone.0036826

Del Frari, G., Cabral, A., Nascimiento, T., Coavida, F. R., and Oliveira, H. (2019). *Epiccocum layuense* a potential biocontrol agent od associated fungi in grapevine. *PLoS One* 14:e0213273. doi: 10.1371/journal.pone.0213273

Dennis, C., and Webster, J. (1971). Antagonistic properties of species-groups of *Trichoderma*. *Trans. Br. Mycol. Soc.* 57, 25–IN3. doi: 10.1016/s0007-1536(71)80077-3

Díaz, G. A., Auger, J., Besoain, X., Bordeu, E., and Latorre, B. A. (2013). Prevalence and pathogenicity of fungi associated with grapevine trunk diseases in chilean vineyards. *Cienc. Investig. Agrar.* 40, 327–339. doi: 10.4067/RCIA.V40I2.1101

Díaz, G. A., and Latorre, B. A. (2013). Efficacy of paste and liquid fungicide formulations to protect pruning wounds against pathogens associated with grapevine trunk diseases in chile. *Crop Protect.* 46, 106–112. doi: 10.1016/j.cropro.2013.01.001

Díaz, G. A., and Latorre, B. A. (2014). Infection caused by *Phaeomoniella chlamydospora* associated with Esca-like symptoms in grapevine in Chile. *Plant Dis.* 98, 351–360. doi: 10.1094/PDIS-12-12-1180-RE

Díaz, G. A., Prehn, D., Besoain, X., Chávez, E. R., and Latorre, B. A. (2011a). *Neofusicoccum parvum* associated with grapevine trunk diseases in Chile. *Plant Dis.* 95, 1032–1032. doi: 10.1094/PDIS-03-11-0260

Díaz, G. A., Prehn, D., and Latorre, B. A. (2011b). First report of *Cryptovalsa ampelina* and *Eutypella leprosa* associated with grapevine trunk diseases in Chile. *Plant Dis.* 95, 490–490. doi: 10.1094/PDIS-12-10-0919

Felzensztein, C. (2014). The chilean wine industry: new international strategies for 2020. *Emerald Emerg. Mark. Case Stud.* 4, 1–12. doi: 10.1108/EEMCS-2014-2222

Gao, K., Liu, X., Kang, Z., and Mendgen, K. (2005). Mycoparasitism of *Rhizoctonia solani* by endophytic *Chaetomium spirale* ND35: ultrastructure and cytochemistry of the interaction. *J. Phytopathol.* 153, 280–290. doi: 10.1111/j.1439-0434.2005.00970.x

Gramaje, D., and Armengol, J. (2011). Importance and impact of fungal trunk pathogens in young vineyards. *Plant Dis.* 95, 1040–1055. doi: 10.1074/jbc.M309555200

Gramaje, D., Urbez-Torres, J. R., and Sosnowski, M. R. (2018). Managing grapevine trunk diseases with respect to etiology and epidemiology: current strategies and future prospects. *Plant Dis.* 102, 12–39. doi: 10.1094/PDIS-04-17-0512-FE

Halleen, F., Fourie, P. H., and Lombard, P. J. (2010). Protection of grapevine pruning wounds against *Eutypa lata* by biological and chemical methods. *South Afric. J. Enol. Viticult.* 31, 125–132.

Hardoim, P. R., Van Overbeek, L. S., Berg, G., Pirttilä, A. M., Compant, S., Campisano, A., et al. (2015). The hidden world within plants: ecological and evolutionary considerations for defining functioning of microbial endophytes. *Microbiol. Mol. Biol. Rev.* 79, 293–320. doi: 10.1128/MMBR.00050-14

Hardoim, P. R., Van Overbeek, L. S., and Van Elsas, J. D. (2008). Properties of bacterial endophytes and their proposed role in plant growth. *Trends Microbiol.* 16, 463–471. doi: 10.1016/j.tim.2008.07.008

Hirsch, G., and Braun, U. (1992). "Communities of parasitic microfungi," in *Fungi in Vegetation Science. Handbook of Vegetation Science*, Vol. 19, ed. W. Winterhoff (Dordrecht: Springer), doi: 10.1007/978-94-011-2414-0_8

Howell, C. R. (2003). Mechanisms employed by *Trichoderma* species in the biological control of plant diseases: the history and evolution of current concepts. *Plant Dis.* 87, 4–10. doi: 10.1094/pdis.2003.87.1.4

Hung, P. M., Wattanachai, P., Soytong, K., and Poeaim, S. (2015). Efficacy of *Chaetomium* species as biological control agents against *Phytophthora nicotianae* root rot in citrus. *Mycobiology* 43:288. doi: 10.5941/MYCO.2015.43.3.288

Huu Phong, N., Pongnak, W., and Soytong, K. (2016). Antifungal activities of *Chaetomium* Spp. against *Fusarium* Wilt of Tea. *Plant Protect. Sci.* 52, 10–17. doi: 10.17221/34/2015-PPS

Ichi-Ishi, A., and Inoue, H. (2005). Cloning, nucleotide sequence, and expression of Tef-1, the gene encoding translation elongation factor 1.ALPHA (EF-1.ALPHA.) of *Neurospora crassa*. *Jpn. J. Genet.* 70, 273–287. doi: 10.1266/jjg.70.273

Inch, S., and Gilbert, J. (2007). Effect of *Trichoderma harzianum* on perithecial production of *Gibberella zeae* on Wheat Straw. *Biocontrol Sci. Technol.* 17, 635–646. doi: 10.1080/09583150701408865

Iqbal, M., Dubey, M., McEwan, K., Menzel, U., Andersson Franko, M., Viketoft, M., et al. (2017). Evaluation of *Clonostachys rosea* for control of plant-parasitic nematodes in soil and in roots of carrot and wheat. *Phytopathology* 108, 52–59. doi: 10.1094/phyto-03-17-0091-r

John, S., Scott, E. S., Wicks, T. J., and Hunt, J. S. (2004). Interactions between *Eutypa lata* and *Trichoderma harzianum*. *Phytopathol. Mediterra.* 43, 95–104.

Kaplan, J., Travadon, R., Cooper, M., Hillis, V., Lubell, M., and Baumgartner, K. (2016). Identifying economic hurdles to early adoption of preventative practices: the case of trunk diseases in california winegrape vineyards. *Wine Econom. Policy* 5, 127–141. doi: 10.1016/j.wep.2016.11.001

Karlsson, M., Brandström Durling, M., Choi, J., Kosawang, C., Lackner, G., Tzelepis, L., et al. (2015). Insights on the evolution of *Mycoparasitism* from the genome of *Clonostachys rosea*. *Genome Biol. Evol.* 7, 465–480. doi: 10.1093/gbe/evu292

Kaul, S., Gupta, S., Ahmed, M., and Dhar, M. K. (2012). Endophytic fungi from medicinal plants: a treasure hunt for bioactive metabolites. *Phytochem. Rev.* 11, 487–505. doi: 10.1007/s11101-012-9260-6

Köhl, J., Kolnaar, R., and Ravensberg, W. J. (2019). Mode of action of microbial biological control agents against plant diseases: relevance beyond efficacy. *Front. Plant Sci.* 10:845. doi: 10.3389/fpls.2019.00845

Köhl, J., Scheer, C., Holb, I. J., Masny, S., and Molhoek, W. (2015). Toward an integrated use of biological control by *Cladosporium cladosporioides* H39 in Apple Scab (*Venturia Inaequalis*) management. *Plant Dis.* 99, 535–543. doi: 10.1094/PDIS-08-14-0836-RE

Latorre, G. B. (2018). *Compendio de las Enfermedades de las Plantas*, 1st Edn, Madrid: Ediciones UC.

Latz, M. A. C., Jensen, B., Collinge, D. B., and Jørgensen, H. J. L. (2018). Endophytic fungi as biocontrol agents: elucidating mechanisms in disease suppression. *Plant Ecol. Divers.* 11, 555–567. doi: 10.1080/17550874.2018.1534146

Lehtonen, P. T., Helander, M., Siddiqui, S. A., Lehto, K., and Saikkonen, K. (2006). Endophytic fungus decreases plant virus infections in meadow ryegrass (*Lolium pratense*). *Biol. Lett.* 2, 620–623. doi: 10.1098/rsbl.2006.0499

Lombard, L., Van Der Merwe, N. A., Groenewald, J. Z., and Crous, P. W. (2014). Lineages in Nectriaceae: re-evaluating the generic status of Ilyonectria and allied genera. *Phytopathol. Mediterra.* 53, 515–532.

López-Fernández, S., Compant, S., Vrhovsek, U., Bianchedi, P. L., Sessitsch, A., Pertot, I., et al. (2016). Grapevine colonization by Endophytic bacteria shifts secondary metabolism and suggests activation of defense pathways. *Plant Soil* 405, 155–175. doi: 10.1007/s11104-015-2631-1

Massonnet, M., Figueroa-Balderas, R., Galarneau, E. R. A., Miki, S., Lawrence, D. P., Sun, Q., et al. (2017). *Neofusicoccum parvum* colonization of the grapevine woody stem triggers asynchronous host responses at the site of infection and in the leaves. *Front. Plant Sci.* 8:1117. doi: 10.3389/fpls.2017.01117

Mondello, V., Songy, A., Battiston, E., Pinto, C., Coppin, C., Trotel-Aziz, P., et al. (2018). Grapevine trunk diseases: a review of fifteen years of trials for their control with chemicals and Biocontrol agents. *Plant Dis.* 102, 1189–1217. doi: 10.1094/PDIS-08-17-1181-FE

Moraga-Suazo, P., Sanfuentes, E., and Le-Feuvre, R. (2016). Induced systemic resistance triggered by *Clonostachys rosea* against *Fusarium circinatum* in *Pinus radiata*. *For. Res. Open Access* 5, 1–4. doi: 10.4172/2168-9776.1000174

Morandi, M. A. B., Maffia, L. A., and Sutton, J. C. (2001). Development of *Clonostachys rosea* and interactions with *Botrytis cinerea* in rose leaves and residues. *Phytoparasitica* 29, 103–113. doi: 10.1007/bf02983954

Morales-Cruz, A., Amrine, K. C. H., Blanco-Ulate, B., Lawrence, D. P., Travadon, R., Rolshausen, P. E., et al. (2015). Distinctive expansion of gene families associated with plant cell wall degradation, secondary metabolism and nutrient uptake in the genomes of grapevine trunk pathogens. *BMC Genomics* 16:469. doi: 10.1186/s12864-015-1624-z

Mousa, W. K., and Raizada, M. N. (2013). The diversity of anti-microbial secondary metabolites produced by fungal Endophytes: an interdisciplinary perspective. *Front. Microbiol.* 4:65. doi: 10.3389/fmicb.2013.00065

Mugnai, L. (2011). Editor's note and dedication. *Phytopathol. Mediterra.* 50, S3–S4.

Munkvold, G. P., Duthie, J. A., and Marois, J. J. (1994). Reductions in yield and vegetative growth of grapevines due to *Eutypa* dieback. *Am. Phytopathol. Soc.* 84, 186–192. doi: 10.1094/Phyto-84-186

Nilsson, R. H., Larsson, K. H., Taylor, A. F. S., Bengtsson-Palme, J., Jeppesen, T. S., Schigel, D., et al. (2019). The UNITE database for molecular identification of fungi: handling dark taxa and parallel taxonomic classifications. *Nucleic Acids Res.* 47, D259–D264. doi: 10.1093/nar/gky1022

Pancher, M., Ceol, M., Corneo, P. E., Oliveira Longa, C. M., Yousaf, S., Pertot, I., et al. (2012). Fungal endophytic communities in grapevines (*Vitis vinifera* L.) respond to crop management. *Appl. Environ. Microbiol.* 78, 4308–4317. doi: 10.1128/AEM.07655-11

Petrini, O. (1991). "Fungal endophytes of tree leaves," in *Microbial Ecology of Leaves. Brock/Springer Series in Contemporary Bioscience*, eds J. H. Andrews, and S. S. Hirano (New York, NY: Springer), 179–197. doi: 10.1007/978-1-4612-3168-4_9

Petzoldt, C. H. (1981). *Eutypa* dieback of grapevine: seasonal differences in infection and duration of susceptibility of pruning wounds. *Phytopathology* 71, 540–543. doi: 10.1094/phyto-71-540

Pieterse, C. M. J., Zamioudis, C., Berendsen, R. L., Weller, D. M., Van Wees, S. C. M., and Bakker, P. A. H. M. (2014). Induced systemic resistance by beneficial microbes. *Annu. Rev. Phytopathol.* 52, 347–375. doi: 10.1146/anurev-phyto-082712-102340

Pizarro, M. J. (2018). *Boletín Del Vino: Producción, Precios y Comercio Exterior. Avance a Octubre de 2018*. Chile: ODEPA, Ministerio de Agricultura.

Rodriguez, M. A., Cabrera, G., Gozzo, F. C., Eberlin, M. N., and Godeas, A. (2011). *Clonostachys rosea* BAFC3874 as a *Sclerotinia sclerotiorum* antagonist: mechanisms involved and potential as a biocontrol agent. *J. Appl. Microbiol.* 110, 1177–1186. doi: 10.1111/j.1365-2672.2011.04970.x

Rolshausen, P. E., and Gubler, W. D. (2005). Use of boron for the control of *Eutypa* dieback of grapevines. *Plant Dis.* 89, 734–738. doi: 10.1094/PD-89-0734

Rolshausen, P. E., Urbez-Torres, J. R., Rooney-Latham, S., Eskalen, A., Smith, R. J., and Gubler, W. D. (2010). Evaluation of pruning wound susceptibility and protection against fungi associated with grapevine trunk diseases. *Am. J. Enol. Viticult.* 61, 113–119.

Schindelin, J., Arganda-Carreras, I., Frise, E., Kaynig, V., Longair, M., Pietzsch, T., et al. (2012). Fiji: an open-source platform for biological-image analysis. *Nat. Methods* 9:676. doi: 10.1038/nmeth.2019

Schöneberg, A., Musa, T., Voegele, R. T., and Vogelgsang, S. (2015). The potential of antagonistic fungi for control of *Fusarium graminearum* and *Fusarium crookwellense* varies depending on the experimental approach. *J. Appl. Microbiol.* 118, 1165–1179. doi: 10.1111/jam.12775

Schulz, B., and Boyle, C. (2005). The endophytic continuum. *Mycol. Res.* 109, 661–686. doi: 10.1017/S095375620500273X

Sharmini, J., Scott, E. S., Wicks, T. J., and Hunt, J. S. (2004). Interactions between *Eutypa lata* and *Trichoderma harzanium*. *Phytopathol. Mediterr.* 43, 95–104.

Solano Castillo, T. F., Castillo Ávila, M. L., Medina Medina, J. V., and Del Pozo Núñez, E. M. (2014). Efectividad de hongos nematófagos sobre *Meloidogyne incognita* (Kofoid y White) chitwood en tomate en condiciones de campo, Loja, ecuador effectiveness of nematophagous fungi on *Meloidogyne incognita* (Kofoid and White) chitwood on tomato in field conditions in Loja, ecuador. *Rev. Protecc. Veg.* 29, 192–196.

Sosnowski, M. R., and Mundy, D. C. (2018). Pruning wound protection strategies for simultaneous control of *Eutypa* and *Botryosphaeria* dieback in New Zealand. *Plant Dis.* 103, 1–26. doi: 10.1007/978-3-319-23534-9_1

Sosnowski, M. R., and Mundy, D. C. (2019). Pruning wound protection strategies for simultaneous control of *Eutypa* and *Botryosphaeria* Dieback in New Zealand. *Plant Dis.* 103, 519–525. doi: 10.1094/PDIS-05-18-0728-RE

Stone, J. K., Bacon, C. W., and White, J. F. (2000). "An overview of endophytic microbes," in *Microbial Endophytes*, eds C. W. Bacon, and J. F. White, Jr. (New York: Marcel Dekker), 3–30.

Surico, G., Mugnai, L., and Marchi, G. (2006). Older and more recent observations on Esca: a critical overview. *Phytopathol. Mediterra.* 45(Suppl. 1), 68–86. doi: 10.14601/PHYTOPATHOL_MEDITERR-1847

Tan, Y., Cui, Y., Li, H., Kuang, A., Li, X., Wei, Y., et al. (2017). Rhizospheric soil and root endogenous fungal diversity and composition in response to continuous *Panax notoginseng* cropping practices. *Microbiol. Res.* 194, 10–19. doi: 10.1016/j.micres.2016.09.009

Thampi, A., and Suseela, B. R. (2017). Rizosphere actinobacteria for combating *Phytophthora capsici* and *Sclerotium rolfsii*, the major soil borne pathogens of black pepper (*Piper nigrum L.*) *Biol. Control* 109, 1–13. doi: 10.1016/j.biocontrol.2017.03.006

Travadon, R., Lecomte, P., Diarra, B., Lawrence, D. P., Renault, D., Ojeda, H., et al. (2016). Grapevine pruning systems and cultivars influence the diversity of wood-colonizing fungi. *Fungal Ecol.* 24, 82–93. doi: 10.1016/j.funeco.2016.09.003

Trouillas, F. P., Úrbez-Torres, J. R., and Gubler, W. D. (2010). Diversity of Diatrypaceous fungi associated with grapevine canker in California. *Mycologia* 102, 319–336. doi: 10.3852/08-185

Úrbez-Torres, J. R. (2011). The status of *Botryosphaereaceae* species infecting grapevines. *Phytopathol. Mediterra.* 50, S5–S45. doi: 10.14601/Phytopathol_Mediterr-9316

USDA Foreign Agricultural Center (2019). *Grapes, Fresh Table: Production, Supply and Distribution*. https://apps.fas.usda.gov/psdonline/reporthandler.ashx?reportId=2419&templateId=3&format=html&fileName=Grapes (accessed March 11, 2019).

Wagschal, I., Abou-Mansour, E., Petit, A. N., Clement, C., and Fontaine, F. (2008). Wood diseases of grapevine: a review on *Eutypa* dieback and Esca. *Res. Signpost* 37, 661–686.

Waite, H., and Morton, L. (2007). Hot water treatment, trunk diseases and other critical factors in the production of high-quality grapevine planting material. *Phytopathol. Mediterra.* 46, 5–17. doi: 10.14601/phytopathol_mediterr-1857

Weber, E. A., Trouillas, F. P., and Gubler, W. D. (2007). Double pruning of grapevines: a cultural practice to reduce infections by *Eutypa lata*. *Am. J. Enol. Viticult.* 58, 61–66.

White, J. F., Bacon, C. W., and Hinton, D. M. (1997). Modifications of host cells and tissues by the biotrophic endophyte *Epichloë amarillans* (*Clavicipitaceae*; *Ascomycotina*). *Can. J. Bot.* 75, 1061–1069. doi: 10.1139/b97-117

White, T. J., Bruns, T., Lee, S. W., and Taylor, J. W. (1990). ""Amplification and direct sequencing of fungal ribosomal RNA genes for phylogenetics," in *PCR Protocols: A Guide to Methods and Applications*, eds M. A. Innis, D. H. Gelfand, J. J. Sninsky, and T. J. White (New York, NY: Academic Press Inc), 315–322. doi: 10.1016/b978-0-12-372180-8.50042-1

Wicaksono, W. A., Jones, E. E., Monk, J., and Ridgway, H. J. (2017). Using bacterial endophytes from a New Zealand native medicinal plant for control of grapevine trunk diseases. *Biol. Control* 114, 65–72. doi: 10.1016/j.biocontrol.2017.08.003

Wightwick, A., Walters, R., Allinson, G., Reichman, S., and Menzies, N. (2010). *Environmental Risks of Fungicides Used in Horticultural Production Systems. Fungicides*. doi: 10.5772/13032 Available at: https://www.intechopen.com/books/fungicides/environmental-risks-of-fungicides-used-in-horticultural-production-systems doi: 10.1016/j.biocontrol.2017.08.003

Zabalgogeazcoa, I. (2008). Fungal endophytes and their interaction with plant pathogens. *Span. J. Agric. Res.* 6, 138–146. doi: 10.5424/sjar/200806S1-382

Conflict of Interest: The authors declare that the research was conducted in the absence of any commercial or financial relationships that could be construed as a potential conflict of interest.

frontiers in Microbiology

ORIGINAL RESEARCH
published: 10 February 2021
doi: 10.3389/fmicb.2021.623735

Proteome-Wide Analysis of Lysine 2-Hydroxyisobutyrylated Proteins in *Fusarium oxysporum*

*Hengwei Qian[1,2], Lulu Wang[1], Xianliang Ma[3], Xingling Yi[3], Baoshan Wang[2] and Wenxing Liang[1]**

[1] College of Plant Health and Medicine, Qingdao Agricultural University, Qingdao, China, [2] College of Life Sciences, Shandong Normal University, Jinan, China, [3] Micron Biotechnology Co., Ltd., Hangzhou, China

Protein lysine 2-hydroxyisobutyrylation (K_{hib}), a new type of post-translational modification, occurs in histones and non-histone proteins and plays an important role in almost all aspects of both eukaryotic and prokaryotic living cells. *Fusarium oxysporum*, a soil-borne fungal pathogen, can cause disease in more than 150 plants. However, little is currently known about the functions of K_{hib} in this plant pathogenic fungus. Here, we report a systematic analysis of 2-hydroxyisobutyrylated proteins in *F. oxysporum*. In this study, 3782 K_{hib} sites in 1299 proteins were identified in *F. oxysporum*. The bioinformatics analysis showed that 2-hydroxyisobutyrylated proteins are involved in different biological processes and functions and are located in diverse subcellular localizations. The enrichment analysis revealed that K_{hib} participates in a variety of pathways, including the ribosome, oxidative phosphorylation, and proteasome pathways. The protein interaction network analysis showed that 2-hydroxyisobutyrylated protein complexes are involved in diverse interactions. Notably, several 2-hydroxyisobutyrylated proteins, including three kinds of protein kinases, were involved in the virulence or conidiation of *F. oxysporum*, suggesting that K_{hib} plays regulatory roles in pathogenesis. Moreover, our study shows that there are different K_{hib} levels of *F. oxysporum* in conidial and mycelial stages. These findings provide evidence of K_{hib} in *F. oxysporum*, an important filamentous plant pathogenic fungus, and serve as a resource for further exploration of the potential functions of K_{hib} in *Fusarium* species and other filamentous pathogenic fungi.

Keywords: lysine 2-hydroxyisobutyrylation, post-translational modification, *Fusarium oxysporum*, proteomics, virulence

OPEN ACCESS

Edited by:
Amin Uddin Mridha, University of Chittagong, Bangladesh

Reviewed by:
Xiaogang Li, Nanjing Forestry University, China
Wei-Hua Tang, Institute of Plant Physiology and Ecology, Shanghai Institutes for Biological Sciences (CAS), China
Jianping Xie, Southwest University, China
Khaled Abbas El-Tarabily, United Arab Emirates University, United Arab Emirates

***Correspondence:**
Wenxing Liang
wliang1@qau.edu.cn

Specialty section:
This article was submitted to Microbe and Virus Interactions with Plants, a section of the journal Frontiers in Microbiology

Received: *30 October 2020*
Accepted: *21 January 2021*
Published: *10 February 2021*

Citation:
Qian H, Wang L, Ma X, Yi X, Wang B and Liang W (2021) Proteome-Wide Analysis of Lysine 2-Hydroxyisobutyrylated Proteins in Fusarium oxysporum. Front. Microbiol. 12:623735. doi: 10.3389/fmicb.2021.623735

INTRODUCTION

Post-translational modifications (PTMs) of proteins play key roles in diverse biological processes of cells and are dynamic and reversible modification reactions occurring during or after biosynthesis, including amino acid synthesis, protein interaction networks, and energy metabolism (Zhou et al., 2016; Liu et al., 2018a). In recent years, with the development of mass spectrometry (MS) (Huang et al., 2014), lysine (K) has been identified as a primary residue for PTMs, including crotonylation (K_{cr}), acetylation (K_{ac}), malonylation (K_{ma}), succinylation (K_{su}), methylation (K_{me}), butyrylation (K_{bu}), and glutarylation (K_{glu}), which were named lysine acylation (Chen et al., 2007;

Peng et al., 2011; Peach et al., 2012; Tan et al., 2014; Li D. et al., 2016; Li Y. et al., 2016; Zhang et al., 2017; Cheng et al., 2020). Several types of lysine acylation occur because lysine is an alkaline amino acid that contains an unstable ε-NH_2 side chain that can interact with diverse chemical groups (Xu et al., 2017). Many PTMs have been discovered to modulate chromatin packaging by changing the charge of lysine slide chains. In addition, PTMs may regulate enzyme activity or protein structure, further affecting protein functions (Huang et al., 2015).

Recently, lysine 2-hydroxyisobutyrylation (K_{hib}), a type of lysine modification, was discovered in histones and is conserved from yeast to humans (Dai et al., 2014; Huang et al., 2017, 2018). In a mass spectrometry analysis, the reporter indicated that K_{hib} has a mass shift of +86.03 Da because of the ε-NH_2 side chain of K_{hib} (Dai et al., 2014). Recently, K_{hib} was identified as a new histone mark in eukaryotic cells, and 63 K_{hib} sites on histone proteins have been identified by MS analysis and biochemical methods in humans and mice (Dai et al., 2014; Cheng et al., 2020). In this study, histone H4K8$_{hib}$ was found to regulate gene transcriptional activity and was a better indicator of high gene expression than H4K8$_{ac}$. In addition, K_{hib} exists in the N-termini of histone proteins and the main globular domain, but acetylation mainly occurs in the N-termini of histone proteins. Obviously, 2-hydroxyisobutyrylation structurally differs from acetylation (Dai et al., 2014; Cluntun et al., 2015). A proteome-wide analysis of K_{hib} in *Saccharomyces cerevisiae* identified 1458 K_{hib} sites on 369 histones and non-histone proteins, and a bioinformatics analysis showed that K_{hib} was enriched in the glycolysis/gluconeogenesis pathway. Interestingly, the histone H4K8$_{hib}$ was regulated by glucose homeostasis and influenced cell proliferation in *S. cerevisiae* (Huang et al., 2017). In prokaryotic cells, K_{hib} is widely distributed, and 4735 K_{hib} sites on 1051 proteins were identified in *Proteus mirabilis* by affinity enrichment with two-dimensional liquid chromatography (LC) separation and MS analysis. The most 2-hydroxyisobutyrylated proteins were involved in diverse biological processes based on the bioinformatics analysis; importantly, central metabolism enzymes were found to be 2-hydroxyisobutyrylated in *P. mirabilis* (Dong et al., 2018). In a study of developing rice seeds, which was the first report of K_{hib} in plant, 9916 K_{hib} sites on 2512 proteins were identified. Functional annotation analyses indicated that 2-hydroxyisobutyrylated lysine is essential for various biological processes, including the TCA cycle, starch biosynthesis, lipid metabolism, and protein biosynthesis (Meng et al., 2017). Using a specific antibody combined with LC-MS/MS, a total of 11 976 K_{hib} sites in 3001 proteins were found in *Physcomitrella patens*, an important plant model system used for physiological studies. A systematic analysis of K_{hib} sites in *P. patens* histone proteins demonstrated some conserved sites in histone H3 and H4 proteins and revealed unknown sites in histone H1, H2A, and H2B proteins (Vidali and Bezanilla, 2012; Yu et al., 2017).

Histone acetylation and deacetylation of lysine residues are reversible processes and are catalyzed by histone acetyltransferases (HATs) and histone deacetylases (HDACs), respectively (Lv et al., 2016). In addition to acetylation and deacetylation catalysis, HATs and HDACs can also catalyze other acylation or deacylation reactions such as 2-hydroxyisobutyrylation, implying that the functions of new acylations may be similar to or redundant with histone acetylation (Cheng et al., 2009; Sabari et al., 2015). The HAT Esa1p and its human homolog Tip60 could catalyze K_{hib} reaction *in vitro* and *in vivo* (Huang et al., 2018). In addition, the HDACs HDAC1, HDAC2, and HDAC3 function as reverse enzymes to remove K_{hib} in both *in vitro* and *in vivo* reactions in mammalian cells. The findings of K_{hib} transferase and de-2-hydroxyisobutyrylation enzymes greatly increase the knowledge of K_{hib} and expand the perspective of protein functions (Dai et al., 2014; Huang et al., 2017).

However, to date, no evidence of K_{hib} has been reported in filamentous plant pathogenic fungi. *Fusarium* species are the most diverse and widely dispersed filamentous plant pathogentic fungi in the world that causes the economic loss and reduces the crop yields. Some *Fusarium* species, such as *Fusarium graminearum*, *Fusarium asiaticum*, and *Fusarium verticillioides*, could infect the predominantly the cereals, but the *Fusarium oxysporum* has a broad host range (Ma et al., 2010; Alwahshi et al., 2019). *F. oxysporum* is a soil-borne phytopathogenic fungus that can cause root rot or wilting disease in more than 150 different plants, including tomato, potato, banana, melon, pine, and date palm (*Phoenix canariensis*) (Mohali, 1996; Pietro et al., 2003; Perez-Nadales and Di Pietro, 2011; Lan et al., 2020). At first, the conidia of *F. oxysporum* adhere to the surface of the host plant and then invade and colonize the roots, thereby absorbing nutrients and water, resulting in a reduction in plant growth or even plant cell death (Michielse and Rep, 2009; Rana et al., 2017). Individual *F. oxysporum* strains were defined as forma specialis (f. sp.) based on various hosts, for instance, *F. oxysporum* f. sp. *Lycopersici*, also called *Fol*, is a tomato pathogen (Kashiwa et al., 2016; Rana et al., 2017). K_{hib}, as a type of PTM, occurs on lysine residues and is expected to play important roles in biological processes and molecular functions in *F. oxysporum*. To test this hypothesis, we performed the first global analysis of K_{hib} in *F. oxysporum*. In total, 3782 K_{hib} sites in 1299 proteins were identified and involved in various biological processes. The results of a bioinformatics analysis showed that the 2-hydroxyisobutyrylated proteins were localized in multiple cellular compartments, including the cytoplasm, nucleus, mitochondria and plasma membrane, with diverse molecular functions. Importantly, we found that several 2-hydroxyisobutyrylated proteins play a regulatory role in the virulence or conidiation of *F. oxysporum*. This work provides insights into the lysine 2-hydroxyisobutyrylome in *F. oxysporum* and serves as a dataset for exploring the function of 2-hydroxyisobutyrylated proteins in this pathogen.

MATERIALS AND METHODS

Fungal Strain and Culture

The *F. oxysporum* f. sp. *lycopersici* strain 4287 was used in this study (Ma et al., 2010). The *F. oxysporum* was cultured in potato Dextrose agar (PDA) (Solarbio, Beijing, China) at 25°C for 3 days, and then was taken from the colony and transferred into PDB (Potato Dextrose Broth) medium to produce conidia.

The conidia were harvested and incubated in YEPD medium at 25°C with shaking at 180 rpm for 14 h. The harvested mycelia were immediately frozen in liquid nitrogen and stored at −80°C.

Protein Extraction and Trypsin Digestion

The mycelia were ground into powder in liquid nitrogen (Zhou et al., 2016; Liu et al., 2018a). Next, the powder sample was suspended in 5 mL lysis buffer containing 8 M urea, 1% Triton X-100, 65 mM dithiothreitol (DTT), 0.1% protease inhibitor cocktail, 50 mM nicotinamide, 2 mM EDTA, and 3 μM Trichostatin A (Solarbio, Beijing, China) and then sonicated for three times on ice using a high intensity ultrasonic processor (Scienta, Ningbo, China) (Lv et al., 2016). The cell debris was separated by centrifugation at 15 000 × *g* and 4°C for 15 min, and the proteins were precipitated with 15% cold TCA (Sigma, Darmstadt, Germany) at 4°C for 2 h. After centrifugation at 4°C for 15 min, the supernatant was discarded, and the remaining protein was washed three times with cold acetone (Yuandong, Yantai, China). Finally, the target protein was redissolved in 8 M urea supplemented with 100 mM $(NH_4)_2CO_3$ (PH 8.0) and the protein concentration was determined with 2-D Quant kit (GE, Fairfield, CT, United States) according to the manufacturer's instructions. The protein solution was reduced with 5 mM DTT (Solarbio, Beijing, China) at 37°C for 1 h and alkylated with 30 mM iodoacetamide (IAA) (Solarbio, Beijing, China) for 45 min at 25°C in darkness. For digestion, the protein was diluted with 100 mM $(NH_4)_2CO_3$ to reduce urea concentration. Trypsin (Thermo Fisher Scientific, Waltham, MA, United States) was added into the reaction overnight at 1:50 trypsin-to-protein mass ratio (Liu et al., 2018b). In order to ensure digested completely, trypsin was added again into reaction at 1:100 trypsin-to-protein mass ratio and the mixture reaction was incubated for other 4 h.

HPLC Fractionation

The sample was separated into fractions by high pH reverse-phase HPLC (Shimadzu, Kyoto, Japan) using Agilent 300 Extend C18 column (5 μM particles, 4.6 mm ID, and 250 mm length). The peptides were separated firstly into 80 fractions with a gradient of 2 to 60% acetonitrile (Solarbio, Beijing, China) in 10 mM $(NH_4)_2CO_3$ (pH 10.0). Then, the peptides were combined into eight fractions and dried by vacuum centrifuging (Meng et al., 2017; Yin et al., 2019).

Affinity Enrichment of Lysine 2-Hydroxyisobutyrylated Peptides

For K_{hib} peptides enrichment, the tryptic peptides were dissolved in NETN buffer (50 mM Tris–HCl, 100 mM NaCl, 1 mM EDTA, 0.5% NP-40, pH 8.0) and then separated into several fractions. Each fraction was incubated with pre-washed agarose beads conjugated with 2-hydroxyisobutyryllysine antibody (PTM-801) (PTM Biolabs, Hangzhou, China) overnight at 4°C with gentle shaking. Then the beads were washed three times with NETN buffer and twice with cold ddH_2O. The K_{hib} peptides bound to the beads were eluted with 0.1% trifluoroacetic acid (TFA) and then rinsed with C18 Zip Tips (Millipore, Burlington, MA, United States).

LC-MS/MS Analysis

The K_{hib} peptides were reconstituted in 0.1% formic acid (FA) and loaded on a reversed-phase pre-column (Acclaim PepMap 100 C18 column) (Thermo Fisher Scientific, Waltham, MA, United States), and then separated using a reversed-phase analytical column (Acclaim PepMap RSLC C18 column) (Thermo Fisher Scientific, Waltham, MA, United States) on UPLC system. The gradient was composed of an increase from 2 to 10% solvent (0.1% formic acid in 98% acetonitrile) for 6 min, 10 to 20% for 45 min, 20% climbing to 80% in 7 min and then holding at 80% at least for 4 min, all maintaining a flow rate of 250 nl/min. The peptides were subjected to ESI/NSI sources followed by MS/MS in Q ExactiveTM Plus (Thermo Fisher Scientific, Waltham, MA, United States) coupled online to UPLC. Whole peptides and ion fragments were detected in the Orbitrap at a resolution of 70 000 and 17 500, respectively, with NCE setting at 30. The electrospray voltage was set at 2.0 kV to analyze. In order to generate MS/MS spectra, the automatic gain control (AGC) was used to prevent overfilling of the ion trap. The m/z range was from 350 to 1800 for MS scans. The MS fixed first mass was set at 100 m/z.

Database Cearch

MaxQuant integrated with Andromeda search engine (v.1.5.1.8) was used to analyze the raw data of MS/MS. The tandem mass spectra collected were searched against UniProt *F. oxysporum* f. sp. *lycopersici* database (17 735 sequences) concatenated with reverse decoy database. Mass errors of precursor and fragment ions were set as 10 ppm and 0.02 Da, respectively. Trypsin/P was specified as cleavage enzyme allowing up to four missing cleavage, five modifications per peptide and five charges. Carbamidomethylation on Cysteine was specified as fixed modification. Oxidation of methionine and 2-hydroxyisobutyrylation both on lysine and protein N-terminal were fixed as variable modifications. The minimal peptide was set to seven, and the false discovery rate (FDR) threshold for modification sites and peptides were set as 1%. The K_{hib} site localization probability of <0.75 was excluded.

Bioinformatics Analysis

Gene ontology (GO) of 2-hydroxyisobutyrylation proteome was derived from the UniProt-GOA database[1]. Firstly, converting the identified protein ID to UniProt ID and then mapping to GO IDs by protein ID. If the identified proteins were not annotated by UniProt-GOA database, the InterProScan soft would be used to annotate protein's GO functional based on protein sequence alignment method (Jiao et al., 2012). Then proteins were classified by GO annotation based on three categories: biological process, cellular component, and molecular function. The software WoLF PSORT was used to predict the subcellular localization of the 2-hydroxyisobutyrylated proteins. Protein secondary structures (α-helix, β-strand, and coil) were analyzed by the online tool NetSurfP (Klausen et al., 2019). Soft MoMo (motif-x algorithm) was used to analyze the sequences model of 2-hydroxyisobutyrylated proteins

[1]http://www.ebi.ac.uk/GOA/

constituted with amino acids in specific positions of modify-21-mers (10 amino acids upstream and downstream of the site) in all protein sequences (Chou and Schwartz, 2011). Minimum number of occurrences was set to 20. To define the evolutionary conservation of 2-hydroxyisobutyrylation, the BLASTP was used to compare the 2-hydroxyisobutyrylated protein sequences of *F. oxysporum* with *Homo sapiens*, *P. patens*, *Oryza sativa*, *S. Cerevisiae*, and *Toxoplasma gondii*. InterProScan was used to annotate functional description of protein domains based on protein sequences alignment method and the InterPro domain database[2]. Kyoto Encyclopedia of Genes and Genomes (KEGG) database was used to annotate protein pathway description. A two-tailed Fisher's exact test was used to verify the enrichment of lysine 2-hydroxyisobutyrylated proteins against all database proteins. The protein–protein interaction networks for the 2-hydroxyisobutyrylated proteins were analyzed by using STRING database and visualized in Cytoscape. All projects with a corrected p-value < 0.05 is considered significant.

Generation of the FoFGB1-GFP Strains of *F. oxysporum* and Western Blot Analysis

The coding domain sequence (CDS) of *FoFGB1* was cloned into pYF11-GFP overexpression vector to construct FoFGB1-GFP strains using protoplast transformation of *F. oxysporum*. Total proteins were extracted from conidia and mycelia using lysis buffer (25 mM Tris–HCl pH 8.0, 150 mM NaCl, 0.5 mM EDTA, 0.5% NP-40, 0.5% Triton X-100, 5% glycerol). The protein concentration was determined by BCA protein assay kit (PC0020) (Solarbio, Beijing, China) using BSA as the protein standard. To purify the fusion protein FoFGB1-GFP, 5 mg of total protein was incubated with 25 μL (bead volume) of anti-GFP agarose beads (KT, Shenzhen, China) according the manufacturer's instructions at 4°C for 3 h. After centrifugation, the beads were washed three times with 1 mL washing buffer (50 mM Tris–HCl pH 7.5, 150 mM NaCl, 0.5 mM EDTA), and the target proteins were eluted completely. The proteins were separated on 12% SDS-PAGE and subjected to immunoblotting using anti-K_{hib} (1:5 000 dilution) (PTM-801) (PTM Biolabs, Hangzhou, China) and anti-GFP antibodies (1:10 000 dilution) (ab290) (Abcam, Cambridgeshire, United Kingdom), respectively.

RESULTS

Identification of Lysine 2-Hydroxyisobutyrylated Proteins in *F. oxysporum*

Three repeated experiments for identifying 2-hydroxyisobutyrylated proteins and sites were carried out by using a specific antibody and LC-MS/MS analysis, resulting in 5917 sites in 1616 proteins, 6047 sites in 1653 proteins and 5931 sites in 1648 proteins (**Supplementary Table 1**), respectively. In total, 3782 lysine 2-hydroxyisobutyrylated sites in 1299 proteins were identified from all three replicates (**Supplementary Figure 1B** and **Supplementary Table 2**), which account for 7.3% (1299/17 735) of total proteins in *F. oxysporum*. The number of identified 2-hydroxyisobutyrylated proteins in *F. oxysporum* was less than that in rice seed (*O. sativa*) (Meng et al., 2017) and *P. patens* (Yu et al., 2017) but more than that in *S. cerevisiae* (Huang et al., 2017) and *P. mirabilis* (Dong et al., 2018). Together with the identification of 2-hydroxyisobutyrylated proteins in other species, K_{hib} is suggested to be a widespread PTM, and this research is the first to report K_{hib} in *F. oxysporum*.

Analysis of 2-Hydroxyisobutyrylated Sites

To understand the distribution of 2-hydroxyisobutyrylated sites, the number of modified sites in each identified protein was calculated in *F. oxysporum*. The result shows that each protein has one or more modified sites, as shown in **Figure 1A**. From the results, we found that 43.6% of the 2-hydroxyisobutyrylated proteins have only one 2-hydroxyisobutyrylated site and that 56.4% of them contain two or more modified sites.

To determine the relationship between K_{hib} and the protein structure in *F. oxysporum*, an analysis of the secondary structure of 2-hydroxyisobutyrylated proteins was performed using the NetSurfP program. The results showed that approximately 34.8% of 2-hydroxyisobutyrylated sites were located in regions with ordered secondary structure, including 28.4% of them located in alpha-helices and 6.4% in beta-strands; however, the 65.2% of 2-hydroxyisobutyrylated sites were distributed in disordered and random coil regions. Furthermore, 2-hydroxyisobutyrylated sites tended to be located in disordered regions when comparing the similarity of the distribution pattern between 2-hydroxyisobutyrylated lysines and all lysines in *F. oxysporum* proteins (**Figure 1B**), and this result was similar to that from a previous study (Meng et al., 2017). It is suggested that modified 2-hydroxyisobutyrylated lysines are easily located in a folded polypeptide chain because of the flexibility of the disordered regions, and this distribution pattern is similar to that found in *O. sativa*. In addition, the results of the surface accessibility of 2-hydroxyisobutyrylated lysine showed that 36.23% of the modified lysine sites and 37.56% of all residues were exposed to the protein surface (**Figure 1C**), indicating that K_{hib} could slightly affect the surface accessibility of 2-hydroxyisobutyrylated proteins in *F. oxysporum*.

To better identify the amino acid sequences around the 2-hydroxyisobutyrylated lysine sites in *F. oxysporum*, the frequency of motifs in all identified K_{hib} peptides were examined by the Motif-x tool. A total of 12 motifs were identified from 2820 K_{hib} peptides, which contain sequences from the −10 to +10 position around the 2-hydroxyisobutyrylated lysine (**Figure 2A**). The different motifs exhibited diverse proportions, and the EK_{hib}, KK_{hib}, and $K_{hib}E$ motifs had large proportions. There were 481, 381, and 344 K_{hib} peptides with these motifs, accounting for 17.1, 13.5, and 12.2% of all K_{hib} peptides, respectively (**Figure 2B**). From the results, we can learn that the amino acids with negatively charged side chains, aspartic acid (D), and glutamic

[2]http://www.ebi.ac.uk/interpro/

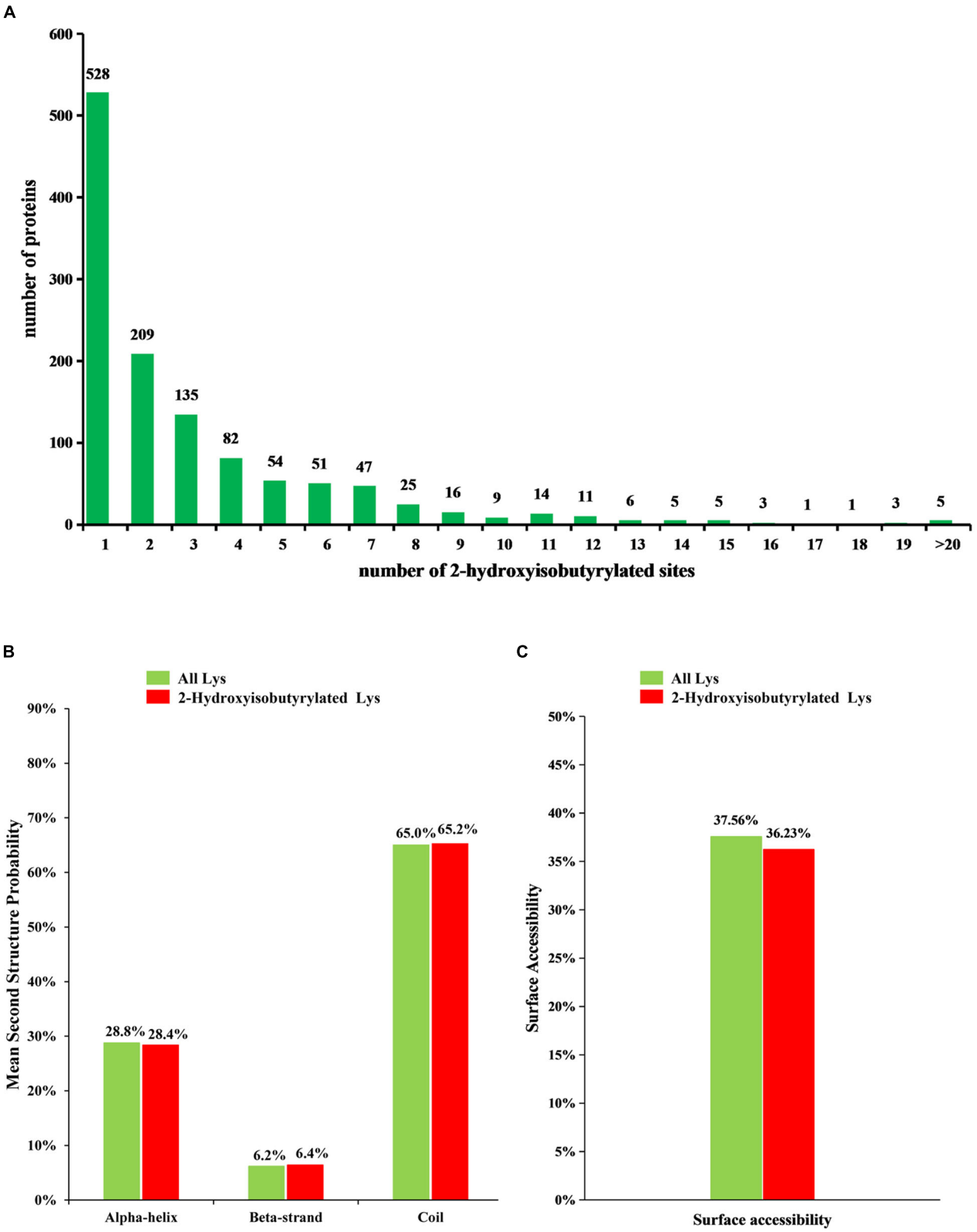

FIGURE 1 | Analysis of 2-hydroxyisobutyrylated sites in *Fusarium oxysporum*. **(A)** Distribution of K_{hib} sites in the 2-hydroxyisobutyrylated proteins. The *x*-axis indicates the number of K_{hib} sites in protein, whereas the *y*-axis means the proteins number which containing the K_{hib} sites. **(B)** Probabilities of lysine 2-hydroxyisobutyrylation in different protein secondary structures (alpha-helix, beta-strand and coil). **(C)** Predicted surface accessibility of 2-hydroxyisobutyrylated lysine was compared with all lysine in *F. oxysporum*.

acid (E), have a high tendency to be located around the 2-hydroxyisobutyrylated lysine sites. Consistent with this finding, the motifs EK_{hib}, $K_{hib}E$, and DK_{hib} were also found in other species, including rice, indicating that K_{hib} is a conserved PTM in different species. As shown in the heat map of the amino acid compositions around the 2-hydroxyisobutyrylated sites, the frequencies of arginine (R) at positions −4 to −1 and S (serine) at positions −10 to +10 were the lowest. In addition to D and E, lysine (K) at the −10 to −5 and +4 to +10 positions, valine (V) at the +3 positions and glycine (G) at the −1 position were preferred sites for K_{hib} (**Figure 2C** and **Supplementary Table 3**).

Conservation Analysis of 2-Hydroxyisobutyrylated Proteins

In this report, using BLASTP, the orthologous 2-hydroxyisobutyrylated protein sequences in *F. oxysporum* were searched against five organisms: *H. sapiens*, *P. patens*, *O. sativa*, *S. cerevisiae*, and *T. gondii*. In total, 2799 orthologs of the 2-hydroxyisobutyrylated proteins in *F. oxysporum* were identified in these five organisms (**Figure 3A** and **Supplementary Table 4**). The results showed that 839 2-hydroxyisobutyrylated proteins have orthologs in *T. gondii*, *S. cerevisiae*, *P. patens*, *O. sativa*, and *H. sapiens* and that the numbers of proteins were 503, 564, 596, 565, and 571, respectively, accounting for 69.3% (839/1210) of the total 2-hydroxyisobutyrylated proteins in *F. oxysporum*. **Figure 3B** shows the conservation of 2-hydroxyisobutyrylated proteins in *F. oxysporum* depending on the number of orthologous proteins in the other five organisms. The pie chart shows that the proportion of completely conserved proteins (with orthologs in all five organisms) was 23.0% (278/1210 proteins). Well-conserved proteins (with orthologs in four organisms) accounted for 13.0% (157/1210 proteins); conserved proteins (with orthologs in three organisms) and poorly conserved proteins (with orthologs in 1 to 2 organisms) accounted for 10.6% (128/1210 proteins) and 22.8% (276/1210 proteins), respectively. In addition, the percentage of novel proteins was 30.7% (371/1210 proteins), these 2-hydroxyisobutyrylated proteins in *F. oxysporum* did not have an ortholog in any of the other five organisms. According to these results, we found that K_{hib} is widely conserved in prokaryotes and eukaryotes, but unique 2-hydroxyisobutyrylated proteins are observed in different organisms or species.

Function Classification and Subcellular Location Analysis of 2-Hydroxyisobutyrylated Proteins in *F. oxysporum*

To further explore the function of K_{hib} in *F. oxysporum*, we performed a GO-term classification analysis of all identified 2-hydroxyisobutyrylated proteins according to their biological process, molecular function and cellular component. The results of the GO analysis of the 2-hydroxyisobutyrylome indicated that the 2-hydroxyisobutyrylated proteins have a large range of biological processes, molecular functions and cellular components (**Supplementary Table 5**). Based on the biological process analysis, the most modified proteins were associated with cellular metabolism (13%) and organic substance metabolism (13%) processes (**Figure 4A**). According to the molecular function classification analysis, the most 2-hydroxyisobutyrylated proteins were involved in organic cyclic compound and heterocyclic compound binding, accounting for 16 and 15% of all 2-hydroxyisobutyrylated proteins, respectively (**Figure 4B**). As shown in **Figure 4C**, the results of the cellular component analysis revealed that the most 2-hydroxyisobutyrylated proteins were distributed in intracellular space (21%), intracellular organelles (18%), and membrane-bounded organelles (16%). These GO functional classification results suggest that K_{hib} may be related to the diverse molecular functions of modified proteins and may control the different biological processes in diverse cellular components in *F. oxysporum*.

Based on the subcellular localization prediction analysis of the 2-hydroxyisobutyrylated proteins in *F. oxysporum*, most proteins were located in the cytoplasm (32.89%) and mitochondria (23.88%) (**Figure 4D**). Importantly, 27.27% of the 2-hydroxyisobutyrylated proteins were located in the nucleus, and these included histone H3, H2A, H2B, and H4 (**Supplementary Table 6**), revealing the key PTMs role of K_{hib}. In addition, other 2-hydroxyisobutyrylated proteins were located in both the cytoplasm and nucleus (5.79%), in the extracellular space (3.29%) and in the plasma membrane (3.22%). A very small percentage of 2-hydroxyisobutyrylated proteins were predicted to localize in the cytoskeleton (2.23%) and other locations (0.74%). These results suggest that 2-hydroxyisobutyrylated proteins have a widespread distribution in *F. oxysporum*.

Functional Enrichment Analysis

Gene ontology (biological processes, molecular functions, and cellular components), KEGG pathway and protein domain enrichment analyses were performed to further understand the characteristics of 2-hydroxyisobutyrylated proteins in *F. oxysporum*. In the biological processes category, a large number of 2-hydroxyisobutyrylated proteins were mainly enriched in cytoplasmic translation, metabolic and biosynthetic processes, indicating that 2-hydroxyisobutyrylated proteins may have a potential function in protein biosynthesis and processing (**Figure 5A** and **Supplementary Tables 7–9**). Consistent with these findings, an enrichment analysis of the molecular functions suggested that these modified proteins were mainly involved in the structural constituent of ribosomes and in binding and translation activities. In the cellular compound enrichment analysis, most of the proteins were enriched in the cytosol and ribosome.

The KEGG pathway enrichment analysis revealed that most 2-hydroxyisobutyrylated proteins were significantly enriched in 13 pathways. In agreement with the GO enrichment analysis, the ribosome pathway (map03010), which is a highly conserved pathway, was the significantly enriched pathway, suggesting an important role of K_{hib} in protein biosynthesis. Remarkably, several energy production-related pathways were also enriched, and these included oxidative phosphorylation (map00190), the TCA cycle (map00020) and 2-oxocarboxylic acid metabolism

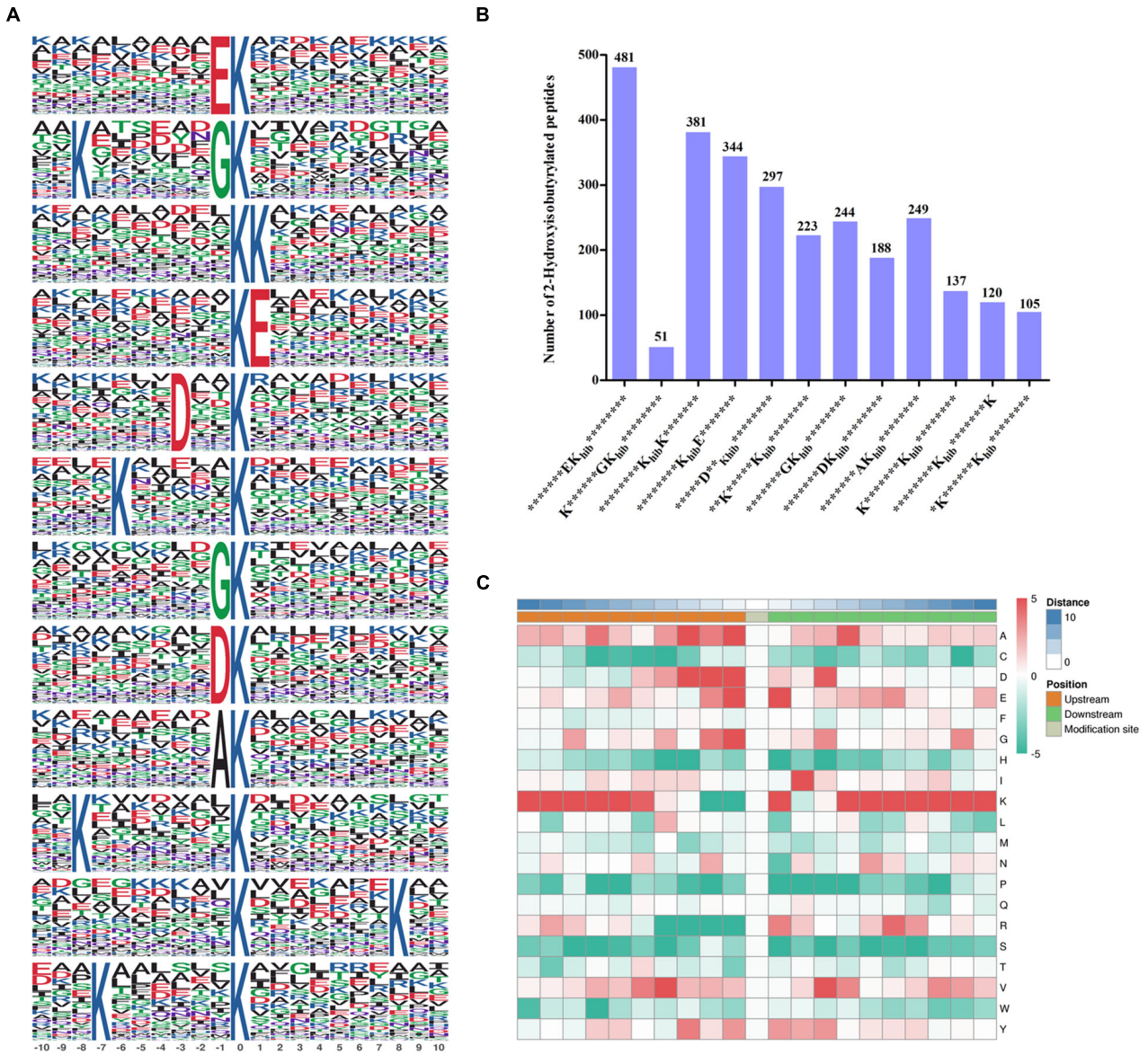

FIGURE 2 | Properties of 2-hydroxyisobutyrylated peptides in *Fusarium oxysporum*. **(A)** 2-hydroxyisobutyrylated motifs and conserved motifs around the 2-hydroxyisobutyrylated sites. **(B)** Frequency of identified 2-hydroxyisobutyrylated peptides in each motif. The ordinate indicates the number of conserved motifs in *x*-axis and the numbers of peptides in different motifs were displayed on top of the columns. K_{hib} represents 2-hydroxyisobutyrylated lysine, and * represents a random amino acid residue. **(C)** Heat map of the amino acid compositions of the 2-hydroxyisobutyrylated sites. The middle square represents the K_{hib} sites, left and right squares represent the upstream and downstream residues of K_{hib} sites, respectively. The red indicates high frequency and green indicates low frequency.

(map012102). Based on the pathway enrichment analysis, the 2-hydroxyisobutyrylated proteins of *S. cerevisiae* were also enriched in the ribosome pathway and some metabolic pathways, and these results are consistent with findings in this study (**Figure 5C** and **Supplementary Table 10**).

The enrichment analysis of the protein domain demonstrated that the proteasome subunit, RNA polymerase Rpb2, elongation factor Tu GTP-binding and LSM domains were all enriched and tended to be 2-hydroxyisobutyrylated in *F. oxysporum* proteins (**Figure 5B** and **Supplementary Table 11**). Taken together, these results showed that 2-hydroxyisobutyrylated proteins are widely distributed in cells and associated with diverse pathways, suggesting that K_{hib} plays an important role in cell metabolism and amino acid biosynthesis.

Protein–Protein Interaction Network of 2-Hydroxyisobutyrylated Proteins in *F. oxysporum*

To further investigate the cellular processes regulated by K_{hib} in *F. oxysporum*, the protein–protein interaction network was established using the STRING database. The interaction

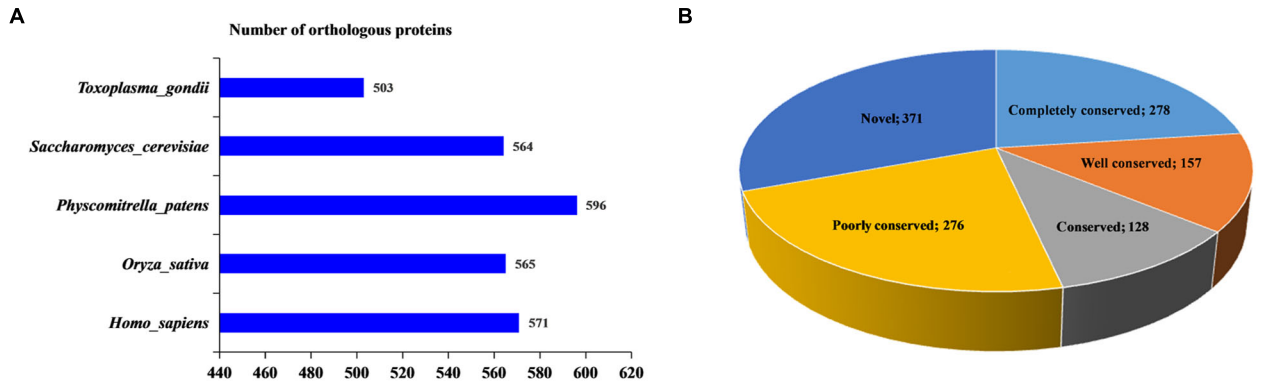

FIGURE 3 | Conservation analysis of 2-hydroxyisobutyrylated proteins in *Fusarium oxysporum* compared with other species. **(A)** Number of orthologous 2-hydroxyisobutyrylated proteins in *Homo sapiens*, *Physcomitrella patens*, *Oryza sativa*, *Saccharomyces cerevisiae*, and *Toxoplasma gondii* with their reported 2-hydroxyisobutyrylomes. The horizontal axis represents the number of orthologous proteins in the species. **(B)** A pie chart of conservation of 2-hydroxyisobutyrylated proteins in five organisms. Grouping was performed as follows: Completely conserved, 5 orthologs; Well conserved, 4 orthologs; Conserved, 3 orthologs; Poorly conserved, 1 to 2 orthologs; and Novel, 0 orthologs.

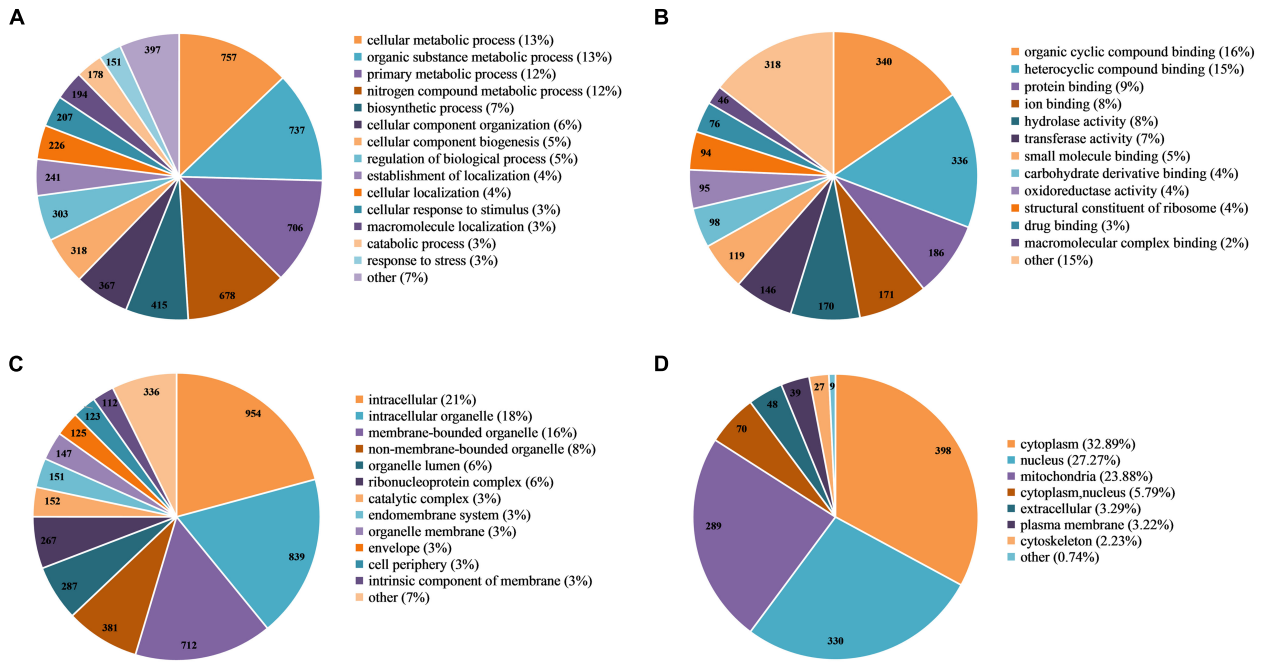

FIGURE 4 | Functional classification of 2-hydroxyisobutyrylated proteins in *Fusarium oxysporum*. **(A)** Classification of the 2-hydroxyisobutyrylated proteins according to biological process. **(B)** Classification of the 2-hydroxyisobutyrylated proteins according to molecular function. **(C)** Classification of the 2-hydroxyisobutyrylated proteins according to cellular component. **(D)** Subcellular localization of the 2-hydroxyisobutyrylated proteins in *F. oxysporum*.

network from STRING was visualized in the Cytoscape program (**Supplementary Table 12**). The results showed that 325 2-hydroxyisobutyrylated proteins were mapped to the protein–protein interaction network, which presents how protein 2-hydroxyisobutyrylation performs diverse pathways in *F. oxysporum*. According to the Cytoscape program, nine highly interconnected clusters of 2-hydroxyisobutyrylated proteins were retrieved, and the top five identified clusters (clusters 1–5) included proteins associated with ribosome, ribosome biogenesis in eukaryotes, proteasome, nucleosome core, and spliceosome (**Figure 6** and **Supplementary Figure 2**). The greater the degree is, the more proteins it interacts with, revealing that the protein is more important in the interaction network. The protein–protein interaction network demonstrated that K_{hib} was related to the ribosome, proteasome, and spliceosome and regulated a variety of pathways in *F. oxysporum*.

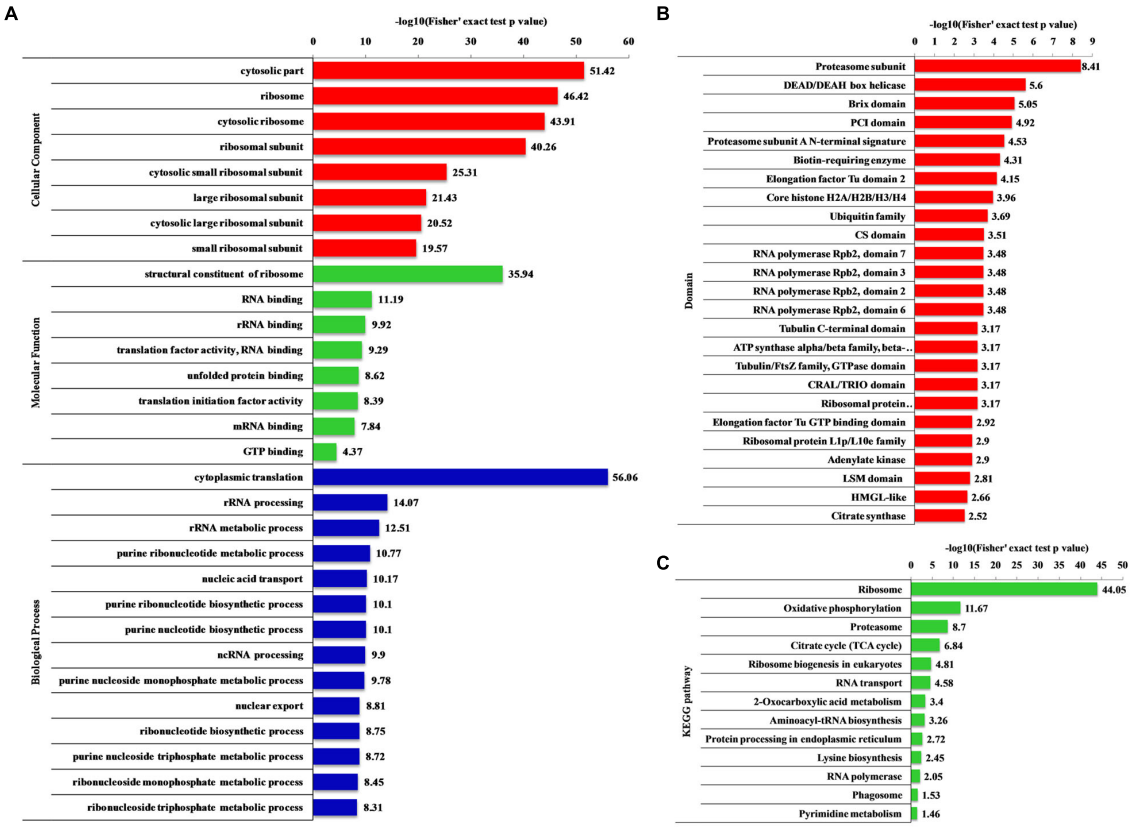

FIGURE 5 | Enrichment analysis of the 2-hydroxyisobutyrylated proteins in *Fusarium oxysporum*. **(A)** GO-based enrichment analysis in terms of biological process (blue), molecular function (green) and cell component (red). **(B)** Domain-based enrichment analysis of the 2-hydroxyisobutyrylated proteins. **(C)** KEGG pathway-based enrichment analysis of the 2-hydroxyisobutyrylated proteins. The value of –log10 (Fisher's test *p* value) is shown on right of the columns.

Analysis of 2-Hydroxyisobutyrylated Proteins Involved in Virulence and Conidiation in *F. oxysporum*

In this study, we found that several 2-hydroxyisobutyrylated proteins were involved in the virulence and conidiation of *F. oxysporum* (**Table 1**), including a G protein beta subunit (FoFGB1), which was implicated in cell growth, conidiation, and virulence (Jain et al., 2003). Among these identified proteins, FoFmk1 and FoHog1, two MAP kinase signaling proteins, are critical for the virulence of *F. oxysporum* (Pareek and Rajam, 2017). In addition, the GTP-binding protein FoRho1, a key enzyme for cell wall biosynthesis, was also found to be 2-hydroxyisobutyrylated and contains four 2-hydroxyisobutyrylated sites (Martinez-Rocha et al., 2008). FoPtc1, a serine/threonine phosphatase, regulates phosphorylation of the high osmolarity glycerol response (HOG) pathway in response to osmotic stress and is involved in conidiation (Lemos et al., 2018). It was also found that K_{hib} occurs in the two-component histidine kinase Fhk1, which is associated with the virulence-related function in *F. oxysporum* (Rispail and Di Pietro, 2010). In conclusion, these results reveal that K_{hib} plays an important role in virulence and conidiation in *F. oxysporum*.

The K_{hib} Levels in Conidia and Mycelia of *F. oxysporum*

To determine the differences in K_{hib} levels in various growth stages of *F. oxysporum*, we carried out immunoblotting of 2-hydroxyisobutyrylated proteins in conidia and mycelia. As shown in **Figure 7A**, a large number of protein bands were observed, and the K_{hib} level in mycelia of *F. oxysporum* was higher than that in conidia. Remarkably, the K_{hib} level of FoFGB1 was also higher in mycelia than in conidia (**Figure 7B**). These results suggested that K_{hib} occurred in various growth stages in *F. oxysporum*, but the level was higher in the vegetative growth stage. It is worthwhile characterizing the functions and mechanisms of the 2-hydroxyisobutyrylated proteins in different growth stages in future research.

DISCUSSION

Lysine 2-hydroxyisobutyrylation is one of the most common PTMs in both prokaryotes and eukaryotes, which play key roles in diversified biological processes with multiple functions. First, K_{hib} was found in mouse and human histone proteins (Dai et al., 2014; Cheng et al., 2020), and then in *P. patens*

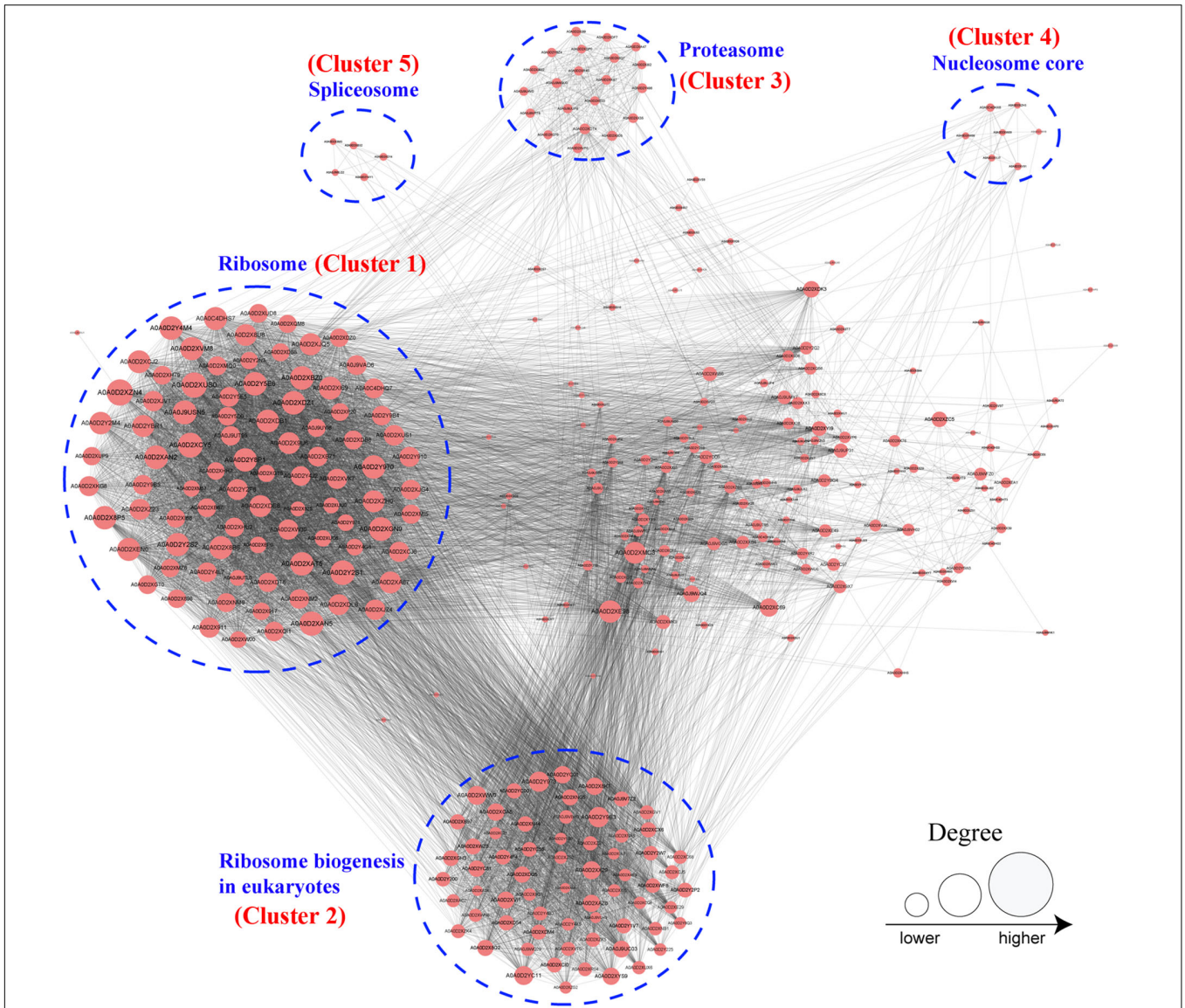

FIGURE 6 | Analysis of protein–protein interaction networks of the 2-hydroxyisobutyrylated proteins in *Fusarium oxysporum*. The top five clusters were shown in blue dotted circle. And the size of the circle indicated number of 2-hydroxyisobutyrylated sites.

TABLE 1 | The 2-hydroxyisobutyrylated proteins involved in virulence and conidiation of *Fusarium oxysporum*.

Protein	Gene name	Annotation	Positions	Function	References
FoFGB1	FOXG_11532	G protein beta subunit	36	Virulence, conidiation	Jain et al., 2003
FoFmk1	FOXG_08140	CMGC/MAPK protein kinase	193	Virulence	Pareek and Rajam, 2017
FoHog1	FOXG_06318	Mitogen-activated protein kinase	49, 285	Virulence	Pareek and Rajam, 2017
FoRho1	FOXG_13835	GTP-binding protein rhoA	126, 137, 155, 162	Virulence	Martinez-Rocha et al., 2008
FoPtc1	FOXG_11525	Protein phosphatase	356	Conidiation	Lemos et al., 2018
FoFhk1	FOXG_01684	Two-component histidine kinase	602	Virulence	Rispail and Di Pietro, 2010

(Yu et al., 2017) and rice (Meng et al., 2017) on both histones and non-histones. Although the K_{hib} is widely distributed in different species, knowledge about this modification in filamentous fungi is still limited.

In this study, we determined the K_{hib} sites in *F. oxysporum* using a specific antibody and high-resolution LC-MS/MS analysis (**Supplementary Figure 1A**) and a total of 3782 K_{hib} sites in 1299 proteins were identified, accounting for about 7% of

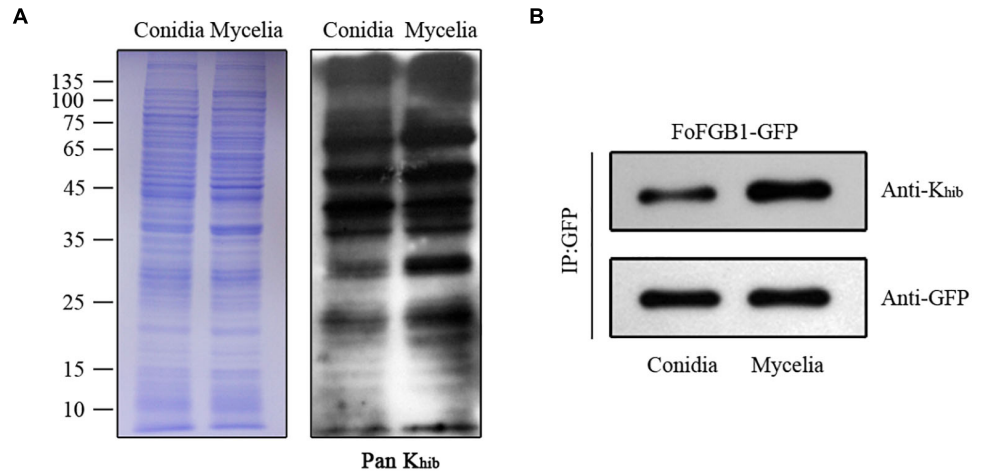

FIGURE 7 | The K_{hib} levels of *Fusarium oxysporum* in conidial and mycelial stages. **(A)**. Immunoblot analysis of 2-hydroxyisobutyrylated proteins with pan anti-K_{hib} antibody of *F. oxysporum* in conidial and mycelial stages. The loading control by coomassie blue staining was used to ensure that equal amounts of protein were loaded in each lane. **(B)** The FoFGB1-GFP was immunoprecipitated by anti-GFP beads. Anti-GFP and anti-K_{hib} antibodies were used to detect FoFGB1-GFP and its K_{hib} level, respectively.

the *F. oxysporum* proteome. And the western blot assay also suggested that the K_{hib} was occurred in *F. oxysporum* (**Figure 7**). Most proteins contain one K_{hib} site, accounting for 43.6% of all 2-hydroxyisobutyrylated proteins, and the sites were distributed in different protein secondary structures in *F. oxysporum* (**Figure 1**). In addition, the identification of several particular amino acid motifs near K_{hib} sites by bioinformatics analysis indicated the substrate preference of K_{hib} in *F. oxysporum*. For example, the amino acids D (Aspartic acid) and E (Glutamic acid), which containing the negatively charged side chains, showed a strong bias around the positions of K_{hib} in *F. oxysporum* (**Figure 2**). In the rice seed, the amino acids D and E have a trendency to be located around the K_{hib} sites (Meng et al., 2017). The negative charge amino acids, D and E, were also strongly preferred around the 2-hydroxyisobutyrylated sites in the *P. patens* (Vidali and Bezanilla, 2012). These results indicated that the position of lysine and the amino acid around the site plays important roles in K_{hib} modification.

In order to confirm the conservation of the K_{hib}, we have searched against the five organisms with 2-hydroxyisobutyrylated protein sequences in *F. oxysporum*, the results showed that the K_{hib} is distributed widely and conserved in a variety of organisms. Furthermore, the protein–protein interaction network analysis suggested that a large range of protein interactions were regulated by K_{hib}. Functional classification analysis showed that 2-hydroxyisobutyrylated proteins were distributed in almost all part of cellular component and involved in various biological processes in *F. oxysporum* (**Figure 4**). GO and KEGG pathway enrichment analyses showed that most 2-hydroxyisobutyrylated proteins were involved in the ribosome and oxidative phosphorylation pathways (**Supplementary Figure 3**), which are critical in living organisms or cells. It is suggested that the K_{hib} was related to multiple biological processes and molecular functions in *F. oxysporum*.

Lysine 2-hydroxyisobutyrylation levels were both highly abundant in conidia and mycelia of *F. oxysporum*, but differences still occurred in the two different growth stages. The results of a comparison of conidia and mycelia indicated that most 2-hydroxyisobutyrylated proteins and sites were specific for each stage. The K_{hib} level in the mycelial stage was higher than that in the conidial stage, and the different concentrations of substrate and 2-hydroxyisobutyryl-CoA in different stages may contribute to difference in K_{hib} abundance. To elucidate whether the different K_{hib} levels in the two stages were due to differences in protein abundance, FoFGB1 (with GFP tag), a G protein beta subunit that is important in development and conidia formation, was extracted and purified from conidia and mycelia. **Figure 7B** shows that the K_{hib} level of FoFGB1 was highly significant in the mycelial stage and was not associated with protein abundance. In *Trichophyton rubrum*, the concentration of propionyl-CoA affects the differences in propionylation levels in the conidial and mycelial stages (Xu et al., 2019). In *F. oxysporum*, the concentration of 2-hydroxyisobutyryl-CoA may contribute to the different K_{hib} levels between the conidial and mycelial stages.

When fungal pathogens invade host plant tissues, the maintenance of the cell wall integrity is essential for the host root penetration and virulence (Di Pietro et al., 2001; Li et al., 2014). Moreover, several proteins related to the cell wall integrity and virulence of *F. oxysporum* was found to be 2-hydroxyisobutyrylated in this study. Rho-type GTPases could control the expression of cell wall biosynthesis genes through signaling pathways (Levin, 2005). FoRhoI, containing four K_{hib} sites, function as cell wall biosynthesis, and the absence of the gene could reduce the virulence of *F. oxysporum* (**Table 1**; Martinez-Rocha et al., 2008). In some plant fungal pathogens, such as *Botrytis cinerea* (Zheng et al., 2000), *Colletotrichum lagenarium* (Takano et al., 2000), and *Claviceps purpurea* (Mey et al., 2002), the genes of mitogen-activated

protein kinase (MAPK) pathway are essential for pathogenicity (Hamel et al., 2012). In this study, we identified several 2-hydroxyisobutyrylated proteins related to the virulence of *F. oxysporum*, including two components of the MAPK pathway: FoFmk1 (K193) and FoHog1 (K49, K285) (Pareek and Rajam, 2017). In the previous research, the deletion of the *fmk1* gene resulted in loss of virulence in tomato plants but no significant difference in conidiation. These results indicated that K_{hib} of FoFmk1 may play a key role in virulence of *F. oxysporum*. In addition, the phosphatase Ptc1, which contains one K_{hib} site in *F. oxysporum*, responses to stress depend on the regulation of two MAPK pathways (Lemos et al., 2018). Apart from the abovementioned 2-hydroxyisobutyrylated protein, there are other identified proteins were enriched in the MAPK pathway (**Supplementary Table 10**). Although additional experiments are needed to explain the relationship between K_{hib} and the biological functions of *F. oxysporum*, these findings provide some clues and ideas for the exploration of K_{hib}.

Acyltransferases and deacylases regulate the reversible rection of each PTM *in vivo*, such as KATs and KDACs, which are responsible for acetylation. KATs could transfer the acetyl group to the lysine residue and KDACs have the ability to remove the acetyl group from lysine (Lv et al., 2016). Recent studies have shown that KATs and KDACs have the same function on 2-hydroxyisobutyrylation as acetylation, and KATs can catale the K_{hib} and KDACs to remove K_{hib}. In budding yeast, *S. cerevisiae* and humans (Sapountzi et al., 2006), HAT has K_{hib} transferase activity both *in vitro* and *in vivo*. HDAC2 and HDAC3 can catalyze de-2-hydroxyisobutyrylation reactions *in vitro* and *in vivo* in mammalian cells (Huang et al., 2018). Further studies are needed to verify the acyltransferases and deacylases of 2-hydroxyisobutyrylated proteins in *F. oxysporum* and offer a rich source for studying the roles of 2-hydroxyisobutyrylation in different biological processes.

Fusarium oxysporum is a soil-borne fungal pathogen and could cause the wilt diseases in more than 150 different plants, including many important crops and trees (Mohali, 1996; Pietro et al., 2003; Perez-Nadales and Di Pietro, 2011; Alwahshi et al., 2019; Lan et al., 2020), that lead to severe losses of production. Integrated disease management (IDM) which is a disease control approach containing the chemical, biological and genetic strategies should be used to control the diseases caused by *F. oxysporum* (Saeed et al., 2017; Kamil et al., 2018). In this study, we found that some 2-hydroxyisobutyrylated proteins were involved in infection and pathogenicity processes of *F. oxysporum* (**Table 1**). Therefore, identification and analysis of virulence associated proteins which occurring K_{hib} modification will be help to widen the comprehensive views of K_{hib} in *F. oxysporum* and open up principally new possibilities for disease control in the field.

CONCLUSION

Our study is the first report of K_{hib} in *F. oxysporum* and provides a resource for further exploration of the potential functions of K_{hib} in plant pathogenic fungi. This finding provides some insights into the function of K_{hib} in several processes of *F. oxysporum* and detects the abundance of K_{hib} in conidial and mycelial stages. This study will improve our comprehension of K_{hib} in conidiation and virulence of *F. oxysporum* and other fungal plant pathogens. Although K_{hib} proteins play important roles in the virulence and conidiation of *F. oxysporum*, further studies are needed to uncover the detailed mechanism.

DATA AVAILABILITY STATEMENT

The datasets presented in this study can be found in online repositories. The names of the repository/repositories and accession number(s) can be found in the article/ **Supplementary Material**.

AUTHOR CONTRIBUTIONS

WL designed the research. HQ and LW performed the research. XM and XY contributed new reagents or analytic tools. HQ, LW, BW, and WL analyzed the data. HQ and WL wrote the manuscript. All authors contributed to the article and approved the submitted version.

FUNDING

This research was financially supported by the Ministry of Agriculture of China (2016ZX08009003-001), the National Natural Science Foundation of China (31722044 and 31972213), Taishan Scholar Construction Foundation of Shandong Province (tshw20130963), and "First Class Grassland Science Discipline" program in Shandong Province, China.

SUPPLEMENTARY MATERIAL

The Supplementary Material for this article can be found online at: https://www.frontiersin.org/articles/10.3389/fmicb.2021.623735/full#supplementary-material

Supplementary Figure 1 | Overview of identification of lysine 2-hydroxyisobutyrylation (K_{hib}) proteome in *Fusarium oxysporum*. **(A)** Schematic representation of the experimental procedures used in *F. oxysporum*. **(B)** Venn diagram showed the number of K_{hib} proteins and overlaps in all three repeated experiments.

Supplementary Figure 2 | Interaction network of 2-hydroxyisobutyrylated proteins associated with ribosome, ribosome biogenesis in eukaryotes, proteasome, nucleosome core, and spliceosome in *Fusarium oxysporum*.

Supplementary Figure 3 | Significantly enriched KEGG pathways in *Fusarium oxysporum*. 2-hydroxyisobutyrylated proteins involved in **(A)** Ribosome **(B)** Oxidative phosphorylation. The identified 2-hydroxyisobutyrylated proteins were highlighted in red.

Supplementary Table 1 | The 2-hydroxyisobutyrylated sites identified in the three experiments in *Fusarium oxysporum*.

Supplementary Table 2 | The number of identified 2-hydroxyisobutyrylated sites in *Fusarium oxysporum*.

Supplementary Table 3 | Amino acid sequence analysis from the −10 to +10 positions around the 2-hydroxyisobutyrylated lysine in *Fusarium oxysporum*.

Supplementary Table 4 | Conservation of lysine 2-hydroxyisobutyrylated proteins in *Fusarium oxysporum*.

Supplementary Table 5 | The distribution of proteins of *Fusarium oxysporum* in GO terms.

Supplementary Table 6 | Subcellular localizations of the 2-hydroxyisobutyrylation proteins in *Fusarium oxysporum*.

Supplementary Table 7 | Protein GO enrichment based on biological process in *Fusarium oxysporum*.

Supplementary Table 8 | Protein GO enrichment based on molecular function in *Fusarium oxysporum*.

Supplementary Table 9 | Protein GO enrichment based on cellular component in *Fusarium oxysporum*.

Supplementary Table 10 | KEGG pathway enrichment analysis in *Fusarium oxysporum*.

Supplementary Table 11 | Protein domain enrichment analysis in *Fusarium oxysporum*.

Supplementary Table 12 | Node information in protein–protein interaction network in *Fusarium oxysporum*.

REFERENCES

Alwahshi, K., Saeed, E., Sham, A., Alblooshi, A., Alblooshi, M., El-Tarabily, K., et al. (2019). Molecular identification and disease management of date palm sudden decline syndrome in the United Arab Emirates. *Int. J. Mol. Sci.* 20:923. doi: 10.3390/ijms20040923

Chen, Y., Sprung, R., Tang, Y., Ball, H., Sangras, B., Kim, S., et al. (2007). Lysine propionylation and butyrylation are novel post-translational modifications in histones. *Mol. Cell. Proteomics* 6, 812–819.

Cheng, Y., Peng, Z., Chen, H., Pan, T., Hu, X., Wang, F., et al. (2020). Posttranslational lysine 2-hydroxyisobutyrylation of human sperm tail proteins affects motility. *Hum. Reprod.* 35, 494–503. doi: 10.1093/humrep/dez296

Cheng, Z., Tang, Y., Chen, Y., Kim, S., Liu, H., Li, S., et al. (2009). Molecular characterization of propionyllysines in non-histone proteins. *Mol. Cell. Proteomics* 8, 45–52. doi: 10.1074/mcp.M800224-MCP200

Chou, M. F., and Schwartz, D. (2011). Biological sequence motif discovery using motif-x. *Curr. Protoc. Bioinformatics* 13, 15–24. doi: 10.1002/0471250953.bi1315s35

Cluntun, A. A., Huang, H., Dai, L., Liu, X., Zhao, Y., and Locasale, J. (2015). The rate of glycolysis quantitatively mediates specific histone acetylation sites. *Cancer Metab.* 3:10. doi: 10.1186/s40170-015-0135-3

Dai, L., Peng, C., Montellier, E., Lu, Z., Chen, Y., Ishii, H., et al. (2014). Lysine 2-hydroxyisobutyrylation is a widely distributed active histone mark. *Nat. Chem. Biol.* 10, 365–370. doi: 10.1038/nCHeMBIO.1497

Di Pietro, A., García-Maceira, F., Méglecz, E., and Roncero, M. (2001). A MAP kinase of the vascular wilt fungus *Fusarium oxysporum* is essential for root penetration and pathogenesis. *Mol. Microbiol.* 39, 1140–1152. doi: 10.1111/j.1365-2958.2001.02307.x

Dong, H., Guo, Z., Feng, W., Zhang, T., Zhai, G., Palusiak, A., et al. (2018). Systematic identification of lysine 2-hydroxyisobutyrylated proteins in *Proteus mirabilis*. *Mol. Cell. Proteomics* 17, 482–494. doi: 10.1074/mcp.RA117.000430

Hamel, H. P., Nicole, M. C., Duplessis, S., and Ellis, B. E. (2012). Mitogen-activated protein kinase signaling in plant-interacting fungi: distinct messages from conserved messengers. *Plant Cell* 24, 1327–1351. doi: 10.1105/tpc.112.096156

Huang, H., Lin, S., Garcia, B. A., and Zhao, Y. (2015). Quantitative proteomic analysis of histone modifications. *Chem. Rev.* 115, 2376–2418. doi: 10.1021/cr500491u

Huang, H., Luo, Z., Qi, S., Huang, J., Xu, P., Wang, X., et al. (2018). Landscape of the regulatory elements for lysine 2-hydroxyisobutyrylation pathway. *Cell Res.* 28, 111–125. doi: 10.1038/cr.2017.149

Huang, H., Sabari, B. R., Garcia, B. A., Allis, C. D., and Zhao, Y. (2014). SnapShot: histone modifications. *Cell* 159, 458–458.e1. doi: 10.1016/j.cell.2014.09.037

Huang, J., Luo, Z., Ying, W., Cao, Q., Huang, H., Dong, J., et al. (2017). 2-Hydroxyisobutyrylation on histone H4K8 is regulated by glucose homeostasis in *Saccharomyces cerevisiae*. *Proc. Natl. Acad. Sci. U.S.A.* 114, 8782–8787. doi: 10.1073/pnas.1700796114

Jain, S., Akiyama, K., Kan, T., Ohguchi, T., and Takata, R. (2003). The G protein beta subunit FGB1 regulates development and pathogenicity in *Fusarium oxysporum*. *Curr. Genet.* 43, 79–86. doi: 10.1007/s00294-003-0372-9

Jiao, X., Sherman, B., Huang, D., Stephens, R., Baseler, M. W., Lane, H., et al. (2012). DAVID-WS: a stateful web service to facilitate gene/protein list analysis. *Bioinformatics* 28, 1805–1806. doi: 10.1093/bioinformatics/bts251

Kamil, F., Saeed, E., El-Tarabily, K., and AbuQamar, S. (2018). Biological control of mango dieback disease caused by *Lasiodiplodia theobromae* using streptomycete and non-streptomycete actinobacteria in the United Arab Emirates. *Front. Microbiol.* 9:829. doi: 10.3389/fmicb.2018.00829

Kashiwa, T., Suzuki, T., Sato, A., Akai, K., Teraoka, T., Komatsu, K., et al. (2016). A new biotype of *Fusarium oxysporum* f. sp. lycopersici race 2 emerged by a transposon-driven mutation of avirulence gene AVR1. *FEMS Microbiol. Lett.* 363:fnw132. doi: 10.1093/femsle/fnw132

Klausen, M. S., Jespersen, M. C., Nielsen, H., Jensen, K. K., Jurtz, V. I., Sønderby, C. K., et al. (2019). NetSurfP-2.0: improved prediction of protein structural features by integrated deep learning. *Proteins* 87, 520–527. doi: 10.1002/prot.25674

Lan, C., Dai, Y., Gan, L., Yao, J., and Yang, X. (2020). First report of *Fusarium oxysporum* f. sp. *canariensis* causing *Fusarium wilt* on Canary Island date palm (*Phoenix canariensis* Hort. Ex Chabaud) in China. *J. Plant Pathol.* 102, 569–570. doi: 10.1007/s42161-019-00458-5

Lemos, P., Ruiz-Roldan, C., and Hera, C. (2018). Role of the phosphatase Ptc1 in stress responses mediated by CWI and HOG pathways in *Fusarium oxysporum*. *Fungal Genet. Biol.* 118, 10–20. doi: 10.1016/j.fgb.2018.05.004

Levin, D. E. (2005). Cell wall integrity signaling in *Saccharomyces cerevisiae*. *Microbiol. Mol. Biol. Rev.* 69, 262–291. doi: 10.1128/MMBR.69.2.262-291.2005

Li, D., Lv, B., Tan, L., Yang, Q., and Liang, W. (2016). Acetylome analysis reveals the involvement of lysine acetylation in diverse biological processes in *Phytophthora sojae*. *Sci. Rep.* 6:29897. doi: 10.1038/srep29897

Li, M., Xie, X., Lin, X., Shi, J., Ding, Z., Ling, J., et al. (2014). Functional characterization of the gene FoOCH1 encoding a putative α-1,6-mannosyltransferase in *Fusarium oxysporum* f. sp. cubense. *Fungal Genet. Biol.* 65, 1–13. doi: 10.1016/j.fgb.2014.01.005

Li, Y., Sabari, B. R., Panchenko, T., Wen, H., Zhao, D., Guan, H., et al. (2016). Molecular coupling of histone crotonylation and active transcription by AF9 YEATS domain. *Mol. Cell* 62, 181–193. doi: 10.1016/j.molcel.2016.03.028

Liu, J., Wang, G., Lin, Q., Liang, W., Gao, Z., Mu, P., et al. (2018a). Systematic analysis of the lysine malonylome in common wheat. *BMC Genomics* 19:209. doi: 10.1186/s12864-018-4535-y

Liu, S., Xue, C., Fang, Y., Chen, G., Peng, X., Zhou, Y., et al. (2018b). Global involvement of lysine crotonylation in protein modification and transcription regulation in rice. *Mol. Cell. Proteomics* 17, 1922–1936. doi: 10.1074/mcp.RA118.000640

Lv, B., Yang, Q., Li, D., Liang, W., and Song, L. (2016). Proteome-wide analysis of lysine acetylation in the plant pathogen *Botrytis cinerea*. *Sci. Rep.* 6:29313. doi: 10.1038/srep29313

Ma, L., van der Does, H. C., Borkovich, K. A., Coleman, J. J., Daboussi, M. J., Pietro, A. D., et al. (2010). Comparative genomics reveals mobile pathogenicity chromosomes in *Fusarium*. *Nature* 464, 367–373. doi: 10.1038/nature08850

Martinez-Rocha, A. L., Roncero, M. I., Lopez-Ramirez, A., Marine, M., Guarro, J., Martínez-Cadena, G., et al. (2008). Rho1 has distinct functions in morphogenesis, cell wall biosynthesis and virulence of *Fusarium oxysporum*. *Cell. Microbiol.* 10, 1339–1351. doi: 10.1111/j.1462-5822.2008.01130.x

Meng, X., Xing, S., Perez, L. M., Peng, X., Zhao, Q., Redoña, D. E., et al. (2017). Proteome-wide analysis of lysine 2-hydroxyisobutyrylation in developing rice (*Oryza sativa*) seeds. *Sci. Rep.* 7:17486. doi: 10.1038/s41598-017-17756-6

Mey, G., Oeser, B., Lebrun, M. H., and Tudzynski, P. (2002). The biotrophic, non-appressorium-forming grass pathogen *Claviceps purpurea* needs a Fus3/Pmk1 homologous mitogen-activated protein kinase for colonization of rye ovarian tissue. *MPMI* 15, 303–312. doi: 10.1094/MPMI.2002.15.4.303

Michielse, C. B., and Rep, M. (2009). Pathogen profile update: *Fusarium oxysporum*. *Mol. Plant Pathol.* 10, 311–324. doi: 10.1111/J.1364-3703.2009.00538.X

Mohali, S. R. (1996). First report of *Fusarium oxysporum* and *Fusarium solani* associated with root disease of Caribbean pine in Venezuela. *Plant Dis.* 80:959. doi: 10.1094/PD-80-0959C

Pareek, M., and Rajam, M. V. (2017). RNAi-mediated silencing of MAP kinase signalling genes (*Fmk1*, *Hog1*, and *Pbs2*) in *Fusarium oxysporum* reduces pathogenesis on tomato plants. *Fungal Biol.* 121, 775–784. doi: 10.1016/j.funbio.2017.05.005

Peach, S. E., Rudomin, E. L., Udeshi, N. D., Carr, S. A., and Jaffe, J. D. (2012). Quantitative assessment of chromatin immunoprecipitation grade antibodies directed against histone modifications reveals patterns of co-occurring marks on histone protein molecules. *Mol. Cell. Proteomics* 11, 128–137.

Peng, C., Lu, Z., Xie, Z., Cheng, Z., Chen, Y., Tan, M., et al. (2011). The first identification of lysine malonylation substrates and its regulatory enzyme. *Mol. Cell. Proteomics* 10, M111.012658. doi: 10.1074/mcp.M111.012658

Perez-Nadales, E., and Di Pietro, A. (2011). The membrane mucin Msb2 regulates invasive growth and plant infection in *Fusarium oxysporum*. *Plant Cell* 23, 1171–1185. doi: 10.1105/tpc.110.075093

Pietro, A. D., Madrid, M. P., Caracuel, Z., Delgado-Jarana, J., and Roncero, M. (2003). *Fusarium oxysporum*: exploring the molecular arsenal of a vascular wilt fungus. *Mol. Plant Pathol.* 4, 315–325. doi: 10.1046/J.1364-3703.2003.00180.X

Rana, A., Sahgal, M., and Johri, B. N. (2017). "*Fusarium oxysporum*: genomics, diversity and plant–host interaction," in *Developments in Fungal Biology and Applied Mycology*, eds T. Satyanarayana, S. Deshmukh, and B. Johri (Singapore: Springer), 159–199. doi: 10.1007/978-981-10-4768-8_10

Rispail, N., and Di Pietro, A. (2010). The two-component histidine kinase Fhk1 controls stress adaptation and virulence of *Fusarium oxysporum*. *Mol. Plant Pathol.* 11, 395–407. doi: 10.1111/J.1364-3703.2010.00612.X

Sabari, B. R., Tang, Z., Huang, H., Yong-Gonzalez, V., Molina, H., Kong, H., et al. (2015). Intracellular crotonyl-CoA stimulates transcription through p300-catalyzed histone crotonylation. *Mol. Cell* 58, 203–215. doi: 10.1016/j.molcel.2015.02.029

Saeed, E., Sham, A., Salmin, Z., Abdelmowla, Y., Iratni, R., El-Tarabily, K., et al. (2017). *Streptomyces globosus* UAE1, a potential effective biocontrol agent for black scorch disease in date palm plantations. *Front. Microbiol.* 8:1455. doi: 10.3389/fmicb.2017.01455

Sapountzi, V., Logan, I. R., and Robson, C. N. (2006). Cellular functions of TIP60. *Int. J. Biochem. Cell Biol.* 38, 1496–1509. doi: 10.1016/j.biocel.2006.03.003

Takano, Y., Kikuchi, T., Kubo, Y., Hamer, J. E., Mise, K., and Furusawa, I. (2000). The *Colletotrichum lagenarium* MAP kinase gene CMK1 regulates diverse aspects of fungal pathogenesis. *Mol. Plant Microbe Interact.* 13, 374–383. doi: 10.1094/MPMI.2000.13.4.374

Tan, M., Peng, C., Anderson, K. A., Chhoy, P., Xie, Z., Dai, L., et al. (2014). Lysine glutarylation is a protein posttranslational modification regulated by SIRT5. *Cell Metab.* 19, 605–617. doi: 10.1016/j.cmet.2014.03.014

Vidali, L., and Bezanilla, M. (2012). *Physcomitrella patens*: a model for tip cell growth and differentiation. *Curr. Opin. Plant Biol.* 15, 625–631. doi: 10.1016/j.pbi.2012.09.008

Xu, H., Zhou, J., Lin, S., Deng, W., Zhang, Y., and Xue, Y. (2017). PLMD: an updated data resource of protein lysine modifications. *J. Genet. Genomics* 44, 243–250. doi: 10.1016/j.jgg.2017.03.007

Xu, X., Cao, X., Yang, J., Chen, L., Liu, B., Liu, T., et al. (2019). Proteome-wide identification of lysine propionylation in the conidial and mycelial stages of *Trichophyton rubrum*. *Front. Microbiol.* 10:2613. doi: 10.3389/fmicb.2019.02613

Yin, D., Jiang, N., Zhang, Y., Wang, D., Sang, X., Feng, Y., et al. (2019). Global lysine crotonylation and 2-hydroxyisobutyrylation in phenotypically different *Toxoplasma gondii* Parasites. *Mol. Cell. Proteomics* 18, 2207–2224. doi: 10.1074/mcp.RA119.001611

Yu, Z., Ni, J., Sheng, W., Wang, Z., and Wu, Y. (2017). Proteome-wide identification of lysine 2-hydroxyisobutyrylation reveals conserved and novel histone modifications in *Physcomitrella patens*. *Sci. Rep.* 7:15553. doi: 10.1038/s41598-017-15854-z

Zhang, Y., Wang, G., Song, L., Mu, P., Wang, S., Liang, W., et al. (2017). Global analysis of protein lysine succinylation profiles in common wheat. *BMC Genomics* 18:309. doi: 10.1186/s12864-017-3698-2

Zheng, L., Campbell, M., Murphy, J., Lam, S., and Xu, J. (2000). The BMP1 gene is essential for pathogenicity in the gray mold fungus *Botrytis cinerea*. *MPMI* 13, 724–732. doi: 10.1094/mpmi.2000.13.7.724

Zhou, S., Yang, Q., Yin, C., Liu, L., and Liang, W. (2016). Systematic analysis of the lysine acetylome in *Fusarium graminearum*. *BMC Genomics* 17:1019. doi: 10.1186/s12864-016-3361-3

Conflict of Interest: XM and XY were employed by the company Micron Biotechnology Co., Ltd.

The remaining authors declare that the research was conducted in the absence of any commercial or financial relationships that could be construed as a potential conflict of interest.

frontiers in Microbiology

ORIGINAL RESEARCH
published: 12 February 2021
doi: 10.3389/fmicb.2021.616932

Intercropping With Aromatic Plants Increased the Soil Organic Matter Content and Changed the Microbial Community in a Pear Orchard

Yan Zhang[1,2,3†], Mingzheng Han[1,2,3†], Mengni Song[1,2,3†], Ji Tian[1,2,3], Beizhou Song[1,2,3], Yujing Hu[1,2,3], Jie Zhang[1,2,3*] and Yuncong Yao[1,2,3*]*

[1] Beijing Advanced Innovation Center for Tree Breeding by Molecular Design, Beijing University of Agriculture, Beijing, China, [2] College of Plant Science and Technology, Beijing University of Agriculture, Beijing, China, [3] Beijing Key Laboratory for Agricultural Application and New Technique, Beijing, China

OPEN ACCESS

Edited by:
Yong Wang,
Guizhou University, China

Reviewed by:
Wei Qinping,
Beijing Academy of Agriculture and Forestry Sciences, China
Roberta Fulthorpe,
University of Toronto Scarborough, Canada
Joanna Dames,
Rhodes University, South Africa

***Correspondence:**
Yuncong Yao
yaoyc_20@126.com
Jie Zhang
anyzj034@126.com
Yan Zhang
360873096@qq.com

[†] These authors have contributed equally to this work

Specialty section:
This article was submitted to Microbe and Virus Interactions with Plants, a section of the journal Frontiers in Microbiology

Received: 13 October 2020
Accepted: 25 January 2021
Published: 12 February 2021

Citation:
Zhang Y, Han M, Song M, Tian J, Song B, Hu Y, Zhang J and Yao Y (2021) Intercropping With Aromatic Plants Increased the Soil Organic Matter Content and Changed the Microbial Community in a Pear Orchard. Front. Microbiol. 12:616932. doi: 10.3389/fmicb.2021.616932

Intercropping influences the soil microbiota via litter and root exudate inputs, but the mechanisms by which root exudates mediate the soil microbial community and soil organic matter (SOM) are still unclear. In this study, we selected three aromatic plants (*Ocimum basilicum*, Tr1; *Satureja hortensis*, Tr2; *Ageratum houstonianum*, Tr3) as intercrops that separately grew between rows of pear trees, and no plants were grown as the control in a pear orchard during the spring–summer season for 3 years. The soil from each plot was collected using a stainless-steel corer by five-point sampling between rows of pear trees. The bacterial and fungal communities of the different aromatic intercrops were analyzed by 16S and ITS rRNA gene amplicon sequencing; their functional profiles were predicted by PICRUSt and FUNGuild analyses. The root exudates of the aromatic plants were analyzed by a liquid chromatography-tandem mass spectrometry (LC-MS) system. Compared with the control treatment, all intercropping treatments with aromatic plants significantly increased SOM and soil water content and decreased pH values. The contents of total nitrogen and alkali-hydrolyzable nitrogen in Tr1 and Tr2 were higher than those in Tr3. In Tr3 soil, the relative content of saccharides increased little, whereas the changes in amine (increases) and alcohols (decreases) were rapid. *Ageratum houstonianum* intercropping decreased the microbial community diversity and significantly influenced the relative abundances of the dominant microbiota (Actinobacteria, Verrucomicrobia, Gemmatimonadetes, Cyanobacteria, Ascomycota, and Basidiomycota) at the phylum, class, and order levels, which increased the assemblage of functional groups (nitrite ammonification, nitrate ammonification, and ureolysis groups). Our study suggested that the main root exudates from aromatic plants shaped the microbial diversity, structure, and functional groups related to the N cycle during SOM mineralization and that intercropping with aromatic plants (especially basil and summer savory) increased N release in the orchard soil.

Keywords: aromatic plants, root exudates, microbial community, soil nutrients, woody-herbaceous intercropping system

INTRODUCTION

Soil organic matter (SOM) transformation has the dual benefits of improving soil fertility and maintaining the stability of the soil system (Scholes and Noble, 2001). Understanding the mechanisms of SOM transformation by the microbial community is therefore important, as the capacity of soil carbon (C) and nitrogen (N) cycling may be constrained by aboveground plant species (especially invasive plants) and may thereby influence soil nutrient availability (Chen and Stark, 2000; Sardans et al., 2017).

Soil nutrients are generally delivered by plant litter and root exudates, which are slowly released into the soil through microbial processes and SOM mineralization. These processes can alter the degree of nutrient availability through the mineralization of organic compounds (Arancon et al., 2006; Sharma et al., 2011). The functional gene structure of soil microbial communities could influence the decomposition of SOM and consequently regulate the supply of soil nutrients (Gourmelon et al., 2016; Cheng et al., 2017; Waldrop et al., 2017). Many studies have reported that the structure, composition and diversity of the soil microbial community are influenced by plant species, with plant species differences in litter type and root exudates contributing to variation in the physicochemical properties of soil (Gourmelon et al., 2016; Fitzpatrick et al., 2018; Chen et al., 2020). Consequently, these processes drive different modes of ecological functions and services related to nutrient availability in the soil ecosystem (Lekberg et al., 2013).

Fitzpatrick et al. (2018) found that greater similarity in root microbiomes between hosts leads to negative effects on plant performance through soil feedback, with specific microbial taxa in the endosphere and rhizosphere potentially causing competitive interactions among plant species. Reduced crop productivity in field systems repeatedly planted with the same or closely related plant species is a common phenomenon and has been named replanted disease (Mazzola and Manici, 2012). To avoid replanted disease, intercropping is often used in agroecosystems. Interactions between plants and microbes continue to benefit plants by increasing the acquisition of nutrients, producing growth hormones, and defending against enemies (Berendsen et al., 2012). Economically valuable herbs (e.g., forage and flowering ground cover-plants) are often used as intercrops. The influence of plant species and even different genotypes of the same species on the composition of soil microorganisms is considered to be the largest driving factor for soil C and N cycles (Marschner et al., 2005; Koutika et al., 2007; DeHaan et al., 2010). Many studies have shown that intercropping with ground-cover plants can provide valuable organic C accumulation and has positive effects on soil texture and nutrient availability, with feedback regulating plant growth and crop yield (Atucha et al., 2011; Chen et al., 2014). Intercropping with kura clover in the alleys of a pecan orchard increased the content of soil organic carbon (SOC) and the activity of soil enzymes improved the soil structure and reduced soil erosion (Kremer and Kussman, 2011). Ramos et al. (2010) showed that intercropping in almond (*Prunus dulcis* L.) orchards improved soil quality by increasing SOC, soil aggregate stability and microbial activity. The influence of such plant species on soil C accumulation through the regulation of microbial communities has received increasing attention.

Plants used primarily for their aromatic properties in perfumery are defined as aromatic plants in the EU, and they are a source of essential oils, cosmetics and biocides (Lubbe and Verpoorte, 2011; Tang et al., 2013; Song et al., 2014). Intercropping with aromatic plants in an orchard can increase the stability of agroecosystems (Tripathi et al., 2019). Intercropping with certain species of aromatic plants can improve soil quality. For example, intercropping with basil (*Ocimum basilicum* L.) and summer savory (*Satureja hortensis* L.) was found to significantly increase soil organic nitrogen and available nitrogen contents in our previous study (Chen et al., 2014). However, only a limited understanding exists of how this intercropping model directly influences the features of the soil microbial community related to the C and N cycles via root exudates and plant litter and the subsequent impacts on soil nutrient availability.

In this study, to reveal the mechanisms by which root exudates mediate the soil microbial community and regulate SOM transformation and nutrient cycling in an intercroppings system, three species of aromatic plants were selected as intercrops in a pear orchard. The aims were to determine the following: (i) the influences of root exudates from different aromatic plants on soil nutrient cycling; (ii) the effects of these components on the structure, composition, diversity and function of the soil microbial community; (iii) the correlations among root exudates, the soil microbial community and the soil C and N framework in a woody-herbaceous ecosystem; and (iv) the differences among the three intercropping treatments.

MATERIALS AND METHODS

Experimental Site and Design

The field experiment was conducted during the spring-summer season 2008-2010 in an organic pear orchard located in the district of Daxing (39°73′N, 116°33′E), south of Beijing, China. This region is classified as having a temperate, semihumid continental monsoon climate, with a mean annual rainfall of 500 mm and a mean annual temperature of 11.6°C. Approximately 76% of the annual precipitation falls in summer. The orchard, containing 15-year-old *Pyrus pyrifolia* "Huangjin"/*P. betulaefolia* rootstock trees planted at a spacing of 3 × 5 m, has been farmed using organic methods since 2005 and has been managed to meet the organic certification standards set by the Organic Food Development Center of China in 2007. During the natural growth of the pear trees, artificial and physical methods were mainly used to control the pear pests in the whole orchard. The soil type is brown soil according to the classification and codes for Chinese soil (GB/T17296-2009). Before the experimental treatments, the topsoil had a pH of 7.79, SOM content of 10.30 g kg^{-1}, alkali-hydrolyzable nitrogen (AN) content of 151.07 mg kg^{-1}, available phosphorus (AP) content of 49.16 mg kg^{-1}, and available potassium (AK) content of 378.61 mg kg^{-1}.

The experiment included four treatments: (i) a control, which was a monocropping system of pear tree (no plants were grown between the rows of pear trees, with naturally occurring weeds removed once a month); (ii) Tr1, an intercropping system of pear tree and basil (*Ocimum basilicum* L); (iii) Tr2, an intercropping system of pear tree and summer savory (*Satureja hortensis* L.); and (iv) Tr3, an intercropping system of pear trees and blue mink (*Ageratum houstonianum* Mill.) (**Supplementary Figure S1A**). There were 12 plots in total, with three plots in each treatment. Each plot was 5 m wide and 30 m long and included 20 pear trees (**Supplementary Figure S1B**). The different treatments were separated from adjacent plots by a 10 m isolation belt (**Supplementary Figure S1A**). The intercrops were sown in a greenhouse, and seedlings (approximately 10 cm in height) were transplanted into the pear orchard in mid-March. The intercrops were grown with a spacing of 0.2 × 0.3 m between the rows of pear trees. During the growing period, intertillage weeding was carried out to keep the intercropping area free of weeds. The aromatic plants in the intercropped plots were mowed in late September annually, with the plant residues left *in situ*.

Soil Sampling and Processing

Soils from all plots were collected in mid-September 2010 after 3 years of intercropping with aromatic plants (ICAP) or no plants (control). Five soil cores (**Supplementary Figure S1C**) from each plot were collected using a stainless-steel corer (4.5 cm inner diameter, depth 0–20 cm) and then mixed to obtain a composite sample for each plot. Thus, each treatment had three replicates of soil samples. The composite samples were immediately sieved (<2 mm) and divided into three subsamples, which were immediately stored at −80°C for subsequent DNA extraction and soil microbial biomass carbon (MBC) and soil microbial biomass nitrogen (MBN) determination; stored at 4°C for analyses of enzymatic activity and the soil water content (SWC); and air dried and stored at room temperature prior to chemical analysis.

Soil Physicochemical Properties and Enzyme Activity Analysis

Soil moisture content was determined gravimetrically by drying at 105°C for 24 h, and the soil pH was determined in a mixture of soil and water suspension (1:2.5) with a pH meter (Mettler Toledo FiveEasy Plus, Switzerland) (Lu, 2000). The SOC was determined using the Walkley-Black method, with slight modifications (Nelson and Sommers, 1996). SOM was calculated as SOC × 1.724 (Pribyl, 2010). Total nitrogen (TN) was determined by the Kjeldahl method (Bremner, 1996), and the total phosphorus was determined by the Olsen method (Olsen and Sommers, 1982). AN was detected using the alkaline hydrolysis diffusion method (Lu, 2000). Soil invertase, catalase (CAT), and urease activities were determined in accordance with the method described by Jin et al. (2009).

The soil MBC and MBN were measured by the fumigation-extraction method (Vance et al., 1987). Briefly, 20 g of fresh soil (dry weight equivalent) was fumigated with CH_3Cl for 24 h, and then both fumigated and non-fumigated soils were extracted with 75 mL of 0.5 M K_2SO_4. The extracted solutions were then filtered and analyzed with a Multi N/C 3100 TOC analyzer (Analytik, Jena, Germany). The soil MBC and MBN were calculated as the difference in extractable organic C and inorganic N contents, respectively, between fumigated and non-fumigated samples using a conversion factor of 0.45 for both C and N (Brookes et al., 1985).

Soil DNA Extraction and Sequencing

Genomic DNA was extracted from a 0.25 g soil sample using a TIANamp Soil DNA Kit (Tiangen Biotech, Beijing, China) following the manufacturer's procedures. The quality and quantity of DNA were determined by the A260/280 ratio using a NanoDrop device (NanoDrop 2000, Germany) and electrophoresis (1% agarose gel, including a 1 kb plus ladder). The DNA samples from the soils of the same plot were pooled together and stored at −80°C until PCR amplification. The V3-V4 hypervariable regions of bacterial 16S rRNA was amplified using barcoded primers 341F and 785R (Klindworth et al., 2013), and fungal ITS2 regions (ITS3_KYO2F and ITS4_KYO3R) was targeted for amplification through two rounds of PCR (Toju et al., 2012). The purified PCR amplicons were sequenced using the Illumina MiSeq (300 bp paired-end reads) platform from Ori-Gene Technology Co., Ltd. (Beijing, China) in 2016. The high-quality paired-end reads of the 16S and ITS sequences were merged using FLASH software (Magoč and Salzberg, 2011) and Mothur[1] to filter the sequences and remove barcodes. The operational taxonomic units (OTUs) were obtained using the UPARSE pipeline based on the merged sequences (Edgar, 2013), and sequences with ≥ 97% similarity were assigned to the same OTU. To obtain the taxonomic information of the OTUs, representative sequences of each OTU were generated and aligned against the SILVA and UNITE databases using the RDP classifier[2] for the 16S and ITS sequences, respectively (Pruesse et al., 2007). The raw sequences were deposited in NCBI's Sequence Read Archive (SRA) under BioProject PRJNA685959.

Alpha-diversity indices, including the number of species observed (Sobs) and the Chao and Shannon indices were calculated with Mothur v.1.34.4 (Schloss et al., 2009). The functional profiles of the bacteria were generated from the Functional Annotation of Prokaryotic Taxa (FAPROTAX) database and associated software[3] (Louca et al., 2016). Trophic classification of pathotrophs, saprotrophs, and symbiotrophs (for fungi) was performed by FUNGuild[4] with the use of OTUs as described by Nguyen et al. (2016).

Root Exudate Collection

The rhizosphere soils of six randomly selected aromatic plants in each plot were pooled into a single rhizosphere soil sample. After shaking off the loosely adhering soil, the tightly adhering

[1]https://mothur.org

[2]https://rdp.cme.msu.edu/

[3]www.zoology.ubc.ca/louca/FAPROTAX

[4]http://www.stbates.org/guilds/app.php

TABLE 1 | Basic physicochemical parameters, soil nutrient contents, and enzyme activities in treated and control soil.

Parameter	Control	Tr1	Tr2	Tr3
pH	7.81 ± 0.13 a	7.67 ± 0.16 b	7.73 ± 0.04 b	7.67 ± 0.10 b
SWC	8.89 ± 0.90 b	11.70 ± 2.37 a	10.62 ± 1.56 a	10.55 ± 1.47 a
SOM	15.21 ± 0.77 b	20.33 ± 1.38 a	20.46 ± 1.59 a	20.62 ± 1.33 a
MBC	252.44 ± 20.09 b	361.54 ± 37.20 a	330.38 ± 59.90 a	318.90 ± 47.90 a
MBN	73.38 ± 1.17 d	88.74 ± 0.97 b	94.21 ± 1.27 a	85.83 ± 1.44c
MBC/MBN	3.26 ± 0.09 c	4.14 ± 0.22 a	3.54 ± 0.09 b	3.66 ± 0.11 b
TN	0.83 ± 0.08 c	1.54 ± 0.09 ab	1.63 ± 0.05 a	1.41 ± 0.05 b
TP	0.59 ± 0.02 b	0.73 ± 0.04 a	0.76 ± 0.03 a	0.65 ± 0.04 b
AN	99.91 ± 5.79c	133.57 ± 13.72 ab	138.16 ± 3.26 a	122.79 ± 3.51 b
C/N	10.54 ± 0.38 a	7.67 ± 0.56 bc	7.30 ± 0.85 c	8.47 ± 0.32 b
N/P	1.23 ± 0.05 c	2.24 ± 0.01 b	2.35 ± 0.10 b	2.42 ± 0.05 a
INV	5.08 ± 0.60 b	7.24 ± 1.16 a	6.75 ± 1.42 a	7.16 ± 1.09 a
CAT	5.05 ± 0.44 b	8.01 ± 0.74 a	7.74 ± 1.31 a	7.75 ± 1.13 a
URE	13.00 ± 1.63 b	18.98 ± 3.19 a	18.45 ± 3.33 a	22.62 ± 3.04 a

Note: Values are the mean ± SD (n = 3). Different letters indicate significant differences at $P < 0.05$ based on Duncan's multiple range tests. SWC, soil water content (%); SOM, soil organic matter (g kg^{-1}); MBC, microbial biomass carbon (mg kg^{-1}); MBN, microbial biomass nitrogen (mg kg^{-1}); TN, total nitrogen (g kg^{-1}); TP, total phosphorus (g kg^{-1}); AN, alkali-hydrolyzable nitrogen (mg kg^{-1}); C/N, soil organic carbon/TN; N/P, TN/TP; INV, invertase (mg glucose g^{-1} soil h^{-1}); CAT, catalase (0.1 mol L^{-1} KMnO4 g^{-1} soil h^{-1}); URE, urease (mg NH_4^+–N g^{-1} soil 24 h^{-1}). Control, monocropping system with clean tillage; Tr1, intercropping with basil (Ocimum basilicum L.); Tr2, intercropping with summer savory (Satureja hortensis L.); Tr3, intercropping with blue mink (Ageratum houstonianum Mill.).

rhizosphere soil was collected with a brush and passed through a 4 mm sieve. Then, the rhizosphere soils were placed on ice and immediately transported to the laboratory. In the monocropping system (control), we collected the bare soil between the rows of pear trees in the same way as the rhizosphere soil. Ten grams of each soil sample was stored at −80°C for root exudate collection (Jiang et al., 2017). The stored rhizosphere soil samples (200 mg) were thawed on ice, and metabolites were extracted with 1 mL of 50% methanol buffer. Briefly, the mixed solution was vortexed for 1 min, subjected to ultrasound for 20 min (on ice) and centrifuged (4°C, 10000 rpm, 15 min), and then 200 μL of supernatant extraction mixture was stored overnight at −20°C. All samples were analyzed by an AB SCIEX nano LC-MS system (Triple TOF 5600 plus) (SCIEX, United Kingdom) following the manufacturer's instructions. Root exudate determination was carried out by Sugar Pharma Technology Co., Ltd. (Beijing).

Statistical Analysis

Soil physicochemical properties, soil enzyme activity, soil microbial community alpha-diversity and composition, and root exudate data were submitted to one-way ANOVA followed by Duncan's multiple range test. Differences at $P < 0.05$ were regarded as statistically significant. Principal component analysis (PCA) and distance-based redundancy analysis (dbRDA) were used to visualize the associations among soil microbial community parameters, root exudates and environmental variables. Spearman correlation coefficients of pairwise correlations between microbial relative abundance, diversity indicators, soil chemistry, and root exudates were obtained. The statistical analyses and figures were performed using R[5].

[5]v3.5.1, https://www.r-project.org

RESULTS

Soil Physicochemical Parameters and Enzyme Activities

The soil physicochemical properties in all treatments are summarized in **Table 1**. SOM and SWC increased, and pH was decreased significantly in the intercropping system compared with the monocropping system (control) values in the pear orchard. The SOM content was increased by 33.6% (Tr1), 34.5% (Tr2), and 35.5% (Tr3) in the intercropping treatments compared with the control. MBC contents increased to a greater extent than MBN content in the intercropping system soil relative to the monocropping system soil values, resulting in an improvement in soil MBC/MBN in the former. The total phosphorus content was increased only in Tr1 and Tr2. Moreover, TN and AN contents and N/P were significantly increased, and C/N was significantly decreased in the intercropping system soil (Tr1, Tr2 and Tr3) relative to the monocropping system soil. TN and AN contents were higher in Tr1 and Tr2 than in Tr3. In addition, the activities of soil enzymes (invertase, urease, and CAT) were significantly enhanced in the intercropping system soil compared with control soil (**Table 1**).

Root Exudates of Aromatic Plants in Rhizosphere Soil

Metabolomics analysis of the relative contents of the root exudates of aromatic plants revealed that the exudates consisted predominantly of saccharides (up to 24.6%), alcohols (up to 10.5%), organic acids (OA, up to 10.0%), lipids (up to 7.8%), and aromatic compounds (AC, up to 5.7%) (**Figure 1**). Root exudation was strongly influenced by the intercropping species. In the intercropping systems, compared with the control, the saccharide, OA and lipid contents were increased, but the

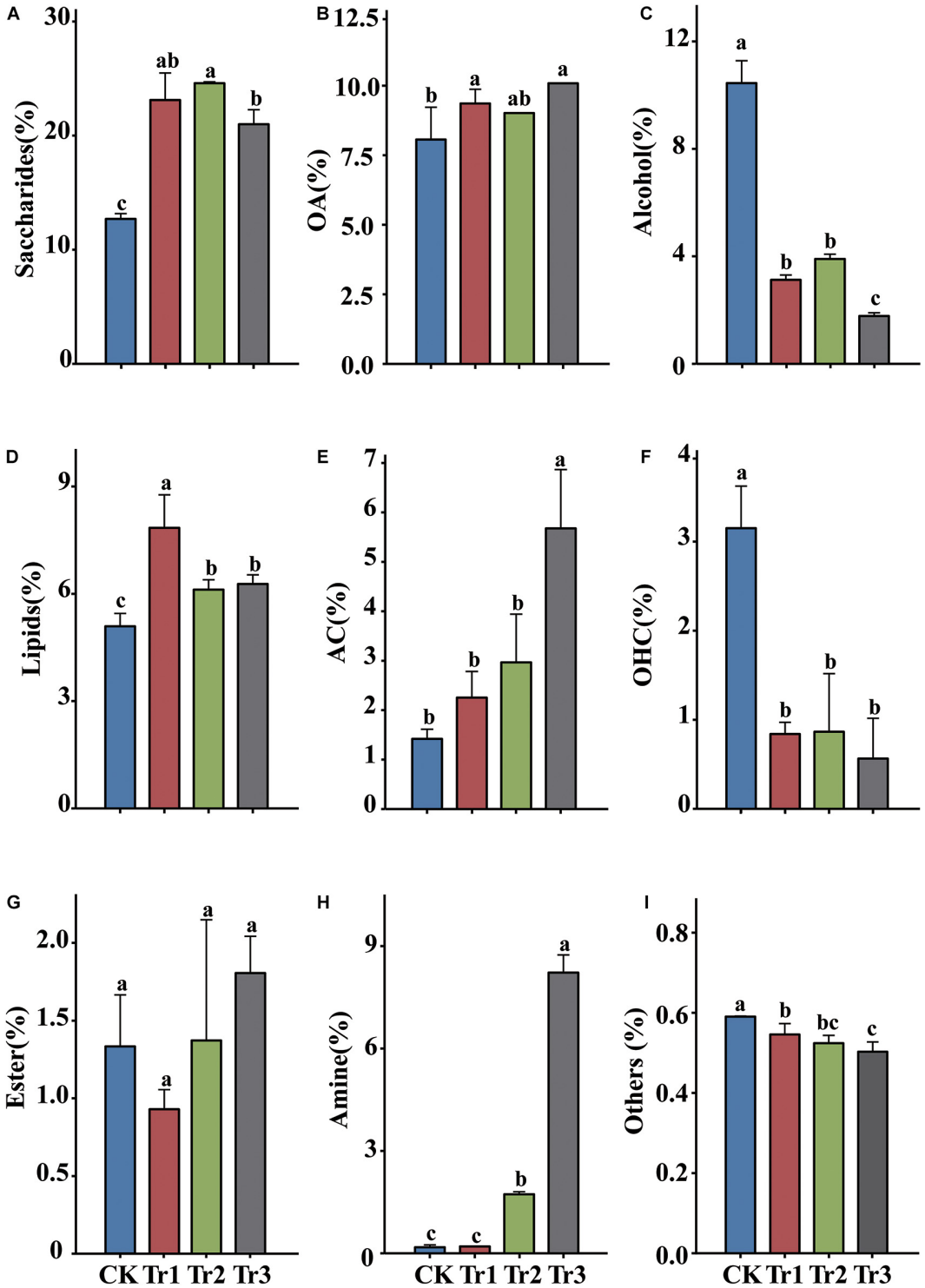

FIGURE 1 | The relative contents of the main root exudate components in rhizosphere soil in intercropping treatments with different species of aromatic plants. **(A)** Saccharides, **(B)** organic acids (OA), **(C)** alcohol, **(D)** lipids, **(E)** aromatic compounds (AC), **(F)** organic heterocyclic compounds (OHC), **(G)** esters, **(H)** amine, and **(I)** others. Values are the mean ± SD (n = 3). Different letters indicate significant differences at $P < 0.05$ based on Duncan's multiple range test.

alcohol and organic heterocyclic compound (OHC) contents were reduced significantly. The alcohol and OHC contents were highest in the control, and the amine and AC contents were highest in Tr3 (**Figure 1**).

The PCA results revealed that the significant differences between the intercropping and monocropping systems were associated with PC1, and that the significant differences among the three aromatic plant intercropping systems were associated with PC2. The PC1 and PC2 components accounted for 59.9% and 15.4% of the total variation, respectively (**Figure 2A**). The C/N ratio, pH, alcohol and OHC contents were significantly positively correlated with each other, while the SWC, SOM, contents of root exudates (AC, saccharides, OA, lipids, amine), contents of C and N compounds, and enzyme activities displayed significant positive correlations. The RDA results indicated that soil pH was positively associated with the contents of root exudates (i.e., alcohols, esters, OHC) and was negatively correlated with the contents of soil C and N compounds and enzyme activities. In addition, SWC was associated with the contents of N compounds, saccharides, OA, and AC, and SOM was associated with the contents of C compounds, saccharides, lipids and amine compounds and CAT activities in the intercropping soil (**Figure 2B**). The contents of root exudates (saccharides, lipids, OA, AC, amine) were positively related to most soil physicochemical parameters (including soil C and N compounds and the activities of associated enzymes) and negatively correlated with soil pH and the C/N ratio; however, alcohol and OHC contents were positively associated with pH and the C/N ratio (**Figure 2C**).

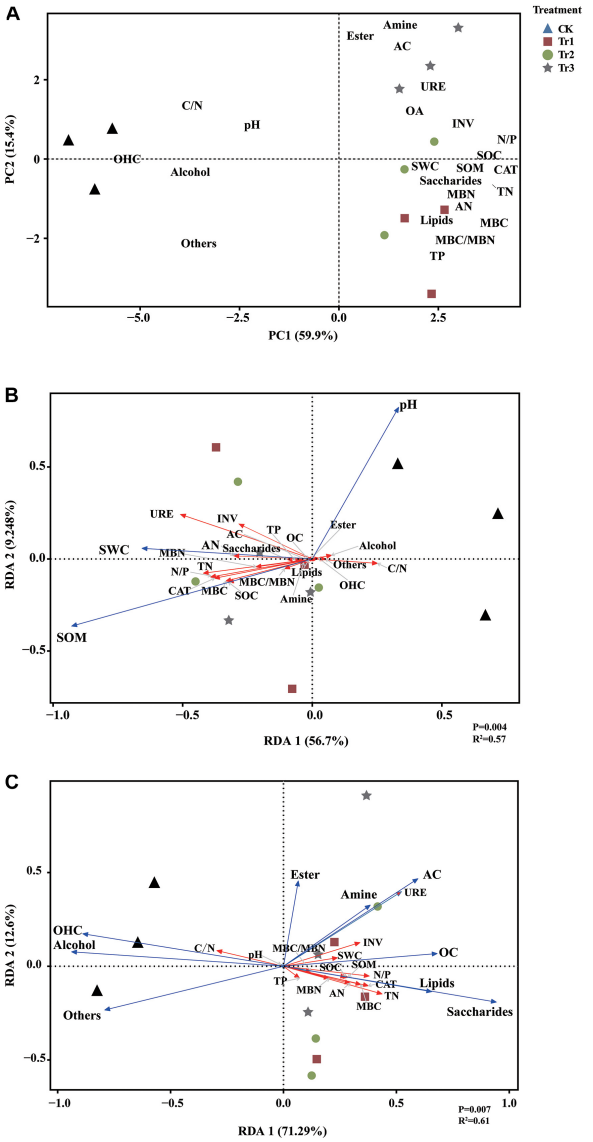

FIGURE 2 | Principal component analysis (PCA) based on the root exudates, soil physicochemical parameters and soil nutrients **(A)** and redundancy analysis (RDA) of soil nutrient variables constrained by basic physicochemical parameters (pH, SWC, and SOM) **(B)** and by root exudates **(C)**.

Composition, Structure, and Diversity of the Soil Bacterial Community

We sequenced the V3-V4 region of the 16S rRNA gene and obtained a total of 1,968,069 sequences from 12 soil samples (n = 3) after filtering. The number of reads ranged from 108,994 to 204,788, with a mean read count of 164,006 ± 28,453. Rarefaction curves implied that the sequencing coverage was sufficient as plateaus were reached for soil communities. Based on the total bacterial community estimated as the number of OTUs, the species richness (Chao index) and alpha-diversity (Shannon index) were enhanced significantly in the intercropping systems with basil and summer savory (Tr1 and Tr2) but not in the intercropping system with plants of blue mink plants (Tr3) compared with the control (**Figure 3A**).

In all intercropping treatments, nine phyla were dominant: Proteobacteria (26.28%), Acidobacteria (14.56%), Actinobacteria (10.14%), Bacteroidetes (8.96%), Planctomycetes (7.63%), Verrucomicrobia (5.70%), Gemmatimonadetes (5.31%), Chloroflexi (3.64%), and Cyanobacteria (1.76%) (**Figure 3B**). The intercropping effect of Tr3 on bacterial community composition was more significant than those of Tr1 or Tr2. Intercropping with blue mink (Tr3) significantly increased the relative abundances (RAs) of Actinobacteria and its dominant classes, orders and families, especially Micrococcales and Micrococcaceae, which both increased in abundance to levels approximately three times those of the control. However, there was no significant difference in bacterial community composition between the intercropping treatments with basil and summer savory (Tr1 and Tr2) and the control. Tr3 also significantly increased the RAs of the phylum Verrucomicrobia and its member classes, orders and families and the RAs of the phylum Cyanobacteria and its member classes. Furthermore, Tr3 significantly reduced the RAs of the phylum Gemmatimonadetes and its member classes and genera and those of the class Cytophagia, order Cytophagales, family Cytophagaceae, and genus *Ohtaekwangia* in the phylum Bacteroidetes. Tr1 significantly increased the RAs of the phylum Verrucomicrobia and its dominant classes, orders and families and those of the phylum Bacteroidetes and its class

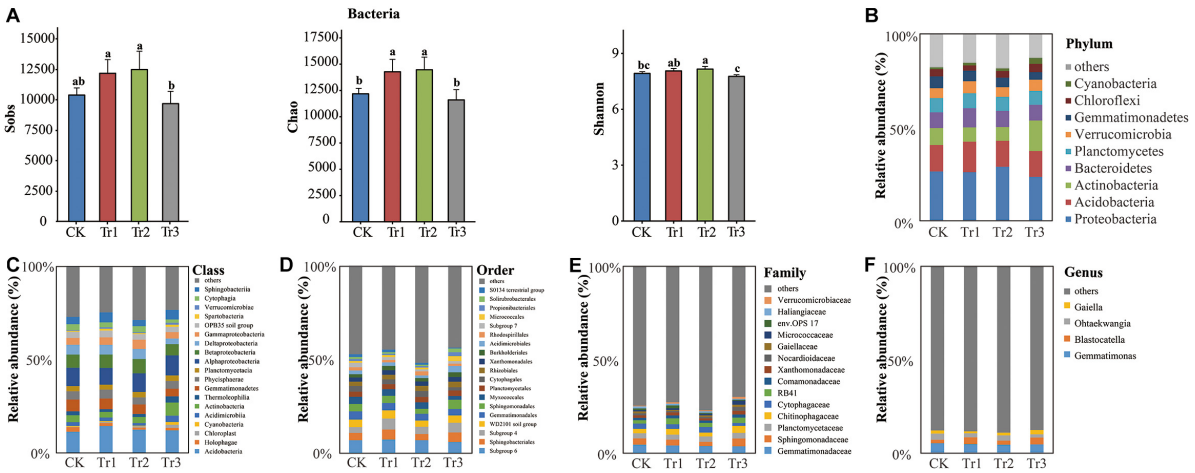

FIGURE 3 | Sobs, Chao, and Shannon indices and phylum-genus composition of the bacterial communities in soil with different species of intercropped aromatic plants, based on the OTUs obtained from 16S rRNA sequencing. **(A)** Sobs, Chao, and Shannon indices; **(B)** phylum; **(C)** class; **(D)** order; **(E)** family; and **(F)** genus. Values are the mean ± SD (n = 3). Different letters indicate significant differences ($P < 0.05$) based on Duncan's multiple range test. Sobs indicates the number of observed species or operational taxonomic units (OTUs). Chao indicates the non-parametric estimation of asymptotic species richness. Shannon's index was used to assess community diversity.

Sphingobacteriia and order Sphingobacteriales. Tr2 significantly reduced the RAs of the phylum Gemmatimonadetes and its member classes but increased the RA of Gammaproteobacteria. In all of the ICAP treatments, the RA of Holophagae in the phylum Acidobacteria was reduced relative to that in the control by 36.7% (Tr1), 54.6% (Tr2), and 43.3% (Tr3) (**Figures 3B–F**, **Supplementary Figure S2A** and **Supplementary Table S1**).

Based on the FAPROTAX database, we observed that several functions related to the C cycle were significantly altered by ICAP (**Figures 4A,D**). Compared with the control, all intercropping treatments significantly reduced the assemblage of fumarate respiration, knallgas bacteria, and ligninolysis groups. In addition, Tr3 promoted the assemblage of cyanobacteria, methylotrophy, and methanol oxidation groups, and Tr1 increased the assemblage of cyanobacteria, chitinolysis, and cellulolysis groups (**Figures 4A,D**). In addition, the assemblage of AC degradation groups showed the largest RA in Tr3 (**Figure 4A**). With respect to the assemblage of functional groups related to N cycling, the nitrite ammonification and nitrate ammonification groups were reduced significantly by ICAP compared with the control, and they were reduced more significantly in Tr3 than in Tr1 and Tr2. The nitrification and aerobic ammonia oxidation groups were reduced, whereas the ureolysis groups were significantly promoted only in Tr3 (**Figures 4B,E**). The type of intercropping impacted the structure of the functional groups related to C cycling (**Figure 4D**) more significantly than that of the functional groups related to N cycling (**Figure 4E**).

Composition, Structure, and Diversity of the Soil Fungal Community

A total of 359,913 quality-filtered fungal ITS2 sequences were obtained from 12 soil samples (n = 3). The number of reads ranged from 16,663 to 36,167 with a mean read count of 29,993 ± 5244. Rarefaction curves implied that the sequencing coverage was sufficient as plateaus were reached for soil communities. Based on the total fungal community estimated as the OTUs, the Sobs, species richness (Chao index) and alpha-diversity (Shannon index) were enhanced significantly by Tr1 and Tr2, while the Shannon index was reduced by Tr3 compared with the control (**Figure 5A**).

The composition of the total fungal community was dominated by the following phyla: Ascomycota (37.95%), Basidiomycota (9.75%), Zygomycota (4.63%), Glomeromycota (2.20%), Chytridiomycota (1.15%), and Ciliophora (0.96%) (**Figure 5B**). The RAs of the phylum Ascomycota and its five genera (*Ciliophora, Myrothecium, Gibberella, Trichocladium,* and *Podospora*) were all significantly reduced by ICAP relative to the control. The RAs of class Sordariomycetes, order Sordariales, family Chaetomiaceae, and genus *Mortierella* of Zygomycota were reduced in Tr3 relative to the control, whereas the RA of order Xylariales was promoted significantly by Tr3. Tr1 also influenced the RAs of these taxa and significantly increased the RAs of Basidiomycota and its member taxa Tremellomycetes, Cystofilobasidiales, Cystofilobasidiaceae, and *Guehomyces*; the RAs of Chytridiomycota and its member class Chytridiomycetes; and the RA of *Glomus* of Glomeromycota (**Figures 5B–F**, **Supplementary Figure S2B** and **Supplementary Table S2**).

Based on the FUNGuild database, the analyzed OTUs were assigned to the following guilds: saprotroph, pathotroph, pathotroph-saprotroph-symbiotroph, saprotroph-symbiotroph, symbiotroph, pathotroph-saprotroph, pathogen-saprotroph-symbiotroph, and pathotroph-symbiotroph (**Figure 4C**). Compared with those in the control, the pathotrophic and saprotrophic groups in ICAP were both reduced significantly. The symbiotic group was promoted by Tr1 and Tr2 but reduced by Tr3 (**Figure 4C**). The structure of the fungal functional groups

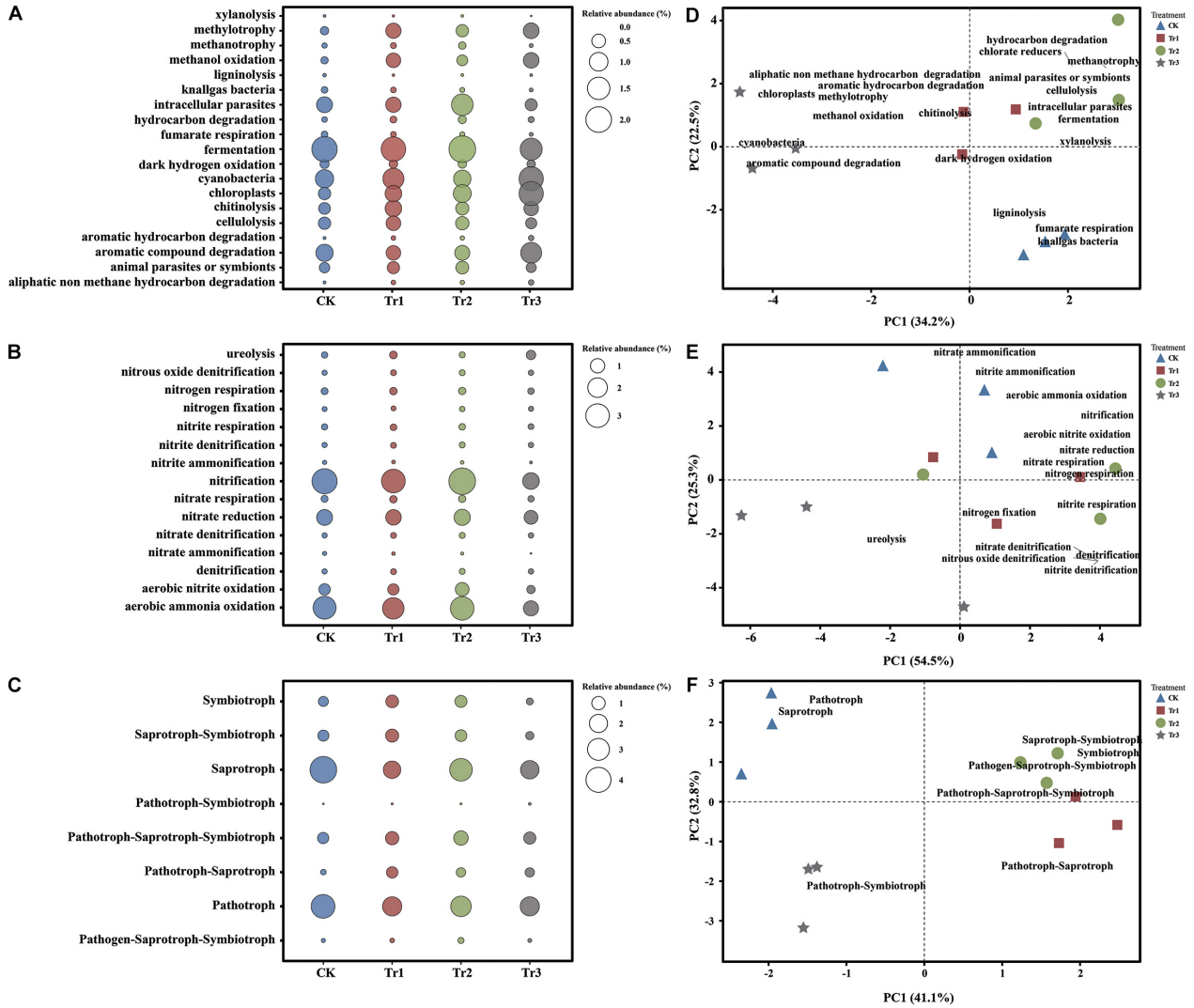

FIGURE 4 | Functional groups in soil with different species of intercropped aromatic plants, identified based on the OTUs obtained from 16S rRNA sequencing. Panels **(A)**, **(B)**, and **(C)** show the changes in functional groups related to the C and N cycles of the bacterial community and the trophic pattern of the fungal community. Panels **(D)**, **(E)**, and **(F)** show the functional group structure related to the C and N cycles of the bacterial community and the trophic pattern of the fungal community.

related to trophic patterns indicated a clear separation among the four treatments. The pathotrophic and saprotrophic groups were mainly clustered in the control (**Figure 4F**).

Relationships Among Soil Properties, Root Exudates, and Microbial Communities

Analyses of the correlations of root exudates and soil properties revealed that saccharide and OA contents were positively correlated with SOM, TN content and CAT activity, whereas alcohol and OHC contents were negatively correlated with these parameters (**Figures 6A–E**). Regarding microbial diversity, saccharide content was positively correlated with the Sobs and Chao indices of both bacteria and fungi, whereas lipid content was positively correlated with these indices only in fungi. The alcohol content was negatively correlated with the Chao index of fungi, and the amine content was negatively correlated with the Shannon index values of both bacteria and fungi (**Figures 6A–G**). The contents of seven main root exudates (in this study) were associated with the RAs of the dominant soil microbes. For example, saccharide content was mainly positively correlated with the RAs of Basidiomycota and half of its member taxa and negatively correlated with the RAs of Gemmatimonadales and its member families and genera and some taxa of Ascomycota (though it was positively correlated with Leotiomycetes RA) (**Figure 6A**). OA content was positively correlated with the RAs of Verrucomicrobiae and its orders and families and negatively correlated with those of Cytophagia and its corresponding orders and families, and most taxa in Ascomycota (**Figure 6B**). With

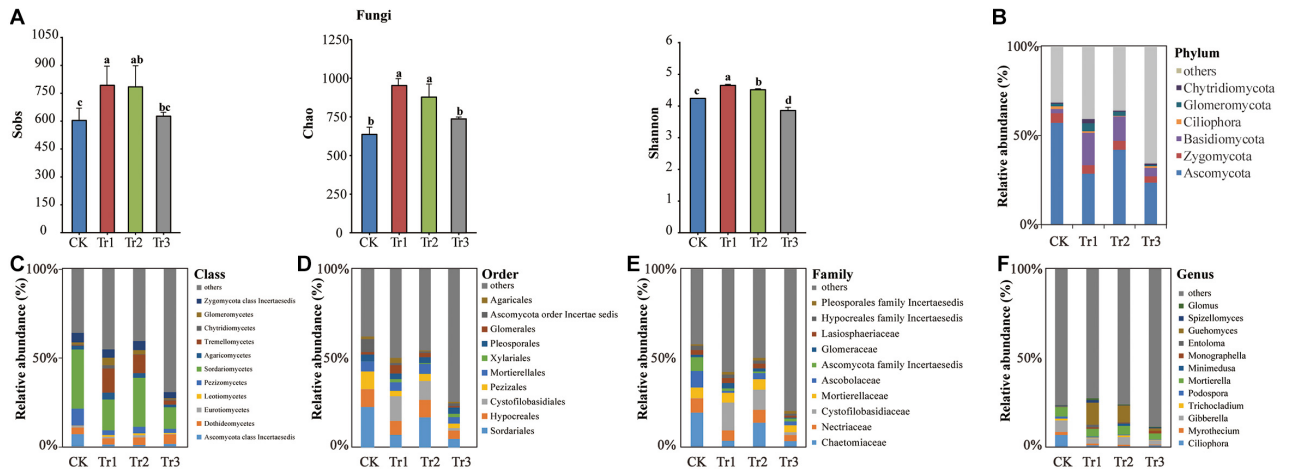

FIGURE 5 | The Sobs, Chao, and Shannon indices and phylum-genus composition of the fungal communities in soil with different species of intercropped aromatic plants, based on the OTUs obtained from ITS rRNA sequencing. **(A)** Sobs, Chao, and Shannon indices; **(B)** phylum; **(C)** class, **(D)** order; **(E)** family; and **(F)** genus. Values are the mean ± SD (n = 3). Different letters indicate significant differences ($P < 0.05$) based on Duncan's multiple range test. Sobs indicates the number of observed species or operational taxonomic units (OTUs). Chao indicates the non-parametric estimation of asymptotic species richness. Shannon's index was used to assess community diversity.

respect to the functional groups of microbial communities, both saccharide content and OA content correlated negatively with the RAs of ligninolysis, knallgas bacteria, and fumarate respiration groups related to the C cycle; nitrite ammonification and nitrate ammonification groups related to the N cycle; and saprotrophic and pathotrophic groups in the fungal trophic structure. Interestingly, the relationships between alcohols and the RAs of the taxonomic groups and functional groups of dominant microbes were largely opposite those between OA content and the RAs of these groups. In addition, the amine content was positively correlated with the RA of a functional group involved in ureolysis and related to the N cycle (**Figure 6D**). The AC content was significantly positively correlated with the RAs of Micrococcales and Micrococcaceae (**Figure 6G**).

Soil organic matter was positively correlated with the contents of OA and saccharides and negatively correlated with the contents of OHC and alcohols in root exudates (**Figure 6H**). In addition, SOM was positively related to fungal alpha-diversity (Chao). With respect to the RAs of members of the soil microbial community, SOM was mainly negatively correlated with the RAs of Gemmatimonadetes and its member classes, orders, families and genera and most dominant species of Ascomycota, whereas it was only positively correlated with the RAs of the subgroup 4 of order in Acidobacteria and Leotiomycetes of Ascomycota (**Figure 6H**). Furthermore, SOM was positively correlated with the RAs of some functional groups, such as those involved in aromatic hydrocarbon degradation and aliphatic non-methane hydrocarbon degradation in the bacterial community, and was negatively correlated with the RAs of others, such as saprotrophic groups of the fungal community and the ligninolysis, fumarate respiration, nitrite ammonification, and nitrate ammonification groups of the bacterial community (**Figure 6H**).

Soil pH was positively correlated with the RAs of Rhodospirillales and Zygomycota (including Mortierellales and Mortierellaceae) and negatively correlated with the RAs of Bacteroidetes (including Sphingobacteriia, Sphingobacteriales, and Chitinophagaceae) and Spartobacteria in Verrucomicrobia, as evaluated by genomics analysis (**Figure 6I**).

DISCUSSION

Root Exudates Shape the Soil C and N Framework After Intercropping

Problems with replanting fruit trees (replant disease) have been reported in numerous fruit-growing areas of the world. In tree fruit production, replant problems have been consistently used to describe conditions of poor tree growth resulting from a plethora of potential factors, including diminished soil fertility, degraded soil structure, and residual herbicide activity (Browne et al., 2006). Culture management should emphasize on improving soil microbial and faunal diversity as well as habitat quality rather than focusing on soil disinfection (Winkelmann et al., 2019). Intercropping is often used in orchards of China because it can mitigate disease and increase fruit yield. Intercropping with Tagetes, conventionally used against nematodes, revealed increased growth of apple in two apple replant disease soils, both in a biotest and in field trials (Yim et al., 2017). Plant diversity in experimental systems often enhances ecosystem productivity, but the mechanisms causing this overyielding are only partly understood (Li et al., 2016). In this study, the root system of intercrops (aromatic plants) is mainly distributed at a depth of 0–20 cm, while that of pear trees are mainly distributed at a depth of 20–60 cm. Thus, there is a complementarity between the root distribution depths of the species. Intercropping, the simultaneous cultivation of multiple crop species in a single field, increases aboveground productivity by enhancing soil C and N due to species complementarity (Cong et al., 2015). High

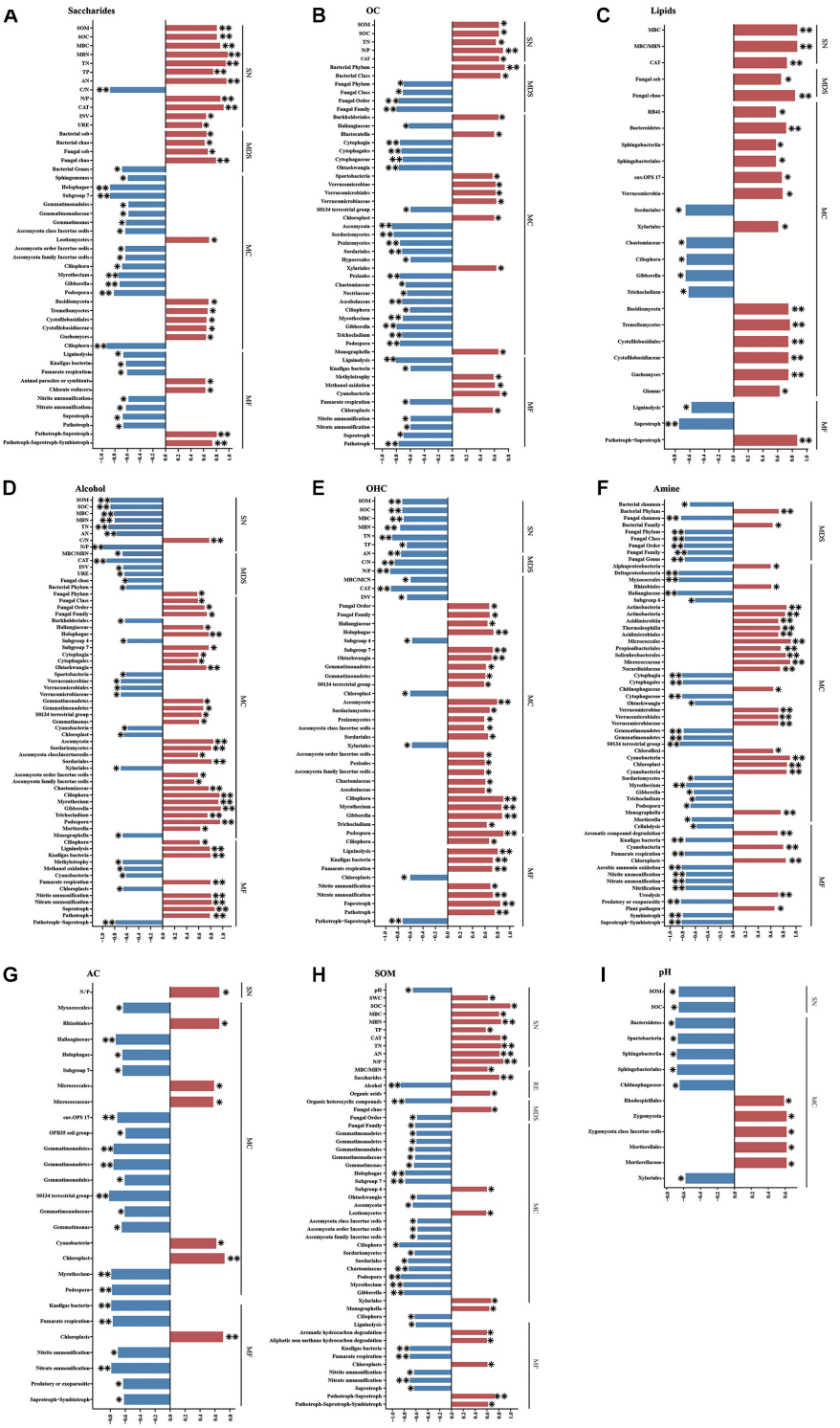

FIGURE 6 | Spearman's correlation coefficients among soil basic physicochemical parameters, root exudates, microbial communities, and soil nutrients. **(A)** Saccharides and other variables, **(B)** OA and other variables, **(C)** lipids and other variables, **(D)** alcohol and other variables, **(E)** OHC and other variables, **(F)** amine and other variables, **(G)** AC and other variables, **(H)** SOM and other variables, **(I)** pH and other variables. SN, soil nutrients; RE, root exudates; MDS, the diversity and structure of the total microbial community; MC, the composition of the microbial community; MF, functional groups of the microbial community. $^{*}P < 0.05$, $^{**}P < 0.01$.

C and N stocks in the soil are correlated with soil productivity (Latati et al., 2017).

In this study, ICAP significantly increased the SOM content and promoted the soil enzyme activities (**Table 1**). These alterations may have been caused by litter and root exudate inputs from the aromatic plants. Previous studies showed that the total amount of soil C inputs in the undergraded grassland (with high aboveground biomass and living root biomass) was higher than that in degraded grassland due to long-term overgrazing, and root turnover was suggested to be the primary source of soil C inputs (Shen et al., 2020). In our study, the saccharide and OA contents increased while the alcohol and OHC contents decreased after ICAP compared with monocropping. Interestingly, we also found that saccharide and OA contents were positively correlated with SOM, whereas alcohol and OHC contents were negatively correlated with SOM (**Figures 6A–E**). These results indicated that the changes in root exudates were beneficial for increasing SOM after ICAP. Similarly, a previous study found that SOM can be mobilized by different root exudates (Nardi et al., 2000). Intercropping can contribute to multiple agroecosystem services by increasing yield and improving soil quality and soil C sequestration (Cong et al., 2015). In addition, the input of litter from aromatic plants may have been responsible for the increase in SOM content under intercropping. Castellano et al. (2015) suggested that plant litter was the primary source of all SOM. However, the processes of litter decomposition and SOM stabilization are often considered separate (Sollins et al., 2007). Carrington et al. (2012) found that plant litter quantity rather than quality is the main determinant of the amount of physicochemically stabilized SOM.

The soil nutrient framework was distinct between the intercropping treatments and the control (**Figure 2A**). Furthermore, the use of different species in the intercropping system resulted in significant differences in the N cycle, with higher TN, AN, and MBN contents and a lower C/N ratio in the soil associated with basil and summer savory plants (Tr1 and Tr2) than in that associated with blue mink plants (Tr3) in the intercropping systems. These differences might be caused by variations in the quantity and quality of plant litter and root exudates among intercrops. High-quality plant litters with high N concentrations and low C/N ratios, accelerated greater mineralization efficiency than low-quality litters (Castellano et al., 2015). In addition, plant root exudates can profoundly modify soil microbial communities and influence their N transformations (Coskun et al., 2017; Meier et al., 2017).

The amount and composition of root exudates varies with the taxonomic status of the host (Chaparro et al., 2014; Mönchgesang et al., 2016; Sasse et al., 2018). In our study, the relative content of AC varied among the different ICAP treatments, with the highest value observed in the Tr3 treatment. One reason for this finding is that among the intercrops, *Ageratum houstonianum* (Tr3) had the highest aboveground and root biomass per plant (data not shown). Previous studies showed that higher plant biomass usually induced higher SOM fraction contents (e.g., particulate organic matter, rhizodeposition), which could act as major sources and energy for microorganisms (Tian et al., 2013).

Root Exudates From Different Aromatic Plants Contributed to the Distinct Properties of Microbial Community

Some studies have shown that the traits of the soil microbial community are influenced by root exudates (Shi et al., 2011; Hu et al., 2018; Sasse et al., 2018). Additionally, root exudate diversity has been identified as a crucial link between plant diversity and soil microorganisms (Steinauer et al., 2016). We found that intercropping with basil and summer savory (Tr1 and Tr2) improved the species richness and alpha-diversity (Chao index) of the bacterial and fungal communities, whereas no significant difference in these measures was observed between the intercropping treatment with blue mink (Tr3) and the control (**Figures 3**, **5**). These differences might be associated with the higher SOM content and lower pH induced by different aromatic plants. A long-term grassland biodiversity experiment showed that bacterial and fungal diversity increased with higher plant diversity (Lange et al., 2015). Another study showed that intercropping increased microbial OTU richness and fungal community diversity and that the diversity of the soil bacterial community varied among seven intercropping systems (Li and Wu, 2018). These observations show that the intercropping species affects the soil microbial community.

The soil bacterial community displayed two distinct clusters according to the two taxonomic families of the intercrops after ICAP (**Supplementary Figure S2A**). This finding suggested that the difference in bacterial composition due to interfamily intercropping was larger than that due to intrafamily intercropping. The root exudates of plant species significantly shaped the structure of the rhizosphere bacterial community (Haichar et al., 2008; Sasse et al., 2018). The potential of cropping systems and species identity to modify soil bacterial communities, subsequently modify plant growth and crop-weed competition (Ishaq et al., 2017).

The composition of bacteria was influenced more markedly by blue mink (Tr3) than by basil and summer savory (Tr1 and Tr2) (**Supplementary Figure S2A**). This might have been due to the contents of aromatic AC, OA and amine being highest in the blue mink (Tr3) rhizosphere. A previous study also indicated that OA in root exudates played a significant role in shaping soil bacterial communities (Shi et al., 2011). Furthermore, SOC and AN have been identified as the key factors shaping bacterial communities in the rhizosphere (Cui et al., 2018). In our study, intercropping with blue mink (Tr3) significantly increased the AC content (**Figure 1E**), the RAs of the phylum Actinobacteria and its order (Micrococcales) and family (Micrococcaceae) (**Figures 3B,D,E**). Correlation analysis further revealed that the AC content was significantly correlated with Micrococcales and Micrococcaceae (**Figure 6G**). We suspected that these groups are involved in the degradation of AC. A previous study found strains resistant to heavy metals in nine of the 15 families belonging to the order Micrococcales (Alvarez et al., 2017). With respect to the fungal community, all ICAP treatments significantly reduced the RAs

of Ascomycota and some of its dominant genera, and the effect of intercropping with blue mink (Tr3) was more significant than that of intercropping with basil and summer savory (Tr1 and Tr2) (**Figure 5B** and **Supplementary Figure S2B**).

The different aromatic plants induced distinct effects on the functional groups of bacteria involved in soil C and N cycling (**Figure 4**). In terms of the functional groups related to C cycling, all ICAP treatments significantly recruited the cyanobacteria, the RA of cyanobacteria was increased significantly in Tr3 (**Figures 4A,D**). Cyanobacteria form the most ancient group of biocrusts and contribute to soil C and N cycling (DeBruyn et al., 2011; Chamizo et al., 2012; Zhao et al., 2015; Muñoz-Rojas et al., 2018; Ma et al., 2019). The three intercropping treatments reduced the assemblage of nitrite ammonification and nitrate ammonification groups, and intercropping with blue mink (Tr3) significantly promoted the assemblage of the ureolysis group (**Figure 4B**). In addition, intercropping significantly reduced the saprotrophic and pathotrophic groups of fungal trophic types; such reductions might reduce plant disease. Intercropping has been widely used for its beneficial effects in controlling disease and improving nutrition in the field (Lian et al., 2019; Misra et al., 2019).

Relationships Among SOM, Root Exudates, and Microbial Communities

Soil bacterial and fungal richness (Sobs and Chao indices) was positively correlated with saccharide content (**Figure 6A**), whereas the alpha-diversity (Shannon index) was negatively correlated with the content of amine compounds (**Figure 6F**). These results indicated that saccharide compounds increased the richness of the microbial population while amine compounds inhibited the diversity of the microbial community. A previous study found that OA, amine and alcohol compounds were associated with microbial structure (Zhalnina et al., 2018). These observations suggest that root exudates can stimulate microbes to decompose SOM and release N with litter input (Strickland et al., 2015; Meier et al., 2017). The relationships between root exudates and the dominant microbial and functional communities identified based on Spearman analysis differed among the treatments (**Figure 6**). Therefore, different aromatic plants recruit different dominant microbes in intercropping systems; for example, Tr3 significantly increased the RA of Actinobacteria. Yuan et al. (2015) found that banana root exudates, especially OA, played a crucial role in attracting plant-growth promoting rhizobacteria (PGPR) and initiating their colonization on the host roots.

Soil organic matter was negatively correlated with the RAs of three main bacterial taxa: phylum Gemmatimonadetes and its members Holophagae (belonging to Acidobacteria) and *Ohtaekwangia* (belonging to Bacteroidetes) (**Figure 6H**). However, pH was negatively correlated with the RAs of many members of Bacteroidetes and Spartobacteria of Verrucomicrobia and was positively correlated with the RA of Rhodospirillales of Proteobacteria (**Figure 6I**). Verrucomicrobial elevational distribution was strongly influenced by soil pH and carbon/nitrogen ratio (Shen et al., 2017). Malik et al. (2018) discovered distinct pH controls of microbial mechanisms of carbon accumulation. This finding indicated that the combined effect of SOM and pH shaped the soil decomposition pattern of the dominant bacteria (Hernández et al., 2015; Malik et al., 2018; Martínez-García et al., 2018; Wan et al., 2020).

Additionally, for the fungal community, SOM was positively correlated with fungal alpha-diversity (Chao) and negatively correlated with the RAs of most members of the phylum Ascomycota, whereas pH was positively correlated with the RAs of some members of Zygomycota. These results are in line with the finding that SOM was more important than pH in inhibiting the dominant fungi involved in degrading organic materials and in inhibiting pathogen growth (Tian et al., 2016). Furthermore, SOM was positively correlated with the RAs of some functional groups related to the C cycle and negatively correlated with the RAs of ligninolysis, fumarate respiration, nitrite ammonification, and nitrate ammonification groups of the bacterial community and pathotrophic groups of fungi, whereas pH was not correlated with the RAs of functional groups (**Figure 6**). These results suggested that SOM was the main driver of microbial functional groups. Changes in SOM and pH mediating the microbial community were associated with increases in saccharide and OA contents and decreases in OHC and alcohol compounds (Tian et al., 2016; Cui et al., 2018; Li et al., 2018).

CONCLUSION

In conclusion, we found that root exudates from aromatic plants shaped the diversity, structure, composition and function of the soil microbial community, which regulated C and N nutrients during SOM decomposition. Intercropping significantly reduced the RAs of saprotrophic and pathotrophic groups. The TN and AN contents, species richness alpha-diversity of bacterial community, and the symbiotic group of the fungal community were higher in Tr1 and Tr2 than in Tr3. We suggest that intercropping with basil and summer savory is more beneficial to pear orchards than intercropping with blue mink. However, the biomass of the intercrops was not determined in this study. To identify the main beneficial factors in intercropping systems, the contents of root exudates and the biomass of intercrops both need to be studied.

DATA AVAILABILITY STATEMENT

The data presented in the study are deposited in the NCBI repository, accession number (PRJNA685959).

AUTHOR CONTRIBUTIONS

MH, MS, JT, BS, and YH contributed to the data curation. YY contributed to the funding acquisition. YZ, MH, and MS contributed to the investigation. YZ and JZ contributed to the writing (original draft). YY contributed to the writing (review and

editing). All authors contributed to the article and approved the submitted version.

FUNDING

Financial support was provided by the National Key Project of the Research and Development Plan (2016YFD0201116), the Beijing Key Project of the Science and Technology Plan (Z181100002418003/004), Beijing Natural Science Found-Municipal Education Commission (KZ201910020022). The Construction of Beijing Science and Technology Innovation and Service Capacity in Top Subjects (CEFF-PXM2019_014207_000032) and Beijing Key Laboratory of New Techniques in Agricultural Application (NYYYKF201901).

ACKNOWLEDGMENTS

We thank the Beijing Collaborative Innovation Center for Eco-environmental Improvement of Forestry and Fruit Trees; the Key Laboratory of Pomology, Beijing Nursery Engineering Research Center for Fruit Crops; the Key Laboratory of Agricultural Applications at the Beijing University of Agriculture; and the technicians from the Changping District Forestry Administration in Beijing.

SUPPLEMENTARY MATERIAL

The Supplementary Material for this article can be found online at: https://www.frontiersin.org/articles/10.3389/fmicb.2021.616932/full#supplementary-material

REFERENCES

Alvarez, A., Saez, J. M., Davila Costa, J. S., Colin, V. L., Fuentes, M. S., Cuozzo, S. A., et al. (2017). Actinobacteria: current research and perspectives for bioremediation of pesticides and heavy metals. *Chemosphere* 166, 41–62. doi: 10.1016/j.chemosphere.2016.09.070

Arancon, N. Q., Edwards, C. A., and Bierman, P. (2006). Influences of vermicomposts on field strawberries: part 2. effects on soil microbiological and chemical properties. *Bioresour. Technol.* 97, 831–840. doi: 10.1016/j.biortech.2005.04.016

Atucha, A., Merwin, I. A., and Brown, M. G. (2011). Long-term effects of four groundcover management systems in an apple orchard. *Hortscience* 46, 1176–1183. doi: 10.21273/HORTSCI.46.8.1176

Berendsen, R. L., Pieterse, C. M. J., and Bakker, P. A. H. M. (2012). The rhizosphere microbiome and plant health. *Trends Plant Sci.* 17, 478–486. doi: 10.1016/j.tplants.2012.04.001

Bremner, J. M. (1996). "Nitrogen-total," in *Methods of Soil Analysis*, ed. D. L. Sparks (Madison: American Society of Agronomy Inc), 1085–1122.

Brookes, P. C., Landman, A., Pruden, G., and Jenkinson, D. S. (1985). Chloroform fumigation and the release of soil nitrogen: a rapid direct extraction method to measure microbial biomass nitrogen in soil. *Soil Biol. Biochem.* 17, 837–842. doi: 10.1016/0038-0717(85)90144-0

Browne, G. T., Connell, J. H., and Schneider, S. M. (2006). Almond replant disease and its management with alternative pre-plant soil Fumigation treatments and rootstocks. *Plant Dis.* 90, 869–876. doi: 10.1094/PD-90-0869

Carrington, E. M., Hernes, P. J., Dyda, R. Y., Plante, A. F., and Six, J. (2012). Biochemical changes across a carbon saturation gradient: lignin, cutin, and suberin decomposition and stabilization in fractionated carbon pools. *Soil Biol. Biochem.* 47, 179–190. doi: 10.1016/j.soilbio.2011.12.024

Castellano, M. J., Mueller, K. E., Olk, D. C., Sawyer, J. E., and Six, J. (2015). Integrating plant litter quality, soil organic matter stabilization, and the carbon saturation concept. *Global Change Biol.* 21, 3200–3209. doi: 10.1111/gcb.12982

Chamizo, S., Cantón, Y., Miralles, I., and Domingo, F. (2012). Biological soil crust development affects physicochemical characteristics of soil surface in semiarid ecosystems. *Soil Biol. Biochem.* 49, 96–105. doi: 10.1016/j.soilbio.2012.02.017

Chaparro, J. M., Badri, D. V., and Vivanco, J. M. (2014). Rhizosphere microbiome assemblage is affected by plant development. *ISME J.* 8, 790–803. doi: 10.1038/ismej.2013.196

Chen, J., and Stark, J. M. (2000). Plant species effects and carbon and nitrogen cycling in a sagebrush–crested wheatgrass soil. *Soil Biol. Biochem.* 32, 47–57. doi: 10.1016/S0038-0717(99)00124-8

Chen, X., Song, B., Yao, Y., Wu, H., Hu, J., and Zhao, L. (2014). Aromatic plants play an important role in promoting soil biological activity related to nitrogen cycling in an orchard ecosystem. *Sci. Total Environ.* 472, 939–946. doi: 10.1016/j.scitotenv.2013.11.117

Chen, Y., Bonkowski, M., Shen, Y., Griffiths, B. S., Jiang, Y., Wang, X., et al. (2020). Root ethylene mediates rhizosphere microbial community reconstruction when chemically detecting cyanide produced by neighbouring plants. *Microbiome* 8:4. doi: 10.1186/s40168-019-0775-6

Cheng, L., Zhang, N., Yuan, M., Xiao, J., Qin, Y., Deng, Y., et al. (2017). Warming enhances old organic carbon decomposition through altering functional microbial communities. *ISME J.* 11:1825. doi: 10.1038/ismej.2017.48

Cong, W., Hoffland, E., Li, L., Six, J., Sun, J., Bao, X., et al. (2015). Intercropping enhances soil carbon and nitrogen. *Global Change Biol.* 21, 1715–1726. doi: 10.1111/gcb.12738

Coskun, D., Britto, D. T., Shi, W., and Kronzucker, H. J. (2017). How plant root exudates shape the nitrogen cycle. *Trends Plant Sci.* 22, 661–673. doi: 10.1016/j.tplants.2017.05.004

Cui, X., Zhang, Y., Gao, J., Peng, F., and Gao, P. (2018). Long-term combined application of manure and chemical fertilizer sustained higher nutrient status and rhizospheric bacterial diversity in reddish paddy soil of Central South China. *Sci. Rep.* 8:16554. doi: 10.1038/s41598-018-34685-0

DeBruyn, J. M., Nixon, L. T., Fawaz, M. N., Johnson, A. M., and Radosevich, M. (2011). Global biogeography and quantitative seasonal dynamics of Gemmatimonadetes in soil. *Appl. Environ. Microbiol.* 77, 6295–6300. doi: 10.1128/AEM.05005-11

DeHaan, L. R., Weisberg, S., Tilman, D., and Fornara, D. (2010). Agricultural and biofuel implications of a species diversity experiment with native perennial grassland plants. *Agr. Ecosyst. Environ.* 137, 33–38. doi: 10.1016/j.agee.2009.10.017

Edgar, R. C. J. (2013). UPARSE: highly accurate OTU sequences from microbial amplicon reads. *Nat. Methods* 10:996. doi: 10.1038/nmeth.2604

Fitzpatrick, C. R., Copeland, J., Wang, P. W., Guttman, D. S., Kotanen, P. M., and Johnson, M. T. (2018). Assembly and ecological function of the root microbiome across angiosperm plant species. *Proc. Natl. Acad. Sci. U.S.A.* 115, E1157–E1165. doi: 10.1073/pnas.1717617115

Gourmelon, V., Maggia, L., Powell, J. R., Gigante, S., Hortal, S., Gueunier, C., et al. (2016). Environmental and geographical factors structure soil microbial diversity in New Caledonian ultramafic substrates: a metagenomic approach. *PloS one* 11:e0167405. doi: 10.1371/journal.pone.0167405

Haichar, F. E. Z., Marol, C., Berge, O., Rangel-Castro, J. I., Prosser, J. I., Balesdent, J., et al. (2008). Plant host habitat and root exudates shape soil bacterial community structure. *ISME J.* 2, 1221–1230. doi: 10.1038/ismej.2008.80

Hernández, M., Dumont, M. G., Yuan, Q., and Conrad, R. (2015). Different bacterial populations associated with the roots and rhizosphere of rice incorporate plant-derived carbon. *Appl. Environ. Microbiol.* 81, 2244–2253. doi: 10.1128/AEM.03209-14

Hu, L., Robert, C., Cadot, S., Zhang, X., Ye, M., Li, B., et al. (2018). Root exudate metabolites drive plant-soil feedbacks on growth and defense by shaping the rhizosphere microbiota. *Nat. Commun.* 9:2738. doi: 10.1038/s41467-018-05122-7

Ishaq, S. L., Johnson, S. P., Miller, Z. J., Lehnhoff, E. A., Olivo, S., Yeoman, C. J., et al. (2017). Impact of cropping systems, soil inoculum, and plant species identity on soil bacterial community structure. *Microb. Ecol.* 73, 417–434. doi: 10.1007/s00248-016-0861-2

Jiang, Y., Liu, M., Zhang, J., Chen, Y., Chen, X., Chen, L., et al. (2017). Nematode grazing promotes bacterial community dynamics in soil at the aggregate level. *ISME J.* 11, 2705–2717. doi: 10.1038/ismej.2017.120

Jin, K., Sleutel, S., Buchan, D., De Neve, S., Cai, D. X., Gabriels, D., et al. (2009). Changes of soil enzyme activities under different tillage practices in the Chinese Loess Plateau. *Soil Till. Res.* 104, 115–120. doi: 10.1016/j.still.2009.02.004

Klindworth, A., Pruesse, E., Schweer, T., Peplies, J., Quast, C., Horn, M., et al. (2013). Evaluation of general 16S ribosomal RNA gene PCR primers for classical and next-generation sequencing-based diversity studies. *Nucleic Acids Res.* 41:e1. doi: 10.1093/nar/gks808

Koutika, L. S., Vanderhoeven, S., Chapuis-Lardy, L., Dassonville, N., and Meerts, P. (2007). Assessment of changes in soil organic matter after invasion by exotic plant species. *Biol. Fert. Soils* 44, 331–341. doi: 10.1007/s00374-007-0210-1

Kremer, R. J., and Kussman, R. D. (2011). Soil quality in a pecan–kura clover alley cropping system in the Midwestern USA. *Agroforest. Syst.* 83, 213–223. doi: 10.1007/s10457-011-9370-y

Lange, M., Eisenhauer, N., Sierra, C. A., Bessler, H., Engels, C., Griffiths, R. I., et al. (2015). Plant diversity increases soil microbial activity and soil carbon storage. *Nat. Commun.* 6:6707. doi: 10.1038/ncomms7707

Latati, M., Aouiche, A., Tellah, S., Laribi, A., Benlahrech, S., Kaci, G., et al. (2017). Intercropping maize and common bean enhances microbial carbon and nitrogen availability in low phosphorus soil under Mediterranean conditions. *Eur. J. Soil Biol.* 80, 9–18. doi: 10.1016/j.ejsobi.2017.03.003

Lekberg, Y., Gibbons, S. M., Rosendahl, S., and Ramsey, P. W. (2013). Severe plant invasions can increase mycorrhizal fungal abundance and diversity. *ISME J.* 7:1424. doi: 10.1038/ismej.2013.41

Li, B., Li, Y., Wu, H., Zhang, F., Li, C., Li, X., et al. (2016). Root exudates drive interspecific facilitation by enhancing nodulation and N_2 fixation. *Proc. Natl Acad. Sci.* 113, 6496–6501. doi: 10.1073/pnas.1523580113

Li, Q., Liu, C., Wang, X., Jin, Z., Song, A., Liang, Y., et al. (2018). Influence of altered microbes on soil organic carbon availability in karst agricultural soils contaminated by Pb-Zn tailings. *Front. Microbiol.* 9:2062. doi: 10.3389/fmicb.2018.02062

Li, S., and Wu, F. (2018). Diversity and co-occurrence patterns of soil bacterial and fungal communities in seven intercropping systems. *Front. Microbiol.* 9:1521. doi: 10.3389/fmicb.2018.01521

Lian, T., Mu, Y., Jin, J., Ma, Q., Cheng, Y., Cai, Z., et al. (2019). Impact of intercropping on the coupling between soil microbial community structure, activity, and nutrient-use efficiencies. *PeerJ* 7:e6412. doi: 10.7717/peerj.6412

Louca, S., Parfrey, L. W., and Doebeli, M. (2016). Decoupling function and taxonomy in the global ocean microbiome. *Science* 353, 1272–1277. doi: 10.1126/science.aaf4507

Lu, R. K. (2000). *Methods of Soil and Agro-Chemical Analysis (in Chinese)*. Beijing: China Agricultural Science and Technology Press.

Lubbe, A., and Verpoorte, R. (2011). Cultivation of medicinal and aromatic plants for specialty industrial materials. *Ind. Crop. Prod.* 34, 785–801. doi: 10.1016/j.indcrop.2011.01.019

Ma, X., Zhang, Q., Zheng, M., Gao, Y., Yuan, T., Hale, L., et al. (2019). Microbial functional traits are sensitive indicators of mild disturbance by lamb grazing. *ISME J.* 13, 1370–1373. doi: 10.1038/s41396-019-0354-7

Magoč, T., and Salzberg, S. L. (2011). FLASH: fast length adjustment of short reads to improve genome assemblies. *Bioinformatics* 27, 2957–2963. doi: 10.1093/bioinformatics/btr507

Malik, A. A., Puissant, J., Buckeridge, K. M., Goodall, T., Jehmlich, N., Chowdhury, S., et al. (2018). Land use driven change in soil pH affects microbial carbon cycling processes. *Nat. Commun.* 9:3591. doi: 10.1038/s41467-018-05980-1

Marschner, P., Grierson, P. F., and Rengel, Z. (2005). Microbial community composition and functioning in the rhizosphere of three Banksia species in native woodland in Western Australia. *Appl. Soil Ecol.* 28, 191–201. doi: 10.1016/j.apsoil.2004.09.001

Martínez-García, L. B., Korthals, G., Brussaard, L., Jørgensen, H. B., and De Deyn, G. B. (2018). Organic management and cover crop species steer soil microbial community structure and functionality along with soil organic matter properties. *Agr. Ecosyst. Environ.* 263, 7–17. doi: 10.1016/j.agee.2018.04.018

Mazzola, M., and Manici, L. M. (2012). Apple replant disease: role of microbial ecology in cause and control. *Annu. Rev. Phytopathol.* 50, 45–65. doi: 10.1146/annurev-phyto-081211-173005

Meier, I. C., Finzi, A. C., and Phillips, R. P. (2017). Root exudates increase N availability by stimulating microbial turnover of fast-cycling N pools. *Soil Biol. Biochem.* 106, 119–128. doi: 10.1016/j.soilbio.2016.12.004

Misra, P., Maji, D., Awasthi, A., Pandey, S. S., Yadav, A., Pandey, A., et al. (2019). Vulnerability of soil microbiome to monocropping of medicinal and aromatic plants and its restoration through intercropping and organic amendments. *Front. Microbiol.* 10:2604. doi: 10.3389/fmicb.2019.02604

Mönchgesang, S., Strehmel, N., Schmidt, S., Westphal, L., Taruttis, F., Müller, E., et al. (2016). Natural variation of root exudates in *Arabidopsis thaliana*-linking metabolomic and genomic data. *Sci. Rep.* 6:29033. doi: 10.1038/srep29033

Muñoz-Rojas, M., Román, J. R., Roncero-Ramos, B., Erickson, T. E., Merritt, D. J., Aguila-Carricondo, P., et al. (2018). Cyanobacteria inoculation enhances carbon sequestration in soil substrates used in dryland restoration. *Sci. Total Environ.* 636, 1149–1154. doi: 10.1016/j.scitotenv.2018.04.265

Nardi, S., Concheri, G., Pizzeghello, D., Sturaro, A., Rella, R., and Parvoli, G. (2000). Soil organic matter mobilization by root exudates. *Chemosphere* 41, 653–658. doi: 10.1016/s0045-6535(99)00488-9

Nelson, D. W., and Sommers, L. E. (1996). "Total carbon, organic carbon, and organic matter," in *Methods of Soil Analysis*, ed. D. L. Sparks (Madison: American Society of Agronomy Inc), 961–1010.

Nguyen, N. H., Song, Z., Bates, S. T., Branco, S., Tedersoo, L., Menke, J., et al. (2016). FUNGuild: an open annotation tool for parsing fungal community datasets by ecological guild. *Fungal Ecol.* 20, 241–248. doi: 10.1016/j.funeco.2015.06.006

Olsen, S. R., and Sommers, L. E. (1982). "Phosphorous," in *Methods of Soil Analysis*, eds A. L. Page, R. H. Miller, and D. R. Keeney (Madison: American Society of Agronomy Inc), 403–427.

Pribyl, D. W. (2010). A critical review of the conventional SOC to SOM conversion factor. *Geoderma* 156, 75–83. doi: 10.1016/j.geoderma.2010.02.003

Pruesse, E., Quast, C., Knittel, K., Fuchs, B. M., Ludwig, W., Peplies, J., et al. (2007). SILVA: a comprehensive online resource for quality checked and aligned ribosomal RNA sequence data compatible with ARB. *Nucleic Acids Res.* 35, 7188–7196. doi: 10.1093/nar/gkm864

Ramos, M. E., Benítez, E., García, P. A., and Robles, A. B. (2010). Cover crops under different managements vs. frequent tillage in almond orchards in semiarid conditions: effects on soil quality. *Appl. Soil Ecol.* 44, 6–14. doi: 10.1016/j.apsoil.2009.08.005

Sardans, J., Bartrons, M., Margalef, O., Gargallo-Garriga, A., Janssens, I. A., Ciais, P., et al. (2017). Plant invasion is associated with higher plant-soil nutrient concentrations in nutrient-poor environments. *Global Change Biol.* 23, 1282–1291. doi: 10.1111/gcb.13384

Sasse, J., Martinoia, E., and Northen, T. (2018). Feed your friends: do plant exudates shape the root microbiome? *Trends Plant Sci.* 23, 25–41. doi: 10.1016/j.tplants.2017.09.003

Schloss, P. D., Westcott, S. L., Ryabin, T., Hall, J. R., Hartmann, M., Hollister, E. B., et al. (2009). Introducing mothur: open-source, platform-independent, community-supported software for describing and comparing microbial communities. *Appl. Environ. Microbiol.* 75, 7537–7541. doi: 10.1128/AEM.01541-09

Scholes, R. J., and Noble, I. R. (2001). Storing carbon on land. *Science* 294, 1012–1013.

Sharma, A., Tiwari, K. N., and Bhadoria, P. B. S. (2011). Effect of land use land cover change on soil erosion potential in an agricultural watershed. *Environ. Monit. Assess.* 173, 789–801. doi: 10.1007/s10661-010-1423-6

Shen, C., Ge, Y., Yang, T., and Chu, H. (2017). Verrucomicrobial elevational distribution was strongly influenced by soil pH and carbon/nitrogen ratio. *J. Soil Sediment* 17, 2449–2456. doi: 10.1007/s11368-017-1680-x

Shen, X., Yang, F., Xiao, C., and Zhou, Y. (2020). Increased contribution of root exudates to soil carbon input during grassland degradation. *Soil Biol. Biochem.* 146:107817. doi: 10.1016/j.soilbio.2020.107817

Shi, S., Richardson, A. E., O'Callaghan, M., DeAngelis, K. M., Jones, E. E., Stewart, A., et al. (2011). Effects of selected root exudate components on soil bacterial

communities. *FEMS Microbiol. Ecol.* 77, 600–610. doi: 10.1111/j.1574-6941.2011.01150.x

Sollins, P., Swanston, C., and Kramer, M. (2007). Stabilization and destabilization of soil organic matter—a new focus. *Biogeochemistry* 85, 1–7. doi: 10.1007/s10533-007-9099-x

Song, B., Jiao, H., Tang, G., and Yao, Y. (2014). Combining repellent and attractive aromatic plants to enhance biological control of three tortricid species (Lepidoptera: Tortricidae) in an apple orchard. *Fla. Entomol.* 97, 1679–1689. doi: 10.1653/024.097.0442

Steinauer, K., Chatzinotas, A., and Eisenhauer, N. (2016). Root exudate cocktails: the link between plant diversity and soil microorganisms? *Ecol. Evol.* 6, 7387–7396. doi: 10.1002/ece3.2454

Strickland, M. S., McCulley, R. L., Nelson, J. A., and Bradford, M. A. (2015). Compositional differences in simulated root exudates elicit a limited functional and compositional response in soil microbial communities. *Front. Microbiol.* 6:817. doi: 10.3389/fmicb.2015.00817

Tang, G. B., Song, B. Z., Zhao, L. L., Sang, X. S., Wan, H. H., Zhang, J., et al. (2013). Repellent and attractive effects of herbs on insects in pear orchards intercropped with aromatic plants. *Agroforest. Syst.* 87, 273–285. doi: 10.1007/s10457-012-9544-2

Tian, J., Dippold, M., Pausch, J., Blagodatskaya, E., Fan, M., Li, X., et al. (2013). Microbial response to rhizodeposition depending on water regimes in paddy soils. *Soil Biol. Biochem.* 65, 195–203. doi: 10.1016/j.soilbio.2013.05.021

Tian, J., Wang, J., Dippold, M., Gao, Y., Blagodatskaya, E., and Kuzyakov, Y. (2016). Biochar affects soil organic matter cycling and microbial functions but does not alter microbial community structure in a paddy soil. *Sci. Total Environ.* 556, 89–97. doi: 10.1016/j.scitotenv.2016.03.010

Toju, H., Tanabe, A. S., Yamamoto, S., and Sato, H. (2012). High-coverage ITS primers for the DNA-based identification of ascomycetes and basidiomycetes in environmental samples. *PloS one* 7:e40863. doi: 10.1111/1462-2920.13133.x

Tripathi, P., Shah, S., Kashyap, S. D., and Tripathi, A. (2019). Fruit yield and quality characteristics of high density *Prunus persica* (L.) Batsch plantation intercropped with medicinal and aromatic plants in the Indian Western Himalayas. *Agroforest. Syst.* 93, 1717–1728. doi: 10.1007/s10457-018-0276-9

Vance, E. D., Brookes, P. C., and Jenkinson, D. S. (1987). An extraction method for measuring soil microbial biomass C. *Soil Biol. Biochem.* 19, 703–707. doi: 10.1016/0038-0717(87)90052-6

Waldrop, M. P., Holloway, J. M., Smith, D. B., Goldhaber, M. B., Drenovsky, R. E., Scow, K. M., et al. (2017). The interacting roles of climate, soils, and plant production on soil microbial communities at a continental scale. *Ecology* 98, 1957–1967. doi: 10.1002/ecy.1883

Wan, W., Tan, J., Wang, Y., Qin, Y., He, H., Wu, H., et al. (2020). Responses of the rhizosphere bacterial community in acidic crop soil to pH: changes in diversity, composition, interaction, and function. *Sci. Total Environ.* 700:134418. doi: 10.1016/j.scitotenv.2019.134418

Winkelmann, T., Smalla, K., Amelung, W., Baab, G., Grunewaldt-Stocker, G., Kanfra, X., et al. (2019). Apple replant disease: causes and mitigation strategies. *Curr. Issues Mol. Biol.* 30, 89–106. doi: 10.21775/cimb.030.089

Yim, B., Nitt, H., Wrede, A., Jacquiod, S., Sørensen, J., Winkelmann, T., et al. (2017). Effects of soil pre-treatment with Basamid§granules, *Brassica juncea*, *Raphanus sativus* and *Tagetes patula* on bacterial and fungal communities at two replant disease sites. *Front. Microbiol.* 8:1604.

Yuan, J., Zhang, N., Huang, Q., Raza, W., Li, R., Vivanco, J. M., et al. (2015). Organic acids from root exudates of banana help root colonization of PGPR strain *Bacillus amyloliquefaciens* NJN-6. *Sci. Rep.* 5:13438. doi: 10.1038/srep13438

Zhalnina, K., Louie, K. B., Hao, Z., Mansoori, N., da Rocha, U. N., Shi, S., et al. (2018). Dynamic root exudate chemistry and microbial substrate preferences drive patterns in rhizosphere microbial community assembly. *Nat. Microbiol.* 3:470. doi: 10.1038/s41564-018-0129-3

Zhao, J., Zeng, Z., He, X., Chen, H., and Wang, K. (2015). Effects of monoculture and mixed culture of grass and legume forage species on soil microbial community structure under different levels of nitrogen fertilization. *Eur. J. Soil Biol.* 68, 61–68. doi: 10.1016/j.ejsobi.2015.03.008

Conflict of Interest: The authors declare that the research was conducted in the absence of any commercial or financial relationships that could be construed as a potential conflict of interest.

frontiers in Microbiology

ORIGINAL RESEARCH
published: 19 February 2021
doi: 10.3389/fmicb.2021.627785

Role of the Type VI Secretion System in the Pathogenicity of *Pseudomonas syringae* pv. *actinidiae*, the Causative Agent of Kiwifruit Bacterial Canker

Nana Wang[1,2†], Ning Han[1,3†], Runze Tian[1,3], Jiliang Chen[1,3], Xiaoning Gao[4], Zhiran Wu[1,3], Yuqi Liu[1,2] and Lili Huang[1,3]*

[1] State Key Laboratory of Crop Stress Biology for Arid Areas, Northwest A&F University, Yangling, China, [2] College of Life Science, Northwest A&F University, Yangling, China, [3] College of Plant Protection, Northwest A&F University, Yangling, China, [4] Institute of Bioengineering, Guangdong Academy of Sciences, Guangzhou, China

The type VI secretion system (T6SS), a macromolecular machine, plays an important role in the pathogenicity of many Gram-negative bacteria. However, the role of T6SS in the pathogenicity of *Pseudomonas syringae* pv. *actinidiae* (*Psa*), the pathogen of kiwifruit bacterial canker, is yet to be studied. Here, we found a T6SS gene cluster consisting of 13 core genes (A-J) in the genome of *Psa* M228 based on a genome-wide analysis. To determine whether the T6SS gene cluster affects the pathogenicity of *Psa* M228, T6SS and its 13 core gene deletion mutants were constructed and their pathogenicity was determined. The deletion mutants showed different degrees of reduction in pathogenicity compared with the wild-type strain M228; in *tssM* and *tssJ* mutants, pathogenicity was significantly reduced by 78.7 and 71.3%, respectively. The pathogenicity results were also confirmed by electron microscopy. To further confirm that the reduction in pathogenicity is related to the function of T6SS, we selected the T6SS gene cluster, comprising *tssM* and *tssJ*, for further analyses. Western blot results revealed that *tssM* and *tssJ* were necessary for hemolytic co-regulatory protein secretion, indicating that they encode a functional T6SS. Further, we explored the mechanism by which T6SS affects the pathogenicity of *Psa* M228. The ability of bacterial competition, biofilm formation, hydrogen peroxide tolerance, and proteolytic activity were all weakened in the deletion mutants M228ΔT6SS, M228ΔtssM, and M228ΔtssJ. All these properties of the two gene complementation mutants were restored to the same levels as those of the wild-type strain, M228. Quantitative real-time results showed that during the interaction between the deletion mutant M228ΔT6SS and the host, expression levels of T3SS transcriptional regulatory gene *hrpR*, structural genes *hrpZ*, *hrcC*, *hopP1*, and effector genes *hopH1* and *hopM1* were down-regulated at different levels. Taken together, our data provide evidence for the first time that the T6SS plays an important role in the pathogenicity of *Psa*, probably via effects on bacterial competition, biofilm formation, and environmental adaptability. Moreover, a complicated relationship exists between T6SS and T3SS.

Keywords: pathogenicity, type VI secretion system, Kiwifruit bacterial canker, type III secretion system, competition, biofilm formation, environmental adaptability

OPEN ACCESS

Edited by:
Jia Liu,
Chongqing University of Arts and Sciences, China

Reviewed by:
Giorgio Mariano Balestra, University of Tuscia, Italy
Angelo Mazzaglia, University of Tuscia, Italy

****Correspondence:***
Lili Huang
huanglili@nwsuaf.edu.cn

† These authors share first authorship

Specialty section:
This article was submitted to Microbe and Virus Interactions with Plants, a section of the journal Frontiers in Microbiology

Received: *10 November 2020*
Accepted: *29 January 2021*
Published: *19 February 2021*

Citation:
Wang N, Han N, Tian R, Chen J, Gao X, Wu Z, Liu Y and Huang L (2021) Role of the Type VI Secretion System in the Pathogenicity of Pseudomonas syringae pv. actinidiae, the Causative Agent of Kiwifruit Bacterial Canker. Front. Microbiol. 12:627785. doi: 10.3389/fmicb.2021.627785

INTRODUCTION

The bacterial canker of kiwifruit is caused by the virulent form of *Pseudomonas syringae* pv. *actinidiae* (*Psa*) and is the most prevalent disease in the kiwifruit industry (Pinheiro et al., 2020). *Psa* can enter the plant through stomata, water holes, lenticels, wounds (caused by birds, insects, and/or human contact) and can colonize the plant (including branches, leaves, buds, leaf marks, and pruned diseased branches) for a long time without inducing external symptoms, until a suitable environmental condition is developed (Donati et al., 2020). Systemic infection occurs through various pathways (Stefani and Giovanardi, 2011; Tontou et al., 2014). *Psa* can infect young twigs systemically within a few minutes (Michelotti et al., 2018). Therefore, pathogenic bacteria can infect kiwifruits repeatedly, breed in cortex, expand up and down, and even move to the xylem and central column of the plant, causing severe pathogenicity under appropriate conditions (Gao et al., 2016). Due to the latent and short-term outbreak characteristics of *Psa*, bacterial canker has been identified as a destructive disease of kiwifruit, which results in production losses worldwide. Recently, this disease has received more attention in the main kiwifruit planting areas owing to the huge economic losses (Vanneste, 2017; Hang et al., 2018; Kim et al., 2019; Williams et al., 2020). Therefore, identifying the pathogenic mechanism will play a vital role in effective prevention and control of the disease.

Bacterial phytopathogens usually infect their host plants by various extracellular proteins or secretion of effectors through secretory systems (Khan et al., 2018; Deb et al., 2019). These secretion systems are a class of complex nanomolecular machines that can transport the virulence proteins to the external environment or host cells directly or indirectly (Costa et al., 2015; Wen et al., 2018). To date, at least six different types of secretion systems (I–VI) have been identified in Gram-negative pathogenic bacteria (Mcquade and Stock, 2018). Among them, a newly discovered secretion system, the type VI secretion system (T6SS), has been shown to play an important role in pathogenicity (Agnetti et al., 2019; Zhu et al., 2020) and has also been implicated in bacterial interactions or environmental adaptations such as colonization, biofilm formation, resistance, and survival (Mathias et al., 2017; Wu et al., 2018; Ben-aakov and Salomon, 2019; Asolkar and Ramesh, 2020). T6SS comprises 13 core genes (*tssA* to *tssM*) usually encoded within the same gene cluster (Leiman et al., 2009; Catarina et al., 2011; Kapitein et al., 2013; Kudryashev et al., 2015; Cianfanelli et al., 2016). Among them, hemolytic co-regulatory protein (Hcp) of bacteriophage T4 (Pell et al., 2009; Nguyen et al., 2018) is one of the major substrates secreted by T6SS. Since the secretion of Hcp is T6SS-dependent, it is often a reliable indicator of whether T6SS functions appropriately (Pukatzki et al., 2009).

Multiple studies have found that T6SS was closely related to the pathogenicity in many pathogenic bacteria strains. Mattinen et al. (2010) found that there was four H in the extract from pathogenic bacterium *Pectobacterium atrosepticum*, when it was cultured in minimal medium supplemented with host extract. Overexpression mutants of the *hcp* genes were constructed. The pathogenicity of the mutant strains was enhanced compared with that of the wild-type strain. Hcp may act as a new virulence factor in *P. atrosepticum* (Mattinen et al., 2010). Since the secretion of Hcp is dependent on the T6SS secretion system, the results indicates that T6SS plays an important role in *P. atrosepticum*. The crown gall disease caused by *Agrobacterium tumefaciens* is a worldwide tumor forming disease of the plants and is a major problem for plant nursery industries. It can cause great economic loss in fruit plants (Habbadi et al., 2017). Wu et al. (2018) found that the pathogenicity of *A. tumefaciens* is closely related to T6SS. *Pantoea ananatis* LMG 2665 is the most prevalent pathogenic bacterium found in pineapple fruit and onions. Shyntum et al. (2015) found that two sets of T6SS in its genome, namely T6SS-1 and T6SS-3. T6SS-1 is closely related to the pathogenicity and competitiveness of the strain *P. ananatis* LMG 2665, while T6SS-3 has no effect on its pathogenicity. This indicates that T6SS-1 is an important virulence factor in *P. ananatis*. In addition, the core genes *tssM* (Zhang et al., 2012) and *tssB* (Zhang et al., 2014) of T6SS are essential for the pathogenicity of *Ralstonia solanacearum*. This indicates that T6SS plays an important role in an increasing number of plant bacterial diseases, where the core genes of T6SS have different functions. The bacterial canker of kiwifruit, caused by *Psa*, is the most prevalent disease in the kiwifruit industry; however, the function of T6SS in the pathogenicity of *Psa* is still unclear. In this study, we found a T6SS gene cluster consisting of 13 core genes (A-J) in the genome of *Psa* M228 based on a genome-wide analysis. We studied the role of T6SS in the pathogenicity of *Psa* by mutant construction through homologous recombination technology and conducted a preliminary exploration of its mechanism. The results showed that T6SS is an important pathogenic determinant in *Psa* M228 and plays a role in bacterial competition, biofilm formation, hydrogen peroxide tolerance, proteolytic ability, and T3SS function. Our results provide insights into the functions of T6SS in the pathogenic mechanism of *Psa*.

MATERIALS AND METHODS

Bacterial Strains, Plasmids, and Reagents

Pseudomonas syringae pv. *actinidiae* strain M228 (*Psa* M228) was isolated from kiwi leaves in the Meixian, Shaanxi Province of China in 2010 (Gao et al., 2016). Deletion and complementation mutants were constructed in this study. The strain *Psa* M228 and mutants were grown on Luria-Bertani (LB) agar plates or cultured in LB liquid medium at 25 ± 1°C. *Escherichia coli* DH5α was grown in LB medium at 37°C. For gene cloning, *E. coli* S17-1λpir was cultured under the same conditions for bacterial gene transfer. When necessary, ampicillin (Amp, 10 μg/mL), kanamycin (Km, 10 μg/mL), tetracycline (Tcr, 10 μg/mL), erythromycin (Em, 10 μg/mL), and nalidixic acid (NAL, 10 μg/mL) were used. All strains used in this study were provided by the Plant Pathology Laboratory at Northwest A&F University, Yangling, and PRC. All reagents and solvents were of analytical grade. Antibiotics were purchased from Sigma (United States). Plasmid pK18mobsacB was used for gene deletion, and purchased from Biovector Science Lab, Inc.

(Beijing, China); pDSK-GFPuV was used for fluorescently labeled strains construction, and was provide by Ph.D. Mysore (The Samuel Roberts Noble Foundation, United States); pMarA was used for *Bacillus* transformation, and provided by Professor Qi Wang (China Agricultural University, Beijing, China); pDSK was used for gene complementation, pBR322 was used for *E. coli* DH5α transformation, and these two plasmids were provided by Professor Xi-Hui Shen (Northwest A&F University, Yangling, China).

T6SS Bioinformatics Analysis of *Psa* M228

The whole genome of *Psa* M228 has been sequenced by our laboratory, and the genome data have been registered on NCBI (ANJI00000000.2). The gene *tssC* sequence of *Psa* M228 was obtained through bioinformatics analysis, and an evolutionary tree was constructed from the *tssC* sequence of 68 species in 38 genera that contain T6SS. There are three representative types of T6SS and from the evolutionary tree; the species containing them were selected. Subsequently, a phylogenetic tree was constructed to determine the type of T6SS *Psa* M228 belonged to. The evolutionary history was inferred using the Maximum Likelihood method based on the Le_Gascuel_2008 model (Le and Gascuel, 1993). The bootstrap consensus tree inferred from 1000 replicates was used to represent the evolutionary history of the taxa analyzed (Felsenstein, 1985). Branches corresponding to partitions reproduced in less than 60% bootstrap replicates were collapsed. The percentage of replicate trees in which the associated taxa clustered together in the bootstrap test (1000 replicates) is shown next to the branches (Felsenstein, 1985). The initial tree(s) for the heuristic search were obtained automatically by applying Neighbor-Join and BioNJ algorithms to a matrix of pairwise distances estimated using a JTT model, and the topology with a superior log likelihood value was selected. A discrete Gamma distribution was used to model evolutionary rate differences among sites [five categories (+G, parameter = 2.4316)]. The analysis involved 34 amino acid sequences. All positions containing gaps and missing data were eliminated. A total of 443 positions in the final dataset was obtained. Evolutionary analyses were conducted in MEGA6 (Tamura et al., 2013).

According to the phylogenetic tree, the T6SS structural genes of *Psa* M228 were annotated. The database of Clusters of Orthologous Groups of proteins (COGs) was obtained from the National Center of Biotechnology Information[1]. A schematic diagram of the T6SS structure was constructed using the *Pseudomonas aeruginosa* PAO1 gene structure map as a reference (Sana et al., 2016).

Generation of *Psa* M228 Mutant Strains

Mutant strains with deletions of T6SS and its 13 core genes were constructed by the homologous recombination method (Kvitko and Collmer, 2011). In brief, PCR primer synthesis and DNA sequencing were performed by TsingKe Biotech Co., Ltd. (Beijing, China). *Psa* genomic and plasmid DNAs were isolated using an E.Z.N.A. TM Bacterial DNA Kit (OMEGA, United States) and Plasmid Mini Kit I (OMEGA, United States), respectively. Restriction enzymes were purchased from TaKaRa (Dalian, China). Deletion mutants were constructed using the suicide vector pK18mobSacB (Schafer et al., 1994). The gene fragments including their left and right arms were amplified using the corresponding primers (**Supplementary Table S1**). The DNA fragments were digested with *Eco*RI/*Hin*dIII and ligated to pK18mobsacB. The vector pK18mobsacB carrying each target gene fragment was inserted by the Km resistance gene and deletion vectors were constructed. Then, the vectors were introduced into the M228 strain by conjugal mating experiments. The first recombinant mutants were screened on LB (Km10-NAL10-Amp 10 μg/mL) and PCR detected using primers SacB-F/R (**Supplementary Table S2**). The mutant candidates were then screened to remove the suicide plasmid, using LB agar plates containing 20% sucrose without sodium chloride. The results of target gene deletion were confirmed by PCR amplification and DNA sequencing.

Complementation of *Psa* M228ΔtssM and M228ΔtssJ in Deletion Mutants

The complement mutants were constructed as follows: primers TssM-C-F/R and TssJ-C-F/R (**Supplementary Table 1**) were used to amplify the full-length *tssM* (3849 bp) and *tssJ* (474 bp) genes from the *Psa* M228 genome, as well as the upstream putative promoters. The PCR products were cloned into the *Bam*HI and *Nde*I sites of plasmid PDSK, and the plasmids were transformed into *E. coli* DH5α. The complementation plasmids PDSK-tssM and PDSK-tssJ were extracted from *E. coli* DH5α according to the manufacturer's instructions in the Plasmid Mini Kit I (OMEGA, United States), and then electroporated into mutants M228ΔtssM and M228ΔtssJ, respectively. The complement mutants were screened by kanamycin resistance on LB agar.

Spread Assays

The spreading ability of the strain *Psa* M228 and its mutant M228ΔT6SS was determined as previously described (Gao et al., 2016). In brief, the strains *Psa* M228 and its mutant M228ΔT6SS were successfully transformed with pDSK-GFPuV by electroporation (Huang et al., 2013). Kiwi branches (cv. "Hongyang") were surface-disinfected by rinsing with running water, soaked in 0.6% sodium hypochlorite solution for 5 min, and rinsed with sterile water again. The base of the petiole was wrapped with absorbent cotton to avoid evaporation. Punctures were made at the main leaf vein 1–2 cm away from the petiole, and GFPuv labeled bacterial culture of 10 μL (diluted to OD_{600} = 0.1, concentration = 1×10^8 CFU/mL) were dripped onto the wound. The inoculated materials were placed in an artificial climate incubator (photoperiod L/D: 16/8 h; day and night temperature: 16/4°C, relative humidity 95%). The results were observed using a stereo fluorescence microscope (Leica MZ10F, Leica Microsystems, Germany) after 2 days.

[1] ftp://ftp.ncbi.nih.gov/pub/COG/COG2014/static/lists/listAciave.html

Pathogenicity Assays

Pathogenicity of the strain *Psa* M228 and its mutants was determined in kiwi (cv. "Hongyang"), as described previously (Zhao et al., 2019). Healthy branches of kiwi (cv. "Hongyang") were cut into short branches of about 15 cm each and rinsed with sterile water; the ends were sealed with paraffin to avoid evaporation. In each test, a wound deep to the phloem within a width of 2 mm was cut with a blade in the middle of the branch, and 10 μL of the substance (OD_{600} = 0.1, the concentration = 1×10^8 CFU/mL) was inoculated, while using sterile water as a negative control. Each strain was inoculated with five branches, and each experiment was repeated three times. The branches were maintained in an artificial climate incubator at a temperature of 25°C under natural day and night cycles. The lesion lengths of the branches were measured after 30 days. The lesion length is the average of three replicates. Statistical significance was determined by Student's *t*-test.

Electron Microscopic Observation

Healthy leaves from kiwifruit (cv. "Hongyang") were inoculated separately with bacterial suspensions of *Psa* M228 and its mutant strains M228ΔtssM and M228ΔtssJ, using the same method as described in section "Pathogenicity Assays." Scanning electron microscopy (SEM) samples were prepared by taking the leaf blade (5–7 mm) from the edge of sick and healthy junctions after 48 and 96 h. Carefully processed as described by Kang (1995), the colonization of bacterial pathogens in leaf tissue was observed using a JSH 6360 SEM (JEOL Ltd., Tokyo, Japan) at 15 kV. Transmission electron microscope (TEM) samples from 96 h culture were prepared in the same way as described by Kang (1995), and alterations in the ultrastructure of the leaf tissue infested by pathogenic bacteria were observed using an HT7700 TEM (HITACHI Company, Tokyo, Japan).

Western Blot Assays

To explore whether the T6SS gene cluster encodes a functioning T6SS, Hcp secretion was assayed by western blot. The wild-type strains *Psa* M228 and mutants M228ΔT6SS, M228ΔtssM, and M228ΔtssJ were cultured as described in section "Electron Microscopic Observation." The supernatant and cells were obtained by centrifugation at 13,000 × *g* for 10 min at 4°C. The protein content was determined using a Micro BCA™ Protein Assay Kit (Thermo Fisher Scientific, United States). Extracellular and intracellular proteins were subjected to 12% SDS PAGE and then transferred to PVDF membranes. The immunoblot analysis was performed using anti-VSV-G-tag monoclonal antibody (VSVG) (CB100151, Cali-Bio, United States) and anti-RNA polymerase (RNAP) antibody (W0023, NeoClone, Beijing, China) at a dilution of 1:1000 as the primary and secondary antibodies were goat anti-mouse horseradish peroxidase (HRP) (DY60203) (DIYI BIO TECHNOLOGY, Shanghai, China) and goat anti-rabbit HRP (DY60202) (DIYI BIO TECHNOLOGY, Shanghai, China), respectively, at a dilution of 1:10,000. The differences between the bands of intracellular and extracellular proteins were compared between M228 and the mutants, using RNAP as a control.

Bacterial Competition Assays

Escherichia coli DH5α was transformed with plasmid pBR322 to confer tetracycline resistance and *Bacillus* was transformed with plasmid pMarA to confer erythromycin resistance used for the competition studies. The competition assays were carried out as per the protocol described by MacIntyre et al. (2010). Competitor strains were grown overnight in LB broth supplemented with tetracycline (10 μg/mL) or erythromycin (10 μg/mL). The cells were centrifuged and washed twice with fresh sterile LB broth (10,000 × *g*, 1 min). The washed cells were resuspended in LB broth (OD_{600} = 0.1, concentration = 1×10^8 CFU/mL) and combined with the *Psa* M228 wild-type or mutant strain M228ΔT6SS at a ratio of 1:1. The mixture was cultured at 25°C for 24 h, and then spotted on LB agar plates and incubated at 30°C for 12 h for the competition strain bacterial analysis.

Biofilm Assays

Biofilm assays were performed using the method described by Stepanovic et al. (2000). The results were determined by measuring the absorbance at 570 nm (OD_{570}) using a Thermo Multiskan EX Micro plate Photometer (Thermo Fisher Scientific Inc., United States). The experiments were repeated three times with six replicates per treatment. The absorbance at 570 nm was the average of six replicates. Statistical significance was determined by Student's *t*-test.

Environmental Adaptability Assays

The hydrogen peroxide (H_2O_2) tolerance and proteolytic ability were evaluated in accordance with previously described procedures (Molina et al., 2005). The bacterial solutions (diluted to OD_{600} = 0.1, concentration = 1×10^8 CFU/mL) were inoculated into LB broth medium containing H_2O_2 solution (10 mL, 0.06 mol/L) at a ratio of 1:100. Bacterial growth was measured at 600 nm absorbance every 12 h.

A total of 2 μL of the bacterial solution (diluted to OD_{600} = 0.1, concentration = 1×10^8 CFU/mL) was inoculated in the acid hydrolyzed case in a medium plate (1%w/v). Colony diameter was measured after culturing at 25°C for 14 days. All assays were repeated three times, and each treatment was performed in triplicate. Statistical significance was determined by Student's *t*-test.

Quantitative Real-Time Assays

Healthy branches from kiwifruit (cv. "Hongyang") were prepared as described in section "Pathogenicity Assays." Suspension of *Psa* M228 and mutant M228ΔT6SS (diluted to OD_{600} = 0.5, concentration = 5×10^8 CFU/mL, 10 μL) were inoculated into the wound made in advance, and cultivated in an artificial climate incubator (the illumination time was 16 h and the dark time was 8 h). The bark of the inoculated wound (deep to phloem) was taken at 2 and 16 h after inoculation. Operations for bacterial RNA extraction, cDNA synthesis, and qPCR were performed as previously described (Broms et al., 2009). The reference genes were *gyrB* (DNA gyrase subunit B), *dusA* (tRNA dihydrouridine synthase), and *ftrA* (transcriptional regulator) (Hirose et al., 2020). Data were analyzed following the protocol

of the comparative critical threshold (CT) method (Zhang et al., 2014). The expression levels of the target genes (*hrpR*, *hrpZ, hrcC*, *hopP1, hopH1*, and *hopM1*) at different inoculation times were calculated relative to endogenous control genes using the relative quantification method (Lopez and Pardo, 2005). Quantitative data were presented as fold change mutant strain M228ΔT6SS compared to wild-type (WT) M228 levels at 2 and 16 h. Error bars represent the standard deviation of the ΔΔC value. Statistical significance was determined by Student's *t*-test. The quantitative real-time PCR (qRT-PCR) was performed in triplicate for technical replicates.

RESULTS

T6SS Gene Structure Diagram of *Psa* M228

According to the results of the phylogenetic tree constructed from the *tssC* sequence of 68 species in 38 genera (**Supplementary Figure 1**), and its simplified phylogenetic tree (**Figure 1A**), one complete T6SS was found in *Psa* M228 and belonged to the same branch as the *P. aeruginosa* PAO1 H3-T6SS (HIS-III) gene cluster. Then, the T6SS gene structure diagram in M228 was obtained.

As shown in **Figure 1B**, there are 13 conserved structural genes such as *tssA-tssM* necessary for T6SS in M228. The COGs of the cluster are impA, impB, impC, hcp, impF, impG, impH, clpV, vgrG, lip, impJ, impK, and impL, all of which are located in the M228 genome sequence contig054. Among them, *tssB* and *tssC* are the needle-sheath structural genes, *tssD* is the needle-tube structural gene, and *tssM*, *tssJ*, and *tssL* are transmembrane structural genes. However, there is a frameshift mutation in the transmembrane structural protein gene *tssM* (1272 codons) and the ATP hydrolase gene *tssH* (854 codons) (**Figure 1B**).

Construction of T6SS Gene Cluster and 13 Core Genes Deletion Mutants in *Psa* M228

The previous sequence analysis showed that there is a T6SS gene cluster in the *Psa* M228 genome, which consists of 13 core genes (*tssA-tssM*). The function of the gene cluster and core genes in *Psa* has not been studied yet. Thus, in this study, we began by deleting the T6SS gene cluster and its individual 13 core genes of *Psa* M228 using λ Red-recombineering technique (Kvitko and Collmer, 2011), yielding strains M228ΔT6SS and 13 mutants from M228ΔtssA to M228ΔtssM.

T6SS of *Psa* M228 Is Required for Spreading

The spreading ability of mutant M228ΔT6SS in leaf veins was significantly different from that of wild-type M228. The spreading range of M228 in leaf veins increased with an increase in incubation time, and fluorescence began to weaken after 12 days. However, the spreading ability of M228ΔT6SS in leaf veins was significantly weakened; it failed to expand rapidly in the leaf veins and indicated only weak fluorescence near the inoculation point (**Figure 2B**).

T6SS of *Psa* M228 Is Required for Pathogenicity

To clarify the role of T6SS in the pathogenicity of M228, the pathogenicity of mutants lacking the T6SS gene cluster or 13 core genes were assessed by conducting pathogenicity tests on healthy branches of kiwi (cv. "Hongyang"), as described previously (Zhao et al., 2019). The pathogenicity of the mutant M228ΔT6SS was reduced by 69.65% compared with that of the wild-type strain M228 (**Figure 2A**). All the deletion mutants of 13 core genes of T6SS showed different degrees of pathogenicity reduction compared with that of the wild-type strain M228 (**Figure 3A**), especially gene *tssM* and *tssJ* (**Figure 3B**). The pathogenicity of mutants M228ΔtssM and M228ΔtssJ mutants were significantly reduced by 78.7 and 71.3%, respectively. However, the complemented strain M228ΔtssM-R and M228ΔtssJ-R restored the pathogenicity to wild-type levels (**Figure 3B**).

The difference in pathogenicity between M228 and the mutants was also confirmed by SEM (**Figure 4**) and TEM (**Figure 5**). After 4 days of inoculation of the host kiwifruit leaves using wild-type strain M228, a large number of pathogens could be observed in the host tissue (**Figure 4B**).Serious plasmolysis occurred in the host cells of the pathogenic bacteria colonized area, and electron density of the host cell wall decreased and its chloroplast was degraded (**Figures 5B,C**). After inoculation of the mutants M228ΔtssM (**Figure 4C**) and M228ΔtssJ (**Figure 4E**), only a small amount of bacterial colonization was found in the host tissue at 4 days. The host cell was intact, and the organelles were not significantly degraded due to pathogen colonization (**Figures 5D,F**). However, there was no significant difference in the colonization and infection ability between the wild-type strain M228 and the complemented strain M228ΔtssM-R (**Figures 4D**, **5E**) and M228ΔtssJ-R (**Figures 4F**, **5G**). The mutants can cause a similar phenomenon to the host cell, indicating that its infection ability is restored to the wild-type level. The results showed that the T6SS gene cluster played an important role in the pathogenicity of *Psa* in kiwifruit, especially the core genes *tssM* and *tssJ*.

T6SS Gene Cluster Encodes a Functioning T6SS in *Psa* M228

To investigate the function of T6SS, M228 and the deletion mutant strain, M228ΔT6SS, M228ΔtssM, and M228ΔtssJ were examined for the secretion of Hcp, which is an indication of functional T6SS in many bacterial species (Ma and Mekalanos, 2010). As shown in **Figure 6**, Hcp was detected by western blot from both cells and supernatants for the wild-type strain *Psa* M228, but only detected in the cells and not in the supernatant for mutant strains M228ΔT6SS, M228ΔtssM, and M228ΔtssJ. This result demonstrated that T6SS is essential for the secretion of Hcp in *Psa* M228. The results also showed that T6SS in the pathogenic strain *Psa*M228 is functional, and its core genes

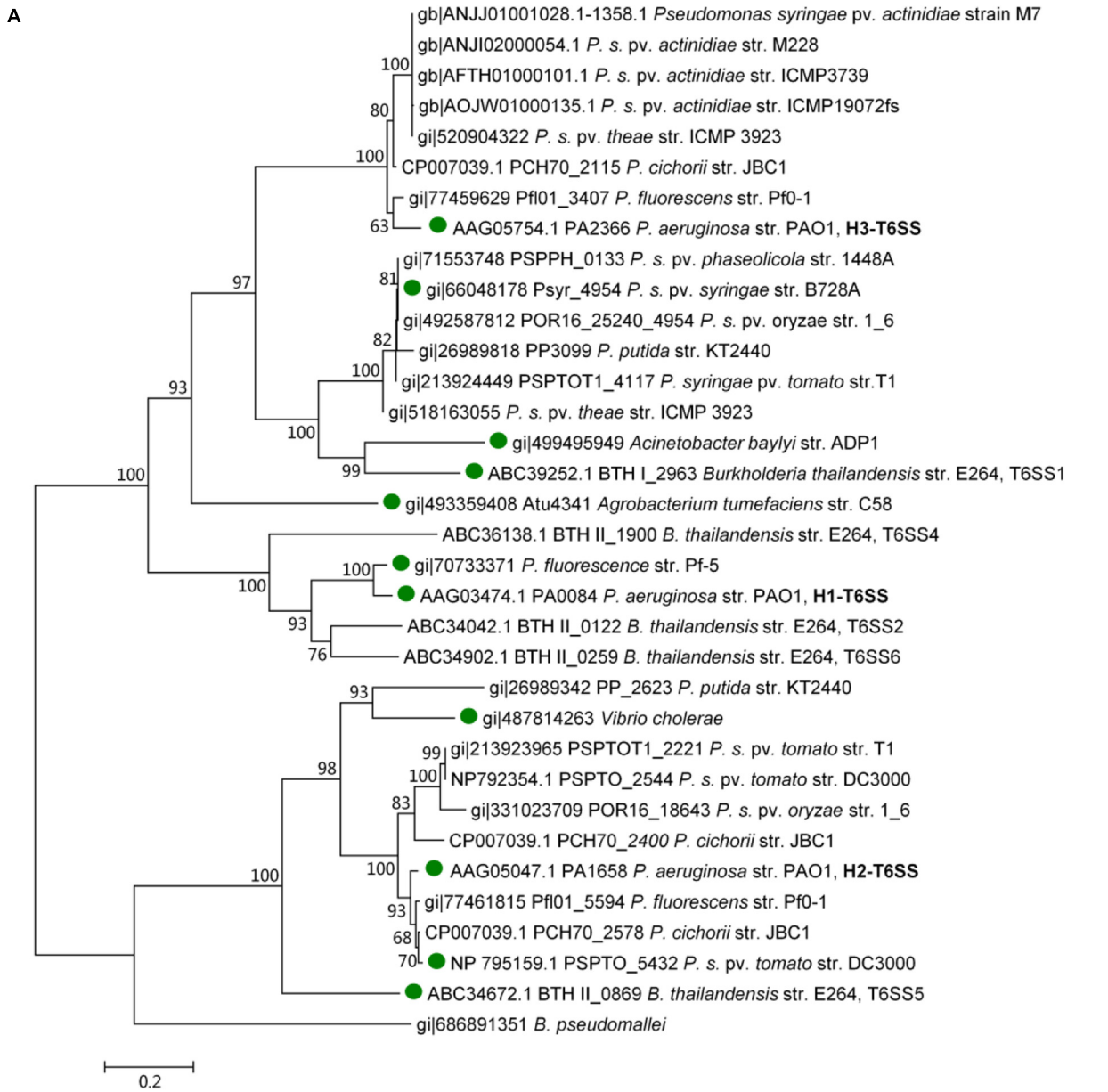

FIGURE 1 | Structure of T6SS gene cluster analysis of the pathogenic strain *Psa* M228. **(A)** Molecular phylogenetic analysis by Maximum Likelihood method. The evolutionary history was inferred using the Maximum Likelihood method based on the Le_Gascuel_2008 model (Le and Gascuel, 1993). The bootstrap consensus tree inferred from 1000 replicates was used to represent the evolutionary history of the taxa analyzed (Felsenstein, 1985). Branches corresponding to partitions reproduced in less than 60% bootstrap replicates were collapsed. The percentage of replicate trees in which the associated taxa clustered together in the bootstrap test (1000 replicates) is shown next to the branches (Felsenstein, 1985). The initial tree(s) for the heuristic search were obtained automatically by applying

(Continued)

FIGURE 1 | Continued
Neighbor-Join and BioNJ algorithms to a matrix of pairwise distances estimated using a JTT model, and the topology with a superior log likelihood value was selected. A discrete Gamma distribution was used to model evolutionary rate differences among sites [five categories (+G, parameter = 2.4316)]. The analysis involved 34 amino acid sequences. All positions containing gaps and missing data were eliminated. A total of 443 positions in the final dataset was obtained. Evolutionary analyses were conducted in MEGA6 (Tamura et al., 2013). According to the results of the phylogenetic tree, one complete T6SS was found in *Psa* M228 and belonged to the same branch as that of the *P. aeruginosa* PAO1 H3-T6SS (HIS-III) gene cluster. "●" indicates the functional T6SS that has been reported. **(B)**. Schematic diagram of theT6SS gene cluster of the pathogenic strain *Psa* M228. The name of the core genes of T6SS in Psa M228 are indicated by arrows. The direction of the arrows represents the direction of transcription of the genes in the genome. "//" indicates the presence of other genes not belonging to T6SS. "*" indicates the presence of frameshift mutation. The gene products are shown below the arrows. The database of Clusters of Orthologous Groups of proteins (COGs) was obtained from the National Center of Biotechnology Information (see text footnote 1).

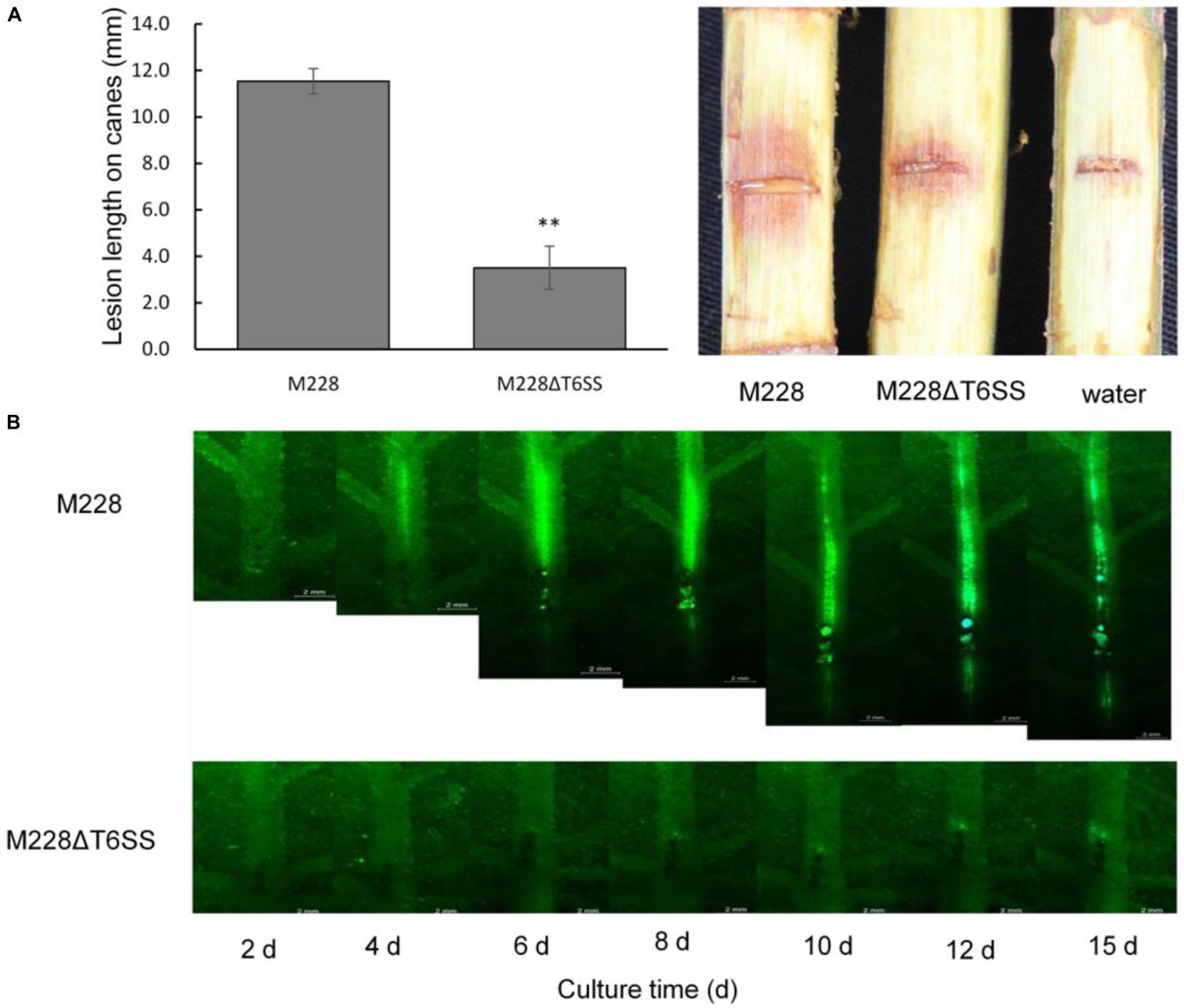

FIGURE 2 | Pathogenicity and spreading ability analysis of the pathogenic strain M228 and its mutants M228ΔT6SS. **(A)** Pathogenicity analysis. The pathogenicity of the mutant M228ΔT6SS mutant was reduced by 69.65% compared with that of the wild-type strain. The lesion length is the average of five replicates. Statistical significance was determined by Student's *t*-test. "**" Means the difference is significant at the 0.01 level. **(B)** Spreading ability analysis+. The spreading ability of mutant M228ΔT6SS in leaf veins was significantly different from that of wild-type M228. The spreading range of M228 in leaf veins increased with an increase in incubation time, and fluorescence began to weaken after 12 days. However, the spreading ability of M228ΔT6SS in leaf veins was significantly weakened, and it failed to expand rapidly in leaf veins, and only showed weak fluorescence near the inoculation point.

tssM and *tssJ* are critical for Hcp secretion and pathogenicity. The internal control protein RNAP was stably expressed in the cell, but was not detected in the supernatant, confirming the reliability of the results.

The T6SS of *Psa* M228 Is Used to Compete Against Bacteria

In order to determine whether the T6SS is functional in competition between bacterial species, a competitive test was

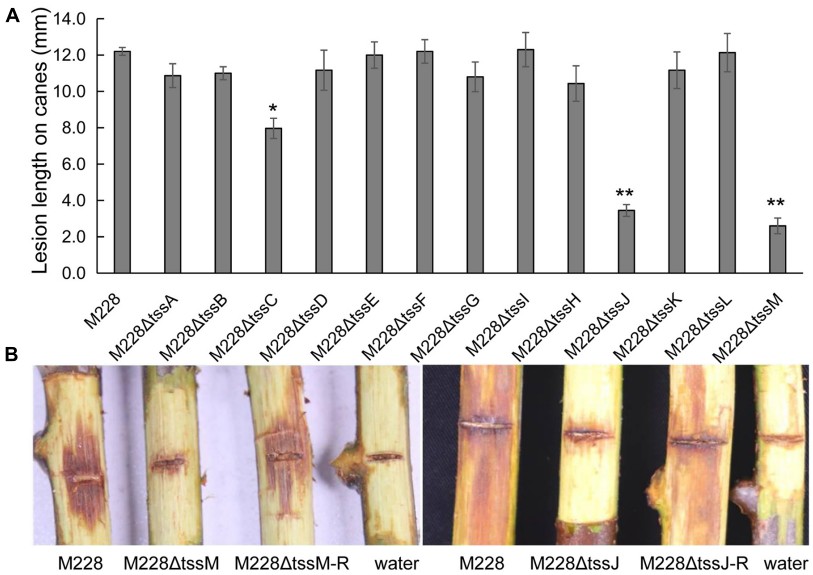

FIGURE 3 | Pathogenicity analysis of the deletion mutant strains of 13 core genes constitute T6SS. **(A)** The lesion lengths analysis of the deletion mutants infecting on branches of kiwi. All the deletion mutants of 13 core genes of T6SS showed different degrees of pathogenicity reduction compared with that of the wild-type strain M228, especially gene *tssM* and *tssJ*. The pathogenicity of mutants M228ΔtssM and M228ΔtssJ mutants were significantly reduced by 78.7 and 71.3%, respectively. However, the complemented strain M228ΔtssM-R and M228ΔtssJ-R restored the pathogenicity to wild-type levels. The lesion lengths are the average of three replicate. Statistical significance was determined by Student's *t*-test. "*" Means the difference is significant at the 0.05 level; "**" means the difference is significant at the 0.01 level. **(B)** The lesion observation of mutant strain M228ΔtssM and M228ΔtssJ infecting on branches of kiwi.

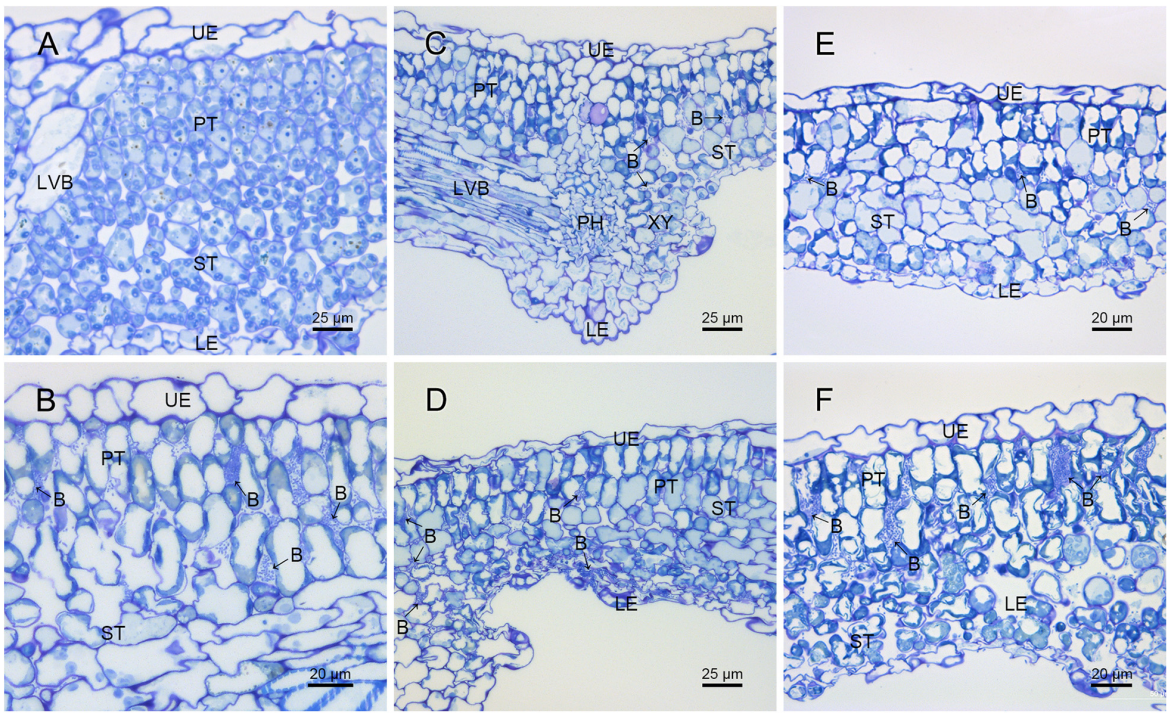

FIGURE 4 | Histological observation of the pathogenic strain M228 and its mutants infecting leaves of kiwi by SEM. **(A)** Healthy kiwi leaves; **(B)** after 4 days of inoculation of the host kiwifruit leaves using wild-type strain M228, a large number of pathogens could be observed in the host tissue. **(C,E)** After 4 days of inoculation of the host kiwifruit leaves using the mutants M228ΔtssM and M228ΔtssJ, only a small amount of bacterial colonization was found in the host tissue; **(D,F)** after 4 days of inoculation of the host kiwifruit leaves using the mutantsM228ΔtssM-R and M228ΔtssJ-R, a large number of pathogens could be observed in the host tissue, and there was no significant difference in the colonization and infection ability between the wild-type strain M228 and the complemented strains. UE, upper epidermis; PT, palisade tissue; ST, sponge tissue; PH, phloem; XY, xylem; LE, lower epidermis; LVB, lateral vein; B, pathogenic bacteria.

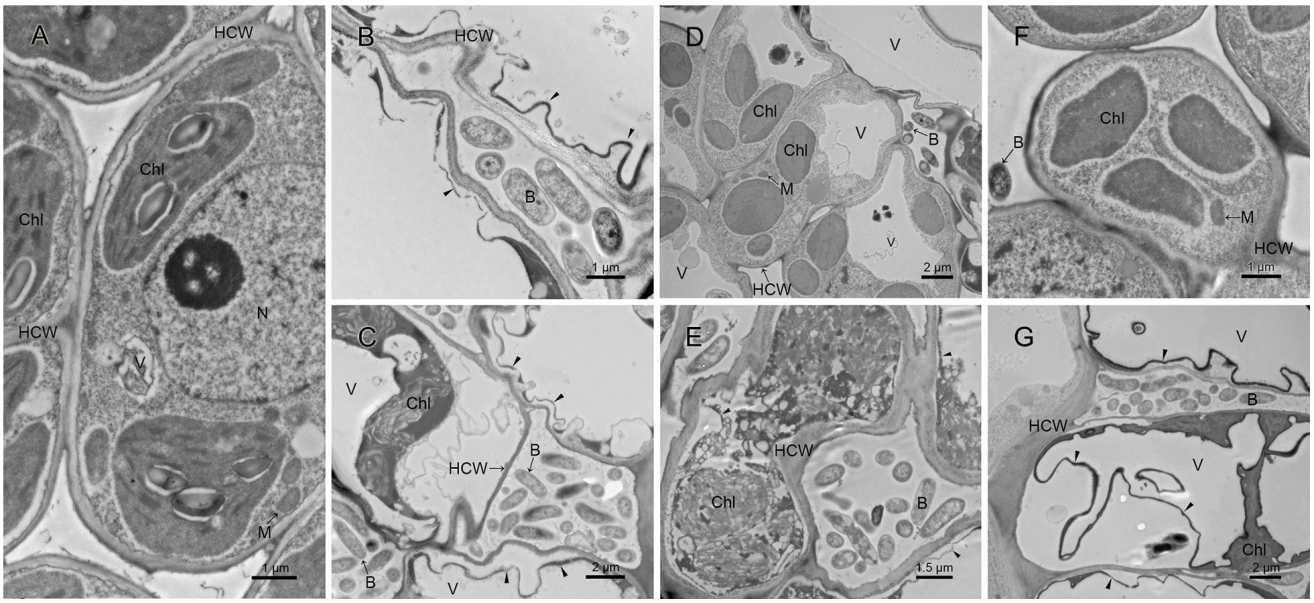

FIGURE 5 | Ultrastructure analysis of kiwi leaves infected by the pathogenic strain M228 and its mutants by TEM. **(A)** Healthy kiwi leaves; **(B,C)** after 4 days of inoculation of the host kiwifruit leaves using wild-type strain M228, serious plasmolysis occurred in the host cells of the pathogenic bacteria colonized area, and electron density of the host cell wall decreased and its chloroplast was degraded; **(D,F)** after 4 days of inoculation of the host kiwifruit leaves using the mutants M228ΔtssM and M228ΔtssJ, the host cell was intact, and organelles were not significantly degraded due to pathogen colonization. **(E,G)** After 4 days of inoculation of the host kiwifruit leaves using the mutants M228ΔtssM-R and M228ΔtssJ-R, serious plasmolysis occurred in the host cells of the pathogenic bacteria colonized area, and electron density of the host cell wall decreased and its chloroplast was degraded; the mutants could cause a similar phenomenon to the host cell with wild-type strain M228. HCW, host cell wall; N, nucleus; V, vacuole; Chl, chloroplast; M, mitochondria; B, pathogenic bacteria; CW, bacterial cell wall; "▲," host cell plasmolysis.

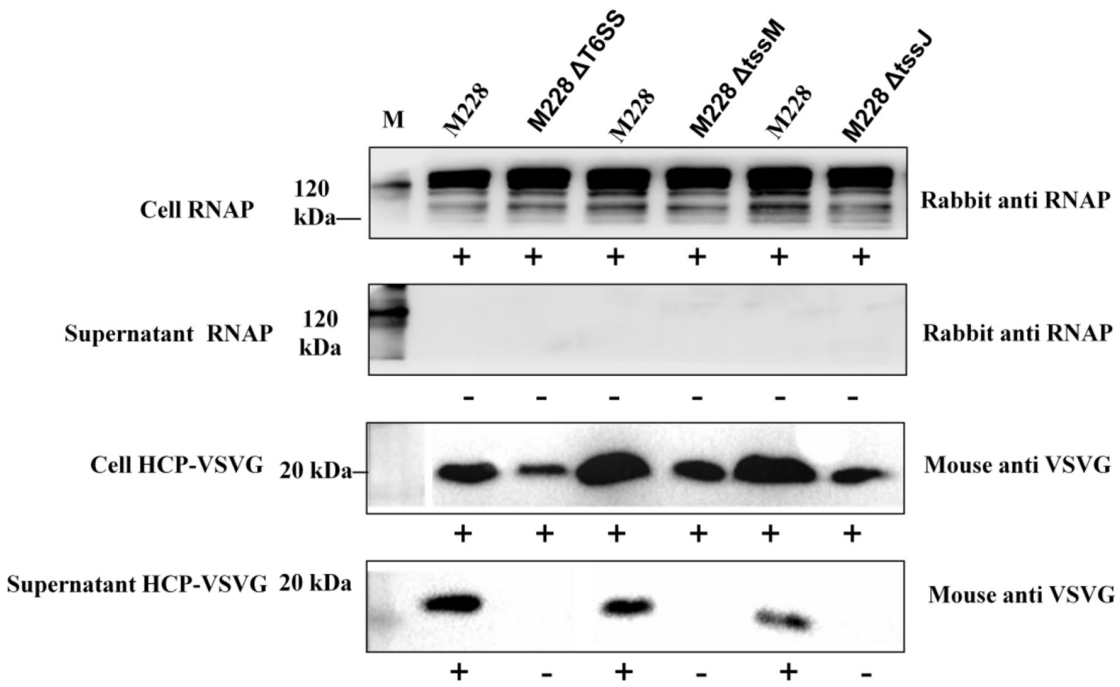

FIGURE 6 | Immunoblot analysis of *Psa* M228 and mutants M228ΔT6SS, M228ΔtssM, and M228ΔtssJ Hcp export. Hcp was detected by western blot from both cells and supernatant for the wild-type strain Psa M228, but was only detected in the cells and not in the supernatant for mutant strain M228ΔT6SS, M228ΔtssM, and M228ΔtssJ. The internal control protein RNAP was stably expressed in the cell, but was not detected in the supernatant, confirming the reliability of the results. Lane M, protein marker.

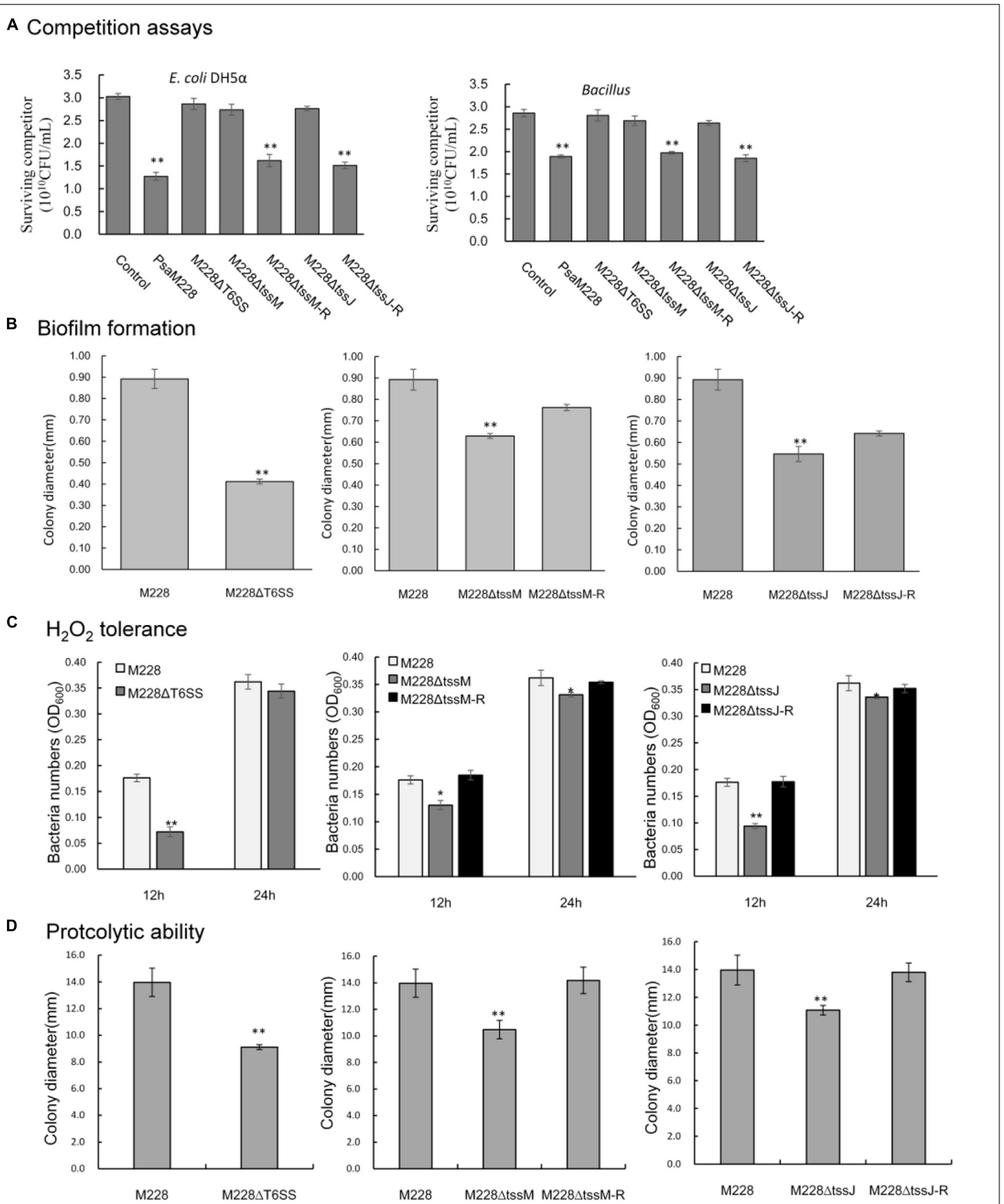

FIGURE 7 | Competitive, biofilm formation, and environmental adaptability analysis of wild-type strain M228 and mutants M228ΔT6SS, M228ΔtssM, and M228ΔtssJ. **(A)** Bacterial competition assay. When the competitor strains were cocultured with wild-type *Psa* M228 or the complementation mutants M228ΔtssM-R and M228ΔtssJ-R, the viable cell numbers showed an obvious drop from 46.5, 58.0 to 31.0, and 35.2%, respectively. In contrast, when the competitor strains were cocultured with deletion mutants M228ΔT6SS, M228ΔtssM, and M228ΔtssJ, the survival of competitor bacteria increased up to the same

(Continued)

FIGURE 7 | Continued
level as that of the control. **(B)** Biofilm assays. The biofilm formation ability of the three mutants M228ΔT6SS, M228ΔtssM, and M228ΔtssJ was significantly lower than that of the wild-type strain M228 and decreased by 53.8, 29.5, and 38.7%, respectively. The biofilm formation ability was restored to the same level as that of M228 when the deletion genes were restored. **(C)** H_2O_2 tolerance assay. The H_2O_2 tolerance of mutant strains M228ΔT6SS, M228ΔtssM, and M228ΔtssJ was significantly lower than that of the wild-type strain M228, decreased by 59.1, 26.1, and 46.6% at 12 h, respectively, and decreased by 5.0, 8.5, and 7.2% at 24 h, respectively. The H_2O_2 tolerance was restored when the deletion genes were restored to the same level as that of M228 when the deletion genes were restored. **(D)** Proteolytic ability assay. The proteolytic ability of mutant strains M228ΔT6SS, M228ΔtssM, and M228ΔtssJ was significantly lower than that of the wild-type strain M228, and decreased by 34.8, 25.0, and 20.66%, respectively. The proteolytic ability was restored when the deletion genes were restored to the same level as that of M228. Statistical significance was determined by Student's *t*-test. "*" Means the difference is significant at the 0.05 level; "**" means the difference is significant at the 0.01 level.

conducted in order to examine whether the mutants lacking the T6SS gene clusters could reduce the number of *E. coli* DH5α and *Bacillus* strains on agar plates. When the competitor strains were cocultured with wild-type *Psa* M228 or the complementation mutants M228ΔtssM-R and M228ΔtssJ-R, viable cell numbers showed an obvious drop from 46.5, 58.0 to 31.0, and 35.2%, respectively. In contrast, when the competitor strains were cocultured with deletion mutants M228ΔT6SS, M228ΔtssM, and M228ΔtssJ, the survival of competitor bacteria was increased up to the same level as that of the control (**Figure 7A**). Overall, the results showed that the T6SS gene cluster is related to bacterial competition in *Psa* M228.

T6SS of *Psa* M228 Is Required for Biofilm Formation

To investigate the function of T6SS, M228, and the deletion mutant strains, M228ΔT6SS, M228ΔtssM, and M228ΔtssJ were examined for biofilm formation. As shown in **Figure 7B**, the biofilm formation ability of the three mutants was significantly lower than that of the wild-type strain M228 ($P < 0.05$): M228ΔT6SS decreased by 53.8%, M228ΔtssM by 29.5%, and M228ΔtssJ by 38.7%. After the deletion genes were restored, the biofilm formation ability of the mutants was restored to the same level as that of M228.

The T6SS of *Psa* M228 Is Required for H_2O_2 Tolerance and Proteolytic Ability

In order to determine whether the T6SS is functional in environmental adaptability of *Psa* M228, we examined whether the mutants lacking the T6SS gene clusters could weaken the H_2O_2 tolerance and proteolytic ability.

The H_2O_2 tolerance results of mutants M228ΔT6SS, M228ΔtssM, and M228ΔtssJ was significantly lower than that of the wild-type strain M228, decreased by 59.1, 26.1, and 46.6% at 12 h, respectively, and decreased by 5.0, 8.5, and 7.2% at 24 h, respectively (**Figure 7C**). The hydrogen peroxide tolerance was significantly affected by T6SS in the early stages. The proteolytic ability of mutants M228ΔT6SS, M228ΔtssM, and M228ΔtssJ was significantly lower than that of the wild-type strain M228 ($P < 0.01$), and decreased by 34.8, 25.0, and 20.66%, respectively (**Figure 7D**). The H_2O_2 tolerance and proteolytic ability were all restored when the deletion genes were restored.

T3SS-Related Genes Show Down-Regulated Expression in *Psa* M228ΔT6SS

The qRT-PCR technique was used to analyze the relationship between the T6SS cluster gene and T3SS-related gene expression. During the interaction between the mutant strain M228ΔT6SS and the host, expression levels of T3SS transcriptional regulatory genes *hrpR*, structural genes *hrpZ*, *hrcC*, *hopP1*, and effector genes *hopM1* and *hopH1*were regulated. Following interaction for 2 h, T3SS-related genes *hrpR*, *hrpZ*, *hrcC*, *hopP1*, *hopH1*, and *hopM1* of the mutant M228ΔT6SS, were down-regulated by 2.01, 1.48, 1.46, 1.14, 1.05, and 1.2 times compared to the wild-type strain; following interaction for 16 h, the expression of the genes was down-regulated by 2.71, 1.76, 1.70, 1.48, 1.78, and 1.83 times, using *gyrB* as an internal reference. A similar down-regulation result was obtained using *dusA* and *ftrA* as internal reference genes (**Figure 8**). The expression levels of the T3SS related genes were significantly affected by T6SS in the later stage.

DISCUSSION

The protein secretion system plays an important role in the pathogenicity and host infection process of many bacterial pathogens (Gerlach and Hensel, 2007). Among them, T3SS plays a vital role in the pathogenicity of many pathogenic bacteria and can directly transfer effectors from pathogenic bacteria to host cells and exerts pathogenic functions (Cornelis et al., 2006; Zhang et al., 2018). Many studies have confirmed that T3SS plays an important role in the phytopathogenic bacteria of a variety of economic crops. Our previous studies also indicated that T3SS promoters are important pathogenic factors (Zhao et al., 2019) by the differential proteome data of strong and weak pathogenic strains. However, in this study, a T6SS cluster consisting of 13 core genes (A-J) was found in *Psa* M228. Although there is a frameshift mutation in the transmembrane structural protein gene *tssM* (1272 codons) and the ATP hydrolase gene *tssH* (854 codons), the pathogenicity was weaker in all deletion mutants, including mutants M228ΔtssM and M228ΔtssH, than in the wild-type strain M228. It seems that the frameshift mutations of these two genes did not affect their function. This mechanism requires further research.

We further explored whether the gene cluster in *Psa* 228 is a functional T6SS and plays a similar function in pathogenicity as it does in other pathogenic bacteria. Western blot results

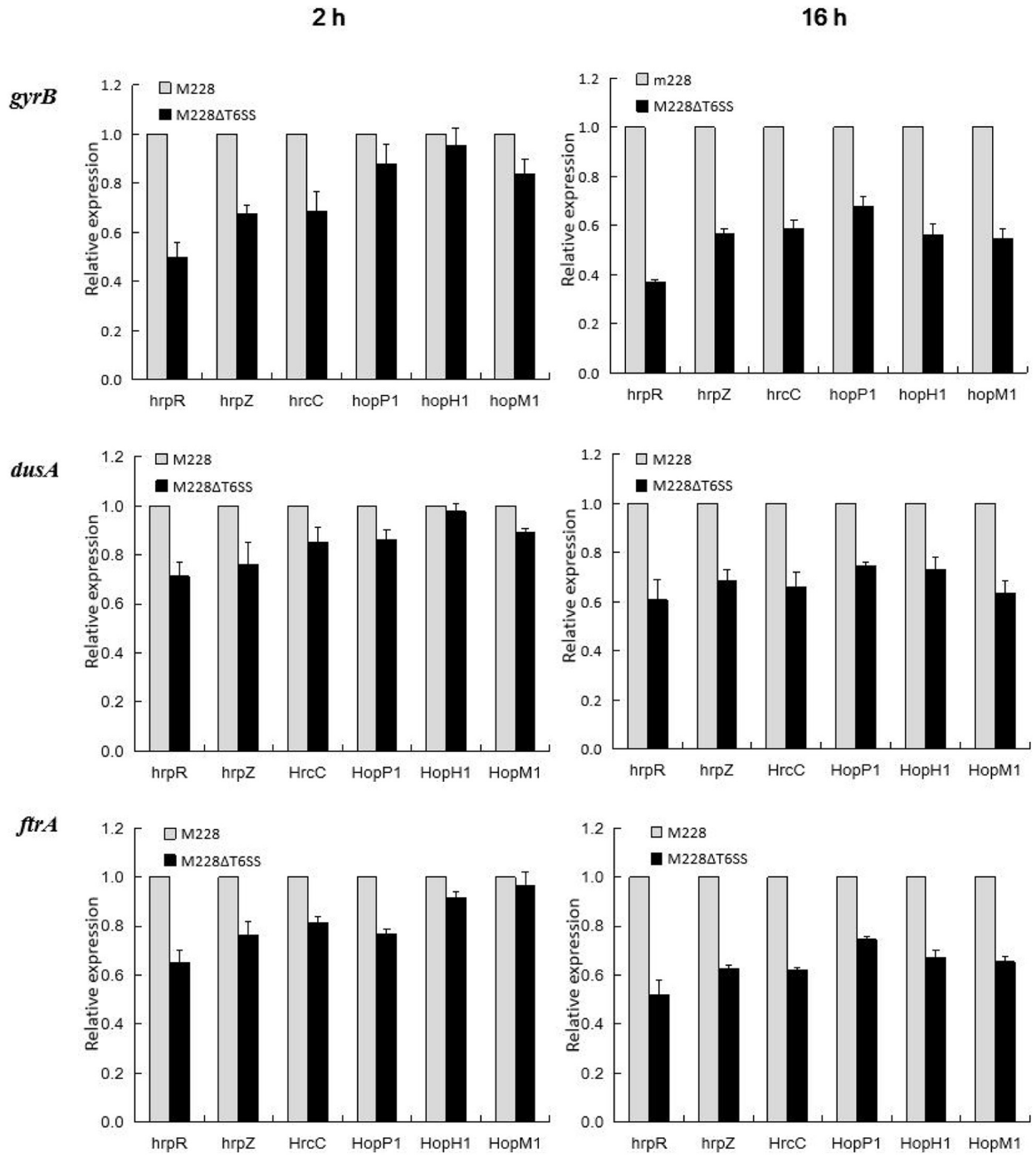

FIGURE 8 | Differential expression of T3SS-related genes analysis in the process of pathogenic strain *Psa* M228 and its mutant M228ΔT6SS infecting kiwi branches. During the interaction between the mutant strain M228ΔT6SS and the host, the expression levels of the T3SS transcriptional regulatory genes *hrpR*, structural genes *hrpZ*, *hrcC*, *hopP1*, and effector genes *hopM1* and *hopH1*were regulated. Following interaction for 2 h, T3SS-related genes *hrpR*, *hrpZ*, *hrcC*, *hopP1*, *hopH1*, and *hopM1* of the mutant M228ΔT6SS, were down-regulated by 2.01, 1.48, 1.46, 1.14, 1.05, and 1.2 times compared to the wild-type strain; following interaction for 16 h, the expression of the genes was down-regulated by 2.71, 1.76, 1.70, 1.48, 1.78, and 1.83 times, using *gyrB* as internal reference; a similar downregulation result was obtained using *dusA* and *ftrA* as internal reference genes.

showed that the T6SS was necessary for Hcp secretion, showing that the T6SS gene cluster in M228 is functional. To determine whether the observed decrease in pathogenicity is related to a functioning T6SS, we generated 13 core genes of T6SS gene cluster deletion mutants. These mutations all led to attenuated pathogenesis and weakened the spread ability of kiwi plants

at different levels, especially *tssM* and *tssJ*. All these properties of the two gene complementation mutants were restored to the same level as those of the wild-type strain M228. The results indicate that the pathogenicity reduction is related to T6SS. To find out whether the effect of T6SS on pathogenicity is related to T3SS, we also conducted a preliminary study. Quantitative real-time results showed that T3SS genes related to pathogenicity were all down regulated in mutant M228ΔT6SS compared to those in the wild-type strain *Psa* M228, especially in the later stages of infection. Further research is needed to understand whether T6SS affects pathogenicity by regulating the T3SS-related genes expressed indirectly or by secreting virulence factors directly. The study results are consistent with the experimental results of a single T6SS gene mutation in *R. solanacearum* (Luo et al., 2016) and the relationship between T3SS and T6SS in the pathogenicity of *Edwardsiella tarda* (Zhang et al., 2016).

In nature or in the host, microorganisms usually exist in complex environmental conditions. For their own survival, they must compete with other organisms for limited nutrients and space. Studies have shown that many Gram-negative bacteria can kill or inhibit other bacteria through T6SS (Alcoforado et al., 2015). For example, the human pathogen *Vibrio cholerae* kills *E. coli* by secreting virulence factors through T6SS (MacIntyre et al., 2010). In addition, recent studies have shown that T6SS plays an important role in *P. aeruginosa* and *E. coli* cells. A variety of antibacterial toxins that plays an important role in bacterial competition can be delivered to the target cell through T6SS (Basler et al., 2013; Brunet et al., 2013; Durand et al., 2014; Alcoforado et al., 2015). It has been reported that *E. coli* is susceptible to T6SS and can be killed by the antibacterial toxin secreted by T6SS. Therefore, *E. coli* is often used as an ideal competitor (MacIntyre et al., 2010; Zheng et al., 2011; Weber et al., 2013). *Bacillus* is one of the most abundant species of plant endophytes (Gadhave et al., 2018; Gordon et al., 2020). Therefore, in this work, we used *E. coli* and *Bacillus* as competitors. Our results showed that T6SS is required for efficient bacterial competition. Moreover, how the competition is carried out *in vitro* requires further research and needs to be confirmed using *in vivo* survival assays. In addition, we investigated the role of the T6SS in bacterial biofilm formation, which is essential during infection and pathogenic processes (Yu et al., 2016). Our research indicated that T6SS plays an important role in the pathogenicity of *Psa* M228. These results present novel insights regarding the pathogenesis of *Psa*.

The adaptability of plants to various pressures from the natural environment needs to be achieved by regulating the pressure signal transduction pathways. When plants are attacked by pathogenic bacteria, it produces a series of stress responses, including the oxidative burst (Nicaise and Candresse, 2017; Kanwar and Jha, 2019; Guo and Li, 2000). Previous studies have suggested that these reactive oxygen species have pathological functions such as inhibiting the growth of bacterial and fungal pathogens (Jiang et al., 2011). Our study showed that compared to the wild-type strain M228, the growth of the deletion mutants M228ΔT6SS, M228ΔtssM, and M228ΔtssJ was significantly inhibited under H_2O_2 stress. The deletion of T6SS, *tssM*, and *tssJ* from *Psa* M228 may lead to reduced tolerance to H_2O_2, thereby affecting the survival of the pathogenic bacteria. The results indicate that T6SS may be associated with resistance to environmental stress in pathogenic bacteria. However, this requires further investigation.

CONCLUSION

Here, we found a T6SS gene cluster consisting of 13 core genes (A-M) in the genome of *Psa* M228 based on a genome-wide analysis. We provide evidence that T6SS plays an important role in pathogenesis, bacterial competition, biofilm formation, and environmental adaptability. The next step is to clarify the assembly and secretion mechanism of T6SS and identify the virulence factors secreted by T6SS in *Psa*. This research has deepened our understanding of the pathogenic mechanism of *Psa*.

DATA AVAILABILITY STATEMENT

The raw data supporting the conclusions of this article will be made available by the authors, without undue reservation.

AUTHOR CONTRIBUTIONS

NW, NH, and LH designed the research. NW, NH, RT, XG, JC, ZW, and YL performed the experiments. NW, NH, RT, ZW, and YL analyzed the data. NW and NH wrote the manuscript. All authors contributed to the article and approved the submitted version.

FUNDING

This work was financially supported by the Special Support Plan for High-level Talent of Shaanxi Province, the National Key Research and Development Plan (2018TSCXL-NY-01-04), and Key Innovation Project in Shaanxi, China (2017ZDCXL-NY-03-02).

ACKNOWLEDGMENTS

We thank Prof. Xi-Hui Shen at Northwest A&F University, and Associate Professor Zhi-Bo Zhao at Guizhou University for helpful suggestions to improve this article.

SUPPLEMENTARY MATERIAL

The Supplementary Material for this article can be found online at: https://www.frontiersin.org/articles/10.3389/fmicb.2021.627785/full#supplementary-material

REFERENCES

Agnetti, J., Seth-Smith, H. M. B., Ursich, S., Reist, J., Basler, M., and Nickel, C. (2019). Clinical impact of the type VI secretion system on virulence of *Campylobacter* species during infection. *BMC Infect. Dis.* 19:237. doi: 10.1186/s12879-019-3858-x

Alcoforado, D. J., Liu, Y. C., and Coulthurst, S. J. (2015). Molecular weaponry: Diverse effectors delivered by the Type VI secretion system. *Cell Microbiol.* 17, 1742–1751. doi: 10.1111/cmi.12532

Asolkar, T., and Ramesh, R. (2020). The involvement of the type six secretion system (T6SS) in the virulence of *Ralstonia solanacearum* on brinjal. 3. *Biotech* 10:324. doi: 10.1007/s13205-020-02311-4

Basler, M., Ho, B. T., and Mekalanos, J. J. (2013). Tit-for-tat: Type VI secretion system counterattack during bacterial cell-cell interactions. *Cell* 152, 884–894. doi: 10.1016/j.cell.2013.01.042

Ben-aakov, R., and Salomon, D. (2019). The regulatory network of *Vibrio parahaemolyticus* type VI secretion system. *Environ. Microbiol.* 21, 2248–2260. doi: 10.1111/1462-2920.14594

Broms, J. E., Lavander, M., and Sjo-stedt, A. (2009). A conserved a-helix essential for a type VI secretion-like system of *Francisella tularensis*. *J. Bacteriol.* 191, 2431–2446. doi: 10.1128/jb.01759-08

Brunet, Y. R., Espinosa, L., Harchouni, S., Mignot, T., and Cascales, E. (2013). Imaging type VI secretion-mediated bacterial killing. *Cell Rep.* 3, 36–41. doi: 10.1016/j.celrep.2012.11.027

Catarina, F. R., Eric, D., Marie-Stéphanie, A., Stéphanie, B., Miguel, O. L., Badreddine, D., et al. (2011). Towards a structural comprehension of bacterial type VI secretion systems: characterization of the TssJ-TssM complex of an *Escherichia coli* pathovar. *PLoS Pathog.* 7:e1002386. doi: 10.1371/journal.ppat.1002386

Cianfanelli, F. R., Monlezun, L., and Coulthurst, S. J. (2016). Aim, load, fire: the Type VI secretion system, a bacterial nanoweapon. *Trends Microbiol.* 24, 51–62. doi: 10.1016/j.tim.2015.10.005

Cornelis, G. R., Agrain, C., and Sorg, I. (2006). Length control of extended protein structures in bacteria and bacteriophages. *Curr. Opin. Microbiol.* 9, 201–206. doi: 10.1016/j.mib.2006.01.002

Costa, T. R. D., Felisberto-Rodrigues, C., Meir, A., Prevost, M. S., Redzej, A., Trokter, M., et al. (2015). Secretion systems in gram-negative bacteria: Structural and mechanistic insights. *Nat. Rev. Microbiol.* 13, 343–359. doi: 10.1038/nrmicro3456

Deb, S., Gupta, M. K., Patel, H. K., and Sonti, R. V. (2019). *Xanthomonasoryzae* pv. *oryzaexopq* protein suppresses rice immune responses through interaction with two 14-3-3 proteins but its phosphor-null mutant induces rice immune responses and interacts with another 14-3-3 protein. *Mol. Plant Patholmol. Plant Pathol.* 20, 976–989. doi: 10.1111/mpp.12807

Donati, I., Cellini, A., Sangiorgio, D., Vanneste, J. L., and Spinelli, F. (2020). *Pseudomonas syringae* pv. *actinidiae*: ecology, infection dynamics and disease epidemiology. *Microb. Ecol.* 80, 1–22. doi: 10.1007/s00248-019-01459-8

Durand, E., Cambillau, C., Cascales, E., and Journet, L. (2014). VgrG, Tae, Tle, and beyond: The versatile arsenal of type VI secretion effectors. *Trends Microbiol.* 22, 498–507. doi: 10.1016/j.tim.2014.06.004

Felsenstein, J. (1985). Confidence limits on phylogenies: An approach using the bootstrap. *Evolution* 39, 783–791. doi: 10.1111/j.1558-5646.1985.tb00420.x

Gadhave, K. R., Devlin, P. F., Ebertz, A., Ross, A., and Gange, A. C. (2018). Soil inoculation with *Bacillus* spp. modifies root endophytic bacterial diversity, evenness, and community composition in a context-specific manner. *Microb. Ecol.* 76, 741–750. doi: 10.1007/s00248-018-1160-x

Gao, X., Huang, Q., Zhao, Z., Han, Q., Ke, X., Qin, H., et al. (2016). Studies on the infection, colonization, and movement of *Pseudomonas syringae* pv. *Actinidiae* in kiwifruit tissues using a GFPuv-Labeled strain. *PLoS One* 11:e0151169. doi: 10.1371/journal.pone.0151169

Gerlach, R. G., and Hensel, M. (2007). Protein secretion systems and adhesins: The molecular armory of gram-negative pathogens. *Int. J. Med. Micobiol.* 297, 401–415. doi: 10.1016/j.ijmm.2007.03.017

Gordon, W., Mullins, A. J., Edward, C. O., Arun, R., Bai, A. J., and Eshwar, M. (2020). Culturable diversity of bacterial endophytes associated with medicinal plants of the Western Ghats, india. *FEMS Microbiol. Ecol.* 9:147. doi: 10.1093/femsec/fiaa147

Guo, Z., and Li, D. (2000). Active oxygen species in plant disease resistance. *J. Integr. Plant Biol.* 42, 881–891.

Habbadi, K., Benkirane, R., Benbouazza, A., Bouaichi, A., and Achbani, E. H. (2017). Biological control of grapevine crown gall caused by allorhizobiumvitis using bacterial antagonists. *IJSR* 6, 1390–1397. doi: 10.21275/ART20174478

Hang, C., Yue, H., Qin, K., Yang, X., Jia, Z., and Li, Q. (2018). A serological approach for the identification of the effector hopz5 of *Pseudomonas syringae* pv. *actinidiae*: a tool for the rapid immune detection of kiwifruit bacterial canker. *J. Plant Pathol.* 100, 171–177. doi: 10.1007/s42161-018-0041-y

Hirose, K., Ishiga, Y., and Fujikawa, T. (2020). Phytotoxin synthesis genes and type III effector genes of *Pseudomonas syringae* pv. *Actinidiae* biovar 6 are regulated by culture conditions. *PEERJ* 8:e9697. doi: 10.7717/peerj.9697

Huang, Q. L., Gao, X. N., Zhao, Z. B., Qin, H. Q., and Huang, L. L. (2013). Transformed GFPuv into *Pseudomonas syringae* pv. *actinidiae* and its biological characteristics and colonization in soil and roots of kiwifruit. *Scient. Agricult. Sin.* 46, 282–291.

Jiang, S. J., Liu, Z., Yu, H., Zhang, G. Q., and Fan, W. Y. (2011). Research on oxidative stress Induced by Tenuazonic Acid from Alternaria augustiovoide and Changes in Antioxidant enzyme activities in leaves of Echinochloacrus-gall. *J. Agr. Sci. Tech. Iran* 2011, 792–798. doi: 10.16175/j.cnki.1009-4229.2011.06.019

Kang, Z. S. (1995). *Ultrastructure of plant pathogenic fungi*. Beijing: China Science and Technology Press.

Kanwar, P., and Jha, G. (2019). Alterations in plant sugar metabolism: signatory of pathogen attack. *Planta* 249, 305–318. doi: 10.1007/s00425-018-3018-3

Kapitein, N., Bonemann, G., Pietrosiuk, A., Seyffer, F., € Hausser, I., Locker, J. K., et al. (2013). ClpV recycles VipA/VipB tubules and prevents non-productive tubule formation to ensure efficient type VI protein secretion. *Mol. Microbiol.* 87, 1013–1028. doi: 10.1111/mmi.12147

Khan, M., Seto, D., Subramaniam, R., and Desveaux, D. (2018). Oh, the places they'll go! A survey of phytopathogen effectors and their host targets. *Plant J. Cell Mol. Biol.* 93, 651–663. doi: 10.1111/tpj.13780

Kim, M. J., Chae, D. H., Cho, G., Kim, D. R., and Kwak, Y. S. (2019). Characterization of antibacterial strains against kiwifruit bacterial canker pathogen. *Plant Pathol. J.* 35, 1–13. doi: 10.5423/PPJ.OA.05.2019.0154

Kudryashev, M., Wang, R. Y.-R., Brackmann, M., Scherer, S., Maier, T., and Baker, D. (2015). Structure of the type VI secretion system contractile sheath. *Cell* 160, 952–962. doi: 10.1016/j.cell.2015.01.037

Kvitko, B. H., and Collmer, A. (2011). Construction of *Pseudomonas syringae*pv. *Tomato* DC3000 mutant and polymutant strains. *Methods Mol. Biol.* 712:109. doi: 10.1007/978-1-61737-998-7_10

Le, S. Q., and Gascuel, O. (1993). An improved general amino acid replacement matrix. *Mol. Biol. Evol.* 25, 1307–1320. doi: 10.1093/molbev/msn067

Leiman, P. G., Basler, M., Ramagopal, U. A., Bonanno, J. B., Sauder, J. M., and Pukatzki, S. (2009). Type VI secretion apparatus and phage tail-associated protein complexes share a common evolutionary origin. *Proc. Natl. Acad. Sci. U S A.* 106, 4154–4159. doi: 10.1073/pnas.0813360106

Lopez, I., and Pardo, M. A. (2005). Application of relative quantification taqman real-time polymerase chain reaction technology for the identification and quantification of *Thunnus alalunga* and *Thunnus albacares*. *J. Agr. Food Chem.* 53, 4554–4560. doi: 10.1021/jf0500841

Luo, Y., Xu, J., Xu, J., Zhang, H., and Feng, J. (2016). Functional analysis of a T6SS cluster of *Ralstonia solanacearum* po82. *Plant Prot. Sci.* 6, 38–45.

Ma, A. T., and Mekalanos, J. J. (2010). In vivo actin cross-linking induced by *Vibrio cholerae* type VI secretion system is associated with intestinal inflammation. *Proc. Natl. Acad. Sci U S A.* 107, 4365–4370. doi: 10.1073/pnas.0915156107

MacIntyre, D. L., Miyata, S. T., Kitaoka, M., and Pukatzki, S. (2010). The *Vibrio cholerae* type VI secretion system displays antimicrobial properties. *Proc. Natl. Acad. Sci. U S A.* 107, 19520–19524. doi: 10.1073/pnas.1012931107

Mathias, G., Victorien, D., Corinne, B., Thibaut, R., and Annabelle, M. (2017). Contribution of the *Pseudomonas fluorescens* mfe01 type VI secretion system to biofilm formation. *PLoS One* 12:e0170770. doi: 10.1371/journal.pone.0170770

Mattinen, L., Nissinen, R., and Riipi, T. (2010). Host-extract induced changes in the secretome of the plant pathogenic bacterium *Pectobacterium atrosepticum*. *Proteomics* 7, 3527–3537. doi: 10.1002/pmic.200600759

Mcquade, R., and Stock, S. (2018). Secretion systems and secreted proteins in gram-negative entomopathogenic bacteria: their roles in insect virulence and beyond. *Insects* 9:68. doi: 10.3390/insects9020068

Michelotti, V., Lamontanara, A., Burian, G., Orrù, L., Cellini, A., Donati, I., et al. (2018). Comparative transcriptome analysis of the interaction between *Actinidiachinensis* var. *chinensis* and *Pseudomonas syringae*pv. *actinidiae* in absence and presence of acibenzolar-s-methyl. *BMC Genomics* 19:585. doi: 10.1186/s12864-018-4967-4

Molina, L., Rezzonico, F., Défago, G., Duffy, B. (2005). Autoinduction in erwinia amylovora: evidence of an acyl-homoserine lactone signal in the fire blight pathogen. *J. Bacteriol.* 187, 3206–3213. doi: 10.1128/JB.187.9.3206-3213.2005

Nguyen, V. S., Douzi, B., Durand, E., Roussel, A., Cascales, E., and Cambillau, C. (2018). Towards a complete structural deciphering of type VI secretion system. *Curr. Opin. Struc. Biol.* 49, 77–84. doi: 10.1016/j.sbi.2018.01.007

Nicaise, V., and Candresse, T. (2017). Plum pox virus capsid protein suppresses plant pathogen-associated molecular pattern (pamp)-triggered immunity. *Mol. Plant Pathol.* 18, 878–886. doi: 10.1111/mpp.12447

Pell, L. G., Kanelis, V., Donaldson, L. W., Howell, P. L., and Davidson, A. R. (2009). The phage lambda major tail protein structure reveals a common evolution for long-tailed phages and the type VI bacterial secretion system. *Proc. Natl. Acad. Sci. U S A.* 106, 4160–4165. doi: 10.1073/pnas.0900044106

Pinheiro, L. A. M., Pereira, C., Barreal, M. E., Gallego, P. P., and Almeida, A. (2020). Environmental biotechnology use of phage ϕ6 to inactivate *Pseudomonas syringae* pv. *actinidiae* in kiwifruit plants: in vitro and ex vivo experiments. *Appl. Microbiol. Biot.* 104, 1319–1330. doi: 10.1007/s00253-019-10301-7

Pukatzki, S., McAuley, S. B., and Miyata, S. T. (2009). The type VI secretion system: translocation of effectors and effector-domains. *Curr. Opin. Microbiol.* 12, 11–17. doi: 10.1016/j.mib.2008.11.010

Sana, T. G., Benjamin, B., and Sophie, B. (2016). The T6SS of *Pseudomonas aeruginosa* strain PAO1 and their effectors: beyond bacterial-cell targeting. *Front. Cell Infect. Microbiol.* 6:61. doi: 10.3389/fcimb.2016.00061

Schafer, A., Tauch, A., Jager, W., Kalinowski, J., Thierbach, G., and Puhler. (1994). A Small mobilizable multi-purpose cloning vectors derived from the *Escherichia coli* plasmids pK18 and pK19: selection of defined deletions in the chromosome of *Coryne bacterium glutamicum*. *Gene* 145, 69–73. doi: 10.1016/0378-1119(94)90324-7

Shyntum, D. Y., Theron, J., Moleleki, L. N., Toth, I. K., and Coutinho, T. A. (2015). *Pantoeaananatis* utilizes a type VI secretion system for pathogenesis and bacterial competition. *Mol. Plant Microbe Interact.* 28, 420–431. doi: 10.1094/MPMI-07-14-0219-R

Stefani, E., and Giovanardi, D. (2011). Dissemination of *Pseudomonas syringae* pv. *actinidiae* through pollen and its epiphytic life on leaves and fruits. *Phytopathol. Mediterr.* 50, 489–496. doi: 10.1016/j.phymed.2011.09.068

Stepanovic, S., Vukovic, D., Dakic, I., Savic, B., and Svabic-Vlahovic, M. (2000). A modified microtiter-plate test for quantification of staphylococcal biofilm formation. *J. Microbiol. Meth.* 40, 175–179. doi: 10.1016/S0167-7012(00)00122-6

Tamura, K., Stecher, G., Peterson, D., Filipski, A., and Kumar, S. (2013). MEGA6: Molecular evolutionary genetics analysis version 6.0. *Mol. Biol. Evol.* 30, 2725–2729. doi: 10.1093/molbev/mst197

Tontou, R., Giovanardi, D., and Stefani, E. (2014). Pollen as a possible pathway for the dissemination of *Pseudomonas syringae* pv. *actinidiae* and bacterial canker of kiwifruit. *Phytopathol. Mediterr.* 53, 333–339. doi: 10.14601/Phytopathol_Mediterr-13757

Vanneste, J. L. (2017). The scientific, economic, and social impacts of the New Zealand outbreak of bacterial canker of kiwifruit (*Pseudomonas syringae* pv. *actinidiae*). *Annu. Rev. Phytopathol.* 55, 377–399. doi: 10.1146/annurev-phyto-080516-035530

Weber, B. S., Miyata, S. T., Iwashkiw, J. A., Mortensen, B. L., Pukatzki, S., and Feldman, M. F. (2013). Genomic and functional analysisof the type VI secretion system in *Acinetobacter*. *PLoS One* 8:e55142. doi: 10.1371/journal.pone.0055142

Wen, Z., Yan, G., Qian, C., Qi, Z., Lin, F., and Zheng, J. (2018). Decorin is a pivotal effector in the extracellular matrix and tumour microenvironment. *Oncotarget* 9, 5480–5491. doi: 10.18632/oncotarget.23869

Williams, H., Ting, C., Nejati, M., Jones, M. H., Penhall, N., and Lim, J. Y. (2020). Improvements to and large-scale evaluation of a robotic kiwifruit harvester. *J. Robotic Syst.* 37, 187–201. doi: 10.1002/rob.21890

Wu, C. F., Smith, D. A., Lai, E. M., and Chang, J. H. (2018). The agrobacterium type VI secretion system: a contractile nanomachine for interbacterial competition. *Curr. Top Microbiol.* 418, 215–231. doi: 10.1007/82_2018_99

Yu, Q., Li, J., Zhang, Y., Wang, Y., Liu, L., and Li, M. (2016). Inhibition of gold nanoparticles (aunps) on pathogenic biofilm formation and invasion to host cells. *Sci Rep. U K.* 6:26667. doi: 10.1038/srep26667

Zhang, L., Ni, C., Xu, W., Dai, T., and Liu, Q. (2016). Intra macrophage infection reinforces the virulence of *Edward siellatarda*. *J. Bacteriol.* 198, 1534–1542. doi: 10.1128/JB.00978-15

Zhang, L., Xu, J., Xu, J., Chen, K., He, L., and Feng, J. (2012). TssM is essential for virulence and required for type VI secretion in *Ralstonia solanacearum*. *J. Plant Dis. Protect.* 119, 125–134. doi: 10.1007/BF03356431

Zhang, L., Xu, J., Xu, J., Zhang, H., He, L., and Feng, J. (2014). TssB is essential for virulence and required for Type VI secretion system in *Ralstonia solanacearum*. *Microb. Pathog.* 74, 1–7. doi: 10.1016/j.micpath.2014.06.006

Zhang, Y., Liu, Y., Wang, T., Deng, X., and Chu, X. (2018). Natural compound sanguinarine chloride targets the type III secretion system of *Salmonella entericasero* var *typhimurium*. *Biochem. Biophys. Rep.* 14, 149–154. doi: 10.1016/j.bbrep.2018.04.011

Zhao, Z., Chen, J., Gao, X., Zhang, D., Zhang, J., Wen, J., et al. (2019). Comparative genomics reveal pathogenicity-related loci in *Pseudomonas syringae* pv. A*ctinidiae* biovar 3. *Mol. Plant Pathol.* 20, 923–942. doi: 10.1111/mpp.12803

Zheng, J., Ho, B., and Mekalanos, J. J. (2011). Genetic analysis of antiamoebae and anti-bacterial activities of the type VI secretion system in *Vibriocholerae*. *PLoS One* 6:e23876. doi: 10.1371/journal.pone.0023876

Zhu, P. C., Li, Y. M., Zou, H. F., Niu, X. N., Xu, L. H., Jiang, W., et al. (2020). Type VI secretion system is not required for virulence on rice but for inter-bacterial competition in *Xanthomonasoryzae* pv. *Oryzicola*. *Res. Microbiol.* 171, 64–73. doi: 10.1016/j.resmic.2019.10.004

Conflict of Interest: The authors declare that the research was conducted in the absence of any commercial or financial relationships that could be construed as a potential conflict of interest.

frontiers in Microbiology

ORIGINAL RESEARCH
published: 08 March 2021
doi: 10.3389/fmicb.2021.629387

CgNPG1 as a Novel Pathogenic Gene of *Colletotrichum gloeosporioides* From *Hevea brasiliensis* in Mycelial Growth, Conidiation, and the Invasive Structures Development

*Chen Liang†, Bei Zhang†, Yun Zhou, Hongyan Yin, Bang An, Daozhe Lin, Chaozu He and Hongli Luo**

Hainan Key Laboratory for Sustainable Utilization of Tropical Bioresource, College of Tropical Crops, Hainan University, Haikou, China

OPEN ACCESS

Edited by:
Yong Wang,
Guizhou University, China

Reviewed by:
Zhibo Zhao,
Guizhou University, China
Oded Yarden,
Hebrew University of Jerusalem, Israel

***Correspondence:**
Hongli Luo
hlluo@hainanu.edu.cn

† These authors have contributed equally to this work

Specialty section:
This article was submitted to Microbe and Virus Interactions with Plants, a section of the journal Frontiers in Microbiology

Received: *14 November 2020*
Accepted: *02 February 2021*
Published: *08 March 2021*

Citation:
Liang C, Zhang B, Zhou Y, Yin H, An B, Lin D, He C and Luo H (2021) CgNPG1 as a Novel Pathogenic Gene of Colletotrichum gloeosporioides From Hevea brasiliensis in Mycelial Growth, Conidiation, and the Invasive Structures Development. Front. Microbiol. 12:629387. doi: 10.3389/fmicb.2021.629387

The rubber tree (*Hevea brasiliensis*) is a tropical perennial crop for the primary source of natural rubber. *Colletotrichum gloeosporioides* from *Hevea brasiliensis* (*C. gloeosporioides* Hb) and *Colletotrichum acutatum* from *Hevea brasiliensis* (*C. acutatum* Hb) are the causal agents of rubber tree anthracnose and lead to serious loss of natural rubber production. Inoculation tests showed that *C. gloeosporioides* Hb possessed higher pathogenicity than *C. acutatum* Hb to the rubber tree. Genomic analysis revealed that an unknown gene, named *CgNPG1* (a Novel Pathogenic Gene 1), was presented in the genome of *C. gloeosporioides* Hb but not identified in *C. acutatum* Hb. *CgNPG1* was predicted to encode a small secretory protein without any conserved domain. To investigate the functions of *CgNPG1* in *C. gloeosporioides* Hb and in *C. acutatum* Hb, the gene deletion and overexpression mutants were generated. The phenotype analysis showed that deletion of *CgNPG1* led to changed conidia morphology, decreased mycelial growth, conidiation, conidia germination rate, appressorium formation rate, and pathogenicity of *C. gloeosporioides* Hb to the rubber tree. Meanwhile, heterogeneous expression of *CgNPG1* in *C. acutatum* Hb significantly changed the conidia morphology and improved the mycelial growth rate, conidiation, conidia germination rate, appressorium formation rate, and the pathogenicity of *C. acutatum* Hb to the rubber tree. Consistently, *CgNPG1* increased the expression level of *CaCRZ1* and *CaCMK1* in *C. acutatum* Hb. These data suggested that *CgNPG1* contributed to mycelial growth, conidiation, the development of invasive structures, and the pathogenicity of *Colletotrichum* to the rubber tree, which might be related to the modulation of CaCRZ1 and mitogen-activated protein kinase CMK1. Our results provided new insight into *CgNPG1* in regulating growth and pathogenicity of the *Colletotrichum* spp.

Keywords: *Colletotrichum gloeosporioides*, *Colletotrichum acutatum*, CgNPG1, mycelial growth, conidiation, pathogenicity

INTRODUCTION

Colletotrichum as asexual genus is classified into fungi imperfecti, coelomycetes (Dean et al., 2012). As one of the most common and important genus of filamentous phytopathogenic fungi, *Colletotrichum* caused anthracnose on a wide variety of herbaceous and woody plants in tropical, subtropical, and temperate climates, resulting in serious economic losses (Cannon et al., 2012; Dean et al., 2012; Crouch et al., 2014; Baroncelli et al., 2016). Most *Colletotrichum* species feed on hemibiotrophy, exhibiting initially a brief biotrophic phase with large intracellular primary hyphae and later a destructive, necrotrophic phase with narrower secondary hyphae, which ramify throughout the host tissue (Münch et al., 2008; Dean et al., 2012). Among these *Colletotrichum* species, *Colletotrichum acutatum*, and *Colletotrichum gloeosporioides* are frequently mentioned and reported because of early taxonomic confusion (Dean et al., 2012).

Although multiple inoculation investigations have demonstrated that most isolates of *Colletotrichum* spp. are relatively non-host-specific, there are still some differences in host and tissue pathogenicity between species (Peres et al., 2005; de Souza et al., 2013). For example, *C. acutatum* isolates from pine were non-pathogenic or weakly pathogenic to lupine and vice versa, and the isolates from fruits were not pathogenic on either pine or lupine (Lardner et al., 1999; Peres et al., 2005). In plant pathogens, host specificity is often attributed to pathogen virulence factors, including specialized secondary metabolites (SSM), toxin, cell wall-degrading enzymes, and small-secreted protein (SSP) effectors (Stukenbrock and McDonald, 2007; Brunner et al., 2013; Poppe et al., 2015; Buiate et al., 2017). Recently, several reports have revealed that horizontal gene transfer (HGT) and horizontal chromosome transfer (HCT) between plant pathogenic fungi affect their host range and virulence (Mehrabi et al., 2011; Jaramillo et al., 2014).

Mitogen-activated protein (MAP) kinase signal transduction pathways were involved in fungal pathogenesis (Dickman and Yarden, 1999), and some virulence-involved transcription factors (TFs) played important roles in fungal infection to plant (Dickman and Yarden, 1999; Son et al., 2011). For example, MAP kinase *Cpmk2* from ascomycete *Claviceps purpurea* and *mps1* from *Magnaporthe grisea* contributed to conidiation and virulence (Xu et al., 1998; Mey et al., 2002). MoCRZ1 from rice blast fungus *Magnaporthe oryzae* was essential for cell wall integrity, conidiation, pathogenicity, and Ca^{2+}-dependent vegetative growth (Choi et al., 2009). The infection process of *Colletotrichum* includes germination, formation of melanized appressoria, appressorial penetration, and subsequent invasive growth in host plants. In *C. lagenarium*, *CMK1* regulated conidial germination, appressorium formation, and pathogenicity (Takano et al., 2000). In *C. gloeosporioides*, CgCrzA as the homolog of CRZ1, was involved in regulating cell wall integrity and infection-related morphogenesis. Deletion of the *CgCRZA* in *C. gloeosporioides* showed severe cell wall integrity defects and inhibited the vegetative growth, conidiation, appressorial formation rate, and lost pathogenicity to plant hosts (Wang et al., 2020). These data suggested that both CMK1 and CRZ1 in *Colletotrichum* were involved in fungal development and pathogenesis.

The rubber tree (*Hevea brasiliensis*) is a tropical perennial crop for natural rubber; however, rubber latex production is seriously affected by rubber tree anthracnose (Pu et al., 2007; Cao et al., 2017), which are caused by *C. gloeosporioides* and *C. acutatum* (Brown and Soepena, 1994; Saha et al., 2002). In China, *C. gloeosporioides* was considered as the only pathogen of rubber tree anthracnose at first, until *C. acutatum* was first reported as a causal agent of rubber tree anthracnose in Yunnan Province in 2008 and in Hainan in 2010 (Zhang et al., 2008; Li et al., 2010). Further research revealed that both *C. gloeosporioides* and *C. acutatum* can induce typical water-soaked, darker, and circular lesions on rubber tree leaves, but the colony growth rate of *C. gloeosporioides* is significantly higher than that of *C. acutatum* (Cao et al., 2017). So far, little is known about the pathogenic mechanism of *C. gloeosporioides* and *C. acutatum* to rubber trees. In this study, *C. gloeosporioides* Hb and *C. acutatum* Hb were isolated from the leaves of rubber trees infected with anthracnose in Hainan province, and the following analysis showed that *C. gloeosporioides* Hb possesses significantly higher pathogenicity than that of *C. acutatum* Hb to rubber tree leaves. In order to explain the difference of pathogenicity to the rubber tree, the specific genes of *C. gloeosporioides* Hb, but not in *C. acutatum* Hb, were screened, especially *CgNPG1* (a Novel Pathogenic Gene of *C. gloeosporioides*). Further, the biological functions of *CgNPG1* have been characterized through construction of *CgNPG1* deletion mutant in *C. gloeosporioides* Hb and *CgNPG1* heterologous expression in *C. acutatum* Hb. These results not only extend our understanding of the pathogenesis of *C. gloeosporioides* Hb to the rubber tree but also provide novel insight into the host specificity mechanism of *C. gloeosporioides* Hb and *C. acutatum* Hb to the rubber tree.

MATERIALS AND METHODS

Fungal Strains and Culture Conditions

Colletotrichum gloeosporioides from *Hevea brasiliensis* and *Colletotrichum acutatum* from *Hevea brasiliensis* strains were isolated from the leaves of *Hevea brasiliensis* with anthracnose in Hainan province. Both strains were grown on potato dextrose agar (PDA) at 28°C in the dark.

In silico Analysis of *CgNPG1*

The amino acid sequence of CgNPG1 was deduced by DNASTAR software. Prediction of signal peptides was performed online by SignalP 5.0 analysis tool[1]. Prediction of conserved domain

[1]http://www.cbs.dtu.dk/services/SignalP/

and motif were performed by Motif Scan[2]. The bootstrap neighbor-joining phylogenetic tree was constructed using Clustal X 2.0 and MEGA X.

Vector Constructions

For the construction of the gene deletion vector, the 5′ and 3′ flanking region nucleotides of the *CgNPG1* were amplified from genomic DNA and ligated into the vector pCB1532 carrying the acetolactate synthase gene (SUR) cassette from *M. oryzae* conferred resistance to chlorimuron ethyl (a sulfonylurea herbicide) (**Supplementary Figure 1A**). For construction of the complementation vector, the open read frame of *CgNPG1* was amplified from cDNA, fused with the 3 X FLAG coding sequence, and cloned into the vector harboring the promoter of *ToxA*, the terminator of nos, and the hygromycin phosphotransferase gene (HPH) (**Supplementary Figure 2A**).

Transformation of *Colletotrichum gloeosporioides* and *Colletotrichum acutatum*

Protoplast preparation and transformation were carried out as described in our previous work (Wang et al., 2018). The deletion mutants were analyzed by two round PCR analyses, which were diagnostic tests for homologous integration of the 5′ part and 3′ part. Then the correct transformants were purified by single conidia isolations and analyzed by Southern blot. For Southern blot analysis, genomic DNA of wild type and the deletion mutant was extracted and digested with *HindIII*, and the upstream flanking region of *CgNPG1* was amplified and used as probe. Another PCR was conducted for screening existence of *CgNPG1*. The complementation mutant of *C. gloeosporioides* Hb and the heterogeneous expression mutant of *C. acutatum* Hb were identified by PCR analysis, and the *CgNPG1* expression level of the mutants was estimated by RT-PCR.

RNA Isolation, cDNA Synthesis, and qRT-PCR

RNA was extracted from the mycelium of *C. gloeosporioides* Hb and *C. acutatum* Hb using the CTAB-LiCl method (Yang et al., 2020). The contaminating DNA was eliminated using RNase-free DNase, and the first-strand cDNA was synthesized using Revert Aid First Strand cDNA Synthesis Kit (Thermo Fisher). Quantitative RT-PCR analysis was performed with the LightCycler 96 System (Roche). The beta-tubulin-1 (β-tub1) gene was used as an endogenous control for normalization. Relative expression levels of target genes were estimated using the $2^{-\Delta\Delta Ct}$ method.

Fungal Growth Assay

For the vegetate growth assay, 5-mm-diameter disks of mycelium together with agar were inoculated on fresh potato dextrose agar medium and cultured for 9 days. The diameters of the colonies were recorded, and the growth rates were calculated. The experiment was repeated three times. Statistical analysis was performed by SPSS software (version 20), with $P < 0.05$ as statistically significant.

Conidiation and Appressorium Formation Assay

For the conidiation assay, conidia were harvested from the strains growing on PDA medium for 8 days and inoculated into 50-ml liquid CMC medium to the final concentration of 10^4/ml, respectively. Then all samples were cultured at 28°C, 150 rpm, and the conidia numbers were calculated under a microscope after incubation for 2 days.

For appressorium formation assays, 20-μl drops of conidial suspensions were placed on nylon membrane and incubated at 28°C. After 4 and 8 h post-incubation, the percentages of conidial

[2]http://myhits.isb-sib.ch/cgi-bin/motif_scan

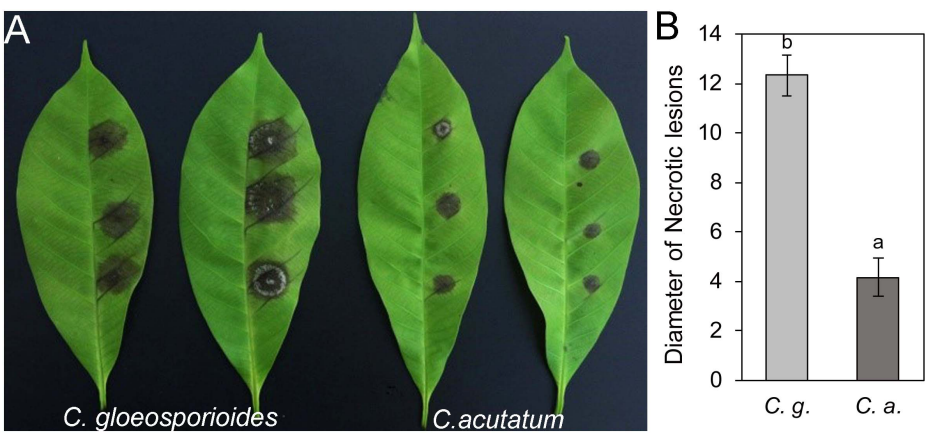

FIGURE 1 | Pathogenicity assay of *Colletotrichum gloeosporioides* Hb and *Colletotrichum acutatum* Hb on rubber tree leaves. **(A)** Disease symptoms of rubber-tree leaves at 3 days post-inoculation with *C. gloeosporioides* Hb and *C. acutatum* Hb mycelium. **(B)** Lesion diameters at 3 day post-inoculation. Error bars indicated standard deviation, and columns with different letters indicate significant difference ($P < 0.05$).

germination and appressorium formation were determined under a microscope, respectively. The experiment was repeated three times, and at least 100 conidia were detected per replicate.

Pathogenicity Test

For the pathogenicity test, conidia suspension was used to inoculate the rubber tree variety 7–33–97 leaves at the "light green" stage. Conidia were harvested from mycelium grown on potato dextrose agar medium for 12 days in a 28°C incubator, washed with double-distilled H_2O, filtered through a filter membrane (Miracloth, Millipore), and resuspended in a solution of 5% Sabouraud Maltose Broth (Difco) to a final concentration of 2×10^5 conidia/ml. Then 10 μl of the conidial suspensions were inoculated onto the wounded rubber tree leaves. The inoculated leaves were kept in a moist chamber at 28°C under natural illumination for 4 days,

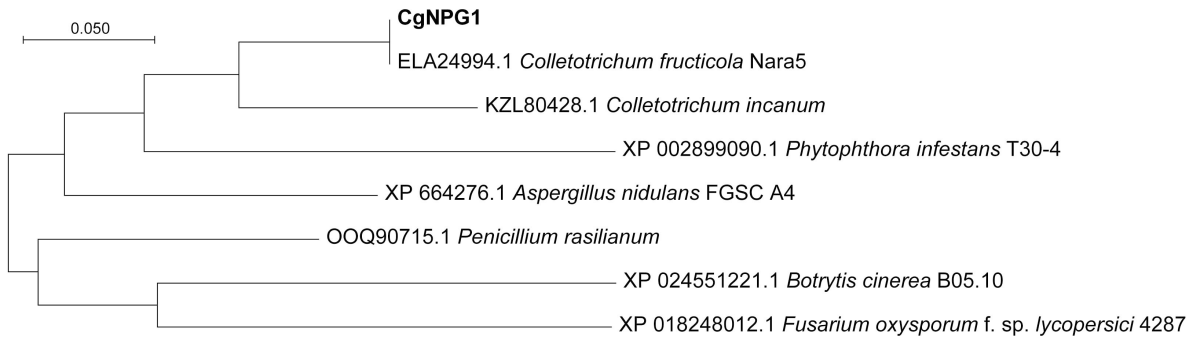

FIGURE 2 | Phylogenetic analysis of a Novel Pathogenic Gene 1 (CgNPG1). Phylogenetic analysis of CgNPG1 and another seven orthologs by neighbor-joining methods using MEGA X software.

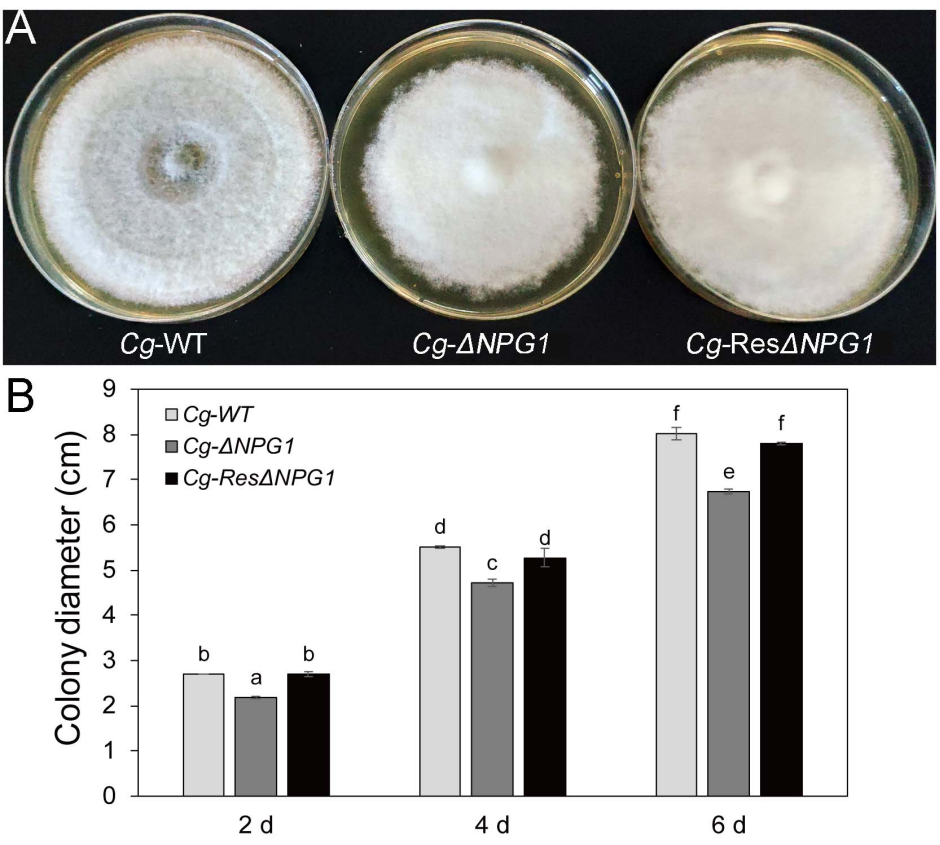

FIGURE 3 | Growth rate assays of *CgNPG1* deletion and complementation mutants of *C. gloeosporioides* Hb. **(A)** Colonial morphology of wild type strain (Cg-WT), the *CgNPG1* deletion mutant (Cg-ΔNPG1), and complementation mutant (Cg-ResΔNPG1) after culture for 8 day on potato dextrose agar. **(B)** Colony diameters at 2, 4, and 6 day post-inoculation. Error bars indicated standard deviation, and columns with different letters indicate significant difference ($P < 0.05$).

and the disease symptoms were scored. Each treatment contained three replicates of nine leaves, and the entire experiment was repeated three times. Statistical analysis was performed by SPSS software (version 20), with $P < 0.05$ as statistically significant.

RESULTS

Pathogenicity Difference of *Colletotrichum gloeosporioides* Hb and *Colletotrichum acutatum* Hb on Rubber Tree Leaves

Colletotrichum gloeosporioides from *Hevea brasiliensis* and *Colletotrichum acutatum* from *Hevea brasiliensis* were isolated and characterized from rubber trees in Hainan province of China. When the detached "light green" rubber tree leaves from variety 73–3–97 were inoculated with *C. gloeosporioides* Hb and *C. acutatum* Hb, respectively, the necrotic lesions were obviously observed on the 4th day (**Figure 1A**). The mean size of the disease lesion was about 1.3 cm in *C. gloeosporioides* Hb, while that of *C. acutatum* Hb was only about 0.4 cm (**Figure 1B**), suggesting that *C. gloeosporioides* Hb possesses higher pathogenicity to the rubber tree than *C. acutatum* Hb.

Cloning and Analysis of Specific Pathogenic Genes of *Colletotrichum gloeosporioides* Hb

Genome sequencing of *C. gloeosporioides* Hb and *C. acutatum* Hb was produced by Illumina Hiseq2000. Both of the genome sequences have been uploaded to the NCBI database (Bioproject ID: PRJAN690880). In order to reveal the mechanism of the different pathogenicities of *C. gloeosporioides* Hb and *C. acutatum* Hb to the rubber tree, the genes encoding secretory proteins were predicted. Among these genes, three genes encoded proteins with no putative conserved domains and were specific to *C. gloeosporioides* Hb than to *C. acutatum* Hb. One of them was named *CgNPG1* (a Novel Pathogenic Gene of *C. gloeosporioides* Hb). *CgNPG1* contains a 435-bp open reading frame encoding a polypeptide of 144 amino acids with a molecular weight of approximately 15.0 kDa and a theoretical pI of 4.28. The CgNPG1 protein contained 10 cysteines, accounting for 6.9% of the total number of amino acids. Signal peptide was predicted at the N-terminal of 1 to 16 amino acids (**Supplementary Figure 1**). In addition, the

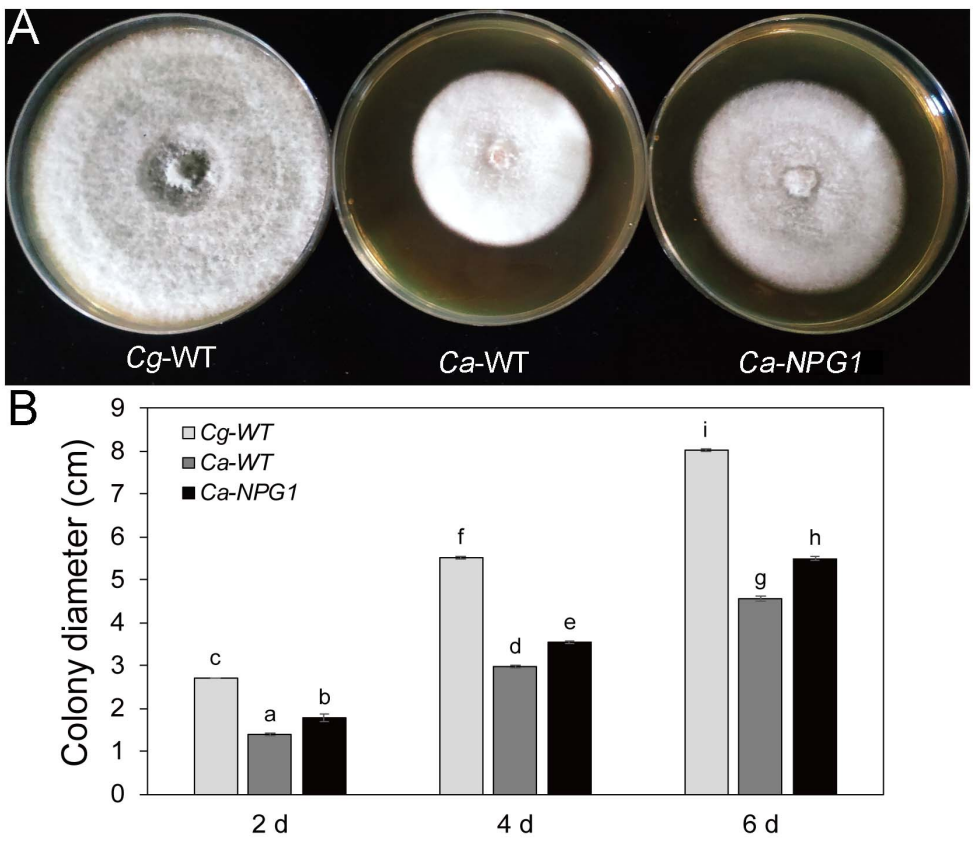

FIGURE 4 | Growth rate assays of *C. acutatum* Hb strains expressing *CgNPG1*. **(A)** Colonial morphology of *C. gloeosporioides* Hb wild type strain (Cg-WT), *C. acutatum* Hb wild type strain (Ca-WT), and the *CgNPG1* heterologous expression mutant (Ca-*NPG1*). **(B)** Colony diameters at 2, 4, and 6 day post-inoculation. Error bars indicated standard deviation, and columns with different letters indicate significant difference ($P < 0.05$).

transmembrane domain and any known conserved domains were not found in the CgNPG1 protein. In addition, the protein sequences of CgNPG1 and some highly homologous protein sequences of representative hemibiotrophic fungi, necrotrophic fungi, and oomycetes from Blastp were used to generate a phylogenetic tree. Phylogenetic tree analysis showed that the homologous proteins of CgNPG1 widely exist in hemibiotrophic fungi, necrotrophic fungi, and oomycetes, and CgNPG1 is the closest, homologous to *Colletotrichum* and oomycetes (**Figure 2**).

Generation of *CgNPG1* Deletion and Complementary Mutant in *Colletotrichum gloeosporioides*, and Heterogeneous Expression Mutant in *Colletotrichum acutatum*

To investigate the functions of *CgNPG1* in *C. gloeosporioides* Hb, the *CgNPG1* gene deletion and complementation mutants were generated. In addition, the *CgNPG1* heterogeneous expression mutant of *C. acutatum* Hb was generated to investigate its roles on *C. acutatum* Hb. The *CgNPG1* deletion mutant of *C. gloeosporioides* Hb (Cg-Δ*NPG1*) was generated by homologous recombination strategy (**Supplementary Figure 2A**). PCR diagnostic analysis showed that *CgNPG1* was successfully deleted from the *C. gloeosporioides* Hb genome (**Supplementary Figure 2B**). Southern blot assays revealed that the *CgNPG1* had only one copy and was deleted in the Cg-Δ*NPG1* mutant (**Supplementary Figure 2C**). The complementation strain (Cg-ResΔ*NPG1*) was generated by expressing *CgNPG1* driven by a ToxA promoter in the Cg-Δ*NPG1* mutant (**Supplementary Figure 3A**). PCR and semi-quantitative RT-PCR analysis showed that *CgNPG1* was restored in the complementary strain (**Supplementary Figures 3B,C**). The complementary vector of *CgNPG1* was used to transform *C. acutatum* Hb to generate the heterogeneous expression mutant (Ca-*NPG1*). PCR and semiquantitative RT-PCR analysis showed that *CgNPG1* was successfully integrated into the genome and expressed in *C. acutatum* Hb (**Supplementary Figure 4**).

CgNPG1 Contributes to Colony Growth of *Colletotrichum gloeosporioides* Hb and *Colletotrichum acutatum* Hb

Growth analysis showed that the deletion of *CgNPG1* obviously decreased the colony growth rate in *C. gloeosporioides* Hb, with the colony diameter decreased to 6.5 cm in Cg-Δ*NPG1* in comparison to 8 cm in Cg-WT at 8 days after inoculation. Meanwhile, the Cg-Δ*NPG1* showed different colonial morphology with more aerial hyphae compared with Cg-WT. In addition, complementation of *CgNPG1* restored the growth rate of Cg-Δ*NPG1* (**Figure 3**). Heterologous expression of *CgNPG1* significantly promoted the colony growth rate in *C. acutatum* Hb (**Figure 4**). These results suggested that CgNPG1 contributed to the vegetative growth of *C. gloeosporioides* Hb and *C. acutatum* Hb.

CgNPG1 Contributes to Conidia Morphology and Conidiation of *C. gloeosporioides* Hb and *C. acutatum* Hb

The morphological observation showed that the Conidia of Cg-Δ*NPG1* were significantly shorter than that of Cg-WT and complemented strains Cg-ResΔ*NPG1*, and heterologous expression of *CgNPG1* in *C. acutatum* Hb caused more than 65% of conidia to become blunt round at both ends and fatter compared with Ca-WT (**Figure 5A**). Conidiation assay showed that the conidia production of Δ*CgNPG1* was drastically reduced to less than half of Cg-WT and Cg-ResΔ*NPG1* (**Figure 5B**), and heterologous expression of *CgNPG1* in *C. acutatum* Hb doubled the conidia yield of Ca-WT (**Figure 5C**).

CgNPG1 Is Involved in Conidia Germination and Appressorium Formation

The processes of conidia germination and appressorium formation was observed and counted on nylon membrane. In

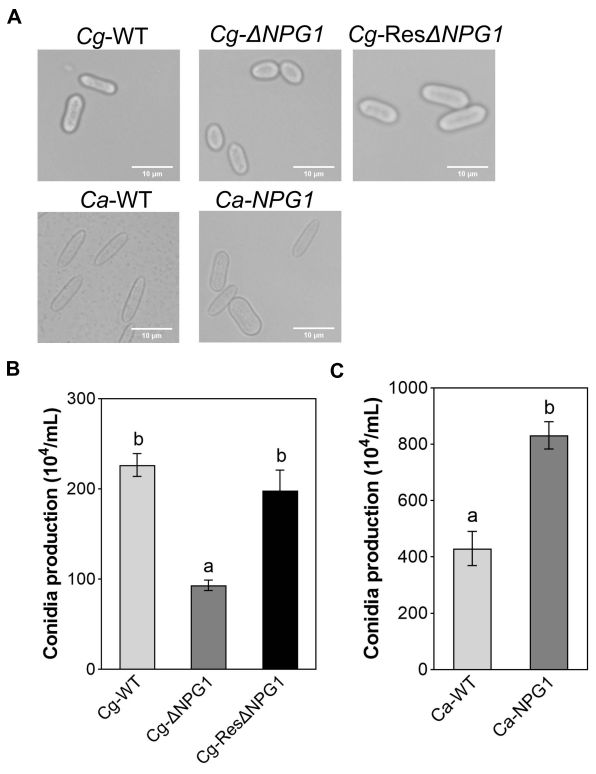

FIGURE 5 | Conidia morphology observation and conidiation assay of *CgNPG1* deletion mutant, *CgNPG1* complementation mutant, and *CgNPG1* heterologous expression mutant. **(A)** Conidial morphology of Cg-WT, Cg-Δ*NPG*, Cg-ResΔ*NPG1*, Ca-WT, and Ca-*NPG1*. **(B)** The number of conidia developed by the Cg-WT, Cg-Δ*NPG*, Cg-ResΔ*NPG1*. **(C)** The number of conidia developed by the Ca-WT and Ca-*NPG1*. Error bars indicated standard deviation, and columns with different letters indicate significant difference ($P < 0.05$).

Cg-WT and Cg-Res1Δ*NPG1*, more than 80% of the conidia germinated after 4 h of post-incubation, compared with less than 30% in Cg-Δ*NPG1* (**Figures 6A,B**). In the Cg-Δ*NPG1*mutant, over 70% of conidia failed to form abnormal appressoria after 8 h of post-incubation, compared with Cg-WT and Cg-Res1Δ*NPG1* strains, which formed normal appressoria (**Figures 6A,D**). Additionally, after 4 h of post-incubation, the conidia germination rate of Ca-*NPG1* strain was about 90%, which was significantly higher than that of wild type Ca-WT that was about 80% (**Figure 6C**). After 8 h of post-incubation, the appressorium information rate of Ca-*NPG1* strain was more than 95%, which was significantly higher than that of the

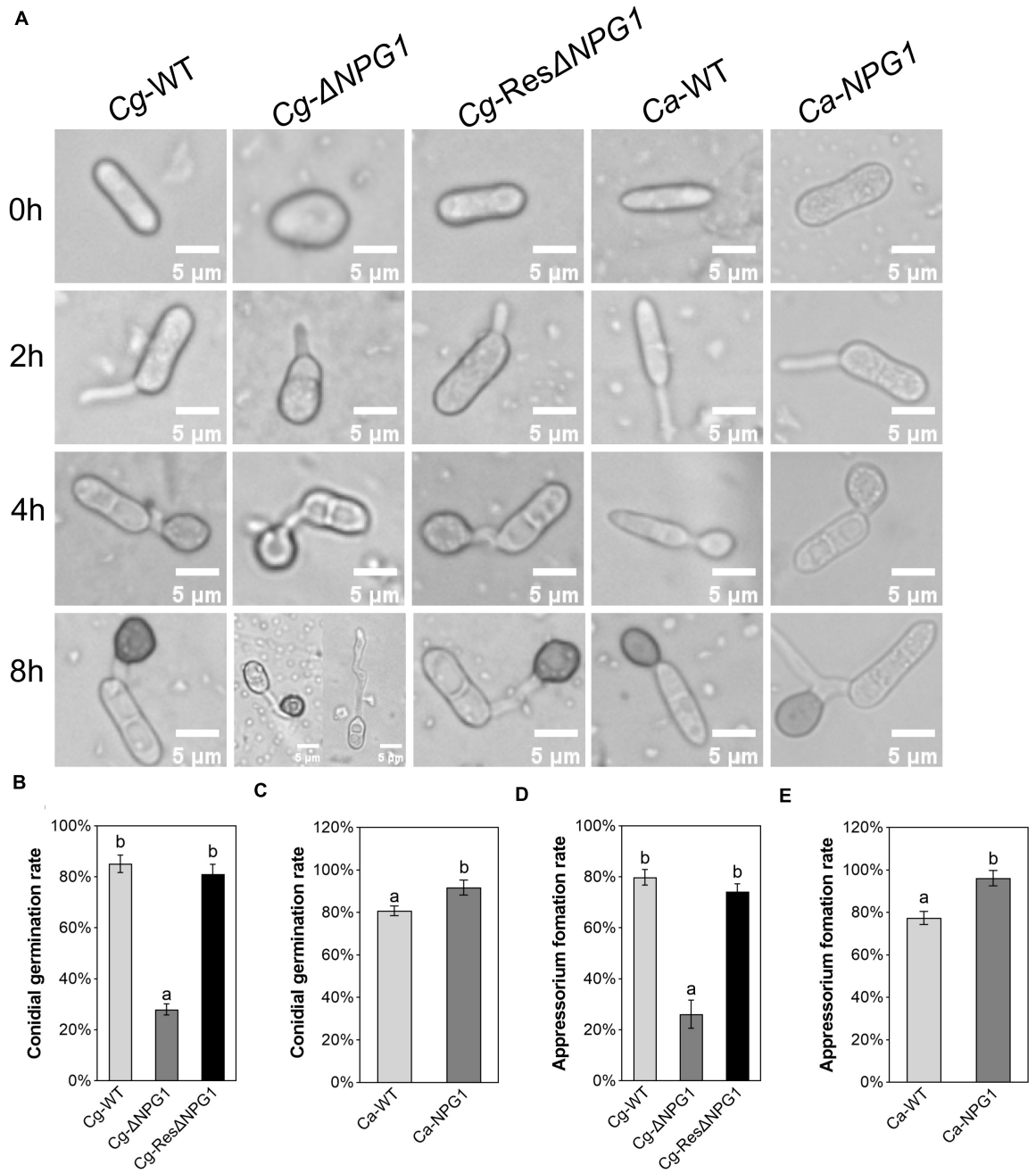

FIGURE 6 | Conidial germination and appressorium formation assay of *CgNPG1* deletion mutant and *CgNPG1* heterologous expression mutant. **(A)** Appressorium development progress of Cg-WT, Cg-Δ*NPG*, Cg-Res1Δ*NPG1*, Ca-WT, and Ca-*NPG1*. **(B)** Conidia germination rates of Cg-WT, Cg-Δ*NPG*, Cg-Res1Δ*NPG1* at 4 h time intervals. **(C)** Conidia germination rates of Ca-WT and Ca-*NPG1* at 4 h time intervals. **(D)** Appressorium formation rates of Cg-WT, Cg-Δ*NPG*, Cg-Res1Δ*NPG1* at 8 h time intervals. **(E)** Appressorium formation rates of Ca-WT and Ca-*NPG1* at 8 h time intervals. Error bars indicated standard deviation, and columns with different letters indicate significant difference ($P < 0.05$).

wild type Ca-WT strain, which was nearly 80% (**Figure 6E**). These data indicated that *CgNPG1* was involved in the invasive structure development of *C. gloeosporioides* Hb, including conidia germination and normal appressorium formation, and heterologous expression of *CgNPG1* in *C. acutatum* Hb promoted conidia germination and appressorium formation.

CgNPG1 Is Required for the Virulence of *Colletotrichum gloeosporioides* Hb and Increases the Virulence of *Colletotrichum acutatum* Hb on Rubber Tree

Detached rubber tree leaves were used for pathogenicity analysis. After inoculation for 4 day, both Cg-Δ*NPG1* and Cg-ResΔ*NPG1* caused typical anthracnose symptoms as well as Cg-WT (**Figure 7A**), but the mean lesion diameter caused by Cg-Δ*NPG1* (only 0.9 cm) was obviously smaller than that caused by Cg-WT (over 1.4 cm) (**Figure 7B**). Meanwhile, Cg-ResΔ*NPG1* basically restored the pathogenicity of Cg-Δ*NPG1*, with a lesion diameter of 1.3 cm after inoculation at 4 days. Interestingly, heterologous expression of *CgNPG1* in *C. acutatum* Hb significantly increase the pathogenicity of *C. acutatum* Hb to rubber tree leaves, with lesion diameters of 1.3 cm in Ca-*NPG1*; in contrast, the mean lesion diameter of Ca-WT was only 0.4 cm (**Figures 7C,D**). These data demonstrated that *CgNPG1* play important roles in the pathogenicity of *C. gloeosporioides* Hb and *C. acutatum* Hb to rubber tree.

CgNPG1 Increased the Expression of *CaCRZ1* and *CaCMK1* in *Colletotrichum acutatum* Hb

CRZ1 and CMK1 act as regulators of the upstream signals to control the growth, conidiation, invasive structures development, and pathogenicity in fungal pathogens (Mey et al., 2002; Wang et al., 2020). Here, heterologous expression of *CgNPG1* in *C. acutatum* Hb obviously upregulated the transcription of *CaCRZ1* and *CaCMK1*, with the expression level of *CaCRZ1* increased to twofold and *CaCMK1* to 1.3-fold (**Figure 8**), indicating that the effect of *CgNPG1* on *C. acutatum* Hb might be related to the modulation of CaCRZ1 and CaCMK1.

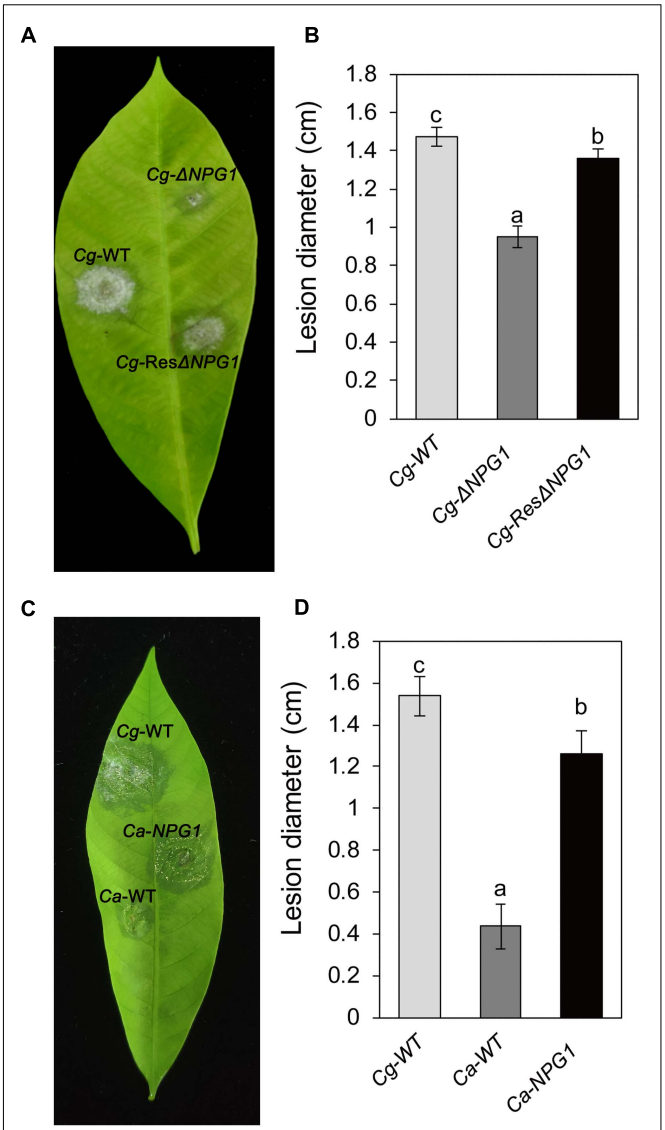

FIGURE 7 | Pathogenicity assay of *CgNPG1* deletion mutant and *CgNPG1* heterologous expression mutant on rubber tree leaves. **(A)** Disease symptoms of rubber tree leaves at 4 days post-inoculation with conidia of *C. gloeosporioides* Hb wild type (Cg-WT), the *CgNPG1* deletion mutant (Cg-Δ*NPG1*), and complementation mutant (Cg-ResΔ*NPG1*) strains. **(B)** Lesion diameters at 4 day post-inoculation with conidia of Cg-WT, Cg-Δ*NPG1,* and Cg-ResΔ*NPG1* strains. **(C)** Disease symptoms of rubber tree leaves at 4 days post-inoculation with conidia of *C. gloeosporioides* Hb wild type (Cg-WT), *C. acutatum* Hb wild type (Ca-WT), and the *CgNPG1* heterologous expression mutant (Ca-*NPG1*) strains. **(D)** Lesion diameters at 4 day post-inoculation with conidia of Cg-WT, Ca-WT, and Ca-*NPG1* strains. Error bars indicated standard deviation, and columns with different letters indicate significant difference ($P < 0.05$).

DISCUSSION

Colletotrichum spp. is one of the most common and important genera of plant pathogenic fungi, causing anthracnose on important staple food crops (Dean et al., 2012). Although both *C. gloeosporioides* and *C. acutatum* could cause typical anthracnose on rubber tree (*Hevea brasiliensis*) (Zhang et al., 2008; Li et al., 2010), there is virulence difference between the two pathogens. Consistently, the anthracnose caused by *C. gloeosporioides* Hb was more severe than that by *C. acutatum* Hb, suggesting that *C. gloeosporioides* Hb possesses higher pathogenicity. For the same race of plant pathogens, individual pathogenic isolates possesses different abilities to infect just one or a few host species, and these different isolates are conventionally merged into infraspecific assemblages, known as formae speciales (ff. spp.). Different isolates of the same formae speciales could be further separated into different virulence groups. Genomic analysis revealed that the weakly virulent isolates often lack some virulence factors, including TFs, effectors, cell wall-degrading enzymes, and toxins

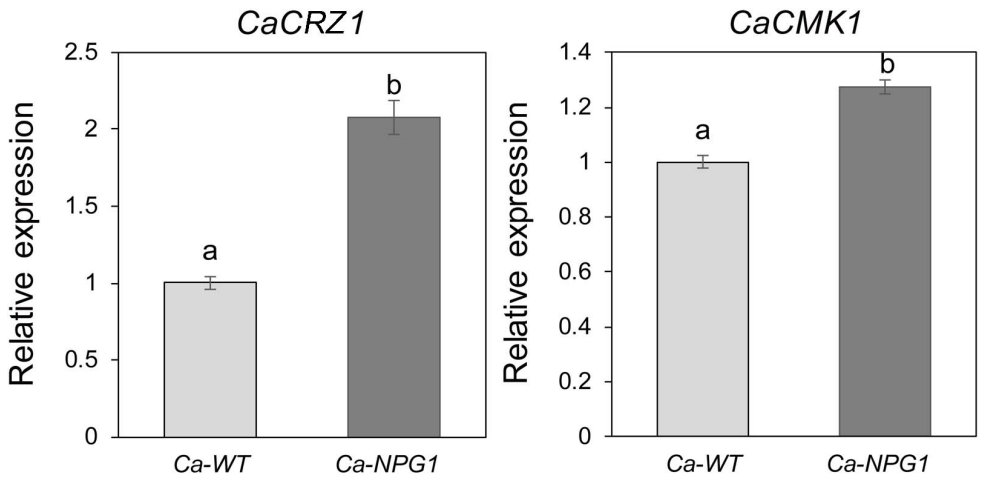

FIGURE 8 | Quantitative RT-PCR analysis. Relative expression levels of *CaCRZ1* and *CaCMK1* were estimated using the $2^{-\Delta\Delta Ct}$ method with *beta-tubulin* 1 as the reference gene. Error bars indicated standard deviation, and columns with different letters indicate significant difference ($P < 0.05$).

(Stukenbrock and McDonald, 2007; de Vega-Bartol et al., 2011; Brunner et al., 2013; Poppe et al., 2015; Buiate et al., 2017). Notably, the presence of particular small secreted proteins is associated with the determination of host range in some phytopathogenic fungi, including *Alternaria* spp., *Cochliobolus* spp., and *Fusarium* spp. (Ito et al., 2004; Houterman et al., 2008; Bhadauria et al., 2015). Therefore, the objective of this study was to investigate whether there are special virulence factors that contribute to the virulence difference between *C. gloeosporioides* Hb and *C. acutatum* Hb, especially *CgNPG1* as a potential specific pathogenic factor in *C. gloeosporioides* Hb. Although no conserved domains was identified in CgNPG1, phylogenetic tree analysis showed that the homologous proteins of CgNPG1 widely existed in plant pathogens, including the most common fungal pathogens and oomycetes (*Phytophthora infestans*), and human pathogens (*Aspergillus nidulans* and *Penicillium brasilianum*) (**Figure 2**). CgNPG1 contained 144 amino acids, of which 10 cysteines accounted for 6.9% and did not have any transmembrane domain except a signal peptide at the N-terminal of 1 to 16 amino acids (**Supplementary Figure 1**). Usually, the SSPs classified as effectors had the following characteristics: the sequence length of $\leq$300 amino acids and $\geq$4 cysteines, and function as key infection factors in suppressing host defense responses and modulating its physiology (Feldman et al., 2020). In our study, CgNPG1 matched the above sequence characteristics and effects in mycelial growth, conidiation, invasive structure development, and pathogenesis (**Figures 3–7**). Moreover, the prediction results by EeffectorP1.0 software showed that CgNPG1 was an effector. Based on the above data, CgNPG1 could be considered as an effector.

To investigate the function of *CgNPG1*, its nucleotide sequence was deleted from the genome of *C. gloeosporioides* Hb and heterogeneously expressed in *C. acutatum* Hb. *In vitro* test showed that mycelial growth of Cg-Δ*NPG1* mutant on PDA medium decreased slightly but was still comparable to that of the wild type, and growth rate recovered to the wild type level in the restored transformants (**Figure 3**). Heterogeneous expression of *CgNPG1* in *C. acutatum* Hb obviously increased the colony growth rate (**Figure 4**). Leaf inoculation tests showed that deletion of *CgNPG1* in *C. gloeosporioides* Hb resulted in significant decreased pathogenicity. Although Cg-Δ*NPG1* mutant could infect the leaves and develop necrotic lesions, but the lesion diameters decreased by about 50% compared to that of the WT and the restored transformants (**Figures 7A,B**). Heterogeneous expression of *CgNPG1* in *C. acutatum* Hb significantly increased the pathogenicity of *C. acutatum* Hb to the rubber tree (**Figures 7C,D**), with the disease severity of *Ca-NPG1* increased by about 60% compared with the Ca-WT strain. Interestingly, the deletion of *CgNPG1* in *C. gloeosporioides* Hb decreased the conidiation and changed the conidia morphology, and heterogeneous expression of *CgNPG1* in *C. acutatum* Hb increased the conidiation and also changed the morphology. In addition, we also found that the deletion of *CgNPG1* could affect conidia germination and appressorium formation (**Figure 6**). Since *CgNPG1* was required for the mycelial growth, conidiation, conidia morphology, and germination, and pathogenicity of *C. gloeosporioides* Hb and *C. acutatum* Hb, the deletion of *CgNPG1* in *C. acutatum* Hb might contribute to the poor pathogenicity to the rubber tree, at least partially.

Specialization to a new host is possible through advantageous mutations, vertical inheritance, and gene transfer events. Gene transfer (HGT and HCT) is associated with host specificity (Jaramillo et al., 2014). In *Fusarium oxysporum*, transfer of lineage-specific chromosomes between strains by HCT could even convert a non-pathogenic strain into a pathogen (Ma et al., 2010). For HGT, the candidate transferred genes are those constantly subject to gene duplication and gene loss. In *Pezizomycotina*, although no evidence of a burst of HGT events coinciding with major geological events was found, HGT appears to be occurring at a steady

rate during their evolution (Jaramillo et al., 2014). Between two vegetative incompatible biotypes of *C. gloeosporioides*, it has been proved that HCT can occur during co-cultivation under laboratory conditions and most likely in nature (Masel et al., 1996; He et al., 1998). Moreover, 11 HGT events from bacteria into *Colletotrichum* or their ancestors have been identified, and some of the genes play roles in virulence (Jaramillo et al., 2014). In our case, to explore the possibility of HGT event in *Colletotrichum*, we constructed the phylogenetic relationships among the fungi close to *C. gloeosporioides* based on their 28S ribosomal sequences (**Supplementary Figure 5**). Referring to the phylogenetic tree, none homolog of *NPG1* was further found in these close organisms other than *Colletotrichum.* However, the high similarity was found between *NPG1* genes in *Colletotrichum* and *Phytophthora* (**Supplementary Figure 6**). Collectively, the results indicated the occurrence of HGT events.

Perception of environmental signals initiates intracellular signal transduction pathways and promote infection-related morphogenesis in phytopathogens. Ca^{2+}-calmodulin signal transduction pathways controls a wide array of processes in cell growth and development (Berridge et al., 2003) through the mediation of transcription factors (Cyert, 2003). As a major component of Ca^{2+} signaling pathway, MoCRZ1 was involved in growth, conidiation, and pathogenicity (Choi et al., 2009). As CRZ1 homolog in *C. gloeosporioides* s.s. strain SMCG1#C, CgCrzA was also involved in vegetative growth, conidiation, appressorial formation rate, and lost pathogenicity to plant hosts (Wang et al., 2020). In addition, MAP kinase cascades are also an important regulatory system in cells (Dean, 1997). In *C. lagenarium*, CMK1 regulates the conidiation, appressoria formation, and pathogenic growth (Takano et al., 2000). Here, our results showed that the mutant heterogeneously expressing *CgNPG1* (Ca-*NPG1*) exhibited changed conidia morphology (**Figure 5A**), enhanced mycelia growth rate (**Figure 4**), conidiation (**Figure 5C**), conidia germination rate, appressorial formation rate (**Figures 6C,E**), and pathogenicity to rubber trees (**Figures 7C,D**). These results suggested that the function of CgNPG1 was similar to the function of CgCrzA and CMK1. Besides that, our results also showed that heterogeneous expression of *CgNPG1* significantly increased the expression level of *CaCRZ1* and induced the transcription of *CaCMK1* in *C. acutatum* Hb (**Figure 8**), suggesting that the regulation of *CgNPG1* on *C. acutatum* Hb might be related to *CaCRZ1* and *CaCMK1*.

Taken together, these data suggested that *C. gloeosporioides* Hb-specific *CgNPG1* played important roles in controlling mycelial growth, conidiation, and the development of invasive structures, such as conidia morphology and germination, appressorium formation, and pathogenicity.

DATA AVAILABILITY STATEMENT

The original contributions presented in the study are included in the article/**Supplementary Material**, further inquiries can be directed to the corresponding author.

AUTHOR CONTRIBUTIONS

CL carried out most of the experiments and analyzed the data. BZ carried out the complementation experiments and the data assay. YZ cloned the *CgNPG1* gene. HY completed the bioinformatics analysis of HGT. CL, BA, and HL wrote the manuscript. CH revised the manuscript. All authors read and approved the final manuscript.

FUNDING

This study was supported by grants from the National Natural Science Foundation of China (Grant Nos. 31860478 and 32060591).

SUPPLEMENTARY MATERIAL

The Supplementary Material for this article can be found online at: https://www.frontiersin.org/articles/10.3389/fmicb.2021.629387/full#supplementary-material

Supplementary Figure 1 | Nucleotide sequence and deduced amino acid sequence of *CgNPG1*. The predicted signal peptide is shaded by medium gray.

Supplementary Figure 2 | Generation and molecular confirmation of *CgNPG1* deletion mutant (Cg-Δ*NPG1*). **(A)** The gene deletion strategy. **(B)** Diagnostic PCR analysis for correct integration of recombinant fragment into the *CgNPG1* locus. **(C)** Southern blot analysis of wild type and Cg-Δ*NPG1* mutant.

Supplementary Figure 3 | Generation and molecular confirmation of *CgNPG1* complementation mutant (Cg-*Res*Δ*NPG1*). **(A)** The diagram of complementation vector. **(B)** Diagnostic PCR analysis for integration of *CgNPG1* into the genome of the *CgNPG1* deletion mutant. **(C)** Semi-quantitative RT-PCR analysis of *CgNPG1* expression level in Cg-ΔNPG1 and Cg-ResΔ*NPG1*.

Supplementary Figure 4 | Generation and molecular identification of mutant with heterogenous Expression of *CgNPG1* in *C. acutatum* Hb (Ca-*NPG1*). **(A)** Diagnostic PCR analysis for integration of *CgNPG1* open read frame into the genome of *C. acutatum* Hb. **(B)** Semi-quantitative RT-PCR analysis of *CgNPG1* expression level in Ca-*NPG1*strains.

Supplementary Figure 5 | Phylogenetic tree of top 600 fungi with close relationships to *C. gloeosporioides* Hb utilizing 28 s sequences (Ribosomal Database Project, Release 11, http://rdp.cme.msu.edu).

Supplementary Figure 6 | Phylogenetic tree of top 10 sequences with close relationships to *CgNPG1*.

REFERENCES

Baroncelli, R., Amby, D. B., Zapparata, A., Sarrocco, S., Vannacci, G., Floch, G. L., et al. (2016). Gene family expansions and contractions are associated with host range in plant pathogens of the genus *Colletotrichum*. *BMC Genomics* 17:555. doi: 10.1186/s12864-016-2917-6

Berridge, M. J., Bootman, M. D., and Roderick, H. L. (2003). Calcium signaling: dynamics, homeostasis and remodeling. *Nat. Rev. Mol. Cell Biol.* 4, 517–529. doi: 10.1038/nrm1155

Bhadauria, V., Maclachlan, R., Pozniak, C., and Banniza, S. (2015). Candidate effectors contribute to race differentiation and virulence of the lentil anthracnose pathogen *Colletotrichum* lentis. *BMC Genomics* 16:628. doi: 10.1186/s12864-015-1836-2

Brown, A., and Soepena, H. (1994). Pathogenicity of *Colletotrichum acutatum* and C. gloeosporioide on leaves of Hevea spp. *Mycol. Res.* 98, 264–266. doi: 10.1016/S0953-7562(09)80453-X

Brunner, P. C., Torriani, S. F. F., Croll, D., Stukenbrock, E. H., and McDonald, B. A. (2013). Coevolution and life cycle specialization of plant cell wall degrading enzymes in a hemibiotrophic pathogen. *Mol. Biol. Evol.* 30, 1337–1347. doi: 10.1093/molbev/mst041

Buiate, E. A. S., Xavier, K. V., Moore, N., Torres, M. F., Farman, M. L., Schardl, C. L., et al. (2017). A comparative genomic analysis of putative pathogenicity genes in the host-specific sibling species *Colletotrichum graminicola* and *Colletotrichum* sublineola. *BMC Genomics* 18:67. doi: 10.1186/s12864-016-3457-9

Cannon, P. F., Damm, U., Johnston, P. R., and Weir, B. S. (2012). *Colletotrichum*-current status and future directions. *Stud. Mycol.* 73, 181–213. doi: 10.3114/sim0014

Cao, X., Xu, X., Che, H., West, S. J., and Luo, D. (2017). Distribution and fungicide sensitivity of *Colletotrichum* species complexes from rubber tree in Hainan, China. *Plant Dis.* 101, 1774–1780. doi: 10.1094/PDIS-03-17-0352-RE

Choi, J., Kim, Y., Kim, S., Park, J., and Lee, Y. H. (2009). MoCRZ1, a gene encoding a calcineurin-responsive transcription factor, regulates fungal growth and pathogenicity of *Magnaporthe* oryzae. *Fungal Genet. Biol.* 46, 243–254. doi: 10.1016/j.fgb.2008.11.010

Crouch, J., O'Connell, R., Gan, P., Buiate, E., Torres, M. F., Beirn, L., et al. (2014). "The genomics of *Colletotrichum*," in *Genomics of Plant-Associated Fungi: Monocot Pathogens*, eds R. A. Dean, A. Lichens-Park, and C. Kole. Berlin: Springer, 69–102. doi: 10.1007/978-3-662-44053-7_3

Cyert, M. (2003). Calcineurin signaling in *Saccharomyces* cereviside: how yeast go crazy in response to stress. *Biochem. Biophys. Res. Commun.* 311, 1143–1150. doi: 10.1016/S0006-291X(03)01552-3

de Souza, A., Delphino Carboni, R. C., Wickert, E., De Macedo, L. E. G., and de Goes, A. (2013). Lack of host specificity of *Colletotrichum* spp. isolates associated with anthracnose symptoms on mango in Brazil. *Plant Pathol.* 62, 1038–1047. doi: 10.1111/ppa.12021

de Vega-Bartol, J. J., Martín-Dominguez, R., Ramos, B., García-Sánchez, M. A., and Díaz-Mínguez, J. M. (2011). New virulence groups in *Fusarium oxysporum* f. sp. phaseoli: the expression of the gene coding for the transcription factor FTF1 correlates with virulence. *Phytopathology* 101, 470–479. doi: 10.1094/PHYTO-09-10-0252

Dean, R., Kan, J. A. V., Pretorius, Z. A., Hammond-Kosack, K. E., Di Pietro, A., Spanu, P. D., et al. (2012). The top 10 fungal pathogens in molecular plant pathology. *Mol. Plant Pathol.* 13, 414–430. doi: 10.1111/j.1364-3703.2012.00822.x

Dean, R. A. (1997). Signal pathways and appressorium morphogenesis. *Annu. Rev. Phytopathol.* 35, 211–234. doi: 10.1146/annurev.phyto.35.1.211

Dickman, M. B., and Yarden, O. (1999). Serine/threonine protein kinases and phosphatases in filamentous fungi. *Fungal Genet. Biol.* 26, 99–117. doi: 10.1006/fgbi.1999.1118

Feldman, D., Yarden, O., and Hadar, Y. (2020). Seeking the roles for fungal small-secreted proteins in affecting saprophytic lifestyles. *Front. Microbiol.* 11:455. doi: 10.3389/fmicb.2020.00455

He, C., Rusu, A. G., Poplawski, A. M., Irwin, J. A. G., and Manners, J. M. (1998). Transfer of a supernumerary chromosome between vegetatively incompatible biotypes of the fungus *Colletotrichum gloeosporioides*. *Genetics* 150, 1459–1466. doi: 10.1017/S0016672398003528

Houterman, P. M., Cornelissen, B. J. C., and Rep, M. (2008). Suppression of plant resistance gene-based immunity by a fungal effector. *PLoS Pathog.* 4:e1000061. doi: 10.1371/journal.ppat.1000061

Ito, K., Tanaka, T., Hatta, R., Yamamoto, M., and Tsuge, T. (2004). Dissection of the host range of the fungal plant pathogen *Alternaria alternata* by modification of secondary metabolism. *Mol. Microbiol.* 52, 399–411. doi: 10.1111/j.1365-2958.2004.04004.x

Jaramillo, V. D. A., Sukno, S. A., and Thon, M. R. (2014). Identification of horizontally transferred genes in the genus *Colletotrichum* reveals a steady tempo of bacterial to fungal gene transfer. *BMC Genomics* 16:2. doi: 10.1186/1471-2164-16-2

Lardner, R., Johnston, P. R., Plummer, K. M., and Pearson, M. N. (1999). Morphological and molecular analysis of *Colletotrichum* acutatum sensu lato. *Mycol. Res.* 103, 275–285. doi: 10.1017/S0953756298007023

Li, J. F., Liu, X. B., Cai, J. M., Lin, C. H., and Huang, G. X. (2010). Identification and the internal transcribed spacer regions analysis of pathogen causing rubber anthracnose. *Chin. Agricul. Sci. Bull.* 26, 221–226.

Ma, L. J., van der Does, H. C., Borkovich, K. A., Coleman, J. J., Daboussi, M., Di Pietro, A., et al. (2010). Comparative genomics reveals mobile pathogenicity chromosomes in *Fusarium*. *Nature* 464, 367–373. doi: 10.1038/nature08850

Masel, A. M., He, C. Z., Poplawski, A. M., Irwin, J. A. G., and Manners, J. M. (1996). Molecular evidence for chromosome transfer between biotypes of *Colletotrichum gloeosporioides*. *Mol. Plant Microbe* Interact. 9, 339–348. doi: 10.1094/MPMI-9-0339

Mehrabi, R., Bahkali, A. H., Abd-Elsalam, K. A., Moslem, M., M'Barek, S. B., Gohari, A. M., et al. (2011). Horizontal gene and chromosome transfer in plant pathogenic fungi affecting host range. *FEMS Microbiol. Rev.* 35, 542–554. doi: 10.1111/j.1574-6976.2010.00263.x

Mey, G., Held, K., Scheffe, R. J., Tenberge, K. B., and Tudzynski, P. (2002). CPMK2, an SLT2-homologous mitogen-activated protein (MAP) kinase, is essential for pathogenesis of Claviceps purpurea on rye: evidence for a second conserved pathogenesis-related MAP kinase cascade in phytopathogenic fungi. *Mol. Microbiol.* 46, 305–318. doi: 10.1046/j.1365-2958.2002.03133.x

Münch, S., Lingner, U., Floss, D. S., Ludwing, N., Sauer, N., and Desing, H. B. (2008). The hemibiotrophic lifestyle of *Colletotrichum* species. *Plant Physiol.* 165, 41–51. doi: 10.1016/j.jplph.2007.06.008

Peres, N. A., Adaskaveg, J. E., and Correll, J. C. (2005). Life styles of *Colletotrichum* acutatum. *Plant Dis.* 89, 784–796. doi: 10.1094/PD-89-0784

Poppe, S., Dorsheimer, L., Happel, P., and Stukenbrock, E. H. (2015). Rapidly evolving genes are key players in host specialization and virulence of the fungal wheat pathogen *Zymoseptoria tritici* (*Mycosphaerella graminicola*). *PLoS Pathog.* 11:e1005055. doi: 10.1371/journal.ppat.1005055

Pu, J. J., Zhang, X., Qi, Y. X., Xie, Y. X., Zhang, H. Q., and Zhang, H. (2007). First record of Corynespora leaf fall disease of Hevea rubber tree in China. *Australas. Plant Dis. Notes* 2, 35–36. doi: 10.1071/DN07017

Saha, T., Kumar, A., Ravindran, M., Jacob, C. K., Roy, B., and Nazeer, M. A. (2002). Identification of *Colletotrichum* acutatum from rubber using random amplified polymorphic DNAs and ribosomal DNA polymorphisms. *Mycol. Res.* 106, 215–221. doi: 10.1017/S0953756201005342

Son, H., Seo, Y. S., Min, K., Park, A. R., Lee, J., Jin, J. M., et al. (2011). A phenome-based functional analysis of transcription factors in the cereal head blight fungus, *Fusarium graminearum*. *PLoS Pathog.* 7:e1002310. doi: 10.1371/journal.ppat.1002310

Stukenbrock, E. H., and McDonald, B. A. (2007). Geographical variation and positive diversifying selection in the host-specific toxin SnToxA. *Mol. Plant Pathol.* 8, 321–332. doi: 10.1111/j.1364-3703.2007.00396.x

Takano, Y., Kikuchi, T., Kubo, Y., John, E. H., Mise, K., and Furusawa, I. (2000). The *Colletotrichum* lagenarium MAP kinase gene CMK1 regulates diverse aspects of fungal pathogenesis. *Mol. Plant Microbe Interact.* 13, 374–383. doi: 10.1094/MPMI.2000.13.4.374

Wang, P., Li, B., Pan, Y., Zhang, Y., Li, D., and Huang, L. (2020). Calcineurin-responsive transcription factor CgCrzA is required for cell wall integrity and infection-related morphogenesis in *Colletotrichum gloeosporioides*. *Plant Pathol. J.* 36, 385–397. doi: 10.5423/PPJ.OA.04.2020.0071

Wang, Q., An, B., Hou, X., Guo, Y., Luo, H., and He, C. (2018). Dicer-like proteins regulate the growth, conidiation, and pathogenicity of *Colletotrichum gloeosporioides* from Hevea brasiliensis. *Front. Microbiol.* 8:2621. doi: 10.3389/fmicb.2017.02621

Xu, J. R., Staiger, C. J., and Hamer, J. E. (1998). Inactivation of the mitogen-activated protein kinase Mps1 from the rice blast fungus prevents

penetration of host cells but allows activation of plant defense responses. *Proc. Natl. Acad. Sci. U. S. A.* 95, 12713–12718. doi: 10.1073/pnas.95.21.12713

Yang, J., Wang, Q., Luo, H., He, C., and An, B. (2020). HbWRKY40 plays an important role in the regulation of pathogen resistance in Hevea brasiliensis. *Plant Cell Rep.* 39:1095-1107. doi: 10.1007/s00299-020-02551-x

Zhang, C. X., He, M. X., Li, J. Z., Cai, Z. Y., and Wang, J. Q. (2008). Identification of the pathogen causing *Colletotrichum* leaf disease on rubber in Xishuangbanna Yunnan. *Plant Prot.* 34, 103–106.

Conflict of Interest: The authors declare that the research was conducted in the absence of any commercial or financial relationships that could be construed as a potential conflict of interest.

frontiers in Microbiology

ORIGINAL RESEARCH
published: 22 March 2021
doi: 10.3389/fmicb.2021.623799

Comparative Metagenomics Reveals Microbial Signatures of Sugarcane Phyllosphere in Organic Management

Ahmad Nuruddin Khoiri[1], Supapon Cheevadhanarak[1,2], Jiraporn Jirakkakul[2], Sudarat Dulsawat[2], Peerada Prommeenate[3], Anuwat Tachaleat[2], Kanthida Kusonmano[1,4], Songsak Wattanachaisaereekul[2,5] and Sawannee Sutheeworapong[2]**

[1] School of Bioresources and Technology, King Mongkut's University of Technology Thonburi, Bangkok, Thailand, [2] Pilot Plant Development and Training Institute, King Mongkut's University of Technology Thonburi, Bangkok, Thailand, [3] Biochemical Engineering and Systems Biology Research Group, National Center for Genetic Engineering and Biotechnology, National Science and Technology Development Agency at King Mongkut's University of Technology Thonburi, Bangkok, Thailand, [4] Bioinformatics and Systems Biology Program, School of Bioresources and Technology, King Mongkut's University of Technology Thonburi, Bangkok, Thailand, [5] Faculty of Food Industry, King Mongkut's Institute of Technology Ladkrabang, Bangkok, Thailand

OPEN ACCESS

Edited by:
Amin Uddin Mridha, University of Chittagong, Bangladesh

Reviewed by:
Elle M. Barnes, Fordham University, United States
Yong Wang, Guizhou University, China

***Correspondence:**
Sawannee Sutheeworapong
sawannee.sut@mail.kmutt.ac.th
Songsak Wattanachaisaereekul
songsak.wa@kmitl.ac.th

Specialty section:
This article was submitted to Microbe and Virus Interactions with Plants, a section of the journal Frontiers in Microbiology

Received: *30 October 2020*
Accepted: *01 February 2021*
Published: *22 March 2021*

Citation:
Khoiri AN, Cheevadhanarak S, Jirakkakul J, Dulsawat S, Prommeenate P, Tachaleat A, Kusonmano K, Wattanachaisaereekul S and Sutheeworapong S (2021) Comparative Metagenomics Reveals Microbial Signatures of Sugarcane Phyllosphere in Organic Management. Front. Microbiol. 12:623799. doi: 10.3389/fmicb.2021.623799

Converting conventional farms to organic systems to improve ecosystem health is an emerging trend in recent decades, yet little is explored to what extent and how this process drives the taxonomic diversity and functional capacity of above-ground microbes. This study was, therefore, conducted to investigate the effects of agricultural management, i.e., organic, transition, and conventional, on the structure and function of sugarcane phyllosphere microbial community using the shotgun metagenomics approach. Comparative metagenome analysis exhibited that farming practices strongly influenced taxonomic and functional diversities, as well as co-occurrence interactions of phyllosphere microbes. A complex microbial network with the highest connectivity was observed in organic farming, indicating strong resilient capabilities of its microbial community to cope with the dynamic environmental stressors. Organic farming also harbored genus *Streptomyces* as the potential keystone species and plant growth-promoting bacteria as microbial signatures, including *Mesorhizobium loti*, *Bradyrhizobium* sp. SG09, *Lactobacillus plantarum*, and *Bacillus cellulosilyticus*. Interestingly, numerous toxic compound-degrading species were specifically enriched in transition farming, which might suggest their essential roles in the transformation of conventional to organic farming. Moreover, conventional practice diminished the abundance of genes related to cell motility and energy metabolism of phyllosphere microbes, which could negatively contribute to lower microbial diversity in this habitat. Altogether, our results demonstrated the response of sugarcane-associated phyllosphere microbiota to specific agricultural managements that played vital roles in sustainable sugarcane production.

Keywords: agricultural shift, microbial signatures, phyllosphere, sugarcane, farming practices

INTRODUCTION

Over the past decades, conventional farming practice that mainly relies on agrochemical inputs has significantly increased the global *per capita* agricultural production (Pretty, 2008). However, this effort not only raises production costs but also causes serious problems to the environment including soil contamination and degradation, emission of fertilizers and pesticides, loss of biodiversity, and several negative impacts on human health (Rivera et al., 2017). Therefore, alternative methods are needed for improving agricultural outputs or reducing dependency on agrochemicals and equilibrating productivity with sustainability.

Converting conventional farms to organic management systems, known as transition farming, could potentially be a solution to improve biodiversity and sustainably increase food production (Gonthier et al., 2014). However, how long it takes to recover the loss of biodiversity and functionality caused by unsustainable farming practices remains questionable. Organic farming is one kind of farming practice intended to reduce the need for chemical inputs to improve overall ecosystem health. It relies on animal waste, green manure, biological pest control, and some techniques including crop rotation and multiple cropping to enhance soil nutrients and crop fertility (Pimentel et al., 2005). Compared to conventional farming, organic farming is much closer to natural ecosystems because it depends less on agrochemicals and increases more on nutrient recycling systems. Hence, this farming has been shown to be more effective in reducing the negative impacts of agricultural practices on the environment and promoting biodiversity (Bengtsson et al., 2005). Previous studies have demonstrated that organic farming could promote more diverse below-ground microbial communities (i.e., soil and root niches) compared with conventional farming (Lupatini et al., 2017; Hartman et al., 2018). Another research also showed that organic fertilization improved the abundance of microbial nitrogen (N)-cycle genes, which were associated with N availability in the soil (Morugán-Coronado et al., 2019).

Phyllosphere, the above parts of plant compartments dominated by leaves, is densely colonized by numerous microbial taxa such as bacteria, fungi, and yeasts (Müller and Ruppel, 2014). Phyllosphere microbial community has been known to participate in nutrient cycles, e.g., carbon (Knief et al., 2012) and nitrogen (Fürnkranz et al., 2008), and degradation of air pollutants (Ali et al., 2012). Microbes residing in this environment have also been thought to play important roles in plant health and ecosystem productivity (Laforest-Lapointe et al., 2017). For instance, microbial colonizers can promote the growth of their host through phytohormone production (Taghavi et al., 2009), foliar pathogen protection (Ritpitakphong et al., 2016), and stress tolerance enhancement (Redman et al., 2002). Besides, as an open system, the phyllosphere habitat can be easily invaded by exogenous microbes through transmission from the atmosphere, soil, and insects (Vorholt, 2012; Maignien et al., 2014), including phytopathogens. Thus, maintaining homeostasis of phyllosphere microbiota will be critical for the survival of the host plant (Chen et al., 2020). With all these traits, harnessing beneficial phyllosphere microbiota as new alternatives of biofertilizers, biopesticides, or biostimulants seems to be a promising target for improving plant and environmental fitness, which leads to sustainable agriculture to feed the continuously growing global population. However, a comprehensive understanding of phyllosphere microbial diversity and functionality in response to agricultural shift remains to be elucidated and will be an important step to achieve these goals.

Sugarcane (*Saccharum officinarum* L.) is a C4 grass plant that has approximately 50% higher photosynthesis efficiency than C3 plants (Kajala et al., 2011). It is also one of the most economically important crops used as a major source for sugar and bioethanol production (Waclawovsky et al., 2010). This plant is grown in tropical and subtropical countries in which Brazil is the world's largest producer, followed by India, China, and Thailand (FAO, 2018). However, to increase sugarcane yield, a high rate of synthetic N fertilizers is commonly applied as well as pesticides for plant protection against phytopathogen infections (Robinson et al., 2011), resulting in ecological damages. Besides, previous sugarcane microbiome studies have mainly focused on the below-ground compartments (i.e., soil, rhizosphere, and root) using amplicon sequencing such as 16S rRNA and ITS barcoding regions (Paungfoo-Lonhienne et al., 2014, 2015; Dong et al., 2018), which are limited to the taxonomic classification at the genus level and are biased by the PCR amplification process. Moreover, the important roles of phyllosphere microbial community have been less explored than those of other niches, especially in correlation with farming management practices, despite their potential benefits on agricultural productivity.

Previous studies have demonstrated that organic farming promoted higher species richness of wheat phyllosphere fungal microbiome than conventional farming (Karlsson et al., 2017). Moreover, different agricultural inputs in organic and conventional farms would directly and/or indirectly influence the phyllosphere microbial community. Karlsson et al. (2014) showed that fungicides negatively affected fungal community composition on wheat leaves. Perazzolli et al. (2014) reported that the richness and diversity of bacterial and fungal communities of graphene leaves were altered by penconazole fungicide and biological control agent (*Lysobacter capsici* AZ78) treatments. Similarly, Cernava et al. (2019) exhibited that pest and pathogen management practices, i.e., pesticides and biological treatments, shaped the microbial population of tea leaves. In addition, Xiang et al. (2020) suggested that functional traits of phyllosphere microorganisms were more sensitive to land use and anthropogenic disturbance compared with soil microbiota. Thus, we hypothesized that different farming practices would have impacts on the taxonomic diversity and functional capacity of the above-ground microbial community and promote distinct microbial profiles with unique signatures.

To gain deeper insights into how taxonomic diversity and functional capacity of phyllosphere microbial community are shaped by farming practices, we performed shotgun metagenome sequencing on sugarcane leaves collected from organic farming where a bio-compost and swine manure were applied as input and conventional farming that has long been treated with agrochemicals. We also included transition farming that had been switched to the organic system 2 years before

our sample collection to observe how phyllosphere microbes are involved in this transformation process. We aimed to observe structural changes of phyllosphere microbiota regarding agricultural management types and identify beneficial microbes that could be potentially used as biostimulants to replace agrochemicals to transform the conventional practices toward organic systems for more sustainable farming.

MATERIALS AND METHODS

Study Area, Sample Collection, and Storage

In this study, sugarcane leaves (plant age: 10 months old; maturing; and ripening stage) were sampled in April 2019 from three different farming practices in Thailand. These sampling sites included organic farming (OP) at Rai Sukphoang, Chom Bueng District, Ratchaburi (13°35′42.5″N 99°34′58.0″E); transition farming (TP) at Rai Sarot, Rang Bua, Chom Bueng District, Ratchaburi (13°37′52.8″N 99°33′10.7″E); and conventional farming (CP) at Rai Pramote, Photharam District, Ratchaburi (13°44′34.2″N 99°54′16.6′E) (**Supplementary Table 1** and **Supplementary Figure 1**). In total, nine samples of sugarcane Khon Kaen 3 (KK3) cultivar were collected for three replicates (i.e., three different sugarcane tillers from the same field) per farm. Based on Kuijper's leaf numbering system (Kuijper, 1915), leaves number +1 to +4 were chosen, and the leaf sheath and the leaf tip were removed using a surface-sterilized scissor. All samples were then stored in a sterile zipper locking plastic bag and kept cool during field collection and transported at 4°C, then frozen at −80°C until used for downstream processes.

DNA Extraction

Sugarcane leaf samples were ground using mortars and pestles under liquid nitrogen to accelerate the grinding process. Phyllosphere microbial DNA from 0.2 *g* of leaf powder was extracted using the innuPREP Plant DNA Kit (AnalytikJena AG, Berlin, Germany) according to the manufacturer's instructions. The DNA was eluted in a Tris-EDTA (TE) buffer, then stored at −80°C for subsequent steps. Total genomic DNA samples were qualitatively and quantitatively measured by using gel electrophoresis and a NanoDrop spectrophotometer (Thermo Scientific, Wilmington, DE, United States), respectively. The obtained phyllosphere microbial DNA samples comprise both epiphytic and endophytic microbial DNA.

Library Preparation and Sequencing

Phyllosphere microbial DNA samples were sent for sequencing to ZymoBIOMICS® Shotgun Metagenomic Sequencing Service (Zymo Research Corp., Irvine, CA, United States) assisted by S.M.Chemical Supplies Co., Ltd., Thailand. Briefly, a metagenome sequencing library was prepared from up to 100 ng of genomic DNA using Nextera® DNA Flex Library Prep Kit (Illumina, San Diego, CA, United States) according to the manufacturer's instructions. The library was tagged with internal dual-index 8-bases barcodes and Nextera® adapters (Illumina, San Diego, CA, United States), then quantified using TapeStation® (Agilent Technologies, Santa Clara, CA, United States) and equally pooled. The resulting DNA pool was measured using quantitative PCR (qPCR). In addition, a negative control (i.e., blank library preparation control) was used during the metagenome library preparation process. Finally, 11 metagenome libraries including a mock sample (ZymoBIOMICS™ Microbial Community DNA Standard II, Catalog No. D6311) were sequenced on Illumina HiSeq 1500 platform paired-end sequencing (2 × 100 bp).

Metagenomic Analysis

Quality Control and Host DNA Removal

In order to maximize the quality of the datasets, the following steps were performed. First, sequence reads were subjected to quality checking using FastQC version 0.11.9 (Andrews, 2010) and MultiQC version 1.8 (Ewels et al., 2016). Furthermore, the remaining adapters and the low quality of reads with Phred score less than 15 were trimmed, and the short reads less than 50 bp were discarded using Trimmomatic version 0.39 (Bolger et al., 2014) with the parameters as follows: NexteraPE-PE.fa:2:30:10:2:keepBothReads, SLIDINGWINDOW 4:15, and MINLEN: 50. High-quality reads were subsequently aligned with the publicly available sugarcane genome (*Saccharum spontaneum* cultivar AP85-441: GenBank accession number: GCA_003544965.1, downloaded as of March 24, 2020) using Bowtie2 version 2.3.5.1 (Langmead and Salzberg, 2012) to identify and filter out host contaminant sequences.

Taxonomic Profiling and Diversity Analysis

Non-host sequences were taxonomically assigned using Kraken2 version 2.0.8-beta (Wood et al., 2019) against a custom Kraken2 database consisting of archaeal, bacterial, fungal, plasmid, and viral sequences (downloaded from NCBI RefSeq as of August 15, 2020). Bracken version 2.5.0 (Lu et al., 2017) was further used to re-estimate the microbial abundance at the species level. The microbial abundance table generated from metagenome taxonomic profiling with Kraken2 + Bracken was used as an input for diversity analyses. These were performed on R program version 3.6.2 (R Core Team, 2019) with *vegan* version 2.5-6 (Oksanen et al., 2019), *ggplot2* version 3.3.0 (Wickham, 2016), and *phyloseq* version 1.28.0 (McMurdie and Holmes, 2013) packages. Briefly, a one-way ANOVA test was computed based on a Shannon estimator to determine the species diversity and the Pielou index for quantifying species evenness in each sample (α-diversity). Furthermore, the differences of overall microbial profiles among farming practices (β-diversity) were estimated by performing unconstrained principal coordinate analysis (PCoA) using the Bray–Curtis distance. The statistical significance of β-diversity was then determined by PERMANOVA test with 999 permutations, followed by a multivariate homogeneity of group dispersions (variances) test (BETADISPER) to check whether the investigated groups are homogeneously dispersed in relation to their microbial taxa. Geographical location (district) was also included in these statistical assessments of β-diversity as a potential confounding effect. In addition, the adequacy of

sampling was quantified by calculating Good's coverage index and by plotting an α-rarefaction curve.

Metagenome Functional Annotation

Functional analysis of metagenome was performed with sequence similarity searches using SqueezeMeta version 1.2.0 with function "sqm_reads.pl" (Tamames and Puente-Sánchez, 2019). In brief, sequence reads were functionally assigned against the Kyoto Encyclopedia of Genes and Genomes (KEGG) Orthology (KO) database, downloaded as of August 18, 2020 (Kanehisa and Goto, 2000; Kanehisa et al., 2016) using the DIAMOND (blastx) algorithm (Buchfink et al., 2015) with default options (maximum *E*-value = 1e-03 and minimum percent identity = 50). Finally, the function of fun3 in the SqueezeMeta program was employed for functional assignments. In addition, only sequences that were previously assigned as archaea, bacteria, fungi, and viruses were kept for functional analyses. Thus, the other sequences that could not be assigned for both taxonomy and function were discarded.

The generated KO abundance table was subsequently preprocessed following the workflow of the previous study (Yurgel et al., 2019). First, the count matrix was normalized to the Reads Per Kilobase per Genome equivalent (RPKG) method using MicrobeCensus version 1.1.0 (Nayfach and Pollard, 2015). MinPath (Ye and Doak, 2009) and the function "pathway_pipeline.py" in PICRUSt2 version 2.3.0-b (Douglas et al., 2020) were then employed to map a normalized KO table to KEGG pathways with the "–no_regroup" setting. The predicted pathways were further manually grouped into the levels of KEGG BRITE hierarchy termed as the KEGG category and the KEGG pathway. Furthermore, gene diversity at the KO level was estimated using the Shannon index. Functional β-diversity was calculated by projecting the data onto the unconstrained PCoA plot using Bray–Curtis dissimilarity, followed by PERMANOVA with 999 permutations and BETADISPER tests, in which farming practices and districts were the main and confounding effects, respectively. In addition, one-way ANOVA was used to statistically test whether metabolic processes at the level of the KEGG category and the KEGG pathway were affected by farming practices.

Core Feature Identification and Differential Abundance Analysis

Core taxonomic and functional metagenomes were quantified using the "core_members" function in R package *microbiome* version 1.6.0 (Lahti and Shetty, 2019) with the following criteria: detection = 0.001 and prevalence = 95%. Furthermore, the differential abundance of taxonomic and functional metagenomes among farming practices was statistically examined using the linear discriminant analysis (LDA) effect size (LEfSe) method as implemented in the LEfSe version 1.0.8 (Segata et al., 2011). LEfSe employs a non-parametric Kruskal–Wallis sum-rank test to detect any differentially abundant feature between groups. Biological consistency is then examined with a set of pairwise tests using an unpaired Wilcoxon rank-sum test. Finally, the effect size of significantly abundant features is estimated using the LDA test. In this study, LEfSe parameters such as the LDA score and the Wilcoxon *p*-value were set to 2.0 and 0.05, respectively. The results were then visualized in bar graphs using R package *ggplot2* version 3.3.0 (Wickham, 2016).

Microbial Co-occurrence Network Construction

A microbial co-occurrence network was constructed based on the Sparse Correlations for Compositional data (SparCC) algorithm (Friedman and Alm, 2012) using FastSpar version 0.0.10 (Watts et al., 2018). The microbial abundance matrix, in which rows and columns represent taxa and samples, respectively, was used as an input and was preprocessed as follows. First, the data were divided into three subsets based on their origin (Organic, Transition, and Conventional). Microbial species (features) present in less than 2 out of 3 samples and the abundances lower than 11 were removed out from the count table. To avoid comparison biases caused by unequal numbers of features after the filtering step, only 500 features of each filtered dataset were randomly selected for network analysis. Empirical SparCC correlation coefficients (*p*-value) were calculated by a bootstrapping method with 1,000 iterations, and three farming-specific co-occurrence networks were then constructed. Cytoscape version 3.8.0 (Shannon et al., 2003) was employed to visualize the networks with the following criteria: strong correlation ($|r| > 0.6$) and p-value < 0.05. In addition, the Girvan–Newman algorithm was executed to find network modules using the Cytoscape app *clusterMaker2* version 1.3.1 (Morris et al., 2011), while other network topological features were examined using available functions in R package *igraph* version 1.2.4.2 (Csardi and Nepusz, 2006). Microbial taxa (nodes) with degree > 10 and betweenness centrality < 0.1 were considered as the hub species as explained in the previous research (Berry and Widder, 2014). Node attributes of each network were quantified by a bootstrapping method with 10,000 iterations and were subsequently compared with the two-sample Kolmogorov–Smirnov test using the "ks.test" function in the *stats* R package.

RESULTS

General Information of Metagenome Dataset

A total of 118,535,073 raw sequence reads from 9 shotgun metagenome libraries were generated by the Illumina platform, ranging from 9,892,628 to 29,216,274 reads per sample. The mean sequence length of paired-end reads was 100 bp with an average Phred score above 30. After quality-filtering, i.e., host decontamination and base quality trimming, approximately 93% of reads were discarded, remaining 8,176,818 high-quality sequences for subsequent analyses (**Supplementary Table 2**). In addition, around 250,000 reads could be taxonomically assigned belonging to archaeal, bacterial, fungal, and viral species.

Taxonomic Composition of Sugarcane Phyllosphere Microbiota

Read-based metagenome taxonomic profiling on Kraken2 followed by microbial abundance re-estimation with Bracken yielded 6,572 overall microbial taxa across all samples.

Particularly, 5,488 bacterial species (OP: 5,255; TP: 4,968; and CP: 4,945), 331 fungal species (OP: 330; TP: 330; and CP: 331), 287 archaeal species (OP: 272; TP: 252; and CP: 251), and 466 viral species (OP: 319; TP: 218; and CP: 189) were observed. At the domain level, bacteria (70.6%) were the most abundant microbial colonizers inhabiting sugarcane phyllosphere habitat, followed by eukaryotic, i.e., fungal (27%), archaeal (1.8%), and viral (0.6%) communities (**Figure 1A**). On the level of phylum, Proteobacteria, Ascomycota, Actinobacteria, Firmicutes, Bacteroidetes, Basidiomycota, Cyanobacteria, Mucoromycota, Euryarchaeota, and Tenericutes were the top 10 predominant microbial phyla (**Figure 1B**).

Functional Potentials of Sugarcane Phyllosphere Microbiota

In total, 3,797 KEGG orthologs (KOs) consisting of 185 KEGG pathways and 36 KEGG categories were observed across all samples. Gene functions related to metabolism were the most abundant, accounting for 69.4% of overall annotated sequences (**Supplementary Figure 2**). Specifically, amino acid metabolism (12.1%), energy metabolism (11%), carbohydrate metabolism (9.4%), glycan biosynthesis and metabolism (8.1%), biosynthesis of other secondary metabolites (7.3%), metabolism of terpenoids and polyketides (5.3%), lipid metabolism (4.8%), and metabolism of cofactors and vitamins (4.8%) were among the top KEGG functional categories (**Supplementary Figure 3**). At the level of the KEGG pathway, other glycan degradation (ko00511) was the predominant pathway, followed by photosynthesis (ko00195), valine, leucine, and isoleucine biosynthesis (ko00290), phenylpropanoid biosynthesis (ko00940), aminoacyl-tRNA biosynthesis (ko00970), oxidative phosphorylation (ko00190), and biosynthesis of ansamycins (ko01051), complementing the dominant pathways with abundances higher than 2% (**Supplementary Figure 4**).

Farming Practices Significantly Induced Distinct Taxonomic and Functional β-Diversities

Prior to taxonomic diversity analyses, the number of reads was rarefied to 19,000 for each sample to avoid comparison biases caused by an unequal library size (**Supplementary Figure 5**). After this process, an average Good's coverage was reported as 95% (**Supplementary Table 3**), indicating that the sample size was still enough for downstream analyses. Species diversity was the highest in organic farming and gradually decreased in transition and conventional farms, respectively (**Figure 2A**), while the evenness index showed the opposite trend with organic farming being the lowest (**Figure 2B**). Similarly, functional diversity on the gene level using the Shannon index also revealed that organic farming had the greatest microbial functions than the other two farming practices (**Figure 2C**). However, no statistical significance was observed for α-diversity estimation.

β-Diversity was estimated by plotting unconstrained PCoA and executing PERMANOVA test based on Bray–Curtis dissimilarity on the level of species and KO for taxonomy and functional potential, respectively. The PCoA plots showed that microbial communities and their gene functions were clearly separated along the first principle coordinate according to types of farming practices (**Figure 3**). PERMANOVA results further confirmed the observed differences among the three microbial habitats ($R^2 = 0.27, p < 0.01$ and $R^2 = 0.28, p < 0.05$ for taxonomic and functional diversity, respectively) (**Supplementary Table 4**). However, the significant output of the BETADISPER test in taxonomic profile ($p < 0.01$), but not in functional potential ($p > 0.05$), suggested that differences of taxonomic β-diversity might be also slightly influenced by within-group dispersion (**Supplementary Table 4**). The PERMANOVA analysis also provided the top 50 most influential taxa, which potentially contribute to the differentiation of taxonomic profile regarding farming practices (**Supplementary Figure 6**). In addition, we also

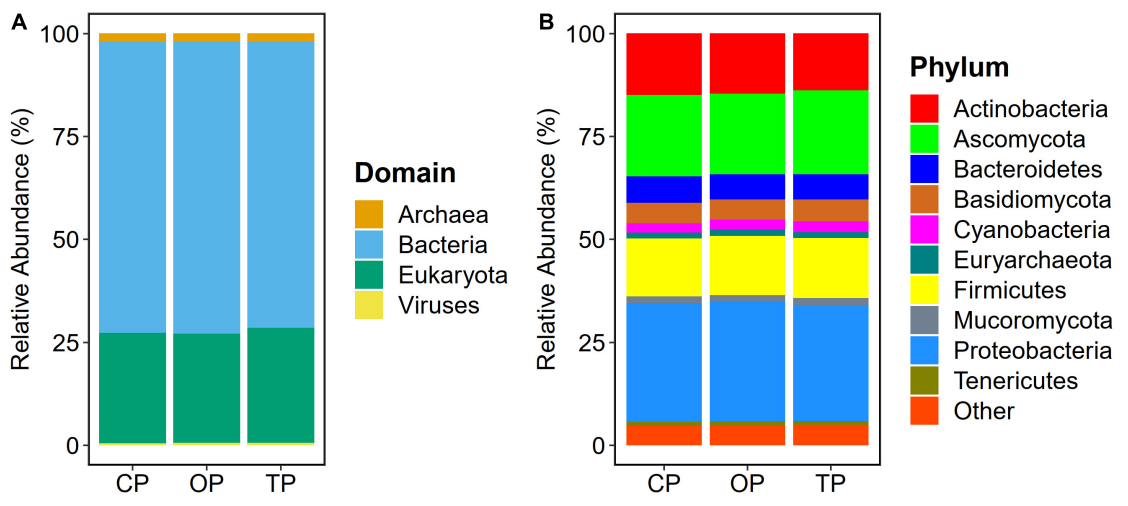

FIGURE 1 | Microbial taxonomic composition of sugarcane phyllosphere. Relative abundance at **(A)** domain and **(B)** phylum levels in conventional (CP), organic (OP), and transition (TP) farming practices.

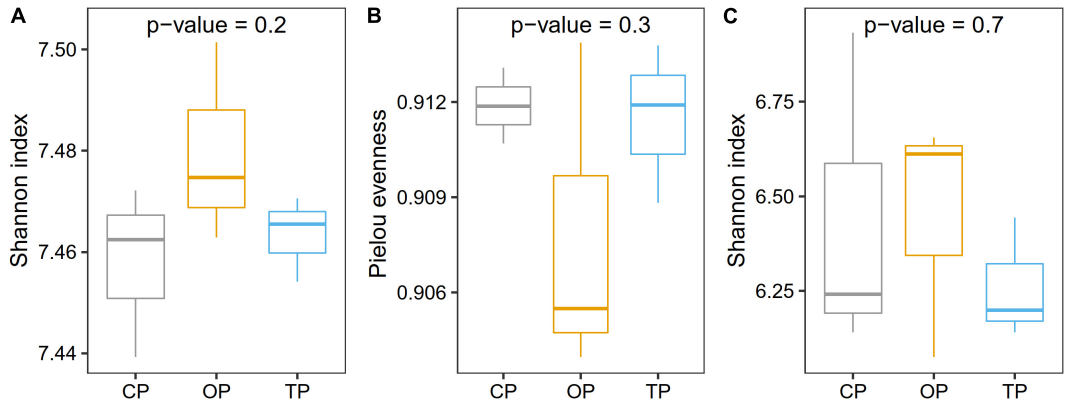

FIGURE 2 | Effect of farming practices on taxonomic α-diversity determined using **(A)** the Shannon index and **(B)** Pielou evenness, and **(C)** microbial gene diversity estimated with the Shannon index. Statistical analysis was performed on one-way ANOVA.

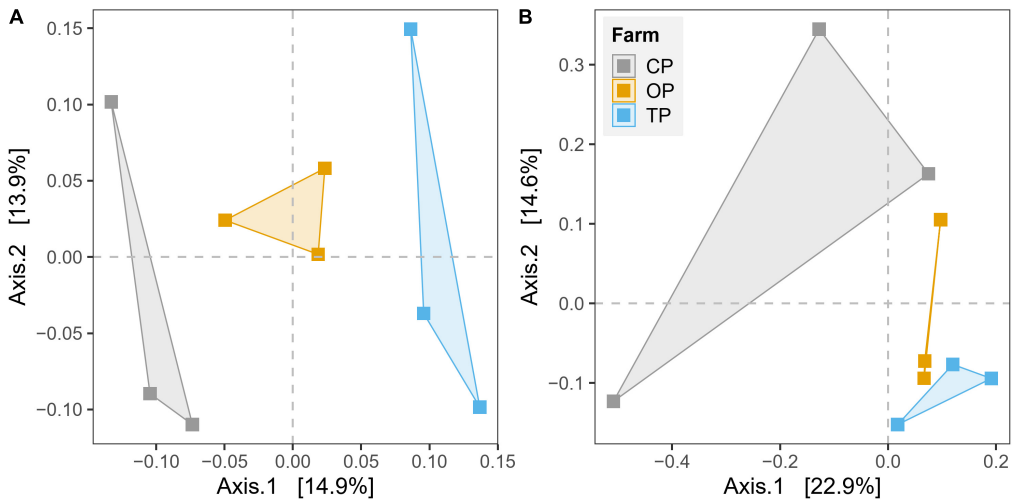

FIGURE 3 | Unconstrained principal coordinate analysis (PCoA) based on Bray–Curtis distance for the effect of agricultural practices on **(A)** taxonomic diversity and **(B)** gene function.

found a significant effect of the district (geographical location) from the PERMANOVA test of both taxonomic β-diversity (R^2 = 0.14, $p < 0.05$) and functional β-diversity (R^2 = 0.17, $p < 0.05$) (**Supplementary Table 4**).

Cell Motility and Energy Metabolism Significantly Depleted Under Conventional Farming

Functional metagenome analysis at the level of the KEGG category and the KEGG pathway showed that microbial gene abundances related to cell motility and energy metabolism were significantly affected by farming practices. Particularly, the abundance of cell motility was the highest in organic farming (ANOVA, $p < 0.05$). In terms of energy metabolism, transition farming was prominent (ANOVA, $p < 0.05$), specifically the photosynthesis pathway (ko00195) (ANOVA, $p < 0.05$). For amino acid metabolism, both transition and organic farms were slightly higher than conventional farming (ANOVA, $p > 0.1$). Specifically, the valine, leucine, and isoleucine biosynthetic pathway (ko00290) was significantly predominant in organic farming and was the lowest in the conventional one (ANOVA, $p < 0.05$). Further, conventional farming hosted lightly greater numbers of microbial genes associated with carbohydrate metabolism (ANOVA, $p > 0.1$), xenobiotics biodegradation and metabolism (ANOVA, $p < 0.1$), and infectious disease: bacterial (ANOVA, $p > 0.1$) (**Figure 4** and **Supplementary Figures 3**, **4**).

Organic Farming Harbored a Complex Phyllospere Microbial Network With Streptomyces as the Major Hub Taxa

Co-occurrence network analysis showed that organic farming harbored the greatest network connectivity (**Figure 5**), number of edges, and network density (**Supplementary Table 5**). Similarly, the number of hub species identified was the highest in organic

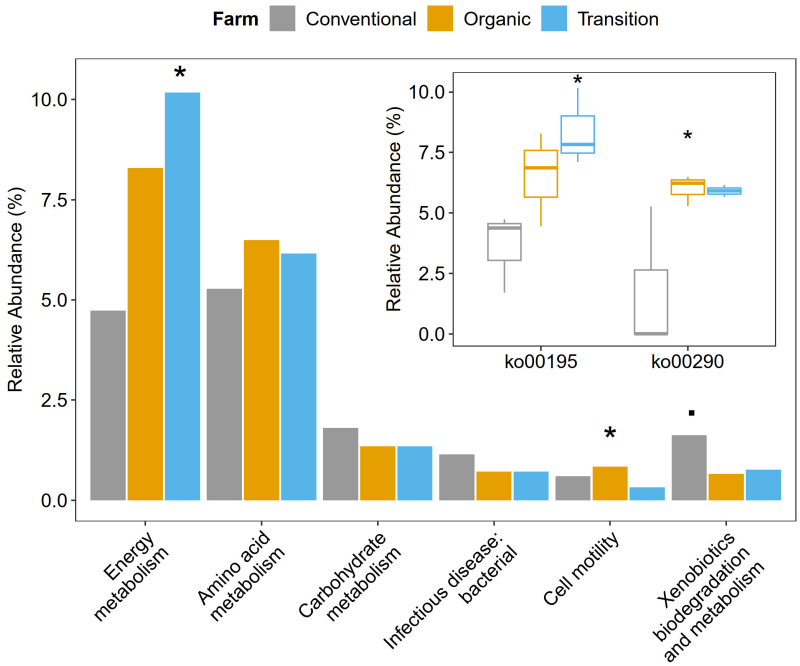

FIGURE 4 | The impacts of farming practices on metabolic processes at the second and third levels of KEGG hierarchy. The statistical test was performed using one-way ANOVA in which *p*-values < 0.05 were considered significant as represented by the (*) symbol, while the (.) character reflected *p*-value < 0.1.

farming (19 species) compared to 6 and 2 species in transition and conventional farms, respectively (**Supplementary Figure 7**). The hub species of the organic network was dominated by 4 bacterial species belonging to the genus *Streptomyces*, followed by nitrogen-fixing bacteria [i.e., carotenoid-producing *Calothrix* sp. 336/3 (Kosourov et al., 2016), *Paraburkholderia* sp. CCGE1002 (Ormeño-Orrillo et al., 2012), and *Azoarcus* sp. DD4 (Deng et al., 2019)], polysaccharide-degrading *Lacinutrix* sp. 5H-3-7-4 (Klippel et al., 2011), 1,4-dioxane-degrading *Mycobacterium dioxanotrophicus* (He et al., 2017), hydrogen-producing *Ethanoligenens harbinense* (Li et al., 2019), and ammonia-oxidizing archaeon *Candidatus Nitrosocosmicus franklandus* (Lehtovirta-Morley et al., 2016). In the transition network, six hub species included mushroom pathogenic *Janthinobacterium agaricidamnosum* (Graupner et al., 2015), human pathogenic *Raoultella ornithinolytica* (Morais et al., 2009), ochratoxin A-producing *Aspergillus homomorphus* (Varga et al., 2011), riboflavin-producing *Eremothecium gossypii* (Ledesma-Amaro et al., 2015), *Curtobacterium* sp. csp3, and *Micromonospora tulbaghiae,* whereas two bacterial species of oil hydrocarbon-degrading *Pedobacter cryoconitis* (Margesin et al., 2003) and *Flavobacterium branchiophilum* were the hubs in the conventional network.

Beneficial Microbes Were Identified as Core Species and Agricultural Practices Induced Specific Microbial Compositions

Core microbes were identified by selecting the most abundant (detection) and ubiquitous (prevalence) taxa across all samples. We observed 28 bacteria and 32 fungi as core species of sugarcane phyllosphere, accounting for 0.9% of total observed taxa and 19.4% of overall relative abundance (**Supplementary Figure 8**). These core bacterial species consisted of plant growth-promoting bacteria [i.e., *Bacillus cereus* (Zhang et al., 2019), *B. thuringiensis* (Raddadi et al., 2008), *Pseudomonas aeruginosa* (Radhapriya et al., 2015), *Rhodopseudomonas palustris* (Xu et al., 2018), and *Methylobacterium radiotolerans* (Eevers et al., 2015)], antibiotic-producing *Streptomyces venezuelae* (Kim et al., 2019), cellulolytic *Sorangium cellulosum* (Wang et al., 2012), photosynthetic *Scytonema* sp. NIES-4073 (Will et al., 2019), catechol-degrading *P. resinovorans* (Nojiri et al., 2002), indole acetic acid (IAA)-producing *Acinetobacter baumannii* (Lin et al., 2018), and several animal- and human-associated pathogens. Fungal core taxa were dominated by four species of *Aspergillus* including *Aspergillus niger, A. neoniger, A. thermomutatus,* and *A. heteromorphus*, followed by two species of *Fusarium* such as *Fusarium proliferatum* and *F. oxysporum*. Similar to bacterial core species, several human pathogenic fungi as well as phytopathogens were also members of the core species in the sugarcane phyllosphere.

Apart from identifying common species of sugarcane phyllosphere, we also investigated whether farming practices could promote the abundance of specific taxa as their representatives (microbial signatures). In this case, LEfSe analysis (LDA score > 2.0) was used to statistically detect any microbial species of which their abundances were significantly different among farming practices (farming-specific taxa). In terms of the bacterial community, transition farming had the highest number of enriched taxa (16 species), while organic and conventional

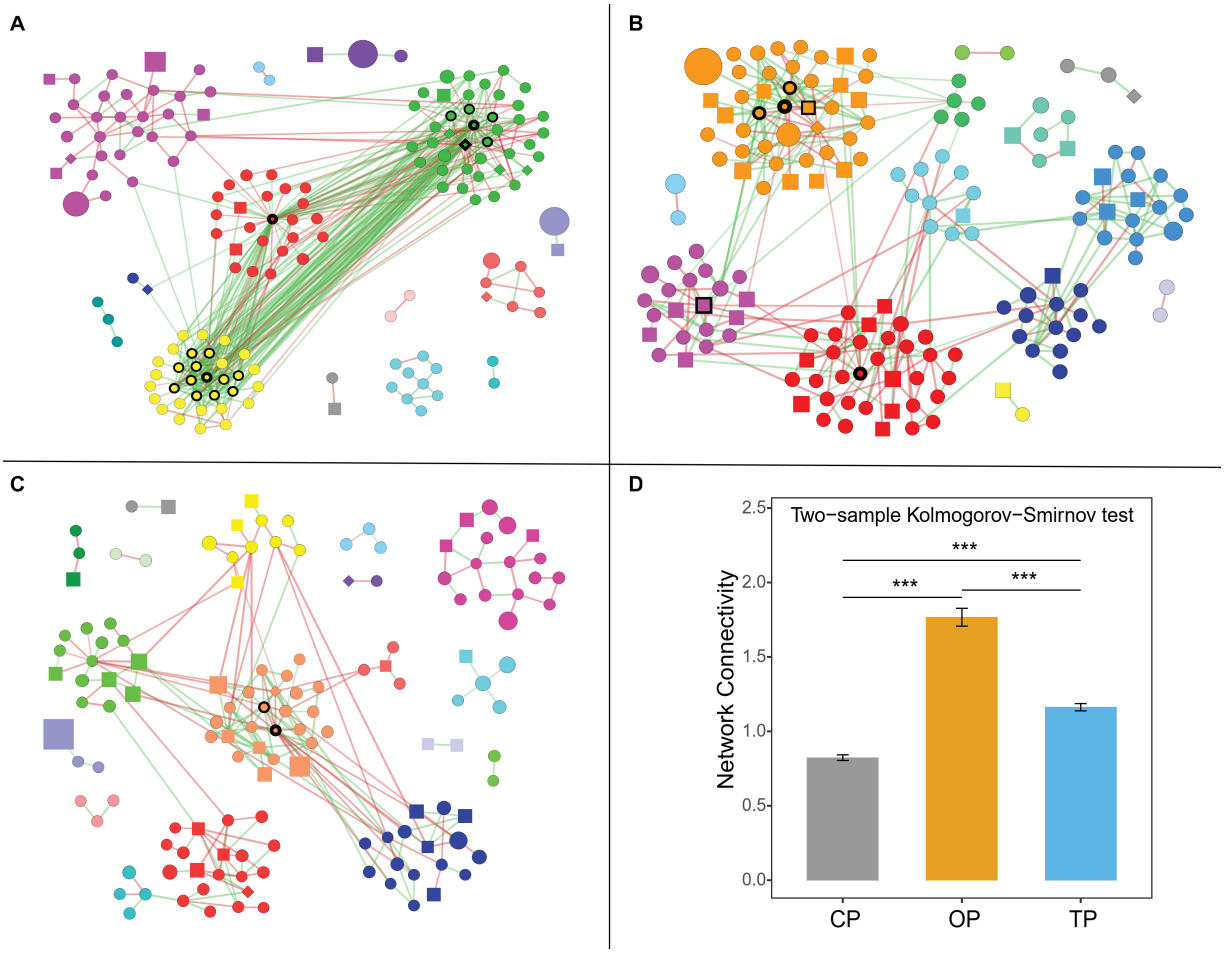

FIGURE 5 | Farming-specific co-occurrence networks of **(A)** organic, **(B)** transition, and **(C)** conventional farming practices. Green and red colors of the edges represent positive and negative relationships, respectively, while the color of nodes demonstrates network modules. The shape of vertices reflects microbial domains (i.e., circle: bacteria; square: fungi; and diamond: archaea), and the size of nodes refers to abundances. In addition, the nodes with black borders were assigned as hub taxa, and the width of the border reflects the node degree score. Note: only nodes with at least 1 connection are visualized. **(D)** Network connectivity or node degree represents the number of edges connected to a node. The symbol (***) represents statistical significance of p-value < 0.0001.

farms equally hosted 7 unique bacterial species (**Figure 6**). These bacterial species included plant growth-promoting bacteria, xenobiotic degraders, and pathogens. For the archaeal domain, seven species were identified, including three associated with conventional farming, two with organic farming, and two with transition farming (**Figure 6**). Furthermore, only two fungal taxa were observed, specifically one species in both organic and transition farms (**Figure 6**). However, no farming-specific fungi were observed in conventional farming.

Highly Conserved and Unique Microbial Gene Functions Were Observed in Each Farming Practice

Similarly, we also noticed that the sugarcane phyllosphere microbial community shared common functions across all three farming practices. Specifically, 32 KOs were identified as core functions from overall samples (**Supplementary Figure 9**). Among them, genes associated with oxidative phosphorylation and photosynthesis were the most abundant, including F-type H^+/Na^+-transporting ATPase subunit alpha and beta (K02111 and K02112), F-type H^+-transporting ATPase subunit alpha (K02132), cytochrome c oxidase subunit 1 (K02256), photosystem I P700 chlorophyll a apoprotein A1 and A2 (K02689 and K02690), photosystem II P680 reaction center D1 protein (K02703), nitrite reductase (NADH)-ubiquinone oxidoreductase chain 5 (K03883), NADH dehydrogenase (ubiquinone) Fe-S protein 2 (K03935), NAD(P)H-quinone oxidoreductase subunit 2 (K05573), and ribulose-bisphosphate carboxylase large chain (K01601). Genes involved in stress responses were also members of core functions such as heat shock 70 kDa protein 1/2/6/8 (K03283), molecular chaperone DnaJ (K03686), molecular chaperone HtpG (K04079), and a calcium permeable stress-gated cation channel (K21989).

For farming-specific microbial functions, 31 unique KOs in total were identified by the LEfSe program with LDA

FIGURE 6 | LEfSe analysis of taxonomic abundance among organic (green), transition (blue), and conventional (red) farming practices at the species level.

score > 2.0, including 12 KOs associated with organic farming, 11 with conventional farming, and 8 with transition farming (**Supplementary Figure 10**). At the KEGG pathway level, bacterial chemotaxis (ko02030) and a hedgehog signaling pathway (ko04340) were uniquely enriched in organic farming, while three farming-specific pathways in conventional farming included amoebiasis (ko05146), nitrogen metabolism (ko00910), and MAPK signaling pathway-yeast (ko04011) (**Figure 7**). However, no significantly abundant pathway was found in transition farming.

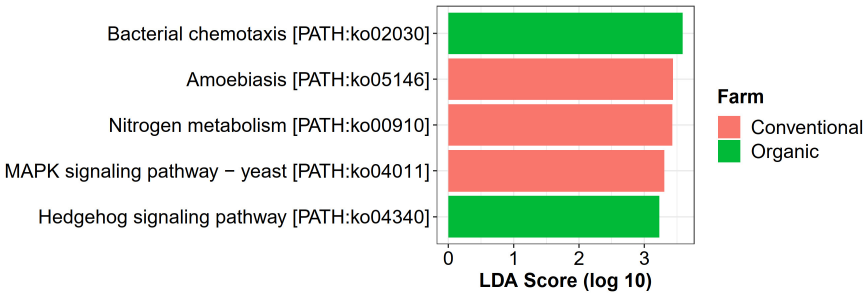

FIGURE 7 | LEfSe analysis of functional abundance based on the KEGG pathway in all farming practices.

DISCUSSION

Phyllosphere is described as the aerial parts of plant organs dominated by leaves (Turner et al., 2013). This habitat was tightly inhabited by up to 1×10^8 bacterial cells g^{-1} fresh weight of leaves (Remus-Emsermann et al., 2014), and these associated microbiota were suggested to have great importance on the survivability of the host plants (Vorholt, 2012; Peñuelas and Terradas, 2014). In the present study, shotgun metagenome sequencing was used to investigate the effect of agricultural shift on taxonomic diversity and functional capacity of sugarcane phyllosphere microbial community. This approach directly sequences the entire genomic DNA in a sample, thus providing a minimally biased quantification of the absolute abundance of microbes.

Read-based taxonomic profiling exhibited that the composition of phyllosphere microbial community was mainly composed of the bacterial phyla Proteobacteria, Actinobacteria, and Firmicutes, and the fungal phyla Ascomycota and Basidiomycota in all three farming practices. The predominant bacterial and fungal phyla observed in this work were similar to the previously reported study of sugarcane using 16S rRNA and ITS amplicons (Hamonts et al., 2018), as well as in other plant species including tomato (Toju et al., 2019), and grapevine (Perazzolli et al., 2014). These results supported the earlier finding of highly conserved phyllosphere microbial communities across host species (Massoni et al., 2020).

Diversity analyses revealed that farming practices significantly influenced the taxonomic and functional profiles of phyllosphere microbiota (β-diversity). Organic farming was slightly more diverse (Shannon index) than transition and conventional farms, while this practice was also the lowest in terms of species evenness (Pielou index). Theoretically, more diverse microbial communities would potentially increase the resistance of the host plant to pathogen invasion with the support of beneficial microbial symbionts (Kinkel et al., 2011). *Streptomyces* sp. GF20 and *Lactobacillus plantarum* were identified as microbial signatures of organic farming by LEfSe, and these bacteria were also among the top 100 most abundant taxa in the overall organic samples. It indicated that these species might contribute to the decrease in the evenness index through their dominancy, which would be useful for the host performance. Notably, a similar response has been observed on the soil microbial community as reported by the previous research (Hartmann et al., 2014), indicating that above-ground microbes responded to agricultural managements in the same way as those colonizing below-ground compartments. The Shannon diversity index of functional potentials also tended to increase in organic farming compared with the other two farming practices. However, no statistical significance of taxonomic and functional α-diversities was detected. In addition, the district was also found to have a significant effect on both taxonomic and functional β-diversities. Although the influence of farming practice was stronger than that of the district based on the PERMANOVA *p*-value, the farming practice was not the sole factor structuring the composition and functional potentials of phyllosphere microbial communities.

Core microbiome was thought to be tightly associated and evolved with terrestrial plants for the long term (Yeoh et al., 2017), in which their gene functions were essential for plant growth and productivity (Lemanceau et al., 2017). Core species of sugarcane phyllosphere were comprised of plant growth-promoting bacteria including N_2-fixing, antibiotic-producing, and IAA-producing species, highlighting the important roles of phyllosphere microbes to the fitness of host plants. Many of them have been cultivated *in vitro* (Raddadi et al., 2008; Radhapriya et al., 2015; Xu et al., 2018; Zhang et al., 2019). The presence of ammonia-oxidizing, cellulolytic, and photosynthetic bacteria as core members of sugarcane phyllosphere microbes further indicated their contributions to global nitrogen and carbon cycles, while the existence of a catechol-degrading bacterium showed phylloremediation potentials. For fungi, members of *Aspergillus* and *Fusarium* were the most predominant core taxa. Fungal species of *Aspergillus* have been studied for their plant growth-promoting properties including *Aspergillus niger*, which can solubilize phosphorous (P) (Mendes et al., 2015) and potassium (K) (Lopes-Assad et al., 2010). In contrast, *Fusarium* is one of the devastating phytopathogens that can adapt to a wide range of environments and affects various economic crops worldwide (Perincherry et al., 2019). Notably, by linking taxonomy and function, we found that beneficial genes possessed by core species mentioned above were commonly found in all samples. However, some of these genes were more abundant in organic and transition farms, while they were decreased in the conventional farm. Altogether, these core microbes emphasized the essential roles of phyllosphere microbial communities

in ensuring plant growth and productivity, leading to the enhancement of the health of the entire host ecosystem.

Similar to the previous report of neotropical trees (Lajoie et al., 2020), conserved metabolic functions of phyllosphere microbes were also found in this work. Specifically, amino acid and carbohydrate metabolisms were enriched in all samples, indicating that these two functions were of prominent importance for the phyllosphere microbes to access the nutrients in this habitat (Müller et al., 2016), in that polysaccharides and proteins were parts of leaf exudates secreted by glandular trichomes, which also functioned in plant–microbe interactions (Schlechter et al., 2019). At the level of KO, oxidative phosphorylation, photosynthesis, and stress responses represented core phyllosphere microbial functions. It is thus not surprising that photosynthetic genes were part of the core functions as many core microbial species were photosynthetic bacteria. This also suggested that phyllosphere microbes might use light as an alternative source of energy upon nutrient deficit (Vorholt, 2012; Stiefel et al., 2013). Furthermore, a highly dynamic and extreme condition of the phyllosphere environment, including exposure to UV light and high temperatures, which varied during the entire day, enforced phyllosphere microbes to activate a number of genes associated with stress responses to successfully colonize and thrive on the leaf surface (Vorholt, 2012). In this study, we found numerous genes encoding heat-shock proteins as core functions, indicating that these genes might play critical roles in the adaptation and survival of phyllosphere microbes in this harsh habitat. These results were in accordance with previous studies that reported conserved functions related to phototrophy and microbial adaptation of phyllosphere microbial communities in different types of plants (Finkel et al., 2016; Lambais et al., 2017; Flores-Núñez et al., 2020).

Co-occurrence network analysis was subsequently performed to compare the structure and complexity of phyllosphere microbial communities in response to farming practices. Network topology assessments showed that organic network had the highest number of edges, density, and connectivity, which might be linked to the strong resilience capabilities of the phyllosphere microbiota under this farm to disturbances or invasion of exogenous microbes (Mendes et al., 2018; Banerjee et al., 2019; Liao et al., 2019). Moreover, greater complexity and connectivity in the organic network were followed by the number of hub species identified, while unsustainable farming was in contrast. This pattern was similar to the previous study of wheat root microbiome (Banerjee et al., 2019). Interestingly, the three farming practices harbored completely distinct hub species, illustrating that agricultural conversion shifted the central taxa in the community. Hub species of the organic network were dominated by *Streptomyces* spp., which are well-known antibiotic-producing bacteria (Kong et al., 2019). Most of the edges associated with Streptomyces hubs were positive (56 positive edges and 3 negative edges), including inter- and intraspecies associations. This indicated that *Streptomyces* could coexist and inhibit the growth of other microbes in regulating the composition and structure of the organic network. Hu et al. (2020) suggested that *Streptomyces* application could promote the growth of tomato by reshaping the rhizosphere microbial community and could positively increase the abundance of other beneficial bacteria. Cyanobacterial *Calothrix* sp. 336/3, which had abilities to fix atmospheric carbon and nitrogen (Kosourov et al., 2016), was the most connected node in the organic network, followed by polysaccharide-degrading *Lacinutrix* sp. 5H-3-7-4 (Klippel et al., 2011) and ammonia-oxidizing archaeon *Candidatus Nitrosocosmicus franklandus* (Lehtovirta-Morley et al., 2016). With their capabilities, these three hub species could be placed at a higher trophic level and were positively connected with the *Streptomyces* hubs, explaining the essential role of *Streptomyces*, which could therefore be assigned as potential keystone species in the organic network. In the transition network, bacterial pathogens of mushroom, plant, and human were the hub species, while the conventional network had the lowest number of hub taxa, comprising of oil hydrocarbon-degrading *Pedobacter cryoconitis* (Margesin et al., 2003) and pathogenic *Flavobacterium branchiophilum* (Good et al., 2015). In short, the identified keystone species of phyllosphere microbes might play important ecological roles in their respective agricultural practices, which provided a future direction of study. However, further experimental validation regarding the biological process governing microbial networks is required, such as using a synthetic community.

Differential abundant analysis revealed that conventional practice induced the abundance of pathogenic species and microbes that could tolerate the harsh environments, while organic farming was characterized by the enrichment of beneficial species for the host plant. Conventional-specific taxa comprised of metal-mobilizing *Metallosphaera cuprina* (Liu et al., 2011), environmental extremes-resistant *Halorubrum* sp. BOL3-1 (DasSarma et al., 2019), and human pathogenic bacteria such as *Elizabethkingia miricola* (Zdziarski et al., 2017), and *Mycolicibacterium smegmatis* (Yamada et al., 2018). Organic-specific taxa consisted of plant growth-promoting bacteria including N_2-fixing bacteria [i.e., *Mesorhizobium loti* (Shimoda et al., 2016) and *Bradyrhizobium* sp. SG09 (Wasai-Hara et al., 2020)], lactic acid bacterium *L. plantarum*, which had the capability to behave as a biocontrol agent against phytopathogens (Daranas et al., 2019), and cellulase-degrading *Bacillus cellulosilyticus* (Mead et al., 2013). The number of transition-specific taxa was the highest, suggesting that many microbes might act as intermediate agents of agricultural transformation from conventional practices to organic systems. These species were dominated by toxic compound degraders including pyridine-degrading *Rhodococcus pyridinivorans* (Yoon et al., 2000), dye-decolorizing *Shewanella decolorationis* (Xu et al., 2005), metal-reducing *Pelosinus* sp. UFO1 (Brown et al., 2014), Fe(II)-oxidizing *Leptothrix cholodnii* (Kunoh et al., 2016), as well as phytopathogenic *Pantoea ananatis* (Stice et al., 2018), and enteropathogenic *Arcobacter butzleri* (Prouzet-Mauléon et al., 2006). One possible explanation was that residues of applied agrochemicals in the previous practice of transition farming remained in the soil and were absorbed by plants and then distributed to the leaves (Myers et al., 2016). As a response, the abundance of these microbes was increased, which could help to remediate those toxic substances. Thus, these beneficial

sugarcane microbiomes could be utilized as a promising approach for accelerating the conversion of conventional farming to organic management. Remarkably, several species belonging to genus *Streptomyces* were found in all farming practices by LEfSe analysis, identified as core species across all samples, and assigned as potential keystone species in the organic network. It thus suggested that *Streptomyces* spp. were well-adapted taxa in various conditions and might play crucial roles in the sugarcane growth and productivity (Sousa and Olivares, 2016; Wang et al., 2019).

Besides driving microbial composition, farming practices also significantly affected cell motility and energy metabolism of phyllosphere microbes. Cell motility was predominant in organic farming, particularly bacterial chemotaxis, suggesting that the active movement of microbial species in organic farming was greater than those in transition and conventional farms. Chemotaxis signaling allowed motile phyllosphere microorganisms to exploit chemical gradients to find nutrient resources such as leaf exudates released by the host plant or to escape noxious compounds (Scharf et al., 2016). Thus, the limitation of nutrients on the leaf surface made this property critical for the epiphytes to survive in this oligotrophic habitat (Vorholt, 2012; Scharf et al., 2016). Energy metabolism by means of the photosynthetic pathway was the highest in transition farming followed by organic farming and was significantly decreased in conventional farming, suggesting that higher energy was required to transform the agrochemical-polluted land into healthier farmland. This also indicated that the application of agrochemicals, especially herbicides, in the conventional practice reduced the photosynthetic potentials of the overall phyllosphere microbial communities (Broser et al., 2011; Crouzet et al., 2019). Furthermore, fertilization in the conventional farm could also alter the composition of leaf exudates (Barunawati et al., 2013), which might not favor its associated phyllosphere colonizers. In addition, valine, leucine, and isoleucine biosynthesis, also known as branched-chain amino acids (BCAAs), was also depleted in conventional farming. BCAAs were global transcriptional regulators in bacteria, which were importantly involved in the response to nutrient availability and metabolic reprogramming upon nutrient depletion (Kaiser and Heinrichs, 2018). Taken together, these might be the reason for the decrease in microbial diversity in conventional farming as some of the phyllosphere microbes lose these essential abilities to grow and survive.

Conventional farming, in contrast, slightly increased the abundance of xenobiotics biodegradation and metabolism, while organic farming was the lowest. This supported the idea that conventional farming, which relied on synthetic agrochemical usages (i.e., herbicides and NPK fertilizers), provided a toxic environment for the microbes, and xenobiotic-degrading genes were increased as a response (Liao et al., 2019). It also elevated the nitrogen metabolism of the phyllosphere microbes, including glutamine synthetase (K01915) and nitrite reductase (NADH) large subunit (K00362), which were identified as conventional-specific functions by LEfSe. The latter was reported to participate indirectly in nitric oxide (NO) production through the denitrification process (Härtig and Zumft, 1999; Ruiz et al., 2019). Interestingly, human pathogenic genes involved in the amoebiasis pathway were specifically enriched under conventional farming, emphasizing the harmful effect of unsustainable practices not only to the environment but also to human health.

While it was apparent that farming practices significantly influenced the taxonomic diversity and functional capacity of phyllosphere microbial communities, our experimental design in which triplicate samples of a particular farming type were collected from the same field could not clearly separate the effects of agricultural practices and farmland areas. Therefore, the study of the impacts of geographical location with similar farming practices, including soil properties and environmental and seasonal conditions, is warranted in the future to elucidate the essential roles of phyllosphere microbial communities for agricultural conversion toward sustainable farming.

CONCLUSION

This study revealed that organic farming promoted a higher microbial diversity with a more complex and stable network structure. Greater numbers of plant growth-promoting bacteria were also enriched as farming-specific taxa in this practice. Transition farming was predominated by numerous toxic compound degraders, which might importantly contribute to the restoration of damaged agroecosystems such as remediation of agrochemical residues. Conventional farming, which had the lowest diversity index, increased the abundance of extremes-resistant and human pathogenic species. Decreased microbial diversity in conventional farming might be attributed to diminished cell motility and energy metabolism, which were essentially required for the phyllosphere microbes to survive and thrive under stressful conditions in the phyllosphere habitat, including nutrient limitation. Overall, our results highlighted that shifting agricultural managements induced community changes and distinct functional profiles of phyllosphere microbial community, demonstrating the potential use of phyllosphere microbiota as signatures for improving agrochemical-derived farming to healthier and more sustainable systems. In addition, our work provided a basis for future research on the response of sugarcane-associated phyllosphere microbiota to agricultural land conversion and their prospects for enhancing crop productivity and global ecosystem health.

DATA AVAILABILITY STATEMENT

The datasets presented in this study can be found in online repositories. The names of the repository/repositories and accession number(s) can be found below: https://www.ebi.ac.uk/ena, PRJEB38470.

AUTHOR CONTRIBUTIONS

AK, SW, and SC designed the experiment. AK, JJ, AT, PP, and SD performed sample collection. AK and SD conducted DNA extraction. SW, JJ, and SD arranged the sequencing process. AK,

SS, and KK carried out the shotgun metagenome data analysis. AK, SC, SS, and SW contributed to data interpretation. AK wrote the first draft of the manuscript. All authors critically revised and approved the final version of the manuscript to be published.

FUNDING

This work was supported by the research fund from the King Mongkut's University of Technology Thonburi, Thailand (Project ID: 21850).

ACKNOWLEDGMENTS

AK was financially supported by the "Petchra Pra Jom Klao Master's Degree Research Scholarship from King Mongkut's University of Technology Thonburi" and Fungal Biotechnology Laboratory. We thank the Fungal Biotechnology Laboratory and Systems Biology and Bioinformatics Laboratory, Pilot Plant Development and Training Institute (PDTI), King Mongkut's University of Technology Thonburi (KMUTT) for the facilities. We appreciate Rai Sukphoang, Rai Sarot, and Rai Pramote for providing invaluable leaf samples for this research. We acknowledge Asst. Prof. Sansanalak Rachdawong (Mitr Phol Group and KMUTT) and Dr. Laddawan Potprommane (PDTI, KMUTT) for their contributions to funding acquisition. We thank Mr. Thanawat Duangfoo (PDTI, KMUTT), Mr. Sumate Tancharoen (PDTI, KMUTT), and Mr. Nipon Jeankawkham (PDTI, KMUTT) for helping to collect the samples.

SUPPLEMENTARY MATERIAL

The Supplementary Material for this article can be found online at: https://www.frontiersin.org/articles/10.3389/fmicb.2021.623799/full#supplementary-material

Supplementary Figure 1 | Map of sampling locations created with Google maps.

Supplementary Figure 2 | Relative abundance of the KEGG major category visualized by histogram in three different farming practices.

Supplementary Figure 3 | Relative abundance of the KEGG category from the highest (top) to the lowest (bottom) in three different farming practices.

Supplementary Figure 4 | Top 25 relative abundances of the KEGG pathway in three different farming practices.

Supplementary Figure 5 | α-Rarefaction curves, drawn based on the abundance of microbial communities in conventional, organic, and transition farming practices represented by red, green, and blue, respectively.

Supplementary Figure 6 | Top 50 most influential microbial species to the community differences among farming practices. The *x*-axis values are based on the coefficient score of the PERMANOVA test. The *y*-axis (microbial species) highlighted by green color are microbial signatures of organic farming identified by LEfSe.

Supplementary Figure 7 | Keystone species observed in the three farming-specific microbial co-occurrence networks. The table shows the node degree of each taxon. Rows represent microbial species and columns represent farming practices. Horizontal and vertical dendrograms were constructed by the hierarchical clustering method.

Supplementary Figure 8 | Core phyllosphere microbes of sugarcane sampled from three different farming practices.

Supplementary Figure 9 | Core gene functions of phyllosphere microbes associated with sugarcane in organic, transition, and conventional farming practices.

Supplementary Figure 10 | LEfSe test of functional abundance based on KEGG orthology (KO) in organic, transition, and conventional farming practices.

Supplementary Table 1 | Description of three sugarcane farming practices sampled in this study.

Supplementary Table 2 | Number of reads remaining before and after QC processes.

Supplementary Table 3 | Good's coverage values of all samples in three farming practices.

Supplementary Table 4 | PERMANOVA and BETADISPER analysis results.

Supplementary Table 5 | Co-occurrence network attributes in three different farming practices.

REFERENCES

Ali, N., Sorkhoh, N., Salamah, S., Eliyas, M., and Radwan, S. (2012). The potential of epiphytic hydrocarbon-utilizing bacteria on legume leaves for attenuation of atmospheric hydrocarbon pollutants. *J. Environ. Manage.* 93, 113–120. doi: 10.1016/j.jenvman.2011.08.014

Andrews, S. (2010). *FastQC: A QualityControl Tool for High Throughput Sequence Data*. Available online at: https://www.bioinformatics.babraham.ac.uk/projects/fastqc/ (accessed January 31, 2020).

Banerjee, S., Walder, F., Büchi, L., Meyer, M., Held, A. Y., Gattinger, A., et al. (2019). Agricultural intensification reduces microbial network complexity and the abundance of keystone taxa in roots. *ISME J.* 13, 1722–1736. doi: 10.1038/s41396-019-0383-2

Barunawati, N., Hettwer Giehl, R. F., Bauer, B., and Von Wirén, N. (2013). The influence of inorganic nitrogen fertilizer forms on micronutrient retranslocation and accumulation in grains of winter wheat. *Front. Plant Sci.* 4:320. doi: 10.3389/fpls.2013.00320

Bengtsson, J., Ahnström, J., and Weibull, A.-C. (2005). The effects of organic agriculture on biodiversity and abundance: a meta-analysis. *J. Appl. Ecol.* 42, 261–269. doi: 10.1111/j.1365-2664.2005.01005.x

Berry, D., and Widder, S. (2014). Deciphering microbial interactions and detecting keystone species with co-occurrence networks. *Front. Microbiol.* 5:219. doi: 10.3389/fmicb.2014.00219

Bolger, A. M., Lohse, M., and Usadel, B. (2014). Trimmomatic: a flexible trimmer for Illumina sequence data. *Bioinformatics* 30, 2114–2120. doi: 10.1093/bioinformatics/btu170

Broser, M., Glöckner, C., Gabdulkhakov, A., Guskov, A., Buchta, J., Kern, J., et al. (2011). Structural basis of cyanobacterial photosystem II Inhibition by the herbicide terbutryn. *J. Biol. Chem.* 286, 15964–15972. doi: 10.1074/jbc.M110.215970

Brown, S. D., Utturkar, S. M., Magnuson, T. S., Ray, A. E., Poole, F. L., Lancaster, W. A., et al. (2014). Complete genome sequence of *Pelosinus* sp. strain UFO1 assembled using single-molecule real-time DNA sequencing technology. *Genome Announc.* 2:e00881-14. doi: 10.1128/genomeA.00881-14

Buchfink, B., Xie, C., and Huson, D. H. (2015). Fast and sensitive protein alignment using DIAMOND. *Nat. Methods* 12, 59–60. doi: 10.1038/nmeth.3176

Cernava, T., Chen, X., Krug, L., Li, H., Yang, M., and Berg, G. (2019). The tea leaf microbiome shows specific responses to chemical pesticides and biocontrol applications. *Sci. Total Environ.* 667, 33–40. doi: 10.1016/j.scitotenv.2019.02.319

Chen, T., Nomura, K., Wang, X., Sohrabi, R., Xu, J., Yao, L., et al. (2020). A plant genetic network for preventing dysbiosis in the phyllosphere. *Nature* 580, 653–657. doi: 10.1038/s41586-020-2185-0

Crouzet, O., Consentino, L., Pétraud, J.-P., Marrauld, C., Aguer, J.-P., Bureau, S., et al. (2019). Soil photosynthetic microbial communities mediate aggregate stability: influence of cropping systems and herbicide use in an agricultural soil. *Front. Microbiol.* 10:1319. doi: 10.3389/fmicb.2019.01319

Csardi, G., and Nepusz, T. (2006). The igraph software package for complex network research. *InterJ. Comp. Syst.* 1695, 1–9.

Daranas, N., Roselló, G., Cabrefiga, J., Donati, I., Francés, J., Badosa, E., et al. (2019). Biological control of bacterial plant diseases with *Lactobacillus plantarum* strains selected for their broad-spectrum activity. *Ann. Appl. Biol.* 174, 92–105. doi: 10.1111/aab.12476

DasSarma, P., Anton, B. P., DasSarma, S., Laye, V. J., Guzman, D., Roberts, R. J., et al. (2019). Genome sequence and methylation patterns of *Halorubrum* sp. strain BOL3-1, the first haloarchaeon isolated and cultured from Salar de Uyuni, Bolivia. *Microbiol. Resour. Announc.* 8:e00386-19. doi: 10.1128/MRA.00386-19

Deng, D., Li, F., Ye, L., and Li, M. (2019). Complete genome sequence of *Azoarcus* sp. strain DD4, a gram-negative propanotroph that degrades 1,4-Dioxane and 1,1-Dichloroethylene. *Microbiol. Resour. Announc.* 8:e00775-19. doi: 10.1128/mra.00775-19

Dong, M., Yang, Z., Cheng, G., Peng, L., Xu, Q., and Xu, J. (2018). Diversity of the bacterial microbiome in the roots of four *Saccharum* species: *S. spontaneum*, *S. robustum*, *S. barberi*, and *S. officinarum*. *Front. Microbiol.* 9:267. doi: 10.3389/fmicb.2018.00267

Douglas, G. M., Maffei, V. J., Zaneveld, J. R., Yurgel, S. N., Brown, J. R., Taylor, C. M., et al. (2020). PICRUSt2 for prediction of metagenome functions. *Nat. Biotechnol.* 38, 685–688. doi: 10.1038/s41587-020-0548-6

Eevers, N., Van Hamme, J. D., Bottos, E. M., Weyens, N., and Vangronsveld, J. (2015). Draft genome sequence of *Methylobacterium radiotolerans*, a DDE-degrading and plant growth-promoting strain isolated from *Cucurbita pepo*. *Genome Announc.* 3:e00488-15. doi: 10.1128/genomeA.00488-15

Ewels, P., Magnusson, M., Lundin, S., and Käller, M. (2016). MultiQC: summarize analysis results for multiple tools and samples in a single report. *Bioinformatics* 32, 3047–3048. doi: 10.1093/bioinformatics/btw354

FAO (2018). *Top Sugarcane Production: Food and Agriculture Organization of the United Nations*. Available online at: http://www.fao.org/faostat/en/#data/QC/visualize (accessed June 28, 2020)

Finkel, O. M., Delmont, T. O., Post, A. F., and Belkin, S. (2016). Metagenomic signatures of bacterial adaptation to life in the phyllosphere of a salt-secreting desert tree. *Appl. Environ. Microbiol.* 82, 2854–2861. doi: 10.1128/aem.00483-16

Flores-Núñez, V. M., Fonseca-García, C., Desgarennes, D., Eloe-Fadrosh, E., Woyke, T., and Partida-Martínez, L. P. (2020). Functional signatures of the epiphytic prokaryotic microbiome of agaves and cacti. *Front. Microbiol.* 10:3044. doi: 10.3389/fmicb.2019.03044

Friedman, J., and Alm, E. J. (2012). Inferring correlation networks from genomic survey data. *PLoS Comput. Biol.* 8:e1002687. doi: 10.1371/journal.pcbi.1002687

Fürnkranz, M., Wanek, W., Richter, A., Abell, G., Rasche, F., and Sessitsch, A. (2008). Nitrogen fixation by phyllosphere bacteria associated with higher plants and their colonizing epiphytes of a tropical lowland rainforest of Costa Rica. *ISME J.* 2, 561–570. doi: 10.1038/ismej.2008.14

Gonthier, D. J., Ennis, K. K., Farinas, S., Hsieh, H. Y., Iverson, A. L., Batary, P., et al. (2014). Biodiversity conservation in agriculture requires a multi-scale approach. *Proc. Biol. Sci.* 281:20141358. doi: 10.1098/rspb.2014.1358

Good, C., Davidson, J., Wiens, G. D., Welch, T. J., and Summerfelt, S. (2015). *Flavobacterium branchiophilum* and *F. succinicans* associated with bacterial gill disease in rainbow trout *Oncorhynchus mykiss* (Walbaum) in water recirculation aquaculture systems. *J. Fish Dis.* 38, 409–413. doi: 10.1111/jfd.12249

Graupner, K., Lackner, G., and Hertweck, C. (2015). Genome sequence of mushroom soft-rot pathogen *Janthinobacterium agaricidamnosum*. *Genome Announc.* 3:e00277-15. doi: 10.1128/genomeA.00277-15

Hamonts, K., Trivedi, P., Garg, A., Janitz, C., Grinyer, J., Holford, P., et al. (2018). Field study reveals core plant microbiota and relative importance of their drivers. *Environ. Microbiol.* 20, 124–140. doi: 10.1111/1462-2920.14031

Härtig, E., and Zumft, W. G. (1999). Kinetics of *nirS* expression (cytochrome cd1 nitrite reductase) in *Pseudomonas stutzeri* during the transition from aerobic respiration to denitrification: evidence for a denitrification-specific nitrate- and nitrite-responsive regulatory system. *J. Bacteriol.* 181, 161–166. doi: 10.1128/JB.181.1.161-166.1999

Hartman, K., van der Heijden, M. G. A., Wittwer, R. A., Banerjee, S., Walser, J.-C., and Schlaeppi, K. (2018). Cropping practices manipulate abundance patterns of root and soil microbiome members paving the way to smart farming. *Microbiome* 6:14. doi: 10.1186/s40168-017-0389-9

Hartmann, M., Frey, B., Mayer, J., Mäder, P., and Widmer, F. (2014). Distinct soil microbial diversity under long-term organic and conventional farming. *ISME J.* 9, 1177–1194. doi: 10.1038/ismej.2014.210

He, Y., Wei, K., Si, K., Mathieu, J., Li, M., and Alvarez, P. J. J. (2017). Whole-genome sequence of the 1,4-Dioxane-degrading bacterium *Mycobacterium dioxanotrophicus* PH-06. *Genome Announc.* 5:e00625-17. doi: 10.1128/genomeA.00625-17

Hu, D., Li, S., Li, Y., Peng, J., Wei, X., Ma, J., et al. (2020). *Streptomyces* sp. strain TOR3209: a rhizosphere bacterium promoting growth of tomato by affecting the rhizosphere microbial community. *Sci. Rep.* 10:20132. doi: 10.1038/s41598-020-76887-5

Kaiser, J. C., and Heinrichs, D. E. (2018). Branching out: alterations in bacterial physiology and virulence due to branched-chain amino acid deprivation. *mBio* 9:e01188-18. doi: 10.1128/mBio.01188-18

Kajala, K., Covshoff, S., Karki, S., Woodfield, H., Tolley, B. J., Dionora, M. J. A., et al. (2011). Strategies for engineering a two-celled C4 photosynthetic pathway into rice. *J. Exp. Bot.* 62, 3001–3010. doi: 10.1093/jxb/err022

Kanehisa, M., and Goto, S. (2000). KEGG: Kyoto encyclopedia of genes and genomes. *Nucleic Acids Res.* 28, 27–30. doi: 10.1093/nar/28.1.27

Kanehisa, M., Sato, Y., Kawashima, M., Furumichi, M., and Tanabe, M. (2016). KEGG as a reference resource for gene and protein annotation. *Nucleic Acids Res.* 44, D457–D462. doi: 10.1093/nar/gkv1070

Karlsson, I., Friberg, H., Kolseth, A.-K., Steinberg, C., and Persson, P. (2017). Organic farming increases richness of fungal taxa in the wheat phyllosphere. *Mol. Ecol.* 26, 3424–3436. doi: 10.1111/mec.14132

Karlsson, I., Friberg, H., Steinberg, C., and Persson, P. (2014). Fungicide effects on fungal community composition in the wheat phyllosphere. *PLoS One* 9:e111786. doi: 10.1371/journal.pone.0111786

Kim, J.-E., Choi, J.-S., and Roe, J.-H. (2019). Growth and differentiation properties of pikromycin-producing *Streptomyces venezuelae* ATCC15439. *J. Microbiol.* 57, 388–395. doi: 10.1007/s12275-019-8539-3

Kinkel, L. L., Bakker, M. G., and Schlatter, D. C. (2011). A coevolutionary framework for managing disease-suppressive soils. *Annu. Rev. Phytopathol.* 49, 47–67. doi: 10.1146/annurev-phyto-072910-095232

Klippel, B., Lochner, A., Bruce, D. C., Davenport, K. W., Detter, C., Goodwin, L. A., et al. (2011). Complete genome sequences of *Krokinobacter* sp. strain 4H-3-7-5 and *Lacinutrix* sp. strain 5H-3-7-4, polysaccharide-degrading members of the family *Flavobacteriaceae*. *J. Bacteriol.* 193, 4545–4546. doi: 10.1128/JB.05518-11

Knief, C., Delmotte, N., Chaffron, S., Stark, M., Innerebner, G., Wassmann, R., et al. (2012). Metaproteogenomic analysis of microbial communities in the phyllosphere and rhizosphere of rice. *ISME J.* 6, 1378–1390. doi: 10.1038/ismej.2011.192

Kong, D., Wang, X., Nie, J., and Niu, G. (2019). Regulation of antibiotic production by signaling molecules in *Streptomyces*. *Front. Microbiol.* 10:2927. doi: 10.3389/fmicb.2019.02927

Kosourov, S., Murukesan, G., Jokela, J., and Allahverdiyeva, Y. (2016). Carotenoid biosynthesis in *Calothrix* sp. 336/3: composition of carotenoids on full medium, during diazotrophic growth and after long-term H_2 photoproduction. *Plant Cell Physiol.* 57, 2269–2282. doi: 10.1093/pcp/pcw143

Kuijper, J. (1915). DeGroei van Bladschijf, Bladscheede em Stengel van het suikerriet. *Arch. Suikerind Ned Indië* 23, 528–556.

Kunoh, T., Hashimoto, H., McFarlane, I. R., Hayashi, N., Suzuki, T., Taketa, E., et al. (2016). Abiotic deposition of Fe complexes onto *Leptothrix* sheaths. *Biology* 5:26. doi: 10.3390/biology5020026

Laforest-Lapointe, I., Paquette, A., Messier, C., and Kembel, S. W. (2017). Leaf bacterial diversity mediates plant diversity and ecosystem function relationships. *Nature* 546, 145–147. doi: 10.1038/nature22399

Lahti, L., and Shetty, S. (2019). *Microbiome R Package*. Available online at: http://microbiome.github.io (accessed February 17, 2020).

Lajoie, G., Maglione, R., and Kembel, S. W. (2020). Adaptive matching between phyllosphere bacteria and their tree hosts in a neotropical forest. *Microbiome* 8:70. doi: 10.1186/s40168-020-00844-7

Lambais, M. R., Barrera, S. E., Santos, E. C., Crowley, D. E., and Jumpponen, A. (2017). Phyllosphere metaproteomes of trees from the Brazilian Atlantic Forest show high levels of functional redundancy. *Microb. Ecol.* 73, 123–134. doi: 10.1007/s00248-016-0878-6

Langmead, B., and Salzberg, S. L. (2012). Fast gapped-read alignment with Bowtie 2. *Nat. Methods* 9, 357–359. doi: 10.1038/nmeth.1923

Ledesma-Amaro, R., Serrano-Amatriain, C., Jiménez, A., and Revuelta, J. L. (2015). Metabolic engineering of riboflavin production in *Ashbya gossypii* through pathway optimization. *Microb. Cell Fact.* 14:163. doi: 10.1186/s12934-015-0354-x

Lehtovirta-Morley, L. E., Ross, J., Hink, L., Weber, E. B., Gubry-Rangin, C., Thion, C., et al. (2016). Isolation of '*Candidatus Nitrosocosmicus franklandus*', a novel ureolytic soil archaeal ammonia oxidiser with tolerance to high ammonia concentration. *FEMS Microbiol. Ecol.* 92:fiw057. doi: 10.1093/femsec/fiw057

Lemanceau, P., Blouin, M., Muller, D., and Moënne-Loccoz, Y. (2017). Let the core microbiota be functional. *Trends Plant Sci.* 22, 583–595. doi: 10.1016/j.tplants.2017.04.008

Li, H., Mei, X., Liu, B., Xie, G., Ren, N., and Xing, D. (2019). Quantitative proteomic analysis reveals the ethanologenic metabolism regulation of *Ethanoligenens harbinense* by exogenous ethanol addition. *Biotechnol. Biofuels* 12:166. doi: 10.1186/s13068-019-1511-y

Liao, J., Xu, Q., Xu, H., and Huang, D. (2019). Natural farming improves soil quality and alters microbial diversity in a cabbage field in Japan. *Sustainability* 11:3131. doi: 10.3390/su11113131

Lin, H.-R., Shu, H.-Y., and Lin, G.-H. (2018). Biological roles of indole-3-acetic acid in *Acinetobacter baumannii*. *Microbiol. Res.* 216, 30–39. doi: 10.1016/j.micres.2018.08.004

Liu, L.-J., You, X.-Y., Guo, X., Liu, S.-J., and Jiang, C.-Y. (2011). *Metallosphaera cuprina* sp. nov., an acidothermophilic, metal-mobilizing archaeon. *Int. J. Syst. Evol. Microbiol.* 61, 2395–2400. doi: 10.1099/ijs.0.026591-0

Lopes-Assad, M. L., Avansini, S. H., Rosa, M. M., de Carvalho, J. R. P., and Ceccato-Antonini, S. R. (2010). The solubilization of potassium-bearing rock powder by *Aspergillus niger* in small-scale batch fermentations. *Can. J. Microbiol.* 56, 598–605. doi: 10.1139/W10-044

Lu, J., Breitwieser, F. P., Thielen, P., and Salzberg, S. L. (2017). Bracken: estimating species abundance in metagenomics data. *PeerJ Comput. Sci.* 3:e104. doi: 10.7717/peerj-cs.104

Lupatini, M., Korthals, G. W., de Hollander, M., Janssens, T. K. S., and Kuramae, E. E. (2017). Soil microbiome is more heterogeneous in organic than in conventional farming system. *Front. Microbiol.* 7:2064. doi: 10.3389/fmicb.2016.02064

Maignien, L., DeForce, E. A., Chafee, M. E., Eren, A. M., and Simmons, S. L. (2014). Ecological succession and stochastic variation in the assembly of *Arabidopsis thaliana* phyllosphere communities. *mBio* 5:e0068213. doi: 10.1128/mBio.00682-13

Margesin, R., Spröer, C., Schumann, P., and Schinner, F. (2003). *Pedobacter cryoconitis* sp. nov., a facultative psychrophile from alpine glacier cryoconite. *Int. J. Syst. Evol. Microbiol.* 53, 1291–1296. doi: 10.1099/ijs.0.02436-0

Massoni, J., Bortfeld-Miller, M., Jardillier, L., Salazar, G., Sunagawa, S., and Vorholt, J. A. (2020). Consistent host and organ occupancy of phyllosphere bacteria in a community of wild herbaceous plant species. *ISME J.* 14, 245–258. doi: 10.1038/s41396-019-0531-8

McMurdie, P. J., and Holmes, S. (2013). phyloseq: an R package for reproducible interactive analysis and graphics of microbiome census data. *PLoS One* 8:e6121717. doi: 10.1371/journal.pone.0061217

Mead, D., Drinkwater, C., and Brumm, P. J. (2013). Genomic and enzymatic results show *Bacillus cellulosilyticus* uses a novel set of LPXTA carbohydrases to hydrolyze polysaccharides. *PLoS One* 8:e61131. doi: 10.1371/journal.pone.0061131

Mendes, G. D. O., da Silva, N. M. R. M., Anastácio, T. C., Vassilev, N. B., Ribeiro, J. I. Jr., da Silva, I. R., et al. (2015). Optimization of *Aspergillus niger* rock phosphate solubilization in solid-state fermentation and use of the resulting product as a P fertilizer. *Microb. Biotechnol.* 8, 930–939. doi: 10.1111/1751-7915.12289

Mendes, L. W., Raaijmakers, J. M., de Hollander, M., Mendes, R., and Tsai, S. M. (2018). Influence of resistance breeding in common bean on rhizosphere microbiome composition and function. *ISME J.* 12, 212–224. doi: 10.1038/ismej.2017.158

Morais, V. P., Daporta, M. T., Bao, A. F., Campello, M. G., and Andrés, G. Q. (2009). Enteric fever-like syndrome caused by *Raoultella ornithinolytica* (*Klebsiella ornithinolytica*). *J. Clin. Microbiol.* 47, 868–869. doi: 10.1128/jcm.01709-08

Morris, J. H., Apeltsin, L., Newman, A. M., Baumbach, J., Wittkop, T., Su, G., et al. (2011). clusterMaker: a multi-algorithm clustering plugin for Cytoscape. *BMC Bioinformatics* 12:436. doi: 10.1186/1471-2105-12-436

Morugán-Coronado, A., García-Orenes, F., McMillan, M., and Pereg, L. (2019). The effect of moisture on soil microbial properties and nitrogen cyclers in Mediterranean sweet orange orchards under organic and inorganic fertilization. *Sci. Total Environ.* 655, 158–167. doi: 10.1016/j.scitotenv.2018.11.174

Müller, D. B., Schubert, O. T., Röst, H., Aebersold, R., and Vorholt, J. A. (2016). Systems-level proteomics of two ubiquitous leaf commensals reveals complementary adaptive traits for phyllosphere colonization. *Mol. Cell. Proteomics* 15, 3256–3269. doi: 10.1074/mcp.M116.058164

Müller, T., and Ruppel, S. (2014). Progress in cultivation-independent phyllosphere microbiology. *FEMS Microbiol. Ecol.* 87, 2–17. doi: 10.1111/1574-6941.12198

Myers, J. P., Antoniou, M. N., Blumberg, B., Carroll, L., Colborn, T., Everett, L. G., et al. (2016). Concerns over use of glyphosate-based herbicides and risks associated with exposures: a consensus statement. *Environ. Health* 15:19. doi: 10.1186/s12940-016-0117-0

Nayfach, S., and Pollard, K. S. (2015). Average genome size estimation improves comparative metagenomics and sheds light on the functional ecology of the human microbiome. *Genome Biol.* 16:51. doi: 10.1186/s13059-015-0611-7

Nojiri, H., Maeda, K., Sekiguchi, H., Urata, M., Shintani, M., Yoshida, T., et al. (2002). Organization and transcriptional characterization of catechol degradation genes involved in carbazole degradation by *Pseudomonas resinovorans* strain CA10. *Biosci. Biotechnol. Biochem.* 66, 897–901. doi: 10.1271/bbb.66.897

Oksanen, J., Blanchet, F. G., Friendly, M., Kindt, R., Legendre, P., McGlinn, D., et al. (2019). *vegan: Community Ecology Package.* R Package Version 2.5-6. Available online at: https://CRAN.R-project.org/package=vegan (accessed February 17, 2020).

Ormeño-Orrillo, E., Rogel, M. A., Chueire, L. M. O., Tiedje, J. M., Martínez-Romero, E., and Hungria, M. (2012). Genome sequences of *Burkholderia* sp. strains CCGE1002 and H160, isolated from legume nodules in Mexico and Brazil. *J. Bacteriol.* 194:6927. doi: 10.1128/jb.01756-12

Paungfoo-Lonhienne, C., Lonhienne, T. G. A., Yeoh, Y. K., Webb, R. I., Lakshmanan, P., Chan, C. X., et al. (2014). A new species of *Burkholderia* isolated from sugarcane roots promotes plant growth. *Microb. Biotechnol.* 7, 142–154. doi: 10.1111/1751-7915.12105

Paungfoo-Lonhienne, C., Yeoh, Y. K., Kasinadhuni, N. R. P., Lonhienne, T. G. A., Robinson, N., Hugenholtz, P., et al. (2015). Nitrogen fertilizer dose alters fungal communities in sugarcane soil and rhizosphere. *Sci. Rep.* 5:8678. doi: 10.1038/srep08678

Peñuelas, J., and Terradas, J. (2014). The foliar microbiome. *Trends Plant Sci.* 19, 278–280. doi: 10.1016/j.tplants.2013.12.007

Perazzolli, M., Antonielli, L., Storari, M., Puopolo, G., Pancher, M., Giovannini, O., et al. (2014). Resilience of the natural phyllosphere microbiota of the grapevine to chemical and biological pesticides. *Appl. Environ. Microbiol.* 80, 3585–3596. doi: 10.1128/AEM.00415-14

Perincherry, L., Lalak-Kańczugowska, J., and Stępień, Ł (2019). *Fusarium*-produced mycotoxins in plant-pathogen interactions. *Toxins* 11:664. doi: 10.3390/toxins11110664

Pimentel, D., Hepperly, P., Hanson, J., Douds, D., and Seidel, R. (2005). Environmental, energetic, and economic comparisons of organic and conventional farming systems. *BioScience* 55, 573–582. doi: 10.1641/0006-35682005055[0573:EEAECO]2.0.CO;2

Pretty, J. (2008). Agricultural sustainability: concepts, principles and evidence. *Philos. Trans. R. Soc. Lond. B Biol. Sci.* 363, 447–465. doi: 10.1098/rstb.2007.2163

Prouzet-Mauléon, V., Labadi, L., Bouges, N., Ménard, A., and Mégraud, F. (2006). *Arcobacter butzleri*: underestimated enteropathogen. *Emerg. Infect. Dis.* 12, 307–309. doi: 10.3201/eid1202.050570

R Core Team (2019). *R: A Language and Environment for Statistical Computing*. Available online at: https://www.R-project.org/ (accessed February 7, 2020).

Raddadi, N., Cherif, A., Boudabous, A., and Daffonchio, D. (2008). Screening of plant growth promoting traits of *Bacillus thuringiensis*. *Ann. Microbiol.* 58, 47–52. doi: 10.1007/BF03179444

Radhapriya, P., Ramachandran, A., Anandham, R., and Mahalingam, S. (2015). *Pseudomonas aeruginosa* RRALC3 enhances the biomass, nutrient and carbon contents of *Pongamia pinnata* seedlings in degraded forest soil. *PLoS One* 10:e0139881. doi: 10.1371/journal.pone.0139881

Redman, R. S., Sheehan, K. B., Stout, R. G., Rodriguez, R. J., and Henson, J. M. (2002). Thermotolerance generated by plant/fungal symbiosis. *Science* 298:1581. doi: 10.1126/science.1078055

Remus-Emsermann, M. N., Lücker, S., Müller, D. B., Potthoff, E., Daims, H., and Vorholt, J. A. (2014). Spatial distribution analyses of natural phyllosphere-colonizing bacteria on *Arabidopsis thaliana* revealed by fluorescence in situ hybridization. *Environ. Microbiol.* 16, 2329–2340. doi: 10.1111/1462-2920.12482

Ritpitakphong, U., Falquet, L., Vimoltust, A., Berger, A., Métraux, J. P., and L'Haridon, F. (2016). The microbiome of the leaf surface of *Arabidopsis* protects against a fungal pathogen. *New Phytol.* 210, 1033–1043. doi: 10.1111/nph.13808

Rivera, X. C. S., Bacenetti, J., Fusi, A., and Niero, M. (2017). The influence of fertiliser and pesticide emissions model on life cycle assessment of agricultural products: the case of Danish and Italian barley. *Sci. Total Environ.* 592, 745–757. doi: 10.1016/j.scitotenv.2016.11.183

Robinson, N., Brackin, R., Vinall, K., Soper, F., Holst, J., Gamage, H., et al. (2011). Nitrate paradigm does not hold up for sugarcane. *PLoS One* 6:e19045. doi: 10.1371/journal.pone.0019045

Ruiz, B., Le Scornet, A., Sauviac, L., Rémy, A., Bruand, C., and Meilhoc, E. (2019). The nitrate assimilatory pathway in *Sinorhizobium meliloti*: contribution to NO production. *Front. Microbiol.* 10:1526. doi: 10.3389/fmicb.2019.01526

Scharf, B. E., Hynes, M. F., and Alexandre, G. M. (2016). Chemotaxis signaling systems in model beneficial plant–bacteria associations. *Plant Mol. Biol.* 90, 549–559. doi: 10.1007/s11103-016-0432-4

Schlechter, R. O., Miebach, M., and Remus-Emsermann, M. N. P. (2019). Driving factors of epiphytic bacterial communities: a review. *J. Adv. Res.* 19, 57–65. doi: 10.1016/j.jare.2019.03.003

Segata, N., Izard, J., Waldron, L., Gevers, D., Miropolsky, L., Garrett, W. S., et al. (2011). Metagenomic biomarker discovery and explanation. *Genome Biol.* 12:R60. doi: 10.1186/gb-2011-12-6-r60

Shannon, P., Markiel, A., Ozier, O., Baliga, N. S., Wang, J. T., Ramage, D., et al. (2003). Cytoscape: a software environment for integrated models of biomolecular interaction networks. *Genome Res.* 13, 2498–2504. doi: 10.1101/gr.1239303

Shimoda, Y., Hirakawa, H., Sato, S., Saeki, K., and Hayashi, M. (2016). Whole-genome sequence of the nitrogen-fixing symbiotic rhizobium *Mesorhizobium loti* strain TONO. *Genome Announc.* 4:e01016-16. doi: 10.1128/genomeA.01016-16

Sousa, J. A. D. J., and Olivares, F. L. (2016). Plant growth promotion by *Streptomycetes*: ecophysiology, mechanisms and applications. *Chem. Biol. Technol. Agric.* 3:24. doi: 10.1186/s40538-016-0073-5

Stice, S. P., Stumpf, S. D., Gitaitis, R. D., Kvitko, B. H., and Dutta, B. (2018). *Pantoea ananatis* genetic diversity analysis reveals limited genomic diversity as well as accessory genes correlated with onion pathogenicity. *Front. Microbiol.* 9:184. doi: 10.3389/fmicb.2018.00184

Stiefel, P., Zambelli, T., and Vorholt, J. A. (2013). Isolation of optically targeted single bacteria by application of fluidic force microscopy to aerobic anoxygenic phototrophs from the phyllosphere. *Appl. Environ. Microbiol.* 79, 4895–4905. doi: 10.1128/AEM.01087-13

Taghavi, S., Garafola, C., Monchy, S., Newman, L., Hoffman, A., Weyens, N., et al. (2009). Genome survey and characterization of endophytic bacteria exhibiting a beneficial effect on growth and development of poplar trees. *Appl. Environ. Microbiol.* 75, 748–757. doi: 10.1128/AEM.02239-08

Tamames, J., and Puente-Sánchez, F. (2019). SqueezeMeta, a highly portable, fully automatic metagenomic analysis pipeline. *Front. Microbiol.* 9:3349. doi: 10.3389/fmicb.2018.03349

Toju, H., Okayasu, K., and Notaguchi, M. (2019). Leaf-associated microbiomes of grafted tomato plants. *Sci. Rep.* 9:1787. doi: 10.1038/s41598-018-38344-2

Turner, T. R., James, E. K., and Poole, P. S. (2013). The plant microbiome. *Genome Biol.* 14:209. doi: 10.1186/gb-2013-14-6-209

Varga, J., Frisvad, J. C., Kocsubé, S., Brankovics, B., Tóth, B., Szigeti, G., et al. (2011). New and revisited species in *Aspergillus* section *Nigri*. *Stud. Mycol.* 69, 1–17. doi: 10.3114/sim.2011.69.01

Vorholt, J. A. (2012). Microbial life in the phyllosphere. *Nat. Rev. Microbiol.* 10, 828–840. doi: 10.1038/nrmicro2910

Waclawovsky, A. J., Sato, P. M., Lembke, C. G., Moore, P. H., and Souza, G. M. (2010). Sugarcane for bioenergy production: an assessment of yield and regulation of sucrose content. *Plant Biotechnol. J.* 8, 263–276. doi: 10.1111/j.1467-7652.2009.00491.x

Wang, S.-Y., Hu, W., Lin, X.-Y., Wu, Z.-H., and Li, Y.-Z. (2012). A novel cold-active xylanase from the cellulolytic myxobacterium *Sorangium cellulosum* So9733-1: gene cloning, expression, and enzymatic characterization. *Appl. Microbiol. Biotechnol.* 93, 1503–1512. doi: 10.1007/s00253-011-3480-3

Wang, Z., Solanki, M. K., Yu, Z.-X., Yang, L.-T., An, Q.-L., Dong, D.-F., et al. (2019). Draft genome analysis offers insights into the mechanism by which *Streptomyces chartreusis* WZS021 increases drought tolerance in sugarcane. *Front. Microbiol.* 9:3262. doi: 10.3389/fmicb.2018.03262

Wasai-Hara, S., Hara, S., Morikawa, T., Sugawara, M., Takami, H., Yoneda, J., et al. (2020). Diversity of *Bradyrhizobium* in non-leguminous sorghum plants: *B. ottawaense* isolates unique in genes for N_2O reductase and lack of the type VI secretion system. *Microbes Environ.* 35:ME19102. doi: 10.1264/jsme2.ME19102

Watts, S. C., Ritchie, S. C., Inouye, M., and Holt, K. E. (2018). FastSpar: rapid and scalable correlation estimation for compositional data. *Bioinformatics* 35, 1064–1066. doi: 10.1093/bioinformatics/bty734

Wickham, H. (2016). *ggplot2: Elegant Graphics for Data Analysis*. New York: Springer-Verlag.

Will, S. E., Henke, P., Boedeker, C., Huang, S., Brinkmann, H., Rohde, M., et al. (2019). Day and night: metabolic profiles and evolutionary relationships of six axenic non-marine *Cyanobacteria*. *Genome Biol. Evol.* 11, 270–294. doi: 10.1093/gbe/evy275

Wood, D. E., Lu, J., and Langmead, B. (2019). Improved metagenomic analysis with Kraken 2. *Genome Biol.* 20:257. doi: 10.1186/s13059-019-1891-0

Xiang, Q., Chen, Q.-L., Zhu, D., Yang, X.-R., Qiao, M., Hu, H.-W., et al. (2020). Microbial functional traits in phyllosphere are more sensitive to anthropogenic disturbance than in soil. *Environ. Pollut.* 265:114954. doi: 10.1016/j.envpol.2020.114954

Xu, J., Feng, Y., Wang, Y., and Lin, X. (2018). Effect of rhizobacterium *Rhodopseudomonas palustris* inoculation on *Stevia rebaudiana* plant growth and soil microbial community. *Pedosphere* 28, 793–803. doi: 10.1016/S1002-0160(18)60043-8

Xu, M., Guo, J., Cen, Y., Zhong, X., Cao, W., and Sun, G. (2005). *Shewanella decolorationis* sp. nov., a dye-decolorizing bacterium isolated from activated sludge of a waste-water treatment plant. *Int. J. Syst. Evol. Microbiol.* 55, 363–368. doi: 10.1099/ijs.0.63157-0

Yamada, H., Yamaguchi, M., Igarashi, Y., Chikamatsu, K., Aono, A., Murase, Y., et al. (2018). *Mycolicibacterium smegmatis*, basonym *Mycobacterium smegmatis*, expresses morphological phenotypes much more similar to *Escherichia coli* than *Mycobacterium tuberculosis* in quantitative structome analysis and CryoTEM examination. *Front. Microbiol.* 9:1992. doi: 10.3389/fmicb.2018.01992

Ye, Y., and Doak, T. G. (2009). A parsimony approach to biological pathway reconstruction/inference for genomes and metagenomes. *PLoS Comput. Biol.* 5:e1000465. doi: 10.1371/journal.pcbi.1000465

Yeoh, Y. K., Dennis, P. G., Paungfoo-Lonhienne, C., Weber, L., Brackin, R., Ragan, M. A., et al. (2017). Evolutionary conservation of a core root microbiome across plant phyla along a tropical soil chronosequence. *Nat Commun.* 8:215. doi: 10.1038/s41467-017-00262-8

Yoon, J. H., Kang, S. S., Cho, Y. G., Lee, S. T., Kho, Y. H., Kim, C. J., et al. (2000). *Rhodococcus pyridinivorans* sp. nov., a pyridine-degrading bacterium. *Int. J. Syst. Evol. Microbiol.* 50, 2173–2180. doi: 10.1099/00207713-50-6-2173

Yurgel, S. N., Nearing, J. T., Douglas, G. M., and Langille, M. G. I. (2019). Metagenomic functional shifts to plant induced environmental changes. *Front. Microbiol.* 10:1682. doi: 10.3389/fmicb.2019.01682

Zdziarski, P., Paściak, M., Rogala, K., Korzeniowska-Kowal, A., and Gamian, A. (2017). *Elizabethkingia miricola* as an opportunistic oral pathogen associated with superinfectious complications in humoral immunodeficiency: a case report. *BMC Infect. Dis.* 17:763. doi: 10.1186/s12879-017-2886-7

Zhang, L.-N., Wang, D.-C., Hu, Q., Dai, X.-Q., Xie, Y.-S., Li, Q., et al. (2019). Consortium of plant growth-promoting rhizobacteria strains suppresses sweet pepper disease by altering the rhizosphere microbiota. *Front. Microbiol.* 10:1668. doi: 10.3389/fmicb.2019.01668

Conflict of Interest: The authors declare that the research was conducted in the absence of any commercial or financial relationships that could be construed as a potential conflict of interest.

frontiers in Microbiology

ORIGINAL RESEARCH
published: 23 March 2021
doi: 10.3389/fmicb.2021.621875

Research on the Interaction Mechanism Between α Mino-Phosphonate Derivative Q-R and Harpin-Binding Protein 1 in Tobacco (*Nicotiana tabacum*) Plants

Maoxi Huang[1†], Yunlong Yan[1,2†], Li Wang[1,2†], Jun Chen[1,2], Tao Liu[1], Xin Xie[2] and Xiangyang Li[1]*

[1] State Key Laboratory Breeding Base of Green Pesticide and Agricultural Bioengineering, Key Laboratory of Green Pesticide and Agricultural Bioengineering, Ministry of Education, Guizhou University, Guiyang, China, [2] College of Agriculture, Guizhou University, Guiyang, China

OPEN ACCESS

Edited by:
Jia Liu,
Chongqing University of Arts and Sciences, China

Reviewed by:
Orlando Borras-Hidalgo,
Qilu University of Technology, China
Xusheng Shao,
East China University of Science and Technology, China

***Correspondence:**
Xiangyang Li
xyli1@gzu.edu.cn;
xiangyangli83@126.com

† These authors have contributed equally to this work

Specialty section:
This article was submitted to Microbe and Virus Interactions with Plants, a section of the journal Frontiers in Microbiology

Received: *27 October 2020*
Accepted: *24 February 2021*
Published: *23 March 2021*

Citation:
Huang M, Yan Y, Wang L, Chen J, Liu T, Xie X and Li X (2021) Research on the Interaction Mechanism Between α Mino-Phosphonate Derivative Q-R and Harpin-Binding Protein 1 in Tobacco (Nicotiana tabacum) Plants. Front. Microbiol. 12:621875. doi: 10.3389/fmicb.2021.621875

Amino-phosphonate derivative R-diphenyl-1-(4-methylbenzothiazole-2-amino)-1-(thiphene-2-yl)-methylphosphonate (Q-R) has a high protective anti-tobacco mosaic virus (TMV) activity. However, the mechanism responsible for Q-R's effect on TMV infection is largely unknown. Here, we studied the expression levels of harpin-binding protein 1 (HrBP1) and pathogenesis-related protein-1a (PR-1a) in TMV-infected tobacco plants by using reverse transcription quantitative real-time PCR. Then, we verified the interactions between Q-R and the HrBP1 protein from *Escherichia coli* using isothermal titration calorimetry and studied the Q-R-associated assembly of HrBP1 using size-exclusion chromatography. The results showed that the expression levels of HrBP1 and PR-1a genes were significantly increased by Q-R at the transcriptional level in TMV-infected tobacco plants, and the *E. coli*-expressed HrBP1 protein was assembled into oligomers by Q-R via binding to HrBP1 with a dissociation constant of 1.19 μM. We, therefore, concluded that Q-R activated the HrBP1 and PR-1a genes and enhanced the ability of HrBP1 to assemble in tobacco plants.

Keywords: Q-R, HrBP1, PR-1a, interaction, binding

INTRODUCTION

Harpin induces hypersensitive responses to plants and induces the defensive processes of pathogen-associated immunity in plant roots (El-Maarouf et al., 2001; Aljaafri et al., 2017; Lawaju et al., 2018).

Harpin-binding protein (HrBP1) is a protein receptor of Harpin. HrBP1 was first discovered in planting cell walls. HrBP1 induces systemic acquired resistance to plants (El-Maarouf et al., 2001). HrBP1 can be selectively up-regulate several signaling pathways, including those of salicylic acid (SA), ethylene and the jasmonic acid. In the SA pathway, the genes encoding enhanced disease susceptibility 1, non-expressor of pathogenesis- related 1, pathogenesis-related protein-1a

(PR-1a), pathogenesis related- protein-2, pathogenesis-related protein-5, and alternative oxidase were activated. In the ethylene and jasmonic acid pathways, PDF1.2 and Thi2.1 were activated. In addition, HrBP1 generates disease resistance by up-regulating the harpin-induced gene related to the *mitogen-activated protein kinase* gene (Lee et al., 2001; Wang et al., 2002; Liu et al., 2006; Penmetsa et al., 2008; Camehl et al., 2010). HrBP1 expression results in the hypersensitive reaction and systemic acquired resistance related to the *non-race-specific disease resistance* and *enhanced disease susceptibility-1* genes (Peng et al., 2003; Gopalan, 2008). Thus, HrBP1 can generate anti-viral responses in plants.

In a previous study, we found that dufulin-associated activation of HrBP1 leads to the SA signaling pathway and produces antiviral responses from the tobacco plants (Chen et al., 2012). Amino-phosphonate derivative (R)-diphenyl-1-(4-methylbenzothiazole-2-amino)-1-(thiphene-2-yl)-methylphosphonate (Q-R) is a derivative compound of dufulin with high bioactivities on tobacco mosaic virus (TMV) and cucumber mosaic virus (Song et al., 2009; Zhang et al., 2016, 2017). However, the mechanism of Q-R that affects TMV infection is largely unknown. The structure of Q-R is similar to that of dufulin (**Figure 1**). To further to investigate the protective mechanism of Q-R, we studied the expression levels of the *HrBP1* and *PR-1a* genes in TMV-infected tobacco (*Nicotiana tabacum*) plant treated with Q-R. Then, we studied the mechanism of Q-R affecting by HrBP1 protein.

Abbreviations: Q-R, R-diphenyl-1-(4-methylbenzothiazole-2-amino)-1-(thiphene-2-yl)-methylphosphonate; TMV, tobacco mosaic virus; HrBP1, harpin-binding protein 1; PR-1a, pathogenesis-related protein-1a; BTH, Benzo-1, 2, 3-thiadiazole-7-carbothioic acid S-methyl ester; SA, salicylic acid; IPTG, isopropyl-β-D-galactopyranoside; SEC, Size-exclusion chromatography; SDS-PAGE, sodium dodecyl sulfate-polyacrylamide gel electrophoresis.

MATERIALS AND METHODS

Antiviral Agents and Plant Materials

The chiral α-aminophosphonate derivative Q-R (99%) and dufulin (99%) was synthesized in our laboratory (Zhang et al., 2016). Benzo-1, 2, 3-thiadiazole-7-carbothioic acid S-methyl ester (BTH) (99%) was purchased from Aladdin Biochemical Technology Co. (Shanghai, China) (Sleiman et al., 2017). The structural formulae of these compounds are presented in **Figure 1**. In total, ∼30 *Nicotiana tabacum* K326 seeds were placed in a growth chamber at 25°C, after 12 weeks, the tobacco plants were used for the study. The TMV was purified as previously described by Gooding (Gooding and Hebert, 1967). The 12-weeks-old tobacco plants were sprayed with 5 mL of 500-μg/mL Q-R three times for 1-d intervals (500-μg/mL dufulin and BTH were positive control). Then, the plants were inoculated with TMV and grown for 5 days. The leaf

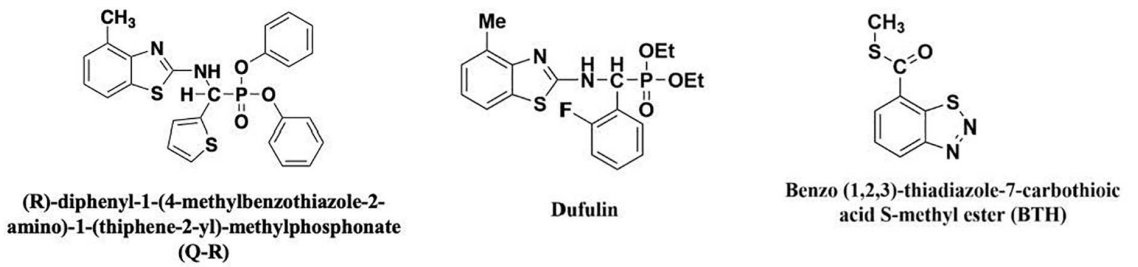

FIGURE 1 | The chemical structures of antiviral agents.

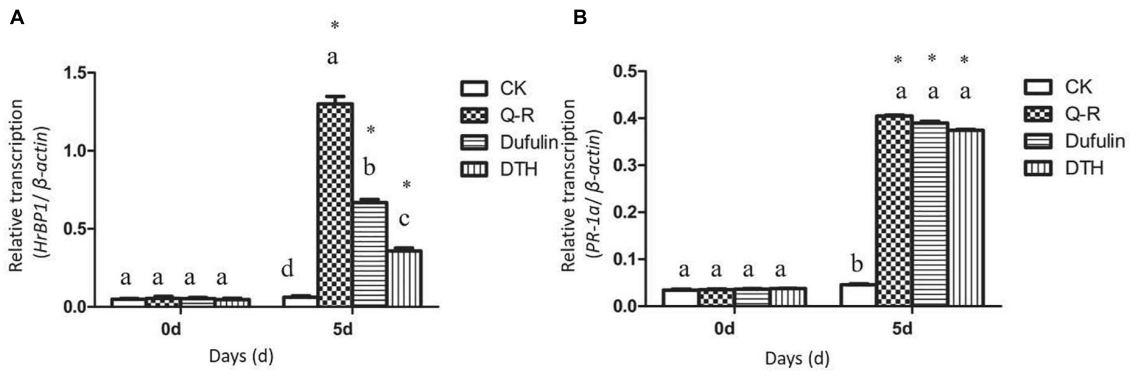

FIGURE 2 | Antiviral response genes expression analysis by qPCR using gene-specific primers (**Supplementary Table 1**). Relative expression of the *HrBP1* **(A)** and *PR-1a* **(B)** genes in TMV-infection plants treated with Q-R, dufulin and BTH at 500 μg/mL at 5 days. Asterisks represent the significantly different between agent treatment and control ($P < 0.05$). The different lowercase letters represent *HrBP1*/*PR-1a* genes expression values in the different treatment groups ($P < 0.05$).

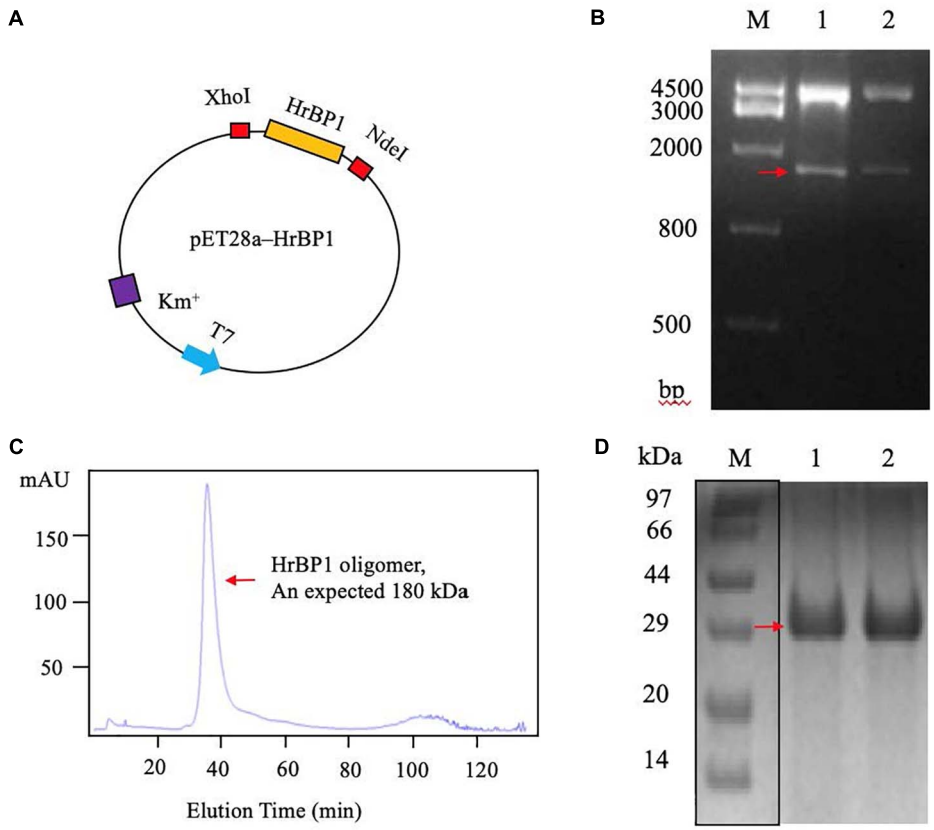

FIGURE 3 | The *HrBP1* gene determination and HrBP1 protein expression and purification. **(A)** Recombinant vector pET28a-HrBP1 was digested by *Nde*I and *Xho*I. **(B)** The *HrBP1* gene size (ca. 831 bp) was confirmed by 1% agarose gel electrophoresis. Lane M is a DNA marker; Lanes 1 and 2 shows the digestion of *HrBP1* gene by *Nde*I and *Xho*I in the pET28a-HrBP1 recombinant plasmid; the red arrow shows bands of HrBP1 bands. **(C)** HrBP1 oligomer protein with expected size 180 kDa between 440 kDa (Ferritin) and 158 kDa (IgG). **(D)** M is protein Marker; Lanes 1 and 2 are HrBP1 purification proteins in 12% SDS-PAGE; the red arrow shows HrBP1 bands.

samples of tobacco plants were harvested for further analyses. Three independent experimental replicates were conducted. The control tobacco plants, not exposed to TMV, were kept in another growth chamber.

Relative Expression Levels of Activated Response Genes After TMV-Infected Tobacco Were Treated With Antiviral Agents as Assessed by Reverse Transcription Quantitative Real-Time PCR (qPCR)

To verify the effects of Q-R on the expression of antiviral response genes in the TMV-infected tobacco plants, the expression levels of the *HrBP1* and *PR-1a* genes were examined using qPCR. Briefly, 100 mg total RNA from tobacco samples (treated with 500 μg/mL of an antiviral agent) was extracted using the TRIzol reagent kit, independently (TakaRa, Japan), and cDNAs were synthesized using a Reverse Transcription System kit (TakaRa). Then, qPCR was performed using SYBR Premix Ex TaqII (TaKaRa). Gene expression levels were normalized using β-*actin* as the internal control (**Supplementary Table 1**; Chen et al., 2012; Gao et al., 2019). The relative expression gene levels were calculated using the $2^{-\Delta\Delta Ct}$ method (Livak and Schmittgen, 2001; Wang et al., 2019).

HrBP1 Plasmid Constructs

The sequence (GenBank accession no. 107762961) for *N. tabacum HrBP1* was used to design a forward primer containing a *Nde*I (underlined) restriction site in (5′-GGAAT TCCATATGGCTTCTCTACTTCAGTACTCTACACT-3′) and a *Xho*I (underlined) restriction site in reverse primers (5′- CCGC TCGAGTGAGATAACGAAAACTCTAAGCTCTC-3′). The full-length *N. tabacum HrBP1* gene (831 bp) was inserted into pET28a (Novagen, United States), resulting in the plasmid pET28a-HrBP1. The *N. tabacum HrBP1* gene was confirmed by 1% agarose gel electrophoresis and the *N. tabacum HrBP1* DNA sequence was confirmed at the Shanghai Sangon Company (Chen et al., 2012).

HrBP1 Expression and Purification

The plasmid pET28a-HrBP1 in a culture of *E. coli* strains BL21(DE3) (Novagen) was transferred to 1 L of Luria broth (30-μg/mL kanamycin). When the OD_{600} of Luria broth reached

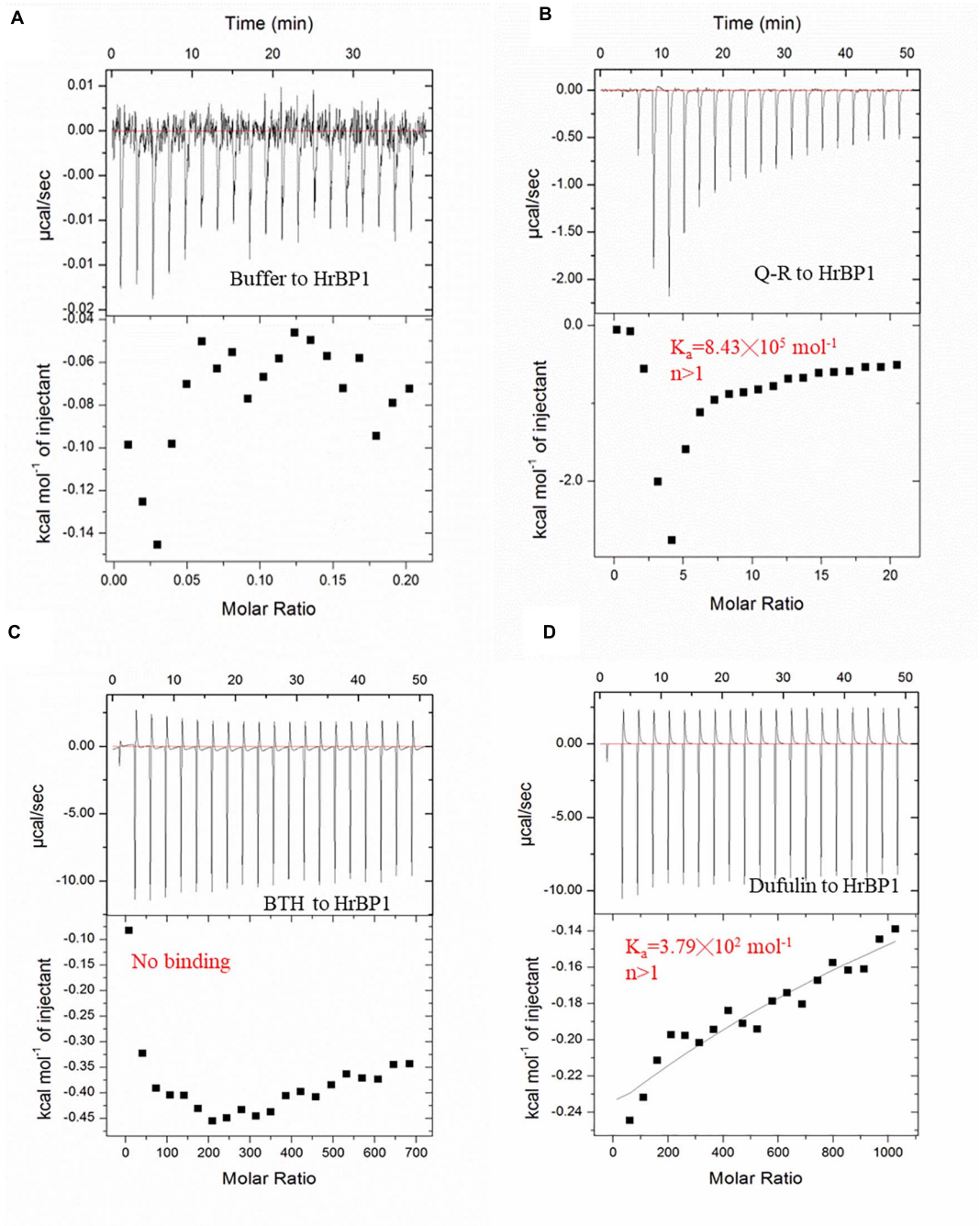

FIGURE 4 | ITC studies of Q-R, dufulin, BTH and HrBP1 purification protein. **(A)** control. **(B)** Q-R and HrBP1. **(C)** BTH and HrBP1. **(D)** Dufulin and HrBP1.

0.65, the temperature was decreased to 16°C, and 0.8–1.0 mM isopropyl-β-D-galactopyranoside (IPTG) was supplemented in Luria broth. HrBP1 protein was expressed in Luria broth overnight. Then, the cells containing HrBP1 protein were collected, harvested, and resuspended in 50 mM Tris-HCl, 150 mM NaCl and 1 mM β-mercaptoethanol buffer (pH 7.5) and the cells were lysed at 4°C using sonication (Li et al., 2013, 2015a). The whole cells were centrifuged at 12,000 g for 30 min at 4°C, the soluble supernatants were collected and loaded onto a 5-mL HisTrap high-performance column attached to an AKTA purifier protein liquid chromatography system (GE Healthcare, United States), and the protein was eluted by 20 mM Tris-HCl and 300-mM imidazole buffer (pH 7.5). Eluate fractions were collected and analyzed by 12% sodium dodecyl sulfate (SDS)-polyacrylamide gel electrophoresis (PAGE), and the crude protein were extracted at 4°C using a

desalting column (GE Healthcare), and the eluate fractions were pooled and concentrated by ultrafiltration (10-kDa cut-off). The protein amount was detected by absorbance at 280 nm using a Genequant100 (GE Healthcare).

Size-Exclusion Chromatography (SEC), PAGE and High-Resolution Mass Spectrometry

At 4°C, SEC was performed using Superdex 200 10/300 GL column (GE Healthcare) attached to an AKTA purifier protein liquid chromatography system (GE Healthcare) (Li et al., 2015b). The column was equilibrated using a buffer containing 20 mM Tris-HCl and 100 mM NaCl (pH 7.5). Myoglobin (17 kDa), ovalbumin (43 kDa), albumin (67 kDa), IgG (158 kDa), and ferritin (440 kDa) was used as the molecular mass standards (Bio-Rad, United States). The protein content was detected at a wavelength of 280 nm. The purified protein was confirmed by 8% enriching gel and 12% SDS-PAGE, and then stained with Coomassie brilliant blue (Li et al., 2015a).

The purified HrBP1 proteins were digested using trypsin, the digested products were analyzed using a Nano LC-1DTM plus system (Eksigent Technologies, United States) and TripleTOF 5600 MS (AB SCIEX, United States) (Gopalan, 2008; MacLean et al., 2010; Chen et al., 2015; Yang et al., 2017; Shi et al., 2018; Yu et al., 2018). The achieved peptide masses were searched and blasted using UniProt database without any species or peptide limits. Multiple peptide fragments matched the reported HrBP1 segments (Uniprot accession no.: Q5QJB2). High-resolution masses spectrometry data were extracted and retrieved using PeakView (AB SCIEX) and ProteinPilot (AB SCIEX). The trypsin cleaved sites and the predicted m/z values were analyzed using Skyline (AB SCIEX) (Huntley et al., 2014).

Isothermal Titration Calorimetry (ITC)

At 25°C, ITC-based binding experiments were performed using an ITC 200 Micro Calorimeter (GE Healthcare). The HrBP1 protein was in the buffer containing 20-mM Tris-HCl and 100-mM sodium chloride (pH 7.5). The 2 mM Q-R compound was titrated into the HrBP1 protein (0.1 mM) in a 200-μL sample cell as follows: 0.4 μL for the first injection and 2 μL for the next 19 injections using a 40-μL microsyringe, the intervals of each injection was150 s. According to the manufacturer's instructions, the integrated heat data were analyzed using the one-set-of-sites model. The first data point was not required in the analysis. The binding parameters reaction including enthalpy change, ΔH (cal·mol^{-1}), binding constant K (mol^{-1}) and number of molecules per HrBP1 protein (n) was floating in the fit. The binding free energy and reaction entropy was calculated (Kumar et al., 2014). The dissociation constant K_d was determined as 1/K (Kumar et al., 2014).

Statistical Analyses

Data were submitted to an analysis of variance (ANOVA) using Duncan's multiple range test by SPSS 19.0 software (IBM, United States). $P < 0.05$ was identified as the significance level.

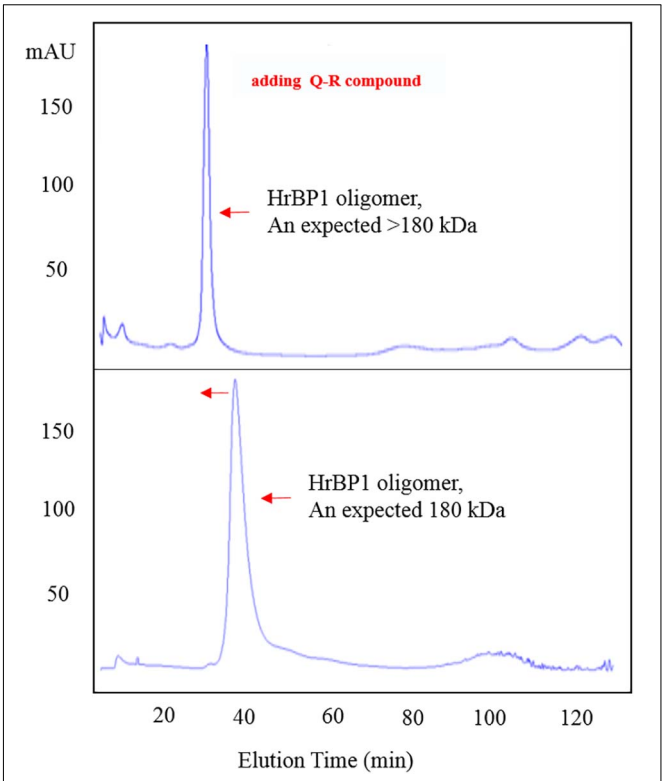

FIGURE 5 | Q-R induced the assembly of HrBP1 large oligomer protein with expected size > 180 kDa between 440 kDa (Ferritin) and 158 kDa (IgG).

RESULTS AND DISCUSSION

Relative Expression Levels of Antiviral Response Genes After Q-R Treatment in TMV-Infected Tobacco as Assessed by qPCR

To investigate whether Q-R inhibits the antiviral response genes' expression levels in TMV-infected tobacco plants, we detected the relative expression of *HrBP1* and *PR-1a* utilizing the qPCR assay. The expression levels of the *HrBP1* and *PR-1a* genes in TMV-infected tobacco plants significantly increased compared with the CK ($P < 0.05$) at the transcriptional level after exposure to by 500 μg/mL of Q-R on 5 days (**Figure 2**). Compared with dufulin and BTH, the expression levels of the *HrBP1* genes were significantly ($P < 0.05$) promoted by compound Q-R (**Figure 2A**).

Cloning of the HrBP1 Gene

To obtain the code sequence of the HrBP1 gene in tobacco plant, we amplified the full-length cDNA sequence of HrBP1 and cloned it into the pET28a plasmid (**Figure 3A**). Electrophoresis and furthering sequence of the fragment confirmed the HrBP1 gene having an expected 831-bp size and nucleotide sequence (**Figure 3B** and **Supplementary Figure 1**) as reported (Chen et al., 2012).

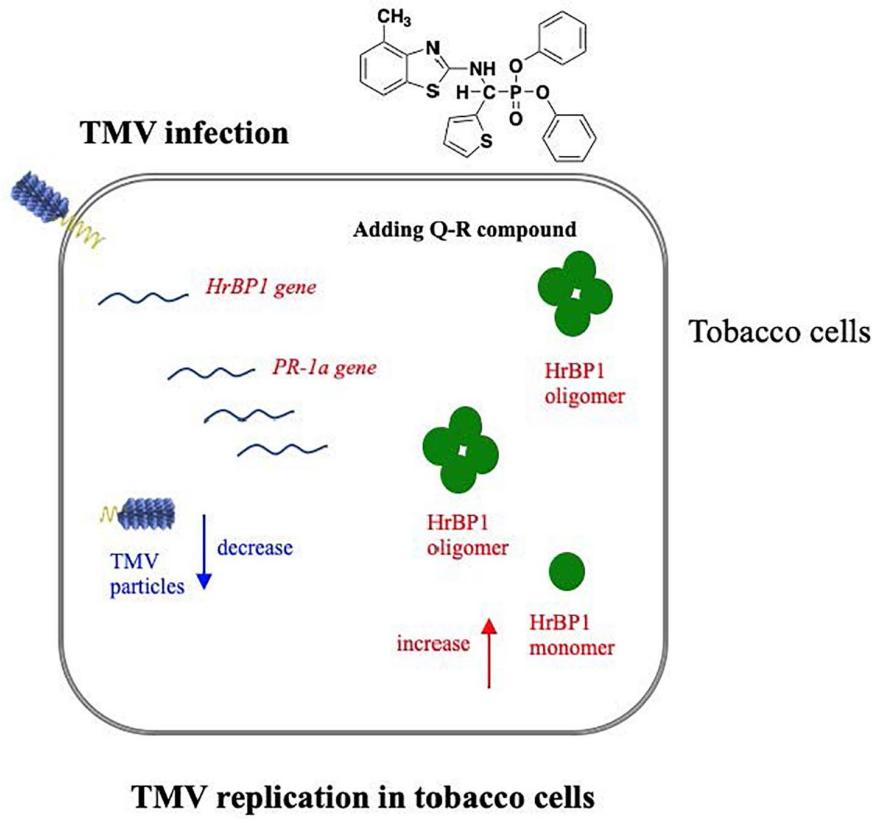

FIGURE 6 | Hypothetical pathway wherein the HrBP1 protein of tobacco plant was induced by Q-R through promotes the expression of the *HrBP1* and *PR-1a* genes in tobacco plants, which leads to Q-R induces antiviral responses and inhibits the duplication of TMV in TMV-infected tobacco plant. Red indicate the up-regulated genes/protein, blue indicate the down-regulated genes/protein.

Expression and Purification of HrBP1 Using the pET28a Vector

To obtain sufficient quantities of HrBP1 protein for further analyses, we designed the pET28a expression vector including the HrBP1 gene and transformed it into *E. coli* strain BL21(DE3). The expressed protein was supported by SDS-PAGE analysis to be 30 kDa. The HrBP1 protein was overexpressed after exposure to 0.8 mM isopropyl-β-D-galactopyranoside (IPTG) at 16°C for 16 h (**Figures 3C,D**). The expressed HrBP1 proteins (approximately 90%) was purified and concentrated on subsequent analysis.

Identification and Analysis of the Expressed HrBP1 Protein

To further determine the amino acid composition of the expressed HrBP1 protein through a polypeptide analysis. The 18.1% fraction of the obtained polypeptide fragments covered the entire 276 amino acids, and the sequence was equally expected.

The SEC results showed that the HrBP1 recombinant protein was an oligomer. The HrBP1 protein was elected and calculated to be approximately 180 kDa based on a reference size (**Figure 3C**). The SDS-PAGE analysis results showed that the size of the collected protein was approximately 30 kDa (**Figure 3D**), which indicated that the HrBP1 oligomer was destroyed by SDS *in vitro*.

Interactions Between Q-R and the HrBP1 Protein

To examine the interaction between Q-R and the HrBP1 protein, we analyzed the binding affinity between Q-R to HrBP1 protein using ITC. The binding affinity with Q-R to the HrBP1 protein was stronger than that of the control of antiviral agents BTH and dufulin. Q-R on the HrBP1 protein had a Kd value of 1.19 μM (8.43×10^5 mol^{-1}, **Figures 4A,B**). The titration data indicated an apparent negative enthalpy values ($\Delta G \approx -8.08$) during the binding of Q-R to the HrBP1 protein. While no binding occurred between the BTH and HrBP1 protein (**Figures 4A,C**), and weak binding occurred between the dufulin and HrBP1 protein (**Figures 4A,D**). Thus, the HrBP1–Q-R complex was stable, implying that Q-R had the ability to bind the HrBP1 protein.

Confirmation of the Protein-Ligand Interactions Between Q-R and HrBP1

To confirm the interaction between Q-R and the HrBP1 protein, we analyzed the HrBP1 protein's state of aggregation after being treated by Q-R using the SEC. Q-R induced the assembly of

a large HrBP1 protein oligomer. Briefly, the HrBP1 protein formed functional aggregates. After adding Q-R, the protein samples were examined by SEC. We further assessed the effects of Q-R on the biochemical properties of the HrBP1 protein. As expecting, the HrBP1 protein was present in a large aggregated state (**Figure 5**). Thus, we deduced that Q-R induces the assembly of the HrBP1 protein and the further formation of the HrBP1–Q-R complex (**Figure 6**), which agreed with the ITC studies.

CONCLUSION

In summary, our study clarified the mechanism by which Q-R produces antiviral responses associated with the HrBP1 protein expressed in *E. coli* (*In vitro*) and tobacco plants (*In vivo*). *In vitro*, a strong affinity existed on Q-R and the HrBP1 protein. *In vivo*, Q-R promoted the expression of the HrBP1 gene in tobacco plants. Thus, Q-R produces antiviral responses by activating the HrBP1 gene and protein in tobacco plants.

DATA AVAILABILITY STATEMENT

The data presented in the study are deposited in the NCBI repository, accession number MW256718.

AUTHOR CONTRIBUTIONS

XL designed this study. MH carried out the clone and protein expression studies, participated in the sequence alignment, and drafted the manuscript. YY, LW, JC, and TL performed MST and qPCR tests. XX and XL critically revised the manuscript. All authors read and approved the final version of the manuscript.

FUNDING

This work was supported by the National Key Research and Development Program of China (No. 2017YFD0200503-3), the National Natural Science Foundation of China (No. 31960546), and Program of Introducing Talents of Discipline to Universities of China (111 Program, D20023).

ACKNOWLEDGMENTS

We thank International Science Editing (http://www.internationalscienceediting.com) for editing this manuscript.

SUPPLEMENTARY MATERIAL

The Supplementary Material for this article can be found online at: https://www.frontiersin.org/articles/10.3389/fmicb.2021.621875/full#supplementary-material

Supplementary Figure 1 | Nucleotide sequence and amino acid sequence of *HrBP1* sequence from *Nicotiana tabacum*.

Supplementary Table 1 | Primer sequences used in qPCR.

REFERENCES

Aljaafri, W. A., McNeece, B. T., Lawaju, B. R., Sharma, K., Niruala, P. M., Pant, S. R., et al. (2017). A harpin elicitor induces the expression of a coiled-coil nucleotide binding leucine rich repeat (CC-NB-LRR) defense signaling gene and others functioning during defense to parasitic nematodes. *Plant Physiol. Biochem.* 121, 161–175. doi: 10.1016/j.plaphy.2017.10.004

Camehl, I., Sherameti, I., Venus, Y., Bethke, G., Varma, A., Lee, J., et al. (2010). Ethylene signalling and ethylene-targeted transcription factors are required to balance beneficial and nonbeneficial traits in the symbiosis between the endophytic fungus Piriformospora indica and *Arabidopsis thaliana*. *New Phytol.* 185, 1062–1073. doi: 10.1111/j.1469-8137.2009.03149.x

Chen, Z., Chen, B. H., Guo, Q., Shi, L., He, M., Qin, Z., et al. (2015). A Time-course proteomic analysis of rice triggered by plant activator BTH. *J. Plant Growth Regul.* 34, 392–409. doi: 10.1007/s00344-015-9476-y

Chen, Z., Zeng, M. J., Song, B. A., Hou, C., Hu, D., Li, X., et al. (2012). Dufulin activates HrBP1 to produce antiviral responses in tobacco. *PLoS One* 7:e37944. doi: 10.1371/journal.pone.0037944

El-Maarouf, H., Barny, M. A., Rona, J. P., and Bouteau, F. (2001). Harpin, a hypersensitive response elicitor from *Erwinia amylovora*, regulates ion channel activities in Arabidopsis thaliana suspension cells. *FEBS Lett.* 497:82. doi: 10.1016/S0014-5793(01)02441-3

Gao, D., Wang, D. M., Chen, K., Huang, M., Xie, X., and Li, X. (2019). Activation of biochemical factors in CMV-infected tobacco by ningnanmycin. *Pest. Biochem. Physiol.* 156, 116–122. doi: 10.1016/j.pestbp.2019.02.012

Gooding, G. J., and Hebert, T. T. (1967). A simple technique for purification of tobacco mosaic virus in large quantities. *Phytopathology* 57:1285. doi: 10.1098/rstl.1767.0047

Gopalan, S. (2008). Reversal of an immunity associated plant cell death program by the growth regulator auxin. *BMC Res.* 1:126. doi: 10.1186/1756-0500-1-126

Huntley, R. P., Sawford, T., Mutowo-Meullenet, P., Shypitsyna, A., Bonilla, C., Martin, M. J., et al. (2014). The GOA database: gene ontology annotation updates for 2015. *Nucleic Acid Res.* 43, 1057–1063. doi: 10.1093/nar/gku1113

Kumar, R. R., Singh, G. P., Goswami, S., Pathak, H., and Rai, R. D. (2014). Proteome analysis of wheat (*Triticum aestivum*) for the identification of differentially expressed heat-responsive proteins. *Aus. J. Crop Sci.* 8, 973–986.

Lawaju, B. R., Lawrence, K. S., Lawrence, G. W., and Klink, V. P. (2018). Harpin-inducible defense signaling components impair infection by the ascomycete *Macrophomina phaseolina*. *Plant Physiol. Biochem.* 129, 331–348. doi: 10.1016/j.plaphy.2018.06.020

Lee, J., Klessig, D. F., and Nürnberger, T. (2001). A harpin binding site in tobacco plasma membranes mediates activation of the pathogenesis-related gene HIN1 independent of extracellular calcium but dependent on mitogen-activated protein kinase activity. *Plant Cell* 13, 1079–1093. doi: 10.1105/tpc.13.5.1079

Li, X. Y., Liu, J., Yang, X., Ding, Y., Wu, J., Hu, D., et al. (2015a). Studies of binding interactions between dufulin and southern rice black-streaked dwarf virus P9-1. *Bioorg. Med. Chem.* 23, 3629–3637. doi: 10.1016/j.bmc.2015.04.008

Li, X. Y., Song, B. A., Chen, X., Wang, Z. C., Zeng, M. J., Yu, D. D., et al. (2013). Crystal structure of a four-layer aggregate of engineered TMV CP implies the importance of terminal residues for oligomer assembly. *PLoS One* 8:e77717. doi: 10.1371/journal.pone.0077717

Li, X. Y., Zhang, W. Y., Ding, Y., Wang, Z., Wu, Z., Yu, L., et al. (2015b). Characterization of the importance of terminal residues for southern rice black-streaked dwarf virus P9-1 viroplasm formations. *Pro. Exp. Purif.* 111, 98–104. doi: 10.1016/j.pep.2015.04.003

Liu, F. Q., Liu, H. X., Jia, Q., Wu, X., Guo, X., Zhang, S., et al. (2006). The internal glycine-rich motif and cysteine suppress several effects of the HpaGXooc protein in plants. *Phytopathology* 96, 1052–1059.

Livak, K. J., and Schmittgen, T. D. (2001). Analysis of relative gene expression data using real-time quantitative PCR and the 2(-delta delta c(t)) method. *Methods* 25, 402–408. doi: 10.1006/meth.2001.1262

MacLean, B., Tomazela, D. M., Shulman, N., Chambers, M., Finney, G. L., Frewen, B., et al. (2010). Skyline: an open source document editor for creating and analyzing targeted proteomics experiments. *Bioinformatics* 26, 966–968.

Peng, J. L., Dong, H. S., Dong, H. P., Delaney, T. P., Bonasera, J. M., and Beer, S. V. (2003). Harpin-elicited hypersensitive cell death and pathogen resistance require the NDR1 and EDS1 genes. *Physiol. Mol. Plant Pathol.* 62, 317–326. doi: 10.1016/S0885-5765(03)00078-X

Penmetsa, R. V., Uribe, P., Anderson, J., Lichtenzveig, J., Gish, J. C., Woo, Y., et al. (2008). The *Medicago truncatula* ortholog of *Arabidopsis* EIN2, SICKLE, is a negative regulator of symbiotic and pathogenic microbial associations. *Plant J.* 55, 580–595. doi: 10.1111/j.1365-313X.2008.03531.x

Shi, J., Yu, L., and Song, A. B. (2018). Proteomics analysis of xiangcaoliusuobingmi-treated *Capsicum annuum* L. infected with cucumber mosaic virus. *Pestic. Biochem. Physiol.* 149, 113–122. doi: 10.1016/j.pestbp.2018.06.008

Sleiman, M., Claire, P. D. S., and Richard, C. (2017). Heterogeneous photochemistry of agrochemicals at the leaf surface: a case study of plant activator acibenzolar-S-methyl. *J. Agric. Food. Chem.* 65, 7653–7660. doi: 10.1021/acs.jafc.7b02622

Song, B. A., Yang, S., Jin, L. H., and Bhadury, S. (2009). *Environment Friendly Anti-plant Viral Agent*. Berlin: Springer Press, 234–253.

Wang, D. M., Xie, X., Gao, D., Chen, K., Chen, Z., Jin, L., et al. (2019). Dufulin intervenes the viroplasmic proteins as the mechanism of action against southern rice black-streaked dwarf virus. *J. Agric. Food Chem.* 67, 11380–11387. doi: 10.1021/acs.jafc.9b05793

Wang, K. L., Li, H., and Ecker, J. R. (2002). Ethylene biosynthesis and signaling networks. *Plant Cell* 14, 131–151. doi: 10.1105/tpc.001768

Yang, A. M., Yu, L., Zhuo, C., Zhang, S., Shi, J., Zhao, X., et al. (2017). Label-free quantitative proteomic analysis of chitosan oligosaccharide-treated rice infected with southern rice black-streaked dwarf virus. *Viruses J.* 9:115. doi: 10.3390/v9050115

Yu, L., Wang, W. L., Zeng, S., Chen, Z., Yang, A., Shi, J., et al. (2018). Label-free quantitative proteomics analysis of cytosinpeptidemycin responses in southern rice black-streaked dwarf virus-infected rice. *Pestic. Biochem. Physiol.* 147, 20–26. doi: 10.1016/j.pestbp.2017.06.005

Zhang, G. P., Hao, G. F., Pan, J. K., Zhang, J., Hu, D., and Song, B. (2016). Asymmetric synthesis and bioselective activities of α-amino-phosphonates based on the dufulin motif. *J. Agric. Food Chem.* 64, 4207–4213. doi: 10.1021/acs.jafc.6b01256

Zhang, W. Y., Li, X. Y., Zhang, G. P., Ding, Y., Ran, L., Luo, L., et al. (2017). Binding interactions between enantiomeric-aminophosphonate derivatives and tobacco mosaic virus coat protein. *Int. J. Biol. Macromol.* 94(Pt A), 603–610. doi: 10.1016/j.ijbiomac.2016.10.027

Conflict of Interest: The authors declare that the research was conducted in the absence of any commercial or financial relationships that could be construed as a potential conflict of interest.

frontiers in Microbiology

ORIGINAL RESEARCH
published: 25 March 2021
doi: 10.3389/fmicb.2021.650099

Genetic Causes of Non-pathogenic *Pseudomonas syringae* pv. *actinidiae* Isolates in Kiwifruit Orchards

Yue Li[1†], Qiaomei Zhu[1†], Taihui Zhi[1], Rong Fan[2], Ting Xie[1], Zhibo Zhao[1,2], Youhua Long[2*] and Zhong Li[1]*

[1] Department of Plant Pathology, College of Agriculture, Guizhou University, Guiyang, China, [2] Kiwifruit Engineering and Technology Research Center, Guizhou University, Guiyang, China

Bacterial canker disease has become the largest threat to kiwifruit cultivation and production. A monomorphic subpopulation of *Pseudomonas syringae* pv. *actinidiae* biovar 3 (Psa3) is responsible for the pandemic worldwide. Diversity in pathogenicity has been found in the pandemic subpopulation and in other Psa3 subpopulations causing epidemics in China. However, the genetic bases have not yet been elucidated. In this study, 117 Psa3 isolates were identified by Psa- and Psa3-specific primers, and evaluated for pathogenicity. Three isolates G4, G40, and S2 are not pathogenic to kiwifruit and do not elicit hypersensitivity responses (HRs) in non-host *Nicotiana benthamiana* leaves. Two isolates, G25 and G35, exhibited attenuated HR-eliciting activity in non-host *N. benthamiana*, but they exhibited greatly and slightly reduced pathogenicity in host plants, respectively. The genomes of the five isolates were sequenced and compared with closely related isolates revealed by MLVA and whole-genome typing methods. The candidate genetic loci responsible for the changes in pathogenicity and HR elicitation, were further evaluated by allele replacement experiments. We found that the three non-pathogenic isolates were formed due to the independent, identical insertion events of ISPsy36 transposon in the *hrpR* gene, encoding a key regulator of type III secretion system (T3SS) and type III effectors (T3Es). In the symptomatic sample from which G4 was isolated, 27% HR negative isolates were detected. In isolate G25, transposon insertion of ISPsy32 at the non-coding sequence upstream of the *hrpR* gene was detected, similar to a previously reported low-virulent Psa3 strain M227. In isolate G35, we detected disruptions of T3Es hopBB1-1 and hopBB1-2, which induce HR in *N. benthamiana* leaves revealed by *Agrobacterium tumefaciens* infiltration. These phenotype-changed isolates were formed at low frequencies during the course of pathogen infection in host plants, supported by the binding assay of ISPsy32 and the non-coding DNA sequences upstream of the *hrpR* gene, the co-isolation of the virulent isolates belonging to the same MLVA clade, and the low levels of transcription of the transposon genes. Taken together, in terms of short-term field evolution, transposon insertions in the T3SS-related genes resulted in the formation of non-pathogenic and low-virulent Psa3 isolates.

Keywords: non-pathogenic, bacterial canker of kiwifruit, transposable elements, comparative genomics, T3SS, *hrpR*

OPEN ACCESS

Edited by:
Amin Uddin Mridha, University of Chittagong, Bangladesh

Reviewed by:
Joel L. Vanneste, The New Zealand Institute for Plant and Food Research Ltd., New Zealand
Jose Sebastian Rufian, Chinese Academy of Sciences (CAS), China

***Correspondence:**
Zhibo Zhao
zbzhao@gzu.edu.cn
Youhua Long
gzlyh126@126.com

† These authors have contributed equally to this work and share first authorship

Specialty section:
This article was submitted to Microbe and Virus Interactions with Plants, a section of the journal Frontiers in Microbiology

Received: *06 January 2021*
Accepted: *08 March 2021*
Published: *25 March 2021*

Citation:
Li Y, Zhu Q, Zhi T, Fan R, Xie T, Zhao Z, Long Y and Li Z (2021) Genetic Causes of Non-pathogenic Pseudomonas syringae pv. actinidiae Isolates in Kiwifruit Orchards. Front. Microbiol. 12:650099. doi: 10.3389/fmicb.2021.650099

INTRODUCTION

Kiwifruit (*Actinidia* spp.) is an economically important fruit plant cultivated in many countries, such as New Zealand, China, and Italy. However, bacterial canker disease, caused by *Pseudomonas syringae* pv. *actinidiae* (Psa) has spread across all the key kiwifruit production areas, and represents the largest threat to kiwifruit cultivation and production (Vanneste, 2017). Many efforts have been made to uncover the population structure of Psa, and at least five biovar populations (biovar 1, 2, 3, 5, and 6) within Psa has been identified, of which biovar 3 (Psa3) is responsible for the global pandemic (Vanneste et al., 2013; McCann et al., 2017; Sawada and Fujikawa, 2019). These biovars diverged many years ago and became distributed in different countries. For instance, the first recorded population, biovar 1, was detected in Japan, Italy, and Korea, and now is widely distributed in Japan; biovar 2 was only found in Korea, and biovars 5 and 6 occurred on a small scale in Japan (Sawada and Fujikawa, 2019).

Psa3 was thought to be the most aggressive biovar to kiwifruit, and remarkable differences in the composition of pathogenicity-related genes among these biovars have been observed (McCann et al., 2013). However, the molecular mechanisms underlying the emergence and rapid spread of Psa3 has not been fully elucidated. Psa3 was found in China in 1986 and has formed several distinct clonal-complexes related to geographical distribution (McCann et al., 2017; He et al., 2019; Zhao et al., 2019b). Notably, variations in pathogenicity were observed amongst strains within each genetically monomorphic clonal-complex, and the pathogenic determinants of Psa3 might be identified via a genomic comparison of phenotypically different strains within each clade (Zhao et al., 2019a). Similarly, the global clade within Psa3 which emerged in Italy in 2008, is genetically monomorphic (McCann et al., 2017), but an increase of virulence and genetic diversity of the Psa3 strains in Northern Italy has been described (Prencipe et al., 2018). Fitness increases of plant bacterial pathogen within host has been evidenced by experimental evolution as well (Guidot et al., 2014; Perrier et al., 2016). This supports the notion that Psa3 has evolved rapidly in agricultural ecosystems.

Genotypic diversity has been shown to arise within clonal populations during plant colonization by *P. syringae* (Barrett et al., 2011; Lovell et al., 2011; Bartoli et al., 2015). During the initial infection, non-pathogenic variants might benefit from co-existence with virulent pathogens (Barrett et al., 2011; Rufián et al., 2018). Non-pathogenic isolates may be the products of negative mutations during short-term evolution of the pathogen, and may be eliminated quickly due to their poor survivability in host plants. However, loss-of-function was also thought to be an adaptive strategy for pathogens and can be strongly selected *in planta* (Hottes et al., 2013; Perrier et al., 2016; Peyraud et al., 2016). For instance, the non-pathogenic variants in *Ralstonia solanacearum* populations exhibited better growth than their wild-type ancestor *in planta* (Peyraud et al., 2016; Perrier et al., 2019). The underlying genetic causes for the formation of non-pathogenic variants may provide clues for their biological significance. Meanwhile, non-pathogenic Psa3 isolates can be used for identification of pathogenic determinants of Psa3.

In this study, we obtained 117 Psa3 isolates from 15 kiwifruit orchards in China, and evaluated their pathogenicity in kiwifruit plants and their ability to elicit hypersensitivity responses (HRs) in non-host *Nicotiana benthamiana* leaves. The genetic causes of the non-pathogenic and reduced virulence isolates within Psa3 were identified by comparative genomics, and further evidenced by allele replacement experiments. The driving factor underlying the emergence of non-pathogenic variants, and the interaction between pathogenic and non-pathogenic variants within the host are discussed.

MATERIALS AND METHODS

Plants, Bacterial Strains, and Growth Conditions

N. benthamiana plants and 3-years-old pot-grown plants of kiwifruit (*Actinidia chinensis* var. *chinensis* cultivar "Hongyang") were cultivated in a phytotron at 24°C with a 12-h day/night cycle.

The Psa3 strains ICMP 18884 (Genome accessions CP011972.2, CP011973.1) and M227 (WGS accession MDXF01) were used in comparative genomic analyses. The 117 Psa3 isolates were identified from the symptomatic canes, leaves, and flowers of kiwifruit with bacterial canker disease as previously described (Zhao et al., 2013). The bacteria were grown in Luria–Bertani (LB) medium at 25°C for Psa strains, 28°C for *Agrobacterium tumefaciens* strains, and 37°C for *Escherichia coli* strains with appropriate antibiotics. The following concentrations (mg/L) of antibiotics were used: kanamycin, 50; nalidixic acid, 10; and ampicillin, 100. When necessary, Psa was cultured in HDM (*hrp*-derepressing medium) (Stauber et al., 2012), mimicing *in-planta* conditions, at 25°C.

MLVA and Whole-Genome Typing for the Psa3 Isolates

The 117 Psa3 isolates were confirmed by PCR detection methods using the Psa-specific primers PsaF/R (Balestra et al., 2013) and Psa3-specific primers P0F/P6R (Gallelli et al., 2014). All the isolates were clustered by a previously established Multilocus Variable-Number of Tandem Repeats (VNTR) Analysis (MLVA) method (Zhao et al., 2019b). Briefly, 10 VNTR-related DNA products were PCR amplified for each isolate, and the repeat number in each locus was determined by capillary electrophoresis using a high-resolution automatic electrophoresis platform Qsep-1 (Bioptic Inc., Taiwan, China). The majority UPGMA tree was constructed by BioNumerics software (version 8.0; Applied Maths, St-Martens-Latem, Belgium) based on MLVA data for 117 Psa3 isolates. The genome tree was built based on the bulk of non-recombination SNPs from the genomic data of 57 representative Psa3 isolates, of which 14 were included in the MLVA analyses, using the panX pipeline (Ding et al., 2018).

Pathogenicity Assays and Bacterial Infiltration in *N. benthamiana* Leaves

Pathogenicity tests of the Psa3 isolates were performed according to previously described methods: (1) wound inoculation on

detached dormant kiwifruit canes with 10^8 CFU/mL bacteria, (2) vacuum infiltration inoculation on leaf discs with 10^4 CFU/mL bacteria (Zhao et al., 2019a). At least 15 canes or leaves were used in a pathogenicity trial, and the disease rating for each strain was calculated as a mean for three independent trials. Based on the pathogenicity data, a hierarchical cluster analysis was performed with the Ward's method in SPSS 19.0. Analysis of variance (ANOVA) was performed to compare pathogenicity between strains using SPSS 19.0.

To test the ability to elicit HR in non-host plants, Psa3 isolates and mutants were cultured, suspended in 10 mM $MgCl_2$ solution, and infiltrated into the upper leaves of 4-weeks-old *N. benthamiana* plants. The bacterial concentrations of the isolates used in the infiltration assay were designated in the figure legends.

Agro-infiltration assays were carried out following a previously described procedure (Zhao et al., 2019a). The *A. tumefaciens* strain GV3101 carrying an expression plasmid (pCAMIBA1300-effector) was cultured and infiltrated into *N. benthamiana* leaves. Cell death symptoms were evaluated and photographed after trypan blue staining 3–4 days post infiltration. Each assay was performed in triplicate.

DNA Insertion and Mutant Generation

We performed comparative genomics as previously described (Zhao et al., 2019a). The candidate loci relating to pathogenicity were confirmed by allele replacement assays. The ISPsy36 transposon were naturally inserted at the 573-bp inside of *hrpR* gene, so we artificially inserted an 841-bp *gfp* fragment at the same location of the *hrpR* gene in the high-virulent Psa3 isolate G1, resulting in a mutant G1-*gfp*. The mutant was constructed using a previously described *SacB*-based unmarked mutagenesis method (Kvitko and Collmer, 2011; Zhao et al., 2019a). Briefly, a 2,499 bp fusion DNA fragment containing an 873 bp upstream flank (using primers hrpRN-F/R), an 841 bp *gfp* fragment amplified from pDSK-GFPuv (using primers gfpF/R) (Wang et al., 2007), and a 784 bp downstream flank (using primers hrpRC-F/R), was constructed by crossover-PCR and subsequently cloned into the *EcoR1*/*Hin*dIII sites on the suicide plasmid pK18*mobSacB*. Then, the fragment replaced the corresponding sequence in G1 as described in Zhao et al. (2019a), resulting in a mutant designated G1-*gfp*. The mutant was confirmed by PCR using hrpR_RTF/R primers and fluorescence using a NIKON CI-E + Ri2 fluorescence microscope (Nikon Instruments, Japan). The genes *hopBB1-1* (IYO_003727 in CP011972.2) and *hopBB1-2* (IYO_003675 in CP011972.2) were PCR amplified from G1 and inserted in the *Nde*I/*Pst*I locus of *Pseudomonas*-expressing plasmid pDSK-GFPuv (Wang et al., 2007), and the recombinant plasmids were electro-transformed into Psa3 isolate G35, resulting in overexpression mutants G35 pHopBB1-1 and G35 pHopBB1-2.

qRT-PCR Analysis of Gene Expression

Bacteria were cultured in KB at the designated 0 h, and subsequently transferred into HDM medium with a final concentration of 0.02 OD_{600}. The bacteria were sampled at the designated time and pretreated using the RNAprotect Bacteria Reagent (Qiagen). The total RNA was extracted with the RNeasy Protect Bacteria Mini kit (Qiagen). RNA integrity was evaluated by capillary electrophoresis with Qsep-1 (Bioptic Inc., Taiwan, China), and reverse transcription of the RNAs was performed with the RevertAid RT Reverse Transcription Kit (Thermo Fisher Scientific™). Quantitative real time PCR was performed in a thermal cycler (CFX96, BioRad Inc., United States) using Fast SYBR™ Green Master Mix (Applied Biosystems). Two house-keeping genes *gyrA* and *gyrB*, which constitutively expressed in bacteria, were used as the internal control in the RT-PCR examination. Primers used for qPCR are listed in **Supplementary Table 1**. Three replicates were performed for each sample. The relative expression levels of the *hrpL* gene of G1, G4, and G1-*gfp*, cultured in HDM, were analyzed using the $2^{-\Delta\Delta CT}$ method (Livak and Schmittgen, 2001).

DNA Pull-Down Assay

This assay was carried out as described previously (Jutras et al., 2012). Briefly, the 1,076-bp non-coding DNA sequence upstream of the *hrpR* gene in Psa3 isolate G1 was synthesized and labeled by desthiobiotin at the 5′-end. The bioinylated DNA probe then bound to the Streptavidin-coated magnetic beads (Dynabeads M-280, Invitrogen), and the probe-bead complex was incubated with the cytoplasmic extracts of G1 cultivated in HDM. Finally, the probe-bead-protein complex was eluted and detected by SDS-PAGE. The binding proteins were identified by LC-MS/MS on a TripleTOF 5600 plus mass spectrometer (AB Sciex, Framingham, MA) coped with an ProteinPilot 5.0v software in Lianchuan Bio-company (Hangzhou, China).

RESULTS

Diverse Clonal Populations Within Psa3 Spreading in China

We identified 108 Psa3 isolates from an emerging kiwifruit cultivation region in China (Guizhou Province), and 9 Psa3 isolates from the largest kiwifruit cultivation region in the country (Shaanxi Province), in which the Psa3 population has been extensively investigated (Zhao et al., 2019a). All 117 isolates were confirmed as Psa3 by Psa- and Psa3-specific primers. We then evaluated the genetic diversity of Psa3 in the emerging region using a previously established MLVA method (Zhao et al., 2019b), and found 3–4 clonal populations in each area (**Figure 1**). The clustering result was further supported by whole-genome analysis (**Figure 2**). Seven clonal populations, which differed from each other with 200–300 non-recombinant SNPs at the genomic-wide level, have been described in China (McCann et al., 2017; Zhao et al., 2019a), and a novel clonal population, MLVA clade 8, was identified in this study. The clustering information was furthered used for the selection of reference strains in the subsequent comparative genomics between high and low (or non-) pathogenic isolates, and also for tracking the formation of the non-pathogenic isolates.

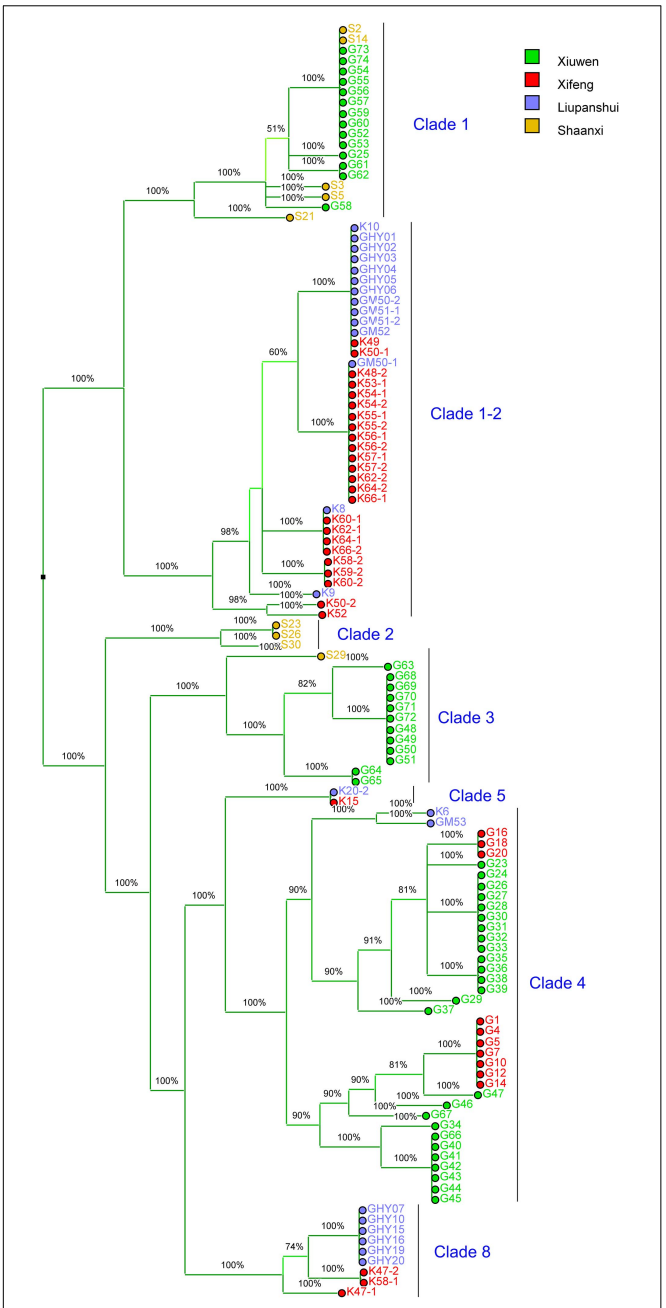

FIGURE 1 | Majority UPGMA dendrogram constructed using Bionumerics 8.0 software based on MLVA data for 117 *Pseudomonas syringae* pv. *actinidiae* biovar 3 isolates from Guizhou and Shaanxi Province, China. The MLVA clustering method is as per Zhao et al. (2019b). The colored squares indicate the geographical source of the isolates. Xiuwen, Xifeng and Liupanshui are three main kiwifruit cultivating areas in Guizhou Province. The clade-populations are designated based on both MLVA typing results and whole-genome analysis.

Three Non-pathogenic and Two Virulence-Reduced Variants Identified

The pathogenicity test of the 54 Psa3 isolates revealed variations in pathogenicity within each of the clonal populations (**Figure 3A**). Three isolates G4, G40, and S2 are not pathogenic, and two isolates G42 and G25 are less virulent to kiwifruit leaves (**Figure 3B**). The pathogenicity results were also evidenced on kiwifruit dormant canes using the wound inoculation method (**Figures 3C,D**). We further investigated the ability of the 117 isolates to elicit HR in non-host *N. benthamiana* leaves. None of the three non-pathogenic isolates showed any HR elicitation activity, while the two low-virulent isolates and another isolate G35 exhibited attenuated HR-eliciting activity in *N. benthamina* leaves (**Figure 4**). However, G35 showed moderate pathogenicity in host plants (**Figure 3**).

Genetic Causes of the Phenotypically Changed Isolates

To uncover the genetic causes of the phenotypically changed isolates, comparative genomics were performed. The genomes of the six isolates were sequenced, and the reference high-virulent isolates were selected according to the MLVA clustering tree. Isolates S2 and G25, belonging to the Clade-1 population, were compared with the high-virulent strains ICMP 18884 (McCann et al., 2013) and M7 (Zhao et al., 2019a); isolates G4, G40, G42, and G35, belonging to the Clade-4 population, were compared with G1.

In the three non-pathogenic isolates (S2, G4, and G40), the insertion events of 1,666-bp ISPsy36 transposon (IS1182 family) were detected at the same position (573-bp) of the *hrpR* gene (**Figure 5A**), encoding the key regulator of type III secretion system (T3SS) and type III effectors (T3Es). We artificially inserted an 841-bp *gfp* fragment in the same location of the *hrpR* gene in G1, resulting in a mutant G1-*gfp*. The mutant exhibited no pathogenicity on kiwifruit canes (**Figure 5B**), and lost the ability to elicit HR in *N. benthamina* leaves (**Figure 5C**). Given the presence of the "HrpR/S-HrpL-T3SS/T3Es" hierarchical regulatory cascade in *P. syringae* (Xie et al., 2019), we detected the *hrpL* transcripts of the three strains in HDM, mimicking *in-planta* conditions. As expected, *hrpL* transcription in G4 and G1-*gfp* were no longer induced in HDM (**Figure 5D**). These results indicated that the transposon disruption of the *hrpR* gene is the cause of the phenotype of the above-mentioned non-pathogenic isolates. Two Italian Psa3 isolates, IPV-BO 8893 and IPV-BO 9286, were hitherto shown to be HR negative, but the genetic causes were not identified (Biondi et al., 2017). We reviewed the genomic data of the two HR negative isolates, and found transposon-insertion events at the same location in the *hrpR* gene.

In the low-virulent isolate G25, insertion of an 1,176-bp ISPsy32 transposon (IS630 family) was detected upstream of the *hrpR* gene (**Figure 5A**), identical to a previously reported low-virulent strain M227 (Zhao et al., 2019a). The insertion caused disorder expression of the *hrpR/S* gene and resulted in attenuated expression and secretion of T3SS and T3Es (Zhao et al., 2019a). However, we could not identify the genetic cause of G42, which is phenotypically very similar to G25.

In the isolate G35, we found that two T3E genes, *hopBB1-1* and *hopBB1-2*, were incomplete. It has been reported that HopBB1-2 is localized in nucleocytoplasmic, and does not trigger

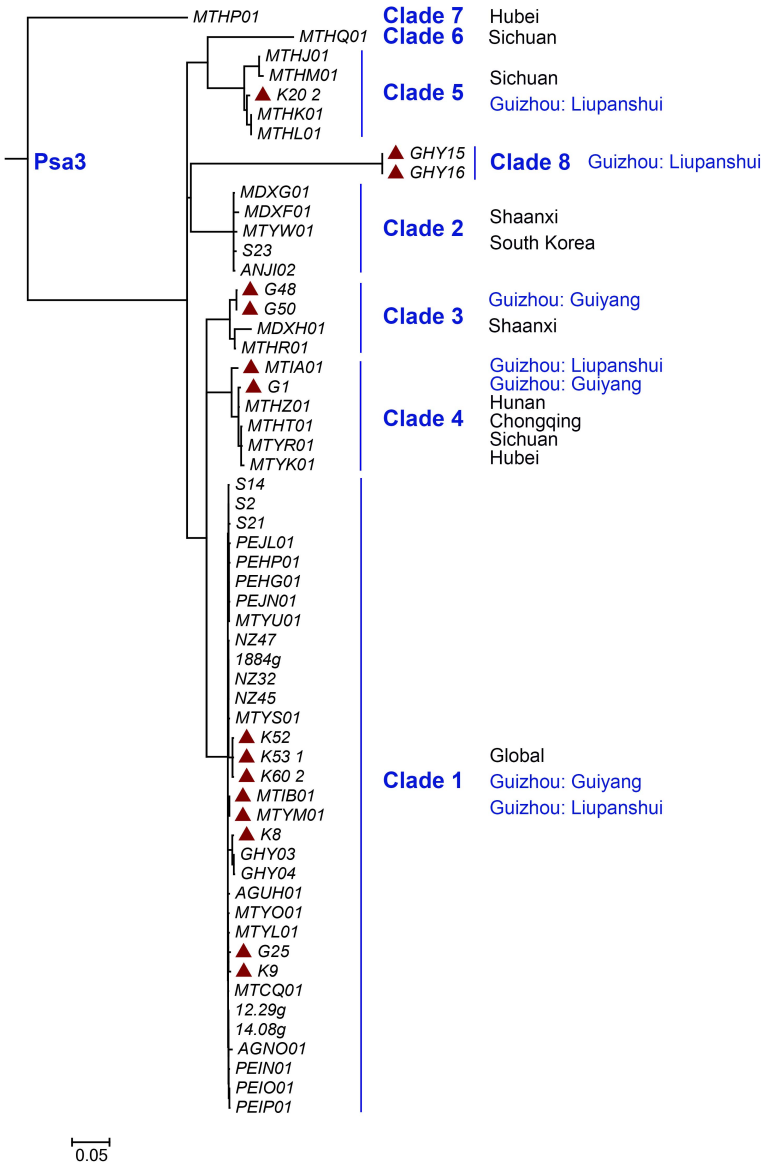

FIGURE 2 | Maximum likelihood tree of 57 representative isolates within *Pseudomonas syringae* pv. *actinidiae* biovar 3 (Psa3) based on whole genome data. The tree was built based on the bulk of non-recombination SNPs from Psa3 genome data using the panX pipeline (Ding et al., 2018). The red solid triangle indicates Psa3 strains from Guizhou Province, China.

HR in *N. benthamina* and *N. tabacum* Wisconsin 3 leaves (Choi et al., 2017). However, in this study we found that both HopBB1-1 and HopBB1-2 induced HR in *N. benthamiana* leaves (**Figure 6A**).Moreover, the G35 mutants expressing either *hopBB1-1* or *hopBB1-2* exhibited increased HR-eliciting activity (**Figure 6B**), but not pathogenicity (**Figures 6C,D**).

Phenotypically-Changed Psa3 Isolates Formed During the Course of Pathogen Infection

We investigated whether the phenotypically-changed isolates were formed during the course of pathogen infection. In the symptomatic sample from which G4 was isolated, 27% HR negative isolates were detected, and both HR-negative and HR-positive isolates showed identical MLVA typing data and genomic sequences (**Figure 1**). The HR-negative isolate G40 and HR-positive isolate G41 were co-isolated and showed identical MLVA patterns (**Figure 1**). This indicated that the HR negative clones were formed during the course of infection, and could reach a high population level in host tissue.

The phenotypically-changed Psa3 isolates were caused by the potential active transposons. There are 48 complete ISPsy32 and 14 complete ISPsy36 transposons, respectively, presented in the Psa3 strain ICMP 18884 (Genome accession no. CP011972.2). We performed an *in vitro* DNA pull-down assay to detect

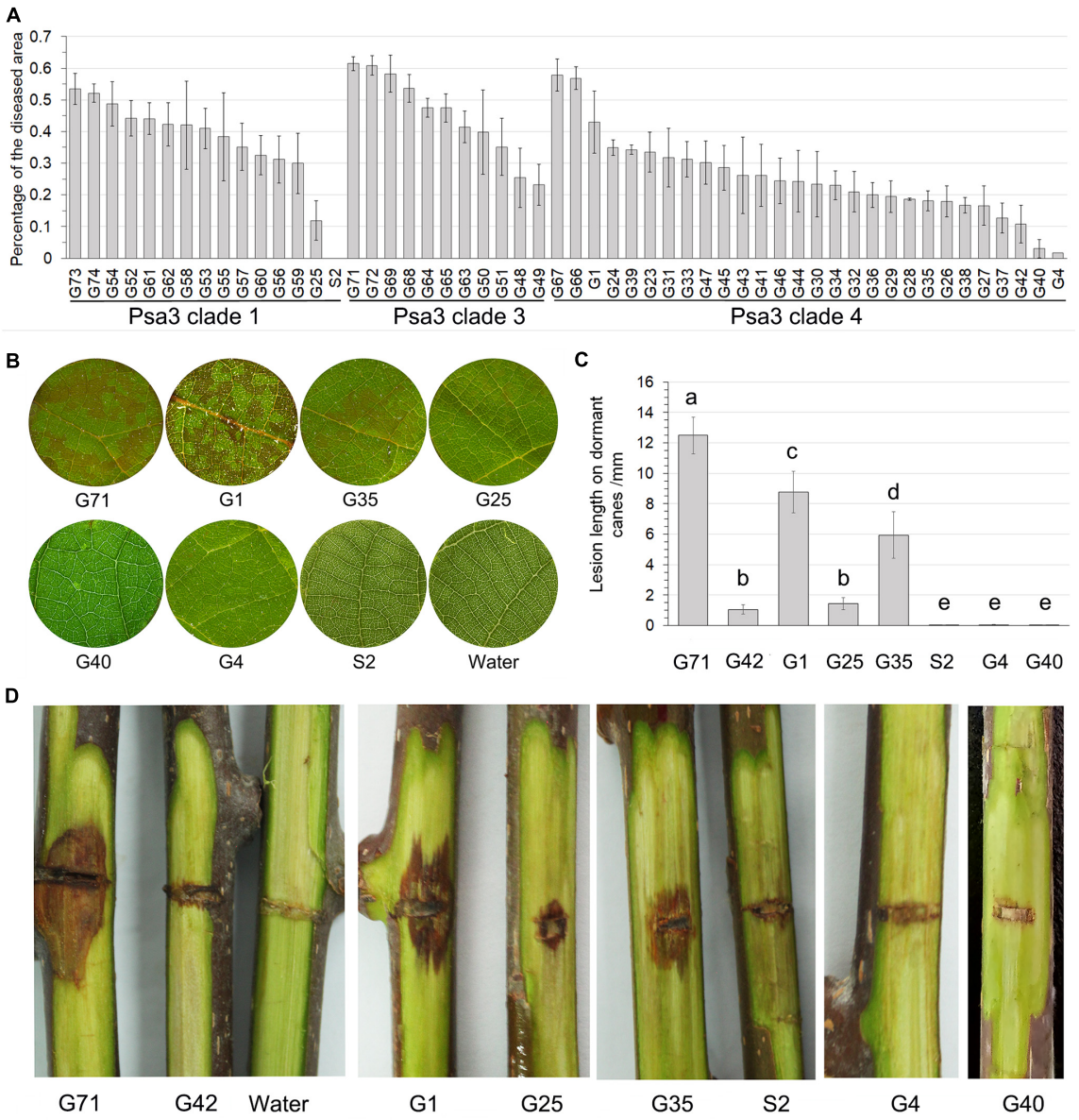

FIGURE 3 | Non-pathogenic and very low-virulent isolates within *Pseudomonas syringae* pv. *actinidiae* biovar 3 (Psa3) were identified. **(A)** Diverse pathogenicity of the Psa3 isolates. The pathogenicity patterns of 54 Psa3 isolates from Guizhou Province were determined using a vacuum-infiltration inoculation method on leaf discs of *Actinidia chinensis* var. *chinensis* "Hongyang." **(B)** Representative photographs of the non-pathogenic and very low-virulent isolates on kiwifruit leaf discs. **(C,D)** The pathogenicity of the non-pathogenic and very low-virulent isolates were confirmed by wound inoculation on detached dormant woody canes of kiwifruit cultivar "Hongyang." Values are means ± standard deviations (SDs). The experiments were repeated three times with similar results.

the proteins binding to the upstream non-coding sequence of the *hrpR* gene in G1, and identified two transposon-associated proteins, ISPsy32 (IS630 family) and ISPsy34 (IS66 family) (**Supplementary Table 3**).

DISCUSSION

An important issue in plant-microbe co-evolution is how pathogens evolve within crop plants in natural conditions, but very few studies have investigated the trajectories of pathogen evolution (Arnold and Jackson, 2011). The emergence of Psa3 in China in the 1980s, concomitant with domestication and cultivation of kiwifruit, offers a rare opportunity to understand the short-term evolution of the pathogen and the responding evolutionary factors (McCann et al., 2017; Zhao et al., 2019b). In terms of the evolution of bacterial pathogenicity, we focused on the non-pathogenic and very low-virulent Psa3 isolates formed in Chinese kiwifruit orchards, and investigated the genetic causes of these isolates. Our results revealed that

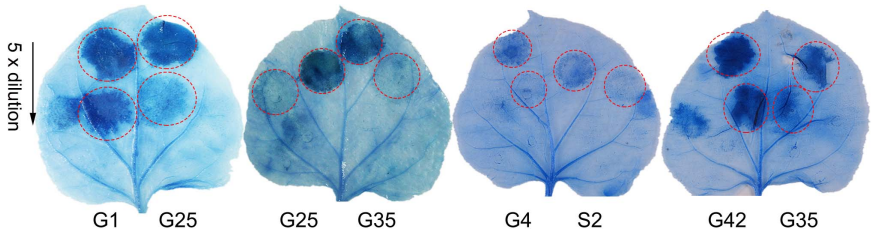

FIGURE 4 | Non-pathogenic and very low-virulent isolates within *Pseudomonas syringae* pv. *actinidiae* biovar 3 (Psa3) showed attenuated capacity to elicit a hypersensitivity response (HR) in non-host *Nicotiana benthamina* leaves. Four zones in half a leaf were injected with fivefold diluted bacteria (10^7 CFU/mL as the initial concentration), and three leaves from three independent plants were treated with each isolate. Photographs were taken 3 days post infiltration. Experiments were repeated at least twice with similar results.

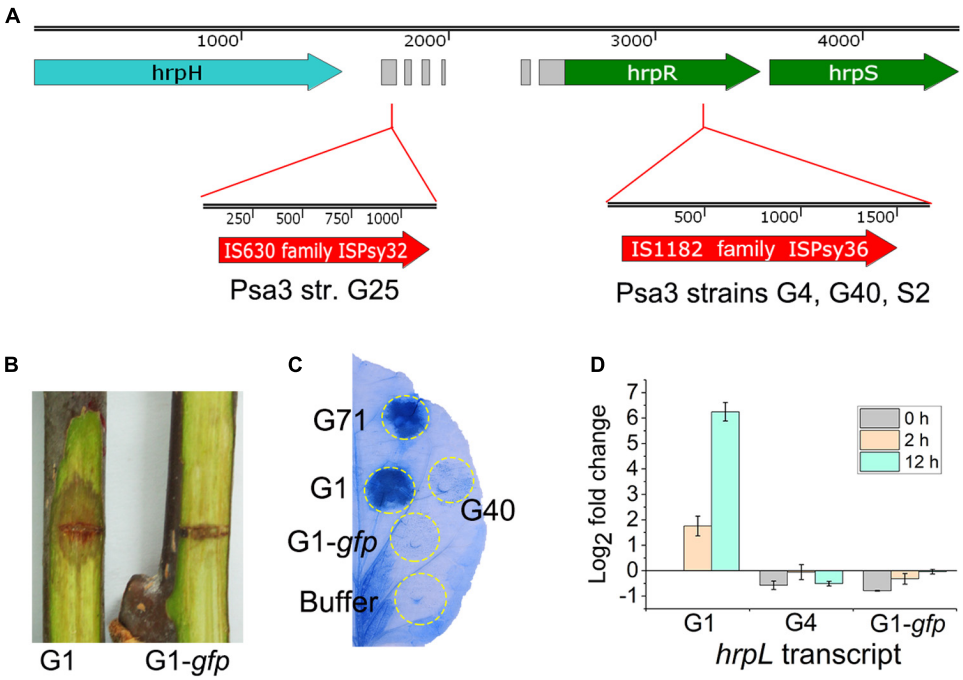

FIGURE 5 | Genetic causes of the phenotypically-changed isolates within *Pseudomonas syringae* pv. *actinidiae* biovar 3 (Psa3). **(A)** ISPsy32 and ISPsy36 were inserted in the conserved region upstream and inside the *hrpR* gene, resulting in the low-virulent and non-pathogenic Psa3 isolates, respectively. The gray modules between the *hrpH* and *hrpR* genes represent the conserved sequences among diverse *P. syringae* pathovars. **(B,C)** An artificial mutant G1-*gfp* exhibited no pathogenicity on kiwifruit canes, and lost the ability to elicit a hypersensitivity response (HR) in non-host *Nicotiana benthamina* leaves. G1-*gfp* was constructed by an 841-bp *gfp* fragment insertion in the same location (as the ISPsy36 insertion in G25) of the *hrpR* gene in the high-virulent isolate G1. The *N. benthamina* leaves were infiltrated with bacterial suspensions (10^8 CFU/mL) and photographed at 36-hour post infiltration. **(D)** The qRT-PCR results indicated that transcriptional patterns of the *hrpL* gene in G4 and G1-*gfp* were similar in the *hrp*-derepressing medium (HDM), while different from that of G1. Two house-keeping genes *gyrA* and *gyrB*, which constitutively expressed in bacteria, were used as the internal control. The experiments were repeated three times with similar results.

transposition events of the transposable elements (TEs) in the T3SS cluster were leading causes for these phenotypically-changed isolates.

Independent, Identical TE Transposition Events Occurred During Pathogen Infection

The non-pathogenic Psa3 isolates were isolated in geographically different places, and were categorized into different MLVA clades (**Figure 1**). For instance, isolates G4 and G40 within the Clade-4 population, and S2 within Clade-1, were formed in two kiwifruit cultivated regions (Guizhou and Shaanxi Province), respectively (**Figure 1**). However, their changed phylotype and also a previously reported HR negative isolate in Italy (Firrao et al., 2018), were caused by identical transposition events of ISPsy36. Meanwhile, independent transposition events of ISPsy32 were found in the two low-virulent Psa3 isolates G25 and M227. The low-virulent G25 within Clade-1 and M227 within Clade-2 were isolated from Guizhou Province and Shaanxi Province, respectively (**Figure 2**). This is very interesting that the same mobile element was inserted at the exact same

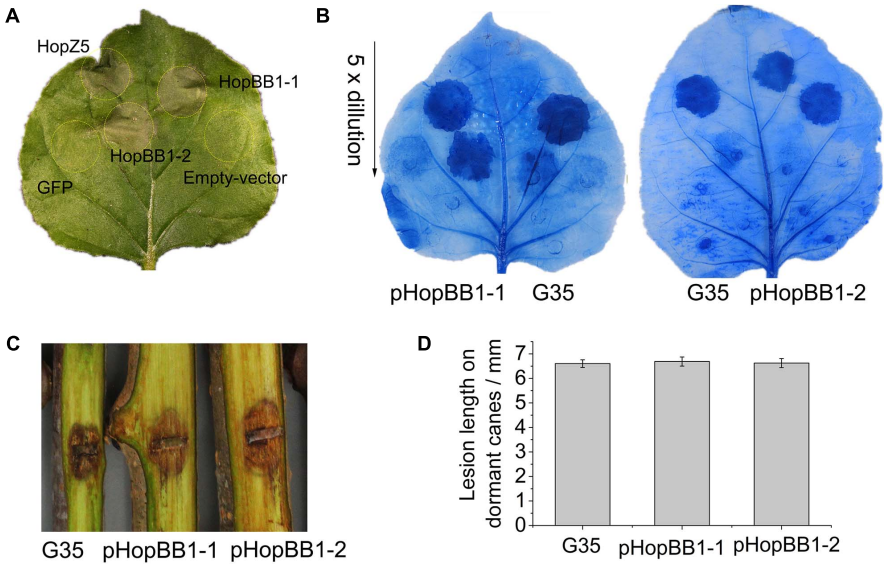

FIGURE 6 | Type III effectors HopBB1-1 and HopBB1-2 induce hypersensitivity response (HR) in non-host *Nicotiana benthamina* leaves and enhance the HR-inducing ability of G35. **(A)** HR induction of heterologously expressed HopBB1-1 and HopBB1-2. The type III effector HopZ5 is used as the positive control, while the GFP and the empty-vector pCAMIBA1300 are used as the negative control. Four-weeks-old *N. benthamina* leaves were infiltrated with *Agrobacterium tumefaciens* strain GV3101 carrying certain plasmid at a concentration of 10^8 CFU/mL, and were photographed at 36-hour post infiltration. The experiments were repeated three times with similar results. **(B)** Constitutively expressed HopBB1-1 or HopBB1-2 in G35 enhanced HR-inducing ability. **(C,D)** HopBB1-1 and HopBB1-2 constitutively expressed alone in G35 did not increase the pathogenicity of the pathogen on kiwifruit.

location in Psa3 strains isolated at different time and at different places. The target DNA sequences of ISPsy36 and ISPsy32 are "GGCC" and "CTAG" repeats, respectively. These two TEs and the corresponding targets are presented in all Psa pathovars, indicating the potential presence of phenotypically-changed isolates caused by TE insertions in other Psa pathovars.

These TEs are potentially active in Psa3, and the phenotype-changed isolates were formed during the course of pathogen infection in host plants. This was evidenced by an *in vitro* DNA pull-down assay, mimicking *in-planta* environments, and revealing that ISPsy32 indeed binds to the non-coding DNA sequences upstream of the *hrpR* gene in the T3SS cluster, which occurred in the formation of G25 and M227. Moreover, the co-isolation of the virulent and the phenotype-changed isolates, belonging to the same MLVA clade, further supported this view. However, the TE-associated genes showed low levels of transcription and were not upregulated during pathogen infection (McAtee et al., 2018), which accords with the observation that non-pathogenic isolates were only identified at low frequency during Psa3 isolation.

The Fate or Biological Role of the Non-pathogenic Isolates

The non-pathogenic Psa3 variants might reach a high population level, together with the original high-virulent bacteria, in the initial infection, but might be eliminated due to natural selection. In a mixed infection, T3Es secreted by the virulent bacteria can favorably modify the host environment for the non-pathogenic variants, while the T3SS-deficient non-pathogenic strain may trigger the PTI (PAMP-triggered immunity)-based defense, impeding the spread of the virulent strain (Barrett et al., 2011; Rufián et al., 2018). Before now, the HR-negative isolates had never been identified alone in symptomatic samples. The non-pathogenic isolates may have decreased fitness in host plants.

However, it has been reported that less aggressive variants of *P. syringae* have a fitness advantage in non-host environments and are maintained in the field (Barrett et al., 2011). Thus, the non-pathogenic variants of Psa3 may play a role in adaptation to other stages of its life cycle.

The emergence of the non-pathogenic variants may also be interpreted by another scenario whereby a resource allocation trade-off mechanism exists in plant pathogenic bacteria (Peyraud et al., 2016; Perrier et al., 2019). For instance, the non-pathogenic variants of *R. solanacearum* were caused by a gene mutation of the quorum-sensing-dependent regulatory protein PhcA, and showed enhanced metabolic versatility compared to the wild-type (Perrier et al., 2019). Expression of T3SS represents a significant cost for Psa3, and the maintenance of a pathogenicity trait can be challenging. This would be verified by the discovery of the reversion of the natural non-pathogenic variant to the wild-type form after *in-planta* multiplication, as per that of *R. solanacearum* (Poussier et al., 2003).

The Central Role of T3SS in Psa3 Pathogenicity

All the above results clearly support the central role of T3SS during the interaction of Psa3 with host and non-host plants. T3SS and T3E genes were induced in the early phase of Psa3

infection, and were required for pathogenicity (McAtee et al., 2018; Zhao et al., 2019a). It has been reported that Psa3 strain C17 naturally lacks the T3SS cluster and is highly compromised in its ability to grow in host plants (McCann et al., 2017). Moreover, a recent comparative transcriptional profiling exercise revealed that T3SS genes were strongly activated in Psa3 responding to apoplast-like conditions, compared with those in Psa1 and Psa2, which are responsible for the epidemics in Japan and Korea, respectively (Vandelle et al., 2020). Several T3Es secreted by the T3SS apparatus have been reported to be involved in pathogenicity in Psa3, such as HopZ5 (Zhao et al., 2019a), AvrE1, and HopR1 (Jayaraman et al., 2020). In this study, we found that T3Es HopBB1-1 and HopBB1-2 were incomplete in Psa3 isolate G35, which showed attenuated HR-eliciting activity in *N. benthamina* leaves and moderate pathogenicity in host plants. The two T3Es indeed induce HR in *N. benthamina* leaves, which evidenced by heterologous expression mediated by *A. tumefaciens*, and over-expression in G35. However, over-expression of HopBB1-1 or HopBB1-2 could not enhance the virulence of G35. The mobile DNA, including transposons, plasmids, or genomic islands (GIs) have been reported to be involved in T3E evolution, and genetic variation affecting T3E genes, and thus bacterial virulence and host specialization, can arise during interaction with the plant host (McCann and Guttman, 2008; Tampakaki et al., 2010; Arnold and Jackson, 2011; Karasov et al., 2014; Frantzeskakis et al., 2020). However, although there are remarkable differences in the composition of T3Es among different Psa biovars (McCann et al., 2013; Sawada and Fujikawa, 2019), only the T3SS apparatus and regulator, and not T3E genes, were involved in the rapid short-term evolution of Psa3 pathogenesis in kiwifruit orchards.

DATA AVAILABILITY STATEMENT

The datasets presented in this study can be found in online repositories. The names of the repository/repositories and accession number(s) can be found below: https://www.ncbi.nlm.nih.gov/bioproject, PRJNA693644 and http://www.proteomexchange.org/, PXD023722.

AUTHOR CONTRIBUTIONS

YuL and QZ carried out most of the experiments. TZ, TX, and RF conducted the data analysis and prepared the figures and tables. ZZ and YoL designed and supervised the experiments. ZZ and ZL wrote the manuscript. All authors reviewed and approved the manuscript.

FUNDING

This study was supported by grants (Grant Nos. 31860486 and 32001864) from the National Natural Science Foundation of China, grants [Grant Nos. QKHJC(2019)1062, QKHZC(2020)1Y131, and QKHPTRC(2020)5001] from the Guizhou Science and Technology Department, and Grant No. (2017)55 from Guizhou University.

SUPPLEMENTARY MATERIAL

The Supplementary Material for this article can be found online at: https://www.frontiersin.org/articles/10.3389/fmicb.2021.650099/full#supplementary-material

Supplementary Figure 1 | Hierarchical cluster analysis of pathogenicity data with the Ward's method in SPSS 19.0.

Supplementary Table 1 | Primers used in this study.

Supplementary Table 2 | The detailed information of Psa3 isolates and MLVA typing results.

Supplementary Table 3 | Results of the DNA pull-down assay.

REFERENCES

Arnold, D. L., and Jackson, R. W. (2011). Bacterial genomes: evolution of pathogenicity. *Curr. Opin. Plant Biol.* 14, 385–391. doi: 10.1016/j.pbi.2011.03.001

Balestra, G. M., Taratufolo, M. C., Vinatzer, B. A., and Mazzaglia, A. (2013). A multiplex PCR assay for detection of *Pseudomonas syringae* pv. *Actinidiae* and differentiation of populations with different geographic origin. *Plant Dis.* 97, 472–478. doi: 10.1094/PDIS-06-12-0590-RE

Barrett, L. G., Bell, T., Dwyer, G., and Bergelson, J. (2011). Cheating, trade-offs and the evolution of aggressiveness in a natural pathogen population. *Ecol. Lett.* 14, 1149–1157. doi: 10.1111/j.1461-0248.2011.01687.x

Bartoli, C., Lamichhane, J. R., Berge, O., Varvaro, L., and Morris, C. E. (2015). Mutability in *Pseudomonas viridiflava* as a programmed balance between antibiotic resistance and pathogenicity. *Mol. Plant Pathol.* 16, 860–869. doi: 10.1111/mpp.12243

Biondi, E., Zamorano, A., Vega, E., Ardizzi, S., Sitta, D., De Salvador, R., et al. (2017). Draft whole genome sequence analyses on *Pseudomonas syringae* pv. *Actinidiae* HR negative strains detected from kiwifruit bleeding sap samples. *Phytopathology* 108, 552–560. doi: 10.1094/PHYTO-08-17-0278-R

Choi, S., Jayaraman, J., Segonzac, C., Park, H.-J., Park, H., Han, S.-W., et al. (2017). *Pseudomonas syringae* pv. *Actinidiae* type III effectors localized at multiple cellular compartments activate or suppress innate immune responses in *Nicotiana benthamiana*. *Front. Plant Sci.* 8:2157. doi: 10.3389/fpls.2017.02157

Ding, W., Baumdicker, F., and Neher, R. A. (2018). panX: pan-genome analysis and exploration. *Nucleic Acids Res.* 46:e5. doi: 10.1093/nar/gkx977

Firrao, G., Torelli, E., Polano, C., Ferrante, P., Ferrini, F., Martini, M., et al. (2018). Genomic structural variations affecting virulence during clonal expansion of *Pseudomonas syringae* pv. *Actinidiae* biovar 3 in Europe. *Front. Microbiol.* 9:656. doi: 10.3389/fmicb.2018.00656

Frantzeskakis, L., Di Pietro, A., Rep, M., Schirawski, J., Wu, C. H., and Panstruga, R. (2020). Rapid evolution in plant-microbe interactions-a molecular genomics perspective. *New Phytol.* 225, 1134–1142. doi: 10.1111/nph.15966

Gallelli, A., Talocci, S., Pilotti, M., and Loreti, S. (2014). Real-time and qualitative PCR for detecting *Pseudomonas syringae* pv. *Actinidiae* isolates causing recent outbreaks of kiwifruit bacterial canker. *Plant Pathol.* 63, 264–276. doi: 10.1111/ppa.12082

Guidot, A., Jiang, W., Ferdy, J.-B., Thébaud, C., Barberis, P., Gouzy, J., et al. (2014). Multihost experimental evolution of the pathogen *Ralstonia solanacearum* unveils genes involved in adaptation to plants. *Mol. Biol. Evol.* 31, 2913–2928. doi: 10.1093/molbev/msu229

He, R., Liu, P., Jia, B., Xue, S., Wang, X., Hu, J., et al. (2019). Genetic diversity of *Pseudomonas syringae* pv. *Actinidiae* strains from different geographic regions in China. *Phytopathology* 109, 347–357. doi: 10.1094/phyto-06-18-0188-r

Hottes, A. K., Freddolino, P. L., Khare, A., Donnell, Z. N., Liu, J. C., and Tavazoie, S. (2013). Bacterial adaptation through loss of function. *PLoS Genet.* 9:e1003617. doi: 10.1371/journal.pgen.1003617

Jayaraman, J., Yoon, M., Applegate, E. R., Stroud, E. A., and Templeton, M. D. (2020). AvrE1 and HopR1 from *Pseudomonas syringae* pv. *Actinidiae* are additively required for full virulence on kiwifruit. *Mol. Plant Pathol.* 21, 1467–1480. doi: 10.1111/mpp.12989

Jutras, B. L., Verma, A., and Stevenson, B. (2012). Identification of novel DNA-binding proteins using DNA-affinity chromatography/pull down. *Curr. Protoc. Microbiol.* 24, 1F.1.1–1F.1.13. doi: 10.1002/9780471729259.mc01f01s24

Karasov, T. L., Horton, M. W., and Bergelson, J. (2014). Genomic variability as a driver of plant-pathogen coevolution? *Curr. Opin. Plant Biol.* 18, 24–30. doi: 10.1016/j.pbi.2013.12.003

Kvitko, B. H., and Collmer, A. (2011). "Construction of *Pseudomonas syringae* pv. *tomato* DC3000 mutant and polymutant strains," in *Plant Immunity*, ed. J. McDowell (Totowa, NJ: Humana Press), 109–128. doi: 10.1007/978-1-61737-998-7_10

Livak, K. J., and Schmittgen, T. D. (2001). Analysis of relative gene expression data using real-time quantitative PCR and the $2^{-\Delta\Delta\ C}{}_{T}$ method. *Methods* 25, 402–408. doi: 10.1673/031.012.6001

Lovell, H. C., Jackson, R. W., Mansfield, J. W., Godfrey, S. A., Hancock, J. T., Desikan, R., et al. (2011). In planta conditions induce genomic changes in *Pseudomonas syringae* pv. *Phaseolicola*. *Mol. Plant Pathol.* 12, 167–176. doi: 10.1111/j.1364-3703.2010.00658.x

McAtee, P. A., Brian, L., Curran, B., van der Linden, O., Nieuwenhuizen, N. J., Chen, X., et al. (2018). Re-programming of *Pseudomonas syringae* pv. *Actinidiae* gene expression during early stages of infection of kiwifruit. *BMC Genomics* 19:822. doi: 10.1186/s12864-018-5197-5

McCann, H. C., and Guttman, D. S. (2008). Evolution of the type III secretion system and its effectors in plant–microbe interactions. *New Phytol.* 177, 33–47. doi: 10.1111/j.1469-8137.2007.02293.x

McCann, H. C., Li, L., Liu, Y., Li, D., Pan, H., Zhong, C., et al. (2017). Origin and evolution of the kiwifruit canker pandemic. *Genome Biol. Evol.* 9, 932–944. doi: 10.1093/gbe/evx055

McCann, H. C., Rikkerink, E. H., Bertels, F., Fiers, M., Lu, A., Rees-George, J., et al. (2013). Genomic analysis of the kiwifruit pathogen *Pseudomonas syringae* pv. *Actinidiae* provides insight into the origins of an emergent plant disease. *PLoS Pathog.* 9:e1003503. doi: 10.1371/journal.ppat.1003503

Perrier, A., Barlet, X., Rengel, D., Prior, P., Poussier, S., Genin, S., et al. (2019). Spontaneous mutations in a regulatory gene induce phenotypic heterogeneity and adaptation of *Ralstonia solanacearum* to changing environments. *Environ. Microbiol. Rep.* 21, 3140–3152. doi: 10.1111/1462-2920.14717

Perrier, A., Peyraud, R., Rengel, D., Barlet, X., Lucasson, E., Gouzy, J., et al. (2016). Enhanced in planta fitness through adaptive mutations in EfpR, a dual regulator of virulence and metabolic functions in the plant pathogen *Ralstonia solanacearum*. *PLoS Pathog.* 12:e1006044. doi: 10.1371/journal.ppat.1006044

Peyraud, R., Cottret, L., Marmiesse, L., Gouzy, J., and Genin, S. (2016). A resource allocation trade-off between virulence and proliferation drives metabolic versatility in the plant pathogen *Ralstonia solanacearum*. *PLoS Pathog.* 12:e1005939. doi: 10.1371/journal.ppat.1005939

Poussier, S., Thoquet, P., Trigalet-Demery, D., Barthet, S., Meyer, D., Arlat, M., et al. (2003). Host plant-dependent phenotypic reversion of *Ralstonia solanacearum* from non-pathogenic to pathogenic forms via alterations in the *phcA* gene. *Mol. Microbiol.* 49, 991–1003. doi: 10.1046/j.1365-2958.2003.03605.x

Prencipe, S., Gullino, M. L., and Spadaro, D. (2018). *Pseudomonas syringae* pv. *Actinidiae* isolated from *Actinidia chinensis* var. *deliciosa* in Northern Italy: genetic diversity and virulence. *Eur. J. Plant Pathol.* 150, 191–204. doi: 10.1007/s10658-017-1267-9

Rufián, J. S., Macho, A. P., Corry, D. S., Mansfield, J. W., Ruiz-Albert, J., Arnold, D. L., et al. (2018). Confocal microscopy reveals *in planta* dynamic interactions between pathogenic, avirulent and non-pathogenic *Pseudomonas syringae* strains. *Mol. Plant Pathol.* 19, 537–551. doi: 10.1111/mpp.12539

Sawada, H., and Fujikawa, T. (2019). Genetic diversity of *Pseudomonas syringae* pv. *Actinidiae*, pathogen of kiwifruit bacterial canker. *Plant Pathol.* 68, 1235–1248. doi: 10.1111/ppa.13040

Stauber, J. L., Loginicheva, E., and Schechter, L. M. (2012). Carbon source and cell density-dependent regulation of type III secretion system gene expression in *Pseudomonas syringae* pathovar *tomato* DC3000. *Res. Microbiol.* 163, 531–539. doi: 10.1016/j.resmic.2012.08.005

Tampakaki, A. P., Skandalis, N., Gazi, A. D., Bastaki, M. N., Panagiotis, F. S., Charova, S. N., et al. (2010). Playing the "Harp": evolution of our understanding of *hrp/hrc* genes. *Annu. Rev. Phytopathol.* 48, 347–370. doi: 10.1146/annurev-phyto-073009-114407

Vandelle, E., Colombo, T., Regaiolo, A., Libardi, T., Maurizio, V., Danzi, D., et al. (2020). Transcriptional profiling of three *Pseudomonas syringae* pv. *Actinidiae* biovars reveals different responses to apoplast-like conditions related to strain virulence. *Mol. Plant Microbe Interact.* doi: 10.1094/MPMI-09-20-0248-R

Vanneste, J. (2017). The scientific, economic, and social impacts of the New Zealand outbreak of bacterial canker of kiwifruit (*Pseudomonas syringae* pv. *Actinidiae*.). *Annu. Rev. Phytopathol.* 55, 377–399. doi: 10.1146/annurev-phyto-080516-035530

Vanneste, J. L., Yu, J., Cornish, D. A., Tanner, D. J., Windner, R., Chapman, J. R., et al. (2013). Identification, virulence, and distribution of two biovars of *Pseudomonas syringae* pv. *Actinidiae* in New Zealand. *Plant Dis.* 97, 708–719. doi: 10.1094/PDIS-07-12-0700-RE

Wang, K., Kang, L., Anand, A., Lazarovits, G., and Mysore, K. S. (2007). Monitoring *in planta* bacterial infection at both cellular and whole-plant levels using the green fluorescent protein variant GFPuv. *New Phytol.* 174, 212–223. doi: 10.1111/j.1469-8137.2007.01999.x

Xie, Y., Shao, X., and Deng, X. (2019). Regulation of type III secretion system in *Pseudomonas syringae*. *Environ. Microbiol. Rep.* 21, 4465–4477. doi: 10.1111/1462-2920.14779

Zhao, Z., Chen, J., Gao, X., Zhang, D., Zhang, J., Wen, J., et al. (2019a). Comparative genomics reveal pathogenicity-related loci in *Pseudomonas syringae* pv. *Actinidiae* biovar 3. *Mol. Plant Pathol.* 20, 923–942. doi: 10.1111/mpp.12803

Zhao, Z., Du, S., Li, Y., Yang, W., Fan, R., Wang, Y., et al. (2019b). Establishment and application of MLVA typing for *Pseudomonas syringae* pv. *Actinidiae* biovar 3 populations. *Acta Phytopathol. Sin.* 49, 445–455. (in Chinese),

Zhao, Z., Gao, X., Huang, Q., Huang, L., Qin, H., and Kang, Z. (2013). Identification and characterization of the causal agent of bacterial canker of kiwifruit in the Shaanxi province of China. *J. Plant Pathol.* 95, 155–162.

Conflict of Interest: The authors declare that the research was conducted in the absence of any commercial or financial relationships that could be construed as a potential conflict of interest.

frontiers in Microbiology

ORIGINAL RESEARCH
published: 25 March 2021
doi: 10.3389/fmicb.2021.637068

DNA Metabarcoding Reveals Broad Presence of Plant Pathogenic Oomycetes in Soil From Internationally Traded Plants

*Simeon Rossmann[1], Erik Lysøe[1], Monica Skogen[1], Venche Talgø[1] and May Bente Brurberg[1,2]**

[1]Division of Biotechnology and Plant Health, Norwegian Institute of Bioeconomy Research (NIBIO), Ås, Norway, [2]Department of Plant Sciences, Norwegian University of Life Sciences (NMBU), Ås, Norway

OPEN ACCESS

Edited by:
Sabine Dagmar Zimmermann, Délégation Languedoc Roussillon (CNRS), France

Reviewed by:
Christopher John Grim, United States Food and Drug Administration, United States
Alejandro Rojas, University of Arkansas, United States
Jan Nechwatal, Bayerische Landesanstalt für Landwirtschaft (LfL), Germany

***Correspondence:**
May Bente Brurberg
may.brurberg@nibio.no

Specialty section:
This article was submitted to Microbe and Virus Interactions With Plants, a section of the journal Frontiers in Microbiology

Received: *02 December 2020*
Accepted: *03 March 2021*
Published: *25 March 2021*

Citation:
Rossmann S, Lysøe E, Skogen M, Talgø V and Brurberg MB (2021) DNA Metabarcoding Reveals Broad Presence of Plant Pathogenic Oomycetes in Soil From Internationally Traded Plants. Front. Microbiol. 12:637068. doi: 10.3389/fmicb.2021.637068

Plants with roots and soil clumps transported over long distances in plant trading can harbor plant pathogenic oomycetes, facilitating disease outbreaks that threaten ecosystems, biodiversity, and food security. Tools to detect the presence of such oomycetes with a sufficiently high throughput and broad scope are currently not part of international phytosanitary testing regimes. In this work, DNA metabarcoding targeting the internal transcribed spacer (ITS) region was employed to broadly detect and identify oomycetes present in soil from internationally shipped plants. This method was compared to traditional isolation-based detection and identification after an enrichment step. DNA metabarcoding showed widespread presence of potentially plant pathogenic *Phytophthora* and *Pythium* species in internationally transported rhizospheric soil with *Pythium* being the overall most abundant genus observed. Baiting, a commonly employed enrichment method for *Phytophthora* species, led to an increase of golden-brown algae in the soil samples, but did not increase the relative or absolute abundance of potentially plant pathogenic oomycetes. Metabarcoding of rhizospheric soil yielded DNA sequences corresponding to oomycete isolates obtained after enrichment and identified them correctly but did not always detect the isolated oomycetes in the same samples. This work provides a proof of concept and outlines necessary improvements for the use of environmental DNA (eDNA) and metabarcoding as a standalone phytosanitary assessment tool for broad detection and identification of plant pathogenic oomycetes.

Keywords: baiting, environmental DNA, *Globisporangium*, *Phytophthora*, plant pathogens, *Pythium*

INTRODUCTION

Oomycetes comprise some of the most notorious plant pathogens, such as *Phytophthora infestans*, the pathogen widely known for its central role in the Irish potato famine and a remaining concern in potato production; *Phytophthora ramorum*, damaging a range of wild and cultivated tree and shrub species; *Pythium ultimum*, causing damping off and root rot in a range of important crops like corn, soybean, and potato (Kamoun et al., 2015). Oomycetes form a

taxonomically distinct group of eukaryotic microorganisms that shares some biological features with fungi (e.g., formation of spores and hyphae) but are phylogenetically distant from fungi. The large spectrum of environmental conditions and plant hosts that oomycetes thrive in is reflected in their phylogenetic diversity (Thines, 2014). *Phytophthora*, *Pythium*, and *Globisporangium*, which was recently branched off from *Pythium* (Uzuhashi et al., 2010), are among the phylogenetically most complex oomycete genera and encompass an ever-growing list of species, of which a large number are plant pathogens. Many oomycetes, including various *Phytophthora* and *Pythium* species, overwinter as resting spores (oospores or chlamydospores), and some may remain dormant for several years before resuming a reproductive state (Judelson and Blanco, 2005; Babadoost and Pavon, 2013). Human activity, such as trade with rooted plants, is the predominant pathway of oomycete spread over long, potentially global, distances (Ristaino and Gumpertz, 2000; Cushman and Meentemeyer, 2008; Jung et al., 2016). Soil is also commonly moved locally or over longer distances, e.g., during construction projects, when transplanting trees or bushes from plant nurseries, or as debris on apparel, equipment, and machines. Oomycetes may also spread as airborne (zoosporangia with zoospores) or waterborne (zoospores or resting spores in soil particles) spores, and some can be transported from infected to healthy plants *via* vectors like certain insects (Goldberg and Stanghellini, 1990; Jarvis et al., 1993; Judelson and Blanco, 2005). Considering in addition the longevity of resting spores, the international transport of plant pathogens in contaminated soil presents a major threat to ecosystems, biodiversity, and food security. The risk of catastrophic disease outbreaks caused by oomycetes is especially high when a non-native invasive species, or lineages within a species, are introduced to an ecosystem that is not adapted to it (Fisher et al., 2012; Díaz et al., 2019; Fones et al., 2020). This was likely the case for the recent epidemics caused by *Ph. ramorum* on tanoak (*Notholithocarpus densiflorus*) in the United States and larch (*Larix* spp.) in the United Kingdom (Fry and Goodwin, 1997; Grünwald et al., 2012).

Despite this, phytosanitary measures required in the international transport of plants are commonly limited to a visual inspection for symptoms and do not address oomycete pathogens in rhizospheric soil. A single large individual plant can have a root-soil clump of many kilograms, resulting in thousands of tons of soil being transported internationally. In Europe, routine testing of a limited number of random samples is only done for a few plant pathogenic *Phytophthora* species that are recommended for regulation as quarantine pests in the A1/A2 lists of the European and Mediterranean Plant Protection Organization (EPPO 2018). Moreover, only samples from symptomatic plant tissue are tested and rapid, reliable detection methods for soil samples are currently not available to inspectors. Consequently, detection schemes for oomycetes and other microbial plant pathogens that are not regulated as quarantine pests are not established in international transport of plant material with soil in European countries.

In Norway, a national surveillance program was instated in 2018 and 2019 by the Norwegian Food Safety Authority to analyze for *Phytophthora* spp., in random samples of soil from imported woody ornamental plants, i.e., soil attached to the plants or as loose debris in shipping containers. Sequencing the ribosomal internal transcribed spacer (ITS) region of isolates after enrichment identified 19 distinct *Phytophthora* species from 231 soil samples (Talgø et al., 2019; Pettersson et al., 2020). Sequencing the ITS region of isolates provides reliable identification of oomycetes, but is resource intensive, as it requires DNA isolation from pure cultures before sequencing the marker region. To enrich plant pathogenic oomycetes before isolation, so called "baiting" is often employed. In this approach, healthy leaves or other parts of susceptible plants (e.g., *Rhododendron* spp.) are used as bait for oomycetes (e.g., Telfer et al., 2015). If the bait tissue develops symptoms like spots or lesions (appearing water soaked or necrotic), oomycetes can be isolated from the margin between diseased and healthy tissues. This approach has proven useful for analysis of both soil and water samples (e.g., Roberts et al., 2005; Shrestha et al., 2013). As an alternative, next-generation sequencing of short conserved DNA regions, so called "metabarcoding" or, more generally, "amplicon sequencing," may be used to derive the identity of present oomycetes directly from environmental DNA (eDNA). This approach offers detection and identification of a wide variety of oomycetes and other groups of organisms directly from soil and other sources without requiring prior enrichment and laborious isolation of pure cultures. In the context of phytosanitary measures, establishing reliable metabarcoding routines could drastically improve the scope of controlling for stowaways in international transport of plants, and reduce the threat alien invasive species pose to plant-based industries and endemic vegetation.

In this work, metabarcoding was employed as a tool to detect and identify oomycetes present in soil samples before and after enrichment. The investigated samples comprised soil imported to Norway attached to roots of ornamental trees and shrubs. A particular focus was the presence and dynamics of potentially plant pathogenic oomycete genera and species, such as *Phytophthora* spp., and *Pythium* spp./*Globisporangium* spp. The reproducible analysis workflow for Illumina paired-end oomycete ITS1 metabarcodes used in this work is applicable to future work and can be modified to accommodate additional primer sets. The following hypotheses were tested:

> *Hypothesis* 1: Internationally transported soil attached to plants contains potentially non-native, plant pathogenic oomycetes.
> *Hypothesis* 2: Metabarcoding of the ITS1 region provides reliable detection and identification of oomycetes in soil samples.

Hypothesis 1 was tested by taxonomical and functional classification into potentially plant pathogenic genera for all oomycetes detected by metabarcoding in imported soil samples. Hypothesis 2 was tested by comparing detection and taxonomic identification by metabarcoding of the ITS1 region to isolates obtained through the traditionally used enrichment by baiting.

MATERIALS AND METHODS

Sampling

A total of 73 soil samples were collected from three major entry points for plant import to Norway in 2018. All the soil sampling *in situ* was performed by regional inspectors from the Norwegian Food Safety Authority. The samples, each approximately 1 L, mainly originated from the root zone of woody ornamental plants, while a few constituted debris that had accumulated in the transport containers. A list of the samples with the exporting country, Norwegian region they were collected in, and the host plants are given in **Supplementary Table S1**.

Enrichment of Oomycetes and Identification of Isolates

Oomycetes were enriched by baiting with asymptomatic leaves of *Rhododendron* cv. "Cunningham's White" from greenhouse-grown plants. In preparation for baiting, each soil sample was homogenized in deionized water in suitable plastic trays. After a day, when sediments had settled, leaves were placed on the water surface with the abaxial side down, and incubated for up to a week at room temperature (~20°C). Where water soaked or necrotic lesions developed, sections from the margin between diseased and healthy tissue were dissected (pieces of approx. 0.5 cm^2) using sterile scalpels. The leaf pieces were placed on P_{10}ARPH agar (17 g corn meal agar in 1 L water; with addition of 250 mg ampicillin, 100 mg pentachloronitrobenzene, 35 mg hymexazol, 10 mg pimaricin, 10 mg rifampicin, and 1 ml dimethylsulphoxide), which is selective for *Phytophthora* species.

The agar plates were incubated at room temperature (~20°C) and checked daily for the presence of colonies. Hyphae resembling *Phytophthora* spp., were transferred to potato dextrose agar (PDA) plates to achieve pure cultures. The isolates were identified by sequencing their complete ribosomal ITS DNA region. In brief, DNA of cultured oomycetes was isolated using the DNeasy Plant Mini kit (Qiagen) according to the manufacturer's instructions. The ITS region was amplified using the ITS5 and ITS4 primers (**Supplementary Table S2**) as described by White et al. (1990). The PCR products were submitted to Eurofins (Germany) for Sanger sequencing. Raw sequences were trimmed, assembled, and manually checked, and the final sequences were used to support identification of the isolates based on searches in public databases (GenBank and BOLD Systems).

Metabarcode Sequencing

From each 1 L soil sample, 50 ml was sub-sampled for metabarcode analysis before and after enrichment. The sub-samples were homogenized, and total eDNA was isolated from 250 mg soil per sub-sample using the DNeasy PowerSoil kit (Qiagen). The 250 mg fractions of each sub-sample were chemically lysed in buffer C1 (DNeasy PowerSoil kit) for 10 min before mechanical homogenization using beads in a FastPrep-24 homogenizer (MP Biomedicals) for 2 × 45 s, speed 5.0. After homogenization and centrifugation, DNA isolation from the supernatant was automatized in a QIAcube (Qiagen) using the manufacturer's PowerSoil protocol. Indexed libraries for paired-end sequencing of the ITS1 metabarcoding region were generated using a one-step PCR with indexed Oomycete specific primers from Agler et al. (2016) (see **Supplementary Table S2**). After amplification, the DNA concentrations of the PCR products were measured using a Qubit 2.0 Fluorometer (Invitrogen), and 100 ng DNA per sample was used for library generation. The libraries were purified twice using the MinElute PCR Purification Kit (Qiagen), the DNA concentration measured again using the Qubit Fluorometer, and integrity of the DNA was confirmed in the 2100 Bioanalyzer (Agilent). Sequencing was performed on an Illumina MiSeq System using MiSeq Reagent Kit v3 (600-cycle) chemistry (Illumina), with 15 and 20 pM of the libraries in two separate runs together with 10% PhiX control and sequencing primers. In addition to the soil samples, five replicates of a positive control containing DNA from 12 oomycete species and 11 fungal species were included in the libraries for both sequencing runs. A list of the species included in the positive control as well as the resulting amplicon sequence variants (ASVs) is given in **Supplementary Table S1** (Sheet 2).

Bioinformatics Analysis

Reads were automatically demultiplexed on the MiSeq system by the included MiSeq Reporter software, and the generated fastq files were used in downstream analysis. Adapters in the 3' region were removed from reads using "cutadapt," based on the sequence of the 3' primers and a minimum match length of 15 bp (Martin, 2011). The DADA2 pipeline was used to derive ASVs, largely following Callahan et al. (2016). In short, reads were quality filtered using the "filterAndTrim" function; DADA2 was trained on the error rates for each of the two sequencing runs using the "learnError" function; reads were dereplicated using the "derepFastq" function; error rates were inferred using the "dada" function; paired reads were merged into a single sequence using the "mergePairs" function; the ASV table was generated using the "makeSequenceTable" function; samples "mergeSequenceTables" function; and chimeras were removed using the "removeBinerasDenovo" function.

The taxonomy used in this work was derived from a BLAST search against a local copy of the complete NCBI nucleotide database (nt, version 5), last updated from the FTP server in January 2020 (Tao et al., 2011). BLAST+ commands and derivation of the complete lineage for BLAST hits are documented in the "Blast_lineage_headers" R-Markdown document in the "Additional scripts" subdirectory of the GitLab repository under https://gitlab.nibio.no/simeon/oomycete-metabarcoding-supplementary.

Detailed parameters used in the DADA2 pipeline are found in **Supplementary Material 2** and a full documentation of the data analysis contained in this work, mainly performed using the Phyloseq and tidyverse packages, are given in **Supplementary Material 3**. DADA2 and downstream data analysis scripts were last run in RStudio version 1.3 under R version 4.0; packages used, and their versions are documented in **Supplementary Material 3**.

RESULTS

Metabarcoding Overview

DNA from the rhizospheric soil and debris samples of imported plants was sequenced in two Illumina MiSeq runs (with 20 and 45 samples, respectively). Subsamples before and after enrichment were always sequenced in the same run. The run with fewer samples produced more reads per sample on average, which was expected due to more available space in the flow cell (**Supplementary Figure S1**). Positive controls (a mix of oomycete species, five replicates per flow cell) included with both flow cells showed even and equivalent amplification across sequencing runs (**Supplementary Figure S2**).

After quality filtering and defining ASVs, the samples and controls contained ~35,000 ASV counts on average. Samples with more than 5,000 ASV counts were retained for analysis (**Supplementary Figure S1**).

Of 146 soil sub-samples initially taken in for analysis, (73 before enrichment, 73 after enrichment), 128 sub-samples were sequenced (63 before enrichment, 65 after enrichment), the remainder was disqualified due to insufficient PCR product during library generation. After processing, 58 samples achieved sufficient sequencing depth before and after enrichment (116 sub-samples total), while six samples yielded usable results for only one of the sampling points, for one sample, both sub-samples had to be discarded due to insufficient sequencing depth. As a result, 64 samples were analyzed with full or partial sub-sample coverage and renumbered as S01–S64. A full tabular overview of the samples, processing notes for discarded samples and metadata are provided in **Supplementary Table S1**. A full tabular overview of all ASVs with their taxonomy and ASV counts for each sample is provided in **Supplementary Table S3**.

Oomycetes in eDNA

A total of 5,195 ASVs were identified in the samples, and 1,832 were classified as oomycete sequences, representing ~72% of all reads. This relative dominance of oomycete ASVs was more pronounced in the untreated soil samples than the samples after enrichment (**Figure 1**). The five most abundant taxonomic classes, in order of abundance, were Oomycetes, Chrysophyceae, "uncultured fungi," Bacilliarophyceae, and Dinophyceae, representing ~96% of all reads (**Figure 1**). The 10 most abundant genera covered approx. 87% of all reads. The most abundant genus was *Pythium* (mean 49%), *Globisporangium* and *Phytophthora* were also among the 10 most abundant genera (mean 6% each). The distribution of the top five classes and top 10 genera per sample is shown in **Supplementary Figure S3**. The number of oomycete ASVs and their relative proportion per sample is given in **Table 1**.

Abundance of Putative Plant Pathogenic Oomycetes

To determine the plant pathogenic potential of the identified oomycete ASVs, their taxonomic classification was matched against the FUNGuild database that categorizes organisms into guilds according to their ecological role (Nguyen et al., 2016). While the primary focus of the database is on fungi, it contains entries on several other organism groups, including oomycetes.

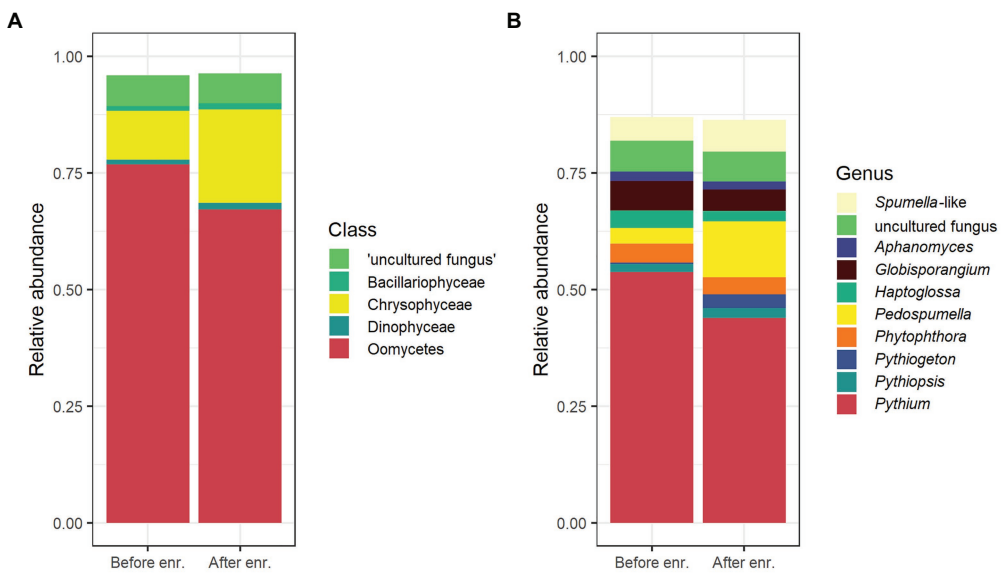

FIGURE 1 | Overview of the most abundant organisms in rhizospheric soil samples detected by oomycete internal transcribed spacer (ITS) metabarcoding, means of all samples. Relative abundance of amplicon sequence variants (ASVs) belonging to the five most abundant taxonomic classes **(A)** and the 10 most abundant genera **(B)** before ("Before enr.") and after enrichment ("After enr."). In **(B)**, *Globisporangium*, *Pythium*, and *Phytophthora* are highlighted in bordeaux, red, and orange, respectively, while *Aphanomyces* and *Phytiogeton* are colored in shades of purple/dark blue. **Supplementary Figure S3** shows a per-sample overview for the top five classes and top 10 genera.

TABLE 1 | Overview of ASVs annotated as oomycetes and potentially plant pathogenic genera in soil samples before and after enrichment, and isolates after enrichment.

				# Oomycete ASVs		% Oomycete ASVs		# PP ASVs		% PP ASVs		
Soil	**Type**	**Country**	**SeqRun**	**Before**	**After**	**Before**	**After**	**Before**	**After**	**Before**	**After**	**Isolates**
S01	Rhiz.	NL	A	83	104	86.8	88.4	55	66	75.1	81.7	–
S02	Rhiz.	NL	A	66	64	85.4	95.5	37	34	77.7	87	2
S03	Debris	NL	A	107	101	99.1	97.2	80	62	96.7	28.5	1
S04	Rhiz.	NL	A	80	101	93.3	80.8	56	72	76.5	66.4	1
S05	Rhiz.	NL	A	75	77	67.3	71.4	58	58	57.1	63	–
S06	Rhiz.	DK	A	19	39	36.9	61.1	11	20	25.6	44.7	–
S07	Rhiz.	NL	A	49	74	97.2	60.6	29	55	81	47.6	–
S08	Rhiz.	NL	A	72	78	96.4	97.6	42	46	73.9	92.1	–
S09	Rhiz.	NL	A	-	65	-	96.7	-	31	-	35.1	1
S10	Rhiz.	NL	A	-	20	-	42.2	-	10	-	38.4	–
S11	Rhiz.	DE	A	19	17	78.9	20.1	11	9	40	13.9	–
S12	Rhiz.	NL	A	-	68	-	90	-	52	-	74.1	–
S13	Rhiz.	IT *via* DK	A	16	57	45	74.4	12	39	44	68.6	–
S14	Rhiz.	NL	A	55	73	98.6	95.2	36	48	93.7	86.5	–
S15	Rhiz.	NL	A	38	43	40.4	58.8	31	36	35.5	55.5	–
S16	Rhiz.	NL	A	38	53	93.3	84.6	25	40	77.1	74.6	–
S17	Rhiz.	NL	A	15	-	91.1	-	14	-	87	-	–
S18	Rhiz.	NL	A	10	-	43.7	-	9	-	43.1	-	–
S19	Rhiz.	NL	A	53	58	73	58.9	38	36	52.8	51.4	–
S20	Rhiz.	NL	B	27	15	74.7	13.9	12	9	49	6.9	–
S21	Rhiz.	NL	B	51	36	72.1	58.8	10	15	4.2	12.2	–
S22	Rhiz.	NL	B	36	22	66.1	65.9	26	12	57.5	50.3	–
S23	Rhiz.	DK	B	53	57	73.4	82.5	32	33	54.7	51.4	–
S24	Rhiz.	NL	B	34	46	74.3	74.2	28	35	63.5	65.6	–
S25	Rhiz.	DE	B	47	25	90.9	74.6	25	16	62.5	32.5	–
S26	Rhiz.	IT *via* DK	B	29	34	97.9	17	17	25	95.1	15.5	–
S27	Rhiz.	NL	B	-	45	-	69.1	-	34	-	57.8	–
S28	Rhiz.	NL	B	22	49	74.2	58	13	33	59.6	45.3	–
S29	Rhiz.	NL	B	72	51	92.4	86.8	57	42	78.6	78.5	2
S30	Rhiz.	NL	B	24	59	89.5	59.7	15	35	61.2	32.8	1
S31	Rhiz.	NL	B	37	25	58.3	59.2	24	20	39.7	39.6	–
S32	Rhiz.	NL	B	36	30	97.1	84.8	24	14	91.1	71.3	–
S33	Rhiz.	PL	B	19	12	6.7	10.1	6	4	0.9	0.5	–
S34	Rhiz.	NL	B	32	49	73.4	43.1	24	37	57.3	38.3	–
S35	Rhiz.	NL	B	52	57	99	97.7	45	44	96.1	94.2	–
S36	Rhiz.	NL	B	47	46	89.8	62.2	27	23	81	41	–
S37	Rhiz.	NL	B	78	77	97.6	94.2	62	60	96	80.4	–
S38	Rhiz.	NL	B	53	21	79	76.9	32	16	58.9	70.4	–
S39	Debris	NL	B	24	24	75	84.8	20	15	70.4	53.1	–
S40	Rhiz.	DK	B	51	64	89.8	77.3	32	39	80.1	66.9	–
S41	Rhiz.	SE	B	59	31	85.9	53.8	47	23	79.4	41.8	–
S42	Rhiz.	NL	B	21	13	6.2	6.9	11	5	3.3	2.3	–
S43	Rhiz.	DK	B	71	61	94	93.8	59	49	84.7	81.2	–
S44	Rhiz.	NL	B	19	7	67.3	39.6	11	3	48.3	37.1	–
S45	Rhiz.	NL	B	26	17	13.1	17	5	5	2.4	1.9	–
S46	Rhiz.	DE	B	49	21	83.4	79.9	32	14	61.5	70.3	1
S47	Rhiz.	DE	B	51	48	94.6	83.9	34	36	57.2	70.8	–
S48	Rhiz.	DK	B	46	67	96	96.7	35	48	90.5	81.4	1
S49	Rhiz.	IT *via* DK	B	26	26	90.9	83.4	20	20	77.7	68.5	–
S50	Rhiz.	IT *via* DK	B	35	47	97.8	79.4	25	32	96.1	72.4	–
S51	Rhiz.	IT *via* DK	B	35	61	65.3	51	25	50	22.7	32	1
S52	Rhiz.	DE	B	32	28	76	71.8	23	20	31.1	33.3	–
S53	Rhiz.	DK	B	41	23	84.3	70.9	31	16	76	54.8	–
S54	Rhiz.	DK	B	44	29	85.5	61.4	37	24	77.8	55.9	–
S55	Rhiz.	NL	B	31	22	83.6	77.4	18	17	55.8	64.9	–
S56	Rhiz.	DK	B	22	32	95.4	64.3	18	22	83.3	52	–
S57	Rhiz.	NL	B	16	21	57.3	26.2	9	13	9.7	13.9	1
S58	Rhiz.	IT *via* DK	B	28	22	94.3	69.2	21	15	31.8	25.6	1
S59	Rhiz.	DE	B	33	45	77.6	27.3	19	24	52.8	10	–
S60	Rhiz.	DE	B	23	60	61.6	73.3	17	40	59.4	61.4	–
S61	Rhiz.	DK	B	52	43	97.1	95.4	36	31	86.9	87.9	–

(Continued)

TABLE 1 | Continued

				# Oomycete ASVs		% Oomycete ASVs		# PP ASVs		% PP ASVs		
Soil	**Type**	**Country**	**SeqRun**	**Before**	**After**	**Before**	**After**	**Before**	**After**	**Before**	**After**	**Isolates**
S62	Debris	DK	B	33	23	97.5	80.8	23	12	71	3.5	–
S63	Rhiz.	SE	B	28	19	15.5	48.1	19	13	6.7	16.3	–
S64	Rhiz.	IT *via* DK	B	67	44	87.6	83.5	41	25	75.8	59.8	–

For each soil sample included in the final analysis (S01–S64) the sample type (rhizospheric soil = "Rhiz." or "Debris"), the exporting country (two letter country code) and the sequencing run ("SeqRun") are given. The number of ASVs (#) and their relative abundance in the sample (in percent) is given for ASVs annotated as oomycetes and ASVs annotated as potentially plant pathogenic genera ("PP") before enrichment ("Before") and after enrichment ("After"). The number of isolates recovered from the soil samples after enrichment is also provided. Missing values due to samples that were discarded because of low read count or unsuccessful amplification are indicated by "-".

Of the 1,832 oomycete ASVs detected in this work, 1,188 were annotated as probable members of the "plant pathogen" guild on a genus level (**Figure 2**). On a species level, 395 ASVs were annotated as probable plant pathogens. The remaining ASVs did not correspond to entries in the FUNGuild database and were therefore not assigned a guild. Since the identification of ASVs to a species level is not possible based on metabarcoding of a single marker with high confidence, the guild classification on a genus level was used as the basis of further analysis. These ASVs are referred to as "potentially plant pathogenic" (abbreviated as "PP") on the genus level below. It is important to note that *Pythium*, the most abundant genus, was annotated as potentially plant pathogenic in FUNGuild, but more than half of the reads belonging to *Pythium* ASVs were not assigned a guild on a species level (**Figure 2**). Likewise, a large number of species belonging to other genera were not assigned any guild, even if the genus they belonged to was classified as a plant pathogen, either because the species were not found in the database or because they lacked guild assignments on the species level (**Figure 2**). The number of PP ASVs and their relative proportion per sample is given in **Table 1**.

Decrease of Potentially Plant Pathogenic Oomycetes During the Enrichment

Mean relative abundance of plant pathogenic oomycetes significantly (p = 0.03) decreased from 60.6% in untreated soil to 50.2% in soil after enrichment ("PP" in **Figure 3**). Unlike plant pathogenic oomycetes, the relative abundance of oomycetes belonging to other genera did not significantly change during enrichment (16.2 and 16.9% mean). The relative decrease of plant pathogenic oomycete genera was largely caused by a significant (p = 0.008) increase in mean relative abundance of golden-brown algae from the class Chrysophyceae, which increased from 10.4% in untreated soil to 20% in enriched soil. This observed shift in mean relative abundance was facilitated by an absolute increase in Chrysophyceae reads, not a decrease in reads from plant pathogenic oomycetes (**Supplementary Figure S4**). Reads from classes other than Oomycetes and Chrysophyceae, including taxonomically not assigned reads, were not significantly impacted by the enrichment process. The full results of the statistical analysis of mean relative abundances can be found in **Supplementary Table S4**. **Table 1** shows that the significantly lower abundance of potentially plant pathogenic oomycetes after enrichment observed for mean values was not observed in all samples equally.

ASVs Corresponding to Isolated Oomycetes Recovered in Metabarcoding

Thirteen isolates recovered from 11 soil samples after enrichment were identified using traditional ITS sequencing and used to assess the accuracy of metabarcoding. The isolates and corresponding ASVs (>98% sequence similarity) were identified as *Phytophthora* and *Phytopythium* species by traditional ITS-sequencing and metabarcoding (**Table 2**). The corresponding ASVs were detected in multiple soil samples by metabarcoding and clustered phylogenetically with the isolate sequences and reference isolates (**Figure 4**). In some soil samples, ASVs corresponding to an isolate sequence were observed either only before or only after enrichment. Most ASVs that were highly similar to isolate sequences were detected at low abundance relative to other ASVs in the soil sample. An exception was ASV6 (*Phytophthora cambivora*) which was detected with a relative abundance of approx. 60% in soil sample S02 before and after enrichment. While all ASVs corresponding to isolates were detected in multiple soil samples, the ASVs were detected in the same soil samples as the isolate was obtained from in only five of 13 cases. The full lineage assigned to ASVs in the taxonomic pipeline and the number of times any ASV was observed in each soil sample is given in **Supplementary Table S3**.

DISCUSSION

Presence of Potentially Plant Pathogenic Oomycetes in Imported Rhizosphere Soil

As described above, nucleotide reads were readily obtained from 128 rhizospheric soil samples using the ITS1 primers optimized for metabarcoding of oomycetes developed by Agler et al. (2016). An additional 18 samples were excluded from the analysis because they did not yield usable DNA or contained too few reads to be analyzed, likely due to unsuccessful processing, not an actual absence of oomycetes in those samples. Two oomycete isolates were obtained from one of these samples after enrichment, but DNA isolation and/or ITS1 PCR were unsuccessful both before and after enrichment. Since problems with DNA isolation and/or PCR amplification most often occurred for both sampling points of the same soils, these

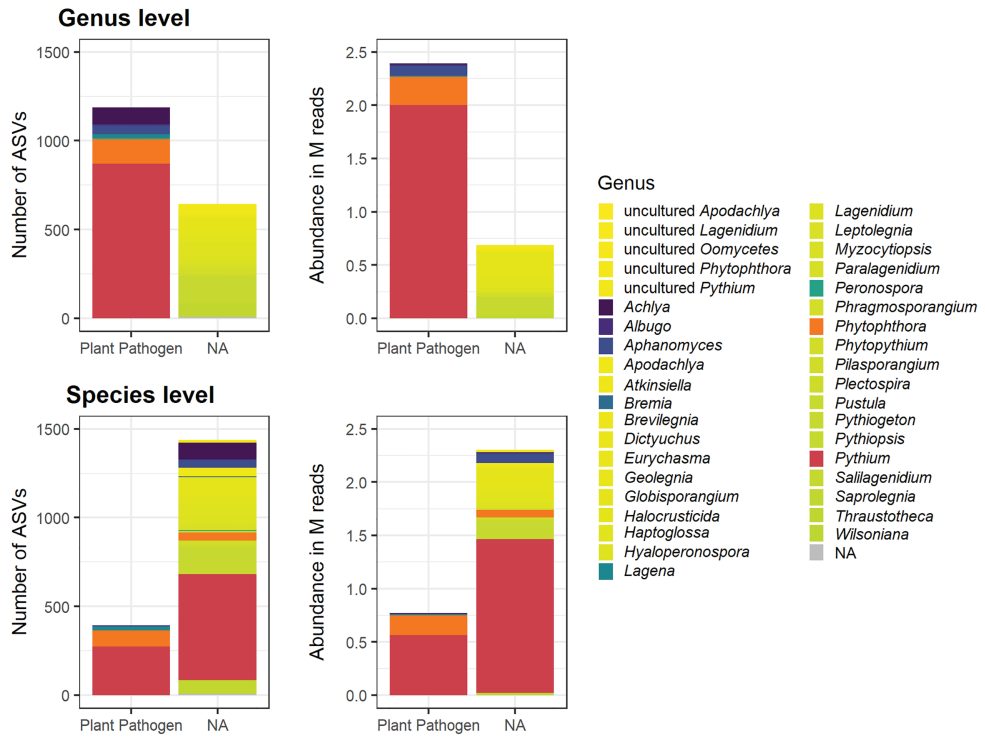

FIGURE 2 | Oomycete ASVs in rhizospheric soil samples detected by ITS metabarcoding, and their classification in the FUNGuild database on a genus and species level. The number of ASVs with a given designation is shown in the left panels and the total abundance of these ASVs in million (M) reads is shown in the right panels. In both the genus and species level plots, the bars are colored according to the genus assignment. *Pythium* and *Phytophthora* are highlighted in red and orange, respectively. Other genera that were assigned to the "plant pathogen" guild and species belonging to them are colored in shades between dark purple and dark green. Oomycete genera that were not assigned any guild in the FUNGuild database ("NA") and the species belonging to them are colored in shades between yellow and lime.

soil samples were either completely free of biomaterial targeted by the ITS1 primers, or, more likely, contained inhibitors that interfered with successful DNA isolation and/or PCR amplification. While this affected only a minority of samples (12%), improvements in the isolation and amplification procedure could likely remedy this, e.g., extra purification steps prior to PCR. The number of samples that were amplified successfully was sufficient to address the aims stated for this work, thus further attempts to amplify the remaining samples were not made. The integrity and evenness of the positive controls over two independent sequencing runs indicate that the PCR amplifications were uniform and reliable. Well-known issues in high throughput sequencing, such as index-hopping resulting in the incorrect assignment of sequences from the true sample to a different sample, or PCR amplification preference for certain ASVs due to primer bias are more likely to affect relative abundance estimates in samples with very few reads. Therefore, six samples with total ASV counts of less than 5,000 were excluded from the analysis. Overall, a large majority of samples yielded a sufficient number of high-quality reads (**Supplementary Figure S1**).

The most abundant ASVs were typically identified as originating from oomycetes, as expected for the employed primer set (**Figure 1**). *Phytophthora* and *Pythium* were among the 10 most abundant genera identified in the samples, with *Pythium* being most abundant (**Figure 1B**). The high prevalence of these two potentially plant pathogenic genera was likely not an effect of primer biases, since previous experiments using this set yielded primarily the oomycetes *Albugo* and *Hyaloperenospora* and far fewer *Pythium* and *Phytophthora* from plant material (Figure S6 in Agler et al., 2016).

Potentially plant pathogenic oomycetes, which are frequently species belonging to the *Phytophthora* genus and, to a lesser extent, *Pythium* species were of particular interest and represented a large part of the detected oomycetes (**Figure 2**). The classification based on the FUNGuild database proved to be a useful tool for automated annotation of this trait but was only reliable to a limited extent. The primary issue was that the FUNGuild database is primarily aimed at functional grouping of fungi, not oomycetes. The oomycete entries are mostly automated imports from the database entries of the American Phytopathological Society (APS) and not curated by humans. This may lead to some degree of false functional classification. The lack of focus on oomycetes in the FUNGuild database also means that some important genera and species have no entry there. This was the case for, e.g., *Globisporangium*, which was recently branched off from *Pythium* and inherited some of the most problematic plant pathogens formerly belonging

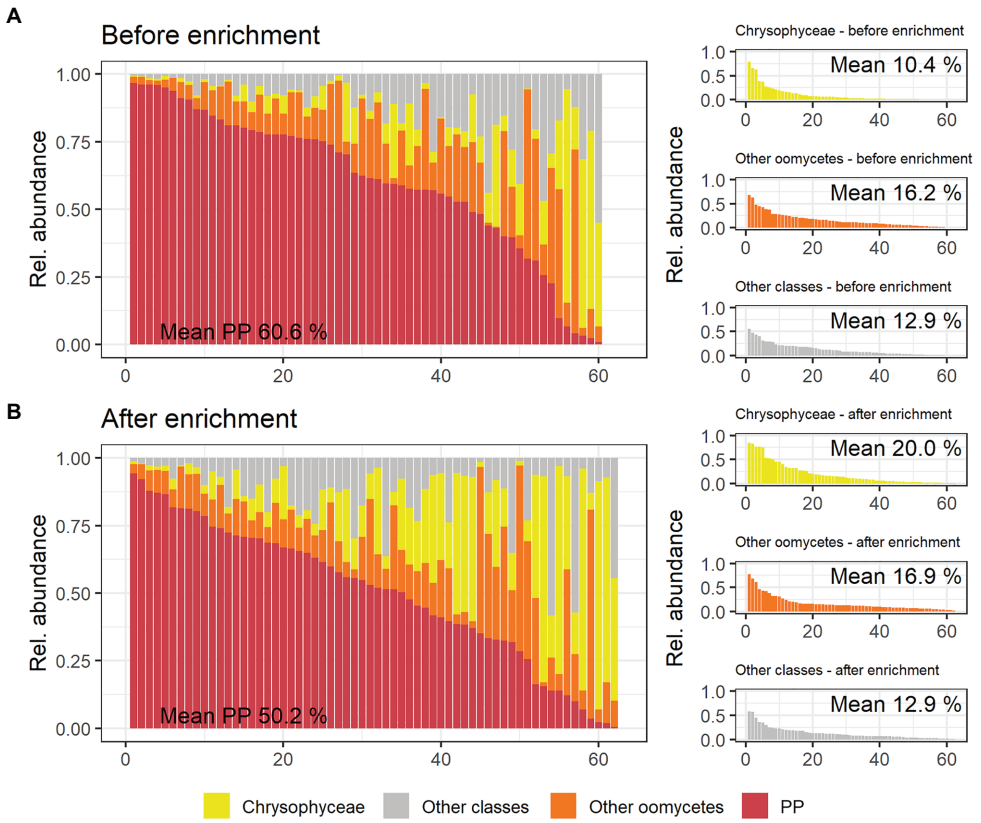

FIGURE 3 | Overview of taxonomic classes of interest and their relative abundance per rhizospheric soil sample detected by metabarcoding using the oomycete ITS1 marker. **(A)** shows the relative abundances in soil samples before enrichment, **(B)** shows corresponding results in soil after enrichment. The large panels show relative abundances of plant pathogenic oomycete genera (PP, red) per sample ranked from the sample with the highest to the lowest relative abundance. The relative abundances of other Oomycetes, Chrysophyceae, and all other classes (including not taxonomically assigned ASVs) are shown in orange, yellow, and gray, respectively. These groups are also shown as separate, smaller graphs in the right panels of **(A)** and **(B)**, with the mean percentages of reads belonging to the different taxonomic classes given in each panel.

TABLE 2 | Thirteen isolates obtained from rhizospheric soil samples after enrichment, their species identities and corresponding ASVs recovered in metabarcoding.

Soil	Isolate ID	Identified as	Most similar ASV	ID%	ASV identified as
S02	2	*Phytophthora plurivora*	ASV117	98.4	*Phytophthora plurivora*
S02	13	*Phytophthora cambivora*	ASV6	100	*Phytophthora cambivora*
S03	8	*Phytophthora gonapodyides*	ASV18	100	*Phytophthora gonapodyides*
S04	10	*Phytopythium citrinum*	ASV385	98.5	*Phytopythium citrinum*
S09	1	*Phytophthora plurivora*	ASV117	100	*Phytophthora plurivora*
S29	9	*Phytophthora plurivora*	ASV117	100	*Phytophthora plurivora*
S29	12	*Phytopythium citrinum*	ASV385	100	*Phytopythium citrinum*
S30	11	*Phytophthora gonapodyides*	ASV18	99.1	*Phytophthora gonapodyides*
S46	6	*Phytopythium vexans*	ASV267	100	*Phytopythium vexans*
S48	3	*Phytophthora cambivora*	ASV6	100	*Phytophthora cambivora*
S51	4	*Phytophthora gonapodyides*	ASV18	99.6	*Phytophthora gonapodyides*
S57	7	*Phytopythium vexans*	ASV286	100	*Phytopythium vexans*
S58	5	*Phytopythium vexans*	ASV286	99.6	*Phytopythium vexans*

For each isolate, the soil sample it was recovered from (S01–S64), the species it was identified as based on the full ITS sequence, and the most similar ASV are given. Percent (ID%) refer to nucleotide similarity between these ASVs and corresponding isolate's ITS sequence (obtained by Sanger sequencing) over the length of the ASV (approximately 170–270 bp).

to *Pythium*, such as the former *Py. irregulare*, *Py. sylvaticum*, and *Py. ultimum* (Uzuhashi et al., 2010). In the NCBI BLAST nucleotide database and corresponding taxonomic database used for the automatic taxonomy pipeline in this work, some but not all these former *Pythium* species, are correctly annotated as *Globisporangium*, meaning that there was only partial correspondence between the annotation obtained in this work and the FUNGuild database. Because of these issues, the

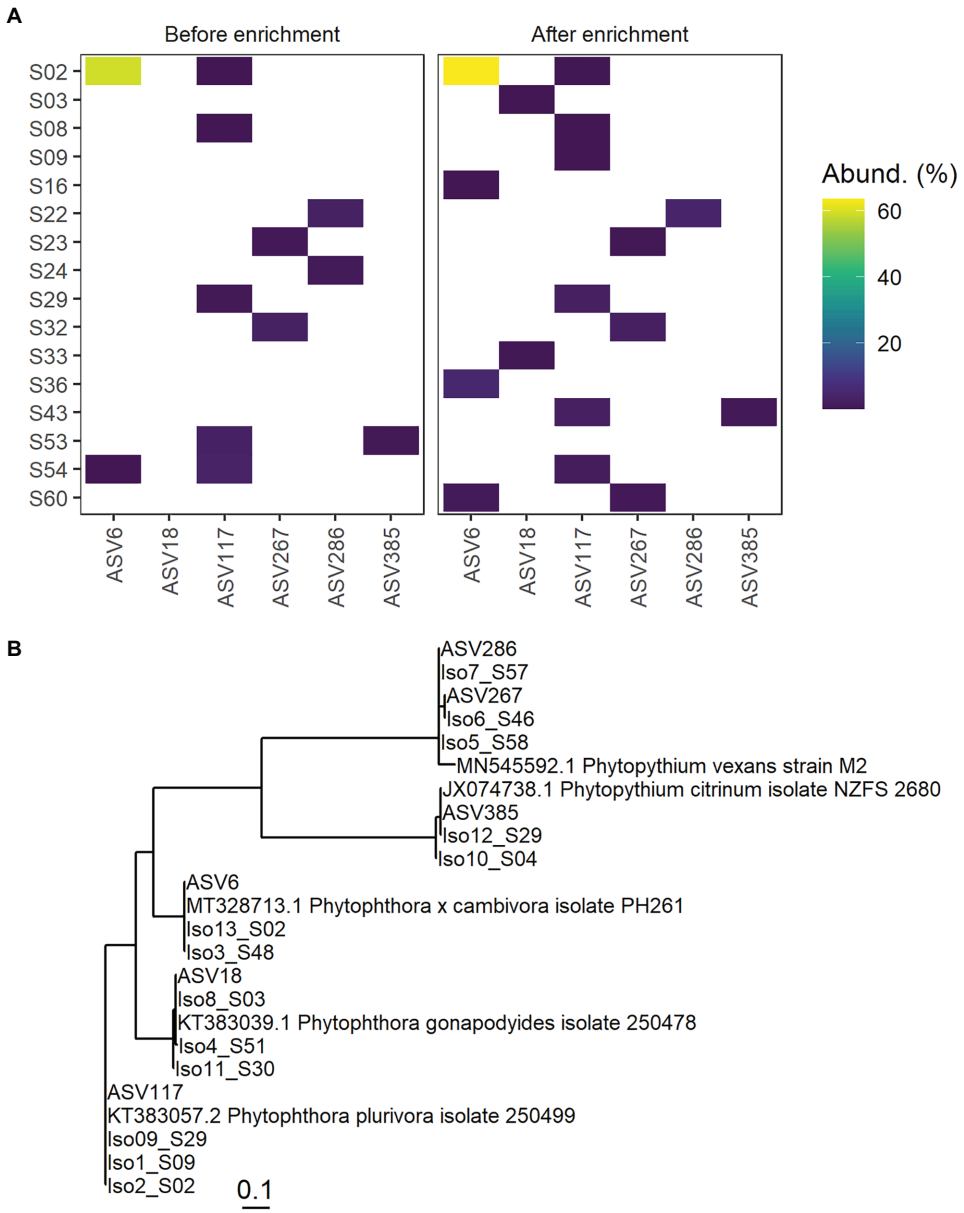

FIGURE 4 | Detection of ASVs corresponding to oomycetes isolated from rhizospheric soil samples. In **(A)**, the left panel shows ASV detection by metabarcoding before enrichment, the right panel after enrichment. ASVs are given on the *x*-axis and soil samples on the *y*-axis. The relative abundance of ASVs in percent of the whole soil sample is indicated on a continuous color scale, no color was assigned if the abundance was 0%. **(B)** shows a phylogenetic tree based on ITS-sequences of isolates, corresponding ASVs, and publicly available sequences for identified strains. Represented in a Neighbor Joining tree fitted with a General time reversible model with discrete Gamma distribution and evolutionarily invariable sites (GTR + G + I). The tree's scale (substitutions per site) is indicated on the bottom.

FUNGuild database when used for oomycete functional classification may have produced a high rate of false negatives, where oomycete ASVs may actually belong to the plant-pathogens but were not assigned a guild. However, in cases where ASVs were classified as originating from plant pathogenic oomycetes, it is reasonable to assume that they were correctly annotated as such, meaning a likely low risk of false positives. The annotation provided by this method therefore offers a conservative functional classification on the genus level in this case. It is important to note that neither the NCBI nt database used for taxonomical annotation, nor the FUNGuild database used for functional annotation were optimal, but currently the best available tools. Alternatives, primarily curated ITS databases such as BOLD and UNITE were tested but performed worse for taxonomical assignment (higher amount of unassigned sequences and lower confidence assignments) due to their relative lack of diverse and well-annotated oomycete sequences (Ratnasingham and Hebert, 2007; Nilsson et al., 2018).

For functional assignment, no suitable alternative databases were found. Future efforts to employ metabarcoding for oomycete detection and identification need to reevaluate the use of these resources and carefully consider whether better, curated databases are available or existing databases like UNITE have been amended sufficiently.

Bias Introduced by Enrichment

The enrichment process significantly reduced the relative abundance of potentially plant pathogenic oomycetes in favor of Chrysophyceae (golden-brown algae). We expected oomycetes, such as *Phytophthora* spp., that are captured by the employed enrichment method to increase rather than decrease, because the biomass of such oomycetes should accumulate drastically. There are two likely causes that may explain the observed dynamics: first, the accumulation of plant pathogenic oomycetes may have been hyperlocalized to the leaves that were used for baiting without affecting the biomass of these oomycetes in the soil samples. Second, the conditions during the enrichment process, with the soil having been submerged in water for approximately a week likely favored the growth of Chrysophyceae, leading to an unintended relative increase of these organisms. Indeed, the absolute number of reads attributed to oomycetes from genera of interest in the soil remained relatively stable while mean Chrysophyceae reads more than doubled during enrichment (**Supplementary Figure S4**). While not a reliable measure of abundance, the absolute number of reads may allow some conclusions on the dynamics when comparing soil samples before and after enrichment since both were always sequenced on the same flow cell.

Reliability and Usefulness of Metabarcoding in Detection

Amplicon sequence variants identical or highly similar to sequences obtained by ITS barcoding of *Phytophthora* and *Phytopythium* isolates were obtained by metabarcoding (**Table 2**; **Figure 4**). For the highly abundant ASV6 before and after enrichment in soil sample S02, a corresponding *Phytophthora cambivora* culture was isolated from that sample. *Phytophthora plurivora* isolates identical or highly similar in sequence to ASV117 were detected by metabarcoding in soil samples S02, S09, and S29 and isolated from those samples. *Phytophthora gonapodyides* was isolated from S03 and the identical ASV18 was detected in the same sample. For the remaining *Phytophthora* isolates and all *Phytopythium* species, the ASVs corresponding to isolates were not observed in the soil samples the isolates were found in. This was likely an effect of the small soil samples (250 mg from 50 ml) used for DNA isolation compared to the large total volume used in the enrichment (approx. 1 L). A hyperlocalization of the infecting oomycete at the leaves without a corresponding increase in the soil during enrichment may also have contributed to lack of ASV detection where isolates were found. To avoid an effect of potential hyperlocalization and get a better correlation with isolates, DNA could be isolated from the water used during enrichment, a higher soil volume should be used for DNA isolation and soil from the entire sample should be homogenized thoroughly before sampling for DNA isolation. In general, submerging soil in water for some time and subsequently filtering the water and extracting DNA from the filter may yield a more representative census of microorganisms in large volumes of soil, even if no enrichment is planned. The use of additional primer sets could also increase detection frequency further by balancing potentially less efficient amplification of some genera.

For identification purposes, traditional isolation-based approaches that employ Sanger sequencing of specific DNA marker regions like ITS have some advantages over metabarcoding in its current form, as they have fewer restrictions on sequence length or targeted region. Additionally, having access to isolates offers the possibility to study morphology, biochemical features, as well as pathogenicity. Purely DNA-based methods like metabarcoding cannot distinguish between DNA from dead and living organisms, although it is likely that DNA from dead organisms in the soil samples tested here would have been degraded by living microorganisms during transport of the plants, and/or during the enrichment. Metabarcoding as a means of simultaneous and sensitive detection and identification of oomycetes in soil will improve with additional primer sets, increased length of sequenced fragments, and dedicated databases for taxonomic and functional assignment. Despite some current shortcomings, metabarcoding showed itself to have several advantages in the detection of potentially plant pathogenic oomycetes, as it produced useful results from untreated soil, negating the need for potentially biased treatment and laborious isolation of pure cultures. It furthermore enabled the agnostic detection of a wide variety of *Phytophthora* and *Pythium*, two genera of high interest. Detection that does not take preconceived notions of relevance into account is important, because *Pythium* (~*Globisporangium*) species like *Py. ultimum*, *Py. irregulare*, and *Py. sylvaticum* are problematic plant pathogens, particularly on tree seeds and seedlings, that are often discarded or ignored in isolation-based screenings because they are less dangerous than *Phytophthora* species after the nursery stage.

While ASV-based processing yields sequences that can be regarded as proxies for unique organisms analogous to "operational taxonomical units" (OTUs), it is challenging to annotate these sequences with traditional taxonomical units on the lowest level, such as species or strains, since species affiliation can only be reliably determined from longer sequences and might include morphological or phenotypical characteristics. Despite stringent quality filtering, and although false-positive rates are lower than with comparable methods, false-positive ASVs may be derived from Illumina-reads due to sequencing errors regardless of the compensation for such errors in the data processing (Callahan et al., 2016). Furthermore, some *Phytophthora* species are identical or highly similar across the ITS region traditionally used for identification of isolates, increasing the chance of incorrect or ambiguous species assignment even when using a longer segment of the ITS region (Yang and Hong, 2018). Even so, annotation of ASVs down to the species level based on DNA sequence similarity is possible and was done in this work (**Supplementary Table S3**). However, genus level assignment of ASV taxonomy is more

reliable than species level annotation and should be focused on when interpreting metabarcoding results without additional information, given the currently available databases. While the approach used in this work produced nearly complete taxonomic lineage annotation and good results, there is a need for a curated and balanced collection of oomycete reference sequences for taxonomic and functional annotation of ASVs. Unlocking the full potential of metabarcoding as an identification tool requires such sequence databases tailored to the organisms of interest (Dormontt et al., 2018; Richardson et al., 2018).

In summary, metabarcoding showed several advantages compared to isolation-based strategies: (1) Unbiased, sensitive, broad detection of all oomycetes; (2) For specific oomycetes, such as *Phytophthora* spp., metabarcoding can give near-complete detection of variants present in a sample, while isolating all variants present in a given sample with a high degree of certainty requires considerable effort, metabarcoding therefore has a lower theoretical false-negative detection rate in routine applications; (3) Shorter turn-around time from sampling to detection in soil without enrichment; (4) Increased amount of samples that can be processed per person-hour; and (5) Less rigid processing schedule as the samples can be frozen for prolonged periods between any of the steps without losing information. There are also major drawbacks of metabarcoding, some of which can be addressed in the future and some that are inherent to the method: (1) There is no definitive proof of the presence of live oomycetes without isolating them; (2) Short amplicon sizes make species identification unreliable, this may be addressed by amplifying with additional primer pairs or by increasing amplicon size with, e.g., PacBio sequencing technology; and (3) Databases for reliable taxonomic and functional identification of oomycetes are lacking, this should be addressed by increased efforts to create new databases and improve existing ones.

The relatively high abundance of *Pythium* and *Phytophthora* detected in this work implies wide-spread presence of considerable amounts of potentially plant pathogenic oomycetes in soil associated with the rhizosphere of woody ornamentals that are traded internationally. Our results therefore strengthen the first hypothesis stated in the introduction. The second hypothesis underlying this work was supported to a large degree by the results presented here, but further improvements on aspects of metabarcoding implementation are needed. Compared to the conventional approach that relies on enrichment and isolation of certain oomycete genera, metabarcoding detected and identified a far larger diversity of oomycetes from untreated soil and showed the growth of undesirable organisms during the enrichment process. With sufficient research data and further development of the underlying technology, metabarcoding can eventually become a valuable standalone tool for direct detection and identification of plant pathogenic oomycetes in phytosanitary control schemes.

DATA AVAILABILITY STATEMENT

The datasets presented in this study can be found in online repositories. All R code and files required to reproduce the analysis of results presented here can be found on the GitLab repository at: gitlab.nibio.no/simeon/oomycete-metabarcoding-supplementary. Raw read data is archived at the European Nucleotide Archive (ENA) under the accession number PRJEB40676 (www.ebi.ac.uk/ena/browser/view/PRJEB40676).

AUTHOR CONTRIBUTIONS

MB, EL, and VT conceived the ideas and designed the methodology. MS and VT collected the data. SR and EL analyzed the data. SR led the writing of the manuscript. All authors contributed to the article and approved the submitted version.

FUNDING

This work was supported by the Research Council of Norway, Grant number 194051, through the SIS BIOIMMIGRANTS.

ACKNOWLEDGMENTS

We are grateful to Dr. Marie Davey, who implemented the initial version of the DADA2 pipeline.

SUPPLEMENTARY MATERIAL

The Supplementary Material for this article can be found online at: https://www.frontiersin.org/articles/10.3389/fmicb.2021.637068/full#supplementary-material

Supplementary Table 1 | Overview of all rhizospheric soil samples, whether they yielded DNA and sufficient PCR amplicons for sequencing, the read counts through the processing and associated metadata. The metadata for each numbered soil sample includes the countries from which the samples were imported, which plant species the soil was imported with and processing notes when samples were discarded. Sheet 2 contains information on the species used as positive controls and whether they were found in sequencing.

Supplementary Table 3 | Occurrence of ASVs in the samples and their full taxonomy. For each ASV, the ASV count is given for all samples. The taxonomy derived from local BLAST against the NCBI nt database is provided on seven taxonomic levels (where available): Kingdom, Phylum, Class, Order, Family, Genus, Species.

Supplementary Material 2 | Complete documentation of the R code used for the DADA2 pipeline. The code and outputs are compartmentalized in chunks for separate processes. The raw reads used as input for DADA2 are deposited on www.ebi.ac.uk/ena/data/view/PRJEB40676. Version information for R, RStudio and the libraries used is found at the bottom of the document. The R Markdown file is available on GitLab under gitlab.nibio.no/simeon/oomycete-metabarcoding-supplementary.

Supplementary Material 3 | Complete data analysis documentation including a clear description of the input data, the code that was used to analyse it and the various outputs as well as version information for R, RStudio and the libraries used. The code and outputs are compartmentalized in chunks for separate processes. The data files used as input for the Phyloseq section and the R Markdown file are available on GitLab under gitlab.nibio.no/simeon/oomycete-metabarcoding-supplementary.

REFERENCES

Agler, M. T., Ruhe, J., Kroll, S., Morhenn, C., Kim, S.-T., Weigel, D., et al. (2016). Microbial hub taxa link host and abiotic factors to plant microbiome variation. *PLoS Biol.* 14:e1002352. doi: 10.1371/journal.pbio.1002352

Babadoost, M., and Pavon, C. (2013). Survival of oospores of *Phytophthora capsici* in soil. *Plant Dis.* 97, 1478–1483. doi: 10.1094/PDIS-12-12-1123-RE

Callahan, B. J., McMurdie, P. J., Rosen, M. J., Han, A. W., Johnson, A. J. A., and Holmes, S. P. (2016). DADA2: high-resolution sample inference from Illumina amplicon data. *Nat. Methods* 13:581. doi: 10.1038/nmeth.3869

Cushman, J., and Meentemeyer, R. K. (2008). Multi-scale patterns of human activity and the incidence of an exotic forest pathogen. *J. Ecol.* 96, 766–776. doi: 10.1111/j.1365-2745.2008.01376.x

Díaz, S., Settele, J., Brondízio, E. S., Ngo, H. T., Agard, J., Arneth, A., et al. (2019). Pervasive human-driven decline of life on earth points to the need for transformative change. *Science* 366:eaax3100. doi: 10.1126/science.aax3100

Dormontt, E. E., van Dijk, K.-J., Bell, K. L., Biffin, E., Breed, M. F., Byrne, M., et al. (2018). Advancing DNA barcoding and metabarcoding applications for plants requires systematic analysis of herbarium collections—an Australian perspective. *Front. Ecol. Evol.* 6:134. doi: 10.3389/fevo.2018.00134

Fisher, M. C., Henk, D. A., Briggs, C. J., Brownstein, J. S., Madoff, L. C., McCraw, S. L., et al. (2012). Emerging fungal threats to animal, plant and ecosystem health. *Nature* 484, 186–194. doi: 10.1038/nature10947

Fones, H. N., Bebber, D. P., Chaloner, T. M., Kay, W. T., Steinberg, G., and Gurr, S. J. (2020). Threats to global food security from emerging fungal and oomycete crop pathogens. *Nature Food* 1, 332–342. doi: 10.1038/s43016-020-0075-0

Fry, W. E., and Goodwin, S. B. (1997). Resurgence of the Irish potato famine fungus. *Bioscience* 47, 363–371. doi: 10.2307/1313151

Goldberg, N., and Stanghellini, M. (1990). Ingestion-egestion and aerial transmission of *Pythium aphanidermatum* by shore flies (Ephydrinae: *Scatella stagnalis*). *Phytopathology* 80, 1244–1246. doi: 10.1094/Phyto-80-1244

Grünwald, N. J., Garbelotto, M., Goss, E. M., Heungens, K., and Prospero, S. (2012). Emergence of the sudden oak death pathogen *Phytophthora ramorum*. *Trends Microbiol.* 20, 131–138. doi: 10.1016/j.tim.2011.12.006

Jarvis, W., Shipp, J., and Gardiner, R. (1993). Transmission of *Pythium aphanidermatum* to greenhouse cucumber by the fungus gnat *Bradysia impatiens* (Diptera: Sciaridae). *Ann. Appl. Biol.* 122, 23–29. doi: 10.1111/j.1744-7348.1993.tb04010.x

Judelson, H. S., and Blanco, F. A. (2005). The spores of *Phytophthora*: weapons of the plant destroyer. *Nat. Rev. Microbiol.* 3, 47–58. doi: 10.1038/nrmicro1064

Jung, T., Orlikowski, L., Henricot, B., Abad-Campos, P., Aday, A. G., Aguín Casal, O., et al. (2016). Widespread *Phytophthora* infestations in European nurseries put forest, semi-natural and horticultural ecosystems at high risk of *Phytophthora* diseases. *For. Pathol.* 46, 134–163. doi: 10.1111/efp.12239

Kamoun, S., Furzer, O., Jones, J. D. G., Judelson, H. S., Ali, G. S., Dalio, R. J. D., et al. (2015). The top 10 oomycete pathogens in molecular plant pathology, 434. *Mol. Plant Pathol.* 16:413. doi: 10.1111/mpp.12190

Martin, M. (2011). Cutadapt removes adapter sequences from high-throughput sequencing reads. *EMBnet J.* 17:3. doi: 10.14806/ej.17.1.200

Nguyen, N. H., Song, Z., Bates, S. T., Branco, S., Tedersoo, L., Menke, J., et al. (2016). FUNGuild: an open annotation tool for parsing fungal community datasets by ecological guild. *Fungal Ecol.* 20, 241–248. doi: 10.1016/j.funeco.2015.06.006

Nilsson, R. H., Larsson, K.-H., Taylor, A. F. S., Bengtsson-Palme, J., Jeppesen, T. S., Schigel, D., et al. (2018). The UNITE database for molecular identification of fungi: handling dark taxa and parallel taxonomic classifications. *Nucleic Acids Res.* 47, D259–D264. doi: 10.1093/nar/gky1022

Pettersson, M., Brurberg, M. B., and Talgø, V. (2020). Delrapport for 2019 i OK-programmet 'Nematoder og *Phytophthora* spp. i jord på importerte planter'. NIBIO Rapport 6.

Ratnasingham, S., and Hebert, P. D. N. (2007). BOLD: the barcode of life data system (http://www.barcodinglife.org). *Mol. Ecol. Notes* 7, 355–364. doi: 10.1111/j.1471-8286.2007.01678.x

Richardson, R. T., Bengtsson-Palme, J., Gardiner, M. M., and Johnson, R. M. (2018). A reference cytochrome c oxidase subunit I database curated for hierarchical classification of arthropod metabarcoding data. *PeerJ* 6:e5126. doi: 10.7717/peerj.5126

Ristaino, J. B., and Gumpertz, M. L. (2000). New frontiers in the study of dispersal and spatial analysis of epidemics caused by species in the genus *Phytophthora*. *Annu. Rev. Phytopathol.* 38, 541–576. doi: 10.1146/annurev.phyto.38.1.541

Roberts, P., Urs, R., French-Monar, R., Hoffine, M., Seijo, T., and McGovern, R. (2005). Survival and recovery of *Phytophthora capsici* and oomycetes in tailwater and soil from vegetable fields in Florida. *Ann. Appl. Biol.* 146, 351–359. doi: 10.1111/j.1744-7348.2005.040120.x

Shrestha, S. K., Zhou, Y., and Lamour, K. (2013). Oomycetes baited from streams in Tennessee 2010–2012. *Mycologia* 105, 1516–1523. doi: 10.3852/13-010

Talgø, V., Pettersson, M., and Brurberg, M. B. (2019). Delrapport for 2018 i OK-programmet 'Nematoder og *Phytophthora* spp. i jord på importerte planter'. NIBIO Rapport 5.

Tao, T., Madden, T., and Christiam, C. (2011). *BLAST FTP Site* [Online]. Bethesda (MD): National Center for Biotechnology Information (US). Available at: https://www.ncbi.nlm.nih.gov/books/NBK62345/ (Accessed November 23, 2020).

Telfer, K. H., Brurberg, M. B., Herrero, M.-L., Stensvand, A., and Talgø, V. (2015). *Phytophthora cambivora* found on beech in Norway. *For. Pathol.* 45, 415–425. doi: 10.1111/efp.12215

Thines, M. (2014). Phylogeny and evolution of plant pathogenic oomycetes—a global overview. *Eur. J. Plant Pathol.* 138, 431–447. doi: 10.1007/s10658-013-0366-5

Uzuhashi, S., Kakishima, M., and Tojo, M. (2010). Phylogeny of the genus *Pythium* and description of new genera. *Mycoscience* 51, 337–365. doi: 10.1007/S10267-010-0046-7

White, T. J., Bruns, T., Lee, S., and Taylor, J. (1990). "Amplification and direct sequencing of fungal ribosomal RNA genes for phylogenetics" in *PCR protocols: A guide to methods and applications. Vol. 18.* eds. M. A. Innis, D. H. Gelfand, J. J. Sninsky and T. J. White (New York: Academic Press, Inc.), 315–322.

Yang, X., and Hong, C. (2018). Differential usefulness of nine commonly used genetic markers for identifying phytophthora species. *Front. Microbiol.* 9:2334. doi: 10.3389/fmicb.2018.02334

Conflict of Interest: The authors declare that the research was conducted in the absence of any commercial or financial relationships that could be construed as a potential conflict of interest.

frontiers in Microbiology

REVIEW
published: 08 April 2021
doi: 10.3389/fmicb.2021.650610

Microbiome Modulation—Toward a Better Understanding of Plant Microbiome Response to Microbial Inoculants

Gabriele Berg[1], Peter Kusstatscher[1], Ahmed Abdelfattah[1], Tomislav Cernava[1] and Kornelia Smalla[2]*

[1] Institute of Environmental Biotechnology, Graz University of Technology, Graz, Austria, [2] Julius Kühn Institute (JKI) Federal Research Centre for Cultivated Plants, Institute for Epidemiology and Pathogen Diagnostics, Braunschweig, Germany

Plant-associated microorganisms are involved in important functions related to growth, performance and health of their hosts. Understanding their modes of action is important for the design of promising microbial inoculants for sustainable agriculture. Plant-associated microorganisms are able to interact with their hosts and often exert specific functions toward potential pathogens; the underlying *in vitro* interactions are well studied. In contrast, *in situ* effects of inoculants, and especially their impact on the plant indigenous microbiome was mostly neglected so far. Recently, microbiome research has revolutionized our understanding of plants as coevolved holobionts but also of indigenous microbiome-inoculant interactions. Here we disentangle the effects of microbial inoculants on the indigenous plant microbiome and point out the following types of plant microbiome modulations: (i) transient microbiome shifts, (ii) stabilization or increase of microbial diversity, (iii) stabilization or increase of plant microbiome evenness, (iv) restoration of a dysbiosis/compensation or reduction of a pathogen-induced shift, (v) targeted shifts toward plant beneficial members of the indigenous microbiota, and (vi) suppression of potential pathogens. Therefore, we suggest microbiome modulations as novel and efficient mode of action for microbial inoculants that can also be mediated *via* the plant.

Keywords: holobiont, microbial diversity, healthy plant microbiome, mode of action, microbiome shift

OPEN ACCESS

Edited by:
Yong Wang,
Guizhou University, China

Reviewed by:
Sara Borin,
University of Milan, Italy
Jay Prakash Verma,
Banaras Hindu University, India

***Correspondence:**
Peter Kusstatscher
peter.kusstatscher@tugraz.at

Specialty section:
This article was submitted to Microbe and Virus Interactions with Plants, a section of the journal Frontiers in Microbiology

Received: *07 January 2021*
Accepted: *19 March 2021*
Published: *08 April 2021*

Citation:
Berg G, Kusstatscher P, Abdelfattah A, Cernava T and Smalla K (2021) Microbiome Modulation—Toward a Better Understanding of Plant Microbiome Response to Microbial Inoculants. Front. Microbiol. 12:650610. doi: 10.3389/fmicb.2021.650610

INTRODUCTION

Plants are naturally associated with specific microorganisms, which fulfill important functions, e.g., nutrient, mineral and vitamin supply, and protection against biotic and abiotic stress (Vandenkoornhuyse et al., 2015; Sánchez-Cañizares et al., 2017; Bakker et al., 2020). Microbiome research has revolutionized our understanding of plant microbiome functioning, and it simultaneously opened new possibilities for applications toward sustainable agriculture (Berg et al., 2020). Advances in engineering of environmental microbiomes are predicted to replace toxic chemicals and fertilizers in agriculture in the future, and stimulate a more sustainable use of environmental resources, as well as improve our food processing (Massart et al., 2015). Currently,

agricultural products based on microorganisms are one of the fastest growing sectors in agronomy with a Compound Annual Growth Rate (CAGR) of 15–18% and a predicted value of over $10 billion United States dollars by 2025 for the whole biocontrol sector (DunhamTrimmer, 2017).

Understanding their modes of action is important for the design of promising applications in the form of microbial inoculants for sustainable agriculture (Berg, 2009; Köhl et al., 2019). Microbial inoculants comprise bioprotectants, biopesticides, and biostimulants, as well as biofertilizers (Lugtenberg and Kamilova, 2009; DunhamTrimmer, 2017). However, these classifications, which are mostly based on to the underlying modes of action, are currently under discussion. Moreover, there are various country-specific as well as continent-specific definitions (ibma-global.org). From the scientific point of view, most of microbial inoculants influence the host plant by stimulating plant defense response, plant hormone production and nutrient uptake (Windisch et al., 2017). Thus, the categories listed above might be important for regulation purposes but are still poorly defined, because inoculants that improve plant growth might also enhance plant resistance toward pathogens. Here, we use the term microbial inoculant without further categorizing it. Many of the currently available inoculants are able to establish interactions by relying on several modes of action, and their interactions depend on environmental conditions (Köhl et al., 2019). Despite this fact, interaction with the indigenous plant microbiome are often not considered at all.

In vitro plant-microbe as well as pathogen-microbe interactions are well studied (reviewed by Whipps et al., 1988; Weller et al., 2002; Berg, 2009; Köhl et al., 2019), while interactions with microbial inoculants *in situ* are not yet fully understood. Here, three-way interactions with the plant, with pathogens and with the indigenous microbiome are possible to induce beneficial effects. In general, the competence of microbial inoculants to colonize plant habitats is essential for successful interactions (Lugtenberg and Kamilova, 2009). Distinct steps during the initiation of such interplay include recognition, adherence, invasion (only endophytes and pathogens), colonization and growth, and several specific strategies to establish interactions (Hardoim et al., 2015). Direct interactions of microbial inoculants with host plants include (i) provision of nutrients and minerals, (ii) balancing the hormonal status of plants, and (iii) priming and induction of resistance (Schenk et al., 2010; Pieterse et al., 2014). Moreover, the ability to suppress pathogens can be an important feature (Weller et al., 2002). Pathogen suppression can be based on (i) antibiosis: inhibition of microbial growth by bioactive substances, (ii) competition (e.g., for iron) and modification of microenvironments, (iii) interference with pathogenicity, and (iv) parasitism and lysis (Lugtenberg et al., 2002; Linares et al., 2006). Furthermore, a meta-analysis by Mawarda et al. (2020) illustrates the impact of microbial inoculants on the native soil community structure and functioning and highlights changes in root exudation as an important underlying mode of action. Here, we summarize the current knowledge related to the effects of microbial inoculants on the indigenous plant microbiome, and suggest this novel, so far mostly unexplored mode of action to be termed "microbiome modulation."

CURRENT KNOWLEDGE RELATED TO PLANT MICROBIOME INTERACTIONS

Plant microbiomes are characteristic microbial communities in habitats that are well-defined by distinct physio-chemical properties, e.g., in the rhizoplane (the surface of the root), rhizosphere (the soil influenced by the root), phyllosphere (stem and leaves) and the endosphere (inner plant parts) (Philippot et al., 2013; Hardoim et al., 2015; Remus-Emsermann and Schlechter, 2018). The plant and its associated microbiome can also be regarded as a meta-organism the so-called "holobiont" (Vandenkoornhuyse et al., 2015). Plant microbiome assembly starts with seeds, which are an important reservoir of microorganisms (Berg and Raaijmakers, 2018). The current model of plant microbiome assembly indicates that both the seed and soil microbiome are able to colonize the plant seedling, which allows to maintain microbial diversity and function but also facilitates adaptation to the local environment (Bergna et al., 2018). The phyllosphere microbiome is also recruited from airborne dust or irrigation water (Vorholt, 2012). Moreover, recent experimental evidences on the seed's role in vertical transmission across plant generations showed high spatial partitioning of the fungal and bacterial community, within both seed and seedling, indicating inheritance, niche differentiation, and divergent transmission routes for the establishment of root and phyllosphere communities (Rezki et al., 2016; Wassermann et al., 2019; Abdelfattah et al., 2021). Distinct microbes from the surrounding environment can colonize the plants surface and tissues, especially in the rhizosphere, which is the soil influenced by the plant root and as such the interface to the soil. Here, the plant species, its specific rhizo-deposits and exudate blend constitute the main factors shaping the microbiome assembled in the vicinity of the roots (Neumann et al., 2014; Schreiter et al., 2014a). However, the plant growth developmental stage, soil properties and diverse agricultural management practices also strongly shape the rhizosphere microbiome and can influence plant microbiome assembly (Paul Chowdhury et al., 2019; Smalla pers. communication).

The plant-associated indigenous microbiome contributes with multiple functions to the holobiont, including (i) germination and growth, (ii) nutrient supply, (iii) resistance against biotic and abiotic stress factors, (iv) production of bioactive metabolites, (v) plant development and flowering, and (vi) attraction of pollinators and of predators and parasites of herbivores (Pieterse et al., 2014; Wagner et al., 2014; Berg et al., 2016; Etemadi et al., 2018). To fulfill these functions, plant-associated microorganisms are embedded in complex networks with microorganisms of the same species as well as with different species, genera, families and domains of life (Wassermann et al., 2019). The cooperation between plants and millions of microorganisms as well as the intra-microbiome interplay requires an intense communication (Venturi and Keel, 2016). A high number of specific genes encoding quorum sensing components and other

signaling molecules were found in plant-associated microbial metagenomes (Bragina et al., 2014); however, the mechanism by which microorganisms interact as a community to confer beneficial traits to plants is still poorly understood. Quorum sensing is an essential communication factor, while a high number of volatile organic compounds are responsible for "microbial small talk," but they can also act as long-distance messengers for interactions with the plant host (Schmidt et al., 2016). A review by Rosier et al. (2016) highlights the importance of chemical signaling, and biochemical and genetic events which determine the efficacy of benign microbes in promoting the development of beneficial traits in plants (Rosier et al., 2016).

WHAT IS A HEALTHY PLANT MICROBIOME?

Although this question is of fundamental importance, we still cannot answer it entirely. Healthy plant microbiomes are characterized by a high microbial diversity and high evenness within the plant-associated indigenous microbial communities (Berg et al., 2017; Trivedi et al., 2020). However, all microhabitats harbor common and specifically adapted microbial communities; the diversity and evenness is generally lower in the rhizoplane (surface of the roots) and in the rhizosphere of crops compared to bulk soils, because only distinct microbes are attracted *via* chemical gradients to the root where they proliferate. Interestingly, all healthy plant microbiomes naturally also contain potential pathogens in seeds as well as in the rhizosphere (Berg et al., 2005; Wassermann et al., 2019). Manzotti et al. (2020) showed that after isolation and re-inoculation, they could exert their pathogenicity on the same host plant (Manzotti et al., 2020). This is an interesting observation underlying the conclusion that the balance and evenness within the plant microbiome is crucial for plant health. Each healthy plant microbiome is characterized by key stone species within the core microbiome and a dense network of positive interactions among the constituents (Berg et al., 2020). Following this perspective, the beneficial interplay of the host and its microbiome is essential for maintaining the health of the holobiont, while diseases are often correlated with a microbial dysbiosis or reduced diversity.

In the context of dysbiosis, the "pathobiome" concept, which integrates pathogenic agents within biotic environments, was established and applied to multiple pathosystems (Vayssier-Taussat et al., 2014). Analyses of pathobiomes often revealed that multiple pathogens and their followers (opportunistic microbes causing secondary infections) might be involved in a severe dysbiosis. Another interesting interpretation of microbial-host interactions is a so-called "Anna Karenina principle" (Zaneveld et al., 2017). It states that, paralleling Leo Tolstoy's dictum that "all happy families look alike; each unhappy family is unhappy in its own way," dysbiotic individuals vary more in microbial community composition than healthy individuals. For instance, infestations by *Bactrocera oleae* in olives was found to alter the natural fungal community into a dysbiotic state that was found to be unique in every geographical location (Abdelfattah et al., 2018). Dysbiosis was also observed in the rhizoplane of apple ("M26") roots exposed to apple replant diseased soil. A strong local plant defense response resulted in phytoalexin accumulation, severe disease symptoms of the roots and in a dysbiosis (reduction of the alpha diversity) of the bacterial community (Balbín-Suárez et al., 2020). These results also suggest that microbial diversity is a key factor in preventing diseases in plants (Berg et al., 2017). Despite numerous studies, defining a "healthy microbiota," the conception of borders between eubiosis and dysbiosis still remains a major challenge for the future of plant microbiome research.

INTERACTIONS OF MICROBIAL INOCULANTS WITH THE PLANT AND ITS MICROBIOME

Establishment of Microbial Inoculants

The establishment of microbial inoculants was studied for a long time, under different perspectives and by applying different methods. The used methodology has a crucial impact on results; highly sensitive methods, e.g., specific qPCR can improve studying colonization rates compared to e.g., cultivation-dependent methods (Verginer et al., 2010). However, the majority of studies revealed only transient establishment or low abundance of the microbial inoculants during plant growth (Scherwinski et al., 2008; Schreiter et al., 2014b; Eltlbany et al., 2019). In order to understand establishment efficiency, it is important to consider rhizosphere and rhizoplane colonization patterns of the inoculant (Götz et al., 2006; Elsayed et al., 2020). A successful establishment depends on strain traits (Adesina et al., 2009), application mode (Götz et al., 2006; Schmidt et al., 2012), and on the structure of the target microbiome (van Elsas et al., 2012). Schreiter et al. (2014b, 2018) showed that the competence of *Pseudomonas* sp. RU47 to colonize field-grown lettuce and potato roots was not influenced by the soil type (Schreiter et al., 2014b, 2018). High microbial diversity was shown to correlate with low colonization rates of typically non-plant/soil microbiome invaders as observed for *E. coli* (van Elsas et al., 2012) and *Salmonella* (Schierstaedt et al., 2020); the indigenous rhizosphere microbiome acts as a barrier or even protection shield of the holobiont against external intruders. Therefore, Adam et al. (2016) suggested the use of minor disturbance, e.g., selectively emptying niches (*via* introduction of bacterial predators, targeted antibiotics or enzymes), combined with timely application of microbial inoculants with or without helper strains to improve their establishment (Adam et al., 2016).

Microbiome Modulation by Microbial Inoculants

The effect of microbial inoculants on the indigenous microbiome of plants has been studied now for more than one decade. Pioneering studies based on microbial fingerprinting techniques already revealed substantial shifts within microbial communities, e.g., caused by *Stenotrophomonas* or *Pseudomonas* treatments (Götz et al., 2006; Adesina et al., 2009; Schmidt et al., 2012). Application of next-generation sequencing techniques in the last

years allowed disentangling these shifts in more detail. Exemplary interactions of microbial inoculants with the plant microbiome, including plant growth promoting bacteria, nitrogen fixing inocula, arbuscular mycorrhizal fungi as well as bacterial and fungal strains with antagonistic activity toward phytopathogens, are listed in **Table 1**.

Schwieger and Tebbe (2000) analyzed the effect of field inoculation with *Sinorhizobium meliloti* L33 on bacterial communities in rhizospheres of *Medicago sativa;* they were the first describing microbiome shifts. Transient microbiome shifts were also reported as response to diverse microbial inoculants in lettuce (Scherwinski et al., 2008). Moreover, a stabilization (increase of resilience to biotic and abiotic stresses) of the microbiome was often described; a specific case during the flowering period was observed after an inoculation of cucumber with *Bacillus subtilis* B579. In this study, *B. subtilis* increased the microbial diversity transiently by promoting the secretion of root exudates during flowering of the host plant. This resulted in an enhanced protection against the pathogen *Fusarium oxysporum* f. sp. *cucumeris*. Disease suppression of Fusarium wilt caused by *Fusarium oxysporum* f. sp. *cubense* (FOC) was observed after inoculation with *Bacillus amyloliquefaciens*, which indirectly supported the growth of the indigenous *Pseudomonas* population (Tao et al., 2020). Interestingly, the response of the indigenous rhizosphere microbiome of field-grown lettuce to the inoculant *Pseudomonas* sp. RU47 was soil type dependent as revealed by amplicon sequencing (Schreiter et al., 2014a). However, it remains to be shown whether the microbiome shifts occur at the sites were inoculants are colonizing or a distant site. The latter would indicate that microbiome modulations are not caused by direct interaction but by changes in the composition and amounts of exudates. Recently, Windisch et al. (2017) showed that both, pathogen inoculation as well as treatments with the bacterial inoculants *Pseudomonas* sp. RU47 or *Serratia plymuthica* 3Re-4-18 resulted in increased concentrations of the antifungal compounds benzoic and lauric acid in a soil type-dependent manner. Bottom rot of lettuce caused by *Rhizoctonia solani* I-IB was least severe in loess loam soil and correlated with the highest concentrations of both antifungal compounds. Obviously, an important factor in the complex interaction below ground is the plant and its chemical response to inoculants, pathogens or the indigenous soil microbiome. A similar holobiont-level mode of action protecting cucumber was shown to rely on the induction of a microbiome shift by *Pseudomonas fluorescens* 2P24 or CPF10 that modify the bacterial community composition toward *Bacillus* spp. (Yin et al., 2013). An additional mode of action was observed with *Pseudomonas* sp. RU47, which stabilized the plant's microbiome. The bioprotectant counteracted diversity losses that are observed in combination of *Rhizoctonia solani* AG1-IB (Adesina et al., 2009). An analogous effect was observed in combination with *R. solani* AG1-IB following a co-inoculation of lettuce with *Serratia plymuthica* 3Re4-18 and *Trichoderma viride* GB7. The combination of these two strains enhanced the biocontrol efficacy and increased the evenness of the plant microbiome (Grosch et al., 2012). Similar effects were observed in tomato plants infected with *Ralstonia solanacearum* B3B through the inoculation of *Bacillus velezensis* B63 or *Pseudomonas fluorescens* P142. Here, a microbiome shift toward genera that comprise multiple strains with plant growth promoting activity such as *Arthrobacter* and *Gaiella (Actinobacteria*) or *Ochrobactrum* (*Alphaproteobacteria*) was observed (Elsayed et al., 2020). *Fusarium* stalk rot in maize caused by *Fusarium graminearum* can be controlled *via* application of *Trichoderma harzianum* CCTCC-RW0024, which resulted in an increase of plant growth promoting *Acidobacteria* (Saravanakumar et al., 2017). Furthermore, a significant increase in microbial activity was observed following the inoculation of pepper plants infected with *Phytophthora capsici* with *Pseudomonas corrugata* CCR80 or *Chryseobacterium indologenes* ISE14. Both biocontrol agents increased the microbial diversity and induced microbial shifts toward *Pseudomonas* and *Actinomycetes* that contain many strains that are well-known for their antagonistic potential (Sang and Kim, 2012). When a bacterial consortium consisting of the PGPR strains *Bacillus cereus* AR156, *Bacillus subtilis* SM21 and *Serratia sp*. XY21 was used for the inoculation of sweet pepper infected with *Phytophthora capsici*, the disease symptoms were significantly reduced. The consortium significantly increased the abundance of the genera *Burkholderia, Comamonas,* and *Ramlibacter*. *Burkholderia* spp. are common antagonists of various plant pathogens, while *Comamonas* spp. commonly have antifungal effects and *Ramlibacter* spp. can potentially improve plant growth under adverse conditions (Zhang et al., 2019). The extent of interferences of microbial inoculants with the plant microbiome can also differ and is likely strain specific. While *Stenotrophomonas rhizophila* SPA P69 was only able to suppress minor fungal pathogens within the rhizosphere microbiome (Schmidt et al., 2012; Kusstatscher et al., 2020), *B. velezensis* FZB42 was observed to generally increase the microbial diversity in the rhizosphere as inferred from 16S rRNA amplicon analyses, which led to the identification of an advanced mode of action against *Rhizoctonia solani* AG1-IB (Erlacher et al., 2014). Chowdhury et al. (2013) reported similar results; they showed that FZB42 treatments resulted in a shift of the indigenous rhizosphere bacterial community although the inoculant was only temporarily present. Interestingly, Lee et al. (2021) were the first to demonstrate that dysbiosis of the protective Gram-positive bacterial community in diseased tomato plants promotes the incidence of disease. This underlines the importance of this novel mode of action. Moreover, the same group showed a plant mediated microbiome shift (*via* volatile organic compounds and root exudates) in neighboring plants to the one inoculated with *Bacillus amyloliquefaciens* GB03 (Kong et al., 2020).

In general, six different types of microbiome modulation were described in literature: (i) transient microbiome shifts, (ii) stabilization or increase of microbial diversity, (iii) stabilization or increase of microbiome evenness, (iv) restoration of a dysbiosis/compensation or reduction of a pathogen-induced shift, (v) targeted shifts toward potential beneficial phyla, and (vi) depletion of potential pathogens. Microbiome modulations are an important response to microbial inoculants, which should be considered in terms of the impact on plants and pathogens (**Figure 1**).

TABLE 1 | Microbial modulators and their influence on the plant microbiome.

Microbial inoculant	Pathosystem, pathogen, plant	Microbiome response	Microbiome modulation concept	References
Sinorhizobium meliloti L33	*Medicago sativa*	Microbiome shift: Decrease of γ-proteobacteria and increased of α-proteobacteria	E, F	Schwieger and Tebbe, 2000
Serratia plymuthica 3Re4-18 *Pseudomonas trivialis* 3Re2-7 *Pseudomonas fluorescens* L13-6-12	*Rhizoctonia solani* AG1-IB—lettuce	Short-time microbiome shift	A	Scherwinski et al., 2008
Pseudomonas jessenii RU47	*Rhizoctonia solani* AG1-IB—lettuce	Stabilization of microbial diversity Reduction of the pathogen-induced shift	B, C, and D	Adesina et al., 2009
Paenibacillus sp. E119 *Methylobacterium mesophilicum* SR1.6/6	Potato	Shift of Alphaproteobacterial and *Paenibacillus* communities	E	Andreote et al., 2010
Stenotrophomonas rhizophila SPA-P69	Cotton, tomato, and sweet pepper	Depletion of potential (minor) pathogens	F	Schmidt et al., 2012
Serratia plymuthica 3RE4-18 *Trichoderma viride* GB7 Consortium of both strains	*Rhizoctonia solani* AG1-IB—lettuce	Stabilization of microbial diversity	B, C	Grosch et al., 2012
Chryseobacterium indologenes ISE14 *Pseudomonas corrugata* CCR80	*Phytophthora capsici*—pepper	Increase of microbial diversity Targeted shifts toward potential beneficial phyla (*Pseudomonads* and *Actinomycetes)*	B, E	Sang and Kim, 2012
Bacillus subtilis B579	*Fusarium oxysporum* f. sp. *cucumerinum*—cucumber	Increase of microbial diversity, especially during flowering	B	Chen et al., 2013
Pseudomonas fluorescens 2P24 *Pseudomonas fluorescens* CPF10	Cucumber	Targeted shifts toward potential beneficial phyla (*Bacillus* spp.)	E	Yin et al., 2013
Bacillus amyloliquefaciens FZB42	*Rhizoctonia solani* AG1-IB—lettuce	Short-time microbiome shift	A	Chowdhury et al., 2013; Kröber et al., 2014
Streptomyces subrutilus Wbn2-11 *Bacillus subtilis* Co1-6 *Paenibacillus polymyxa* Mc5Re-14 *Pseudomonas fluorescens* L13-6-12 *Stenotrophomonas rhizophila* SPA-P69 *Serratia plymuthica* 3Re4-18	Chamomile	Treatment-specific microbiome shift, e.g. *Stenotrophomonas:* increase *Verrucomicrobia; Bacillus:* increase *Acidobacteria*	E	Schmidt et al., 2014
Bacillus amyloliquefaciens FZB42	*Rhizoctonia solani* AG1-IB—lettuce	Increase of microbial diversity Targeted shifts toward potential beneficial phyla (*Acinetobacter* spp. and *Alkanindiges* spp.)	B, E	Erlacher et al., 2014
Ochrobactrum sp. NW-3	Cucumber	Increase of microbial diversity	B	Song et al., 2015
Bacillus amyloliquefaciens NJN-6	Fusarium wilt- banana	Increase of bacterial diversity Microbiome shift: Abundance of *Acidobacteria, Firmicutes*, increased while abundance of *Fusarium* and fungi in general decreased	B, E, and F	Shen et al., 2015
Stenotrophomonas acidaminiphila BJ1	*Vicia faba*	Increase of microbial diversity	B	Zhang et al., 2017

(Continued)

TABLE 1 | Continued

Microbial inoculant	Pathosystem, pathogen, plant	Microbiome response	Microbiome modulation concept	References
Arbuscular mycorrhizal fungus *Rhizophagus intraradices*	Native shrub species	Microbiome shift: *Anaerolineaceae* family was an indicator of AMF-inoculated rhizospheres	A, E	Rodríguez-Caballero et al., 2017
Trichoderma harzianum CCTCC-RW0024	*Fusarium graminearum*—maize	Targeted shifts toward potential beneficial phyla (*Acidobacteria*) Depletion of potential pathogens (*Fusarium graminearum*)	D, E, and F	Saravanakumar et al., 2017
Ensifer sp. NYM3 *Acinetobacter sp.* P16 *Flavobacterium sp.* KYM3	Cucumber	Microbiome shift: Increase of *Gammaproteobacteria, Acidobacteria, Nitrospirae*, and *Armatimonadetes* Decrease of *Actinobacteria* and *Firmicutes* by microbial co-inoculations	E, F	Wang et al., 2018
Bacillus cereus AR156 *Bacillus subtilis* SM21 *Serratia sp.* XY21	*Phytophthora capsici*—pepper	Targeted shifts toward potential beneficial phyla *(Burkholderia spp., Comamonas spp., Ramlibacter spp.)*	E	Zhang et al., 2019
Trichoderma harzianum T-22 *Pseudomonas sp.* DSMZ 13134 *Bacillus amyloliquefaciens* FZB42 *Pseudomonas sp.* RU47	Tomato	Targeted shifts toward potential beneficial phyla (plant growth promoting bacteria)	E	Eltlbany et al., 2019
Stenotrophomonas rhizophilia SPA-P69	Maize	Targeted shifts toward potential beneficial phyla (plant growth promoting bacteria)	E	Kusstatscher et al., 2020
Streptomyces pactum Act12 *Streptomyces rochei* D74	Soil-borne pathogens—monkhood (*Aconitum carmichaelii*)	Strong microbiome shift Decrease of pathogens	A, F	Li et al., 2020
Bacillus velezensis B63 *Pseudomonas fluorescens* P142	*Ralstonia solanacearum* B3B-tomato	Targeted shifts toward potential beneficial phyla (*Actinobacteria, Verrucomicrobia)*	E	Elsayed et al., 2020
Paenibacillus pasadenensis R16 *Pseudomonas syringae* 260-02 *Bacillus amyloliquefaciens strain* CC2	*Rhizoctonia solani* AG1-IB/*Pythium ultimum*—lettuce	Strong microbiome shift Reduction of *Pythium ultimum* symptoms	A, D, and F	Passera et al., 2020
Bacillus amyloliquefaciens W19	*Fusarium oxysporum f. sp. cubense* (FOC) —banana	Targeted shifts toward potential beneficial phyla (*Pseudomonas* spp.)	E	Tao et al., 2020
Brevibacterium frigoritolerans HRS1 *Bacillus niacini* HRS2 *Solibacillus silvestris* HRS3 *Bacillus luciferensis* HRS4	*R. solanacearum*—tomato	Compensation or reduction of the pathogen-induced shift Consortium of functional guilds of healthy plants restoring the dysbiosis	D	Lee et al., 2021
Bacillus amyloliquefaciens strain GB03	*R. solanacearum*—tomato	Microbiome shift which synchronized neighboring plants rhizosphere microbiome (VOC mediated)	A, E	Kong et al., 2020

Microbiome modulation concepts: transient microbiome shifts (A), stabilization or increase of microbial diversity (B), stabilization or increase of plant microbiome evenness (C), restoration of a dysbiosis/compensation or reduction of a pathogen-induced shift (D), targeted shifts toward plant beneficial members of the indigenous microbiota (E), and suppression of potential pathogens (F) are indicated.

Methods to Study Microbiome Modulation by Microbial Inoculants

The detectable inoculation impact on the plant microbiome depends on the time of sampling (days or weeks after inoculation) and more generally on the technical approach (Mawarda et al., 2020). Currently, the state of the art for analyzing plant or rhizosphere microbiome shifts in response to microbial inoculants are total community DNA based methods. Although

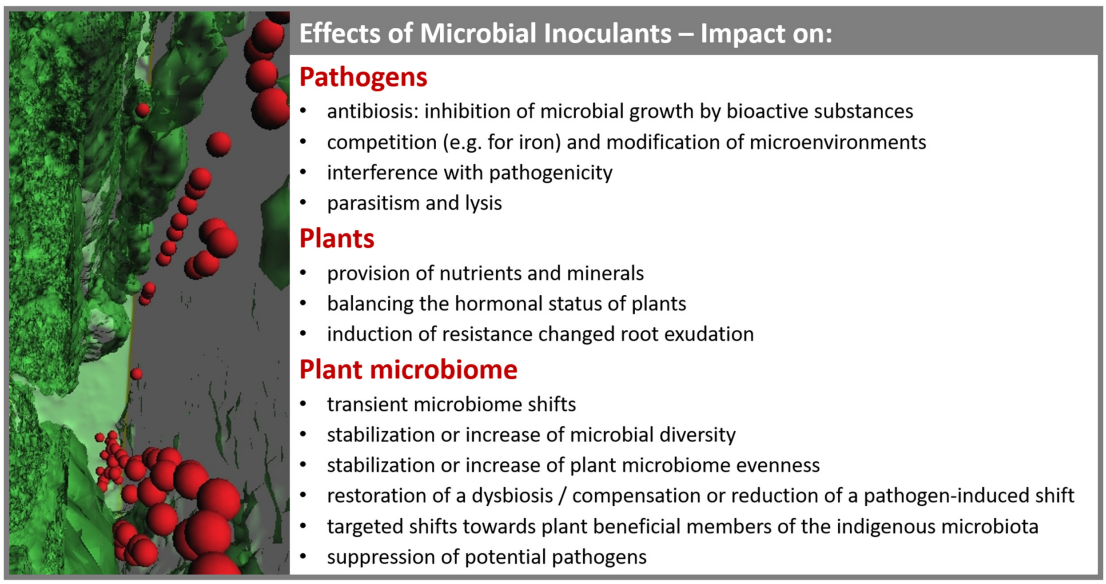

FIGURE 1 | Summary of known effects elicited by microbial inoculants on pathogens, plants and the plant-associated microbiome. Various effects of inoculants on native plant microbiomes are connected to their modes of actions related to plant health and disease prevention. The included 3D reconstruction of a micrograph shows the colonization of a microbial inoculant in plant tissues.

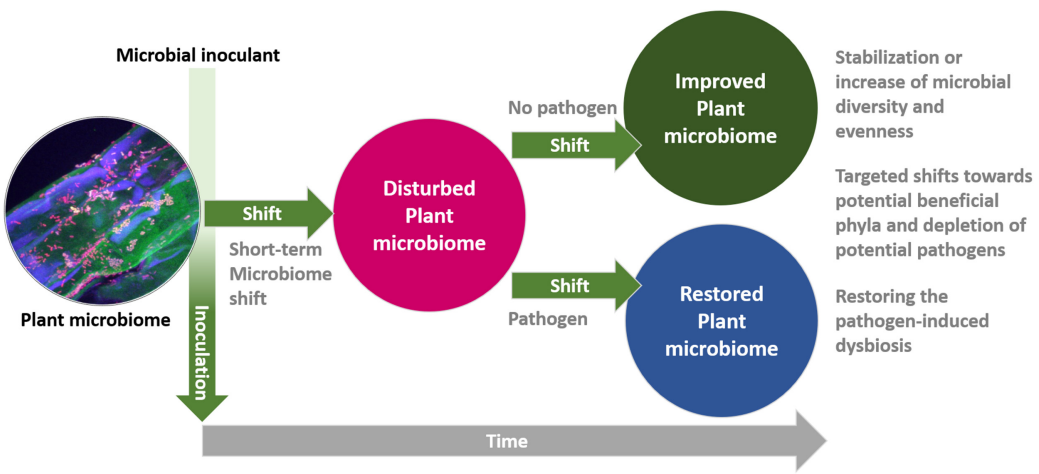

FIGURE 2 | A model for plant microbiome responses to microbial inoculants. Inoculation of microbial inoculants induces short-term shifts and improves or restores a healthy plant microbial community on a long term.

these methods are prevalent, it is important to mention that a large number of publications is available that highlight the bias in DNA extraction and processing procedures for subsequent analysis of microbiomes (Albertsen et al., 2015). PCR-amplified 16S rRNA genes (bacteria, archaea) or ITS fragments amplified from total community DNA were analyzed by fingerprinting methods in the past and presently by amplicon sequencing. The latter method is suitable to unravel the taxonomic composition but also shifts in the relative abundance or diversity changes. So-called responders to the treatments (microbial inoculants)—taxa that significantly increased or decreased in relative abundance—can be determined by comparative analyses of amplicon sequence data from inoculated and non-inoculated treatments. To avoid studying relic DNA or such from dead cells, propidium monoazide (PMA) can be implemented. It can only penetrate membrane-damaged cells, where a photo-induced azide group covalently binds to DNA and effectively inhibits PCR amplification of DNA from dead cells of both Gram-negative and Gram-positive bacteria (Nocker et al., 2006). Short read sequences with typically 150–300 bp read length from Illumina high throughput sequencing should provide sufficient sequencing depth after quality filtering and data processing to obtain taxonomic composition on genus level. Even though the number of reads necessary to obtain full diversity in samples

is impossible to define, beta diversity is usually covered with a lower sequencing depth, while higher read numbers are needed for alpha diversity and rare taxa (Gołębiewski and Tretyn, 2020). Compositional and microbiome shift observations are possible with this data, however, functional predictions based on 16S rRNA and ITS region data should be carefully interpreted. Presently, we mainly compare detected taxa to what is known from isolates of the particular species. However, it is also well known that plant-beneficial traits are typically strain-specific. Strains sharing identical 16S rRNA gene sequences might have diverse plant-beneficial traits. Thus, linking amplicon sequencing with plant-beneficial functions remains challenging. Conducting cultivation-based characterization in parallel has the advantage that strain-specific traits ranging from rhizosphere competence, *in vitro* antagonistic activity, production of extracellular enzymes, siderophores, indol acetic can be determined. Even though, it must be mentioned that *in vitro* effects may not always represent *in vivo* effects of a certain strain. Moreover, whole genome sequencing allows to precisely determine the taxonomy by multi-locus sequencing and comparative genomics (Loper et al., 2012; Kuzmanović et al., 2019). Furthermore, interaction studies with the plant can be performed and the effects on plant hormones, secondary metabolites, root growth mineral uptake, and the indigenous microbiome can be assessed. Metagenome sequencing and single cell genomics (based on Raman or other high throughput isolation and screening techniques) have enormous potential to disentangle inoculant-induced microbiome shifts with cultivation-independent methods (Jansson and Baker, 2016; Song et al., 2017; Zhang et al., 2021). Moreover, evaluating inoculants from a functional perspective using a broad range of omic approaches is important to assess their impact on ecosystem functioning (Mawarda et al., 2020). Most critical is the sensitivity of the cultivation independent methods that will likely detect shifts in the dominant members of the plant microbiome (Blau et al., 2018). Microbiome research is strongly driven by methodological advances and, until now, there is no perfect and universal method. It can be expected that in the future an improved toolbox of technologies will reduce bias resulting from each individual technology and result in a more complete view on the biological system as a whole (Berg et al., 2020).

Assessment and Integration of Microbiome Modulations Into Mode of Action Patterns

Interestingly, no study so far described an enrichment of potential pathogens due to inoculant application, neither for plants nor for humans. In contrast, many studies described an enrichment of well-known plant beneficial bacteria, e.g., *Pseudomonas* (Sang and Kim, 2012; Tao et al., 2020), *Bacillus* (Yin et al., 2013), *Acidobacteria* (Saravanakumar et al., 2017; Wang et al., 2018), *Burkholderia, Comamonas, Ramlibacter* (Zhang et al., 2019), and *Verrucomicrobia* (Schmidt et al., 2014; Eltlbany et al., 2019). In this context, an interesting study was published by Lee et al. (2021). They identified a higher relative abundance of *Actinobacteria* and *Firmicutes* in healthy tomato plants. Representative isolates of the health indicators (*Brevibacterium frigoritolerans* HRS1, *Bacillus niacini* HRS2, *Solibacillus silvestris* HRS3, and *Bacillus luciferensis* HRS4) were able to induce an immune activation and extended plant protection against *R. solanacearum*. In addition, several studies described the depletion of potential pathogens due to inoculant application (Schmidt et al., 2012; Saravanakumar et al., 2017; Elsayed et al., 2020). These studies provide indications that depletion of pathogens might be an accompanying effect to the enrichment of plant-beneficial strains, which together constitutes the observed microbiome shifts. Wang et al. (2018) analyzed different consortia and showed that the microbiome is specifically modulated by distinct microbial strains. Gu et al. (2020) reported that growth inhibitory siderophores secreted by microbial inoculants or members of the indigenous rhizosphere microbiome play an important role in suppressing the bacterial phytopathogen *R. solanacearum* and protecting plant health. They proposed a mechanistic link between microbiome competition for iron and plant protection (Gu et al., 2020). Such observations require further assessments in order to better understand the underlying molecular modes of action. The current knowledge base indicates that microbiome modulations are part of the interaction of microbial inoculants with plant hosts. Together with the ability to suppress pathogens, induce resistance, provide nutrients and minerals, and change/balance the hormonal status of plants, the interaction of microbial inoculants with the indigenous plant microbiome is important to consider. Moreover, secondary effects induced by modulating the native microbiome are possible, e.g., recruitment of other beneficial microbes.

DISCUSSION

Altogether, we have identified and described six different modulations types of the plant microbiome by microbial inoculants. According to available literature, the extent of modulation depends on the sampling time following the application. Directly after the application, strong, transient microbiome shifts are commonly observed. A few weeks after the application, shifts are often not evident anymore; however, at this point a stabilization effect or even an increase in microbial diversity and evenness was often described. This observation is in line with the intermediate disturbance hypothesis in macro-ecology, which suggests that local species diversity is maximized when ecological disturbance is neither too rare nor too frequent (Wilkinson, 1999). On the other hand, if the microbial ecosystem is already substantially disturbed, which is reflected by a severe dysbiosis, distinct microbial inoculants are able to restore the dysbiosis by compensation or a reduction of pathogen-induced microbiome shifts. Considering microbiome composition, all studies that are available so far describe shifts enriching potentially beneficial microbes while simultaneously decreasing potential pathogens. A summary of previous results was integrated in a model for plant microbiome responses to microbial inoculants (**Figure 2**).

Microbial inoculants are only one out of many different possibilities to manage microbiomes. While microbial inoculants are well-defined, formulated single or multi species preparations, highly diverse microbiome transplants from other environments or bio-active metabolites can also be used to directly manage microbiomes. In addition, by changing the environmental conditions, the structure and function of microbiomes can be shifted (Berg and Smalla, 2009). In general, various treatments were shown to induce similar patterns and microbiome shifts (Cernava et al., 2019; Guimarães et al., 2020). Surprisingly, breeding was shown to cause similar, long-term microbiome shifts as well (Pérez-Jaramillo et al., 2018). In the last centuries, plant breeding was directed to high yields and to resistance toward pathogens; high yield cultivars enriched plant growth promoting microorganisms (Pérez-Jaramillo et al., 2018), while resistant cultivars enrich microorganisms antagonistic toward pathogens (Adam et al., 2018; Mendes et al., 2019; Wolfgang et al., 2020). For example, *Rhizoctonia*-tolerant cultivars of sugar beet, mainly mediated by the Fort Collins Resistance (USDA), resulted in an enrichment of bioactive *Pseudomonas* strains in the rhizosphere. Strains of *Pseudomonas* are also able to induce the same resistance under experimental settings (Wolfgang et al., 2020). Only recently two independent studies have shown that microorganisms can shape their host phenotypes by evoking resistance traits that are undistinguishable from innate plant immunity: in sugar beets two members of the native endorhiza microbiota (*Chitinophaga* and *Flavobacterium)* were shown to confer resistance to the host plant against *Rhizoctonia solani* (Carrión et al., 2019) and in rice a seed-endophytic *Sphingomonas melonis* strain was shown to confer disease resistance against *Burkholderia plantarii* that causes seedling blight (Matsumoto et al., 2021). The available evidence for such functions strongly suggests integrating microbiome research into breeding and plant protection strategies. Management can also induce microbiome shifts; for example, biofumigation-modulated soil microbiomes in response to organic amendments and was proposed to be a major mode of action. The effects of biofumigation on apple plant growth were site-dependent and might result from suppression of soil-borne pathogens and changes in soil microbial community compositions and activity through the additional nutrients from the incorporated biomass (Yim et al., 2017). Thus, combining the activation of indigenous beneficial bacteria in the soil and microbial inoculants through suitable organic amendments seems a promising approach for microbiome modulation and enhancing plant growth. However, we have to take into account that also pathogens evolved to manipulate host microbiomes to their advantage by using effector proteins (Snelders et al., 2020).

Direct microbiome modulation by microbial inoculants or such that are mediated by the host plant provide important options for sustainable agriculture and circular bio-economy. The application of microbial inoculants to replace chemical pesticides and to use waste materials (especially agricultural residue) for their production is an important step in counteracting major problems of the future such as climate change, biodiversity loss and changes in biogeochemical cycles. It is highly interesting that similar types of microbiome modulations were detected in plants, animals and humans (Frerejacques et al., 2020; Ojima et al., 2020). The restoration of reduced diversity of the microbiome by administration of specific microorganisms was observed in animals as well as humans. This cross-kingdom similarity was already described for microbiome functioning (Mendes and Raaijmakers, 2015) and control (Berg et al., 2015). Due to their importance, microbiome shifts definitively require a better understanding of the underlying communication and interaction mechanisms within the microbiome. Further experimental evidence, utilizing gnotobiotic plant trials as well as field conditions, is needed to mechanistically explore the underlying mechanisms. Especially the role of the host in the microbiome modulation requires a better understanding, along with the molecular pathways involved in the host response. Multi-omics approaches can help to understand the interaction of microbial inoculants with all possible partners including the host, the microbiome and their interplay (Jansson and Baker, 2016). At least it is proposed to re-think current categories of microbial inoculants and their regulation to open new possibilities for applications toward sustainable agriculture.

AUTHOR CONTRIBUTIONS

GB drafted and refined the manuscript. All authors critically read the article, contributed to the writing, and approved it for publication.

FUNDING

The authors received funding from the European Union's Horizon 2020 research and innovation program under grant agreement No. 817946 (Excalibur) awarded to GB. The research program "Rhizosphere Spatiotemporal Organization—a Key to Rhizosphere Functions" of the German Science Foundation, funded by the German Research Foundation (SM59/19-1) is acknowledged by KS.

REFERENCES

Abdelfattah, A., Ruano-Rosa, D., Cacciola, S. O., Nicosia, M. G. L. D., and Schena, L. (2018). Impact of *Bactrocera oleae* on the fungal microbiota of ripe olive drupes. *PLoS One* 13:e0199403. doi: 10.1371/journal.pone.0199403

Abdelfattah, A., Wisniewski, M., Schena, L., and Tack, A. J. (2021). Experimental evidence of microbial inheritance in plants and transmission routes from seed to phyllosphere and root. *Environ. Microbiol.* doi: 10.1111/1462-2920.15392

Adam, E., Bernhart, M., Müller, H., Winkler, J., and Berg, G. (2018). The *Cucurbita pepo* seed microbiome: genotype-specific composition and implications for breeding. *Plant Soil* 422, 35–49.

Adam, E., Groenenboom, A. E., Kurm, V., Rajewska, M., Schmidt, R., Tyc, O., et al. (2016). Controlling the microbiome: microhabitat adjustments for successful biocontrol strategies in soil and human gut. *Front. Microbiol.* 7:1079. doi: 10.3389/fmicb.2016.01079

Adesina, M. F., Grosch, R., Lembke, A., Vatchev, T. D., and Smalla, K. (2009). In vitro antagonists of *Rhizoctonia solani* tested on lettuce: Rhizosphere

competence, biocontrol efficiency and rhizosphere microbial community response: research article. *FEMS Microbiol. Ecol.* 69, 62–74. doi: 10.1111/j.1574-6941.2009.00685.x

Albertsen, M., Karst, S. M., Ziegler, A. S., Kirkegaard, R. H., and Nielsen, P. H. (2015). Back to basics–the influence of DNA extraction and primer choice on phylogenetic analysis of activated sludge communities. *PLoS One* 10:e0132783. doi: 10.1371/journal.pone.0132783

Andreote, F. D., Rocha, U. N., da.Araújo, W. L., Azevedo, J. L., and van Overbeek, L. S. (2010). Effect of bacterial inoculation, plant genotype and developmental stage on root-associated and endophytic bacterial communities in potato (*Solanum tuberosum*). *Antonie van Leeuwenhoek* 97, 389–399. doi: 10.1007/s10482-010-9421-9

Bakker, P. A., Berendsen, R. L., Van Pelt, J. A., Vismans, G., Yu, K., Li, E., et al. (2020). The soil-borne identity and microbiome-assisted agriculture: looking back to the future. *Mol. Plant* 13, 1394–1401.

Balbín-Suárez, A., Lucas, M., Vetterlein, D., Sørensen, S. J., Winkelmann, T., Smalla, K., et al. (2020). Exploring microbial determinants of apple replant disease (ARD): a microhabitat approach under split-root design. *FEMS Microbiol. Ecol.* 96:fiaa211. doi: 10.1093/femsec/fiaa211

Berg, G. (2009). Plant–microbe interactions promoting plant growth and health: perspectives for controlled use of microorganisms in agriculture. *Appl. Microbiol. Biotechnol.* 84, 11–18. doi: 10.1007/s00253-009-2092-7

Berg, G., and Raaijmakers, J. M. (2018). Saving seed microbiomes. *ISME J.* 12, 1167–1170.

Berg, G., and Smalla, K. (2009). Plant species and soil type cooperatively shape the structure and function of microbial communities in the rhizosphere. *FEMS Microbiol. Ecol.* 68, 1–13. doi: 10.1111/j.1574-6941.2009.00654.x

Berg, G., Köberl, M., Rybakova, D., Müller, H., Grosch, R., and Smalla, K. (2017). Plant microbial diversity is suggested as the key to future biocontrol and health trends. *FEMS Microbiol. Ecol.* 93:fix050. doi: 10.1093/femsec/fix050

Berg, G., Krause, R., and Mendes, R. (2015). Cross-kingdom similarities in microbiome ecology and biocontrol of pathogens. *Front. Microbiol.* 6:1311. doi: 10.3389/fmicb.2015.01311

Berg, G., Krechel, A., Ditz, M., Sikora, R. A., Ulrich, A., and Hallmann, J. (2005). Endophytic and ectophytic potato-associated bacterial communities differ in structure and antagonistic function against plant pathogenic fungi. *FEMS Microbiol. Ecol.* 51, 215–229. doi: 10.1016/j.femsec.2004.08.006

Berg, G., Rybakova, D., Fischer, D., Cernava, T., Vergès, M.-C. C., Charles, T., et al. (2020). Microbiome definition re-visited: old concepts and new challenges. *Microbiome* 8, 1–22.

Berg, G., Rybakova, D., Grube, M., and Köberl, M. (2016). The plant microbiome explored: implications for experimental botany. *J. Exp. Bot.* 67, 995–1002. doi: 10.1093/jxb/erv466

Bergna, A., Cernava, T., Rändler, M., Grosch, R., Zachow, C., and Berg, G. (2018). Tomato seeds preferably transmit plant beneficial endophytes. *Phytobiomes* 2, 183–193. doi: 10.1094/PBIOMES-06-18-0029-R

Blau, K., Bettermann, A., Jechalke, S., Fornefeld, E., Vanrobaeys, Y., Stalder, T., et al. (2018). The transferable resistome of produce. *MBio* 9, e1300–e1318.

Bragina, A., Oberauner-Wappis, L., Zachow, C., Halwachs, B., Thallinger, G. G., Müller, H., et al. (2014). The *Sphagnum* microbiome supports bog ecosystem functioning under extreme conditions. *Mol. Ecol.* 23, 4498–4510.

Carrión, V. J., Perez-Jaramillo, J., Cordovez, V., Tracanna, V., De Hollander, M., Ruiz-Buck, D., et al. (2019). Pathogen-induced activation of disease-suppressive functions in the endophytic root microbiome. *Science* 366, 606–612.

Cernava, T., Chen, X., Krug, L., Li, H., Yang, M., and Berg, G. (2019). The tea leaf microbiome shows specific responses to chemical pesticides and biocontrol applications. *Sci. Total Environ.* 667, 33–40.

Chen, F., Wang, M., Zheng, Y., Li, S., Wang, H., Han, D., et al. (2013). The effect of biocontrol bacteria on rhizosphere bacterial communities analyzed by plating and PCR-DGGE. *Curr. Microbiol.* 67, 177–182. doi: 10.1007/s00284-013-0347-0

Chowdhury, S. P., Dietel, K., Rändler, M., Schmid, M., Junge, H., Borriss, R., et al. (2013). Effects of *Bacillus amyloliquefaciens* FZB42 on lettuce growth and health under pathogen pressure and Its impact on the rhizosphere bacterial community. *PLoS One* 8:e68818. doi: 10.1371/journal.pone.0068818

DunhamTrimmer. (2017). *Biological Control Global Market Overview*. Available online at: http://ir4-test.metro.ucdavis.edu/events/2017_SLR_Meeting/Presentations/GeneralPresentations/1%20Trimmer%20-%20Global%20Biocontrol%20Market%202017.pdf (accessed August 12, 2020).

Elsayed, T. R., Jacquiod, S., Nour, E. H., Sørensen, S. J., and Smalla, K. (2020). Biocontrol of Bacterial Wilt Disease Through Complex Interaction Between Tomato Plant, Antagonists, the Indigenous Rhizosphere Microbiota, and *Ralstonia solanacearum*. *Front. Microbiol.* 10:2835. doi: 10.3389/fmicb.2019.02835

Eltlbany, N., Baklawa, M., Ding, G.-C., Nassal, D., Weber, N., Kandeler, E., et al. (2019). Enhanced tomato plant growth in soil under reduced P supply through microbial inoculants and microbiome shifts. *FEMS Microbiol. Ecol.* 95:fiz124. doi: 10.1093/femsec/fiz124

Erlacher, A., Cardinale, M., Grosch, R., Grube, M., and Berg, G. (2014). The impact of the pathogen *Rhizoctonia solani* and its beneficial counterpart *Bacillus amyloliquefaciens* on the indigenous lettuce microbiome. *Front. Microbiol.* 5:175. doi: 10.3389/fmicb.2014.00175

Etemadi, M., Zuther, E., Müller, H., Hincha, D. K., and Berg, G. (2018). Ecotype-dependent response of bacterial communities associated with *Arabidopsis* to cold acclimation. *Phytobiomes* 2, 3–13.

Frerejacques, M., Rousselle, C., Gauthier, L., Cottet-Emard, S., Derobert, L., Roynette, A., et al. (2020). Human skin bacterial community response to probiotic (*Lactobacillus reuteri* DSM 17938) introduction. *Microorganisms* 8:1223. doi: 10.3390/microorganisms8081223

Gołębiewski, M., and Tretyn, A. (2020). Generating amplicon reads for microbial community assessment with next-generation sequencing. *J. Appl. Microbiol.* 128, 330–354.

Götz, M., Gomes, N. C. M., Dratwinski, A., Costa, R., Berg, G., Peixoto, R., et al. (2006). Survival of gfp-tagged antagonistic bacteria in the rhizosphere of tomato plants and their effects on the indigenous bacterial community. *FEMS Microbiol. Ecol.* 56, 207–218. doi: 10.1111/j.1574-6941.2006.00093.x

Grosch, R., Dealtry, S., Schreiter, S., Berg, G., Mendonça-Hagler, L., and Smalla, K. (2012). Biocontrol of *Rhizoctonia solani*: complex interaction of biocontrol strains, pathogen and indigenous microbial community in the rhizosphere of lettuce shown by molecular methods. *Plant Soil* 361, 343–357. doi: 10.1007/s11104-012-1239-y

Gu, S., Yang, T., Shao, Z., Wang, T., Cao, K., Jousset, A., et al. (2020). Siderophore-mediated interactions determine the disease suppressiveness of microbial consortia. *mSystems* 5, e811–e819. doi: 10.1128/mSystems.00811-19

Guimarães, R. A., Pherez-Perrony, P. E., Müller, H., Berg, G., Medeiros, F. H. V., and Cernava, T. (2020). Microbiome-guided evaluation of *Bacillus subtilis* BIOUFLA2 application to reduce mycotoxins in maize kernels. *Biol. Control* 150:104370. doi: 10.1016/j.biocontrol.2020.104370

Hardoim, P. R., Van Overbeek, L. S., Berg, G., Pirttilä, A. M., Compant, S., Campisano, A., et al. (2015). The hidden world within plants: ecological and evolutionary considerations for defining functioning of microbial endophytes. *Microbiol. Mol. Biol. Rev.* 79, 293–320.

Jansson, J. K., and Baker, E. S. (2016). A multi-omic future for microbiome studies. *Nat. Microbiol.* 1:16049. doi: 10.1038/nmicrobiol.2016.49

Köhl, J., Kolnaar, R., and Ravensberg, W. J. (2019). Mode of action of microbial biological control agents against plant diseases: relevance beyond efficacy. *Front. Plant Sci.* 10:845.

Kong, H. G., Song, G. C., Sim, H.-J., and Ryu, C.-M. (2020). Achieving similar root microbiota composition in neighbouring plants through airborne signalling. *ISME J.* 15, 397–408.

Kröber, M., Wibberg, D., Grosch, R., Eikmeyer, F., Verwaaijen, B., Chowdhury, S. P., et al. (2014). Effect of the strain *Bacillus amyloliquefaciens* FZB42 on the microbial community in the rhizosphere of lettuce under field conditions analyzed by whole metagenome sequencing. *Front. Microbiol.* 5:252. doi: 10.3389/fmicb.2014.00252

Kusstatscher, P., Wicaksono, W. A., Thenappan, D. P., Adam, E., Müller, H., and Berg, G. (2020). Microbiome management by biological and chemical treatments in maize is linked to plant health. *Microorganisms* 8:1506. doi: 10.3390/microorganisms8101506

Kuzmanović, N., Behrens, P., Idczak, E., Wagner, S., Götz, M., Spröer, C., et al. (2019). A novel group of *Rhizobium tumorigenes*-like *Agrobacteria* associated with crown gall disease of *Rhododendron* and blueberry. *Phytopathology®* 109, 1840–1848. doi: 10.1094/PHYTO-05-19-0167-R

Lee, S.-M., Kong, H. G., Song, G. C., and Ryu, C.-M. (2021). Disruption of *Firmicutes* and *Actinobacteria* abundance in tomato rhizosphere causes the

incidence of bacterial wilt disease. *ISME J.* 15, 330–347. doi: 10.1038/s41396-020-00785-x

Li, Y., Guo, Q., He, F., Li, Y., Xue, Q., and Lai, H. (2020). Biocontrol of root diseases and growth promotion of the tuberous plant *Aconitum carmichaelii* induced by *Actinomycetes* are related to shifts in the rhizosphere microbiota. *Microb. Ecol.* 79, 134–147. doi: 10.1007/s00248-019-01388-6

Linares, J. F., Gustafsson, I., Baquero, F., and Martinez, J. (2006). Antibiotics as intermicrobial signaling agents instead of weapons. *Proc. Nat. Acad. Sci.U.S.A.* 103, 19484–19489.

Loper, J. E., Hassan, K. A., Mavrodi, D. V., Ii, E. W. D., Lim, C. K., Shaffer, B. T., et al. (2012). Comparative genomics of plant-associated *Pseudomonas* spp.: insights into diversity and inheritance of traits involved in multitrophic interactions. *PLoS Genetics* 8:e1002784. doi: 10.1371/journal.pgen.1002784

Lugtenberg, B. J. J., Chin-A-Woeng, T. F. C., and Bloemberg, G. V. (2002). Microbe–plant interactions: principles and mechanisms. *Antonie Van Leeuwenhoek* 81, 373–383. doi: 10.1023/A:1020596903142

Lugtenberg, B., and Kamilova, F. (2009). Plant-growth-promoting rhizobacteria. *Annu. Rev. Microbiol.* 63, 541–556. doi: 10.1146/annurev.micro.62.081307.162918

Manzotti, A., Bergna, A., Burow, M., Jørgensen, H. J. L., Cernava, T., Berg, G., et al. (2020). Insights into the community structure and lifestyle of the fungal root endophytes of tomato by combining amplicon sequencing and isolation approaches with phytohormone profiling. *FEMS Microbiol. Ecol.* 96:fiaa052. doi: 10.1093/femsec/fiaa052

Massart, S., Martinez-Medina, M., and Jijakli, M. H. (2015). Biological control in the microbiome era: challenges and opportunities. *Biol. Control* 89, 98–108. doi: 10.1016/j.biocontrol.2015.06.003

Matsumoto, H., Fan, X., Wang, Y., Kusstatscher, P., Duan, J., Wu, S., et al. (2021). Bacterial seed endophyte shapes disease resistance in rice. *Nat. Plants* 7, 60–72. doi: 10.1038/s41477-020-00826-5

Mawarda, P. C., Le Roux, X., Van Elsas, J. D., and Salles, J. F. (2020). Deliberate introduction of invisible invaders: a critical appraisal of the impact of microbial inoculants on soil microbial communities. *Soil Biol. Biochem.* 148:107874.

Mendes, L. W., Gonçalves De Chaves, M. G., da Fonseca, M., de, C., Mendes, R., Raaijmakers, J. M., et al. (2019). Resistance breeding of common bean shapes the physiology of the rhizosphere microbiome. *Front. Microbiol.* 10:2252. doi: 10.3389/fmicb.2019.02252

Mendes, R., and Raaijmakers, J. M. (2015). Cross-kingdom similarities in microbiome functions. *ISME J* 9, 1905–1907. doi: 10.1038/ismej.2015.7

Neumann, G., Bott, S., Ohler, M., Mock, H.-P., Lippmann, R., Grosch, R., et al. (2014). Root exudation and root development of lettuce (*Lactuca sativa* L. cv. Tizian) as affected by different soils. *Front. Microbiol.* 5:2. doi: 10.3389/fmicb.2014.00002

Nocker, A., Cheung, C.-Y., and Camper, A. K. (2006). Comparison of propidium monoazide with ethidium monoazide for differentiation of live vs. dead bacteria by selective removal of DNA from dead cells. *J. Microbiol. Methods* 67, 310–320. doi: 10.1016/j.mimet.2006.04.015

Ojima, M. N., Gotoh, A., Takada, H., Odamaki, T., Xiao, J.-Z., Katoh, T., et al. (2020). *Bifidobacterium bifidum* suppresses gut inflammation caused by repeated antibiotic disturbance without recovering gut microbiome diversity in mice. *Front. Microbiol.* 11:1349. doi: 10.3389/fmicb.2020.01349

Passera, A., Vacchini, V., Cocetta, G., Shahzad, G.-I.-R., Arpanahi, A. A., Casati, P., et al. (2020). Towards nutrition-sensitive agriculture: an evaluation of biocontrol effects, nutritional value, and ecological impact of bacterial inoculants. *Sci. Total Environ.* 724:138127. doi: 10.1016/j.scitotenv.2020.138127

Paul Chowdhury, S., Babin, D., Sandmann, M., Jacquiod, S., Sommermann, L., Sørensen, S. J., et al. (2019). Effect of long-term organic and mineral fertilization strategies on rhizosphere microbiota assemblage and performance of lettuce. *Environ. Microbiol.* 21, 2426–2439.

Pérez-Jaramillo, J. E., Carrión, V. J., de Hollander, M., and Raaijmakers, J. M. (2018). The wild side of plant microbiomes. *Microbiome* 6:143. doi: 10.1186/s40168-018-0519-z

Philippot, L., Raaijmakers, J. M., Lemanceau, P., and van der Putten, W. H. (2013). Going back to the roots: the microbial ecology of the rhizosphere. *Nat. Rev. Microbiol.* 11, 789–799. doi: 10.1038/nrmicro3109

Pieterse, C. M. J., Zamioudis, C., Berendsen, R. L., Weller, D. M., Van Wees, S. C. M., and Bakker, P. A. H. M. (2014). Induced systemic resistance by beneficial microbes. *Annu. Rev. Phytopathol.* 52, 347–375. doi: 10.1146/annurev-phyto-082712-102340

Remus-Emsermann, M. N., and Schlechter, R. O. (2018). Phyllosphere microbiology: at the interface between microbial individuals and the plant host. *N. Phytol.* 218, 1327–1333.

Rezki, S., Campion, C., Iacomi-Vasilescu, B., Preveaux, A., Toualbia, Y., Bonneau, S., et al. (2016). Differences in stability of seed-associated microbial assemblages in response to invasion by phytopathogenic microorganisms. *PeerJ.* 4:e1923.

Rodríguez-Caballero, G., Caravaca, F., Fernández-González, A. J., Alguacil, M. M., Fernández-López, M., and Roldán, A. (2017). Arbuscular mycorrhizal fungi inoculation mediated changes in rhizosphere bacterial community structure while promoting revegetation in a semiarid ecosystem. *Sci. Total Environ.* 584–585, 838–848. doi: 10.1016/j.scitotenv.2017.01.128

Rosier, A., Bishnoi, U., Lakshmanan, V., Sherrier, D. J., and Bais, H. P. (2016). A perspective on inter-kingdom signaling in plant–beneficial microbe interactions. *Plant Mol. Biol.* 90, 537–548.

Sánchez-Cañizares, C., Jorrín, B., Poole, P. S., and Tkacz, A. (2017). Understanding the holobiont: the interdependence of plants and their microbiome. *Curr. Opin. Microbiol.* 38, 188–196.

Sang, M. K., and Kim, K. D. (2012). Plant growth-promoting rhizobacteria suppressive to *Phytophthora* blight affect microbial activities and communities in the rhizosphere of pepper (*Capsicum annuum* L.) in the field. *Appl. Soil Ecol.* 62, 88–97. doi: 10.1016/j.apsoil.2012.08.001

Saravanakumar, K., Li, Y., Yu, C., Wang, Q. Q., Wang, M., Sun, J., et al. (2017). Effect of *Trichoderma harzianum* on maize rhizosphere microbiome and biocontrol of *Fusarium* Stalk rot. *Sci. Rep.* 7:1771. doi: 10.1038/s41598-017-01680-w

Schenk, M. F., Hamelink, R., van der Vlugt, R. A. A., Vermunt, A. M. W., Kaarsenmaker, R. C., and Stijger, I. C. C. M. M. (2010). The use of attenuated isolates of Pepino mosaic virus for cross-protection. *Eur. J. Plant Pathol.* 127, 249–261. doi: 10.1007/s10658-010-9590-4

Scherwinski, K., Grosch, R., and Berg, G. (2008). Effect of bacterial antagonists on lettuce: active biocontrol of *Rhizoctonia solani* and negligible, short-term effects on nontarget microorganisms. *FEMS Microbiol. Ecol.* 64, 106–116.

Schierstaedt, J., Jechalke, S., Nesme, J., Neuhaus, K., Sørensen, S. J., Grosch, R., et al. (2020). *Salmonella* persistence in soil depends on reciprocal interactions with indigenous microorganisms. *Environ. Microbiol.* 22, 2639–2652. doi: 10.1111/1462-2920.14972

Schmidt, C. S., Alavi, M., Cardinale, M., Müller, H., and Berg, G. (2012). *Stenotrophomonas rhizophila* DSM14405 T promotes plant growth probably by altering fungal communities in the rhizosphere. *Biol. Fertil. Soils* 48, 947–960.

Schmidt, R., Etalo, D. W., de Jager, V., Gerards, S., Zweers, H., de Boer, W., et al. (2016). Microbial small talk: volatiles in fungal–bacterial interactions. *Front. Microbiol.* 6:1495. doi: 10.3389/fmicb.2015.01495

Schmidt, R., Köberl, M., Mostafa, A., Ramadan, E., Monschein, M., Jensen, K., et al. (2014). Effects of bacterial inoculants on the indigenous microbiome and secondary metabolites of chamomile plants. *Front. Microbiol.* 5:64. doi: 10.3389/fmicb.2014.00064

Schreiter, S., Babin, D., Smalla, K., and Grosch, R. (2018). Rhizosphere competence and biocontrol effect of *Pseudomonas* sp. RU47 independent from plant species and soil type at the field scale. *Front. Microbiol.* 9:97. doi: 10.3389/fmicb.2018.00097

Schreiter, S., Ding, G.-C., Grosch, R., Kropf, S., Antweiler, K., and Smalla, K. (2014a). Soil type-dependent effects of a potential biocontrol inoculant on indigenous bacterial communities in the rhizosphere of field-grown lettuce. *FEMS Microbiol. Ecol.* 90, 718–730.

Schreiter, S., Sandmann, M., Smalla, K., and Grosch, R. (2014b). Soil type dependent rhizosphere competence and biocontrol of two bacterial inoculant strains and their effects on the rhizosphere microbial community of field-grown lettuce. *PLoS One* 9:e103726. doi: 10.1371/journal.pone.0103726

Schwieger, F., and Tebbe, C. C. (2000). Effect of field inoculation with *Sinorhizobium meliloti* L33 on the composition of bacterial communities in rhizospheres of a target plant *Medicago sativa* and a non-target plant *Chenopodium album*—linking of 16S rRNA gene-based single-strand conformation polymorphism community profiles to the diversity of cultivated bacteria. *Appl. Environ. Microbiol.* 66, 3556. doi: 10.1128/AEM.66.8.3556-3565.2000

Shen, Z., Ruan, Y., Chao, X., Zhang, J., Li, R., and Shen, Q. (2015). Rhizosphere microbial community manipulated by 2 years of consecutive biofertilizer application associated with banana *Fusarium* wilt disease suppression. *Biol. Fertil. Soils* 51, 553–562. doi: 10.1007/s00374-015-1002-7

Snelders, N. C., Rovenich, H., Petti, G. C., Rocafort, M., van den Berg, G. C. M., Vorholt, J. A., et al. (2020). Microbiome manipulation by a soil-borne fungal plant pathogen using effector proteins. *Nat. Plants* 6, 1365–1374. doi: 10.1038/s41477-020-00799-5

Song, X., Ying, L., JingJing, W., TingTing, Y., YiFan, H., XingBiao, W., et al. (2015). Isolation and potential of *Ochrobactrum* sp. NW-3 to increase the growth of cucumber. *Int. J. Agric. Policy Res.* 3, 341–350.

Song, Y., Kaster, A., Vollmers, J., Song, Y., Davison, P. A., Frentrup, M., et al. (2017). Single-cell genomics based on Raman sorting reveals novel carotenoid-containing bacteria in the Red Sea. *Microb. Biotechnol.* 10, 125–137.

Tao, C., Li, R., Xiong, W., Shen, Z., Liu, S., Wang, B., et al. (2020). Bio-organic fertilizers stimulate indigenous soil Pseudomonas populations to enhance plant disease suppression. *Microbiome* 8, 1–14.

Trivedi, P., Leach, J. E., Tringe, S. G., Sa, T., and Singh, B. K. (2020). Plant–microbiome interactions: from community assembly to plant health. *Nat. Rev. Microbiol.* 18, 607–621.

van Elsas, J. D., Chiurazzi, M., Mallon, C. A., Elhottovâ, D., Krištůfek, V., and Salles, J. F. (2012). Microbial diversity determines the invasion of soil by a bacterial pathogen. *Proc. Nat. Acad. Sci.* 109, 1159–1164. doi: 10.1073/pnas.1109326109

Vandenkoornhuyse, P., Quaiser, A., Duhamel, M., Le Van, A., and Dufresne, A. (2015). The importance of the microbiome of the plant holobiont. *N. Phytol.* 206, 1196–1206. doi: 10.1111/nph.13312

Vayssier-Taussat, M., Albina, E., Citti, C., Cosson, J. F., Jacques, M.-A., Lebrun, M.-H., et al. (2014). Shifting the paradigm from pathogens to pathobiome: new concepts in the light of meta-omics. *Front. Cell. Infect. Microbiol.* 4:29. doi: 10.3389/fcimb.2014.00029

Venturi, V., and Keel, C. (2016). Signaling in the rhizosphere. *Trends Plant Sci.* 21, 187–198.

Verginer, M., Siegmund, B., Cardinale, M., Müller, H., Choi, Y., Míguez, C. B., et al. (2010). Monitoring the plant epiphyte *Methylobacterium extorquens* DSM 21961 by real-time PCR and its influence on the strawberry flavor. *FEMS Microbiol. Ecol.* 74, 136–145.

Vorholt, J. A. (2012). Microbial life in the phyllosphere. *Nat. Rev. Microbiol.* 10, 828–840.

Wagner, M. R., Lundberg, D. S., Coleman-Derr, D., Tringe, S. G., Dangl, J. L., and Mitchell-Olds, T. (2014). Natural soil microbes alter flowering phenology and the intensity of selection on flowering time in a wild *Arabidopsis* relative. *Ecol. Lett.* 17, 717–726.

Wang, J., Li, Q., Xu, S., Zhao, W., Lei, Y., Song, C., et al. (2018). Traits-based integration of multi-species inoculants facilitates shifts of indigenous soil bacterial community. *Front. Microbiol.* 9:1692. doi: 10.3389/fmicb.2018.01692

Wassermann, B., Cernava, T., Müller, H., Berg, C., and Berg, G. (2019). Seeds of native alpine plants host unique microbial communities embedded in cross-kingdom networks. *Microbiome* 7:108.

Weller, D. M., Raaijmakers, J. M., Gardener, B. B. M., and Thomashow, L. S. (2002). Microbial populations responsible for specific soil suppressiveness to plant pathogens. *Annu. Rev. Phytopathol.* 40, 309–348. doi: 10.1146/annurev.phyto.40.030402.110010

Whipps, J., Lewis, K., and Cooke, R. (1988). "Mycoparasitism and plant disease control," in *Fungi Biol. Control Syst.* ed. M. Burge (Manchester University Press), 161–187.

Wilkinson, D. M. (1999). The disturbing history of intermediate disturbance. *Oikos* 84, 145–147. doi: 10.2307/3546874

Windisch, S., Bott, S., Ohler, M.-A., Mock, H.-P., Lippmann, R., Grosch, R., et al. (2017). *Rhizoctonia solani* and bacterial inoculants stimulate root exudation of antifungal compounds in lettuce in a soil-type specific manner. *Agronomy* 7:44.

Wolfgang, A., Zachow, C., Müller, H., Grand, A., Temme, N., Tilcher, R., et al. (2020). Understanding the impact of cultivar, seed origin, and substrate on bacterial diversity of the sugar beet rhizosphere and suppression of soil-borne pathogens. *Front. Plant Sci.* 11:1450. doi: 10.3389/fpls.2020.560869

Yim, B., Nitt, H., Wrede, A., Jacquiod, S., Sørensen, S. J., Winkelmann, T., et al. (2017). Effects of soil pre-treatment with Basamid® granules, *Brassica juncea*, *Raphanus sativus*, and *Tagetes patula* on bacterial and fungal communities at two apple replant disease sites. *Front. Microbiol.* 8:1604. doi: 10.3389/fmicb.2017.01604

Yin, D., Wang, N., Xia, F., Li, Q., and Wang, W. (2013). Impact of biocontrol agents *Pseudomonas fluorescens* 2P24 and CPF10 on the bacterial community in the cucumber rhizosphere. *Eur. J. Soil Biol.* 59, 36–42. doi: 10.1016/j.ejsobi.2013.09.001

Zaneveld, J. R., McMinds, R., and Vega Thurber, R. (2017). Stress and stability: applying the Anna Karenina principle to animal microbiomes. *Nat. Microbiol.* 2:17121. doi: 10.1038/nmicrobiol.2017.121

Zhang, J., Liu, Y.-X., Guo, X., Qin, Y., Garrido-Oter, R., Schulze-Lefert, P., et al. (2021). High-throughput cultivation and identification of bacteria from the plant root microbiota. *Nat. Protoc.* 16, 988–1012.

Zhang, L.-N., Wang, D.-C., Hu, Q., Dai, X.-Q., Xie, Y.-S., Li, Q., et al. (2019). Consortium of plant growth-promoting Rhizobacteria strains suppresses sweet pepper disease by altering the *Rhizosphere Microbiota*. *Front. Microbiol.* 10:1668. doi: 10.3389/fmicb.2019.01668

Zhang, Q., Saleem, M., and Wang, C. (2017). Probiotic strain *Stenotrophomonas acidaminiphila* BJ1 degrades and reduces chlorothalonil toxicity to soil enzymes, microbial communities and plant roots. *AMB Exp.* 7:227. doi: 10.1186/s13568-017-0530-y

Conflict of Interest: The authors declare that the research was conducted in the absence of any commercial or financial relationships that could be construed as a potential conflict of interest.

frontiers in Microbiology

ORIGINAL RESEARCH
published: 14 April 2021
doi: 10.3389/fmicb.2021.644046

Evaluation of Phenolic Root Exudates as Stimulants of Saptrophic Fungi in the Rhizosphere

Anna Clocchiatti[1,2], S. Emilia Hannula[1], Marlies van den Berg[1], Maria P. J. Hundscheid[1] and Wietse de Boer[1,2]*

[1] Netherlands Institute of Ecology (NIOO-KNAW), Wageningen, Netherlands, [2] Soil Biology Group, Wageningen University, Wageningen, Netherlands

The rhizosphere microbial community of crop plants in intensively managed arable soils is strongly dominated by bacteria, especially in the initial stages of plant development. In order to establish more diverse and balanced rhizosphere microbiomes, as seen for wild plants, crop variety selection could be based on their ability to promote growth of saprotrophic fungi in the rhizosphere. We hypothesized that this can be achieved by increasing the exudation of phenolic acids, as generally higher fungal abundance is observed in environments with phenolic-rich inputs, such as exudates of older plants and litter leachates. To test this, a rhizosphere simulation microcosm was designed to establish gradual diffusion of root exudate metabolites from sterile sand into arable soil. With this system, we tested the fungus-stimulating effect of eight phenolic acids alone or in combination with primary root metabolites. Ergosterol-based fungal biomass measurements revealed that most phenolic acids did not increase fungal abundance in the arable soil layer. These results were supported by comparison of fungal biomass in the rhizosphere of wild type *Arabidopsis thaliana* plants and mutants with altered phenolic acid metabolism. Salicylic acid was the only phenolic acid that stimulated a higher fungal biomass in the arable soil layer of microcosms, but only when combined with a background of primary root metabolites. However, such effect on rhizosphere fungi was not confirmed for a salicylic acid-impaired *A. thaliana* mutant. For three phenolic acid treatments (chlorogenic acid, salicylic acid, vanillic acid) fungal and bacterial community compositions were analyzed using amplicon sequencing. Despite having little effect on fungal biomass, phenolic acids combined with primary metabolites promoted a higher relative abundance of soil-borne fungi with the ability to invade plant roots (*Fusarium, Trichoderma* and *Fusicolla* spp.) in the simulated rhizosphere. Bacterial community composition was also affected by these phenolic acids. Although this study indicates that phenolic acids do not increase fungal biomass in the rhizosphere, we highlight a potential role of phenolic acids as attractants for root-colonizing fungi.

Keywords: phenolic acids, root exudates, saprotrophic fungi, fungal biomass, fungal community, *Trichoderma*, *Fusarium*

OPEN ACCESS

Edited by:
Yong Wang,
Guizhou University, China

Reviewed by:
Barbara Drigo,
University of South Australia, Australia
Xiaogang Li,
Nanjing Forestry University, China

****Correspondence:***
Anna Clocchiatti
a.clocchiatti@nioo.knaw.nl

Specialty section:
This article was submitted to Microbe and Virus Interactions With Plants, a section of the journal Frontiers in Microbiology

Received: *19 December 2020*
Accepted: *08 March 2021*
Published: *14 April 2021*

Citation:
Clocchiatti A, Hannula SE, van den Berg M, Hundscheid MPJ and de Boer W (2021) Evaluation of Phenolic Root Exudates as Stimulants of Saptrophic Fungi in the Rhizosphere. Front. Microbiol. 12:644046. doi: 10.3389/fmicb.2021.644046

INTRODUCTION

The rhizosphere, the soil volume surrounding plant roots, is a hotspot for microbial activity (Pausch and Kuzyakov, 2018), harboring saprotrophic fungi, alongside bacteria and mycorrhizal fungi (Buée et al., 2009; van der Putten et al., 2016; Hugoni et al., 2018). Rhizosphere saprotrophic fungi can provide multiple services to the plant, such as promotion of plant growth and immunity (Koike et al., 2001; Kohler et al., 2007; Yadav et al., 2011; Naznin et al., 2014; Xia et al., 2019), as well as suppression of infection by soil-borne fungal pathogens. The presence of active saprotrophic fungi can limit root infection by soil-borne pathogens by increasing the competition for resources in the rhizosphere or by direct inhibitory activities such as antibiosis or mycoparasitism (Punja and Utkhede, 2003; Xiong et al., 2017; Latz et al., 2018). Moreover, rhizosphere saprotrophic fungi can influence beneficial rhizosphere bacteria and mycorrhizal fungi, hence indirectly influencing plant performance (Kohler et al., 2007; Saldajeno et al., 2008; de Boer et al., 2015; Qin et al., 2017; Deveau et al., 2018).

Intensively managed arable soils usually harbor low saprotrophic fungal biomass (Djajakirana et al., 1996; de Vries and Bardgett, 2012), which is also reflected in low activity of saprotrophic fungi in the rhizosphere of crop plant seedlings (Hünninghaus et al., 2019). Low fungal biomass in arable soils can be attributed to a combination of factors such as low input of organic resources (van der Wal et al., 2006; Clocchiatti et al., 2020), use of chemical fungicides (Duah-Yentumi and Johnson, 1986; Shao and Zhang, 2017) and intensive tillage. Hence, strategies that promote high saprotrophic fungal biomass and activity in the rhizosphere of crops could be important to enhance the sustainability of agricultural cultivation.

Saprotrophic fungal abundance in the rhizosphere largely depends on the availability of appropriate energy sources. The amendment of arable soils with organic substrates, such as manure, straw, cover crop remainders or sawdust, can be used to increase fungal biomass in the bulk soil (Lucas et al., 2014; Arcand et al., 2016; Clocchiatti et al., 2020) and also may increase fungal abundance and activity in the rhizosphere (Hannula et al., 2012). During the growth of crop plants, rhizodeposits are the main organic input into soil in conventional monocultures. However, high fungal biomass is observed in the crop rhizosphere only at late phenological stages, such as flowering and senescence, and in perennial crops (Hannula et al., 2010; Tavi et al., 2013; Pausch et al., 2016). This can be attributed to the deposition of a larger proportion of cellulose-rich root debris released by older roots (Dennis et al., 2010; Pausch and Kuzyakov, 2018). Moreover, older plants tend to exude a higher proportion of soluble secondary metabolites, including phenolic acids, as compared to younger plants (Gransee and Wittenmayer, 2000; Chaparro et al., 2013; Iannucci et al., 2013; Zhalnina et al., 2018). Hence, in order to increase the contribution of saprotrophic fungi in the rhizosphere of crop seedlings, an approach involving manipulation of the quantity and quality of rhizodeposits may prove useful. For example, the release of fungus-stimulating root exudates could be used as selection criterion for breeding crop varieties.

Phenolic acids exert a strong selection on rhizosphere microbial communities. As phenolic acids are toxic to microbial cells at relatively low concentrations, they act as a deterrent for sensitive microbial groups, whilst they favor those groups that possess metabolic pathways for phenolic degradation (Fierer et al., 2005; Pumphrey and Madsen, 2008). The ability to degrade phenolic acids is very common among saprotrophic fungi, as it is essential to consume or tolerate free aromatic compounds released during lignocellulose depolymerization (Cain et al., 1968; Sampedro et al., 2004; Mäkelä et al., 2015). When soils receive inputs rich in simple phenolics, saprotrophic fungi are among the main microbial utilizers of such compounds (Waldrop and Firestone, 2004; Brant et al., 2006) and this can lead to a large increase in fungal abundance (Zhou et al., 2012; Suseela et al., 2016; Wang et al., 2016). This suggests that phenolic acids in root exudates could promote the colonization by saprotrophic fungi also in the rhizosphere of crop plants. However, as certain groups of bacteria can also utilize phenolic acids (Blum and Shafer, 1988), the relative stimulation of fungi by phenolic root exudates may depend on soil edaphic factors.

The objective of this study was to investigate the effect of phenolic acids on growth and composition of saprotrophic fungi in simulated and real rhizospheres in an arable soil. The first part of this study was conducted with a microcosm system that simulates root exudation via diffusion of artificial metabolite solutions. This rhizosphere simulation system was used to investigate 1) if diffusion of distinct phenolic acid compounds, alone or in combination with primary root exudate metabolites, increases fungal biomass and 2) if this modulates the community composition of fungi and bacteria. In the second part of this study, fungal development in the rhizosphere of *Arabidopsis thaliana* was compared between wild types and mutant lines *pdr2* and *sid2*, altered in the proportion of exuded phenolic acids and biosynthesis of salicylic acid, respectively. The effect of altered exudation of phenolic compounds on the rhizosphere fungal biomass was tested for two plant developmental stages. We hypothesized that the presence of phenolic acids in root exudates promotes the growth of saprotrophic fungi and increases their competitive ability to utilize other energy sources (i.e., primary metabolites) in the rhizosphere.

MATERIALS AND METHODS

The study comprised of two experiments. The first experiment (Exp. 1) was carried out in two-compartment microcosms, which were used to simulate diffusion of root exudates into arable soil (**Figure 1**). Using this set-up, we investigated the effect of eight phenolic acids on abundance and community composition of fungi and bacteria. In the second experiment (Exp. 2), *A. thaliana* mutant lines with altered phenolics exudation patterns and wild-type *A. thaliana* lines were grown in an arable soil. Fungal biomass was measured in the rhizosphere of these plants at two developmental stages.

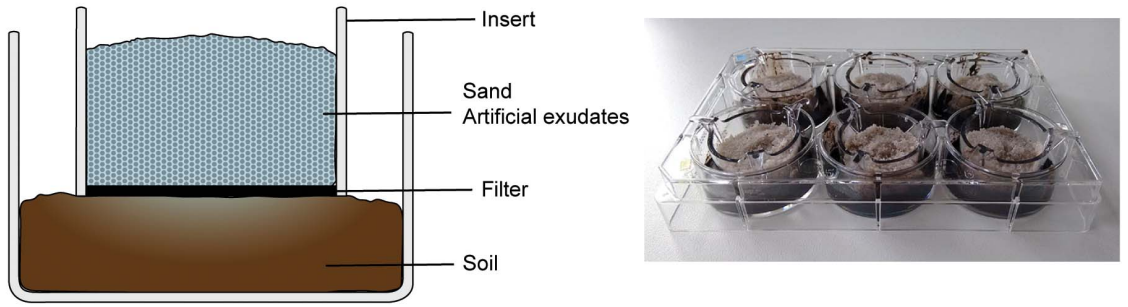

FIGURE 1 | Setup of rhizosphere simulation microcosms in a two-compartment well with insert. **(A)** In a microcosm, the lower compartment contained arable soil, the upper compartment (insert) was filled with sterile sand mixed with artificial exudates. A permeable filter separates the compartments, which allows the diffusion of artificial exudates from the sand in the soil, simulating root exudation. **(B)** Setup of six microcosms in a six-well plate with inserts.

Characteristics of Soil and Sand

Two batches of soil were sampled in October 2016 and July 2019 and were used for Exp. 1 and 2, respectively. The soil was sampled at the experimental farm of Wageningen University & Research located in Vredepeel (N 51 32 19, E 5 51 05, the Netherlands) from the top 10 cm soil layer, within patches of bare soil in between triticale (first batch) and maize plants (second batch), in a plot that was subjected to conventional agricultural management practices. The soil was sandy and had a relatively high organic matter content (6.3%). For more details on soil management and soil characteristics see Quist et al. (2016) and Clocchiatti et al. (2020). The soil samples were sieved through a 4-mm mesh and stored at 4°C until use. Moreover, acid-washed quartz sand (granulation 0.1–0.5 mm; Honeywell Speciality Chemicals Seelze GmbH, Seelze, Germany) was used in Exp. 1. Before use, the sand was autoclaved (121°C for 20 min) and dried under sterile conditions.

Preparation of Artificial Exudates Solutions

The study included eight water-soluble phenolic acid compounds that are commonly found in root exudates (**Table 1**): vanillic acid, syringic acid, gallic acid, salicylic acid, chlorogenic acid, nicotinic acid, ferulic acid and cinnamic acid. A suspension containing 0.5 mg C ml^{-1} in 50 ml sterile demi-water was prepared for each compound. The pH of all suspensions was adjusted to 6 with NaOH/HCl and the suspensions were subjected to sonication for 20 min at 47 kHz, in order to facilitate the dissolution of the phenolic compounds. Half of each phenolic acid solution was filter-sterilized and stored at 4°C and used in Exp. 1. The remaining solution was mixed with a stock solution of primary root exudate metabolites (PM) prepared according to Griffiths et al. (1998) (**Table 1**). The concentration of PM in the working solution was 13.4 M glucose, 13.4 mM fructose, 13.4 mM sucrose, 6.7 mM succinic acid, 6.7 mM malic acid, 3.35 mM arginine, 3.35 mM serine and 3.35 mM cysteine. Solutions containing PM and a phenolic acid had a total carbon content of 5.5 mg C ml^{-1}. These PM + phenolic acid solutions were filter-sterilized and stored at 4°C until use in Exp 1.

Setup of Two-Compartment Rhizosphere Simulation Microcosms

Before the start of Exp. 1, the arable soil was adjusted to 75% water holding capacity (WHC) by adding sterile demi-water and acclimatized at 21°C in a dark climate chamber for 2 days. Six-well plates (6-well CELLSTAR plates and ThinCert cell culture inserts, Greiner Bio-One B.V., the Netherlands) were used for setting up microcosms. Each microcosm was set up in a well containing an insert, so that it had a lower compartment and an upper compartment, separated by a permeable polyethylene terephthalate membrane (**Figure 1**). The membrane had 0.4 μm pores, which enabled the diffusion of dissolved molecules between the two compartments, but hampered the migration of soil microbes. In all microcosms, the lower compartment was filled with soil equivalent to 5 g dry weight. The insert was then placed on top of the soil layer, taking care that the filter membrane adhered to the soil. The upper compartment was filled with 5 g of pure sterilized sand mixed with a solution of either phenolic acids only, PM or PM + phenolic acid. The sand had a moisture of 75% WHC, which was obtained by adding the described metabolites solutions (0.2 ml g^{-1} sand) and demi-water (7.4 μl g^{-1} sand). All the materials in the upper compartment were sterile, thus the soil was the only source of microbes in the microcosm. The metabolites added in the sand compartment diffuse into the soil through the filter, simulating root exudation.

The sand in each unit received either a single phenolic acid, equivalent to 0.1 mg C g^{-1} sand, or a phenolic acid combined with PM, containing in total 1.1 mg C g^{-1} sand. In the latter mixture, the proportion of a phenolic acid was ca. 10% of the total C, which resembles the proportions observed in root exudates (Narasimhan et al., 2003). The experiment had two separate controls, namely sand receiving sterile water only and sand receiving PM only. In total, 18 types of solutions were used (eight phenolic acids × with/without PM + 2 controls). Each treatment was applied in four replicate microcosms, making up a total of 72 microcosms across 12 six-well plates. The solutions were distributed over the plates according to a complete randomized block design.

TABLE 1 | Phenolic acids and primary metabolites used in Exp. 1.

Compound	Concentration in AE solution (mg ml^{-1})	Concentration in sand (mg C g^{-1})	References	Source
Phenolic acids	-	0.1		
Vanillic acid	0.875	0.1	Shukla et al., 2011; Iannucci et al., 2013; Ray et al., 2018; Zhalnina et al., 2018	Sigma-Aldrich, H36001
Syringic acid	0.917	0.1	Shukla et al., 2011; Iannucci et al., 2013; Zhalnina et al., 2018	Sigma-Aldrich, 86230
Gallic acid	0.642	0.1	Shukla et al., 2011; Ray et al., 2018	Sigma-Aldrich 48630
Salicylic acid	0.821	0.1	Badri et al., 2013; Shalaby and Horwitz, 2015; Gao et al., 2018; Zhalnina et al., 2018	Sigma-Aldrich S-7401
Chlorogenic acid	0.922	0.1	Shukla et al., 2011; Shalaby and Horwitz, 2015	Merck 1.59619.0001
Nicotinic acid	0.854	0.1	Shukla et al., 2011; Zhalnina et al., 2018	Sigma-Aldrich 72309
Ferulic acid	0.808	0.1	Badri et al., 2013; Iannucci et al., 2013; Shalaby and Horwitz, 2015; Gao et al., 2018; Ray et al., 2018	Sigma-Aldrich 128708
Cinnamic acid	0.685	0.1	Shukla et al., 2011; Shalaby and Horwitz, 2015; Gao et al., 2018	Sigma-Aldrich C80857
Primary metabolites		1	Griffiths et al., 1998; Shukla et al., 2011	
Glucose	2.42	0.19		Roth 6639
Fructose	2.66	0.19		Sigma-Aldrich F-0127
Sucrose	4.60	0.39		Sigma-Aldrich S-9378
Succinic acid	0.79	0.06		Sigma-Aldrich S3674
Malic acid	0.90	0.06		Sigma-Aldrich M-9138
Arginine	0.58	0.05		Sigma-Aldrich A-8094
Serine	0.35	0.02		Sigma-Aldrich S-5511
Cysteine	0.41	0.02		Sigma-Aldrich C7352

For each compound are displayed: the concentration used for preparing the artificial exudates (AE) solution, the amount of added carbon per gram of sand, references to literature reporting the presence of each compound in root exudates and the product used in this study.

Incubation and Sampling of the Two-Compartment Rhizosphere Simulation Microcosms

Each plate was sealed with surgical tape (Micropore, 3M, Minnesota, United States), which allowed gas exchange, while limiting water evaporation. The two-compartment microcosms were incubated for 2 weeks in a dark climate chamber at 21°C. After 2 weeks, the sand and soil were sampled separately from all microcosms. For sand, 0.5 g samples were obtained from a 2 mm layer close to the membrane filter. These samples were used for ergosterol-based fungal biomass determination, while the rest of the sand present in the inserts was used to measure the moisture content. Similarly, 1 g samples of soil were taken from the 2 mm layer right below the filter. Half of this sample was used to determine fungal biomass with ergosterol and half was stored at −20°C to be used for DNA extraction. Samples for ergosterol extraction were stored in methanol KOH 4% at −20°C. Soil moisture was determined by using the rest of the soil in the lower compartment. Moisture content of sand and soil were measured as weight loss following oven-drying at 105° C overnight.

Fungal Biomass

Ergosterol was extracted from soil and sand samples as described by de Ridder-Duine et al. (2006). Briefly, the extraction method is based on sonication, followed by heat treatment and a subsequent alkaline hydrolysis of esterified ergosterol, aided by mechanical shaking. The ergosterol concentration was quantified in the final methanol-based extract by LC-MS-MS (UHPLC 1290 Infinity II, Agilent Technologies and 6460 Triple Quad LC-MS, Santa Clara, California, United States).

Fungal and Bacterial Community Structure and Bacterial Abundance

DNA was extracted from 0.25 g soil using DNeasy PowerSoil Pro Kit (Qiagen, Germany) according to the manufacturer's instructions. DNA was extracted for a selection of soil samples in Exp. 1, namely from microcosms of vanillic acid -, salicylic acid -, chlorogenic acid - and water treatments, both with and without PM. This selection covered phenolic acids with and without fungal stimulation effects in Exp. 1. Vanillic acid was included in the selection to allow comparisons with the numerous studies that include this compound as a representative of phenolic acids (Waldrop and Firestone, 2004; di Lonardo et al., 2017; Chen et al., 2018). The DNA was subjected to bacterial and fungal amplicon sequencing using Illumina MiSeq PE250, which was performed by McGill University and Génome Québec Innovation Centre, Montréal, Canada, with primers Eub515f/806r (Caporaso et al., 2011) and ITS4r/9f (Ihrmark et al., 2012), for bacteria and fungi, respectively.

The 16S rDNA gene copy number was determined by qPCR for the control soil samples and those treated with vanillic - and salicylic acid, both with and without PM. The qPCR analysis was performed on a Rotor-Gene Q Real-time PCR cycler (Qiagen). The mix comprised 0.5 μl of each primer Eub

338/518 10 μM, 7.5 μl iTaq Universal SYBR green supermix (Bio-Rad Laboratories, California, United States), 2.5 μl Nuclease-Free water (Sigma-Aldrich, Missouri, United States) and 4 μl DNA 2.5 ng μl^{-1}. The qPCR cycling program was 3 min at 95°C followed by 40 cycles of 30 s at 95°C, 30 s at 53°C and 30 s at 72°C. Two standard curves were established for each run (0.23 ng μl^{-1}, 0.023 ng μl^{-1}, 0.0023 ng μl^{-1}, 0.00023 ng μl^{-1}, 0.000023 ng μl^{-1}, 0.0000023 ng μl^{-1}) with a M13 plasmid containing the 16S region obtained from a *Collimonas* pure culture.

Arabidopsis thaliana Varieties

Four *A. thaliana* lines were used in Exp. 2, of which two were wild-type accessions (Col-0 and Col-8) and represented the controls, whereas two mutant lines (*sid2* and *pdr2*) were used to test the response of fungal biomass to altered exudate composition. *Sid2* (salicylic acid induction deficient 2) is a mutant impaired in salicylic acid production. As a consequence of a defect in the isochorismate synthase 1 (ICS1) gene, it fails to accumulate salicylic acid in its tissues (Wildermuth et al., 2001). *Pdr2* (pleiotropic drud resistance 2) is a knockdown mutant for the ATP-binding cassette transporter G30 (ABCG30), which is involved in root exudation. Badri et al. (2009) showed that this results in an altered exudation pattern with higher proportion of phenolic acids, among other secondary metabolites, and a lower proportion of sugars. Seeds of the line Col-0 were obtained from seeds available in house, whereas seeds of Col-8, *sid2* and *pdr2* were obtained from Nottingham *Arabidopsis* Stock Centre (stock IDs N60000, N16438, N66055). Seeds were propagated by growing each line in potting soil, under protective plastic covers, to prevent cross-pollination. Seeds were collected and stored at 15°C until use. Before the start of Exp. 2, seeds of each line were surface-sterilized by soaking in ethanol 70% for 3 min, followed by rinsing three times with sterile-demi water. After that, seeds were laid on wet filters in petri dishes and vernalized by incubation at 4°C for four nights.

Setup of the Bioassay

Fifty pots (polyethylene, Ø 14.5 cm × 11.5 cm) were prepared for Exp. 2 as follows. Vredepeel soil was brought to 60% WHC and mixed with 0.6 g kg^{-1} of a commercial NPK fertilizer (Tuinmest 12-10-18, Pokon Naturado, the Netherlands), corresponding to the addition of 72 mg N kg^{-1}, 60 mg P kg^{-1}, 84 mg K kg^{-1}. Each pot was filled with 1.4 kg soil and sown with 80 *A. thaliana* seeds of the same line. These were distributed over 20 spots (interspace 1 cm) on the soil surface. Each spot contained four seeds. The pots were incubated in a random arrangement (CRBD) in a climate chamber at 21°C, with photoperiod 12:12. 10 days after the start of the growth period, all but one seedling per spot were removed. Hence, a maximum of 20 seedlings were grown in each pot. The experiment comprised of ten replicate pots for each *A. thaliana* line and ten un-planted control pots. Of these, five replicates for each line were harvested 33 days after the start of the experiment, few days before the bolting stage. The other five replicates were harvested after 50 days of incubation, during the flowering stage.

Harvesting of Plants and Sampling

At both developmental stages, plant and soil samples were obtained as follows. Excess soil was removed from the roots by shaking and the soil adhering to the roots was collected by brushing. The rhizosphere soil of all plants in a pot was pooled to form one composite sample. Of this, 1 g was stored in methanol KOH 4% at −20°C until ergosterol extraction. In addition to this, 1 g of bulk soil was sampled from each pot and stored in the same way for ergosterol extraction. Ergosterol was extracted and quantified as described for Exp. 1. Roots and shoots were kept separate from each other but pooled per pot, frozen, freeze-dried and used as a measure of total aboveground and belowground dry biomass produced in each pot.

Statistical and Bioinformatic Analysis

The statistical analyses were carried out in R version 3.4.0. For Exp. 1, three-way ANOVA was performed to compare the ergosterol levels across microcosms that received different types of metabolites. The model comprised the type of phenolic acid, presence/absence of PM and compartment (soil or sand) as factors. The model included block as a factor as well. The assumptions of equality of variances and normality were verified for the model. The ergosterol concentration was compared between each metabolite type and the control by applying planned contrasts to the three-way ANOVA model (R package lsmeans), combined with Dunn–Šidák correction of *p*-values for multiple comparisons (Šidák, 1967). The same method was used to perform a two-way ANOVA, in order to compare 16S copy number as measured in the soil in microcosms receiving phenolic acids with and without PM.

Two-way ANOVA models were carried out for Exp. 2, after checking the assumptions of homoscedasticity and normality. ANOVA models were used for comparing four *A. thaliana* lines at two developmental stages, with block as a random factor, for the following variables: ergosterol concentration in the rhizosphere, ratio of ergosterol in the rhizosphere and bulk soil, aboveground and belowground plant biomass in a pot.

The raw sequencing data contained 2 767 341 sequences for fungi and 374 216 sequences for bacteria. The ITS2 region was extracted with ITSxpress from fungal sequences (Rivers et al., 2018) before analyzing the data with R package DADA2, whereas 16S data was processed directly using the DADA2 pipeline without an extra filtering step. Sequences were quality filtered (maxEE = 2, truncQ = 2, only for bacteria: truncLen = 240), paired-end reads were merged, chimeric sequences were removed, sequencing errors modelled and finally sequence variants (SVs) were identified by the DADA2 algorithm (Callahan et al., 2016). Taxonomy was assigned using the RDP classifier based on the UNITE v2019 database (Abarenkov et al., 2010) for fungi and SILVA v132 for bacteria. After removing non-fungal and non-bacterial sequences from each dataset, the fungal dataset resulted in 1 046 SVs, whereas the bacterial dataset counted 5 992 SVs. Fungal guilds were assigned to each fungal SV when possible, using the FUNGuild database v1.1 (Nguyen et al., 2016). In addition to guild, information about the growth mode and life history traits were retained

in the analysis, in order to distinguish types of saprotrophic fungi (e.g., yeasts, filamentous microfungi and soft rot fungi). Permutational multivariate analysis of variance (PERMANOVA) was used to determine the effect of phenolic acids with and without a background of PM, after checking the homogeneity of multivariate variance (vegan, PERMDISP, Anderson and Walsh, 2013). Differences in relative abundance of fungal taxa between soils treated with different metabolites were analyzed at phylum, class and genus level and for fungal functional guilds. For both fungal and bacterial communities Chao1 and Shannon indexes were calculated. Differences in diversity, as well as in relative abundance were analyzed with two-way ANOVA models, after verification of normality and homoscedasticity of each model. Planned contrasts between each metabolite and the control were performed for ANOVA models to extract the simple effect of a phenolic acid with or without PM. *P*-values were corrected with the Dunn–Šidák method. Differences in bacterial community composition between soil treated with salicylic acid + PM as compared to PM alone were highlighted by differential abundance analysis (R package DESeq2, wald test, $p < 0.01$).

RESULTS

Fungal Biomass

The ergosterol concentration in the arable soil layer of the microcosms (Exp. 1) increased in response to the presence of primary root exudate metabolites (PM) in the upper sand layer (ANOVA, $df = 1$, $F = 186.6$, $p < 0.001$, **Supplementary Table 1A**). Presence of phenolic acids in the upper sand layer had a smaller yet significant effect on ergosterol concentration (ANOVA, $df = 8$, $F = 3.2$, $p < 0.01$). However, the effect of phenolic acids was dependent on the presence of PM (seen as interaction PM x phenolic acid, **Supplementary Table 1A**). Especially, adding salicylic acid together with PM resulted in an extra increase of ergosterol compared to the PM-only control ($p < 0.01$) while salicylic acid alone did not increase ergosterol concentration in the soil as compared to the water only control (**Figure 2**). When compared directly with the controls, none of the other phenolic acids with or without PM had a significant effect on the ergosterol concentration in the soil layer.

Despite the small pore size (0.4 μm) of the insert membrane, fungi in the soil compartment were able to reach the sterile upper sand compartment especially in the treatments in which PM were added together with phenolic acids (**Supplementary Figure 1**). In the sand compartment, salicylic, nicotinic and ferulic acid added together with PM increased ergosterol concentration more than PM added alone (**Supplementary Figure 1**).

Bacterial numbers in the soil were not significantly affected by the addition of vanillic acid and salicylic acid alone (**Figure 3** and **Supplementary Table 1**). The addition of PM alone resulted in a significant increase of bacterial numbers (measured as 16S rDNA copies) in the soil, as compared to the control with addition of only water ($p < 0.05$; **Figure 3**). Salicylic acid combined with PM had a lower bacterial abundance as compared to the addition of PM only ($p < 0.05$, **Figure 3** and **Supplementary Table 1**).

In Exp. 2, ergosterol concentrations were higher in the rhizosphere than the bulk soil for all *A. thaliana* accessions (Tukeys' test, $p < 0.001$ for both developmental stages; **Figure 4B**). Furthermore, ergosterol content was higher in the

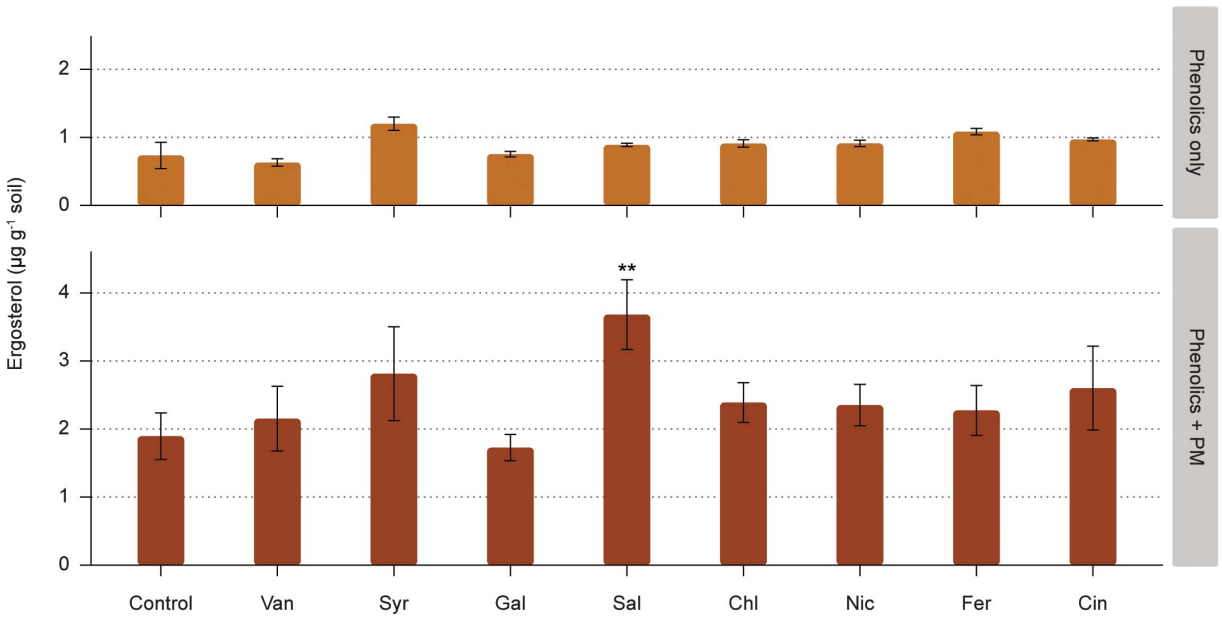

FIGURE 2 | Effect of phenolic acids on fungal biomass, as measured in the soil compartment of rhizosphere simulation microcosms. Phenolic acids were vanillic acid (Van), syringic acid (Syr), gallic acid (Gal), salicylic acid (Sal), chlorogenic acid (Chl), nicotinic acid (Nic), ferulic acid (Fer), and cinnamic acid (Cin). Phenolic acids were added alone or with a background of soluble primary metabolites (PM). Significant differences to the control (water and PM only, respectively) are shown for phenolic acids without and with PM (** $0.01 > p > 0.001$).

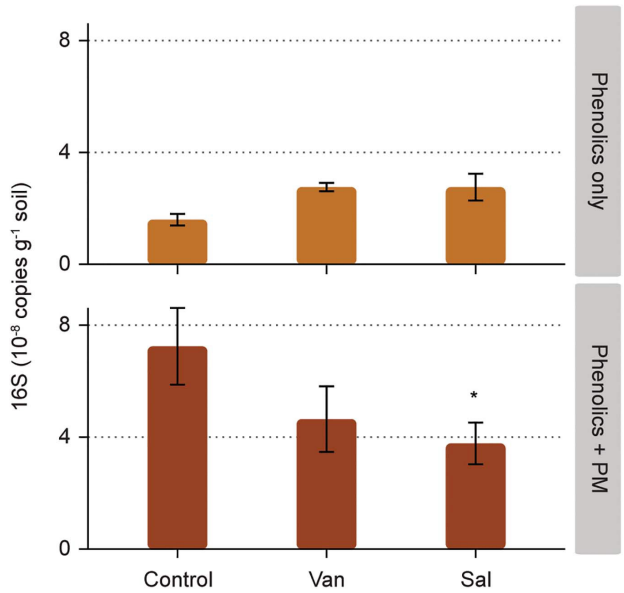

FIGURE 3 | Effect of phenolic acids on bacterial numbers, as measured in the soil compartment of rhizosphere simulation microcosms. Phenolic acids were vanillic acid (Van) and salicylic acid (Sal), applied alone and with a background of soluble primary metabolites (PM). Significant differences to the control (water and PM only, respectively) are shown for phenolic acids without and with PM (* $0.05 > p > 0.01$).

rhizosphere of plants at the first developmental stage (D1) than at the second stage (D2) (Tukeys' test, $p < 0.001$; **Figures 4A,B**). No differences were found in rhizosphere ergosterol levels among the different *A. thaliana* lines (**Figure 4** and **Supplementary Table 2**) and the four *A. thaliana* lines also produced comparable belowground and aboveground biomass (**Figure 4C**).

Fungal and Bacterial Community Structure

In the rhizosphere simulation microcosms, the soil fungal community was dominated by Basidiomycota, in particular Microbotryomycetes. The analysis of fungal communities in control soil and in soil receiving vanillic, salicylic and chlorogenic acid, with and without PM, revealed that the application of PM, but not of the tested phenolics, significantly affected the composition of the fungal community (PERMANOVA, $df = 1$, $F = 0.38$, $R^2 = 0.19$, $p < 0.001$; **Figure 5A** and **Supplementary Table 3**). In treatments with PM, increases in relative abundances were detected for Mortierellomycota ($df = 1$, $F = 64.1$, $p < 0.001$), Ascomycota ($df = 1$, $F = 5.7$, $p < 0.05$) and, among Basidiomycota, for Tremellomycetes ($df = 1$, $F = 9.0$, $p < 0.01$) (**Figures 6A**, **7A**). Among functional guilds, presence of PM resulted in an increase of filamentous fungi classified as saprotrophs (microfungi, pezizoid, soft rot; $df = 1$, $F = 12.4$, $p < 0.01$, **Figure 6B**) and of fungi classified as endophyte-saprotroph ($df = 1$, $F = 63.7$, $p < 0.001$, **Figure 6B**).

Despite the lack of overall effects of the three analyzed phenolic acids treatments on fungal community structure, specific effects were apparent. Treatments with vanillic acid + PM and salicylic acid + PM compared to PM alone had a higher proportion of Sordariomycetes ($p = 0.061$ and $p = 0.053$, respectively) (**Figures 6A** and **7A**). The most abundant Sordariomycetes were *Trichoderma* spp., *Fusarium* spp. and *Fusicolla* spp. (**Figures 7B–D**). When combined with PM, vanillic acid and salicylic acid promoted *Trichoderma* spp. as compared to PM alone ($p < 0.05$ and $p = 0.07$, respectively). Vanillic acid + PM and salicylic acid + PM had a higher average relative abundance of *Fusarium* spp. as compared to PM only, however, this effect was not significant ($p = 0.1$ and $p = 0.3$, respectively). *Fusicolla* spp. increased as compared to PM alone, with vanillic acid + PM and chlorogenic acid + PM ($p < 0.001$ and $p < 0.05$, respectively).

Bacterial community composition was affected by addition of PM and by the three analyzed phenolic acid treatments, (**Figure 5B** and **Supplementary Table 3B**). In particular, PM increased γ-Proteobacteria ($df = 1$, $F = 32.0$, $p < 0.001$), Bacilli ($df = 1$, $F = 40.0$, $p < 0.001$) and Clostridia ($df = 1$, $F = 14.8$, $p < 0.001$) (**Figure 6C**). The phenolic acids examined altered the bacterial community composition both alone ($df = 3$, $F = 0.04$, $R^2 = 0.21$, $p < 0.01$) and with a background of PM ($df = 3$, $F = 1.17$, $R^2 = 0.23$, $p < 0.01$). In particular, salicylic acid + PM had the largest dissimilarity from the control with PM only (**Figure 5B**). Therefore, this treatment was analyzed in more detail. Differential abundance analysis (wald test, $p < 0.01$) showed that 210 SVs were overrepresented in the bacterial community affected by salicylic acid + PM, as compared with PM only. Conversely, 123 SVs were overrepresented in the community affected by PM only, as compared to salicylic acid + PM (**Supplementary Figure 3**). Bacteria favored by salicylic acid + PM or by PM alone were distributed across all the bacterial classes, included α-, γ-, δ-Proteobacteria, Bacilli, Clostridia, Bacteroidia and Actinobacteria (**Supplementary Figure 3**).

DISCUSSION

Effect of Phenolic Acids in Root Exudates on Abundance and Community Composition of Fungi and Bacteria

The effect of individual phenolic acids on fungal biomass was tested in rhizosphere simulation microcosms. We expected that diffusion of phenolic acids from the sterile upper sand layer into arable soil would increase saprotrophic fungal abundance. Yet, we detected no significant effect of added phenolic acids on fungal biomass in the arable soil. Diffusion of primary root exudate metabolites had a strong positive effect of fungal biomass in the arable soil layer, but combination of primary metabolites with phenolic acids did not result in an additional increase, with exception of one phenolic acid, namely salicylic acid. The analysis of fungal sequences revealed that the primary metabolites in artificial root exudates promoted the growth of Mortierellomycota,

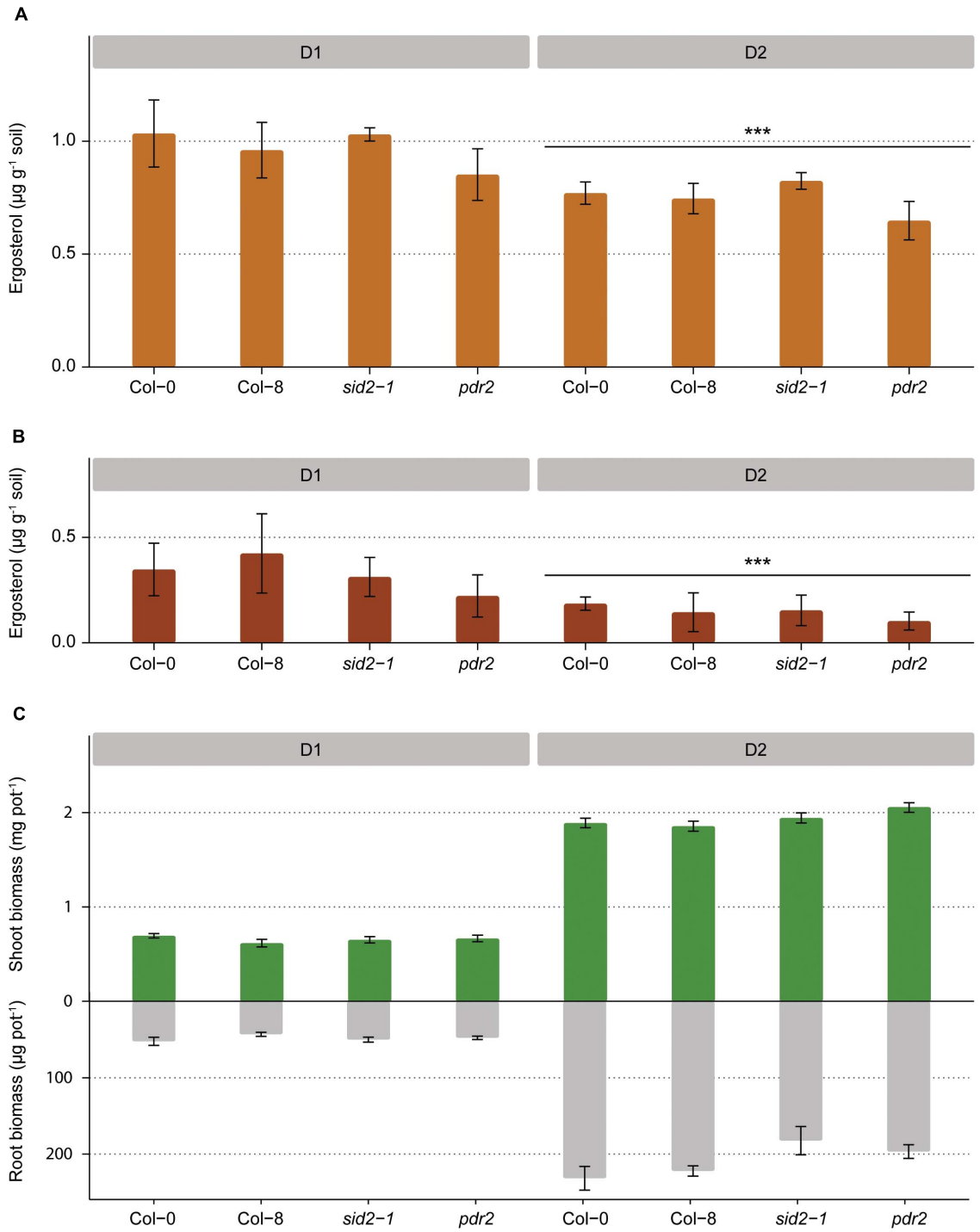

FIGURE 4 | Fungal biomass in the rhizosphere soil of four *Arabidopsis* lines at two developmental stages (D1 and D2) measured as ergosterol concentration **(A)** and increase in ergosterol concentration from the level measured in the bulk soil **(B)**. Aboveground and belowground dry plant biomass collected from each pot for four *Arabidopsis* lines at two developmental stages **(C)** (*** $p < 0.001$).

Ascomycota and basidiomycetal yeasts in the simulated rhizosphere microcosms. This is in line with what is often observed in rhizospheres and reflects the ability of many fungi of these groups to utilize easy degradable carbon compounds (Porras-Alfaro et al., 2011; Kazerooni et al., 2017; Hugoni et al., 2018).

The absence of selective stimulation by most phenolic acids suggests that these compounds were not preferentially consumed

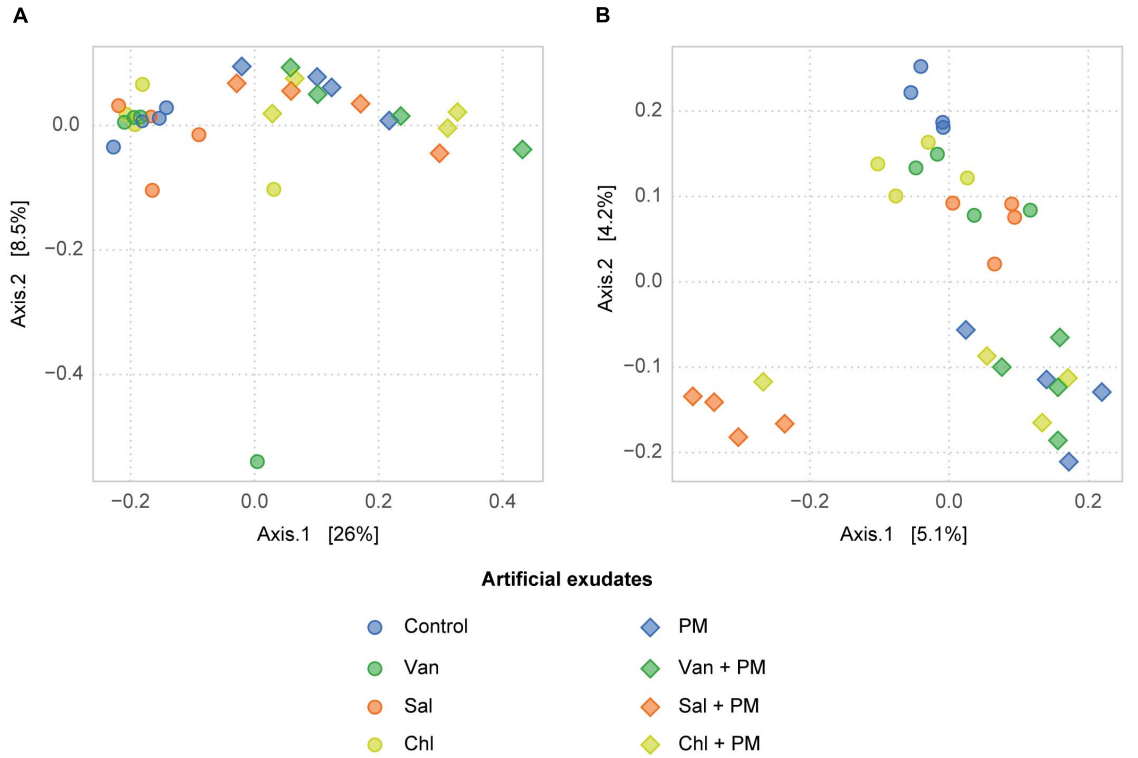

FIGURE 5 | Effect of phenolic acids on fungal **(A)** and bacterial **(B)** communities in the arable soil layer of rhizosphere simulation microcosms. PCoA ordination plot based on Bray-Curtis distances. Four replicates are shown for the control, vanillic acid (Van), salicylic acid (Sal) and chlorogenic acid (Chl), applied alone (phenolics only) and with primary metabolites (phenolics + PM).

by fungi and did also not increase their competitive ability in the simulated rhizosphere. Indeed, previous studies show that both soil fungi and bacteria can metabolize phenolic acids (Blum and Shafer, 1988; Waldrop and Firestone, 2004; di Lonardo et al., 2017; Zwetsloot et al., 2020), although in some cases phenolic acids stimulated fungi to a larger extent than bacteria (Zhou et al., 2012; Zhou and Wu, 2013; Suseela et al., 2016). These differential responses can be ascribed to the observation that the effect of phenolic acids on fungi and bacteria appear to be concentration dependent. In particular, fungi become dominant in soils receiving high loads of simple phenolics (Blum and Shafer, 1988; Zhou and Wu, 2013). In the study of di Lonardo et al. (2017), a stimulation of fungal abundance was observed in an ex-arable soil at a high concentration of vanillic acid (0.8 mg C g^{-1}) and only in combination with supplemental nitrogen, but not at a low vanillic acid concentration (0.1 mg C g^{-1}). In monocropped soils, phenolic acids are usually found at concentrations ranging from 0.02 to 0.2 mg C g^{-1} soil (Zhou et al., 2012). In our study, phenolic acids were added at a concentration of 0.1 mg C g^{-1} soil and represented ca. 10% of the total C when mixed with primary metabolites, as based on the proportion of phenolic acids in root exudates reported by Narasimhan et al., 2003. Hence, the low, yet realistic input of phenolic acids into the arable soil may explain the lack of observable effect on fungal biomass.

Interestingly, fungi were able to invade the upper sterile sand compartment when PM were present. Probably 0.4 μm pores were enlarged as a consequence of a partial decomposition of the polyethylene membrane by soil microbes during the 2 weeks of incubation (Gajendiran et al., 2016). This invasion of fungi in the upper compartment could be considered as a simulation of fungi entering the root interior. It was more pronounced in combination with phenolic acids, especially with salicylic, nicotinic and ferulic acid, indicating that fungi were moving toward the source of these phenolic acids.

Fungal biomass was not stimulated in the rhizosphere of *pdr2 Arabidopsis* plants producing higher proportion of phenolic root exudates than wild type plants (Badri et al., 2009). This supports the results of the simulated rhizosphere microcosms. However, it must be noted that the mutation *pdr2* does not target specifically phenolic acids, but also impacts a number of other secondary and primary metabolites (Badri et al., 2009). In order to have better insight in the role of phenolic acids on saprotrophic fungi in the rhizosphere another possible approach would be to utilize mutants with alterations specific for phenolic acids and/or compare a broader array of plant varieties with contrasting phenolic exudation profiles (Wu et al., 2001; Zwetsloot et al., 2018; Bergelson et al., 2019). Root exudates could also be compared and/or manipulated after extraction from roots and tested in simulated rhizosphere microcosms (de Vries et al., 2019).

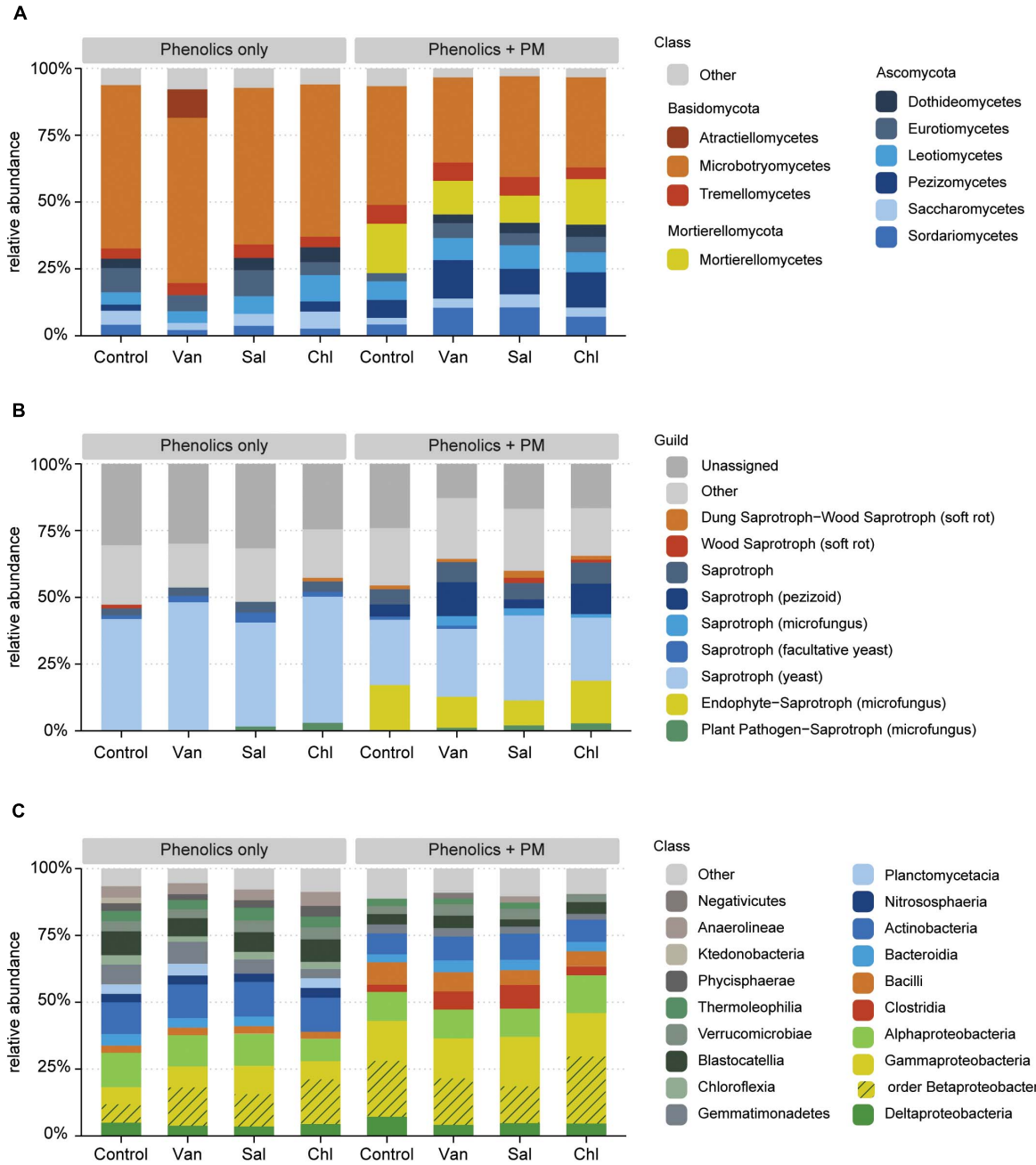

FIGURE 6 | Effect of phenolic acids (phenolics only) and phenolic acids combined with primary metabolites (phenolics + PM) on the relative abundance of fungal classes **(A)**, fungal functional groups **(B)**, and bacterial classes **(C)**, as detected in the arable soil compartment of rhizosphere simulation microcosms. Classes constituting < 2% of each community are displayed as "Other." The result is shown for the control, vanillic acid (Van), salicylic acid (Sal) and chlorogenic acid (Chl).

Although phenolic acids had little effect on the total fungal biomass, fungal community analysis for three phenolic acids revealed that they promoted specific genera, when added in combination with primary root metabolites. The analyzed phenolic acids increased the relative abundance of *Fusarium*, *Trichoderma* and *Fusicolla* spp., as compared to primary metabolites alone. Both *Fusarium* and *Trichoderma* comprise soil-borne fungi able to invade root internal tissues (Chen et al., 2018). Little information is available about *Fusicolla*, however, the close relationship of this genus with *Fusarium* suggests they could share the ability to reach the plant interior (Gräfenhan et al., 2011). Catabolism of phenolic acids, in particular of salicylic acid, is required by endophytic fungi in order to cope with plant immune responses in internal plant tissues (Qi et al., 2012) which could give a competitive advantage to these fungal groups also in the rhizosphere. The ability of

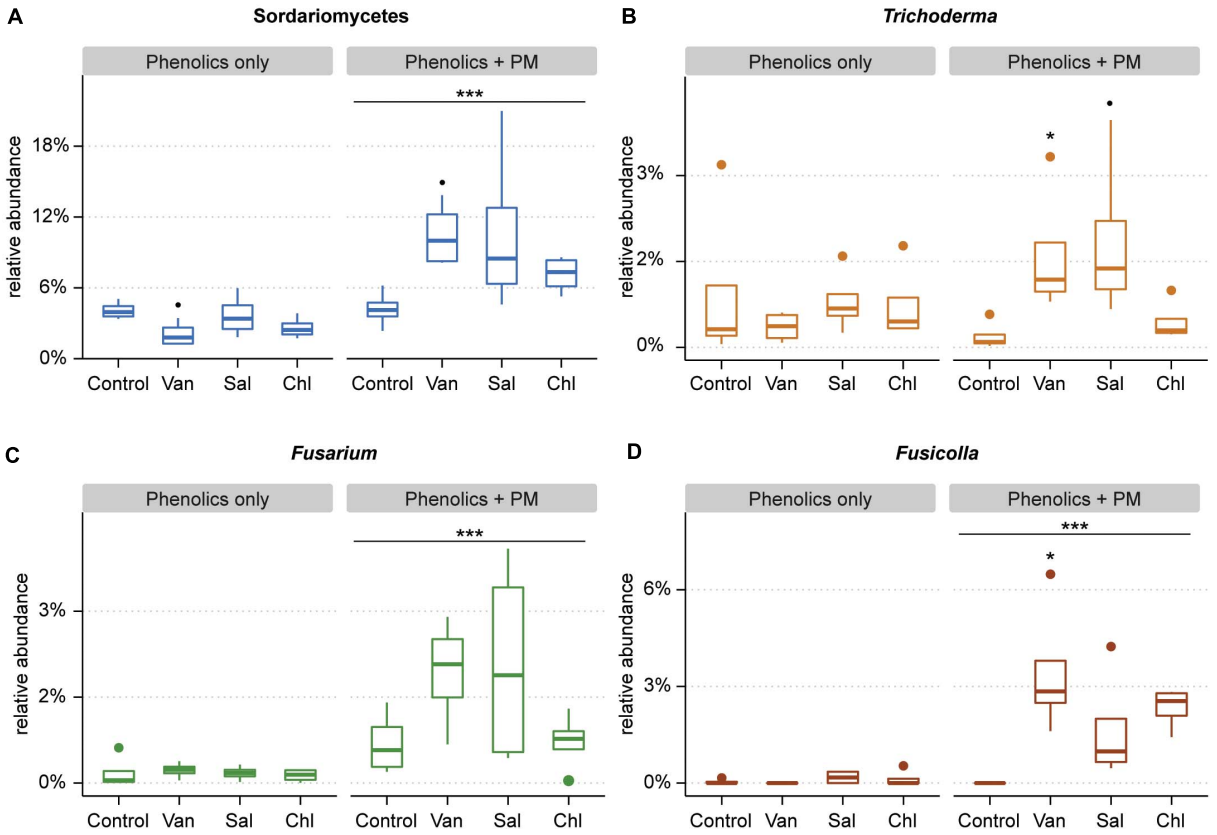

FIGURE 7 | Relative abundance of Sordariomycetes **(A)** and the three most abundant sordariomycetal genera: *Trichoderma* **(B)**, *Fusarium* **(C)**, and *Fusicolla* **(D)**, as found in the soil compartment of in rhizosphere simulation microcosms treated with vanillic acid (Van), salicylic acid (Sal), chlorogenic acid (Chl) or control, with and without primary metabolites (PM). The main effect of primary metabolites is shown, as well as the effect of a phenolic acid as compared to the control (•$0.1 > p > 0.05$, *$0.05 > p > 0.01$, ***$p < 0.001$).

Fusarium spp. to grow in presence of low levels of phenolic acids has been documented (Targoński et al., 1986; Chen et al., 2018). Similarly, *Trichoderma* spp. abundance in the rhizosphere was found to be promoted by vanillic acid in earlier studies (Chen et al., 2018; Zhou and Wu, 2018). Earlier research has indicated the attraction of rhizosphere- and root-inhabiting bacteria by phenolic acids (Li et al., 2012; Badri et al., 2013). Moreover, stress-induced changes in root exudation were also associated with an selective chemoattraction of *Trichoderma* (Lombardi et al., 2018). Our results indicate that phenolic root exudates could play a role in stress-induced attraction of endophytic fungi.

In this study it was not possible to determine if *Fusarium* spp. belonged to pathogenic or non-pathogenic guilds, as they were solely identified based on ITS sequences, that is not a good marker for *Fusaria*. *Trichoderma* spp. are well-known as beneficial facultative endophytes of plants (Kepler et al., 2017; Chen et al., 2018). With regard to *Fusicolla* spp., there is little information on their virulence to plants (Gräfenhan et al., 2011). This potential variety of fungal guilds promoted by phenolic acids is consistent with the evidence that phenolic acid degradation is a virulence factor found in pathogenic fungi, but that mutualistic soil-borne fungi also share this trait (Lahrmann et al., 2015). Hence, phenolic acids appear to affect both non-pathogenic and pathogenic fungal endophytes. Further analyses targeting activity and gene expression, rather than (relative) abundances, are required to get more insight in the response of potential fungal endophytes to phenolic root exudates.

Besides modulating the fungal community composition, the analyzed phenolic acids also affected bacteria in the simulated rhizosphere. Bacteria belonging to all the most abundant classes in soils (i.e., α-, γ-Proteobacteria, Bacilli and Clostridia) were overrepresented in the rhizosphere receiving salicylic acid and primary metabolites, as compared to primary metabolites alone. At the same time, other members of the same classes were underrepresented in the soil receiving salicylic acid and primary metabolites. As indicated above, phenolic acids are known to exert a strong selection on rhizosphere bacterial communities (Pumphrey and Madsen, 2008; Li et al., 2012; Badri et al., 2013; Zhalnina et al., 2018). They favor those groups that possess the specialized metabolism for phenolic degradation, while acting as a deterrent for those sensitive to phenolic acids at relatively low concentrations (Blum and Shafer, 1988; Fierer et al., 2005; Pumphrey and Madsen, 2008). Similar to this study, Lebeis et al. (2015) observed opposing effects among taxonomically closely related bacteria.

Stimulation Fungal Biomass and Decreased Bacterial Numbers by Salicylic Acid

Salicylic acid alone did not increase fungal or bacterial abundance in the simulated rhizosphere. However, salicylic acid combined with primary metabolites increased fungal biomass and decreased bacterial numbers, hence shifting the balance between the two groups. On the other hand, *A. thaliana sid2* plants impaired in the production of salicylic acid harbored similar fungal biomass in their rhizospheres as the wild type. The fungal-stimulating effect observed in the model rhizosphere could be a consequence of a better ability of some fungi to utilize this plant hormone for growth, resulting in a competitive advantage of fungi, as compared to bacteria. Lebeis et al. (2015) showed that salicylic acid and its downstream cascade is not only an important regulator of the plant immune system, but is also a modulator of the root bacterial community composition, as it selectively promoted specific bacterial families, whilst inhibiting others. To our knowledge, saprotrophic fungi have rarely been included in studies on the effect of salicylic acid on root and rhizosphere microbiomes. Our result points at an as-yet-undefined role of salicylic acid in modulating fungal abundances in the rhizosphere. In particular, *Trichoderma* and *Fusarium* spp. are triggered by the combination of salicylic acid in a background of primary metabolites.

Yet, fungal biomass was not affected by the knockdown of salicylic acid synthesis in *sid2 A. thaliana* plants. Therefore, it is not clear whether the fungus-stimulating effect of salicylic acid observed in the rhizosphere simulation microcosm is also occurring *in planta*. Since root exudate composition was not determined, it is not possible to validate if the lack of response of fungi was indeed occurring despite different concentrations of salicylic acid. Lack of fungal biomass stimulation can be affected by the fact that a large difference in salicylic acid accumulation is seen between *sid2* and wild-type plants only after pathogen infection, whereas such a difference is less marked during constitutive salicylic acid biosynthesis (Wildermuth et al., 2001). Moreover, *sid2* plants could partially compensate for the isochorismate synthase knockdown mutation by the upregulation of alternate pathways for salicylic acid production. Considering the limitations of this approach, and apparent contrasting results in the two experiments, it will be of interest to further address whether salicylic acid operates as a modulator of size, composition and activity of the rhizosphere fungal community.

CONCLUSION AND PERSPECTIVES

Our research indicates that phenolic acids, at the concentrations found in root exudates, have little effect on the biomass of saprotrophic fungi inhabiting the rhizosphere. Therefore, selecting crop varieties with a higher exudation of phenolic acids probably does not represent an effective strategy for increasing fungal abundance in the rhizosphere of crop plants growing in fungal-poor arable soils. Nevertheless, this study shows that phenolic acids act as modulators of fungal communities by attracting soil-borne fungal endophytes. These potentially belonged to both pathogenic and mutualistic groups. Further research should indicate if this endophyte-attraction aspect of phenolic acids in root exudates has potential for steering toward improved functioning of rhizosphere- and root microbial communities.

DATA AVAILABILITY STATEMENT

The datasets presented in this study are publicly available at Dryad doi: 10.5061/dryad.573n5tb6z and at the European Nucleotide Archive (sequencing data): accession PRJEB38475(ERP121911).

AUTHOR CONTRIBUTIONS

AC, SEH, and WB conceived and planned the experiments. AC, MB, and MPJH executed the experiments. AC analyzed the data and wrote the manuscript in consultation with SEH and WB. All authors contributed to the article and approved the submitted version.

FUNDING

This research is supported by the Dutch Technology Foundation (STW), a branch of the Netherlands Organization for Scientific Research (NWO; grant number 14012).

ACKNOWLEDGMENTS

We thank Marc Kroonen and Harry Verstegen, who allowed us to take soil samples at the WUR Vredepeel experimental farm. This is publication number 7174 of the NIOO-KNAW Netherlands Institute of Ecology.

SUPPLEMENTARY MATERIAL

The Supplementary Material for this article can be found online at: https://www.frontiersin.org/articles/10.3389/fmicb.2021.644046/full#supplementary-material

Supplementary Figure 1 | Effect of phenolic acids on fungal biomass, as measured in the upper sterile sand compartment of rhizosphere simulation microcosms. Phenolic acids were vanillic acid (Van), syringic acid (Syr), gallic acid (Gal), salicylic acid (Sal), chlorogenic acid (Chl), nicotinic acid (Nic), ferulic acid (Fer) and cinnamic acid (Cin). Phenolic acids were added alone or with a background of soluble primary metabolites (PM) (•$0.1 > p > 0.05$, *$0.05 > p > 0.01$, **$0.01 > p > 0.001$, ***$p < 0.001$).

Supplementary Figure 2 | Effect of phenolic acids (Van = vanillic acid, Sal = salicylic acid, Chl = chlorogenic acid) alone and combined with primary

metabolites (PM) on α-diversity of the soil fungal **(A,B)** and bacterial community **(C,D)** as measured in rhizosphere simulation microcosms. Alpha diversity is shown by Chao1 **(A,C)** and Shannon indexes **(B,D)**. The main effect of PM and the effect of individual phenolic acids are shown (** 0,01 > p > 0,001, *** p < 0,001).

Supplementary Figure 3 | Effect of salicylic acid + PM as compared to PM only on bacterial taxa in the arable soil layer of rhizosphere simulation microcosms. Bacterial SVs over- (log_2 fold change > 0) and under-represented (log_2 fold change < 0) in soil treated with salicylic acid + PM were highlighted by differential abundance analysis (wald test, p < 0,01). Bacterial SVs are grouped by class and bacterial families are specified for the seven most abundant bacterial classes (δ-, γ- and α-Proteobacteria, Bacilli, Clostridia, Bacteroidia and Actinobacteria). SVs belonging to classes with < 2% relative abundance are classified as "Other."

Supplementary Table 1 | Summary of ANOVA results on ergosterol **(A)** and 16S copy number **(B)** as a function of the type of phenolic acid, compartment (soil/sand), and presence or absence of primary metabolites (PM) (Exp. 1). *df*.: degrees of freedon, *SS*: sum of squares, *MS*: mean sum of squares.

Supplementary Table 2 | Summary of ANOVA results on ergosterol as a function of the *Arabidopsis* line (*A.t.* line) and developmental stage (dev. stage) (Exp. 2), shown for ergosterol in the rhizosphere **(A)** and for the ergosterol increase in the rhizosphere from its concentration in the bulk soil **(B)**. *df*: degrees of freedom, *SS*: sum of squares, *MS*: mean sum of squares.

Supplementary Table 3 | Summary of permutational analysis of multivariate variance (PERMANOVA) applied to fungal **(A)** and bacterial **(B)** community data of the arable soil layer in rhizosphere simulation microcosms using Bray-Curtis distances. The PERMANOVA was applied for the total dataset for partitioning the variance according to two factors (type of phenolic acid x presence of additional primary metabolites, PM). The effect of type of phenolic acid was also tested alone on two subsets of data (Phenolic acid with/without PM), as these had a better homogeneity of multivariate variance. *df*: degrees of freedom, *SS*: sum of squares *MS*: mean sum of squares, *p* values based on 999 permutations.

REFERENCES

Abarenkov, K., Henrik Nilsson, R., Larsson, K.-H., Alexander, I. J., Eberhardt, U., Erland, S., et al. (2010). The UNITE database for molecular identification of fungi – recent updates and future perspectives. *New Phytol.* 186, 281–285. doi: 10.1111/j.1469-8137.2009.03160.x

Anderson, M. J., and Walsh, D. C. I. (2013). PERMANOVA, ANOSIM, and the Mantel test in the face of heterogeneous dispersions: what null hypothesis are you testing? *Ecol. Monogr.* 83, 557–574. doi: 10.1890/12-2010.1

Arcand, M. M., Helgason, B. L., and Lemke, R. L. (2016). Microbial crop residue decomposition dynamics in organic and conventionally managed soils. *Appl. Soil Ecol.* 107, 347–359. doi: 10.1016/j.apsoil.2016.07.001

Badri, D. V., Chaparro, J. M., Zhang, R., Shen, Q., and Vivanco, J. M. (2013). Application of natural blends of phytochemicals derived from the root exudates of *Arabidopsis* to the soil reveal that phenolic-related compounds predominantly modulate the soil microbiome. *J. Biol. Chem.* 288, 30503–30503. doi: 10.1074/jbc.A112.433300

Badri, D. V., Quintana, N., El Kassis, E. G., Kim, H. K., Choi, Y. H., Sugiyama, A., et al. (2009). An ABC transporter mutation alters root exudation of phytochemicals that orovoke an overhaul of natural soil microbiota. *Plant Physiol.* 151, 2006. doi: 10.1104/pp.109.147462

Bergelson, J., Mittelstrass, J., and Horton, M. W. (2019). Characterizing both bacteria and fungi improves understanding of the *Arabidopsis* root microbiome. *Sci. Rep.* 9:24. doi: 10.1038/s41598-018-37208-z

Blum, U., and Shafer, S. R. (1988). Microbial populations and phenolic acids in soil. *Soil Biol. Biochem.* 20, 793–800. doi: 10.1016/0038-0717(88)90084-3

Brant, J. B., Sulzman, E. W., and Myrold, D. D. (2006). Microbial community utilization of added carbon substrates in response to long-term carbon input manipulation. *Soil Biol. Biochem.* 38, 2219–2232. doi: 10.1016/j.soilbio.2006.01.022

Buée, M., De Boer, W., Martin, F., van Overbeek, L., and Jurkevitch, E. (2009). The rhizosphere zoo: an overview of plant-associated communities of microorganisms, including phages, bacteria, archaea, and fungi, and of some of their structuring factors. *Plant Soil* 321, 189–212. doi: 10.1007/s11104-009-9991-3

Cain, R. B., Bilton, R. F., and Darrah, J. A. (1968). The metabolism of aromatic acids by micro-organisms. Metabolic pathways in the fungi. *Biochem. J.* 108, 797–828. doi: 10.1042/bj1080797

Callahan, B. J., McMurdie, P. J., Rosen, M. J., Han, A. W., Johnson, A. J. A., and Holmes, S. P. (2016). DADA2: high-resolution sample inference from Illumina amplicon data. *Nat. Methods* 13, 581–583. doi: 10.1038/nmeth.3869

Caporaso, J. G., Lauber, C. L., Walters, W. A., Berg-Lyons, D., Lozupone, C. A., Turnbaugh, P. J., et al. (2011). Global patterns of 16S rRNA diversity at a depth of millions of sequences per sample. *Proc. Natl. Acad. Sci. U.S.A.* 108(Suppl. 1), 4516–4522. doi: 10.1073/pnas.1000080107

Chaparro, J. M., Badri, D. V., Bakker, M. G., Sugiyama, A., Manter, D. K., and Vivanco, J. M. (2013). Root exudation of phytochemicals in Arabidopsis follows specific patterns that are developmentally programmed and correlate with soil microbial functions. *PLoS One* 8:e55731. doi: 10.1371/journal.pone.0055731

Chen, S., Yu, H., Zhou, X., and Wu, F. (2018). Cucumber (*Cucumis sativus* L.) seedling rhizosphere *Trichoderma* and *Fusarium* spp. communities altered by vanillic acid. *Front. Microbiol.* 9:2195. doi: 10.3389/fmicb.2018.02195

Clocchiatti, A., Hannula, S. E., van den Berg, M., Korthals, G., and de Boer, W. (2020). The hidden potential of saprotrophic fungi in arable soil: Patterns of short-term stimulation by organic amendments. *Appl. Soil Ecol.* 147:103434. doi: 10.1016/j.apsoil.2019.103434

de Boer, W., Hundscheid, M. P. J., Klein Gunnewiek, P. J. A., de Ridder-Duine, A. S., Thion, C., van Veen, J. A., et al. (2015). Antifungal rhizosphere bacteria can increase as response to the presence of saprotrophic fungi. *PLoS One* 10:e0137988. doi: 10.1371/journal.pone.0137988

de Ridder-Duine, A. S., Smant, W., van der Wal, A., van Veen, J. A., and de Boer, W. (2006). Evaluation of a simple, non-alkaline extraction protocol to quantify soil ergosterol. *Pedobiologia* 50, 293–300. doi: 10.1016/j.pedobi.2006.03.004

de Vries, F. T., and Bardgett, R. D. (2012). Plant–microbial linkages and ecosystem nitrogen retention: lessons for sustainable agriculture. *Front. Ecol. Environ.* 10:425–432. doi: 10.1890/110162

de Vries, F. T., Williams, A., Stringer, F., Willcocks, R., McEwing, R., Langridge, H., et al. (2019). Changes in root-exudate-induced respiration reveal a novel mechanism through which drought affects ecosystem carbon cycling. *New Phytol.* 224, 132–145. doi: 10.1111/nph.16001

Dennis, P. G., Miller, A. J., and Hirsch, P. R. (2010). Are root exudates more important than other sources of rhizodeposits in structuring rhizosphere bacterial communities? *FEMS Microbiol. Ecol.* 72, 313–327. doi: 10.1111/j.1574-6941.2010.00860.x

Deveau, A., Bonito, G., Uehling, J., Paoletti, M., Becker, M., Bindschedler, S., et al. (2018). Bacterial–fungal interactions: ecology, mechanisms and challenges. *FEMS Microbiol. Rev.* 42, 335–352. doi: 10.1093/femsre/fuy008

di Lonardo, D. P., de Boer, W., Klein Gunnewiek, P. J. A., Hannula, S. E., and van der Wal, A. (2017). Priming of soil organic matter: chemical structure of added compounds is more important than the energy content. *Soil Biol. Biochem.* 108, 41–54. doi: 10.1016/j.soilbio.2017.01.017

Djajakirana, G., Joergensen, R. G., and Meyer, B. (1996). Ergosterol and microbial biomass relationship in soil. *Biol. Fertil. Soils* 22, 299–304. doi: 10.1007/BF00334573

Duah-Yentumi, S., and Johnson, D. B. (1986). Changes in soil microflora in response to repeated applications of some pesticides. *Soil Biol. Biochem.* 18, 629–635. doi: 10.1016/0038-0717(86)90086-6

Fierer, N., Jackson, J. A., Vilgalys, R., and Jackson, R. B. (2005). Assessment of soil microbial community structure by use of taxon-specific quantitative PCR assays. *Appl. Environ. Microbiol.* 71:4117. doi: 10.1128/AEM.71.7.4117-4120.2005

Gajendiran, A., Krishnamoorthy, S., and Abraham, J. (2016). Microbial degradation of low-density polyethylene (LDPE) by *Aspergillus clavatus* strain JASK1 isolated from landfill soil. *3 Biotech* 6:52. doi: 10.1007/s13205-016-0394-x

Gao, X., Zhang, S., Zhao, X., and Wu, Q. (2018). Potassium-induced plant resistance against soybean cyst nematode via root exudation of phenolic acids and plant pathogen-related genes. *PLoS One* 13:e0200903. doi: 10.1371/journal.pone.0200903

Gräfenhan, T., Schroers, H.-J., Nirenberg, H. I., and Seifert, K. A. (2011). An overview of the taxonomy, phylogeny, and typification of nectriaceous fungi in *Cosmospora*, *Acremonium*, *Fusarium*, *Stilbella*, and *Volutella*. *Stud. Mycol.* 68, 79–113. doi: 10.3114/sim.2011.68.04

Gransee, A., and Wittenmayer, L. (2000). Qualitative and quantitative analysis of water-soluble root exudates in relation to plant species and development. *J. Plant Nutr. Soil Sci.* 163, 381–385.

Griffiths, B. S., Ritz, K., Ebblewhite, N., and Dobson, G. (1998). Soil microbial community structure: effects of substrate loading rates. *Soil Biol. Biochem.* 31, 145–153. doi: 10.1016/S0038-0717(98)00117-5

Hannula, S. E., Boschker, H. T. S., de Boer, W., and van Veen, J. A. (2012). 13C pulse-labeling assessment of the community structure of active fungi in the rhizosphere of a genetically starch-modified potato (*Solanum tuberosum*) cultivar and its parental isoline. *New Phytol.* 194, 784–799. doi: 10.1111/j.1469-8137.2012.04089.x

Hannula, S. E., de Boer, W., and van Veen, J. A. (2010). In situ dynamics of soil fungal communities under different genotypes of potato, including a genetically modified cultivar. *Soil Biol. Biochem.* 42, 2211–2223. doi: 10.1016/j.soilbio.2010.08.020

Hugoni, M., Luis, P., Guyonnet, J., and Haichar, F. el Z (2018). Plant host habitat and root exudates shape fungal diversity. *Mycorrhiza* 28, 451–463. doi: 10.1007/s00572-018-0857-5

Hünninghaus, M., Dibbern, D., Kramer, S., Koller, R., Pausch, J., Schloter-Hai, B., et al. (2019). Disentangling carbon flow across microbial kingdoms in the rhizosphere of maize. *Soil Biol. Biochem.* 134, 122–130. doi: 10.1016/j.soilbio.2019.03.007

Iannucci, A., Fragasso, M., Platani, C., and Papa, R. (2013). Plant growth and phenolic compounds in the rhizosphere soil of wild oat (*Avena fatua* L.). *Front. Plant Sci.* 4:509. doi: 10.3389/fpls.2013.00509

Ihrmark, K., Bödeker, I. T. M., Cruz-Martinez, K., Friberg, H., Kubartova, A., Schenck, J., et al. (2012). New primers to amplify the fungal ITS2 region – evaluation by 454-sequencing of artificial and natural communities. *FEMS Microbiol. Ecol.* 82, 666–677. doi: 10.1111/j.1574-6941.2012.01437.x

Kazerooni, E. A., Maharachchikumbura, S. S. N., Rethinasamy, V., Al-Mahrouqi, H., and Al-Sadi, A. M. (2017). Fungal diversity in tomato rhizosphere soil under conventional and desert farming systems. *Front. Microbiol.* 8:1462. doi: 10.3389/fmicb.2017.01462

Kepler, R. M., Maul, J. E., and Rehner, S. A. (2017). Managing the plant microbiome for biocontrol fungi: examples from Hypocreales. *Curr. Opin. Microbiol.* 37, 48–53. doi: 10.1016/j.mib.2017.03.006

Kohler, J., Caravaca, F., Carrasco, L., and Roldán, A. (2007). Interactions between a plant growth-promoting rhizobacterium, an AM fungus and a phosphate-solubilising fungus in the rhizosphere of Lactuca sativa. *Appl. Soil Ecol.* 35, 480–487. doi: 10.1016/j.apsoil.2006.10.006

Koike, N., Hyakumachi, M., Kageyama, K., Tsuyumu, S., and Doke, N. (2001). Induction of systemic resistance in cucumber against several diseases by plant growth-promoting fungi: lignification and superoxide generation. *Eur. J. Plant Pathol.* 107, 523–533. doi: 10.1023/A:1011203826805

Lahrmann, U., Strehmel, N., Langen, G., Frerigmann, H., Leson, L., Ding, Y., et al. (2015). Mutualistic root endophytism is not associated with the reduction of saprotrophic traits and requires a noncompromised plant innate immunity. *New Phytol.* 207, 841–857. doi: 10.1111/nph.13411

Latz, M. A. C., Jensen, B., Collinge, D. B., and Jørgensen, H. J. L. (2018). Endophytic fungi as biocontrol agents: elucidating mechanisms in disease suppression. *Plant Ecol. Divers.* 11, 555–567. doi: 10.1080/17550874.2018.1534146

Lebeis, S. L., Paredes, S. H., Lundberg, D. S., Breakfield, N., Gehring, J., McDonald, M., et al. (2015). Salicylic acid modulates colonization of the root microbiome by specific bacterial taxa. *Science* 349:860. doi: 10.1126/science.aaa8764

Li, P., Ma, L., Feng, Y. L., Mo, M. H., Yang, F. X., Dai, H. F., et al. (2012). Diversity and chemotaxis of soil bacteria with antifungal activity against *Fusarium* wilt of banana. *J. Ind. Microbiol. Biotechnol.* 39, 1495–1505. doi: 10.1007/s10295-012-1163-4

Lombardi, N., Vitale, S., Turrà, D., Reverberi, M., Fanelli, C., Vinale, F., et al. (2018). Root exudates of stressed plants stimulate and attract trichoderma soil fungi. *Mol. Plant Microbe Interact.* 31, 982–994. doi: 10.1094/MPMI-12-17-0310-R

Lucas, S. T., D'Angelo, E. M., and Williams, M. A. (2014). Improving soil structure by promoting fungal abundance with organic soil amendments. *Appl. Soil Ecol.* 75, 13–23. doi: 10.1016/j.apsoil.2013.10.002

Mäkelä, M. R., Marinoviæ, M., Nousiainen, P., Liwanag, A. J. M., Benoit, I., Sipilä, J., et al. (2015). "Aromatic metabolism of filamentous fungi in relation to the presence of aromatic compounds in plant biomass," in *Advances in Applied Microbiology*, eds S. Sariaslani and G. M. Gadd (Cambridge, MA: Academic Press), 63–137. doi: 10.1016/bs.aambs.2014.12.001

Narasimhan, K., Basheer, C., Bajic, V. B., and Swarup, S. (2003). Enhancement of plant-microbe interactions using a rhizosphere metabolomics-driven approach and its application in the removal of polychlorinated biphenyls. *Plant Physiol.* 132, 146–153. doi: 10.1104/pp.102.016295

Naznin, H. A., Kiyohara, D., Kimura, M., Miyazawa, M., Shimizu, M., and Hyakumachi, M. (2014). Systemic resistance induced by volatile organic compounds emitted by plant growth-promoting fungi in *Arabidopsis thaliana*. *PLoS One* 9:e86882. doi: 10.1371/journal.pone.0086882

Nguyen, N. H., Song, Z., Bates, S. T., Branco, S., Tedersoo, L., Menke, J., et al. (2016). FUNGuild: an open annotation tool for parsing fungal community datasets by ecological guild. *Fungal Ecol.* 20, 241–248. doi: 10.1016/j.funeco.2015.06.006

Pausch, J., Kramer, S., Scharroba, A., Scheunemann, N., Butenschoen, O., Kandeler, E., et al. (2016). Small but active – pool size does not matter for carbon incorporation in below-ground food webs. *Funct. Ecol.* 30, 479–489. doi: 10.1111/1365-2435.12512

Pausch, J., and Kuzyakov, Y. (2018). Carbon input by roots into the soil: quantification of rhizodeposition from root to ecosystem scale. *Glob. Change Biol.* 24, 1–12. doi: 10.1111/gcb.13850

Porras-Alfaro, A., Herrera, J., Natvig, D. O., Lipinski, K., and Sinsabaugh, R. L. (2011). Diversity and distribution of soil fungal communities in a semiarid grassland. *Mycologia* 103, 10–21. doi: 10.3852/09-297

Pumphrey, G. M., and Madsen, E. L. (2008). Field-based stable isotope probing reveals the identities of benzoic acid-metabolizing microorganisms and their in situ growth in agricultural soil. *Appl. Environ. Microbiol.* 74, 4111–4118. doi: 10.1128/AEM.00464-08

Punja, Z. K., and Utkhede, R. S. (2003). Using fungi and yeasts to manage vegetable crop diseases. *Trends Biotechnol.* 21, 400–407. doi: 10.1016/S0167-7799(03)00193-8

Qi, P.-F., Johnston, A., Balcerzak, M., Rocheleau, H., Harris, L. J., Long, X.-Y., et al. (2012). Effect of salicylic acid on *Fusarium graminearum*, the major causal agent of fusarium head blight in wheat. *Fungal Biol.* 116, 413–426. doi: 10.1016/j.funbio.2012.01.001

Qin, S., Yeboah, S., Xu, X., Liu, Y., and Yu, B. (2017). Analysis on fungal diversity in rhizosphere soil of continuous cropping potato subjected to different furrow-ridge mulching managements. *Front. Microbiol.* 8:845. doi: 10.3389/fmicb.2017.00845

Quist, C. W., Schrama, M., de Haan, J. J., Smant, G., Bakker, J., van der Putten, W. H., et al. (2016). Organic farming practices result in compositional shifts in nematode communities that exceed crop-related changes. *Appl. Soil Ecol.* 98, 254–260. doi: 10.1016/j.apsoil.2015.10.022

Ray, S., Mishra, S., Bisen, K., Singh, S., Sarma, B. K., and Singh, H. B. (2018). Modulation in phenolic root exudate profile of *Abelmoschus esculentus* expressing activation of defense pathway. *Microbiol. Res.* 207, 100–107. doi: 10.1016/j.micres.2017.11.011

Rivers, A., Weber, K., Gardner, T., Liu, S., and Armstrong, S. (2018). ITSxpress: software to rapidly trim internally transcribed spacer sequences with quality scores for marker gene analysis. *F1000Research* 7:1418. doi: 10.12688/f1000research.15704.1

Saldajeno, M. G. B., Chandanie, W. A., Kubota, M., and Hyakumachi, M. (2008). "Effects of interactions of arbuscular mycorrhizal fungi and beneficial saprophytic mycoflora on plant growth and disease protection," in *Mycorrhizae: Sustainable Agriculture and Forestry*, eds Z. A. Siddiqui, M. S. Akhtar, and K. Futai (Dordrecht: Springer Netherlands), 211–226. doi: 10.1007/978-1-4020-8770-7_9

Sampedro, I., Aranda, E., Martın, J., Garcıa-Garrido, J. M., Garcıa-Romera, I., and Ocampo, J. A. (2004). Saprobic fungi decrease plant toxicity caused by olive mill residues. *Appl. Soil Ecol.* 26, 149–156. doi: 10.1016/j.apsoil.2003.10.011

Shalaby, S., and Horwitz, B. A. (2015). Plant phenolic compounds and oxidative stress: integrated signals in fungal–plant interactions. *Curr. Genet.* 61, 347–357. doi: 10.1007/s00294-014-0458-6

Shao, H., and Zhang, Y. (2017). Non-target effects on soil microbial parameters of the synthetic pesticide carbendazim with the biopesticides cantharidin and norcantharidin. *Sci. Rep.* 7:5521. doi: 10.1038/s41598-017-05923-8

Shukla, K., Sharma, S., Singh, N., Singh, V., Tiwari, K., and Singh, S. (2011). Nature and role of root exudates: efficacy in bioremediation. *Afr. J. Biotechnol.* 10, 9717–9724. doi: 10.5897/AJB10.2552

Šidák, Z. (1967). Rectangular confidence regions for the means of multivariate normal distributions. *J. Am. Stat. Assoc.* 62, 626–633. doi: 10.1080/01621459.1967.10482935

Suseela, V., Alpert, P., Nakatsu, C. H., Armstrong, A., and Tharayil, N. (2016). Plant–soil interactions regulate the identity of soil carbon in invaded ecosystems: implication for legacy effects. *Funct. Ecol.* 30, 1227–1238. doi: 10.1111/1365-2435.12591

Targoński, Z., Rogalski, J., and Szczodrak, J. (1986). Decomposition of 14C-labelled vanillic acid and its related compounds by *Fusarium oxysporum*. *Syst. Appl. Microbiol.* 8, 148–151. doi: 10.1016/S0723-2020(86)80163-1

Tavi, N. M., Martikainen, P. J., Lokko, K., Kontro, M., Wild, B., Richter, A., et al. (2013). Linking microbial community structure and allocation of plant-derived carbon in an organic agricultural soil using 13CO2 pulse-chase labelling combined with 13C-PLFA profiling. *Soil Biol. Biochem.* 58, 207–215. doi: 10.1016/j.soilbio.2012.11.013

van der Putten, W. H., Bradford, M. A., Pernilla Brinkman, E., van de Voorde, T. F. J., and Veen, G. F. (2016). Where, when and how plant–soil feedback matters in a changing world. *Funct. Ecol.* 30, 1109–1121. doi: 10.1111/1365-2435.12657

van der Wal, A., van Veen, J. A., Pijl, A., Summerbell, R., and de Boer, W. (2006). Constraints on development of fungal biomass and decomposition processes during restoration of arable sandy soils. *Soil Biol. Biochem.* 38, 2890–2902. doi: 10.1016/j.soilbio.2006.04.046

Waldrop, M. P., and Firestone, M. K. (2004). Microbial community utilization of recalcitrant and simple carbon compounds: impact of oak-woodland plant communities. *Oecologia* 138, 275–284. doi: 10.1007/s00442-003-1419-9

Wang, Y., Li, C., Wang, Q., Wang, H., Duan, B., and Zhang, G. (2016). Environmental behaviors of phenolic acids dominated their rhizodeposition in boreal poplar plantation forest soils. *J. Soils Sediments* 16, 1858–1870. doi: 10.1007/s11368-016-1375-8

Wildermuth, M. C., Dewdney, J., Wu, G., and Ausubel, F. M. (2001). Isochorismate synthase is required to synthesize salicylic acid for plant defence. *Nature* 414, 562–565. doi: 10.1038/35107108

Wu, H., Haig, T., Pratley, J., Lemerle, D., and An, M. (2001). Allelochemicals in wheat (*Triticum aestivum* L.): cultivar difference in the exudation of phenolic acids. *J. Agric. Food Chem.* 49, 3742–3745. doi: 10.1021/jf010111x

Xia, Y., Sahib, M. R., Amna, A., Opiyo, S. O., Zhao, Z., and Gao, Y. G. (2019). Culturable endophytic fungal communities associated with plants in organic and conventional farming systems and their effects on plant growth. *Sci. Rep.* 9:1669. doi: 10.1038/s41598-018-38230-x

Xiong, W., Li, R., Ren, Y., Liu, C., Zhao, Q., Wu, H., et al. (2017). Distinct roles for soil fungal and bacterial communities associated with the suppression of vanilla *Fusarium* wilt disease. *Soil Biol. Biochem.* 107, 198–207. doi: 10.1016/j.soilbio.2017.01.010

Yadav, J., Verma, J., and Tiwari, K. (2011). Plant growth promoting activities of fungi and their effect on chickpea plant growth. *Asian J. Biol. Sci.* 4, 291–299. doi: 10.3923/ajbs.2011.291.299

Zhalnina, K., Louie, K. B., Hao, Z., Mansoori, N., da Rocha, U. N., Shi, S., et al. (2018). Dynamic root exudate chemistry and microbial substrate preferences drive patterns in rhizosphere microbial community assembly. *Nat. Microbiol.* 3, 470–480. doi: 10.1038/s41564-018-0129-3

Zhou, X., and Wu, F. (2013). Artificially applied vanillic acid changed soil microbial communities in the rhizosphere of cucumber (*Cucumis sativus* L.). *Can. J. Soil Sci.* 93, 13–21. doi: 10.4141/cjss2012-039

Zhou, X., and Wu, F. (2018). Vanillic acid changed cucumber (*Cucumis sativus* L.) seedling rhizosphere total bacterial, *Pseudomonas* and *Bacillus* spp. communities. *Sci. Rep.* 8:4929. doi: 10.1038/s41598-018-23406-2

Zhou, X., Yu, G., and Wu, F. (2012). Soil phenolics in a continuously mono-cropped cucumber (*Cucumis sativus* L.) system and their effects on cucumber seedling growth and soil microbial communities. *Eur. J. Soil Sci.* 63, 332–340. doi: 10.1111/j.1365-2389.2012.01442.x

Zwetsloot, M. J., Kessler, A., and Bauerle, T. L. (2018). Phenolic root exudate and tissue compounds vary widely among temperate forest tree species and have contrasting effects on soil microbial respiration. *New Phytol.* 218, 530–541. doi: 10.1111/nph.15041

Zwetsloot, M. J., Ucros, J. M., Wickings, K., Wilhelm, R. C., Sparks, J., Buckley, D. H., et al. (2020). Prevalent root-derived phenolics drive shifts in microbial community composition and prime decomposition in forest soil. *Soil Biol. Biochem.* 145:107797. doi: 10.1016/j.soilbio.2020.107797

Conflict of Interest: The authors declare that the research was conducted in the absence of any commercial or financial relationships that could be construed as a potential conflict of interest.

frontiers in Microbiology

ORIGINAL RESEARCH
published: 07 May 2021
doi: 10.3389/fmicb.2021.628503

Increased Organic Fertilizer and Reduced Chemical Fertilizer Increased Fungal Diversity and the Abundance of Beneficial Fungi on the Grape Berry Surface in Arid Areas

Linnan Wu[1†], Zhiqiang Li[2†], Fengyun Zhao[1], Benzhou Zhao[1], Fesobi Olumide Phillip[1], Jianrong Feng[1], Huaifeng Liu[1] and Kun Yu[1]*

[1]Department of Horticulture, College of Agriculture, The Key Laboratory of Characteristics of Fruit and Vegetable Cultivation and Utilization of Germoplasm Resources of the Xinjiang Production and Construction Crops, Shihezi University, Shihezi, China, [2]Shihezi Academy of Agricultural Sciences, Shihezi, China

OPEN ACCESS

Edited by:
Jia Liu,
Chongqing University of Arts and Sciences, China

Reviewed by:
Asha Janadaree Dissanayake, University of Electronic Science and Technology of China, China
Yanfang Wang, Shandong Agricultural University, China

***Correspondence:**
Kun Yu
yukun410@163.com

[†]These authors have contributed equally to this work

Specialty section:
This article was submitted to Microbe and Virus Interactions With Plants, a section of the journal Frontiers in Microbiology

Received: *12 November 2020*
Accepted: *12 April 2021*
Published: *07 May 2021*

Citation:
Wu L, Li Z, Zhao F, Zhao B, Phillip FO, Feng J, Liu H and Yu K (2021) Increased Organic Fertilizer and Reduced Chemical Fertilizer Increased Fungal Diversity and the Abundance of Beneficial Fungi on the Grape Berry Surface in Arid Areas. Front. Microbiol. 12:628503. doi: 10.3389/fmicb.2021.628503

Fertilizer practices can significantly impact the fruit quality and microbial diversity of the orchards. The fungi on the surface of fruits are essential for fruit storability and safety. However, it is not clear whether fertilization affects the fungal diversity and community structure on the surface of grape berries. Here, grape quality and the fungal diversity on the surface of grapes harvested from three fertilizer treatments were analyzed shortly after grape picking (T0) and following 8 days of storage (T1). The study involved three treatments: (1) common chemical fertilizer for 2 years (CH); (2) increased organic fertilizer and reduced chemical fertilizer for 1 year (A.O); and (3) increased organic fertilizer and reduced chemical fertilizer for 2 years (B.O). The application of increased organic fertilizer and reduced chemical fertilizer increased the soluble solids content (SSC) of the grape berries and decreased the pH of the grape juice. A total of 827,947 high-quality fungal sequences were recovered and assigned to 527 operational taxonomic units. Members of the *Ascomycota* phylum were dominant in all samples and accounted for 94.41% of the total number of detected sequences, followed by the *Basidiomycota* (5.05%), and unidentified fungi (0.54%). Alpha and beta diversity analyses revealed significantly different fungal populations in the three fertilizer treatments over the two time periods. The fungal diversity and richness on the grape berry surface in the B.O and A.O treatments were higher than those in the CH treatment. Among the detected fungi, the B.O treatments were mainly *Pichia*, *Aureobasidium*, and *Candida* genera, while the CH treatments were *Botrytis*, *Aspergillus*, and *Penicillium*. Moreover, significant differences were revealed between the two assessment times (T0 and T1). The samples from the T0 timepoint had higher fungal richness and diversity than the samples from T1 timepoint. Increasing organic fertilizer usage in grape management could improve grape quality and went on to increase the fungal diversity, as well as the relative abundance (RA) of beneficial fungi on grape berry surfaces. The correlation analysis suggested that the pH of the grape juice was significantly negatively correlated with fungal diversity parameters.

Keywords: organic fertilizer, chemical fertilizer, fungal diversity, beneficial fungi, grape

INTRODUCTION

Increases in global grain and fruit yields in recent decades have been largely dependent on heavy investments in fertilizer (Geng et al., 2019). However, fertilizer can harm marine, freshwater, and terrestrial ecosystems (Tilman et al., 2011). Soil conditions with excess nutrients may result in potential damages to the environment, causing widespread environmental problems (García-Díaz et al., 2017). Excessive fertilizer application aggravated the decline in soil organic matter (SOM) and fertility (Lv et al., 2020; Wu et al., 2020). Therefore, in addition to yields, agricultural production needs to take environmental sustainability into account. Organic fertilizers are often used as basal fertilizer to ensure that SOM and micronutrients play unique roles during grapevine growth and development (Zhao et al., 2019). Organic fertilizer can affect soil moisture-holding capacity by increasing soil infiltration and minimizing soil evaporation (Moreno-Jiménez et al., 2019). Although organic fertilizers are more eco-friendly, they have low nutrient concentrations and nutrient release is too slow to support grape production in a short time (Xiao et al., 2017). The nutrient contents of chemical fertilizers are higher than that of organic ones, but they easily to cause environmental pollution and soil degradation (Song et al., 2020). The partial replacement of chemical fertilizers with organic fertilizers has proven to be a beneficial approach to sustain soil fertility compared to applying chemical or organic fertilizers alone (Song et al., 2020). Studies have shown that the use of inorganic-organic compound fertilizers can not only reduce the use of chemical fertilizer but also improve the efficiency and sustainability of agricultural ecosystems in the long term (Geng et al., 2019).

Numerous studies have found that the combination of chemical fertilizer and organic fertilizer can improve the quality of peaches (Sharma et al., 2017), pears (Wei et al., 2012), grapes (Zhao et al., 2020), and others. Organic fertilizer application increased the soluble sugar content of bananas (Zhang et al., 2020), decreased the titratable acid content of pears (Wei et al., 2012), and significantly affected the pH of the grape juice (Zhao et al., 2020). Through the modification of soil physicochemical properties, fertilization has been found to influence the soil microbial biomass and community composition (Liu et al., 2010). Similar studies also found that the use of organic fertilizer not only affected soil physical properties but also enhanced soil microbial diversity (Hao et al., 2008). Many studies have shown that organic fertilization had positive effects on soil microbial richness and diversity (Zhang et al., 2012; Geng et al., 2019). By contrast, chemical fertilization was bad for microbial diversity (Luan et al., 2020). Plant surfaces host diverse and abundant microbial communities, which are related to specific functions that may affect plant productivity and health (Angeli et al., 2019). Microbial communities associated with grape leaves, flowers, and berries shared a greater proportion of taxa with the soil communities, suggesting that soil may serve as a microbial reservoir (Zarraonaindia et al., 2015). *Ascomycota*, *Basidiomycota*, *Chytridiomycota*, *Blastocladiomycota*, and *Glomeromycota* were main fungal phylum in the soil; *Ascomycota* and *Basidiomycota* were main fungal phylum on the grape berry surface. There were 24.63% of the fungal genera which were common to soil and on the grapes surface (Morrison-Whittle et al., 2017). Martins et al. (2013) also found about 50% of the bacteria genera that were common to soil and grapes. Microbial community structure on the grape surface is mainly controlled by the cultivation environments (Abdelfattah et al., 2016a; Kecskemeti et al., 2016). The microbiota on the surface of grapes are important for the development of plant diseases and might also impact fruit maturity (Buchholz et al., 2018). Barata et al. (2012) identified over 50 bacterial species on grape berries, mainly belonging to two groups, *Proteobacteria* and *Firmicutes*. The bacterial community on the surface of grape berry changed with the ripening of the grapes (Renouf et al., 2005). The majority of research has been focused on the bacterial communities, but fungi are also important (Escribano-Viana et al., 2018). Fungi can profoundly influence plant function, health, and development, through a wide range of interactions acting as biocontrol agents or as pathogens (Oliveira et al., 2018). Some fungi are vital for plant health as well as fruit quality and yield (Ding et al., 2019). Previous studies have mostly focused on the pathogenic fungi causing grape diseases, including *Botrytis cinerea* (Chen et al., 2019), *Penicillium expansum* (Jurick 2nd et al., 2020; Luciano-Rosario et al., 2020), and *Aspergillus japonicus* (Yan and Liu, 2019), the causal agents of grapevine powdery mildew, blue mold, and bitter rot, respectively (Lorenzini et al., 2018). Moreover, researchers have also identified saprophytic molds, such as *Cladosporium* sp., *Aspergillus* sp., and *Penicillium* sp., that could produce mycotoxins, which were indirectly responsible for food spoilage and directly responsible for grape rot (Martins et al., 2014). Several *Botryosphaeriaceae* species were known to occur worldwide, causing dieback, canker, and fruit rot on various hosts (Akila et al., 2020). Grape black rot is caused by *Guignardia bidwellii* and was the grapevine disease attributed to a *botryosphaeriaceous* fungus (Onesti et al., 2017). Macrophoma rot is caused by *Botryosphaeria dothidea* (Úrbez-Torres, 2011; Xu et al., 2015). Both *Botryosphaeria kuwatsukai* and *B. dothidea* are the main causal agents for apple ring rot in China and Japan (Xu et al., 2015). Plant-associated fungi, such as *Aureobasidium pullulans* (Lorenzini and Zapparoli, 2019) and *Candida xylopsoci* (Gao et al., 2019), have also been suggested to have a positive interaction with their host plants. In the production of organic apples and pears, *A. pullulans* is used as a biocontrol agent for fire blight protection (Temple et al., 2020). Utilization of *A. pullulans* was shown to be successful in controlling against both *P. expansum* and *Penicillium digitatum* (Agirman and Erten, 2020). A better understanding of these interactions may provide novel opportunities to develop creative biocontrol methods against plant pathogens (Sebastien et al., 2015). Contemporary studies dealing with the microbiome in grapes and the winemaking process have focused on the effects of vineyard locations and grape varieties (Shen et al., 2020). Subsequently, varieties, management methods, and eco-geographic factors were taken into account to explain their possible impacts on the microbiome associated with grapes (Bokulich et al., 2014). Fungi associated with the winemaking process and grape musts have been extensively documented (Escribano-Viana et al., 2018; Oliveira et al., 2018), however, few studies have concentrated

on the fungal community composition on the table grape berry surface under different fertilizer practices.

Xinjiang is an area with a long history of viticulture, with a planting area of 142,900 ha (Huang, 2019). Located in arid regions in Xinjiang, the orchard environment is fragile, and the long-term unscientific use of chemical fertilizer results in an increased frequency of fungal diseases such as powdery mildew (*Erysiphe necator*) and downy mildew (*Plasmopara viticola*) in vineyards. Previous studies mainly focused on the effects of fertilization on the growth of grapes (Liu et al., 2016) and the soil environment (Zhang et al., 2018; Cheng et al., 2020). The fungi on the surface of the grape berries are essential for the quality and storage of grape berries, which are also very important for people's food safety. However, there is no report on the effects of different fertilization modes on grape berry surface fungal communities. The paper aimed to investigate the grape quality and the fungal diversity on the grape berry surface under three fertilizer treatments at two postharvest timepoints to provide a theoretical basis for improving the ecological environment and promoting the sustainable production of grapes in arid areas.

MATERIALS AND METHODS

Experimental Site and Experimental Design

The experimental site was located in the grape standard experimental orchard (lat. 45°19'N, long. 86°03'E) of Shihezi Agricultural Science Research Institute in Xinjiang. The experimental zone is classified as temperate and arid, with a continental climate. The site's annual precipitation, annual evaporation, and mean annual temperature are 0.23 m, 1.34 m, and 7.8°C, respectively (Tao et al., 2018). The meteorological data (daily temperature and daily rainfall) recorded during the experiment are shown in **Supplementary Figure S1**. The soil was sandy loam soil. The basic soil properties before the beginning of the experiment were as follow: pH, 8.04; SOM, 32.23 g kg^{-1}; total nitrogen (TN), 1.26 g kg^{-1}; alkali-hydrolysed nitrogen (AN), 50.13 mg kg^{-1}; total phosphorus (TP), 0.89 g kg^{-1}; available phosphorus (AP), 42.95 mg kg^{-1}; available potassium (AK), 121.05 mg kg^{-1}; and conductivity, 2.10 ms m^{-1}. The soil pH, SOM, TN, TP, TK, AN, AK, and AP was measured as described (Bao, 2000).

These experiments used table grapes (*Vitis vinifera* L.) from one cultivar (Summer Black) that is widely planted in Xinjiang. Each treatment was repeated three times and randomly assigned to the experimental units. The grape trellis was a V-shaped scaffold (**Figure 1**) placed between the vines. In the spring, organic fertilizer was applied as the base fertilizer, 0.25 m deep (unilateral fertilization, and on one side of the grape line to avoid mutual influence between the grape plants) and 0.30 m away from the central trunk of the grape vine. Chemical fertilizers (drip application) were applied during the growing season. A total of 11 irrigations were carried out during the whole growth period, and the irrigation interval was 7–10 days. The three fertilization treatments had the same irrigation dates and irrigation times. The three treatments were: (1) common chemical fertilizer for 2 years (CH); (2) increased organic fertilizer and reduced chemical fertilizer for 1 year (A.O); and (3) increased organic fertilizer and reduce chemical fertilizer for 2 years (B.O). The study used a randomized complete block designed with three replicates of the three treatments. Rotten cattle manure was used as organic fertilizer containing 2.48% nitrogen, 1.79% phosphorus, and 1.67% potassium. See **Table 1** for the application amount. The amount of chemical fertilizer applied in the CH treatment was determined according to the amount of fertilizer used by local fruit farmers on the vineyard.

Sample Preparation

Grape bunches were chosen to represent the same aspect (orientation to prevailing wind and sun) and position (proximity to the middle of the row), and samples were randomly collected from each vine at 11 a.m. on August 20, 2018. Then, samples were transported to the laboratory, and healthy bunches were selected based on color uniformity and absence of blemishes or disease. The first nine samples (three replicates × three treatments) were analyzed for grape quality and fungal communities on the grape berry surface shortly after grape picking. The other samples of the three fertilizer treatments (five clusters per fertilizer treatment) were packed into three cardboard boxes and stored at room temperature (~20°C) for

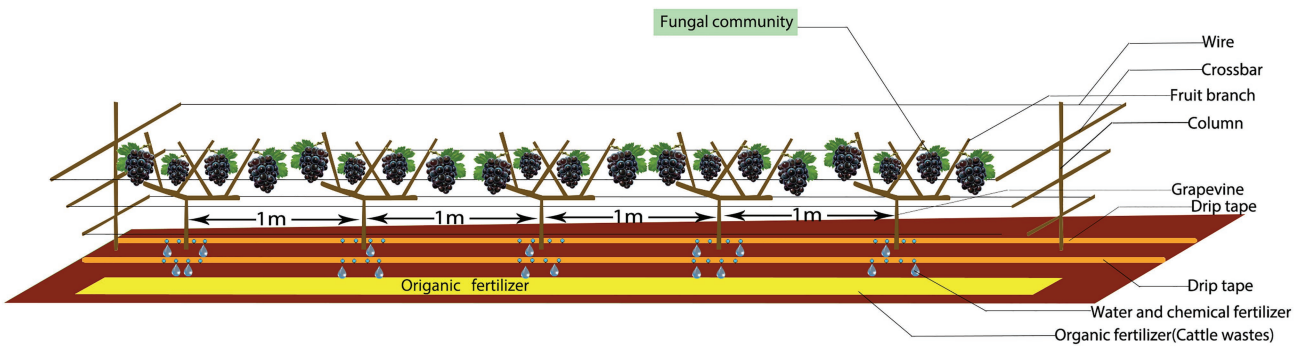

FIGURE 1 | Experimental model.

TABLE 1 | Specific fertilizer application amounts for different treatments and years.

Treatment	2017				2018			
	Chemical fertilizer (kg hm^{-2})			Base fertilizer (kg hm^{-2})	Chemical fertilizer (kg hm^{-2})			Base fertilizer (kg hm^{-2})
	N	P_2O_5	K_2O	Organic fertilizer	N	P_2O_5	K_2O	Organic fertilizer
CH	289.8	172.5	345	0	289.8	172.5	345	0
A.O	217.4	129.3	258.8	0	217.4	129.3	258.8	2921.4
B.O	217.4	129.3	258.8	2921.4	217.4	129.3	258.8	0

The organic fertilizer application amount is consistent with the pure nitrogen nutrient amount provided by chemical fertilizer.

8 days. Table grapes can be stored for 7–12 days at room temperature and some table grapes are sold during this period (Zhu, 2020). Eighteen samples (three replicates × three treatments × two timepoints) of microbial DNA were collected from the grape surfaces. Each treatment consisted of three replications with 50 fresh grape berries per replicate. The microbial samples were gathered by wiping or swabbing each grape with a pre-moistened cotton swab. Swab samples were collected and stored at −80°C before microbial DNA extraction. The wiped grape berries were then used to assess the quality parameters of the grape berries.

Determination of Quality Parameters of Grape Berries

The pH was determined using a Mettler Toledo FE20 Desktop pH Meter (Mettler Toledo Instruments Co. Ltd., Shanghai, China). The SSC was measured with a Pocket Brix-acidity Meter (Atago, PALBX/ACID 5, Tokyo, Japan). Titratable acid content was determined using potentiometric titration with 0.1 N NaOH up to pH = 8.2 and expressed as percentage of tartaric acid (Youssef et al., 2015). The total anthocyanin content (TAC) in berries was determined by the pH differential method (Yang et al., 2020). The berry firmness was performed with a texture analyzer (TA). XT plus (Stable Micro Systems, Surrey, England), analyzing the equatorial position of 15 berries with pedicels per plot (Youssef et al., 2015).

Extraction of Genomeice DNA and PCR Amplification

The MoBio Power Water® DNA Isolation kit (MoBio Laboratories, Inc., Carlsbad, CA, United States) was used to extract microbial genomic DNA from the swabs. The NC 2000 spectrophotometer (Thermo Scientific Fisher, Waltham, MA, United States) and 1.0% agarose gel electrophoresis were used to determine the concentration and molecular size of the extracted DNA, respectively. Then, the DNA extractions were stored at −80°C until further use. Grape berries were analyzed for fungal communities shortly after grape picking, which was referred to as T0. Grape samples stored for 8 days, were referred to as T1. A total of 18 diluted DNA samples were submitted to Shanghai Personal Biotechnology Co., Ltd (Shanghai, China) for internal transcribed spacer (ITS) sequencing using the Illumina HiSeq sequencing platform. The specific pairs were ITS25F (5'-GGAAGTAAAAGTAACAAGG-3') and ITS1R (5'-GCTGCGTTCTTCATGC-3'). The PCR reaction contained 5 U of DNA polymerase (Pyrobest TaKaRa, Japan), 15 pmol of each primer, 2.5 mM of dNTP mixture, 10 μl of 10x Buffer II, and 40 ng of template DNA for a total volume of 25 μl. The PCR amplification series was performed using an ABI 9600 instrument under method of Hao et al. (2016). The obtained ITS1 amplicons were sequenced on the Illumina MiSeq platform at Shanghai Personal Biotechnology Co., Ltd (Shanghai, China).

PCR Product Purification and Library Preparation

According to the concentrations of the PCR products, PCR products were mixed at equal density ratios and then purified using a Qiagen Gel Extraction Kit (Qiagen Company in Germany; Zetsche et al., 2017). The TruSeq® DNA PCR-Free Sample Preparation Kit (Illumina, United States) was used to generate sequencing libraries, and then index codes were added (Noguerol-Pato et al., 2014). The library quality was evaluated using the Qubit@ 2.0 Fluorometer (Thermo Scientific) and an Agilent Bioanalyzer 2100 system (Kao et al., 2016). Finally, the library was sequenced on the Illumina HiSeq 2500 platform and 250 bp paired-end reads were generated.

Bioinformatic Analyses

After completing high-throughput sequencing, paired-end reads were obtained, which were assigned to samples based on their unique barcodes, and then truncated by cutting off the barcode and primer sequences. Using FLASH V1.2.7 spliced the paired-end reads (El-Ashram and Suo, 2017), filtered according to the QIIME V1.7.0 quality control process, and termed the high-quality clean tags. The tags were compared to the reference database using the UCHIME algorithm to detect chimeric sequences, and then removed the chimeric sequences (Li et al., 2018). Finally, we obtained the effective tags. Alpha diversity was evaluated using the QIIME suite of programmes, including the Simpson index, ACE, Shannon diversity, Chao1 richness, and observed species (Marsh et al., 2013). Principal coordinate analysis (PCoA) based on weighted calculations was used to analyze the differences in the community structure of the different treatments and timepoints (Horn et al., 2017). We used flower charts and Venn diagrams to explore the specific and common operational taxonomic units (OTUs) among the different treatments or timepoints. The microbial communities on the grape berry surfaces from the different treatments/timepoints were further compared using analysis of similarities (Anosim) and analysis of molecular variance (Amova). Amova was used to assess the significance

of the fungal community structures among the different treatments. After basic analysis, Origin 2019 and R Studio (version 2.15.3) were used to draw figures (Hayden and Beman, 2016).

Statistical Analysis

SPSS 20.0 software was used to test the significance of the differences in the quality and fungal diversity of grapes, and the data were expressed as the means ± SD of triplicates.

RESULT

The Quality Parameters of Grape Berries

The SSC, pH of the grape juice, and TAC significantly increased after 8 days of storage in grapes from all three fertilizer treatments. At both timepoints, the SSC was significantly higher with the organic fertilizer treatments (A.O and B.O) relative to the chemical fertilizer treatment (CH); the value of the B.O sample was 14.21% higher than that of the CH sample, and the value of the A.O sample increased by 11.76% compared with the CH samples from T1 timepoint (**Figure 2A**). Of the three treatments, the titratable acid content was the highest in grapes from the B.O treatment at both the T0 and T1 timepoints (**Figure 2B**). **Figure 2C** shows the effect of the fertilizer treatments on the pH of the grape juice. At both the T0 and T1 timepoints, the pH of the grape juice in the A.O samples was significantly higher than that in the B.O samples. As seen in **Figure 2D**, at both timepoints, the TAC of the B.O and A.O samples was higher than that of the CH sample. The TAC in the T1.B.O and T1.A.O samples increased by 72.48 and 53.32%, respectively, compared with the T1.CH samples. **Figure 2E** shows that the firmness of the grape flesh

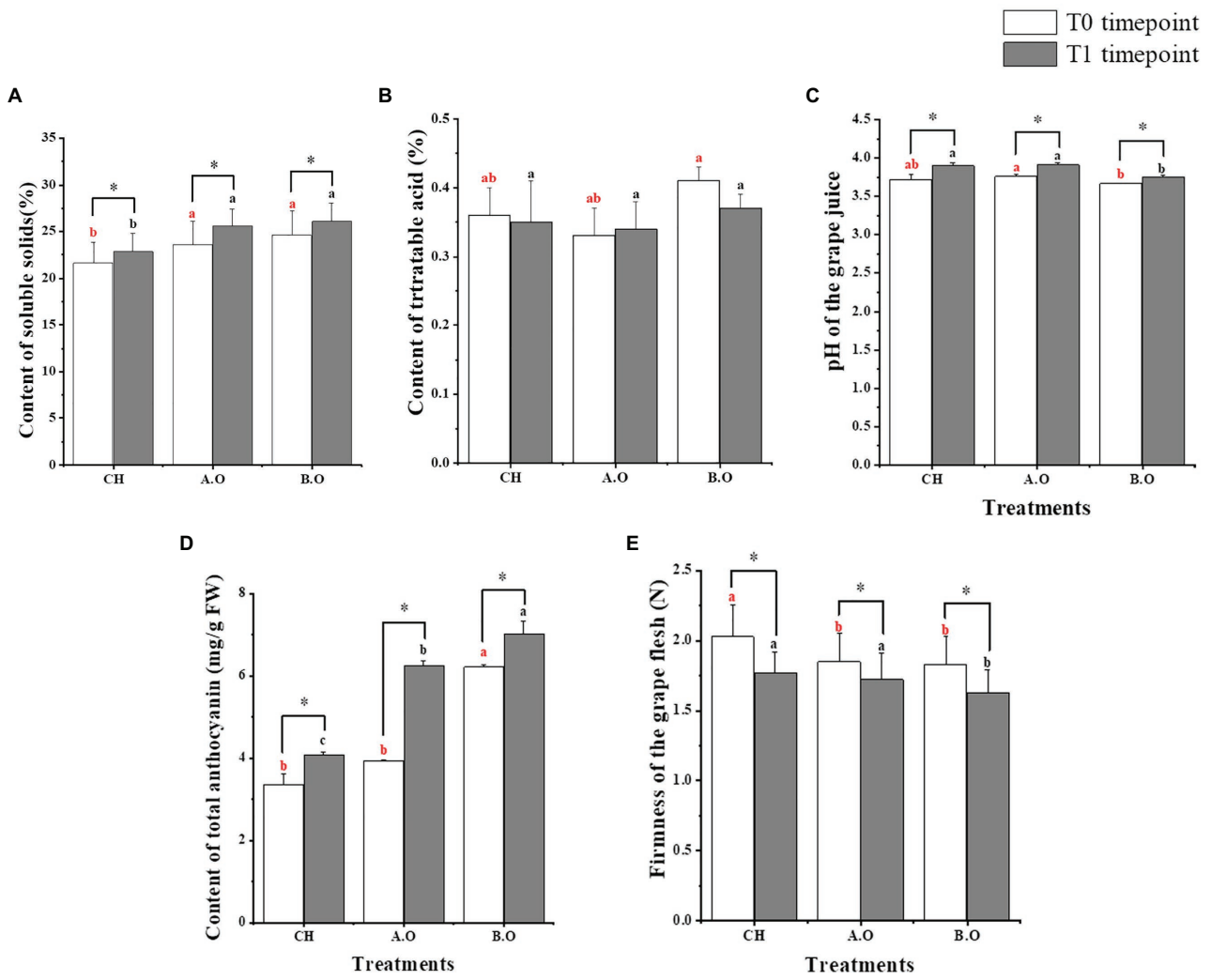

FIGURE 2 | Quality parameters of grape berries. **(A)** Soluble solids content (SSC) of grape berries. **(B)** Titratable acid contents. **(C)** The pH of the grape juice. **(D)** Total anthocyanins contents. **(E)** Firmness of the grape flesh. Values presented are the means ± SD ($n \geq 3$). Vertical bars indicate the SD of the means. Different letters indicate significant differences among treatments from the same timepoint using Duncan's test ($p < 0.05$). * indicates a significant difference between the T0 and T1 timepoint samples of the same treatment using a one-tailed Student's *t*-test ($p < 0.05$).

from the three fertilizer treatments decreased during the storage period. At both timepoints, the firmness of grape flesh in the CH samples was the highest, while the B.O samples were the lowest. The firmness of the grape flesh in the CH samples increased by 8.87 and 9.85% compared with A.O and B.O samples, respectively, at the T0 timepoint.

ITS-Based Fungal Sequencing Data and Fungal Diversity

A total of 848,903 fungal ITS sequences passed quality control. The total number of reads obtained was 415,995 in the grape samples obtained at T0 timepoint and 432,909 in the samples at the T1 timepoint. Then, the high-quality sequences were clustered into OTUs at 97% sequence identity. After filtering rare OTUs, a total of 827,947 sequences were clustered into 527 identified OTUs (**Supplementary Table S1**).

The observed species and Shannon and ACE indexes of the three fertilizer treatment samples were significantly higher at the T0 timepoint than those at the T1 timepoint. At the T0 timepoint, the Shannon index of the B.O and A.O samples was significantly increased by 14.38 and 11.71%, respectively, compared to the CH samples. The observed species and ACE index of the B.O samples were the highest of three fertilizer treatments. At the T1 timepoint, the Shannon index of the B.O samples was higher than that of the A.O and CH samples, and the difference between the B.O samples and the CH samples was significant. The observed species and ACE index were significantly higher in the B.O samples relative to the A.O and CH samples (**Table 2**).

Overall Characteristics of the Fungal Community

The percentages and distributions of the predominant fungi at different classification levels (phylum, class, order, family, genus, and species) are shown in **Figure 3**. *Ascomycota* was the most abundant phylum, accounting for 94.41% of the total sequences. We also detected *Basidiomycota* as a minor phylum (5.05%). Dominant classes included *Saccharomycetes* (48.47%), *Dothideomycetes* (16.63%), and *Tremellomycetes* (3.65%). Dominant orders were *Saccharomycetales* (48.47%), *Pleosporales* (13.46%), *Capnodiales* (2.63%), and *Helotials* (2.57%). Dominant families were *Pichiaceae* (13.01%), *Sclerotiniaceae* (2.57%), and *Davidiellaceae* (2.03%). A total of 99 genera were detected in grape surface samples from the T0 timepoint, and 83 genera were detected in the grape surface samples from the T1 timepoint. The predominant genera of samples from the T0 timepoint were *Botrytis* (3.55%), *Cladosporium* (2.72%), *Cryptococcus* (1.68%), *Pichia* (1.06%), *Aspergillus* (0.98%), and *Aureobasidium* (0.73%). Correspondingly, the predominant genera of samples from the T1 timepoint were *Pichia* (21.26%), *Issatchenkia* (3.07%), *Botryis* (1.58%), *Cladosporium* (1.34%), *Cryptococcus* (1.17%), *Aureobasidium* (0.39%), and *Aspergillus* (0.32%; **Table 3**). Most of these highly detected genera included multiple species. A total of nine species *Cryptococcus* were detected, primarily *C. albidus*, *C. cyanovorans*, *C. heimaeyensis*, and *C. heveanensis*. *Aspergillus* was detected with nine species, mainly of *A. japonicus*, *A. pipers*, *A. cibarius*, *A. subversicolor*, and *A. ochraceus*. Two species of *Aureobasidium*, *A. pullulans* and *A. microstictum* were highly detected in all samples. A total of seven species of *Penicillium* were detected primarily *P. spinulosum*, *P. cinnamopurpureum*, and *P. bialowiezense*. Only one species each of *Pichia*, *Issatchenkia*, *Botrytis*, and *Cladosporium* were detected, *P. kluyveri*, *I. terricola*, *B. caroliniana*, and *C. grevilleae*, respectively (**Supplementary Table S1**).

Fungal Community Variation

The beta diversity results of the weighted UniFrac PCoA showed significant fungal compositional differences between samples from the T0 and T1 timepoints (**Figure 4**). The weighted UniFrac PCoA clustered the samples into two groups; the grape surface fungal community compositions from the T1.B.O, T1.A.O, and T0.CH samples grouped together, while the other treatments were scattered (**Figure 4**). PC1 contributed 73.55% and PC2 contributed 13.70%.

Core Fungal Communities on the Surface of Grape Berries

A total of 157 fungal OTUs were shared by all samples of the three treatments at the T0 and T1 timepoints (**Figure 5A**). There were more OTUs in the samples from the T0 timepoint (472 OTUs) than that of the samples from T1 timepoint (390 OTUs). From the total number of reads at the T0

TABLE 2 | Richness and diversity indexes of the fungal communities on the grape berry surfaces following the three treatments across the two timepoints.

Timepoint	Treatment	Reads	Observed species	Diversity and richness indexes			
				Shannon	Simpson	Chao1	ACE
T0	CH	45,316 ± 3246a	208 ± 15b*	2.99 ± 0.06b*	0.82 ± 0.02a*	228.67 ± 8.08a*	216.67 ± 6.66b*
	A.O	46,222 ± 2490a	227 ± 7ab*	3.34 ± 0.14a*	0.83 ± 0.02a	227.50 ± 7.96a	229.44 ± 9.41ab*
	B.O	47,127 ± 3736a	236 ± 7a*	3.42 ± 0.14a*	0.81 ± 0.02a	232.68 ± 8.08a	233.45 ± 7.77a*
T1	CH	47,199 ± 5444a	145 ± 35b*	2.33 ± 0.45b*	0.66 ± 0.03b*	149.71 ± 23.91b*	153.71 ± 25.07b*
	A.O	47,698 ± 2024a	169 ± 17b*	2.55 ± 0.19ab*	0.74 ± 0.01a	160.31 ± 5.53b	161.63 ± 3.82b*
	B.O	49,405 ± 6490a	218 ± 13a*	2.95 ± 0.12a*	0.75 ± 0.02a	193.00 ± 9.85a	212.92 ± 10.68a*

*Different lowercase letters after data within the same column and timepoint indicate significant differences between the treatments ($p < 0.05$; Duncan's test). All of the values are expressed as the means ± SD of three replicates. *Significant differences between the T0 and T1 timepoints of the same treatment, as determined by a one-tailed Student's t-test ($p < 0.05$).*

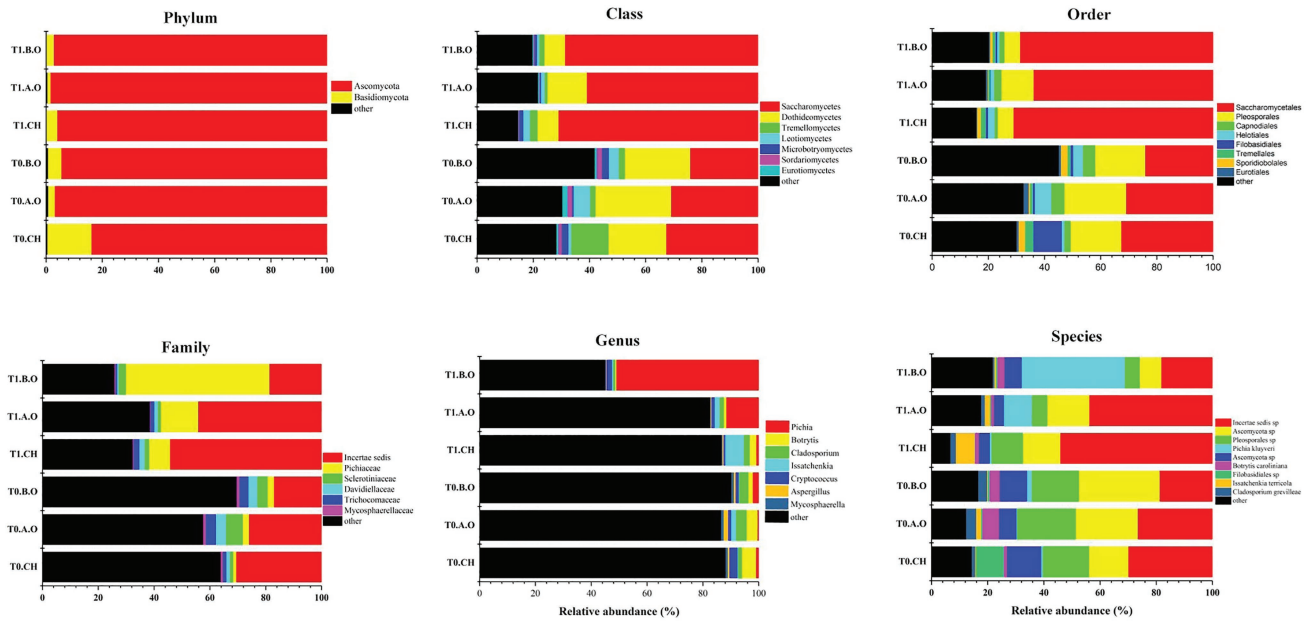

FIGURE 3 | Composition of predominant fungi (abundance ≥ 0.5%) at different taxonomic levels (phylum, class, order, family, genus, and species) from the three fertilizer treatments at the T0 and T1 timepoints.

TABLE 3 | Effects of storage time and fertilizer treatment on the fungal communities on the grape berry surface at the genus level.

Genus (%)	T0			T1		
	CH	A.O	B.O	CH	A.O	B.O
Pichia	0.87 ± 0.21ab	0.33 ± 0.06b*	1.97 ± 0.23a*	0.77 ± 0.40c	11.50 ± 5.64b*	51.80 ± 15.01a*
Botrytis	5.97 ± 2.22a*	3.63 ± 1.84ab*	1.06 ± 0.25b	2.43 ± 0.78a*	1.40 ± 0.53ab*	0.90 ± 0.20b
Cladosporium	3.63 ± 0.45a*	3.23 ± 1.26a*	1.30 ± 0.30b	2.03 ± 0.46a*	1.37 ± 0.40ab*	0.63 ± 0.35b
Cryptococcus	2.87 ± 1.00a	1.07 ± 0.23b	1.10 ± 0.01b	1.87 ± 1.80a	1.07 ± 0.11b	0.57 ± 0.31b
Aspergillus	1.63 ± 0.19a*	0.67 ± 0.40b	0.63 ± 0.21b	0.37 ± 0.21a*	0.37 ± 0.11ab	0.23 ± 0.05b
Aureobasidium	0.43 ± 0.17b	0.63 ± 0.27ab*	1.13 ± 71a	0.12 ± 0.01b	0.17 ± 0.06b*	0.87 ± 0.25a*
Penicillium	0.16 ± 0.07a*	0.09 ± 0.04ab	0.06 ± 0.01b	0.08 ± 0.03a*	0.04 ± 0.03b	0.03 ± 0.02b
Candida	0.08 ± 0.07c	0.11 ± 0.02b*	0.20 ± 0.01a*	0.09 ± 0.04b	0.23 ± 0.02ab*	0.27 ± 0.01a*

*Only fungal genera contributing to at least 0.05% of the total reads with significant differences between the three treatments within one period are shown. Different lowercase letters after data within the same row and timepoint indicate significant differences between treatments ($p < 0.05$; Duncan's test). All of the values are expressed as the means ± SD of three replicates. *Significant differences between the T0 and T1 timepoint within the same treatment, as determined by a one-tailed Student's t-test ($p < 0.05$).*

timepoint, 345 OTUs were identified in the CH treatment, while 323 and 346 OTUs were identified in the A.O and B.O treatments (**Figure 5B**), respectively. A total of 225 fungal OTUs were shared by all the samples at T0 timepoint. For the T1 timepoint, 262, 288, and 237 OTUs were identified in B.O, A.O, and CH treatments (**Figure 5C**), respectively, and 157 fungal OTUs were shared by all the samples at the T1 timepoint. There were significantly more OTUs in the three fertilizer treatments at the T0 timepoint than at the T1 timepoint. The structure of the core fungal community was significantly different between the three treatments at both the T0 and T1 timepoints (**Figures 5D,E**). The dominant species of the core fungal communities of the samples at the T0 timepoint were *Ascomycota* sp., *Pleosporales* sp., *Filobasidiales* sp., and *Botrytis caroliniana*, while those of the samples at the T1 timepoint were *Pichia kluyveri*, *Ascomycota* sp., *Pleosporales* sp., and *Saccharomycetales* sp.

The Fungal Communities at the Genus Level

At the genus level, the relative abundances (RAs) of *Pichia* and *Candida* in the organic fertilizer treatments significantly increased after 8 days of storage. By contrast, the RAs of *Botrytis*, *Cladosporium*, *Cryptococcus*, *Aspergillus*, *Aureobasidium*, and *Penicillium* in the three fertilizer treatments decreased during the storage period (**Table 3**). The RAs of *Botrytis* in the T0.CH and T0.A.O samples significantly decreased by 59.30 and 61.43%, respectively, compared with the T1.CH and T1.A.O samples. The RAs of *Aureobasidium* and *Candida* were the highest of three fertilizer treatments in the B.O samples at

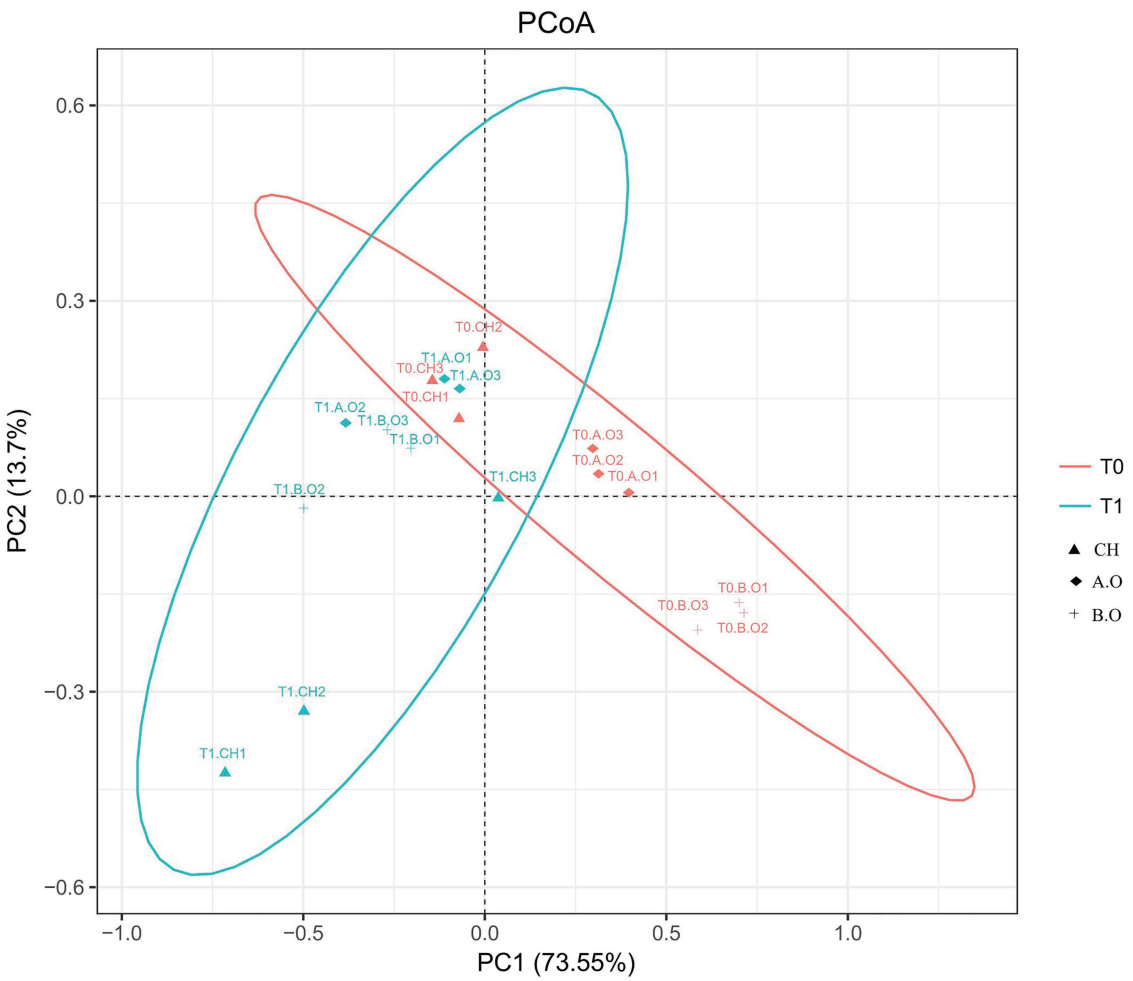

FIGURE 4 | Comparison of fungal communities on the grape berry surface. A principal coordinate analysis (PCoA) based on weighted UniFrac distances was generated with operational taxonomic units (OTUs) (at 97% similarity) present in the three fertilizer treatments. Red colored oval represents samples from the T0 timepoint. Blue colored oval represents samples from the T1 timepoint.

both timepoints. The RA of *Aureobasidium* in the T0.B.O samples was 162.79% higher than that in the T0.CH samples. The RAs of *Botrytis*, *Cladosporium*, and *Penicillium* in the T0.CH samples were significantly higher than those in T0.B.O samples. The RA of *Botrytis* in T0.B.O samples was 82.42% lower than that in the T0.CH samples. The RAs of *Cryptococcus* and *Aspergillus* were significantly higher in the T0.CH samples relative to the T0.B.O and T0.A.O samples. The RA of *Aspergillus* in the T0.CH samples increased by 61.35 and 58.90% compared to the T0.B.O and T0.A.O samples, respectively (**Table 3**).

The Fungal Communities at the Species Level

The dominant fungi at species level were *Ascomycota* sp., *Pleosporales* sp., and *P. kluyver* at both timepoints (**Figures 5D,E**). However, the RAs of these fungi within the fungal community changed. **Table 4** shows that the RA of *P. kluyver* in all three treatments at the T1 timepoint was higher than that at the T0 timepoint, and the same was true for *I. terricola* and *B. caroliniana*. The RA of *P. kluyver* in the T1.A.O and T1.B.O samples was significantly increased by 3509.52 and 1976.68%, respectively, compared to the T0.A.O and T0.B.O samples (**Table 4**). By contrast, the RAs of *Filobasidiales* sp., *A. pullulans*, *C. xylopsoci*, and *A. japonicas* in the three fertilizer treatments decreased during the storage period. *Aureobasidium pullulans* and *C. xylopsoci* RAs were the highest of three fertilizer treatments in the B.O samples at both timepoints. *Aureobasidium pullulans*, *Filpbasidiales* sp., and *C. xylopsoci* RAs were the lowest of three fertilizer treatments in the CH samples at both timepoints. The *A. pullulans* RA in the T0.B.O samples increased by 464.29% compared with the T0.CH samples. The abundance of *A. pullulans* in the T1.B.O samples was 687.50% higher than that in the T1.CH samples. The *B. caroliniana* and *A. japonicus* RAs in the T0.CH samples were significantly higher than those in the T0.B.O samples ($p < 0.05$). The *B. caroliniana* RA in the T0.B.O samples decreased by 59.73% compared with the T0.CH samples. The *I. terricola* RA was significantly higher in the T0.CH samples relative to the T0.B.O and T0.A.O samples. The *I. terricola* RA

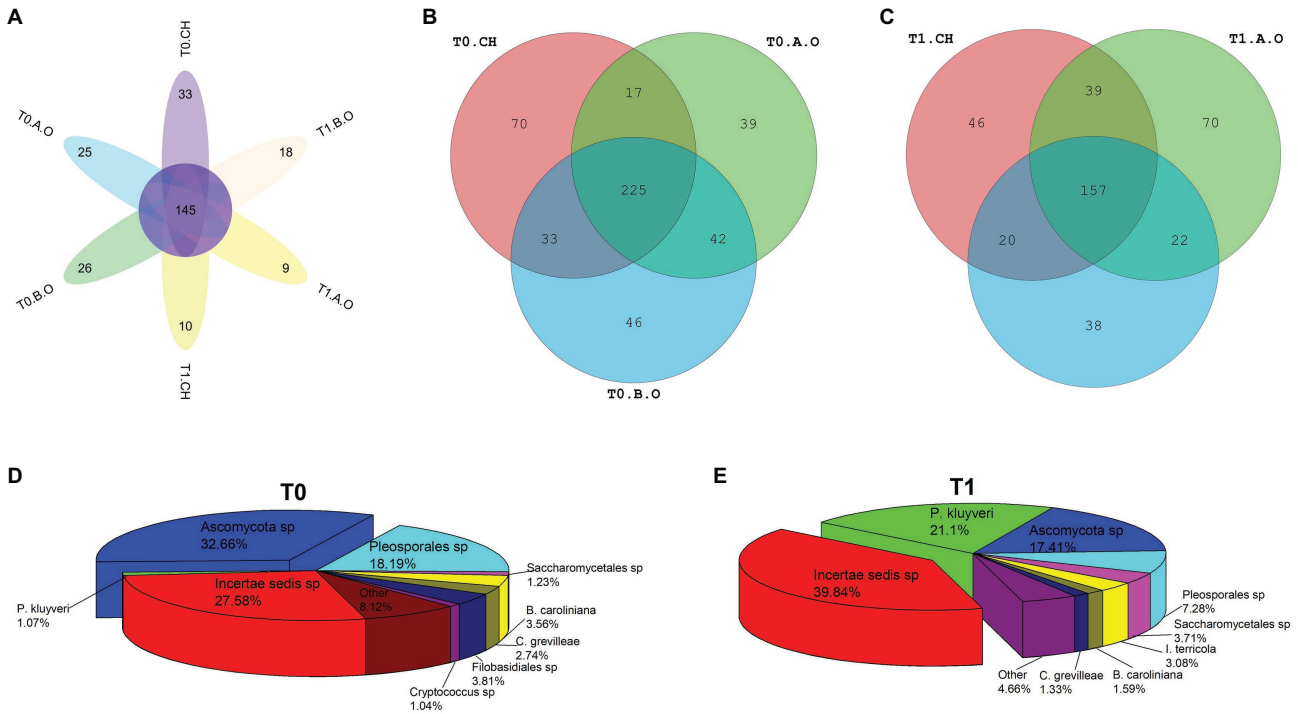

FIGURE 5 | The exclusive and common fungal OTUs on the grape berry surface. **(A)** Flower chart of the three fertilizer treatments at the T0 and T1 timepoints; **(B)** Venn diagram of the three fertilizer treatments at the T0 timepoint; **(C)** Venn diagram of the three fertilizer treatments at the T1 timepoint; **(D)** Composition of the core fungal community of the three fertilizer treatments at the T0 timepoint; and **(E)** Composition of the core fungal community of the three fertilizer treatments at the T1 timepoint.

TABLE 4 | Effects of storage time and fertilizer treatment on the fungal communities on the grape berry surface at the species level.

Species (%)	T0			T1		
	CH	A.O	B.O	CH	A.O	B.O
P. kluyver	0.52 ± 0.17ab	0.21 ± 0.03b*	1.33 ± 0.17a*	0.53 ± 0.27b	7.58 ± 4.31ab*	27.62 ± 18.71a*
I. terricola	1.29 ± 0.72a*	0.14 ± 0.20b*	0.19 ± 0.0.07b*	19.79 ± 2.73a*	5.51 ± 0.71b*	1.65 ± 1.10c*
B. caroliniana	2.93 ± 0.49a*	1.78 ± 0.06b*	1.18 ± 0.35bc	7.34 ± 2.27a*	4.37 ± 2.01ab*	1.31 ± 0.22b
Filobasidiales sp.	0.43 ± 0.23b	0.56 ± 0.60b	7.49 ± 0.69a	0.12 ± 0.01b	0.36 ± 0.13ab	0.49 ± 0.04a
A. pullulans	0.14 ± 0.03c	0.30 ± 0.05b	0.79 ± 0.21a	0.08 ± 0.01b	0.08 ± 0.03b	0.63 ± 0.02a
C. xylopsoci	0.05 ± 0.03b	0.17 ± 0.05ab	0.20 ± 0.06a	0.09 ± 0.04b	0.08 ± 0.03b	0.12 ± 0.03a
A. japonicus	0.19 ± 0.012a	0.18 ± 0.02a	0.12 ± 0.03b	0.07 ± 0.02a	0.06 ± 0.00ab	0.05 ± 0.01b

*Only fungal species contributing at least 0.05% of the total reads with significant differences between the three treatments within a timepoint are shown. Different lowercase letters after data within the same row and timepoint indicate significant differences between treatments ($p < 0.05$; Duncan's test). All of the values are expressed as the means ± SD of three replicates. P. kluyver, Pichia kluyver; I. terricola, Issatchenkia terricola; B. caroliniana, Botrytis caroliniana; A. pullulans, Aureobasidium pullulans; C. xylopsoci, Candida xylopsoci; and A. japonicas, Aspergillus japonicus. *Significant differences between the T0 and T1 timepoints within the same treatment, as determined by a one-tailed Student's t-test ($p < 0.05$).*

in the T0.CH samples increased by 89.15 and 85.27% compared to the T0.A.O and T0.B.O samples, respectively (**Table 4**).

Association Networks Among Fungal Species

Fungal co-occurrence networks among the most abundant fungal species (RA > 0.1%) are shown in **Figures 6, 7**. A total of 82 interaction pairs related to 25 species were obtained from the T0 timepoint, *P. kluyveri* (four linkages), *I. terricola* (four linkages), *B. caroliniana* (eight linkages), *Filobasidiales* sp. (eight linkages), *A. pullulans* (four linkages), *C. xylopsoci* (four linkages), and *A. japonicus* (four linkages) exhibited higher degrees of linkage with other species (**Figure 6**). The species *P. kluyveri* cooperated with *A. pullulans* and competed with *I. terricola*. *Aureobasidium pullulans* competed with *A. japonicus* and *I. terricola*. *Botrytis caroliniana* competed with *C. xylopsoci* and *Filobasidiales* sp. *Candida xylopsoci* cooperated with *Filobasidiales* sp. and *Cryptococcus victoriae*.

As shown in **Figure 7**, a total of 89 interaction pairs related to 26 species were obtained from the T1 timepoint; *P. kluyveri* (10 linkages), *I. terricola* (10 linkages), *B. caroliniana* (seven linkages), *Filobasidiales* sp. (10 linkages), *A. pullulans* (10 linkages),

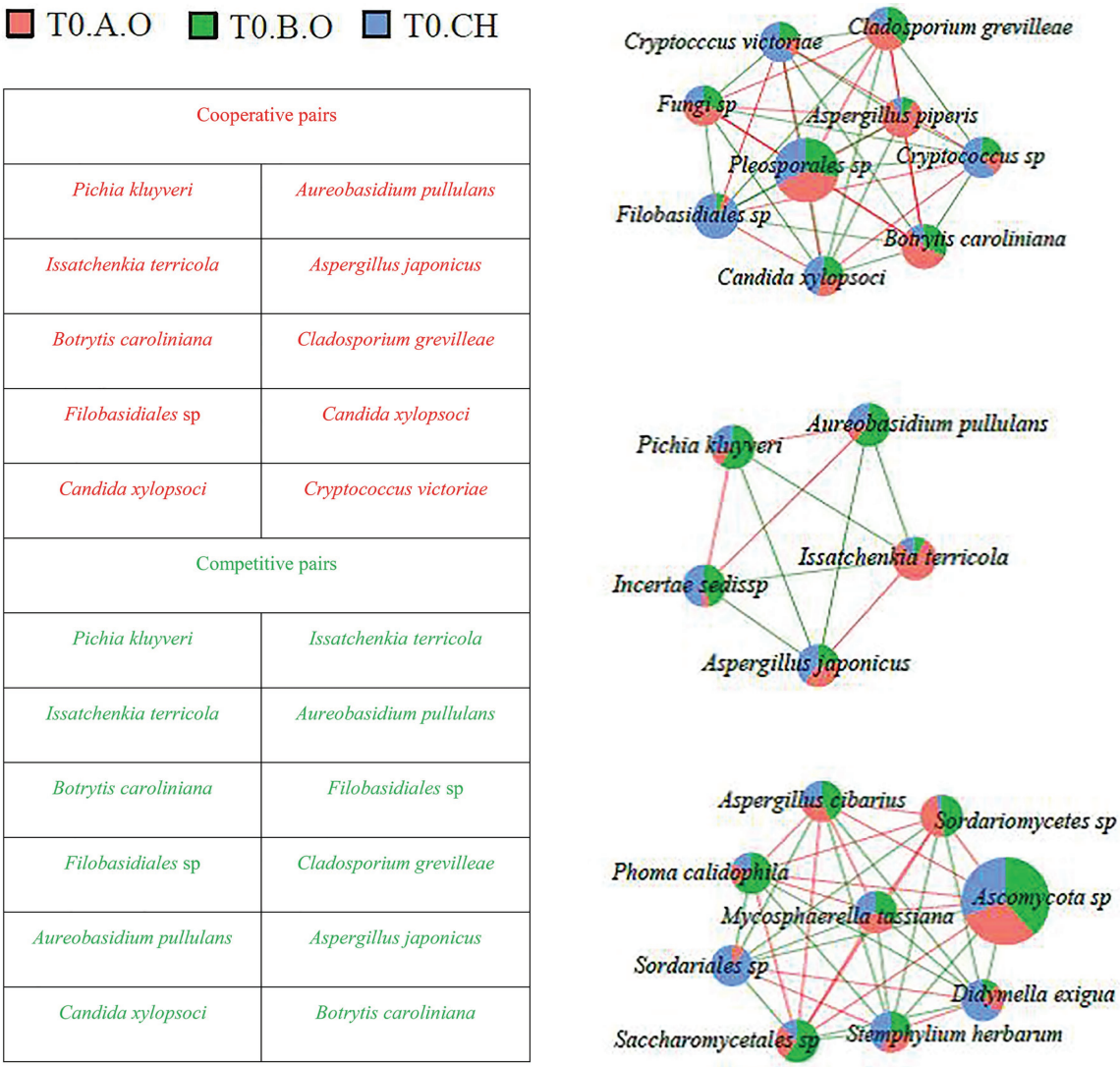

Cooperative pairs	
Pichia kluyveri	*Aureobasidium pullulans*
Issatchenkia terricola	*Aspergillus japonicus*
Botrytis caroliniana	*Cladosporium grevilleae*
Filobasidiales sp	*Candida xylopsoci*
Candida xylopsoci	*Cryptococcus victoriae*
Competitive pairs	
Pichia kluyveri	*Issatchenkia terricola*
Issatchenkia terricola	*Aureobasidium pullulans*
Botrytis caroliniana	*Filobasidiales* sp
Filobasidiales sp	*Cladosporium grevilleae*
Aureobasidium pullulans	*Aspergillus japonicus*
Candida xylopsoci	*Botrytis caroliniana*

FIGURE 6 | Network diagram of dominant species in the T0 timepoint samples (RA > 0.1%) showing cooperative and competitive associations. Green represents a competitive association and red represents a cooperative association.

C. xylopsoci (seven linkages), and *A. japonicus* (10 linkages) exhibited higher degrees of linkage with other species. At the T1 timepoint, the species *Filobasidiales* sp. was observed to cooperate with *Pichia kluyveri* and *Candida xylopsoci*, whereas *Filobasidiales* sp. was observed to compete with *I. terricola*. *Aspergillus japonicus* cooperated with *I. terricola* and *Cryptococcus* sp., whereas *A. japonicus* competed with *P. kluyveri* and *A. pullulans*. *Issatchenkia terricola* competed with *Filobasidiales* sp. and *A. pullulans*.

Correlation Analysis Between the Fungal Diversity on the Grape Berry Surface and Quality Parameters of Grape Berries

The Pearson correlation analysis was used to verify the correlations between the experimental indicators, such as firmness, pH, SSC, titratable acid, anthocyanin, and the Shannon, Simpson, Chao1, and ACE indexes, and the indicators of correlation are listed in **Figure 8**. The firmness of the grape flesh showed a positive correlation with the Chao1, Simpson, ACE, and Shannon indexes, as well as with titratable acid. The firmness of the grape flesh showed a significant negative correlation with anthocyanin and SSC. Moreover, the pH of the grape juice showed a significant negative correlation with the ACE, Chao1, Simpson, and Shannon indexes. Likewise, anthocyanin of grapes had a significant positive correlation with SSC. Additionally, titratable acid showed a positive correlation with the ACE, Chao1, Simpson, and Shannon indexes, and a negative correlation was observed between pH and titratable acid.

DISCUSSION

Organic farming is important to maintain or even improve soil quality (Hondebrink et al., 2017). Although organic farming

T1.A.O T1.B.O T1.CH

Cooperative pairs	
Pichia kluyveri	*Aureobasidium pullulans*
Issatchenkia terricola	*Aspergillus japonicus*
Botrytis caroliniana	*Cladosporium grevilleae*
Filobasidiales sp	*Candida xylopsoci*
Candida xylopsoci	*Cryptococcus victoriae*
Competitive pairs	
Pichia kluyveri	*Issatchenkia terricola*
Issatchenkia terricola	*Aureobasidium pullulans*
Botrytis caroliniana	*Filobasidiales sp*
Aureobasidium pullulans	*Aspergillus japonicus*
Filobasidiales sp	Cladosporium grevilleae
Candida xylopsoci	*Botrytis caroliniana*

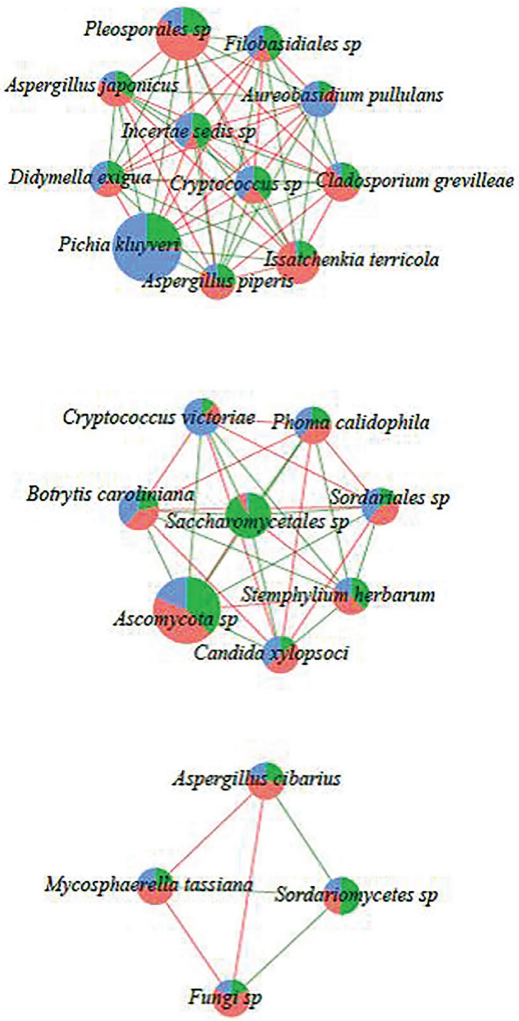

FIGURE 7 | Network diagram of dominant species in the T1 timepoint samples (RA > 0.1%) showing cooperative and competitive associations. Green represents a competitive association and red represents a cooperative association.

is more eco-friendly and can improve the quality of grapes, it cannot meet the requirements for high grape yields in a short period. In recent years, to maintain high yields and protect the environment, the replacement of chemical fertilizers with organic ones has received more and more attention (Geng et al., 2019). In this study, we showed that the SSC of grape berries treated with organic fertilizer was higher than that of control grapes, and grape berries produced higher TAC with organic fertilizer (**Figure 2**). Furthermore, increased application of organic fertilizer along with reduced chemical fertilizer for 2 years induced the most significant improve the contents in the SSC and TAC of grape compared to the control grapes from T0 and T1 timepoints.

Fertilizer practices can have an impact on microbial diversity. Agricultural practices affect the community structure of phyllosphere fungal communities associated with Carménère grapevines. Grapes under organic agricultural management had more fungal species than grapes under conventional agricultural management (Castaneda et al., 2018). There are significant differences in the microbial community compositions on the surface of conventional and organic grapes (Leff and Fierer, 2013). Moreover, significant differences in fungal populations were observed in conventional and organic apples. Several unique taxa have been exclusively detected in organic apples (Abdelfattah et al., 2016a). We observed different level of fungal diversity in the fungal taxonomies obtained from the three fertilizer treatments at two timepoints (**Figure 3**). Also, we found that the Simpson and ACE indexes of the three fertilizer treatments at the T0 timepoint were significantly higher than those of the three fertilizer treatments at the T1 timepoint (**Table 2**). These results indicated that samples of the three fertilizer treatments at T0 timepoint shared a more diverse of fungal community than samples of the three fertilizer treatments at the T1 timepoint. These results indicate that room temperature storage reduces fungal diversity on the grape

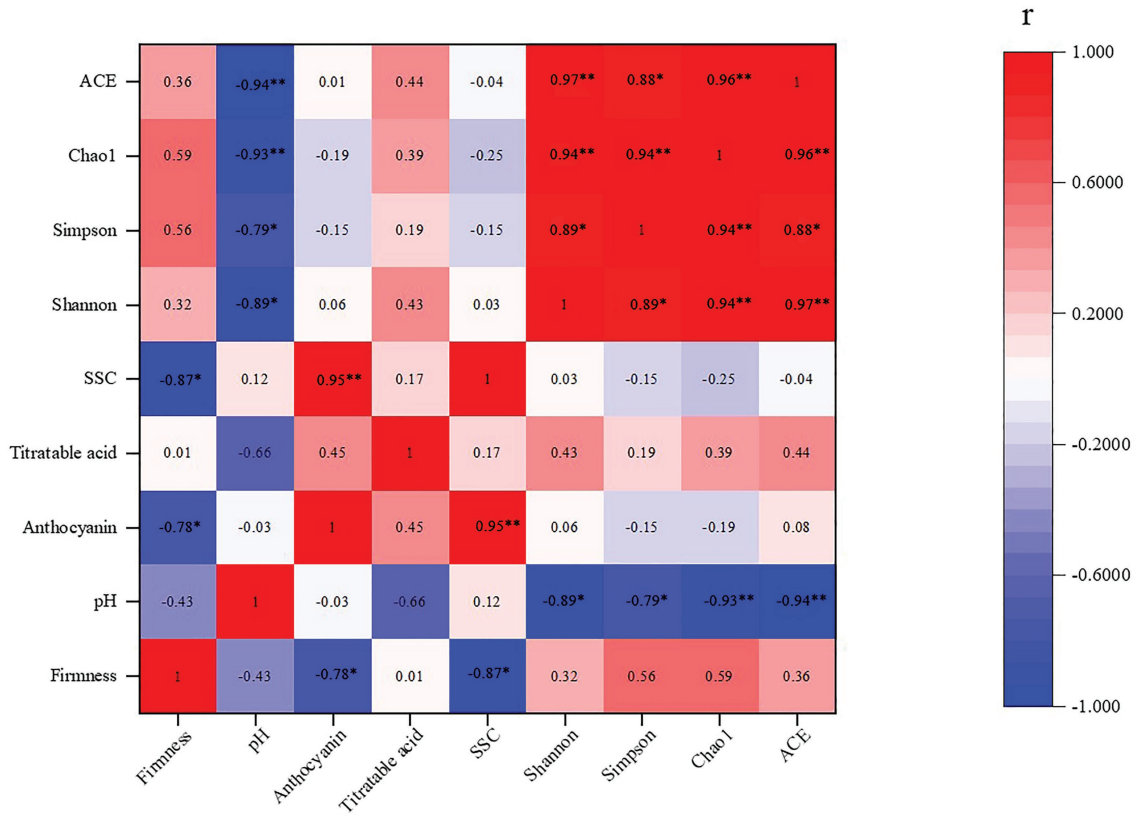

FIGURE 8 | Correlation between the fungal diversity on the grape berry surface and quality parameters of the grape berries. *, ** indicate significant correlations at $p < 0.05$ and 0.01, respectively.

berry surface. Furthermore, the Simpson and ACE indexes of A.O and B.O samples (increased organic fertilizer and reduced chemical fertilizer for 1 and 2 years, respectively) were both higher than the CH samples (application of common chemical fertilizer for 2 years). These results indicate that increasing the application of organic fertilizer and reducing the application of chemical fertilizer in the grape rhizosphere can increase the fungal diversity on the grape berry surface. The majority of vine-associated microbial assemblages originate in the soil, and their distribution reflects the influence of vineyard management (Zarraonaindia et al., 2015). Morrison-Whittle et al. (2017) found 24.63% of the fungal genera which were common to soil and on the grape surface. This result was maybe due to the increased organic matter content in the soil that occurred through the application of organic fertilizer, thereby improving the soil properties and increasing the soil fungal diversity. Aboveground (leaves, flowers, and grapes) fungal communities shared a greater proportion of taxa with soil communities (Zarraonaindia et al., 2015), so the fungal diversity on the grape berry surface increased.

Ascomycota was the most highly detected phylum in this study (94.41%). The high percentage of *Ascomycota* coincided with results from other studies of *Kyoho* grape berries (80.24%; Abdelfattah et al., 2016b) and wine grape (77.00%; Carmichael et al., 2017). Gao et al. (2019) found that the main genera of four different wine grape cultivars were *Aureobasidium*, *Botrytis*, *Alternaria*, *Cladosporium*, *Mucor*, *Hanseniaspora*, and *Cryptococcus*, but their abundances in the different cultivars changed significantly. *Sclerotinia* sp., *Cladosporium* sp., *A. pullulans*, and *A. alternate* were the dominant fungal species in study of Kecskemeti et al. (2016). In our study, the predominant genera of the samples from the T0 timepoint were *Botrytis*, *Cladosporium*, *Cryptooccus*, *Pichia*, and *Aspergillus*. Correspondingly, the predominant genera of the samples from the T1 timepoint were *Pichia*, *Issatchenkia*, *Botryis*, *Cladosporium*, and *Cryptococcus*. The dominant genera of the three fertilizer treatments were almost unchanged between the T0 and T1 timepoints, but their abundances changed significantly. The components of the core fungal communities were significantly different between samples from the T0 and T1 timepoints (**Figures 5D,E**), indicating that the epiphytic fungal community on the grape berry surface at the T0 timepoint was significantly different from that of T1 timepoint.

Different fungal communities on the fruit surface can affect the fruit safety. Peri-urban apples samples carried potential pathogenic risks, whereas rural apple maintained more diverse fungal communities on their surfaces (Shen et al., 2018). We analyzed the dominant genera and

species of the three fertilizer treatments from the T0 and T1 timepoints with RAs greater than 0.05%. We found that the RAs of *Aureobasidium* and *Candida* in the B.O samples were significantly higher than that of the CH samples at both timepoints. The RAs of *Aureobasidium* and *Candida* in the A.O samples were also higher than that of the CH samples at both timepoints, but the difference was not significant (**Table 3**). The epiphytic fungi living in plant tissues, particularly *Aureobasidium* (Ferreira-Pinto et al., 2006), *Candida* (Mewa-Ngongang et al., 2019), and *Pichia* (Mewa-Ngongang et al., 2019), play essential roles in disease control. *Aureobasidium pullulans* was used as a biocontrol agent against *B. cinerea* on grapes (Wang et al., 2018a). Certain fungal genera enriched in the B.O and A.O samples have been reported to exhibit protective functions. Therefore, the soil environment by organic fertilizer may provide certain advantages in maintaining healthier fungal communities on grape surfaces. *Botrytis*, *Cladosporium*, *Cryptococcus*, *Aspergillus*, and *Penicillium* were enriched in the CH samples. Significantly, several of these genera have been reported to exhibit pathogenic features and may be related with fruit decay. Specifically, *Penicillium* and *Aspergillus* are wildly reported to cause fruit deterioration and mycotoxin contamination. *Botrytis* causes gray mold on grapevines and strawberries (Haidar et al., 2016; Dowling et al., 2017). *Penicillium* causes grape losses (Platania et al., 2012; Parafati et al., 2015). *Cladosporium* was most common and important fungal agent of grape bunch rot (Mahdian and Zafari, 2016). *Aspergillus japonicus* is an important black *Aspergillus* species that may cause grape black rot (Xanthopoulou et al., 2018; Apud et al., 2019). So we suggested that CH samples carried more potential microbiological risks. These results indicated that the increased application of organic fertilizer and reduced application of chemical fertilizer to grapes could increase the RAs of beneficial fungal species on the grape surface. Increased organic fertilizer and reduced chemical fertilizer for 2 years had the most significant effect on increasing the beneficial fungal species on the grape surface.

Inter-species interactions are extremely important in shaping fungal dynamics (Shen et al., 2018). The network analysis results are shown in **Figures 6, 7** demonstrate potential intra-species relationships. We observed that *A. pullulans* was competitive with *I. terricola* and *A. japonicas*. *Aureobasidium pullulans* was cooperative with *P. kluyveri* and *C. xylopsoci*. *Candida xylopsoci* competed with *B. caroliniana*. The fungal species with biological control activity cooperated against the pathogenic fungal species (Shen et al., 2018). pH significantly affected the fungal community structure, which was similar to the results of soil fungal and archaeal community structures (Wang et al., 2019) and soil bacterial community structures (Wang et al., 2018b) in an ongoing antimony mine area. The pH of the grape juice was significantly positively correlated with the Shannon, Simpson, Chao1, and ACE indexes (**Figure 8**). The Shannon, Simpson, Chao1, and ACE indexes were positively correlated with firmness and titratable acidity, but the correlations were not significant. Consequently, the pH of the grape juice can be regarded as a key factor affecting the fungal richness and diversity on the grape berry surface. In our past study, we found that increasing the application of organic fertilizer can significantly affect the pH of the grape juice (Zhao et al., 2020). Ren et al. (2019) also found that the fungal community structure of Pinggu peach trees was significantly correlated with pH.

In summary, increasing the application of organic fertilizer to the root zone of grapes decreased the pH of the grape juice and increased the soluble solids of the grapes, and went on to increase the fungal diversity and RAs of *P. kluyver*, *A. pullulans*, and *C. xylopsoci* (beneficial fungi) on the surface of the grape berries at T0 and T1 timepoints. The positive effect of increased organic fertilizer and reduced chemical fertilizer for 2 years was the most significant. Moreover, significant differences were revealed between the two assessment times (T0 and T1). After 8 days of storage at room temperature, the fungal diversity on the surface of the grape berries significantly decreased. The correlation analysis suggested that the pH of the grape juice was significantly negatively correlated with fungal diversity parameters.

DATA AVAILABILITY STATEMENT

The datasets generated can be found in the NCBI SRA under the Bioproject: ID PRJNA678874.

AUTHOR CONTRIBUTIONS

LW, ZL, and KY designed the study. LW performed the experiments and was involved with writing the manuscript. JF, HL, and KY contributed to revising the manuscript. FZ and BZ participated in lab work and helped with data analysis. All authors contributed to the article and approved the submitted version.

FUNDING

This work was supported by the National Key Research and Development Program (2018YFD1000200), the Natural Science Foundation of China (31760550), and the Transformation Project of Scientific and Technological Achievements of the Xinjiang Production and Construction Corps (2020BA006).

ACKNOWLEDGMENTS

We are very grateful to Xiaoxia Sun for excellent technical support.

SUPPLEMENTARY MATERIAL

The Supplementary Material for this article can be found online at: https://www.frontiersin.org/articles/10.3389/fmicb.2021.628503/full#supplementary-material

REFERENCES

Abdelfattah, A., Wisniewski, M., Droby, S., and Schena, L. (2016a). Spatial and compositional variation in the fungal communities of organic and conventionally grown apple fruit at the consumer point-of-purchase. *Hortic. Res.* 3:16047. doi: 10.1038/hortres.2016.47

Abdelfattah, A., Wisniewski, M., Li Destri Nicosia, M. G., Cacciola, S. O., and Schena, L. (2016b). Metagenomic analysis of fungal diversity on strawberry plants and the effect of management practices on the fungal community structure of aerial organs. *PLoS One* 11:e0160470. doi: 10.1371/journal.pone.0160470

Agirman, B., and Erten, H. (2020). Biocontrol ability and action mechanisms of *Aureobasidium pullulans* GE17 and *Meyerozyma guilliermondii* KL3 against *Penicillium digitatum* DSM2750 and *Penicillium expansum* DSM62841 causing postharvest diseases. *Yeast* 37, 437–448. doi: 10.1002/yea.3501

Akila, B.-T., Eddine, M. A., Wassila, A.-M., Milan, Š., Jana, Č., Robert, P., et al. (2020). Lasiodiplodia mitidjana sp. nov. and other Botryosphaeriaceae species causing branch canker and dieback of *Citrus sinensis* in Algeria. *PLoS One* 15:e0232448. doi: 10.1371/journal.pone.0232448

Angeli, D., Sare, A. R., Jijakli, M. H., Pertot, I., and Massart, S. (2019). Insights gained from metagenomic shotgun sequencing of apple fruit epiphytic microbiota. *Postharvest Biol. Technol.* 153, 96–106. doi: 10.1016/j.postharvbio.2019.03.020

Apud, G. R., Aredes-Fernandez, P. A., Kritsanida, M., Grougnet, R., and Sampietro, D. A. (2019). Antifungal activity of Bignoniaceae plants on *Aspergillus carbonarius* and *Aspergillus niger*. *Nat. Prod. Res.* 34, 2656–2659. doi: 10.1080/14786419.2018.1548453

Bao, S. D. (2000). *Soil agrochemical analysis. 3rd Edn.* Beijing: China Agriculture Press.

Barata, A., Malfeito-Ferreira, M., and Loureiro, V. (2012). The microbial ecology of wine grape berries. *Int. J. Food Microbiol.* 153, 243–259. doi: 10.1016/j.ijfoodmicro.2011.11.025

Bokulich, N. A., Thorngate, J. H., Richardson, P. M., and Mills, D. A. (2014). Microbial biogeography of wine grapes is conditioned by cultivar, vintage, and climate. *Proc. Natl. Acad. Sci. U. S. A.* 111, E139–E148. doi: 10.1073/pnas.1317377110

Buchholz, F., Kostic, T., Sessitsch, A., and Mitter, B. (2018). The potential of plant microbiota in reducing postharvest food loss. *Microb. Biotechnol.* 11, 971–975. doi: 10.1111/1751-7915.13252

Carmichael, P. C., Siyoum, N., Chidamba, L., and Korsten, L. (2017). Characterization of fungal communities of developmental stages in table grape grown in the northern region of South Africa. *J. Appl. Microbiol.* 123, 1251–1262. doi: 10.1111/jam.13577

Castaneda, L. E., Miura, T., Sanchez, R., and Barbosa, O. (2018). Effects of agricultural management on phyllosphere fungal diversity in vineyards and the association with adjacent native forests. *PeerJ* 6:e5715. doi: 10.7717/peerj.5715

Chen, X., Wang, Y., Gao, Y., Gao, T., and Zhang, D. (2019). Inhibitory abilities of *Bacillus* isolates and their culture filtrates against the gray mold caused by *Botrytis cinerea* on postharvest fruit. *Plant Pathol. J.* 35, 425–436. doi: 10.5423/PPJ.OA.03.2019.0064

Cheng, H., Zhang, D., Huang, B., Song, Z., Ren, L., Hao, B., et al. (2020). Organic fertilizer improves soil fertility and restores the bacterial community after 1,3-dichloropropene fumigation. *Sci. Total Environ.* 738:140345. doi: 10.1016/j.scitotenv.2020.140345

Ding, S., Li, N., Cao, M. M., Huang, Q. F., Chen, G. P., Xie, S. Y., et al. (2019). Diversity of epiphytic fungi on the surface of Kyoho grape berries during ripening process in summer and winter at Nanning region, Guangxi, China. *Fungal Biol.* 123, 283–289. doi: 10.1016/j.funbio.2018.11.014

Dowling, M. E., Hu, M. J., and Schnabel, G. (2017). Identification and characterization of Botrytis fragariae isolates on strawberry in the United States. *Plant Dis.* 101, 1769–1773. doi: 10.1094/PDIS-03-17-0316-RE

El-Ashram, S., and Suo, X. (2017). Exploring the microbial community (microflora) associated with ovine Haemonchus contortus (macroflora) field strains. *Sci. Rep.* 7:70. doi: 10.1038/s41598-017-07623-9

Escribano-Viana, R., Lopez-Alfaro, I., Lopez, R., Santamaria, P., Gutierrez, A. R., and Gonzalez-Arenzana, L. (2018). Impact of chemical and biological fungicides applied to grapevine on grape biofilm, must, and wine microbial diversity. *Front. Microbiol.* 9:59. doi: 10.3389/fmicb.2018.00059

Ferreira-Pinto, M. M., Moura-Guedes, M. C., Barreiro, M. G., Pais, I., Santos, M. R., and Silva, M. J. (2006). *Aureobasidium pullulans* as a biocontrol agent of blue mold in "Rocha" pear. *Commun. Agric. Appl. Biol. Sci.* 71, 973–978.

Gao, F. F., Chen, J. L., Xiao, J., Cheng, W. D., Zheng, X. J., Wang, B., et al. (2019). Microbial community composition on grape surface controlled by geographical factors of different wine regions in Xinjiang, China. *Food. Res. Int.* 122, 348–360. doi: 10.1016/j.foodres.2019.04.029

García-Díaz, A., Bienes, R., Sastre, B., Novara, A., Gristina, L., and Cerdà, A. (2017). Nitrogen losses in vineyards under different types of soil groundcover. A field runoff simulator approach in Central Spain. *Agric. Ecosyst. Environ.* 236, 257–267. doi: 10.1016/j.agee.2016.12.013

Geng, Y., Cao, G., Wang, L., and Wang, S. (2019). Effects of equal chemical fertilizer substitutions with organic manure on yield, dry matter, and nitrogen uptake of spring maize and soil nitrogen distribution. *PLoS One* 14:e0219512. doi: 10.1371/journal.pone.0219512

Haidar, R., Deschamps, A., Roudet, J., Calvo-Garrido, C., Bruez, E., Rey, P., et al. (2016). Multi-organ screening of efficient bacterial control agents against two major pathogens of grapevine. *Biol. Control* 92, 55–65. doi: 10.1016/j.biocontrol.2015.09.003

Hao, X. H., Liu, S. L., Wu, J. S., Hu, R. G., Tong, C. L., and Su, Y. Y. (2008). Effect of long-term application of inorganic fertilizer and organic amendments on soil organic matter and microbial biomass in three subtropical paddy soils. *Nutr. Cycl. Agroecosyst.* 81, 17–24. doi: 10.1007/s10705-007-9145-z

Hao, D. C., Song, S. M., Mu, J., Hu, W. L., and Xiao, P. G. (2016). Unearthing microbial diversity of Taxus rhizosphere via MiSeq high-throughput amplicon sequencing and isolate characterization. *Sci. Rep.* 6:22006. doi: 10.1038/srep22006

Hayden, C. J., and Beman, J. M. (2016). Microbial diversity and community structure along a lake elevation gradient in Yosemite National Park, California, USA. *Environ. Microbiol.* 18, 1782–1791. doi: 10.1111/1462-2920.12938

Hondebrink, M. A., Cammeraat, L. H., and Cerda, A. (2017). The impact of agricultural management on selected soil properties in citrus orchards in eastern Spain: a comparison between conventional and organic citrus orchards with drip and flood irrigation. *Sci. Total Environ.* 581-582, 153–160. doi: 10.1016/j.scitotenv.2016.12.087

Horn, S., Hempel, S., Verbruggen, E., Rillig, M. C., and Caruso, T. (2017). Linking the community structure of arbuscular mycorrhizal fungi and plants: a story of interdependence? *ISME J.* 11, 1400–1411. doi: 10.1038/ismej.2017.5

Huang, B. (2019). *China rural statistics yearbook 2019*. China: China Statistics Publishing House.

Jurick, W. M. 2nd, Peng, H., Beard, H. S., Garrett, W. M., Lichtner, F. J., Luciano-Rosario, D., et al. (2020). Blistering1 modulates *Penicillium expansum* virulence via vesicle-mediated protein secretion. *Mol. Cell. Proteomics* 19, 344–361. doi: 10.1074/mcp.RA119.001831

Kao, C. M., Liao, H. Y., Chien, C. C., Tseng, Y. K., Tang, P., Lin, C. E., et al. (2016). The change of microbial community from chlorinated solvent-contaminated groundwater after biostimulation using the metagenome analysis. *J. Hazard. Mater.* 302, 144–150. doi: 10.1016/j.jhazmat.2015.09.047

Kecskemeti, E., Berkelmann-Lohnertz, B., and Reineke, A. (2016). Are epiphytic microbial communities in the carposphere of ripening grape clusters (*Vitis vinifera* L.) different between conventional, organic, and biodynamic grapes? *PLoS One* 11:e0160852. doi: 10.1371/journal.pone.0160852

Leff, J. W., and Fierer, N. (2013). Bacterial communities associated with the surfaces of fresh fruits and vegetables. *PLoS One* 8:e59310. doi: 10.1371/journal.pone.0059310

Li, J., Hu, W., Huang, X., and Xu, Y. (2018). Investigation of yeast population diversity and dynamics in spontaneous fermentation of vidal blanc icewine by traditional culture-dependent and high-throughput sequencing methods. *Food Res. Int.* 112, 66–77. doi: 10.1016/j.foodres.2018.06.011

Liu, H. T., Wang, Y. W., Huang, W. D., and Lei, M. (2016). Response of wine grape growth, development and the transfer of copper, lead, and cadmium in soil-fruit system to sludge compost amendment. *Environ. Sci. Pollut. Res. Int.* 23, 24230–24236. doi: 10.1007/s11356-016-7676-z

Liu, E., Yan, C., Mei, X., He, W., Bing, S. H., Ding, L., et al. (2010). Long-term effect of chemical fertilizer, straw, and manure on soil chemical and biological properties in Northwest China. *Geoderma* 158, 173–180. doi: 10.1016/j.geoderma.2010.04.029

Lorenzini, M., Simonato, B., Favati, F., Bernardi, P., Sbarbati, A., and Zapparoli, G. (2018). Filamentous fungi associated with natural infection of noble rot on withered grapes. *Int. J. Food Microbiol.* 272, 83–86. doi: 10.1016/j.ijfoodmicro.2018.03.004

Lorenzini, M., and Zapparoli, G. (2019). Yeast-like fungi and yeasts in withered grape carposphere: characterization of *Aureobasidium pullulans* population and species diversity. *Int. J. Food Microbiol.* 289, 223–230. doi: 10.1016/j.ijfoodmicro.2018.10.023

Luan, H., Gao, W., Huang, S., Tang, J., Li, M., Zhang, H., et al. (2020). Substitution of manure for chemical fertilizer affects soil microbial community diversity, structure and function in greenhouse vegetable production systems. *PLoS One* 15:e0214041. doi: 10.1371/journal.pone.0214041

Luciano-Rosario, D., Keller, N. P., and Jurick, W. M. 2nd (2020). *Penicillium expansum*: biology, omics, and management tools for a global postharvest pathogen causing blue mould of pome fruit. *Mol. Plant Pathol.* 21, 1391–1404. doi: 10.1111/mpp.12990

Lv, F., Song, J., Giltrap, D., Feng, Y., Yang, X., and Zhang, S. (2020). Crop yield and N2O emission affected by long-term organic manure substitution fertilizer under winter wheat-summer maize cropping system. *Sci. Total Environ.* 732:139321. doi: 10.1016/j.scitotenv.2020.139321

Mahdian, S., and Zafari, D. (2016). First report of alternaria cucurbitae causing bunch rot on grape in Iran. *J. Plant Pathol.* 98:185.

Marsh, A. J., O'Sullivan, O., Hill, C., Ross, R. P., and Cotter, P. D. (2013). Sequencing-based analysis of the bacterial and fungal composition of kefir grains and milks from multiple sources. *PLoS One* 8:e69371. doi: 10.1371/journal.pone.0069371

Martins, G., Lauga, B., Miot-Sertier, C., Mercier, A., Lonvaud, A., Soulas, M. -L., et al. (2013). Characterization of epiphytic bacterial communities from grapes, leaves, bark and soil of grapevine plants grown, and their relations. *PLoS One* 8:e73013. doi: 10.1371/journal.pone.0073013

Martins, G., Vallance, J., Mercier, A., Albertin, W., Stamatopoulos, P., Rey, P., et al. (2014). Influence of the farming system on the epiphytic yeasts and yeast-like fungi colonizing grape berries during the ripening process. *Int. J. Food Microbiol.* 177, 21–28. doi: 10.1016/j.ijfoodmicro.2014.02.002

Mewa-Ngongang, M., Plessis, H. W. D., Ntwampe, S. K. O., Chidi, B. S., Hutchinson, U. F., Mekuto, L., et al. (2019). The use of *Candida pyralidae* and *Pichia kluyveri* to control spoilage microorganisms of raw fruits used for beverage production. *Foods* 8:454. doi: 10.3390/foods8100454

Moreno-Jiménez, E., Plaza, C., Saiz, H., Manzano, R., Flagmeier, M., and Maestre, F. T. (2019). Aridity and reduced soil micronutrient availability in global drylands. *Nat. Sustain.* 2, 371–377. doi: 10.1038/s41893-019-0262-x

Morrison-Whittle, P., Lee, S. A., and Goddard, M. R. (2017). Fungal communities are differentially affected by conventional and biodynamic agricultural management approaches in vineyard ecosystems. *Agric. Ecosyst. Environ.* 246, 306–313. doi: 10.1016/j.agee.2017.05.022

Noguerol-Pato, R., Torrado-Agrasar, A., Gonzalez-Barreiro, C., Cancho-Grande, B., and Simal-Gandara, J. (2014). Influence of new generation fungicides on *Saccharomyces cerevisiae* growth, grape must fermentation and aroma biosynthesis. *Food Chem.* 146, 234–241. doi: 10.1016/j.foodchem.2013.09.058

Oliveira, M., Arenas, M., Lage, O., Cunha, M., and Amorim, M. I. (2018). Epiphytic fungal community in *Vitis vinifera* of the portuguese wine regions. *Lett. Appl. Microbiol.* 66, 93–102. doi: 10.1111/lam.12826

Onesti, G., González-Domínguez, E., and Rossi, V. (2017). Production of pycnidia and conidia by *Guignardia bidwellii*, the causal agent of grape black rot, as affected by temperature and humidity. *Phytopathology* 107, 173–183. doi: 10.1094/PHYTO-07-16-0255-R

Parafati, L., Vitale, A., Restuccia, C., and Cirvilleri, G. (2015). Biocontrol ability and action mechanism of food-isolated yeast strains against *Botrytis cinerea* causing post-harvest bunch rot of table grape. *Food Microbiol.* 47, 85–92. doi: 10.1016/j.fm.2014.11.013

Platania, C., Restuccia, C., Muccilli, S., and Cirvilleri, G. (2012). Efficacy of killer yeasts in the biological control of *Penicillium digitatum* on tarocco orange fruits (*Citrus sinensis*). *Food Microbiol.* 30, 219–225. doi: 10.1016/j.fm.2011.12.010

Ren, F., Dong, W., and Yan, D. H. (2019). Organs, cultivars, soil, and fruit properties affect structure of endophytic mycobiota of pinggu peach trees. *Microorganisms* 7:322. doi: 10.3390/microorganisms7090322

Renouf, V., Claisse, O., and Lonvaud-Funel, A. (2005). Understanding the microbial ecosystem on the grape berry surface through numeration and identification of yeast and bacteria. *Aust. J. Grape Wine Res.* 11, 316–327. doi: 10.1111/j.1755-0238.2005.tb00031.x

Sebastien, M., Margarita, M. M., and Haissam, J. M. (2015). Biological control in the microbiome era: challenges and opportunities. *Biol. Control* 89, 98–108. doi: 10.1016/j.biocontrol.2015.06.003

Sharma, S., Sharma, S. D., and Kumar, P. (2017). Response of nectarines to organic fertilization under the rain-fed ecosystem of Northwest Himalayas. *J. Plant Nutr.* 40, 2014–2025. doi: 10.1080/01904167.2017.1346118

Shen, Y., Nie, J., Kuang, L., Zhang, J., and Li, H. (2020). DNA sequencing, genomes and genetic markers of microbes on fruits and vegetables. *Microb. Biotechnol.* 14, 323–362. doi: 10.1111/1751-7915.13560

Shen, Y., Nie, J., Li, Z., Li, H., Wu, Y., Dong, Y., et al. (2018). Differentiated surface fungal communities at point of harvest on apple fruits from rural and peri-urban orchards. *Sci. Rep.* 8:2165. doi: 10.1038/s41598-017-17436-5

Song, H., Wang, J., Zhang, K., Zhang, M., Hui, R., Sui, T., et al. (2020). A 4-year field measurement of N_2O emissions from a maize-wheat rotation system as influenced by partial organic substitution for synthetic fertilizer. *J. Environ. Manag.* 263:110384. doi: 10.1016/j.jenvman.2020.110384

Tao, R., Wakelin, S. A., Liang, Y., Hu, B., and Chu, G. (2018). Nitrous oxide emission and denitrifier communities in drip-irrigated calcareous soil as affected by chemical and organic fertilizers. *Sci. Total Environ.* 612, 739–749. doi: 10.1016/j.scitotenv.2017.08.258

Temple, T. N., Thompson, E. C., Uppala, S., Granatstein, D., and Johnson, K. B. (2020). Floral colonization dynamics and specificity of *Aureobasidium pullulans* strains used to suppress fire blight of pome fruit. *Plant Dis.* 104, 121–128. doi: 10.1094/PDIS-09-18-1512-RE

Tilman, D., Balzer, C., Hill, J., and Befort, B. L. (2011). Global food demand and the sustainable intensification of agriculture. *Proc. Natl. Acad. Sci. U. S. A.* 108, 20260–20264. doi: 10.1073/pnas.1116437108

Úrbez-Torres, J. R. (2011). The status of Botryosphaeriaceae species infecting grapevines. *Phytopathol. Mediterr.* 50, S5–S45.

Wang, X., Glawe, D. A., Kramer, E., Weller, D., and Okubara, P. A. (2018a). Biological control of *Botrytis cinerea*: interactions with native vineyard yeasts from Washington state. *Phytopathology* 108, 691–701. doi: 10.1094/PHYTO-09-17-0306-R

Wang, N., Wang, A., Xie, J., and He, M. (2019). Responses of soil fungal and archaeal communities to environmental factors in an ongoing antimony mine area. *Sci. Total Environ.* 652, 1030–1039. doi: 10.1016/j.scitotenv.2018.10.300

Wang, N., Zhang, S., and He, M. (2018b). Bacterial community profile of contaminated soils in a typical antimony mining site. *Environ. Sci. Pollut. Res.* 25, 141–152. doi: 10.1007/s11356-016-8159-y

Wei, S., Zhang, Y., Wang, H., Wang, H., Gao, H., and Wang, S. (2012). Effect of organic fertilizer and bagging on fruit flavor quality of Yali pear. *Plant Nutr. Fer. Sci.* 18, 1269–1276.

Wu, L., Jiang, Y., Zhao, F., He, X., Liu, H., and Yu, K. (2020). Increased organic fertilizer application and reduced chemical fertilizer application affect the soil properties and bacterial communities of grape rhizosphere soil. *Sci. Rep.* 10:9568. doi: 10.1038/s41598-020-66648-9

Xanthopoulou, A., Ganopoulos, I., Tryfinopoulou, P., Panagou, E. Z., Osanthanunkul, M., Madesis, P., et al. (2018). Rapid and accurate identification of black aspergilli from grapes using high-resolution melting (HRM) analysis. *J. Sci. Food Agric.* 99, 309–314. doi: 10.1002/jsfa.9189

Xiao, L., Sun, Q., Yuan, H., and Lian, B. (2017). A practical soil management to improve soil quality by applying mineral organic fertilizer. *Acta Geochim.* 36, 198–204. doi: 10.1007/s11631-017-0139-5

Xu, C., Wang, C., Ju, L., Zhang, R., Biggs, A. R., Tanaka, E., et al. (2015). Multiple locus genealogies and phenotypic characters reappraise the causal agents of apple ring rot in China. *Fungal Divers.* 71, 215–231. doi: 10.1007/s13225-014-0306-5

Yan, L., and Liu, Y. (2019). Insights into the mechanism and enantioselectivity in the biosynthesis of ergot alkaloid cycloclavine catalyzed by Aj_EasH from *Aspergillus japonicus*. *Inorg. Chem.* 58, 13771–13781. doi: 10.1021/acs.inorgchem.9b01168

Yang, B., He, S., Liu, Y., Liu, B., Ju, Y., Kang, D., et al. (2020). Transcriptomics integrated with metabolomics reveals the effect of regulated deficit irrigation on anthocyanin biosynthesis in cabernet sauvignon grape berries. *Food Chem.* 314:126170. doi: 10.1016/j.foodchem.2020.126170

Youssef, K., Roberto, S. R., Chiarotti, F., Koyama, R., Hussain, I., and de Souza, R. T. (2015). Control of *Botrytis* mold of the new seedless grape 'BRS Vitoria' during cold storage. *Sci. Hortic.* 193, 316–321. doi: 10.1016/j.scienta.2015.07.026

Zarraonaindia, I., Owens, S. M., Weisenhorn, P., West, K., Hampton-Marcell, J., Lax, S., et al. (2015). The soil microbiome influences grapevine-associated microbiota. *MBio* 6, e02527–e02614. doi: 10.1128/mBio.02527-14

Zetsche, B., Heidenreich, M., Mohanraju, P., Fedorova, I., Kneppers, J., DeGennaro, E. M., et al. (2017). Multiplex gene editing by CRISPR-Cpf1 using a single crRNA array. *Nat. Biotechnol.* 35, 31–34. doi: 10.1038/nbt.3737

Zhang, J., Balkovic, J., Azevedo, L. B., Skalsky, R., Bouwman, A. F., Xu, G., et al. (2018). Analyzing and modelling the effect of long-term fertilizer management on crop yield and soil organic carbon in China. *Sci. Total Environ.* 627, 361–372. doi: 10.1016/j.scitotenv.2018.01.090

Zhang, J., Li, B., Zhang, J., Christie, P., and Li, X. (2020). Organic fertilizer application and mg fertilizer promote banana yield and quality in an Udic Ferralsol. *PLoS One* 15:e0230593. doi: 10.1371/journal.pone.0230593

Zhang, Q., Shamsi, I. H., Xu, D., Wang, G., Lin, X., Jilani, G., et al. (2012). Chemical fertilizer and organic manure inputs in soil exhibit a vice versa pattern of microbial community structure. *Appl. Soil Ecol.* 57, 1–8. doi: 10.1016/j.apsoil.2012.02.012

Zhao, Z., Chu, C., Zhou, D., Sha, Z., and Wu, S. (2019). Soil nutrient status and the relation with planting area, planting age and grape varieties in urban vineyards in Shanghai. *Heliyon* 5:e02362. doi: 10.1016/j.heliyon.2019.e02362

Zhao, F., Jiang, Y., He, X., Liu, H., and Yu, K. (2020). Increasing organic fertilizer and decreasing drip chemical fertilizer for two consecutive years improved the fruit quality of 'summer black' grapes in arid areas. *HortScience* 55, 196–203. doi: 10.21273/HORTSCI14488-19

Zhu, Z. (2020). Analysis of Quality Change of Muscat Hamburg Grape From Xinjiang Under Room Temperature and Refrigeration Storage Conditions. dissertation/master's thesis. Shihezi University.

Conflict of Interest: The authors declare that the research was conducted in the absence of any commercial or financial relationships that could be construed as a potential conflict of interest.

frontiers in Microbiology

ORIGINAL RESEARCH
published: 26 May 2021
doi: 10.3389/fmicb.2021.667394

Pulse Frequency in Crop Rotations Alters Soil Microbial Community Networks and the Relative Abundance of Fungal Plant Pathogens

*Tony Yang[1], Bianca Evans[1] and Luke D. Bainard[2]**

[1] Swift Current Research and Development Centre, Agriculture and Agri-Food Canada, Swift Current, SK, Canada, [2] Agassiz Research and Development Centre, Agriculture and Agri-Food Canada, Agassiz, BC, Canada

Including pulse crops in cereal-based cropping systems has become a widely accepted and useful agronomic practice to increase crop diversification and biologically fixed nitrogen in agroecosystems. However, there is a lack of knowledge regarding how the intensification of pulses in crop rotations influence soil microbial communities. In this study, we used an amplicon sequencing approach to examine the bulk and rhizosphere soil bacterial and fungal communities from the wheat (*Triticum aestivum* L.) phase (final year of 4 years rotations) of a long-term pulse intensification field trial in the semi-arid region of the Canadian Prairies. Our results revealed pulse frequency had a minimal impact on microbial α-diversity, but caused a significant shift in the composition of the fungal (rhizosphere and bulk soil) and bacterial (bulk soil) communities. This effect was the most pronounced in the Ascomycete and Bacteroidete communities. Increasing pulse frequency also promoted a higher proportion of fungal pathotrophs in the bulk soil, particularly those putatively identified as plant pathogens. The network analysis revealed that rotations with higher pulse frequency promoted increased competition within the soil microbial networks in the rhizosphere and bulk soil. However, we also detected more negative interactions among the dominant pathotrophic taxa with increased pulse frequency, suggesting higher soil-borne disease potential. These findings highlight the potential drawbacks and reduced sustainability of increasing pulse frequency in crop rotations in semiarid environments.

Keywords: crop rotation, soil-borne disease, pulse frequency, fungal guilds, network analysis

OPEN ACCESS

Edited by:
Yong Wang,
Guizhou University, China

Reviewed by:
Jun Zhao,
Nanjing Normal University, China
Xiaogang Li,
Nanjing Forestry University, China

****Correspondence:***
Luke D. Bainard
luke.bainard@canada.ca

Specialty section:
This article was submitted to Microbe and Virus Interactions with Plants, a section of the journal Frontiers in Microbiology

Received: *12 February 2021*
Accepted: *29 April 2021*
Published: *26 May 2021*

Citation:
Yang T, Evans B and Bainard LD (2021) Pulse Frequency in Crop Rotations Alters Soil Microbial Community Networks and the Relative Abundance of Fungal Plant Pathogens. Front. Microbiol. 12:667394. doi: 10.3389/fmicb.2021.667394

INTRODUCTION

Among agronomic practices used in annual cropping systems, crop rotation is one of the most common management tools used to enhance soil nutrient and water availability, control weeds and pests, and improve the ecological and economic sustainability of cropping systems (Schönhart et al., 2011; Barbieri et al., 2017). Considering the unique capability of legumes to fix atmospheric nitrogen via biological nitrogen fixation (BNF), legume-based rotations have demonstrated many advantages for enhancing the sustainability of agriculture worldwide. As a result, the land base planted to legume crops has gradually increased globally over the past 50 years (Foyer et al., 2016).

This trend has been particularly evident in the Northern Great Plains for pulse crops such as field pea (*Pisum sativum* L.), lentil (*Lens culinaris Medik.*), and chickpea (*Cicer arietinum* L.), which are common grain legume crops that have been used to diversify cereal and oilseed cropping systems (Khakbazan et al., 2020). The globally cultivated area for pea, lentil and chickpea is around 8.1, 6.6, and 14.6 Mha, respectively, which provide about 0.74, 0.36, and 0.66 Tg of annual fixed nitrogen, respectively (Jensen et al., 2020). Including pulses in crop rotations has been documented to provide many economic and ecological benefits including increased soil organic carbon (Liu k. et al., 2020) and nitrogen availability (Jensen et al., 2020), reduced disease pressure (Kirkegaard et al., 2008), increased yield of subsequent crops in rotations (Reckling et al., 2020; Zhao et al., 2020) and overall system productivity (Gan et al., 2015), and improved soil health (Lal, 2017). However, due to the application of synthetic fertilizers and pesticides as well as economic drivers of crop selection, diversification of many crop rotation designs in practice are overly simplified, and improper rotation designs in modern agriculture jeopardize the eco-functionality of agroecosystems and endanger soil biodiversity (Barbieri et al., 2017). It is essential to select the right type of pulse crops for the rotation design and ecosystem, and incorporate them at an appropriate frequency to achieve the potential ecological and economic benefits linked to these crops. However, this type of information is still very limited, particularly from long-term field studies.

In particular, our understanding of how pulse based mid- to long-term rotations and high pulse frequency rotations influence soil microbial community dynamics remains limited. Early evidence from short term studies (<4 years) has shown that pulse frequency in annual crop rotations is an important factor driving shifts in the composition, diversity and functional guilds of soil and root-associated microbial communities (Bainard et al., 2017; Navarro-Borrell et al., 2017; Hamel et al., 2018; Niu et al., 2018). There is evidence that plant species can have selective effects on rhizosphere microbial communities. As a result, enriched pulse frequency in annual crop rotations will likely lead to a gradual enrichment of host specific effects in soil, which can further alter soil microbial communities.

In this study, we used a long term (8 years) crop rotation study in the semiarid region of the Canadian Prairies to explore the impacts of pulse frequency on the diversity, composition and interactions of soil microbial communities. We hypothesized that increasing the pulse frequency in crop rotations will alter the diversity, composition, and network interactions of soil microbial communities.

MATERIALS AND METHODS

Site Description and Experimental Design

A long-term field experiment was established in 2010 with a 4 years crop rotation design located at the Swift Current Research and Development Centre was utilized for this study. The experiment included low (one-pulse phase), medium (two-pulse phases) and high (three-pulse phases) pulse frequency rotations in the long-term rotation design. For this study we selected the following treatments: (i) low pulse frequency rotations, Pea-Wheat-Wheat-Wheat (PWWW) and Chickpea-Wheat-Wheat-Wheat (CWWW); (ii) medium pulse frequency rotations, Pea-Wheat-Pea-Wheat (PWPW) and Chickpea-Wheat-Chickpea-Wheat (CWCW); and (iii) high pulse frequency rotations, Pea-Pea-Pea-Wheat (PPPW), Chickpea-Chickpea-Chickpea-Wheat (CCCW) and Pea-Lentil-Chickpea-Wheat (PLCW) rotations. The first cycle of the rotations was completed in 2013 and repeated again starting in 2014. Due to the development of serious root diseases issues associated with growing chickpea in the same plots for three continuous years during the first cycle, mustard was grown during the second year of the CCCW rotation during the second cycle (i.e., Chickpea-Mustard-Chickpea-Wheat) to limit disease issues. Each treatment was planted into a 4 × 12 m plot and replicated four times in a randomized complete block design. This study was conducted during the 2017 growing season, which was the fourth year of the rotations during the second cycle and all rotations were seeded to wheat (*Triticum aestivum* L.).

All plots received glyphosate spray at 0.45 kg/ha as a pre-seeding burn-off treatment and Trifluralin 10G at 8.5 kg/ha prior to seeding (except for wheat plots) to eliminate weed effects in each year. At the beginning of each rotation cycle (2010 and 2014) all wheat plots received a total of 80 Kg/ha actual N using 46-0-0 mineral fertilizer, and pulse crop plots received 22 kg/ha of actual P using 11-51-0 mineral fertilizer. All pulse plots also received inoculation prior to seeding with a granular rhizobium inoculant (TeamTag®, 4 kg ha^{-1}) annually. All plots were under no-till management practices and were planted with a no-till plot seeder.

Sampling and Chemical Analysis

Soil sampling was conducted at the soft dough stage to assess the soil microbial community and soil chemical properties. Four soil cores (2.5 cm diameter) were randomly collected in each plot to a depth of 15 cm, pooled together and homogenized in a large Ziploc bag to form one composite soil sample per plot. At the same time, four wheat plants were carefully excavated from the same sampling locations as the bulk soil cores in each plot. The loose soil was shaken from the roots and the remaining soil adhering to the roots was carefully brushed off, pooled together and homogenized as one rhizosphere soil sample per plot. There were a total of 28 bulk soil and 28 rhizosphere soil samples collected for this study. Sub-samples were immediately taken from the composite bulk and rhizosphere soil samples and flash frozen in a liquid nitrogen cryo-shipper for molecular analyses. The remaining soil was stored in a cooler with ice for transportation and then stored at 4°C for up to 48 h until further processing. Soil samples were sieved through a 2 mm sieve, and a subsample was used to determine soil moisture content (gravimetric). The remaining soil was air-dried and ground for chemical analyses.

For all soil samples, soil organic carbon and total carbon were determined using the dry combustion method (after acidification with HCl) using an Elementar vario MICRO cube elemental analyzer (Schumacher, 2002). Soil nitrate nitrogen (N), phosphate phosphorus (P) and potassium (K) were determined

using sodium bicarbonate extractions followed by colorimetric analysis using a Technicon Autoanalyzer (Harm et al., 1973; Gentry and Willis, 1988). Soil sulfate sulfur (S) was determined using calcium chloride extractions followed by colorimetric analysis using a Technicon Autoanalyzer (Harm et al., 1973). Soil pH and EC were measured in water saturation paste (Habekost et al., 2008) and paste extracts (Miller and Curtin, 2006). Soil moisture was measured using the gravimetric method.

DNA Extraction, Amplicon Sequencing, and Bioinformatics

Genomic DNA was extracted from 0.25 g of soil in duplicate for each bulk and rhizosphere soil sample using the DNeasy PowerSoil kit (Qiagen) using the QIAcube automated nucleic acid extraction system (Qiagen). DNA was quantified using a Qubit dsDNA BR Assay Kit (Thermo Fisher Scientific, Waltham, MA) and shipped on dry ice to the Genome Quebec Innovation Center (Montreal, Canada) for amplicon library preparation and Illumina MiSeq sequencing. The bacterial 16S rRNA genes were sequenced using primers 515-F and 806-R (Caporaso et al., 2012) and fungal ITS1 region was sequenced using primers ITS1F and 58A2R (Martin and Rygiewicz, 2005). For a full description of the amplicon library preparation and Illumina Miseq sequencing see Delavaux et al. (2020). The raw amplicon sequencing datasets are available in the NCBI Sequence Read Archive under BioProject ID PRJNA694704, PRJNA694839, PRJNA694691, PRJNA694475, PRJNA717779, and PRJNA694448. Raw reads were processed (assembled, trimmed, quality filtered, dereplicated, and clustered) using the UPARSE pipeline of USEARCH v.9 (Edgar, 2013). Sequences were clustered into operational taxonomic units (OTU) based on 97% similarity. Taxonomic identity was assigned with a confidence threshold of 80% using the RDP classifier (Wang et al., 2007) and 16S rRNA training set (version 16) for bacteria and ITS UNITE database for fungi (Kõljalg et al., 2013). FUNGuild was used to parse the fungal community datasets by functional ecological guild (Nguyen et al., 2016). See Bainard et al. (2020) for a full description of the bioinformatics.

Statistical Analysis

All statistical analyses were performed using R packages (version 3.5.1) vegan, breakaway, ecodist and ggplot2 (R Foundation for Statistical Computing, Vienna, Austria). To determine the effect of pulse frequency on α-diversity we estimated the total OTU richness using the package breakaway (Willis and Bunge, 2015). One-way analysis of variance (ANOVA) was used to test the effect of pulse frequency on the soil properties and OTU richness. *Post hoc* comparisons of means were completed using Tukey's HSD procedure at a 5% level of probability. Permutational multivariate analysis of variance (permanova) was used to test the effect of pulse frequency on the wheat rhizosphere and bulk soil microbial communities. Sequence read variability was normalized among samples by randomly resampling to the lowest number of reads for each dataset (i.e., bacteria = 19,682 reads/sample; fungi = 21,468/sample). To eliminate influences of low abundance OTUs which are in many cases artifacts generated through the sequencing process and better compare treatment effects, unclassified OTUs and rare OTUs (OTUs shown in less than 3 soil samples and OTUs with less than 10 reads in total) were removed from downstream analysis. Network analysis was constructed for soil microbial communities related to different pulse frequencies based on their OTU relative abundances, and was performed using the Molecular Ecological Network Analyses (MENA) pipeline: http://ieg4.rccc.ou.edu/mena (Deng et al., 2012) and visualized by Cytoscape 3.6.1. Module-EigenGene network analysis was applied to examine interactions of the soil microbial community with environmental factors. The connectivity of each node was determined based on its within-module connectivity (Zi) and among-module connectivity (Pi), and the node topologies were separated by Zi and Pi with threshold of 2.5 and 0.62 (Guimerà and Nunes Amaral, 2005; Olesen et al., 2007). OTUs with low Zi and low Pi values were considered as specialists (peripherals) which typically only had links within their own modules. OTUs with low Zi and high Pi values (connectors), or high Zi and low Pi values (module hubs) were considered as generalists. This included either module hubs (actively linked with other OTUs within their own module) or connectors (linking with OTUs from other modules). OTUs with high Zi and Pi values were considered as super generalists (network hubs) which act as both connectors among several modules and module hubs within their own modules.

RESULTS

Soil Properties and Wheat Growth

Pulse frequency in the rotations had a minimal impact on the bulk and rhizosphere soil properties. Total C and organic C in rhizosphere soil was significantly higher in rotations with medium pulse frequency compared to rotations with low and high pulse frequency, and soil moisture was highest in rotations with low pulse frequency (**Table 1**). In the bulk soil, rotations with a medium pulse frequency had a significantly higher soil S and P content compared to the high pulse frequency rotations. All other soil properties in the bulk and rhizosphere soil were unaffected by pulse frequency. Pulse frequency also impacted wheat growth. Tiller number and dry biomass of wheat were significantly affected by pulse frequency, with rotations with medium pulse frequency exhibiting the highest biomass production. However, wheat yield, height or seeds per plant did not significantly differ among the rotations with different pulse frequencies (**Supplementary Table 1**).

Soil Microbial Diversity

Pulse frequency did not significantly affect the α–diversity (estimated total richness) of the bacterial community in the rhizosphere or bulk soil (**Figures 1A,B**). However, pulse frequency did significantly affect the estimated total fungal richness in the rhizosphere (highest under low pulse frequency), but not in the bulk soil (**Figures 1C,D**). Among the fungal guilds, pathotrophs were the only group that were significantly affected by pulse frequency (**Table 2**). In the rhizosphere, rotations with medium pulse frequency had the highest proportion of fungal pathotrophs. In the bulk soil, rotations with medium and high

TABLE 1 | ANOVA results of the effect of pulse crop frequency (low, medium, and high) on the wheat rhizosphere and bulk soil properties.

Sample type	Pulse frequency	S (mg kg^{-1})	K (mg kg^{-1})	N (mg kg^{-1})	P (mg kg^{-1})	TC (%)	OC (%)	TN (%)	pH	EC (dS m^{-1})	Moisture (%)
Rhizosphere	Low	1.49 ± 0.10	253.48 ± 8.96	3.73 ± 0.60	27.94 ± 0.95	1.46 ± 0.04^{b}	1.40 ± 0.03^{b}	0.14 ± 0.003	6.34 ± 0.09	0.28 ± 0.02	12.76 ± 0.20^{a}
	Medium	2.21 ± 0.23	267.15 ± 13.69	5.37 ± 0.68	26.85 ± 0.95	1.53 ± 0.02^{a}	1.46 ± 0.02^{a}	0.15 ± 0.002	6.48 ± 0.14	0.40 ± 0.05	11.88 ± 0.60^{b}
	High	1.82 ± 0.10	238.86 ± 9.79	4.88 ± 0.53	31.15 ± 1.28	1.47 ± 0.04^{b}	1.40 ± 0.04^{b}	0.14 ± 0.003	6.60 ± 0.10	0.32 ± 0.03	11.43 ± 0.21^{b}
	P-value	0.224	0.158	0.292	0.738	0.009	0.013	0.215	0.961	0.678	0.017
Bulk soil	Low	2.56 ± 0.22^{ab}	270.45 ± 14.17	6.44 ± 1.49	64.86 ± 3.45^{ab}	1.66 ± 0.04	1.55 ± 0.03	0.16 ± 0.002	6.29 ± 0.07	0.35 ± 0.04	10.10 ± 0.27
	Medium	2.87 ± 0.18^{a}	273.78 ± 12.10	5.42 ± 0.99	68.01 ± 2.17^{a}	1.55 ± 0.03	1.44 ± 0.03	0.15 ± 0.003	6.32 ± 0.10	0.36 ± 0.03	9.22 ± 0.16
	High	2.42 ± 0.15^{b}	242.25 ± 10.68	8.19 ± 1.18	63.37 ± 2.29^{b}	1.51 ± 0.03	1.45 ± 0.03	0.15 ± 0.003	6.29 ± 0.11	0.32 ± 0.02	9.41 ± 0.21
	P-value	0.01	0.207	0.161	0.021	0.365	0.46	0.246	0.235	0.084	0.108

Means (±standard error) for each sample type in the same column with different letters are significantly different ($P < 0.05$).

frequency had the highest proportion of fungal pathotrophs. Of the fungal pathotrophs putatively assigned as plant pathogens in the bulk soil, the rotations with medium and high pulse frequency had nearly twice the proportion of reads compared to the rotations with low pulse frequency.

The permanova indicated that pulse frequency had a significant effect on the fungal community in both the rhizosphere and bulk soil (**Table 3**). This appears to be primarily linked to shifts in the taxa belonging to the Ascomycota in bulk soil, and taxa belonging to the Ascomycota and Mortierellomycota in rhizosphere soil. The principle coordinate analyses (PCoA) revealed that the fungal community from rotations with low pulse frequency were distinct and showed some separation compared to those from medium and high pulse frequency in both the rhizosphere and bulk soil (**Supplementary Figure 1**). This trend is particularly evident for the Ascomycete community in both the rhizosphere and bulk soil. Pulse frequency did not have a significant effect on the bacterial community in either the bulk or rhizosphere soil. However, pulse frequency did significantly influence the rhizosphere Firmicutes community, and bulk soil bacterial communities belonging to the Actinobacteria, Armatimonadetes, Bacteroidetes, candidate division WPS-1, Gemmatimonadetes, and Proteobacteria (**Table 3** and **Supplementary Figure 2**). The strongest effect was observed on the Bacteroidetes community in the bulk soil, with the PCoA showing a distinct separation between samples taken from rotations with low pulse frequency and those from medium and high pulse frequency (**Supplementary Figure 2**).

Soil Microbial Community Networks

The network analysis revealed that increasing the pulse frequency in crop rotations modified the interactions of the soil microbial community (**Table 4**). The top three dominant bacterial phyla (Acidobacteria, Actinobacteria, and Proteobacteria) influenced the structure and interconnectedness of the soil microbial community. The majority of the nodes with high degree in the network analysis in both rhizosphere and bulk soil were linked to these three dominant phyla (Acidobacteria > Actinobacteria > Proteobacteria), and accounted for approximately 50% of the identified dominant nodes (**Figures 2**, **3**). In both rhizosphere and bulk soil, rotations with high pulse frequency had microbial communities with stronger interactions that included a smaller number of nodes, higher number of edges, shorter average path distance, more connectedness, higher betweenness centrality, less modules and more dominant nodes (**Table 4**). These results suggest that high levels of pulse frequency in crop rotations can enhance the soil microbial community interactions.

Increasing pulse frequency also increased phylogenetic diversity of dominant nodes in the rhizosphere (**Figure 2** and **Supplementary Figure 3**), especially taxa that belonged to the Basidiomycota, Chloroflexi, Thaumarchaeota and candidate division WPS-1. The number of nodes from Ascomycota, Gemmatimonadetes, and Proteobacteria were increased while the number of nodes from Acidobacteria and Actinobacteria were decreased with increased pulse frequency. We also observed a higher number of negative interactions between nodes under

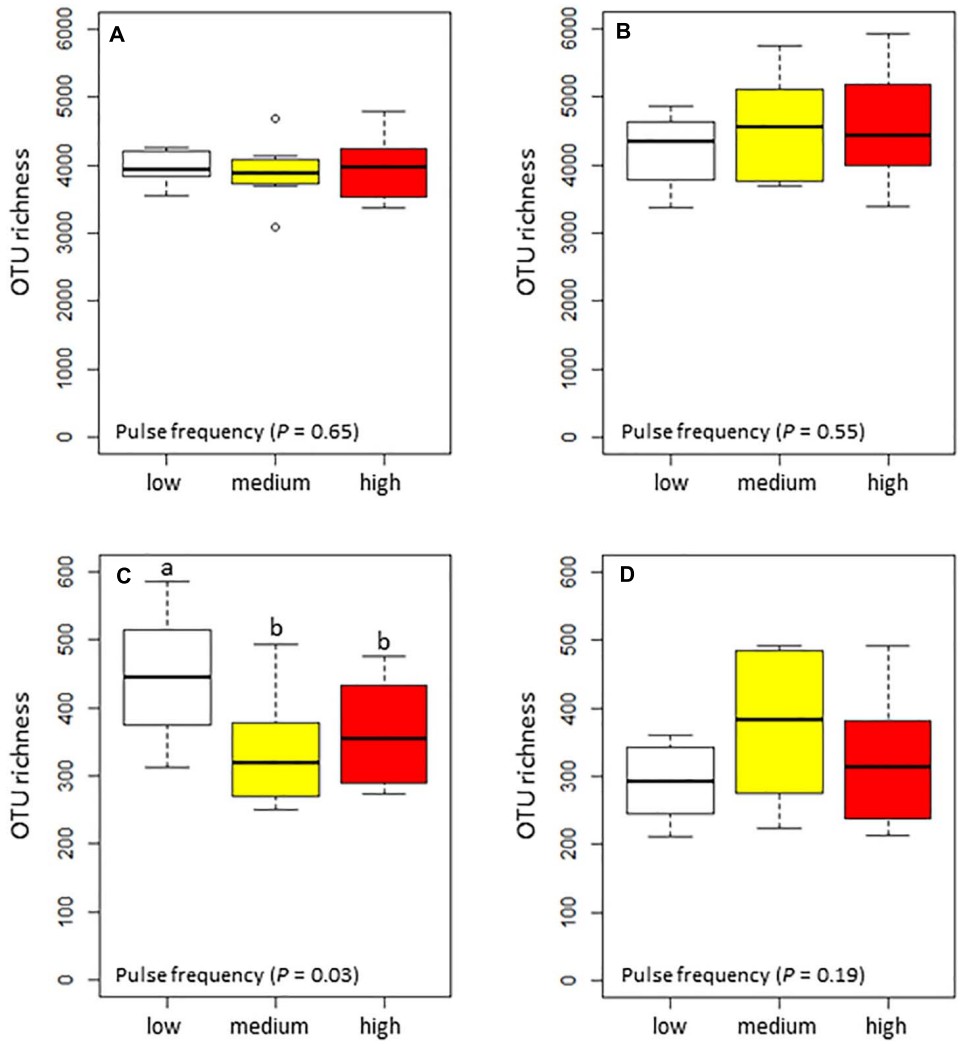

FIGURE 1 | Box plots of the total estimated richness for the bacterial community in the **(A)** wheat rhizosphere and **(B)** bulk soil, and fungal community in the **(C)** wheat rhizosphere and **(D)** bulk soil as influenced by pulse frequency in the crop rotations.

TABLE 2 | ANOVA results of the effect of pulse crop frequency (low, medium, and high) on the proportion (percentage) of reads assigned to fungal guilds in the wheat rhizosphere and bulk soil.

Sample type	Pulse frequency	Pathotrophs (%)	Saprotrophs (%)	Symbiotrophs (%)	Undefined (%)	Plant pathogens (%)
Rhizosphere	Low	21.0 ± 1.2^{b}	52.2 ± 2.6	0.7 ± 0.2	11.3 ± 1.6	14.8 ± 0.8
	Medium	26.5 ± 1.1^{a}	43.4 ± 2.2	1.1 ± 0.4	12.0 ± 2.6	17.1 ± 1.7
	High	21.2 ± 2.1^{b}	44.5 ± 4.2	0.3 ± 0.2	16.4 ± 7.6	17.5 ± 1.7
	P-value	0.035	0.269	0.128	0.722	0.248
Bulk soil	Low	18.6 ± 2.4^{b}	48.2 ± 4.2	1.3 ± 0.8	20.0 ± 4.4	11.9 ± 1.6^{b}
	Medium	29.4 ± 2.0^{a}	38.6 ± 2.9	0.3 ± 0.2	11.2 ± 1.0	20.5 ± 1.6^{a}
	High	26.4 ± 1.7^{a}	42.3 ± 3.0	0.0 ± 0.0	10.3 ± 1.3	21.0 ± 1.2^{a}
	P-value	0.001	0.427	0.142	0.070	<0.001

Means (± standard error) for each sample type in the same column with different letters are significantly different ($P < 0.05$).

high pulse frequency than under low pulse frequency, which may be linked to higher competition between soil microorganisms for limited nutrients and environmental resources, or accumulation of pulse specific pathogens.

In the bulk soil, high pulse frequency led to an increased total phylogenetic diversity of dominant nodes along with a shift in composition compared with low and medium pulse frequency rotations (**Figure 3** and

TABLE 3 | Permanova results of the effect of pulse crop frequency (low, medium, and high) on the wheat rhizosphere and bulk soil fungal and bacterial community composition.

	Rhizosphere soil			Bulk soil		
	F	R^2	*P*	F	R^2	*P*
Fungi						
Total	1.3	0.093	0.05	1.845	0.129	0.001
Ascomycota	1.485	0.106	0.014	2.106	0.144	<0.001
Basidiomycota	0.918	0.068	0.627	1.074	0.079	0.33
Mortierellomycota	0.889	0.066	0.541	1.733	0.122	0.049
Bacteria						
Total	1.371	0.099	0.165	1.632	0.115	0.06
Acidobacteria	1.533	0.109	0.146	1.393	0.1	0.159
Actinobacteria	1.296	0.093	0.208	1.89	0.131	0.031
Armatimonadetes	1.217	0.089	0.234	1.831	0.128	0.031
Bacteroidetes	1.236	0.09	0.176	2.502	0.167	<0.001
Candidate division WPS-1	1.127	0.083	0.318	1.6	0.113	0.042
Chloroflexi	0.898	0.067	0.527	1.316	0.095	0.186
Firmicutes	2.382	0.16	0.037	0.359	0.028	0.904
Gemmatimonadetes	1.305	0.095	0.195	2.155	0.147	0.025
Nitrospirae	2.252	0.153	0.068	1.955	0.135	0.054
Planctomycetes	1.004	0.074	0.397	1.486	0.106	0.06
Proteobacteria	1.482	0.106	0.109	1.986	0.137	0.013
Thaumarchaeota	0.959	0.072	0.454	1.022	0.076	0.417
Verrucomicrobia	1.106	0.081	0.314	1.269	0.092	0.226

Supplementary Figure 4). For example, dominant nodes from Acidobacteria, Actinobacteria, and Gemmatimonadetes were reduced and dominant nodes from Ascomycota, Basidiomycota, Mortierellomycota, Planctomycetes and candidate division WPS-1 were increased in rotations with high pulse frequency. The latter group accounted for approximately half of the total dominant nodes and the majority of the negative interactions with other nodes in the bulk soil microbial community.

Soil Microbial Community Response to Environmental Factors

Module-EigenGene network analysis grouped soil microorganisms into different modules based on their interactions with environmental factors (**Supplementary Figure 5**). In both the rhizosphere and bulk soil, module numbers decreased with an increase in pulse frequency, indicating that rotations with higher frequency of pulses can strength interactions within the microbial community. However, the microbial community in bulk soil and rhizosphere soil reacted to the pulse frequency differently.

In the rhizosphere, S, pH and EC had the strongest influence on the soil microbial community (**Supplementary Figures 5A–C** and **Supplementary Table 1**). This was particularly evident for the bacterial community under low to medium pulse frequency rotations. The modules that contained the keystone OTUs (black framed modules, **Supplementary Figures 5A–C**) were more sensitive to EC and pH under low to medium pulse frequency rotations, but more sensitive to TC and TN under high pulse frequency. This indicated that the influence of pulse crops on microbial keystone taxa in the rhizosphere is co-dependent on the pulse frequency and environmental factors.

In the bulk soil, S, N, and K had the strongest influence on the soil microbial community in low pulse frequency rotations (**Supplementary Figure 5D**), while N had the strongest influence in medium pulse frequency rotations (**Supplementary Figure 5E**). Under high pulse frequency rotations, EC had the strongest effect (**Supplementary Figure 5F**), particularly for the bacterial community (**Supplementary Table 1**). For the modules that include most of the keystone taxa, they had a negative response to S under low pulse frequency, and strong response to N (either negative or positive, depending on the module) under medium pulse frequency, and none of these environmental factors significantly affected these modules under high pulse frequency. These results suggest that in bulk soil, rotations with a high frequency of pulse crops could develop a relatively stable soil microbial community network that is not as responsive to changing environmental conditions.

Impact of Pulse Frequency on Keystone Taxa

To evaluate the topological role of identified nodes in the network, we used within-module connectivity (Zi) and among-module connectivity (Pi) values to separate each network into four ecological modules (**Figure 4**). From the rhizosphere soil (**Figure 4A**), we identified 22 module hubs and 4 connectors in low pulse frequency, 20 module hubs and 17 connectors in medium pulse frequency, 25 module hubs and 11 connectors in high pulse frequency. From bulk soil (**Figure 4B**), we identified 23 module hubs and 2 connectors in low pulse frequency, 18 module hubs and 8 connectors in medium pulse frequency, 14 module hubs, 74 connectors, and 9 network hubs in high pulse frequency.

TABLE 4 | Network topological properties of the microbial community identified in the wheat rhizosphere and bulk soil samples in rotations with low, medium or high pulse frequency.

		Nodes	Edges	R^2 of power law	Average path distance	Average clustering coefficient	Connectedness	Betweenness centrality	Module number	Nodes with degree > 10
Rhizosphere	Low	1,010	1,491	0.889	7.490	0.104	0.537	0.103	26	31
	Medium	816	2,187	0.879	4.746	0.105	0.572	0.060	19	115
	High	787	2,983	0.950	4.355	0.060	0.814	0.110	8	146
Bulk soil	Low	897	1,618	0.882	7.377	0.135	0.476	0.066	30	47
	Medium	843	1,634	0.921	5.669	0.120	0.528	0.088	18	69
	High	831	2,110	0.916	4.327	0.068	0.660	0.101	8	114

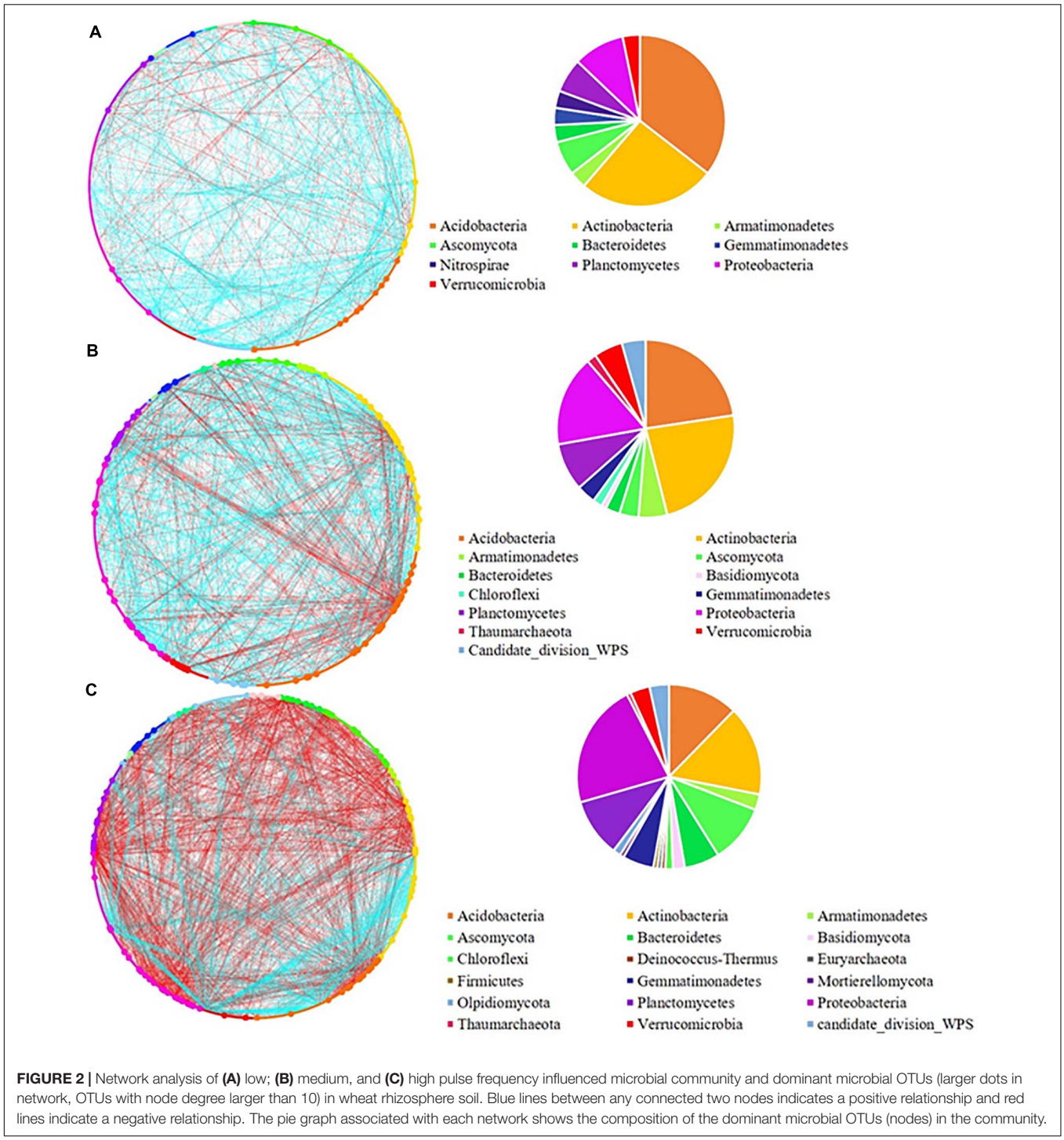

FIGURE 2 | Network analysis of **(A)** low; **(B)** medium, and **(C)** high pulse frequency influenced microbial community and dominant microbial OTUs (larger dots in network, OTUs with node degree larger than 10) in wheat rhizosphere soil. Blue lines between any connected two nodes indicates a positive relationship and red lines indicate a negative relationship. The pie graph associated with each network shows the composition of the dominant microbial OTUs (nodes) in the community.

The higher number of connectors under high pulse frequency indicated that soil microbial taxa were more active within their own modules under low pulse frequency, but tended to build up interactions with OTUs located at different modules under high pulse frequency. These results suggest that higher levels of pulse frequency in crop rotations can enhance the interactions of soil microbial taxa in different subgroups which may carryout different biological and ecological functions.

DISCUSSION

Despite the important role that crop rotations play in sustainable agriculture (Drinkwater et al., 1998; Foyer et al., 2016), there is still a lack of systematic analysis on how pulse crops influence soil microbial community dynamics (Hamel et al., 2018). The results from our study provide insight into how pulse frequency in crop rotations impacts the soil microbial community, their

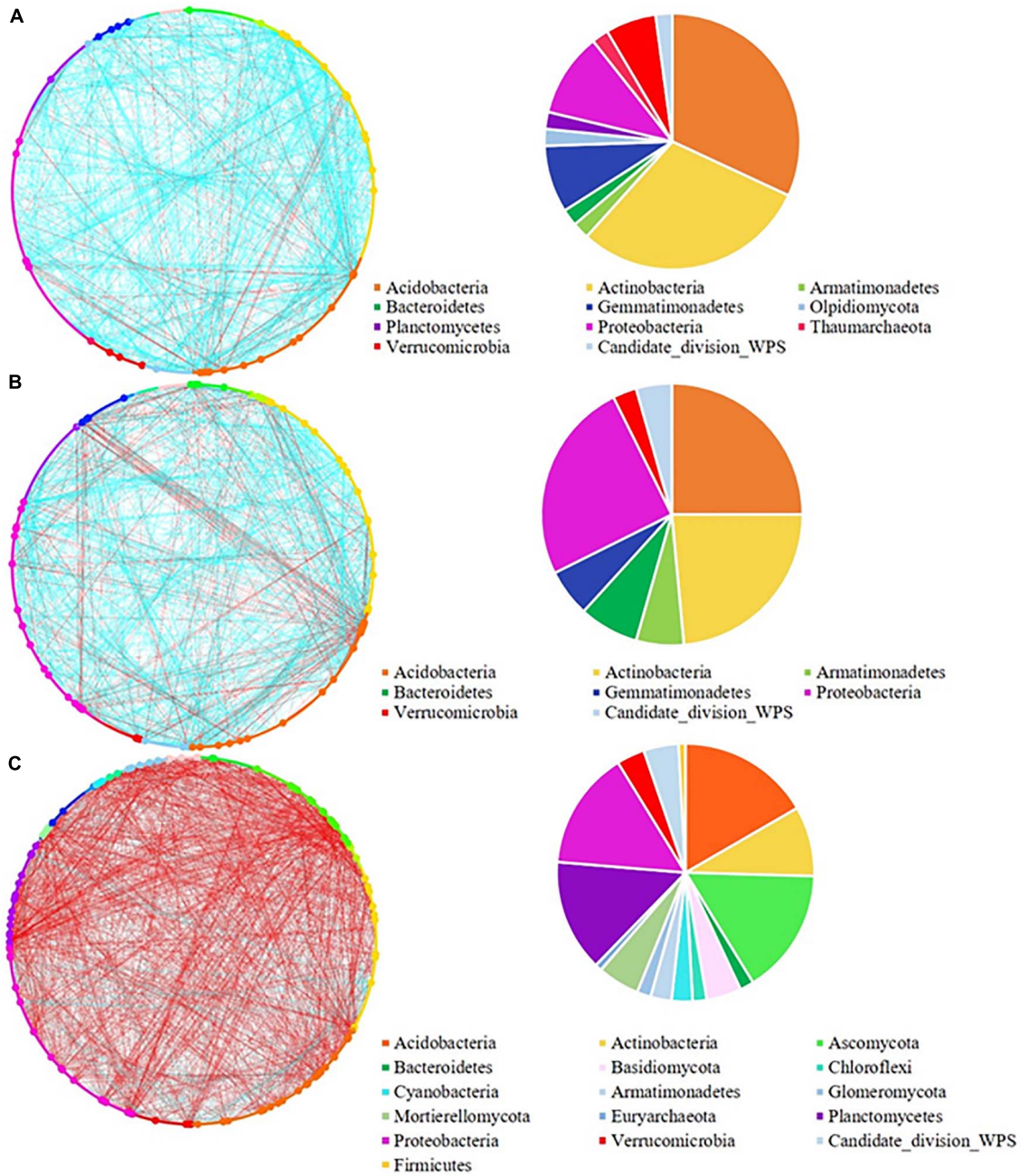

FIGURE 3 | Network analysis of **(A)** low; **(B)** medium, and **(C)** high pulse frequency influenced microbial community and dominant microbial OTUs (larger dots in network, OTUs with node degree larger than 10) in bulk soil. Blue lines between any connected two nodes indicates a positive relationship and red lines indicate a negative relationship. The pie graph associated with each network shows the composition of the dominant microbial OTUs (nodes) in the community.

diversity, interactions, potential eco-functions and relationship with environmental factors.

Soil bacterial diversity did not significantly change in response to increased pulse frequency in the crop rotations. Similar results were observed during the first rotation cycle at the same field trial and phase of the rotation (Hamel et al., 2018), but these results were based on the bacterial community colonizing the wheat roots rather than the rhizosphere or bulk soil. A recent meta-analysis also found that although some rotations can have either a negative or positive impact on soil microbial diversity, the majority of studies observed no significant effect of rotations on soil bacterial diversity, including those with or without legume crops (Venter et al., 2016). Despite the lack of changes in α-diversity, we did observe compositional shifts of certain bacterial phyla in the bulk soil in response to pulse frequency. We sampled during the final year and second cycle

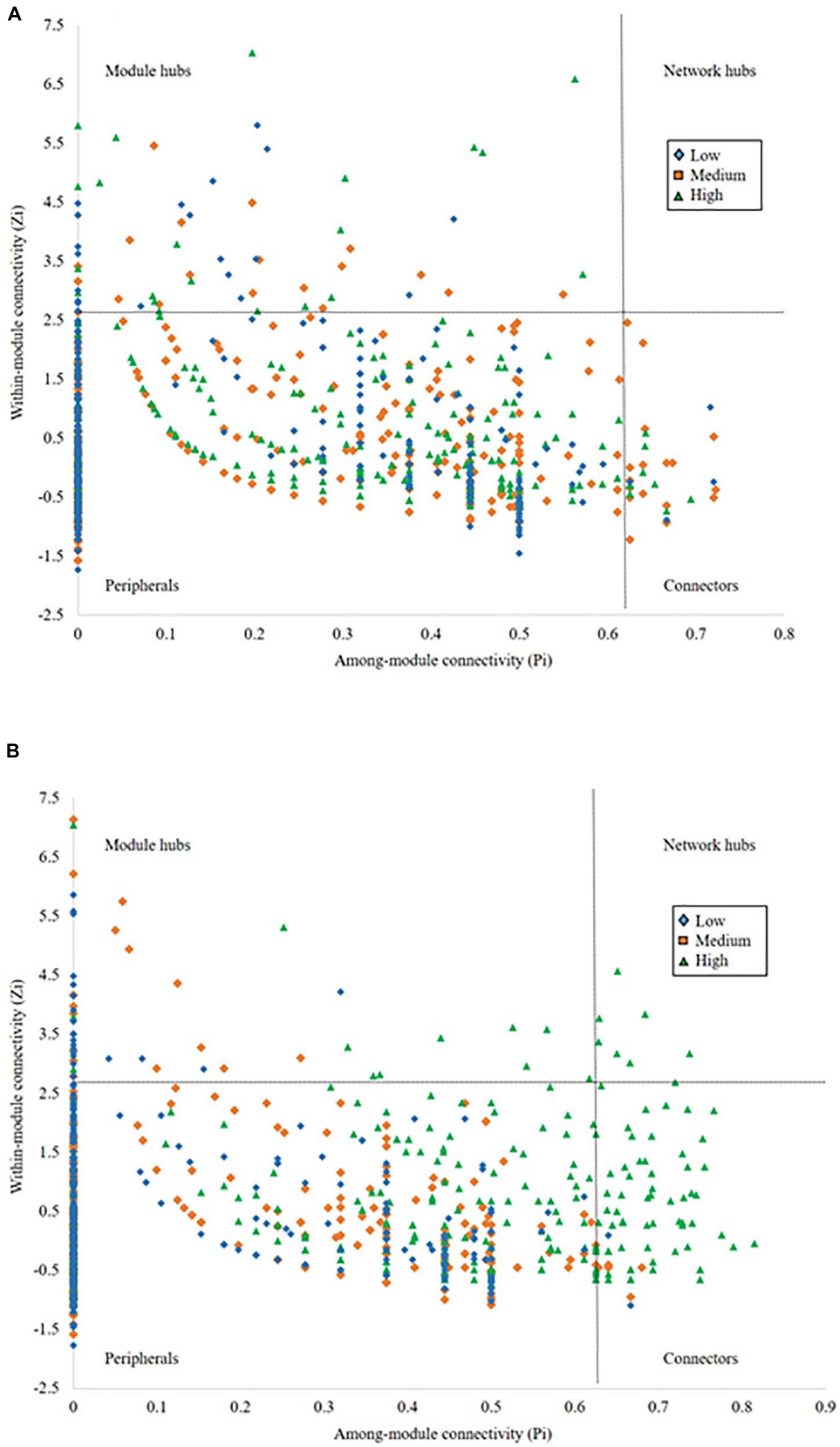

FIGURE 4 | The network nodes of **(A)** rhizosphere and **(B)** bulk soil were separated by within-module connectivity (Zi) and among-module connectivity (Pi).

of the 4 years rotations (i.e., 8th year of the field trial) when all plots were seeded to wheat so these shifts are likely a building legacy effect, particularly for the Bacteriodetes, which exhibited the strongest shift in response to pulse frequency. These shifts may also be related to the increased nitrogen fixation potential and higher residual soil nitrogen associated with higher pulse frequency in the crop rotations (Niu et al., 2017; Clúa et al., 2018; Liu J. et al., 2020).

The fungal community was more sensitive to pulse frequency than the bacterial community in our study, particularly the Ascomycota, which appear to be a dominant node in the soil microbial community network. We also found that putative fungal plant pathogens, which primarily belonged to the Ascomycota, significantly increased in rotations with higher pulse frequencies. Different crops can accumulate and select specific soil microbial taxa in the rhizosphere and bulk soil, which can be linked to either beneficial microbes that form symbiotic relationships with host plants and/or promote plant growth, or pathogens that infect specific host plant species (Zak et al., 2003). The network analysis also showed an increased abundance of dominant (nodes) Ascomycota taxa (including fungal pathotrophs and plant pathogens) that had more competitive interactions with Acidobacteria, Actinobacteria, Proteobacteria, and Planctomycetes in rotations with high pulse frequency. Previous studies have reported that certain pathogens can modify their host plant associated microbial community by building up syntrophic interactions with certain bacteria phyla, which can either directly help pathogen growth or inhibit certain bacterial phyla that have antagonistic influences on pathogens (Snelders et al., 2020; Wen et al., 2020). The competitive interactions between Ascomycota and other soil microbial phyla we identified in our study could be due to selective effects of potential pathogens on the soil microbial community. Overall, our results align with previous studies that showed that including two or more phases of pulse crops in 4 years rotations increases the proportion of fungal plant pathogens in soil, particularly those that belong to the Ascomycota such as *Fusarium* sp. and *Alternaria* sp. (Bainard et al., 2017). The shift in community composition of the Ascomycetes and buildup of fungal plant pathogens was the strongest in the bulk versus the rhizosphere soil, which likely indicates a potential building legacy effect of pulse frequency in this long term rotation experiment.

The network analysis revealed that pulse frequency altered the stability of the soil microbial communities. We found a higher ratio of identified edges to nodes and shorter average path distance under high pulse frequency rotations than low pulse frequency rotations in both the rhizosphere and bulk soil. This indicated that including more pulse crops in rotations could create favorable niches to select specific microbial taxa that can build up more intensive interactions within the community (Shi et al., 2016; Jiang et al., 2017). However, we found more negative interactions, shorter average path distance, lower average clustering coefficient and higher betweenness centrality numbers in the rhizosphere and bulk soil microbial communities under high pulse frequency rotations. This suggests there are more competitive interactions within soil microbial communities under rotations with high pulse frequency than their corresponding networks under rotations with low pulse frequency. This may lead to relatively unstable microbial networks as these increased interactions could be more easily interfered by other factors such as changes in environmental conditions (He et al., 2017).

We also found that higher pulse frequency changed the diversity and composition of keystone taxa of the soil microbial communities. Keystone taxa are highly related to soil microbial community structure and function, especially when these taxa are connectors in the community (Herren and McMahon, 2018). Based on previous studies, keystone taxa can alter the soil microbial community by modifying biotic connectivity within the community and changing the response of the microbial community to abiotic factors and their symbiotic relationships with host plants (Berry and Widder, 2014; Agler et al., 2016; Banerjee et al., 2018; Herren and McMahon, 2018). This can result in changes to the biological and ecological functions of the soil microbial community (Wittwer et al., 2017; Toju et al., 2018; Banerjee et al., 2019). In our study, we found that keystone taxa that functioned as connectors within the rhizosphere and bulk soil microbial communities increased under rotations with high pulse frequency. This may be an indicator that pulse frequency in crop rotations may be a contributing factor to causing functional shifts in the soil microbial community. A high proportion of keystone taxa altered by pulse frequency belonged to Acidobacteria, Proteobacteria, and Actinobacteria, which have been found to play critical biological and ecological functions in various ecosystems, including agroecosystems (Banerjee et al., 2016, 2018). Furthermore, some rare microbial taxa belonging to Bacteroidetes, Cyanobacteria, and Armatimonadetes were identified as keystone taxa (either module hubs or connectors), especially under rotations with high pulse frequency. These rare taxa have recently been reported as critical rare soil microbial species that can be major drivers of ecosystem multifunctionality in long-term agroecosystems (Chen et al., 2020). As a result, changes to these keystone taxa that belong to these bacterial phyla in our study due to high pulse frequency could reflect potential biological and ecological function changes to the soil microbial community.

In rhizosphere soil, we identified pH and EC as the primary environmental factors that influenced the microbial community, which has been commonly reported by other studies (Adviento-Borbe et al., 2006; Geisseler and Scow, 2014; Ratzke et al., 2020). In our study, the effect of pH and EC varied depending on pulse frequency, as modules containing the keystone taxa were more sensitive to pH and EC under low to medium pulse frequency. However, increased pulse frequency did not significantly alter the soil pH and EC in rhizosphere soils. This suggests that pulse frequency may influence the abundance of microbial taxa that are more responsive to pH and EC. Similarly, although bulk soil potassium didn't significantly change with increased pulse frequency, potassium showed more negative interactions on the soil microbial community under low pulse frequency, but more positive interactions with microbes under higher pulse frequency. Overall, the various modules reacted to environmental factors differently, suggesting that microorganisms from these modules may be involved in different ecological functions.

Previous studies have reported that increased pulse phases in crop rotations has been shown to improve levels of soil available nitrogen (Niu et al., 2017), but we found that soil nitrate had stronger negative correlations with microbial modules in both rhizosphere and bulk soil, especially under high pulse frequency. Nitrogen is an essential nutrient for crop growth, but it is usually one of the strongest limiting factors in most agricultural systems worldwide (Stevens, 2019). However, the long-term accumulation of nitrogen inputs has been demonstrated to have inhibiting effects on soil microorganisms and to change the nutrient competition status of plants and microbes, symbiotic status of soil microbes on host plants, and alter C:N ratios, changing the growth rate of fungi and bacteria as they require different C:N ratios in soil (Zhang et al., 2018), which could explain some of the results observed in this study.

Interestingly, we found that soil sulfur showed a significant relationship with many identified microbial modules in this study. These relationships were generally more positive in rhizosphere soil and more negative in bulk soil, with similar results being shown in a study conducted on Luvisolic and Chernozemic soils in Canada (Lupwayi et al., 2001). Soil microorganisms play an important role in soil sulfur cycling. More than 95% of sulfur in soil exists in organic forms such as sulfate esters, sulphonates or amino acid sulfur which can be used by plants only after interconversion into inorganic sulfur by microorganisms (Kertesz and Mirleau, 2004), thus mineralization and immobilization of soil sulfur is largely dependent on the activities of soil microorganisms. Furthermore, sulfur is an essential element for some basic amino acids and enzymes to support the growth of microorganisms, and soil microbial sulfur is tightly related to soil total organic sulfur pools and soil carbon, nitrogen and phosphorus cycling (Banerjee and Chapman, 1996; Bünemann and Condron, 2007; Smolders et al., 2010). Sulfur is critical for legume crops to form nodules and fix nitrogen, which has been documented for decades (Anderson and Spencer, 1949; Reckling et al., 2020). Considering sulfur deficiencies have been reported consistently in modern agriculture (McNeill et al., 2005) and different crop rotation designs can significantly affect soil sulfur (Mohammadi et al., 2011), rotations with different legume:cereal ratios could restructure soil microbial communities through host plant effects. Therefore, these interactions between sulfur and identified microbial modules identified in our study can be the result of either direct nutrient effects or indirect host plant effects, which requires further investigation.

Overall, we found that high pulse frequency in cropping systems can alter the composition and increase network interactions of soil microbial communities in both rhizosphere and bulk soil. The Ascomycetes and Bacteroidetes exhibited the strongest shift under rotations with higher pulse frequencies, particularly in the bulk soil, which may be an indicator of a building legacy effect following two cycles through the 4 years rotation. We also observed an increase in potential fungal pathogens and negative interactions in the soil microbial networks under high pulse frequency, highlighting the risks associated with incorporating pulse crops into crop rotations.

DATA AVAILABILITY STATEMENT

The datasets presented in this study can be found in online repositories. The names of the repository/repositories and accession number(s) can be found below: NCBI BioProject; PRJNA694691, PRJNA694475, PRJNA694839, PRJNA694704, PRJNA717779, and PRJNA694448.

AUTHOR CONTRIBUTIONS

LB and BE designed and were responsible for conducting the field and lab work. TY and LB conducted the data analysis and wrote the manuscript. All authors contributed to editing the manuscript and approved the final version.

FUNDING

The authors declare that this study received funding from Saskatchewan Pulse Growers. The funder was not involved in the study design, collection, analysis, interpretation of data, the writing of this article or the decision to submit it for publication.

ACKNOWLEDGMENTS

We gratefully acknowledge the technical support from Keith Hanson, Lee Poppy, Eric Walker, and multiple summer students in the field. We are grateful for financial support from the Saskatchewan Pulse Growers.

SUPPLEMENTARY MATERIAL

The Supplementary Material for this article can be found online at: https://www.frontiersin.org/articles/10.3389/fmicb.2021.667394/full#supplementary-material

REFERENCES

Adviento-Borbe, M. A., Doran, J. W., Drijber, R. A., and Dobermann, A. (2006). Soil electrical conductivity and water content affect nitrous oxide and carbon dioxide emissions in intensively managed soils. *J. Environ. Qual.* 35, 1999–2010. doi: 10.2134/jeq2006.0109

Agler, M. T., Ruhe, J., Kroll, S., Morhenn, C., Kim, S.-T., Weigel, D., et al. (2016). Microbial hub taxa link host and abiotic factors to plant microbiome variation. *PLoS Biol.* 14:e1002352. doi: 10.1371/journal.pbio.1002352

Anderson, A. J., and Spencer, D. (1949). Molybdenum and sulphur in symbiotic nitrogen fixation. *Nature* 164, 273–274. doi: 10.1038/164273a0

Bainard, L., Evans, B., Malis, E., Yang, T., and Bainard, J. (2020). Influence of annual plant diversity on forage productivity and nutrition, soil chemistry, and soil microbial communities. *Front. Sustain. Food Syst.* 4:560479. doi: 10.3389/fsufs.2020.560479

Bainard, L. D., Navarro-Borrell, A., Hamel, C., Braun, K., Hanson, K., and Gan, Y. (2017). Increasing the frequency of pulses in crop rotations reduces soil fungal diversity and increases the proportion of fungal pathotrophs in a semiarid

agroecosystem. *Agric. Ecosyst. Environ.* 240, 206–214. doi: 10.1016/j.agee.2017.02.020

Banerjee, M. R., and Chapman, S. J. (1996). The significance of microbial biomass sulphur in soil. *Biol. Fert. Soils* 22, 116–125. doi: 10.1007/BF00384442

Banerjee, S., Kirkby, C. A., Schmutter, D., Bissett, A., Kirkegaard, J. A., and Richardson, A. E. (2016). Network analysis reveals functional redundancy and keystone taxa amongst bacterial and fungal communities during organic matter decomposition in an arable soil. *Soil Biol. Biochem.* 97, 188–198. doi: 10.1016/j.soilbio.2016.03.017

Banerjee, S., Schlaeppi, K., and Van Der Heijden, M. G. (2018). Keystone taxa as drivers of microbiome structure and functioning. *Nat. Rev. Microbiol.* 16, 567–576. doi: 10.1038/s41579-018-0024-1

Banerjee, S., Walder, F., Büchi, L., Meyer, M., Held, A. Y., Gattinger, A., et al. (2019). Agricultural intensification reduces microbial network complexity and the abundance of keystone taxa in roots. *ISME J.* 13, 1722–1736. doi: 10.1038/s41396-019-0383-2

Barbieri, P., Pellerin, S., and Nesme, T. (2017). Comparing crop rotations between organic and conventional farming. *Sci. Rep.* 7:13761.

Berry, D., and Widder, S. (2014). Deciphering microbial interactions and detecting keystone species with co-occurrence networks. *Front. Microbiol.* 5:219. doi: 10.3389/fmicb.2014.00219

Bünemann, E. K., and Condron, L. M. (2007). "Phosphorus and sulphur cycling in terrestrial ecosystems," in *Nutrient Cycling in Terrestrial Ecosystems*, eds P. Marschner and Z. Rengel (Berlin: Springer), 65–92. doi: 10.1007/978-3-540-68027-7_3

Caporaso, J. G., Lauber, C. L., Walters, W. A., Berg-Lyons, D., Huntley, J., Fierer, N., et al. (2012). Ultra-high-throughput microbial community analysis on the illumina HiSeq and MiSeq platforms. *ISME J.* 6, 1621–1624. doi: 10.1038/ismej.2012.8

Chen, Q.-L., Ding, J., Zhu, D., Hu, H.-W., Delgado-Baquerizo, M., Ma, Y.-B., et al. (2020). Rare microbial taxa as the major drivers of ecosystem multifunctionality in long-term fertilized soils. *Soil Biol. Biochem.* 141:107686. doi: 10.1016/j.soilbio.2019.107686

Clúa, J., Roda, C., Zanetti, M. E., and Blanco, F. A. (2018). Compatibility between legumes and rhizobia for the establishment of a successful nitrogen-fixing symbiosis. *Genes* 9:125. doi: 10.3390/genes9030125

Delavaux, C. S., Bever, J. D., Karppinen, E. M., and Bainard, L. D. (2020). Keeping it cool: soil sample cold pack storage and DNA shipment up to 1 month does not impact metabarcoding results. *Ecol. Evol.* 10, 4652–4664. doi: 10.1002/ece3.6219

Deng, Y., Jiang, Y. H., Yang, Y., He, Z., Luo, F., and Zhou, J. (2012). Molecular ecological network analyses. *BMC Bioinformatics* 13:113. doi: 10.1186/1471-2105-13-113

Drinkwater, L. E., Wagoner, P., and Sarrantonio, M. (1998). Legume-based cropping systems have reduced carbon and nitrogen losses. *Nature* 396, 262–265. doi: 10.1038/24376

Edgar, R. C. (2013). UPARSE: highly accurate OTU sequences from microbial amplicon reads. *Nat. Methods* 10, 996–998. doi: 10.1038/nmeth.2604

Foyer, C. H., Lam, H. M., Nguyen, H. T., Siddique, K. H., Varshney, R. K., Colmer, T. D., et al. (2016). Neglecting legumes has compromised human health and sustainable food production. *Nat. Plants* 2:16112. doi: 10.1038/nplants.2016.112

Gan, Y., Hamel, C., O'donovan, J. T., Cutforth, H., Zentner, R. P., Campbell, C. A., et al. (2015). Diversifying crop rotations with pulses enhances system productivity. *Sci. Rep.* 5:14625. doi: 10.1038/srep14625

Geisseler, D., and Scow, K. M. (2014). Long-term effects of mineral fertilizers on soil microorganisms – A review. *Soil Biol. Biochem.* 75, 54–63. doi: 10.1016/j.soilbio.2014.03.023

Gentry, C. E., and Willis, R. B. (1988). Improved method for automated determination of ammonium in soil extracts. *Commun. Soil Sci. Plant Anal.* 19, 721–737. doi: 10.1080/00103628809367970

Guimerà, R., and Nunes Amaral, L. A. (2005). Functional cartography of complex metabolic networks. *Nature* 433, 895–900. doi: 10.1038/nature03288

Habekost, M., Eisenhauer, N., Scheu, S., Steinbeiss, S., Weigelt, A., and Gleixner, G. (2008). Seasonal changes in the soil microbial community in a grassland plant diversity gradient four years after establishment. *Soil Biol. Biochem.* 40, 2588–2595. doi: 10.1016/j.soilbio.2008.06.019

Hamel, C., Gan, Y., Sokolski, S., and Bainard, L. D. (2018). High frequency cropping of pulses modifies soil nitrogen level and the rhizosphere bacterial microbiome in 4-year rotation systems of the semiarid prairie. *Appl. Soil Ecol.* 126, 47–56. doi: 10.1016/j.apsoil.2018.01.003

Harm, J., Bettany, J., and Halstead, E. (1973). A soil test for sulphur and interpretative criteria for Saskatchewan. *Commun. Soil Sci. Plant Anal.* 4, 219–231. doi: 10.1080/00103627309366440

He, D., Shen, W., Eberwein, J., Zhao, Q., Ren, L., and Wu, Q. L. (2017). Diversity and co-occurrence network of soil fungi are more responsive than those of bacteria to shifts in precipitation seasonality in a subtropical forest. *Soil Biol. Biochem.* 115, 499–510. doi: 10.1016/j.soilbio.2017.09.023

Herren, C. M., and McMahon, K. D. (2018). Keystone taxa predict compositional change in microbial communities. *Environ. Microbiol.* 20, 2207–2217. doi: 10.1111/1462-2920.14257

Jensen, E. S., Carlsson, G., and Hauggaard-Nielsen, H. (2020). Intercropping of grain legumes and cereals improves the use of soil N resources and reduces the requirement for synthetic fertilizer N: a global-scale analysis. *Agron. Sustain. Dev.* 40:5. doi: 10.1007/s13593-020-0607-x

Jiang, Y., Li, S., Li, R., Zhang, J., Liu, Y., Lv, L., et al. (2017). Plant cultivars imprint the rhizosphere bacterial community composition and association networks. *Soil Biol. Biochem.* 109, 145–155. doi: 10.1016/j.soilbio.2017.02.010

Kertesz, M. A., and Mirleau, P. (2004). The role of soil microbes in plant sulphur nutrition. *J. Exp. Bot.* 55, 1939–1945. doi: 10.1093/jxb/erh176

Khakbazan, M., Gan, Y., Bandara, M., and Huang, J. (2020). Economics of pulse crop frequency and sequence in a wheat-based rotation. *J. Agron.* 112, 2058–2080. doi: 10.1002/agj2.20182

Kirkegaard, J., Christen, O., Krupinsky, J., and Layzell, D. (2008). Break crop benefits in temperate wheat production. *Field Crops Res.* 107, 185–195. doi: 10.1016/j.fcr.2008.02.010

Kõljalg, U., Nilsson, R. H., Abarenkov, K., Tedersoo, L., Taylor, A. F. S., Bahram, M., et al. (2013). Towards a unified paradigm for sequence-based identification of fungi. *Mol. Ecol.* 22, 5271–5277. doi: 10.1111/mec.12481

Lal, R. (2017). "Chapter four – Improving soil health and human protein nutrition by pulses-based cropping systems," in *Advances in Agronomy*, ed. D. L. Sparks (Cambridge, MA: Academic Press), 167–204. doi: 10.1016/bs.agron.2017.05.003

Liu, J., Yu, X., Qin, Q., Dinkins, R. D., and Zhu, H. (2020). The impacts of domestication and breeding on nitrogen fixation symbiosis in legumes. *Front. Genet.* 11:00973. doi: 10.3389/fgene.2020.00973

Liu, K., Bandara, M., Hamel, C., Knight, J. D., and Gan, Y. (2020). Intensifying crop rotations with pulse crops enhances system productivity and soil organic carbon in semi-arid environments. *Field Crops Res.* 248, 107657. doi: 10.1016/j.fcr.2019.107657

Lupwayi, N. Z., Monreal, M. A., Clayton, G. W., Grant, C. A., Johnston, A. M., and Rice, W. A. (2001). Soil microbial biomass and diversity respond to tillage and sulphur fertilizers. *Can. J. Soil Sci.* 81, 577–589. doi: 10.4141/S01-010

Martin, K. J., and Rygiewicz, P. T. (2005). Fungal-specific PCR primers developed for analysis of the ITS region of environmental DNA extracts. *BMC Microbiol.* 5:28. doi: 10.1186/1471-2180-5-28

McNeill, A., Eriksen, J., Bergström, L., Smith, K., Marstorp, H., Kirchmann, H., et al. (2005). Nitrogen and sulphur management: challenges for organic sources in temperate agricultural systems. *Soil Use Manag.* 21, 82–93. doi: 10.1111/j.1475-2743.2005.tb00112.x

Miller, J. J., and Curtin, D. (2006). "Electrical conductivity and soluble ions," in *Soil Sampling and Methods of Analysis*, 2 Edn, eds M. R. Carter and E. G. Gregorich (Boca Raton, FL: CRC Press).

Mohammadi, K., Ghalavand, A., Aghaalikhani, M., Heidari, G., Shahmoradi, B., and Sohrabi, Y. (2011). Effect of different methods of crop rotation and fertilization on canola traits and soil microbial activity. *Aust. J. Crop Sci.* 5:1261.

Navarro-Borrell, A., Shi, Y., Gan, Y., Bainard, L. D., Germida, J. J., and Hamel, C. (2017). Fungal diversity associated with pulses and its influence on the subsequent wheat crop in the Canadian prairies. *Plant Soil* 414, 13–31. doi: 10.1007/s11104-016-3075-y

Nguyen, N. H., Song, Z., Bates, S. T., Branco, S., Tedersoo, L., Menke, J., et al. (2016). FUNGuild: an open annotation tool for parsing fungal community datasets by ecological guild. *Fungal Ecol.* 20, 241–248. doi: 10.1016/j.funeco.2015.06.006

Niu, Y., Bainard, L. D., Bandara, M., Hamel, C., and Gan, Y. (2017). Soil residual water and nutrients explain about 30% of the rotational effect in 4-yr pulse-intensified rotation systems. *Can. J. Plant Sci.* 97, 852–864. doi: 10.1139/cjps-2016-0282

Olesen, J. M., Bascompte, J., Dupont, Y. L., and Jordano, P. (2007). The modularity of pollination networks. *Proc. Natl. Acad. Sci. U.S.A.* 104, 19891–19896. doi: 10.1073/pnas.0706375104

Ratzke, C., Barrere, J., and Gore, J. (2020). Strength of species interactions determines biodiversity and stability in microbial communities. *Nat. Ecol. Evol.* 4, 376–383. doi: 10.1038/s41559-020-1099-4

Reckling, M., Bergkvist, G., Watson, C. A., Stoddard, F. L., and Bachinger, J. (2020). Re-designing organic grain legume cropping systems using systems agronomy. *Eur. J. Agron.* 112:125951. doi: 10.1016/j.eja.2019.125951

Schönhart, M., Schmid, E., and Schneider, U. A. (2011). CropRota – A crop rotation model to support integrated land use assessments. *Eur. J. Agron.* 34, 263–277. doi: 10.1016/j.eja.2011.02.004

Schumacher, B. A. (2002). *Methods for the Determination of Total Organic Carbon (TOC) in Soils and Sediments*. Washington, DC: United States Environmental Protection Agency, 1–24.

Shi, S., Nuccio, E. E., Shi, Z. J., He, Z., Zhou, J., and Firestone, M. K. (2016). The interconnected rhizosphere: high network complexity dominates rhizosphere assemblages. *Ecol. Lett.* 19, 926–936. doi: 10.1111/ele.12630

Smolders, A. J. P., Lucassen, E. C. H. E. T., Bobbink, R., Roelofs, J. G. M., and Lamers, L. P. M. (2010). How nitrate leaching from agricultural lands provokes phosphate eutrophication in groundwater fed wetlands: the sulphur bridge. *Biogeochemistry* 98, 1–7. doi: 10.1007/s10533-009-9387-8

Snelders, N. C., Rovenich, H., Petti, G. C., Rocafort, M., Van Den Berg, G. C., Vorholt, J. A., et al. (2020). Microbiome manipulation by a soil-borne fungal plant pathogen using effector proteins. *Nat. Plants* 6, 1365–1374. doi: 10.1038/s41477-020-00799-5

Stevens, C. J. (2019). Nitrogen in the environment. *Science* 363, 578–580. doi: 10.1126/science.aav8215

Toju, H., Tanabe, A. S., and Sato, H. (2018). Network hubs in root-associated fungal metacommunities. *Microbiome* 6:116. doi: 10.1186/s40168-018-0497-1

Venter, Z. S., Jacobs, K., and Hawkins, H.-J. (2016). The impact of crop rotation on soil microbial diversity: a meta-analysis. *Pedobiologia* 59, 215–223. doi: 10.1016/j.pedobi.2016.04.001

Wang, Q., Garrity, G. M., Tiedje, J. M., and Cole, J. R. (2007). Naive bayesian classifier for rapid assignment of rRNA sequences into the new bacterial taxonomy. *Appl. Environ. Microbiol.* 73, 5261–5267. doi: 10.1128/AEM.00062-07

Wen, T., Zhao, M., Liu, T., Huang, Q., Yuan, J., and Shen, Q. (2020). High abundance of *Ralstonia solanacearum* changed tomato rhizosphere microbiome and metabolome. *BMC Plant Biol.* 20:166. doi: 10.1186/s12870-020-02365-9

Willis, A., and Bunge, J. (2015). Estimating diversity via frequency ratios. *Biom. Methodol.* 71, 1042–1049. doi: 10.1111/biom.12332

Wittwer, R. A., Dorn, B., Jossi, W., and Van Der Heijden, M. G. (2017). Cover crops support ecological intensification of arable cropping systems. *Sci. Rep.* 7:41911. doi: 10.1038/srep41911

Zak, D. R., Holmes, W. E., White, D. C., Peacock, A. D., and Tilman, D. (2003). Plant diversity, soil microbial communities, and ecosystem function: are there any links? *Ecology* 84, 2042–2050. doi: 10.1890/02-0433

Zhang, T. A., Chen, H. Y. H., and Ruan, H. (2018). Global negative effects of nitrogen deposition on soil microbes. *ISME J.* 12, 1817–1825. doi: 10.1038/s41396-018-0096-y

Zhao, J., Yang, Y., Zhang, K., Jeong, J., Zeng, Z., and Zang, H. (2020). Does crop rotation yield more in China? A meta-analysis. *Field Crops Res.* 245:107659. doi: 10.1016/j.fcr.2019.107659

Conflict of Interest: The authors declare that the research was conducted in the absence of any commercial or financial relationships that could be construed as a potential conflict of interest.

frontiers in Microbiology

ORIGINAL RESEARCH
published: 09 June 2021
doi: 10.3389/fmicb.2021.646143

Bacterial Communities Associated With Healthy and Bleached Crustose Coralline Alga *Porolithon onkodes*

*Fangfang Yang[1], Zhiliang Xiao[1,2], Zhangliang Wei[1] and Lijuan Long[1]**

[1] Key Laboratory of Tropical Marine Bio-resources and Ecology, South China Sea Institute of Oceanology, Chinese Academy of Sciences, Guangzhou, China, [2] University of Chinese Academy of Sciences, Beijing, China

Crustose coralline algae (CCA) play vital roles in producing and stabilizing reef structures and inducing the settlement and metamorphosis of invertebrate larvae in coral reef ecosystems. However, little is known about the bacterial communities associated with healthy and bleached CCA and their interactions with coral larval settlement. We collected samples of healthy, middle semi-bleached, and bleached CCA *Porolithon onkodes* from Sanya Bay in the South China Sea and investigated their influences on the larval settlement and metamorphosis of the reef-building coral *Pocillopora damicornis*. The larval settlement/metamorphosis rates all exceeded 70% when exposed to healthy, middle semi-bleached, and bleached algae. Furthermore, the compositions of bacterial community using amplicon pyrosequencing of the V3–V4 region of 16S rRNA were investigated. There were no obvious changes in bacterial community structure among healthy, middle semi-bleached, and bleached algae. *Alphaproteobacteria*, *Bacteroidetes*, and *Gammaproteobacteria* were dominant in all samples, which may contribute to coral larval settlement. However, the relative abundances of several bacterial communities varied among groups. The relative abundances of *Mesoflavibacter*, *Ruegeria*, *Nautella*, and *Alteromonas* in bleached samples were more than double those in the healthy samples, whereas *Fodinicurvata* and unclassified *Rhodobacteraceae* were significantly lower in the bleached samples. Additionally, others at the genus level increased significantly from 8.5% in the healthy samples to 22.93% in the bleached samples, which may be related to algal bleaching. These results revealed that the microbial community structure associated with *P. onkodes* generally displayed a degree of stability. Furthermore, bleached alga was still able to induce larval settlement and metamorphosis.

Keywords: bacterial community, coralline algae, metamorphosis, *Pocillopora damicornis*, *Porolithon onkodes*, settlement

OPEN ACCESS

Edited by:
Yong Wang,
Guizhou University, China

Reviewed by:
Shan-Hua Yang,
National Taiwan University, Taiwan
Zhibo Zhao,
Guizhou University, China

***Correspondence:**
Lijuan Long
longlj@scsio.ac.cn

Specialty section:
This article was submitted to Microbe and Virus Interactions with Plants, a section of the journal Frontiers in Microbiology

Received: *25 December 2020*
Accepted: *05 May 2021*
Published: *09 June 2021*

Citation:
Yang F, Xiao Z, Wei Z and Long L (2021) Bacterial Communities Associated With Healthy and Bleached Crustose Coralline Alga Porolithon onkodes. Front. Microbiol. 12:646143. doi: 10.3389/fmicb.2021.646143

INTRODUCTION

Crustose coralline algae (CCA) are considered as critical structural components of coral reef ecosystems. They play important roles in contributing to primary productivity, producing and stabilizing reef structures through $CaCO_3$ deposition, and functioning as autogenic ecosystem engineers by the provision of three-dimensional habitat structure (Nelson, 2009;

Tebben et al., 2015; van der Heijden and Kamenos, 2015). Furthermore, several CCA species have been shown to positively induce coral larval settlement and metamorphosis through a variety of mechanisms including chemical allelopathy and microbial induction (Morse and Hooker, 1988; Harrington et al., 2004; Gómez-Lemos et al., 2018). There are increasing evidences to suggest that algal–bacterial communities are species-specific and may play vital roles in larval settlement (Sneed et al., 2015; Yang et al., 2021), algal health, response to environmental stress, and defense against diseases (Harder et al., 2012; Singh and Reddy, 2014). However, algal–bacterial associations show highly dynamic relationships in response to environmental stress (Miranda et al., 2013; Quéré et al., 2019). For an improved understanding of the future health of coral reefs, it is important to determine the bacterial communities associated with CCA and how they shift in response to a disease or environmental stress.

Algal bleaching has recently occurred due to anthropogenic stressors and climate change, resulting in algal mortality (Martone et al., 2010; Cornwall et al., 2019). Previous studies have shown differences in bacterial communities between bleached and healthy organisms including corals and non-calcified macroalgae. The presence of some potential pathogens (i.e., *Vibrio shilonii*, *Nautella italica* R11, and *Phaeobacter gallaeciensis* LSS9) is related to bleaching disease (Kushmaro et al., 1996; Meron et al., 2011; Zozaya-Valdes et al., 2015; Rajasabapathy et al., 2020). To date, reports of microbial community variations between healthy and bleached CCA are very limited. Only two studies have investigated the microbiome associated with CCA-diseased tissue (*Neogoniolithon brassica-florida* and *N. mamillare*) (Meistertzheim et al., 2017; Quéré et al., 2019). Moreover, it is unclear whether changes in the bacterial communities associated with CCA affect the settlement of coral larvae.

Porolithon onkodes (Corallinales, Rhodophyta) is commonly found on tropical and subtropical coral reefs and is conspicuous on wave-resistant algal ridges (Dean et al., 2015). The species has been demonstrated to induce coral larval settlement and metamorphosis (Whitman et al., 2020). However, it is also one of the most vulnerable species to environmental change due to its highly soluble Mg-calcite skeleton (Ordoñez et al., 2019). Previous studies have revealed the physiological impacts of bleaching on *P. onkodes*, characterized by the loss of pink surface pigments, which occurs more frequently during summer months when temperatures and light radiation are elevated (Anthony et al., 2008; Bessell-Browne et al., 2017). It is unknown whether algal bleaching influences the larval settlement and distribution of coral populations.

Pocillopora damicornis is one of the most abundant and widespread hermaphrodite reef-building corals (Harriott, 1983) and is commonly used in experimental biology and physiology as a model species. There are many studies focusing on the microbiome of *P. damicornis*, which is mainly affiliated with γ-*Proteobacteria* (Bourne and Munn, 2005; Osman et al., 2020). However, in recent years, *P. damicornis* has suffered a degradation in reef ecosystems (Zheng et al., 2021). The coral recruitment and recovery depend mainly on the successful settlement and metamorphosis of coral larvae. A study has revealed that the larvae of *P. damicornis* preferentially settle on, or locate in close proximity to, a particular species of CCA (Yang et al., 2021). However, the mechanism of larval substrate choice and settlement specificity to CCA is unclear.

The main goal of the study was to investigate the bacterial communities associated with different health statuses of *P. onkodes* and their interactions with coral larval settlement. Our hypotheses are that (1) bacterial community associated with *P. onkodes* plays roles in larval settlement and metamorphosis and (2) bacterial community associated with *P. onkodes* is relatively stable but, however, their relative abundances differed. To test these hypotheses, in this study, healthy, middle semi-bleached, and bleached *P. onkodes* were collected from Sanya Bay, in the South China Sea. Their effects on coral larval survival, settlement, and bacterial community were investigated. The interactions between the bacterial community associated with *P. onkodes* and larval settlement, and potential pathogenic bacteria capable of causing algal bleaching, were analyzed.

MATERIALS AND METHODS

Collection of CCA and Coral Larvae

Healthy, middle semi-bleached, and bleached *P. onkodes* were collected from Luhuitou fringing reef, Sanya Bay (18°12′N, 109°28′E), Hainan Island in the South China Sea in August, 2020. Fragments (3–5 cm) were collected from rocks using a hammer and chisel at 3–5-m depth. Each algal fragment was washed gently to remove epiphytes and then placed in an individual collecting bag in order to avoid contamination between specimens. Samples were then transported immediately to the laboratory. A total of nine samples, including three from healthy specimens (healthy group), three from the middle semi-bleached area between healthy and bleached specimens (middle group), and three from bleached specimens (bleached group), were immediately frozen by N_2 and stored at −80°C for subsequent analysis of the bacterial community associated with *P. onkodes*. Other samples were cultured in flow-through tanks with filtered seawater at the Tropical Marine Biological Research Station in Sanya Bay for the settlement and metamorphosis assays. Ten colonies of coral *P. damicornis* were sampled at 2–3-m depth from Luhuitou fringing reef in August, 2020. Colonies were placed in flow-through buckets with filtered seawater. The released larvae were then collected in a chamber equipped with a 100-μm plankton mesh. The larvae were mixed and cultured with filtered seawater for the settlement and metamorphosis assays.

Experimental Treatment and Larval Settlement Assays

To evaluate the larval settlement and metamorphosis responses to different health statuses of *P. onkodes*, four different treatments were conducted: control, healthy alga, middle alga, and bleached alga. Each experimental treatment had six replicates. Filtered seawater without the addition of alga was used as a negative control group. Fragments of *P. onkodes* were cut into 1 cm^2 standardized surface area samples using a handheld grinding wheel. The effects of the following treated *P. onkodes* and extracts

on larval settlement and metamorphosis were investigated: (i) live thalli extracted with either hot water (autoclave conditions, 121°C, 15 psi), cold water (27°C), ethanol, methanol, or methanol/chloroform (1:2, *v*/*v*). For all extractions, *P. onkodes* was extracted in 25 ml for 60 min; (ii) dried and autoclaved without water; and (iii) pink surface pigments were removed.

Ten *P. damicornis* larvae were randomly selected and added to individual wells of a six-well plate with 10 ml of 0.2 μm filtered seawater. The temperatures of the plates were maintained at 27°C by floating them in a seawater bath. The rates of larvae survival, metamorphosis, and settlement were calculated at 24 h with a dissecting microscope. The values were expressed as mean ± standard deviation. The following categories of larval behavior were observed in the assays: (i) dead larvae that had vanished or showed signs of degradation; (ii) swimming larvae with no response to cues; (iii) metamorphosis larvae that underwent morphological changes from a planula larva to a polyp, but without attachment to the substrate; and (iv) settlement and metamorphosis, defined as planulae firmly attached to the substratum and transforming into the coral primary polyp stage, respectively.

DNA Extraction, PCR Amplification, and Sequencing of Microbial Communities

Bacterial communities of *P. onkodes* were investigated. Specially, microbial DNA was extracted from nine algal samples using the E.Z.N.A.® Soil DNA Kit (Omega Bio-Tek, Norcross, GA, United States) according to manufacturer's protocols. The final DNA concentration and purification were determined by a NanoDrop 2000 UV-Vis spectrophotometer (Thermo Fisher Scientific, Wilmington, DE, United States). DNA quality was checked by 1% agarose gel electrophoresis. The V3–V4 hypervariable regions of bacteria 16S rRNA gene were amplified with primers 338F (5′-ACTCCTACGGGAGGCAGCAG-3′) and 806R (5′-GGACTACHVGGGTWTCTAA T-3′) by a thermocycler polymerase chain reaction (PCR) system (GeneAmp 9700, ABI, Thermo Fisher Scientific, Wilmington, DE, United States) (Li et al., 2018; Yang et al., 2021). The PCR reactions were as follows: 3 min of denaturation at 95°C, 27 cycles of 30 s at 95°C, 30 s for annealing at 55°C, 45 s for elongation at 72°C, and a final extension for 10 min at 72°C. PCR reactions were performed in triplicate 20-μl mixtures containing 0.8 μl of each primer (5 μM), 4 μl of 5 × FastPfu Buffer, 2 μl of 2.5 mM dNTPs, 0.4 μl of FastPfu Polymerase, and 10 ng of template DNA. The PCR products were extracted from a 2% of agarose gel and purified using the AxyPrep DNA Gel Extraction Kit (Axygen Biosciences, Union City, CA, United States). They were then quantified using QuantiFluor™ ST (Promega, Madison, WI, United States) according to the manufacturer's protocols. Purified amplicons were pooled in equimolars and paired-end sequenced (2 × 300) on an Illumina MiSeq platform (Illumina, San Diego, CA, United States) according to the standard protocols by Majorbio Bio-Pharm Technology Co., Ltd. (Shanghai, China). The raw reads were deposited into the NCBI Sequence Read Archive under BioProject ID PRJNA685315 (accession numbers: SAMN17082550, SAMN17082551, SAMN17082552, SAMN17082553, SAMN17082554, SAMN17082555, SAMN17082556, SAMN17082557, and SAMN1 7082558).

Raw FASTQ files were demultiplexed, quality filtered by Trimmomatic, and merged by FLASH using the following criteria: (i) the reads were truncated at any site receiving an average quality score of 20 over a 50-bp sliding window; (ii) primers were exactly matched allowing two nucleotide mismatches, and reads containing ambiguous bases were removed; and (iii) sequences whose overlap exceeded 10 bp were merged according to their overlap sequence. Operational taxonomic units (OTUs) were clustered using UPARSE version 7.1[1], and chimeric sequences were identified and removed using UCHIME (Osman et al., 2020). High-quality filtered tags with ≥97% similarity in nucleotide identity were clustered into same operational taxonomic units by OTU cluster analysis (Latif et al., 2020). The taxonomy of each 16S rRNA gene sequence was analyzed by the RDP Classifier algorithm[2] against the Silva (SSU123) 16S rRNA database with a confidence threshold of 70%. Phylogenetic Investigation of Communities by Reconstruction of Unobserved States (PICRUSt2) software package was employed to predict the potential functional capabilities and differences among bacterial communities associated with different health statuses of *P. onkodes*.

Statistical Analyses

The alpha diversity of bacterial community was analyzed using Shannon, Simpson's, and Ace indices, based on the assigned OTUs (Latif et al., 2020; Osman et al., 2020). The beta diversity of bacterial community among different samples was assessed using a hierarchical cluster tree and principal coordinates analysis (PCoA) based on Bray–Curtis similarity. The relative abundances of bacterial phyla, class, and genera among the three algae groups were statistically analyzed using the Kruskal–Wallis *H*-test followed by the Scheffe's *post hoc* test. Differences in the relative abundances of bacterial community composition between two groups were analyzed using the Welch's *t*-test (White et al., 2009). The values in the settlement and metamorphosis assays were expressed as mean ± standard deviation. $P < 0.05$ was considered statistically significant, while $p < 0.01$ was considered extremely statistically significant.

RESULTS

Responses of Coral Larvae to Healthy, Middle Semi-Bleached, and Bleached *P. onkodes*

The effects of healthy, middle semi-bleached, and bleached *P. onkodes* on the settlement and metamorphosis of *P. damicornis* larvae were investigated. Larval survivorship in all groups was 100% within 24 h. As shown in **Figure 1**, the settlement rate was 76% at 24 h when exposed to healthy alga, which was similar to that in the middle and bleached algae at 78% ($p = 0.32$, **Supplementary Table 1**). Approximately 6% of coral

[1]http://drive5.com/uparse/

[2]http://rdp.cme.msu.edu/

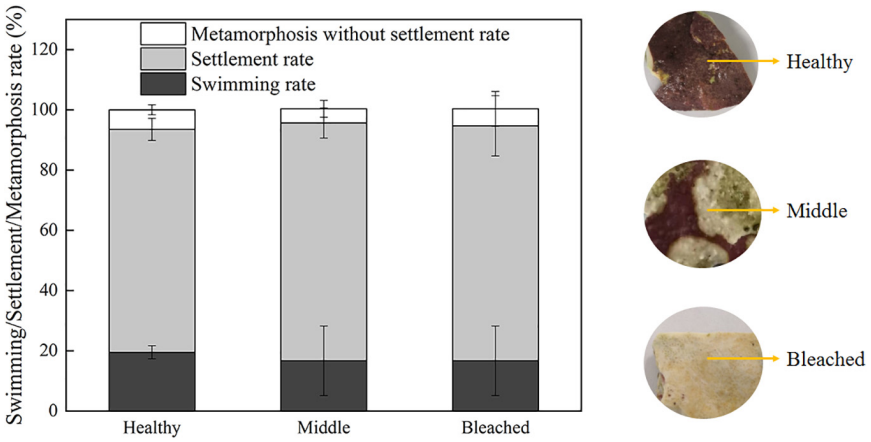

FIGURE 1 | Settlement/metamorphosis rates of *P. damicornis* larvae exposed to different health statuses of *P. onkodes* at 24 h.

larvae underwent morphological changes without attaching to the substratum when exposed to *P. onkodes* (**Supplementary Figure 1**). In the control group without cues, larvae were observed to actively swim throughout the exposure, and the settlement and metamorphosis rate was zero. These results suggested that bleached *P. onkodes* still induced larval settlement and metamorphosis.

As shown in **Figure 2**, *P. onkodes* lacking pink surface pigments induced high levels of settlement and metamorphosis (79%), which was consistent with healthy alga (p = 0.24). The result implied that the algal skeleton induced the settlement and metamorphosis of *P. damicornis* larvae rather than pink surface pigments. However, settlement rates decreased significantly when the larvae were exposed to algal extracts or autoclaved algae, especially those extracted with ethanol, methanol, and methanol/chloroform (0%). The settlement rates were 3, 23, and 26% for autoclaved algae, cold aqueous extracts, and hot aqueous extracts, respectively. Similarly, the metamorphosis rates decreased from 76% (healthy alga) to 53% (aqueous extracts). These results suggested that both the aqueous extracts and bacterial community associated with *P. onkodes* played important roles in larval settlement and metamorphosis.

Bacterial Communities Associated With Different Health Statuses of *P. onkodes*

A total of 2,444 OTUs were predicted across all samples based on the 16S RNA gene database at the cut-off level of 97% (**Supplementary Figure 2**), among which 466 OTUs existed across all groups. The middle group (1,831 OTUs) had the highest number of OTUs, whereas the lowest number of OTUs was observed in the healthy group (848). Similarly, the middle group had the highest number of specific OTUs (828), followed by the bleached (372), and healthy groups (170).

There were significant differences in the alpha diversity of bacterial community associated with different health statuses of *P. onkodes* according to the Shannon index (**Figure 2**). The diversity index of the middle group (4.54) was significantly higher than that of the healthy (4.03) and bleached groups (2.61) (**Figure 3A**, p = 0.001 and 0.042, respectively). Bacterial richness was calculated via the Ace index, which ranged from 607.5 to 1,299.5 (**Figure 3B**). Similarly, bacterial richness differed significantly between the healthy and bleached groups (p = 0.039). A significantly higher Ace index was observed in the bleached group compared with the healthy group. The Simpson's index was significantly higher in the healthy group than in the middle and bleached groups (**Figure 3C**, p = 0.006 and 0.004, respectively). There was no significant difference in the Simpson's index between the middle and bleached groups.

The beta diversity of bacterial community associated with different health statuses of *P. onkodes* was analyzed. Firstly, a

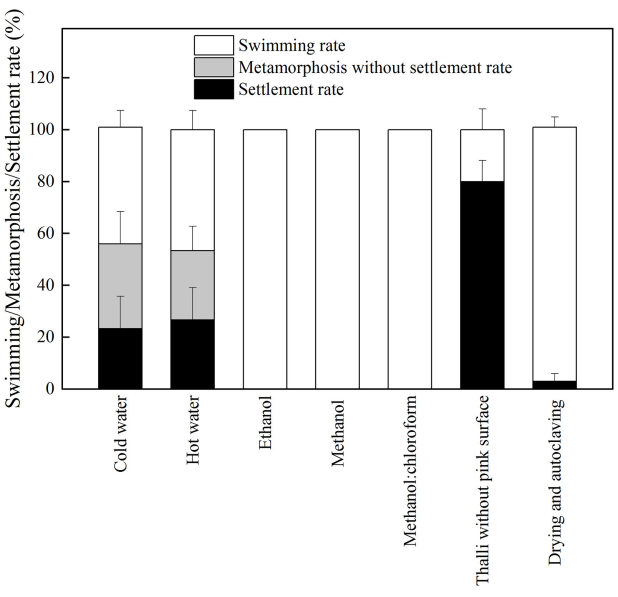

FIGURE 2 | The responses of larval settlement and metamorphosis to the treated *P. onkodes* and algal extracts at 24 h.

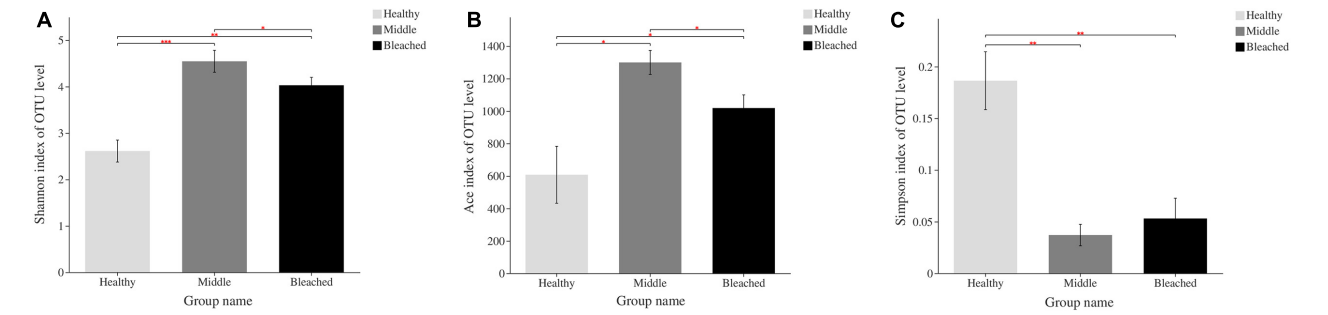

FIGURE 3 | Richness and alpha diversity of bacterial communities associated with *P. onkodes* based on **(A)** Shannon index, **(B)** Ace index, and **(C)** Simpson index. $*p \leq 0.05$, $**p \leq 0.01$, and $***p \leq 0.001$.

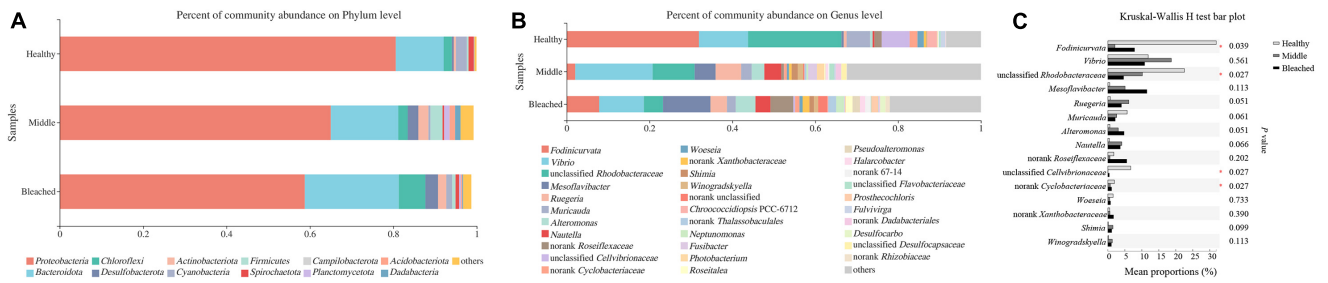

FIGURE 4 | Microbial compositions at **(A)** the phylum level, **(B)** the genus level, and **(C)** the top 15 bacterial genus groups with significant differences among different health statuses of *P. onkodes*.

hierarchical cluster tree of the bacterial community showed that the data were clustered in two distinct groups (**Supplementary Figure 3**). Group 1 contained the healthy samples, while group 2 included the middle and bleached samples. PCoA explained 67.54% of the observed variation and confirmed the output of the first method. The three samples within each group were relatively similar and clustered together. Healthy, middle, and bleached samples were grouped to the right, left, and left of the graph along PC1, respectively. The results of the two methods indicated that the middle and bleached groups had the highest level of similarity in bacterial community composition.

The bacterial community structure associated with different health statuses of *P. onkodes* was analyzed and presented in **Figure 4**. Overall, the structure of microbial communities was relatively stable among the three groups; however, the relative abundances of several bacteria differed. Specifically, the most dominant phylum was *Proteobacteria* with a relative abundance ranging from 59% in the bleached group and 81% in the healthy group (**Figure 4A**). Among *Proteobacteria*, *Alphaproteobacteria* was the predominant class, followed by *Gammaproteobacteria*. The average relative abundances of *Alphaproteobacteria* were 58, 33, and 32% in the healthy, middle, and bleached groups, respectively, while *Gammaproteobacteria* accounted for 22% (healthy group) to 31% (middle group) of the total relative abundance. *Bacteroidota*, mainly *Bacteroidetes*, was the second most dominant phylum with a relative abundance ranging from 12% in the healthy group and 22% in the bleached group. Other phyla with a relative abundance lower than 7%, including *Chloroflexi*, *Desulfobacterota*, *Actinobacteria*, *Cyanobacteria*, *Firmicutes*, and *Planctomycetes*, were also observed among all groups. As shown in **Table 1**, the Kruskal–Wallis *H*-test revealed that *Proteobacteria*, *Planctomycetota*, and *Acidobacteriota* exhibited statistically significant differences among the three groups. Additionally, the relative abundances of *Proteobacteria*, *Desulfobacterota*, *Actinobacteriota*, *Dadabacteria*, *Patescibacteria*, and *Campilobacterota* showed significant differences between the healthy and middle groups. For *Proteobacteria* and *Desulfobacterota*, there was a significant difference in their relative abundance between the healthy and bleached groups. Only the abundance of the phylum *Dadabacteria* differed significantly between the middle and bleached groups; however, the relative abundances were both lower than 2%.

As shown in **Figure 4B**, *Fodinicurvata*, *Vibrio*, *Muricauda*, unclassified *Rhodobacteraceae*, and unclassified *Cellvibrionaceae* were the predominant genera in all groups. Among these, *Fodinicurvata* decreased from 31.9% in the healthy group to 2.1% in the middle group and 7.9% in the bleached group, whereas other genera increased from 8.5% in the healthy group to 32.5% in the middle group and 22.9% in the bleached group. Similarly, the relative abundances of unclassified *Rhodobacteraceae* were 22.6, 10.1, and 4.6% in the healthy, middle, and bleached groups, respectively. The abundance of unclassified *Cellvibrionaceae* ranged from 6.7% in the healthy group to 0.0% in the bleached group. *Muricauda* accounted for 5.7, 2.5, and 2.1% of the healthy, middle, and bleached groups, respectively. The relative abundances of *Mesoflavibacter* and other genera were higher in the bleached and middle groups compared with the healthy group.

TABLE 1 | Statistical analysis of dominant bacterial phyla in bacterial communities associated with *P. onkodes*.

Phylum	*P* value			
	Among three groups	Healthy-middle	Healthy-bleached	Middle-bleached
Proteobacteria	**0.039**	**0.022**	**0.013**	0.248
Planctomycetota	**0.027**	0.059	0.124	0.114
Acidobacteriota	**0.039**	0.165	0.212	0.663
Desulfobacterota	0.061	**0.015**	**0.035**	0.454
Actinobacteriota	0.061	**0.010**	0.196	0.663
Dadabacteria	0.051	**0.021**	0.228	**0.016**
Campilobacterota	0.061	**0.000**	0.117	0.389
Patescibacteria	0.061	**0.043**	0.368	0.863

Bold numbers indicate $p < 0.05$.

Statistical analysis revealed that the relative abundances of four bacterial genera were significantly different at the genus level among the groups, and these comprised *Fodinicurvata*, unclassified *Rhodobacteraceae*, unclassified *Cellvibrionaceae*, and norank *Xanthobacteraceae* ($p < 0.05$, **Figure 4C**). As shown in **Figure 5**, the relative abundance of *Fodinicurvata* was significantly higher in the healthy group compared with the other two groups; however, no significant difference was observed between the bleached and middle groups. The bleached alga had higher percentages of norank unclassified bacteria ($p = 0.031$), *Mesoflavibacter* ($p = 0.224$), *Ruegeria* ($p = 0.088$), *Nautella* ($p = 0.224$), and *Alteromonas* ($p = 0.070$) compared with healthy alga. Additionally, the relative abundances of *Ruegeria* and *Alteromonas* in the healthy group were significantly lower than those in the middle group ($p = 0.024, 0.012$, respectively).

The PICRUSt2 program was used to predict metabolic functions in bacterial communities. At level 1, six pathways including metabolism, environmental information processing, genetic information processing, cellular processes, human diseases, and organismal systems were predicted. At level 2, the predictive pathways mainly focused on membrane transport, signal transduction, translation, carbohydrate metabolism, and infectious disease. **Figure 6A** reveals major predictive pathways at level 3. The biosynthesis of amino acids, ABC transporters, two-component system, carbon metabolism, and quorum sensing was observed in all groups. Among these pathways, quorum sensing, two-component system, bacterial secretion system, and bacterial chemotaxis may be related to larval settlement. As shown in **Figure 6B**, there were no significant differences in these pathways among groups ($p > 0.05$), which may be the main reason for the lack of change in settlement rates when coral larvae were exposed to different health statuses of *P. onkodes*. However, the function of several bacterial flora involved in disease and metabolism changed significantly among different groups (**Figure 6B**). Specifically, the expression of alcoholism, amphetamine addiction, and cocaine addiction in disease pathway; staurosporine biosynthesis and glycan biosynthesis in metabolism pathway; dopaminergic synapse and serotonergic synapse in organismal systems increased significantly in the middle and bleached groups compared with the healthy group

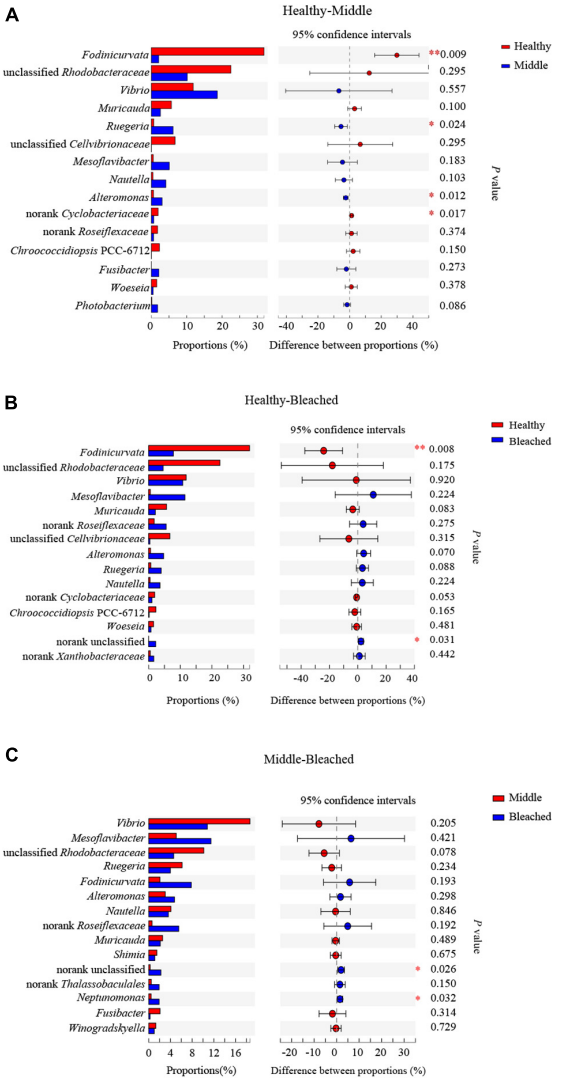

FIGURE 5 | *Post hoc* testing of bacterial genus groups with significant differences **(A)** between healthy and middle groups, **(B)** between healthy and bleached groups, and **(C)** between middle and bleached groups. *$p \leq 0.05$ and **$p \leq 0.01$.

($p < 0.05$). Conversely, the abundances of retinol metabolism, phosphonate and phosphinate metabolism, chloroalkane and chloroalkene degradation, and fluorobenzoate degradation in metabolism pathway were lower in the middle and bleached groups than those in the healthy group ($p < 0.05$).

DISCUSSION

Stability of Bacterial Communities Associated With Different Health Statuses of *P. onkodes*

Crustose coralline algae are the most abundant and important calcified macroalgae worldwide (Nelson, 2009).

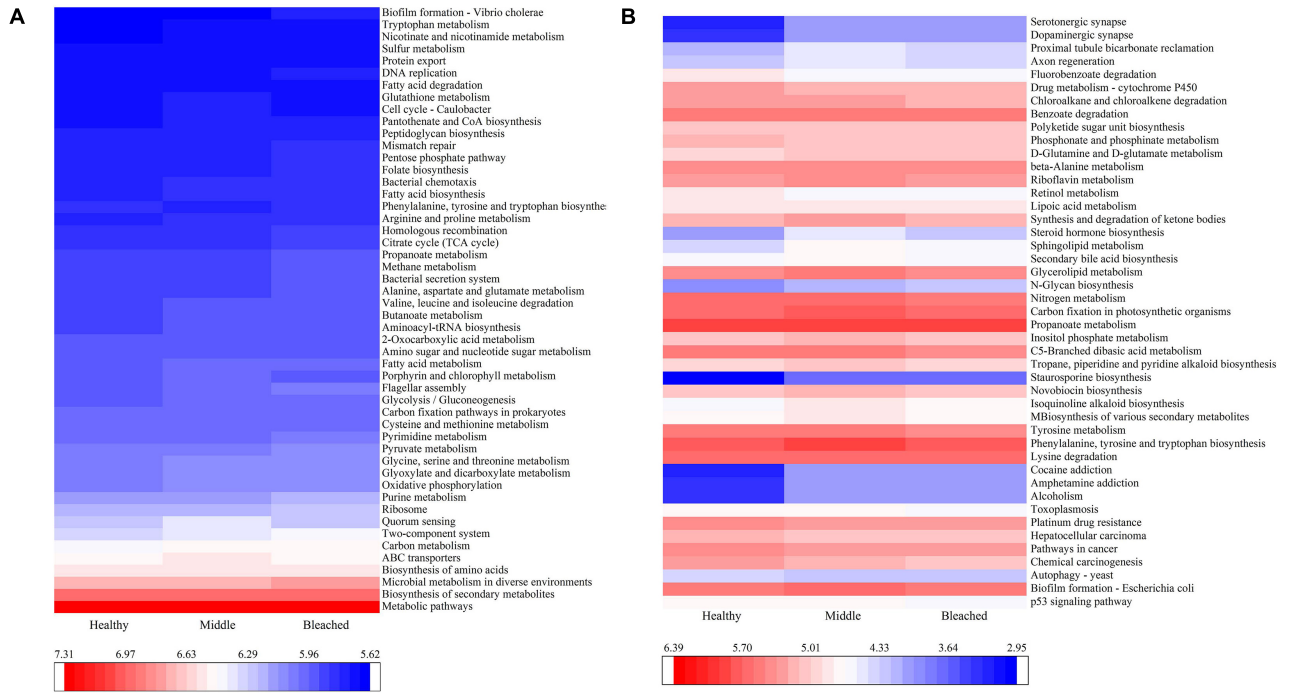

FIGURE 6 | PICRUSt2 function prediction showing **(A)** the abundances of the top 50 of predicted pathways and **(B)** the abundances of the predicted pathways involved in diseases, metabolism, cellular processes, and organismal systems with significant differences among the three *P. onkodes* groups.

It has been demonstrated that each CCA harbors a unique bacterial community (Cavalcanti et al., 2014; Sneed et al., 2015; Brodie et al., 2016). Hollants et al. (2013) reviewed 161 macroalgal–bacterial studies and reported that *Gammaproteobacteria*, *Alphaproteobacteria*, *Bacteroidetes*, *Firmicutes*, and *Actinobacteria* represented the core microbiome of these macroalgae. Sneed et al. (2015) showed that the microbiomes of four CCA species were similarly dominated by *Gammaproteobacteria*, *Alphaproteobacteria*, and *Actinobacteria* but that *Bacteroidetes* was not the most dominant phylum recorded. Different results were observed in *Corallina officinalis*, which had high abundances of *Gammaproteobacteria*, *Alphaproteobacteria*, *Bacteroidetes*, and *Flavobacteria* and a low proportion of *Firmicutes* (Brodie et al., 2016). In the present study, the bacterial communities associated with different health statuses of *P. onkodes* (i.e., healthy, middle, and bleached) were determined. We found that bacterial community compositions were similar among groups. *Alphaproteobacteria*, *Gammaproteobacteria*, and *Bacteroidetes* comprised the core bacterial microbiome members of *P. onkodes*; their relative abundance accounted for 80–90%. Additionally, *P. onkodes* had a relatively low proportion of *Actinobacteria* and lacked *Firmicutes* in its core microbiome, compared with previously reported algal species (Hollants et al., 2013). These results imply that the overall bacterial community composition associated with *P. onkodes* is relatively conserved.

The relative abundances of bacterial communities associated with algae are affected by sea water temperatures, pH, habitats, and disease (Webster et al., 2011; Miranda et al., 2013; Meistertzheim et al., 2017). Brodie et al. (2016) reported that the OTU number, Chao1 richness, and Shannon diversity index of the *C. officinalis* microbiome were significantly affected by different intertidal habitats. Greater abiotic stress experienced in the upper intertidal could enhance the overall richness and diversity in the bacterial community. Our study revealed that diversity and richness of the bacterial community based on the abundance of OTUs were correlated with algal health statuses, which increased when the alga was bleached. Additionally, there were differences in the relative abundances of several bacteria among different groups. For example, the bacterial sequences that were classified as other genera significantly increased in the bleached group, indicating that unknown genera or new pathogens increased when the *P. onkodes* was bleached. These findings suggested that the algal health status affected the relative abundance of several microbial species but did not fundamentally impact the bacterial community structure. This is consistent with the findings of Hadaidi et al. (2017), who found that coral health condition had no significant effect on bacterial community composition but detected a significant difference in abundance.

Roles of *P. onkodes*-Associated Bacterial Communities in Coral Larval Settlement and Metamorphosis

Crustose coralline algae have been shown to facilitate the settlement and metamorphosis of coral larvae (such as *Pocillopora* and *Acropora*) (Tebben et al., 2011, 2015).

However, their capacities to induce coral larval settlement and metamorphosis differ among phylogenetically distinct CCA species. For example, *P. onkodes* (formerly *Hydrolithon onkodes*) and *Porolithon gardineri* induce high levels of larval settlement, whereas *Neogoniolithon fosliei* induces a lower settlement rate at 4.7%. A potential reason for these species-specific differences is that each CCA species might harbor distinct bacterial communities or algal components that affect coral larval settlement and metamorphosis (Johnson et al., 1991; Tebben et al., 2015; Gómez-Lemos et al., 2018; Quinlan et al., 2019). Tebben et al. (2015) found that chemical cues (i.e., glycoglycerolipids and polysaccharides) derived from CCA could trigger larval settlement and metamorphosis. Recent studies have suggested that the bacterial communities associated with CCA play important roles in larval settlement (Sneed et al., 2015; Siboni et al., 2020). Coral larvae may selectively settle on CCA species through the recognition of bacterial communities on CCA (Sneed et al., 2015). To the best of our knowledge, the present study is the first to investigate the larval settlement response to different health statuses of CCA (i.e., healthy, middle, and bleached) and their bacterial community composition. Interestingly, we found that bleached *P. onkodes* could still induce the settlement and metamorphosis of coral larvae. Furthermore, the aqueous extracts of *P. onkodes* could induce larval settlement and metamorphosis; however, the settlement and metamorphosis rates were lower than those associated with healthy alga. This finding indicated that the algal extracts and CCA-associated bacterial communities play vital roles in larval settlement and metamorphosis. This raises the question of which bacteria are associated with the induction. As previously mentioned, the bacterial community composition was similar among the three groups. Furthermore, there were no significant differences in quorum sensing, two-component system, bacterial secretion system, and bacterial chemotaxis pathways among the groups in the PICRUSt2 analysis. Therefore, it is speculated that bacteria involved in these pathways may be related to the larval settlement, which is one of the potential reasons why all three groups significantly induced *P. damicornis* larval settlement.

Importance of Bacterial Communities Associated With *P. onkodes* for Algal Health

Marine bacteria have important functions for the health, performance, and resilience of multicellular organisms, as demonstrated for epiphytic bacteria associated with macroalgae (Harder et al., 2012; Egan et al., 2013; Singh and Reddy, 2014). However, their negative influences are also increasingly recognized in the disease of organisms. When homeostasis in organism-associated bacterial community is disrupted, the organism health can be affected (de Castro et al., 2010; Pollock et al., 2019). In the present study, the abundances of predicted pathways involved in infectious diseases, cell growth and death, immune system, and metabolism of other amino acids significantly changed in the diseased alga compared with healthy alga. This indicates that algal diseases affect the immune system, metabolism, growth, and death. Regarding the question of which bacteria are associated with disease, previous studies have shown that coral or macroalgal diseases are caused by multiple bacteria (Largo et al., 1995; Joyner et al., 2015). Among these bacteria, some genera of *Rhodobacteraceae* and *Rhizobiaceae*, the most dominant families in algae and coral (Wang et al., 2020), have been thought to be highly related to stony coral disease (Cárdenas et al., 2012; Meyer et al., 2019; Rosales et al., 2020). Our study revealed that the relative abundances of *Rhodobacteraceae* and *Rhizobiaceae* differed between the bleached and healthy groups. Therefore, the abundances of *Rhodobacteraceae* and *Rhizobiaceae* may be correlated with algal disease.

Bleaching disease, which is characterized by localized pigment loss, is considered to be a primary algal disease (Campbell et al., 2014). The bleaching disease of *Delisea pulchra* is one of the best-studied models (Fernandes et al., 2012; Cooper and Smith, 2015). Kumar et al. (2016) found that *Alteromonas* sp. belonging to the family *Alteromonadaceae* (*Gammaproteobacteria*) could be an opportunistic pathogen that causes the bleaching of *D. pulchra*, although healthy individuals also had a low abundance of *Alteromonas* sp. A similar result was observed in the present study whereby bleached *P. onkodes* had a higher abundance of *Alteromonas* sp. Additionally, *Nautella* and *Phaeobacter* were also considered as pathogens that cause symptomatic bleaching in algal sporelings during *in vitro* infection assays (Case et al., 2011; Fernandes et al., 2011; Campbell et al., 2014). In the current study, *Nautella* and *Phaeobacter* were not found in the healthy group, but *Nautella* was present in the semi-bleached and bleached groups. Therefore, it is speculated that *Nautella* and *Alteromonas* may be potential pathogens capable of causing algal bleaching. Further investigation into multiple pathogens resulting in algal bleaching is warranted.

In conclusion, relatively stable bacterial communities were observed in bleached, middle semi-bleached, and healthy *P. onkodes*. *Alphaproteobacteria*, *Gammaproteobacteria*, and *Bacteroidetes* were the dominant phyla in all algal samples, although there were apparent differences in the relative abundance of bacterial phyla. These abundant and ubiquitous bacterial taxa were identified as core bacterial microbiome members of *P. onkodes*. Furthermore, and noteworthy, the bleaching of *P. onkodes* did not affect the coral larval settlement of *P. damicornis*, which was likely related to its conserved bacterial communities. Additionally, there was a lower relative abundance of *Fodinicurvata* and higher relative abundances of *Mesoflavibacter*, *Ruegeria*, *Nautella*, and *Alteromonas* in the bleached alga compared with healthy alga. Therefore, *Nautella* and *Alteromonas* may be potential pathogens that result in algal bleaching.

DATA AVAILABILITY STATEMENT

The datasets presented in this study can be found in online repositories. The names of the repository/repositories and

accession number(s) can be found below: https://www.ncbi.nlm.nih.gov/, BioProject ID PRJNA685315.

AUTHOR CONTRIBUTIONS

FY designed and performed the experiments, analyzed the data, and wrote the manuscript. ZX and ZW participated in larval settlement assays. LL conceived the experiments and revised the manuscript. All authors contributed to manuscript writing and provided final approval for publication.

FUNDING

This work was supported by the National Natural Science Foundation of China (41806145), the Strategic Priority Research Program of the Chinese Academy of Sciences (XDA13020203), and the National Key Research and Development Program of China (2018YFC1406505).

SUPPLEMENTARY MATERIAL

The Supplementary Material for this article can be found online at: https://www.frontiersin.org/articles/10.3389/fmicb.2021.646143/full#supplementary-material

Supplementary Figure 1 | Coral larvae exposed to **(A)** healthy, **(B)** middle, and **(C)** bleached *P. onkodes*. Red arrows represent different health statuses of *P. onkodes*, while green arrows indicate coral larvae.

Supplementary Figure 2 | Venn diagram showing the number of OTUs in healthy, middle, and bleached *P. onkodes* based on the 16S RNA gene database at the cut-off level of 97%.

Supplementary Figure 3 | The beta diversity of bacterial communities associated with *P. onkodes* based on a hierarchical cluster tree and principal coordinates analysis (PCoA). The values of axes 1 and 2 represent the percentages that can be explained by the corresponding axis.

Supplementary Table 1 | Analysis of variance on larval settlement/metamorphosis/swimming rates exposed to different health statuses of *P. onkodes*.

REFERENCES

Anthony, K. R. N., Kline, D. I., Diaz-Pulido, G., Dove, S., and Hoegh-Guldberg, O. (2008). Ocean acidification causes bleaching and productivity loss in coral reef builders. *PNAS* 105, 17442–17446. doi: 10.1073/pnas.0804478105

Bessell-Browne, P., Negri, A. P., Fisher, R., Clode, P. L., and Jones, R. (2017). Impacts of light limitation on corals and crustose coralline algae. *Sci. Rep.* 7:11553. doi: 10.1038/s41598-017-11783-z

Bourne, D. G., and Munn, C. B. (2005). Diversity of bacteria associated with the coral Pocillopora damicornis from the Great Barrier Reef. *Environ. Microbiol.* 7, 1162–1174.

Brodie, J., Williamson, C., Barker, G. L., Walker, R. H., Briscoe, A., and Yallop, M. (2016). Characterising the microbiome of Corallina officinalis, a dominant calcified intertidal red alga. *FEMS Microbiol. Ecol.* 92:fiw110.

Campbell, A. H., Vergés, A., and Steinberg, P. D. (2014). Demographic consequences of disease in a habitat-forming seaweed and impacts on interactions between natural enemies. *Ecology* 95, 142–152. doi: 10.1890/13-0213.1

Cárdenas, A., Rodriguez-R, L. M., Pizarro, V., Cadavid, L. F., and Arévalo-Ferro, C. (2012). Shifts in bacterial communities of two Caribbean reef-building coral species affected by white plague disease. *ISME J.* 6, 502–512. doi: 10.1038/ismej.2011.123

Case, R. J., Longford, S. R., Campbell, A. H., Low, A., Tujula, N., Steinberg, P. D., et al. (2011). Temperature induced bacterial virulence and bleaching disease in a chemically defended marine macroalga. *Environ. Microbiol.* 13, 529–537. doi: 10.1111/j.1462-2920.2010.02356.x

Cavalcanti, G. S., Gregoracci, G. B., Santos, E. O. D., Silveira, C. B., Meirelles, P. M., Longo, L. L., et al. (2014). Physiologic and metagenomic attributes of the rhodoliths forming the largest CaCO3 bed in the South Atlantic Ocean. *ISME J.* 8, 52–62. doi: 10.1038/ismej.2013.133

Cooper, M. B., and Smith, A. G. (2015). Exploring mutualistic interactions between microalgae and bacteria in the omics age. *Curr. Opin. Plant. Biol.* 26, 147–153. doi: 10.1016/j.pbi.2015.07.003

Cornwall, C. E., Diaz-Pulido, G., and Comeau, S. (2019). Impacts of ocean warming on coralline algal calcification: meta-analysis, knowledge gaps, and key recommendations for future research. *Front. Mar. Sci.* 6:186. doi: 10.3389/fmars.2019.00186

de Castro, A. P., Araújo, S. D., Reis, A. M. M., Moura, R. L., Francini-Filho, R. B., Pappas, G. Jr., et al. (2010). Bacterial community associated with healthy and diseased reef coral Mussismilia hispida from Eastern Brazil. *Microb. Ecol.* 59, 658–667. doi: 10.1007/s00248-010-9646-1

Dean, A. J., Steneck, R. S., Tager, D., and Pandolfi, J. M. (2015). Distribution, abundance and diversity of crustose coralline algae on the Great Barrier Reef. *Coral Reefs.* 34, 581–594. doi: 10.1007/s00338-015-1263-5

Egan, S., Harder, T., Burke, C., Steinberg, P., Kjelleberg, S., and Thomas, T. (2013). The seaweed holobiont: understanding seaweed–bacteria interactions. *FEMS Microbiol. Rev.* 37, 462–476. doi: 10.1111/1574-6976.12011

Fernandes, N., Case, R. J., Longford, S. R., Seyedsayamdost, M. R., Steinberg, P. D., Kjelleberg, S., et al. (2011). Genomes and virulence factors of novel bacterial pathogens causing bleaching disease in the marine red alga Delisea pulchra. *PLoS One* 6:e27387. doi: 10.1371/journal.pone.0027387

Fernandes, N., Steinberg, P., Rusch, D., Kjelleberg, S., and Thomas, T. (2012). Community structure and functional gene profile of bacteria on healthy and diseased thalli of the red seaweed Deliseapulchra. *PLoS One* 7:e50854. doi: 10.1371/journal.pone.0050854

Gómez-Lemos, L. A., Doropoulos, C., Bayraktarov, E., and Diaz-Pulido, G. (2018). Coralline algal metabolites induce settlement and mediate the inductive effect of epiphytic microbes on coral larvae. *Sci. Rep.* 8:17557.

Hadaidi, G., Röthig, T., Yum, L. K., Ziegler, M., Arif, C., Roder, C., et al. (2017). Stable mucus-associated bacterial communities in bleached and healthy corals of Porites lobate from the Arabian Seas. *Sci. Rep.* 7:45362. doi: 10.1038/srep45362

Harder, T., Campbell, A. H., Egan, S., and Steinberg, P. D. (2012). Chemical mediation of ternary interactions between marine holobionts and their environment as exemplified by the red alga Delisea pulchra. *J. Chem. Ecol.* 38, 442–450. doi: 10.1007/s10886-012-0119-5

Harrington, L., Fabricius, K., De'ath, G., and Negri, A. (2004). Recognition and selection of settlement substrata determine post-settlement survival in corals. *Ecology* 85, 3428–3437. doi: 10.1890/04-0298

Harriott, V. J. (1983). Reproductive seasonality, settlement, and post-settlement mortality of *Pocillopora damicornis* (Linnaeus), at Lizard Island, Great Barrier Reef. *Coral Reefs.* 2, 151–157. doi: 10.1007/BF00336721

Hollants, J., Leliaert, F., De Clerck, O., and Willems, A. (2013). What we can learn from sushi: a review on seaweed-bacterial associations. *FEMS Microbiol. Ecol.* 83, 1–16. doi: 10.1111/j.1574-6941.2012.01446.x

Johnson, C. R., Sutton, D., Olson, R., and Giddins, R. (1991). Settlement of crown-of-thorns starfish: role of bacteria on surfaces of coralline algae and a hypothesis for deepwater recruitment. *Mar. Ecol. Prog. Ser.* 71, 143–162.

Joyner, J. L., Sutherland, K. P., Kemp, D. W., Berry, B., Griffin, A., Porter, J. W., et al. (2015). Systematic analysis of white pox disease in Acropora palmata of the Florida Keys and role of *Serratia marcescens*. *Appl. Environ. Microbiol.* 81, 4451–4457. doi: 10.1128/AEM.00116-15

Kumar, V., Zozaya-Valdes, E., Kjelleberg, S., Thomas, T., and Egan, S. (2016). Multiple opportunistic pathogens can cause a bleaching disease in the red seaweed Delisea pulchra. *Environ. Microbiol.* 18, 3962–3975.

Kushmaro, A., Loya, Y., Fine, M., and Rosenberg, E. (1996). Bacterial infection and coral bleaching. *Nature* 380, 396–396. doi: 10.1038/380396a0

Largo, D. B., Fukami, K., and Nishijima, T. (1995). Occasional pathogenic bacteria promoting ice-ice disease in the carrageenan-producing red algae Kappaphycus alvarezii and Eucheuma denticulatum (Solieriaceae, Gigartinales, Rhodophyta). *J. Appl. Phycol.* 7, 545–554. doi: 10.1007/BF00003941

Latif, S., Bibi, S., Kouser, R., Fatimah, H., Farooq, S., Naseer, S., et al. (2020). Characterization of bacterial community structure in the rhizosphere of Triticum aestivum L. *Genomics* 112, 4760–4768. doi: 10.1016/j.ygeno.2020.07.031

Li, Y. F., Yang, N., Liang, X., Yoshida, A., Osatomi, K., Power, D., et al. (2018). Elevated seawater temperatures decrease microbial diversity in the gut of Mytilus coruscus. *Front. Physiol.* 10:839. doi: 10.3389/fphys.2018.00839

Martone, P. T., Alyono, M., and Stites, S. (2010). Bleaching of an intertidal coralline alga: untangling the effects of light, temperature, and desiccation. *Mar. Ecol. Prog. Ser.* 416, 57–67. doi: 10.3354/meps08782

Meistertzheim, A. L., Nugues, M. M., Quéré, G., and Galand, P. E. (2017). Pathobiomes differ between two diseases affecting reef building coralline algae. *Front. Microbiol.* 8:1686. doi: 10.3389/fmicb.2017.01686

Meron, D., Atias, E., Kruh, L. I., Elifantz, H., Minz, D., Fine, M., et al. (2011). The impact of reduced pH on the microbial community of the coral Acropora eurystoma. *ISME J.* 5, 51–60. doi: 10.1038/ismej.2010.102

Meyer, J. L., Castellanos-Gell, J., Aeby, G. S., Häse, C. C., Ushijima, B., and Paul, V. J. (2019). Microbial community shifts associated with the ongoing stony coral tissue loss disease outbreak on the florida reef tract. *Front. Microbiol.* 10:2244. doi: 10.3389/fmicb.2019.02244

Miranda, L. N., Hutchison, K., Grossman, A. T., and Brawley, S. H. (2013). Diversity and abundance of the bacterial community of the red macroalga Porphyra umbilicalis: did bacterial farmers produce macroalgae? *PLoS One* 8:e58269. doi: 10.1371/journal.pone.0058269

Morse, D. E., and Hooker, N. (1988). Control of larval metamorphosis and recruitment in sympatric agariciid corals. *J. Exp. Mar. Biol. Ecol.* 116, 193–217. doi: 10.1016/0022-0981(88)90027-5

Nelson, W. (2009). Calcified macroalgae–critical to coastal ecosystems and vulnerable to change: a review. *Mar. Freshw. Res.* 60, 787–801.

Ordoñez, A., Wangpraseurt, D., Lyndby, N. H., Kühl, M., and Diaz-Pulido, G. (2019). Elevated CO2 leads to enhanced photosynthesis but decreased growth in early life stages of reef building coralline algae. *Front. Mar. Sci.* 5:495. doi: 10.3389/fmars.2018.00495

Osman, E. O., Suggett, D. J., Voolstra, C. R., Pettay, D. T., Clark, D. R., Pogoreutz, C., et al. (2020). Coral microbiome composition along the northern Red Sea suggests high plasticity of bacterial and specificity of endosymbiotic dinoflagellate communities. *Microbiome* 8:8. doi: 10.1186/s40168-019-0776-5

Pollock, F. J., Lamb, J. B., van de Water, J. A. J. M., Smith, H. A., Schaffelke, B., Willis, B. L., et al. (2019). Reduced diversity and stability of coral-associated bacterial communities and suppressed immune function precedes disease onset in corals. *R. Soc. Open Sci.* 6:190355. doi: 10.1098/rsos.190355

Quéré, G., Intertaglia, L., Payri, C., and Galand, P. E. (2019). Disease specific bacterial communities in a coralline algae of the Northwestern Mediterranean Sea: a combined culture dependent and-Independent approach. *Front. Microbiol.* 10:1850. doi: 10.3389/fmicb.2019.01850

Quinlan, Z. A., Ritson-Williams, R., Carroll, B. J., Carlson, C. A., and Nelson, C. E. (2019). Species-specific differences in the microbiomes and organic exudates of crustose coralline algae influence bacterioplankton communities. *Front. Microbiol.* 10:2397. doi: 10.3389/fmicb.2019.02397

Rajasabapathy, R., Ramasamy, K. P., Manikandan, B., Mohandass, C., and James, R. A. (2020). Bacterial communities associated with healthy and diseased (skeletal growth anomaly) reef coral Acropora cytherea from Palk Bay, India. *Front. Mar. Sci.* 7:92. doi: 10.3389/fmars.2020.00092

Rosales, S. M., Clark, A. S., Huebner, L. K., Ruzicka, R. R., and Muller, E. M. (2020). *Rhodobacterales* and *Rhizobiales* are associated with stony coral tissue loss disease and its suspected sources of transmission. *Front. Microbiol* 11:681. doi: 10.3389/fmicb.2020.00681

Siboni, N., Abrego, D., Puill-Stephan, E., King, W. L., Bourne, D. G., Raina, J. B., et al. (2020). Crustose coralline algae that promote coral larval settlement harbor distinct surface bacterial communities. *Coral Reefs.* 39, 1703–1713. doi: 10.1007/s00338-020-01997-5

Singh, R. P., and Reddy, C. R. K. (2014). Seaweed-microbial interactions: key function of seaweed-associated bacteria. *FEMS Microb. Ecol.* 88, 213–230. doi: 10.1111/1574-6941.12297

Sneed, J. M., Ritson-Williams, R., and Paul, V. J. (2015). Crustose coralline algal species host distinct bacterial assemblages on their surfaces. *ISME J.* 9, 2527–2536. doi: 10.1038/ismej.2015.67

Tebben, J., Motti, C. A., Siboni, N., Tapiolas, D. M., Negri, A. P., Schupp, P. J., et al. (2015). Chemical mediation of coral larval settlement by crustose coralline algae. *Sci. Rep.* 5:10803. doi: 10.1038/srep10803

Tebben, J., Tapiolas, D. M., Motti, C. A., Abrego, D., Negri, A. P., Blackall, L. L., et al. (2011). Induction of larval metamorphosis of the coral Acropora millepora by tetrabromopyrrole isolated from a Pseudoalteromonas bacterium. *PLoS One* 6:e19082. doi: 10.1371/journal.pone.0019082

van der Heijden, L. H., and Kamenos, N. A. (2015). Reviews and syntheses: calculating the global contribution of coralline algae to total carbon burial. *Biogeosciences* 12, 6429–6441. doi: 10.5194/bg-12-6429-2015

Wang, J., Lu, J., Zhang, Y., and Wu, J. (2020). Microbial ecology might serve as new indicator for the influence of green tide on the coastal water quality: assessment the bioturbation of Ulva prolifera outbreak on bacterial community in coastal waters. *Ecol. Indic.* 113:106211. doi: 10.1016/j.ecolind.2020.106211

Webster, N. S., Soo, R., Cobb, R., and Negri, A. P. (2011). Elevated seawater temperature causes a microbial shift on crustose coralline algae with implications for the recruitment of coral larvae. *ISME J.* 5, 759–770. doi: 10.1038/ismej.2010.152

White, J. R., Nagarajan, N., and Pop, M. (2009). Statistical methods for detecting differentially abundant features in clinical metagenomic samples. *PLoS Comput. Biol.* 5:e1000352. doi: 10.1371/journal.pcbi.1000352

Whitman, T. N., Negri, A. P., Bourne, D. G., and Randall, C. J. (2020). Settlement of larvae from four families of corals in response to a crustose coralline alga and its biochemical morphogens. *Sci. Rep.* 10:16397. doi: 10.1038/s41598-020-73103-2

Yang, F., Mo, J., Wei, Z., and Long, L. (2021). Calcified macroalgae and their bacterial community in relation to larval settlement and metamorphosis of reef-building coral Pocillopora damicornis. *FEMS Microbiol. Ecol.* 97:fiaa215. doi: 10.1093/femsec/fiaa215

Zheng, X. Q., Li, Y. C., Liang, J. L., Lin, R. C., and Wang, D. R. (2021). Performance of ecological restoration in an impaired coral reef in the Wuzhizhou Island, Sanya, China. *J. Oceanol. Limnol.* 39, 135–147. doi: 10.1007/s00343-020-9253-z

Zozaya-Valdes, E., Egan, S., and Thomas, T. (2015). A comprehensive analysis of the microbial communities of healthy and diseased marine macroalgae and the detection of known and potential bacterial pathogens. *Front. Microbiol.* 6:146. doi: 10.3389/fmicb.2015.00146

Conflict of Interest: The authors declare that the research was conducted in the absence of any commercial or financial relationships that could be construed as a potential conflict of interest.

frontiers in Microbiology

ORIGINAL RESEARCH
published: 10 June 2021
doi: 10.3389/fmicb.2021.609482

Screening of Tomato Seed Bacterial Endophytes for Antifungal Activity Reveals Lipopeptide Producing *Bacillus siamensis* Strain NKIT9 as a Potential Bio-Control Agent

Ayushi Sharma[1,2], Nutan Kaushik[1], Abhishek Sharma[1], Abhay Bajaj[3†], Mandar Rasane[3], Yogesh S. Shouche[3], Takwa Marzouk[4] and Naceur Djébali[4]*

[1] Amity Food and Agriculture Foundation, Amity University Uttar Pradesh, Noida, India, [2] Amity Institute of Microbial Technology, Amity University Uttar Pradesh, Noida, India, [3] National Centre for Microbial Resource, National Centre for Cell Science, Pune, India, [4] Centre of Biotechnology of Borj Cedria, Laboratory of Bioactive Substances, Hammam-lif, Tunisia

The current study investigates the diversity pattern and fungicidal potential of bacterial endophytes isolated from two different organic varieties of tomato plants (V1 and V2). A total of seventy-five bacterial isolates identified by 16S rRNA gene sequencing revealed a majority of genus as *Bacillus* and one *Planococcus,* which were grouped into eight different species. The Shannon diversity H' (1.56), Simpson's index of diversity (0.93), Magalef' index (2.23), Evenness (0.96), and Species richness (7) indicated the high endophytic bacterial diversity in the V1 variety of the tomato. Bacterial endophytes isolated from both of the varieties were screened for their antifungal activity against five economically critical fungal pathogens (viz., *Botrytis cinerea*, *Rhizoctonia solani*, *Fusarium solani*, *Verticillium lateritium,* and *Alternaria solani*) of tomato crop through dual culture assay. The data revealed *B. siamensis* strain NKIT9 as the most potent antagonist, significantly ($p < 0.05$) inhibiting the mycelial growth between 75 to 90% against selected fungal pathogens. High bioactivity of lipopeptide extract of strain NKIT9 was recorded against *R. solani* with minimum IC_{50} value of 230 μg/ml. The Ultra Performance Liquid Chromatography-High Definition Mass Spectrometry (UPLC-HDMS) analysis of this lipopeptide extract revealed the presence of Surfactin and Bacillomycin D. Furthermore, *in-vitro* results showed that the selected bacterial strain significantly minimized the disease incidence in damping-off assay which makes this strain a promising antifungal bio-control agent. Moreover, in the pot experiment the NKIT9 increased the fruit yield by 59.2% compared with the untreated *R. solani* infested control.

Keywords: crop protection, bio-pesticide, diversity indices, plant growth promotion, UPLC, antagonistic

OPEN ACCESS

Edited by:
Alan John Lander Phillips, Universidade de Lisboa, Portugal

Reviewed by:
George Newcombe, University of Idaho, United States
Prem Lal Kashyap, Indian Institute of Wheat and Barley Research (ICAR), India
Manoj Kumar Solanki, University of Silesia in Katowice, Poland

****Correspondence:***
Nutan Kaushik
kaushikn2008@gmail.com; nkaushik5@amity.edu

†Present address:
Abhay Bajaj, CSIR-National Environmental Engineering Research Institute (CSIR-NEERI), Nagpur, India

Specialty section:
This article was submitted to Microbe and Virus Interactions with Plants, a section of the journal Frontiers in Microbiology

Received: *23 September 2020*
Accepted: *23 April 2021*
Published: *10 June 2021*

Citation:
Sharma A, Kaushik N, Sharma A, Bajaj A, Rasane M, Shouche YS, Marzouk T and Djébali N (2021) Screening of Tomato Seed Bacterial Endophytes for Antifungal Activity Reveals Lipopeptide Producing Bacillus siamensis Strain NKIT9 as a Potential Bio-Control Agent. Front. Microbiol. 12:609482. doi: 10.3389/fmicb.2021.609482

INTRODUCTION

Tomato (*Solanum lycopersicum*) is a well-known vegetable crop due to its high nutritional values, which suffers from various fungal infestation diseases. Its succulent fruit increases its susceptibility toward fungal attacks compared to other crop plants, which is a critical limiting factor in its production (Habiba et al., 2017). The major phytopathogens responsible for damaging this crop include *Rhizoctonia solani*, *Fusarium solani, Botrytis cinerea, Alternaria solani,* and *Verticillium sp.* because of their diverse host spectra and soil-borne existence, fungal phytopathogens are difficult to control (Lamichhane et al., 2017). *R. solani* is one of the most important and widespread soil-borne phytopathogenic fungi causing yield losses in more than 200 crops around the world (Sturrock et al., 2015) via seedling damping-off and crown rot (Montealegre et al., 2010; Zamoum et al., 2017). *A. solani* can cause serious damage during all stages of plant growth (Attia et al., 2020). It has been reported to damage photosynthesis and pigment content, resulting in substantial growth inhibition and thus a major reduction in yield (Agamy et al., 2013). Gray mold, caused by *B. cinerea*, is a significant and persistent threat to tomatoes grown in fields and greenhouses in many countries around the world (Soylu et al., 2010). Site-specific fungicides such as benzimidazoles, dicarboximides, and Nphenylcarbamate were predominantly used to control gray fungus (Leroux et al., 2002). While synthetic fungicides are successful, their prolonged or persistent use has weakened biological control by natural enemies, resulting in disease outbreaks and widespread production of fungicide resistance (Soylu et al., 2010).

Soil-borne diseases caused by fungi such as *F. solani* are often a significant crop production constraint. *F. solani* is responsible for root rot in tomato plants (Shenashen et al., 2017). Chitin-containing pathogens including *F. solani* and *A. solani* cause the most damage to crop plants among fungal pathogens and can become chemical fungicide resistant (Badrhadad et al., 2018). *Verticillium*, a soil-borne fungus, causes serious vascular disease in a wide range of vegetable crops. In dead or dying plant tissues, *Verticillium* species develop long-lasting settling structures such as microsclerotia, chlamydospores, and resting mycelium (Deketelaere et al., 2017). Such resting complexes act as the primary inoculum, forming hyphae that penetrate the roots of host plants directly (Deketelaere et al., 2017). The use of chemical fungicides is the most common strategy to prevent fungal pathogens (Windels and Brantner, 2005). The prolonged use of chemicals has led to the development of resistance in phytopathogens, such as Fluazinam, fentin chloride, fludioxonil, difenoconazole, 28 cyazofamid, chlorothalonil, and 2, 4-dinitrophen, which have all been reported to cause multi drug resistance in *R. solani* (Cheng et al., 2020).

Seeds are the key structures of plants that help them to not only reproduce over time, but also to survive stress in the most effective way possible; as a result, seeds play an important role in agriculture (Guan et al., 2009). Seeds harbor bacterial endophytes (López et al., 2018) which play an essential task in managing plant health and diseases (Hazarika et al., 2019) by reducing pathogen population densities without stimulating hypersensitive reactions in the host (Roy et al., 2017; Hazarika et al., 2019). Bacterial endophyte composition varied among plants, organs, genotypes, tissues, cultivars, soil, and location (Kumar et al., 2020). The rhizosphere or phyllosphere work as a source for several endophytes; nevertheless, some bacterial species have been reported as having vertical transmission through seeds (Truyens et al., 2014). Plants choose unique microbial communities to establish association, such as rice plants grown in neutral-pH soil supporting seed-borne *Pseudomonas oryzihabitans* and *Rhizobium radiobacter*, while plants grown in low-pH soil favor *Enterobacter*-like and *Dyella ginsengisoli* (Hardoim et al., 2012). The potential benefits of endophytic bacteria are close to those of rhizosphere bacteria (Ryan et al., 2008) including serving as biological control agents (Hong and Park, 2016). Many endophytic bacteria, mainly *Bacillus* species, exhibit antagonistic ability toward fungal pathogens. Studies have reported the antifungal ability of *Bacillus subtilis* SCB-1 against diverse fungal pathogens, including the *Alternaria* and *Fusarium* (Hazarika et al., 2019). In another study, volatile organic compounds of highly antagonistic *Bacillus* strains were reported against *Sclerotinia sclerotiorum* (Massawe et al., 2018). *Bacillus* species is becoming an attractive agent for commercial use in modern farming systems (Piggot and Hilbert, 2004; Tiago et al., 2004) due to their heat and UV resistant spore forming capacity which can withstand adverse environmental conditions.

In the present study, the diversity of the endophytic bacteria isolated from the various tissues of two different organic tomato varieties was evaluated for its bio-control potential against tomato pathogens.

MATERIALS AND METHODS

Seed Collection

Two organic tomato varieties were used in this study for the isolation of bacterial endophytes. Both the varieties, i.e., Pusa Ruby (Maharashtra) (V1) and a local variety of Andhra Pradesh (Madanapalle) (V2) were procured from the online garden stores, Ugaoo and Organic Garten, respectively.

Isolation of Bacterial Endophytic Strains

Surface sterilization of tomato seeds was performed following the method described by Kumar et al. (2011). Briefly, seeds were first sterilized with 70% ethanol for 2 min, followed by a 1% sodium hypochlorite solution for 3 min. After that, surface-sterilized seeds were washed three times with autoclaved distilled water and dried with sterile blotting paper. For sterility check, imprints of dry surface-sterilized seeds were taken on Luria-Bertani agar medium (10 g Peptone 140; 5 g Yeast Extract; 5 g Sodium Chloride; 12 g Agar) (Vinodkumar et al., 2018). Seeds were then put for germination on sterile filter paper immersed with autoclaved distilled water in a petri dish at 27°C. For isolation (Chimwamurombe et al., 2016), seedlings obtained after the 9 days of germination were again surface sterilized with the method described above. After the sterility check, each seedling was cut into different sections viz., root, hypocotyl, and cotyledon. Each part was further divided into various

segments and placed on the Luria-Bertani agar plate. Plates were then incubated for 2–3 days at 27°C. Visually distinct bacterial colonies acquired from segmented seedlings were purified and maintained in Nutrient agar slants/plates and glycerol stock at 4 and −80°C, respectively. The identification of the most active strain among the isolates was further confirmed with endospore staining as per the method of Aneja (2003).

Molecular Identification of Bacterial Endophytes and Phylogenetic Analysis

The identification of isolates was carried out at the Sequencing facility of the National Centre for Microbial Resource (NCMR), National Centre for Cell Science, Pune. DNA extraction and purification was done using HiPurA 96 Bacterial Genomic DNA Purification Kit (Himedia), as per the manufacturer's protocol; followed by amplification of the 16S rRNA gene using universal bacterial primers (27F and 1492R). PCR amplification was performed with initial denaturation for 5 min at 94°C followed by 30 cycles of 30 s denaturation at 94°C, 30 s of primer annealing at 55°C, 1 min elongation at 72°C, and final extension of 7 min at 72°C. Amplified products were sequenced by the Sanger method on ABI 3730xl Genetic Analyzer (Applied BioSystems). The sequences were aligned and evaluated for taxonomic identification by BLASTn analysis (Boratyn et al., 2013). The phylogenetic tree was reconstructed by doing alignment using Muscle and the evolutionary history inferred using the neighbor-joining (NJ) method. A tree with 100 bootstrap replicates was constructed using MEGA-7 (Kumar et al., 2016).

Diversity Indices of Bacterial Endophytes

Bacterial endophytes derived from organic tomato seedlings were grouped into their specific isolation sections, such as hypocotyl, root, and cotyledon, which facilitated the comparison between the isolates of the same or other variety. Species diversity was calculated using the Shannon diversity index to measure species evenness and richness (Chowdhary and Kaushik, 2019).

$$H' = -\sum_{i=1}^{s} p_i \mathrm{In}(p_i)$$

Where, S equals the number of species, and pi equals the ratio of individuals of species i divided by all individuals N of all species. The Shannon diversity index ranges typically from 1.5 to 3.5 and rarely reaches 4.5. Simpson's index (D) was calculated to determine the dominance, the higher the value lower in the diversity (Ifo et al., 2016).

$$D = \sum_{i=1}^{s} \left(\frac{\mathrm{n_i}(\mathrm{n_i}-1)}{\mathrm{N}(\mathrm{N}-1)} \right)$$

Where, n_i is the number of individuals in the i^{th} species and N equals the total number of individuals and Simpson's index of diversity was calculated b

$$D' = (1 - D)$$

Other parameters, such as species evenness and richness, were also calculated (Ifo et al., 2016). Margalef's index (d) also indicates the evenness (Kumar et al., 2006).

$$d = \frac{(S-1)}{In(N)}$$

S is the total number of species; N is the number of individuals, and the natural logarithm.

To measure the similarity in the species composition for both varieties of tomato, we used Sorenson's index of similarity using the equation,

$$QS = 2a/(2a + b + C)$$

and, Jaccard's index of similarity using the equation,

$$JS = a/(a + b + C)$$

Whereas, "a" denotes the number of bacterial species commonly shared by both the varieties, "b" denotes the number of bacterial species found in V1, and "c" denotes the number of bacterial species found in V2 (Chowdhary and Kaushik, 2015).

In-vitro Antifungal Activity of Bacterial Endophytes

All the bacterial isolates were screened for their antagonistic activity against major pathogenic fungi of the tomato crop, namely, *R. solani* (ITCC-6430), *F. solani* (ITCC-6731), *B. cinerea* (ITCC-6011), *A. solani* (ITCC-4632), and *V. lateritium* (ITCC-2819) obtained from Indian Type Culture Collection (ITCC) at Indian Agricultural Research Institute (IARI), Pusa, New Delhi, India. Isolates were evaluated by dual culture assay on Potato Dextrose Agar (PDA) medium (Slama et al., 2019). A fully grown 7 mm fungal disc was placed in the center of the PDA plate in an inverted position to aid the contact of the fungal mycelium with the culture medium, while bacterial isolate was streaked on both sides of the fungal disc at equidistance. A PDA plate inoculated only with the fungal disc was kept as the control. After 5–7 days of incubation, plates were observed for the antagonism expressed by endophytic bacteria, and percentage growth inhibition was calculated. Experiment was performed in the replication of three. Growth inhibition (GI) was calculated as per the following:

$$\mathrm{GI} = \{(\mathrm{A} - \mathrm{B})/\mathrm{A}\} \times 100$$

Where, A = radial growth of the plant pathogenic fungus in control; B = radial growth of the plant pathogenic fungus in the presence of endophytic bacterial strain (dual inoculation). Amongst all the isolates, only *B. siamensis* strain NKIT9 showed the highest antifungal activity against all test pathogens. Therefore, the *B. siamensis* strain NKIT9 was selected for further studies.

Extraction and Identification of Lipopeptide

The endophytic bacteria *B. siamensis* strain NKIT9, with the most promising antagonistic activity against all the test pathogenic fungi, was further explored for the production of antifungal lipopeptides. The lipopeptide extraction method involved acid precipitation and solvent extraction, as described

by Romano et al. (2011). Briefly, extraction of lipopeptide from a cell-free supernatant was done by precipitation method at pH 2 using 6N HCl and incubated at 4°C overnight and then centrifuged at 12,000 rpm for 15 min at 4°C. The pellet was dissolved in a solvent mixture of Chloroform: Methanol (2:1, v/v) followed by centrifugation for at 12000 rpm for 15 min at 4°C to remove any undissolved extract. The lipopeptides present in the supernatant were filtered and concentrated to dryness by rotary evaporation. Waters ACQUITY Ultra Performance Liquid Chromatography (UPLC) H-class system with the BEH C18 column was employed for lipopeptide profiling. The lipopeptide extract (10 mg) was dissolved in 10 mL of HPLC grade ethanol and filtered through 0.22 μm PVDF membrane syringe filter (Durapore, Merk), and a 10 μL aliquot of the sample was injected into the column and the column was eluted at a flow rate of 0.3 ml/min with 100% methanol at 0 min and gradually increased the polarity to acetonitrile: methanol (40:60) for 4 min which was further retained for 22 min followed by 100% methanol for 25 min. The lipopeptides were detected by mass spectroscopy using positive ionization electrospray (ESI+) Synapt G2-Si High Definition Mass Spectrometer (HDMS) coupled with the UPLC system.

Antifungal Bioassay of the Lipopeptides

The lipopeptide extracted from cell free supernatant of bacterial *B. siamensis* strain NKIT9 was tested against all five phytopathogenic fungi viz. *R. solani, F. solani, B. cinerea, A. solani*, and *V. lateritium,* by poisoned food technique (Ibrahim et al., 2017). From a 40 mg/ml stock solution prepared in methanol, the extract was added to autoclaved molten PDA at the final extract concentration of 50, 100, 250, 500, and 1000 μg/ml to prepare the agar plates. The fungal pathogens were inoculated by placing a 7 mm agar disc at the center of every petri plate in an inverted position for the greater contact of fungal mycelium and were incubated at 27°C for 5 days under dark conditions. Eight replicates were used for each concentration. In parallel, PDA mixed with 250 μl of methanol inoculated with fungal disc served as the control. Percentage of growth inhibition (% GI) was calculated by comparing the radial distance of fungal growth toward each spot inoculation with ethanol control. IC_{50} was calculated using regression equation analysis.

In vivo Bio-Control Assay

Bio-Priming of Tomato Seeds

Tomato seeds (Pusa Ruby) were surface sterilized by the above described method. Surface sterilized seeds were bio-primed with pure culture of *B. siamensis* strain NKIT9, with the microbial load adjusted to $\geq 10^8$ cfu/ml by diluting with sterile saline water. In contrast, uncoated surface-sterilized seeds were kept as the control. Seeds were then kept for incubation with continuous agitation (150–200 rpm) at 27°C for 24 h (Xia et al., 2015). Bio-primed seeds were placed on sterile blotting paper and air dried in laminar air-flow.

Damping-Off Assay

Based on the in vitro antifungal activities, strain NKIT9 was selected for *in vivo* assay for bio-control of damping-off of tomato seedlings caused by *R. solani*. Experiment was carried out in germination trays (Hyco trays) with ten cavities in each. Six treatments were performed:

T1: Surface-sterilized seeds only (control),

T2: Surface-sterilized seeds + fungal pathogen (*R. solani*),

T3: Bio-primed seeds only (for growth promoting activity),

T4: Bio-primed seeds + fungal pathogen,

T5: Bio-primed seeds + fungal pathogen + soil treatment of the bacterial strain NKIT9,

T6: Chemical treated seeds (Bavistin-Carbendazim) + fungal pathogen (chemical control);

There were nine replicates for each treatment with 10 seedlings in each replicate. In the chemical control, sterilized seeds were treated with Carbendazin 50% WP as recommended by the manufacturer (2 g/kg of sterilized seeds) for 1 h before sowing (Adhikari et al., 2015). For each treatment, one tomato seed was sown per cavity of the tray as per the treatments. Each tray was filled with an autoclaved mix of cocopeat: vermiculite: perlite (2:1:1). The pathogen inoculation was done with sorghum seeds colonized by *R. solani* with a spore density of 10^4 cfu/g (Khan and Anwer, 2007; Paul, 2018). For the application of strain NKIT9 in the soil, 72 h old bacterial culture pellets were washed and re-suspended in distilled water and applied to the tray mix (10^9 CFU/ml) (Szczech and Shoda, 2006). Trays containing tomato seeds were kept under standard conditions in a plant growth room with 23–27°C temperature and 12 h of photo period (Goudjal et al., 2014) and moisture was maintained by spraying tap water as per the requirement for seed germination. After 15 days of germination, germination and disease percentage were calculated, shoot length was measured, and seedling fresh weight was estimated.

Pot Experiment

Pot experiment of the tomato seeds (Pusa Ruby) was carried out in a greenhouse condition with temperatures ranging from 23–30°C and relative humidity from 60–85%, in a Completely Randomized Design (CRD). Six treatments were conducted in pot trial as described above (T1–T6) with 16 replicates for each treatment. However, in this case soil treatment with the pathogen in treatment T2 and T4 and the soil treatment of the bio-control agent in treatment T5 were given in the pot after the transplantation and no treatment was given at the nursery stage except bio-priming of the seed.

Seeds (bio-primed/non-primed seeds) were sown in hyco trays containing an autoclaved mix of cocopeat: vermiculite: perlite (2:1:1). Trays containing tomato seeds were kept under standard conditions in a plant growth room with a maintained temperature of 23–27°C and 12 h of photo period as mentioned above. Trays were watered with spraying tap water as per the requirement to maintain the moisture level favorable for seeds and the seedling. The seedlings were maintained in the trays until the four-leaf stage and then transplanted in the pots as described below.

Sandy loam soil was used for the pot study. Pot mix comprising soil and farm yard manure (2:1) was autoclaved in polypropylene plastic bags. The pots (10 inches) were filled with the pot mix and watered before sowing. For pathogen infested

soil, *R. solani* inoculated sorghum seeds were mixed with the pot mix (3 g/kg) (Asaka and Shoda, 1996). Pots were then watered with sterile distilled water and incubated at room temperature for 5 days to enhance the growth of the pathogen. Plate count method was used to evaluate the density of *R. solani* in the infested soil (10^4 CFU/g). Seedlings from the hyco trays as mentioned above were transplanted into the pots, and each pot contained one seedling. Plants were observed for number of leaves, plant height, number of flowers, and fruit yield for 70 days (from the date of sowing).

Data Analysis

The aligned 16S rRNA gene sequences were curated and trimmed to infer the evolutionary history with 100 bootstrap replicates in the NJ method. Heatmap was produced through online software Heatmapper[1]. The data of in planta assays were analyzed by IBM SPSS Statistics 20. One-way ANOVA analysis of variance was performed for damping-off bio-control assay and pot experiment. To analyze the significant difference among the groups was determined by Post hoc different examination test (Duncan's Multiple Range test).

RESULTS

Isolation, Identification, and Phylogenetic Analysis

Seventy five bacterial endophytes were isolated from the various tissues of root, hypocotyl, and cotyledon of tomato plants of both the organic varieties (V1 and V2) using the culture-dependent technique. The majority of the isolates (60%) were obtained from the V1 variety. All the 75 isolates were grouped into eight species on the basis of 16S rRNA gene sequencing based molecular identification. Comparing the two varieties, Pusa ruby (V1) harbored all the eight species identified while the local variety (V2) possessed less diverse endophytic populations as only four species inhabited it. All the bacterial isolates belonged to the phylum Firmicutes. The details of isolates according to their closest and representative species concerning identification, accession number, similarity percentage, and source are summarized in **Supplementary Table 1**. In the V1 variety, *Bacillus safensis* (strains NKIT1, NKIT2, NKIT4-8, NKIT11, NKIT15-20, NKIT22-23, NKIT25, NKIT27, NKIT30, NKIT31, NKIT34, NKIT35, NKIT37, NKIT41, NKIT43, and NKIT45) and *B. siamensis* (strains NKIT9, NKIT12, NKIT14, NKIT21, NKIT24, NKIT26, NKIT28, and NKIT29) were the dominant species with relative abundance (RA) of 57.8 and 17.8%, respectively. The majority of isolates belong to the genus *Bacillus* except for one non-bacillus species, which was isolated from V1 and was identified as a member of the genus *Planococcus* (NKIT38). In V2, *Bacillus australimaris* (strains NKIT51, NKIT52, NKIT55, NKIT58, NKIT59, NKIT62, NKIT68-70, NKIT72, NKIT73, and NKIT75) and *B. safensis* (strains NKIT46, NKIT48-50, NKIT53, NKIT54, NKIT57, NKIT60, NKIT65, NKIT66, and NKIT74) were the dominant species with RA of 40 and 36.7%, respectively (**Figure 1**). In V1 isolates, only two endophytic bacterial species, namely *B. safensis* and *B. siamensis*, were isolated from all the three parts of tomato seedling such as root (strains NKIT4, NKIT11, NKIT12, NKIT17, NKIT19, NKIT20, NKIT25, NKIT31, NKIT34, and NKIT45), hypocotyls (NKIT1, NKIT2, NKIR6-9, NKIT14-16, NKIT18, NKIT21, NKIT26-29, NKIT35, NKIT37, NKIT41 and NKIT43), and cotyledon (NKIT5, NKIT22, NKIT23, and NKIT24), and other bacterial endophytic species were only exclusive to one or two tissues. However, three out of four species isolated from the V2 variety, namely, *B. safensis*, *B. australimaris,* and *Bacillus zhangzhouensis,* were found to inhabit all the three parts of tomato seedling such as root (NKIT46, NKIT51, NKIT56, NKIT64, NKIT67, NKIT68, and NKIT71), hypocotyls (NKIT49, NKIT50, NKIT55, NKIT59, NKIT60, NKIT62, NKIT63, NKIT66, and NKIT74), and cotyledon (NKIT47, NKIT48, NKIT52-54, NKIT57, NKIT58, NKIT70, NKIT72, NKIT73, and NKIT75), whereas, *Bacillus amyloliquefaciens* (strain NKIT61) was found only in the root region. According to BLAST analysis of sequenced 16S rRNA gene homology and phylogenetic analysis using the NJ approach with 100 bootstrap sampling, strain NKIT9 shared 99.16% identity with a variety of *B. siamensis* strains in the NCBI database. A phylogenetic tree based on 16S rRNA gene sequences was drawn, and it clearly showed strain NKIT9 as *B. siamensis* (**Figure 2**). Moreover, the endospore staining confirmed that it belongs to *Bacillus* genus (**Supplementary Figure 1**).

Distribution, Diversity, and Richness of Bacterial Endophytes

Diversity indices calculated between the bacterial endophytes isolated from each tissue of the two varieties of tomato plants used in the study are shown in **Table 1**. Shannon diversity (H') was maximum in the cotyledon (1.56) and hypocotyls (1.34) of V1 variety. Least diversity was reported in the root region of V1 variety (0.83). Simpson's index of diversity was maximum in the cotyledon (0.93) of V1, followed by root (0.77) of V2. Species richness was determined by counting the number of species in each group and was found at its maximum in hypocotyl ($n = 7$) of V1 variety followed by the cotyledon ($n = 5$) and root ($n = 4$) of V1. Magalef' index, calculated to estimate the evenness between the species of both the types, was found to be highest in cotyledon (2.23) of V1 variety. Species shared between V1 and V2 were highest in hypocotyl, resulting in a high value of Sorenson's similarity index (0.37) (**Table 2**). A Venn diagram illustrated the species' number and the relationship between the isolated species within the same variety (**Figure 3**). Interestingly, the V1 variety of tomato (Pusa Ruby) contains a more diverse population of endophytic bacteria as compared to V2 (**Table 1**).

Antifungal Activity of the Isolated Endophytic Bacteria

All the bacterial endophytes isolated from the two organic tomato varieties were screened for their antifungal activity against five economically important fungal pathogens of tomato crop viz. *R. solani, V. lateritium*, *B. cinerea, A. solani,* and

[1]www.heatmapper.ca

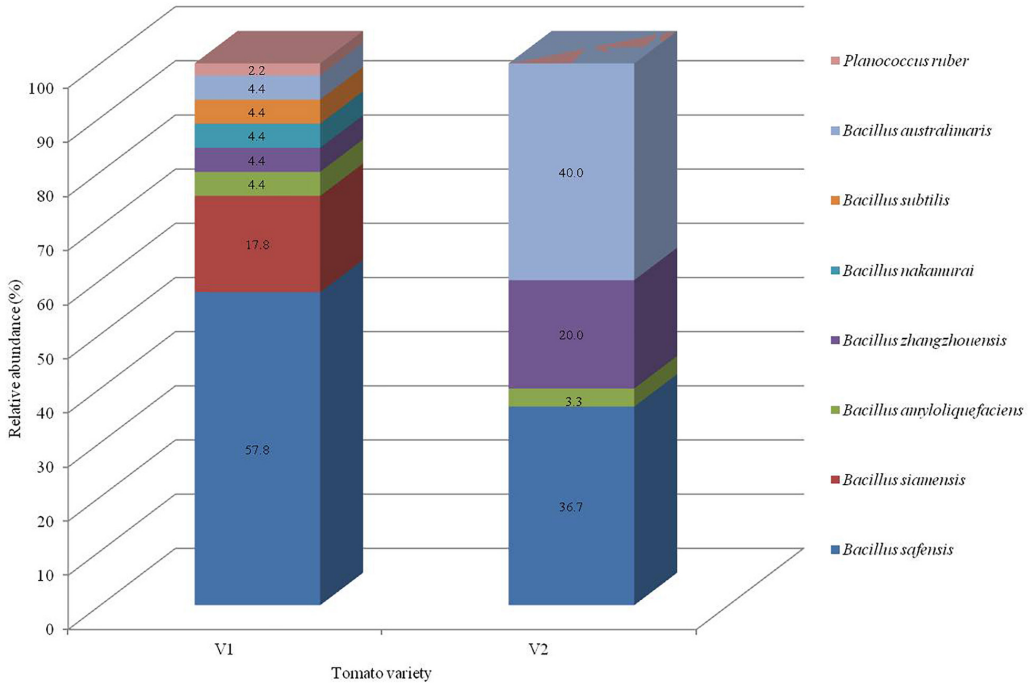

FIGURE 1 | Taxonomic profiles of the bacterial community in each variety at the representative species level with the relative abundance.

F. solani through dual culture assay (**Figures 4A,B** and **Supplementary Tables 2, 3**). The dual culture bioassay's key purpose was based on a bio-prospecting strategy to select potential endophytes with antifungal activity. Among all the isolates of V1, strain NKIT9 exhibited the highest antifungal activity with percentage growth inhibition values ranging from 75-90%, against all the five major pathogens of the tomato crop (**Figure 5**). The zone of inhibition persisted for up to 7 days of inoculation. To the best of our knowledge, this is the first report on the antifungal activity of endophytic *Bacillus siamensis* strain NKIT9 isolated from the organic varieties of tomato.

B. amyloliquefaciens strain NKIT10 was found to be the next best species. The activity pattern of *B. safensis* varied from strain to strain. The most active strain of *B. safensis viz. B. safensis* strain NKIT46 isolated from variety V2 recorded >70% growth inhibition activity against *R. solani* and *A. solani.* Simultaneously, strains of *B. australimaris*, *B. nakamurai*, and *B. zhangzhouensis* showed very low to nil activity against the selected pathogens. Heatmap dendrogram revealed that the antifungal activity of the tested strains against *R. solani* positively correlated with *A. solani* while activity against *B. cinerea* correlated with activity against *F. solani*. It shows the antagonism between the test fungi and the isolated bacterial strain of V1 and V2 (**Supplementary Figure 2**). The z-score clustering facilitates the bacterial species relationship between the isolates in relation to the antifungal activity.

The endophytic population from variety V1 has been observed to be more antagonistic against all the five pathogenic fungi than the V2. None of the endophytes were found active against all the five test pathogens. More than 68% of endophytic bacteria of V1 suppressed the growth of *R. solani* in the dual culture assay with antagonistic activity up to 90%. Meanwhile, 15% of its population showed the antagonistic effect against all the test pathogens with over 60 or more than 60% inhibition.

Antifungal Activity of Extracted Lipopeptide

In this study, the results showed that the lipopeptide extract of the bacterial strain NKIT9 inhibited the growth of all test fungi with an IC_{50} value of 230, 276.2, 346.6, 470.5, and 329.9 μg/ml against *R. solani, V. lateritium, B. cinerea, F. solani,* and *A. solani,* respectively. A dose response with an R^2 value of 0.867 and 100% growth inhibition of *R. solani* was observed at 1000 μg/ml extract of NKIT9 (**Figure 6**). The IC_{50} values were obtained using regression equation (**Supplementary Figures 3A–E**). The lipopeptide extract of strain NKIT9 was found to be most active against *R. solani* as compared to other test fungi with an IC_{50} value of 230 μg/ml. Based on the results of the dual culture assay and lipopeptide bioassay, *R. solani* was selected as the test fungi for *in vivo* tests for damping-off disease control and green house trial.

Lipopeptide Profiling by UPLC-HDMS

To identify the lipopeptides present in the extract obtained from the bacterial strain NKIT9, Chromatographic separation and Mass Spectrometry of lipopeptide extract was performed on UPLC-H class with a Synapt G2-Si-High Definition Mass Spectrometry (HDMS) system. The UPLC total ion chromatogram of the bacterial extract is shown in **Figure 7A**. **Figure 7B** reveals the mass spectrum of the analyte showing

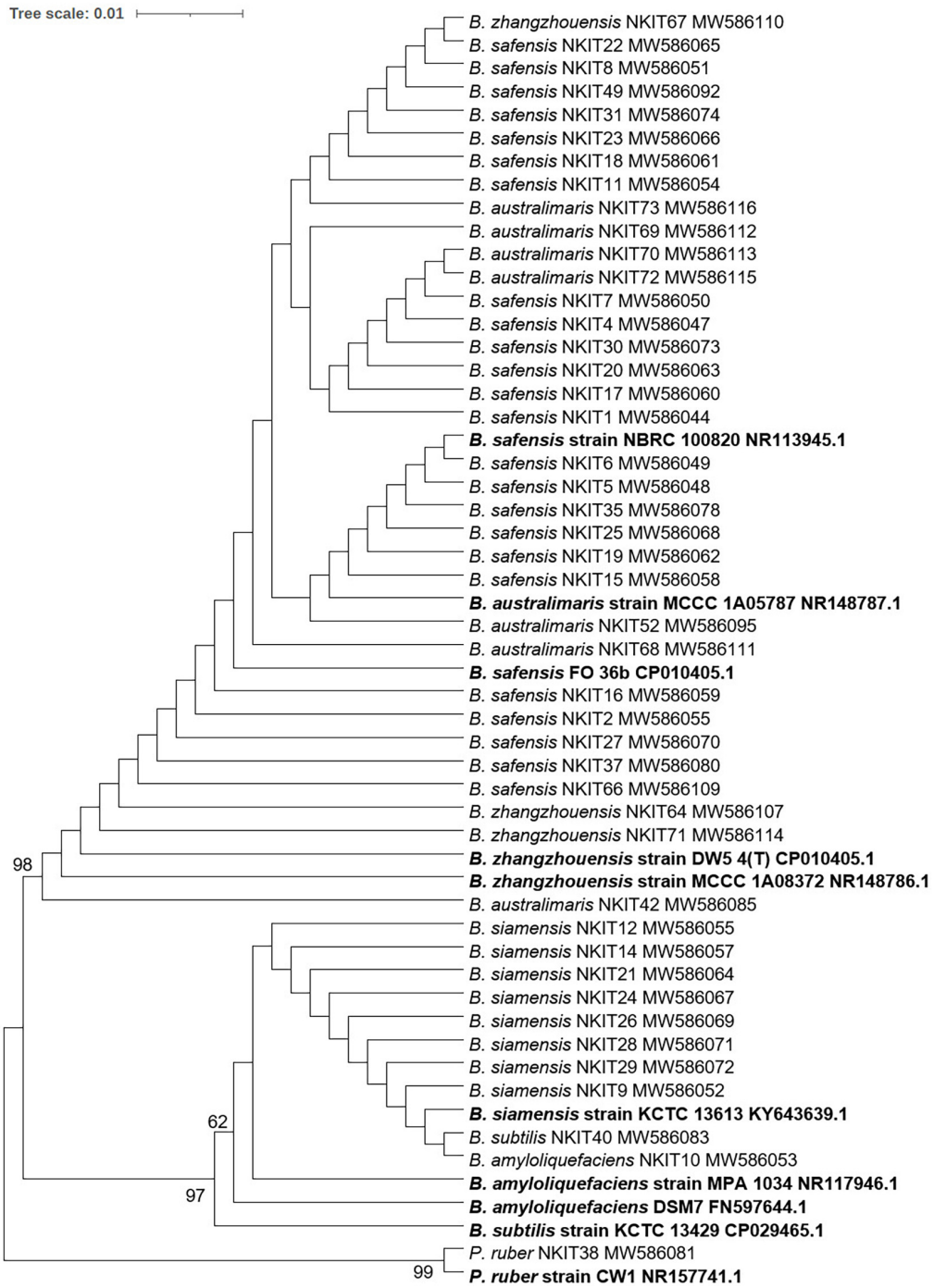

FIGURE 2 | Evolutionary relationships of bacterial isolates investigated in this study: Phylogenetic tree was constructed using 16S rRNA gene sequences and the bootstrap values (100 replicates) are indicated (BS > 50) at the nodes. Closest neighbor of strain NKIT38, *Planococcus ruber* strain CW1 was used outgroup. The evolutionary history was inferred using the NJ method. The optimal tree with the sum of branch length = 0.07256030 is shown. The evolutionary distances were computed using the Maximum Composite Likelihood method and are in the units of the number of base substitutions per site. The analysis involved 55 nucleotide sequences. All positions containing gaps and missing data were eliminated. There were a total of 545 positions in the final dataset. Evolutionary analyses were conducted in MEGA7.

the presence of the molecular peaks at m/z 994.8, 1008.77, 1022.72, 1036.74, 1050.75, 1064.77, 1096.86, 1045.77, 1059.79, and 1079.81. These masses were assigned to C12 Surfactin [M + H+]+, C13 Surfactin [M + H+]+, C14 Surfactin [M + H+]+, C15 Surfactin [M + H+]+, C16, Surfactin [M + H+]+, C17 Surfactin [M + H+]+, linear C18

TABLE 1 | Species diversity analysis of the bacterial isolated from V1 and V2 variety of tomato.

	V1			V2		
	Hypocotyl	Root	Cotyledon	Hypocotyl	Root	Cotyledon
Shannon diversity	1.34	0.83	1.56	0.93	1.28	0.91
Simpson's index	0.34	0.54	0.06	0.36	0.22	0.38
Simpson's index of diversity	0.65	0.45	0.93	0.63	0.77	0.62
Margalef' index	1.82	1.20	2.23	0.91	1.30	0.83
Evenness	0.68	0.59	0.96	0.85	0.92	0.83
Species richness	7.00	4.00	5.00	3.00	4.00	3.00

TABLE 2 | Comparison of different similarity indices among various regions of two organic varieties of tomato.

V1 vs. V2	Species shared	Jaccard's SI	Sorensen's SI
Root	1.00	0.10	0.20
Hypocotyl	3.00	0.23	0.37
Cotyledon	2.00	0.20	0.33

Surfactin and, C15 Bacillomycin D [M + H+]+ respectively (**Supplementary Table 4**). The general molecular structures of the isolated antifungal lipopeptides are presented in **Figure 8**.

Damping-Off Assay

The highest percentage of germination (96.7%) was observed in the treatment T3 (Bio-primed seeds) with no diseased plant. While the highest percentage of the diseased (72.2%) seedlings was observed in the treatment T2 (Surface sterilized seeds treated with fungal pathogen). Desiccation of the roots was observed in germinated seeds and young seedlings due to damping-off symptoms (**Supplementary Figure 4**). Treatments 4 (Bio-primed seeds + fungal pathogen) and T5 (Bio-primed seeds + fungal pathogen + soil treatment of the bacterial strain NKIT9) observed the second best treatment after T3 with only 28.9% and 27.8% diseased plants, respectively (**Table 3**). Chemical treatment was found to be less effective than the introduced bio-control agent in the control of damping-off disease of tomato seedlings. Compared with the positive control, the seed treatment with strain NKIT9 enhanced the seedling shoot length from 2.23 cm to 7.79 cm (**Figure 9A**) and seedling fresh weight from 12.6 mg to 33.2 mg and (**Figure 9B**). These findings suggest that strain NKIT9 can help in protecting tomato seedlings from damping-off and promoting the plant growth.

Pot Experiment

Under greenhouse conditions, the strain NKIT9 showed strong control of *R. solani*. According to the results of plant growth promotion treatment, *B. siamensis* strain NKIT9 had a noticeable effect on tomato plant growth in a greenhouse. Interestingly bio-primed seeds treated with fungal pathogen (T4) recorded highest yield, plant height, buds, flowers, and fruits followed by T3 and T5 (**Table 4**). Fungicide treated seeds recorded yield comparable to T2. The plant height increased by 58.9% and the number of flowers increased by 62.2% as compared to T2 (**Figure 10**). T5 treatment plants showed statistically similar growth patterns compared to the chemical control (T6). These findings suggested that the strain NKIT9 could successfully control the *R. solani in vivo* and could be used as a bio-control agent.

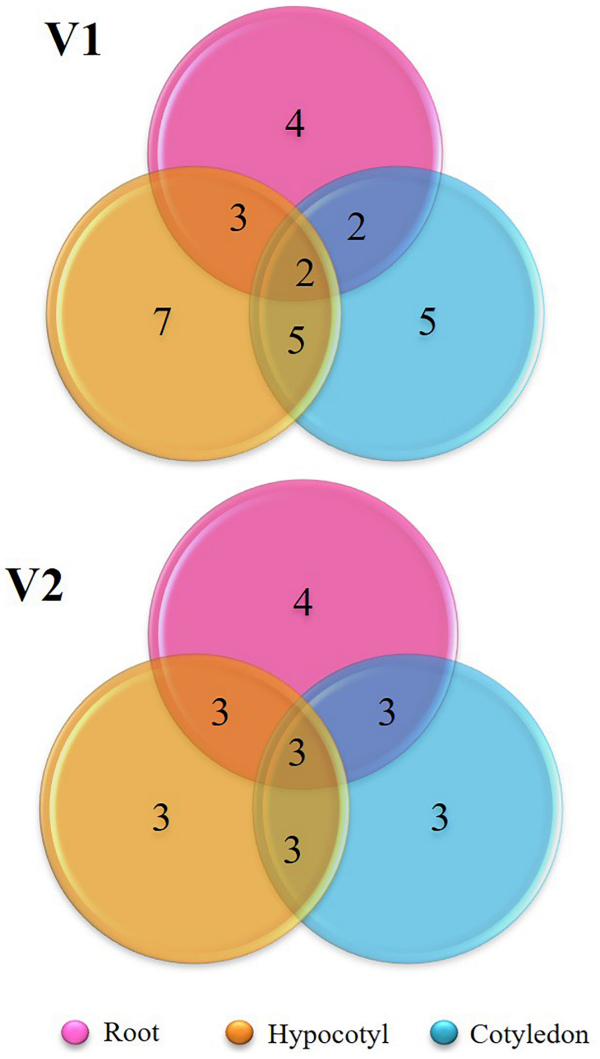

FIGURE 3 | Venn diagram representing the shared species of isolated bacterial endophytes within the variety.

DISCUSSION

The present research explores two organic tomato varieties for diversity of endophytic bacteria and their antifungal ability against selected fungal pathogens. This is the first report on the diversity study of endophytic bacteria from organic tomato plants. The seedlings of the V1 tomato plant variety were

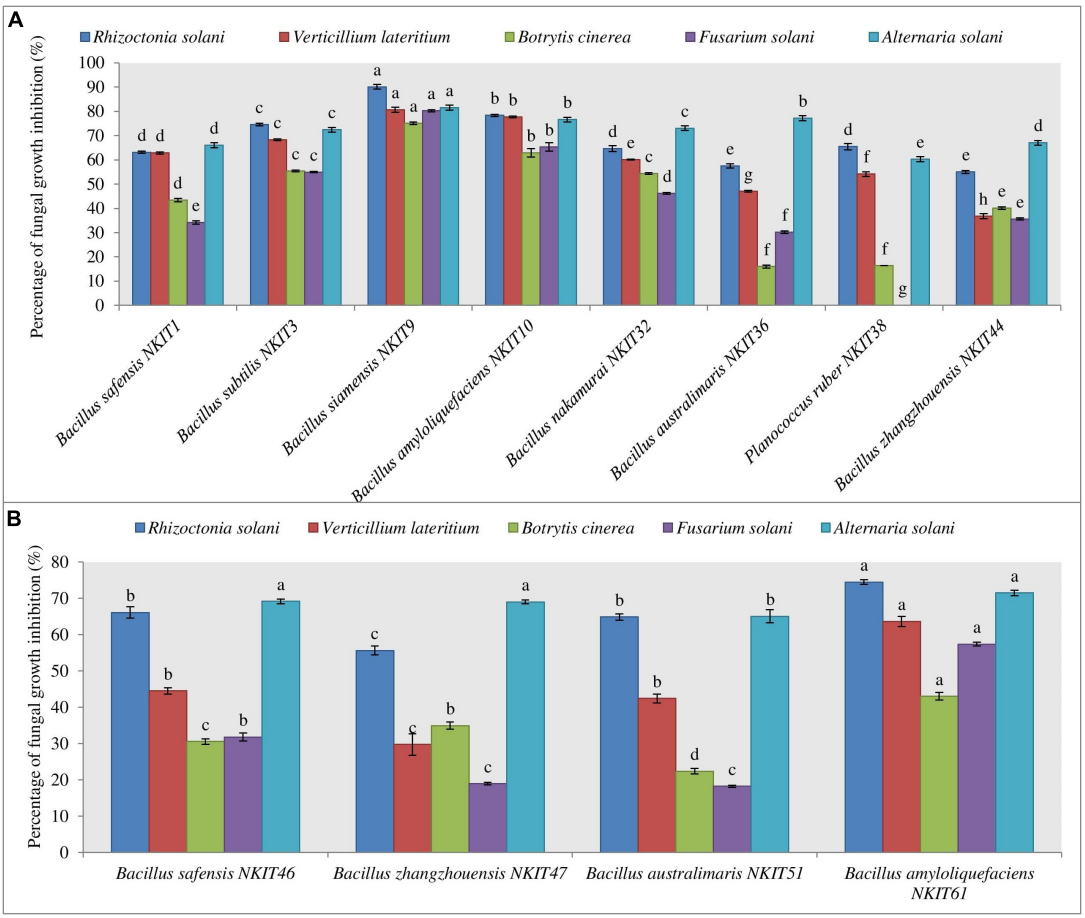

FIGURE 4 | Antagonistic effect against five pathogenic test fungi. **(A)** Graph for the antifungal activity of bacterial endophytes isolated from V1 variety seeds. **(B)** Graph for the antifungal activity of bacterial endophytes isolated from V2 variety seeds. Three replicates were used for the assay. Bars labeled with the same letters are not significantly different according to Duncan Multiple Range Test at $p = 0.05$. Vertical lines represent the standard errors of the mean.

found to have high species abundances and the diversity of bacterial endophytes. The plausible reason for the disparity in endophyte diversity between the two tomato plant varieties could be the variations in the rhizospheric microbiome that probably contribute to differential bacterial colonization in the plant endosphere (Compant et al., 2010; Liu et al., 2017). Species richness was found at its maximum in the hypocotyl of the seedling ($n = 7$) of V1. Evenness was found at its maximum in V1 cotyledon (0.96). A value for evenness approaching zero reflects large differences in the abundance of species, whereas, an evenness of one means all species are equally abundant. These findings indicate that endophytic bacteria can exhibit a tissue-specific distribution, which has also been reported from other systems (Reinhold-Hurek and Hurek, 2011; Thomas and Reddy, 2013; Xia et al., 2015). Previous studies have shown the species specificity of endophytes. The difference in endophytic assemblies in different tissue types can be due to the difference in their potential to use the substrate (Huang et al., 2008; Chowdhary and Kaushik, 2015). Yang et al. (2011) reported 72 bacterial endophytes, including 45 from the stem and 27 from the healthy tomato plant leaves, and found *Brevibacillus brevis* W4, an endophyte antagonistic to *B. cinerea*. We believe that different agro-climatic locations (V1 from Maharashtra and V2 from Andhra Pradesh) resulted in endophytic population variations in the current study. The bacterial strains isolated from the tomato seedlings must contain the same phylum of the bacterial population as those present in seeds (López et al., 2018). These findings indicate that tomato seeds can comprise a fundamental group of bacteria that are likely to reach seeds during their reproductive development, and play specific roles in seed or seedling growth (López et al., 2018). Firmicutes, the phylum that mostly colonizes seeds, grew faster in seedlings, implying that seed germination offers a nutritional benefit that boosts this group's development. Some of the bacteria found in seeds, such *as Bacillus,* are known to produce endospores, which may explain their high occurrence in seeds (López et al., 2018). The host genotype is reported to play an essential role in managing the associated plant microorganisms, particularly the endophytes (Lundberg et al., 2012; Podolich et al., 2015; Upreti and Thomas, 2015). Also,

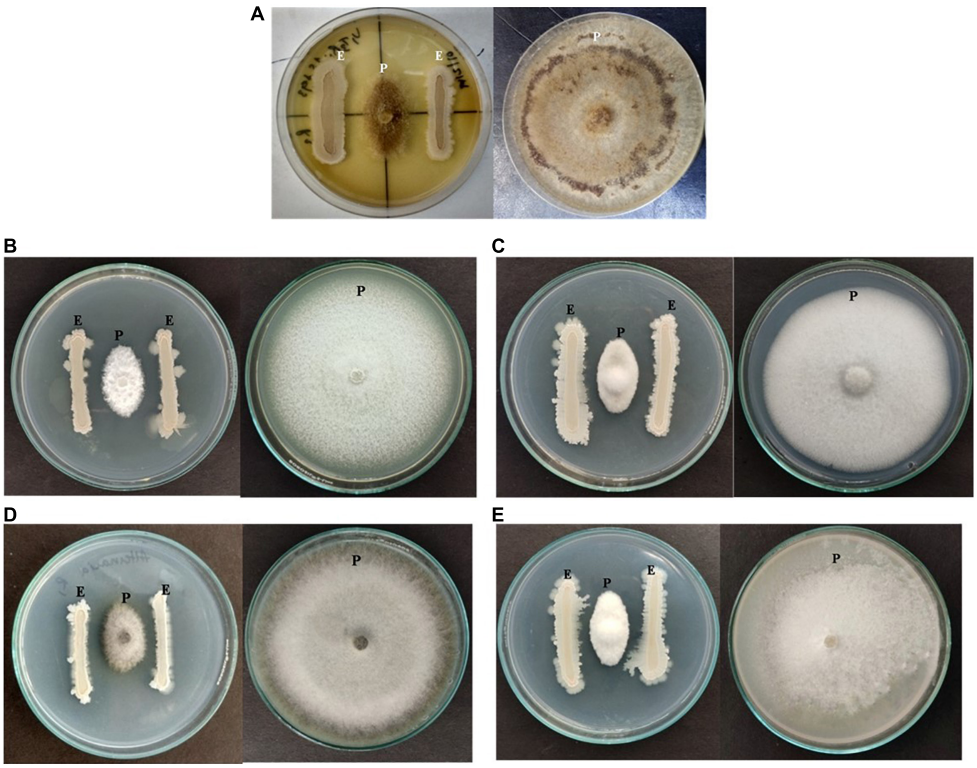

FIGURE 5 | Antagonizing effect of strain NKIT9 against **(A)** *Rhizoctonia solani,* **(B)** *Verticillium lateritium* **(C)** *Botrytis cinerea,* **(D)** *Alternaria solani*, and **(E)** *Fusarium solani* after 6 days of inoculation ("E" represents endophytic bacterial strain whereas "P" represents Pathogenic fungi).

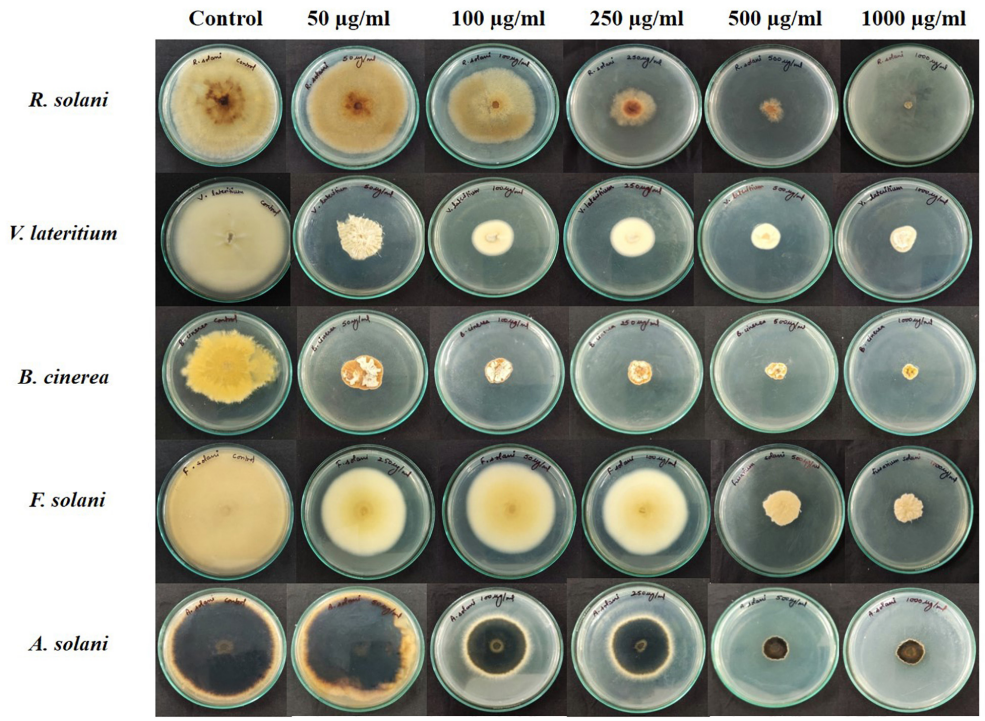

FIGURE 6 | Antifungal bioassay of lipopeptide extracted from *Bacillus siamensis* strain NKIT9 at 5 different concentrations of 50, 100, 250, 500, and 1000 µg/ml against five test pathogenic fungi (*R. solani, F. solani, B. cinerea, A. solani*, and *V. lateritium).*

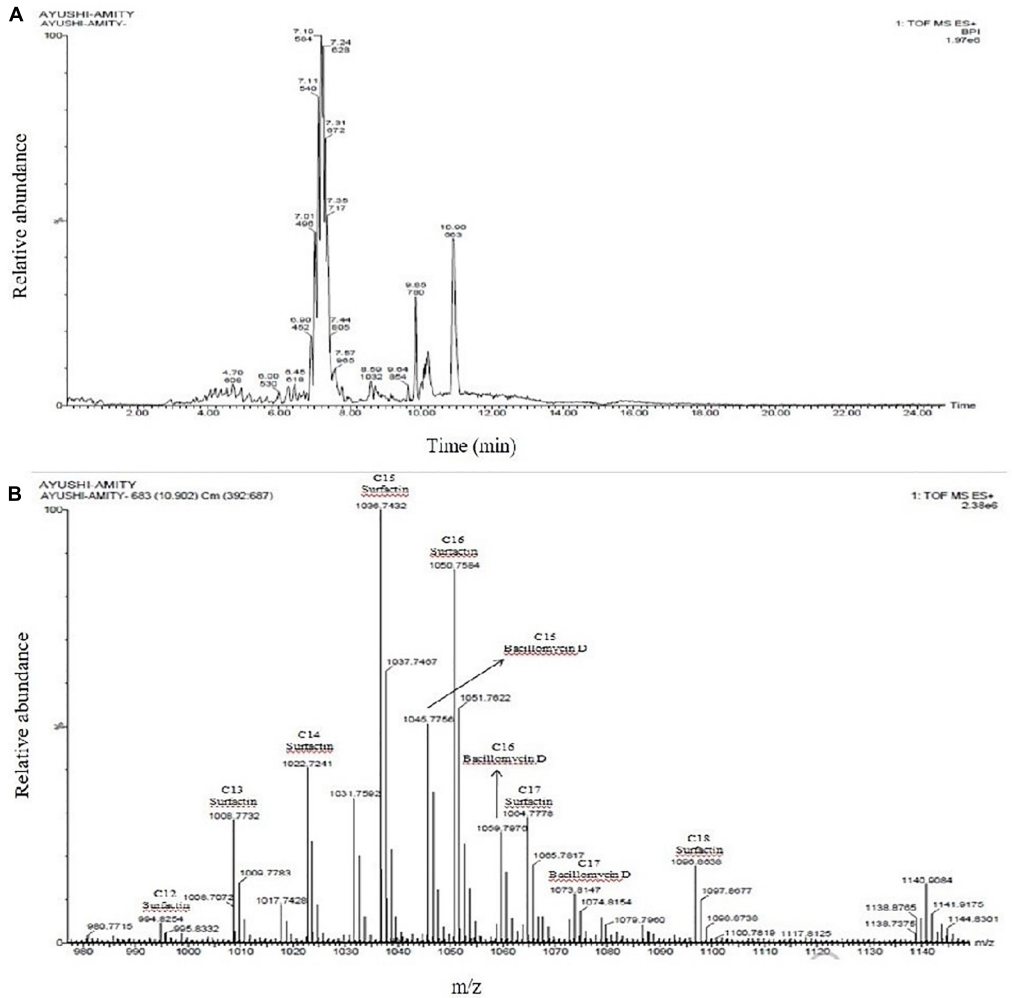

FIGURE 7 | (A) UPLC chromatogram of lipopeptides extracted from *Bacillus siamensis* strain NKIT9; **(B)** HDMS accurate mass revealed the production of Surfactin and Bacillomycin D analogues.

there are indications of endophytic bacterial transmission via seeds, which might clarify their possible integral interaction with a specific host varietal (Truyens et al., 2014). Seeds or associated fruits are ecologically important as units of dispersal, succession, invasion, and survival in the face of adversity. Germination causes fierce competition among seedlings, which shapes wild communities and necessitates management in crop situations (Newcombe et al., 2018).

Despite being identical in the presence of species, our findings show that under regulated conditions, not all bacteria inhibit mycelial growth; however, they vary in their ability to synthesize other inhibitory molecules. In comparison to the endophytes in variety V2, the V1 endophytic population is increasingly antagonistic to all five test fungi. The most potent antagonistic endophyte was identified through 16S rRNA gene sequencing as *B. siamensis* NKIT9. There was no physical contact between the isolates and the pathogen in the inhibition zone, indicating that the isolated active *Bacillus* species may generate definite antifungal substances that impede the mycelial growth (Lee et al., 2008). *B. siamensis* strain NKIT9 exhibits more antagonistic activity than other species against all the selected fungal pathogens. The *z*-score clustering facilitates the bacterial species relationship between the isolates in relation to the antifungal activity. A higher *z*-value suggests that genotypes will be better clustered by function, suggesting a clustering result, which is more biologically important (Bhattacharya et al., 2012). In variety V1, *B. cinerea and F. solani* are less susceptible to antifungal behavior of some endophytic species or have similar responses to most of the bacterial species. Likewise, *R. solani* and *A. solani* linked similar responses with those of *V. lateritium.* This clustering is not by chance but because of the similarity in antifungal activity. However, in variety V2, *B. amyloliquefaciensis* was notable for maximum antifungal activity against all pathogenic fungi.

Frequent and excessive use of fungicides has led to the development of the pathogen's resistant races (Brent and Hollomon, 2007), such as 2-amino-pyrimidineresistant *Blumeria graminis* causing powdery mildew (Brent, 1982), phenylamides

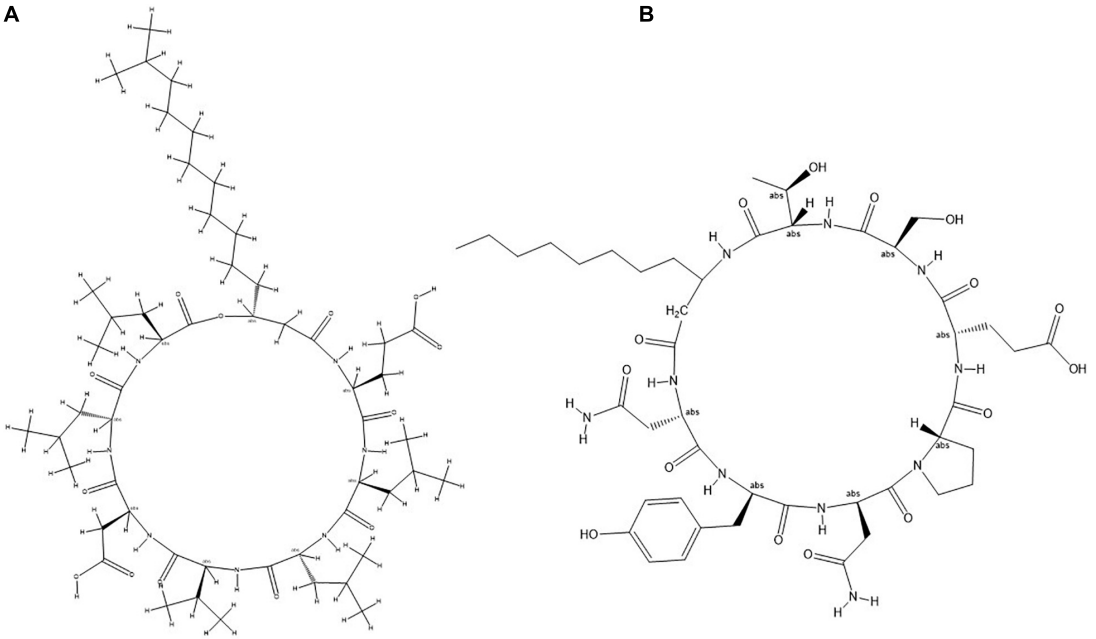

FIGURE 8 | General molecular structure of lipopeptides **(A)** Surfactin and **(B)** Bacillomycin isolated from *B. siamensis* strain NKIT9.

TABLE 3 | Effects of strain NKIT9 on seedling germination, the suppression of damping-off of tomato plants caused by *R. solani* 15 days after planting*.

Treatments	Seedling germination (%)	Diseased plants %
T1: Surface- sterilized seeds only (control)	74.44 ± 0.17c	0 ± 0.00d
T2: Surface-sterilized seeds + fungal pathogen	48.89 ± 0.26d	72.22 ± 0.40a
T3: Bio–primed seeds only (for growth promoting activity)	96.67 ± 0.16a	0 ± 0.00d
T4: Bio- primed seeds + fungal pathogen	81.11 ± 0.20b,c	28.89 ± 0.42c
T5: Bio primed seeds + fungal pathogen + soil treatment of the bacterial strain NKIT9	82.22 ± 0.27b	27.78 ± 0.46c
T6: Chemical treated seeds (Bavistin-Carbendazim) + fungal pathogen (chemical control)	87.78 ± 0.30b	42.22 ± 0.40b

**For each treatment, each datum is an average of results of nine replicates with ± SE. Means in any column with different letters are significantly different (P = 0.05) according to Duncan Multiple Range Test with F-value of 42.387 and 61.938 for seedling germination and disease percentage. Whereas, "a" signifies highest value followed by "b" > "c" > "d."*

resistant *Phytophthora infestans* to (Staub, 1994), Melanin Biosynthesis Inhibitors (Dehydratase) MBI-D resistant rice blast causing *Magnoprthe grisea* (Kaku et al., 2003). Due to the appearance of these resistant strains and rising environmental contamination, seed bio-priming with endophytes is being looked upon as an environmentally friendly option. It has been used as an alternative method for controlling a variety of seed and soil-borne pathogens in recent years. It is an ecological strategy that employs selected fungal antagonists to combat pathogens found in soil and seeds (Reddy, 2012). Seed bio-priming improved the effectiveness of *B. subtilis*, in the control of root rot pathogens (*F. solani* and *R. solani*) in greenhouse trials, with bio-priming seed treatments showing the highest percentages of disease reduction (Reddy, 2012). Many horticultural crops used seed priming as a tool to improve germination speed and uniformity, as well as final stand (Bisen et al., 2015). However, if seeds are infected or damaged with infectious agents, fungal growth can be accelerated during priming, causing negative plant effects (Reddy, 2012). In the study conducted by El-Mohamedy and Abd El-Baky (2008), after 15, 45, and 60 days of sowing of bio-primed pea seeds, the disease incidence reduced by 72.7–84.5, 72.2–82.9, and 67.6–80.0%, respectively, at the pre- and post-emergence stages. Seed priming, either alone or in combination with low-dose fungicides and/or bio-control agents, is being used to improve seed emergence rate and uniformity while reducing damping-off disease (Reddy, 2012). Therefore, formulation or suspension of biological agent can also be used as a booster dose in plant protection. Many endophytic strain treatments of tomato seeds, namely *Rhizobium taibaishanense* (RBEB2), *Pseudomonas psychrotolerance* (REB4), *Microbacterium testaceum* (RBEB1), and *Bacillus subtilis* (RBEB6), have previously shown significantly improved seed germination, seedling growth, vigor index, and biomass production (Karthik et al., 2017). In the present study, the bio-primed tomato seeds showed reduced percentage of damping-off diseased plants when challenged with *R. solani* as compared to the control indicating *B. siamensis* strain NKIT9 treatment exhibited a significant disease resistance ($p < 0.05$).

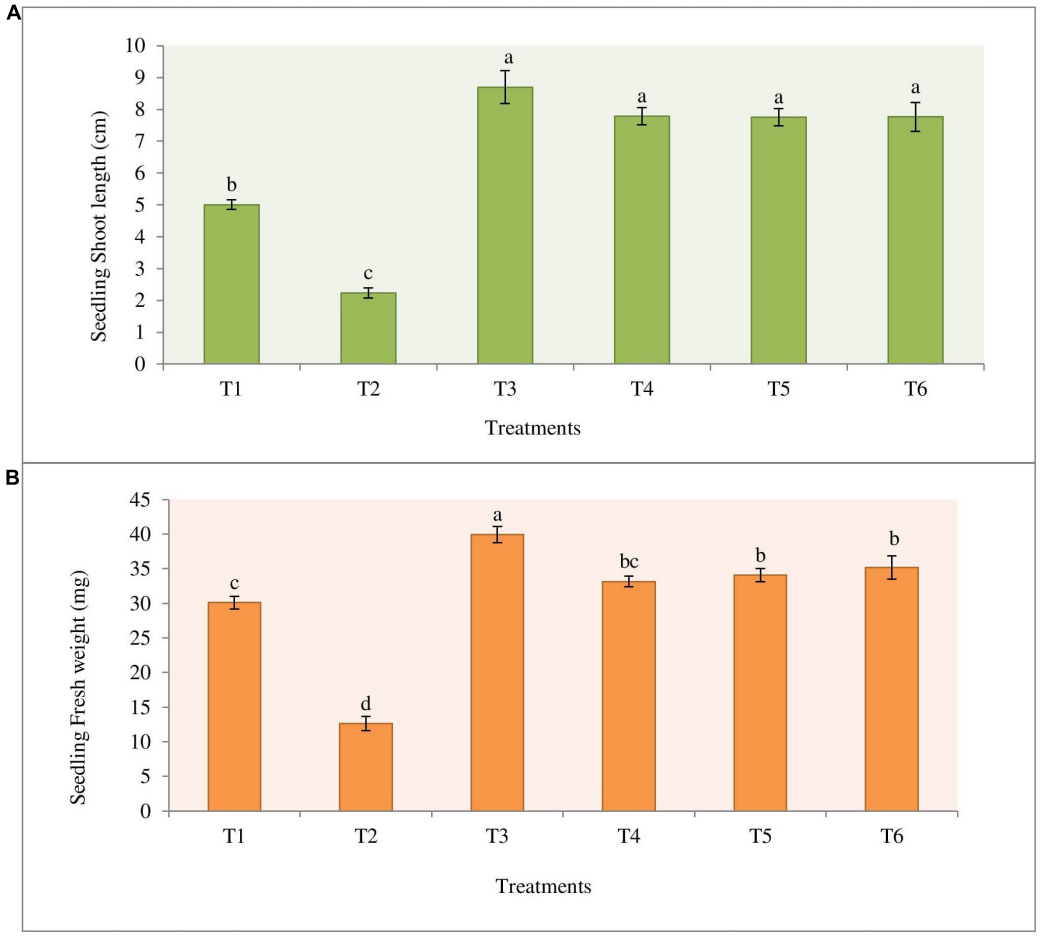

FIGURE 9 | Effect of priming of tomato seeds with strain NKIT9 on the **(A)** shoot length of the seedling (F = 54.109; df = 53) and **(B)** seedling fresh weight (F = 70.928; df = 53). Evaluation was made after 15 days of planting of tomato seeds. Nine replicates were used for the assay with 10 seedlings in each replicate. Bars labeled with the same letters are not significantly different according to Duncan Multiple Range Test at p = 0.05. Vertical lines represent the standard errors of the mean.

Under greenhouse conditions also, the strain NKIT9 suppressed *R. solani* infestation and showed increase in fruit yield by 59.2% compared with the untreated *R. solani* infested control. Increased fruit yield concomitantly led to low disease incidence of *R. solani* in tomato plants. This plant growth promoting properties of endophytic strains makes them a more suitable alternative for chemical agents.

Studies have reported the production of wide variety of structurally different antagonistic secondary metabolites from many endophytic and non-endophytic *Bacillus* spp. including *B. siamensis* (Fira et al., 2018). Interestingly, the strains producing non-ribosomally synthesized lipopeptides and peptides have shown enhanced fungicidal activities (Etchegaray et al., 2008; Dimkiæ et al., 2013). The LC-MS/MS-based analysis of the strain NKIT9 extract further confirmed the product of surfactin derivatives, iturin, and fengycin by *Bacillus* sp. (Jasim et al., 2016). The current study shows the first experimental evidence of the presence of these antifungal lipopeptides in *B. siamensis* isolated from a tomato variety. The IC_{50} value of 230 μg/ml showed the high potency of the crude lipopeptide extract obtained from the pure culture of *B. siamensis* strain NKIT9 to inhibit the growth of *R. solani,* thus, further confirming that the antifungal activity of the *B. siamensis* is due to lipopeptides. Earlier, it was predicted through genome sequencing that *B. siamensis* contains Sufactin and Bacillomycin D genes (Pan et al., 2019). However, in the current study, this is the first time that it has been extracted and confirmed in the culture broth. It is believed that bioactive compounds producing bacterial endophytes can be an effective biological agent and a powerful tool for the development of a formulation against fungal pathogens in crop protection and for promoting plant growth. The mechanism of action of lipopeptides might depend on the structural and functional properties of lipopeptides (Zhang et al., 2013). Bacillomycin L antifungal activity against *R. solani Kühn*, which includes a specific association with intact fungal hyphae, has been extensively investigated using different fluorescent

TABLE 4 | Morphological characters and fruit yield of tomato crops observed with different treatments.

Treatments	Measure of physical parameters per plant				
	Plant height (cm)	**No. of buds**	**No. of flowers**	**No. of fruits (70 DAP*)**	**Fruit yield (g)**
T1: Surface- sterilized seeds only (control)	20.09 ± 2.74d	4.63 ± 1.22a–c	11.35 ± 1.57b,c	5.56 ± 3.43b,c	500.62 ± 71.25b,c
T2: Surface-sterilized seeds + fungal pathogen	20.93 ± 3.43d	1.06 ± 0.34d	8.19 ± 1.65c	4.78 ± 3.43c	430.31 ± 90.55c
T3: Bio–primed seeds only (for growth promoting activity)	46.94 ± 1.98a,b	3.38 ± 0.49b–d	15.81 ± 2.25b	7.90 ± 3.43b	711.56 ± 101.39b
T4: Bio- primed seeds + fungal pathogen	51.00 ± 1.90a	7.06 ± 0.98a	23.44 ± 2.73a	11.72 ± 3.43a	1054.69 ± 123.02a
T5: Bio primed seeds + fungal pathogen + soil treatment of the bacterial strain NKIT9	42.28 ± 1.54b	4.63 ± 1.02a–c	16.93 ± 1.86b	8.46 ± 3.43b	762.19 ± 83.73b
T6: Chemical treated seeds (Bavistin-Carbendazim) + fungal pathogen (chemical control)	23.75 ± 3.41c	5.50 ± 1.06a,b	9.06 ± 1.45d	4.53 ± 3.43c	407.81 ± 65.40c
F-value	*18.99*	*4.26*	*6.87*	*7.42*	*7.42*

Values are mean of 16 replications ± SE. Means followed by a common letter are not significantly different at 5% level by DMRT. Whereas, "a" signifies highest value followed by "b" > "c" > "d." DAP, Days after planting.

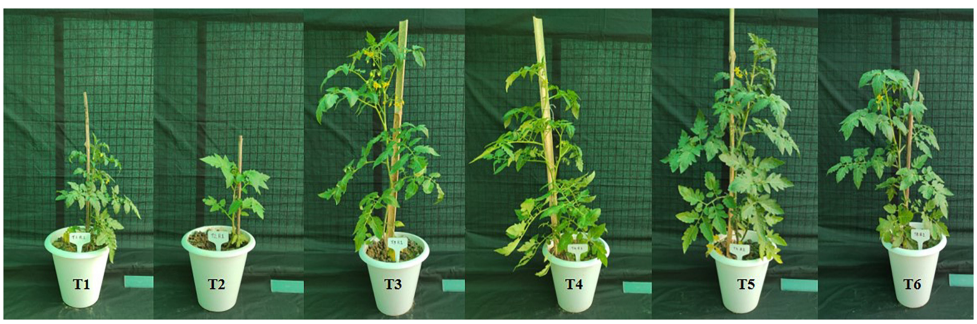

FIGURE 10 | Growth of tomato plants (V1) obtained after 45 days of sowing of tomato seeds of all the treatments: T1 (Surface-sterilized seeds only); T2 (Surface-sterilized seeds + fungal pathogen); T3 (Bio-primed seeds only); T4 (Bio-primed seeds + fungal pathogen); T5 (Bio-primed seeds + fungal pathogen + soil treatment of the bacterial strain NKIT9); T6 (Chemical treated seeds (Bavistin-Carbendazim) + fungal pathogen.

methods, gel retardation experiments, and electron microscopy (Zhang et al., 2013).

Previously, *B. siamensis* strain isolation has been reported from rhizosphere or other sources other than endophytic (Hussain and Khan, 2020; Yoo et al., 2020; Pastor-Bueis et al., 2017; Islam et al., 2019). Recently, Putri et al., 2020, showed antifungal activity of ethyl acetate extract obtained from fermentation filtrate of *B. siamensis* against *Aspergillus niger*. Various *Bacillus* strains, including *B. siamensis,* were previously identified with surfactin gene and produce surfactin like biosurfactants (Mehetre et al., 2019). A similar study by Pan et al. (2019) reported that *B. siamensis* produced sets of bacillibactins, fengycins, bacillomycins, and surfactins through the mining of genome and metabolic profiling. Another PCR based study identified the genes, namely surfactin synthetase D, and bacillomycin synthetase D, involved in cyclic lipopeptide biosynthesis against multidrug-resistant aquatic bacterial pathogens (Xu et al., 2018). Interestingly, no endophytic strain of *B. siamensis* isolated from a tomato variety with antifungal potential has been reported to produce surfactin and Bacillomycin D. Complete isolation and identification of these lipopeptides from *B. siamensis* strain NKIT9 isolated from the varieties of tomato plants. Overall, this indicates that the use of bacteria native to host plants may increase the success rate in screening bio-control agents because these isolates are likely to be better adapted to the host and its associated environmental conditions than other strains selected from culture collections (Köberl et al., 2013; Karimi et al., 2016).

CONCLUSION

The data presented here collectively support the notion that soil properties and rhizospheric microflora can affect the endophytic

microflora. To the best of our knowledge, this is the first report of the isolation and diversification of bacterial endophytes from organic tomato seeds; however, we only found the presence of *Bacillus* species. Comparatively, Pusa Ruby has a more diverse and biologically active endophytic population of bacteria. Results demonstrated that *Bacillus* sp. strain NKIT9 showed the highest *in-vitro* antifungal activity against *R. solani*, which produces bioactive lipopeptide compound as identified through Ultra Performance Liquid-Chromatography High Definition Mass Spectrometry (UPLC-HDMS). In addition, in vitro findings revealed that the strain NKIT9 significantly reduced disease incidence which makes this strain a promising antifungal bio-control agent.

DATA AVAILABILITY STATEMENT

The datasets presented in this study can be found in online repositories. The names of the repository/repositories and accession number(s) can be found in the article/ **Supplementary Material**.

AUTHOR CONTRIBUTIONS

NK and ND conceived the idea, secured funding, planned the work, and guided the AyS. AyS performed the experimental work and wrote the manuscript. AbS helped in data analysis. NK, AbS, and ND read and reviewed the manuscript. AB, MR, and YS conducted the molecular identification of all the bacterial isolates. TM supported in lipopeptide extraction process. All authors contributed to the article and approved the submitted version.

FUNDING

Financial support provided by the Department of Science and Technology, Government of India under Project No. DST/INT/TUNISIA/P-04/2017, Department of Biotechnology, Government of India and Tunisian Ministry of Higher Education and Scientific Research under the TOMendo Project.

ACKNOWLEDGMENTS

The authors are thankful to the Amity University Uttar Pradesh, Noida (India) for providing the infrastructure for the smooth conduction of experiments.

SUPPLEMENTARY MATERIAL

The Supplementary Material for this article can be found online at: https://www.frontiersin.org/articles/10.3389/fmicb.2021.609482/full#supplementary-material

REFERENCES

Adhikari, P. R., Baral, S., and Bhandari, B. (2015). Use of biological agents for disease management of tomato in Bhaktapur of Nepal. *J. Agric. Environ.* 16, 62–76. doi: 10.3126/aej.v16i0.19840

Agamy, R., Alamri, S., Moustafa, M. F., and Hashem, M. (2013). Management of tomato leaf spot caused by *Alternaria tenuissima* Wiltshire using salicylic acid and agrileen. *Int. J. Agric. Biol.* 5, 266–272.

Aneja, K. R. (2003). *Experiments in Microbiology and Plant Pathology*, 4th Edn. New Delhi: New Age International Pvt. Ltd.

Asaka, O., and Shoda, M. (1996). Biocontrol of *Rhizoctonia solani* damping-off of tomato with *Bacillus subtilis* RB14. *Appl. Environ. Microbiol.* 62, 4081–4085.

Attia, M. S., El-Sayyad, G. S., Abd Elkodous, M., and El-Batal, A. I. (2020). The effective antagonistic potential of plant growth-promoting rhizobacteria against *Alternaria solani*-causing early blight disease in tomato plant. *Sci. Hortic.* 266:109289. doi: 10.1016/j.scienta.2020.109289

Badrhadad, A., Nazarian-Firouzabadi, F., and Ismaili, A. (2018). Fusion of a chitin-binding domain to an antibacterial peptide to enhance resistance to *Fusarium solani* in tobacco (*Nicotiana tabacum*). *3 Biotech* 8, 1–10. doi: 10.1007/s13205-018-1416-7

Bhattacharya, A., Chowdhury, N., and Kumar De, R. (2012). Comparative analysis of clustering and biclustering algorithms for grouping of genes: co-function and co-regulation. *Curr. Bioinform.* 7, 63–76. doi: 10.2174/2F157489312799304440

Bisen, K., Keswani, C., Mishra, S., Saxena, A., Rakshit, A., and Singh, H. B. (2015). "Unrealized potential of seed bio-priming for versatile agriculture," in *Nutrient use Efficiency: From Basics to Advances*, eds A. Rakshit, H. B. Singh, and A. Sen (New Delhi: Springer), 193–206.

Boratyn, G. M., Camacho, C., Cooper, P. S., Coulouris, G., Fong, A., Ma, N., et al. (2013). BLAST: a more efficient report with usability improvements. *Nucleic Acids Res.* 41, W29–W33. doi: 10.1093/nar/gkt282

Brent, K. J. (1982). "'Case study 4: powdery mildews of barley and cucumber," in *Fungicide Resistance in Crop Protection*, eds J. Dekker and S. G. Georgopoulos (Wageningen: PUDOC), 219–230.

Brent, K. J., and Hollomon, D. W. (2007). *Fungicide Resistance in crop Pathogens: How Can it be Managed (FRAC Monograph No. 1)"*. Brussels: Fungicide Resistance Action Committee, 98.

Cheng, X., Man, X., Wang, Z., Liang, L., Zhang, F., Wang, Z., et al. (2020). Fungicide SYP-14288 inducing multidrug resistance in *Rhizoctonia solani*. *Plant Dis.* 104, 2563–2570. doi: 10.1094/PDIS-01-20-0048-RE

Chimwamurombe, P. M., Grönemeyer, J. L., and Reinhold-Hurek, B. (2016). Isolation and characterization of culturable seed-associated bacterial endophytes from gnotobiotically grown Marama bean seedlings. *FEMS Microbiol. Ecol.* 92:fiw083. doi: 10.1093/femsec/fiw083

Chowdhary, K., and Kaushik, N. (2015). Fungal endophyte diversity and bioactivity in the Indian medicinal plant *Ocimumsanctum Linn*. *PLoS One* 10:e0141444. doi: 10.1371/journal.pone.0141444

Chowdhary, K., and Kaushik, N. (2019). Biodiversity and In vitro inhibition study of fungal endophytes of *Chlorophytum borivilianum* against selected phytopathogens. *Proc. Natl. Acad. Sci. India Sect. B Biol. Sci.* 89, 113–121. doi: 10.1007/s40011-017-0924-2

Compant, S., Clément, C., and Sessitsch, A. (2010). Plant growth-promoting bacteria in the rhizo-and endosphere of plants: their role, colonization, mechanisms involved and prospects for utilization. *Soil Biol. Biochem.* 42, 669–678. doi: 10.1016/j.soilbio.2009.11.024

Deketelaere, S., Tyvaert, L., França, S. C., and Höfte, M. (2017). Desirable traits of a good biocontrol agent against *Verticillium wilt*. *Front. Microbiol.* 8:1186. doi: 10.3389/fmicb.2017.01186

Dimkiæ, I., Živkoviæ, S., Beriæ, T., Ivanoviæ, Ž, Gavriloviæ, V., Stankoviæ, S., et al. (2013). Characterization and evaluation of two *Bacillus strains*, SS-12.6 and SS-13.1, as potential agents for the control of phytopathogenic bacteria and fungi. *Biol. Control* 65, 312–321. doi: 10.1016/j.biocontrol.2013.03.012

El-Mohamedy, R. S. R., and Abd El-Baky, M. M. H. (2008). Evaluation of different types of seed treatment on control of root rot disease, improvement growth and yield quality of pea plant in Nobaria province. *Res. J. Agric. Biol. Sci.* 4, 611–622.

Etchegaray, A., de Castro Bueno, C., de Melo, I. S., Tsai, S. M., de Fátima Fiore, M., Silva-Stenico, M. E., et al. (2008). Effect of a highly concentrated lipopeptide

extract of *Bacillus subtilis* on fungal and bacterial cells. *Arch. Microbiol.* 190, 611–622. doi: 10.1007/s00203-008-0409-z

Fira, D., Dimkiæ, I., Beriæ, T., Lozo, J., and Stankoviæ, S. (2018). Biological control of plant pathogens by *Bacillus* species. *J. Biotechnol.* 285, 44–55. doi: 10.1016/j.jbiotec.2018.07.044

Goudjal, Y., Toumatia, O., Yekkour, A., Sabaou, N., Mathieu, F., and Zitouni, A. (2014). Biocontrol of *Rhizoctonia* solani damping-off and promotion of tomato plant growth by endophytic actinomycetes isolated from native plants of Algerian Sahara. *Microbiol. Res.* 169, 59–65. doi: 10.1016/j.micres.2013.06.014

Guan, B., Zhou, D., Zhang, H., Tian, Y., Japhet, W., and Wang, P. (2009). Germination responses of *Medicago ruthenica* seeds to salinity, alkalinity, and temperature. *J. Arid Environ.* 73, 135–138. doi: 10.1016/j.jaridenv.2008.08.009

Habiba, R. N., Ali, S. A., Hasan, K. A., Ara, J., Sultana, V., and Ehteshamul-Haque, S. (2017). Protective role of epiphytic fluorescent *Pseudomonas* on natural postharvest decay of tomato at room temperature. *J. Appl. Bot. Food Qual.* 90, 288–297.

Hardoim, P. R., Hardoim, C. C., Van Overbeek, L. S., and Van Elsas, J. D. (2012). Dynamics of seed-borne rice endophytes on early plant growth stages. *PLoS One* 7:e30438. doi: 10.1371/journal.pone.0030438:

Hazarika, D. J., Goswami, G., Gautom, T., Parveen, A., Das, P., Barooah, M., et al. (2019). Lipopeptide mediated biocontrol activity of endophytic *Bacillus subtilis* against fungal phytopathogens. *BMC Microbiol.* 19:71. doi: 10.1186/s12866-019-1440-8

Hong, C. E., and Park, J. M. (2016). Endophytic bacteria as biocontrol agents against plant pathogens: current state-of-the-art. *Plant Biotechnol. Rep.* 10, 353–357. doi: 10.1007/s11816-016-0423-6

Huang, W. Y., Cai, Y. Z., Hyde, K. D., Corke, H., and Sun, M. (2008). Biodiversity of endophytic fungi associated with 29 traditional Chinese medicinal plants. *Fungal Divers.* 33, 61–75.

Hussain, T., and Khan, A. A. (2020). Determining the antifungal activity and characterization of *Bacillus siamensis* AMU03 against *Macrophomina phaseolina* (Tassi) Goid. *Indian Phytopathol.* 73, 507–516. doi: 10.1007/s42360-020-00239-6

Ibrahim, M., Kaushik, N., Sowemimo, A., Chhipa, H., Koekemoer, T., Van de Venter, M., et al. (2017). Antifungal and antiproliferative activities of endophytic fungi isolated from the leaves of *Markhamia tomentosa*. *Pharm. Biol.* 55, 590–595. doi: 10.1080/13880209.2016.1263671

Ifo, S. A., Moutsambote, J. M., Koubouana, F., Yoka, J., Ndzai, S. F., Bouetou-Kadilamio, L. N. O., et al. (2016). Tree species diversity, richness, and similarity in intact and degraded forest in the tropical rainforest of the Congo Basin: case of the Forest of Likouala in the Republic of Congo. *J. For. Res.* 2, 1–12.

Islam, A., Kabir, S., and Khair, A. (2019). Characterization and evaluation *of Bacillus siamensis* isolate for its growth promoting potential in tomato. *Agriculture (Pol'nohospodárstvo).* 65, 42–50. doi: 10.2478/agri-2019-0005

Jasim, B., Sreelakshmi, K. S., Mathew, J., and Radhakrishnan, E. K. (2016). Surfactin, iturin, and fengycin biosynthesis by endophytic *Bacillus* sp. from *Bacopa monnieri*. *Microb. Ecol.* 72, 106–119. doi: 10.1007/s00248-016-0753-5

Kaku, K., Takagaki, M., Shimizu, T., and Nagayama, K. (2003). Diagnosis of dehydratase inhibitors in melanin biosynthesis inhibitor (MBI-D) resistance by primer-introduced restriction enzyme analysis in scylatone dehydratase gene of *Magnaporthe grisea*. *Pest Manag. Sci.* 59, 843–846. doi: 10.002/ps.742

Karimi, E., Safaie, N., Shams-Baksh, M., and Mahmoudi, B. (2016). Bacillus amyloliquefaciens SB14 from rhizosphere alleviates *Rhizoctonia* damping-off disease on sugar beet. *Microbiol. Res.* 192, 221–230. doi: 10.1016/j.micres.2016.06.011

Karthik, M., Pushpakanth, P., Krishnamoorthy, R., and Senthilkumar, M. (2017). Endophytic bacteria associated with banana cultivars and their inoculation effect on plant growth. *J. Hortic. Sci. Biotech.* 92, 568–576. doi: 10.1080/14620316.2017.1310600

Khan, M. R., and Anwer, M. A. (2007). Molecular and biochemical characterization of soil isolates of *Aspergillus niger* aggregate and an assessment of their antagonism against *Rhizoctonia solani*. *Phytopathol. Mediterr.* 46, 304–315.

Köberl, M., Ramadan, E. M., Adam, M., Cardinale, M., Hallmann, J., Heuer, H., et al. (2013). Bacillus and Streptomyces were selected as broad-spectrum antagonists against soilborne pathogens from arid areas in Egypt. *FEMS Microbiol. Lett.* 342, 168–178. doi: 10.1111/1574-6968.12089

Kumar, A., Marcot, B. G., and Saxena, A. (2006). Tree species diversity and distribution patterns in tropical forests of Garo Hills. *Curr. Sci.* 91, 1370–1381. doi: 10.2307/24094061

Kumar, S., Kaushik, N., Edrada-Ebel, R., Ebel, R., and Proksch, P. (2011). Isolation, characterization, and bioactivity of endophytic fungi of *Tylophora indica*. *World J. Microb. Biot.* 27, 571–577. doi: 10.1007/s11274-010-0492-6

Kumar, S., Stecher, G., and Tamura, K. (2016). MEGA7: molecular evolutionary genetics analysis version 7.0 for bigger datasets. *Mol. Biol. Evol.* 33, 1870–1874. doi: 10.1093/molbev/msw054

Kumar, V., Jain, L., Jain, S. K., Chaturvedi, S., and Kaushal, P. (2020). Bacterial endophytes of rice (*Oryza sativa* L.) and their potential for plant growth promotion and antagonistic activities. *S. Afr. J. Bot.* 134, 50–63. doi: 10.1016/j.sajb.2020.02.017

Lamichhane, J. R., Dürr, C., Schwanck, A. A., Robin, M. H., Sarthou, J. P., Cellier, V., et al. (2017). Integrated management of damping-off diseases. A review. *Agron. Sustain. Dev.* 37, 10. doi: 10.1007/s13593-017-0417-y

Lee, K. J., Kamala-Kannan, S., Sub, H. S., Seong, C. K., and Lee, G. W. (2008). Biological control of *Phytophthora* blight in red pepper (*Capsicum annuum* L.) using *Bacillus subtilis*. *World J. Microb. Biot.* 24, 1139–1145. doi: 10.1007/s11274-007-9585-2

Leroux, P., Fritz, R., Debieu, D., Albertini, C., Lanen, C., Bach, J., et al. (2002). Mechanisms of resistance to fungicides in field strains of *Botrytis cinerea*. *Pest Manag. Sci.* 58, 876–888. doi: 10.1002/ps.566

Liu, H., Carvalhais, L. C., Crawford, M., Singh, E., Dennis, P. G., Pieterse, C. M., et al. (2017). Inner plant values: diversity, colonization and benefits from endophytic bacteria. *Front. Microbiol.* 8:2552. doi: 10.3389/fmicb.2017.02552

López, S. M. Y., Pastorino, G. N., Franco, M. E. E., Medina, R., Lucentini, C. G., Saparrat, M. C. N., et al. (2018). Microbial endophytes that live within the seed of two tomato hybrids cultivated in Argentina. *Agronomy* 8:136. doi: 10.3390/agronomy8080136

Lundberg, D. S., Lebeis, S. L., Paredes, S. H., Yourstone, S., Gehring, J., Malfatti, S., et al. (2012). Defining the core *Arabidopsis thaliana* root microbiome. *Nature* 488, 86–90. doi: 10.1038/nature11237

Massawe, V. C., Hanif, A., Farzand, A., Mburu, D. K., Ochola, S. O., Wu, L., et al. (2018). Volatile compounds of endophytic *Bacillus* spp. have biocontrol activity against *Sclerotinia sclerotiorum*. *Phytopathology* 108, 1373–1385. doi: 10.1094/PHYTO-04-18-0118-R

Mehetre, G. T., Dastager, S. G., and Dharne, M. S. (2019). Biodegradation of mixed polycyclic aromatic hydrocarbons by pure and mixed cultures of biosurfactant producing thermophilic and thermo-tolerant bacteria. *Sci. Total Environ.* 679, 52–60. doi: 10.1016/j.scitotenv.2019.04.376

Montealegre, J., Valderrama, L., Sánchez, S., Herrera, R., Besoain, X., and Pérez, L. M. (2010). Biological control of Rhizoctonia solani in tomatoes with *Trichoderma harzianum* mutants. *Electron. J. Biotechnol.* 13, 1–2.

Newcombe, G., Harding, A., Ridout, M., and Busby, P. E. (2018). A hypothetical bottleneck in the plant microbiome. *Front. microbial.* 9:1645. doi: 10.3389/fmicb.2018.01645

Pan, H., Tian, X., Shao, M., Xie, Y., Huang, H., Hu, J., et al. (2019). Genome mining and metabolic profiling illuminate the chemistry driving diverse biological activities of *Bacillus siamensis* SCSIO 05746. *Appl. Microbiol. Biotechnol.* 103, 4153–4165.

Pastor-Bueis, R., Mulas, R., Gómez, X., and González-Andrés, F. (2017). Innovative liquid formulation of digestates for producing a biofertilizer based on *Bacillus siamensis*: field testing on sweet pepper. *J. Plant Nutr. Soil Sc.* 180, 748–758. doi: 10.1002/jpln.201700200

Paul, H. (2018). Re: Hw to Test Pathogenicity of Fusariunlycopersici, Rhizoctonia Solani and Sclerotium Rolfsii on Tomato Crop During off Season or undr in Vitro Cndtion? Available online at: https://www.researchgate.net/post/Hw-to-test-pathogenicity-of-Fusariun-lycopersici-Rhizoctonia-solani-and-Sclerotium-rolfsii-on-Tomato-crop-during-off-season-or-undr-in-vitro-cndtion/5b98836d979fdc1332777dd2/citation/download (accessed March 02, 2021).

Piggot, P. J., and Hilbert, D. W. (2004). Sporulation of *Bacillus subtilis*. *Curr. Opin. Microbiol.* 7, 579–586. doi: 10.1016/j.mib.2004.10.001

Podolich, O., Ardanov, P., Zaets, I., Pirttilä, A. M., and Kozyrovska, N. (2015). Reviving of the endophytic bacterial community as a putative mechanism of plant resistance. *Plant Soil* 388, 367–377.

Putri, B. R., Santoso, I., and Yasman, Y. (2020). "Antagonistic potential of *Bacillus siamensis* LDR against *Aspergillus niger* ABP and ART," in *Proceedings of the AIP Conference*, Vol. 2242, (Melville, NY: AIP Publishing LLC), 050017.

Reddy, P. P. (2012). "Bio-priming of seeds," in *Recent Advances in Crop Protection*, ed. P. P Reddy (New Delhi: Springer), 83–90. doi: 10.1007/978-81-322-0723-8_6

Reinhold-Hurek, B., and Hurek, T. (2011). Living inside plants: bacterial endophytes. *Curr. Opin. Plant Biol.* 14, 435–443. doi: 10.1016/j.pbi.2011.04.004

Romano, A., Vitullo, D., Di Pietro, A., Lima, G., and Lanzotti, V. (2011). Antifungal lipopeptides from *Bacillus amyloliquefaciens* strain BO7. *J. Nat. Prod.* 74, 145–151. doi: 10.1021/np100408y

Roy, S., Chakraborty, S., and Basu, A. (2017). In vitro evaluation for antagonistic potential of some bio control isolates against important foliar fungal pathogens of cowpea. *Int. J. Curr. Microbiol. App. Sci.* 6, 2998–3011.

Ryan, R. P., Germaine, K., Franks, A., Ryan, D. J., and Dowling, D. N. (2008). Bacterial endophytes: recent developments and applications. *FEMS Microbiol. Lett.* 278, 1–9. doi: 10.1111/j.1574-6968.2007.00918.x

Shenashen, M., Derbalah, A., Hamza, A., Mohamed, A., and El Safty, S. (2017). Recent trend in controlling root rot disease of tomato caused by *Fusarium solani* using aluminasilica nanoparticles. *Int. J. Adv. Res. Biol. Sci.* 4, 105–119. doi: 10.22192/ijarbs.2017.04.06.017

Slama, H. B., Cherif-Silini, H., ChenariBouket, A., Qader, M., Silini, A., Yahiaoui, B., et al. (2019). Screening for *Fusarium antagonistic* bacteria from contrasting niches designated the endophyte *Bacillus halotolerans* as plant warden against *Fusarium*. *Front. Microb.* 9:3236. doi: 10.3389/fmicb.2018.03236

Soylu, E. M., Kurt, Ł, and Soylu, S. (2010). In vitro and in vivo antifungal activities of the essential oils of various plants against tomato grey mould disease agent *Botrytis cinerea*. *Int. J. Food Microbiol* 143, 183–189. doi: 10.1016/j.ijfoodmicro.2010.08.015

Staub, T. (1994). "Early experiences with phenylamide resistance and lessons for continued successful use," in *Fungicide Resistance*, eds S. Heaney, D. Slawson, D. W. Hollomon, M. Smith, P. E. Russell, and D. W. Parry (Farnham: British Crop Protection Council), 131–138.

Sturrock, C. J., Woodhall, J., Brown, M., Walker, C., Mooney, S. J., and Ray, R. V. (2015). Effects of damping-off caused by *Rhizoctonia solani* anastomosis group 2-1 on roots of wheat and oil seed rape quantified using X-ray computed tomography and real-time PCR. *Front. Plant. Sci.* 6:461. doi: 10.3389/fpls.2015.00461

Szczech, M., and Shoda, M. (2006). The effect of mode of application of *Bacillus subtilis* RB14-C on its efficacy as a biocontrol agent against *Rhizoctonia solani*. *J. Phytopathol.* 154, 370–377. doi: 10.3389/fpls.2015.00461

Thomas, P., and Reddy, K. M. (2013). Microscopic elucidation of abundant endophytic bacteria colonizing the cell wall-plasma membrane peri-space in the shoot-tip tissue of banana. *AoB Plants* 5, 1–12. doi: 10.1093/aobpla/plt011

Tiago, I., Teixeira, I., Siva, S., Chung, P., Veríssimo, A., and Manaia, C. M. (2004). Metabolic and genetic diversity of mesophilic and thermophilic bacteria isolated from composted municipal sludge on poly- ε -caprolactones. *Curr. Microbiol.* 49, 407–414. doi: 10.1007/s00284-004-4353-0

Truyens, S., Weyens, N., Cuypers, A., and Vangronsveld, J. (2014). Bacterial seed endophytes: genera, vertical transmission and interaction with plants. *Environ. Microbiol. Rep.* 7, 40–50. doi: 10.1111/1758-2229.12181

Upreti, R., and Thomas, P. (2015). Root-associated bacterial endophytes from *Ralstonia solanacearum* resistant and susceptible tomato cultivars and their pathogen antagonistic effects. *Front. Microbiol.* 6:255. doi: 10.3389/fmicb.2015.00255

Vinodkumar, S., Nakkeeran, S., Renukadevi, P., and Mohankumar, S. (2018). Diversity and antiviral potential of rhizospheric and endophytic *Bacillus* species and phyto-antiviral principles against tobacco streak virus in cotton. *Agric. Ecosyst. Environ.* 267, 42–51. doi: 10.1016/j.agee.2018.08.008

Windels, C. E., and Brantner, J. R. (2005). Early-season application of azoxystrobin to sugar beet for control of *Rhizoctonia solani* AG 4 and AG 2-2. *J. Sugar Beet Res.* 42, 1–18.

Xia, Y., DeBolt, S., Dreyer, J., Scott, D., and Williams, M. A. (2015). Characterization of culturable bacterial endophytes and their capacity to promote plant growth from plants grown using organic or conventional practices. *Front. Plant Sci.* 6:490. doi: 10.3389/fpls.2015.00490

Xu, B. H., Lu, Y. Q., Ye, Z. W., Zheng, Q. W., Wei, T., Lin, J. F., et al. (2018). Genomics-guided discovery and structure identification of cyclic lipopeptides from the *Bacillus siamensis* JFL15. *PLoS One* 13:e0202893. doi: 10.1371/journal.pone.0202893

Yang, C. J., Zhang, X. G., Shi, G. Y., Zhao, H. Y., Chen, L., Tao, K., et al. (2011). Isolation and identification of endophytic bacterium W4 against tomato *Botrytis cinerea* and antagonistic activity stability. *Afr. J. Microbiol. Res.* 5, 131–136. doi: 10.5897/AJMR10.815

Yoo, S., Weon, H., Song, J., and Sang, M. (2020). Effects of *Chryseobacterium soldanellicola* T16E-39 and *Bacillus siamensis* T20E-257 on biocontrol against phytophthora blight and bacterial wilt and growth promotion in tomato plants. *Int. J. Agric. Biol.* 23, 534–540. doi: 10.17957/IJAB/15.1320

Zamoum, M., Goudjal, Y., Sabaou, N., Mathieu, F., and Zitouni, A. (2017). Development of formulations based on *Streptomyces rochei* strain PTL2 spores for biocontrol of *Rhizoctonia solani* damping-off of tomato seedlings. *Biocontrol. Sci. Technol.* 27, 723–738. doi: 10.1080/09583157.2017.1334257

Zhang, B., Dong, C., Shang, Q., Han, Y., and Li, P. (2013). New insights into membrane-active action in plasma membrane of fungal hyphae by the lipopeptide antibiotic bacillomycin L. *Biochim. Biophys. Acta Biomembr.* 1828, 2230–2237. doi: 10.1016/j.bbamem.2013.05.033

Conflict of Interest: The authors declare that the research was conducted in the absence of any commercial or financial relationships that could be construed as a potential conflict of interest.

frontiers in Microbiology

ORIGINAL RESEARCH
published: 17 June 2021
doi: 10.3389/fmicb.2021.629793

Effects and Mechanisms of Symbiotic Microbial Combination Agents to Control Tomato *Fusarium* Crown and Root Rot Disease

Xinyue Cai[1], Honghai Zhao[2], Chen Liang[2], Min Li[1] and Runjin Liu[1]*

[1] Institute of Mycorrhizal Biotechnology, Qingdao Agricultural University, Qingdao, China, [2] Key Laboratory of Integrated Crop Pest Management of Shandong Province, College of Plant Health and Medicine, Qingdao Agricultural University, Qingdao, China

OPEN ACCESS

Edited by:
Yong Wang,
Guizhou University, China

Reviewed by:
Zhipeng Hao,
Research Center for Eco-Environmental Sciences Chinese Academy of Sciences (CAS), China
Wei Guo,
Chinese Academy of Agricultural Sciences (CAAS), China

***Correspondence:**
Min Li
minli@qau.edu.cn

Specialty section:
This article was submitted to Microbe and Virus Interactions with Plants, a section of the journal Frontiers in Microbiology

Received: *16 November 2020*
Accepted: *20 May 2021*
Published: *17 June 2021*

Citation:
Cai X, Zhao H, Liang C, Li M and Liu R (2021) Effects and Mechanisms of Symbiotic Microbial Combination Agents to Control Tomato Fusarium Crown and Root Rot Disease. Front. Microbiol. 12:629793. doi: 10.3389/fmicb.2021.629793

This study evaluated the effects and underlying mechanisms of different combinations of plant symbiotic microbes, comprising arbuscular mycorrhizal fungi (AMF), plant growth-promoting rhizobacteria (PGPR), and *Trichoderma* spp., on tomato *Fusarium* crown and root rot (TFCRR) resistance. A total of 54 treatments were applied in a greenhouse pot experiment to tomato (*Solanum lycopersicum*) seedlings inoculated with or without *Funneliformis mosseae* (Fm), *Rhizophagus intraradices* (Ri), *Trichoderma virens* I40012 (Tv), *Trichoderma harzianum* I40015 (Th), *Bacillus subtilis* PS1-3 (Bs), *Pseudomonas fluorescens* PS2-6 (Pf), and *Fusarium oxysporum* f. sp. *radicis-lycopersici* (Fo). The symbioses on the tomato root system were well developed, and the composite symbiont generated by AMF + *Trichoderma* spp. was observed for the first time. Compared with other treatments, Ri + Bs + Tv and Fm + Pf + Tv stimulated the greatest improvements in tomato growth and yield. The combination Ri + Pf + Th + Fo resulted in the strongest biocontrol effects on TFCRR, followed by the treatments Th + Pf + Fo and Ri + Th + Fo. Compared with the Fo treatment, most inoculation treatments improved photosynthetic performance and significantly increased defense enzyme activity in tomato plants, of which the treatment Ri + Pf + Th + Fo showed the highest enzyme activity. Metabolome analysis detected changes in a total of 1,266 metabolites. The number of up-regulated metabolites in tomato plants inoculated with Ri + Pf + Th and Ri + Pf + Th + Fo exceeded that of the Fo treatment, whereas the number of down-regulated metabolites showed the opposite trend. It is concluded that AMF + *Trichoderma* + PGPR is the most effective combination to promote resistance to TFCRR in tomato. The up-regulation and down-regulation of metabolites regulated by symbiotic microbial genes may be an important mechanism by which root symbiotic microorganisms promote plant growth, increase yield, and improve disease resistance.

Keywords: arbuscular mycorrhizal fungi, plant growth-promoting rhizobacteria, *Trichoderma* spp., combined microbe agents, tomato, *Fusarium* crown and root rot

INTRODUCTION

With the increase in prevalence of multiple cropping regimes and aggravation of obstacles to continuous cropping, soil-borne diseases increasingly restrict tomato (*Solanum lycopersicum*) production, especially under protected cultivation. Among such diseases, tomato *Fusarium* crown and root rot (TFCRR) has become a highly destructive soil-borne disease (Kucharek et al., 2000; Hibar et al., 2006; Cao et al., 2018; Li et al., 2018). Tomato production is impacted by TFCRR in more than 10 provinces and cities in China (Li et al., 2018; Wang et al., 2019).

A variety of chemical, cultivation, breeding, microbial, and management measures have been attempted to control TFCRR. At present, fungicides are mainly employed in tomato production to control soil-borne diseases. However, fungicides pollute the environment and directly contribute to toxic residues in food products, thereby endangering human health. Development of green technologies for disease prevention and control is a matter of urgency. Plant metabolites and plant-based derivative treatments have been recently used to reduce incidence of TFCRR and could replace certain chemical fungicides, such as hymexazol and benomyl (Hibar et al., 2007; Murugesan et al., 2011). Selection of resistant cultivars and grafting onto disease-resistant rootstock are effective means of prevention (Thorpe and Jarvis, 1981). However, these methods and approaches have certain limitations. Therefore, it is necessary to develop more efficient and time-saving preventive and control technologies.

Plant roots are colonized with a variety of symbiotic microorganisms, such as mycorrhizal fungi, dark septate endophytes (DSE), *Trichoderma* spp., *Metarhizium* spp., and plant growth-promoting rhizobacteria (PGPR). Each of these plant-symbiotic microorganisms may directly or indirectly inhibit infection by pathogens and promote growth of the host plant (Liu and Wang, 2018; Atalla et al., 2020; Mendes et al., 2020; Rana et al., 2020). Although some biological control agents can effectively control TFCRR in a greenhouse, the effect is more efficient when used in combination with other control measures (Colak and Bicici, 2013). Under a field environment, dual inoculation with arbuscular mycorrhizal fungi (AMF) and *Bacillus* sp. reduces fertilizer application by 50% of the recommended NPK fertilization without compromising crop growth, nutrition, and yield (Nanjundappa et al., 2019). Combined inoculation with *Funneliformis mosseae* + *Bacillus* sp. M3-4, or with *Glomus versiforme*+ *Bacillus* sp. M3-4 promotes the growth of potato and induces an enhanced defense response to control bacterial wilt disease compared with the benefits of single inoculations (Tan et al., 2015). Liu et al. (2016) evaluated the effects of different combinations of the AMF *F. mosseae* (Fm), *Rhizophagus intraradices* (Ri), and *G. versiforme* (Gv) with PGPR PR2-1, PS1-3, PS1-5, PS2-6, and PS3-2 on plant growth, resistance to *Fusarium* wilt, and yield of cucumber in a greenhouse pot experiment. The authors concluded that the combinations Fm + PS1-5, Fm + PS3-2, and Gv + PS2-6 were the most effective for control of *Fusarium* wilt among all tested treatments.

Mutualisms of plant + fungi, plant + bacteria, and fungi + bacteria often represent a reciprocal symbiotic system and form a compound symbiont in a natural ecosystem. Combined symbionts may exert more powerful functions than when inoculated alone. Field experiments show that AMF + *Trichoderma harzianum* effectively reduces the incidence of soil-borne disease and improves the quality of *Salvia miltiorrhiza* (Wang et al., 2014). Liu et al. (2019) observed improved control of tomato root knot nematode by the combined inoculation of *T. harzianum* + *Bacillus cereus* compared with that of the single strain in a field trial. *T. harzianum* mainly inhibits *Rhizoctonia solani* by reparasitism, and *Bacillus subtilis* inhibits *R. solani* by an antagonistic mechanism. The combination of these disparate inhibitory mechanisms effectively prevents potato black scurf by *R. solani* (Pan et al., 2020).

Symbiotic microbial agents in combination may exert their effects by regulating plant physiological metabolism. Inoculation of *Fragaria* × *ananassa* plants with the mycorrhizal preparations Mykoflor (*Rhizophagus irregularis*, *F. mosseae*, and *Claroideoglomus etunicatum*), MYC 800 (*R. intraradices*), and the bacterial preparation Rhizocell C (*Bacillus amyloliquefaciens* IT45) increases the transpiration rate and CO_2 concentration in the intercellular spaces of the leaves, and the total number of bacteria and fungi in the soil is increased. Plants treated with MYC 800 + Rhizocell C show a higher CO_2 assimilation rate than that of the control (Mikiciuk et al., 2019). The combination of AMF + PGPR reduces cucumber *Fusarium* wilt disease incidence and improves the disease resistance of cucumber plants by antagonizing pathogens, promoting synthesis of disease resistance signaling substances, up-regulating defense gene expression, increasing defense enzyme activity, and reducing accumulation of toxic substances in plants (Liu et al., 2017).

Although many previous studies have investigated TFCRR and its prevention, control of soil-borne diseases with chemical pesticides is difficult under a continuous cropping system. Therefore, development of green technologies for prevention and control of soil-borne diseases has attracted considerable research attention. As a symbiotic and active region of plant nutrient acquisition and strong interactions among many organisms, the rhizosphere is an important environment for the development of soil-borne diseases and is the principal location of plant–soil–microorganism interactions. A large number of symbiotic microbes colonize the root zone, restrict and promote each other, and exert diverse physiological and ecological effects. Therefore, it is of theoretical and practical importance to explore the effects and mechanisms of combinations of microbial agents composed of a variety of symbiotic microorganisms. Previously identified biocontrol agents were mostly single strains, but recent studies have revealed that many microbial agents show greater application potential in combination. These results lay a sound theoretical and practical foundation for further research on combination of symbiotic microbial agents. As important members of the plant root symbiotic microbiota, AMF, PGPR, and *Trichoderma* interact with each other and have been extensively studied. Compared with AMF + PGPR, inoculation with AMF + *Trichoderma*, *Trichoderma* + PGPR, and other combinations have been studied less intensively, and even fewer studies have investigated AMF + PGPR + *Trichoderma* combinations.

Metabolomic profiling is an increasingly important technique in the large field of systems biology (Dearth et al., 2018). Yang et al. (2020) used liquid chromatography combined with time-of-flight mass spectrometry (LC/TOF-MS) to analyze the metabolite profile of *Puccinellia tenuiflora* seedlings inoculated with or without AMF under alkali stress. Their findings provide insight into the metabolic mechanisms of *P. tenuiflora* seedlings infected with AMF in alkaline soil and clarify the role of AMF in the molecular regulation of this species under alkali stress. Lu et al. (2020) used ultra-performance liquid chromatography (UPLC) coupled with tandem mass spectrometry (MS/MS) to show that *F. mosseae* alleviates root rot caused by continuous cropping. The increased activity of certain disease-resistant metabolites may partly account for the disease resistance of the plants. The study provides insight into the molecular mechanism by which AMF alleviates root rot of soybean. Hill et al. (2018) performed the first metabolomic investigation into the impact of AMF colonization by *R. irregularis* on the chemical defenses in above- and belowground tissues of ragwort (*Senecio jacobaea*). An increase in the concentrations of four pyrrolizidine alkaloids in roots (but not shoots) of AMF-colonized plants was observed, which may protect colonized plants from attack by belowground organisms.

The objective of the present study was to evaluate the effect of inoculation with AMF, *Trichoderma* spp., and PGPR, either alone or in combinations, on resistance to TFCRR and to explore the possible mechanisms of the biocontrol effects.

MATERIALS AND METHODS

Experimental Materials

Seeds of tomato 'Ginobili' (a cultivar sensitive to TFCRR) were purchased from Qingdao Wufeng Fruit and Vegetable Development Co. Ltd. (Qingdao, China).

The symbiotic AMF *F. mosseae* (Fm), *R. intraradices* (Ri), PGPR *B. subtilis* PS1-3 (Bs), and *P. fluorescens* PS2-6 (Pf) were obtained from the Institute of Mycorrhizal Biotechnology, Qingdao Agricultural University (QAU), China. Spores, mycorrhizal root segments, and culture media of AMF were employed as inocula with inoculation potential units determined following the method of Liu and Luo (1994).

The aforementioned PGPR species were inoculated into nutrient broth (3 g beef extract, 10 g peptone, 5 g NaCl, and distilled water to 1,000 ml) and cultured on a rotating shaker at 30°C for 3 days. The PGPR fermentation broth was diluted to 1×10^8 CFU/ml for inoculation.

Trichoderma virens 140012 (Tv), *T. harzianum* 140015 (Th), and the TFCRR pathogen *F. oxysporum* f. sp. *radicis-lycopersici* (Fo) were provided by the College of Plant Medicine, QAU. The *Trichoderma* spp. were inoculated onto potato dextrose agar (PDA) medium and incubated at 28°C for 10 days. The pellets were filtered, washed, resuspended, and diluted to 1×10^5 CFU/ml for inoculation. Fo was cultured on PDA plates for 5–7 days and a conidia suspension was prepared. The solution was diluted to 10^7 conidia/ml, stored at 4°C, and inoculated within 24 h.

Nutrient broth and PDA were used for isolation and culture of bacteria and fungi, respectively.

Peat (0–6 mm grade; Pindstrup Mosebrug A/S, Ryomgård, Denmark) was sterilized (121°C for 1 h). The chemical characteristics of the peat were pH 6, electrical conductivity 40 mS/m, NO_3^--N 70 g/m^3, NH_4^+-N 50 g/m^3, P_2O_5 140 g/m^3, K_2O 240 g/m^3, MgO 23 g/m^3, B 0.4 g/m^3, Mo 2.04 g/m^3, Cu 1.7 g/m^3, Mn 2.9 g/m^3, Zn 0.9 g/m^3, and Fe 8.4 g/m^3. The 2.5-L pots were surface-sterilized before filling with the peat.

Experimental Design, Inoculation, and Management

A greenhouse pot experiment was conducted with tomato seedlings inoculated with (alone or in combination) the symbiotic microbes and the pathogen, and a total of 54 treatments were designed (**Supplementary Table 1**). A complete randomized block design was used with five replicates for each treatment. The 54 treatments comprised inoculation with or without AMF, PGPR, and *Trichoderma*, respectively. First, 50 g of AMF inoculum (12,000 inoculation potential units), 10 ml (1×10^8 CFU/ml) of each PGPR species inoculum, and/or 10 ml (1×10^5 CFU/ml) of *Trichoderma* inoculum were mixed into the peat for the inoculation treatments, respectively. The same volume of sterilized inoculum was added for the non-inoculation treatment (control). Five seeds were sown in each pot. Subsequently, three seedlings were retained in each pot. At the 2–3 leaves stage, the seedlings were inoculated by irrigation with 10 ml of Fo conidial suspension applied to the root zone. Pots were watered three times weekly and, once per week, plants were fertigated with Hoagland's nutrient solution. The volume of nutrient solution applied to each seedling in one application was 250 ml. During the growing period, the average day/night temperatures were 19°C/27°C.

Determination of AMF Colonization, Physiological Parameters, and Metabolome Analysis of Tomato Plants

AMF Colonization and Associated Indices

Colonization by AMF was determined following the method described by Biermann and Linderman (1981). For PGPR population measurement, 1.0 g dry soil collected from the rhizosphere was added to sterilized water to prepare a soil solution. The PGPR numbers in the rhizosphere soil were counted using a dilution plate method after incubation at 30°C for 3 days (Bashan et al., 1993; Zhao and He, 2002). For *Trichoderma* colonization measurement, 1 g fine roots were cleaned and surface sterilized, cut into small segments and slices, and placed on PDA for culture at 25°C for 7 days. The number of effective colonies was recorded daily. The disease grade was classified as follows: grade 0, the root showed normal color; grade 1, root slightly discolored with the discolored area as much as 25% of the total root area; grade 2, roots with 26–50% of the total area showing discoloration; grade 3, 51–75% of the total root area showing discoloration; grade 4, more than 76% of the total root area is discolored or the plant is dead. The aforementioned parameters were measured at harvest.

Measurements of Plant Growth Indices and Photosynthetic Characteristics

Conventional methods were used to measure plant height, dry mass weight, fruit yield, and fruit weight per plant. Leaf photosynthetic parameters were measured using a portable photosynthesis system (LI-6400; LI-COR, Inc., Lincoln, NE, United States) between 08:00 and 11:30. Leaf gas exchange measurements were conducted on three leaves. The sampled leaves were frozen in liquid nitrogen and stored at −80°C for subsequent measurements of antioxidant enzyme activities.

Antioxidant Enzyme Activities

Fresh leaf samples (0.5 g) from tomato plants at the fruit-setting stage were homogenized with a pestle in an ice-cold mortar containing 10 ml of ice-cold 50 mM phosphate buffer (pH 7.0). The homogenate was filtered through gauze and then centrifuged at 1,500 × *g* for 20 min at 4°C. The supernatant (enzyme extract) was collected and used for the measurement of superoxide dismutase (SOD), catalase (CAT), peroxidase (POD), and phenylalanine ammonia-lyase (PAL) activities. Each sample was measured three times. The activities of SOD, CAT, POD, and PAL were determined according to the methods described by Wang (2006).

Metabolome Analysis

Samples of stems with young and mature leaves, and of the fine feeding roots of tomato plants at the fruit-setting stage were frozen in liquid N_2 and stored at −80°C. Metabolome analysis was performed by Biomarker Technologies Co., Ltd. (Beijing, China) using non-target liquid chromatography–mass spectrometry (LC-MS; Biomarker Technologies) to identify differences in the metabolite profile among treatments. The specific experimental methods were as follows. The sample (50 mg) was added to 1 ml extract containing an internal standard (1000:2) (methanol/acetonitrile/water, 2:2:1, v/v/v; internal standard concentration 2 mg/L), swirled, and mixed for 30 s. Porcelain beads were added and the sample was homogenized at 45 Hz for 10 min, then treated with ultrasound for 10 min in an ice water bath. After standing for 1 h at −20°C, the homogenate was centrifuged at 4°C and 13,000 × *g* for 15 min. A sample (500 μl) of the supernatant was carefully removed from the tube. The extract was dried in a vacuum concentrator. An aliquot (150 μl) of the extract (acetonitrile/water, 1:1, v/v) was added to the dried metabolites for resolution. After vortexing for 30 s, the solution was treated with ultrasound for 10 min in an ice water bath. The solution was centrifuged at 4°C and 13,000 × *g* for 15 min. A sample (120 μl) of the supernatant was carefully transferred to a 2-ml injection flask and mixed with 10 μl from each sample of the QC sample for analysis. KEGG database was used for annotation and enrichment analysis of differential metabolites.

Data Analysis

The data were statistically analyzed by ANOVA with DPS 7.05 software. Fisher's protected least significant difference (LSD) was used to compare the means at 5% level of significance. The data in the table were mean ± SE.

RESULTS

Root Symbionts Formed With the Symbiotic Microbes

The tested AMF, PGPR, *Trichoderma* spp., and their combinations colonized tomato roots and the rhizosphere soil. Among these microorganisms, under the condition of single inoculation and Fo inoculation, the colonization frequency of *T. virens* was significantly higher than that of *T. harzianum*, which were 1.1 and 1.2 times of that, respectively. Both Fm and Pf increased colonization by the other microorganism. Inoculation with Fm, Ri, and Pf enhanced the colonization frequency of *T. harzianum*, whereas Fo reduced colonization by AMF, PGPR, and *Trichoderma* spp. to different degrees. The AMF and *Trichoderma* sp. simultaneously colonized roots to form dual symbionts (**Table 1**).

Effects of Symbiotic Microbes on Plant Growth, Development, and TFCRR

Inoculation with Fm, Ri, Bs, Pf, Th, Tv, and their combination treatments increased the growth of tomato plants, and promoted early flowering, percentage fruit set, number of fruit, and yield per plant to various degrees. The treatments Ri + Bs + Tv and Fm + Pf + Tv showed the most highly significant effects. Under the condition of Fo inoculation, the effect of the treatment Ri + Pf + Th was greatest (**Table 2**).

Single inoculation, and the combinations of two or three symbiotic microorganisms, reduced the incidence and disease index of TFCRR, but the effects differed among treatments. The treatment Ri + Pf + Th + Fo showed the most significant effect, followed by the Th + Pf + Fo and Ri + Th + Fo treatments. Multivariate analysis of variance showed that there were significant interactions among AMF, PGPR, and *Trichoderma* spp. (**Table 3**).

Effects of Symbiotic Microbes on Photosynthesis and Antioxidant Enzyme Activities in Tomato Leaves

Most of the photosynthesis parameters, such as net photosynthetic rate (P_n), stomatal conductance (G_s), intercellular carbon dioxide concentration (C_i), and transpiration rate (T_r), of tomato leaves treated with Ri, Bs, Tv + Bs, Tv + Pf, Ri + Bs + Tv, and Ri + Pf + Tv were significantly higher than those of the non-inoculated control. Compared with the Fo treatment, most of the inoculation treatments showed improved photosynthetic performance (**Table 4**).

In addition, most of the inoculation treatments significantly increased the antioxidant enzyme activity of tomato plants. Among these enzymes, POD, SOD, CAT, and PAL showed the highest activity in the treatment Ri + Pf + Th + Fo, followed by Fm + Pf + Th + Fo, Fm + Pf + Tv + Fo, Ri + Bs + Tv + Fo, Ri + Th + Fo, and Th + Pf + Fo (**Table 5**).

TABLE 1 | Colonization of AMF, PGPR, and *Trichoderma* spp. on tomato roots.

Treatments	AM (%)	Arbuscule (%)	PGPR (10^6 CFU·g^{-1})	*Trichoderma* spp. (10^4 CFU·g^{-1})
Control	–	–	–	–
Fm	84.9 ± 2.3bcd	65.5 ± 2.1ab	–	–
Ri	88.4 ± 1.1ab	44.3 ± 1.1hi	–	–
Bs	–	–	8.1 ± 0.4de	–
Pf	–	–	9.0 ± 0.4bc	–
Th	–	–	–	7.2 ± 0.3def
Tv	–	–	–	7.9 ± 0.3abc
Fm + Bs	74.6 ± 2.1hijk	56.3 ± 1.7cd	6.7 ± 0.2jkl	–
Fm + Pf	91.6 ± 2.1a	70.8 ± 2.9a	9.7 ± 0.1a	–
Ri + Bs	68.1 ± 1.5lm	48.5 ± 1.8gh	6.7 ± 0.2jkl	–
Ri + Pf	90.7 ± 1.4a	61.1 ± 1.2bc	9.0 ± 0.2b	–
Fm + Th	78.2 ± 1.3fghi	60.4 ± 1.1bc	–	8.1 ± 0.2ab
Fm + Tv	83.5 ± 1.0cde	65.8 ± 1.4ab	–	7.8 ± 0.1abc
Ri + Th	89.4 ± 1.1ab	60.4 ± 1.1bc	–	8.0 ± 0.2abc
Ri + Tv	78.1 ± 1.7ghi	50.2 ± 3.5efg	–	6.6 ± 0.4gh
Th + Bs	–	–	7.7 ± 0.2efg	6.7 ± 0.2fgh
Th + Pf	–	–	8.9 ± 0.2bc	8.2 ± 0.2a
Tv + Bs	–	–	7.7 ± 0.2efg	7.5 ± 0.3cde
Tv + Pf	–	–	8.9 ± 0.2bc	7.8 ± 0.1abcd
Fm + Bs + Th	67.1 ± 2.9m	40.9 ± 2.4ijk	5.8 ± 0.1mno	4.4 ± 0.2m
Fm + Bs + Tv	75.7 ± 1.1hij	48.2 ± 1.7gh	6.3 ± 0.1lm	5.5 ± 0.1l
Ri + Pf + Th	87.5 ± 1.2abc	59.0 ± 0.7cd	9.0 ± 0.1b	7.9 ± 0.2abc
Ri + Pf + Tv	78.0 ± 1.3ghi	44.2 ± 3.7hi	8.0 ± 0.2de	5.8 ± 0.2kl
Ri + Bs + Th	67.1 ± 2.0m	33.6 ± 1.2lmn	6.8 ± 0.1ijkl	5.7 ± 0.2l
Ri + Bs + Tv	58.0 ± 2.1n	29.8 ± 1.2mn	6.4 ± 0.2kl	5.5 ± 0.2l
Fm + Pf + Th	70.9 ± 1.3jklm	49.3 ± 4.2gh	6.5 ± 0.2kl	7.8 ± 0.2abcd
Fm + Pf + Tv	79.1 ± 1.8efgh	58.9 ± 2.7cd	7.8 ± 0.2def	8.3 ± 0.1a
Fo	–	–	–	–
Fm + Fo	70.4 ± 1.6klm	55.9 ± 2.6cde	–	–
Ri + Fo	73.5 ± 1.3ijk	40.1 ± 1.0ijk	–	–
Bs + Fo	–	–	6.5 ± 0.1kl	–
Pf + Fo	–	–	7.5 ± 0.1efgh	–
Th + Fo	–	–	–	5.9 ± 0.2jkl
Tv + Fo	–	–	–	6.8 ± 0.2fgh
Fm + Bs + Fo	59.1 ± 1.0n	38.9 ± 2.2ijkl	5.6 ± 0.3no	–
Fm + Pf + Fo	85.1 ± 2.7bcd	68.3 ± 1.0a	6.8 ± 0.1ijkl	–
Ri + Bs + Fo	57.1 ± 2.2n	28.3 ± 1.4n	5.4 ± 0.2o	–
Ri + Pf + Fo	84.5 ± 2.2bcd	53.2 ± 1.0defg	8.4 ± 0.2cd	–
Fm + Th + Fo	70.7 ± 0.8klm	49.9 ± 1.2fgh	–	5.7 ± 0.2kl
Fm + Tv + Fo	78.1 ± 1.5ghi	56.5 ± 1.9cd	–	6.6 ± 0.2ghi
Ri + Th + Fo	81.1 ± 2.3defg	55.8 ± 3.2cde	–	6.4 ± 0.1hij
Ri + Tv + Fo	68.1 ± 1.5lm	35.2 ± 2.1klm	–	5.7 ± 0.2kl
Th + Bs + Fo	–	–	6.9 ± 0.2hijk	5.8 ± 0.2kl
Th + Pf + Fo	–	–	8.9 ± 0.1bc	7.5 ± 0.2bcde
Tv + Bs + Fo	–	–	6.7 ± 0.2jkl	6.3 ± 0.1hijk
Tv + Pf + Fo	–	–	7.7 ± 0.2efg	7.1 ± 0.2efg
Fm + Bs + Th + Fo	48.8 ± 1.9o	30.4 ± 1.8mn	5.8 ± 0.3mno	4.8 ± 0.2m
Fm + Bs + Tv + Fo	60.6 ± 1.2n	41.4 ± 1.1ij	5.8 ± 0.2mno	5.4 ± 0.2l
Ri + Pf + Th + Fo	83.0 ± 1.6cdef	55.4 ± 2.7cdef	9.0 ± 0.1bc	7.5 ± 0.2bcde
Ri + Pf + Tv + Fo	72.0 ± 1.8jkl	36.4 ± 1.8jkl	7.1 ± 0.4ghij	6.8 ± 0.1fgh
Ri + Bs + Th + Fo	57.1 ± 2.0n	28.0 ± 1.3n	6.2 ± 0.2lmn	5.5 ± 0.3l
Ri + Bs + Tv + Fo	61.0 ± 1.5n	29.6 ± 1.3mn	5.7 ± 0.2mno	5.8 ± 0.2jkl
Fm + Pf + Th + Fo	58.9 ± 0.7n	38.1 ± 1.5jkl	7.4 ± 0.1fghi	6.8 ± 0.2fgh
Fm + Pf + Tv + Fo	66.6 ± 2.4m	48.2 ± 2.0gh	6.6 ± 0.4jkl	6.0 ± 0.1ijkl

Fm, Funneliformis mosseae; Ri, Rhizophagus intraradices; Bs, Bacillus subtilis PS1-3; Pf, Pseudomonas fluorescens PS2-6; Tv, Trichoderma virens 140012; Th, Trichoderma harzianum 140015; Fo, Fusarium oxysporum f. sp. radicis-lycopersici. Mean data ± SE of 54 treatments are presented. For each column, data followed by the same letter are not significantly different at $p < 0.05$ (LSD test).

TABLE 2 | Influences of AMF, PGPR, *Trichoderma* spp., and *Fusarium oxysporum* f. sp. *radicis-lycopersici* on tomato growth and yield.

Inoculation	Plant height (cm)	Dry mass of stem with leaves (g)	Dry mass of roots (g)	Fruit weight per plant (g)	Number of fruits per plant
Control	42.2 ± 4.3gh	26.7 ± 1.3u	4.2 ± 0.2opqrst	20.5 ± 6.4lm	1.7 ± 0.3de
Fm	46.3 ± 1.9cdefgh	35.2 ± 1.1pqrs	4.6 ± 0.2mnopqr	35.7 ± 0.6fghijkl	1.7 ± 0.3de
Ri	45.6 ± 3.2cdefgh	36.5 ± 1.8lmnopqr	4.5 ± 0.4mnopqrs	66.6 ± 15abc	2.0 ± 0.6cde
Bs	50.5 ± 4.5abcdefgh	42.5 ± 1.9cdefghij	6.2 ± 0.2ab	31.6 ± 3.2hijklm	2.0 ± 0.0cde
Pf	46.9 ± 2.6bcdefgh	34.4 ± 3.0qrst	4.5 ± 0.2mnopqrs	36.4 ± 3.6efghijkl	2.0 ± 0.0cde
Th	53.2 ± 2.6abcdef	44.0 ± 1.7bcdef	6.8 ± 0.3a	28.0 ± 8.0hijklm	2.0 ± 0.6cde
Tv	46.3 ± 3.8cdefgh	36.4 ± 3.0lmnopqr	5.3 ± 0.3efghijkl	68.5 ± 4.2ab	2.0 ± 0.0cde
Fm + Bs	55.8 ± 3.9abc	47.6 ± 2.9bcd	6.0 ± 0.1bc	18.9 ± 3.2lm	1.7 ± 0.3de
Fm + Pf	50.2 ± 4.0abcdefgh	45.4 ± 3.0bcdef	5.3 ± 0.3efghijkl	48.8 ± 4.4bcdefghij	2.3 ± 0.3bcde
Ri + Bs	49.9 ± 4.5bcdefgh	43.3 ± 2.2bcdefghij	5.3 ± 0.3defghijk	63.5 ± 8.5abcd	2.3 ± 0.3bcde
Ri + Pf	51.5 ± 4.5abcdefgh	46.3 ± 2.2bcdef	5.6 ± 0.3cdefgh	50.8 ± 5.7bcdefgh	3.0 ± 0.0abcd
Fm + Th	54.4 ± 1.8abcd	48.4 ± 1.8bc	5.9 ± 0.2bcde	26.6 ± 8.5ijklm	3.0 ± 0.0abcd
Fm + Tv	49.3 ± 5.0bcdefgh	44.1 ± 1.2bcdef	5.0 ± 0.1ghijklmn	41.1 ± 8.4defghijkl	2.7 ± 0.3bcde
Ri + Th	46.6 ± 3.6bcdefgh	36.3 ± 3.0lmnopqr	4.5 ± 0.3mnopqrs	36.4 ± 5.9efghijkl	1.7 ± 0.7de
Ri + Tv	47.4 ± 3.5bcdefgh	37.7 ± 2.2ghijklmnopq	4.7 ± 0.2klmnopq	55.4 ± 6.3abcdefg	2.0 ± 0.0cde
Th + Bs	50.5 ± 7.9abcdefgh	43.6 ± 2.0bcdefg	5.7 ± 0.3bcdef	40.5 ± 6.6defghijkl	2.7 ± 1.2bcde
Th + Pf	51.4 ± 2.2abcdefgh	46.6 ± 3.1bcde	5.9 ± 0.2bcde	47.5 ± 7.3bcdefghijk	2.3 ± 0.3bcde
Tv + Bs	50.3 ± 3.9abcdefgh	42.6 ± 2.4cdefghij	5.4 ± 0.3defghijk	59.9 ± 14abcde	2.3 ± 0.3bcde
Tv + Pf	49.5 ± 3.6bcdefgh	41.2 ± 2.3efghijklmno	4.7 ± 0.2klmnopq	66.6 ± 9.4abc	2.7 ± 0.3bcde
Fm + Bs + Th	47.7 ± 3.9bcdefgh	36.5 ± 1.8klmnopqr	4.3 ± 0.2nopqrst	36.4 ± 5.4efghijkl	3.0 ± 0.6abcd
Fm + Bs + Tv	51.6 ± 3.5abcdefgh	46.4 ± 1.3bcde	5.7 ± 0.3bcdef	45.6 ± 4.8bcdefghijk	2.3 ± 0.3bcde
Ri + Pf + Th	43.4 ± 2.8fgh	34.7 ± 1.8pqrs	4.4 ± 0.2nopqrst	37.0 ± 8.0efghijkl	2.0 ± 1.0cde
Ri + Pf + Tv	45.2 ± 3.5defgh	35.6 ± 1.1nopqr	4.6 ± 0.2lmnopqr	41.8 ± 6.0defghijkl	2.7 ± 0.3bcde
Ri + Bs + Th	53.5 ± 2.4abcdef	45.3 ± 3.0bcdef	5.6 ± 0.3bcdefg	36.5 ± 3.1efghijkl	2.3 ± 0.9bcde
Ri + Bs + Tv	60.5 ± 1.4a	57.5 ± 0.7a	6.0 ± 0.3bcd	50.1 ± 2.2bcdefghi	3.3 ± 0.3abc
Fm + Pf + Th	48.6 ± 4.2bcdefgh	42.8 ± 2.3bcdefghij	5.5 ± 0.2cdefghi	32.7 ± 4.9ghijkl	2.0 ± 0.0cde
Fm + Pf + Tv	56.7 ± 1.6ab	54.7 ± 0.8a	5.4 ± 0.1cdefghij	76.7 ± 8.1a	3.0 ± 0.6abcd
Fo	42.4 ± 4.1gh	28.6 ± 1.3tu	4.8 ± 0.2jklmnop	29.1 ± 8.6hijklm	2.7 ± 0.7bcde
Fm + Fo	43.3 ± 4.0fgh	33.5 ± 1.8qrst	3.2 ± 0.1w	29.1 ± 13hijklm	2.0 ± 0.0cde
Ri + Fo	49.8 ± 4.6bcdefgh	42.4 ± 1.8cdefghijk	4.1 ± 0.2qrst	24.9 ± 7.2klm	1.7 ± 0.3de
Bs + Fo	47.3 ± 4.7bcdefgh	40.4 ± 2.3fghijklmnop	4.3 ± 0.1opqrst	38.8 ± 12efghijkl	2.0 ± 0.6cde
Pf + Fo	44.5 ± 4.8defgh	36.2 ± 1.8lmnopqr	4.2 ± 0.1pqrst	27.2 ± 4.4ijklm	2.0 ± 0.0cde
Th + Fo	43.6 ± 4.0efgh	35.7 ± 1.3mnopqr	3.8 ± 0.2tuv	32.4 ± 3.1ghijklm	2.0 ± 0.0cde
Tv + Fo	41.7 ± 2.2h	29.4 ± 1.2stu	3.5 ± 0.2uvw	27.8 ± 1.9hijklm	2.0 ± 0.6cde
Fm + Bs + Fo	47.4 ± 3.4bcdefgh	41.5 ± 1.7efghijklmn	4.0 ± 0.2rstu	37.8 ± 4.9efghijkl	1.7 ± 0.3de
Fm + Pf + Fo	49.7 ± 4.1bcdefgh	41.6 ± 2.1efghijklm	3.9 ± 0.1tuv	57.9 ± 16abcdef	1.7 ± 0.3de
Ri + Bs + Fo	50.1 ± 1.2bcdefgh	43.6 ± 2.0bcdefgh	4.5 ± 0.2nopqrst	25.4 ± 2.8jklm	1.7 ± 0.3de
Ri + Pf + Fo	49.4 ± 4.0bcdefgh	42.4 ± 2.2cdefghijk	4.4 ± 0.2nopqrst	39.5 ± 3.4efghijkl	2.0 ± 0.6cde
Fm + Th + Fo	44.6 ± 4.5defgh	37.6 ± 1.2hijklmnopq	3.4 ± 0.2vw	31.9 ± 5.3ghijklm	2.0 ± 0.0cde
Fm + Tv + Fo	41.5 ± 2.1h	31.2 ± 1.2rstu	3.0 ± 0.1w	38.4 ± 14efghijkl	1.3 ± 0.3e
Ri + Th + Fo	45.2 ± 3.5defgh	37.7 ± 1.6ghijklmnopq	3.9 ± 0.2stuv	49.0 ± 5.1bcdefghij	2.0 ± 0.0cde
Ri + Tv + Fo	49.8 ± 4.6bcdefgh	41.7 ± 2.4efghijkl	4.3 ± 0.1nopqrst	35.2 ± 17fghijkl	3.0 ± 1.0abcd
Th + Bs + Fo	47.7 ± 3.6bcdefgh	48.7 ± 3.3b	5.2 ± 0.3efghijkl	37.1 ± 6.2efghijkl	2.0 ± 0.6cde
Th + Pf + Fo	45.6 ± 3.8cdefgh	37.6 ± 1.2ijklmnopq	4.8 ± 0.1klmnopq	30.1 ± 9.2hijklm	1.7 ± 0.3de
Tv + Bs + Fo	52.4 ± 4.5abcdefg	44.6 ± 2.5bcdef	5.8 ± 0.2bcde	32.3 ± 6.5ghijklm	2.0 ± 0.6cde
Tv + Pf + Fo	43.5 ± 4.5efgh	35.4 ± 2.2opqr	4.8 ± 0.2ijklmno	19.5 ± 3.7lm	1.7 ± 0.3de
Fm + Bs + Th + Fo	45.8 ± 3.4cdefgh	37.5 ± 1.3jklmnopq	4.3 ± 0.2opqrst	9.1 ± 0.5m	2.0 ± 0.0cde
Fm + Bs + Tv + Fo	50.5 ± 3.3abcdefgh	43.5 ± 2.3bcdefghi	5.2 ± 0.1fghijklm	44.6 ± 12cdefghijk	2.0 ± 0.0cde
Ri + Pf + Th + Fo	53.8 ± 2.4abcde	45.5 ± 2.7bcdef	4.3 ± 0.1opqrst	49.2 ± 22bcdefghi	4.3 ± 2.3a
Ri + Pf + Tv + Fo	48.6 ± 3.4bcdefgh	42.5 ± 2.9cdefghij	4.4 ± 0.1nopqrst	37.8 ± 4.2efghijkl	2.0 ± 0.0cde
Ri + Bs + Th + Fo	47.7 ± 3.6bcdefgh	41.7 ± 2.4defghijkl	4.2 ± 0.3opqrst	38.8 ± 15efghijkl	3.7 ± 0.9ab
Ri + Bs + Tv + Fo	51.4 ± 4.0abcdefgh	44.6 ± 2.1bcdef	4.6 ± 0.3mnopqr	38.2 ± 4.0efghijkl	3.0 ± 0.6abcd
Fm + Pf + Th + Fo	49.6 ± 4.6bcdefgh	42.5 ± 2.3cdefghij	4.1 ± 0.2rstu	40.1 ± 5.8defghijkl	2.7 ± 0.3bcde
Fm + Pf + Tv + Fo	49.6 ± 4.2bcdefgh	43.5 ± 2.9bcdefghi	4.9 ± 0.3hijklmn	39.1 ± 5.5efghijkl	2.7 ± 0.3bcde

Fm, Funneliformis mosseae; Ri, Rhizophagus intraradices; Bs, Bacillus subtilis PS1-3; Pf, Pseudomonas fluorescens PS2-6; Tv, Trichoderma virens 140012; Th, Trichoderma harzianum 140015; Fo, Fusarium oxysporum f. sp. radicis-lycopersici. Mean data ± SE of 54 treatments are presented. For each column, data followed by the same letter are not significantly different at $p < 0.05$ (LSD test).

TABLE 3 | Effects of AMF, PGPR, and *Trichoderma* spp. on TFCRR disease.

Inoculation	Disease incidence (%)	Disease index	Relative control effects (%)
Fo	75.7 ± 1.2a	53.1 ± 1.6a	–
Fm + Fo	35.0 ± 2.4hi	34.0 ± 2.5defgh	35.9 ± 4.8efghi
Ri + Fo	33.6 ± 1.8hi	31.6 ± 1.1ghi	40.4 ± 2.1def
Bs + Fo	53.1 ± 0.8bc	41.4 ± 0.6b	22.0 ± 1.0k
Pf + Fo	49.5 ± 1.0cd	38.3 ± 1.3bcd	28.0 ± 2.5ijk
Th + Fo	41.2 ± 1.3fg	34.1 ± 2.7defgh	35.7 ± 5.1efghi
Tv + Fo	56.7 ± 2.1b	37.8 ± 2.3bcde	28.8 ± 4.3hijk
Fm + Bs + Fo	38.3 ± 1.7ghi	35.6 ± 2.3cdefg	32.9 ± 4.3fghij
Fm + Pf + Fo	33.9 ± 1.9hi	31.5 ± 1.0ghi	40.6 ± 1.8def
Ri + Bs + Fo	47.9 ± 1.3de	39.8 ± 1.7bc	25.1 ± 3.2jk
Ri + Pf + Fo	28.2 ± 1.5jk	24.1 ± 2.5jk	54.7 ± 4.8bc
Fm + Th + Fo	44.4 ± 2.5def	40.7 ± 1.0b	23.4 ± 1.9k
Fm + Tv + Fo	38.5 ± 3.3gh	34.8 ± 2.3defgh	34.5 ± 4.4efghi
Ri + Th + Fo	26.5 ± 1.9k	22.7 ± 0.7kl	57.3 ± 1.3ab
Ri + Tv + Fo	48.3 ± 1.0cde	37.7 ± 1.2bcdef	29.0 ± 2.2ghijk
Th + Bs + Fo	33.6 ± 1.9hi	27.9 ± 1.3ij	47.5 ± 2.5cd
Th + Pf + Fo	26.1 ± 1.6k	21.9 ± 1.6kl	58.7 ± 3.1ab
Tv + Bs + Fo	48.0 ± 1.3cde	39.9 ± 1.4bc	24.8 ± 2.7jk
Tv + Pf + Fo	44.0 ± 2.5ef	30.5 ± 1.1hi	42.6 ± 2.0de
Fm + Bs + Th + Fo	38.1 ± 1.4ghi	33.8 ± 1.5defgh	36.4 ± 2.9efghi
Fm + Bs + Tv + Fo	42.6 ± 1.3fg	33.5 ± 1.1efgh	37.0 ± 2.1efgh
Ri + Pf + Th + Fo	12.8 ± 1.6l	18.1 ± 1.3l	65.8 ± 2.5a
Ri + Pf + Tv + Fo	33.4 ± 1.9hi	30.4 ± 1.1hi	42.8 ± 2.1de
Ri + Bs + Th + Fo	35.2 ± 2.1hi	30.2 ± 1.9hi	43.1 ± 3.6de
Ri + Bs + Tv + Fo	41.7 ± 2.3fg	32.9 ± 0.9fgh	38.0 ± 1.6efg
Fm + Pf + Th + Fo	35.3 ± 1.6hi	23.8 ± 2.7jk	55.1 ± 5.0bc
Fm + Pf + Tv + Fo	33.3 ± 1.4ij	23.8 ± 1.1jk	55.1 ± 2.1bc
ANOVA			
F(AMF)	**	**	**
F(PGPR)	**	**	**
F(*Trichoderma*)	**	**	**
F(AMF × PGPR)	**	**	**
F(AMF × *Trichoderma*)	**	**	**
F(PGPR × *Trichoderma*)	NS	NS	NS
F(AMF × PGPR × *Trichoderma*)	**	**	**

*Fm, Funneliformis mosseae; Ri, Rhizophagus intraradices; Bs, Bacillus subtilis PS1-3; Pf, Pseudomonas fluorescens PS2-6; Tv, Trichoderma virens 140012; Th, Trichoderma harzianum 140015; Fo, Fusarium oxysporum f. sp. radicis-lycopersici. Mean data ± SE of 28 treatments are presented. For each column, data followed by the same letter are not significantly different ($p < 0.05$). NS means no significant difference; **means extremely significant difference at $p < 0.01$ level.*

Effects of Symbiotic Microbes on Physiological Metabolism of Tomato Plants

Using non-target LC-MS, metabolome analysis was conducted on the shoots (S) and roots (R) of control (1), Ri + Pf + Th (22), Fo (28), and Ri + Pf + Th + Fo (49) treatments. Principal component analysis (PCA) and partial least squares discriminant analysis were used to analyze the detected MS data to determine the final difference in charge-to-mass ratio, which was then compared with the KEGG metabolite database, and the difference in metabolite content and species among treatments was identified.

Overview of Metabolite Profiles Using PCA and Hierarchical Cluster Analysis

Principal component analysis was performed to reduce the dimensionality of the data and visualize the relationships among the 24 samples. The first principal component (PC1) explained 87.99% of the total variation and the second principal component (PC2) explained 3.24% of the variation across the data set (**Figure 1**). The responses of the aboveground and underground organs to the different inoculation treatments were well separated by PC1. Regardless of the control group and the treatment group, no significant difference in the metabolites of the aboveground or underground organs was detected, whereas the metabolites differed between the aboveground and underground organs, indicating that aboveground and belowground metabolism of the plant differed significantly. In addition, the biological replicates were projected closely in multidimensional space, which indicated that the replicates showed a strong correlation. Cluster heat map analysis was conducted for 24 samples, of which all samples were clustered into four main groups and the samples from the same organ were clustered together (**Figure 2**). A higher number of metabolites were up-regulated in the shoot, whereas a greater number of metabolites were down-regulated in the root of tomato plants (**Figure 2**). Thus, significant differences in metabolism between aboveground and underground organs of the plant were demonstrated. Correlation analysis among the 24 samples showed that each treatment showed high repeatability. Collectively, these results indicated that the data were reliable and the experiment was meaningful.

Differential Metabolite Analysis

A total of 1,266 differential metabolites were detected in the metabolome analysis. With regard to the aboveground organs of tomato, compared with the S1 group, the number of up-regulated metabolites in the S22 treatment group exceeded the number of down-regulated metabolites, whereas the number of down-regulated metabolites in the S28 treatment group was significantly increased and was 44 times higher than that of up-regulated metabolites. The number of metabolites down-regulated in the S49 treatment group was more than the number that were up-regulated. However, after inoculation with Ri + Pf + Th, in tomato shoots the number of down-regulated metabolites decreased and the number of up-regulated metabolites increased (**Figure 3** and **Supplementary Figure 2**).

With regard to the roots of tomato, the number of up-regulated metabolites in the R22, R28, and R49 treatment groups was significantly higher than that in the R1 group, and the number of up-regulated metabolites in the R22 treatment group was 40 times higher than the number of down-regulated metabolites. However, compared with the plants inoculated with Fo, the number of up-regulated metabolites increased by 63 and the number of down-regulated metabolites decreased by 6 in tomato inoculated with Ri + Pf + Th (**Figure 3** and **Supplementary Figure 2**).

TABLE 4 | Influences of AMF, PGPR, *Trichoderma* spp., and *Fusarium oxysporum* f. sp. *radicis-lycopersici* on tomato leaf photosynthetic performance.

Inoculation	P_n ($\mu mol \cdot m^{-2} \cdot s^{-1}$)	G_s ($mol \cdot m^{-2} \cdot s^{-1}$)	C_i ($\mu mol \cdot mol^{-1}$)	T_r ($mmol \cdot m^{-2} \cdot s^{-1}$)
Control	9.3 ± 0.1ij	0.21 ± 0.06ij	265.5 ± 2.9defgh	2.3 ± 0.1hijklm
Fm	12.5 ± 1.1bcdefghi	0.32 ± 0.01bcdefgh	308.9 ± 0.5abcd	3.6 ± 0.1abcdefg
Ri	13.8 ± 0.6bc	0.38 ± 0.01bcd	319.0 ± 1.8a	4.7 ± 0.2a
Bs	13.8 ± 0.8bc	0.35 ± 0.07bcdef	313.3 ± 8.7abc	4.6 ± 0.6ab
Pf	10.1 ± 0.3ghij	0.25 ± 0.07fghi	294.8 ± 15abcdefg	2.9 ± 0.2efghijklm
Th	10.2 ± 0.2fghij	0.29 ± 0.08cdefghi	314.0 ± 5.1abc	3.5 ± 1.0abcdefgh
Tv	13.5 ± 1.6bcde	0.31 ± 0.05bcdefghi	306.7 ± 2.0abcd	4.2 ± 0.4abcd
Fm + Bs	13.0 ± 1.3bcdefgh	0.30 ± 0.03cdefghi	310.4 ± 3.1abcd	4.0 ± 0.2abcde
Fm + Pf	12.8 ± 1.1bcdefgh	0.33 ± 0.06bcdef	314.8 ± 7.1ab	4.4 ± 0.5abc
Ri + Bs	12.9 ± 0.6bcdefgh	0.34 ± 0.03bcdef	314.4 ± 4.6ab	3.7 ± 0.7abcdef
Ri + Pf	10.2 ± 0.3efghij	0.34 ± 0.16bcdef	299.1 ± 31abcdef	2.8 ± 0.1fghijklm
Fm + Th	13.2 ± 1.8bcdefg	0.26 ± 0.06fghi	289.8 ± 12abcdefg	3.1 ± 0.9defghijk
Fm + Tv	13.2 ± 1.0bcdefg	0.30 ± 0.03cdefghi	307.8 ± 9abcd	4.1 ± 0.2abcde
Ri + Th	10.3 ± 3.5efghij	0.32 ± 0.01bcdefgh	299.5 ± 10abcdef	2.9 ± 1.1efghijklm
Ri + Tv	12.3 ± 0.8bcdefghi	0.35 ± 0.01bcdef	284.9 ± 3.2abcdefgh	3.2 ± 0.2cdefghijk
Th + Bs	12.5 ± 0.3bcdefghi	0.36 ± 0.01bcde	304.0 ± 1.1abcde	3.8 ± 0.1abcdef
Th + Pf	14.1 ± 1.1ab	0.27 ± 0.05efghi	288.9 ± 9.3abcdefg	3.7 ± 0.5abcdef
Tv + Bs	12.8 ± 0.6bcdefgh	0.41 ± 0.01ab	317.6 ± 11ab	3.6 ± 0.2abcdefg
Tv + Pf	17.3 ± 2.5a	0.37 ± 0.01bcde	294.8 ± 3.3abcdefg	4.7 ± 0.6a
Fm + Bs + Th	10.1 ± 2.7ghij	0.35 ± 0.01bcdef	306.5 ± 13abcd	3.1 ± 1.2defghijkl
Fm + Bs + Tv	12.4 ± 1.6bcdefghi	0.37 ± 0.01bcde	301.7 ± 8.7abcdef	3.2 ± 0.5cdefghijk
Ri + Pf + Th	12.3 ± 0.5bcdefghi	0.31 ± 0.01bcdefghi	188.0 ± 30j	2.9 ± 0.1efghijklm
Ri + Pf + Tv	13.0 ± 0.4bcdefgh	0.33 ± 0.01bcdefg	304.4 ± 7.3abcd	3.8 ± 0.3abcdef
Ri + Bs + Th	10.6 ± 1.4cdefghi	0.38 ± 0.01abc	276.1 ± 20abcdefgh	2.3 ± 0.8hijklm
Ri + Bs + Tv	13.6 ± 1.3bcd	0.48 ± 0.01a	291.9 ± 12abcdefg	2.3 ± 0.4ijklmn
Fm + Pf + Th	11.1 ± 2.2bcdefghi	0.30 ± 0.01cdefghi	278.3 ± 21abcdefgh	2.1 ± 0.7jklmn
Fm + Pf + Tv	12.1 ± 0.7bcdefghi	0.31 ± 0.01bcdefghi	303.4 ± 18abcdef	3.4 ± 1.1bcdefghi
Fo	7.3 ± 0.1j	0.14 ± 0.01j	212.9 ± 1.5ij	1.1 ± 0.1n
Fm + Fo	11.6 ± 0.7bcdefghi	0.33 ± 0.03bcdef	256.6 ± 29fghi	2.0 ± 0.2klmn
Ri + Fo	12.6 ± 0.8bcdefghi	0.29 ± 0.01cdefghi	248.7 ± 26ghi	1.8 ± 0.1mn
Bs + Fo	13.5 ± 1.0bcde	0.27 ± 0.01defghi	270.9 ± 32bcdefgh	2.0 ± 0.1jklmn
Pf + Fo	11.7 ± 1.4bcdefghi	0.25 ± 0.01fghi	279.4 ± 12abcdefgh	1.8 ± 0.1mn
Th + Fo	9.8 ± 0.2hij	0.27 ± 0.01efghi	288.3 ± 21abcdefg	1.9 ± 0.1lmn
Tv + Fo	10.8 ± 1.2bcdefghi	0.26 ± 0.01efghi	266.9 ± 34cdefgh	2.0 ± 0.1jklmn
Fm + Bs + Fo	13.5 ± 1.0bcdef	0.28 ± 0.05defghi	317.6 ± 14ab	2.2 ± 0.1ijklmn
Fm + Pf + Fo	12.9 ± 0.6bcdefgh	0.29 ± 0.01cdefghi	306.8 ± 5.4abcd	2.2 ± 0.1ijklmn
Ri + Bs + Fo	11.9 ± 1.7bcde	0.32 ± 0.01bcdefgh	309.9 ± 9.7abcd	2.3 ± 0.1hijklmn
Ri + Pf + Fo	12.6 ± 0.7bcdefghi	0.23 ± 0.03ghij	301.0 ± 7.2abcdef	2.3 ± 0.1hijklmn
Fm + Th + Fo	11.5 ± 0.7bcde	0.25 ± 0.01fghi	275.2 ± 16abcdefgh	2.3 ± 0.1hijklmn
Fm + Tv + Fo	12.6 ± 0.9bcdefghi	0.27 ± 0.01defghi	289.8 ± 23abcdefg	2.4 ± 0.1ghijklm
Ri + Th + Fo	11.3 ± 1.2bcdefghi	0.26 ± 0.01efghi	281.0 ± 13abcdefgh	2.3 ± 0.1hijklm
Ri + Tv + Fo	12.5 ± 0.8bcdefghi	0.22 ± 0.09hij	282.7 ± 22abcdefgh	1.8 ± 0.1mn
Th + Bs + Fo	13.0 ± 1.1bcdefgh	0.32 ± 0.02bcdefgh	308.7 ± 11abcd	3.2 ± 0.1cdefghij
Th + Pf + Fo	12.7 ± 0.4bcdefgh	0.28 ± 0.01cdefghi	312.4 ± 12abcd	2.9 ± 0.1efghijklm
Tv + Bs + Fo	11.5 ± 0.8bcdefghi	0.33 ± 0.01bcdefg	238.7 ± 22hi	2.3 ± 0.1ijklmn
Tv + Pf + Fo	10.6 ± 0.7cdefghij	0.28 ± 0.01cdefghi	256.9 ± 51efghi	1.9 ± 0.1lmn
Fm + Bs + Th + Fo	11.6 ± 0.9bcdefghi	0.26 ± 0.01efghi	276.6 ± 10abcdefgh	2.4 ± 0.1ghijklm
Fm + Bs + Tv + Fo	10.7 ± 0.8cdefghi	0.31 ± 0.01bcdefghi	317.0 ± 11ab	2.2 ± 0.1ijklmn
Ri + Pf + Th + Fo	12.4 ± 0.7bcdefghi	0.33 ± 0.02bcdef	299.5 ± 9.3abcdef	2.3 ± 0.1ijklmn
Ri + Pf + Tv + Fo	10.5 ± 0.7cdefghij	0.26 ± 0.01efghi	298.3 ± 4.3abcdef	1.9 ± 0.1lmn
Ri + Bs + Th + Fo	10.3 ± 0.6efghij	0.32 ± 0.01bcdefgh	307.8 ± 5.4abcd	2.1 ± 0.1jklmn
Ri + Bs + Tv + Fo	11.6 ± 0.5bcde	0.26 ± 0.01efghi	296.0 ± 15abcdef	2.3 ± 0.1hijklmn
Fm + Pf + Th + Fo	10.3 ± 1.7defghij	0.25 ± 0.01fghi	291.4 ± 19abcdefg	1.8 ± 0.1mn
Fm + Pf + Tv + Fo	12.1 ± 0.7bcdefghi	0.28 ± 0.01cdefghi	292.0 ± 21abcdefg	2.3 ± 0.1hijklmn

Fm, Funneliformis mosseae; Ri, Rhizophagus intraradices; Bs, Bacillus subtilis PS1-3; Pf, Pseudomonas fluorescens PS2-6; Tv, Trichoderma virens 140012; Th, Trichoderma harzianum 140015; Fo, Fusarium oxysporum f. sp. radicis-lycopersici. Mean data ± SE of 54 treatments are presented. For each column, data followed by the same letter are not significantly different at $p < 0.05$ (LSD test).

TABLE 5 | Influences of AMF, PGPR, *Trichoderma*, and *Fusarium oxysporum* f. sp. *radicis-lycopersici* on the antioxidant enzyme activity in tomato leaves.

Inoculation	POD activity (U/g·min)	SOD activity (U/g)	CAT activity (U/g·min)	PAL activity (U/g·min)
Control	10.6 ± 0.8n	57.3 ± 0.9o	82.8 ± 0.6p	10.4 ± 0.7p
Fm	23.2 ± 1.1k	85.3 ± 0.5lm	117.8 ± 0.8n	18.2 ± 0.6lmn
Ri	23.8 ± 0.7k	87.0 ± 0.6kl	117.6 ± 0.6n	19.4 ± 0.3jkl
Bs	18.4 ± 1.5m	80.0 ± 1.6n	110.0 ± 0.8o	15.3 ± 0.3o
Pf	18.7 ± 1.3m	82.5 ± 1.4mn	112.1 ± 0.6o	16.8 ± 0.6mno
Th	18.5 ± 1.2m	81.9 ± 1.4n	112.1 ± 0.9o	16.4 ± 0.6no
Tv	19.9 ± 1.3lm	81.5 ± 1.2n	112.1 ± 0.8o	16.9 ± 1.1mno
Fm + Bs	23.8 ± 0.5k	86.9 ± 0.8kl	129.2 ± 0.8l	19.4 ± 0.6jkl
Fm + Pf	29.8 ± 1.1hij	88.5 ± 0.3k	136.8 ± 0.8j	23.4 ± 0.7h
Ri + Bs	23.3 ± 1.0k	85.3 ± 0.8lm	122.4 ± 0.7m	18.5 ± 0.6klm
Ri + Pf	27.5 ± 0.6j	89.2 ± 0.6k	132.0 ± 1.2k	20.3 ± 0.6jk
Fm + Th	23.8 ± 1.2k	87.2 ± 0.7kl	127.7 ± 0.6l	19.4 ± 0.6jkl
Fm + Tv	28.8 ± 0.9ij	89.5 ± 0.9k	135.2 ± 0.4j	21.2 ± 0.7ij
Ri + Th	27.6 ± 0.8j	88.7 ± 1.3k	131.7 ± 0.7k	20.2 ± 0.5jk
Ri + Tv	23.5 ± 0.4k	85.3 ± 0.7lm	131.8 ± 0.8k	18.5 ± 0.8klm
Th + Bs	21.1 ± 1.2klm	80.5 ± 0.4n	122.2 ± 0.9m	18.2 ± 0.6lmn
Th + Pf	21.5 ± 1.0kl	82.5 ± 0.9mn	123.4 ± 0.7m	19.3 ± 1.2jkl
Tv + Bs	21.5 ± 1.2kl	81.6 ± 1.5n	124.2 ± 0.5m	18.2 ± 0.7lmn
Tv + Pf	28.5 ± 0.6ij	88.7 ± 1.1k	132.0 ± 0.8k	20.4 ± 0.6jk
Fm + Bs + Th	31.0 ± 0.7ghi	97.0 ± 1.1ij	142.1 ± 0.8hi	24.4 ± 0.5h
Fm + Bs + Tv	32.1 ± 0.9fgh	97.1 ± 1.1ij	144.1 ± 0.5h	26.7 ± 0.6g
Ri + Pf + Th	37.8 ± 0.9cd	110.5 ± 1.1fg	152.1 ± 1.2g	32.7 ± 0.5de
Ri + Pf + Tv	32.1 ± 0.9fgh	102.1 ± 0.8h	144.2 ± 1.1h	26.6 ± 0.5g
Ri + Bs + Th	30.0 ± 1.1hij	95.4 ± 0.8j	139.9 ± 0.9i	21.2 ± 0.6ij
Ri + Bs + Tv	30.0 ± 1.1hij	95.7 ± 0.6j	139.9 ± 0.7i	22.6 ± 0.7hi
Fm + Pf + Th	32.1 ± 1.1fgh	98.6 ± 0.8i	144.1 ± 0.6h	27.4 ± 0.8g
Fm + Pf + Tv	33.5 ± 1.4fg	102.0 ± 0.8h	144.2 ± 0.5h	29.7 ± 0.5f
Fo	20.1 ± 1.7lm	79.8 ± 1.2n	117.3 ± 1.3n	16.7 ± 0.7mno
Fm + Fo	30.9 ± 1.1ghi	98.5 ± 0.5i	135.4 ± 0.6j	20.6 ± 0.6j
Ri + Fo	33.2 ± 0.8fg	102.2 ± 1.0h	140.0 ± 0.9i	24.2 ± 0.5h
Bs + Fo	28.6 ± 1.1ij	94.6 ± 0.8j	128.2 ± 0.5l	20.0 ± 0.5jkl
Pf + Fo	28.6 ± 0.4ij	94.7 ± 1.4j	128.5 ± 0.4l	20.6 ± 0.7j
Th + Fo	31.2 ± 0.7ghi	98.5 ± 1.4i	136.8 ± 0.6j	23.4 ± 0.6h
Tv + Fo	30.3 ± 0.8hij	97.1 ± 1.0ij	131.6 ± 0.8k	22.7 ± 0.6hi
Fm + Bs + Fo	34.7 ± 0.4ef	108.8 ± 0.9g	144.0 ± 0.7h	27.3 ± 0.6g
Fm + Pf + Fo	36.5 ± 1.3de	112.1 ± 1.5f	153.2 ± 0.8g	30.5 ± 0.9f
Ri + Bs + Fo	36.4 ± 1.1de	110.7 ± 0.9fg	142.1 ± 0.6hi	27.5 ± 0.7g
Ri + Pf + Fo	38.2 ± 1.1cd	112.4 ± 1.3f	157.6 ± 0.7f	29.8 ± 0.5f
Fm + Th + Fo	34.7 ± 0.6ef	108.7 ± 0.9g	142.1 ± 0.9hi	27.5 ± 0.7g
Fm + Tv + Fo	36.5 ± 0.8de	109.0 ± 0.7g	152.3 ± 1.2g	26.9 ± 0.6g
Ri + Th + Fo	40.4 ± 1.5bc	120.0 ± 1.4d	162.1 ± 1.1e	33.2 ± 0.5de
Ri + Tv + Fo	34.9 ± 0.6ef	108.4 ± 0.9g	153.3 ± 0.6g	24.4 ± 0.8h
Th + Bs + Fo	36.8 ± 0.8de	110.3 ± 0.8fg	157.8 ± 0.8f	27.0 ± 0.9g
Th + Pf + Fo	40.4 ± 1.4bc	119.9 ± 1.1d	161.6 ± 0.9e	32.8 ± 0.6de
Tv + Bs + Fo	36.4 ± 1.0de	112.0 ± 1.5f	143.7 ± 0.6h	27.3 ± 1.0g
Tv + Pf + Fo	36.8 ± 0.8de	112.7 ± 0.6f	157.7 ± 0.8f	30.3 ± 0.7f
Fm + Bs + Th + Fo	38.5 ± 0.4cd	115.9 ± 0.8e	164.9 ± 1.1d	31.5 ± 0.6ef
Fm + Bs + Tv + Fo	38.1 ± 0.3cd	116.4 ± 1.4e	165.1 ± 0.8d	31.5 ± 0.6ef
Ri + Pf + Th + Fo	48.5 ± 1.1a	135.4 ± 1.2a	204.8 ± 1.1a	42.7 ± 1.2a
Ri + Pf + Tv + Fo	42.9 ± 1.3b	122.6 ± 1.2cd	181.9 ± 1.0b	34.6 ± 0.6cd
Ri + Bs + Th + Fo	40.5 ± 0.6bc	122.6 ± 0.7cd	177.9 ± 0.8c	34.6 ± 0.5cd
Ri + Bs + Tv + Fo	42.3 ± 1.4b	122.7 ± 0.8cd	177.4 ± 1.2c	34.6 ± 1.2cd
Fm + Pf + Th + Fo	42.5 ± 1.0b	125.4 ± 0.8bc	181.7 ± 0.9b	36.4 ± 0.8c
Fm + Pf + Tv + Fo	42.8 ± 1.1b	127.9 ± 1.2b	181.0 ± 0.9b	38.5 ± 0.4b

Fm, Funneliformis mosseae; Ri, Rhizophagus intraradices; Bs, Bacillus subtilis PS1-3; Pf, Pseudomonas fluorescens PS2-6; Tv, Trichoderma virens 140012; Th, Trichoderma harzianum 140015; Fo, Fusarium oxysporum f. sp. radicis-lycopersici. Mean data ± SE of 54 treatments are presented. For each column, data followed by the same letter are not significantly different at p < 0.05 (LSD test).

Thus, it was noted that symbiotic microorganisms or pathogens mainly affected the amount of down-regulated metabolites in the shoots of tomato and participated in the metabolic regulation of aboveground organs. In contrast, in the roots of tomato plants, the number of up-regulated metabolites was more strongly affected by symbiotic microorganisms or pathogens. In addition, significant differences in secondary metabolism between the shoots and roots of tomato plants were observed (**Figure 3** and **Supplementary Figure 2**).

We screened the differential metabolites using the criteria variable importance plot >1 and p-value < 0.05 based on a partial least squares-discriminant analysis model of the shoots and roots from different treatments (**Supplementary Figure 1**).

For the shoot of tomato, it was observed that nine of the top 20 differential metabolites were detected in the Ri + Pf + Th treatment compared with the Fo treatment, comprising four up-regulated and five down-regulated metabolites. Inoculation with Ri + Pf + Th promoted the synthesis of acetylspiramycin and 6-hydroxypentadecanedioic acid, but inhibited the production of glucocaffeic acid, vanillic acid-4-*O*-glucuronide, and 6-caffeoylsucrose (**Table 6**). In addition, compared with the Fo treatment, 13 of the top 20 differential metabolites were detected in the shoot in the Ri + Pf + Th + Fo group, comprising four up-regulated and nine down-regulated metabolites. Inoculation with Ri + Pf + Th promoted the synthesis of fucosyllactose, zidovudine, and dihydrovaltrate, but inhibited the production of picolinic acid, curcumin, indoleacetic acid, buchanine, and other metabolites (**Table 7**).

Compared with inoculation with Fo, 10 of the top 20 differential metabolites were detected in the root after Ri + Pf + Th + Fo inoculation. The metabolites lactosamine, lucuminic acid, cyclomorusin, primidone, icaceine, and 3β,15α-diacetoxylanosta-8,24-dien-26-oic acid were up-regulated, whereas argiopinin I, 16-hydroxyhexadecanoic acid, pantoyllactone glucoside, and sinapoylspermine were down-regulated in the Ri + Pf + Th treatment (**Table 8**). In addition, compared with the Fo treatment, 11 of the top 20 differential metabolites were detected in the Ri + Pf + Th + Fo treatment. The metabolites lucuminic acid, cyclomorusin, and lactosamine were highly accumulated, whereas quercetin 3-arabinoside 7-glucoside, quercetin 3-glucoside 7-xyloside, and 3-hexadecanoyloleanolic acid were down-regulated in Ri + Pf + Th + Fo treatment (**Table 9**).

A KEGG enrichment analysis was performed (**Supplementary Figure 3**). Nicotinate and nicotinamide metabolism pathways were the most abundant pathways in tomato shoots after inoculation with Ri + Pf + Th and constituted 28% of the differential metabolites detected. After single inoculation with Fo, arginine and proline metabolism was most strongly enriched pathway in the shoots and comprised 15% of the metabolites, followed by nicotinate and nicotinamide metabolism and butanoate metabolism (12%). After inoculation with Ri + Pf + Th + Fo, 17% of the total metabolites were mainly enriched in the histidine metabolism, glycerophospholipid metabolism, and tyrosine metabolism pathways in tomato shoots (**Figure 4**).

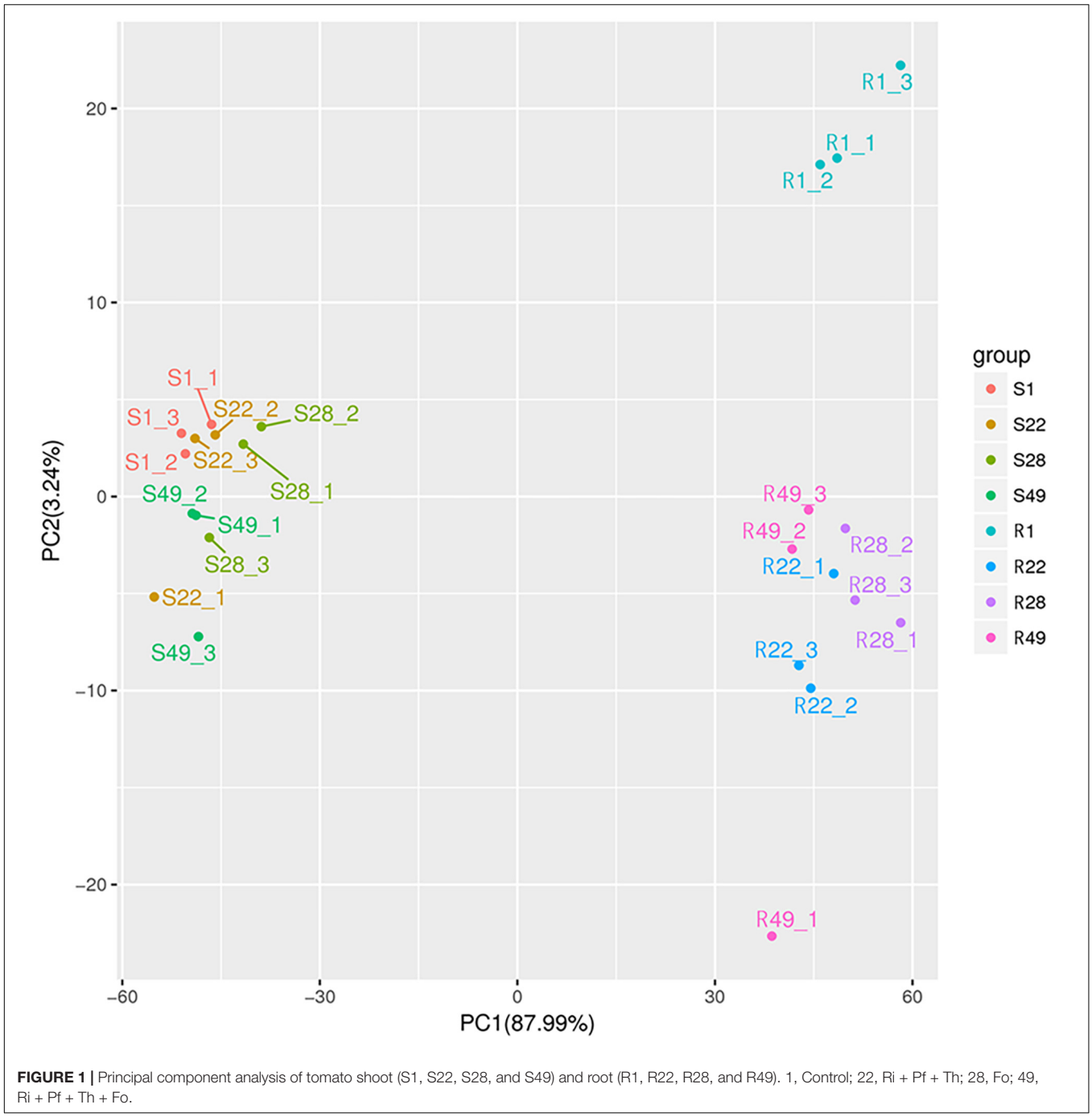

FIGURE 1 | Principal component analysis of tomato shoot (S1, S22, S28, and S49) and root (R1, R22, R28, and R49). 1, Control; 22, Ri + Pf + Th; 28, Fo; 49, Ri + Pf + Th + Fo.

Among the top 10 enriched pathways, 18% of the total metabolites were involved in biosynthesis of amino acids in tomato roots inoculated with Ri + Pf + Th, and 12% of the metabolites were enriched with the tyrosine metabolism and glycerophospholipid metabolism pathways. After single inoculation with Fo, 24% of the metabolites in the roots were enriched in the pyrimidine metabolism and glycerophospholipid metabolism pathways, and 18% of the metabolites were enriched in the arginine biosynthesis and amino acid biosynthesis pathways. The amino acid biosynthesis and ABC transporters pathways were the most strongly enriched pathways in tomato roots after inoculation with Ri + Pf + Th + Fo, accounting for 21% of the total metabolites, whereas 14% of the metabolites were involved in the tyrosine metabolism pathway (**Figure 4**). It was speculated that the amino acid biosynthesis pathway played an important role in promoting root growth and development of tomato, and the ABC transporters pathway may play a pivotal role in resistance to pathogenic bacteria in tomato roots.

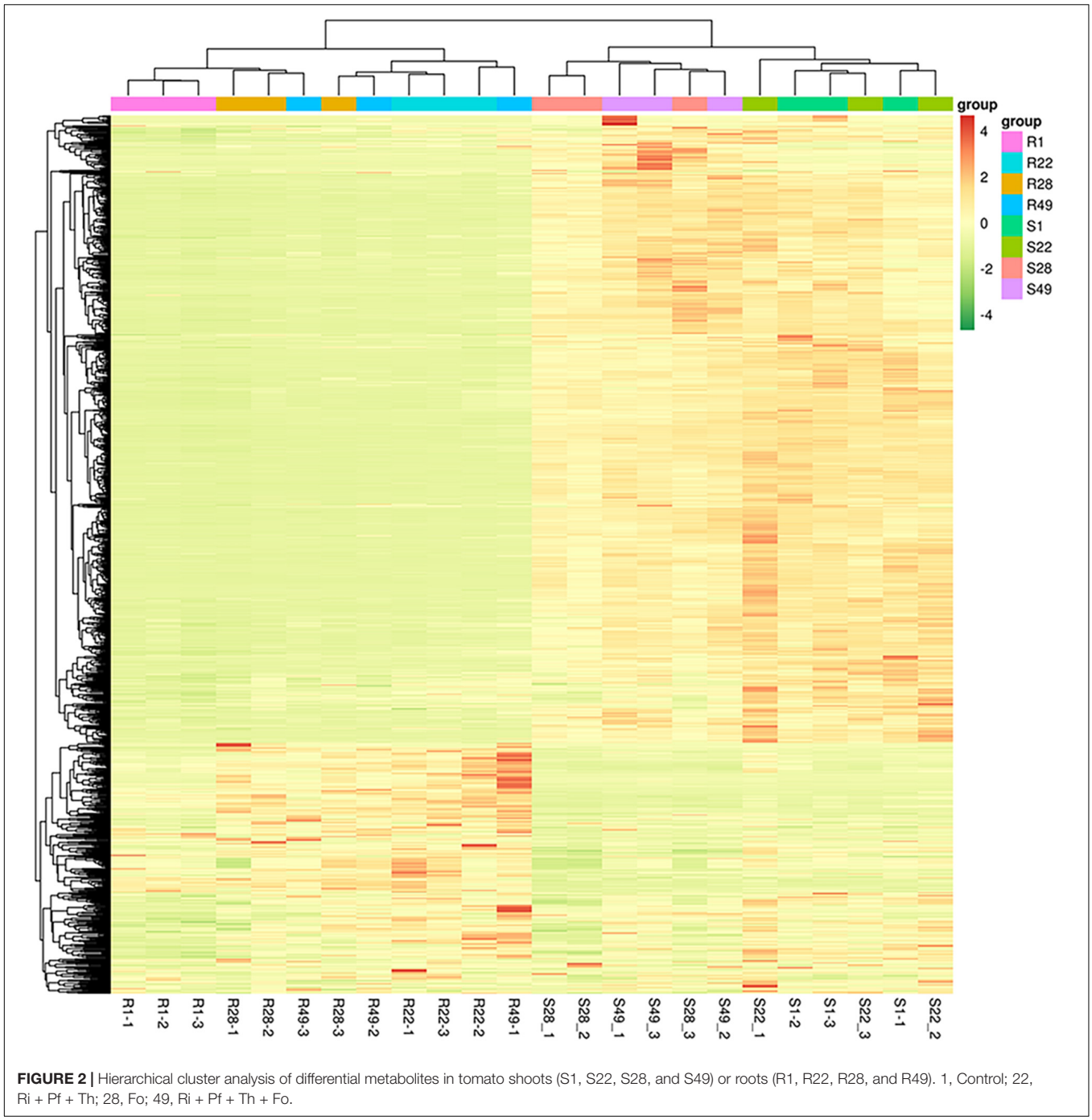

FIGURE 2 | Hierarchical cluster analysis of differential metabolites in tomato shoots (S1, S22, S28, and S49) or roots (R1, R22, R28, and R49). 1, Control; 22, Ri + Pf + Th; 28, Fo; 49, Ri + Pf + Th + Fo.

DISCUSSION

Increasing research attention is focused on disease control by symbiotic microbe combinations. Kabdwal et al. (2019) conducted growth promotion and disease control experiments on tomato using *T. harzianum* (Th43), *P. fluorescens* (Pf173), *R. intraradices*, and mancozeb, which was applied in different combinations as a soil application, seedling treatment, or foliar spray. The authors observed that soil treated with Th43 + Pf173 + *R. intraradices* and seedlings treated with Th43 + Pf173 + three applications of mancozeb as a foliar spray were highly effective in reducing plant mortality, promoting plant growth, and increasing yield. A field trial by Kumar et al. (2018) showed that *Glomus mosseae* and *Glomus fasciculatum* + *Trichoderma viride* (TR) + *Azotobacter chroococcum* (AZ) combinations had the strongest effect on litchi growth. In the present study, we observed that the combinations Ri + Bs + Tv and Fm + Pf + Tv had the greatest growth-promoting effects on tomato, whereas the combination Ri + Pf + Th had the greatest biological

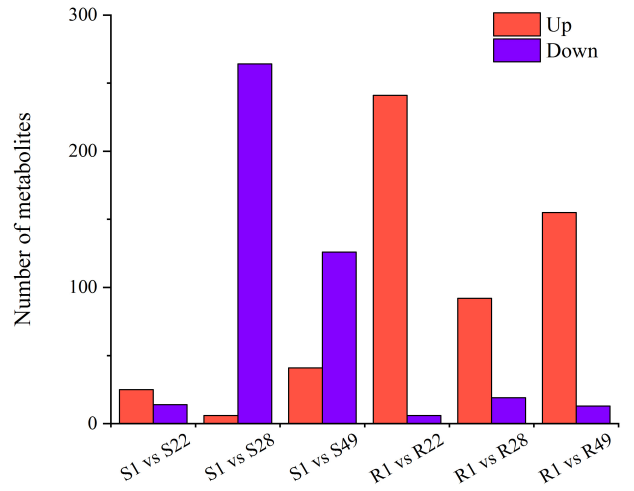

FIGURE 3 | Differential metabolites of S1 vs. S22, S1 vs. S28, S1 vs. S49, R1 vs. R22, R1 vs. R28, and R1 vs. R49. 1, Control; 22, Ri + Pf + Th; 28, Fo; 49, Ri + Pf + Th + Fo.

control effect against Fo. Differing from non-symbiotic microbial biocontrol agents, symbiotic microorganisms were used in the present experiment. These AMF, PGPR, and *Trichoderma* spp. colonized the rhizosphere as well as the root system, thereby forming a mutual symbiosis. *Trichoderma* spp. not only exist widely in the soil but also colonize the surface and internal tissues of plant roots, stems, and leaves. Zhang et al. (2013) observed that *T. harzianum* T-E5 colonized the root system of cucumber in a hydroponic culture system; first, the mycelia covered the root surface, then gradually extended into the cortex of the root, and survived in the epidermis and exodermis of the root for a long period. In the present experiment, both *T. viride* and *T. harzianum* colonized tomato root cortical cells but differed in their colonization ability, especially after inoculation with a pathogenic fungus. The colonization frequency of *T. viride* was higher than that of *T. harzianum*, thus it could be inferred that the colonization ability of the former species was stronger, which may affect the capability to prevent and control disease. The present results also confirmed this point. This finding is of great importance and warrants further systematic investigation. Furthermore, we observed that *Trichoderma* spp. colonized tomato roots together with AMF to form complex symbionts, and played a synergistic role with AMF, or concurrently exerted an ecological effect in collaboration with AMF + PGPR. This is the first observation of a complex symbiont formed by AMF + *Trichoderma*. The present experiment not only confirmed the aforementioned effects of *Trichoderma* but further demonstrated that *Trichoderma* played a synergistic role in combination with AMF or formed a biologically effective collaboration with AMF + PGPR. Therefore, it is of practical importance to further investigate the physiological and ecological functions and mechanism of the AMF + *Trichoderma* + PGPR symbiosis.

Symbiotic microorganisms function by direct synthesis of secondary metabolites, such as phytohormones and antibiotics, regulation of plant-related gene expression, and regulation of the community structure of other organisms. In the

TABLE 6 | Nine differential metabolites detected in the Ri + Pf + Th treatment compared with Fo treatment from tomato shoots.

Compounds	Description	Metabolic level	Fold change
Meta_8261	Unknown	Up	2.44
Meta_9662	Acetylspiramycin	Up	1.62
Meta_9336	PS [20:3(8Z,11Z,14Z)/18:1(9Z)]	Up	1.48
Meta_2302	6-Hydroxypentadecanedioic acid	Up	1.37
Meta_3569	Glucocaffeic acid	Down	−1.62
Meta_3474	Vanillic acid-4-*O*-glucuronide	Down	−1.7
Meta_6199	6-Caffeoylsucrose; clindamycin phosphate	Down	−1.71
Meta_5782	6-Caffeoylsucrose; clindamycin phosphate	Down	−1.79
Meta_5869	6-Caffeoylsucrose; clindamycin phosphate	Down	−2.18

TABLE 7 | Thirteen differential metabolites detected in the Ri + Pf + Th + Fo treatment compared with Fo treatment from tomato shoots.

Compounds	Description	Metabolic level	Fold change
Meta_5617	Fucosyllactose	Up	3.05
Meta_5869	6-Caffeoylsucrose; clindamycin phosphate	Up	2.97
Meta_6354	Zidovudine	Up	2.75
Meta_4498	Dihydrovaltrate	Up	2.7
Meta_1432	Methyl 3-carbazolecarboxylate	Down	−1.2
Meta_352	Picolinic acid	Down	−1.25
Meta_3652	Curcumin	Down	−1.27
Meta_735	Indoleacetic acid	Down	−1.29
Meta_2237	Buchanine	Down	−1.31
Meta_2915	Polixetonium chloride	Down	−1.66
Meta_8940	Aquifoliunine EIII	Down	−1.72
Meta_6922	Unknown	Down	−1.89
Meta_6762	LysoPC (22:1(13Z))	Down	−2.31

TABLE 8 | Ten differential metabolites detected in the Ri + Pf + Th treatment compared with Fo treatment in tomato roots.

Compounds	Description	Metabolic level	Fold change
Meta_8579	Argiopinin I	Down	−1.11
Meta_2422	16-Hydroxy hexadecanoic acid	Down	−1.22
Meta_3346	Pantoyllactone glucoside	Down	−1.27
Meta_4259	Sinapoylspermine	Down	−1.55
Meta_3155	Lactosamine	Up	4.02
Meta_5127	Lucuminic acid	Up	3.96
Meta_4732	Cyclomorusin	Up	3.83
Meta_1926	Primidone	Up	3.61
Meta_4111	Icaceine	Up	3.59
Meta_8040	3beta,15alpha-Diacetoxylanosta-8,24-dien-26-oic acid	Up	3.39

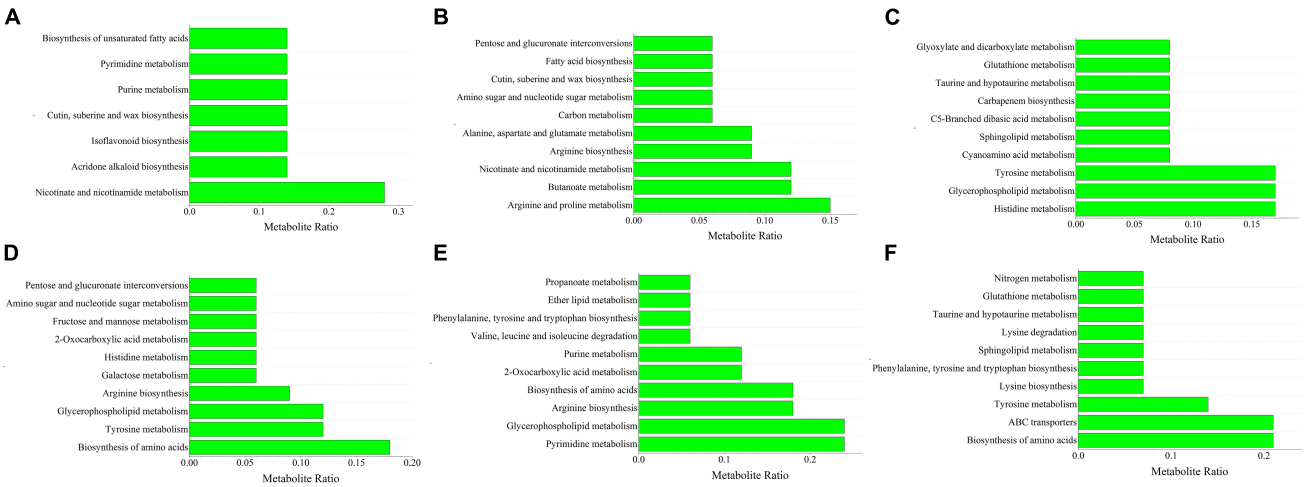

FIGURE 4 | Top 10 metabolites ratio of S1 vs. S22 **(A)**, S1 vs. S28 **(B)**, S1 vs. S49 **(C)**, R1 vs. R22 **(D)**, R1 vs. R28 **(E)**, and R1 vs. R49 **(F)**. 1, Control; 22, Ri + Pf + Th; 28, Fo; 49, Ri + Pf + Th + Fo.

process of coevolution of plants and pathogens, complex and diverse defense systems have developed. Among these systems, many metabolites produced by plant metabolic pathways are an important material basis of plant resistance and play an important role in the plant defense system. Using LC-MS technology, Tian et al. (2019) reported that resistant and susceptible tobacco cultivars infected by *Meloidogyne incognita* both showed significant changes in the metabolic pathways associated with disease resistance. The differential metabolites identified included alkaloids, fatty acids, flavonoids, terpenoids, and polyketones. A total of 1,374 proteins and 33 small molecular metabolites in grape leaves were differentially expressed by 1.5 times ($p < 0.05$) after infection by *Botrytis cinerea* for 3 days. Infection by *B. cinerea* had the greatest influence on expression of chloroplast proteins and mainly affected the three signaling pathways of plant disease interaction, plant hormone synthesis, and alkaloid synthesis. In addition, full activation of the disease resistance signaling pathway mediated by salicylic acid was an effective means to resist infection by *B. cinerea* in grape leaves (Fang et al., 2019). The present metabolome analysis provided results similar to the aforementioned findings, with a total of 1,266 differential metabolites detected and a large number of unknown metabolites. The results showed that AMF + PGPR + *Trichoderma* inoculation promoted the synthesis of secondary metabolites, including antibiotics and acids, in tomato leaves, but inhibited the synthesis of certain hydrocarbons. Furthermore, this combination promoted the synthesis of antibiotics, acids, and other hydrocarbons in the roots, but inhibited the secretion of acids, glycosides, and certain nitrogen-containing compounds by the roots. In contrast, AMF + PGPR + *Trichoderma* + Fo co-inoculation promoted the synthesis of secondary metabolites, including saccharides, nucleoside compounds, and hydrocarbons in tomato leaves, but inhibited the synthesis of certain pigments, auxin, and bactericide. Furthermore, the combination promoted the synthesis of glycosides and hydrocarbons in roots, but inhibited secretion of certain glycoside compounds by the roots. The number of metabolites up-regulated and down-regulated in each combination differed significantly, but the specific differences in metabolites and metabolic pathways require further study. The results indicated that a compound microbial agent generated by a certain combination of multiple symbiotic microorganisms may be more effective than a single microbial agent. Therefore, in future research and development of green technologies for prevention and control of TFCRR, the screening and evaluation of compound symbiotic bacteria should be a focus.

The present results may help to develop microbial strain resources and to use the advantages of multiple microbial strains. This will contribute to the development of novel

TABLE 9 | Eleven differential metabolites detected in the Ri + Pf + Th + Fo treatment compared with Fo treatment in tomato roots.

Compounds	Description	Metabolic level	Fold change
Meta_5127	Lucuminic acid	Up	4.86
Meta_4732	Cyclomorusin	Up	4.59
Meta_3155	Lactosamine	Up	3.9
Meta_8376	Unknown	Down	−0.9
Meta_6922	Unknown	Down	−0.9
Meta_7076	Quercetin 3-arabinoside 7-glucoside	Down	−1.11
Meta_8227	Quercetin 3-glucoside 7-xyloside	Down	−1.12
Meta_7919	3-Hexadecanoyloleanolic acid	Down	−1.12
Meta_8593	Unknown	Down	−1.29
Meta_8671	Unknown	Down	−1.36
Meta_8579	Argiopinin I	Down	−1.49

microbial pesticides and biofertilizers for effective pest control. It will be helpful to determine whether there are antagonistic effects between the symbiotic microbes, in addition to their growth-promoting effect, when inoculated in combinations. The present study focused on biological disease prevention as a measure to provide a theoretical basis to eliminate the environmental damage caused by abuse of chemical fertilizers and pesticides. The findings also provide guidance for further research and development of green disease prevention and control technologies and promote agricultural sustainability and economic development.

Given the temporal and spatial limitations of the present experiment, environmental factors such as light, moisture, temperature, and insect pests were not considered but may impact on the biocontrol effectiveness of combinations of AMF, PGPR, and *Trichoderma* spp. In addition, the metabolome analysis in this experiment has certain shortcomings, such as less processing number. Therefore, single- and dual-inoculation treatments should be analyzed further in future experiments to obtain more complete metabolite profiles and clarify the metabolic pathways that promote tomato growth and resistance to TFCRR. Simultaneous analysis of gene expression and the transcriptome could be conducted. Optimization of the promotive effect of different types of symbiotic microbes and minimization of antagonistic interactions, thereby producing more effective biocontrol bacterial agents, will further contribute to development of green technologies for disease prevention and control.

CONCLUSION

Applications of symbiotic microbes, alone or in combinations, influence leaf photosynthesis, defense enzyme activities, disease occurrence, growth and development, and yield of tomato. Combinations of AMF, PGPR, and *Trichoderma*, such as *R. intraradices* + *P. fluorescens* + *T. harzianum*, have strong biocontrol effects on TFCRR. Therefore, this symbiotic microbe combination shows potential for development as an effective biocontrol agent.

DATA AVAILABILITY STATEMENT

The original contributions generated for this study are included in the article/**Supplementary Material**, further inquiries can be directed to the corresponding author.

AUTHOR CONTRIBUTIONS

XC and ML conceived, designed, carried out the experiments, and collected and analyzed the data. HZ and CL prepared the experimental materials. XC wrote the first draft of the manuscript. RL and ML revised the manuscript. All authors approved the final version of the article for publication.

FUNDING

This research was supported by the Major Scientific Innovation Project of Shandong Province (2019JZZY010715) and the Key technology Research and Development of Shandong Province (2019GNC106043).

ACKNOWLEDGMENTS

We thank Robert McKenzie, from Liwen Bianji, Edanz Editing China (www.liwenbianji.cn/ac), for editing the English text of a draft of this article. We also thank Yinglong Chen, from University of Western Australia for his comments on the draft of this work.

SUPPLEMENTARY MATERIAL

The Supplementary Material for this article can be found online at: https://www.frontiersin.org/articles/10.3389/fmicb.2021.629793/full#supplementary-material

Supplementary Figure 1 | Differential multiple histogram. Top 20 differential metabolites of S1 vs. S22 **(A)**, S1 vs. S28 **(B)**, S1 vs. S49 **(C)**, R1 vs. R22 **(D)**, R1 vs. R28 **(E)**, and R1 vs. R49 **(F)**. 1, Control; 22, Ri + Pf + Th; 28, Fo; 49, Ri + Pf + Th + Fo.

Supplementary Figure 2 | Volcanic map of differential metabolites. Differential metabolite volcanic maps of S1 vs. S22 **(A)**, S1 vs. S28 **(B)**, S1 vs. S49 **(C)**, R1 vs. R22 **(D)**, R1 vs. R28 **(E)**, and R1 vs. R49 **(F)**. 1, Control; 22, Ri + Pf + Th; 28, Fo; 49, Ri + Pf + Th + Fo.

Supplementary Figure 3 | The most enriched KEGG pathway of differential metabolites, as analyzed via pairwise comparisons between different treatments. Different metabolites KEGG enrichment maps of S1 vs. S22 **(A)**, S1 vs. S28 **(B)**, S1 vs. S49 **(C)**, R1 vs. R22 **(D)**, R1 vs. R28 **(E)**, and R1 vs. R49 **(F)**. 1, Control; 22, Ri + Pf + Th; 28, Fo; 49, Ri + Pf + Th + Fo.

Supplementary Table 1 | The list of treatments.

Supplementary Table 2 | Metabolites_full_table (NEG).

Supplementary Table 3 | Metabolites_full_table (POS).

REFERENCES

Atalla, S. M. M., Abdel-Kader, M. M., El-Gamal, N. G., and El-Mougy, N. S. (2020). Using maize wastes, fermented by co-cultures of *Trichoderma harzianum* and *Pseudomonas fluorescens*, as grain dressing against m maize diseases under field conditions. *Egypt. J. Biol. Pest Control* 30:37. doi: 10.1186/s41938-020-00236-x

Bashan, Y., Holguin, G., and Lifshitz, R. (1993). "Isolation and characterization of plant growth-promoting rhizobacteria," in *Methods in Plant Molecular Biology and Biotechnology*, eds B. R. Glick and J. E. Thompson (Boca Raton, FL: CRC Press).

Biermann, B., and Linderman, R. G. (1981). Quantifying vercular-arbuscular mycorrhizas: a proposed method towards standardization. *New Phytol.* 87, 63–67. doi: 10.1111/j.1469-8137.1981.tb01690.x

Cao, H., Li, X., Wang, X., Bai, H., Mu, W., and Liu, F. (2018). Control efficacy of pyraclostrobin and triazole fungicides against tomato crown and root rot. *Sci. Agric. Sin.* 51, 4065–4075. doi: 10.3864/j.issn.0578-1752.2018.21.006

Colak, A., and Bicici, M. (2013). Integrated disease management of *Fusarium* crown and root rot of greenhouse-grown tomato in eastern Mediterranean region of turkey. *Tarim Bilim. Derg.* 19, 89–100.

Dearth, S. P., Castro, H. F., Venice, F., Tague, E. D., Novero, M., Bonfante, P., et al. (2018). Metabolome changes are induced in the arbuscular mycorrhizal fungus *Gigaspora margarita* by germination and by its bacterial endosymbiont. *Mycorrhiza* 28, 421–433. doi: 10.1007/s00572-018-0838-8

Fang, X., He, Y., Xi, X., Zha, Q., Zhang, L., and Jiang, A. (2019). Multi-omics reveals the resistance mechanism of grape leaves in response to *Botrytis cinerea*. *J. Zhejiang Univ. (Agric. Life Sci.)* 45, 306–316. doi: 10.3785/j.issn.1008-9209.2018.11.121

Hibar, K., Daami-Remadi, M., Ayed, F., and Mahjoub, M. E. (2007). *Fusarium* crown and root rot of tomato and its chemical control. *Int. J. Agric. Res.* 2, 687–695. doi: 10.3923/ijar.2007.687.695

Hibar, K., Daami-Remadi, M., Hamada, W., and El-Mahjoub, M. (2006). Bio-fungicides as an alternative for tomato *Fusarium* crown and root rot control. *Tunis. J. Plant Prot.* 1, 19–29.

Hill, E. M., Robinson, L. A., Abdul-Sada, A., Vanbergen, A. J., Hodge, A., and Hartley, S. E. (2018). Arbuscular mycorrhizal fungi and plant chemical defence: effects of colonisation on aboveground and belowground metabolomes. *J. Chem. Ecol.* 44, 198–208. doi: 10.1007/s10886-017-0921-1

Kabdwal, B. C., Sharma, R., Tewari, R., Tewari, A. K., Singh, R. P., and Dandona, J. K. (2019). Field efficacy of different combinations of *Trichoderma harzianum*, *Pseudomonas fluorescens*, and arbuscular mycorrhiza fungus against the major diseases of tomato in Uttarakhand (India). *Egypt. J. Biol. Pest Control* 29:1. doi: 10.1186/s41938-018-0103-7

Kucharek, T., Jones, J. P., Hopkins, D., and Strandberg, I. (2000). *Some disease of vegetables and agronomic crops caused by Fusarium in Florida*. Circular 1025, Florida Cooperative Extension Service. Gainesville, FL: Institute of Food and Agricultural Sciences, University of Florida.

Kumar, V., Anal, A. K. D., and Nath, V. (2018). Growth response of litchi to arbuscular mycorrhizal co-inoculation with *Trichoderma viride*, *Azotobacter chroococcum* and *Bacillus megatarium*. *Indian Phytopath.* 71, 65–74. doi: 10.1007/s42360-018-0010-6

Li, J., Sun, Y., Zhao, T., Jiang, J., and Xu, X. (2018). Separation identification and biological characteristics of pathogen causing *Fusarium* crown and root rot of tomato. *J. Northeast Agric. Univ.* 49, 22–30.

Liu, B., Wang, Y., Hu, J., Li, J., and Yang, H. (2019). Biocontrol effect evaluation of combined of *Trichoderma harzianum* and *Bacillus cereus* against root-knot nematode *Meloidogyne* ssp. on tomatoes. *Shandong Sci.* 32, 71–75. doi: 10.3976/j.issn.1002-4026.2019.05.008

Liu, D., Li, M., Sun, W., and Liu, R. (2016). Selection of combinations of arbuscular mycorrhizal fungi and plant growth-promoting rhizobacteria against cucumber *Fusarium* wilt disease. *Acta Phytopathol. Sin.* 46, 821–832. doi: 10.13926/j.cnki.apps.2016.06.012

Liu, D., Li, M., Sun, W., and Liu, R. (2017). Mechanism of increasing resistance of cucumber plants to *Fusarium* wilt disease by combined inoculation with arbuscular mycorrhizal fungi and plant growth-promo- ting rhizobacteria. *Acta Phytopathol. Sin.* 47, 832–841.

Liu, R., and Luo, X. (1994). A new method to quantify the inoculum potential of arbuscular mycorrhizal fungi. *New Phytol.* 128, 89–92. doi: 10.1111/j.1469-8137.1994.tb03990.x

Liu, R., and Wang, L. (2018). *Biological Symbiotics*. Beijing: Science press.

Lu, C. C., Guo, N., Yang, C., Sun, H. B., and Cai, B. Y. (2020). Transcriptome and metabolite profiling reveals the effects of *Funneliformis mosseae* on the roots of continuously cropped soybeans. *BMC Plant Biol.* 20:479. doi: 10.1186/s12870-020-02647-2

Mendes, J. B. S., da Costa Neton, V. P., de Sousa, C. D. A., de Carvalho Filho, M. R., Rodrigues, A. C., and Bonifacio, A. (2020). *Trichoderma* and bradyrhizobia act synergistically and enhance the growth rate, biomass and photosynthetic pigments of cowpea (*Vigna unguiculata*) grown in controlled conditions. *Symbiosis* 80, 133–143. doi: 10.1007/s13199-019-00662-y

Mikiciuk, G., Sas-Paszt, L., Mikiciuk, M., Derkowska, E., Trzciński, P., Głuszek, S., et al. (2019). Mycorrhizal frequency, physiological parameters, and yield of strawberry plants inoculated with endomycorrhizal fungi and rhizosphere bacteria. *Mycorrhiza* 29, 489–501. doi: 10.1007/s00572-019-00905-2

Murugesan, S., Vijayakumar, R., and Panneerselvam, A. (2011). Antifungal activity of medicinal plants against plant pathogenic fungus *Fusarium oxysporum*. *J. Pharm. Res.* 4, 843–844.

Nanjundappa, A., Bagyaraj, D. J., Saxena, A. K., Kumar, M., and Chakdar, H. (2019). Interaction between arbuscular mycorrhizal fungi and *Bacillus* spp. in soil enhancing growth of crop plants. *Fungal Biol. Biotechnol.* 6:23. doi: 10.1186/s40694-019-0086-5

Pan, X., Chang, R., Mu, K., and Chen, Q. (2020). Inhibition effects of *Trichoderma harzianum* VT9-3r and Bacillus subtilis VT4-1x on three potato pathogens. *J. China Agric. Univ.* 25, 72–81.

Rana, K. L., Kour, D., Kaur, T., Devi, R., Yadav, A. N., and Yadav, N. (2020). Endophytic microbes: biodiversity, plant growth-promoting mechanisms and potential applications for agricultural sustainability. *Antonie van Leeuwenhoek* 113, 1075–1107. doi: 10.1007/s10482-020-01429-y

Tan, S., Sun, W., and Liu, R. (2015). Combination of *Glomus* spp. and *Bacillus* sp. M3-4 promotes plant resistance to bacterial wilt in potato. *Acta Phytopathol. Sin.* 45, 661–669.

Thorpe, H. J., and Jarvis, W. R. (1981). Grafted tomatoes escape *Fusarium* foot and root rot. *Can. J. Plant Sci.* 61, 1027–1028. doi: 10.4141/cjps81-157

Tian, P., Li, X., He, W., Duan, D., Xu, S., and Yang, T. (2019). Metabonomics analysis of resistant susceptible tobacco varieties before and after infection by *Meloidogyne incognita*. *Acta Tabacaria Sin.* 25, 81–92. doi: 10.16472/j.chinatobacco.2018.261

Wang, J., Ren, P., Zhang, F., Hong, B., Chang, Q., Liu, C., et al. (2019). "Isolation and identification of pathogen of tomato Fusarium crown and root rot in greenhouse," in *Proceedings of the 2019 Annual Meeting of the Society for Plant Protection China Society of Plant Protection*, 81–86.

Wang, X., Chen, M., Yang, G., Li, X., Li, P., and Chen, M. (2014). Effect of *Glomus versiforme* and *Trichodema harzianum* on growth and quality of *Salvia miltiorrhiza*. *China J. Chin. Mater. Med.* 39, 1574–1578. doi: 10.4268/cjcmm20140906

Wang, X. K. (2006). *Principles and Techniques of Plant Physiological Biochemical Experimental*. Beijing: Higher Education Press.

Yang, C. X., Zhao, W. N., Wang, Y. N., Zhang, L., Huang, W. C., and Lin, J. X. (2020). Metabolomics analysis reveals the alkali tolerance mechanism in *Puccinellia tenuiflora* Plants inoculated with arbuscular mycorrhizal fungi. *Microorganisms* 8:327. doi: 10.3390/microorganisms8030327

Zhang, F., Zhu, Z., Wang, B., and Wang, P. (2013). Optimization of *Trichoderma harzianum* T-E5 biomass and determining the degradation sequence of biopolymers by FTIR in solid-state fermentation. *Ind. Crops Prod.* 49, 619–627. doi: 10.1016/j.indcrop.2013.05.037

Zhao, B., and He, S. (2002). *Microbiology Experiments*. Beijing: Science Press.

Conflict of Interest: The authors declare that the research was conducted in the absence of any commercial or financial relationships that could be construed as a potential conflict of interest.

frontiers in Microbiology

ORIGINAL RESEARCH
published: 06 July 2021
doi: 10.3389/fmicb.2021.658113

Whole Genome Sequence of *Bacillus velezensis* Strain GUMT319: A Potential Biocontrol Agent Against Tobacco Black Shank Disease

Haixia Ding[1,2], Weidi Mo[1], Shui Yu[3], Huanhuan Cheng[1], Lijuan Peng[3] and Zuoyi Liu[2,4]**

[1] Department of Plant Pathology, College of Agriculture, Guizhou University, Guiyang, China, [2] Guizhou Academy of Agricultural Sciences, Guiyang, China, [3] College of Tobacco Science, Guizhou University, Guiyang, China, [4] Guizhou Key Laboratory of Agricultural Biotechnology, Guizhou Academy of Agricultural Sciences, Guiyang, China

Phytophthora nicotianae causes black shank, a serious soil-borne disease, in tobacco. In this study, the *Bacillus* strain GUMT319 was isolated from the rhizosphere of healthy tobacco plants grown in a field in Guizhou with a high incidence of tobacco black shank. Genome sequencing revealed that GUMT319 contained a single circular chromosome 3,940,023 bp in length, with 4,053 predicted genes and an average GC content of 46.6%. Based on phylogenomic analyses, GUMT319 was designated as *Bacillus velezensis*. The genome of GUMT319 contained more than 60 genes and 13 gene clusters that have previously been found to be active in antifungal mechanisms, biofilm formation, and chemotaxis motility. Additionally, confocal laser scanning microscopy and scanning electron microscopy showed that GUMT319 formed a spatially organized biofilm *in vivo*. In addition, lauric acid negatively regulated biofilm formation. This is the first study to report that nicotine in tobacco root exudates was a chemoattractant for biocontrol *Bacillus* strains. In this study, we identified new interactions between beneficial microorganisms and tobacco roots in the rhizosphere. Moreover, dual culture tests *in vitro* showed that GUMT319 inhibited the growth of *P. nicotianae* and also displayed inhibitory effects against eight other plant pathogens, namely, *Colletotrichum scovillei*, *Colletotrichum capsici*, *Fusarium carminascens*, *Sclerotinia sclerotiorum*, *Alternaria alternata*, *Phomopsis* sp., *Phyllosticta sorghina*, and *Exserohilum turcicum*. Furthermore, GUMT319 exhibited > 70% control efficiency against tobacco black shank in field experiments conducted in 2018–2020. Thus, GUMT319 was more effective in controlling the incidence of tobacco black shank than other treatments including fungicide application. Overall, these results suggested that GUMT319 (*B. velezensis*) could be used as a potential biocontrol agent against tobacco black shank.

Keywords: tobacco black shank, *Bacillus velezensis*, biocontrol, genome sequencing, antifungal

OPEN ACCESS

Edited by:
Amin Uddin Mridha, University of Chittagong, Bangladesh

Reviewed by:
Khaled Abbas El-Tarabily, United Arab Emirates University, United Arab Emirates
Orlando Borras-Hidalgo, Qilu University of Technology, China

****Correspondence:***
Lijuan Peng
296430006@qq.com
Zuoyi Liu
gzliuzuoyi@163.com

Specialty section:
This article was submitted to Microbe and Virus Interactions with Plants, a section of the journal Frontiers in Microbiology

Received: *25 January 2021*
Accepted: *25 May 2021*
Published: *06 July 2021*

Citation:
Ding H, Mo W, Yu S, Cheng H, Peng L and Liu Z (2021) Whole Genome Sequence of Bacillus velezensis Strain GUMT319: A Potential Biocontrol Agent Against Tobacco Black Shank Disease. Front. Microbiol. 12:658113. doi: 10.3389/fmicb.2021.658113

INTRODUCTION

Tobacco black shank, caused by the fungal pathogen *Phytophthora nicotianae*, is a serious disease of flue-cured tobacco, which is an economically important crop in Guizhou, China. The severity of tobacco black shank continues to increase each year, causing significant economic losses. In the field, tobacco black shank affects the stem base (Han et al., 2016; Guo et al., 2020) and the chemical

fungicide metalaxyl is generally used for disease control. However, this practice is not conducive to the development of sustainable tobacco agriculture, as it creates an excessive dependence on chemical agents, leaves fungicide residues, and causes environmental pollution (Han et al., 2016; Guo et al., 2020). As an alternative, biological control agents (BCAs) offer safe alternative methods for controlling tobacco black shank (Zhang et al., 2017a; Srikhong et al., 2018).

Biocontrol has proved to be a promising strategy for the management of many plant diseases (Chowdhury et al., 2015; Han et al., 2016; Zhang et al., 2017c; Fan et al., 2018, Mao et al., 2020). Numerous BCAs have been studied, but only a limited number of strains, such as those of *Bacillus* species, have been commercially developed (Chowdhury et al., 2015; Fan et al., 2018; Ye et al., 2020). *Bacillus* spp. are ubiquitous bacteria widely distributed in natural environments, especially in the rhizosphere and plant roots. They are also excellent candidates for BCAs since they produce heat- and desiccation-resistant endospores that are easily stored and transported as stable products (Weng et al., 2013; Fan et al., 2018). However, the use of BCAs remains a challenge since their effect in the field is frequently inconsistent (Weng et al., 2013).

Bacillus spp. employ a number of mechanisms in their effective biocontrol of pathogens, such as antagonism, systemic resistance induction, and plant growth promotion (Chowdhury et al., 2015). In previous studies, *Bacillus* strains exhibited biological activity against various plant pathogens by producing different types of antimicrobial compounds, such as cell wall-degrading enzymes and non-ribosomally synthesized antibiotics, as well as secondary metabolites that trigger induced systemic resistance (ISR), thus protecting the plants against pathogen attack (Chowdhury et al., 2015; Fan et al., 2018; Yan et al., 2020).

Successful root colonization of BCAs is the key to effective biocontrol and is considered to be the main factor responsible for consistent performance in the field (Weng et al., 2013; Xu et al., 2013; Liu et al., 2014). Root colonization is divided into two steps: chemotaxis toward the root and subsequent biofilm formation on the root surface (Zhang et al., 2017b; Feng et al., 2018, 2019). *Bacillus* spp. colonize the roots of many plant species and form a biofilm, which contributes to their biocontrol efficacy (Gao et al., 2015a). Chemotaxis-mediated response to root exudates enhances the colonization and beneficial effects of plant growth-promoting *Bacillus* strains (Feng et al., 2018).

Bacillus velezensis is an important member of the plant growth-promoting rhizobacteria (PGPR), which are known to enhance plant growth and control soil-borne diseases (Chowdhury et al., 2015; Fan et al., 2018). *B. velezensis* FZB42 was the first strain to be sequenced (Chen et al., 2007). It was initially identified as a *Bacillus amyloliquefaciens* strain, but was later recognized as a *B. velezensis* strain and as a model of gram-positive plant growth-promoting and biocontrol rhizobacteria (Fan et al., 2018). Approximately 130 whole genome sequences of *B. velezensis* have been deposited in GenBank to date. *B. velezensis* strains have their own specific genomic characteristics, because these strains reside in different host plants and environments (Wang et al., 2019). For instance, *B. velezensis* SQR9 isolated from the cucumber rhizosphere has been used as a BCA against fungal pathogens, mainly because of its ability to trigger ISR (Borriss et al., 2018; Wu et al., 2018), while *B. velezensis* HAB-2 isolated from cotton has been used as a biological pesticide against bacterial pathogens (Xu et al., 2020).

In this study, we isolated *B. velezensis* GUMT319 from the rhizosphere of healthy tobacco plants growing in high-incidence tobacco black shank fields in Guizhou, China. Previous research has shown that GUMT319 produces enzymes with biocontrol activity, such as proteases, cellulases, siderophores, and phosphatases, and inhibits the mycelial growth of *P. nicotianae in vitro* (Luo et al., 2019). Here, we aimed to investigate the biocontrol effects of GUMT319 in the field and to gain insights into the underlying mechanisms. Genome sequencing of GUMT319 revealed the presence of genes involved in plant growth promotion, biofilm formation, chemotaxis, and antifungal activity. In addition, confocal laser scanning microscopy and scanning electron microscopy analyses of the GUMT319 strain labeled with green fluorescent protein (GFP) revealed its patterns of tobacco root colonization. Overall, this study highlights the excellent potential of GUMT319 as a BCA against the tobacco black shank disease.

MATERIALS AND METHODS

Strains and Culture Conditions

Bacillus strain GUMT319 was grown at 37°C in Luria–Bertani medium (LB). The GFP-labeled GUMT319 (GUMT319-gfp) was maintained in LB supplemented with 10 mg/mL tetracycline. The fungal pathogens used in this study included *P. nicotianae*, *Colletotrichum scovillei*, *Colletotrichum capsici*, *Fusarium carminascens*, *Sclerotinia sclerotiorum*, *Alternaria alternata*, *Phomopsis* spp., *Phyllosticta sorghina*, and *Exserohilum turcicum*. These were maintained on potato dextrose agar (PDA) medium at the Department of Plant Pathology, Guizhou University. To store these pathogens, hyphae were sampled from the growing zone of mycelia in agar disks (1 cm diameter), and they were mixed with 15% glycerol and stored in a 4°C freezer.

Sequencing and Phylogenetic Analysis

A single bacterial colony was inoculated in 5 mL of LB broth and grown for 12 h at 37°C with agitation at 200 rpm. Then, 2 mL of the bacterial culture was centrifuged at 10,000 rpm for 1 min, and bacterial genomic DNA was isolated using an Ezup Column Bacteria Genomic DNA Purification Kit [Sangon Biotech (Shanghai) Co., Ltd., China], in accordance with the manufacturer's protocol. Subsequently, *16S rRNA* and *gyrA* genes were amplified by PCR using sequence-specific primers: 27F (5′-AGAGTTTGATCCTGGCTCAG-3′) and 1492R (5′-GGTTACCTTGTTACGACTT-3′) for amplifying approximately 1,400 bp of the *16S rRNA* gene and *gyrA*-F (5′-CAGTCAGGAAATGCGTACGTCCTT-3′) and *gyrA*-R (5′-CAAGGTAATGCTCCAGGCATTGCT-3′) for amplifying approximately 1,000 bp of the *gyrA* gene (Chen et al., 2016). Each 25-μL PCR mixture contained 1 unit of Pfu DNA Polymerase (Sangon Biotech), 1 × PCR buffer, 1 mM $MgCl_2$, 100 μM dNTPs, 1 μM of each primer, 50 ng of genomic DNA template,

and ultrapure water. PCR was performed using the following conditions: initial denaturation at 95°C for 10 min, followed by 30 cycles of denaturation at 94°C for 30 s, annealing at 56°C for 30 s, and extension at 72°C for 90 s, with a final extension at 72°C for 10 min. The PCR products were sequenced at Sangon Biotech. Sequences of the *16S rRNA* and *gyrA* gene fragments were searched in the National Center for Biotechnology Information (NCBI) nucleotide database using Blastn to determine the closest taxonomic relatives. Subsequently, phylogenetic analysis of *16S rRNA* and *gyrA* gene sequences was performed in MEGA 6.0 using the maximum likelihood method to estimate the evolutionary position of GUMT319 relative to other *Bacillus* strains (**Supplementary Table 1**).

Genome Sequencing and Annotation

The genomic DNA of GUMT319 was sequenced at Beijing Novogene Bioinformatics Technology Co., Ltd. using an Illumina PE150 system and PacBio RSII high-throughput sequencing technology. Low-quality reads were filtered using SMRT Link v5.0.1, and the filtered reads were assembled into one contig without gaps. The complete genome sequence of GUMT319 was annotated using the Prokaryotic Genomes Annotation Pipeline (PGAP) at NCBI, and gene functions were predicted using five databases, namely, Gene Ontology (GO), Kyoto Encyclopedia of Genes and Genomes (KEGG), Clusters of Orthologous Groups (COG), Non-Redundant (NR) protein sequences, and Swiss-Prot, based on whole genome Blast search (*E*-value < 1e-5; minimal alignment length > 40%) against each database.

Construction of GFP-Labeled GUMT319

The *GFP* plasmid pGFP78, an *Escherichia coli–Bacillus subtilis* shuttle vector containing the 78 promoter-controlled *GFP* gene (Zhang et al., 2017c), was electroporated into electrocompetent cells of strain GUMT319, as described previously (Zhang et al., 2012). Briefly, the cells were grown in liquid LB medium at 37°C and were harvested during the exponential growth phase by centrifugation at 10,000 rpm for 10 min at 4°C. The harvested cells were washed five times with an equal volume of cold electroporation buffer containing 0.5 M sorbitol, 0.5 M mannitol, and 10% glycerol (pH 7.0). Subsequently, 100 μL of competent cells were electroporated on ice with 1 mg of pGFP78 DNA using a 1.8-kV electric shock. After electroporation, the cell suspension was diluted with 900 μL of LB medium and incubated at 37°C on an agitator at 120 rpm for 3 h to allow the expression of antibiotic resistance markers. The cell suspension was then spread on LB agar medium supplemented with tetracycline (10 mg/mL). The GFP-labeled cells were selected for tetracycline for three generations, and this was confirmed by fluorescence microscopy (Gao et al., 2015b).

Plant Material and Growth Conditions

Seeds of tobacco (*Nicotiana tabacum*) cultivar Yunyan 87, native to China, were surface-sterilized by soaking in 2% sodium hypochlorite for 15 min and then washed thoroughly with distilled water. The sterilized seeds were sown in axenic tissue culture bottles containing vermiculite, and seedlings grew for 15–20 days in a growth chamber at 25°C day/20°C night temperature and a 16-h light/8-h dark photoperiod. Then, seedlings were aseptically transplanted into 250-mL flasks (one seedling per flask) containing 100 mL sterile liquid 25% sucrose-free Murashige and Skoog (MS) medium, which was renewed every other day during the growth period. The hydroponic system was placed on an agitator and gently shaken at 50 rpm for 2 h each day. Before inoculating the MS medium with *B. velezensis* GUMT319-gfp, 100-μL aliquots of the MS medium were sampled from each flask and spread onto solid LB medium to verify the absence of contamination (Han et al., 2016).

Root Colonization Assay

To perform the root colonization assay, GUMT319-gfp was grown overnight in liquid LB medium and was subsequently resuspended in sterile double-distilled water. Roots of tobacco plants were inoculated with 100 mL of GUMT319-gfp (OD_{600} = 0.5) *via* drench application for 2 h; 10 replicates were performed. The plants were then transferred to fresh MS medium and cultivated for an additional 2 days without agitation. Roots were rinsed with sterile double-distilled water. To visualize colonization by GUMT319-gfp and GUMT319, at least 20 root tips were observed under a confocal laser scanning microscope (CLSM) and scanning electron microscope (SEM), as described previously (Weng et al., 2013).

Collection and Analysis of Root Exudates

Seeds of tobacco cultivar Yunyan 87 and pepper cultivar Dangwu were germinated, and the seedlings were grown for approximately 15–20 days in MS medium, as described above. Before starting the collection of root exudates, plant roots were washed with sterile double-distilled water to avoid contamination from the nutrient solution. The plants were then transferred to a flask, with the roots submerged in sterile water, and the flasks were placed in a growth chamber for 24 h at 25°C and a 16-h light/8-h dark photoperiod, with gentle agitation (50 rpm). The root exudates collected were filtered through a 0.45-μm membrane and lyophilized. The freeze-dried powder of tobacco root exudates was dissolved in ethanol and concentrated 50-fold. To ensure that the root exudates were free from contamination, 100 μL of the filtered root exudate was plated on LB agar medium, and the plates were incubated at 30°C for 24 h.

GC-TOF-MS (Nanjing Zoonbio Biotechnology Co., Ltd., Nanjing, China) was performed to qualitatively analyze the freeze-dried root exudates using an Agilent 7890 gas chromatograph system coupled with a Pegasus HT time-of-flight mass spectrometer. Chroma TOF 4.3X software (LECO Corporation, St. Joseph, MI, United States) and the LECO-Fiehn Rtx5 database were used to extract raw peaks, data baseline filtering, and calibration of the baseline, peak alignment, deconvolution analysis, peak identification, and integration of the peak area. Both the mass spectrum match and retention index match were considered during metabolite identification.

Motility Assay

B. velezensis GUMT319 was grown in LB broth until reaching an OD_{600} of 0.8. Subsequently, 10 mL of the culture was

centrifuged. The cell pellet was washed twice with distilled water and resuspended in 100 μL. Then, 15 mL of LB (0.7% agar) medium was poured into a Petri dish (90 mm diameter), and a 5-μL drop of concentrated bacterial culture was dispensed at the center of the dish. The Petri dish was incubated at 37°C, and the appearance of the bacterial zone was observed after 12 h (de Weert et al., 2002).

Chemotaxis Assay

B. velezensis GUMT319 was grown and harvested as described above. Then, 15 mL of LB (0.7% agar) medium with the 50-fold concentrated root exudates (or 200 μM different composition of root exudates) was poured into a 90-mm-diameter Petri dish. A 5-μL drop of concentrated bacterial culture was added to the center of the dish and incubated at 37°C for 12 h to check for the appearance of the bacterial zone (de Weert et al., 2002; Weng et al., 2013).

Biofilm Formation Assay

The biofilm formation efficiency of *B. velezensis* GUMT319 was quantified using the microtiter plate test. Briefly, GUMT319 was grown in 5 mL of LB broth at 37°C until reaching an OD_{600} value of 0.8. Each well of a sterile 12-well PVC microtiter plate was filled with 2 mL of LB broth and 4 μL of bacterial suspension; 2 mL of LB broth with the 50-fold concentrated root exudate (or 200 μM different composition of root exudates) and 4 μL of bacterial suspension were considered as one treatment. Wells containing only 2 mL of LB broth were used as negative controls. The microtiter plates were incubated at 37°C for 3 days without agitation (Weng et al., 2013).

Fungal Growth Inhibition Assays

The effect of GUMT319 on hyphal growth was tested using the dual culture method. Interaction experiments were performed using PDA and LB media. An agar plug (0.5 cm diameter) of actively growing fungi was placed at the center of a PDA plate and incubated for 1 day. GUMT319 was then inoculated at two points, each at a distance of 2 cm from the plug, and plates were photographed after 7 days (Li et al., 2014). This experiment was conducted for five replicates.

Determination of Disease Control Efficacy Under Field Conditions

To determine the disease control efficacy of GUMT319 under field conditions, experiments were conducted during 2018–2020 in a field naturally infested with tobacco black shank disease. The experimental field was located in Meitan, Zunyi (107°41′N, 27°47′E), Guizhou, China. Roots taken from tobacco seedlings of cultivar Yunyan 87 were soaked in GUMT319 suspension (10^8 CFU/mL) for 1 h and then transplanted. During growth, each tobacco plant was irrigated with 100 mL of GUMT319 suspension (10^8 CFU/mL) at 7, 14, and 21 days post-transplantation, and the disease index was measured at 50 and 60 days post-transplantation. Due to frequent rain during the growing season, the GUMT319 suspension was applied more often when appropriate. At 21 days post-transplantation, tobacco plants that had been irrigated with 100 mL of 1:400 of 58% metalaxyl manganese zinc WP (Haixun Agri-Biotech Co., Ltd., Shandong, China) and 1:700 of 10^{10} CFU/g *Bacillus* spp. (Green Conway WP, Sino Green Agri-Biotech Co., Ltd., Beijing, China) were used as controls, and plants irrigated with water were designated as blank controls. In 2018 and 2019, the field experiments were performed in an approximately 0.1-ha demonstration area. Tobacco plants were planted in randomized blocks and each block contained 100 plants. Each of the four treatments was replicated four times. In 2020, the field experiments were performed on an approximately 0.67-ha demonstration area and each treatment contained over 2,000 plants. The appearance of tobacco black shank disease symptoms and the cumulative number of infected plants were recorded at 45 days post-transplantation.

The disease incidence was calculated as the percentage of diseased plants relative to the total number of plants growing in each block; evaluation took place when the disease emerged. Disease severity was scored on a scale of 0–9, as follows: 0, no symptoms; 1, less than one-third of the total leaves wilted; 3, one-third to one-half of the total leaves wilted; 5, one-half to two-thirds of the total leaves wilted; 7, more than two-thirds of total leaves wilted; and 9, plant dead. The disease index was calculated using the following equation:

$$\text{Disease index} = \frac{\left[(a \times 0) + (b \times 1) + (c \times 3) + (d \times 5) + (e \times 7) + (f \times 9)\right]}{(a + b + c + d + e + f) \times 9} \times 100 \quad (1)$$

where a, b, c, d, e, and f are the number of plants in each disease category.

Data Analysis

Data were statistically analyzed using SPSS v.24.0 (SPSS Inc., Chicago, IL, United States). Mean values of the control and treatment groups were compared using Duncan's new multiple range test at a significance level of 5% ($P < 0.05$). All percentage data were subjected to arc-sine transformation before statistical analysis.

RESULTS

Identification of Strain GUMT319

The GUMT319 strain was deposited in the China Center for Type Culture Collection (CCTCC Accession No.: M 2018871). Strain GUMT319 was previously classified as *B. amyloliquefaciens* (Luo et al., 2019). Here, phylogenetic analysis of *16S rRNA* and *gyrA* sequences using the maximum likelihood method placed GUMT319 in a well-supported cluster with *B. velezensis* FZB42 (**Figure 1A**). BLASTn analysis of *16S rRNA* and *gyrA* sequences amplified from GUMT319 returned a match to the reference strain *B. velezensis* FZB42, with >99% identity. Annotation using the NR protein database indicated that sequences amplified from GUMT319 were most similar to sequences of *B. velezensis* and *B. amyloliquefaciens* (**Figure 1B**). Thus, taking into account

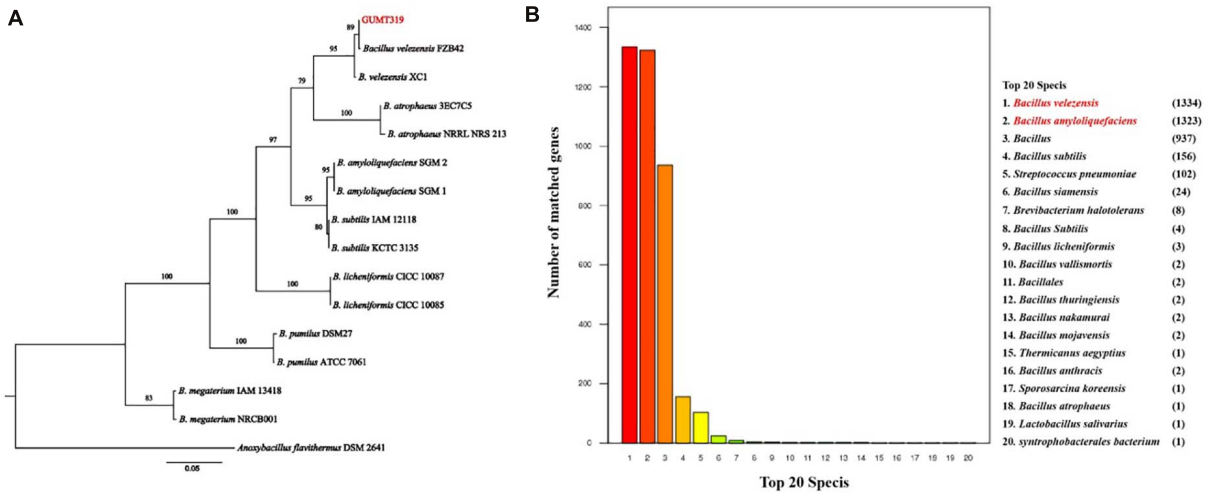

FIGURE 1 | Identification of *Bacillus velezensis* strain GUMT319. **(A)** Phylogenetic tree based on the nucleotide sequences of *16S rRNA* and *gyrA* genes. **(B)** Non-redundant (NR) protein database annotation.

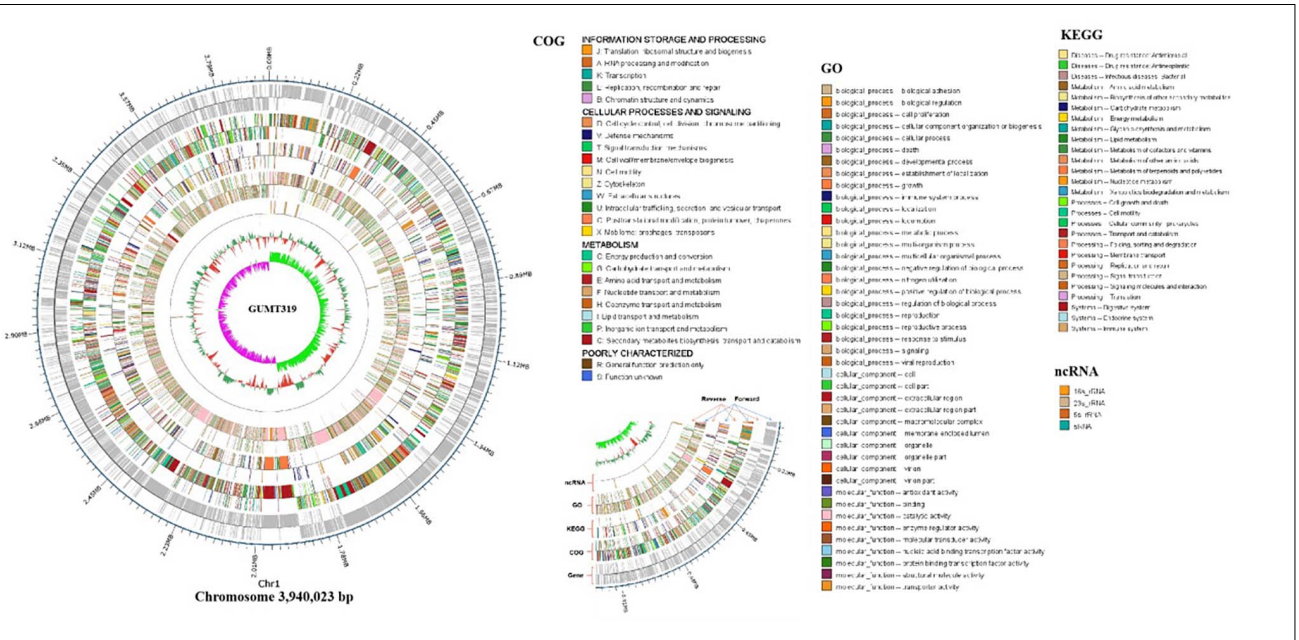

FIGURE 2 | Circular genome map of *B. velezensis* GUMT319. The scale is shown in the outermost circle. The second and third circles indicate genes in forward and reverse orientations, respectively. The outer to inner rings represent forward and reverse DNA sequences of protein-coding genes annotated according to COG, KEGG, and GO databases and ncRNA. The 10th circle shows the GC content, and the 11th circle shows the GC skew in green and purple.

the *16S rRNA* and *gyrA* gene sequences as well as the whole genome sequence comparisons, GUMT319 was identified as a *B. velezensis* strain.

B. velezensis GUMT319 Genome Sequencing and Analysis

To investigate the biocontrol mechanisms of *B. velezensis* GUMT319 and its application for sustainable agriculture, its complete genome sequence was determined. The *B. velezensis* GUMT319 genome consisted of a single circular chromosome 3,940,023 bp in length, with an average GC content of 46.6% (**Figure 2**), and did not harbor any plasmids. The whole genome of GUMT319 was predicted to contain 4,053 protein-coding genes covering 90.0% of the genome, with an average gene length of 875 bp, as well as 27 rRNAs and 86 tRNAs. Principal features of the genomes of *B. velezensis* GUMT319 and model strains, *B. velezensis* FZB42 and SQR9, are summarized in **Table 1** (Chen et al., 2007; Zhang et al., 2015). We performed a collinearity analysis to further compare the genomic similarities and differences between the genome

TABLE 1 | Genomic features of *Bacillus velezensis* strains GUMT319, SQR9, and FZB42.

Strains	GUMT319	SQR9	FZB42
Location of isolation	Tobacco rhizosphere	Cucumber rhizosphere	Sugar beet rhizosphere
Genome size (bp)	3,940,023	4,117,023	3,918,596
GC content (%)	46.6	46.1	46.4
No. of protein-coding genes	4,053	3,902	3,687
Percent coding region	89.1	89.0	88.0
No. of rRNA genes	27	21	29
No. of tRNA genes	86	72	88
No. of phage-associated genes	671	218	44
NCBI Accession No.	NZ_CP068563	NZ_CP006890	NC_009725

of GUMT319 and those of FZB42 and SQR9 (**Figure 3**). The results showed that the GUMT319 genome displayed different synteny to those of the other strains. GUMT319 showed the highest synteny with *B. velezensis* FZB42, indicating that their evolutionary stages were the closest, and their genomes were closely related. Amino acid sequence similarity searches against various databases with an E-value threshold of 1e-5 revealed that 3,915 (96.6%), 3,874 (95.6%), 3,293 (81.2%), 2,884 (71.2%), and 2,623 (64.7%) protein-coding genes showed matches in the NR, KEGG, Swiss-Prot, COG, and GO databases, respectively. Abnormal hyphae of plant pathogens were reported in dual cultures with GUMT319, which could be due to the production of secondary metabolites (Luo et al., 2019). Bioinformatics analyses showed that the GUMT319 genome contained 13 putative gene clusters involved in the biosynthesis of secondary metabolites with potential antimicrobial activities (**Table 2**), most of which were conserved in all *B. velezensis* strains (bacilysin, surfactin, macrolactin, fengycin, bacillaene, difficidin, and terpene; **Supplementary Figure 1**; Grady et al., 2019). Among these gene clusters, five encoded non-ribosomal peptide synthetases (NRPSs), four encoded trans-acyl transferase polyketide synthetases (transAT-PKSs), and one encoded type III polyketide synthetase (T3PKS), while two clusters were involved in terpene biosynthesis, and one cluster was involved in lantipeptide biosynthesis (**Table 2**). In contrast, the clusters predicted to produce lantipeptide had not typically been found in other *Bacillus* spp. (**Supplementary Figure 1**).

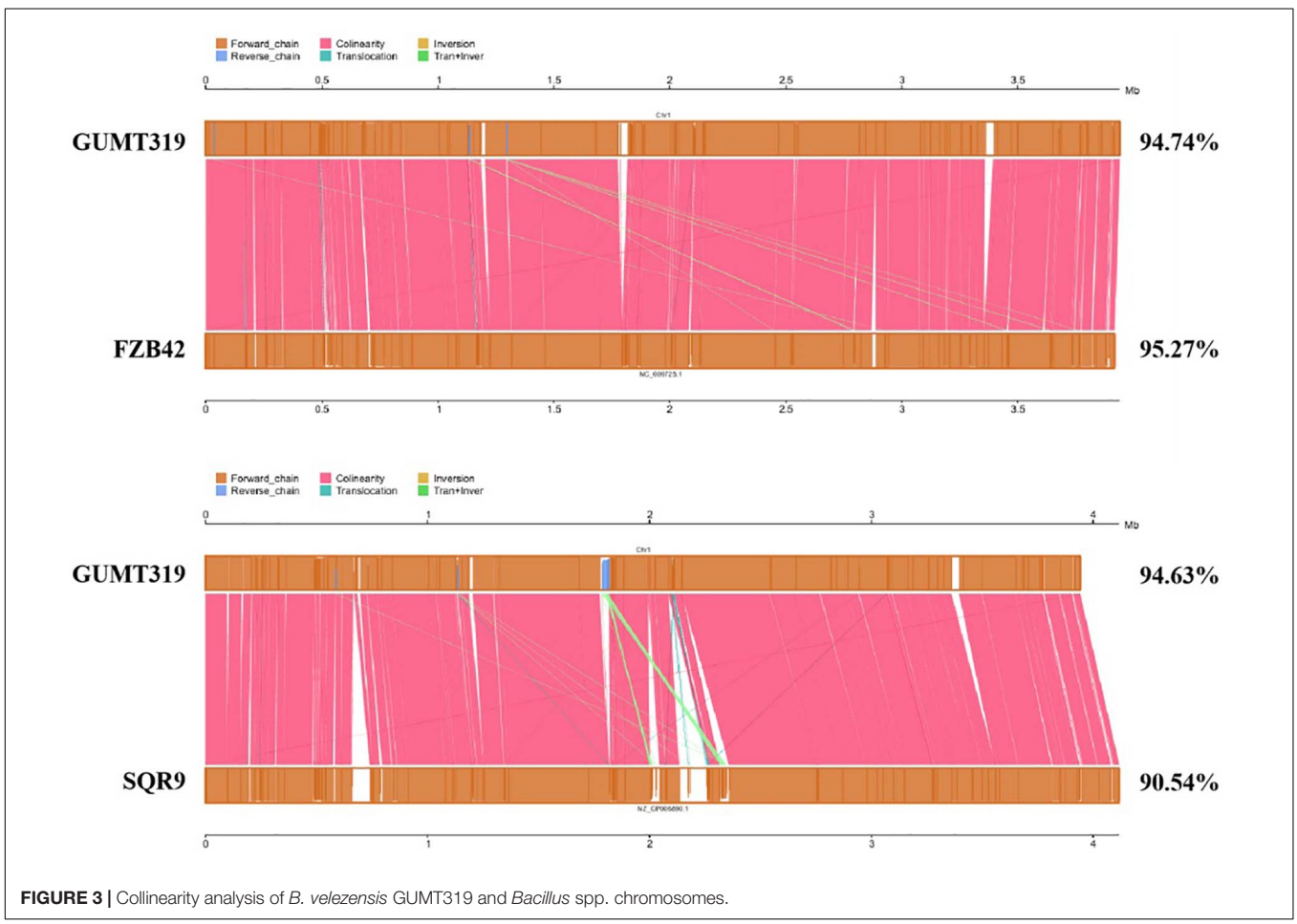

FIGURE 3 | Collinearity analysis of *B. velezensis* GUMT319 and *Bacillus* spp. chromosomes.

TABLE 2 | Antimicrobial gene clusters present in *B. velezensis* GUMT319.

Number	Predicted product	Enzyme complex	Genome location
Cluster 1	Lantipeptide		GUMT319_GM000192-GM000216
Cluster 2	Surfactin	nrps	GUMT319_GM000316-GM000362
Cluster 3	Unknown	Otherks	GUMT319_GM000931-GM000977
Cluster 4	Terpene		GUMT319_GM001059-GM001083
Cluster 5	Macrolactin	Transatpks	GUMT319_GM001461-GM001509
Cluster 6	Bacillaene	Transatpks; nrps	GUMT319_GM001737-GM001789
Cluster 7	Fengycin (iturin)	Transatpks; nrps	GUMT319_GM001911-GM001981
Cluster 8	Terpene		GUMT319_GM002014-GM002037
Cluster 9	Unknown	t3pks	GUMT319_GM002126-GM002183
Cluster 10	Difficidin (polyketide)	Transatpks	GUMT319_GM002319-GM002375
Cluster 11	Bacteriocin	nrps	GUMT319_GM003069-GM003138
Cluster 12	Surfactin (cyclic lipopeptide)	nrps	GUMT319_GM003432-GM003473
Cluster 13	Bacilysin		GUMT319_GM003703-GM003751

Analysis of GUMT319 Genes Involved in Plant Root Colonization

When *B. velezensis* GUMT319 was grown in liquid culture without agitation, it formed robust pellicles at the liquid–air interface (Luo et al., 2019). The genome of *B. velezensis* GUMT319 contained a complete set of genes implicated in biofilm formation, including 15 genes belonging to the exopolysaccharide (EPS) operon *epsA-O* and *tapA-sipW-tasA* operon, which are required for the production of EPS and TasA fibers, which hold chains of cells together in bundles (Chen et al., 2007; Gao et al., 2015a; Al-Ali et al., 2018; **Table 3**). *B. velezensis* GUMT319 displayed a robust swarming phenotype (**Supplementary Figure 2**), and the protein encoded by *swrA* was essential for swarming. The genome of *B. velezensis* GUMT319 contained a complete set of genes implicated in chemotaxis and motility, including six MCPS genes, 25 flagellin gene clusters, and nine chemotaxis protein genes (Liu et al., 2020; **Table 3**). A previous study shows that GUMT319 produces siderophores, which facilitate rhizosphere competition and growth promotion (Gu et al., 2020). The genome of *B. velezensis* GUMT319 contained genes involved in siderophore biosynthesis, such as *dhbB*, *dhbE*, *dhbF*, and *entC*. GUMT319 also contained master global transcriptional regulators, such as AbrB and Spo0A, as well as the quorum-sensing regulators LuxS/AI-2 and ComA/ComP, which regulate biofilm formation, chemotaxis, and root colonization (Comella and Grossman, 2005; Weng et al., 2013; Yan et al., 2016; Xiong et al., 2020; **Table 3**).

Root Colonization

Root colonization of the rhizosphere by antagonistic bacteria is a prerequisite for effective biological control (Liu et al., 2014). In this study, we investigated the colonization of healthy tobacco and pepper seedling roots by *B. velezensis* GUMT319. After 2 days of incubation in the hydroponic system, root colonization by *B. velezensis* GUMT319 and GUMT319-gfp was investigated using SEM and a CLSM. The SEM images showed that GUMT319 cells were rod-shaped (**Figures 4A,C**). Additionally, a complex biofilm structure consisting of GUMT319 cells (**Figure 4C**) and GUMT319-gfp cells (**Figure 4D**) was formed on the tobacco root surface, and colonization occurred preferentially in the elongation region of tobacco roots (**Figure 4**). We also found that GUMT319 (**Figure 4A**) and GUMT319-gfp (**Figure 4B**) could colonize pepper roots, although to a much lesser extent than in tobacco roots (**Figure 4**).

Chemotactic Response to Root Exudates and Biofilm Formation

Root exudates are known to play an important role in plant–microbe interaction in the rhizosphere. The different compositions of root exudates from different plants are directly related to the chemotaxis reaction, biofilm formation, and colonizing behavior of bacterial strains originating from the respective rhizosphere (Zhang et al., 2014). We wanted to identify the different components of the root exudates that mediate the interaction between biocontrol *Bacillus* spp. and plant roots, which influenced their root colonization. To this end, root exudates from tobacco and pepper plants were collected and analyzed. Qualitative analyses of the freeze-dried tobacco and pepper root exudates were performed by GC-TOF-MS, and 248 peaks (**Supplementary Figure 2**) were detected, including amino acids, organic acids, and others (data not shown). Here, some organic acids (cinnamic acid, fumaric acid, phthalic acid, benzoic acid, and lauric acid) and nicotine were selected as the targets for evaluation of their roles on *B. velezensis* GUMT319 (Zhang et al., 2014; Feng et al., 2018; Ma et al., 2018). Cinnamic acid, fumaric acid, and benzoic acid were detected both in tobacco and pepper root exudates. Phthalic acid and nicotine were found only in tobacco root exudates and lauric acid was found only in pepper root exudates.

To investigate the cause of root colonization by *B. velezensis* GUMT319, the chemotactic reaction and biofilm formation response of GUMT319 to two root exudates and six components were determined. After the 12-h incubation period, the LB (0.7% agar) plate was almost fully covered by GUMT319 cells (**Supplementary Figure 2**), indicating that GUMT319 was highly proficient in swarming. We measured the chemotaxis activity of strain GUMT319 using tobacco root exudates, pepper root exudates, organic acids (cinnamic acid, fumaric acid, phthalic acid, benzoic acid, and lauric acid), and nicotine as attractants. The root exudates induced a positive chemotactic response in *B. velezensis* GUMT319, and cells showed faster migration toward all the attractants than toward the control after a 6-h incubation (**Figure 5**). The biofilm formation activity of strain GUMT319 was also examined using the qualitative biofilm experiment with tobacco root exudates, pepper root exudates, organic acids (cinnamic acid, fumaric acid, phthalic acid, benzoic acid, and lauric acid), and nicotine as attractants. The results showed that only lauric acid could be involved in the negative regulation of biofilm formation. No obvious difference was observed in biofilm formation among other treatments conducted with or without

TABLE 3 | List of root colonization-associated genes identified in the GUMT319 genome.

Colonization traits	Gene ID	Gene name	Function
Chemotaxis and motility	GUMT319_GM001681	*cheA*	Chemotaxis protein, sensor kinase
	GUMT319_GM001680	*cheB*	Chemotaxis response regulator protein, glutaminase
	GUMT319_GM001683	*cheC*	Chemotaxis protein, CheY-P-specific phosphatase
	GUMT319_GM002228	*cheR*	Chemotaxis protein methyltransferase
	GUMT319_GM001423	*cheV*	Chemotaxis protein
	GUMT319_GM001682	*cheW*	Chemotaxis protein, purine-binding protein
	GUMT319_GM001671	*cheY*	Chemotaxis protein
	GUMT319_GM003009	*tlpB*	Methyl-accepting chemotaxis protein
	GUMT319_GM003010	*mcpA*	Methyl-accepting chemotaxis protein
	GUMT319_GM003011	*tlpA*	Methyl-accepting chemotaxis protein
	GUMT319_GM003012	*mcpB*	Methyl-accepting chemotaxis protein
	GUMT319_GM000730	*yfmS*	Methyl-accepting chemotaxis protein
	GUMT319_GM001414	*mcpC*	Methyl-accepting chemotaxis protein
	GUMT319_GM001382	*motA*	Flagellar motor protein, chemotaxis protein
	GUMT319_GM001381	*motB*	Flagellar motor protein, chemotaxis protein
	GUMT319_GM001655–GM001679	*fla*	Flagellin gene clusters, flagellar biosynthesis
	GUMT319_GM003455	*swrA*	Swarming motility protein
Biofilm	GUMT319_GM000044	*abrB*	Transition state regulatory protein
	GUMT319_GM002412	*spo0A*	Stage 0 sporulation protein A, quorum sensing
	GUMT319_GM002455	*tapA*	Amyloid fiber anchoring and assembly protein, biofilm formation
	GUMT319_GM002454	*sipW*	Signal peptidase, biofilm formation
	GUMT319_GM002453	*tasA*	Spore coat-associated protein, biofilm formation
	GUMT319_GM002452	*sinR*	HTH-type transcriptional regulator, master regulator for biofilm formation
	GUMT319_GM002451	*sinI*	Anti-repressor of *sinR*
	GUMT319_GM003356–GM003370	*epsA-O*	Polysaccharide biosynthesis protein
Siderophores	GUMT319_GM003092	*entC*	Biosynthesis of siderophore group non-ribosomal peptides
	GUMT319_GM003091	*dhbE*	Siderophore group non-ribosomal peptide synthetase
	GUMT319_GM003090	*dhbB*	Biosynthesis of siderophore group non-ribosomal peptides
	GUMT319_GM003089	*dhbF*	Siderophore group non-ribosomal peptide synthetase
Quorum sensing	GUMT319_GM002966	*luxS*	Quorum-sensing autoinducer 2 (AI-2) synthesis protein
	GUMT319_GM003062	*comA*	Two-component transcriptional regulator, quorum sensing
	GUMT319_GM003063	*comP*	Sensor histidine kinase, quorum sensing

root exudates. The pellicles formed by GUMT319 were similar in all other groups (**Figure 6**).

Antagonistic Effects of GUMT319 on Plant Pathogens *in vitro*

In this study, it was found that GUMT319 displayed strong antagonistic activity against *P. nicotianae*, *C. scovillei*, *C. capsici*, *F. carminascens*, *S. sclerotiorum*, *A. alternata*, *Phomopsis* sp., *P. sorghina*, and *E. turcicum* (**Figure 7** and **Supplementary Table 2**), indicating that *B. velezensis* GUMT319 was effective against a relatively broad spectrum of oomycetes and ascomycetes.

Effects of GUMT319 on Tobacco Black Shank in Field Experiments

We further investigated the efficiency of control of GUMT319 on tobacco black shank in field experiments. In those conducted in 2018, the disease incidence of tobacco plants treated with sterile water was 20.48%, while the disease incidence of plants treated independently with GUMT319 suspension, 58% metalaxyl manganese zinc WP, and Green Conway WP decreased, having control efficacy on tobacco black shank of 77.15, 76.43, and 65.59%, respectively (**Table 3**). Tobacco plants treated with strain GUMT319 showed the lowest disease incidence, with a control efficiency significantly higher than those treated with Green Conway WP. In the 2019 field experiments, the disease incidence of tobacco plants treated with water was 15.42%, while the control efficacy on tobacco black shank of those plants treated independently with GUMT319, 58% metalaxyl manganese zinc WP, and Green Conway WP were 71.97, 71.59, and 66.47%, respectively (**Table 3**). In the 2020 field experiments, the disease incidence of tobacco plants treated with water reached 79.09%, while the control efficacy on tobacco black shank of those plants treated independently with GUMT319, 58% metalaxyl manganese zinc WP, and Green Conway WP were 79.54, 76.98, and 62.31%, respectively (**Table 4** and **Supplementary Figure 4**). Thus, the control effect of GUMT319 suspension was significantly higher than that of 58% metalaxyl manganese zinc WP and Green Conway WP ($P < 0.05$),

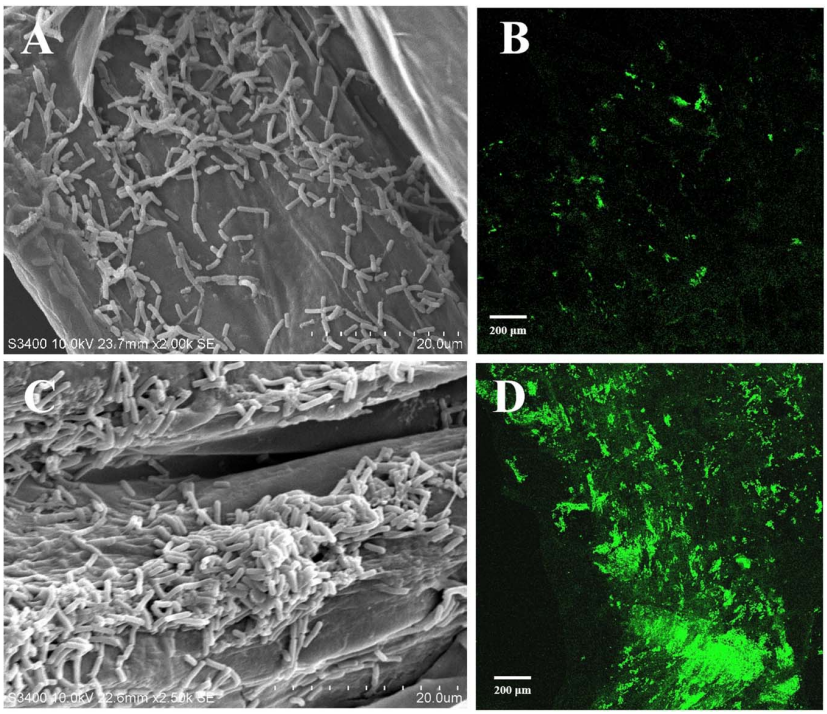

FIGURE 4 | Root colonization assay of *B. velezensis* GUMT319. **(A)** Scanning electron microscope (SEM, HITACHI S-3400N) images of pepper seedling roots colonized by strain GUMT319. **(B)** Confocal laser scanning microscope (CLSM, Olympus FV10i) images of pepper seedling roots colonized by GUMT319-gfp. **(C)** SEM images of tobacco seedling roots colonized by strain GUMT319. **(D)** Confocal laser scanning microscope (CLSM) images of tobacco seedling roots colonized by GUMT319-gfp. The green fluorescence signal depicts live cells colonizing the tobacco roots.

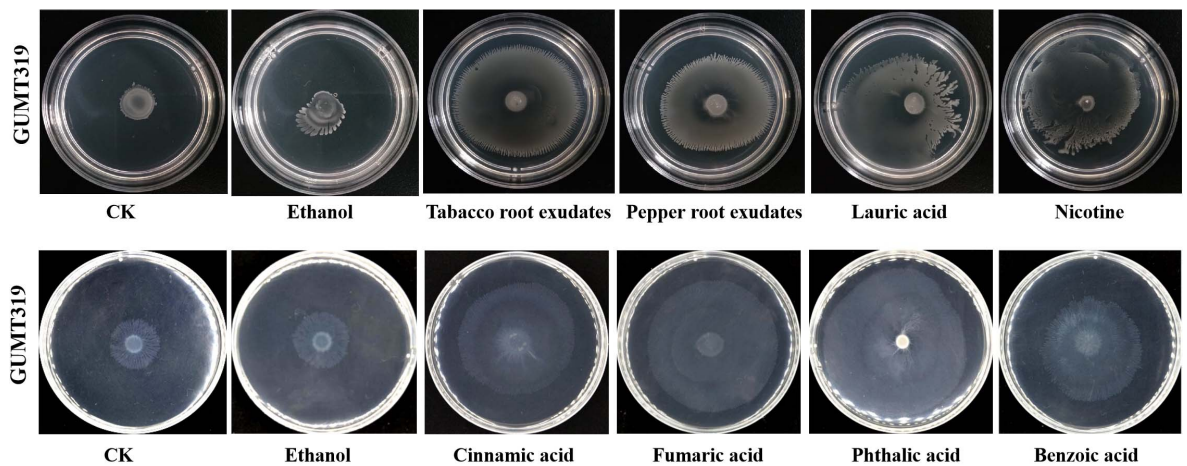

FIGURE 5 | Chemotactic response of *B. velezensis* GUMT319 to root exudates.

suggesting that GUMT319 could be used as a potential BCA for tobacco black shank.

DISCUSSION

The tobacco black shank control efficiency of several *Bacillus* strains, such as *B. subtilis* Tpb55 and *B. velezensis* Ba168, has been tested previously. Tobacco black shank, caused by *P. nicotianae*, is destructive to almost all flue-cured tobacco cultivars and is widespread in many tobacco-growing countries. *Bacillus* strains represent a promising strategy for the management of this soil-borne disease (Han et al., 2016; Zhang et al., 2017a; Srikhong et al., 2018; Guo et al., 2020). In this study, we identified another *B. velezensis* isolate, GUMT319, from a healthy tobacco rhizosphere in the fields

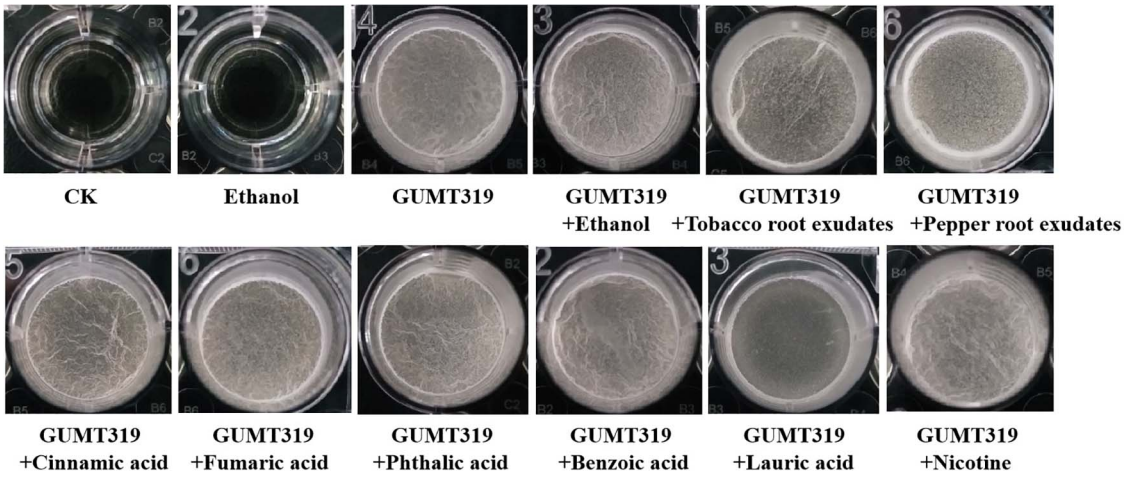

FIGURE 6 | Biofilm formation assay of *B. velezensis* GUMT319.

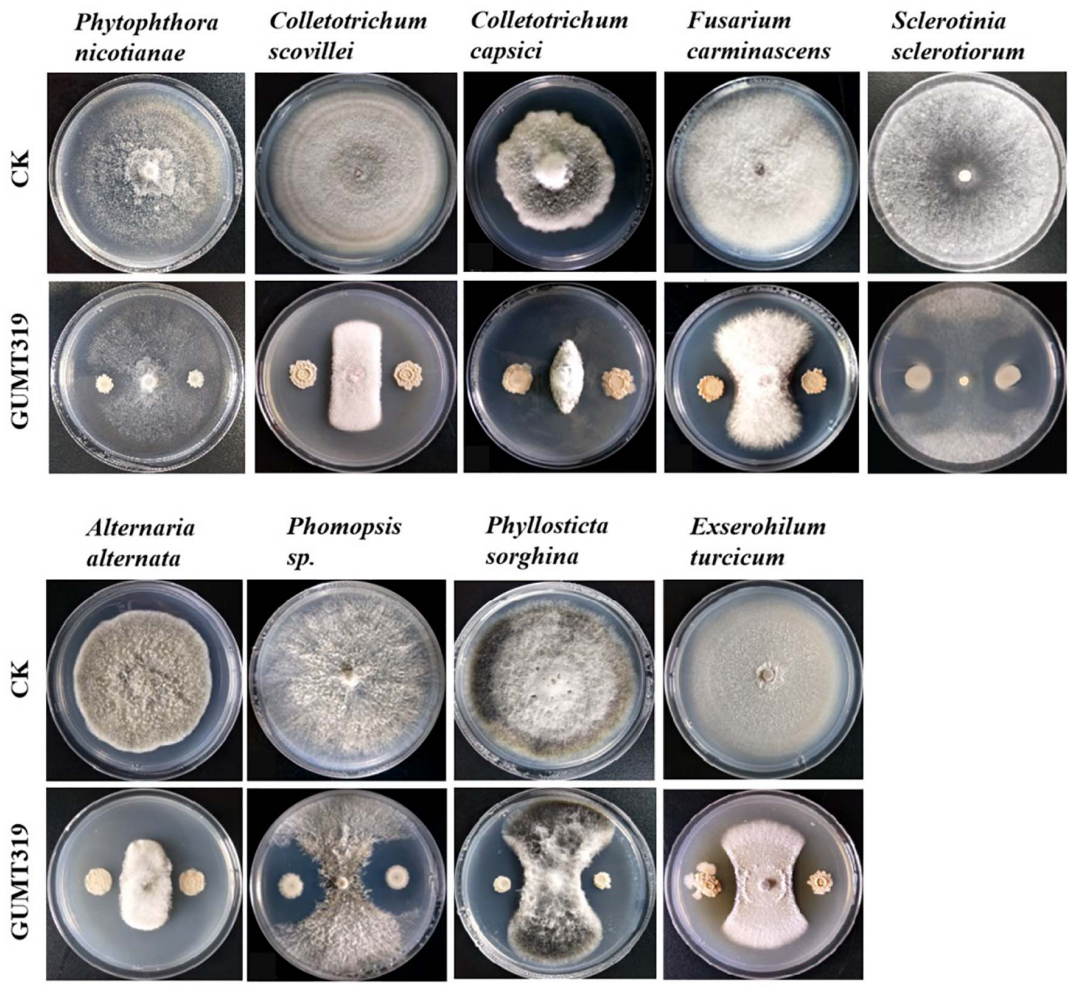

FIGURE 7 | Antagonistic activity of *B. velezensis* GUMT319 against nine plant pathogens in dual-culture test.

TABLE 4 | Control efficacy of strain GUMT319 against tobacco black shank in the field.

Treatments	2018			2019			2020		
	Disease incidence (%)	Disease index	Control efficacy (%)	Disease incidence (%)	Disease index	Control efficacy (%)	Disease incidence (%)	Disease index	Control efficacy (%)
Water (control)	20.48 ± 1.52a	5.93 ± 0.24a	–	15.42 ± 0.44a	5.14 ± 0.09a	–	79.09 ± 0.48a	19.57 ± 0.13a	–
GUMT319	5.26 ± 0.63b	6.17 ± 0.18c	77.15 ± 2.60a(A)	5.17 ± 0.81b	1.48 ± 0.15b	70.97 ± 2.98a(A)	11.66 ± 0.16d	4.01 ± 0.04d	79.54 ± 0.18a(A)
58% metalaxyl manganese zinc WP	7.16 ± 0.92b	1.20 ± 0.13c	76.43 ± 3.48a(A)	4.63 ± 0.39b	1.45 ± 0.08b	71.59 ± 1.60a(A)	22.61 ± 0.43c	4.51 ± 0.11c	76.98 ± 0.54b(B)
Green Conway WP	8.65 ± 2.86b	1.76 ± 0.14b	65.59 ± 2.78b(A)	4.95 ± 0.22b	1.71 ± 0.07b	66.47 ± 1.37a(A)	43.68 ± 0.37b	7.39 ± 0.08b	62.31 ± 0.43c(C)

The data are means ± SDs. The different lowercase and uppercase letters in the same column indicate significant difference at the $P < 0.05$ and $P < 0.1$ levels, respectively, using Duncan's new multiple range test. All percentage data were subjected to arc-sine transformation before statistical analysis.

in Guizhou with a high incidence of tobacco black shank. The control efficiency of GUMT319 against tobacco black shank was greater than 70% in field experiments conducted in Meitan in 2018–2020, which was significantly higher than that obtained using other treatments including fungicide application (**Table 4** and **Supplementary Figure 4**). Hence, GUMT319 could potentially be used as a BCA for tobacco black shank in Guizhou.

GUMT319 was previously identified as a *B. amyloliquefaciens* strain; however, *16S rRNA* and *gyrA* sequences and whole genome sequence comparisons in the current study revealed that GUMT319 is a *B. velezensis* strain (**Figure 1**). Similarly, SQR9 and FZB42, which were previously classified as *B. amyloliquefaciens* strains, are now recognized as *B. velezensis* strains and considered as the model strains for gram-positive plant growth-promoting and biocontrol rhizobacteria (Chen et al., 2007; Zhang et al., 2015; Fan et al., 2018). We support the theory that many strains currently classified as *B. amyloliquefaciens* are actually *B. velezensis*.

In this study, we identified and classified *B. velezensis* strain GUMT319 based on genomic data generated using second- and third-generation sequencing technologies. Strain GUMT319 contained a single circular chromosome 3,940,023 bp in length, with 4,053 predicted genes and an average GC content of 46.6% (**Figure 2**). The genome of GUMT319 is smaller than that of SQR9 (4,117,023 bp) but comparable to that of FZB42 (3,918,596 bp). The three strains were identical in terms of the number of protein-coding genes but differed in the number and size of prophage regions as well as gene clusters encoding secondary metabolites. The majority of genes unique to GUMT319 (i.e., absent in SQR9 and FZB42) were phage related (**Table 1** and **Figure 3**).

The ability of *B. velezensis* GUMT319 to efficiently colonize the surface of tobacco roots was a prerequisite for biocontrol. Many beneficial bacteria form biofilms on plant roots, which play an important role in their antagonistic activities and biocontrol efficacy (Chen et al., 2013). Rhizosphere competence of bacteria is associated with their ability to form sessile, multicellular communities (biofilms) and their chemotaxis motility (Niu et al., 2017; Liu et al., 2020). The genome of GUMT319 contains more than 60 genes and 13 putative gene clusters related to secondary metabolites, which have previously been described as being involved in biofilm formation, chemotaxis motility, growth promotion, and antifungal activity (**Tables 2**, **3**).

B. velezensis has been widely researched because of its potential to produce bacteriostatic secondary metabolites (Fan et al., 2018). *B. velezensis* strain GUMT319 has been reported to produce cell wall-degrading enzymes such as proteases, cellulases, and phosphatases as well as siderophores, which facilitate rhizosphere competition and plant growth promotion and show strong inhibitory activity against *P. nicotianae* as well as eight other plant pathogens *in vitro* (Luo et al., 2019). The GUMT319 genome contained 13 putative gene clusters that were expected to participate in antimicrobial production, including bacilysin, surfactin, macrolactin, fengycin, bacillaene, difficidin, and terpene (**Table 3** and **Supplementary Figure 1**; Grady et al., 2019); the majority of these gene

clusters are conserved in all *B. velezensis* strains. However, clusters predicted to produce lantipeptides were not typical in other *Bacillus* spp. (**Supplementary Figure 3**). Lantipeptides are ribosomally synthesized peptides that are extensively post-translationally modified. It is suggested that lantipeptides are the antimicrobial compounds produced by gram-positive bacteria (Grady et al., 2019).

The ability of *Bacillus* to colonize plant roots and proliferate in the rhizosphere is important for stable, long-lasting disease prevention (Han et al., 2016). To examine the ability of GUMT319 to colonize plant roots, we labeled the strain with GFP. In the present study, GUMT319 and GUMT319-gfp colonized the surface of tobacco roots, forming microcolonies and complex biofilm structures. The root elongation zone was colonized to a greater extent than other areas of the root. We also found that GUMT319 and GUMT319-gfp could colonize on pepper roots, but lesser than that on tobacco roots (**Figure 4**). As a signal to attract or repel microbes, the root exudates serve as a carbon source for soil microorganisms. In addition, they play significant roles in chemotaxis, biofilm formation, and colonization of *Bacillus* strains on plant roots (Feng et al., 2018). The composition of root exudates is closely related to plant species, soil environment, climate factors, microorganisms, nutritional status, etc. Among them, plant species is the most important (Zhang et al., 2014). Therefore, we speculated that some substances in tobacco root exudates (not pepper) play a key role. The root exudates from tobacco and pepper plants were collected and analyzed using GC-TOF-MS (**Supplementary Figure 3**). It was found that organic acids were the most represented class of compounds in both plants. Hence, some organic acids (cinnamic acid, fumaric acid, phthalic acid, benzoic acid, and lauric acid) (Zhang et al., 2014; Feng et al., 2018) and nicotine (Ma et al., 2018) were selected as targets for the evaluation of their roles on *B. velezensis* GUMT319. Cinnamic acid, fumaric acid, and benzoic acid were detected both in tobacco and pepper root exudates, phthalic acid and nicotine in tobacco root exudates, and lauric acid only in pepper root exudates.

In this study, in tobacco root exudates, pepper root exudates, organic acids (cinnamic acid, fumaric acid, phthalic acid, benzoic acid, and lauric acid), and nicotine as attractants, it was found that GUMT319 moved faster toward all root exudates than toward the control (**Figure 5**). Lauric acid could be involved in the negative regulation of biofilm formation. There was no obvious difference among other treatments conducted with or without root exudates in biofilm formation (**Figure 6**). Compared with other root-secreted compounds, it was first reported that nicotine in the root exudates of tobacco was a chemoattractant for *B. velezensis* GUMT319. Previous research shows that nicotine from tobacco root exudates has the ability to enhance chemotaxis, growth, biocontrol efficiency, and colonization by *Pseudomonas aeruginosa* NXHG29 (Ma et al., 2018). However, we do not know how *B. velezensis* GUMT319 recognizes nicotine and regulates chemotaxis and root colonization.

Overall, this study showed that the beneficial function of GUMT319 in controlling tobacco black shank disease is through its ability to inhibit the mycelial growth of plant pathogens and to successfully colonize tobacco roots. Hence, *B. velezensis* GUMT319 could be used as a potential BCA against tobacco black shank.

DATA AVAILABILITY STATEMENT

The datasets presented in this study can be found in online repositories. The names of the repository/repositories and accession number(s) can be found below: https://www.ncbi.nlm.nih.gov/genbank/, CP068563.

AUTHOR CONTRIBUTIONS

HD, LP, and ZL designed the research and wrote the manuscript. HD, WM, SY, HC, and LP performed all the experiments. HD and WM analyzed the data. All authors reviewed the final manuscript.

FUNDING

This work was supported by the China Postdoctoral Science Foundation (Grant No. 2020M683658XB), the Development Project of Young Scientific and Technological Talents of Guizhou Province (Grant No. QJH-KY[2018]101), and the Science and Technology Project of Zunyi, Guizhou Tobacco Company (Grant No. 201706).

ACKNOWLEDGMENTS

We gratefully acknowledge Prof. Yong Wang for useful discussions about this article.

SUPPLEMENTARY MATERIAL

The Supplementary Material for this article can be found online at: https://www.frontiersin.org/articles/10.3389/fmicb.2021.658113/full#supplementary-material

REFERENCES

Al-Ali, A., Deravel, J., Krier, F., Béchet, M., Ongena, M., and Jacques, P. (2018). Biofilm formation is determinant in tomato rhizosphere colonization by *Bacillus velezensis* FZB42. *Environ. Sci. Pollut. Res.* 25, 29910–29920. doi: 10.1007/s11356-017-0469-1

Borriss, R., Danchin, A., Harwood, C. R., Médigue, C., Rocha, E. P. C., Sekowska, A., et al. (2018). *Bacillus subtilis*, the model Gram-positive bacterium: 20 years of annotation refinement. *Microb. Biotechnol.* 11, 3–17. doi: 10.1111/1751-7915.13043

Chen, X., Zhang, Y., Fu, X., Li, Y., and Wang, Q. (2016). Isolation and characterization of *Bacillus amyloliquefaciens* PG12 for the biological control

of apple ring rot. *Postharvest Biol. Technol.* 115, 113–121. doi: 10.1016/j.postharvbio.2015.12.021

Chen, X. H., Koumoutsi, A., Scholz, R., Eisenreich, A., Schneider, K., Heinemeyer, I., et al. (2007). Comparative analysis of the complete genome sequence of the plant growth–promoting bacterium *Bacillus amyloliquefaciens* FZB42. *Nat. Biotechnol.* 25, 1007–1014. doi: 10.1038/nbt1325

Chen, Y., Yan, F., Chai, Y., Liu, H., Kolter, R., Losick, R., et al. (2013). Biocontrol of tomato wilt disease by *Bacillus subtilis* isolates from natural environments depends on conserved genes mediating biofilm formation. *Environ. Microbiol.* 15, 848–864. doi: 10.1111/j.1462-2920.2012.02860.x

Chowdhury, S. P., Hartmann, A., Gao, X., and Borriss, R. (2015). Biocontrol mechanism by root-associated *Bacillus amyloliquefaciens* FZB42 – a review. *Front. Microbiol.* 6:780. doi: 10.3389/fmicb.2015.00780

Comella, N., and Grossman, A. D. (2005). Conservation of genes and processes controlled by the quorum response in bacteria: characterization of genes controlled by the quorum-sensing transcription factor ComA in *Bacillus subtilis*. *Mol. Microbiol.* 57, 1159–1174. doi: 10.1111/j.1365-2958.2005.04749.x

de Weert, S., Vermeiren, H., Mulders, I. H., Kuiper, I., Hendrickx, N., Bloemberg, G. V., et al. (2002). Flagella-driven chemotaxis towards exudate components is an important trait for tomato root colonization by *Pseudomonas fluorescens*. *Mol. Plant Microbe Interact.* 15, 1173–1180. doi: 10.1094/MPMI.2002.15.11.1173

Fan, B., Wang, C., Song, X., Ding, X., Wu, L., Wu, H., et al. (2018). *Bacillus velezensis* FZB42 in 2018: the gram-positive model strain for plant growth promotion and biocontrol. *Front. Microbiol.* 9:2491. doi: 10.3389/fmicb.2018.02491

Feng, H., Zhang, N., Du, W., Zhang, H., Liu, Y., Fu, R., et al. (2018). Identification of chemotaxis compounds in root exudates and their sensing chemoreceptors in plant-growth-promoting rhizobacteria *Bacillus amyloliquefaciens* SQR9. *Mol. Plant-Microbe Inter.* 31, 995–1005. doi: 10.1094/MPMI-01-18-0003-R

Feng, H., Zhang, N., Fu, R., Liu, Y., Krell, T., Du, W., et al. (2019). Recognition of dominant attractants by key chemoreceptors mediates recruitment of plant growth-promoting rhizobacteria. *Environ. Microbiol.* 21, 402–415. doi: 10.1111/1462-2920.14472

Gao, T., Foulston, L., Chai, Y., Wang, Q., and Losick, R. (2015a). Alternative modes of biofilm formation by plant-associated *Bacillus cereus*. *MicrobiologyOpen* 4, 452–464. doi: 10.1002/mbo3.251

Gao, T., Greenwich, J., Li, Y., Wang, Q., and Chai, Y. (2015b). The bacterial tyrosine kinase activator TkmA contributes to biofilm formation largely independently of the cognate kinase PtkA in *Bacillus subtilis*. *J. Bacteriol.* 197, 3421–3432. doi: 10.1128/JB.00438-15

Grady, E. N., MacDonald, J., Ho, M. T., Weselowski, B., McDowell, T., Solomon, O., et al. (2019). Characterization and complete genome analysis of the surfactin-producing, plant-protecting bacterium *Bacillus velezensis* 9D-6. *BMC Microbiol.* 19:5. doi: 10.1186/s12866-018-1380-8

Gu, S., Wei, Z., Shao, Z., Friman, V. P., Cao, K., Yang, T., et al. (2020). Competition for iron drives phytopathogen control by natural rhizosphere microbiomes. *Nat. Microbiol.* 5, 1002–1010. doi: 10.1038/s41564-020-0719-8

Guo, D., Yuan, C., Luo, Y., Chen, Y., Lu, M., Chen, G., et al. (2020). Biocontrol of tobacco black shank disease (*Phytophthora nicotianae*) by *Bacillus velezensis* Ba168. *Pestic. Biochem. Physiol.* 165:104523. doi: 10.1016/j.pestbp.2020.01.004

Han, T., You, C., Zhang, L., Feng, C., Zhang, C., Wang, J., et al. (2016). Biocontrol potential of antagonist *Bacillus subtilis* Tpb55 against tobacco black shank. *Biocontrol* 61, 195–205. doi: 10.1007/s10526-015-9705-0

Li, B., Li, Q., Xu, Z., Zhang, N., Shen, Q., and Zhang, R. (2014). Responses of beneficial *Bacillus amyloliquefaciens* SQR9 to different soilborne fungal pathogens through the alteration of antifungal compounds production. *Front. Microbiol.* 5:636. doi: 10.3389/fmicb.2014.00636

Liu, Y., Feng, H., Fu, R., Zhang, N., Du, W., Shen, Q., et al. (2020). Induced root-secreted d-galactose functions as a chemoattractant and enhances the biofilm formation of *Bacillus velezensis* SQR9 in an McpA-dependent manner. *Appl. Microbiol. Biotechnol.* 104, 785–797. doi: 10.1007/s00253-019-10265-8

Liu, Y., Zhang, N., Qiu, M., Feng, H., Vivanco, J. M., Shen, Q., et al. (2014). Enhanced rhizosphere colonization of beneficial *Bacillus amyloliquefaciens* SQR9 by pathogen infection. *FEMS Microbiol. Lett.* 353, 49–56. doi: 10.1111/1574-6968.12406

Luo, Y., Peng, L., Ding, J., Fu, S., and Li, Y. (2019). Screening and field control effect of biological control *Bacillus* strains against tobacco black shank. *Guizhou Agric. Sci. North. Hort.* 47, 59–64.

Ma, L., Zheng, S. C., Zhang, T. K., Liu, Z. Y., Wang, X. J., Zhou, X. K., et al. (2018). Effect of nicotine from tobacco root exudates on chemotaxis, growth, biocontrol efficiency, and colonization by *Pseudomonas aeruginosa* NXHG29. *Antonie Van Leeuwenhoek* 111, 1237–1257. doi: 10.1007/s10482-018-1035-7

Mao, T., Chen, X., Ding, H., Chen, X., and Jiang, X. (2020). Pepper growth promotion and Fusarium wilt biocontrol by *Trichoderma hamatum* MHT1134. *Biocontrol Sci. Technol.* 30, 1228–1243. doi: 10.1080/09583157.2020.1803212

Niu, B., Paulson, J. N., Zheng, X., and Kolter, R. (2017). Simplified and representative bacterial community of maize roots. *Proc. Natl. Acad. Sci. U.S.A.* 114, E2450–E2459.

Srikhong, P., Lertmongkonthum, K., Sowanpreecha, R., and Rerngsamran, P. (2018). Bacillus sp. strain M10 as a potential biocontrol agent protecting chili pepper and tomato fruits from anthracnose disease caused by *Colletotrichum capsici*. *Biocontrol* 63, 833–842. doi: 10.1007/s10526-018-9902-8

Wang, J., Xing, J., Lu, J., Sun, Y., Zhao, J., Miao, S., et al. (2019). Complete genome sequencing of *Bacillus velezensis* WRN014, and comparison with genome sequences of other *Bacillus velezensis* strains. *J. Microbiol. Biotechnol.* 29, 794–808. doi: 10.4014/jmb.1901.01040

Weng, J., Wang, Y., Li, J., Shen, Q., and Zhang, R. (2013). Enhanced root colonization and biocontrol activity of *Bacillus amyloliquefaciens* SQR9 by *abrB* gene disruption. *Appl. Microbiol. Biotechnol.* 97, 8823–8830. doi: 10.1007/s00253-012-4572-4

Wu, G., Liu, Y., Xu, Y., Zhang, G., Shen, Q., and Zhang, R. (2018). Exploring elicitors of the beneficial rhizobacterium *Bacillus amyloliquefaciens* SQR9 to induce plant systemic resistance and their interactions with plant signaling pathways. *Mol. Plant Microbe Interact.* 31, 560–567. doi: 10.1094/mpmi-11-17-0273-r

Xiong, Q., Liu, D., Zhang, H., Dong, X., Zhang, G., Liu, Y., et al. (2020). Quorum sensing signal autoinducer-2 promotes root colonization of *Bacillus velezensis* SQR9 by affecting biofilm formation and motility. *Appl. Microbiol. Biotechnol.* 104, 7177–7185. doi: 10.1007/s00253-020-10713-w

Xu, P., Xie, S., Liu, W., Jin, P., Wei, D., Yaseen, D. G., et al. (2020). Comparative genomics analysis provides new strategies for bacteriostatic ability of *Bacillus velezensis* HAB-2. *Front. Microbiol.* 11:594079. doi: 10.3389/fmicb.2020.594079

Xu, Z., Shao, J., Li, B., Yan, X., Shen, Q., and Zhang, R. (2013). Contribution of bacillomycin D in *Bacillus amyloliquefaciens* SQR9 to antifungal activity and biofilm formation. *Appl. Environ. Microbiol.* 79, 808–815. doi: 10.1128/AEM.02645-12

Yan, F., Li, C., Ye, X., Lian, Y., Wu, Y., and Wang, X. (2020). Antifungal activity of lipopeptides from *Bacillus amyloliquefaciens* MG3 against *Colletotrichum gloeosporioides* in loquat fruits. *Biol. Control* 146:104281. doi: 10.1016/j.biocontrol.2020.104281

Yan, F., Yu, Y., Wang, L., Luo, Y., Guo, J., and Chai, Y. (2016). The *comer* gene plays an important role in biofilm formation and sporulation in both *Bacillus subtilis* and *Bacillus cereus*. *Front. Microbiol.* 7:1025. doi: 10.3389/fmicb.2016.01025

Ye, X., Li, Z., Luo, X., Wang, W., Li, Y., Li, R., et al. (2020). A predatory myxobacterium controls cucumber *Fusarium* wilt by regulating the soil microbial community. *Microbiome* 8:49. doi: 10.1186/s40168-020-00824-x

Zhang, C., Gao, J., Han, T., Tian, X., and Wang, F. (2017a). Integrated control of tobacco black shank by combined use of riboflavin and *Bacillus subtilis* strain Tpb55. *Biocontrol* 62, 835–845. doi: 10.1007/s10526-017-9849-1

Zhang, G., Wang, W., Deng, A., Sun, Z., Zhang, Y., Liang, Y., et al. (2012). A mimicking-of-DNA-methylation-patterns pipeline for overcoming

the restriction barrier of bacteria. *PLoS Genet*. 8:e1002987. doi: 10.1371/journal.pgen.1002987

Zhang, N., Wang, D., Liu, Y., Li, S., Shen, Q., and Zhang, R. (2014). Effects of different plant root exudates and their organic acid components on chemotaxis, biofilm formation and colonization by beneficial rhizosphere-associated bacterial strains. *Plant Soil* 374, 689–700. doi: 10.1007/s11104-013-1915-6

Zhang, N., Yang, D., Wang, D., Miao, Y., Shao, J., Zhou, X., et al. (2015). Whole transcriptomic analysis of the plant-beneficial rhizobacterium *Bacillus amyloliquefaciens* SQR9 during enhanced biofilm formation regulated by maize root exudates. *BMC Genomics* 16:685. doi: 10.1186/s12864-015-1825-5

Zhang, R., Vivanco, J. M., and Shen, Q. (2017b). The unseen rhizosphere root-soil-microbe interactions for crop production. *Curr. Opin. Microbiol.* 37, 8–14. doi: 10.1016/j.mib.2017.03.008

Zhang, X., Zhou, Y., Li, Y., Fu, X., and Wang, Q. (2017c). Screening and characterization of endophytic *Bacillus* for biocontrol of grapevine downy mildew. *Crop Prot*. 96, 173–179. doi: 10.1016/j.cropro.2017.02.018

Conflict of Interest: The authors declare that the research was conducted in the absence of any commercial or financial relationships that could be construed as a potential conflict of interest.

frontiers in Microbiology

ORIGINAL RESEARCH
published: 16 July 2021
doi: 10.3389/fmicb.2021.715773

Alternative Splicing of *MoPTEN* Is Important for Growth and Pathogenesis in *Magnaporthe oryzae*

*Shaowei Wang[1], Hao Liang[1], Yi Wei[1,2,3], Penghui Zhang[1], Yuejia Dang[2,3], Guihua Li[1] and Shi-Hong Zhang[1,2,3]**

[1] College of Plant Sciences, Jilin University, Changchun, China, [2] Center for Extreme-Environmental Microorganisms, Shenyang Agricultural University, Shenyang, China, [3] College of Plant Protection, Shenyang Agricultural University, Shenyang, China

Human PTEN, a dual-phosphatase tumor suppressor, is frequently dysregulated by alternative splicing. Fungi harbor *PTEN* homologs, but alternative splicing of fungal *PTENs* has not been reported as far as we know. Here, we described an alternative splicing case in the *PTEN* homolog of *Magnaporthe oryzae* (*MoPTEN*). Two splice variants of *MoPTEN* were detected and identified, which are resulted from an intron retention and exclusion (*MoPTEN-1/2*). Both proteins were different in lipid and protein phosphatase activity and in expression patterns. The *MoPTEN* deletion mutant (Δ*MoPTEN*) showed the defects in conidiation, appressorium formation, and pathogenesis. Δ*MoPTEN* could be completely restored by *MoPTEN*, but rescued partially by *MoPTEN-1* in the defect of conidium and appressorium formation, and by *MoPTEN-2* in the defect of invasive development. Assays to assess sensitivity to oxidative stress reveal the involvement of *MoPTEN-2* in scavenging exogenous and host-derived H_2O_2. Taken together, *MoPTEN* undergoes alternative splicing, and both variants cooperatively contribute to conidium and appressorium development, and invasive hyphae growth in plant cells, revealing a novel disease development pathway in *M. oryzae*.

Keywords: alternative splicing, *MoPTEN*, growth, pathogenesis, *Magnaporthe oryzae*

OPEN ACCESS

Edited by:
Yong Wang,
Guizhou University, China

Reviewed by:
Vijai Bhadauria,
China Agricultural University, China
Wensheng Zhao,
China Agricultural University, China

***Correspondence:**
Shi-Hong Zhang
zhangsh89@syau.edu.cn

Specialty section:
This article was submitted to Microbe and Virus Interactions with Plants, a section of the journal Frontiers in Microbiology

Received: *27 May 2021*
Accepted: *24 June 2021*
Published: *16 July 2021*

Citation:
Wang S, Liang H, Wei Y, Zhang P, Dang Y, Li G and Zhang S-H (2021) Alternative Splicing of MoPTEN Is Important for Growth and Pathogenesis in Magnaporthe oryzae. Front. Microbiol. 12:715773. doi: 10.3389/fmicb.2021.715773

INTRODUCTION

Protein phosphorylation, co-regulated by kinase and phosphatase, plays multiple important roles in eukaryotic organisms (Zolnierowicz and Bollen, 2000; Bauman and Scott, 2002). Kinase catalyzes the transfer of phosphate from a donor to a protein resulting in phosphorylated proteins; conversely, phosphatase hydrolyses phosphorylated proteins leading to the removal of phosphate (dephosphorylation). Based on the homology, structure, and substrates, protein phosphatases are divided into two families: serine/threonine protein phosphatases and protein tyrosine phosphatases (PTPs) (Pao et al., 2007; Shi, 2009). Protein tyrosine phosphatase family is very complicated,

Abbreviations: CM, complete minimal media; DAB, 3,3′-diaminobenzidine; dpi, days post-inoculation; DPI, diphenyleneiodonium; hpi, hours post-inoculation; OTA, oatmeal-tomato agar; PDA, potato dextrose agar; PIP2, phosphatidylinositol-4,5-diphosphate; PIP3, phosphatidylinositol-3,4,5-trisphosphate; PTP, protein tyrosine phosphatase; ROS, reactive oxygen species.

and it can be subdivided into several classes, such as specific protein-tyrosine phosphatases and dual-specificity phosphatases (Andersen et al., 2001; Moorhead et al., 2007; Pao et al., 2007).

The human tumor suppressor, PTEN/MMAC1/TEP1 (PTEN, phosphatase deleted on chromosome ten; MMAC1, mutated in multiple advanced cancers; TEP1, tensin-like phosphatase) is a dual-specificity phosphatase based on the conserved catalytic domain (Li et al., 1997a; Steck et al., 1997). As a protein phosphatase, PTEN dephosphorylates the corresponding phosphorylated proteins (Shi et al., 2014; Shinde and Maddika, 2016). However, different from the classic dual-specificity phosphatases, PTEN catalyzes the dephosphorylation of both protein and non-protein substrates and preferentially dephosphorylates the secondary messenger phosphatidylinositol-3,4,5-trisphosphate (PIP3) to phosphatidylinositol-4,5-diphosphate (PIP2), which is essential for regulating the highly oncogenic pro-survival phosphatidylinositol-3-phosphate kinase (PI3K) signaling pathway (Lee et al., 1999; Salmena et al., 2008).

PTEN protein is encoded by a unique gene (Liang et al., 2014). However, alternative splicing increases the number of transcripts. More splice variants, by intron retention or exon exclusion, have been detected to be inactive forms of PTEN (Sharrard and Maitland, 2000; Agrawal and Eng, 2006). PTEN plays multiple important roles in many cellular activities. In addition to tumor suppression, it is also involved in metabolism, tissue homeostasis, differentiation, and neurological diseases (Ramaswamy et al., 1999; Rademacher and Eickholt, 2019). PTEN and homologs are evolutionarily conserved in humans and mammals, but a small number of PTEN homologs have been found in fungi. *TEP1* (YNL128w), the first fungal *PTEN* gene, was cloned in the budding yeast *Saccharomyces cerevisiae* (Li et al., 1997b). The yeast PTEN homolog, like the mammalian counterpart, functions in the phosphatidylinositol pathway; but differently, the *PTEN*/*TEP1* is required for yeast sporulation (Heymont et al., 2000). In filamentous fungal pathogens, homologs of *TEP1*/*PTEN* appear to be associated with conidium formation and pathogenesis (Zhang et al., 2010; Vijayakrishnapillai et al., 2018; Wang et al., 2021).

Magnaporthe oryzae is the causal agent of rice blast worldwide. Host cell invasion is initiated by developed conidia, which occurs outside plant cells and involves conidium germination, tube elongation, appressorium maturation and differentiation (Howard et al., 1991; Talbot, 2003). After penetration, successful development of invasive hyphae determines the severity of blast (Heath et al., 1990; Kankanala et al., 2007). In a whole cycle of disease development, multiple phosphorylation dependent signaling pathways are required, which include the Pmk1 mitogen-activated protein (MAP) kinase, cyclic AMP dependent protein kinase A and Pkc1-Mps1 MAP kinase pathways (Li et al., 2012). Considering the balance of phosphorylation, dephosphorylation with different phosphatases are inevitably activated (Franck et al., 2015). So far, serine/threonine protein phosphatase PP2Ac (Du et al., 2013) and MoPpe1 (Qian et al., 2018) were demonstrated to play vital roles in the pathogenic development of *M. oryzae*. Recently, Sun et al. (2018) reported in the rice blast fungus that Target-of-Rapamycin (TOR) nutrient-signaling pathway plays an important role in mediating plant-fungal biotrophic interface membrane integrity and inhibiting the formation of appressorium in *M. oryzae* by suppressing the downstream of the cPKA pathway (Marroquin-Guzman and Wilson, 2015). Importantly, a dual-specificity phosphatase MoYvh1 was shown to play important roles in scavenging of host-derived reactive oxygen species (ROS) and subverting rice defense in *M. oryzae* (Liu et al., 2018).

Despite the importance of TEP1/PTEN in fungi, there are only a few reports on the function and regulation of its homologs in the filamentous fungi. In this research, we biologically analyzed the PTEN-like gene through creating several mutant strains in the rice blast fungus *M. oryzae*. Biological and molecular data reveal that an alternative splicing of *MoPTEN* is important for growth, development, and pathogenesis in *M. oryzae*.

MATERIALS AND METHODS

Fungal Strains and Growth Conditions

The wild-type strain *M. oryzae* JL0910 was previously isolated and purified from the rice cultivar Jijing88, which is widely planted in Jilin Province, China (Li et al., 2015). All strains, including the four strains generated in this study, were cultured on complete media (CM) agar plates (1 g/L yeast extract, 0.5 g/L enzyme hydrolyzed casein, 0.5 g/L acid hydrolyzed casein, 10 g/L glucose, 1 g/L $Ca(NO_3)_2{\cdot}4H_2O$, 0.2 g/L KH_2PO_4, 0.25 g/L $MgSO_4{\cdot}7H_2O$, 0.15 g/L NaCl, and 15 g/L agar), or potato dextrose agar (PDA) (200 g/L peeled potatoes, 20 g/L glucose, and 15 g/L agar), and stored on filter paper at −20°C. The strains were cultured for 7 days on CM for assessment of their growth rates. Each test was repeated at least three times. Mycelia used for nucleic acid extraction were prepared by growing the relevant strains in 100 mL liquid CM for 3 days at 25°C with gentle rocking at 150 rpm under bright light. For sporulation analysis and conidia harvesting, the strains were inoculated on oatmeal-tomato agar medium (OTA) and incubated at 25°C for 10 days in the dark (Cui et al., 2015). After the aerial hyphae of the colonies had been washed away using sterilized distilled water, the strains were continually grown for 3 days under a fluorescent light.

Saccharomyces cerevisiae BY4743 and the *TEP1/PTEN* deletion mutant strains (Invitrogen, Beijing, China) were used for functional complementation test. The PI3K inhibitor wortmannin (KY12420, Sigma, Beijing, China) was prepared in dimethylsulfoxide (DMSO) as stock solution (25 mg/mL) and stored at −20°C. The yeast *S. cerevisiae* transformation was performed by the lithium acetate procedure. For yeast gene expression, YPB-ADHpt promoter and terminator regions of ADH1 gene in YPB1 was used (Bertram et al., 1996). All yeast strains were cultured according to Li et al. (2018).

DNA, RNA, and Protein Manipulations

Total RNA or DNA were extracted using RNA or DNA extraction kits (Sangon Biotech, Shanghai, China). First-strand cDNA was synthesized from 2.0 μg of total RNA using Avian Myeloblastosis Virus reverse transcriptase (Promega, Madison,

WI, United States). The cDNA samples were 10-fold diluted and used as templates for RT-PCR.

PCR DIG Probe Synthesis Kit (Sigma-Aldrich, Shanghai, China) was used for Southern blot. The fragment with the hygromycin B phosphotransferase gene (*HPH*) was used as a hybridization probe, and the *HPH* probe fragment was amplified by using primer pair HPH1 and HPH2 (**Supplementary Table 1**). The genomic DNA of S28515 was digested with *Eco*RV and *Xba*I, respectively.

The flanking sequence of T-DNA insertion locus of S28515 was isolated by Thermal asymmetric interlaced PCR (Tail-PCR) (Liu and Whittier, 1995), and amplified by arbitrary degenerate primers (AD4) and T-DNA specific primers (RB1-3). The PCR used high-fidelity polymerase (TaKaRa, Dalian, China) for amplification. All the PCR fragments were sequenced (Sangon Biotech, Shanghai, China) and analyzed through NCBI BLAST[1]. Transcript analysis of the *MoPTEN* gene was performed based on semi-quantitative RT-PCR (semi-qRT-PCR). RNA samples were extracted from the vegetative mycelia, conidia, germinated conidia, appressoria at different developmental stages, and diseased leaves at certain hours post-inoculation (hpi), respectively. Total RNA was used to synthesize the first-strand cDNA. The *MoACTIN* gene (MGG_03982) was used as an endogenous control. The primers semi-YP-F/R were used for the *MoPTEN* gene, and the primers semi-actin-F/R were used for the actin gene. Agarose gel electrophoresis (2%) was used to display the *MoPTEN* expression level and pattern. The experiments were independently repeated twice with three biological replicates, and all primer pairs used herein are listed in **Supplementary Table 1**.

For the recombinant protein preparation, the full-length fragments of *MoPTEN-1* (1,974 bp) and *MoPTEN-2* (1,890 bp) were amplified using PCR with a pair of primers (MBD-F/R) containing *Eco*RI and *Hind*III restriction sites. The PCR product was subcloned into the pMD-18T vector (TaKaRa, Dalian, China), and the fragment containing the *MoPTEN-1* or *MoPTEN-2* gene ORF was cloned in-frame into the pET-28a (+) vector (Novagen, Shanghai, China). Using the same strategy, other expression vectors harboring the gene fragments corresponding to either *MoPTEN-1* or *MoPTEN-2* were generated using the primers listed in **Supplementary Table 1**. *Escherichia coli* strains BL21 and DH5α were used as hosts for the plasmid DNA amplification and protein expression, and *E. coli* cells harboring the pET-28a::*MoPTEN-1* or *MoPTEN-2* plasmid were grown in LB medium at 30°C. Once the OD_{600} reached 0.6, IPTG (isopropylthio-β-D-galactoside) was added to a final concentration of 1 mM, and the cells were cultured for another 5–6 h. Recombinant protein was purified from *E. coli* cells using a Ni^{2+}-NTA purification kit according to the manufacturer's instructions (Novagen, Shanghai, China).

Lipid-/Protein-Phosphatase Activity Assays

The lipid-/protein-phosphatase activity of the recombinant MoPTEN-1 and MoPTEN-2 proteins were assayed on a soluble PIP3 or a synthetic phosphopeptide (DADEpYLIPQQG) by using a malachite green- or a molybdenum blue-reaction colorimetry phosphatase assay system (GENMED Scientifics, Shanghai, China) according to the manufacturer's instructions. The substrates were diluted to series of concentrations in phosphate free buffer (25 mM Tris, 100 mM NaCl pH 7.6). All reactions were incubated at 37°C for 30 min and terminated by adding 2 μL NaOH (10 M). A 50 μL of malachite green or molybdenum blue (BIOMOL Enzo Life Sciences, Shenzhen, China) were used to detect the released phosphate. Absorption at 620 or 660 nm was quantified in a NanoPhotometer-N50 microplate spectrophotometer (München, Germany). Phosphate standards were utilized to quantify the phosphate released by each sample. Samples were run in triplicate and results were normalized to a water control. Recombinant human PTEN (BioVision4838-5, San Francisco, CA, United States) or human PTP1B (P6244, Sigma-Aldrich, United States) was used as positive control.

Generation of the *GFP::PTEN* Gene, *PTEN* Gene Deletion and Complementation Strains

The vector pCAMBIA1303 containing promoter-MoPTEN-GFP fusion gene was constructed (**Supplementary Figure 1**). Promoter-MoPTEN (3,107 bp) was amplified using primers Prom-PTEN-F/R, then ligated into the pCAMBIA1303 (*Spe* I restricted), generating pCAMBIA1303-MoPTEN-GFP. The *Agrobacterium tumefaciens* mediated transformation (ATMT) protocol was conducted according to Khan et al. (2014). Transformants were screened on PDA plates with 200 μg/mL HygB. The GFP tag was amplified with the GFP-F/R primers for identification. The fusion gene expression was amplified with primers Mq-YP-F/R. The *MoACTIN* gene (MGG_03982) was amplified with the primers Mq-actin-F/R to serve as an endogenous reference.

To generate the *MoPTEN* deletion strain Δ*MoPTEN*, the *MoPTEN* gene was replaced by the hygromycin resistant cassette (*HPH*). To construct the replacement vector, the flanking sequences were amplified with their corresponding primer pairs (MGG-qc-LF/LR and MGG-qc-RF/RR), treated with restriction enzymes and ligated into the *Eco*RI – *Kpn*I and *Xba*I – *Sal*I sites of the pXEH 2.0 vector to construct a knockout vector (**Supplementary Figures 2A,B**). The three pairs of specific primers MoPTEN-F/R, HYG-YZ-F/R, and M-L-F/R were used to detect the genomes of transformants. The expression level of the subcellular deletion strains was detected using qRT-PCR (**Supplementary Figure 2C**).

Three complementation strains of Δ*MoPTEN* were constructed by using the full-length DNA sequence of the *MoPTEN* gene (2,114 bp), the *MoPTEN-1* (1,974 bp) cDNA containing two synonymous mutation sites at $T^{981}A$ and $A^{1062}T$, and the *MoPTEN-2* (1,890 bp) cDNA (second intron spliced form). These three fragments were, respectively, amplified by using the primers MGG-hb-F/R, and ligated into the *Sma*I restricted site of the pKD7-Red vector (G418-resistance) (a kind gift from Dr. Hongkai Wang and Dr. Jianping Lu, Zhejiang University, China) (**Supplementary Figures 3A,B**).

[1]https://blast.ncbi.nlm.nih.gov/Blast.cgi

The recombinant vectors were introduced into the Δ*MoPTEN* strains using *A. tumefaciens* mediated transformation method. Complementation transformants were screened on PDA agar plates supplemented with 300 μg/mL G418 and were confirmed using PCR and semi-qRT-PCR (**Supplementary Figures 3C,D**). The synonymous mutation was performed using TaKaRa MutanBEST Kit (TaKaRa, Japan, Dalian), a pair of primers MoPTEN-1(SM)-F/R with nucleotide substitution were showed in **Supplementary Table 1**.

Conidiation Quantification, Appressorium Induction, and Inoculation

After 10 days of cultivation on OTA, conidia were collected with 5 mL of distilled water, filtered through three layers of lens paper (Sealee, Japan), and counted with a hemacytometer under a Nikon Eclipse Ni-U microscope (Nikon, Tokyo, Japan). Conidial germination and appressorium formation were measured on a hydrophobic surface (plastic cover slips or gel-bond films) and onion epidermal cells. Conidial suspensions of 30 μL (1×10^5 conidia/mL) were dropped onto a hydrophobic surface or onion epidermal cells and were placed in a moistened box at 25°C. Appressorium formation rate was then calculated under the microscope at 12 hpi while photographs were taken at 24 hpi. More than 100 appressoria were counted for each strain and the experiment was repeated three times.

For the leaf drop-inoculation assay, 10 μL of a conidial suspension (1×10^5 conidia/mL) was dropped onto 10-cm leaf fragments cut from 2-week-old rice seedlings. Leaves pre-abraded with blade or unwounded were used for drop-inoculation. The inoculated leaves were placed on plastic plates with 90% humidity at 25°C for 24 h in the dark, then incubated in a 12-h light/12-h dark cycle until the large lesions appeared. For the inoculation of intact rice leaves, a conidial suspension (1×10^5 conidia/mL) was sprayed onto the leaves using an air sprayer. The inoculated plants were placed in a high humidity of 90% chamber at 25°C for 24 h in the dark, then transferred to a growth chamber with a 16-h light/8-h dark photoperiod. The different types of lesions on the 4 cm^2 leaves were counted and photographed at 7–9 days post-inoculation (dpi). These experiments were performed in triplicate and repeated three times for each strain.

For microscopic observation of cuticle penetration and invasive hyphae growth, leaf sheaths and inoculation were prepared as described in Koga et al. (2004), and inoculated with 300 μL of conidial suspension (1×10^5 conidia/mL) on the inner leaf sheath cuticle cells. After 48 h incubation under the 90% humid conditions at room temperature, the leaf sheaths were observed under a microscope.

H_2O_2 Stress Test, DAB Staining and DPI Treatment Assay

The wild type, mutant and complementation strains were continuously cultured on CM plates with concentrations of 2.5 and 5 mM H_2O_2 in the dark for 7 days at 25°C, and the fungal colonies were observed. The CM medium supplemented without H_2O_2 (0 mM) served as the control.

The 3,3′-diaminobenzidine (DAB) and diphenyleneiodonium (DPI) were used to detect the accumulation of H_2O_2 in plant cells infected by the different strains of *M. oryzae*. Rice leaf sheaths were injected with a conidial suspension at a concentration of 1×10^5 conidia/mL. For DAB staining assay, the infected leaf sheaths were sliced after 48 hpi, and stained in DAB dye solution (1 mg/mL; pH 3.8) for 8 h and destained with ethanol/acetic acid (94:4, v/v) for 1 h (Marroquin-Guzman et al., 2017), and then observed under a microscope. For DPI treatment test, the conidia of wild type, mutant and complementation strains were treated with a concentration of 0.4 μM DPI, which will inhibit plant NADPH oxidase (NOX) but not to affect fungal physiology (Fernandez et al., 2014), before infecting leaf sheaths. At 48 hpi, the infected rice leaves were observed under a microscope. These experiments were performed in triplicate and repeated three times for each strain.

Determination of Appressorial Melanin

Germinated conidia with or without appressoria were collected as samples to measure appressorial melanin, respectively. A 50 mg dried sample pellet was suspended in 6 mL NaOH solution (1 M) and continually heated at 121°C for 20 min. With 1 M NaOH as a blank control, the absorbance was measured at 405 nm with an ultraviolet spectrophotometer (Bio-Rad SmartSpec Plus, CA, United States) (Suryanarayanan et al., 2004). These experiments were performed in triplicate and repeated three times for each strain.

Statistical Analysis

All quantitative data provided in this study represent the results of triplicate experiments independently performed at least three times. Origin 7.0 software (OriginLab Corp., Northampton, MA, United States) was used to analyze the data and determine the mean ± SD of enzyme activity, conidiation, rate of conidial germination, rate of appressorial formation, colony diameters, relative expression and different types of disease. The significance of the data was assessed using the Student's *t*-test. $P < 0.05$ was considered statistically significant. Error bars represent the standard deviation.

RESULTS

Identification of the H_2O_2 Sensitive and Virulence Defective Strain S28515

During host-pathogen interactions, the increased ROS in rice cells is a threat to *M. oryzae*. Accumulation of ROS such as H_2O_2 is known to govern the pathogen and host interaction. Most mutants with pathogenicity defect are impaired in antioxidation (Ding et al., 2010; Marroquin-Guzman et al., 2017; Liu et al., 2018; Li et al., 2020), thus we planned to obtain non-pathogenic mutants based on H_2O_2 primary screening.

From an *A. tumefaciens* mediated T-DNA insertion library, we screened a mutant S28515 that was sensitive to 2.5 mM H_2O_2 on CM plate (**Figure 1A**). In addition, the S28515 mutant failed to cause typical blast lesions and instead caused some pinhead-sized

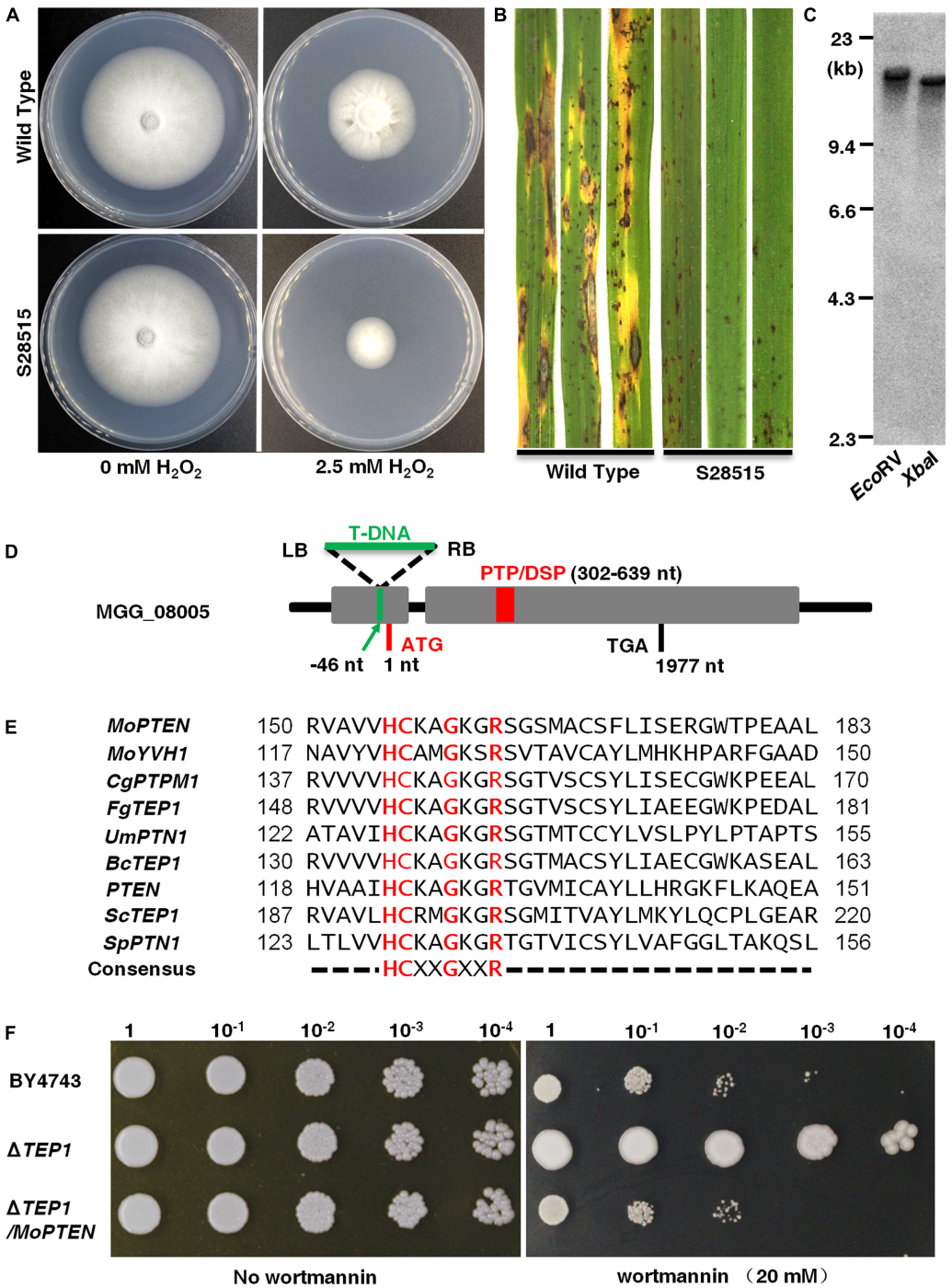

FIGURE 1 | Identification of a screened H_2O_2 sensitive mutant S28515. **(A)** S28515 is more sensitive to 2.5 mM H_2O_2. The wild type and S28515 strains were cultured on complete media (CM) plates or CM containing H_2O_2 (2.5 mM) plates in the dark for 10 days at 25°C and then representative colonies were photographed 7 days post-inoculation (dpi). **(B)** S28515 is defective in pathogenicity. Conidial suspensions of the wild type and S28515 strains were sprayed on rice seedlings. Diseased leaves were photographed 7 dpi. **(C)** Southern blot analysis of S28515. The total genomic DNA was digested with *Eco*RV and *Xba*I, and probed with the partial *HPH* fragment. **(D)** Insertion site analysis. The green arrow indicates the MGG_08005 T-DNA insertion site. The gray area represents the mRNA transcriptional region of the gene MGG_08005. The red rectangle represents PTP/DSP domain. The capital letters ATG and TGA represent the translation start and stop sites, respectively. **(E)** Sequence alignment. The catalytic domain of *MoPTEN* was compared with the phosphatase catalytic domains of reported species, which include *Magnaporthe oryzae* Guy11, *Colletotrichum graminicola* M1.001, *Fusarium graminearum* PH-1, *Ustilago maydis* 521, *Botrytis cinerea* B05.10, *Homo sapiens*, *Saccharomyces cerevisiae* S288C, and *Schizosaccharomyces pombe*. **(F)** Functional complementation of *MoPTEN* for *ScTEP1* in *S. cerevisiae*. A 10 μL droplets containing the indicated concentration of yeast cells were inoculated on to the solid YPD medium plates (20 mM wortmannin added). Wortmannin resistant phenotype of Δ*TEP1* was restored to sensitivity by transferring the *MoPTEN* gene in the yeast. Representative plates were photographed 3 dpi.

brown specks and restricted disease lesions (**Figure 1B**). Southern blot analysis indicated that a single-copy T-DNA fragment was inserted in the genome of S28515 (**Figure 1C**), confirming the phenotype is caused by the single T-DNA insertion.

Tail-PCR analysis was carried out to clone the disrupted locus. According to the bio-information of flanking sequences of the T-DNA insertion, the insertion site was determined to be 46 bp upstream of the start codon in MGG_08005 fragment (**Figure 1D**). The MGG_08005 locus, located on chromosome II of *M. oryzae*, has one intron and transcribes a length of 2,955 bp mRNA[2]. The open reading frame (ORF, 1,977 bp) encodes a protein of 658 amino acid residues with a predicted molecular mass of 72.6 kDa, which contains the consensus active site motif "HCXXGXXR" in most protein tyrosine phosphatases (**Figure 1E**; **Supplementary Figure 4A**).

Phylogenetic analysis showed that MGG_08005 protein and several selected homologs of PTEN/TEP1 were contained in the same clade (**Supplementary Figure 4B**), sharing 54% identity and 65% similarity with CgPTPM1, and 55% identity and 66% similarity with FgTEP1, but only 27% identity and 40% similarity with ScTep1, and 31% identity and 49% similarity with mammalian PTEN, suggesting a comparatively close genetic relationship with PTEN (termed MoPTEN). However, the *MoPTEN* gene could functionally complement the *ScTEP1* deletion mutant from resistant phenotype to sensitive phenotype against 20 mM wortmannin added in solid media (**Figure 1F**). These results indicated that *MoPTEN* is a homolog of *TEP1/PTEN*, and S28515 is the PTEN gene disrupted mutant.

Expression, Alternative Splicing, and Dual-Phosphatase Activity in MoPTEN

To determine the expression pattern, regulation, and localization of the *MoPTEN* gene, a *MoPTEN-GFP* fusion gene driven by its native promoter was transferred into the wild type (**Supplementary Figure 1**). Fluorescent microscopic observation was carried out in the growing hyphae (6 days), conidia, germinated conidia with germ tube (6 h), appressoria (12 h), and invasive hyphae (12, 48 hpi). Green fluorescence signals of the MoPTEN-GFP protein were detected with slightly weak in growing hyphae and rather strong in conidia, appressoria and invasive hyphae (**Figure 2**). By comparison, in the wild type or untransformed strains, the background green fluorescence was too weak to be detected (data not shown). This result suggests that MoPTEN expression is upregulated with the development of the infection process of *M. oryzae*.

Semi-qRT-PCR was performed using total RNA isolated from the different growing mycelia (4, 6, 8 days), newly produced mature conidia, germinated conidia, developing appressoria (6, 12, 24 h), and infected leaves with growing invasive hyphae (24, 48, 72 hpi). The results showed the *MoPTEN* gene expression gradually increased and reached a peak in the 12-h developed appressoria, and then decreased and disappeared until at infection stage (**Supplementary Figure 5A**). Unexpectedly, according to the ORF length of *MoPTEN* (1,977 bp), there appeared an additional band below the *MoPTEN* gene in the developing appressoria and invasive hyphae. In addition, the lower band gradually became the main band as the upper band disappeared within 72 hpi (**Supplementary Figure 5A**).

In order to clarify the additional band, the two bands were excised and sequenced, respectively. The results indicated that both sequences were all derived from the *MoPTEN* gene (**Figure 3A**). The upper band (*MoPTEN-1*) is 1,977 nt long, which is the previously deduced ORF of *MoPTEN* gene; and the lower band (*MoPTEN-2*) is a truncated fragment of *MoPTEN*. In comparison with the DNA sequence of *MoPTEN*, *MoPTEN-2* was 84 nt shorter than *MoPTEN-1*, in which a fragment (between 1,116 and 1,201 nt) was spliced (**Figure 3B**). The two ends of the 84 nt fragment also have the classic splicing sites "GU-AG," suggesting *MoPTEN-1* is an intron retention transcript form.

Compared with the *MoPTEN-1*, the *MoPTEN-2* gene encodes a protein of 630 amino acid residues with a predicted molecular mass of 69.4 kDa. The three-dimensional (3D) structures of MoPTEN-1 and MoPTEN-2 were predicted using the web-based server I-TASSER[3]. Both proteins form an unusually deep and wide pocket (**Supplementary Figure 5B**), which allows PTEN to accommodate the bulky phosphatidylinositol 3,4,5-trisphosphate substrate (Lee et al., 1999). In the pocket, two domains of PTEN, a protein tyrosine phosphatase (PTP) domain and a C2 domain, constitute a single unit; and the PTP domain contains the conserved motif "HCKAGKGR." The main difference between two forms is that MoPTEN-1 has a calcium ion binding site (A_{184}-F_{186}-K_{220}-E_{305}), but MoPTEN-2 has a zinc ion binding site (V_{53}- D_{57}) (**Supplementary Figure 5B**). The different ion binding sites may affect the activity and stability of both proteins, and eventually, lead to difference in biochemical properties.

As a dual-specificity phosphatase, PTEN catalyzes the dephosphorylation of protein and lipid substrates and preferentially dephosphorylates PIP3 to PIP2 (Ramaswamy et al., 1999). Recombinant proteins of MoPTEN-1 and MoPTEN-2 were expressed in *E. coli* and purified to homogeneity with a single-step process using a Ni^{2+}-NTA column (**Figure 3C**). Lipid or PTP-specificity phosphatase activity of MoPTEN-1 and MoPTEN-2 was detected with PIP3 or phosphorylated polypeptide Ac-DADE(pY)LIPQQG-NH_2 as substrate (GENMED Scientifics, Shanghai, China). As a result, MoPTEN-1 activity was significantly higher than that of MoPTEN-2 and the positive control (recombinant human PTEN) when PIP3 was used as substrate (**Figure 3D**). On the contrary, when the substrate was replaced by phosphorylated polypeptide, MoPTEN-2 activity was significantly higher than that of MoPTEN-1 and the positive control (recombinant human PTP-1B) (**Figure 3E**). Collectively, these results suggest that alternatively spliced MoPTEN variants possess the distinct expression patterns and dual-phosphatase activity.

MoPTEN-1 Is Important for Conidium and Appressorium Formation

To investigate the roles of *MoPTEN-1* and *MoPTEN-2*, we genetically created the knockout mutant strains of *MoPTEN* (Δ*MoPTEN*) (**Supplementary Figure 2**). Base on Δ*MoPTEN*,

[2]https://www.ncbi.nlm.nih.gov/; http://fungi.ensembl.org/Magnaporthe_oryzae/

[3]http://zhanglab.ccmb.med.umich.edu/I-TASSER/

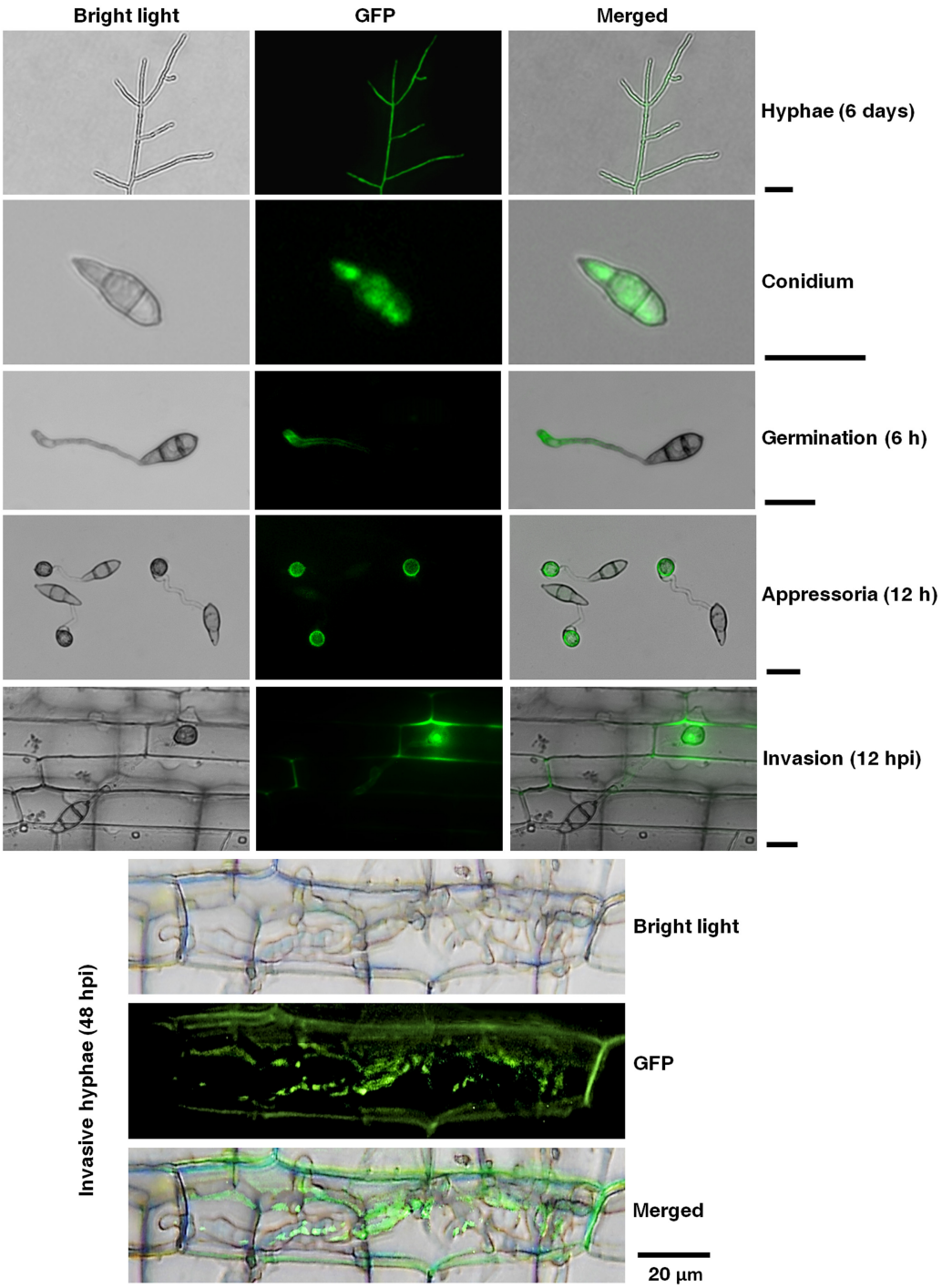

FIGURE 2 | Temporal and spatial dynamics of the *MoPTEN* gene expression in *M. oryzae*. Green fluorescence signals of the MoPTEN-GFP protein were examined by epifluorescence (GFP) microscopy in different developmental stages of *M. oryzae*. All the hyphae, conidia, appressoria and invasive hyphae in leaf-sheath cells were transferred to cover slips before green fluorescence signals observation. The 6-day-old hyphae grown on potato dextrose agar (PDA), conidia harvested from the 10-day-old colonies grown on oatmeal-tomato agar (OTA) media, germinated conidia (6 h), appressoria (12 h), invasive hyphae at 12 h post-inoculation (hpi), and invasive hyphae at 48 hpi were used for green fluorescence signals observation on Nikon Eclipse Ni-U microscope (Nikon, Tokyo, Japan). Scale bar = 20 μm.

we further created three complemented strains harboring Δ*MoPTEN* and the *MoPTEN* gene (Δ*MoPTEN*/*MoPTEN*), the *MoPTEN-1* gene with two synonymous mutations at $T^{981}A$ and $A^{1062}T$ (Δ*MoPTEN*/*MoPTEN-1*, which cannot be further spliced), and the *MoPTEN-2* gene (Δ*MoPTEN*/*MoPTEN-2*) (**Supplementary Figure 3**).

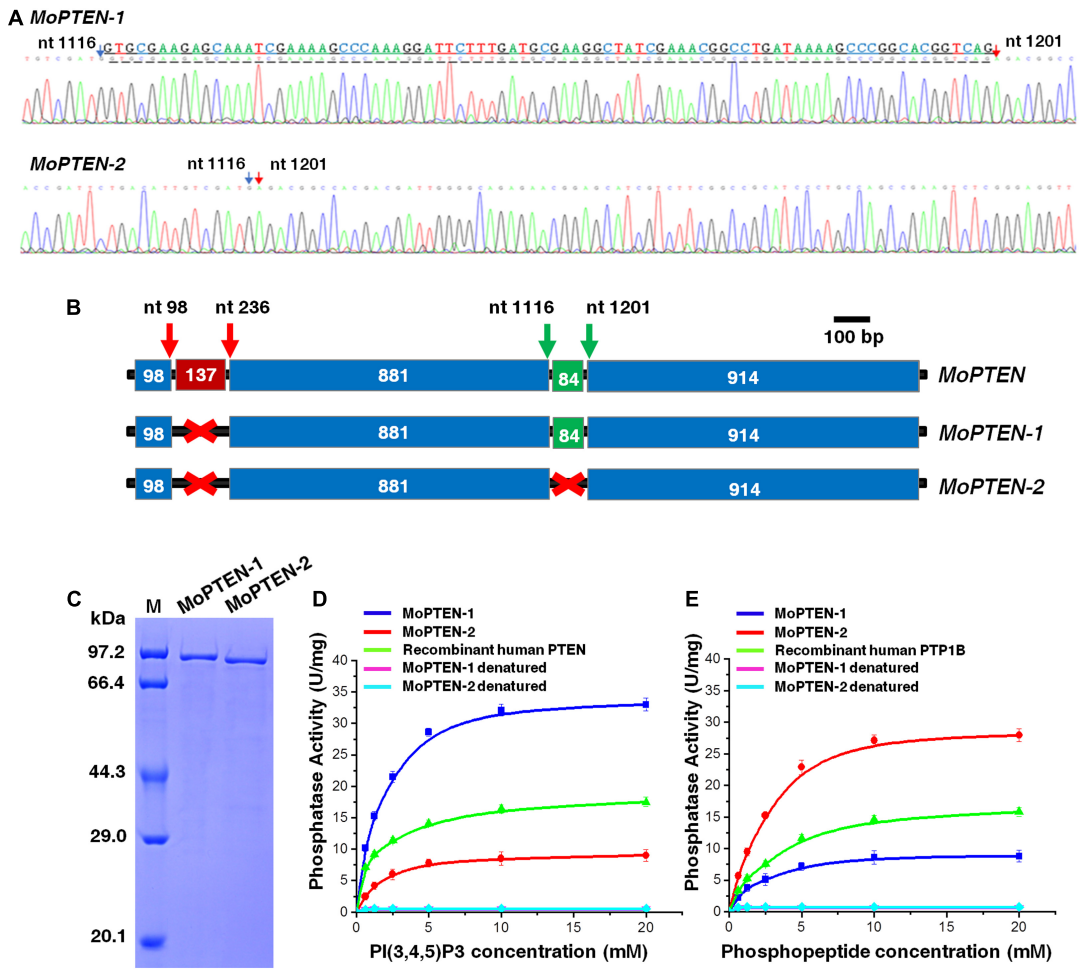

FIGURE 3 | Identification of two alternative splicing variants of *MoPTEN*. **(A)** Sequencing of two transcripts of the *MoPTEN* gene. The partial sequencing results of the two transcripts were shown. The retained intron is underlined, and the numbered arrows indicate two ends of an exon. **(B)** Schematic representation of the *MoPTEN* gene and its splice variants. Alternative splicing occurs in the second intron of *MoPTEN*. The retention or splicing of the second intron leads to two transcript forms, *MoPTEN-1* and *MoPTEN-2*. The upper number stands for the two ends of an exon. **(C)** MoPTEN-1/2 expressed in *Escherichia coli*. Purified both MoPTEN-1/2 were indicated in SDS-PAGE. **(D,E)** Measurement of lipid and protein phosphatase activity. PIP3 and phosphopeptide were used as substrates for activity measurement, respectively; the denatured recombinant proteins were used as negative control, and the recombinant human PTEN and PTP1B were used as positive controls. Error bars represent ± SD of three independent repeated samples.

The growth and development of these strains were assessed. When *M. oryzae* was cultivated on PDA and CM plates at 25°C, all the four created strains grew at a rate similar to that of the wild type, and their colony morphologies exhibited little difference (**Supplementary Figures 6A,B**). However, the deletion of *MoPTEN* significantly decreased conidial production (**Figures 4A,B**). The complementation of Δ*MoPTEN* with either *MoPTEN* or synonymously mutated *MoPTEN-1* could reverse conidia production to the wild-type level, but Δ*MoPTEN*/*MoPTEN-2* could not (**Figures 4A,B**). The conidium germination rate of all strains including the wild type was similar at 6 h, although Δ*MoPTEN* and Δ*MoPTEN*/*MoPTEN-2* appeared to be slow in conidium germination at 2 h (57 ± 2.1%, 66 ± 3%) and 4 h (76 ± 3.1%, 84 ± 3.2%) (**Figure 4C**). In terms of appressorium formation, Δ*MoPTEN*/*MoPTEN* and Δ*MoPTEN*/*MoPTEN*-1 had the formation rate similar as the wild type did; but Δ*MoPTEN* and Δ*MoPTEN*/*MoPTEN-2* were severely affected when induced by artificial hydrophobic film (**Figure 4D**) or by onion epidermis surface (**Figure 4E**). These data suggest that *MoPTEN*, in the form of *MoPTEN-1* (the second intron cannot be spliced), is especially involved in fungal growth and development prior to plant infection.

MoPTEN-2 Is Important for Invasive Hyphal Growth in Rice Cells

In order to characterize the function of *MoPTEN* in pathogenic development, pathogenicity assays were carried out using conidia collected from the four created strains and the wild type. When intact susceptible rice seedlings were spray-inoculated, at 7 dpi, some acute expansive disease lesions were formed in rice leaves by the wild type and Δ*MoPTEN*/*MoPTEN*;

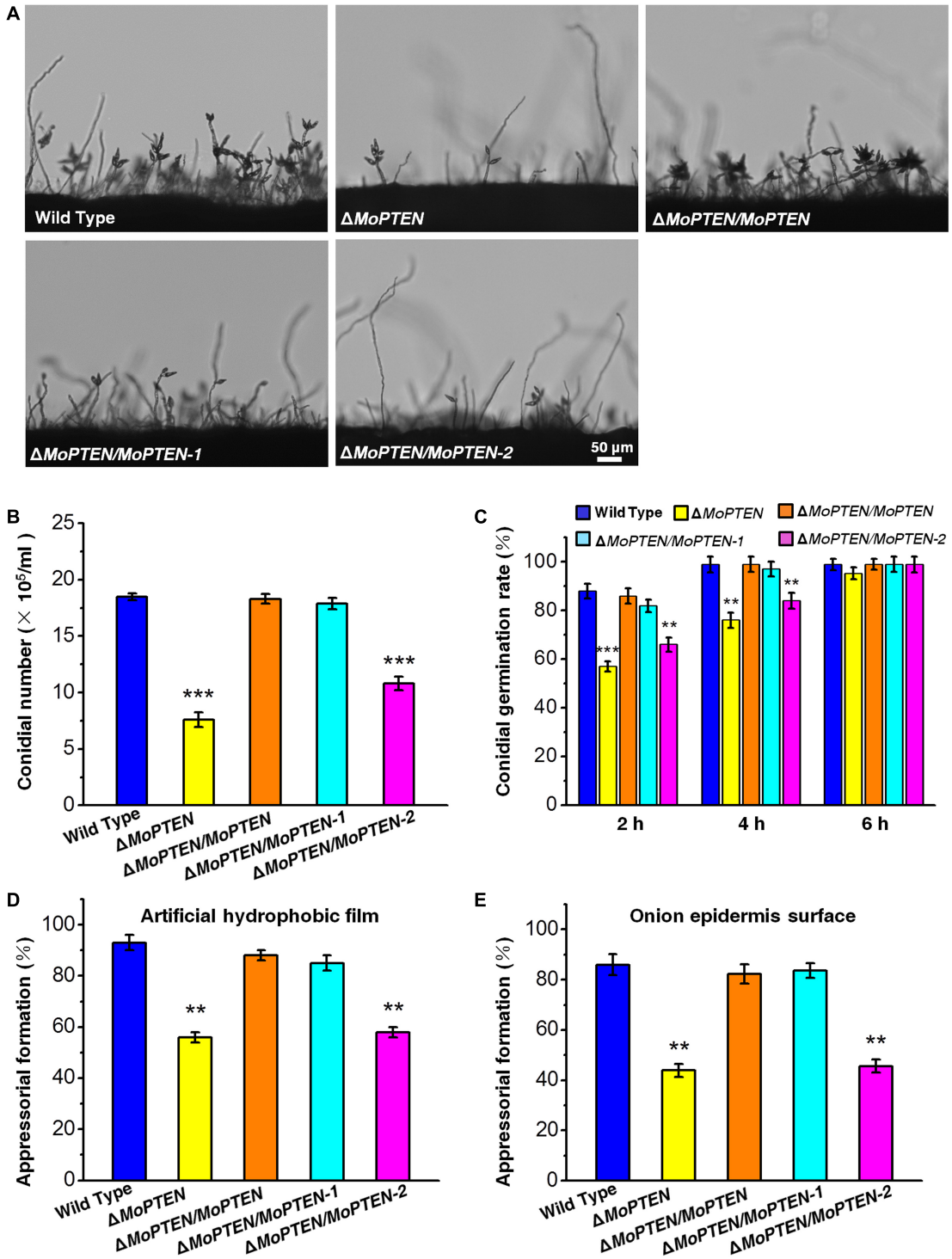

FIGURE 4 | Conidium and appressorium development analysis of the wild type and created strains. **(A)** Conidia formation on conidiophores. Conidia of the wild type and the four created strains (Δ*MoPTEN*, Δ*MoPTEN/MoPTEN*, Δ*MoPTEN/MoPTEN-1*, and Δ*MoPTEN/MoPTEN-2*) from 10-day-old OTA were transferred to cover slips, induced for 48 h, and observed and counted under a light microscope at room temperature. **(B)** Statistical analysis of conidial productivity. The conidia were harvested from the 10-day-old colonies grown on OTA media, and counted using a hemocytometer for all the 5 strains. **(C)** Conidial germination rate. Conidial germination was measured on a hydrophobic surface (plastic cover slips or gel-bond films) and onion epidermal cells and was calculated under the microscope at 2, 4, and 6 hpi. **(D**,**E)** Appressorial formation rate. Appressorial formation was measured on a hydrophobic cover slips and onion epidermis surface and was calculated under the microscope at 12 hpi. Error bars represent ± SD of three independent repeated samples. Two asterisks (**) represent an extremely significant difference at $0.001 < P < 0.01$, and three asterisks (***) represent an extremely significant differences at $P < 0.001$. Scale bar = 50 μm.

but no expansive but restricted lesions were formed in rice leaves by the Δ*MoPTEN*, Δ*MoPTEN*/*MoPTEN-1* and Δ*MoPTEN*/*MoPTEN-2* strains (**Figure 5A**; **Supplementary Figure 6C**). Similarly, when drop-inoculation was assayed, only the wild type and Δ*MoPTEN*/*MoPTEN* strains still showed pathogenicity (**Figure 5B**). Interestingly, when abraded leaves were drop-inoculated, Δ*MoPTEN*/*MoPTEN-2* caused the similar size lesions as the wild type or Δ*MoPTEN*/*MoPTEN* did (**Figure 5C**), suggesting the Δ*MoPTEN*/*MoPTEN-2* is incompetent in rice penetration, but competent in invasive hyphal growth in rice cells.

Leaf sheath infection assays were performed to examine the infection effects of the *MoPTEN* and its splice variants in rice host. At 48 hpi, the majority of appressoria of the wild-type

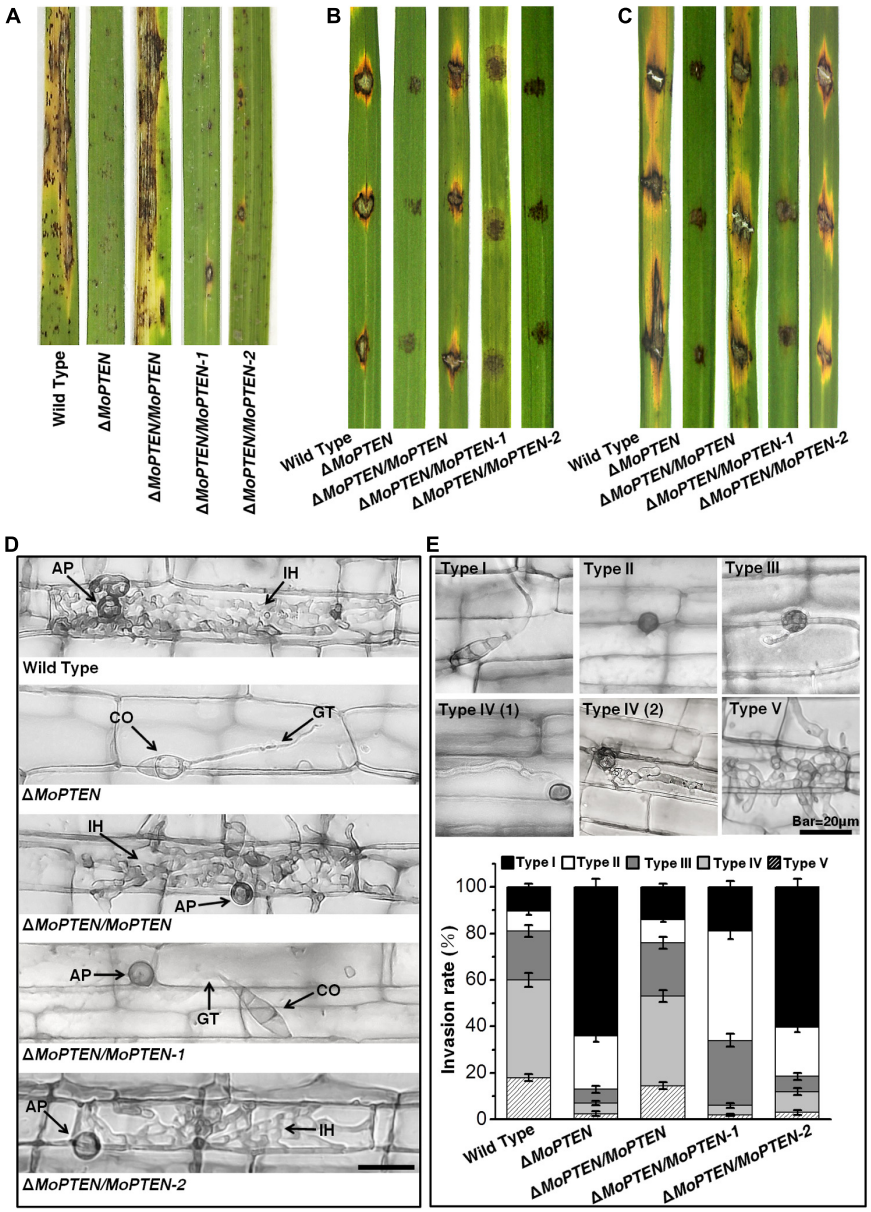

FIGURE 5 | Pathogenesis analysis of the wild type and created strains. **(A)** Spray-inoculation assay. Disease symptoms at 7 dpi of leaves by spraying with conidia (1×10^5/mL). **(B)** Drop-inoculation on unwounded leaves. Disease symptoms following the inoculation of rice leaves with 10-μL droplets of conidia (1×10^5/mL). Representative leaves were photographed at 7 dpi. **(C)** Drop-inoculation on abraded leaves. Disease symptoms following the inoculation of rice leaves with 10-μL droplets of conidia (1×10^5/mL). Representative leaves were photographed at 7 dpi. **(D)** Rice leaf sheath infection assay. The conidial suspension of indicated strains was dropped onto a rice sheath. Representative photographs of invasive hyphae were taken after 48 h of incubation at 25°C. Scale bar = 20 μm. IH, invasive hyphae; CO, conidium; GT, germ tube; AP, appressorium. **(E)** The infection rate was calculated according to the number of type I to type V events. The infection status of more than 100 germinated conidia per leaf sheath was scored at 48 hpi. The experiments were repeated three times and error bars represent ± SD of three independent repeated samples.

and Δ*MoPTEN*/*MoPTEN* invaded rice cells and formed invasive hyphae, but most of the mutant Δ*MoPTEN* did not due to its defect in appressorium formation (**Figure 5D**). Although Δ*MoPTEN*/*MoPTEN-1* was like the wild type in appressorium formation and the well-developed appressoria appeared to be able to penetrate rice cells, the primary invasive hyphal growth was restricted around infection site (**Figure 5D**). Although partial appressoria of Δ*MoPTEN*/*MoPTEN-2* were restricted in formation, the normally developed appressoria could then develop into invasive hyphae (**Figure 5D**).

To decipher the exact action of *MoPTEN* during pathogenic development, we defined the five types of invasive hyphae according to their developmental morphologies (type I, conidia with germ tube; type II, mature appressoria; type III, primary hyphae formed; type IV(1/2), invasive hyphae extended and branched in one cell; type V, invasive hyphae crossing to neighboring cells). Then we quantified the proportion of the five types of invasive hyphae based on 100 germinated conidia in the inoculated leaf sheath (**Figure 5E**). As a result, more than 80% of inoculated conidia from wild type (89.5 ± 4.4%), Δ*MoPTEN*/*MoPTEN* (86.0 ± 4.0%), and Δ*MoPTEN*/*MoPTEN-1* (81 ± 4.6%) formed mature appressoria, further indicating *MoPTEN-1* is responsible for appressorium development. Most appressoria of the wild type (60.0 ± 3.4%) and complementation strain Δ*MoPTEN*/*MoPTEN* (53.0 ± 2.9%) could form invasive hyphae of type IV and V, but this situation is only 6.0 ± 1.1% for Δ*MoPTEN*/*MoPTEN-1*. Of the germinated conidia in Δ*MoPTEN*/*MoPTEN-1*, 47.0 ± 3.5% did not form invasive hyphae after forming mature appressoria, and 28.0 ± 2.5% formed growth-restricted primary hyphae (type III), suggesting *MoPTEN-1* has little effect on the development of invasive hyphae. Similar to the mutant (64.0 ± 3.5%), most of the germinated conidia in Δ*MoPTEN*/*MoPTEN-2* (60.5 ± 3.1%) cannot form mature appressoria, however, the proportion of Δ*MoPTEN*/*MoPTEN-2* can form appressoria and continue to develop into invasive hyphae type IV and V has reached 12.0 ± 1.8%, which is about twice that of the mutant Δ*MoPTEN* (7.0 ± 1.4%) and Δ*MoPTEN*/*MoPTEN-1* (6.0 ± 1.1%) (**Figure 5E**), and these results also indicate the importance of *MoPTEN-2* for invasive hyphae growth in plant cells.

MoPTEN-2 Is Crucial for Scavenging Exogenous and Plant Endogenous H_2O_2

Mutant S28515 was sensitive to 2.5 mM exogenous H_2O_2 (**Figure 1A**), thus we predict *MoPTEN* is associated with resistance to H_2O_2. The four created strains and the wild type were cultivated on CM plates supplemented with H_2O_2. We found that the addition of 2.5 mM or 5.0 mM H_2O_2 to the growth media seriously inhibited the growth of the Δ*MoPTEN* and Δ*MoPTEN*/*MoPTEN-1* strains in comparison with the remained strains (**Figure 6A**), suggesting that *MoPTEN-2, not MoPTEN-1*, is able to rescue the defect of Δ*MoPTEN* in H_2O_2 resistance.

As rice plant accumulates more H_2O_2 during pathogen-rice interaction, and *MoPTEN-2* expression increases with pathogenic development of *M. oryzae*, we speculate that MoPTEN-2 is responsible for the clearance of host-derived H_2O_2 during infection. To test this, DAB staining was used to identify the endogenous ROS accumulated in the cells of rice leaf sheath infected by *M. oryzae* at 48 hpi (**Figure 6B**). In the leaf sheaths inoculated by the Δ*MoPTEN* and Δ*MoPTEN*/*MoPTEN-1* strains, more than 80 and 50% of the infected cells investigated were stained dark brown, respectively; in contrast, less than 25% of the infected cells were stained light brown or colorless as wild type, Δ*MoPTEN*/*MoPTEN* and Δ*MoPTEN*/*MoPTEN*-2 (**Figures 6B,C**), displaying loss of H_2O_2 scavenging function in Δ*MoPTEN* and Δ*MoPTEN*/*MoPTEN-1*. These results reveal that *MoPTEN-2* is crucial for scavenging exogenous and plant-derived H_2O_2.

In order to further verify whether the restricted development of the invasive hyphae of the mutant is related to the inability to scavenge the H_2O_2 produced by host cells, we used NADPH oxidase inhibitor DPI to treat conidia before infecting leaf sheaths. After incubation at 25°C for 48 h, the infected rice leaf sheath cells were observed through an optical microscope. Without treatment of DPI, the growth and development of the invasive hyphae of Δ*MoPTEN* and Δ*MoPTEN*/*MoPTEN-1* was restricted, and granular deposits could be observed in the infected cells, while those of wild type, Δ*MoPTEN*/*MoPTEN* and Δ*MoPTEN*/*MoPTEN-2* could grow normally and extend to adjacent cells (**Figure 6D**). After inhibiting the production of ROS in host cells with DPI, the invasive hyphae of Δ*MoPTEN* and Δ*MoPTEN*/*MoPTEN-1* could also grow normally and extend to neighboring cells. Meanwhile the granular deposits in Δ*MoPTEN* and Δ*MoPTEN*/*MoPTEN-1*-infected rice cells decreased (**Figure 6D**). This result also proved that the *MoPTEN*, in the form of *MoPTEN-2*, participates in the process of removing host-generated ROS, and this may also be an important reason for the decreased virulence and the restriction of the growth and development of invasive hyphae.

DISCUSSION

PTEN has been extensively studied in humans and mammals (Malaney et al., 2017). To suppress tumor effectively, PTEN must be expressed in a normal level and pattern (Abou Faycal et al., 2016; Malaney et al., 2017). However, PTEN and its homologs are often regulated by alternative splicing and formed aberrant variants (Agrawal and Eng, 2006; Sarquis et al., 2006; David and Manley, 2010). Different from the human PTEN, fungal homologs play roles in sporulation and pathogenesis (Di Stasio et al., 2009; Zhang et al., 2010; Vijayakrishnapillai et al., 2018), but the relationships between the fungal PTEN and alternative splicing are largely unknown. In this research, we identified a filamentous fungal homolog of PTEN in a model phytopathogen *M. oryzae*. The *MoPTEN* was associated with H_2O_2 resistance and pathogenicity in the blast fungus. Alternative splicing occurred in the second intron results in the intron retained form MoPTEN-1 and spliced an isoform MoPTEN-2.

Generally, PTEN and its homologous proteins contain the conserved N-terminal PTP catalytic domain (Haynie and Xue, 2015). Amino acid sequence analysis reveals that *MoPTEN* is closely associated with the filamentous fungal homologs of *PTEN*,

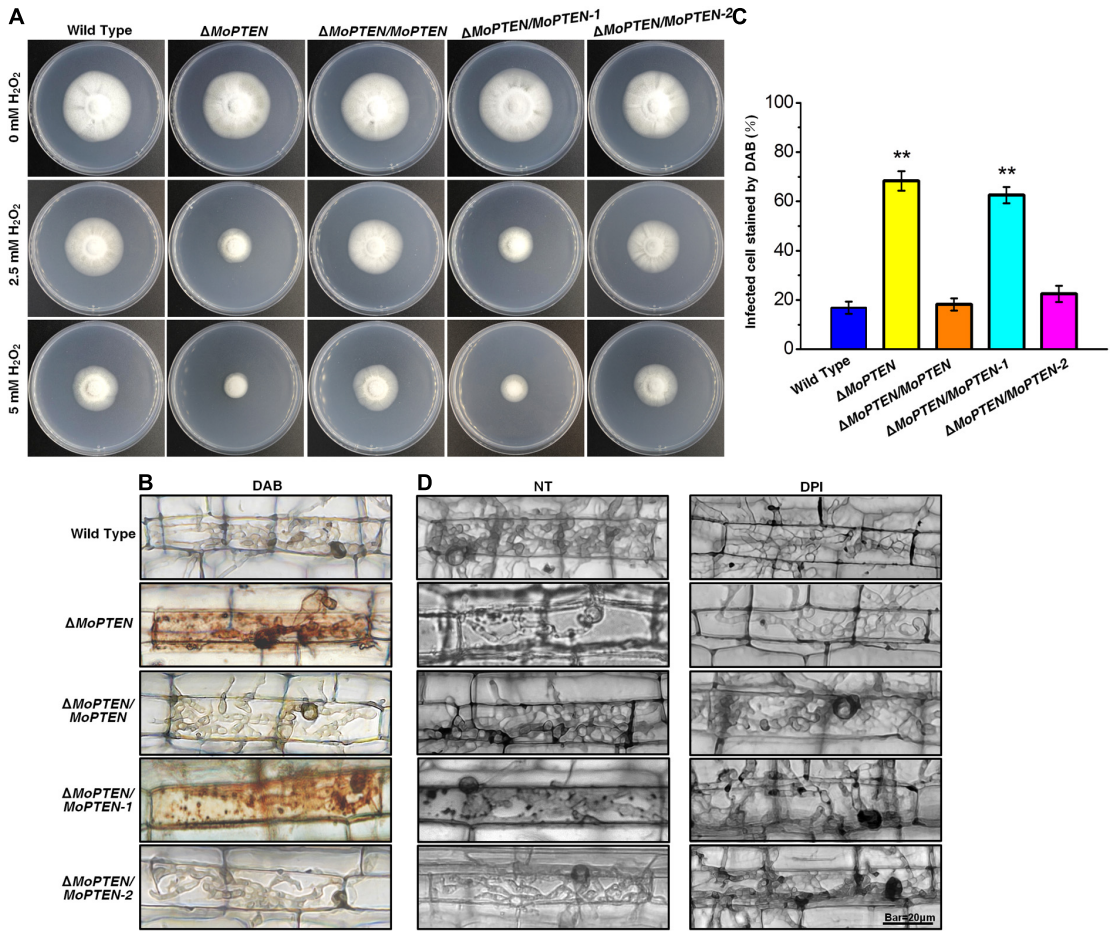

FIGURE 6 | H_2O_2 stress assay, DAB staining and DPI treatment of the wild type and created strains. **(A)** Mycelium growth assay. The five strains indicated were cultured on CM supplemented with or without 2.5 mM or 5 mM H_2O_2 for 7 days. **(B)** The 3,3′-diaminobenzidine (DAB) staining of leaf sheath cells of rice infected by wild type, mutant and complementation strains at 48 hpi. **(C)** Statistical analysis of DAB staining of leaf sheath cells infected by different strains. **(D)** Rice leaf sheaths were inoculated with conidial suspension (1×10^5 conidia/mL) of wild type, mutant and complementation strains after treatment without (NT) or with 0.4 μM diphenyleneiodonium (DPI) at 48 hpi. The experiments were repeated three times and error bars represent the ± SD of three independent repeated samples for each strain. Two asterisks (**) represent an extremely significant difference at $0.001 < P < 0.01$. Scale bar = 20 μm.

such as *FgTEP1* (**Figure 1E**; **Supplementary Figure 4B**). As a lipid and protein phosphatase, PTEN is a non-redundant negative regulator of the PI3K/AKT pathway. Therefore, yeast cells deleted for *TEP1/PTEN* are resistant to the PI3K inhibitor wortmannin (Heymont et al., 2000). The *MoPTEN* could functionally rescue the defective phenotype of the *TEP1/PTEN* deletion strains of yeast, confirming that *MoPTEN* has the basic biological functions of *PTEN* that depends on the lipid phosphatase activity. On the other hand, MoPTEN lacks of several conserved domains, such as PDZ and PEST in the Carboxyl-terminal of PTEN (**Supplementary Figure 4A**) although MoPTEN has the similar pocket-shaped structure to human PTEN (**Supplementary Figure 5B**). In addition, the retention or exclusion of the second intron sequence (84 nt) caused the changes of metal ion binding sites (**Supplementary Figure 5B**), suggesting that MoPTEN is a distinctive homolog of PTEN.

More alternative splicing cases occurred in PTEN and homologs have been reported in humans (Agrawal and Eng, 2006; Sarquis et al., 2006; David and Manley, 2010; Malaney et al., 2017), suggesting the human PTEN is more susceptible to alternative splicing; but *PTEN* alternative splicing has never been described in fungi before this research. For the first time we discovered a case of alternative splicing occurred in *PTEN* gene in *M. oryzae* (**Figures 3A,B**; **Supplementary Figure 5A**). In addition, both splice variants were expressed in a relay manner: the previously deduced *MoPTEN-1*, with the second intron retained, was expressed mainly in conidia and appressoria (fungal development pre-plant infection); and the spliced form *MoPTEN-2* was expressed mainly in growing invasive hyphae (fungal development post-plant infection) (**Figure 7**).

Although PTEN contains the dual specificity lipid and protein phosphatase catalytic domain, the most extensively studied tumor-suppressive function of PTEN is its lipid phosphatase activity (Ramaswamy et al., 1999). Both MoPTEN-1 and MoPTEN-2 have the same lipid and protein phosphatase

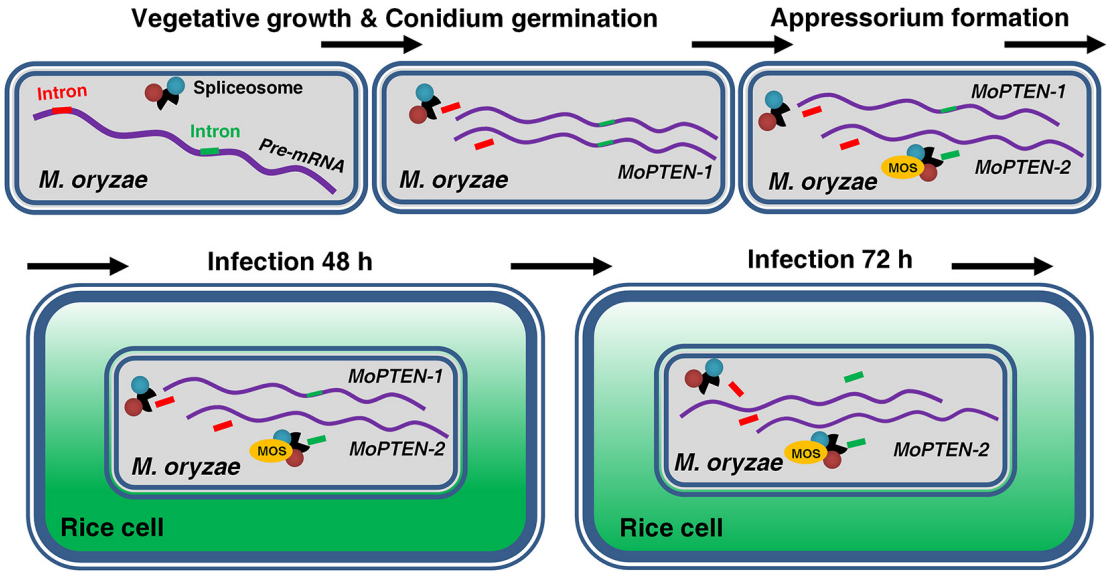

FIGURE 7 | Alternative splicing of *MoPTEN*. *MoPTEN* alternative splicing variants were formed in a phased manner, which, respectively, played a phased role. *MoPTEN-1*, with the second intron retained, was expressed mainly in conidia and appressoria, and the spliced form *MoPTEN-2* was expressed mainly in growing invasive hyphae.

catalytic domain (**Figures 1D,E**); however, they are different in the catalytic substrates: MoPTEN-1 preferred to catalyze lipid substrates but MoPTEN-2 preferred to catalyze phosphorylated proteins (**Figures 3D,E**). The addition of exogenous H_2O_2 or the intracellular production of this metabolite in response to certain stressors affects the activities of phosphatases (Finkel, 1998). Exposure of purified PTEN or of cells to H_2O_2 resulted in inactivation of PTEN (Lee et al., 2002; Kwon et al., 2004). Therefore, we analyzed the activities of both MoPTEN-1/2 proteins in response to H_2O_2 treatment. The activity of MoPTEN-2 was not affected significantly, but MoPTEN-1 was inhibited by up to 80% when treated using 0.4 mM H_2O_2 (**Supplementary Figure 7**), indicating that MoPTEN-2 is more stable than MoPTEN-1 and crucial under H_2O_2 stress derived in pathogen-host interaction.

As a second messenger, PIP3 is involved in multiple physiological processes in many eukaryotic cells (Falasca and Maffucci, 2009). In *Phytophthora* pathogens, PIP3 is required for full virulence (Lu et al., 2013), and mediates the entry of eukaryotic pathogen effectors into plant and animal host cells (Kale et al., 2010). PTEN dephosphorylates the secondary messenger PIP3 to PIP2, and then regulates cell proliferation, differentiation, and survival by blocking the PI3K/AKT pathway (Gil et al., 1999; Huang et al., 1999; Solari et al., 2005; Serezani et al., 2012; Liu and Chin-Sang, 2015). Therefore, it seems that the dephosphorylation activity of PTEN should be detrimental to oomycete pathogenesis due to the shift of PIP3 to PIP2. However, in this study, MoPTEN-1, with high lipid phosphatase activity, were expressed in high levels during conidium and appressorium development, implying MoPTEN-1 promotes plant infection. Considering the differences between *Ascomycetes* and *Oomycetes*, it raises a possibility that *M. oryzae* probably adopts a different pathogenic pathway from *Phytophthora* species, in which MoPTEN-1 is responsible for the balance of PIP3 and PIP2, and then suitable for plant infection. Introns are mediators of cell response to starvation (Parenteau et al., 2019), MoPTEN-1 may be involved in second metabolic regulation, especially the synthesis of melanin (**Supplementary Figure 8A**) due to the intron retention, for we know melanin is one of the most important factors for appressoria differentiation and infection (Kawamura et al., 1997; Manfiolli et al., 2019; Harata et al., 2020). In this research we found that MoPTEN-1 could rescue the defect of Δ*MoPTEN* in melanin production (**Supplementary Figure 8A**); and actually, several melanin synthesis related genes were upregulated in Δ*MoPTEN/MoPTEN-1* (**Supplementary Figure 8B**).

In plant fungal pathogens, reversible protein phosphorylation by protein kinase, such as the central factors of MAP kinase (MAPK), calcium, and cAMP signaling pathways, is a major mechanism for the regulation of pathogenic development (Lee et al., 2003; Zhao et al., 2007; Nguyen et al., 2008; Manfiolli et al., 2019). Quantitative evidence indicates that PTPs are also key regulators in pathogenic signaling transduction (Lee and Levin, 2018; Liu and Levin, 2018). The dual specificity MAPK phosphatase, Rok1, is involved in mating, filamentation, appressorium formation and subsequent disease development by regulating the activities of Kpp2 and Kpp6 in *Ustilago maydis* (Di Stasio et al., 2009). In another case, loss of *FgTEP1* reduces pathogenicity in *Fusarium graminearum* (Zhang et al., 2010). Recently, the requirement of *TEP1/PTEN* homolog has also been shown in virulence of *U. maydis* and *Colletotrichum graminicola* (Vijayakrishnapillai et al., 2018; Wang et al., 2021). Consistently, deletion of the *MoPTEN* gene caused reduced pathogenicity in *M. oryzae* (**Figures 5A,B**). Individual splice

variants of *MoPTEN* could not rescue the defect of virulence in Δ*MoPTEN* (**Figures 5A,B**) although MoPTEN-2 contains protein phosphatase activity (**Figure 3E**). However, when the wounded leaves were used for inoculation, Δ*MoPTEN/MoPTEN-2* virulence was restored, reflecting its defect in plant penetration (**Figure 5C**). Once the pathogen entering plant cells, partial intracellular hyphae enable grow and extend in host cells (**Figures 5C,D,E**).

Protein phosphatase activity of MoPTEN-2 is stable to H_2O_2 treatment (**Supplementary Figure 7**). Δ*MoPTEN/MoPTEN-2*, like the wild type or complementation strain Δ*MoPTEN/MoPTEN*, was resistant to H_2O_2 (**Figure 6A**). Therefore, we propose that the stable *MoPTEN-2* is also capable of scavenging host-derived ROS. Indeed, in Δ*MoPTEN/MoPTEN-2* infected rice cells, DAB staining signals were hard to be detected, but strong in Δ*MoPTEN* and Δ*MoPTEN/MoPTEN-1* (**Figures 6B,C**). In Δ*MoPTEN* and Δ*MoPTEN/MoPTEN-1* strains, several selected degradation genes of H_2O_2 were significantly downregulated, but Δ*MoPTEN/MoPTEN-2* maintained a level as high as the wild type or Δ*MoPTEN/MoPTEN* (**Supplementary Figure 9**). In addition, after being treated by DPI, the invasive hyphae of Δ*MoPTEN* and Δ*MoPTEN*/*MoPTEN-1*, which are restricted in growth and development without treatment of DPI, can grow normally (**Figure 6D**). The above results suggest that *MoPTEN-2* is realted in regulation of ROS degradation.

The pathogenic process of the rice blast fungus can be divided into two phases: pre-plant and post-plant infection, while the later also includes biotrophic growth and necrotrophic growth. Conidium and appressorium formation occurs outside plant cells, and invasive hyphae extension occurs inside host (Talbot, 2003; Kankanala et al., 2007). For a successful infection cycle, *MoPTEN-1* and *MoPTEN-2* served pathogenic development of *M. oryzae* in a relay model (**Figure 7**). According to our research results, it can be seen that *MoPTEN-1* mainly regulates the conidial formation and development of appressorium of *M. oryzae*, while *MoPTEN-2* plays a dominant role in the development and extension of invasive hyphae. Therefore, we analyzed that the occurrence of alternative splicing of *MoPTEN* may be affected by some factors in the post-plant infection process. For example, after infecting host cells, Δ*MoPTEN*/*MoPTEN-1*, similar to mutant Δ*MoPTEN*, could not effectively scavenge H_2O_2 produced by host cells, while Δ*MoPTEN*/*MoPTEN-2* could eliminate H_2O_2 as well as wild type and Δ*MoPTEN*/*MoPTEN* strains (**Figures 6B,C**). Therefore, ROS produced by plant defense response during pathogen infection may be one of the inducements for alternative splicing of *MoPTEN*. In addition, the alternative splicing process of *MoPTEN* may also be regulated by some other genes in *M. oryzae*. Many studies reported that the survival motor neuron (SMN) protein undergoes alternative splicing, and through which it is involved in cellular activities (Liang et al., 2015). On the other hand, SMN functions in the cytoplasmic assembly of Sm-class snRNPs, core particles of the spliceosome (Pellizzoni et al., 2002; Li et al., 2014; Matera and Wang, 2014), exhibiting a role in regulating pre-mRNA alternative splicing. Reduced levels of SMN protein result in a common neuromuscular disorder (SMA) in humans (Lefebvre et al., 1995; Schrank et al., 1997). In fungi, a SMN homolog is associated with pathogenesis in the disease development of rice blast; particularly, the *SMN/MOS* deletion strains of *M. oryzae* shows similar defects to Δ*MoPTEN* in many aspects, such as fewer sporulation, sensitivity to H_2O_2 and reduced pathogenicity (Liang et al., 2015). And because PTEN can interact with the spliceosomal proteins and drive pre-mRNA splicing (Song et al., 2011; Shen et al., 2018), we assume there exists a regulative relationship between MoPTEN and SMN/MOS (**Figure 7**). Indeed, in the previous research, we found that *MoPTEN* is regulated by *SMN/MOS* through transcriptome sequencing, and we have obtained some research results that the expression of *MoPTEN* in Δ*MOS* is down-regulated from that in Δ*MOS/MOS* (data not shown). The splicing process is carried out by the large spliceosome complex consisting of RNA and proteins (Wahl et al., 2009; Shen et al., 2018). The precise regulation of *MoPTEN* alternative splicing should require more factors than *SMN*, by exploring which we will decipher the regulatory mechanism.

DATA AVAILABILITY STATEMENT

The original contributions presented in the study are included in the article/**Supplementary Material**, further inquiries can be directed to the corresponding author/s.

AUTHOR CONTRIBUTIONS

S-HZ and YW designed the research. SW performed the research. HL, YD, and PZ assisted in part of the experimental process. SW, GL, and S-HZ analyzed the data. S-HZ and SW wrote the manuscript. All authors contributed to the article and approved the submitted version.

FUNDING

This research was funded by the National Natural Science Foundation of China (Grant Nos. 31670141 to YW and 31671972 to S-HZ) and the Ministry of Science and Technology of China (Grant No. 2016YFD0300703 to S-HZ).

ACKNOWLEDGMENTS

We thank Liang Yue for helpful advice on this manuscript, and Hongkai Wang and Jianping Lu for providing the pKD7-Red vector. We wish to thank the reviewers for their valuable comments.

SUPPLEMENTARY MATERIAL

The Supplementary Material for this article can be found online at: https://www.frontiersin.org/articles/10.3389/fmicb.2021.715773/full#supplementary-material

REFERENCES

Abou Faycal, C., Gazzeri, S., and Eymin, B. (2016). RNA splicing, cell signaling, and response to therapies. *Curr. Opin. Oncol.* 28, 58–64. doi: 10.1097/CCO.0000000000000254

Agrawal, S., and Eng, C. (2006). Differential expression of novel naturally occurring splice variants of PTEN and their functional consequences in Cowden syndrome and sporadic breast cancer. *Hum. Mol. Genet.* 15, 777–787. doi: 10.1093/hmg/ddi492

Andersen, J. N., Mortensen, O. H., Peters, G. H., Drake, P. G., Iversen, L. F., Olsen, O. H., et al. (2001). Structural and evolutionary relationships among protein tyrosine phosphatase domains. *Mol. Cell. Biol.* 21, 7117–7136.

Bauman, A. L., and Scott, J. D. (2002). Kinase- and phosphatase-anchoring proteins: harnessing the dynamic duo. *Nat. Cell Biol.* 4, E203–E206. doi: 10.1038/ncb0802-e203

Bertram, G., Swoboda, R. K., Gooday, G. W., Gow, N. A., and Brown, A. J. (1996). Structure and regulation of the *Candida albicans ADH1* gene encoding an immunogenic alcohol dehydrogenase. *Yeast* 12, 115–127. doi: 10.1002/(sici)1097-0061(199602)12:2<115::aid-yea889<3.0.co;2-e

Cui, X., Wei, Y., Wang, Y. H., Li, J., Wong, F. L., Zheng, Y. J., et al. (2015). Proteins interacting with mitochondrial ATP-dependent Lon protease (MAP1) in *Magnaporthe oryzae* are involved in rice blast disease. *Mol. Plant Pathol.* 16, 847–859. doi: 10.1111/mpp.12242

David, C. J., and Manley, J. L. (2010). Alternative pre-mRNA splicing regulation in cancer: pathways and programs unhinged. *Genes Dev.* 24, 2343–2364. doi: 10.1101/gad.1973010

Di Stasio, M., Brefort, T., Mendoza-Mendoza, A., Münch, K., and Kahmann, R. (2009). The dual specificity phosphatase Rok1 negatively regulates mating and pathogenicity in *Ustilago maydis*. *Mol. Microbiol.* 73, 73–88. doi: 10.1111/j.1365-2958.2009.06747.x

Ding, S. L., Liu, W. D., Iliuk, A., Ribot, C., Vallet, J., Tao, A., et al. (2010). The Tig1 Histone Deacetylase Complex Regulates Infectious Growth in the Rice Blast Fungus *Magnaporthe oryzae*. *Plant Cell* 22, 2495–2508. doi: 10.1105/tpc.110.074302

Du, Y. X., Shi, Y., Yang, J., Chen, X. L., Xue, M. F., Zhou, W., et al. (2013). A serine/threonine-protein phosphatase PP2A catalytic subunit is essential for asexual development and plant infection in *Magnaporthe oryzae*. *Curr. Genet.* 59, 33–41. doi: 10.1007/s00294-012-0385-3

Falasca, M., and Maffucci, T. (2009). Rethinking phosphatidylinositol 3-monophosphate. *Biochim. Et. Biophys. Acta Mol. Cell Res.* 1793, 1795–1803. doi: 10.1016/j.bbamcr.2009.10.003

Fernandez, J., Marroquin-Guzman, M., Nandakumar, R., Shijo, S., Cornwell, K. M., Li, G., et al. (2014). Plant defence suppression is mediated by a fungal sirtuin during rice infection by *Magnaporthe oryzae*. *Mol. Microbiol.* 94, 70–88. doi: 10.1111/mmi.12743

Finkel, T. (1998). Oxygen radicals and signaling. *Cur.r Opin. Cell Biol.* 10, 248–253. doi: 10.1016/s0955-0674(98)80147-6

Franck, W. L., Gokce, E., Randall, S. M., Oh, Y., Eyre, A., Muddiman, D. C., et al. (2015). Phosphoproteome analysis links protein phosphorylation to cellular remodeling and metabolic adaptation during *Magnaporthe oryzae* appressorium development. *J. Proteome Res.* 14:2408–2424. doi: 10.1021/pr501064q

Gil, E. B., Link, E. M., Liu, L. X., Johnson, C. D., and Lees, J. A. (1999). Regulation of the insulin-like developmental pathway of *Caenorhabditis elegans* by a homolog of the *PTEN* tumor suppressor gene. *Proc. Natl. Acad. Sci. U.S.A.* 96, 2925–2930.

Harata, K., Daimon, H., and Okuno, T. (2020). Trade-off relation between fungicide sensitivity and melanin biosynthesis in plant pathogenic fungi. *iScience* 23:101660. doi: 10.1016/j.isci.2020.101660

Haynie, D. T., and Xue, B. (2015). Superdomains in the protein structure hierarchy: the case of PTP-C2. *Protein Sci.* 24, 874–882. doi: 10.1002/pro.2664

Heath, M. C., Valent, B., Howard, R. J., and Chumley, F. G. (1990). Interactions of two strains of *Magnaporthe grisea* with rice, goosegrass, and weeping lovegrass. *Can. J. Bot.* 68, 1627–1637. doi: 10.1139/b90-209

Heymont, J., Berenfeld, L., Collins, J., Kaganovich, A., Maynes, B., Moulin, A., et al. (2000). *TEP1*, the yeast homolog of the human tumor suppressor gene PTEN/MMAC1/TEP1, is linked to the phosphatidylinositol pathway and plays a role in the developmental process of sporulation. *Proc. Nat. Acad. Sci. U.S.A.* 97, 12672–12677. doi: 10.1073/pnas.97.23.12672

Howard, R. J., Ferrari, M. A., Roach, D. H., and Money, N. P. (1991). Penetration of hard substrates by a fungus employing enormous turgor pressures. *Proc. Natl. Acad. Sci. U.S.A* 88, 11281–11284. doi: 10.1073/pnas.88.24.11281

Huang, H., Potter, C. J., Tao, W. F., Li, D. M., Brogiolo, W., Hafen, E., et al. (1999). PTEN affects cell size, cell proliferation and apoptosis during *Drosophila* eye development. *Development* 126:5365–5372.

Kale, S. D., Gu, B. A., Capelluto, D. G. S., Dou, D. L., Feldman, E., Rumore, A., et al. (2010). External lipid PI3P mediates entry of eukaryotic pathogen effectors into plant and animal host cells. *Cell* 142, 284–295. doi: 10.1016/j.cell.2010.06.008

Kankanala, P., Czymmek, K., and Valent, B. (2007). Roles for rice membrane dynamics and plasmodesmata during biotrophic invasion by the blast fungus. *Plant Cell* 19, 706–724. doi: 10.1105/tpc.106.046300

Kawamura, C., Moriwaki, J., Kimura, N., Fujita, Y., Fuji, S., Hirano, T., et al. (1997). The melanin biosynthesis genes of *Alternaria alternata* can restore pathogenicity of the melanin-deficient mutants of *Magnaporthe grisea*. *Mol. Plant Microbe. Interact.* 10, 446–453. doi: 10.1094/MPMI.1997.10.4.446

Khan, I. A., Wang, Y., Li, H. J., Lu, J. P., Liu, X. H., and Lin, F. C. (2014). Disruption and molecular characterization of calpains-related (*MoCAPN1*, *MoCAPN3* and *MoCAPN4*) genes in *Magnaporthe oryzae*. *Microbiol. Res.* 169, 844–854. doi: 10.1016/j.micres.2014.03.003

Koga, H., Dohi, K., Nakayachi, O., and Mori, M. (2004). A novel inoculation method of *Magnaporthe grisea* for cytological observation of the infection process using intact leaf sheaths of rice plants. *Physiol. Mol. Plant Pathol.* 64, 67–72. doi: 10.1016/j.pmpp.2004.07.002

Kwon, J., Lee, S. R., Yang, K. S., Ahn, Y., Kim, Y. J., Stadtman, E. R., et al. (2004). Reversible oxidation and inactivation of the tumor suppressor PTEN in cells stimulated with peptide growth factors. *Proc. Natl. Acad. Sci. U.S.A* 101, 16419–16424. doi: 10.1073/pnas.0407396101

Lee, J., and Levin, D. E. (2018). Intracellular mechanism by which arsenite activates the yeast stress MAPK Hog1. *Mol. Biol. Cell* 29, 1904–1915. doi: 10.1091/mbc.E18-03-0185

Lee, J. O., Yang, H. J., Georgescu, M. M., Di Cristofano, A., Maehama, T., Shi, Y. G., et al. (1999). Crystal structure of the PTEN tumor suppressor: implications for its phosphoinositide phosphatase activity and membrane association. *Cell* 99, 323–334. doi: 10.1016/S0092-8674(00)81663-3

Lee, N., D'Souza, C. A., and Kronstad, J. W. (2003). Of smuts, blasts, mildews, and blights: cAMP signaling in phytopathogenic fungi. *Ann. Rev. Phytopathol.* 41, 399–427. doi: 10.1146/annurev.phyto.41.052002.095728

Lee, S. R., Yang, K. S., Kwon, J., Lee, C., Jeong, W., and Rhee, S. G. (2002). Reversible inactivation of the tumor suppressor PTEN by H2O2. *J. Biol. Chem.* 277, 20336–20342. doi: 10.1074/jbc.M111899200

Lefebvre, S., Bürglen, L., Reboullet, S., Clermont, O., Burlet, P., Viollet, L., et al. (1995). Identification and characterization of a spinal muscular atrophy-determining gene. *Cell* 80, 155–165. doi: 10.1016/0092-8674(95)90460-3

Li, D. K., Tisdale, S., Lotti, F., and Pellizzoni, L. (2014). SMN control of RNP assembly: from post-transcriptional gene regulation to motor neuron disease. *Semin. Cell Dev. Biol.* 32, 22–29. doi: 10.1016/j.semcdb.2014.04.026

Li, G., Qi, X. B., Sun, G. C., Rocha, R. O., Segal, L. M., Downey, K. S., et al. (2020). Terminating rice innate immunity induction requires a network of antagonistic and redox-responsive E3 ubiquitin ligases targeting a fungal sirtuin. *New Phytol.* 226, 523–540. doi: 10.1111/nph.16365

Li, G. T., Zhou, X. Y., and Xu, J. R. (2012). Genetic control of infection-related development in *Magnaporthe oryzae*. *Curr. Opin. Microbiol.* 15, 678–684. doi: 10.1016/j.mib.2012.09.004

Li, J., Liang, X. L., Wei, Y., Liu, J. L., Lin, F. C., and Zhang, S. H. (2015). An ATP-dependent protease homolog ensures basic standards of survival and pathogenicity for *Magnaporthe oryzae*. *Eur. J. Plant Pathol.* 141, 703–716. doi: 10.1007/s10658-014-0572-9

Li, J., Yen, C., Liaw, D., Podsypanina, K., Bose, S., Wang, S. I., et al. (1997a). PTEN, a putative protein tyrosine phosphatase gene mutated in human brain, breast, and prostate cancer. *Science* 275, 1943–1947. doi: 10.1126/science.275.5308.1943

Li, L. W., Ernsting, B. R., Wishart, M. J., Lohse, D. L., and Dixon, J. E. (1997b). A family of putative tumor suppressors is structurally and functionally conserved in humans and yeast. *J. Biol. Chem.* 272, 29403–29406. doi: 10.1074/jbc.272.47.29403

Li, Z. Q., Pei, X., Zhang, Z. Y., Wei, Y., Song, Y. Y., Chen, L. N., et al. (2018). The unique GH5 cellulase member in the extreme halotolerant fungus *Aspergillus glaucus* CCHA is an endoglucanase with multiple tolerance to salt, alkali and heat: prospects for straw degradation applications. *Extremophiles* 22, 675–685. doi: 10.1007/s00792-018-1028-5

Liang, H., He, S., Yang, J., Jia, X., Wang, P., Chen, X., et al. (2014). PTENα, a PTEN Isoform translated through alternative initiation, regulates mitochondrial function and energy metabolism. *Cell Metab.* 19, 836–848. doi: 10.1016/j.cmet.2014.03.023

Liang, X. L., Liu, J. L., Liu, S. S., Liang, X. N., and Zhang, S. H. (2015). Alternatively spliced *SMN* orthologue in *Magnaporthe oryzae* is required for stress resistance and disease development. *Eur. J. Plant Pathol.* 142, 427–439. doi: 10.1007/s10658-015-0623-x

Liu, J., and Chin-Sang, I. D. (2015). *C. elegans* as a model to study PTEN's regulation and function. *Methods* 7, 180–190. doi: 10.1016/j.ymeth.2014.12.009

Liu, L., and Levin, D. E. (2018). Intracellular mechanism by which genotoxic stress activates yeast SAPK Mpk1. *Mol. Biol. Cell* 29, 2898–2909. doi: 10.1091/mbc.E18-07-0441

Liu, X. Y., Yang, J., Qian, B., Cai, Y. C., Zou, X., Zhang, H. F., et al. (2018). MoYvh1 subverts rice defense through functions of ribosomal protein MoMrt4 in *Magnaporthe oryzae*. *PLoS Pathog.* 14:e1007016. doi: 10.1371/journal.ppat.1007016

Liu, Y. G., and Whittier, R. F. (1995). Thermal asymmetric interlaced PCR: automatable amplification and sequencing of insert end fragments from P1 and YAC clones for chromosome walking. *Genomics* 25, 674–681. doi: 10.1016/0888-7543(95)80010-J

Lu, S., Chen, L. L., Tao, K., Sun, N. N., Wu, Y. R., Lu, X. X., et al. (2013). Intracellular and Extracellular Phosphatidylinositol 3-Phosphate Produced by *Phytophthora* Species Is Important for Infection. *Mol. Plant* 6, 1592–1604. doi: 10.1093/mp/sst047

Malaney, P., Uversky, V. N., and Davé, V. (2017). PTEN proteoforms in biology and disease. *Cell. Mol. Life Sci.* 74, 2783–2794. doi: 10.1007/s00018-017-2500-6

Manfiolli, A. O., Siqueira, F. S., dos Reis, T. F., Van Dijck, P., Schrevens, S., Hoefgen, S., et al. (2019). Mitogen-activated protein kinase cross-talk interaction modulates the production of melanins in *Aspergillus fumigatus*. *mbio* 10, e00215–e00219. doi: 10.1128/mBio.00215-19

Marroquin-Guzman, M., Hartline, D., Wright, J. D., Elowsky, C., Bourret, T. J., and Wilson, R. A. (2017). The *Magnaporthe oryzae* nitrooxidative stress response suppresses rice innate immunity during blast disease. *Nat. Microbiol.* 2:17054. doi: 10.1038/nmicrobiol.2017.54

Marroquin-Guzman, M., and Wilson, R. A. (2015). GATA-dependent glutaminolysis drives appressorium formation in *Magnaporthe oryzae* by suppressing TOR inhibition of cAMP/PKA signaling. *PLoS Pathog.* 11:e1004851. doi: 10.1371/journal.ppat.1004851

Matera, A. G., and Wang, Z. F. (2014). A day in the life of the spliceosome. *Nat. Rev. Mol. Cell Biol.* 15, 108–121. doi: 10.1038/nrm3742

Moorhead, G. B. G., Trinkle-Mulcahy, L., and Ulke-Lemee, A. (2007). Emerging roles of nuclear protein phosphatases. *Nat. Rev. Mol. Cell Biol.* 8, 234–244. doi: 10.1038/nrm2126

Nguyen, Q. B., Kadotani, N., Kasahara, S., Tosa, Y., Mayama, S., and Nakayashiki, H. (2008). Systematic functional analysis of calcium-signalling proteins in the genome of the rice-blast fungus, *Magnaporthe oryzae*, using a high-throughput RNA-silencing system. *Mol. Microbiol.* 68, 1348–1365. doi: 10.1111/j.1365-2958.2008.06242.x

Pao, L. I., Badour, K., Siminovitch, K. A., and Neel, B. G. (2007). Nonreceptor protein-tyrosine phosphatases in immune cell signaling. *Ann. Rev. Immun.* 25, 473–523. doi: 10.1146/annurev.immunol.23.021704.115647

Parenteau, J., Maignon, L., Berthoumieux, M., Catala, M., Gagnon, V., and Abou Elela, S. (2019). Introns are mediators of cell response to starvation. *Nature* 565, 612–617. doi: 10.1038/s41586-018-0859-7

Pellizzoni, L., Yong, J., and Dreyfuss, G. (2002). Essential role for the SMN complex in the specificity of snRNP assembly. *Science* 298, 1775–1779. doi: 10.1126/science.1074962

Qian, B., Liu, X. Y., Jia, J., Cai, Y. C., Chen, C., Zhang, H. F., et al. (2018). MoPpe1 partners with MoSap1 to mediate TOR and cell wall integrity signalling in growth and pathogenicity of the rice blast fungus *Magnaporthe oryzae*. *Environ. Microbiol.* 20, 3964–3979. doi: 10.1111/1462-2920.14421

Rademacher, S., and Eickholt, B. J. (2019). PTEN in autism and neurodevelopmental disorders. *Cold Spring Harb. Perspect. Med.* 9:a036780. doi: 10.1101/cshperspect.a036780

Ramaswamy, S., Nakamura, N., Vazquez, F., Batt, D. B., Perera, S., Roberts, T. M., et al. (1999). Regulation of G1 progression by the PTEN tumor suppressor protein is linked to inhibition of the phosphatidylinositol 3-kinase/Akt pathway. *Proc. Natl. Acad. Sci. U.S.A* 96, 2110–2115. doi: 10.1073/pnas.96.5.2110

Salmena, L., Carracedo, A., and Pandolfi, P. P. (2008). Tenets of PTEN tumor suppression. *Cell* 133, 403–414. doi: 10.1016/j.cell.2008.04.013

Sarquis, M. S., Agrawal, S., Shen, L., Pilarski, R., Zhou, X. P., and Eng, C. (2006). Distinct expression profiles for *PTEN* transcript and its splice variants in Cowden syndrome and Bannayan-Riley-Ruvalcaba syndrome. *Am. J. Hum. Genet.* 79, 23–30.

Schrank, B., Götz, R., Gunnersen, J. M., Ure, J. M., Toyka, K. V., Smith, A. G., et al. (1997). Inactivation of the survival motor neuron gene, a candidate gene for human spinal muscular atrophy, leads to massive cell death in early mouse embryos. *Proc. Natl. Acad. Sci. U.S.A* 94, 9920–9925. doi: 10.1073/pnas.94.18.9920

Serezani, C. H., Kane, S., Medeiros, A. I., Cornett, A. M., Kim, S. H., Marques, M. M., et al. (2012). PTEN directly activates the actin depolymerization factor cofilin-1 during PGE2-mediated inhibition of phagocytosis of fungi. *Sci. Signal.* 5:ra12. doi: 10.1126/scisignal.2002448

Sharrard, R. M., and Maitland, N. J. (2000). Alternative splicing of the human PTEN/MMAC1/TEP1 gene. *Biochim. Biophys. Acta* 1494, 282–285.

Shen, S. M., Ji, Y., Zhang, C., Dong, S. S., Yang, S., Xiong, Z., et al. (2018). Nuclear PTEN safeguards pre-mRNA splicing to link Golgi apparatus for its tumor suppressive role. *Nature Communications* 9, 2392. doi: 10.1038/s41467-018-04760-1

Shi, Y. G. (2009). Serine/threonine phosphatases: mechanism through structure. *Cell* 139, 468–484. doi: 10.1016/j.cell.2009.10.006

Shi, Y. J., Wang, J. R., Chandarlapaty, S., Cross, J., Thompson, C., Rosen, N., et al. (2014). PTEN is a protein tyrosine phosphatase for IRS1. *Nat. Struct. Mol. Biol.* 21, 522–527. doi: 10.1038/nsmb.2828

Shinde, S. R., and Maddika, S. (2016). PTEN modulates EGFR late endocytic trafficking and degradation by dephosphorylating Rab7. *Nat. Commun.* 7:10689. doi: 10.1038/ncomms10689

Solari, F., Bourbon-Piffaut, A., Masse, I., Payrastre, B., Chan, A. M. L., and Billaud, M. (2005). The human tumour suppressor PTEN regulates longevity and dauer formation in *Caenorhabditis elegans*. *Oncogene* 24, 20–27. doi: 10.1038/sj.onc.1207978

Song, M. S., Carracedo, A., Salmena, L., Song, S. J., Egia, A., Malumbres, M., et al. (2011). Nuclear PTEN regulates the APC-CDH1 tumor-suppressive complex in a phosphatase-independent manner. *Cell* 144, 187–199. doi: 10.1016/j.cell.2010.12.020

Steck, P. A., Pershouse, M. A., Jasser, S. A., Yung, W. K., Lin, H., Ligon, A. H., et al. (1997). Identification of a candidate tumour suppressor gene, *MMAC1*, at chromosome 10q23.3 that is mutated in multiple advanced cancers. *Nat. Genet.* 15, 356–362. doi: 10.1038/ng0497-356

Sun, G. C., Elowsky, C., Li, G., and Wilson, R. A. (2018). TOR-autophagy branch signaling via Imp1 dictates plant-microbe biotrophic interface longevity. *PLoS Genet.* 14:e1007814. doi: 10.1371/journal.pgen.1007814

Suryanarayanan, T. S., Ravishankar, J. P., Venkatesan, G., and Murali, T. S. (2004). Characterization of the melanin pigment of a cosmopolitan fungal endophyte. *Mycol. Res.* 108, 974–978. doi: 10.1017/S0953756204000619

Talbot, N. J. (2003). On the trail of a cereal killer: exploring the biology of *Magnaporthe grisea*. *Annu. Rev. Microbiol.* 57, 177–202. doi: 10.1146/annurev.micro.57.030502.090957

Vijayakrishnapillai, L. M. K., Desmarais, J. S., Groeschen, M. N., and Perlin, M. H. (2018). Deletion of *ptn1*, a *PTEN/TEP1* orthologue, in *Ustilago maydis* reduces pathogenicity and teliospore development. *J. Fungi (Basel)* 5:1. doi: 10.3390/jof5010001

Wahl, M. C., Will, C. L., and Luhrmann, R. (2009). The spliceosome: design principles of a dynamic RNP machine. *Cell* 136, 701–718. doi: 10.1016/j.cell.2009.02.009

Wang, S. W., Li, G. H., Wei, Y., Wang, G., Dang, Y. J., Zhang, P. H., et al. (2021). Involvement of the mitochondrial protein tyrosine phosphatase PTPM1 in the

promotion of conidiation, development, and pathogenicity in *Colletotrichum graminicola*. *Front. Microbiol.* 11:605738. doi: 10.3389/fmicb.2020.605738

Zhang, D. J., Fan, F. Y., Yang, J. R., Wang, X. L., Qiu, D. W., and Jiang, L. H. (2010). FgTep1p is linked to the phosphatidylinositol-3 kinase signalling pathway and plays a role in the virulence of *Fusarium graminearum* on wheat. *Mol. Plant Pathol.* 11, 495–502. doi: 10.1111/J.1364-3703.2010.00626.X

Zhao, X. H., Mehrabi, R., and Xu, J. R. (2007). Mitogen-activated protein kinase pathways and fungal pathogenesis. *Eukaryot. Cell* 6, 1701–1714. doi: 10.1128/Ec.00216-07

Zolnierowicz, S., and Bollen, M. (2000). Protein phosphorylation and protein phosphatases. De Panne, Belgium, September 19-24, 1999. *EMBO J.* 19, 483–488. doi: 10.1093/emboj/19.4.483

Conflict of Interest: The authors declare that the research was conducted in the absence of any commercial or financial relationships that could be construed as a potential conflict of interest.

frontiers in Microbiology

ORIGINAL RESEARCH
published: 19 July 2021
doi: 10.3389/fmicb.2021.684888

Efficacy of Plant Growth-Promoting Bacteria *Bacillus cereus* YN917 for Biocontrol of Rice Blast

Hu Zhou[1,2,3†], Zuo-hua Ren[1,2†], Xue Zu[1], Xi-yue Yu[1], Hua-jun Zhu[1], Xiao-juan Li[4], Jie Zhong[1] and Er-ming Liu[1,2,3]*

[1] College of Plant Protection, Hunan Agricultural University, Changsha, China, [2] Hunan Provincial Key Laboratory for Biology and Control of Plant Diseases and Insect Pests, Changsha, China, [3] Southern Regional Collaborative Innovation Center for Grain and Oil Crops in China, Changsha, China, [4] Hunan Academy of Agricultural Sciences, Institute of Plant Protection, Changsha, China

Bacillus cereus YN917, obtained from a rice leaf with remarkable antifungal activity against *Magnaporthe oryzae*, was reported in our previous study. The present study deciphered the possible biocontrol properties. YN917 strain exhibits multiple plant growth-promoting and disease prevention traits, including production of indole-3-acetic acid (IAA), ACC deaminase, siderophores, protease, amylase, cellulase, and β-1,3-glucanase, and harboring mineral phosphate decomposition activity. The effects of the strain YN917 on growth promotion and disease prevention were further evaluated under detached leaf and greenhouse conditions. The results revealed that *B. cereus* YN917 can promote seed germination and seedling plant growth. The growth status of rice plants was measured from the aspects of rice plumule, radicle lengths, plant height, stem width, root lengths, fresh weights, dry weights, and root activity when YN917 was used as inoculants. YN917 significantly reduced rice blast severity under detached leaf and greenhouse conditions. Genome analysis revealed the presence of gene clusters for biosynthesis of plant promotion and antifungal compounds, such as IAA, tryptophan, siderophores, and phenazine. In summary, YN917 can not only be used as biocontrol agents to minimize the use of chemical substances in rice blast control, but also can be developed as bio-fertilizers to promote the rice plant growth.

Keywords: ***Magnaporthe oryzae*, *Bacillus cereus*, biological control, plant growth promoting, antagonistic activities**

OPEN ACCESS

Edited by:
Alan John Lander Phillips, Universidade de Lisboa, Portugal

Reviewed by:
Yoshihiro Yamaguchi, Osaka City University, Japan
José David Flores Félix, Universidade da Beira Interior, Portugal

***Correspondence:**
Er-ming Liu
ermingliu@163.com

† These authors have contributed equally to this work

Specialty section:
This article was submitted to Microbe and Virus Interactions with Plants, a section of the journal Frontiers in Microbiology

Received: *24 March 2021*
Accepted: *09 June 2021*
Published: *19 July 2021*

Citation:
Zhou H, Ren Z-h, Zu X, Yu X-y, Zhu H-j, Li X-j, Zhong J and Liu E-m (2021) Efficacy of Plant Growth-Promoting Bacteria Bacillus cereus YN917 for Biocontrol of Rice Blast. Front. Microbiol. 12:684888. doi: 10.3389/fmicb.2021.684888

INTRODUCTION

Rice blast is considered as a devastating disease of rice plants caused by *Magnaporthe oryzae* (Miah et al., 2017). The disease has been reported throughout the world wherever rice is intensively cultivated including Europe (Isaac et al., 2010), Africa (Mgonja et al., 2016), Central America (Farman et al., 2017), Oceania, India (Jagadeesh et al., 2018), and China (Xu et al., 2019).

At present, the main measures to prevent and cure rice blast are breeding blast-resistant varieties, changing cultivation patterns (Mottaleb et al., 2019), and applying chemical fungicides. Breeding blast-resistant cultivars has proven to be the most effective, economical, and environment-friendly strategy for disease control, but there are restrictions such as long breeding cycles and variation of physiological races that might result in loss of blast resistance. The breeding

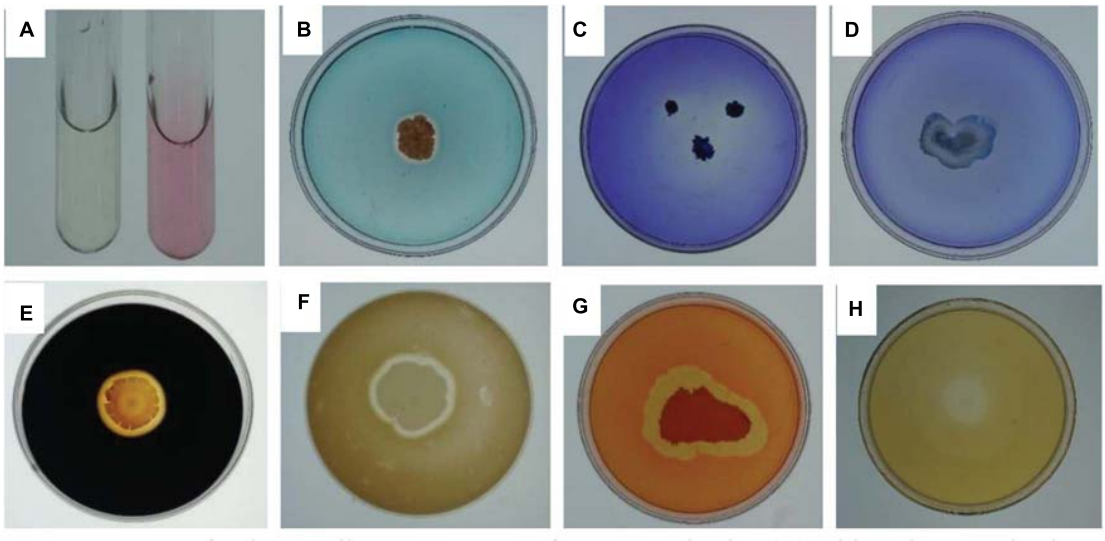

FIGURE 1 | Assays for the *Bacillus cereus* YN917 for IAA production **(A)**. Siderophore production **(B)**. Phosphate solubilization activity **(C)**. Potassium solubilization activity of YN917 **(D)**. Amylase production **(E)**. Protease production **(F)**. Cellulase production **(G)**. β-1,3-glucanase production **(H)**.

of resistant varieties has been proven to be the most effective and economical strategy to control the rice blast, but the long breeding cycle and the loss of resistance due to the variation of physiological races are limiting factors. Up to now, the control of rice blast primarily relies on chemical fungicide, such as tricyclazole, isoprothiolane, tetrachlorobenzene, ediphenphos, blastin, carbendazim, and strobilurin (Wu et al., 2014). Although chemicals are widely available, the excessive dependence on chemical fungicides will cause high fungicide residues and environmental pollution, which is not conducive to the sustainable development of rice agriculture. Microbial fungicides can not only reduce the occurrence of diseases, but also maintain the ecological equilibrium (Zhou et al., 2019). Previous studies have reported that *Bacillus cereus* strains exhibited antifungal activity against *M. oryzae in vitro* or *in vivo*, which is expected to be developed as fungicides to control rice blast, such as the *B. cereus* HS24 (Huang et al., 2020), *B. cereus* AR156 (Jiang et al., 2020), and *B. cereus* KF822666 (Hassan et al., 2019). These studies provided a background for the development of biocides.

In our previous study, a bio-control strain of *B. cereus* YN917 (16S rRNA GenBank: MT990515.1) was isolated from a healthy rice leaf sample of the susceptible rice cultivar Xiangzaoxian No. 24 and stored in China Center for Type Culture Collection, Wuhan, China (CCTCC No. M2020655) (Zhou et al., 2021). To explore the biocontrol potential of strain YN917, this strain was investigated for plant growth-promoting and disease prevention traits, such as the secretion of IAA, ACC deaminase, siderophores, and enzymes, as well as decomposition of mineral phosphate and potassium. The biocontrol effects of strain YN917 in controlling rice blast and growth-promoting properties on rice under detached leaf and greenhouse conditions were evaluated. Moreover, its genomic properties such as the genes associated with production of various antifungal and plant growth-promoting compounds are described.

RESULTS

Plant Growth-Promoting Activities

Indole acetic acid (IAA) production in the *B. cereus* YN917 was determined qualitatively and quantitatively. YN917 was confirmed to produce IAA through the pink chromogenic reaction (**Figure 1A**), and the IAA production seemed to be high according to the pink color (**Table 1**). The IAA production of YN917 was further quantified by the calculated standard curve equation y = 0.0039x-0.0019 (R^2 = 0.9913, y is the absorbance and x is IAA concentration). YN917 showed the maximum 22.54 μg/ml IAA content at the second day of incubation (**Figure 2**). These results suggest that *B. cereus* YN917 could produce IAA even in the absence of exogenous tryptophan.

Spectrophotometric analysis revealed that strain YN917 grows better on ADF medium when compared with the control DF medium. These results suggested that YN917 has the ability to produce ACC deaminase.

Several traits of YN917 involved in plant growth promotion and disease prevention were tested *in vitro* (**Figure 1**). After 7 days of incubation at appropriate temperature, clear and

TABLE 1 | Rice seed growth-promoting effects of *Bacillus cereus* YN917.

Treatments	Germination (%)	Plumule length (cm)	Radicle length (cm)
Control	91.33 ± 0.99 a	0.65 ± 0.14 b	0.97 ± 0.15 b
LB	92.00 ± 0.73 a	0.72 ± 0.03 b	1.08 ± 0.10 b
YN917	91.67 ± 1.21 a	1.31 ± 0.16 a	1.72 ± 0.21 a

Control, LB, and YN917 are the treatments where the rice seedlings were treated with water, LB, and YN917, respectively. The germination, plumule length, and radicle length are represented as the means ± SE of at least three independent experiments. Different letters in each column indicate that the differences are significant ($p < 0.05$) using Duncan's multiple range test.

distinct hydrolytic halos were individually formed around the YN917 colonies that were grown on solid medium containing CAS (**Figure 1B**), $Ca_3(PO_4)_2$ (**Figure 1C**), soluble starch (**Figure 1E**), skimmed milk (**Figure 1F**), CMC (**Figure 1G**), and glucanase (**Figure 1H**). Therefore, it was suggested that *B. cereus* YN917 could secrete siderophore, amylase, protease, cellulase, and β-1, 3-glucanase, as well as have the potential to decompose mineral phosphate. However, there are obvious hydrolytic halos formed around YN917 colonies, which indicated that YN917 has no potential to solubilize potassium (**Figure 1D**).

Growth-Promoting Efficacy of *B. cereus* YN917

The growth-promoting efficacy of YN917 on rice seed were examined, and the results are shown in **Table 1**. It revealed that endophytic bacterial YN917 displayed a growth-promoting effect on seed growth, significantly increasing plumule and radicle lengths ($p > 0.05$), but had no significant effect on germination rate. The average plumule length was 1.31 ± 0.16 cm, which was equivalent to an increase by 101.54% relative to the control when YN917 was inoculated. Meanwhile, it gave rise to the average radicle length of 1.72 ± 0.21 cm, which was equivalent to a 77.32% increase compared with the control. After inoculation with YN917 for 30 days, the growth parameters of rice seedlings (plant height, root length, stem circumference, root length, fresh weight, dry weight, and root activity) were significantly improved relative to control seedlings (**Table 2**). The quantitative results showed that the plant height, stem circumference, root length, fresh weight, dry weight, and root activity of rice seedlings treated with YN917 increased by 49.67, 17.39, 159.46, 30.29, 35.71, and 56.75%, respectively, when compared with those treated only by water. LB medium also improved rice plant growth, but the efficiency was minor and not significant. Overall, these results revealed that *B. cereus* YN917 enabled the inoculated rice seedlings to grow better than the non-inoculated control rice seedlings.

Biocontrol Efficacy of *B. cereus* YN917

The biocontrol efficacy of *B. cereus* YN917 against *M. oryzae* was assayed on detached leaves and in pot experiments. The biocontrol efficacy determined in the detached leaf assays is shown in **Table 3**. Both for the prevention and treatment of disease, strain YN917 showed good anti-blast activity. In the prevention experiments, leaves treated with YN917 and 20% tricyclazole WP developed significant smaller lesions than leaves treated with water or LB (**Figure 3**). In the curative experiments, the leaf lesions were reduced when treated with YN917. Similar results were obtained in the disease treatment experiments. Furthermore, leaves treated with LB showed the longest rice blast lesions.

The results of the biocontrol efficacy in pot experiments are shown in **Table 4**. Compared with the treatments of 40% isoprothiolane WP or YN917 fermentation broth, the untreated rice seedlings showed the most serious rice blast, with a disease index of 60.04%. In the prevention experiments, rice seedlings treated with YN917 had a disease index of 18.68%, which was similar to that treated with tricyclazole and significantly lower than that treated with isoprothiolane (33.67%). Disease treatment

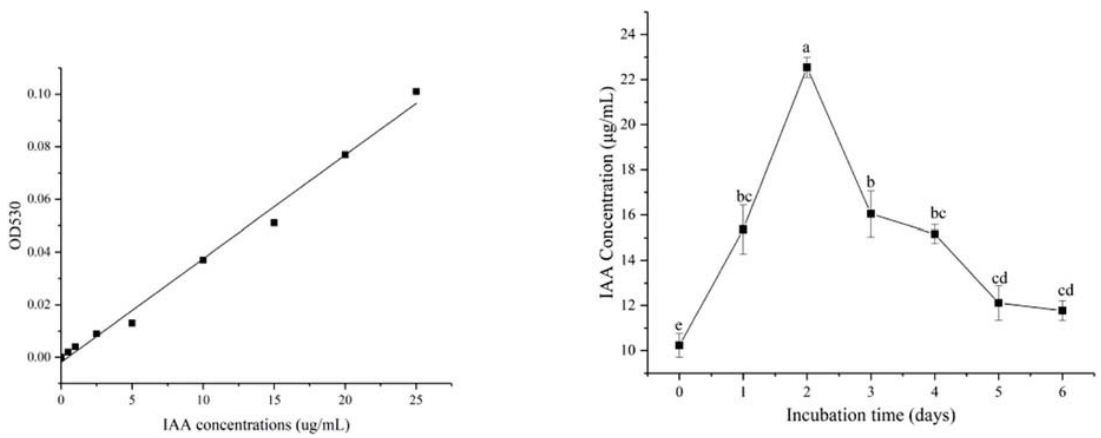

FIGURE 2 | Levels of IAA produced by *B. cereus* YN917 under shaking conditions.

TABLE 2 | Growth parameters of rice plants noted 30 days after their inoculation with *Bacillus cereus* YN917 compared with control.

Treatments	Plant height (cm)	Steam width (mm)	Root length (cm)	Fresh weight (g)	Dry weight (g)	Root activity
Control	22.65 ± 1.95 b	4.83 ± 0.02 c	2.98 ± 0.04 b	1.75 ± 0.05 c	0.70 ± 0.02 a	59.40 ± 1.14 b
LB	25.86 ± 0.98 b	5.04 ± 0.01 b	3.40 ± 0.13 b	1.83 ± 0.08 b	0.78 ± 0.02 a	63.13 ± 1.40 b
YN917	33.69 ± 1.27 a	5.67 ± 0.02 a	7.68 ± 0.35 a	2.28 ± 0.10 a	0.95 ± 0.03 a	93.11 ± 1.57 a

Control, LB, and YN917 are the treatments where the rice seedlings were treated with water, LB, and YN917, respectively. Data represent the means ± SD from 3 independent replicates. Different letters in each column indicate that the differences are significant ($p < 0.05$) using Duncan's multiple range test.

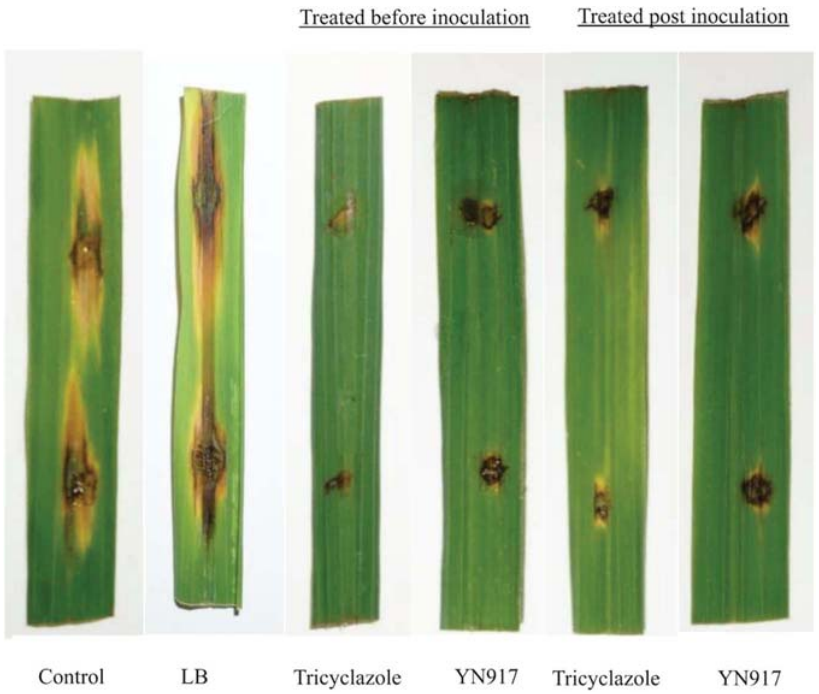

FIGURE 3 | Lesion development 5 days after inoculation with strain *Bacillus cereus* YN917 following protective and therapeutic droplet treatments.

experiments showed that the disease index of YN917 treatments was 20.65%, which was significantly lower than that of the isoprothiolane treatment (34.88%).

Analysis of the Genome Sequence

Because *B. cereus* YN917 was able to produce IAA, ACC-deaminase, and siderophores and solubilize inorganic phosphate and phosphate, to obtain insights into the mechanisms of antifungal and growth-promoting properties of *B. cereus* YN917, the genomic information of *B. cereus* YN917 was analyzed.

The complete genome sequence of strain YN917 (the GenBank accession number is IPRJNA687285 for the BioProject) includes multiple genes taking part in the synthesis of secondary metabolites and organic compounds that contribute to the antifungal activities against pathogens and plant growth promotion. According to the genomic annotation, the *phz*, *pcn*, and *hcn* gene clusters, which are associated with production of antifungal compounds, such as phenazine, were predicted in the YN917 genome. The 2-oxoglutarate dehydrogenase *sucA*, tryptophan 2,3-dioxygenase *TDO2*, arylformamidase *kynB*, kynureninase *kynU*, acyltransferase *atoB*, and amidase amiE, which are associated with hydrolyzing indole acetamide to indoleacetic acid, were predicted in the KEGG pathway of tryptophan metabolism of YN917 genome. The indole-3-glycerol phosphate synthase, *trpC*, tryptophan synthase beta chain, *trpB*, and tryptophan synthase alpha chain, *trpA*, which are associated with tryptophan, synthesize by themselves and several enzymes related to tryptophan synthesis were predicted in the YN917 genome. The genome also contains *pstSCAB-phoU* and beta-glucosidase genes that are involved in plant growth.

TABLE 3 | Incidence rate of leaf blast development 5 days after inoculation with strain *Bacillus cereus* YN917 following protective and therapeutic droplet treatments.

Treatments	Treated before inoculation	Treated after inoculation
Control	98.00 ± 1.15 a	95.67 ± 2.33 a
LB	97.50 ± 2.50 a	96.00 ± 2.31 a
Tricyclazole	9.50 ± 0.76 b	15.33 ± 1.76 b
YN917	13.83 ± 1.30 b	20.67 ± 2.60 b

Control, LB, tricyclazole, and YN917 are the treatments where the rice seedlings were treated with water, LB, 20% tricyclazole, and YN917, respectively. Data represent the means ± SD from 3 independent replicates. Different letters in each column indicate that the differences are significant ($p < 0.05$) using Duncan's multiple range test.

Six genes related to siderophore were found in ABC transporter pathway of *B. cereus* YN917, and five genes were found in porphyrin and chlorophyll metabolism, which are associated with the synthesis of these molecules as well as with the interaction and transport of iron, including iron complex transport system ATP-binding protein, iron complex transport system permease protein, iron complex transport system substrate-binding protein, iron (III) transport system ATP-binding protein, iron (III) transport system permease protein, iron (III) transport system substrate-binding protein, protoporphyrinogen coproporphyrinogen III oxidase, and Fe-coproporphyrin III decarboxylase. Genes related to siderophore have been identified, including *entA*, *entB*, *entC*, and *entE*, and genes related to iron metabolism regulated by IdeR were also identified, including *nuoA*, *nuoB*, *nuoC*, *nuoD*, *nuoH*, *nuoI*, *nuoJ*,

TABLE 4 | Disease index development 7 days after inoculation with strain *Bacillus cereus* YN917 following protective and therapeutic spray treatments.

Treatments	Treated before inoculation			Treated after inoculation		
	Disease incidence (%)	Disease index	Efficacy (%)	Disease incidence (%)	Disease index	Efficacy (%)
Control	89.49 ± 3.38 a	58.65 ± 4.81 a	–	96.73 ± 0.58 a	60.04 ± 2.88 a	–
LB	93.41 ± 3.33 a	52.27 ± 4.06 a	–	91.81 ± 2.70 a	56.16 ± 3.74 a	–
Tricyclazole	58.65 ± 0.68 b	13.79 ± 1.00 c	76.49	60.60 ± 9.32 b	14.12 ± 3.81 c	76.48
YN917	61.52 ± 5.00 b	18.68 ± 3.21 c	68.15	61.17 ± 3.67 b	20.65 ± 3.18 c	65.61

Control, LB, tricyclazole, and YN917 are the treatments where the rice seedlings were treated with water, LB, 20% tricyclazole, and YN917, respectively. Data represent the means ± SD from 3 independent replicates. Different letters in each column indicate that the differences are significant ($p < 0.05$) using Duncan's multiple range test.

nuoK, *nuoL*, *nuoM*, and *nuoN*. Overall, strain YN917 has a great potential as a biocontrol agent in rice cultivation.

DISCUSSION

The biocontrol activity of *Bacillus* spp. against rice blast has been confirmed in previous studies. Compared with the application of fungicides, the biological control of rice blast has the advantages of a low cost and environmental friendliness. In this study, the anti-blast activity of *B. cereus* YN917 was evaluated under detached and greenhouse conditions. The results indicated that strain YN917 was a potential biocontrol agent against rice blast. Notably, in a pot experiment, prevention treatment had a lower disease index than curative treatment; therefore, spraying YN917 in advance is the most effective measure to prevent rice blast. In general, biocontrol strain can induce plant systemic resistance by themselves (Tahir et al., 2017). On the other hand, it was evident that *B. cereus* YN917 efficiently promoted rice growth.

The excellent bio-control effects of YN917 could result from the production of bioactive secondary metabolites or compounds with antimicrobial properties. YN917 produced IAA, ACC deaminase, siderophores, and phosphate-solubilizing and major enzymes such as protease, amylase, cellulase, and β-1,3-glucanase. YN917 showed the production of IAA and ACC deaminase, an important trait of plant growth-promoting microorganisms (Velmurugan et al., 2015). IAA is a phytohormone, which regulates the growth of plant roots by stimulating the proliferation and elongation of root cells, but has no obvious role in bacteria itself (Lwin et al., 2012). ACC is a precursor for ethylene, one of the most important regulatory hormones of plant growth (Bernard, 2005; Glick, 2014; Torbaghan et al., 2016). ACC deaminases can synergistically interact with IAA and enhance plant growth.

In addition, strain YN917 showed the ability to produce siderophores. The production of siderophore is one of the most vital mechanisms to prevent the plant pathogens (Etesami and Maheshwari, 2018). In this study, the ability of YN917 to inhibit mycelium growth of *M. oryzae* was probably associated with the production of siderophore, and further analysis by antiSMASH revealed that a cluster involved in siderophore could be found. Iron is indispensable for DNA synthesis and respiration in organisms. However, the bioavailability of iron in the natural environment is limited by its low solubility of Fe^{3+} in soil. Siderophore is strong enough to remove iron from the environment and convert it into available substances for microbial cell growth (Sasirekha and Shivakumar, 2016). Antagonistic microorganisms could promote their colonization in plants by producing siderophores, as well as assist in obtaining iron nutrition, and limit and inhibit the growth of plant pathogens through iron competition (Eljounaidi et al., 2016).

Generally, bio-control microorganisms can interact with phytopathogens through a series of mechanisms, including the production of antibiotics and lytic enzymes, competition for nutrients, and ecological niches (Berg and Hallmann, 2006). In a previous study, Li et al. (2018) has reported that producing cellulase ability in antagonistic bacteria is essential for entrancing into the plant tissues. YN917 could be developed as a fungicide due to its ability to produce enzymes, which can provide an environment-friendly alternative method to safeguard from phytopathogens.

Genome analysis revealed that the genome of strain YN917 includes the genes associated with antifungal activities and plant growth promotion, such as phenazine, IAA, tryptophan, and siderophore. The genome sequence of *B. cereus* YN917 will contribute to elucidation of genetic mechanisms of the disease prevention and plant growth promotion.

CONCLUSION

In the current study, we investigated a biocontrol strain that could be used as an alternative agent for controlling rice blast, and the experiment results also enhanced our comprehensive understanding toward the possible antifungal mechanisms of *B. cereus* YN917. It has potential to be developed as bio-agents and as bio-fertilizers due to their capabilities in the production of IAA, ACC deaminase, siderophore, and enzymes. The complete genome sequence and annotation of YN917 are summarized, and its genomic properties like the genes associated with production of antifungal activities and plant growth-promoting compounds are described.

MATERIALS AND METHODS

Materials

B. cereus strain YN917 was maintained in 50% glycerol and stored at −80°C. Unless otherwise specified, the strain was grown on Luria–Bertani medium at 28°C (Lagier et al., 2015). *B. cereus*

YN917 was grown on LB medium at 28°C, 180 rpm for 12 h, and the culture was diluted by sterile distilled water and adjusted to an optical density OD 600 = 1 before inoculation.

Magnaporthe oryzae was previously isolated and preserved by our laboratory, and maintained in potato dextrose agar (PDA) plates. Suspension was collected from 7-day-old cultures grown on PDA by washing with water, and then these were transferred to new tomato oatmeal agar plates cultured for 7 day to produce spores. The spores were washed off the plates with 0.1% (v/v) Tween 20 in sterile distilled water and adjusted to 10^5 conidia/ml using a hemocytometer.

The seeds used in this study were Lijiangheituanxingu (Japonica cultivar) and indica cultivar Xiangwanxian No. 12 (Indica rice cultivar; Gold Non-gfeng Seed Industry Technology Co., Ltd., China), which were susceptible to rice blast and were used as the test rice varieties. The seeds were provided by Hunan Academy of Agricultural Sciences, Changsha, Hunan, China.

The commercial fungicide used in this study was 20% tricyclazole WP (750 times dilution; Jiangsu Changqing Agrochemical Co., Ltd., China).

Plant Growth Promotion Assays

Indole-3-Acetic Acid (IAA) Production

Qualitative assay of IAA production was determined by the method described by Bano and Musarrat (2003). *B. cereus* YN917 was inoculated in LB medium and incubated in a shaker (180 rpm, 28°C) for 6 days. One milliliter of the culture was mixed with 2 ml of Salkowski reagent. Appearance of pink color indicates IAA production. The non-inoculated broth medium was used as a control. All treatments consisted of three replicates and were repeated twice.

For quantitative assay of IAA production, a 5-ml aliquot was withdrawn periodically from each culture flask at 0, 1, 2, 3, 4, 5, and 6 days, respectively, and centrifugated (10,000 rpm for 5 min). After that, 2 ml of YN917 supernatant was mixed with 2 drops of phosphoric acid and 4 ml Salkowski's reagent. The optical density of per sample was measured at 530 nm and the amount of YN917 IAA produced was calculated by comparing with the standard IAA curve.

1-Aminocyclopropane-1-Carboxylate (ACC) Deaminase Production

The 1-aminocyclopropane-1-carboxylic acid deaminase activity of *B. cereus* YN917 was detected by using DF medium and ADF medium (Beijing Baiaolaibo Technology Co., Ltd., China) (Dworkin and Foster, 1958; Elżbieta and Stanisław, 2015; Chandra and Sharma, 2016). These mediums were inoculated with 1% (v/v) fresh YN917 cultures and incubated in a shaker (180 rpm, 28°C) for 5 days. The optical density was measured at 600 nm by a spectrophotometer from three replicates; it was considered positive for ACC deaminase production for YN917 that grew in ADF medium and showed no growth on DF medium.

Siderophore Production

Chrome Azurol-S (CAS) detection medium (Qingdao Hope Bio-Technology Co., Ltd., China) was used to qualitatively analyze the YN917 siderophore production (You et al., 2005). These plates were spot inoculated with YN917 and kept at 28°C for 7 days. A yellow-orange halo around YN917 colony was considered as an indicator of siderophore production. The non-inoculated plates were used as control.

Phosphate Solubilization

Pikovskaya (PVK) agar plates were used to qualitatively determine the YN917 insoluble organic phosphate solubilization (Sunita, 2016). The medium consists of 10 g glucose, 0.5 g yeast extract, 0.5 g ammonium sulfate $(NH_4)_2SO_4$, 0.2 g NaCl, 0.2 g KCl, 0.1 g $MgSO_4{\cdot}7H_2O$, 2 mg $MnSO_4$, 2 mg $FeSO_4{\cdot}7H_2O$, 25 mg bromophenol blue, 20 g agar, and 0.5% tricalcium phosphate $Ca_3(PO_4)_2$ in 1 L of distilled water. These plates were spot inoculated with YN917 and kept at 28°C for 7 days. The clear halo around YN917 colony indicated positive phosphate solubilization. The non-inoculated plates were used as control.

Potassium Solubilization

Potassium feldspar agar plates were used to qualitatively determine the YN917 potassium-solubilizing capability. The medium consists of 5 g sucrose, 5 g potassium feldspar powder, 2 g Na_2HPO_4, 0.5g $MgSO_4{\cdot}7H_2O$, 0.1 g $CaCO_3$, 5 mg $FeCl_3$, 25 mg bromophenol blue, and 20 g agar in 1 L of distilled water, pH 7.2, inoculated with YN917, and incubated at 28°C for 7 days. The clear halo around YN917 colony on potassium feldspar agar plates was considered indicative of potassium solubilization. The non-inoculated plates were used as control.

Assay for Enzyme Production

Protease production was determined on skimmed milk LB agar medium (10 g tryptone, 10 g NaCl, 5 g yeast extract, 20 g agar, and 10% sterile skimmed milk in 1 L distilled water, pH 7.4). A positive reaction was read after 2–7 days of incubation at 28°C, with the formation of halo zone surrounding YN917 colonies indicating positive result for protease production. The non-inoculated plates were used as control.

Amylase production was determined by soluble starch agar medium (10 g peptone, 5 g yeast extract, 2 g soluble starch, and 20 g agar in 1 L distilled water, pH 7.0). After 2 days of incubation at 28°C, the ability of YN917 to hydrolyze amylase was determined by the appearance of a halo zone around the colonies and confirmed by Lugol's iodine solution for 15 min and 70% ethanol. The non-inoculated plates were used as control.

Cellulase production was determined by the carboxymethyl cellulose (CMC) agar (10 g peptone, 10 g yeast extract, 10 g CMC, 5 g NaCl, 1 g KH_2PO_4, and 20 g agar in 1 L distilled water, pH 7.0). After 5 days of incubation at 28°C, the ability of isolates to hydrolyze cellulose was determined by the appearance of a clear zone around the colonies and confirmed after pouring 0.1% Congo Red solution into 1 M NaCl (Thomas et al., 2018). The non-inoculated plates were used as control.

β-1,3-Glucanase production was determined by medium (peptone 10 g, yeast extract 5 g, NaCl 10 g, Congo Red 0.04 g, and agar 20 g in 1 L distilled water, pH 7.0). A positive reaction was read after 7 days of incubation at 28°C, with the formation of halo zone surrounding YN917 colonies indicating a positive

result for β-1,3-glucanase production (Srividya et al., 2012). The non-inoculated plates were used as control.

Evaluation of Plant Growth-Promoting Ability of *B. cereus* YN917

Rice Seed Sterilization

Healthy seeds of rice variety Xiangzaoxian No. 24 were selected and disinfected by a 2-min wash in 75% alcohol, and rinsed three times in sterile distilled water (Oyebanji et al., 2009).

Seed Germination Assay

The sterilized seeds were completely soaked in 20 ml YN917 suspension for 12 h to make YN917 colonize on the rice seeds, followed by three rinses of sterile distilled water, and then transferred to Petri plates containing two water-soaked filter papers (50 seeds per replicate) at 28°C for germination. Seeds soaked in LB medium or distilled water served as un-inoculated controls. Germination percentage was recorded at the second day. Rice plumule and radicle lengths were measured at the third day.

Pot Experiment

The plant growth-promoting effects of *B. cereus* YN917 were investigated on Xiangzaoxian No. 24 in the greenhouse. For the pot experiment, the surface-sterilized rice seeds with normal and healthy appearance were selected and planted to every pot (20 cm × 15 cm × 10 cm) filled with field soil and kept in the cultivation greenhouse. The planting soil was taken from Liuyang River in Hunan Agricultural University, Hunan Province, China, and used after disinfection under 121°C for 15 min. Seedlings were grown in natural conditions and irrigated daily. Meanwhile, each pot was irrigated with 50 ml YN917 suspension or water or LB medium once every 10 days. The experiment was conducted three times. Planting for 30 days, the seedlings of each treatment were collected for detection of plant height, root length, stem circumference, fresh weight, and dry weight at the same time.

Biocontrol Assays

Antifungal Activity on Detached Rice Leaves

The biocontrol effect of *B. cereus* YN917 was tested by using punch inoculation on rice leaves of Lijiangheituanxingu which is a rice blast–susceptible variety. Fresh leaves (5-leaf stage) about 7 cm were cut from rice plants. To reinforce the inoculation, a sterilized needle was used to slightly scratch but not puncture the leaf surface. Then 5 μl conidial suspension was added to the wounds, and 5 μl of YN917, sterile water (negative control), LB, or 750 times dilution of 20% tricyclazole WP was added to inoculation points at 24 h before inoculation, as protective test (or 24 h post-inoculation, therapeutic test). The treated materials were placed to 85–100% relative humidity and temperature is 28°C with a 12-h photoperiod. Lesion length was measured at the seventh day after inoculation. All treatments were repeated three times independently (Kunova et al., 2013).

Antifungal Activity in Greenhouse

The biocontrol effect of *B. cereus* YN917 on rice blast was studied by leaf-spraying inoculation with Xiangzaoxian No. 24. When the rice seedlings at the 3-leaf stage were challenge inoculated with conidia suspension (5 ml/pot), 5 ml of YN917 fermentation broth, 20% tricyclazole WP LB, or sterile water was sprayed at 24 h before inoculation, as protective test (or 24 h post-inoculation, therapeutic test). Completely randomized design (CRD) with three replications was used to conduct the experiment. These experiments were carried out in two independent batches. Rice seedlings were incubated in a moist chamber with a 12-h photoperiod, with temperatures ranging 25–32°C. The disease index (DI) was calculated according to the Standard Evaluation System (SES) for International Rice Research Institute (IRRI) (Marta et al., 2011) as follows at 7 days post-inoculation by collecting 50 rice leaves randomly.

Genome Sequencing and Analysis

B. cereus YN917 genomic DNA was extracted using CTAB method, and whole genome sequencing was performed using the PacBio platform and Illumina HiSeq platform at Majorbio Bio-Pharm Technology Co., Ltd. (Shanghai, China). Six databases were used for general function annotation: GO (Gene Ontology) (Moura et al., 2009), KEGG (Kyoto Encyclopedia of Genes and Genomes) (Kanehisa and Goto, 2000), COG (Clusters of Orthologous Groups) (Juhl et al., 2008), NR (Non-Redundant Protein database) (Hossain et al., 2018), Swiss-Prot (Bairoch and Apweiler, 2000), and Pfam (Mistry et al., 2021).

Data Analysis

All statistical analysis was performed using IBM SPSS Statistics 20.0 software with one-way ANOVA. All values are expressed as the mean ± SD of at least three independent experiments.

DATA AVAILABILITY STATEMENT

The datasets presented in this study can be found in online repositories. The names of the repository/repositories and accession number(s) can be found below: NCBI BioProject, accession no: PRJNA687285.

AUTHOR CONTRIBUTIONS

HZ and Z-HR designed the experiment. HZ, XZ, X-YY, and H-JZ performed the experiment. X-JL, Z-HR, and E-ML contributed reagents and materials. HZ, Z-HR, JZ, and E-ML wrote the manuscript. All authors contributed to the article and approved the submitted version.

FUNDING

This work was funded by the National Key R&D Program of China (2016YFD0300700), Central Government Financed Projects, China (2014ZX0800102B), and the Public Welfare Industry (Agriculture) Special Scientific Research Projects, China (201203014).

REFERENCES

Bairoch, A., and Apweiler, R. (2000). The SWISS-PROT protein sequence database and its supplement TrEMBL in 2000. *Nucleic Acids Res.* 28, 45–48. doi: 10.1093/nar/28.1.45

Bano, N., and Musarrat, J. (2003). Characterization of a new *Pseudomonas aeruginosa* strain NJ-15 as a potential biocontrol agent. *Curr. Microbiol.* 46, 324–328. doi: 10.1007/s00284-002-3857-8

Berg, G., and Hallmann, J. (2006). "Control of plant pathogenic fungi with bacterial endophyte," in *Microbial Root Endophytes*, eds B. J. E. Schulz, C. J. C. Boyle, and T. N. Sieber (Berlin: Springer) Vol. 9, 53–70 doi: 10.1007/3-540-33526-9_4

Bernard, R. G. (2005). Modulation of plant ethylene levels by the bacterial enzyme ACC deaminase. *FEMS Microbiol. Lett.* 251, 1–7. doi: 10.1016/j.femsle.2005.07.030

Chandra, D., and Sharma, A. K. (2016). Isolation and characterization of plant growth promoting bacteria containing ACC deaminase from soil collected from central Himalayan region of Uttarakhand, India. *Int. J. Curr. Microbiol. Appl. Sci.* 5, 436–445. doi: 10.20546/ijcmas.2016.508.047

Dworkin, M., and Foster, J. (1958). Experiments with some microorganisms which utilize ethane and hydrogen. *J. Bacteriol.* 75, 592–603. doi: 10.1128/jb.75.5.592-603.1958

Eljounaidi, K., Lee, S. K., and Bae, H. (2016). Bacterial endophytes as potential biocontrol agents of vascular wilt diseases-review and future prospects. *Biol. Control* 103, 62–68. doi: 10.1016/j.biocontrol.2016.07.013

Elżbieta, G. M., and Stanisław, J. P. (2015). Various effects of fluorescent bacteria of the genus *Pseudomonas* containing ACC deaminase on wheat seedling growth. *Microbiol. Res.* 181, 112–119. doi: 10.1016/j.micres.2015.04.005

Etesami, H., and Maheshwari, D. K. (2018). Use of plant growth promoting rhizobacteria (PGPRs) with multiple plant growth promoting traits in stress agriculture: action mechanisms and future prospects. *Ecotoxicol. Environ. Saf.* 156, 225–246. doi: 10.1016/j.ecoenv.2018.03.013

Farman, M., Peterson, G., Chen, L., Starnes, J., Valent, B., Bachi, P., et al. (2017). The *Lolium* pathotype of *Magnaporthe* oryzae recovered from a single blasted wheat plant in the United States. *Plant Dis.* 101, 684–692. doi: 10.1094/pdis-05-16-0700-re

Glick, B. R. (2014). Bacteria with ACC deaminase can promote plant growth and help to feed the world. *FEMS Microbiol. Rev.* 169, 30–39. doi: 10.1016/j.micres.2013.09.009

Hassan, E., Hossein, A. A., and Hossein, M. H. (2019). Root bacterial endophytes as potential biological control agents against fungal rice pathogens. *Arch. Phytopathol. Plant Prot.* 52, 560–581. doi: 10.1080/03235408.2018.1557884

Hossain, M. U., Omar, T. M., Alam, I., Das, K. C., Mohiuddin, A. K. M., Keya, C. A., et al. (2018). Pathway based therapeutic targets identification and development of an interactive database CampyNIBase of *Campylobacter* jejuni RM1221 through non-redundant protein dataset. *PLoS One* 13:e0198170. doi: 10.1371/journal.pone.0198170

Huang, W., Liu, X., Zhou, X., Wang, X., and Liu, H. (2020). Calcium signaling is suppressed in *Magnaporthe* oryzae conidia by *Bacillus cereus* HS24. *Phytopathology* 110, 309–316.

Isaac, L. L., Didier, T., and Mercedes, C. M. (2010). Evidence for rapid changes in the population genetic structure of *Magnaporthe* oryzae in Southern Spain. *J. Phytopathol.* 158, 785–791. doi: 10.1111/j.1439-0434.2010.01699.x

Jagadeesh, D., Prasanna Kumar, M. K., and Devaki, N. S. (2018). Population analysis of *Magnaporthe* oryzae by using endogenous repetitive DNA sequences and mating-type alleles in different districts of Karnataka, India. *J. Appl. Genet.* 59, 365–375. doi: 10.1007/s13353-018-0453-6

Jiang, C. H., Fan, Z. L., Li, Z. J., Niu, D. D., Li, Y., Zheng, M. Z., et al. (2020). *Bacillus cereus* AR156 triggers induced systemic resistance against *Pseudomonas syringae* pv. *tomato* DC3000 by suppressing miR472 and activating CNLs-mediated basal immunity in *Arabidopsis*. *Mol. Plant Pathol.* 21, 854–870. doi: 10.1111/mpp.12935

Juhl, J. L., Philippe, J., Michael, K., Christian, M., Jean, M., Tobias, D., et al. (2008). eggNOG: automated construction and annotation of orthologous groups of genes. *Nucleic Acids Res.* 36(suppl. 1), 250.

Kanehisa, M., and Goto, S. (2000). KEGG: kyoto encyclopedia of genes and genomes. *Nucleic Acids Res.* 28, 27–30.

Kunova, A., Pizzatti, C., and Cortesi, P. (2013). Impact of tricyclazole and azoxystrobin on growth, sporulation and secondary infection of the rice blast fungus, *Magnaporthe* oryzae. *Pest Manage. Sci.* 69, 278–284. doi: 10.1002/ps.3386

Lagier, J. C., Edouard, S., Pagnier, I., Mediannikov, O., Drancourt, M., and Raoult, D. (2015). Current and past strategies for bacterial culture in clinical microbiology. *Clin. Microbiol. Rev.* 28, 208–236. doi: 10.1128/cmr.00110-14

Li, D. X., Ni, K. K., Zhang, Y. C., Lin, Y. L., and Yang, F. (2018). Influence of lactic acid bacteria, cellulase, cellulase-producing *Bacillus pumilus* and their combinations on alfalfa silage quality. *J. Integr. Agric.* 17, 172–186.

Lwin, K. M., Myint, M. M., Tar, T., and Aung, W. Z. M. (2012). Isolation of plant hormone (Indole-3-Acetic Acid-IAA) producing rhizobacteria and study on their effects on maize seedling. *Eng. J.* 16, 137–144. doi: 10.4186/ej.2012.16.5.137

Marta, C. C. F., Gisele, B. D. S., Valácia, L. S., Márcio, V. C., Alessandra, J. G. M., and Anne, S. P. (2011). Leaf blast (*Magnaporthe oryzae*) suppression and growth promotion by rhizobacteria on aerobic rice in Brazil. *Biol. Control.* 58, 160–166. doi: 10.1016/j.biocontrol.2011.04.016

Mgonja, E. M., Balimponya, E. G., Kang, H. X., Bellizzi, M., Park, C. H., Li, Y., et al. (2016). Genome-Wide association mapping of rice resistance genes against *Magnaporthe* oryzae Isolates from Four African Countries. *Phytopathology* 106, 1359–1365. doi: 10.1094/phyto-01-16-0028-r

Miah, G., Rafiii, M. Y., Ismail, M. R., Sahebi, M., Hashemi, F. S. G., Yusufffff, O., et al. (2017). Blast disease intimidation towards rice cultivation: a review of pathogen and strategies to control. *J. Anim. Plant Sci.* 27, 1058–1066.

Mistry, J., Chuguransky, S., Williams, L., Qureshi, M., Salazar, G. A., Sonnhammer, E. L. L., et al. (2021). Pfam: the protein families database in 2021. *Nucleic Acids Res.* 49, 412–419.

Mottaleb, K. A., Govindan, V., Singh, P. K., Sonder, K., He, X. Y., Singh, R. P., et al. (2019). Economic benefits of blast-resistant biofortified wheat in Bangladesh: the case of BARI Gom 33. *Crop Prot.* 123, 45–58. doi: 10.1016/j.cropro.2019.05.013

Moura, A., Soares, M., Pereira, C., Leitão, N., Henriques, I., and Correia, A. (2009). INTEGRALL: a database and search engine for integrons, integrases and gene cassettes. *Bioinformatics* 25, 1096–1098. doi: 10.1093/bioinformatics/btp105

Oyebanji, O. B., Nweke, O., Odebunmi, O., Galadima, N. B., Idris, M. S., Nnodi, U. N., et al. (2009). Simple, effective and economical explant-surface sterilization protocol for cowpea, rice and sorghum seeds. *Afr. J. Biotechnol.* 8, 5395–5399.

Sasirekha, B., and Shivakumar, S. (2016). Siderophore production by *Pseudomonas aeruginosa* FP6, a biocontrol strain for *Rhizoctonia* solani and *Colletotrichum* gloeosporioides causing diseases in chilli. *Agric. Nat. Resour.* 50, 250–256. doi: 10.1016/j.anres.2016.02.003

Srividya, S., Thapa, A., Bhat, D. V., Golmei, K., and Dey, N. (2012). Streptomyces sp. 9p as effective biocontrol against chilli soil borne fungal pathogens. *Eur. J. Exp. Biol.* 2, 163–173.

Sunita, G. (2016). Phosphate dissolving fungi: mechanism and application in alleviation of salt stress in wheat. *Microbiol. Res.* 193, 94–102. doi: 10.1016/j.micres.2016.09.005

Tahir, H. A. S., Gu, Q., Wu, H., Niu, Y., Huo, R., and Gao, X. (2017). Bacillus volatiles adversely affect the physiology and ultra-structure of *Ralstonia solanacearum* and induce systemic resistance in tobacco against bacterial wilt. *Sci. Rep.* 7:40481.

Thomas, L., Ram, H., and Singh, V. P. (2018). Inducible cellulase production from an organic solvent tolerant *Bacillus* sp. SV1 and evolutionary divergence of endoglucanase in different species of the genus *Bacillus*. *Braz. J. Microbiol.* 49, 429–442. doi: 10.1016/j.bjm.2017.05.010

Torbaghan, M. E., Lakzian, A., Astaraei, A. R., Fotovat, A., and Besharati, H. (2016). Quantitative comparison of ammonia and 3-indoleacetic acid production in halophilic, alkalophilic and haloalkalophilic bacterial isolates in soil. *J. Fundam. Appl. Sci.* 3, 194–202.

Velmurugan, A., Sakthivel, K., Swarnam, T. P., Rachael, S., and Roy, D. S. (2015). Assessment of the plant growth promotion and phosphorus solubilization by rhizosphere bacteria isolated from Troporthents soils of Bay Island. *Trends Biosci.* 8, 2888–2892.

Wu, W. H., Wang, L., Zhang, S., Liang, Y. Q., Zheng, X. L., and He, C. P. (2014). Assessment of sensitivity and virulence fitness costs of the AvrPik alleles from *Magnaporthe* oryzae to isoprothiolane. *Genet. Mol. Res. GMR* 13, 9701–9709. doi: 10.4238/2014.november.24.1

Xu, T., Cao, L. D., Zeng, J. R., Christopher, M. M. F., Yang, Y. Z., Hu, X. C., et al. (2019). Plant root exudates are involved in *Bacillus* cereus AR156 mediated biocontrol against *Ralstonia* solanacearum. *Front. Microbiol.* 10:98. doi: 10.3389/fmicb.2019.00098

You, J. L., Cao, L. X., Liu, G. F., Zhou, S. N., Tan, H. M., and Lin, Y. C. (2005). Isolation and characterization of actinomycetes antagonistic to pathogenic *Vibrio* spp. From nearshore marine sediments. *World J. Microbiol. Biotechnol.* 21, 679–682. doi: 10.1007/s11274-004-3851-3

Zhou, G. Y., Zhou, Q., and Zhu, Y. H. (2019). The antifungal action mode of the rice endophyte *Streptomyces* hygroscopicus OsiSh-2 as a potential biocontrol agent against the rice blast pathogen. *Pestic. Biochem. Physiol.* 160, 58–69.

Zhou, H., Zhu, H., Hu, L., Yu, X., Ren, Z., and Liu, E. (2021). Characterization and inhibitory effects of an antifungal protein from the *Bacillus* cereus strain YN917. *Int. J. Agric. Biol.* 25, 1153–1160.

Conflict of Interest: The authors declare that the research was conducted in the absence of any commercial or financial relationships that could be construed as a potential conflict of interest.

frontiers in Microbiology

ORIGINAL RESEARCH
published: 05 August 2021
doi: 10.3389/fmicb.2021.666761

Lauric Acid Is a Potent Biological Control Agent That Damages the Cell Membrane of *Phytophthora sojae*

Changhui Liang[1], Wenteng Gao[1], Ting Ge[1], Xinwei Tan[1], Jiayu Wang[1], Huaxin Liu[1], Yong Wang[2], Chao Han[1], Qian Xu[3] and Qunqing Wang[1,3]**

[1] Shandong Province Key Laboratory of Agricultural Microbiology, Department of Plant Pathology, College of Plant Protection, Shandong Agricultural University, Tai'an, China, [2] Shimadzu (China) Co., Ltd., Beijing, China, [3] State Key Laboratory of Crop Biology, Shandong Agricultural University, Tai'an, China

Sustainable management of plant pathogens is becoming more challenging, and novel solutions are needed. Plant biologically active secondary metabolites are important sources of novel crop protection chemistry. Effective individual compounds of these natural products have the potential to be successful new agrochemicals. In this study, we identified lauric acid (LA) from soybean defense leaf volatiles. LA inhibited the growth of *Phytophthora sojae*, the causal agent of soybean root rot. It influenced mycelial development, sporangium formation, and zoospore generation and germination by damaging the *P. sojae* cell membrane. Additionally, we showed that LA and several of its derivatives, such as glycerol monolaurate (GML), had similar biological activities. Both LA and GML were safe to soybean plants when used at less than 0.3 g a.i./plant and could promote soybean growth, implying their potential as eco-friendly biological control agents.

Keywords: lauric acid, leaf volatile compounds, *Phytophthora sojae*, cell membrane damage, biological control

OPEN ACCESS

Edited by:
Yong Wang,
Guizhou University, China

Reviewed by:
Maofeng Jing,
Nanjing Agricultural University, China
Tofazzal Islam,
Bangabandhu Sheikh Mujibur Rahman Agricultural University, Bangladesh

****Correspondence:***
Qian Xu
xuqian@sdau.edu.cn
Qunqing Wang
wangqunqing@163.com

Specialty section:
This article was submitted to Microbe and Virus Interactions with Plants, a section of the journal Frontiers in Microbiology

Received: *11 February 2021*
Accepted: *24 June 2021*
Published: *05 August 2021*

Citation:
Liang C, Gao W, Ge T, Tan X, Wang J, Liu H, Wang Y, Han C, Xu Q and Wang Q (2021) Lauric Acid Is a Potent Biological Control Agent That Damages the Cell Membrane of Phytophthora sojae. Front. Microbiol. 12:666761. doi: 10.3389/fmicb.2021.666761

INTRODUCTION

Oomycetes are fungus-like eukaryotic organisms that belong to the class Saprolegniomycetidae of the kingdom Stramenopila (Yutin et al., 2008). They encompass notorious plant disease agents, including *Phytophthora*, *Pythium*, and *Albugo*, and a group of downy mildews (Tyler, 2001). Oomycetes have a negative impact on natural and farm ecosystems due to their strong pathogenicity and infectivity (Kamoun et al., 2015). In addition to the well-known potato late blight caused by *Phytophthora infestans*, which led to the 19th-century Irish famine, the persistence of sudden oak death caused by *Phytophthora ramorum* and grape downy mildew caused by *Plasmopara viticola* demonstrate that oomycete phytopathogens are a persistent threat to subsistence and commercial farming and destructive to native plants (Erwin and Ribeiro, 1996). Soybean (*Glycine max* L.) root rot caused by *Phytophthora sojae* is the leading cause of global soybean production loss (Tyler, 2007). Agrochemicals are largely used to control oomycete diseases, resulting in the emergence of resistant strains and resurgence events (Randall et al., 2014). The effective and sustainable control of oomycete-driven diseases requires the identification of novel pharmaceuticals and pesticides to drive the design of fungicides compatible with integrated pest management (IPM) approaches (Gessler et al., 2011).

Environmental-friendly botanical fungicides are valuable because of their higher efficiency, lower residue, and lower toxicity. Multiple interdisciplinary studies and abundant resources have been applied to find new and effective alternatives for the IPM of various oomycete species. Historically, traditional healers have used plants to prevent or cure infections, and active elements for disease control have been identified in various species. For example, artemisinin, present in sweet wormwood (*Artemisia annua*), a Chinese medicinal plant, is an effective antimalarial agent (Tu, 2011). Medium-chain fatty acids (MCFAs), including octanoic acid (C8), capric acid (C10), and lauric acid (LA) (C12), distilled from virgin coconut oil, inhibit various bacterial, fungal, and viral pathogens and have been widely used in human and veterinary medicine (Kabara et al., 1972; Bartolotta et al., 2001; Rouse et al., 2005; Yang et al., 2009, 2018; Shilling et al., 2013; Fortuoso et al., 2019). For example, capric acid kills *Candida albicans* quickly and effectively (Bergsson et al., 2001). LA is the most active MCFA at lower concentrations and after longer incubation times (Bergsson et al., 2001; Lalouckova et al., 2021). Additionally, LA has antimicrobial activity against both Gram-positive and Gram-negative pathogens, including *Staphylococcus aureus*, *Streptococcus mutans*, *Streptococcus pyogenes*, *Escherichia coli*, and *Helicobacter pylori* (Kabara et al., 1972; Rouse et al., 2005). In addition to their effect on human and animal pathogens, MCFAs also inhibit mycelial growth and spore germination of four plant pathogenic fungi: *Alternaria solani*, *Colletotrichum lagenarium*, *Fusarium oxysporum* f. sp. *Cucumerinum*, and *F. oxysporum* f. sp. *lycopersici* (Liu et al., 2008). These observations suggest that MCFAs may be useful for developing alternative IMP approaches for the control of phytopathogens.

Phytochemicals have a long history as sources of novel agrochemicals. Phytopathologists search for natural products (NPs) that can be developed into pesticides for the treatment of plant diseases. For example, poacic acid, which is commonly found in grass lignocellulosic hydrolyzates, inhibits the growth of *Sclerotinia sclerotiorum* and *A. solani* fungi and *P. sojae* oomycetes (Piotrowski et al., 2015). There is considerable evidence for direct protective effects of chemicals isolated from plant root or leaf exudates and leaf or fruit volatile organic compounds (VOCs) in various organisms. For example, ε-viniferin, isolated from *Vitis vinifera* canes, has antifungal activity against *P. viticola* and *Botrytis cinerea* (Schnee et al., 2013). Secomicromelin, 7-methoxy-8-(4′-methyl-3′-furanyl) coumarin, micromarin B, and isomicromelin, present in *Micromelum falcatum* fruits, inhibit *Pythium insidiosum* mycelial growth (Suthiwong et al., 2014). Cuminic acid, present in *Cuminum cyminum* L. seeds, inhibits *Phytophthora capsici* mycelial growth and zoospore germination (Wang et al., 2016). Gossypol, which is naturally present in cotton root tissues, has a strong inhibitory activity on the growth of various soil-borne oomycetes and fungi, including *Pythium irregulare*, *Pythium ultimum*, and *F. oxysporum* (Mellon et al., 2014). Several leaf VOCs are produced and emitted rapidly when plants respond to stresses, such as herbivore or mechanical damage or attack by necrotrophic fungi (Cowan, 1999; Scala et al., 2013; Matsui and Koeduka, 2016; Tanaka et al., 2018; Wang et al., 2020). These phytochemicals may contribute directly to plant defense by preventing pathogen invasion (Matsui, 2006; Kishimoto et al., 2008).

Here, we analyzed soybean leaf volatiles derived from compatible (disease-producing) and incompatible (successful plant defense) interactions with *P. sojae*, the causal agent of soybean root and stem rot disease. LA was identified by headspace solid-phase microextraction coupled with gas chromatography–mass spectrometry (HS-SPME-GC–MS) among the incompatible interaction-produced volatiles. Both LA and glycerol monolaurate (GML), a chemical compound formed from LA and glycerol, inhibited the mycelial growth of *P. sojae* in Petri dish assays. GML also disrupted or disintegrated the *P. sojae* plasma membrane, leading to shrunken mycelia and cytoplasmic electrolyte leakage. We provide a conclusion about the functions and the protective mechanisms of LA as a potential oomycete biological control agent.

MATERIALS AND METHODS

Plant and *P. sojae* Cultivation

Soybean plants were cultivated in a growth chamber at 25°C, with a cycle of 16 h of high light intensity and 8 h of darkness. *P. sojae* strains were grown on 10% V8 medium (10% V8 juice, 0.02% $CaCO_3$, and 1.5% agar) at 25°C in the dark. Hyphal plugs were cultured in V8 liquid medium for mycelial harvest. The mycelia were washed with sterile tap water three times and cultured in the darkness at 25°C for 6 h for zoosporangium incubation and zoospore release. Finally, the concentration of the zoospore suspension was adjusted to 1×10^5 mL.

GC–MS Analysis

Soybean leaves inoculated with *P. sojae* were placed in a 20-mL headspace bottle. An AOC-6000 Multifunctional Autosampler (Shimadzu, Kyoto, Japan) was used for SPME injection, and a GCMS-TQ8040 NX (Shimadzu) was used for detection using the following standard SPME parameters: SPME fiber, FIB-C-WR-95/10; aging temperature, 240°C; aging time before extraction, 30 min; equilibration temperature, 40°C; equilibration time, 5 min; extraction time, 30 min; injection port temperature, 250°C; desorption time, 2 min; and aging time after extraction, 5 min. The GC–MS parameters used were as follows: column, inert cap pure-wax, 30 m × 0.25 mm × 0.25 m; oven program, 50°C(5 min) and 10°C/min 250°C(10 min); carrier gas pressure, 83.5 kPa; injection mode, split; split ratio, 5:1; ion-source temperature, 200°C; interface temperature, 250°C; detector voltage, tuning voltage +0.3 kV; and acquisition mode, MRM.

Inhibitory Effects of LA and Its Derivatives on *P. sojae* Growth

Hyphal plugs with a 6 mm were cultured in V8 liquid medium containing different concentrations (0.5, 1, 1.5, 2, and 2.5 mM) of LA, its derivatives–GML, methyl laurate (MEL), and ethyl laurate (ETL)–or the same volume of sterile water as a control reference (CK). The inoculated medium was incubated in the darkness at

25°C for 5 days. Then, the colony diameter was measured, and the mycelium status was observed under a light microscope.

Effects of LA and Its Derivatives on *P. sojae* Zoosporangium Forming and Zoospores Release

Different concentrations of LA or its derivatives, GML, MEL, and ETL, were added into washed mycelia cultured in V8 liquid medium. After incubation at 25°C for 6 h, the number of zoosporangia was determined under a light microscope.

Lauric acid and its derivatives were added into the same number of sporangium culture dishes without zoospore release. The zoospores were cultured at 25°C, and the number of zoospores was determined under a light microscope.

Effects of LA and Its Derivatives on *P. sojae* (R2) Zoospore Germination

A 0.1-mL spore suspension was evenly coated on V8 medium containing different concentrations of LA or its derivatives, GML, MEL, and ETL. After incubation at 25°C for 4 days, colony formation was analyzed visually.

Damage of the *P. sojae* Cell Membrane by LA and Its Derivatives

Mycelia were cultured in V8 liquid medium for 3 days before different concentrations of LA, and its derivatives, GML, MEL, and ETL, were added to the medium. After 1–2 h of treatment, 1/10 of the total volume of propidium iodate (PI) was added to the culture. After 20 min of incubation, the mycelia were rinsed with PBS 2–3 times. The mycelium was observed under a fluorescence microscope.

The same mycelia were placed in liquid V8 medium containing different concentrations of LA or its derivatives, and the concentrations of DNA and protein, and the electrical conductivity, were measured every 2 h and plotted for analysis.

Safety of LA and Its Derivatives on Soybean Plants

Different concentrations (0.5, 1, 1.5, 2, and 2.5 mM) of LA or its derivatives, GML, MEL, and ETL, were mixed with the same volume of soil. Sterile water was used as a blank control (CK), and each treatment was repeated three times. The growth and development of soybean seedlings were recorded 7 and 14 days after planting.

Use of LA and Its Derivatives as Preplant Soil Fumigants

Different concentrations (0.5, 1, 1.5, 2, and 2.5 mM) of LA or its derivatives, GML, MEL, and ETL, were mixed with the same volume of soil. Sterile water was used as a blank control. The soil was covered with a plastic film; after 15 days, the plastic film was removed, and the soil was ventilated for 2 days. Soybeans were then planted, and their height was measured after 5 days.

RESULTS

Lauric Acid Is Induced in Incompatible Soybean–*P. sojae* Interactions

Soybean is the main host of *P. sojae*. Therefore, soybean cultivars that contain resistance genes to *P. sojae* (*Rps*) are important resources in agricultural production. Resistance genes provide defense ability against pathogen varieties and induce the emergence of hypersensitive responses and the production of secondary metabolites.

We analyzed the leaf volatiles produced during incompatible soybean–*P. sojae* interactions. After inoculation with *P. sojae*, the main constituents of the volatiles produced from the leaves of the susceptible soybean cultivar Williams (without *Rps* genes) and the resistant cultivar Williams 82 (with the resistance gene *Rps1k*) were determined by GC–MS. The LA concentration in the leaf volatiles of Williams 82 was significantly higher than that of Williams (**Supplementary Figure 1**), suggesting that LA contributes to the defense response of soybean to *P. sojae*.

Lauric Acid Is Toxic to *P. sojae*

We measured the radial growth diameters of different *P. sojae* races grown on V8 medium containing different concentrations of LA; the toxicity of LA to *P. sojae* was conspicuous (**Figure 1** and **Supplementary Table 1**). After 5 days' growing on V8 medium with 0.5 mM LA, the diameter of Race2 (strain P6497) hypha was 26.27 mm, and the bacteriostatic rate was 54.21%. Furthermore, the bacteriostatic rates of Race7 (strain P7064), Race17 (strain P7074), and Race19 (strain P7076) were 30.87, 28.22, and 23.33%, respectively. On the medium containing 2.5 mM LA, the bacteriostatic rates for Race2, Race 7, Race17, and Race19 were 64.84, 57.06, 42.16, and 62.86%, respectively. Higher concentrations of LA exacerbated its toxicity to various *P. sojae* races.

Lauric Acid Derivatives Had Lower Toxicity to *P. sojae*

Fatty acids can merge into cell membranes, and their hydrophilicity and lipophilicity likely affect their antimicrobial activity. To verify this hypothesis, we analyzed the mycelial growth diameter of *P. sojae* (Race2) grown under different concentrations of LA and its derivatives, GML, MEL, and ETL. The diameters and bacteriostatic rates of mycelia treated with GML, MEL, and ETL at 0.5 mM were 50.80, 57.53, and 57.37 mm, and 27.32, 17.70, and 17.93%, respectively. For LA, the corresponding values were 45.40 mm and 35.05%, indicating that its toxicity is higher than that of the three derivatives tested (**Figure 2** and **Supplementary Table 2**). The inhibitory effect of LA of *P. sojae* was the most significant at the lowest concentration (0.5 mM). In summary, the toxicity effects to *P. sojae* were the highest for LA, followed by GML, ETL, and MEL.

Lauric Acid Effects on the Development of *P. sojae* Mycelia and Sporangium

We observed the morphology of *P. sojae* hyphae with an optical microscope. LA treatments led to hyphae with more branches,

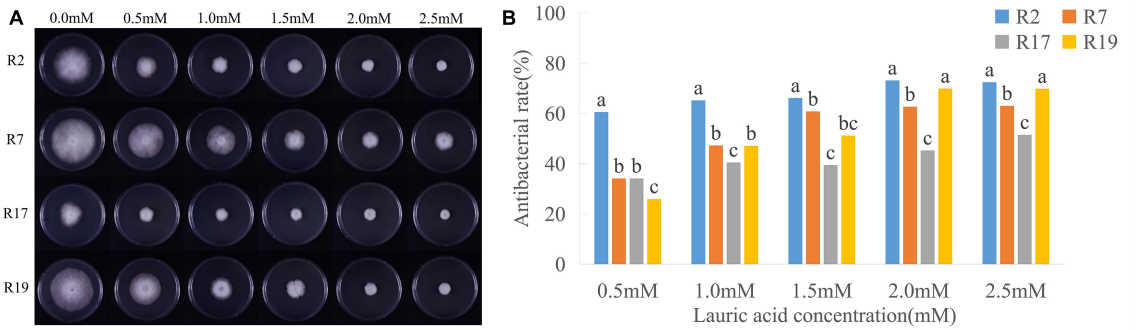

FIGURE 1 | Inhibitory effects of lauric acid (LA) to various *P. sojae* species. **(A)** Four different *P. sojae* races (Race2, Race7, Race17, and, Race19) were cultured on V8 medium with different concentrations of LA for 5 days. The experiment was repeated three times with similar results. **(B)** The diameter of each colony was measured and statistical analyzed via software Statistical Product and Service Solutions (SPSS). Means with different letters are significantly different ($p < 0.05$).

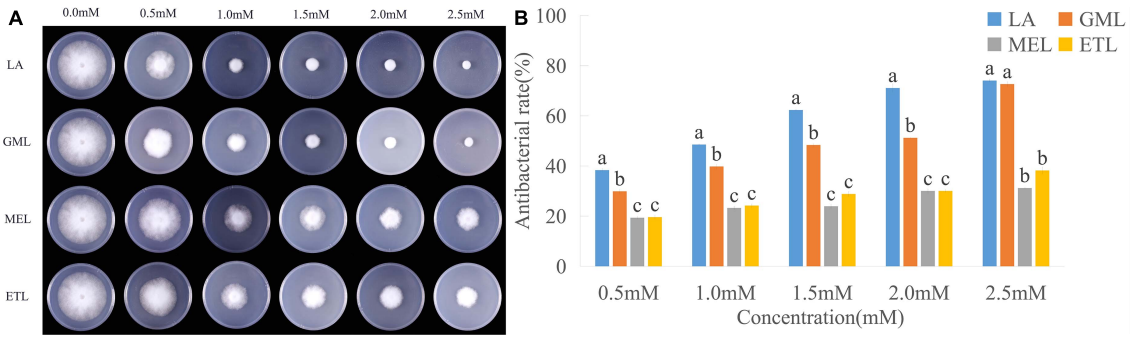

FIGURE 2 | Inhibitory effects of lauric acid (LA) and its derivatives to *P. sojae*. **(A)** The mycelia of *P. sojae* (Race2) were cultured on media containing LA, glycerol monolaurate (GML), methyl laurate (MEL), or ethyl laurate (ETL) for 5 days. **(B)** The diameter of each colony was measured and statistical analyzed via software Statistical Product and Service Solutions (SPSS). Means with different letters are significantly different ($p < 0.05$).

distortions, bending, and nodules than those in the control group. Moreover, LA-treated hyphae had few zoosporangia (**Figure 3**).

To explore how LA and its derivatives affect *P. sojae* zoosporangium formation and zoospore release, we determined the number of zoosporangia formed and calculated the inhibition effect of each chemical. The number of zoosporangia was reduced with 0.16 mM LA or GML when compared with the water control; no zoosporangia were observed with 0.64 mM treatments. With 1.28 mM MEL or ETL, a small number of zoosporangia were obtained (**Supplementary Table 3**).

Zoosporangia formed in the water could not release zoospores when the LA or GML concentration increased to 0.64 mM. Interestingly, almost no zoospores were released from zoosporangia treated with 0.32 mM GML, which was significantly lower than what we observed for LA, MEL, or ETL (**Supplementary Table 3**).

Lauric Acid and Its Derivatives Affect the Germination of *P. sojae* Zoospores

To explore the influence of LA and its derivatives on *P. sojae* zoospore germination, we evenly daubed zoospore suspensions onto media containing various concentrations of LA, GML, MEL, or ETL. Compared to the V8 medium control, LA and GML at 0.08 mM significantly inhibited zoospore germination, and few zoospores could form individual colonies (**Figure 4**). However, MEL and ETL had weak inhibitory effects on zoospore germination at the maximum concentration of 1.28 mM (**Figure 4** and **Supplementary Table 4**).

Lauric Acid Induced Cell Membrane Damage and Cell Substance Leakage in *P. sojae*

Propidium iodate is a DNA-binding and a cell-membrane–impermeable dye, usually used as a marker for membrane integrity and cell viability; PI cannot cross the membrane of live cells but can penetrate and stain the cell nucleus red if the cell membrane is damaged. We PI-stained *P. sojae* hyphae nuclei after exposure to LA and observed that the cell membrane was severely damaged, resulting in red fluorescence in the nucleus (**Figure 5A**).

To further investigate the potential damage to the cell membrane, we analyzed cell substance leakage in *P. sojae* mycelia treated with LA and its derivatives, GML, MEL, and ETL. Total DNA and protein concentrations were monitored every 2 h in the growth media. DNA and protein contents increased significantly over time and gradually flattened out in LA and

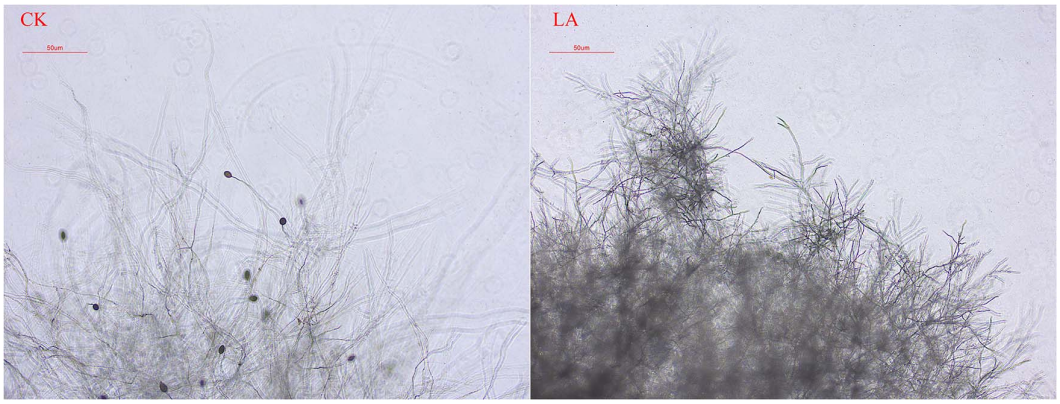

FIGURE 3 | Effect of LA on *P. sojae* mycelial morphology. Mycelia were treated with LA or the same volume of water (CK) for 2 h before their morphology was analyzed. Mycelial growth after LA treatment was disorderly, the terminal branch number increased significantly, and the formation of zoosporangium was inhibited. In CK, the mycelium grew normally and expanded without any distortion, bending, or increased terminal branching. The experiment was repeated three times with similar results.

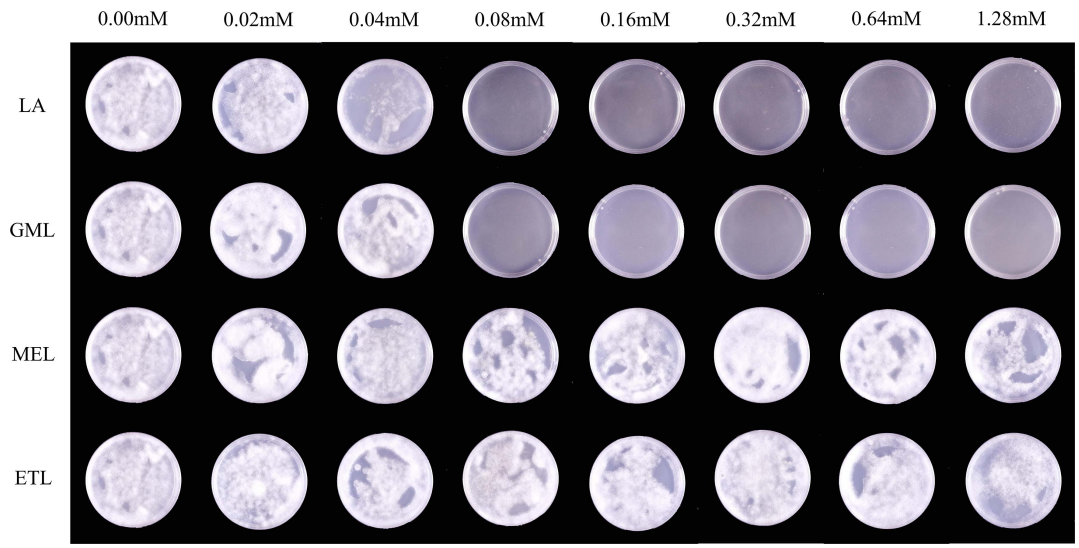

FIGURE 4 | The effects of LA and its derivatives on *P. sojae* zoospore germination. To observe zoospore germination, zoospore suspensions were smeared on V8 medium containing LA, GML, MEL, or ETL at different concentrations. The experiment was repeated three times with similar results. Means with different letters are significantly different (Statistical Product and Service Solutions (SPSS), $p < 0.05$).

GML solutions but changed only slightly in CK, MEL, or ETL solutions (**Figures 5B, C**). The conductibility of the five tested solutions increased in the first 2 h, but it was significantly higher in LA and GML than in CK, MEL, or ETL (**Figure 5D**). The results indicated that the *P. sojae* DNA and proteins penetrated the solution upon treatment with LA or GML, probably because the cell membrane was damaged or destroyed.

Host Security of Treatments With LA and Its Derivatives on Soybean Plants

To understand the security of LA and its derivatives on host plants, we applied different concentrations of LA, GML, MEL, or ETL in the pot-planting holes; soybean seedling height was measured at 7 and 14 days after planting. When LA and GML concentrations were lower than 0.3 g a.i./plant, the treatments promoted soybean growth, whereas the application of 0.3 g a.i./plant did not influence plant growth, and there was no significant difference in height compared with the control group. At 0.6 g a.i./plant, MEL and ETL treatments did not significantly affect plant growth compared to the control at the two time points. However, concentrations higher than 0.6 g a.i./plant were harmful to plants and inhibited their growth (**Supplementary Table 5**).

Potential of LA and Its Derivatives as Biological Control Agents

The mycelium and oospores of *P. sojae* formed on V8 medium were homogenized using a blender and mixed with potted

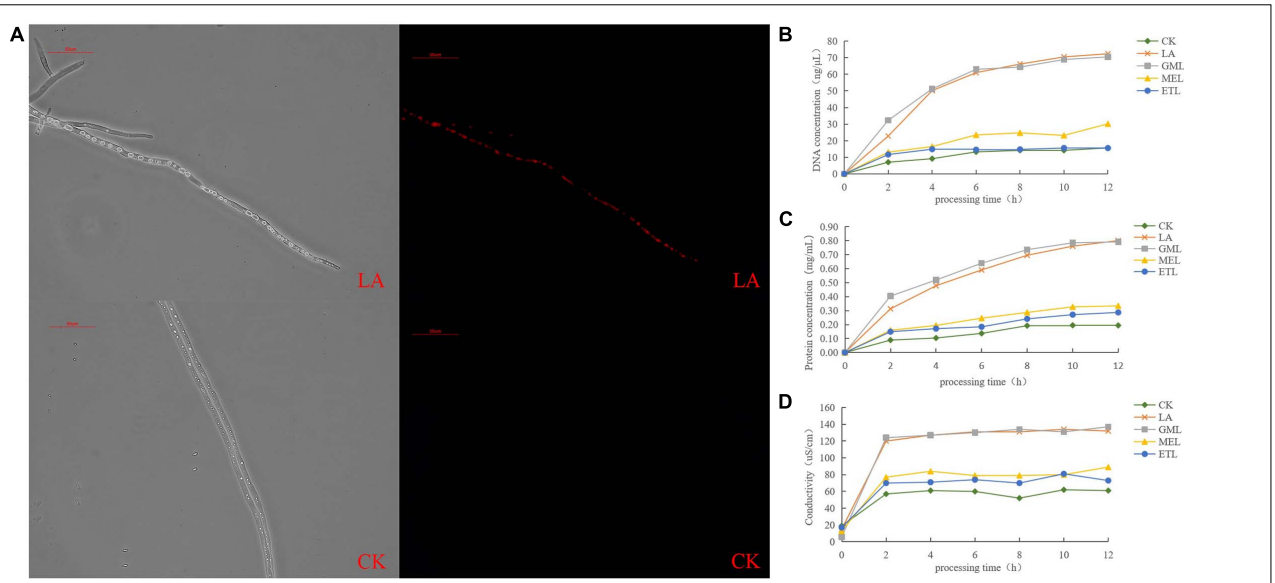

FIGURE 5 | Effect of LA on *P. sojae* cell membrane integrity. **(A)** *P. sojae* hyphae nuclei stained with propidium iodide (PI) after exposure to LA (upper image) or the same amount of water (lower image) and observed under a microscope. **(B)** Effects of LA and its derivatives, GML, MEL, or ETL, on DNA content. **(C)** Effects of LA GML, MEL, and ETL on protein content. **(D)** Effects of LA, GML, MEL, and ETL on solution conductivity. Means with different letters are significantly different (SPSS, $p < 0.05$).

soil before LA, and its derivatives, GML, MEL, or ETL, were added to the pots. Seeds of the *P. sojae*–susceptible soybean cultivar Williams (lacking *Rps* resistance genes) were sowed in the processed soil, and soybean height was measured after 5 days. Potted soybean plants grown in soil treated with LA or its derivatives had similar growth patterns than those in sterilized soil (CK2). However, most seedlings were killed by *P. sojae* in inoculated soil when plants were planted without LA, GML, MEL, or ETL treatments (CK1) (**Figure 6**).

DISCUSSION

Because of the expanding global population and the increasingly stringent environmental, toxicological, and regulatory requirements, plant pathogen control remains a constant need, and the products suitable for phytopathogen management are further limited. NPs are primary or secondary metabolites produced by living cells and have been an important source and template for the development of novel environmental-friendly agrochemicals. The metabolites synthesized in response to pathogen infection, such as leaf VOCs, have been particularly important and have functional benefits in multiple aspects of plant defense. Several VOCs are produced and emitted rapidly when plants respond to biotic stress, and such compounds require further exploration as leads for novel crop protection chemistry. VOCs tend to be chemically complex, and few are used directly for agricultural pathogen control. Nevertheless, it is technically possible to identify the effective constituents in VOCs and modify them as commercial products, transforming many NPs into agriculturally suitable molecules for pathogen control.

Here, we identified the components of soybean leaf volatiles produced in incompatible interactions and compatible interactions with *P. sojae* and found that LA was emitted specificity in a resistant cultivar. As previously reported, LA inhibits the mycelial growth of phytopathogenic fungi. Additionally, LA significantly reduces the *R. solani* and *P. ultimum* mycelial growth in agar culture at the concentration of 100 μm or greater, whereas no fungal growth occurred in liquid culture at concentrations greater than 50 μm (Walters et al., 2003). In this study, *P. sojae* mycelia growth was suppressed by LA, and the formation of zoosporangium was inhibited. This study provides the first report of the activity of LA against a *Phytophthora* pathogen and indicates the need for further research of its mechanism of action.

Lauric acid-treated mycelia grew disorderly, and the number of terminal branches increased significantly. Furthermore, the plasma membrane of *P. sojae* was disrupted or disintegrated by LA. MCFAs and monoglycerides are single-chain lipid amphiphiles that interact with phospholipid membranes as part of various biological activities. For example, they can have membrane-disruptive behavior against microbial pathogens on the human skin surface (Valle-González et al., 2018). LA has a minimum bactericidal concentration to *E. coli* at 1 mM (Kim and Rhee, 2013). Here, we found that LA can inhibit *P. sojae* growth at 0.5 mM, which means it has a greater effect on *Phytophthora* than on *E. coli*. Additionally, the concentration of cell substances, including DNA and protein, in water culture increased after LA treatment, and PI staining of the nucleus indicated that the *P. sojae* cell membrane was damaged.

It has been proposed that the hydrophilic and lipophilic characteristics of fatty acid derivatives affect their antibacterial activities according to their ability to incorporate into the

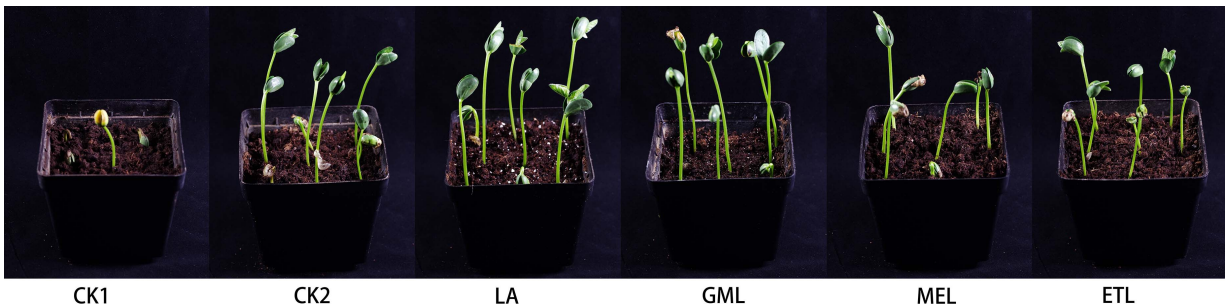

FIGURE 6 | Potted experiment of *P. sojae* control by LA and its derivatives. The soil was treated with LA, GML, MEL, or ETL. In CK1, no agent added to the soil. In CK2, no *P. sojae* mycelium was added to the soil. Plant height was measured 5 days after planting. The experiment was repeated three times with similar results. Means with different letters are significantly different (SPSS, $p < 0.05$).

bacterial cell membrane (Park et al., 2018; Valle-González et al., 2018). To verify this hypothesis, we selected three kinds of LA derivatives esterified with different non–fatty acid moieties and investigated whether the antibacterial activity from their precursor (i.e., LA) was retained or lost. GML had comparative bacteriostatic and bactericidal effects against *P. sojae* to LA, whereas MEL and ETL had weaker inhibitory activity. The antimicrobial properties of LA, GML, and their ester derivatives may be attributed to physicochemical processes and their interference with various cellular processes. GML is 200 times more effective than LA in bactericidal activity (Schlievert and Peterson, 2012), but, in this study, LA had similar effects to *P. sojae*, which suggests differences in the inhibitory mechanisms involved.

Glycerol monolaurate has a potent antimicrobial activity, and LA has the ability to convert into GML, which can destroy the lipid membrane of bacteria (Jin et al., 2021). The high levels of activity of capric and lauric acids, and particularly that of monocaprin, are notable and suggest that these lipids have specific antichlamydial activities (Bergsson et al., 1998). A recent study demonstrated that the potencies of saturated FAs increased sharply by lowering the pH, and a decrease of only 0.5 pH units could cause a change from non-lethal to lethal conditions. Conversely, the bactericidal action of GLM was not pH-dependent (Sun et al., 2003). That means GML is more environmentally stable and likely more suitable for crop protection.

As the main component of coconut oil and breast milk, LA is usually part of regular diets and feed additives, showing potent antimicrobial effects and lack of toxicity (Zeiger et al., 2017; Khan et al., 2020; Zhang et al., 2020). In the host security test, with concentrations lower than 0.3 g a.i./plant, both LA and GML could promote soybean growth; however, higher concentrations may negatively influence host growth.

None of the natural and eco-friendly chemical alternatives currently registered and available have the full spectrum of activity and versatility of methyl bromide as preplant soil fumigants (Duniway, 2002). Based on the results described here, LA and GML have potent antimicrobial effects and positive effects regulating plant growth. Hence, they may be promising substitutes for traditional anti-*Phytophthora* agents.

DATA AVAILABILITY STATEMENT

The original contributions presented in the study are included in the article/**Supplementary Material**, further inquiries can be directed to the corresponding authors.

AUTHOR CONTRIBUTIONS

QW and QX designed the experiments. CH, TG, and WG wrote the manuscript, performed the experiments, and analyzed the data. YW performed the GC–MS experiments and analyzed the data. QX, JW, and XT participated in manuscript revision or experiments. QW revised the manuscript and provided the funding for this research. All authors contributed to the article and approved the submitted version.

FUNDING

This work was supported by grants from the Key R&D projects in Shandong Province (2019GNC106060), Major Basic Research Program of the Shandong Natural Science Foundation 2019JZZY020608, National Natural Science Foundation of China (31972249), and National Key Research and Development Project of China (No. 2016YFD0100602).

ACKNOWLEDGMENTS

We thank the Phytohormone Analysis Platform, Agronomy College of SDAU, for providing technical support and suggestions for this work.

SUPPLEMENTARY MATERIAL

The Supplementary Material for this article can be found online at: https://www.frontiersin.org/articles/10.3389/fmicb.2021.666761/full#supplementary-material

REFERENCES

Bartolotta, S., Garcia, C. C., Candurra, N. A., and Damonte, E. B. (2001). Effect of fatty acids on arenavirus replication: inhibition of virus production by lauric acid. *Arch. Virol.* 146, 777–790. doi: 10.1007/s007050170146

Bergsson, G., Arnfinnsson, J., Karlsson, S. M., Steingrimsson, O., and Thormar, H. (1998). In vitro inactivation of Chlamydia trachomatis by fatty acids and monoglycerides. *Antimicrob. Agents Chemother.* 42, 2290–2294. doi: 10.1128/aac.42.9.2290

Bergsson, G., Arnfinnsson, J., Steingrimsson, O., and Thormar, H. (2001). In vitro killing of Candida albicans by fatty acids and monoglycerides. *Antimicrob. Agents Chemother.* 45, 3209–3212. doi: 10.1128/aac.45.11.3209-3212.2001

Cowan, M. (1999). Plant Products as Antimicrobial Agents. *Clin. Microbiol. Rev.* 12, 564–582. doi: 10.1128/cmr.12.4.564

Duniway, J. M. (2002). Status of Chemical Alternatives to Methyl Bromide for Pre-Plant Fumigation of Soil. *Phytopathology* 92, 1337–1343. doi: 10.1094/phyto.2002.92.12.1337

Erwin, D. C., and Ribeiro, O. K. (1996). *Phytophthora Diseases Worldwide*. USA: The American Phytopathological Society.

Fortuoso, B. F., Dos Reis, J. H., Gebert, R. R., Barreta, M., Griss, L. G., Casagrande, R. A., et al. (2019). Glycerol monolaurate in the diet of broiler chickens replacing conventional antimicrobials: impact on health, performance and meat quality. *Microb. Pathog.* 129, 161–167. doi: 10.1016/j.micpath.2019.02.005

Gessler, C., Pertot, I., and Perazzolli, M. (2011). Plasmopara viticola: a review of knowledge on downy mildew of grapevine and effective disease management. *Phytopathol. Mediterr.* 50, 3–44.

Jin, X., Zhou, J., Richey, G., Wang, M., Hong, S. M. C., and Hong, S. H. (2021). Undecanoic Acid, Lauric Acid, and N-Tridecanoic Acid Inhibit *Escherichia coli* Persistence and Biofilm Formation. *J. Microbiol. Biotechnol.* 31, 130–136. doi: 10.4014/jmb.2008.08027

Kabara, J. J., Swieczkowski, D. M., Conley, A. J., and Truant, J. P. (1972). Fatty acids and derivatives as antimicrobial agents. *Antimicrob. Agents Chemother.* 2, 23–28. doi: 10.1128/aac.2.1.23

Kamoun, S., Furzer, O., Jones, J. D., Judelson, H. S., Ali, G. S., Dalio, R. J., et al. (2015). The Top 10 oomycete pathogens in molecular plant pathology. *Mol. Plant Pathol.* 16, 413–434. doi: 10.1111/mpp.12190

Khan, H. U., Aamir, K., Sisinthy, S. P., Nagojappa, N. B. S., and Arya, A. (2020). Food additive "lauric acid" possess non-toxic profile on biochemical, haematological and histopathological studies in female Sprague Dawley (SD) rats. *PeerJ* 8:e8805. doi: 10.7717/peerj.8805

Kim, S. A., and Rhee, M. S. (2013). Marked synergistic bactericidal effects and mode of action of medium-chain fatty acids in combination with organic acids against *Escherichia coli* O157:H7. *Appl. Environ. Microbiol.* 79, 6552–6560. doi: 10.1128/aem.02164-13

Kishimoto, K., Matsui, K., Ozawa, R., and Takabayashi, J. (2008). Direct fungicidal activities of C6-aldehydes are important constituents for defense responses in Arabidopsis against Botrytis cinerea. *Phytochemistry* 69, 2127–2132. doi: 10.1016/j.phytochem.2008.04.023

Lalouckova, K., Skrivanova, E., Rondevaldova, J., Frankova, A., Soukup, J., and Kokoska, L. (2021). In vitro antagonistic inhibitory effects of palm seed crude oils and their main constituent, lauric acid, with oxacillin in Staphylococcus aureus. *Sci. Rep.* 11:177.

Liu, S., Ruan, W., Li, J., Xu, H., Wang, J., Gao, Y., et al. (2008). Biological control of phytopathogenic fungi by fatty acids. *Mycopathologia* 166, 93–102. doi: 10.1007/s11046-008-9124-1

Matsui, K. (2006). Green leaf volatiles: hydroperoxide lyase pathway of oxylipin metabolism. *Curr. Opin. Plant Biol.* 9, 274–280. doi: 10.1016/j.pbi.2006.03.002

Matsui, K., and Koeduka, T. (2016). Green Leaf Volatiles in Plant Signaling and Response. *Subcell. Biochem.* 86, 427–443. doi: 10.1007/978-3-319-25979-6_17

Mellon, J. E., Dowd, M. K., Beltz, S. B., and Moore, G. G. (2014). Growth inhibitory effects of gossypol and related compounds on fungal cotton root pathogens. *Lett. Appl. Microbiol.* 59, 161–168. doi: 10.1111/lam.12262

Park, K. M., Lee, S. J., Yu, H., Park, J. Y., Jung, H. S., Kim, K., et al. (2018). Hydrophilic and lipophilic characteristics of non-fatty acid moieties: significant factors affecting antibacterial activity of lauric acid esters. *Food Sci. Biotechnol.* 27, 401–409. doi: 10.1007/s10068-018-0353-x

Piotrowski, J. S., Okada, H., Lu, F., Li, S. C., Hinchman, L., Ranjan, A., et al. (2015). Plant-derived antifungal agent poacic acid targets beta-1,3-glucan. *Proc. Natl. Acad. Sci. U. S. A.* 112, E1490–E1497.

Randall, E., Young, V., Sierotzki, H., Scalliet, G., Birch, P. R., Cooke, D. E., et al. (2014). Sequence diversity in the large subunit of RNA polymerase I contributes to Mefenoxam insensitivity in Phytophthora infestans. *Mol. Plant Pathol.* 15, 664–676. doi: 10.1111/mpp.12124

Rouse, M. S., Rotger, M., Piper, K. E., Steckelberg, J. M., Scholz, M., Andrews, J., et al. (2005). In vitro and in vivo evaluations of the activities of lauric acid monoester formulations against Staphylococcus aureus. *Antimicrob. Agents Chemother.* 49, 3187–3191. doi: 10.1128/aac.49.8.3187-3191.2005

Scala, A., Allmann, S., Mirabella, R., Haring, M. A., and Schuurink, R. C. (2013). Green leaf volatiles: a plant's multifunctional weapon against herbivores and pathogens. *Int. J. Mol. Sci.* 14, 17781–17811. doi: 10.3390/ijms140917781

Schlievert, P. M., and Peterson, M. L. (2012). Glycerol monolaurate antibacterial activity in broth and biofilm cultures. *PLoS One* 7:e40350. doi: 10.1371/journal.pone.0040350

Schnee, S., Queiroz, E. F., Voinesco, F., Marcourt, L., Dubuis, P. H., Wolfender, J. L., et al. (2013). Vitis vinifera canes, a new source of antifungal compounds against Plasmopara viticola, Erysiphe necator, and Botrytis cinerea. *J. Agric. Food Chem.* 61, 5459–5467. doi: 10.1021/jf4010252

Shilling, M., Matt, L., Rubin, E., Visitacion, M. P., Haller, N. A., Grey, S. F., et al. (2013). Antimicrobial effects of virgin coconut oil and its medium-chain fatty acids on Clostridium difficile. *J. Med. Food* 16, 1079–1085. doi: 10.1089/jmf.2012.0303

Sun, C. Q., O'Connor, C. J., and Roberton, A. M. (2003). Antibacterial actions of fatty acids and monoglycerides against *Helicobacter* pylori. *FEMS Immunol. Med. Microbiol.* 36, 9–17. doi: 10.1016/s0928-8244(03)00008-7

Suthiwong, J., Sriphana, U., Thongsri, Y., Promsuwan, P., Prariyachatigul, C., and Yenjai, C. (2014). Coumarinoids from the fruits of Micromelum falcatum. *Fitoterapia* 94, 134–141. doi: 10.1016/j.fitote.2014.02.004

Tanaka, T., Ikeda, A., Shiojiri, K., Ozawa, R., Shiki, K., Nagai-Kunihiro, N., et al. (2018). Identification of a Hexenal Reductase That Modulates the Composition of Green Leaf Volatiles. *Plant Physiol.* 178, 552–564. doi: 10.1104/pp.18.00632

Tu, Y. (2011). The discovery of artemisinin (qinghaosu) and gifts from Chinese medicine. *Nat. Med.* 17, 1217–1220. doi: 10.1038/nm.2471

Tyler, B. M. (2001). Genetics and genomics of the oomycete-host interface. *Trends Genet.* 17, 611–614. doi: 10.1016/s0168-9525(01)02517-3

Tyler, B. M. (2007). Phytophthora sojae: root rot pathogen of soybean and model oomycete. *Mol. Plant Pathol.* 8, 1–8. doi: 10.1111/j.1364-3703.2006.00373.x

Valle-González, E. R., Jackman, J. A., Yoon, B. K., Park, S., Sut, T. N., and Cho, N. J. (2018). Characterizing how acidic pH conditions affect the membrane-disruptive activities of lauric acid and glycerol monolaurate. *Langmuir* 34, 13745–13753. doi: 10.1021/acs.langmuir.8b02536

Walters, D. R., Walker, R. L., and Walker, K. C. (2003). Lauric Acid Exhibits Antifungal Activity Against Plant Pathogenic Fungi. *J. Phytopathol.* 151, 228–230. doi: 10.1046/j.1439-0434.2003.00713.x

Wang, X., Wang, S., Yi, J., Li, Y., Liu, J., Wang, J., et al. (2020). Three Host Plant Volatiles, Hexanal, Lauric Acid, and Tetradecane, are Detected by an Antenna-Biased Expressed Odorant Receptor 27 in the Dark Black Chafer Holotrichia parallela. *J. Agric. Food Chem.* 68, 7316–7323. doi: 10.1021/acs.jafc.0c00333

Wang, Y., Sun, Y., Zhang, Y., Zhang, X., and Feng, J. (2016). Antifungal activity and biochemical response of cuminic acid against phytophthora capsici leonian. *Molecules* 21:756. doi: 10.3390/molecules21060756

Yang, D., Pornpattananangkul, D., Nakatsuji, T., Chan, M., Carson, D., Huang, C. M., et al. (2009). The antimicrobial activity of liposomal lauric acids against Propionibacterium acnes. *Biomaterials* 30, 6035–6040. doi: 10.1016/j.biomaterials.2009.07.033

Yang, H.-T., Chen, J.-W., Rathod, J., Jiang, Y.-Z., Tsai, P.-J., Hung, Y.-P., et al. (2018). Lauric Acid Is an Inhibitor of Clostridium difficile Growth in Vitro and Reduces Inflammation in a Mouse Infection Model. *Front. Microbiol.* 8:2635. doi: 10.3389/fmicb.2017.02635

Yutin, N., Makarova, K. S., Mekhedov, S. L., Wolf, Y. I., and Koonin, E. V. (2008). The deep archaeal roots of eukaryotes. *Mol. Biol. Evol.* 25, 1619–1630. doi: 10.1093/molbev/msn108

Zeiger, K., Popp, J., Becker, A., Hankel, J., Visscher, C., Klein, G., et al. (2017). Lauric acid as feed additive - An approach to reducing Campylobacter spp. in broiler meat. *PLoS One* 12:e0175693. doi: 10.1371/journal.pone.0175693

Zhang, S., Xiong, J., Lou, W., Ning, Z., Zhang, D., and Yang, J. (2020). Antifungal Effect of Triglycerol Monolaurate Synthesized by Lipozyme 435-Mediated Esterification. *J. Microbiol. Biotechnol.* 30, 561–570. doi: 10.4014/jmb.1910.10043

Conflict of Interest: YW was employed by company Shimadzu (China) Co., Ltd.

The remaining authors declare that the research was conducted in the absence of any commercial or financial relationships that could be construed as a potential conflict of interest.

Publisher's Note: All claims expressed in this article are solely those of the authors and do not necessarily represent those of their affiliated organizations, or those of the publisher, the editors and the reviewers. Any product that may be evaluated in this article, or claim that may be made by its manufacturer, is not guaranteed or endorsed by the publisher.

frontiers in Microbiology

ORIGINAL RESEARCH
published: 20 August 2021
doi: 10.3389/fmicb.2021.652062

Species Diversity and Chemotypes of *Fusarium* Species Associated With Maize Stalk Rot in Yunnan Province of Southwest China

Kaifei Xi[1,2†], Liuying Shan[1,2†], Yini Yang[3], Guoqing Zhang[4], Jun Zhang[1,2] and Wei Guo[1,2]*

[1]*Institute of Food Science and Technology, Chinese Academy of Agricultural Sciences, Beijing, China,* [2]*Key Laboratory of Agro-Products Quality and Safety Control in Storage and Transport Process, Ministry of Agriculture and Rural Affairs, Beijing, China,* [3]*The Central Agricultural Broadcasting and Television School, Beijing, China,* [4]*General Office of the Ministry of Agriculture and Rural Affairs, Beijing, China*

Maize stalk rot caused by *Fusarium* species is one of the most important fungal diseases of maize throughout the world. The disease is responsible for considerable yield losses and has also been associated with mycotoxin contamination of the crop. In this study, a survey of maize stalk rot was performed in seven locations of Yunnan Province in China during the cropping season of 2015 and 2016. Based on morphological and molecular characteristics, 204 isolates belonging to 12 *Fusarium* spp. from symptomatic stalks of maize were identified. Among the isolated strains, 83 were identified as *Fusarium meridionale* (40.5%), 46 as *Fusarium boothii* (22.5%), 34 as *Fusarium temperatum* (16.5%), 12 as *Fusarium equiseti* (5.9%), 10 as *Fusarium asiaticum* (4.9%), six as *Fusarium proliferatum* (3.0%), four as *Fusarium verticillioides* (2.0%), four as *Fusarium incarnatum* (2.0%), two as *Fusarium avenaceum* (1.0%), one as *Fusarium cerealis* (0.5%), one as *Fusarium graminearum* (0.5%), and one as *Fusarium cortaderiae* (0.5%). *Fusarium cortaderiae* was the first report on the causal agent of maize stalk rot disease in China. These isolates were divided into five chemotypes: nivalenol (NIV), deoxynivalenol (DON), beauvericin (BEA), zearalenone (ZEN), and fumonisin (FUM). Phylogenetic analysis based on partial sequences of the translation elongation factor 1α (*TEF1*-α) showed a high degree of interspecific polymorphisms among the isolates. Pathogenicity analysis on maize stalks indicated that all the 12 species of *Fusarium* were able to cause the disease symptoms with different aggressiveness. This study on population, pathogenicity, and toxigenic chemotypes of *Fusarium* species associated with maize stalk rot in Yunnan Province of southwest China, will help design an effective integrated control strategy for this disease.

Keywords: maize stalk rot, *Fusarium* spp., diversity, pathogenicity, chemotypes

OPEN ACCESS

Edited by:
Yong Wang,
Guizhou University, China

Reviewed by:
Hai-Lei Wei,
Institute of Agricultural Resources and Regional Planning, Chinese Academy of Agricultural Sciences (CAAS), China
Muhammad Inam Ul Haq,
Pir Mehr Ali Shah Arid Agriculture University, Pakistan
Yun Chen,
Zhejiang University, China

***Correspondence:**
Wei Guo
guowei01@caas.cn

†These authors have contributed equally to this work

Specialty section:
This article was submitted to Microbe and Virus Interactions With Plants, a section of the journal Frontiers in Microbiology

Received: *11 January 2021*
Accepted: *21 July 2021*
Published: *20 August 2021*

Citation:
Xi K, Shan L, Yang Y, Zhang G, Zhang J and Guo W (2021) Species Diversity and Chemotypes of Fusarium Species Associated With Maize Stalk Rot in Yunnan Province of Southwest China. Front. Microbiol. 12:652062. doi: 10.3389/fmicb.2021.652062

INTRODUCTION

In the Yunnan Province of southwest China, maize plays a crucial role in local agricultural production. In this region, the maize crop's yield and quality are particularly affected by stalk rot diseases caused by *Fusarium* species. *Fusarium* is an important plant pathogenic fungus with a wide range of hosts, including corn, wheat, rice, and other cereal crops (Boutigny et al., 2011). These pathogens cause ear and stalk rot disease, potentially damaging to crop yield and food safety. Different *Fusarium* species can produce toxic chemicals known as mycotoxins, which can be an important risk to both animal and human health if accumulated to an unsafe level (Sampietro et al., 2012; Kuhnem et al., 2016).

Fusarium genus has numerous species, which are morphologically indistinguishable, so they are very difficult to identify at the species level (Thomas et al., 2019). *Fusarium graminearum* species complex (FGSC) has been divided into biogeographically distinct lineages consisting of at least 16 species. Members of the FGSC are also classified into the broader *Fusarium sambucinum* species complex (FSAMSC; Starkey et al., 2007; O'Donnell et al., 2008, 2013; Sarver et al., 2011). Various members of FGSC show different geographic distribution and host preferences (Lee et al., 2015). Among different species in FGSC, *F. graminearum* is considered as an important pathogen of maize (Moreno-González et al., 2004). Earlier studies have reported that *F. graminearum* could cause seedling blight and root rot (Du et al., 1997; Munkvold and O'Mara, 2002). However, a previous study reported the presence of *Fusarium culmorum*, *Fusarium solani*, *Fusarium semitectum*, *Fusarium verticillioides*, and *F. graminearum* from the lodged maize plants (Ares et al., 2004). Another study showed that *F. graminearum* was the most aggressive strain during pathogenicity tests on maize (Lamprecht et al., 2011). In addition, *F. graminearum* is a dominant pathogen associated with *Fusarium* head blight (FHB) in North America and Europe (O'Donnell et al., 2004; Starkey et al., 2007), whereas *Fusarium asiaticum* has been found as a major species in Asia (Qiu et al., 2014). *Fusarium graminearum* is often found on wheat, but *Fusarium boothii* and *Fusarium meridionale* are frequent pathogens of maize, and *Fusarium asiaticum* is commonly reported from rice (Maier et al., 2006). Besides, *F. verticillioides* is one of the most common pathogens causing ear and stalk rot in maize. This species is widespread in areas with relatively warm and dry weather (Czembor et al., 2019), including the European and the Kansas state of the United States. In China, many *Fusarium* species are associated with ear and stalk rot diseases of maize, which resulted in significant yield losses and mycotoxin contamination problems. In China, the notable *Fusarium* species isolated from maize are *F. verticillioides*, *F. graminearum*, *F. meridionale*, and *Fusarium temperatum* (Duan et al., 2016). *Fusarium temperatum* is also an important maize pathogen and described as a new species causing disease in maize crop (Scauflaire et al., 2011). These pathogens can produce different toxigenic chemotypes, demonstrating the tremendous potential of this species for mycotoxin contamination (Duan et al., 2016). Moreover, isolates of *F. asiaticum*, isolated from head blight infected wheat plants produced 3A-deoxynivalenol (DON) or nivalenol (NIV). It was also showed that the isolates producing different mycotoxins also have differences in growth rate, pathogenicity, conidial length, fecundity, trichothecene accumulation and showed a varying degree of resistance to benzimidazole (Zhang et al., 2012). Although, many *Fusarium* species have been reported to responsible for maize ear and stalk rot disease in China, no detailed studies have been done in Yunnan Province based on composition, pathogenicity, and toxigenic chemotypes.

As the largest grain crop in Yunnan Province, maize is distributed throughout the province. Yunnan has diverse environmental conditions and topography, where the maize planted in areas have temperature ranging from 9 to 30°C and altitude ranging from 700 to 2,400 m. So, climatic conditions, soil type, water availability, farming system, and planting habits vary significantly throughout the province. Besides, different maize varieties planted in different parts of Yunnan have various growth characteristics, and the yield also varies considerably among the different areas of the province. In this study, diseased stalks of maize were collected from seven locations of Yunnan Province during the cropping season of 2015 and 2016. The study aimed to determine species diversity, pathogenicity, and toxigenic chemotypes of the *Fusarium* species causing maize stalk rot in Yunnan Province to design an effective integrated control strategy for this disease.

MATERIALS AND METHODS

Fungal Isolation, Purification, and Morphological Characterization

Stalks of maize showing typical rot symptoms were collected from seven maize-planting locations in Yunnan Province of China during the cropping season of 2015 and 2016 (**Figure 1**). The diseased samples were cut into small pieces (approximately 5 mm^2) and soaked in 75% ethanol for 2 min. Subsequently, washed three times with sterile water and dried using autoclaved tissue towels. Later, the samples were placed onto potato dextrose agar (PDA) plates, which were supplemented with streptomycin sulfate (150 μg/ml) and kanamycin (150 μg/ml). The PDA plates were incubated at 25°C for 2–3 days in darkness. Fungal colonies showing various morphological features were selected. Fungal isolates were grown on PDA after single spore purification by following the procedure described by Xi et al. (2019). Morphological features of the fungal isolates were observed on PDA and carnation leaf agar (CLA). The appearance of the fungal colonies was recorded after the mycelium fully covered the whole PDA plate. Six *Fusarium* species including *Fusarium avenaceum*, *Fusarium cerealis*, *Fusarium equiseti*, *F. graminearum*, *F. proliferatum*, and *F. verticillioides* were confirmed by following the details mentioned in The *Fusarium* Laboratory Manual (Leslie and Summerell, 2006). For the identification of the other six species such as *F. meridionale*, *F. boothii*, *F. temperatum*, *F. asiaticum*, *Fusarium incarnatum*, and *Fusarium cortaderiae*, recently published materials were followed (Lamprecht et al., 2011; Scauflaire et al., 2011;

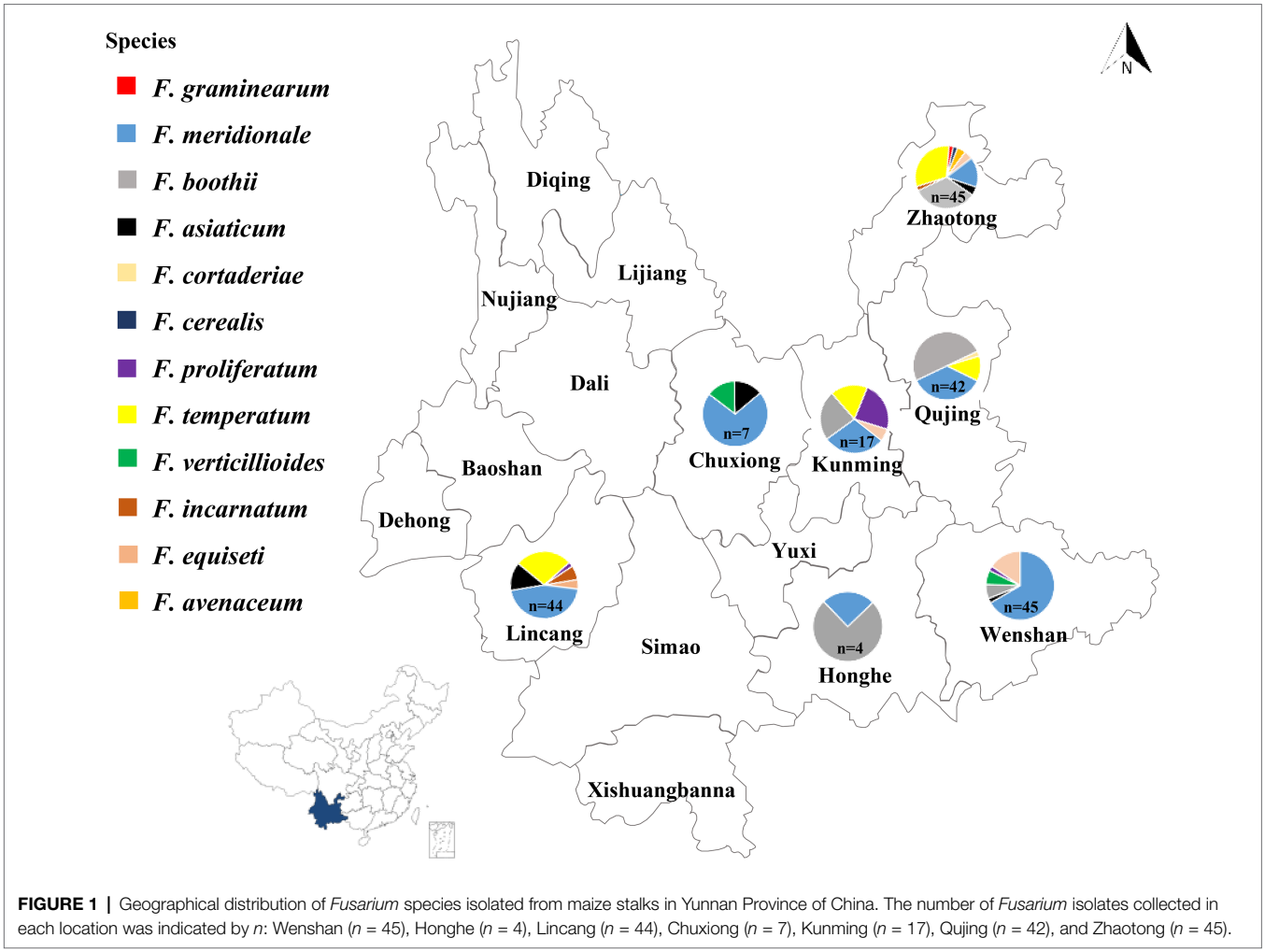

FIGURE 1 | Geographical distribution of *Fusarium* species isolated from maize stalks in Yunnan Province of China. The number of *Fusarium* isolates collected in each location was indicated by *n*: Wenshan (*n* = 45), Honghe (*n* = 4), Lincang (*n* = 44), Chuxiong (*n* = 7), Kunming (*n* = 17), Qujing (*n* = 42), and Zhaotong (*n* = 45).

Castañares et al., 2016; Walkowiak et al., 2016; Avila et al., 2019). The size of microconidia and macroconidia were taken as average from 50 measurements of each isolate.

Species and Chemotype Determination

About 10 mm mycelial plugs from the colony's edge were inoculated to CM liquid medium and incubated in a shaker without light (175 rpm, 25°C) for 5 days. After incubation, the mycelia were collected by centrifugation (4,000 rpm, 5 min) and stored at −80°C until the subsequent use. Total DNA was extracted using a ZR fungal DNA Kit (ZYMO Research, United States) by following the manufacturer's instruction and stored at −20°C until the subsequent use. Sequences of the translation elongation factor 1α (*TEF-1α*) from each isolate were amplified using primers EF-1 (5'-ATGGGTAAGGARGACAAGAC-3'), and EF-2 (5'-GGARGTACCAGTSATCATGTT-3'; Geiser et al., 2004). The resulted sequences were compared with the NCBI database[1] and *Fusarium* database (FUSARIUM-ID v.1.0 database)[2] for species determination.

To identify each isolate's chemotypes, six specific mycotoxin-producing genes were amplified by PCR using specific primers as previous described (Ward et al., 2002; Jennings et al., 2004; Kulik et al., 2007; Meng et al., 2010; Duan et al., 2016). The sequence of primers used to amplify these genes has been mentioned in **Supplementary Table S1**. The PCR was done in a 20 μl reaction mixtures including 1 μl of template DNA, 10 μl of 2× DreamTaq PCR Mix (Thermo Fisher Scientific, United States), 7 μl of sterile water, and 1 μl of each primer (10 μM). Amplification reactions were carried out in a C1000 Touch thermal cycler (Applied Biosystems, BIO-RAD, United States).

Phylogenetic Analysis of the *TEF-1α* Gene Sequence Data

The *TEF1-α* gene always appeared to have a single copy in *Fusarium* and showed high levels of sequence polymorphism in closely related species (Geiser et al., 2004). All of the

[1]https://www.ncbi.nlm.nih.gov/

[2]http://isolate.fusariumdb.org/blast.php

sequences (n = 204) were aligned online using the MAFFT alignment program (Katoh and Standley, 2013). Alignments were adjusted manually using Clustal X (Thompson et al., 1994). A phylogenetic tree from multiple alignments of the 204 sequences was constructed using the neighbor-joining method calculated with MEGA X (Sudhir et al., 2018). The Interactive Tree of Life[3] was used to beautify the phylogenetic tree. Clade support was inferred from 1,000 bootstrap replicates.

Pathogenicity Tests on Maize Stalks

B73 maize plants were inoculated at the 10-leaves stage by punching a hole in the stalk at the second or third internode above the soil line using a sterile toothpick. Then 20 μl conidia suspension was injected from representative isolates at a concentration of 10^6/ml. Mock-inoculated maize stalks were treated with sterilized water. The inoculation site was wrapped using a piece of sterilized gauze to conserve moisture and avoid any contamination. Each representative isolate and control were inoculated on three plants. After 7 days post-inoculation (dpi), the stalks of inoculated plants were split along the longitudinal direction for symptom measurements. The longitudinal brown infected areas were measured as the necrosis area to calculate each identified *Fusarium* species' virulence using ImageJ software (Zhang et al., 2016).

RESULTS

Isolation and Morphological Identification of *Fusarium* Species

Based on the morphological and molecular characteristics, 204 isolates were identified from seven major maize producing regions of Yunnan Province (**Figure 1**). Twelve *Fusarium* species were found including, 83 isolates as *F. meridionale* (40.5%), 46 isolates were *F. boothii* (22.5%), 34 isolates identified as *F. temperatum* (16.5%), 12 as *F. equiseti* (5.9%), 10 isolates were *F. asiaticum* (4.9%), six were *F. proliferatum* (3.0%), four as *F. verticillioides* (2.0%), four as *F. incarnatum* (2.0%), two as *F. avenaceum* (1.0%), one as *F. cerealis* (0.5%), one as *F. graminearum* (0.5%), and one as *F. cortaderiae* (0.5%; **Figure 1**).

All of the 12 species showed typical *Fusarium* morphological characteristics, which were consistent with the previous reports. *Fusarium graminearum*, *F. meridionale*, *F. boothii*, *F. asiaticum*, *F. cortaderiae*, and *F. cerealis* belonged to the FSAMSC and shared similar morphological characteristics. They had woolly aerial hyphae and formed red pigment in the PDA plates. At later stages, yellow hyphae were produced in the center of the colony, and the bottom of the plates became dark-red to black-red (**Figures 2A–F**). Mycelial growth rates of the members of FSAMSC were faster than the other six *Fusarium* species, and the *F. graminearum* showed the fastest growth rate. All members of this complex produced macroconidia, but no microconidia were observed. Macroconidia were curved at the base and apex and usually contained three or five septa. The average sizes of macroconidia (N = 50) were 35.9–72.7 μm long × 3.6–5.6 μm wide, 32.5–68.6 μm long × 2.2–4.4 μm wide, 33.8–61.2 μm long × 2.0–4.0 μm wide, 37.3–69.7 μm long × 2.7–5.3 μm wide, 31.7–66.3 μm long × 3.5–5.5 μm wide, and 25.8–55.9 μm long × 3.0–7.0 μm wide for *F. graminearum*, *F. meridionale*, *F. boothii*, *F. asiaticum*, *F. cortaderiae*, and *F. cerealis*, respectively (**Figure 2**; **Supplementary Table S2**).

Fusarium proliferatum, *F. temperatum*, and *F. verticillioides* belonged to *Fusarium fujikuroi* species complex (FFSC) and shared similar morphological characteristics (**Figures 2G–I**). They had woolly aerial hyphae, and the colonies showed spider-web like arrangement but produced different pigments. *Fusarium proliferatum* was white or light purple in the early stages. Later, it became dark purple or grayish purple (**Figure 2G**). *Fusarium temperatum* was light orange at the start of the growth. It later became dark purple (**Figure 2H**). *Fusarium verticillioides* was initially white or light purple. At the later stages, it became dark purple (**Figure 2I**). Compared to the species of FSAMSC, mycelial growth rates of *F. proliferatum*, *F. temperatum*, and *F. verticillioides* were slow. They could produce macroconidia and microconidia on CLA. The macroconidia of *F. proliferatum* were sickle-shaped, straight, and slender, 3–5 septa, and 35.5–55.5 μm long × 2.5–4.5 μm wide (**Figure 2G**). The microconidia of *F. proliferatum* were ovate or mallet, usually aseptate, concentric or pseudo cephalic, and 5.0–16.7 μm long × 1.8–3.5 μm wide. The macroconidia of *F. temperatum* were slender, mainly possessed four septa, and 26.0–67.5 μm long × 3.6–5.0 μm wide (**Figure 2H**). The microconidia of *F. temperatum* were long elliptic, pseudo cephalic, 0–1 septum, and 5.5–16.5 μm long × 2.0–4.0 μm wide. The macroconidia of *F. verticillioides* were sickle-shaped, straight, and slender, 3–5 septa, and 30.4–52.3 μm long × 2.6–4.0 μm wide (**Figure 2I**). The microconidia of *F. verticillioides* were clubbed shaped, 0–1 septum, and were 4.4–11.1 μm long × 1.5–3.7 μm wide.

Fusarium incarnatum and *F. equiseti* belonged to *Fusarium incarnatum-equiseti* species complex (FIESC) and exhibited similar morphology. Colony appearance of *F. incarnatum* and *F. equiseti* was abundant mycelium that initially white but became yellowish-brown with age (**Figures 2J,K**). *Fusarium incarnatum* produces straight to slightly curved macroconidia without obvious foot-shaped base cells (**Figure 2J**). The species also produces abundant microconidia. There was no apparent boundary between macroconidia and microconidia of *F. incarnatum*, possessed 3–5 septa, 27.5–40.5 μm long × 3.5–5.5 μm wide (**Figure 2J**). However, *F. equiseti* only produces macroconidia. The macroconidia of *F. equiseti* were sickle-shaped, slender, and curved, apical cells slender and a prominent heel, generally 3–6 septa, and 35.5–60.0 μm long × 3.0–5.0 μm wide (**Figure 2K**). *Fusarium avenaceum* belonged to *Fusarium tricinctum* species complex (FTSC). On PDA plates, aerial mycelia were compact and woolly, having white to light yellow color with central spore mass pale orange to brown and the colony reverse was carmine (**Figure 2L**). The macroconidia of *F. avenaceum* were slender and straight,

[3]https://itol.embl.de

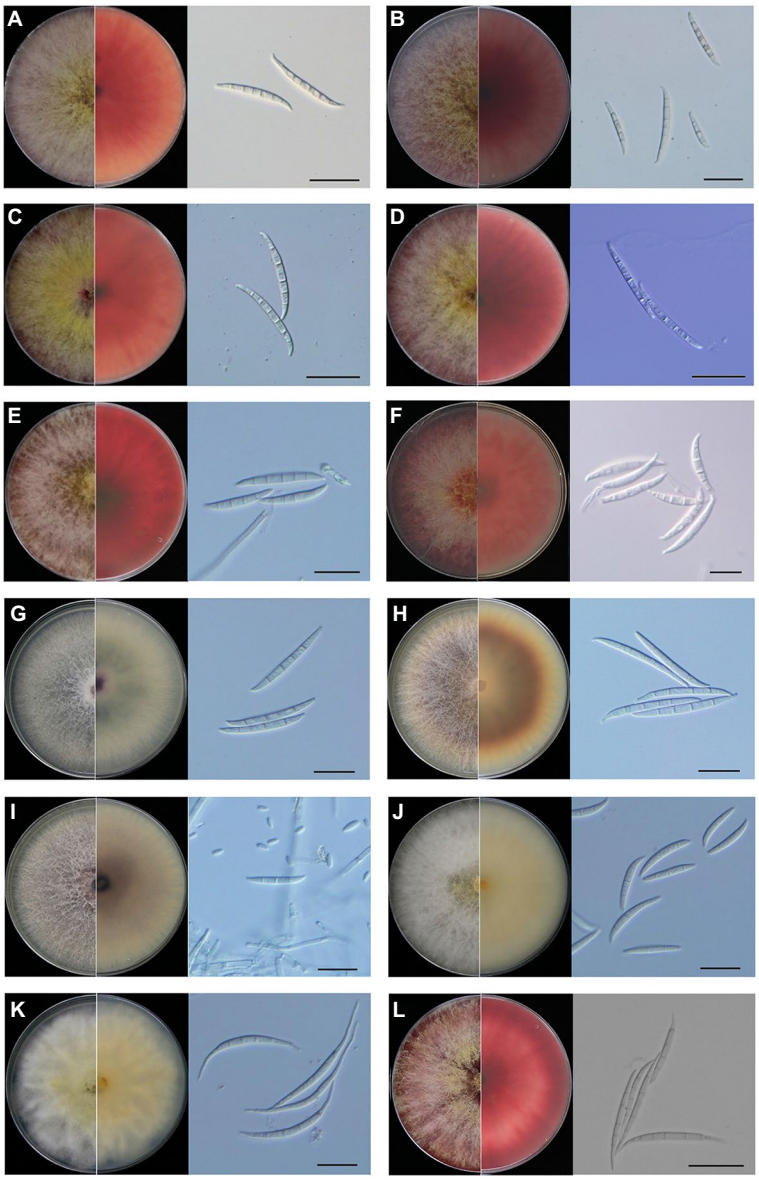

FIGURE 2 | Morphological characteristics of *Fusarium* species isolated from maize stalk rot disease in Yunnan Province, China. Typical colonies of the representative *Fusarium* isolates were observed on potato dextrose agar (PDA) plates at 5 days post-inoculation (dpi). Microscopic features of macroconidia of each *Fusarium* species. **(A)** *Fusarium graminearum*, **(B)** *Fusarium meridionale*, **(C)** *Fusarium boothii*, **(D)** *Fusarium asiaticum*, **(E)** *Fusarium cortaderiae*, **(F)** *Fusarium cerealis*, **(G)** *Fusarium proliferatum*, **(H)** *Fusarium temperatum*, **(I)** *Fusarium verticillioides*, **(J)** *Fusarium incarnatum*, **(K)** *Fusarium equiseti*, and **(L)** *Fusarium avenaceum*. Scale bar = 20 μm.

linear, 4–6 septa, and 45.5–65.5 μm long × 3.5–4.5 μm wide (**Figure 2L**). Microconidia were fusoid, 1–2 septa, and ranged from 13.4–24.6 μm long × 2.6–4.8 μm wide. The morphological details of the colony, macroconidia and microconidia of these *Fusarium* species and the growth diameter of each *Fusarium* colony on PDA plates after 3 days has also been shown in **Supplementary Table S2**.

Analysis of Toxigenic Chemotypes

In FGSC, the *Tri* genes cluster is responsible for the production of different types of toxins. Three primers based on *Tri3*, *Tri7*, and *Tri8* intergenic sequences, Tri315F/R, nivPF/R, and MinusTri7F/R, were used to amplify specific 15-AcDON fragments of 864 bp, NIV fragments of 450 bp, and 3-AcDON fragments of 483 bp, respectively. Similarly, the *FUM1* gene was used to detect the Fumonisins (FBs) with a fragment of 750 bp. Whereas the *esyn1* gene was used to detect the beauvericin (BEA) with a fragment of 600 bp. Also, the PKS4 gene was used to detect the zearalenone (ZEN) with a fragment of 280 bp.

The PCR amplification results showed that all of the 12 *Fusarium* species can synthesize mycotoxins and the

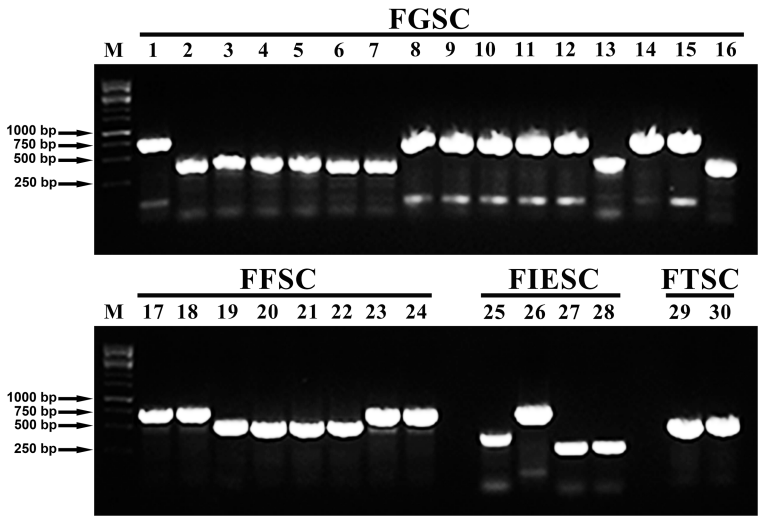

FIGURE 3 | Visualization of PCR-based chemotype analysis from all of the 12 *Fusarium* species using representative isolates. Lane M: Marker; Lanes 1: detection of 15Ac-deoxynivalenol (DON) chemotypes produced by the *F. graminearum* isolate (YNF16-37); Lanes 2–7: detection of nivalenol (NIV) chemotypes produced by *F. meridionale* isolates (YNF15-50, YNF15-21, YNF15-78, YNF15-29, YNF16-19, and YNF16-55); Lanes 8–12: detection of 15Ac-DON chemotypes produced by *F. boothii* isolates (YNF15-23, YNF15-40, YNF16-17, YNF16-68, and YNF16-113); Lanes 13: detection of NIV chemotypes produced by the *Fusarium asiaticum* isolate (YNF15-56); Lanes 14: detection of 15Ac-DON chemotypes produced by the *F. asiaticum* isolate (YNF15-59); Lanes 15: detection of 15Ac-DON chemotypes produced by the *Fusarium cortaderiae* isolate (YNF16-101); Lanes 16: detection of NIV chemotypes produced by the *F. cerealis* isolate (YNF16-22); Lanes 17–18: detection of fumonisin (FUM) chemotypes produced by *F. proliferatum* isolates (YNF15-10 and YNF16-118); Lanes 19–22: detection of beauvericin (BEA) chemotypes produced by *F. temperatum* isolates (YNF15-67, YNF16-04, YNF16-77, and YNF16-116); Lanes 23–24: detection of FUM chemotypes produced by *F. verticillioides* isolates (YNF15-04 and YNF15-98); Lanes 25: detection of 3Ac-DON chemotypes produced by the *F. incarnatum* isolate (YNF15-87); Lanes 26: detection of 15Ac-DON chemotypes produced by the *F. incarnatum* isolate (YNF15-93); Lanes 27–28: detection of zearalenone (ZEN) chemotypes produced by *F. equiseti* isolates (YNF15-01 and YNF15-64); Lanes 29–30: detection of BEA chemotypes produced by *F. avenaceum* isolates (YNF16-15 and YNF16-14).

amplification results of the representative isolates were shown in **Figure 3**. Among all of 204 isolates, 53 isolates produced the DON chemotype, 93 isolates had the NIV chemotype, 10 isolates potentially produced FB1, 12 isolates had ZEN chemotype, and 36 isolates potentially produced BEA. Interestingly, all of *F. cerealis* and *F. meridionale* isolates produced the NIV chemotype. Similarly, the chemotypes of *F. boothii*, *F. cortaderiae*, *F. incarnatum*, and *F. graminearum* were categorized as the DON chemotype. Among the DON-producing isolates, all of *F. boothii*, *F. cortaderiae*, and *F. graminearum* isolates potentially produced 15-AcDON. However, one *F. incarnatum* isolate possessed the 15-AcDON chemotypes, the other three isolates represented the 3-AcDON chemotype. Conversely, all *F. equiseti* isolates were the ZEN chemotype, although *F. incarnatum* and *F. equiseti* belonged to the same species complexes. Also, most of *F. asiaticum* isolates mainly belonged to the NIV chemotype, and only one was categorized as the 15-AcDON chemotype. All of the isolates of *F. verticillioides* and *F. proliferatum* were the fumonisin chemotype. However, all of *F. temperatum* isolates like *F. avenaceum* isolates were the BEA chemotype (**Table 1**).

Phylogenetic Analysis Based on the Partial *TEF-1α* Sequences

For phylogenetic analysis, a neighbor-joining tree was constructed using the partial *TEF-1α* gene sequences, including all isolates in this study (**Figure 4**). The GenBank accession numbers for the *TEF-1α* gene sequences of all the 204 strains are listed in **Supplementary Table S3**. The phylogenetic analysis showed that isolates of *F. graminearum*, *F. meridionale*, *F. boothii*, *F. asiaticum*, *F. cortaderiae*, and *F. cerealis* belonging to the FSAMSC were clustered into one big branch. It is worth noting that the isolates of *F. asiaticum*, *F. boothii*, *F. cortaderiae*, *F. graminearum*, and *F. meridional* showed a closer phylogenetic relationship compared to the isolate of *F. cerealis* because these isolates belonged to the FGSC, which is a part of FSAMSC. The isolates of *F. proliferatum*, *F. temperatum*, and *F. verticillioides* formed an independent branch in the phylogenetic tree owing to these isolates belonging to the FFSC. Similarly, isolates of *F. incarnatum* and *F. equiseti* formed an independent branch because of these isolates belonging to the FIESC. Likewise, isolates of *F. avenaceum* classified into FTSC showed another independent branch in the tree (**Figure 4**). These results indicated that isolates of *Fusarium* species showed a high degree of interspecific polymorphisms variation and was unrelated to geographic distribution.

Pathogenicity Tests on Maize Stalks

To test the pathogenicity of the 12 isolated *Fusarium* species, the stalks of B73 maize plants at the 10-leaf stage were inoculated with each representative fungal species. The symptoms and severity of the disease were recorded at the 7 dpi. The results showed that all of the *Fusarium* species are pathogenic to maize stalks and showed distinct discoloration

of internal stalk tissues around the inoculation site (**Figure 5A**). The longitudinal brown infected areas of maize stalks were measured to evaluate the virulence of each identified *Fusarium* species (**Figure 5B**). The results indicated that isolates of *F. meridionale* are the most aggressive among all of the isolates. Pathogenicity of these isolates was confirmed by reisolating the fungus from symptomatic tissues but not from the control plants.

TABLE 1 | Chemotypes of *Fusarium* species identified in this study.

Species	Percentage (%)	Number	Toxigenic chemotypes				
			NIV	DON	BEA	FUM	ZEN
Fusarium asiaticum	5	10	9	1	0	0	0
Fusarium boothii	22.5	46	0	46	0	0	0
Fusarium cortaderiae	0.5	1	0	1	0	0	0
Fusarium graminearum	0.5	1	0	1	0	0	0
Fusarium meridionale	40.5	83	83	0	0	0	0
Fusarium cerealis	0.5	1	1	0	0	0	0
Fusarium verticillioides	2	4	0	0	0	4	0
Fusarium proliferatum	3	6	0	0	0	6	0
Fusarium temperatum	16.5	34	0	0	34	0	0
Fusarium equiseti	6	12	0	0	0	0	12
Fusarium incarnatum	2	4	0	4	0	0	0
Fusarium avenaceum	1	2	0	0	2	0	0
Total	100	204	93	53	36	10	12

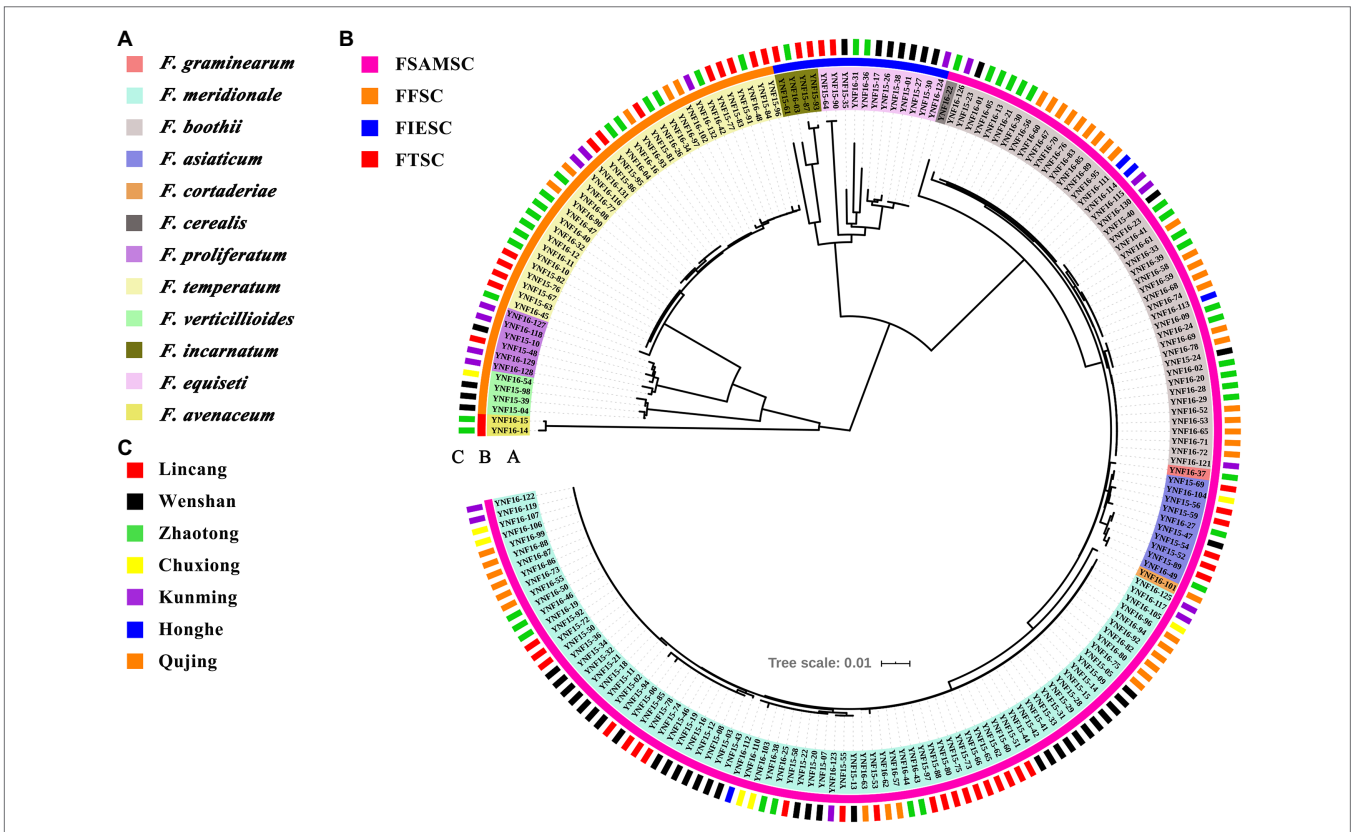

FIGURE 4 | Phylogenetic analysis of *Fusarium* species associated with maize stalk rot disease in Yunnan Province of China. The tree was constructed by the neighbor-joining method based on partial translation elongation factor 1α (*TEF-1*α) sequences. Clade support was inferred from 1,000 bootstrap replicates. The Interactive Tree of Life (see footnote 3) was used to beautify the phylogenetic tree. **(A)** Species information about each *Fusarium* isolates identified in this study and their corresponding color information. **(B)** The abbreviation of *Fusarium* species complexes. FSAMSC means *Fusarium sambucinum* species complex. FFSC means *Fusarium fujikuroi* species complex. FIESC means *Fusarium incarnatum-equiseti* species complex. FTSC means *Fusarium tricinctum* species complex. **(C)** The geographical location of each *Fusarium* isolates identified in this study.

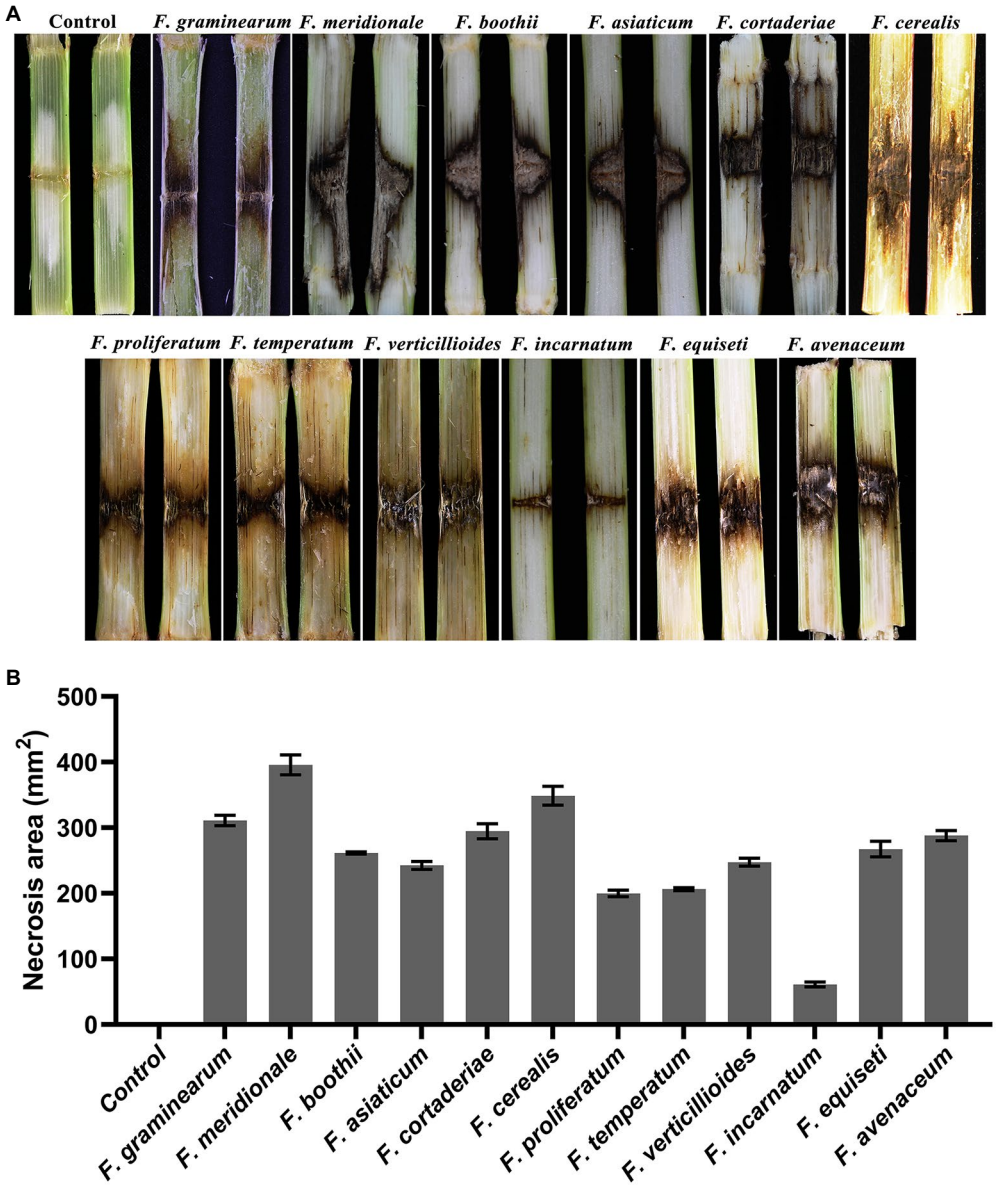

FIGURE 5 | Symptoms on maize stalks inoculated with representative *Fusarium* isolates. **(A)** Symptoms of maize stalks inoculated with representative *Fusarium* isolate at 7 dpi. No symptoms were observed in the control plants. **(B)** Statistical analysis of necrotic areas around the insertion point inoculated with representative *Fusarium* isolates at 7 dpi. The longitudinal brown infected areas were used to evaluate the virulence of each identified *Fusarium* species. Each assay was performed on three independent biological repeats.

DISCUSSION

Fusarium spp. can cause various diseases at different growth stages of maize, such as root, seedling, stalk, and ear rot, leading to yield losses, and reduction of grain quality (Pfordt et al., 2020). Most of *Fusarium* spp. can produce different mycotoxins to contaminate small grain crops from pre-harvest to post-harvest stages. The gene of *TEF1-α* always appeared to have a single copy in *Fusarium*. It showed high levels of sequence polymorphism in closely related species, and the DNA sequence based on the *TEF1-α* was often used to identify the putative *Fusarium* species (Geiser et al., 2004; Berruezo et al., 2018; Fang et al., 2020; Wang et al., 2021). In this study, 12 *Fusarium* species were isolated and identified from symptomatic maize stalks based on morphological characteristics, phylogenetic analysis (*TEF1-α*), and Koch's postulates. Among them, *F. meridionale* (40.5%), *F. boothii* (22.5%), and *F. temperatum* (16.5%) were more prevalent. For the consecutive two cropping seasons of 2015 and 2016, we find the *F. meridionale*, *F. boothii*, *F. asiaticum*, *F. proliferatum*, *F. temperatum*, *F. verticillioides*, *F. incarnatum*, and *F. equiseti* from various locations of the Yunnan Province. Previous

studies reported *F. meridionale*, *F. graminearum*, and *F. cortaderiae* were found from diseased maize plants in Brazil, and *F. meridionale* was the dominant (Kuhnem et al., 2016). Our results showed that *F. meridionale* was distributed throughout the seven-sampling locations and was also the major pathogen causing maize stalk rot disease in Yunnan Province of China. These results indicate that the environmental conditions were suitable for *F. meridionale* in Yunnan Province. However, only two isolates were individually identified as *F. graminearum* and *F. cortaderiae* in the present study. *Fusarium cortaderiae* was identified for the first time from maize in China. Previous study on the pathogenic *Fusarium* spp. causing maize ear rot in China showed that *F. verticillioides*, *F. graminearum*, *F. meridionale*, and *F. boothii* were dominant *Fusarium* species (Duan et al., 2016). However, only a few samples were taken from Yunnan Province in that study, which cannot represent the diversity of *Fusarium* spp. associated with maize ear rot disease in the whole province. In contrast, present studies focused on providing useful information of dominant pathogenic *Fusarium* species and their potential mycotoxins associated with maize in Yunnan Province. In this study, we found that *F. meridionale* and *F. boothii* were prevalent to cause maize stalk rot. However, the percentage of *F. verticillioides* and *F. graminearum* in this survey was unexpected. Notably, *F. temperatum*, a new species recently separated from *Fusarium subglutinans*, need to pay more attention in the future. *Fusarium* species can infect the stalk during the whole vegetation period by systemic spread after colonization of the roots (Murillo-Williams and Munkvold, 2008), through young leaf sheaths, by seed transmission and *via* wounds caused by hail or insect feeding (Gai et al., 2018). Stalk rot of maize results in defective grain filling, premature senescence, and lodging, which negatively affects production, harvesting, and yield (Quesada-Ocampo et al., 2016). In the present study, the pathogenicity tests showed that all of the *Fusarium* isolates could cause severe symptoms of maize stalk rot, but the extent of lesion spread was different. *Fusarium meridionale* was the most aggressive species to infect maize stalks. So, we have reasons to believe that differences in compositions of *Fusarium* spp. associated with maize stalk rot disease in Yunnan Province were caused by local climatic conditions.

To investigate the ability to produce mycotoxins of *Fusarium* species causing maize stalk rot in Yunnan Province, the toxigenic chemotypes were also evaluated by specific PCR assays. The pathogenicity analysis showed that there was no relationship between the pathogenicity and the type of mycotoxin production. Generally, pathogenicity was not influenced by the type of mycotoxin produced (Adams and Hart, 1989; Goswami and Kistler, 2005). However, the pathogenicity of the *F. graminearum* to wheat plant has a relationship with the type of the mycotoxin (Shin et al., 2018). Another study on FSAMSC reported that the aggressiveness of the pathogen was related to the type of mycotoxin produced by the pathogen (Laraba et al., 2021). Our results indicated that 45.6% (93/204) strains were NIV producers, whereas 26.0% (53/204) stains were DON producers. So, the contaminations of NIV and DON in maize-related agro-products should be given particular attention in Yunnan Province of China. Besides, the identification of *F. cortaderiae*, *F. cerealis*, and *F. avenaceum* are reported for the first from Yunnan Province, which needs urgent attention to prevent their widespread. These results will provide useful information to design an effective strategy for the control of disease caused by *Fusarium* species in Yunnan Province of China.

CONCLUSION

In the 2 years of investigation, *F. meridionale* (40.5%), *F. boothii* (22.5%), and *F. temperatum* (16.5%) were the most frequent *Fusarium* species to cause maize stalk rot disease in Yunnan Province of China. The dominance of the NIV chemotype among isolates needs to pay more attention to food safety and animal health because of the more significant toxic potential of NIV relative to DON. Besides, *F. temperatum* associated with BEA mycotoxins represented a toxigenic risk for maize production. The current results on species diversity of *Fusarium* spp. and mycotoxin contaminations associated with maize stalk rot disease will provide valuable information to design effective strategies to control the disease caused by *Fusarium* spp.

DATA AVAILABILITY STATEMENT

The datasets presented in this study can be found in online repositories. The names of the repository/repositories and accession number(s) can be found in the article/ **Supplementary Material**.

AUTHOR CONTRIBUTIONS

WG conceived and designed the experiments. WG and JZ collected the samples in the field. YY and GZ provided substantial assistance to collect the samples in the field. KX and LS performed the experiments. KX and WG wrote and edited the manuscript. All authors contributed to the article and approved the submitted version.

FUNDING

This work was supported by the National Key R&D Program of China (2017YFC1600903), National Natural Science Foundation of China (32072377 and 31670143), Beijing Natural Science Foundation (6192023), and Agricultural Science and Technology Innovation Program (CAAS-ASTIP-2020-IFST-03).

SUPPLEMENTARY MATERIAL

The Supplementary Material for this article can be found online at: https://www.frontiersin.org/articles/10.3389/fmicb.2021.652062/full#supplementary-material

REFERENCES

Adams, G. C., and Hart, L. P. (1989). The role of deoxynivalenol and 15-acetyldeoxynivalenol in pathogenesis by *Gibberella zeae* as elucidated through protoplast fusions between toxigenic and non-toxigenic strains. *Phytopathology* 79, 404–408. doi: 10.1094/Phyto-79-404

Ares, J. L. A., Ferro, A., Ramírez, L. C., and González, J. M. (2004). *Fusarium graminearum* Schwabe, a maize root and stalk rot pathogen isolated from lodged plants in northwestern Spain. *Span. J. Agric. Res.* 2, 249–252. doi: 10.5424/sjar/2004022-82

Avila, C. F., Moreira, G. M., Nicolli, C. P., Gomes, L. B., Abreru, L. M., Pfenning, L. H., et al. (2019). *Fusarium incarnatum-equiseti* species complex associated with Brazilian rice: phylogeny, morphology, and toxigenic potential. *Int. J. Food Microbiol.* 306:108267. doi: 10.1016/j.ijfoodmicro.2019.108267

Berruezo, L. A., Mercado, C. E., Guadalupe, E., Harries, E. D. M., Stenglein, S. A., Curti, R. N., et al. (2018). Characterization of *Fusarium* species associated with tobacco diseases in Northwestern Argentina. *Eur. J. Plant Pathol.* 151, 1065–1079. doi: 10.1007/s10658-018-1443-6

Boutigny, A. L., Ward, T. J., Coller, G. J. V., Flett, B., Lamprecht, S. C., O'Donnell, K., et al. (2011). Analysis of the *Fusarium graminearum* species complex from wheat, barley and maize in South Africa provides evidence of species-specific differences in host preference. *Fungal Genet. Biol.* 48, 914–920. doi: 10.1016/j.fgb.2011.05.005

Castañares, E., Dinolfo, M. I., Del Ponte, E. M., Pan, D., and Stenglein, S. A. (2016). Species composition and genetic structure of *Fusarium graminearum* species complex populations affecting the main barley growing regions of South America. *Plant Pathol.* 65, 930–939. doi: 10.1111/ppa.12470

Czembor, E., Waskiewicz, A., Piechota, U., Puchta, M., Czembor, J. H., and Stepien, Ł. (2019). Differences in ear rot resistance and *Fusarium verticillioides*-produced fumonisin contamination between polish currently and historically used maize inbred lines. *Front. Microbiol.* 10:449. doi: 10.3389/fmicb.2019.00449

Du, T. L., Kirby, H. W., and Pedersen, W. (1997). Evaluation of an aeroponics system to screen maize genotypes for resistance to *Fusarium graminearum* seedling blight. *Plant Dis.* 81, 175–179. doi: 10.1094/PDIS.1997.81.2.175

Duan, C., Qin, Z., Yang, Z., Li, W., Sun, S., Zhu, Z., et al. (2016). Identification of pathogenic *Fusarium* spp. causing maize ear rot and potential mycotoxin production in China. *Toxins* 8:186. doi: 10.3390/toxins8060186

Fang, D. Z., Liu, X. L., Chen, X. R., Yan, W. W., He, Y. L., Cheng, Y., et al. (2020). *Fusarium* species and *Fusarium oxysporum* species complex genotypes associated with yam wilt in South-Central China. *Front. Microbiol.* 11:1964. doi: 10.3389/fmicb.2020.01964

Gai, X., Dong, H., Wang, S., Liu, B., Zhang, Z., Li, X., et al. (2018). Infection cycle of maize stalk rot and ear rot caused by *Fusarium verticillioides*. *PLoS One* 13:e0201588. doi: 10.1371/journal.pone.0201588

Geiser, D. M., Jiménez-Gasco, M. M., Kang, S., Makalowska, I., Veeraraghavan, N., Ward, T. J., et al. (2004). FUSARIUM-ID v. 1.0: a DNA sequence database for identifying *Fusarium*. *Eur. J. Plant Pathol.* 110, 473–479. doi: 10.1023/B:EJPP.0000032386.75915.a0

Goswami, R. S., and Kistler, H. C. (2005). Pathogenicity and in planta mycotoxin accumulation among members of the *Fusarium graminearum* species complex on wheat and rice. *Phytopathology* 95, 1397–1404. doi: 10.1094/PHYTO-95-1397

Jennings, P., Coates, M. E., Turner, J. A., and Nicholson, P. (2004). Determination of deoxynivalenol- and nivalenol-producing chemotypes of *Fusarium graminearum* isolated from wheat crops in England and Wales. *Plant Pathol.* 53, 643–652. doi: 10.1111/j.0032-0862.2004.01061.x

Katoh, K., and Standley, D. M. (2013). Mafft multiple sequence alignment software version 7: improvements in performance and usability. *Mol. Biol. Evol.* 30, 772–780. doi: 10.1093/molbev/mst010

Kuhnem, P. R., Ward, T. J., Silva, C. N., Spolti, P., Ciliato, M. L., Tessmann, D. J., et al. (2016). Composition and toxigenic potential of the *Fusarium graminearum* species complex from maize ears, stalks and stubble in Brazil. *Plant Pathol.* 65, 1185–1191. doi: 10.1111/ppa.12497

Kulik, T., Pszczółkowska, A., Fordoński, G., and Olszewski, J. (2007). PCR approach based on the esyn1 gene for the detection of potential enniatin-producing *Fusarium* species. *Int. J. Food Microbiol.* 116, 319–324. doi: 10.1016/j.ijfoodmicro.2007.02.003

Lamprecht, S. C., Tewoldemedhin, Y. T., Botha, W. J., and Calitz, F. J. (2011). *Fusarium graminearum* species complex associated with maize crowns and roots in the KwaZulu-Natal Province of South Africa. *Plant Dis.* 95, 1153–1158. doi: 10.1094/PDIS-02-11-0083

Laraba, I., McCormick, S. P., Vaughan, M. M., Geiser, D. M., and O'Donnell, K. (2021). Phylogenetic diversity, trichothecene potential, and pathogenicity within *fusarium sambucinum* species complex. *PLoS One* 16:e0245037. doi: 10.1371/journal.pone.0245037

Lee, T., Zhang, H., Diepeningenc, A., and Waalwijka, C. (2015). Biogeography of *Fusarium graminearum* species complex and chemotypes: a review. *Food Addit. Contam.* 32, 453–460. doi: 10.1080/19440049.2014.984244

Leslie, J. F., and Summerell, B. A. (2006). *The Fusarium Laboratory Manual*. Oxford: Blackwell Publishing.

Maier, F. J., Miedaner, T., Hadeler, B., Felk, A., Salomon, S., Lemmens, M., et al. (2006). Involvement of trichothecenes in fusarioses of wheat, barley and maize evaluated by gene disruption of the trichodiene synthase (Tri5) gene in three field isolates of different chemotype and virulence. *Mol. Plant Pathol.* 7, 449–461. doi: 10.1111/j.1364-3703.2006.00351.x

Meng, K., Wang, Y., Yang, P., Luo, H., Bai, Y., Shi, P., et al. (2010). Rapid detection and quantification of zearalenone-producing fusarium species by targeting the zearalenone synthase gene pks4. *Food Control* 21, 207–211. doi: 10.1016/j.foodcont.2009.05.014

Moreno-González, J., Ares, J. L. A., Ferro, R. A., and Ramírez, L. C. (2004). Genetic and statistical models for estimating genetic parameters of maize seedling resistance to *Fusarium graminearum* Schwabe root rot. *Euphytica* 137, 55–61. doi: 10.1023/B:EUPH.0000040502.10811.64

Munkvold, G. P., and O'Mara, J. K. J. (2002). Laboratory and growth chamber evaluation of fungicidal seed treatments for maize seedling blight caused by *Fusarium* species. *Plant Dis.* 86, 143–150. doi: 10.1094/PDIS.2002.86.2.143

Murillo-Williams, A., and Munkvold, G. P. (2008). Systemic infection by *Fusarium verticillioides* in maize plants grown under three temperature regimes. *Plant Dis.* 92, 1695–1700. doi: 10.1094/PDIS-92-12-1695

O'Donnell, K., Rooney, A. P., Proctor, R. H., Brown, D. W., McCormick, S. P., Ward, T. J., et al. (2013). Phylogenetic analyses of RPB1 and RPB2 support a middle cretaceous origin for a clade comprising all agriculturally and medically important fusaria. *Fungal Genet. Biol.* 52, 20–31. doi: 10.1016/j.fgb.2012.12.004

O'Donnell, K., Ward, T. J., Aberra, D., Kistler, H. C., Aoki, T., Orwig, N., et al. (2008). Multilocus genotyping and molecular phylogenetics resolve a novel head blight pathogen within the *Fusarium graminearum* species complex from Ethiopia. *Fungal Genet. Biol.* 45, 1514–1522. doi: 10.1016/j.fgb.2008.09.002

O'Donnell, K., Ward, T. J., Geiser, D. M., Kistler, H. C., and Aoki, T. (2004). Genealogical concordance between the mating type locus and seven other nuclear genes supports formal recognition of nine phylogenetically distinct species within the *Fusarium graminearum* clade. *Fungal Genet. Biol.* 41, 600–623. doi: 10.1016/j.fgb.2004.03.003

Pfordt, A., Romero, L. R., Schiwek, S., Karlovsky, P., and Tiedemann, A. V. (2020). Impact of environmental conditions and agronomic practices on the prevalence of *Fusarium* species associated with ear- and stalk rot in maize. *Pathogens* 9:236. doi: 10.3390/pathogens9030236

Qiu, J., Xu, J., and Shi, J. (2014). Molecular characterization of the *Fusarium graminearum* species complex in Eastern China. *Eur. J. Plant Pathol.* 139, 811–823. doi: 10.1007/s10658-014-0435-4

Quesada-Ocampo, L. M., Al-Haddad, J., Scruggs, A. C., Buell, C. R., and Trail, F. (2016). Susceptibility of maize to stalk rot caused by *Fusarium graminearum* deoxynivalenol and zearalenone mutants. *Phytopathology* 106, 920–927. doi: 10.1094/PHYTO-09-15-0199-R

Sampietro, D. A., Ficoseco, M. E. A., Jimenez, C. M., Vattuone, M. A., and Catalán, C. A. (2012). Trichothecene genotypes and chemotypes in *Fusarium graminearum* complex strains isolated from maize fields of Northwest Argentina. *Int. J. Food Microbiol.* 153, 229–233. doi: 10.1016/j.ijfoodmicro.2011.10.029

Sarver, B. A. J., Ward, T. J., Gale, L. R., Broz, K., Kistler, H. C., Aoki, T., et al. (2011). Novel *Fusarium* head blight pathogens from Nepal and Louisiana revealed by multilocus genealogical concordance. *Fungal Genet. Biol.* 48, 1096–1107. doi: 10.1016/j.fgb.2011.09.002

Scauflaire, J., Gourgue, M., and Munaut, F. (2011). *Fusarium temperatum* sp. nov. from maize, an emergent species closely related to *Fusarium subglutinans*. *Mycologia* 103, 586–597. doi: 10.3852/10-135

Shin, S., Son, J. H., Park, J. C., Kim, Y. H., Yoon, Y. M., Cheong, Y. K., et al. (2018). Comparative pathogenicity of *Fusarium graminearum* isolates from wheat kernels in Korea. *Plant Pathol. J.* 34, 347–355. doi: 10.5423/PPJ.OA.01.2018.0013

Starkey, D. E., Ward, T. J., Takayuki, A., Gale, L. R. H., Corby, K., Geiser, D. M., et al. (2007). Global molecular surveillance reveals novel *Fusarium* head blight species and trichothecene toxin diversity. *Fungal Genet. Biol.* 44, 1191–1204. doi: 10.1016/j.fgb.2007.03.001

Sudhir, K., Glen, S., Michael, L., Christina, K., and Koichiro, T. (2018). Mega x: molecular evolutionary genetics analysis across computing platforms. *Mol. Biol. Evol.* 35, 1547–1549. doi: 10.1093/molbev/msy096

Thomas, B., Audonneau, N. C., Machouart, M., and Debourgogne, A. (2019). Molecular identification of *Fusarium* species complexes: which gene and which database to choose in clinical practice? *J. Mycol. Med.* 29, 56–58. doi: 10.1016/j.mycmed.2019.01.003

Thompson, J. D., Higgins, D. G., and Gibson, T. J. (1994). Improving the sensitivity of progressive multiple sequence alignment through sequence weighting, position-specific gap penalties and weight matrix choice. *Nucleic Acids Res.* 22, 4673–4680. doi: 10.1093/nar/22.22.4673

Walkowiak, S., Rowland, O., Rodrigue, N., and Subramaniam, R. (2016). Whole genome sequencing and comparative genomics of closely related *Fusarium* Head Blight fungi: *Fusarium graminearum*, *F. meridionale* and *F. asiaticum*. *BMC Genomics* 17:1014. doi: 10.1186/s12864-016-3371-1

Wang, W., Wang, B., Sun, X., Qi, X., and Gong, G. (2021). Symptoms and pathogens diversity of corn *Fusarium* sheath rot in Sichuan province, China. *Sci. Rep.* 11:2835. doi: 10.1038/s41598-021-82463-2

Ward, T. J., Bielawski, J. P., Kistler, H. C., Sullivan, E., and O'Donnell, K. (2002). Ancestral polymorphism and adaptive evolution in the trichothecene mycotoxin gene cluster of phytopathogenic *Fusarium*. *Proc. Natl. Acad. Sci. U. S. A.* 99, 9278–9283. doi: 10.1073/pnas.142307199

Xi, K., Haseeb, H. A., Shan, L., Guo, W., and Dai, X. (2019). First report of *Fusarium commune* causing stalk rot on maize in Liaoning Province, China. *Plant Dis.* 103:773. doi: 10.1094/PDIS-09-18-1674-PDN

Zhang, Y., He, J., Jia, L., Yuan, L., Zhang, D., Guo, Y., et al. (2016). Cellular tracking and gene profiling of *Fusarium graminearum* during maize stalk rot disease development elucidates its strategies in confronting phosphorus limitation in the host apoplast. *PLoS Pathog.* 12:e1005485. doi: 10.1371/journal.ppat.1005485

Zhang, H., Van der Lee, T., Waalwijk, C., Chen, W., Xu, J., Xu, J., et al. (2012). Population analysis of the *Fusarium graminearum* species complex from wheat in China show a shift to more aggressive isolates. *PLoS One* 7:e31722. doi: 10.1371/journal.pone.0031722

Conflict of Interest: The authors declare that the research was conducted in the absence of any commercial or financial relationships that could be construed as a potential conflict of interest.

Publisher's Note: All claims expressed in this article are solely those of the authors and do not necessarily represent those of their affiliated organizations, or those of the publisher, the editors and the reviewers. Any product that may be evaluated in this article, or claim that may be made by its manufacturer, is not guaranteed or endorsed by the publisher.

frontiers in Microbiology

ORIGINAL RESEARCH
published: 01 September 2021
doi: 10.3389/fmicb.2021.714750

Endophytes of Brazilian Medicinal Plants With Activity Against Phytopathogens

Jucélia Iantas[1†], Daiani Cristina Savi[2,3], Renata da Silva Schibelbein[1], Sandriele Aparecida Noriler[1], Beatriz Marques Assad[3], Guilherme Dilarri[4], Henrique Ferreira[4], Jürgen Rohr[5†], Jon S. Thorson[5,6†], Khaled A. Shaaban[5,6†] and Chirlei Glienke[1,3*†]*

[1] Postgraduate Program of Microbiology, Parasitology and Pathology, Department of Pathology, Federal University of Paraná, Curitiba, Brazil, [2] Department of Biomedicine, Centro Universitário Católica de Santa Catarina, Joinville, Brazil, [3] Postgraduate Program of Genetics, Federal University of Paraná, Curitiba, Brazil, [4] Department of General and Applied Biology, Biosciences Institute, State University of São Paulo, Rio Claro, Brazil, [5] Department of Pharmaceutical Sciences, College of Pharmacy, University of Kentucky, Lexington, KY, United States, [6] Center for Pharmaceutical Research and Innovation, College of Pharmacy, University of Kentucky, Lexington, KY, United States

Plant diseases caused by phytopathogens are responsible for significant crop losses worldwide. Resistance induction and biological control have been exploited in agriculture due to their enormous potential. In this study, we investigated the antimicrobial potential of endophytic fungi of leaves and petioles of medicinal plants *Vochysia divergens* and *Stryphnodendron adstringens* located in two regions of high diversity in Brazil, Pantanal, and Cerrado, respectively. We recovered 1,304 fungal isolates and based on the characteristics of the culture, were assigned to 159 phenotypes. One isolate was selected as representative of each phenotype and studied for antimicrobial activity against phytopathogens. Isolates with better biological activities were identified based on DNA sequences and phylogenetic analyzes. Among the 159 representative isolates, extracts from 12 endophytes that inhibited the mycelial growth (IG) of *Colletotrichum abscissum* (≥40%) were selected to expand the antimicrobial analysis. The minimum inhibitory concentrations (MIC) of the extracts were determined against citrus pathogens, *C. abscissum*, *Phyllosticta citricarpa* and *Xanthomonas citri* subsp. *citri* and the maize pathogen *Fusarium graminearum*. The highest activity against *C. abscissum* were from extracts of *Pseudofusicoccum stromaticum* CMRP4328 (IG: 83% and MIC: 40 μg/mL) and *Diaporthe vochysiae* CMRP4322 (IG: 75% and MIC: 1 μg/mL), both extracts also inhibited the development of post-bloom fruit drop symptoms in citrus flowers. The extracts were promising in inhibiting the mycelial growth of *P. citricarpa* and reducing the production of pycnidia in citrus leaves. Among the isolates that showed activity, the genus *Diaporthe* was the most common, including the new species *D. cerradensis* described in this study. In addition, high performance liquid chromatography, UV detection, and mass spectrometry and thin layer chromatography analyzes of extracts produced by endophytes that showed high activity, indicated *D. vochysiae* CMRP4322 and *P. stromaticum* CMRP4328 as promising strains that

OPEN ACCESS

Edited by:
Jia Liu,
Chongqing University of Arts and Sciences, China

Reviewed by:
Sunil Kumar Deshmukh,
The Energy and Resources Institute (TERI), India
Madhuree Kumari,
Indian Institute of Science (IISc), India

***Correspondence:**
Khaled A. Shaaban
khaled_shaaban@uky.edu
Chirlei Glienke
ch.glienke@gmail.com

†ORCID:
Chirlei Glienke
orcid.org/0000-0003-3394-0659
Jucélia Iantas
orcid.org/0000-0002-1203-7543
Jürgen Rohr
orcid.org/0000-0001-6447-5951
Jon S. Thorson
orcid.org/0000-0002-7148-0721
Khaled A. Shaaban
orcid.org/0000-0001-7638-4942

Specialty section:
This article was submitted to Microbe and Virus Interactions with Plants, a section of the journal Frontiers in Microbiology

Received: *25 May 2021*
Accepted: *03 August 2021*
Published: *01 September 2021*

Citation:
Iantas J, Savi DC, Schibelbein RdS, Noriler SA, Assad BM, Dilarri G, Ferreira H, Rohr J, Thorson JS, Shaaban KA and Glienke C (2021) Endophytes of Brazilian Medicinal Plants With Activity Against Phytopathogens. Front. Microbiol. 12:714750. doi: 10.3389/fmicb.2021.714750

produce new bioactive natural products. We report here the capacity of endophytic fungi of medicinal plants to produce secondary metabolites with biological activities against phytopathogenic fungi and bacteria. The description of the new species *D. cerradensis*, reinforces the ability of medicinal plants found in Brazil to host a diverse group of fungi with biotechnological potential.

Keywords: phytopathogens, endophytes, secondary metabolites, natural product, endophytic fungi

INTRODUCTION

Plant diseases caused by microorganisms lead to significant crop losses worldwide (Oerke, 2006; Cantrell et al., 2012; Tan et al., 2018; Sang and Kim, 2020). It is estimated that the fungal diseases cause approximately 20% of yield reductions in commercial crops and major foods worldwide (Wang et al., 2016; Fisher et al., 2018; Zhao et al., 2020). In Brazil, economically important crops such as citrus and maize are affected by different phytopathogens that can cause losses in production or render products unviable for export (Ferrigo et al., 2016; Guarnaccia et al., 2017; Ference et al., 2018).

The production of citrus is an important agricultural activity, and in Brazil it occupies a relevant position in the production of fruit, both for the fresh fruit market and to produce concentrate orange juice (Carvalho et al., 2019; González-González et al., 2020). However, this important crop is affected by different pathogens, such as *Colletotrichum abscissum*, *Phyllosticta citricarpa, Xanthomonas citri* subsp. *citri* (Silva-junior et al., 2014; Guarnaccia et al., 2017; Behlau, 2021). The post-bloom fruit drop (PDF) is caused by *C. abscissum* and affects citrus crops at the blossom stage, causing petal lesions, and abscission of young fruits (De Menezes et al., 2014; Silva-junior et al., 2014). The pathogen *P. citricarpa* causes the citrus black spot (CBS) disease, which affects fruits and leaves of citrus, and cause early fruit drop (Glienke et al., 2011; Guarnaccia et al., 2019; Hendricks et al., 2020). Moreover, citrus canker, caused by *X. citri* subsp. *citri*, is a major bacterial disease affecting citrus production in Brazil (Ference et al., 2018).

Maize production stands out in Brazilian agriculture. The country is the third largest global producer and the second largest maize exporter (Allen and Valdes, 2016). However, several species within the *Fusarium graminearum* species complex are the cause of major diseases in maize crops including *F. graminearum*, an important phytopathogen in maize crops, that frequently infects cobs and stalks of maize (*Zea mays* L.) causing the disease fusarium head blight (FHB). This pathogen results in visibly damaged kernels that can lower the grade, and, therefore, the value of the harvested crop (Ferrigo et al., 2016; Walder et al., 2017; Pfordt et al., 2020).

The control or prevention of pathogens is mainly based on the application of synthetic agrochemicals and the use of cultural practices. Although agrochemicals used represent 50% of citrus production costs, control of citrus pathogens is often unsatisfactory (Agostini et al., 2006; Qin et al., 2016; Schreuder et al., 2018; Guarnaccia et al., 2019; Hendricks et al., 2020), and the presence of agrochemicals residues may limit the export of these products (Food and Drug Administration, 2012). The continuous use of agrochemicals also led to an increase in the occurrence and selection of resistant fungal pathogens (Rodrigues et al., 2007; Deising et al., 2008; Hendricks et al., 2013). In addition, synthetic agrochemicals also led to concerns about environmental contamination and human health (Dayan et al., 2009; Kim et al., 2018). In this context, the discovery of new and safer compounds with activity against citrus and maize pathogens is desired.

Potential sources of new secondary metabolites are endophytic fungi that can produce chemically diverse compounds with a broad range of bioactivities (Aly et al., 2011; Tan et al., 2018). Endophytes are microorganisms that reside within the internal tissues of living plants, without visibly harming the host (Quiroga et al., 2001; Hardoim et al., 2015). These microorganisms, when associated with medicinal plants, possess high potential to produce new bioactive metabolites (Savi et al., 2018, 2019a; Singh et al., 2021). Microorganisms have been regarded as a promising source with the most potential for structurally novel antifungal metabolites because of the isolation of many natural fungicides from the microbial resource (Copping and Duke, 2007; Pham et al., 2019).

Among the endophytic fungi, the genus *Diaporthe* has been isolated from different host plants, and is reported as great source of compounds, especially with antibacterial and antifungal activities (Gomes et al., 2013; Santos et al., 2016; Noriler et al., 2019). *Diaporthe* species are commonly isolated from medicinal plants, found in a range of biomes and recent studies have demonstrated antifungal activity of *Diaporthe* endophytes isolated from medicinal plants against citrus phytopathogens such as *C. abscissum* and *P. citricarpa* (Tonial et al., 2017; Noriler et al., 2018, 2019; Savi et al., 2020). However, only a small fraction of the approximately one million known endophytes have been investigated (Savi et al., 2019a; Manganyi and Ateba, 2020). In addition, several rare medicinal plants produce important bioactive compounds to survive in unique environments and may host new and diverse fungal endophytes (Strobel, 2003), which have rarely been isolated and characterized (Tan et al., 2018).

The Cerrado (savanna) and Pantanal (wetland) are recognized as Brazilian biomes with high diversity of species (Myers et al., 2000; Strassburg et al., 2017; Guerreiro et al., 2019). *Stryphnodendron adstringens* (Martius) Coville (Forero, 1972) is a native plant in the Brazilian savanna, recognized by medicinal properties and was added in the "Plants for the Future Initiative Midwest region," an action of the Brazilian Ministry of the Environment (Souza-Moreira et al., 2018; Pellenz et al., 2019; de Souza et al., 2020). This species has been harbored a richness endophytic fungi community with biotechnological potential (Carvalho et al., 2012; Noriler et al., 2018). Additionally, *Vochysia*

divergens Pohl (Vochysiaceae) is one of the main medicinal tree species in the Pantanal region (de Carvalho Filho et al., 2021). Endophytic fungi reported by *V. divergens* have been showed antimicrobial, antifungal and cytotoxicity activities (Hokama et al., 2016; Savi et al., 2018; Noriler et al., 2018, 2019). Considering the need for more effective treatments of plant diseases caused by citrus and maize pathogens, the present study identified fungal endophytes of two medicinal plants, *V. divergens* and *S. adstringens*, and investigated their antimicrobial potential against the citrus pathogens *C. abscissum*, *P. citricarpa*, and *X. citri* subsp. *citri*, as well as against the maize pathogen *F. graminearum*.

MATERIALS AND METHODS

Biological Material

Pathogens Cultures

The pathogens *C. abscissum* (CMRP704 – Ca142), *P. citricarpa* (CMRP06) and *F. graminearum* (LGMF1703) are deposited in the CMRP Taxonline Microbiological Collections of Paraná Network, at the Federal University of Paraná, Brazil[1] and *X. citri* subsp. *citri* (*X. citri*; isolate 306 – IBSBF 1594) deposited in the IBSBF (culture collection of the Biological Institute Culture Collection of Phytopathogenic Bacteria).

Plants

The leaves and petioles of *V. divergens* and *S. adstringens* used for the isolation of endophytes were collected in January 2018 from two Brazilian regions: the Pantanal that is a wetland characterized by periods of flood and drought (Ivory et al., 2019), and the Cerrado that is a savannah characterized by the natural presence of fire (Strassburg et al., 2017). The leaves and petioles of *V. divergens* were collected in the Miranda River of the Pantanal (19°36′35″S 56°58′35″W) and on the Red River in Corumbá, Mato Grosso do Sul, Brazil. *S. adstringens* leaves and petioles were collected in the Cerrado along the BR262 (20°18′10.8″S 56°15′44.3″W). Samples were collected from 20 plants of *S. adstringens* and 20 plants of *V. divergens*. For both species, five leaves and five petioles were collected of each individual plant. The plant tissues were stored at 4°C and the isolation of endophytes was performed within 72 h.

Isolation of Endophytes

The leaves and petioles used for the isolation of endophytic fungi were processed using the protocol described by Petrini (1986), with modifications: the leaves and petioles were submerged in autoclaved water for 1 min, immersion in 70% ethanol (v/v) for 1 min, then for 3 min in sodium hypochlorite 3% (v/v), then for 1 min in 70% ethanol (v/v), and then, washed in sterilized distilled water for 1 min. After surface sterilization, the samples were cut into five pieces of 8 × 8 mm and aseptically transferred to Petri dishes containing potato dextrose agar (PDA) supplemented with nalidixic acid (50 μg/mL), at pH 5.8. The Petri dishes were incubated at 28°C for 30 days. The growth of endophytes was checked daily, and emerging mycelia were transferred to culture tubes containing PDA for further identification. To test the efficacy of surface disinfection method the last rinsed distilled water was collected and plated on the PDA plates and incubated at 28°C. The absence of fungal colonies growth from the last rinsed water plates indicates the efficacy of the surface sterilization procedure and confirming that the isolates were endophytes originated from within the host plant tissues.

After macroscopic characteristic analysis, the isolates were grouped into phenotypes according to colony color, growth rate, hyphal aspect, and presence/absence of spores. One isolate of each phenotype was randomly selected for molecular identification and bioprospecting. For each representative of the phenotypes, a pure culture was obtained from a single spore or hyphal tip according to Gilchrist-Saavedra et al. (2006).

DNA Extraction, PCR Amplification, Sequencing, and Phylogenetic Analyses

Genomic DNA was extracted from 3-day old cultures using the method described by Raeder and Broda (1985). PCR amplification of partial regions of ITS (internal transcribed spacer) using corresponding primer pairs V9G/ITS4 (White et al., 1990; De Hoog and Gerrits van den Ende, 1998). For the *Diaporthe* genus were also used partial sequences of beta-tubulin (*tub2*), translation elongation factor 1-α (*tef1*), calmodulin (*cal*), and histone H3 (*his3*) genes using corresponding primer pairs, e.g., Bt2a/Bt2b (Glass and Donaldson, 1995), EF1-728F/EF1-986R (Carbone and Kohn, 1999), CAL- 228F/CAL-737R (Carbone and Kohn, 1999), and CYLH3F/H3-1b (Glass and Donaldson, 1995; Crous et al., 2004), respectively. PCR reaction was performed using Top Taq Master Mix (QIAGEN), purified with the Exo1 and FastAP enzymes (Thermo Fisher Scientific, United States) and sequenced using the BigDye Terminator Cycle Sequencing Kit v 3.1 Kit. The products were purified with Sephadex G50 and submitted to an ABI3500® automated sequencer (Applied Biosystems, Foster City, CA, United States). Chromatograms were inspected using the MEGA 7 software (Kumar et al., 2015) and the consensus sequences were compared to those available in the NCBI/GenBank database (National Center for Biotechnology Information – http://www.ncbi.nlm.nih.gov/BLAST/) using the Blast tool, limiting to the sequences of the type strains.

The species found were also compared to the list of validated species of the MycoBank database[2]. The alignment was performed using the MAFFT version 7 (Katoh and Toh, 2008) and phylogeny based on Bayesian inference was performed in the MrBayes version 3.2.1 (Ronquist et al., 2011), using two parallel runs with one cold and three heated chains each, using the number of generations needed to reach split frequencies of ≤0.01 and a sampling frequency set to every 100 generations. The phylogenetic analyzes of *Diaporthe* genus were performed following the clades described by Gomes et al. (2013); Gao et al. (2017); Guarnaccia et al. (2018); Yang et al. (2018); Manawasinghe et al. (2019); Guo et al. (2020), and Hilário et al. (2021). In the present study we analyzed 173 *Diaporthe*

[1]www.cmrp-taxonline.com

[2]http://www.mycobank.org/

isolates (**Supplementary Table 1**) (eight endophytic isolates from this study).

All the identified isolates were deposited in the CMRP Taxonline Microbiological Collections of Paraná Network (see text footnote 1) at the Federal University of Paraná (UFPR).

Taxonomy

The isolate CMRP4331 was cultivated in different culture media: PDA, oatmeal agar (OA), and 2% malt extract agar (MEA) at 25°C in darkness and colony diameters were measured 14 days after inoculation (Crous et al., 2009). Colony colors were rated according to Rayner (1970). To induce sporulation, the isolates were cultured on 2% tap water agar supplemented with sterile pine needles (PNA). Cultures were incubated at 25°C with a 12/12 h fluorescent light/dark cycle. 50 alpha conidia and 36 beta conidia were measured to calculate the mean size and standard deviation (SD). Moreover, the morphological characteristics were examined captured using an Olympus microscope equipped with an SC30 camera. Descriptions were deposited in the MycoBank database[3].

Antifungal Activity

Production of Extracts

A total of 159 isolates representing each phenotype were used to prepare the extracts. The isolates were cultured for 7 days on PDA dishes, pH 5.8 at 28°C. Three mycelial disks (1.2 cm) of endophytes were inoculated into Erlenmeyer flasks (250 mL) containing 100 mL ME (Malt extract; Schulz et al., 1995) and cultured under agitation (180 rpm, 28°C) for 14 days. The mycelium was separated from the culture medium by filtration with Whatman n°4 filter paper. The fermentative liquid was mixed with 4% (w/v) XAD-16 resin and stirred overnight, followed by centrifugation. The resin was washed with distilled water (three times) and then extracted with MeOH (three times). The obtained methanol extract was dried using rotary evaporator at 40°C. The generated dry extracts of 159 isolates were diluted in methanol to a final concentration of 10 mg/mL (Savi et al., 2020).

Evaluation of Mycelial Growth Inhibition Against Pathogenic Fungi

The first screening of antifungal activity was evaluated against *C. abscissum*. 100 μL of the extract was added to a Petri dish with PDA medium, and a pathogen mycelial disk (8 mm) was subsequently placed in the center of the plate. The fungicide Carbendazim (Derosal®; 1.0 mg/mL) and methanol were used as positive and negative controls, respectively. The plates were incubated in BOD (Biochemical Oxygen Demand) at 24°C for 7 days. The inhibition of pathogen growth caused by each extract was evaluated by comparing the treatments with the controls (Savi et al., 2015, 2020; Hokama et al., 2016). The experiment was performed in triplicate and the data were submitted to Mann Whitney test in GraphPad Prims v. 6.01. The percentage of inhibition (Quiroga et al., 2001) was calculated with the following formula: Pi = (Cd – Td)/Cd, where: Pi = Percent inhibition; Cd = control growth diameter; Td = treatment growth diameter.

[3]www.MycoBank.org

The extracts that showed the elite results in inhibiting the growth of the pathogen *C. abscissum* were selected for all other tests, including the evaluation of mycelial growth inhibition of *P. citricarpa* and *F. graminearum* that followed the same experimental design. The growth inhibition rates were analyzed 7 and 21 days after inoculation for *F. graminearum* and *P. citricarpa,* respectively. The experiments were performed in triplicate.

Determination of the Minimum Inhibitory Concentration for Pathogenic Fungi

The minimum inhibitory concentrations (MIC) analyzes were performed adapted from Tonial et al. (2017). MIC was determined in 96-well plates, with 100 μL malt extract medium in each well (*C. abscissum* and *P. citricarpa*). Potato dextrose medium was used for *F. graminearum*. 50 μL of the extract were pipetted into the adjacent well for serial dilutions, and 10 μL of conidial suspension of the pathogens *C. abscissum*, *P. citricarpa*, and *F. graminearum* (10^6 conidia/mL) were added in each well. The experiments were performed in triplicate and the plates were incubated at 28°C for 14 days. The MIC was determined as the lowest concentration of the extract capable of completely inhibiting pathogen growth (Hörner et al., 2008).

Determination of the Minimum Inhibitory Concentration for Pathogenic Bacteria

To perform tests against *X. citri* subsp. *citri,* this pathogen was cultivated in NYG/NYG-agar medium (nitrogen-yeast-glycerol: 5 gL^{-1} of peptone, 3 gL^{-1} of yeast extract, 2% glycerol; solid medium bacterial agar was added to 15 gL^{-1}) at 29°C (Zamuner et al., 2020). The inhibitory concentration values (IC) of the extracts for *X. citri* were determined using the Resazurin Microtiter Assay Plate (REMA) adapted by Silva et al. (2013). Stock solutions were prepared by dissolving the extracts in NYG medium containing 1% DMSO (v/v) to the final concentration of 100 μg/mL. Exposure of the cells was done in 96-multiwell plates, in which each of the extracts was serially diluted per column of the plate (example: A1-H1, A2-H2, etc.) using NYG medium as the diluent to the resulting concentration range varying from 100 to 0.78 μg/mL. Cells of *X. citri* were cultivated in NYG from the starting $OD_{600\ nm}$ of ∼0.1 until the $OD_{600\ nm}$ of ∼0.40 (which contains 10^7 cells/mL). A fraction of this culture was added to each of the wells in order to give the final concentration of 10^5 cells/well in a total volume of 100 μL per well. The negative control was NYG medium without any extract, whereas the positive control was kanamycin at 20 μg/mL. The control of vehicle was 1% DMSO (v/v) mixed in the NYG medium. The REMA plates were incubated for 16 h at 29 ± 1°C. Development was performed by adding 15 μL of 0.1 mg/mL resazurin (Sigma-Aldrich, Germany) solution into each well, followed by 2-h incubation at 29 ± 1°C. Cell respiration was monitored by the fluorescence of resorufin (the reduced form of resazurin in the presence of NADH) using the BioTek plate reader Synergy H1N1 set to the excitation and emission wavelengths of 530 and 590 nm, respectively. The percentages of cell growth inhibition per extract

concentration were plotted using the software Microcal Origin 8.0, and polynomial regression was used to estimate IC values (concentrations of extracts able to inhibit 100% of the cells in culture; Morão et al., 2018). To determine if an extract has bactericidal or bacteriostatic effect, aliquots from REMA were transferred to NYG-agar plates before resazurin was added by using a 96-plate replicator (8 × 12 Sigma-Aldrich, Germany). Plates were incubated at 29°C for 48 h to verify the ability of the treated cells to resume growth. Three independent experiments were performed in triplicates each.

Inhibition of Post-Bloom Fruit Drop Development in Citrus Flowers

To evaluate the ability of 12 extracts into inhibit the PFD development, citrus flowers were collected at the UFPR, Curitiba, Paraná, Brazil. Flowers without PFD symptoms were added in Petri dishes containing water agar medium (15 g of agar per 1 L of deionized H_2O). In a petal of each flower were added 5 μL of endophyte extracts and 5 μL of conidial suspension of *C. abscissum* (10^6 conidia/mL). Methanol was used as negative control and fungicide Carbendazim (Derosal®; 1.0 mg/mL) was the positive control. The dishes were kept at 28°C for 48 h, and the qualitative analysis was performed. The presence of PFD symptoms in the flower was considered a negative activity against PFD, and the absence of symptoms was considered a positive activity of extract. The test was performed in triplicate (Savi et al., 2020).

Inhibition of *Phyllosticta citricarpa* Pycnidia Development in Citrus Leaves

To evaluate the potential of 12 extracts to inhibit the development of *P. citricarpa* pycnidia, autoclaved *Citrus sinensis* leaves were used (20 min; 120°C; 1 atm). Leaves disks (Ø 10 mm) with 10 μL of the extract were placed on Petri dishes with water agar medium. Four disks of 2 mm *P. citricarpa* mycelia were inoculated close to each leaf fragment. Methanol was used as negative control and fungicide Carbendazim (Derosal®; 1.0 mg/mL) was the positive control. The Petri dishes were maintained for 21 days at 28°C with 12 h photoperiod. The pycnidia of *P. citricarpa* formed above the leaves were counted under a stereoscopic microscope. This test was performed in triplicate (Santos et al., 2016).

General Experimental Procedures

High performance liquid chromatography, UV detection, and mass spectrometry (HPLC-UV/MS) analyses were accomplished with an Agilent *Infinity Lab LC/MSD* mass spectrometer (*MS* Model G6125B; Agilent Technologies, Santa Clara, CA, United States) equipped with an Agilent 1260 Infinity II Series Quaternary LC system and a Phenomenex NX-C18 column (250 × 4.6 mm, 5 μm) [Method: solvent A: H_2O/0.1% formic acid, solvent B: CH_3CN; flow rate: 0.5 mL/min; 0–30 min, 5–100% B (linear gradient); 30–35 min, 100% B; 35–36 min, 100–5% B; 36–40 min, 5% B]. Thin layer chromatography (TLC) was carried out using Polygram SIL G/UV254 (Macherey-Nagel and Co., Dueren, Germany).

RESULTS

Phenotypes and Screening of the Antifungal Activity

A high number (1,304) of cultivable endophytic fungi were isolated from *V. divergens* and *S. adstringens,* and the isolates were grouped into 159 phenotypes based on morphological characteristics. The antifungal activity of the extracts produced from the fermentation of the 159 representative isolates (one of each phenotype) was determined (**Supplementary Table 2**). Twelve endophytic fungi produced metabolites that inhibited mycelial growth (IG) of the pathogen *C. abscissum* equal to or greater than 40%: CMRP4328 – IG: 83%, CMRP4323 – IG: 80%, CMRP4322 – IG: 75.3%, CMRP4325 – IG: 72.6%, CMRP4330 – IG: 71.3%, CMRP4332 – IG: 65.3%, CMRP4327 – IG: 51.3%, CMRP4324 – IG: 48.6%, CMRP4321 – IG: 46%, CMRP4326 – IG: 46%, CMRP4329 – IG: 40% and CMRP4331 – IG: 40% (**Supplementary Table 2**, **Figure 1**, and **Supplementary Figures 1**, **2**).

Of the 12 isolates selected, seven were isolated from plants of *S. adstringens* (six from leaves and one from a petiole) located in the Cerrado biome, and five isolates were obtained from plants of *V. divergens* (two from leaves and three from petioles) of the Pantanal biome in Brazil (**Supplementary Table 3**).

Identification of Isolates

The 12 isolates were identified based on phylogenetic analysis using ITS (in addition to other loci) sequences as belonging to the Ascomycota phylum, with ten isolates belonging to the Sordariomycetes class, one to Eurotiomycetes and one to the Dothideomycetes class. *Diaporthe* was the genus with the highest number of isolates with antifungal potential, represented by eight isolates (**Supplementary Table 3**): the isolates CMRP4321, CMRP4322, CMRP4326, and CMRP4332 (*D. sojae* complex; **Supplementary Figure 3**), the CMRP4329 isolate (**Supplementary Figure 4**), the isolate CMRP4330 (*D. arecae* complex; **Supplementary Figure 5**) and CMRP4324 and CMRP4331 isolates (**Figure 2**). The other isolates were identified as *Aspergillus* section *Flavi A.* nomius-clade (CMRP4327; **Supplementary Figure 6**), *Coniochaeta* sp. (CMRP4325; **Supplementary Figure 7**), *Nemania primolutea* (CMRP4323; **Supplementary Figure 8**), and *Pseudofusicoccum stromaticum* (CMRP4328; **Supplementary Figure 9** and **Supplementary Table 4**).

Phylogenetic Analyses

Diaporthe genus

Diaporthe vochysiae (CMRP4321, CMRP4322, CMRP4326, and CMRP4332). In the *D. sojae* species complex, 60 representatives of the complex including the outgroup sequences of *Diaporthe amygdali* (CBS126679) were subjected to multi-locus phylogenetic analyses with concatenated ITS, *tub2*, *tef1*, *his3*, and *cal* sequences. A total of 2,439 characters including gaps (593 for ITS, 442 for *tub2,* 369 for *tef1*, 516 for *his3*, and 519 for *cal*) were used in the phylogenetic analysis, 647

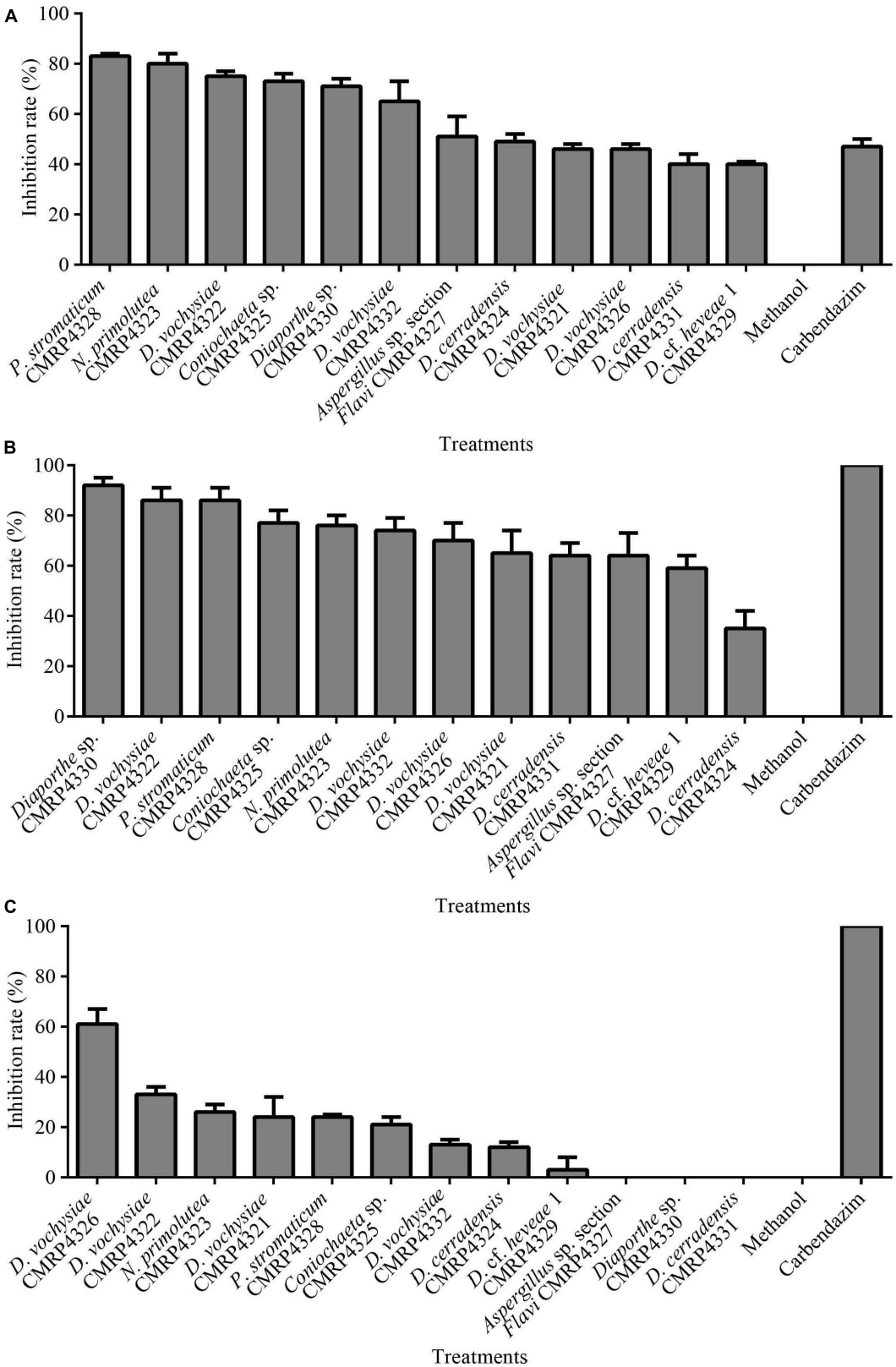

FIGURE 1 | Mean values of mycelial growth inhibition (in%) of the pathogens *Colletotrichum abscissum* **(A)**, *Phyllosticta citricarpa* **(B)**, and *Fusarium graminearum* **(C)** in the presence of 100 μL of extracts obtained after culture of endophytes in malt extract medium. Note: Fungicide: 100 μL Carbendazim (Derosal; 0.1 mg/mL) was used as positive control.

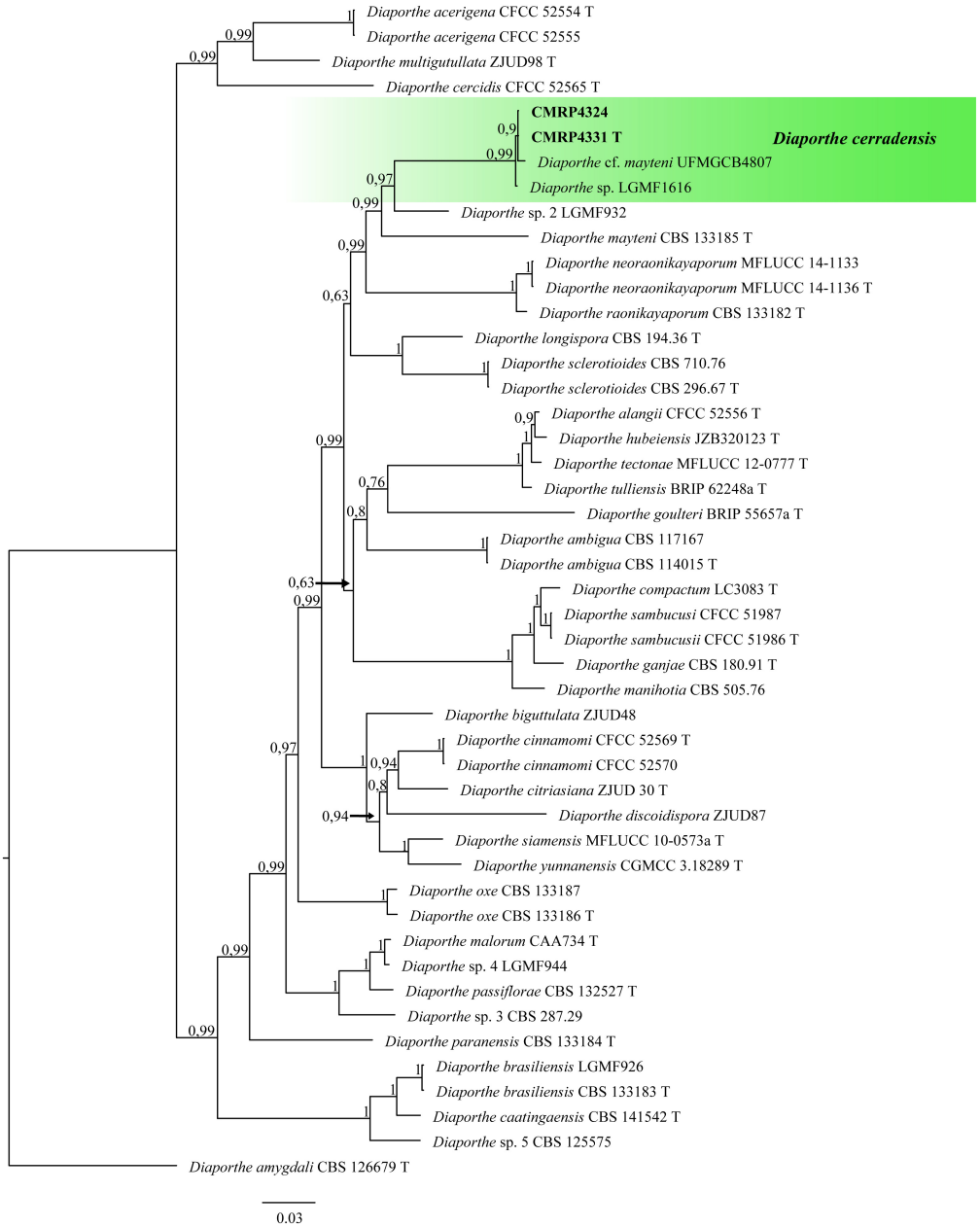

FIGURE 2 | Bayesian Inference phylogenetic tree of *Diaporthe* species based on multiple alignment of ITS, *tub2*, *tef1*, *his3,* and *cal* partial sequences. The data matrix had 47 taxa and 2,133 characters. The species *Diaporthe amygdali* (CBS 126679 T) was used as outgroup. Strains marked with a "*T*" correspond to type sequences. The scale bar of 0.03 represents the number of changes. The sequence of the isolates here studied is presented with its isolation code (CMRP4331 and CMRP4324) highlighted in bold.

characters were parsimony-informative, 921 were variable and 1453 characters were conserved.

In this clade, the isolates CMRP4321, CMRP4322, CMRP4326, and CMRP4332 were closely related to the type strain of *D. vochysiae* (**Supplementary Figure 3**), and therefore, we suggest them as belonging to this species.

Diaporthe cf. heveae 1 (CMRP4329). The multi-locus phylogenetic analyses with 29 representative isolates including the outgroup sequences of *D. perjuncta* (CBS 114435 T). A total of 2,160 characters including gaps (525 for ITS, 396 for *tub2*, 326 for *tef1*, 451 for *his3*, and 459 for *cal*) with 620 characters being parsimony-informative, 792 were variable, and 1,315 characters were conserved. The isolate CMRP4329 was assigned as *Diaporthe* cf. *heveae* 1 (**Supplementary Figure 4**).

D. arecae species complex (CMRP4330). The isolate CMRP4330 was aligned with 49 representative isolates from *D. arecae* species

complex including *D. caulivora* (CBS 127268 T) as outgroup. Were analyzed and 2,112 characters including gaps (517 for ITS, 340 for *tub2*, 323 for *tef1*, 457 for *his3*, and 475 for *cal*) were included in the multi-locus dataset, 474 characters were parsimony-informative, 721 were variable, and 1,361 characters were conserved. The CMRP4330 isolate was positioned on a single branch and, therefore, we suggest that this isolate belongs to a new species of the genus *Diaporthe*, named *Diaporthe* sp. (**Supplementary Figure 5**), since all attempts to produce are productive structure have failed.

Diaporthe cerradensis (CMRP4331 and CMRP4324). The phylogenetic tree to *D. cerradensis* was obtained with 47 representative isolates including the outgroup sequences of *D. amygdali* (CBS 126679 T), a total of 2,133 characters including gaps (505 for ITS, 399 for *tub2*, 356 for *tef1*, 469 for *his3*, and 404 for *cal*). 761 characters were parsimony-informative, 926 were variable, and 1,157 characters were conserved. Based on these multi-locus phylogenic analyses, the isolates CMRP4324 and CMRP4331 were described as a new species and named *D. cerradensis* (**Figure 2**). In addition to these, the results for the first 10 megablast sequences using GenBank[4] are in **Supplementary Tables 5–9**. The highest similarity was for the isolate *Diaporthe* cf. *mayteni* for the partial *tef1* (99.69%) and *tub* (99.59%). There are no *his* and *cal* sequences for *Diaporthe* cf. *mayteni*. Two endophytic strains were clustered in the same clade of *D. cerradensis*, the strain *Diaporthe* cf. *mayteni* UFMGCB4807 isolated from a leaf of *Carapa guianensis* (Ferreira et al., 2015) and *Diaporthe* sp. LGMF1616 isolated from a leaf of *S. adstringens* (Noriler et al., 2018), both also isolated in the Cerrado biome, Brazil. Below, we describe these new species.

Species Description

Diaporthe cerradensis CMRP4331

Diaporthe cerradensis: Iantas, Noriler & Glienke, *sp. nov*. MycoBank 839350;

Etymology: Named after the region where the strain was collected (Cerrado, Brazilian biome)

Pycnidial conidiomata globose, conical or irregular, solitary or aggregated, exposed on the PNA surface, dark brown to black, cream translucent conidial drops exuded from the ostioles, 170–350 μm diameter. *Conidiophores* hyaline, densely aggregated, unbranched, aseptate, subcylindrical to cylindrical, 4.5–6.5 × 2–4.3 μm. *Conidiogenous cells* hyaline and subcylindrical, tapering toward the apex 12.2–15.1 × 2–3.5 μm. *Alpha conidia* common, hyaline, fusiform, biguttulate, 6.4–8.3 × 2–3 μm, mean ± SD = 7.32 ± 0.38 × 2.31 ± 0.18 (n = 50). *Beta conidia* less common hyaline, aseptate, filiform, curved 18.8–29.6 × 1–1.6 μm, mean ± SD = 24.8 ± 2.7 × 1.4 ± 0.1 μm (n = 36). *Gamma conidia* not observed.

Culture characteristics: Colonies on flat PDA, aerial mycelium forming concentric rings with cotton texture, white and light yellow on the surface, colonies reaching 72 mm in diameter after 2 weeks at 25°C; reverse yellow amber. In flat OA, with a white aerial mycelium, olive gray on the surface, colonies reaching 65 mm in diameter; reverse white, gray and greenish olivaceous. In the flat MEA, aerial white mycelium and amber patches on the surface, colonies reaching 52 mm diameter; reverse brown (**Figure 3**).

Specimen examined: Brazil, Miranda, Cerrado, Mato Grosso do Sul, 20°18′10.8″S, 56°15′44.3″W, endophytic species isolated from a leaf of *S. adstringens* (popular name Barbatimão), January 05, 2018 by C. Glienke and D. C. Savi. Holotype: UPCB97125 (Herbarium of the Department of Botany code, University Federal of Paraná), ex-type culture CMRP4331 CMRP – Taxonline Microbiological Collections of Paraná Network (see text footnote 1) at the UFPR.

Notes: *Diaporthe cerradensis* forms a well-supported and independent clade distinct from the previously described species of *Diaporthe*. *D. cerradensis* is most closely related to the species *D. mayteni*, *D. raonikayaporum*, and *D. neoraonikayaporum*. However, *D. cerradensis* differs from these species in the ITS sequences (36 different unique fixed alleles by *D. mayteni*, 30 by *D. raonikayaporum,* and 29 by *D. neoraonikayaporum*), *tef1* (27 different unique fixed alleles by *D. mayteni*, 45 by *D. raonikayaporum,* and 41 by *D. neoraonikayaporum*), *tub2* (19 different unique fixed alleles by *D. mayteni*, 26 by *D. raonikayaporum*, 23 by *D. neoraonikayaporum*), *his3* (30 different unique fixed alleles by *D. mayteni* and 40 by *D. raonikayaporum*), and *cal* (21 different unique fixed alleles by *D. mayteni*, 28 by *D. raonikayaporum*, 26 by *D. neoraonikayaporum*) loci. Furthermore, *D. cerradensis* differs from *D. mayteni* in having larger conidiogenous cells (12.2–15.1 × 2–3.5 vs 10–13 × 2–3 μm) and alpha conidia (6.4–8.3 × 2–3 vs 5–7 × 2–3 μm; Gomes et al., 2013). Conidiogenous cells of *D. cerradensis* are also larger than those of *D. raonikayaporum* (12.2–15.1 × 2–3.5 vs 5–10 × 2–3 μm; Gomes et al., 2013). In addition, alpha conidia of *D. cerradensis* are larger than those of *D. neoraonikayaporum* (6.4–8.3 × 2–3 vs 4–6 × 1.4–1.9 μm; Doilom et al., 2017).

Aspergillus sp. section Flavi A. nomius-clade (CMRP4327)

The isolate CMRP4327 was aligned with 54 sequences of 37 accepted species of the genus *Aspergillus* section *Flavi*, and *Aspergillus muricatus* (NRRL35674 T) was used as the outgroup. The alignment of the partial sequences of ITS consisted of 610 characters, 426 of these were conserved, 83 were parsimony informative, and 161 were uninformative. In the phylogenetic tree, the isolate CMRP4327 is closely related to the species *A. nomius* and *A. pseudonomius* (**Supplementary Figure 6**) and therefore, was denominated as belonging to the *A. nomius* clade.

Coniochaeta sp. (CMRP4325)

The phylogenetic analysis comprises the isolate CMRP4325, 35 species accepted in the *Coniochaeta* genus, and *Cheatosphaeria garethjonessi* MFLU161019 that was used as outgroup. The alignment of partial sequence of the ITS consisted of 612 characters, of which 331 were conserved, 171 were parsimony informative, and 261 uninformative. In the phylogenetic analysis, the isolate CMRP4325 is in the same branch as the *Coniochaeta boothii* species but seems to be a distinct form (**Supplementary Figure 7**). Multigene analysis will be necessary for the identification of this isolate.

[4]https://blast.ncbi.nlm.nih.gov

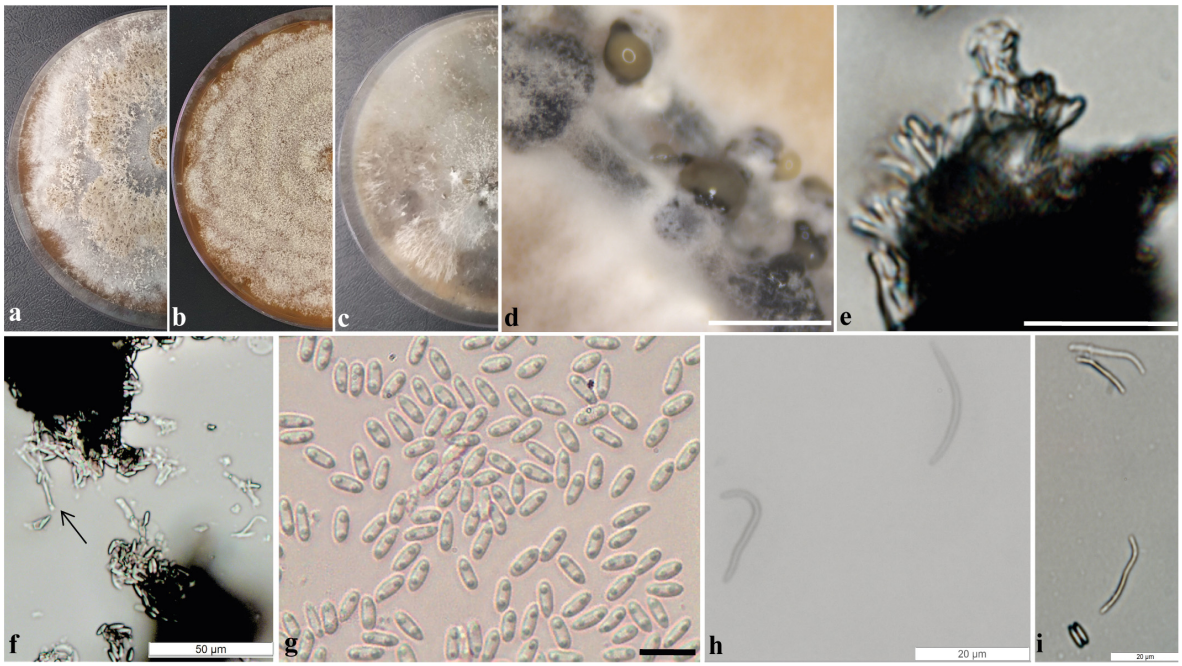

FIGURE 3 | *Diaporthe cerradensis* (CMRP4331). **(a–c)** Colonies on PDA, MEA, and OA, respectively; **(d)** conidiomata sporulating on PNA; **(e)** conidiophores; **(f)** conidiogenous cells; **(g)** alpha conidia; **(h)** beta conidia; and **(i)** alpha and beta conidia. — Scale bars: ***d*** = 200 μm; ***e*** = 50 μm; and ***g*** = 10 μm.

Nemania primolutea (CMRP4323)

The alignment consisted of the isolate CMRP4323, 13 accepted species of the *Nemania* genus, and *Biscogniauxia nummularia* (MUCL51395) as the outgroup taxa. The ITS analysis comprises of 679 characters, which 322 were conserved, 175 were parsimony informative, and 290 were uninformative. Based on this phylogenetic analysis, the isolate CMRP4323 was identified as *N. primolutea* (**Supplementary Figure 8**).

Pseudofusicoccum stromaticum (CMRP4328)

The phylogenetic analysis was performed with the partial sequences of ITS and *tef1* of the isolate CMRP4328 and 15 sequences of 9 accepted species of the *Pseudofusicoccum* genus and using *Endomelanconiopsis microspora* (CBS353.97) as the outgroup taxa. The alignment of the partial sequence of ITS consisted of 575 characters, with 491 conserved sites, 16 were parsimony informative, and 74 uninformative. The partial *tef1* (Translation elongation factor 1 alpha) alignment consisted of 308 characters, with 211 conserved sites, 16 were parsimony informative, and 95 uninformative. In the phylogenetic tree the isolate CMRP4328 grouped with *P. stromaticum* and therefore, it was identified as belonging to this species (**Supplementary Figure 9**).

Biological Activity

Extracts From Endophytic Fungi Inhibit the Mycelial Growth and Germination of Conidia of Plant Pathogens

In the screening for antifungal activity among the 159 extracts evaluated, 12 extracts showed highest mycelium growth inhibition against *C. abscissum* (**Figure 1A**) and were selected to be evaluated for their activity against the pathogens *P. citricarpa* and *F. graminearum*. Seven extracts inhibited more than 70% of the mycelial growth of the pathogen *P. citricarpa* (**Figure 1B**): *Diaporthe* sp. CMRP4330 (IG: 92%, p = 0.01), *P. stromaticum* CMRP4328 (IG: 86%, p = 0.01), *D. vochysiae* CMRP4322 (IG: 86%, p = 0.01), *Coniochaeta* sp. CMRP4325 (IG: 77%, p = 0.05), *N. primolutea* CMRP4323 (IG: 76%, p = 0.05), *D. vochysiae* CMRP4332 (IG: 74%, p = 0.05), and *D. vochysiae* CMRP4326 (IG: 70%, p = 0.05). Against the maize pathogen *F. graminearum* the extract from *D. vochysiae* CMRP4326 inhibited 61% of mycelial growth (p = 0.01; **Figure 1C**). *D. cerradensis* CMRP4324 and CMRP4331 inhibited the mycelial growth of citrus pathogens *C. abscissum* (IG = 49 and 40%, respectively) and *P. citricarpa* (IG = 35 and 64%, respectively).

For the 12 selected extracts, we also evaluated the minimum concentrations that inhibit the germination of the conidia of the pathogens. The values are showed in **Table 1**, and the underlined values represent extracts that also showed evidenced activity in the inhibition of mycelium growth (**Figure 1** and **Supplementary Figure 2**). The extracts produced by the isolates *D. vochysiae* CMRP4322 completely inhibited the conidial germination of *C. abscissum* with the MIC value 1 μg/mL, and other isolates such as *N. primolutea* CMRP4323 (MIC: 40 μg/mL), *D. cerradensis* CMRP4331 (MIC: 40 μg/mL), *D. vochysiae* CMRP4326 (MIC: 40 μg/mL), and *P. stromaticum* CMRP4328 (MIC: 40 μg/mL) showed the lowest MIC values against *C. abscissum*.

The lowest MIC values (10 μg/mL) that inhibit the germination of *P. citricarpa* conidia were produced by four

TABLE 1 | Minimum inhibitory concentration (μg/mL) of extracts produced by the endophytes against the pathogens *Colletotrichum abscissum, Phyllosticta citricarpa*, *Fusarium graminearum,* and *Xanthomonas citri* subsp. *citri* (in bold extracts with bactericidal activity), post-bloom fruit drop (PFD) symptoms in the presence of extracts and number of pycnidia produced in leaves by *P. citricarpa* in the presence of extracts.

		C. abscissum		*P. citricarpa*		*F. graminearum*	*X. citri*
Treatments		**MIC μg/mL**	**PDF symptoms**	**MIC μg/mL**	**Pycnidia**	**MIC μg/mL**	**MIC μg/mL**
D. vochysiae	CMRP4321	120	+	36	154 ± 7^{a}	110	**85**
	CMRP4322	1	–	10	$83 \pm 6^{*c}$	40	100
	CMRP4326	40	+	40	138 ± 8^{b}	10	101
	CMRP4332	36	+	36	$33 \pm 7^{*e}$	36	**99**
D. cerradensis	CMRP4331	40	+	10	$91 \pm 9^{*c}$	110	101
	CMRP4324	36	+	36	$89 \pm 16^{*c}$	110	100
D. cf. *heveae* 1	CMRP4329	36	+	36	155 ± 4^{a}	110	106
Diaporthe sp.	CMRP4330	36	+	10	$22 \pm 5^{*e}$	36	100
Coniochaeta sp.	CMRP4325	36	+	40	148 ± 11^{a}	36	101
N. primolutea	CMRP4323	40	–	40	$52 \pm 4^{*d}$	40	100
P. stromaticum	CMRP4328	40	–	10	$42 \pm 10^{*e}$	10	**79**
Aspergillus sp. section *Flavi*	CMRP4327	36	+	36	171 ± 12^{a}	110	92
Carbendazim (control)		NE	–	NE	0^{f}	NE	NE
Control with methanol		NE	+	NE	168 ± 14^{a}	NE	NE

Underlined MIC – extracts with higher mycelial growth inhibition values, MIC against X. citri (in bold extracts with bactericidal activity), - absence of symptoms, + presence of symptoms, and NE not evaluated.

**Samples that were significant in the reduction of growth compared to the control in the ANOVA ($p < 0.01$). The same subscript letter in the same column means the values are not different.*

isolates, including the new species *D. cerradensis* CMRP4331, and *D. vochysiae* CMRP4322, *Diaporthe* sp. CMRP4330, and *P. stromaticum* CMRP4328 (**Table 1**). The extracts of the isolates *D. vochysiae* CMRP4326 and *P. stromaticum* CMRP4328 inhibited the conidia germination of *F. graminearum* with MIC values of 10 μg/mL.

Extracts of Endophytic Fungi Have Activity Against Citrus Pathogenic Bacteria

Four extracts showed inhibitory activity against *X. citri* subsp. *citri* in which the IC values were below 100 μg/mL: *P. stromaticum* CMRP4328 (MIC: 79 μg/mL), *D. vochysiae* CMRP4321 (MIC: 85 μg/mL) *Aspergillus* sp. section *Flavi* (MIC: 92 μg/mL), and *D. vochysiae* CMRP4332 (MIC: 99 μg/mL). Extracts from *D. vochysiae* CMRP4321, *P. stromaticum* CMRP4328, and *D. vochysiae* CMRP4332 displayed bactericidal action (**Table 1**).

Inhibition of Post-Bloom Fruit Drop Development in Citrus Flowers

The ability of the 12 extracts, which showed great antifungal activity against *C. abscissum*, to inhibit the PFD symptoms in citrus flowers, was evaluated. This qualitative analysis assesses the presence or absence of symptoms of PFD (typical peach-orange necrotic lesions). After 48 h of inoculation, the extracts produced by *D. vochysiae* CMRP4322, *N. primolutea* CMRP4223, and *P. stromaticum* CMRP4328 completely inhibit symptoms in flowers (**Supplementary Table 1** and **Figure 4**). The lesions observed in the flowers treated with the other extracts are similar to the typical PFD lesion shown in **Figure 4a**.

Inhibition of *P. citricarpa* Pycnidia Development in Citrus Leaves

We also evaluated the ability of extracts to inhibit the formation of *P. citricarpa* pycnidia in citrus leaves, and five extracts were able to inhibit more than 50% of pycnidia production (**Supplementary Table 1** and **Figure 5**), *Diaporthe* sp. CMRP4330 (86%; **Figure 5d**), *D. vochysiae* CMRP4332 (81%; **Figure 5e**), *P. stromaticum* CMRP4328 (75%; **Figure 5f**), and *N. primolutea* CMRP4323 (69%; **Figure 5g**). We highlight the extracts from strains *Diaporthe* sp. CMRP4330 and *P. stromaticum* CMRP4328 that were able to reduce pycnidia formation and the mycelial growth.

HPLC-UV/MS and TLC Analyses of Selected Fungal Extracts

The bioactive extracts produced by the top interesting 12 endophytic fungi (*D. vochysiae* CMRP4321, CMRP4322, CMRP4326, and CMRP4332, *D. cerradensis* CMRP4324 and CMRP431, *D.* cf. *heveae* 1 CMRP4329, *Diaporthe* sp. CMRP4330, *N. primolutea* CMRP4323, *Coniochaeta* sp. CMRP4325, *Aspergillus* sp. section *Flavi* CMRP4327, and *P. stromaticum* CMRP4328) have been subjected for chemical screening (TLC and HPLC-UV/MS analyses) followed by metabolite data analysis. The extracts generated from the small-scale fermentations of these fungal strains have been dissolved in MeOH and subjected to HPLC-UV/MS and TLC analyses. The major class of compounds are aflatoxins and xanthones (**Figure 6**). The HPLC-UV/MS analyses of these extracts displayed several interesting UV/vis and MS peaks (**Supplementary Figures 10–42**). For example, HPLC-UV/MS

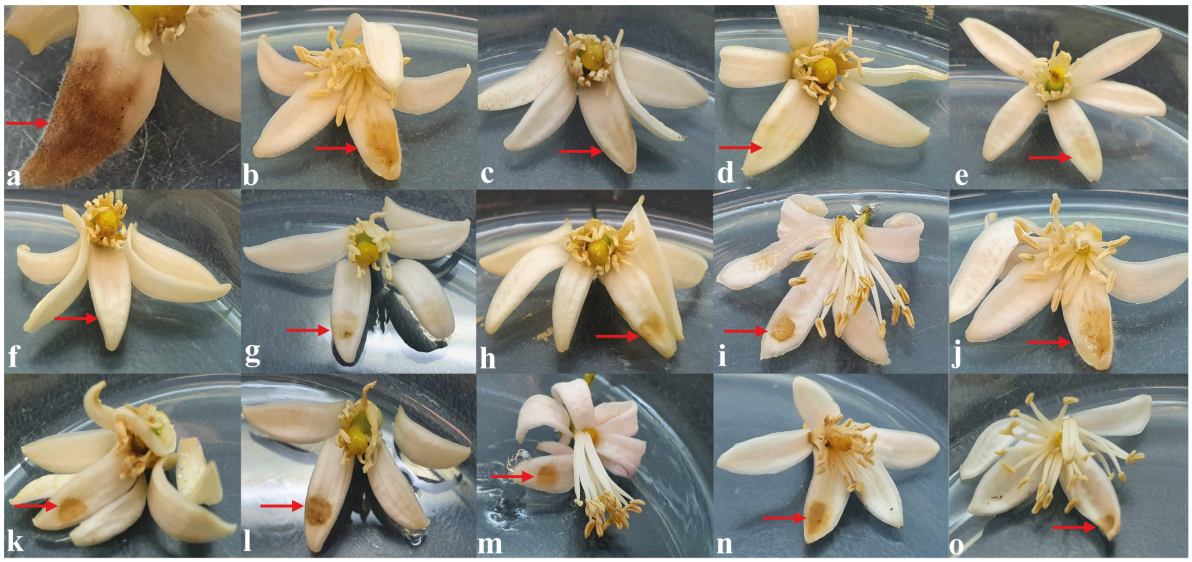

FIGURE 4 | *In vitro* assay to evaluate the activity of the extracts to inhibit the development of post-bloom fruit drop (PFD) in citrus flowers, 48 h after inoculation with 5 μL of conidial suspension of *Colletotrichum abscissum* (10^6 conidia/mL; red arrows) added with: **(a)** 5 μL of saline solution (showing the characteristic symptom of PDF), **(b)** 5 μL of methanol (control), **(c)** 10 μL with carbendazim (Derosal – control), and 5 μL of each endophytic extracts: **(d)** *Diaporthe vochysiae* CMRP4322, **(e)** *Nemania primolutea* CMRP4323, **(f)** *Pseudofusicoccum stromaticum* CMRP4328, **(g)** *D. vochysiae* CMRP4321, **(h)** *D. vochysiae* CMRP4326, **(i)** *D. vochysiae* CMRP4332, **(j)** *D. cerradensis* CMRP4331, **(k)** *D. cerradensis* CMRP4324, **(l)** *D.* cf. *heveae* 1 CMRP4329, **(m)** *Diaporthe* sp. CMRP4330, **(n)** *Coniochaeta* sp. CMRP4325, and **(o)** *Aspergillus* sp. section *Flavi* CMRP4327.

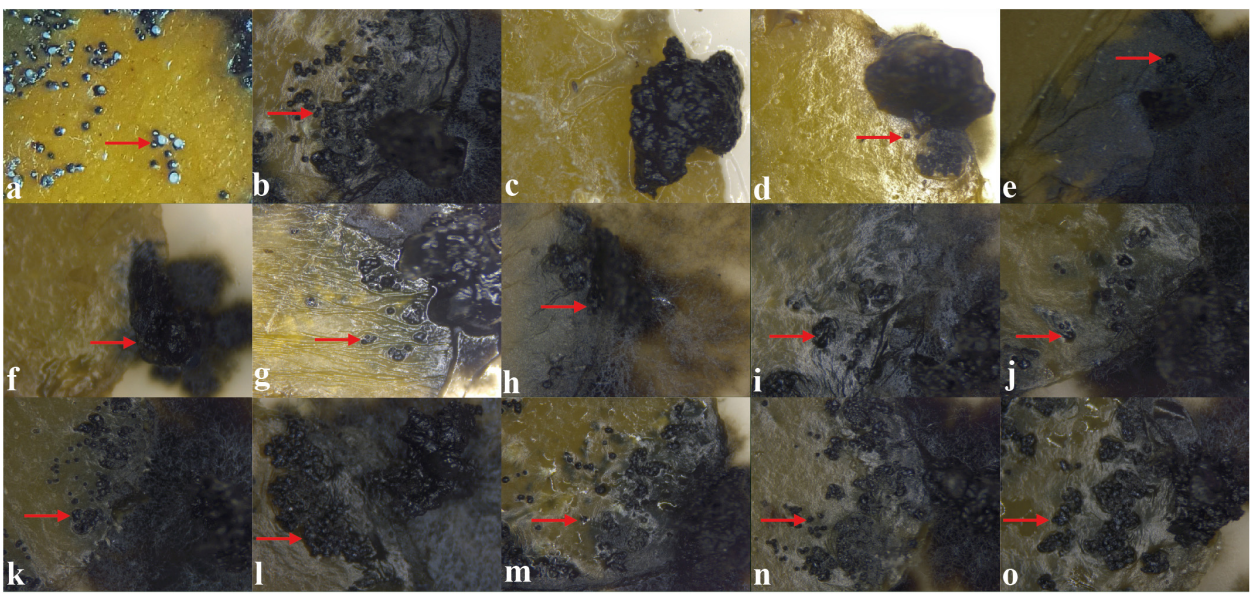

FIGURE 5 | *In vitro* assay to evaluate the activity of the extracts to inhibit the development of pycnidia in citrus leaves, 21 days after the inoculation of mycelial disks of *Phyllosticta citricarpa* added with: **(a)** 10 μL of saline solution (showing characteristic pycnidia), **(b)** 10 μL of methanol (control), **(c)** 10 μL of carbendazim (Derosal; control), and 10 μL of each endophytic extracts: **(d)** *Diaporthe* sp. CMRP4330, **(e)** *D. vochysiae* CMRP4332, **(f)** *Pseudofusicoccum stromaticum* CMRP4328, **(g)** *Nemania primolutea* CMRP4323, **(h)** *D. vochysiae* CMRP4322, **(i)** *D. cerradensis* CMRP4324, **(j)** *D. cerradensis* CMRP4331, **(k)** *D. vochysiae* CMRP4326, **(l)** *Coniochaeta* sp. CMRP4325, **(m)** *D. vochysiae* CMRP4321, **(n)** *D.* cf. *heveae* 1 CMRP4329, and **(o)** *Aspergillus* sp. section *Flavi* CMRP4327. The red arrows represent the pycnidia formation.

analyses of the extracts produced by four strains (*D. vochysiae* CMRP4321, CMRP4322, and CMRP4332, and *P. stromaticum* CMRP4328) indicate the presence of several interesting compounds with similar UV/vis chromophores (**Supplementary Figures 10–16, 30, 31, 38–41**). In the same manner, the LCMS analysis of the fungus *Coniochaeta* sp. CMRP4325 extract showed

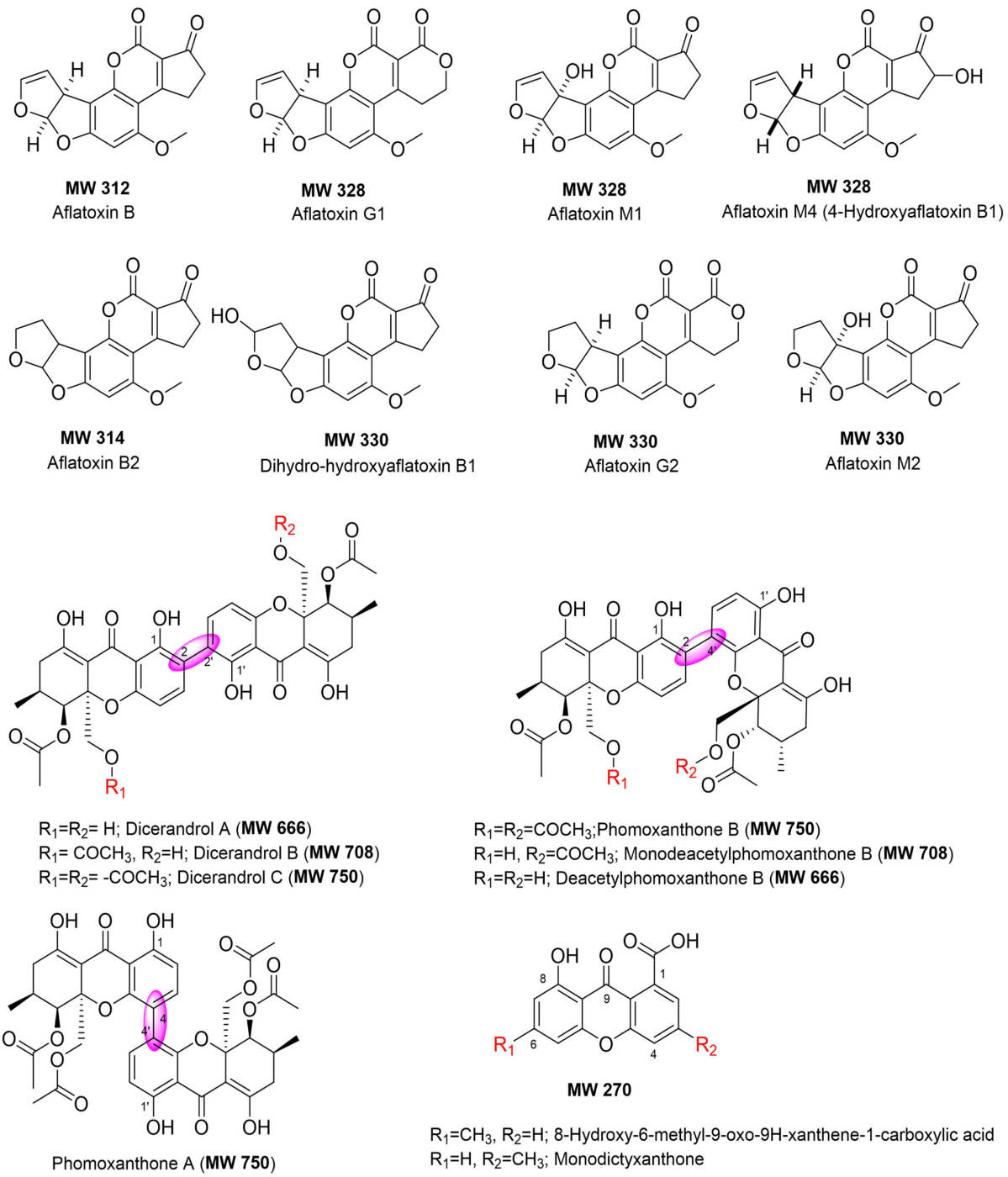

FIGURE 6 | Chemical structures of compounds identified in the extracts of selected endophytic fungi (using HPLC-UV/vis, MS and TLC analyses, and AntiBase search).

two major peaks with molecular weights of 324 and 306 Daltons, respectively, with $\Delta m/z$ = 18 Daltons difference, consistent with loss of water. AntiBase (Laatsch, 2017) search afforded no matched hits, which likely indicates two new fungal metabolites (**Supplementary Figures 22**, **23**). The HPLC-UV/MS analysis of another fungus extract (*Aspergillus* sp. section *Flavi* CMRP4327) was very rich in terms of its metabolites (**Supplementary Figures 26–29**) and shows several peaks with similar UV/vis that matched with the aflatoxin class of compounds (**Figure 6**). The LC mass spectra of these peaks revealed three peaks with different retention times, but the same molecular weight (MW 338) as well as other major peaks with MW of 354, 312, and

422 Daltons. In addition, the TLC of the *Aspergillus* sp. section *Flavi* CMRP4327 extract (**Supplementary Figure 42**) displayed several blue-fluorescent UV bands at 254/365 nm. The extract of *D.* cf. *heveae* 1 CMRP4329 showed three major HPLC peaks with similar UV/vis chromophores, with a major peak of MS = 324 Daltons. No mass match for these compounds were found in an AntiBase search, indicating new compounds in this crude extract. The fungus strain *Diaporthe* sp. CMRP4330 displayed two major peaks (HPLC R_t = 20.96 and 21.19 min) with a similar UV/vis spectrum and the same molecular weight (MW 338; **Supplementary Figure 34**). An AntiBase search showed no hits matching the molecular weights and UV/vis of these two HPLC peaks, which indicates novelty of these two compounds. The generated extracts by the remaining fungal strains (*N. primolutea* CMRP4323, *D. cerradensis* CMRP4324 and CMRP4331, and *D. vochysiae* CMRP4326) did not show major peaks in the HPLC-MS analyses, however, they might contain some none-UV/vis bioactive compounds, or the extracts produced from these strains did not contain compound with good solubility in MeOH.

DISCUSSION

Plant diseases caused by microorganisms remain one of the major obstacles in agriculture, and more effective treatments for diseases caused by pathogens of citrus and maize are necessary. An ecologically attractive alternative to control plant diseases is the use of secondary metabolites produced by endophytes (Khare et al., 2018; Savi et al., 2019a). In the past decade we isolated a large number of endophytic fungi from leaves and petioles of the medicinal plants *V. divergens* and *S. adstringens*, respectively, located in two highly diverse biomes in Brazil: Pantanal and Cerrado (Carvalho et al., 2012; Hokama et al., 2016; Noriler et al., 2018). Here, we report on 12 endophytes producing secondary metabolites that were able to inhibit the mycelial growth of important pathogens of citrus (*C. abscissum*, *P. citricarpa*, and *X. citri*). We also report on extracts that inhibited the maize pathogenic fungus *F. graminearum*.

The isolates with biological activity (**Supplementary Table 3**) belong to the Ascomycota phylum, one of the most prevalent eukaryotic groups in the world (Park et al., 2017). In addition, Sordariomycetes was the most prevalent class among the endophytes selected. *Diaporthe* was the dominant genus among the endophytes that showed potential for production of compounds with antifungal activity. The genus *Diaporthe* belongs to the family Diaporthaceae and is composed of hundreds of species (Chepkirui and Stadler, 2017). We performed multilocus DNA sequence analyses using five loci (ITS, *tef1*, *tub2*, *his3*, and *cal*) commonly used in previous phylogenetic studies of *Diaporthe* species (Gomes et al., 2013; Guarnaccia et al., 2018; Yang et al., 2018; Guo et al., 2020). The final phylogenetic trees distinguished four species of the *Diaporthe* genus that showed potential against plant pathogens, including the new species *D. cerradensis* described in this study. This species was collected in the Cerrado, the Brazilian savanna and the extracts produced by two representatives of this species (CMRP4324 and CMRP4331) showed interesting results, especially against the pathogenic citrus fungi *C. abscissum* and *P. citricarpa*.

The genus *Diaporthe* is a rich source of bioactive secondary metabolites, including volatile and non-volatile compounds, which have been shown to be effective against plant pathogens (Singh et al., 2011; Noriler et al., 2019; Savi et al., 2020; Xu et al., 2021). This genus has also been recognized as a producer of several new compounds of great interest in biotechnology (Nicoletti and Fiorentino, 2015; Santos et al., 2016; Tahir et al., 2017). Santos et al. (2016) reported that endophytic isolates of *D. terenbinthifolii* were able to colonize citrus plants and produce secondary metabolites with activity against *P. citricarpa*, suggesting that this species could be used as a potential biological controller of the CBS disease. The multilocus phylogenetic analyses revealed four isolates belonging to the *D. vochysiae* species. This species was described by Noriler et al. (2019), in which compounds produced by the isolate LGMF1583 were characterized and tested, showing compounds with activity against human pathogenic bacteria.

Fungi endophytes isolates from two Brazilian biomes, Cerrado and Pantanal showed potential to produce secondary metabolites with activity against phytopathogens. In the present study, we isolated the endophyte *D. vochysiae* from both biomes and four strains showed potential to inhibit the growth of both target phytopathogens of this study. This species was initially isolated from the Pantanal biome as an endophyte of *V. divergens* (Noriler et al., 2019) and the extract produced from this isolate showed activities against human pathogens. The four strains belonging to the new species *D. cerradensis* were isolated from plants of the Cerrado biome, two obtained in this study, one (LGMF1616) obtained by Noriler et al. (2018) also from *S. adstringens* leaves and one isolate (UFMGCB4807, previously called *Diaporthe* cf. *mayteni*) was obtained as an endophyte from plant leaves of *C. guianensis* by Ferreira et al. (2015).

Both plant tissues (leaf and petiole) harbored endophytes producers of secondary metabolites with biological activity. One example is the species *D.* cf. *heveae* 1 isolated in the present study as an endophyte of petiole of *S. adstringens*, and isolated from leaf of *S. adstringens* by Noriler et al. (2018). The secondary metabolites from both strains showed activity against plant pathogens (Noriler et al., 2018; Savi et al., 2020). Our data reinforces the importance of both Brazilian biomes as a source of endophytes with biotechnological potential. Further studies can provide more information about fungi endophytic community structures across tissues and biomes.

Extracts produced by the isolates *D. vochysiae* CMRP4322, *P. stromaticum* CMRP4328, and *N. primolutea* CMRP4323 also inhibited the mycelial growth of *C. abscissum* more than the fungicide carbendazim, demonstrating the potential of the metabolites from these endophytic isolates to control citrus pathogens. These same extracts inhibited the development of PFD symptoms in the flowers (**Figures 1A**, **4**). These results are promising since the treatment with the fungicide carbendazim can reduce, but not eliminate the phytopathogen development in field (Savi et al., 2020). In addition to the inhibition of mycelial growth, the isolate *D. vochysiae* CMRP4322 also inhibited the germination of *C. abscissum* conidia at lower than 1 μg/mL

concentrations. These results are quite interesting due to the PFD cycle caused by the production of conidia in already infected flowers, which are then splashed on surrounding leaves, twigs and floral buds that remain after the blossom period (Agostini et al., 1992; Silva-junior et al., 2014; Pinho et al., 2015; Silva A. O. et al., 2016; Savi et al., 2019b). In Brazil, PDF disease leads to large losses in citrus production, estimated 80%, when rainy periods occur during the bloom phase (Goes et al., 2008; Silva A. O. et al., 2016).

Isolates *D. vochysiae* CMRP4322, *Diaporthe* sp. CMRP4330, and *P. stromaticum* CMRP4328 produced extracts that significantly inhibited the mycelial growth of *P. citricarpa*. We also showed that these extracts considerably reduced the formation of pycnidia on leaf surfaces (**Figures 1B**, **5**). *P. citricarpa* affects fruit, leaves and twigs of several citrus hosts causing diverse symptoms (Kotzé, 2000; Guarnaccia et al., 2019). To control the CBS several fungicide applications may be necessary, leading to an increase in the costs of citrus production. However, if this disease is not fully controlled, it depreciates the commercial value of the fruits (Silva G. J. et al., 2016; Schreuder et al., 2018; Hendricks et al., 2020). In addition, citrus fruits with CBS symptoms are subject to quarantine regulations in the European Union restricting market access for countries with the presence of CBS disease and reduce the availability of citrus fruits to consumers in the off-season in Europe (Agostini et al., 2006; EU, 2015; Moyo et al., 2020).

Four isolates, *D. vochysiae* CMRP4322, *Diaporthe* sp. CMRP4330, *D. cerradensis* CMRP4331, and *P. stromaticum* CMRP4328 showed low values of MIC (10 μg/mL) capable of inhibiting the germination of *P. citricarpa* conidia. According to Sposito et al. (2011) and Tran et al. (2018), conidia are important sources of inoculum of *P. citricarpa* and play an important role in increasing the prevalence and spread of CBS disease. Therefore, these four extracts may be explored as an alternative option for CBS control. Endophytic microorganisms or their secondary metabolites can be used as alternatives to reduce the application of fungicides in the control of CBS and PFD (Santos et al., 2016; Tonial et al., 2017; Savi et al., 2020).

Three extracts analyzed (*D. vochysiae* CMRP4321 and CMRP4332, as well as *P. stromaticum* CMRP4328) were bactericidal against *X. citri* subsp. *citri*. This pathogenic bacterium causes citrus canker, a serious disease that affects citrus production worldwide (Fu et al., 2020). *X. citri* can colonize all above ground tissues of citrus plants, including young leaves, thorns, shoots, and fruits (Ferreira et al., 2016; Ference et al., 2018). As one of the most important citrus pathogens, *X. citri* causes serious economic losses due to reduced crop yield and quality, the costs of eradication measures, containment and obstacles to fruit exports. Moreover, the control of this bacterium results in an important environmental alert related to increased use of copper-based pesticides and the development of resistance to antimicrobials (Miller et al., 2009; Robène et al., 2020; Behlau, 2021).

The isolate *D. vochysiae* CMRP4326 inhibited the mycelial growth of a maize pathogen *F. graminearum*. Moreover, two extracts of isolates *D. vochysiae* CMRP4326 and *P. stromaticum* CMRP4328 completely inhibited the germination of conidia of this pathogen at low concentration (10 μg/mL). *F. graminearum* is an important pathogen affecting the yield and production of cereals, including maize and wheat worldwide (Schöneberg et al., 2016). In addition to causing direct yield loss through tissue rotting, *F. graminearum* can also cause crop contamination with mycotoxins, rendering the grain unsafe for human and livestock consumption and imposing higher costs on producers (Arunachalam and Doohan, 2013; Maresca, 2013; Pfordt et al., 2020). Different strategies are used to reduce the impact of FBH, including crop rotation, tillage practices, and fungicide application and planting of less susceptible cultivars (Jones et al., 2018). These strategies reached only low to moderate success (Wegulo et al., 2011; Mousa et al., 2015). Therefore, our results point to a promising alternative since secondary metabolites reported here prevent the germination of asexual spores, which is essential to break the cycle of the diseases.

HPLC-UV/MS analyses of the extracts produced by four strains (*D. vochysiae* CMRP4321, CMRP4322, and CMRP4332, and *P. stromaticum* CMRP4328) indicate the presence of several interesting compounds with similar UV/vis chromophores. AntiBase (Laatsch, 2017) search using MS and UV/vis, resulted in several xanthone-analogs (**Figure 6**) that matches with MS and UV/vis, including dicerandrol A (MW 666), dicerandrol B (MW 708), dicerandrol C (MW 750); phomoxanthone B (MW 750), or its mono- or di-deacetylated analogs (MW 708 and 666, respectively), all of them have been reported previously as fungal metabolites (Isaka et al., 2001; Wagenaar and Clardy, 2001; Zhang et al., 2008; Cao et al., 2012; Choi et al., 2013; Ding et al., 2013; Ronsberg et al., 2013; Kumla et al., 2017). The HPLC-UV/MS analysis of another fungus extract (*Aspergillus* sp. section *Flavi* CMRP4327) was very rich in metabolites (**Supplementary Figures 26–29**). AntiBase (Laatsch, 2017) and literature search using the aforementioned data indicates that this strain is a potential producer of aflatoxins (Asao et al., 1965; Benkerroum, 2020; Zhang and Banerjee, 2020). However, no aflatoxin analogs have been reported previously with MW 338, which designates this strain a potential producer of new aflatoxin-analogs (Laatsch, 2017).

Based on the aforementioned LCMS and TLC results, this work highlights that some of the selected strains including *D. vochysiae* CMRP4322, *D.* cf. *heveae* 1 CMRP4329, and *Diaporthe* sp. CMRP4330, *Coniochaeta* sp. CMRP4325, *Aspergillus* sp. section *Flavi* CMRP4327, and *P. stromaticum* CMRP4328, can now be considered promising strains for potential discovery of new bioactive natural products, and have been selected for future studies (including scale-up fermentations, isolation, and structure elucidation of the new bioactive compounds produced by these strains). Results will be published later somewhere else.

The compounds produced by endophytic microorganisms have been showing promise as a more environmentally friendly alternative (Wang et al., 2019). We reported here the capacity of 12 endophytic fungi isolated from tissues of the medicinal plants *V. divergens* and *S. adstringens* to produce secondary metabolites with biological activities against phytopathogenic fungi and bacteria. These metabolites directly affect the mycelium growth, germination of conidia, or symptoms development of important fungi pathogens of citrus (*C. abscissum* and *P. citricarpa*), and

act also inhibiting the mycelial growth of the maize pathogen *F. graminearum*. In addition, some of these metabolites revealed bactericidal activity against an important pathogenic bacterium of citrus, *X. citri* subsp. *citri*. The herein described *D. cerradensis* is a new species of the *Diaporthe* genus. Its discovery again shows the capacity of medicinal plants found in Brazil to host a diverse group of fungi with biotechnological potential. Further studies are needed to identify the bioactive compounds and also for the field evaluation of the endophytes or their metabolites in the control of plant pathogens.

DATA AVAILABILITY STATEMENT

The datasets presented in this study can be found in online repositories. The names of the repository/repositories and accession number(s) can be found below: [Diaporthe cerradensis MB#839350 – (https://www.mycobank.org/)].

AUTHOR CONTRIBUTIONS

CG, DS, JI, and KS: conceived and designed the experiments. JI, RS, SN, BA, GD, and HF: performed the experiments. JI, DS, KS, and CG: analyzed the data. JI, DS, CG, KS, GD, and HF: writing – original draft. JI, DS, CH, JR, KS, and JT: writing – review and editing. CG, JR, KS, and JT: supervision. All authors read and approved the final manuscript.

FUNDING

This work was supported by the INCT Citrus CNPq 465440/2014-2 Brazil and CNPq grant 309971/2016-0 and 424738/2016-3 to CG, CAPES-Brazil – grant to JI, and FAPESP 2015/50162-2 – grant to HF. This work was also supported by National Institutes of Health grants R01 CA243529, R01 GM115261, the Center of Biomedical Research Excellence (COBRE) in Pharmaceutical Research and Innovation (CPRI, NIH P20 GM130456), the University Professorship in Pharmacy (to JR), the University of Kentucky College of Pharmacy and the National Center for Advancing Translational Sciences (UL1TR000117 and UL1TR001998).

SUPPLEMENTARY MATERIAL

The Supplementary Material for this article can be found online at: https://www.frontiersin.org/articles/10.3389/fmicb.2021.714750/full#supplementary-material

REFERENCES

Agostini, J. P., Peres, N. A., Mackenzie, S. J., Adaskaveg, J. E., and Timmer, L. W. (2006). Effect of fungicides and storage conditions on postharvest development of citrus sblack spot and survival of *Guignardia* citricarpa in fruit tissues. *Plant Dis.* 90, 1419–1424. doi: 10.1094/PD-90-1419

Agostini, J. P., Timmer, L. W., and Mitchell, D. J. (1992). Morphological and pathological characteristics of strains of Colletotrichum gloeosporioides form Citrus. *APS* 82, 1377–1382.

Allen, E., and Valdes, C. (2016). *Brazil's corn industry and the effect on the seasonal pattern of U.S. corn exports*. U.S. Department of Agriculture, Economic Research Service.

Aly, A. H., Debbab, A., and Proksch, P. (2011). Fungal endophytes: unique plant inhabitants with great promises. *J. Appl. Microbiol. Biotechnol.* 90, 1829–1845. doi: 10.1007/s00253-011-3270-y

Arunachalam, C., and Doohan, F. M. (2013). Trichothecene toxicity in eukaryotes: Cellular and molecular mechanisms in plants and animals. *Toxicol. Lett.* 217, 149–158. doi: 10.1016/j.toxlet.2012.12.003

Asao, T., Büchi, G., Abdel-Kader, M. M., Chang, S. B., Wick, E. L., and Wogan, G. N. (1965). The structures of aflatoxins B and G1. *J. Am. Chem. Soc.* 87, 882–886. doi: 10.1021/ja01082a031

Behlau, F. (2021). An overview of citrus canker in Brazil. *Trop. Plant Pathol.* 46, 1–12. doi: 10.1007/s40858-020-00377-2

Benkerroum, N. (2020). Aflatoxins: producing-molds, structure, health issues and incidence in Southeast Asian and Sub-Saharan African Countries. *Int. J. Environ. Res. Public Health* 17:1215. doi: 10.3390/ijerph17041215

Cantrell, C. L., Dayan, F. E., and Duke, S. O. (2012). Natural products as sources for new pesticides. *J. Nat. Prod.* 75, 1231–1242. doi: 10.1021/np300024u

Cao, S., McMillin, D. W., Tamayo, G., Delmore, J., Mitsiades, C. S., and Clardy, J. (2012). Inhibition of tumor cells interacting with stromal cells by xanthones isolated from a Costa Rican *Penicillium* sp. *J. Nat. Prod.* 75, 793–797. doi: 10.1021/np2009863

Carbone, I., and Kohn, L. M. (1999). A method for designing primer sets for speciation studies in filamentous ascomycetes. *Mycol.* 91, 553–556. doi: 10.1080/00275514.1999.12061051

Carvalho, C. R., Gonçalves, V. N., Pereira, C. B., Johann, S., Galliza, I. V., and Rosa, C. A. (2012). The diversity, antimicrobial and anticancer activity of endophytic fungi associated with the medicinal plant *Stryphnodendron* adstringens (Mart.) Coville (Fabaceae) from the Brazilian savannah. *Symbiosis* 57, 95–107. doi: 10.1007/s13199-012-0182-2

Carvalho, S. A. D., Girardi, E. A., Mourão Filho, F. D. A. A., Ferrarezi, R. S., and Coletta Filho, H. D. (2019). Advances in citrus propagation in Brazil. *Rev. Bras. Frutic.* 41:e422. doi: 10.1590/0100-29452019422

Chepkirui, C., and Stadler, M. (2017). The genus *Diaporthe*: a rich source of diverse and bioactive metabolites. *Mycol. Prog.* 16, 477–494. doi: 10.1007/s11557-017-1288-y

Choi, J. N., Kim, J., Ponnusamy, K., Lim, C., Kim, J. G., Muthaiya, M. J., et al. (2013). Identification of a new phomoxanthone antibiotic from Phomopsis longicolla and its antimicrobial correlation with other metabolites during fermentation. *J. Antibiot.* 66, 231–233. doi: 10.1038/ja.2012.105

Copping, L. G., and Duke, S. O. (2007). Natural products that have been used commercially as crop protection agents. *Pest Manag. Sci.* 63, 524–554. doi: 10.1002/ps.1378

Crous, P. W., Groenewald, J. Z., and Risède, J. (2004). Calonectria species and their cylindrocladium anamorphs species with sphaeropedunculate vesicles. *Stud. Mycol.* 50, 415–430.

Crous, P. W., Verkley, G. J. M., and Groenewald, J. Z. (2009). *Fungal Biodiversity. CBS Laboratory Manual Series 1*. Utrecht, Netherlands: Westerdijk Fungal Biodiversity Institute.

Dayan, F. E., Cantrell, C. L., and Duke, S. O. (2009). Natural products in crop protection. *Bioorg. Med. Chem.* 17, 4022–4034. doi: 10.1016/j.bmc.2009.01.046

de Carvalho Filho, C. G., Kellner Filho, L. C., Picão, B. W., Ragozoni, A. A., Ribeiro, A. B., Nicolella, H. D., et al. (2021). Chemical composition and in vitro cytotoxicity of *Corynespora olivacea* (V18) associated with *Vochysia* divergens. *BASR* 2, 1244–1254. doi: 10.34115/basrv5n2-046

De Hoog, G. S., and Gerrits van den Ende, A. H. (1998). Molecular diagnostics of clinical strains of filamentous Basidiomycetes. *Mycoses* 41, 183–189. doi: 10.1111/j.1439-0507.1998.tb00321.x

De Menezes, H. D., Rodrigues, G. B., Teixeira, S. P., Massola, N. S. Jr., Bachmann, L., Wainwright, M., et al. (2014). In vitro photodynamic inactivation of plant-pathogenic fungi *Colletotrichum* acutatum and *Colletotrichum* gloeosporioides

with novel phenothiazinium photosensitizers. *Appl. Environ. Microbiol.* 80, 1623–1632. doi: 10.1128/AEM.02788-13

de Souza, U. J. B., Vitorino, L. C., and Bessa, L. A. (2020). Trends in the scientific literature on Stryphnodendron adstringens (Leguminosae): an important Brazilian medicinal tree. *Multi. Sci. J.* 1, 8–15. doi: 10.33837/msj.v3i1.1108

Deising, H. B., Reimann, S., and Pascholati, S. F. (2008). Mechanisms and significance of fungicide resistance. *Braz. J. Microbiol.* 39, 286–295. doi: 10.1590/s1517-83822008000200017

Ding, B., Yuan, J., Huang, X., Wen, W., Zhu, X., Liu, Y., et al. (2013). New dimeric members of the phomoxanthone family: phomolactonexanthones A, B and deacetylphomoxanthone C isolated from the fungus *Phomopsis* sp. *Mar. Drugs* 11, 4961–4972. doi: 10.3390/md11124961

Doilom, M., Dissanayake, A. J., Wanasinghe, D. N., Boonmee, S., Liu, J. K., Bhat, D. J., et al. (2017). Microfungi on tectona grandis (teak) in Northern Thailand. *Fungal Divers* 1, 107–182. doi: 10.1007/s13225-016-0368-7

EU. (2015) *Guidelines for Phyllosticta citricarpain the Union Territory*. Available Online at: https://gd.eppo.int/taxon/GUIGCI/distribution/BD.

Ference, C. M., Gochez, A. M., Behlau, F., Wang, N., Graham, J. H., and Jones, J. B. (2018). Recent advances in the understanding of *Xanthomonas citri* ssp. citri pathogenesis and citrus canker disease management. *Mol. Plant Pathol.* 19, 1302–1318. doi: 10.1111/mpp.12638

Ferreira, M. C., Vieira, M. D. L. A., Zani, C. L., de Almeida Alves, T. M., Junior, P. A. S., Murta, S. M., et al. (2015). Molecular phylogeny, diversity, symbiosis and discover of bioactive compounds of endophytic fungi associated with the medicinal Amazonian plant *Carapa* guianensis Aublet (Meliaceae). *Biochem. Syst. Ecol.* 59, 36–44. doi: 10.1016/j.bse.2014.12.017

Ferreira, R. M., Moreira, L. M., Ferro, J. A., Soares, M. R. R., Laia, M. L., Varani, A. M., et al. (2016). Unravelling potential virulence factor candidates in *Xanthomonas citri*. subsp. citri by secretome analysis. *Peer J.* 4:e1734. doi: 10.7717/peerj.1734

Ferrigo, D., Raiola, A., and Causin, R. (2016). Fusarium toxins in cereals: occurrence, legislation, factors promoting the appearance and their management. *Molecules* 21:627. doi: 10.3390/molecules21050627

Fisher, M. C., Hawkins, N. J., Sanglard, D., and Gurr, S. J. (2018). Worldwide emergence of resistance to antifungal drugs challenges human health and food security. *Science* 360, 739–742. doi: 10.1126/science.aap7999

Food and Drug Administration (2012). *Carbendazim in Orange Juice Products*. Available Online at: http://www.fda.gov/food/foodborneillnesscontaminants/pesticides/ucm288004.htm

Forero, E. (1972). Studies in Stryphnodendron (Leguminosae Mimosoideae) including two new taxa. *Brittonia* 24, 143–147. doi: 10.2307/2805864

Fu, H., Zhao, M., Xu, J., Tan, L., Han, J., Li, D., et al. (2020). Citron C-05 inhibits both the penetration and colonization of *Xanthomonas* citri subsp. citri to achieve resistance to citrus canker disease. *Hortic. Res.* 7, 1–12. doi: 10.1038/s41438-020-0278-4

Gao, Y., Liu, F., Duan, W., Crous, P. W., and Cai, L. (2017). Diaporthe is paraphyletic. *IMA Fungus* 1, 153–187. doi: 10.5598/imafungus.2017.08.01.11

Gilchrist-Saavedra, L., Fuentes-Dávila, G., Martinez-Cano, C., López-Atilano, R. M., and Duveiller, E. (2006). *Practical Guide to the Identification of Selected Diseases of Wheat and Barley*, 2nd Edn. Mexico: CIMMYT.

Glass, N. L., and Donaldson, G. C. (1995). Development of primer sets designed for use with the PCR to amplify conserved genes from filamentous ascomycetes. *ASM* 61, 1323–1330.

Glienke, C., Pereira, O. L., Stringari, D., Fabris, J., Kava-Cordeiro, V., and Galli-Terasawa, L. (2011). Endophytic and pathogenic Phyllosticta species, with reference to those associated with citrus black spot. *Persoonia* 26, 47–56. doi: 10.3767/003158511X569169

Goes, A., Garrido, R. B. O., Reis, R. F., Baldassari, R. B., and Soares, M. A. (2008). Evaluation of fungicide applications to sweet orange at different flowering stages for control of postbloomfruit drop caused by *Colletotrichum* acutatum. *Crop Prot.* 27, 71–76. doi: 10.1016/j.cropro.2007.04.007

Gomes, R. R., Glienke, C., Videira, S. I. R., Lombard, L., Groenewald, J. Z., and Crous, P. W. (2013). Diaporthe: a genus of endophytic, saprobic and plant pathogenic fungi. *Persoonia* 31, 1–41. doi: 10.3767/003158513X666844

González-González, M. G., Gómez-Sanchis, J., Blasco, J., Soria-Olivas, E., and Chueca, P. (2020). Citrus Yield: a dashboard for mapping yield and fruit quality of citrus in precision agriculture. *Agronomy* 10:128. doi: 10.3390/agronomy10010128

Guarnaccia, V., Gehrmann, T., Silva-Junior, G. J., Fourie, P. H., Haridas, S., and Vu, D. (2019). Phyllosticta citricarpa and sister species of global importance to *Citrus*. *Mol. Plant Pathol.* 20, 1619–1635. doi: 10.1111/mpp.12861

Guarnaccia, V., Groenewald, J. Z., Li, H., Glienke, C., Carstens, E., and Hattingh, V. (2017). First report of Phyllosticta citricarpa and description of two new species, P. paracapitalensis and P. paracitricarpa, from citrus in Europe. *Stud. Mycol.* 87, 161–185. doi: 10.3767/003158515X688433

Guarnaccia, V., Groenewald, J. Z., Woodhall, J., Armengol, J., Cinelli, T., and Eichmeier, A. (2018). Diaporthe diversity and pathogenicity revealed from a broad survey of grapevine diseases in Europe. *Persoonia Mol. Phylogeny Evol. Fungi.* 40, 135–153. doi: 10.3767/persoonia.2018.40.06

Guerreiro, R. L., Bergier, I., McGlue, M. M., Warren, L. V., de Abreu, U. G. P., Abrahão, J., et al. (2019). The soda lakes of Nhecolândia: a conservation opportunity for the Pantanal wetlands. *PECON* 1, 9–18. doi: 10.1016/j.pecon.2018.11.002

Guo, Y. S., Crous, P. W., Bai, Q., Fu, M., Yang, M. M., and Wang, X. H. (2020). High diversity of Diaporthe species associated with pear shoot canker in China. *Persoonia* 45, 132–162. doi: 10.3767/persoonia.2020.45.05

Hardoim, P. R., Van Overbeek, L. S., Berg, G., Pirttilä, A. M., Compant, S., and Campisano, A. (2015). The hidden world within plants: ecological and evolutionary considerations for defining function of microbial endophytes. *Microbiol. Mol. Biol. Rev.* 79, 293–320. doi: 10.1128/MMBR.00050-14

Hendricks, K. E., Christman, M. C., and Roberts, P. D. (2020). The effect of weather and location of fruit within the tree on the incidence and severity of citrus black spot on Fruit. *Sci. Rep.* 10, 1–12. doi: 10.1038/s41598-020-58188-z

Hendricks, K. E. M., Donahoo, R. S., Roberts, P. D., and Christman, M. C. (2013). Effect of copper on growth characteristics and disease control of the recently introduced *Guignardia* citricarpa on citrus in Florida. *Am. J. Plant Sci.* 4, 282–290. doi: 10.4236/ajps.2013.42037

Hilário, S., Santos, L., and Alves, A. (2021). *Diaporthe* amygdali, a species complex or a complex species? *Fungal Biol.* 7, 505–518. doi: 10.1016/j.funbio.2021.01.006

Hokama, Y., Savi, D. C., Assad, B., Aluizio, R., Gomes-Figueiredo, J., and Adamoski, D. (2016). "Endophytic fungi isolated from Vochysia divergens in the Pantanal, Mato Grosso do Sul: diversity, phylogeny and biocontrol of Phyllosticta citricarpa," in *Endophytic Fungi: Diversity, Characterization and Biocontrol*, 4th Edn, ed. E. Hughes (Hauppauge, NY: Nova), 1–25.

Hörner, M., Giglio, V. F., Santos, A. J. R. W. A., Westphalen, A. B., Iglesias, B. A., Martins, P. R., et al. (2008). Triazenes and antibacterial activity. *Rev. Bras. Cienc. Farm.* 44, 441–449. doi: 10.1590/S1516-93322008000300014

Isaka, M., Jaturapat, A., Rukseree, K., Danwisetkanjana, K., Tanticharoen, M., and Thebtaranonth, Y. (2001). Phomoxanthones A and B, novel xanthone dimers from the endophytic fungus *Phomopsis* species. *J. Nat. Prod.* 64, 1015–1018. doi: 10.1021/np010006h

Ivory, S. J., McGlue, M. M., Spera, S., Silva, A., and Bergier, I. (2019). Vegetation, rainfall, and pulsing hydrology in the Pantanal, the world's largest tropical wetland. *Environ. Res. Lett.* 14:124017. doi: 10.1088/1748-9326/ab4ffe

Jones, S., Farooqi, A., Foulkes, J., Sparkes, D., Linforth, R., and Ray, R. V. (2018). Canopy and ear traits associated with avoidance of *Fusarium* head blight in wheat. *Front. Plant Sci.* 9:1021. doi: 10.3389/fpls.2018.01021

Katoh, K., and Toh, H. (2008). Recent developments in the MAFFT multiple sequence alignment program. *Brief. Bioinform.* 9, 286–298. doi: 10.1093/bib/bbn013

Khare, E., Mishra, J., and Arora, N. K. (2018). Multifaceted interactions between endophytes and plant: developments and prospects. *Front. Microbiol.* 9:2732. doi: 10.3389/fmicb.2018.02732

Kim, B., Han, J. W., Ngo, M. T., Le Dang, Q., Kim, J. C., Kim, H., et al. (2018). Identification of novel compounds, oleanane-and ursane-type triterpene glycosides, from Trevesiapalmata: Their biocontrol activity against phytopathogenic fungi. *Sci. Rep.* 8:1452. doi: 10.1038/s41598-018-32956-4

Kotzé, J. M. (2000). "Black spot," in *Compendium of Citrus Diseases*, eds L. W. Timmer, S. M. Garnsey, and J. H. Graham (St. Paul, MN: American Phytopathological Society Press Inc), 23–25.

Kumar, S., Stecher, G., and Tamura, K. (2015). MEGA7: molecular evolutionary genetics analysis version 7 for bigger datasets. *Mol. Biol. Evol.* 33, 1870–1874. doi: 10.1093/molbev/msw054

Kumla, D., Shine Aung, T., Buttachon, S., Dethoup, T., Gales, L., Pereira, J. A., et al. (2017). A new dihydrochromone dimer and other secondary metabolites from cultures of the marine sponge-associated Fungi *Neosartorya* fennelliae KUFA 0811 and *Neosartorya* tsunodae KUFC 9213. *Mar. Drugs* 15:375. doi: 10.3390/md15120375

Laatsch, H. (2017). *AntiBase. "The natural compound identifier"*. Weinheim, Germany: Wiley-VCH.

Manawasinghe, I. S., Dissanayake, A. J., Li, X., Liu, M., Wanasinghe, D. N., Xu, J., et al. (2019). High genetic diversity and species complexity of Diaporthe associated with grapevine dieback in China. *Front. Microbiol.* 10:1936. doi: 10.3389/fmicb.2019.01936

Manganyi, M. C., and Ateba, C. N. (2020). Untapped potentials of endophytic fungi: a review of novel bioactive compounds with biological applications. *Microorganisms* 8:1934. doi: 10.3390/microorganisms8121934

Maresca, M. (2013). From the gut to the brain: Journey and pathophysiological effects of the food associated trichothecene mycotoxin deoxynivalenol. *Toxins* 5, 784–820.

Miller, S. A., Beed, F. D., and Harmon, C. L. (2009). Plant disease diagnostic capabilities and networks. *Annu. Rev. Phytopathol.* 47, 15–38.

Morão, L. G., Polaquini, C. R., Kopacz, M., Torrezan, G. S., Ayusso, G. M., Dilarri, G., et al. (2018). A simplified curcumin targets the membrane of Bacillus subtilis. *Microbiol. Open* 8:e683. doi: 10.1002/mbo3.683

Mousa, W. K., Shearer, C. R., Limay-Rios, V., Zhou, T., and Raizada, M. N. (2015). Bacterial endophytes from wild maize suppress Fusarium graminearum in modern maize and inhibit mycotoxin accumulation. *Front. Plant Sci.* 6:805. doi: 10.3389/fpls.2015.00805

Moyo, P., Fourie, P. H., Masikane, S. L., de Oliveira Fialho, R., Mamba, L. C., du Plooy, W., et al. (2020). The effects of postharvest treatments and sunlight exposure on the reproductive capability and viability of *Phyllosticta* citricarpa in citrus black spot fruit lesions. *Plants* 9:1813. doi: 10.3390/plants9121813

Myers, N., Mittermeier, R. A., Mittermeier, C. G., Da Fonseca, G. A., and Kent, J. (2000). Biodiversity hotspots for conservation priorities. *Nature* 6772, 853–858. doi: 10.1038/35002501

Nicoletti, R., and Fiorentino, A. (2015). Plant bioactive metabolites and drugs produced by endophytic fungi of Spermatophyta. *Agriculture* 5, 918–970. doi: 10.3390/agriculture5040918

Noriler, S. A., Savi, D. C., Aluizio, R., Palácio-Cortes, A. M., Possiede, Y. M., and Glienke, C. (2018). Bioprospecting and structure of fungal endophyte communities found in the Brazilian Biomes, Pantanal, and Cerrado. *Front. microbiol.* 9:1526. doi: 10.3389/fmicb.2018.01526

Noriler, S. A., Savi, D. C., Ponomareva, L. V., Rodrigues, R., Rohr, J., Thorson, J. S., et al. (2019). Vochysiamides A and B: Two new bioactive carboxamides produced by the new species *Diaporthe* vochysiae. *Fitoterapia* 138:104273. doi: 10.1016/j.fitote.2019.104273

Oerke, E. C. (2006). Crop losses to pests. *J. Agric. Sci.* 144, 31–43.

Park, Y. H., Kim, Y., Mishra, R. C., and Bae, H. (2017). Fungal endophytes inhabiting mountain-cultivated ginseng (Panax ginseng Meyer): Diversity and biocontrol activity against ginseng pathogens. *Sci. Rep.* 7, 1–10. doi: 10.1038/s41598-017-16181-z

Pellenz, N. L., Barbisan, F., Azzolin, V. F., Marques, L. P. S., Mastella, M. H., Teixeira, C. F., et al. (2019). Healing activity of Stryphnodendron adstringens (Mart.), a Brazilian tannin-rich species: A review of the literature and a case series. *Wound Med.* 1:100163. doi: 10.1016/j.wndm.2019.100163

Petrini, O. (1986). *Taxonomy of Endophytic Fungi of Aerial Plant Tissues. Microbiology of the Phyllosphere*. Cambridge: Cambridge University Press, 175–187.

Pfordt, A., Ramos Romero, L., Schiwek, S., Karlovsky, P., and von Tiedemann, A. (2020). Impact of environmental conditions and agronomic practices on the prevalence of Fusarium species associated with ear-and stalk rot in maize. *Pathogens* 9:236. doi: 10.3390/pathogens9030236

Pham, J. V., Yilma, M. A., Feliz, A., Majid, M. T., Maffetone, N., Walker, J. R., et al. (2019). A review of the microbial production of bioactive natural products and biologics. *Front. Microbiol.* 10:1404. doi: 10.3389/fmicb.2019.01404

Pinho, D. B., Lopes, U. P., Pereira, O. L., Silveira, A. L., and de Goes, A. (2015). Colletotrichum abscissum Pinho., O.L. *Pereira*, sp. nov. fungal planet description sheets. *Persoonia* 34, 236–237. doi: 10.3767/003158515X688433

Qin, C. F., He, M. H., Chen, F. P., Zhu, W., Yang, L. N., and Wu, E. J. (2016). Comparative analyses of fungicide sensitivity and SSR marker variations indicate a low risk of developing azoxystrobin resistance in Phytophthora infestans. *Sci. Rep.* 6:20483. doi: 10.1038/srep20483

Quiroga, E. N., Sampietro, A. R., and Vattuone, M. (2001). Screening antifungal activity of selected medicinal plants. *J. Ethnopharmacol.* 74, 89–96. doi: 10.1016/S0378-8741(00)00350-0

Raeder, J., and Broda, P. (1985). Rapid preparation of DNA from filamentous fungi. *Let. Appl. Microbiol.* 1, 17–20. doi: 10.1111/j.1472-765X.1985.tb01479.x

Rayner, R. W. (1970). *A mycological colour chart*. Kew, UK: Commonwealth Mycological Institute.

Robène, I., Maillot-Lebon, V., Chabirand, A., Moreau, A., Becker, N., Moumène, A., et al. (2020). Development and comparative validation of genomic-driven PCR-based assays to detect Xanthomonas citripv. citri in citrus plants. *BMC Microbiol.* 20:296. doi: 10.1186/s12866-020-01972-8

Rodrigues, M. B. C., Andreote, F. D., Sposito, M. B., Aguillar-Vildoso, C. I., Araujo, W. L., and Pizzirani-Kleiner, A. A. (2007). Resistência a benzimidazois por Guignardia citricarpa. *Pesq. Agropec. Bras.* 42, 323–327. doi: 10.1590/S0100-204X2007000300004

Ronquist, F., Teslenko, M., Van Der Mark, P., Ayres, D. L., and Darling, A. (2011). MrBayes 3.2: efficient Bayesian phylogenetic inference and model choice across a large model space. *Syst. Biol.* 61, 539–542. doi: 10.1093/sysbio/sys029

Ronsberg, D., Debbab, A., Mandi, A., Vasylyeva, V., Bohler, P., Stork, B., et al. (2013). Pro-apoptotic and immunostimulatory tetrahydroxanthone dimers from the endophytic fungus Phomopsis longicolla. *J. Org. Chem.* 78, 12409–12425. doi: 10.1021/jo402066b

Sang, H., and Kim, J. I. (2020). Advanced strategies to control plant pathogenic fungi by host-induced gene silencing (HIGS) and spray-induced gene silencing (SIGS). *Plant Biotechnol. Rep.* 14, 1–8. doi: 10.1007/s11816-019-00588-3

Santos, P. J. C., Savi, D. C., Gomes, R. R., Goulin, E. H., da costa Senkiv, C., and Tanaka, F. A. (2016). Diaporthe endophytica and D. terebinthifolii from medicinal plants for biological control of *Phyllosticta* citricarpa. *Microbiol. Res.* 186, 153–160. doi: 10.1016/j.micres.2016.04.002

Savi, D. C., Aluizio, R., and Glienke, C. (2019a). Brazilian plants: an unexplored source of endophytes as producers of active metabolites. *Planta Med.* 1, 1–12. doi: 10.1055/a-0847-1532

Savi, D. C., Haminiuk, C. W. I., Sora, G. T. S., Adamoski, D. M., Kensiki, J., and Winnischofer, S. M. B. (2015). Antitumor, antioxidant and antibacterial activities of secondary metabolites extracted by endophytic actinomycetes isolated from *Vochysia* divergens. *Int. J. Pharm. Chem. Biol. Sci.* 5, 347–356.

Savi, D. C., Noriler, S., Ponomareva, L. V., Thorson, J., Rohr, J., Glienke, C., et al. (2020). Dihydroisocoumarins produced by Diaporthe cf. heveae LGMF1631 inhibiting citrus pathogens. *Folia Microbiol.* 65, 381–392. doi: 10.1007/s12223-019-00746-8

Savi, D. C., Rossi, B. J., Rossi, G. R., Ferreira-Maba, L. S., Bini, I. H., da Silva Trindade, E., et al. (2019b). Microscopic analysis of colonization of *Colletotrichum* abscissum in citrus tissues. *Microbiol. Res.* 226, 27–33. doi: 10.1016/j.micres.2019.05.005

Savi, D. C., Shaaban, K. A., Gos, F. M. W. R., Ponomareva, L. V., Thorson, J. S., Glienke, C., et al. (2018). Phaeophleospora vochysiae Savi&Glienke sp. nov. Isolated from *Vochysia* divergens found in the pantanal, Brazil, produces bioactive secondary metabolites. *Sci. Rep.* 8:3122. doi: 10.1038/s41598-018-21400-2

Schöneberg, T., Martin, C., Wettstein, F. E., Bucheli, T. D., Mascher, F., and Bertossa, M. (2016). Fusarium and mycotoxin spectra in Swiss barley are affected by various cropping techniques. *Food Addit. Contam. Part A Chem. Anal. Control.* 33, 1608–1619. doi: 10.1080/19440049.2016.1219071

Schreuder, W., du Plooy, W., Erasmus, A., Savage, C., Basson, E., Lennox, C., et al. (2018). Postharvest fungicide treatments and cold storage control citrus black spot infections. *Crop. Prot.* 112, 332–342. doi: 10.1016/j.cropro.2018.06.020

Schulz, K. F., Chalmers, I., Hayes, R. J., and Altman, D. G. (1995). Empirical evidence of biasdimensions of methodological quality associated with estimates of treatment effects in controlled trials. *JAMA* 273, 408–412. doi: 10.1001/jama.273.5.408

Silva, A. O., Savi, D. C., Gomes, F. B., Gos, F. M. W. R., Silva, G. J., and Glienke, C. (2016). Identification of *Colletotrichum* species associated with postbloom fruit

drop in Brazil through GAPDH sequencing analysis and multiplex PCR. *Eur. J. Plant Pathol.* 147, 731–748. doi: 10.1007/s10658-016-1038-z

Silva, C. I, Regasini, L. O., Petronio, M. S., Silva, D. H., Bolzani, V. S., Belasque, J. Jr., et al. (2013). Antibacterial activity of alkylgallates against Xanthomonas citrisubsp. citri. *J. Bacteriol. Res.* 195, 85–94. doi: 10.1128/JB.01442-12

Silva, G. J. Jr., Scapin, M. S., Silva, F. P., Silva, A. R. P., Behlau, F., and Ramos, H. H. (2016). Spray volume and fungicide rates for citrus black spot control based on tree canopy volume. *Crop Prot.* 85, 38–45. doi: 10.1016/j.cropro.2016.03.014

Silva-junior, G. J., Spósito, M. B., Marin, D. R., and Amorim, L. (2014). Efficacy and timing of application of fungicides for control of citrus postbloom fruit drop. *Crop. Prot.* 59, 51–56. doi: 10.1016/j.cropro.2014.01.012

Singh, A., Singh, D. K., Kharwar, R. N., White, J. F., and Gond, S. K. (2021). Fungal endophytes as efficient sources of plant-derived bioactive compounds and their prospective applications in natural product drug discovery: insights, avenues, and challenges. *Microorganisms* 9:197. doi: 10.3390/microorganisms9010197

Singh, S. K., Strobel, G. A., Knighton, B., Geary, B., Sears, J., and Ezra, D. (2011). An endophytic Phomopsis sp. possessing bioactivity and fuel potential with its volatile organic compounds. *Microb. Ecol.* 61, 729–739. doi: 10.1007/s00248-011-9818-7

Souza-Moreira, T. M., Queiroz-Fernandes, G. M., and Pietro, R. C. (2018). Stryphnodendron species known as "barbatimão": a comprehensive report. *Molecules* 4:910. doi: 10.3390/molecules23040910

Sposito, M. B., Amorim, L., Bassanezi, R. B., Yamamoto, P. T., Felippe, M. R., and Czermainski, A. B. C. (2011). Relative importance of inoculum sources of guignardiacitricarpa on the citrus black spot epidemic in Brazil. *Crop Prot.* 30, 1546–1552. doi: 10.1016/j.cropro.2011.08.007

Strassburg, B. B. N., Brooks, T., Feltran-Barbieri, R., Iribarrem, A., Crouzeilles, R., Loyola, R., et al. (2017). Moment of truth for the Cerrado hotspot. *Nat. Ecol. Evol.* 1, 1–3. doi: 10.1038/s41559-017-0099

Strobel, G. A. (2003). Endophytes as sources of bioactive products. *Microbes Infect.* 5, 535–544. doi: 10.1016/S1286-4579(03)00073-X

Tahir, H. A., Gu, Q., Wu, H., Niu, Y., Huo, R., and Gao, X. (2017). Bacillus volatiles adversely affect the physiology and ultra-structure of *Ralstonia* solanacearum and induce systemic resistance in tobacco against bacterial wilt. *Sci. Rep.* 7:40481. doi: 10.1038/srep40481

Tan, X., Zhou, Y., Zhou, X., Xia, X., Wei, Y., and He, L. (2018). Diversity and bioactive potential of culturable fungal endophytes of *Dysosma* versipellis; a rare medicinal plant endemic to China. *Sci. Rep.* 8:5929. doi: 10.1038/s41598-018-24313-2

Tonial, F., Maia, B. H. L. N. S., Savi, D. C., Vicente, V. A., and Gomes, R. R. (2017). Biological activity of Diaporthe terebinthifolii extracts against *Phyllosticta* citricarpa. *FEMS Microbiol. Lett.* 364:fnx026. doi: 10.1093/femsle/fnx026

Tran, N. T., Miles, A. K., Smith, M. W., Dietzgen, R. G., and Drenth, A. (2018). Pathogenicity of phyllostictacitricarpa ascospores on *Citrus* spp. *Plant Dis.* 102, 1386–1393. doi: 10.1094/PDIS-08-17-1331-RE

Wagenaar, M. M., and Clardy, J. (2001). Dicerandrols, new antibiotic and cytotoxic dimers produced by the fungus Phomopsis longicolla isolated from an endangered mint. *J. Nat. Prod.* 64, 1006–1009. doi: 10.1021/np010020u

Walder, F., Schlaeppi, K., Wittwer, R., Held, A. Y., Vogelgsang, S., and Van der Heijden, M. G. (2017). Community profiling of Fusarium in combination with other plant-associated fungi in different crop species using SMRT sequencing. *Front. Plant Sci.* 8:2019. doi: 10.3389/fpls.2017.02019

Wang, H., Tian, R., Tian, Q., Yan, X., Huang, L., and Ji, Z. (2019). Investigation on the antifungal ingredients of Saccharothrix yanglingensis Hhs. 015, an antagonistic endophytic actinomycete isolated from cucumber plant. *Molecules* 24:3686. doi: 10.3390/molecules24203686

Wang, J. F., He, W. J., Huang, X. L., Tian, X. P., Liao, S. R., Yang, B., et al. (2016). Antifungal new oxepine-containing alkaloids and xanthones from the deep-sea-derived fungus *Aspergillus* versicolor SCSIO 05879. *J. Agr. Food. Chem.* 64, 2910–2916. doi: 10.1021/acs.jafc.6b00527

Wegulo, S. N., Bockus, W. W., Nopsa, J. H., De Wolf, E. D., Eskridge, K. M., and Peiris, K. H. (2011). Effects of integrating cultivar resistance and fungicide application on fusarium head blight and deoxynivalenol in winter wheat. *Plant Dis.* 95, 554–560. doi: 10.1094/PDIS-07-10-0495

White, T. J., Bruns, T., Lee, J., and Taylor, J. (1990). "Amplification and direct sequencing of fungal ribosomal RNA genes for phylogenetics," in *PCR Protocols: A Guide to Methods and Applications*, eds M. A. Innis, D. H. Gelfand, J. J. Sninsky, and T. J. White (San Diego, CA: Academic Press), 315–322.

Xu, T. C., Lu, Y. H., Wang, J. F., Song, Z. Q., Hou, Y. G., Liu, S. S., et al. (2021). Bioactive secondary metabolites of the genus diaportheand anamorph phomopsis from terrestrial and marine habitats and endophytes: 2010–2019. *Microorganisms* 9:217. doi: 10.3390/microorganisms9020217

Yang, Q., Fan, X. L., Guarnaccia, V., and Tian, C. M. (2018). High diversity of *Diaporthe* species associated with dieback diseases in China, with twelve new species described. *MycoKeys.* 39:97. doi: 10.3897/mycokeys.39.26914

Zamuner, C. F. C., Dilarri, G., Cavalca, L. B., Behlau, F., Silva, T. G., Bacci, M. Jr., et al. (2020). A cinnamaldehyde-based formulation as an alternative to sodium hypochlorite for post-harvest decontamination of citrus fruit. *Trop. Plant Pathol.* 45, 701–709. doi: 10.1007/s40858-020-00338-9

Zhang, K., and Banerjee, K. (2020). A review: sample preparation and chromatographic technologies for detection of aflatoxins in foods. *Toxins (Basel)* 12:539. doi: 10.3390/toxins12090539

Zhang, W., Krohn, K., Zia, U., Florke, U., Pescitelli, G., Di Bari, L., et al. (2008). New mono- and dimeric members of the secalonic acid family: blennolides A-G isolated from the fungus Blennoria sp. *Chemistry.* 14, 4913–4923. doi: 10.1002/chem.200800035

Zhao, M., Guo, D. L., Liu, G. H., Fu, X., Gu, Y. C., Ding, L. S., et al. (2020). Antifungal halogenated cyclopentenones from the endophytic fungus *Saccharicola* bicolor of *Bergenia* purpurascens by the one strain-many compounds strategy. *J. Agric. Food Chem.* 68, 185–192. doi: 10.1021/acs.jafc.9b06594

Conflict of Interest: The authors declare that the research was conducted in the absence of any commercial or financial relationships that could be construed as a potential conflict of interest.

Publisher's Note: All claims expressed in this article are solely those of the authors and do not necessarily represent those of their affiliated organizations, or those of the publisher, the editors and the reviewers. Any product that may be evaluated in this article, or claim that may be made by its manufacturer, is not guaranteed or endorsed by the publisher.

frontiers in Microbiology

ORIGINAL RESEARCH
published: 30 September 2021
doi: 10.3389/fmicb.2021.757719

A Comparative Analysis of the Microbiome of Kiwifruit at Harvest Under Open-Field and Rain-Shelter Cultivation Systems

Yuan Sui[1†], Qianhua Zhao[2†], Zhenshuo Wang[3,4†], Jia Liu[1], Mingguo Jiang[5], Junyang Yue[6], Jianbin Lan[1], Jing Liu[1], Qinhong Liao[1], Qi Wang[3], Qiya Yang[2] and Hongyin Zhang[2*]*

[1] Chongqing Key Laboratory of Economic Plant Biotechnology, College of Landscape Architecture and Life Science/Institute of Special Plants, Chongqing University of Arts and Sciences, Yongchuan, Chongqing, China, [2] School of Food and Biological Engineering, Jiangsu University, Zhenjiang, China, [3] Department of Plant Pathology, MOA Key Lab of Pest Monitoring and Green Management, College of Plant Protection, China Agricultural University, Beijing, China, [4] Engineering Research Center of Plant Growth Regulators/Crop Chemical Control Research Center, Department of Agronomy, College of Agronomy and Biotechnology, China Agricultural University, Beijing, China, [5] Guangxi Key Laboratory for Polysaccharide Materials and Modifications, School of Marine Sciences and Biotechnology, Guangxi University for Nationalities, Nanning, China, [6] College of Horticulture, Anhui Agricultural University, Hefei, China

OPEN ACCESS

Edited by:
Jesús Navas-Castillo, Institute of Subtropical and Mediterranean Horticulture La Mayora, Spain

Reviewed by:
Jia Deng, Southwest Forestry University, China
Tomislav Cernava, Graz University of Technology, Austria

***Correspondence:**
Qiya Yang
yangqiya1118@163.com
Hongyin Zhang
zhanghongyin126@126.com

† These authors have contributed equally to this work

Specialty section:
This article was submitted to Microbe and Virus Interactions with Plants, a section of the journal Frontiers in Microbiology

Received: *12 August 2021*
Accepted: *07 September 2021*
Published: *30 September 2021*

Citation:
Sui Y, Zhao Q, Wang Z, Liu J, Jiang M, Yue J, Lan J, Liu J, Liao Q, Wang Q, Yang Q and Zhang H (2021) A Comparative Analysis of the Microbiome of Kiwifruit at Harvest Under Open-Field and Rain-Shelter Cultivation Systems. Front. Microbiol. 12:757719. doi: 10.3389/fmicb.2021.757719

The composition of microbial communities can directly affect fruit quality, health status, and storability. The present study characterized the epiphytes and endophytes of "Hongyang" and "Cuiyu" kiwifruit at harvest under grown under open-field (OF) and rain-shelter (RS) cultivation systems. Disease incidence in kiwifruit was significantly lower ($p < 0.05$) under the RS system than it was under the OF system. High-throughput sequencing [16S V3-V4 ribosomal region and the fungal internal transcribed spacer (ITS2)] was conducted to compare the composition of the epiphytic and endophytic microbial community of kiwifruit under the two cultivation systems. Results indicated that the abundance of Actinobacteria, Bacteroidetes, Enterobacteriales, Acetobacterales, *Sphingomonas*, *Pseudomonas,* and *Sphingobacterium* was higher under the RS system, relative to the OF system, while the abundance of Capnodiales, Hypocreales, *Vishniacozyma,* and *Plectosphaerella* was also higher under the RS system. Some of these bacterial and fungal taxa have been reported to as act as biocontrol agents and reduce disease incidence. Notably, the α-diversity of the epiphytic bacterial and fungal communities on kiwifruit was higher under RS cultivation. In summary, RS cultivation reduced natural disease incidence in kiwifruit, which may be partially attributed to differences in the structure and composition of the microbial community present in and on kiwifruit.

Keywords: ***Actinidia chinensis*, cultivation mode, disease incidence, microbial community, fruit quality**

INTRODUCTION

Kiwifruit, known as the "king of fruits," has a high nutraceutical value. Kiwifruit is rich in bioactive compounds with antioxidant properties and is a major source of vitamin C (Richardson et al., 2018). Kiwifruit fruits, however, are susceptible to various plant pathogens, including *Botrytis cinerea* and *Alternaria alternata* (Cheng et al., 2019), *Pseudomonas syringae* (Fujikawa et al., 2020), and Actinidia viruses (Zhao L. et al., 2019), which cause a variety of diseases during growth

(Ippolito and Nigro, 2000). In order to reduce disease incidence in plants and increase their economic value, rain-shelters (RS) have been used in the cultivation of several different fruits, including pear (Zhang et al., 2020), grape (Meng et al., 2012), and cherry (Tian et al., 2019). Collectively, studies have demonstrated that RS cultivation prevents excessive rainfall and hail damage to flowers and fruits and reduces disease occurrence, thus providing significant protection (Tian et al., 2019). Meng et al. (2012) reported that RS cultivation significantly reduced the incidence of grape diseases, delayed fruit ripening, and promoted the accumulation of quercetin-3-O-glucose-7-O-rhamnoside in grape skin peels during grape ripening. Claire et al. (2018) also found that RS cultivation reduced the level of fruit rot in strawberries. In the present study, RS cultivation was used to reduce the occurrence of kiwifruit natural disease and to explore the impact of RS cultivation on the microbiome of kiwifruit.

The plant microbiome plays an integral role in plant health and productivity, and has been the subject of a great deal of research in recent years (Turner et al., 2013). While the microbiome of many vegetable and field crops has been explored and characterized, much less attention has been paid to fruit crops (Busby et al., 2017). The epiphytic microbial community has a positive influence on plant health, physiology, and environmental adaptability (Kim et al., 2011; Vorholt, 2012; Dees et al., 2015). Biological control agents (BCAs) represent an environmentally friendly alternative to the use of chemical pesticides for disease control (Spadaro and Droby, 2016). Several epiphytic bacterial species isolated from the phyllosphere have been reported to be strong competitors against plant pathogens, thus acting as BCAs (Enya et al., 2007; Sartori et al., 2017). They can secrete antimicrobial substances (Insuk et al., 2020; López et al., 2020), compete for nutrients and space in a limited space, or interfere with the signaling systems of pathogens (Volksch and May, 2001). Dong et al. (2021) studied the epiphytic and endophytic fungal communities of tomato plant roots, leaves, fruits, and seeds. Some endophytic fungi, including yeast, have been proved to be inhibitors of post-harvest diseases. Endophytic yeast fungi isolated from apple were also found to have an inhibitory effect on *Monilinia fructigena*, the causal agent of soft-rot in apple (Madbouly et al., 2020). The endophytic bacteria present in tomato plants has been reported to play an important role in fostering plant growth and health (López et al., 2020). These reports indicate that microbial community composition is linked to levels of plant disease. Mamphogoro et al. (2020) reported a greater abundance of potential pathogenic bacteria on the fruit surface of immature (green) and mature (red) pepper planted under open field (OF) conditions, compared to peppers planted in a hydroponic system. Their data indicated that the microbial community of plants is affected by cultivation methods. Understanding the distribution and composition of the epiphytic and endophytic microbial community of plants may provide important information on how the RS cultivation of kiwifruit reduces the occurrence of natural disease.

In the present study, high-throughput 16S and fungal ITS amplicon sequencing was used to characterize the microbial community of kiwifruit peel and pulp tissues from fruit that was harvested from OF and RS cultivation systems. The objectives were to (i) profile the bacterial and fungal microbial taxa present in and on kiwifruit, and (ii) determine whether cultivar and the two different cultivation systems (RS and OF) influenced the structure and composition of the resident microbiota in a manner that reduced disease incidence.

MATERIALS AND METHODS

Experimental Site Description

The experimental site in this study was located at Huanggua Mountain, Yongchuan District, Chongqing City, China (29°25′47″N, 105°84′96″E). Two kiwifruit (*Actinidia chinensis*) cultivars, "Hongyang" and "Cuiyu," were grown under OF and RS conditions, with the latter being provided with the use of 0.12-mm anti-fog film (6-m height and 6-m width). A total of 20 plants were covered with polyethylene (PE) film from flowering (April) to fruit harvest (September) while another 20 were left uncovered. Each group (OF and RS) of plants contained 10 plants of "Hongyang" and 10 plants of "Cuiyu." No pesticides were applied to either group of plants over the course of the present study.

Disease Incidence and Sample Preparation

Incidence data was collected in late Septembers (the harvest time of kiwifruit) in the 2 years of 2018 and 2019. Six plants were randomly selected from a group of 10 plants. Disease incidence was assessed on three replicate groups of fruit, with each treatment group comprising 120 fruits. Natural disease incidence was calculated as a percentage [number of fruits with visible disease symptoms (Fruits with visible spots $\geq$ 5 mm in diameter are considered to be infected) divided by the total number of assessed fruits $\times$ 100].

In September 2019, six kiwifruit plants were randomly selected from a planting of kiwifruit growing under OF or RS cultivation systems. A total of 40 mid-size healthy fruits were hand-harvested from each replicate kiwifruit plant and immediately placed in sterile bags that were placed on ice and transferred to the lab for further processing. Each group has three biological replicates. All personnel involved in sample collection wore facial masks and sterile gloves to ensure sterility. Different gloves were strictly used when taking different samples to avoid contamination.

Once in the laboratory, 40 kiwifruits in each replicate group were randomly divided into two groups for the assessment of epiphytes or endophytes. Three biological replicates were used for each of the sampled groups and each replicate comprised 40 fruits. For the collection of epiphytic microbes, sterilized phosphate buffered saline (PBS) solution was added to a sterile bag containing 20 kiwifruits until the fruits were completely covered. The bags were then placed on rotary shaker at 25°C and 100 rpm for 30 min. After shaking, the solution was filtered through a 0.22 μm filter and then the membrane was placed in a centrifuge tube, frozen in liquid nitrogen, and stored at −80°C until further processing. For the collection of endophytic microbes, kiwifruit peels were firstly removed using a sterilized knife. The remaining pulp from 20 kiwifruits were cut into small

pieces and placed in a sterile bag, followed by the addition of enough PBS solution to generously cover the pieces of pulp. The bags were then placed on a rotary shaker at 25°C and 100 rpm for 30 min. After shaking, the solution was filtered with a sieve and then loaded into a centrifuge tube. After centrifugation at 4°C and 7000*g* for 30 min, the supernatant was removed, frozen in liquid nitrogen, and stored at −80°C until further processing.

Library Preparation and Amplicon Sequencing

Total genomic DNA was extracted from each kiwifruit sample using the CTAB method with slight modification (Kim et al., 2019). The quality and quantity of the extracted DNA were evaluated using a NanoDrop spectrophotometer (Thermo Fisher Scientific, Cleveland, OH, United States). The extracted DNA was then eluted in 50 μL of Elution buffer and subsequently used as a template for PCR amplification. The V3-V4 variable regions of the 16S ribosomal RNA (rRNA) gene was amplified for assessing bacterial diversity using the primers 341F (5′-CCTACGGGNGGCWGCAG-3′) and 806R (5′-GGACTACHVGGGTWTCTAAT-3′). The ITS2 variable region of the small-subunit rRNA gene was amplified for assessing fungal-diversity using the primers ITS3-KYO2F (5′-GATGAACGYAGYRAA-3′) and ITS4-2409 (5′-TCCTCCGCTTATTGATATGC-3′). The PCR conditions consisted of an initial denaturation at 94°C for 2 min; followed by 30 cycles consisting of denaturation (98°C for 10 s), annealing at 62°C for 30 s, and extension at 68°C for 30 s; and then final extension at 68°C for 5 min. The expected size of the 16S and ITS2 amplified fragments generated by each pair of primers was 466 and 381 bp, respectively. The 5′ ends of the primers were also tagged with specific barcodes for each sample.

After amplicon generation, the PCR products were assessed using 2% agarose gel electrophoresis and further purified using AMPure XP beads (Beckman Coulter Genomics, Danvers, MA, United States). The obtained amplicons were quantified using a Qubit dsDNA Assay Kit (Invitrogen, Waltham, MA, United States). Equal amounts of purified amplicons from each sample were pooled into libraries for high-throughput sequencing. High-throughput amplicon sequencing assay was performed on an Illumina Novaseq 6000 platform according to standard protocols (Illumina, San Diego, CA, United States).

Data Analysis

The raw, paired-end sequence data were first assigned to their respective samples based on their barcodes. Reads without barcode sequences were discarded. The remaining paired-end reads were merged using FLASH software with default parameters (Reyon et al., 2012). Further processing of the merged reads was done using CLC genomics workbench 20.[1] Clean reads were obtained after trimming the barcodes and primer sequences, removing shorter reads (a minimum size of 300 and 200 bp for 16S and ITS2 amplified fragments, respectively), filtering low quality reads with a quality value (Q) less than 20, and cleaning up contaminated reads through alignment (*E*-value $\leq$ *e*-05 and identity $\geq$ 80%) against the kiwifruit genome[2] (Yue et al., 2015). Chimeric sequences were also identified and filtered using VSEARCH software (version 2.3.4) to obtain high-quality clean reads (Rognes et al., 2016). The UCLUST algorithm in QIIME 1.9.1 software (Caporaso et al., 2010) was used to cluster the high-quality clean reads by alignment to the SILVA Database (version 132) (Pruesse et al., 2007) for 16S rRNA sequences and the UNITE dynamic database (Abarenkov et al., 2010) for ITS sequences. Sequences with ≥97% similarity were assigned to a specific operational taxonomic unit (OTU) and the most abundant sequence was selected as representative of each OTU (Edgar, 2013). The representative OTUs were annotated to varying taxonomic ranks, including phylum, class, order, family, genus, and species. The rarefied OTU data was used to calculate α and β diversity indices. For α diversity, the richness of each sample was evaluated using Chao1 metrics and the diversity within each sample was estimated using the observed richness (Shannon) index. For β diversity, PCoA analysis was conducted based on the Unweighted Unifrac distance, and the principal coordinate combination with the largest contribution rate was selected for plotting. PCoA analysis was conducted using the R project Vegan package (version 2.5.3) and used to compare bacterial and fungal community structure between samples. SPSS was used for significant analysis of the relative abundance of the samples between the groups. Independent sample *T* test was used for comparison between the two groups, and single-factor ANOVA was used for analysis of the samples of the three groups or more, and the significant judgment condition was $p < 0.05$.

RESULTS

Disease Incidence

The disease incidence at harvest was assessed in the two cultivars growing under the two cultivation systems (OF and RS) in 2 different years (2018 and 2019). The predominant causal pathogens were *A. alternata* and *Nigrospora oryzae*. The incidence of fruit disease was significantly lower in both cultivars for both diseases in kiwifruit cultivated under the RS compared to the OF ($p < 0.05$). The disease incidence of the "Hongyang" and "Cuiyu" cultivars was 5.7 and 2.2%, respectively, under RS conditions in 2018, while it was 15.4 and 17.4% in the two cultivars, respectively, under OF conditions (**Table 1A**). Similarly, in 2019, the disease incidence of the "Hongyang" and "Cuiyu" cultivars was 5.3 and 3.3%, respectively, under RS conditions, and 12.3 and 15.6%, respectively, under OF conditions (**Table 1B**).

High-Throughput Amplicon Sequencing

The high-throughput sequencing generated 5192782 16S rRNA and 5103950 fungal ITS raw sequences. A total of 5023302 and 5052962 bacterial and fungal clean reads were obtained, respectively, after the removal of chimeras and low-quality sequences. The resulting clean reads were classified into 3639 bacterial and 2863 fungal OTUs based on a 97% sequence

[1] https://www.qiagenbioinformatics.com/

[2] http://kir.atcgn.com/

TABLE 1 | Pre-harvest incidence of natural disease in "Hongyang" and "Cuiyu" kiwifruit cultivars in 2018 **(A)** and 2019 **(B)** grown under rain-shelter and open-field cultivation systems.

Variety	Cultivation methods	Incidence rate %
A		
Hongyang	rain-shelter	5.7 ± 0.4^{b}
Hongyang	open-field	15.4 ± 1.2^{a}
Cuiyu	rain-shelter	2.2 ± 0.3^{b}
Cuiyu	open-field	17.4 ± 1.5^{a}
B		
Hongyang	rain-shelter	5.3 ± 0.5^{b}
Hongyang	open-field	12.3 ± 1.1^{a}
Cuiyu	rain-shelter	3.3 ± 0.3^{b}
Cuiyu	open-field	15.6 ± 1.2^{a}

No disease management practices were administered during the fruit production season. Significant differences ($p < 0.05$) between rain-shelter and open-field groups within the same cultivar ("Hongyang" or "Cuiyu") are indicated by different letters.

similarity. The bacterial OTUs were assigned to 5 phyla, 16 orders, and 23 genera while the fungal OTUs were assigned to 2 phyla, 18 orders, and 19 genera.

Composition Analysis of the Bacterial Community

The phyla, Proteobacteria, Actinobacteria, Bacteroidetes, Firmicutes, and Chlamydiae accounted for 75, 18, 3, 2, and 0.7% of the assigned OTUs, respectively (**Figure 1A**). The relative abundance of Proteobacteria in RS_epi1 (RainShelter-Epiphytic-"Hongyang") samples was significantly higher ($p < 0.05$) than in RS_epi2 (RainShelter-Epiphytic-"Cuiyu") samples, while the relative abundance of Proteobacteria in RS_endo1 (RainShelter-Endophytic-"Hongyang") samples was significantly lower ($p < 0.05$) than it was in RS_endo2 (RainShelter-Endophytic-"Cuiyu") samples. The proportion of Proteobacteria in OF_epi1 (OpenField-Epiphytic-"Hongyang") samples was significantly ($p < 0.05$) lower than in OF_epi2 (OpenField-Epiphytic-"Cuiyu") samples. The proportion of Actinobacteria in "Cuiyu" samples with RS cultivation was significantly higher ($p < 0.05$) than in "Hongyang" samples, with the order of abundance being RS_epi2 (33.79%) > RS_epi1 (19.01%). The proportion of Actinobacteria in RS samples was significantly higher ($p < 0.05$) than it was in OF samples, except for the relative abundance of OF_endo2 (17.76%), which was significantly higher ($p < 0.05$) than it was in RS_endo2 (9.56%). The highest relative abundance (9.02%) of Bacteroidetes was observed in RS_epi2 samples, followed by OF_epi2 (3.91%), OF_epi1 (3.61%), and RS_epi1 (2.57%). The highest proportion of Bacteroidetes in endophyte samples was observed in the RS_endo1 sample.

At the order level. Enterobacteriaceae was dominant in RS_epi1 samples, having a relative abundance of 42.31% (**Figure 1B**). The relative abundance of Enterobacteriaceae was greater ($p < 0.05$) in RS samples than in corresponding OF samples. In regards to epiphytes, the relative abundance of Enterobacteriaceae was significantly higher ($p < 0.05$) in "Hongyang" than in "Cuiyu," while of the opposite was true for endophytic Enterobacteriaceae. Betaproteobacteriales, an order within the Proteobacteria, was the dominant order in OF_epi2 (53.24%) samples. The relative abundance of Betaproteobacteriales in epiphytic samples was higher in "Cuiyu" than in "Hongyang." The relative abundance of Micrococcales in RS samples was significantly higher than ($p < 0.05$) it was in OF samples, with the exception that the proportion in RS_endo2 samples was significantly lower ($p < 0.05$) than it was in OF_endo2 samples. The relative abundance of Sphingomonadales in RS and OF samples was similar to the distribution observed for the Micrococcales. The percentage of Xanthonadales (13.05%) and Pseudomonadales (5.83%) in RS_epi1 samples was significantly higher ($p < 0.05$) than it was in the other sample groups, and the proportion of the two orders was significantly higher ($p < 0.05$) in "Hongyang" RS samples than it was in OF samples. The relative abundance of Propionibacteriales (5.61%), Pseudonocardiales (5.79%), and Sphingobacteria (8.30%) in RS_epi2 samples was significantly higher ($p < 0.05$) than in other sample groups.

Further analysis at taxonomic rank of genus revealed significant differences in the dominant genera present in the eight different sample groups, with the exception of the unclassified category (**Figure 1C**). *Massilia*, with a relative abundance of 52.62%, was the dominant genus in OF_epi2 samples. The relative abundance of epiphytic *Massilia* was significantly lower ($p < 0.05$) in RS samples than it was in OF samples. The relative abundance of *Methylobacterium* was significantly higher ($p < 0.05$) in "Cuiyu" epiphytic samples than in "Hongyang" epiphytic samples, while the opposite trend was observed in endophytic *Methylobacterium*. The proportion of *Methylobacterium* was significantly higher ($p < 0.05$) in OF samples than in RS samples. The relative abundance of epiphytic *Stenotrophomonas* within the same cultivar, was significantly higher ($p < 0.05$) in RS samples than in OF samples. The relative abundance of *Sphingomonas* was 2.47 and 4.38% in RS_epi1 and RS_epi2, respectively, both of which were significantly higher ($p < 0.05$) than they were in other OF groups. The highest proportion (5.47%) of *Pseudomonas*, among all samples, was observed in RS_epi1 samples, and the relative abundance of *Pseudomonas* was significantly higher ($p < 0.05$) in RS epiphytic samples than in OF epiphytic samples. The highest level of relative abundance (6.68%) of *Sphingobacterium* was observed in RS_epi2 samples while its abundance in other sample groups ranged from 0.06 to 0.79%.

Composition Analysis of the Fungal Community

Ascomycota and Basidiomycota were the dominant phyla in all sample groups. with Ascomycota being the most abundant phylum, accounting for 88.66–98% of the OTUs in all sample groups (**Figure 2A**). The proportion of Ascomycota was significantly higher in RS samples than in OF samples. Within the same cultivation system, the relative abundance of Ascomycota was significantly higher ($p < 0.05$) in "Cuiyu" than in "Hongyang" samples, except

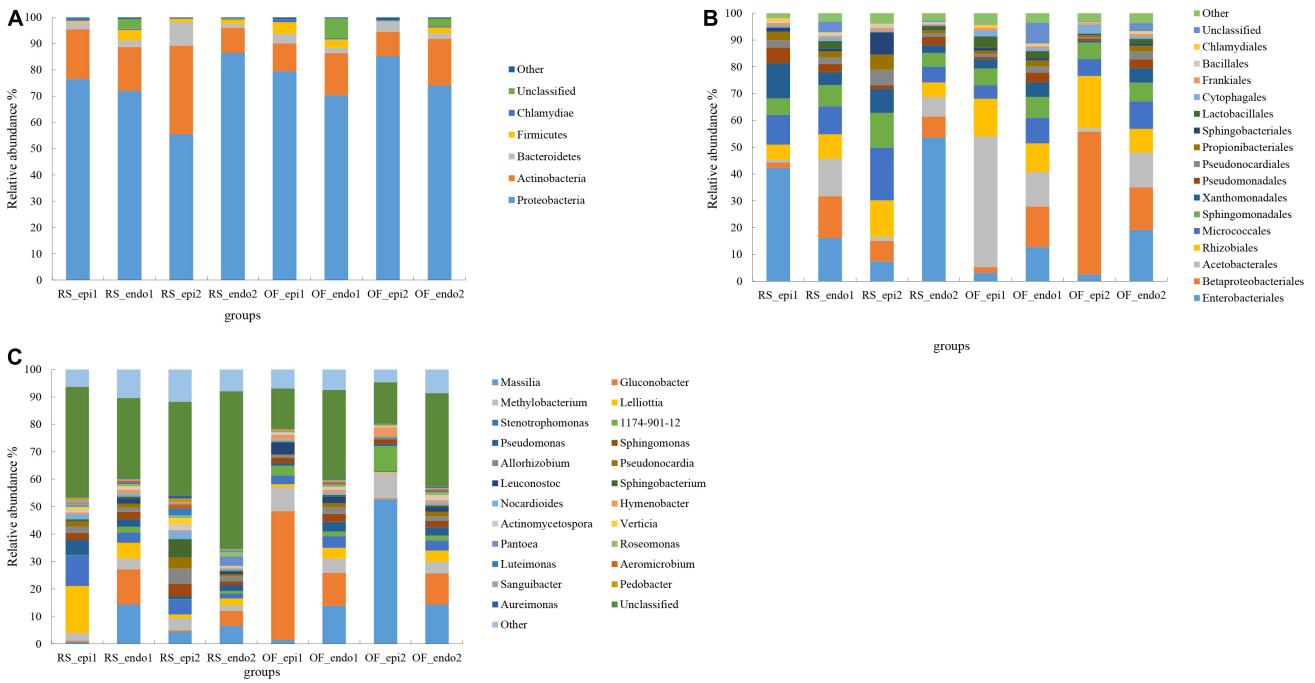

FIGURE 1 | Relative abundance of bacterial taxa at the level of phylum **(A)**, order **(B)**, and genus **(C)**. Bacterial taxa with a relative abundance <1% were grouped together and are designated as "Other." Samples labeled "RS" and "OF" designate rain-shelter (RS) and open-field (OF) samples, respectively. The terms "epi" and "endo" designate epiphytic and endophytic sample groups, respectively, and the designations "1" and "2" indicate "Hongyang" and "Cuiyu" cultivars, respectively. The samples were taken in September 2019.

that the proportion in OF_epi1 ("Hongyang") was higher than it was in OF_epi2 ("Cuiyu"). The relative abundance of Basidiomycota in the sample groups ranged from 1.91 to 9.7%. Notably, the abundance of epiphytic fungi within the same cultivar was significantly lower ($p < 0.05$) in RS samples than in OF samples.

The dominant orders of fungi were Capnodiales, Pleosporales, Botryosphaeriales, Saccharomyceteles, and Hypocreales (**Figure 2B**). The proportion of Capnodiales was higher in RS samples than it was in OF samples, and the relative abundance of epiphytic Capnodiales was significantly higher ($p < 0.05$) in RS_epi1 and RS_epi2 (87.63 and 83.03%, respectively) samples than it was in OF_epi1 and OF_epi2 (42.36 and 33.7%, respectively) samples. Pleosporales accounted for 48.47% of the OTUs in OF_epi2 samples and within the same cultivation system, the proportion of Pleosporales was significantly lower ($p < 0.05$) in "Hongyang" samples than in "Cuiyu" samples. Within the same cultivar, OF samples had a higher level of Pleosporales than RS samples. The relative abundance of Botryosphaeriales was the highest (49.2%) in OF_endo2 samples and the relative abundance of endophytic Botryosphaeriales was significantly higher ($p < 0.05$) than for the relative abundance of epiphytic. Saccharomycetales accounted for 19.43 and 14.3% of the identified OTUs in OF_epi1 and RS_endo2 samples, respectively. The relative abundance of Saccharomycetales was significantly lower ($p < 0.05$) in RS samples than in OF samples, except for RS_endo2. The relative abundance of epiphytic Hypocreales, within the same cultivation system, Hypocreales was significantly lower ($p < 0.05$) in "Hongyang" than it was in "Cuiyu," while the opposite trend was observed for endophytic Hypocreales, the abundance of epiphytic Hypocreales was significantly higher ($p < 0.05$) in RS samples than in OF samples.

Analysis of the composition of the fungal community was also conducted at the genus level (**Figure 2C**). Results revealed that some genera of pathogenic fungi were present in kiwifruit peel and pulp tissues, such as *Botryosphaeria*. The relative abundance of *Botryosphaeria* in OF_endo2 was 49.62%, which was the same proportion observed at level of order. The relative abundance of *Penicillium* in RS_endo2 was 7.04%, which was significantly higher ($p < 0.05$) than its abundance as an epiphyte. The relative abundance of epiphytic *Penicillium*, within the same cultivation system, was significantly higher ($p < 0.05$) in "Hongyang" than it was in "Cuiyu." Within the same cultivar, however, the level of epiphytic *Penicillium* was significantly lower ($p < 0.05$) in RS samples than in OF samples. The relative abundance of *Hansniapora* in OF_epi1 was 19.39%, which was significantly higher ($p < 0.05$) than it was in other groups. *Vishniacozyma* accounted for 0.19–1.1% of the OTUs in all samples, within the same cultivar, the proportion of *Vishniacozyma* was significantly higher ($p < 0.05$) in RS samples than it was in OF samples. The relative abundance of *Vishniacozyma*, within the same cultivation system, was significantly lower ($p < 0.05$) in "Hongyang" than it was in "Cuiyu." The proportion of epiphytic *Plectosphaerella*, within the same cultivar, was significantly higher ($p < 0.05$) in RS samples than it was in OF samples.

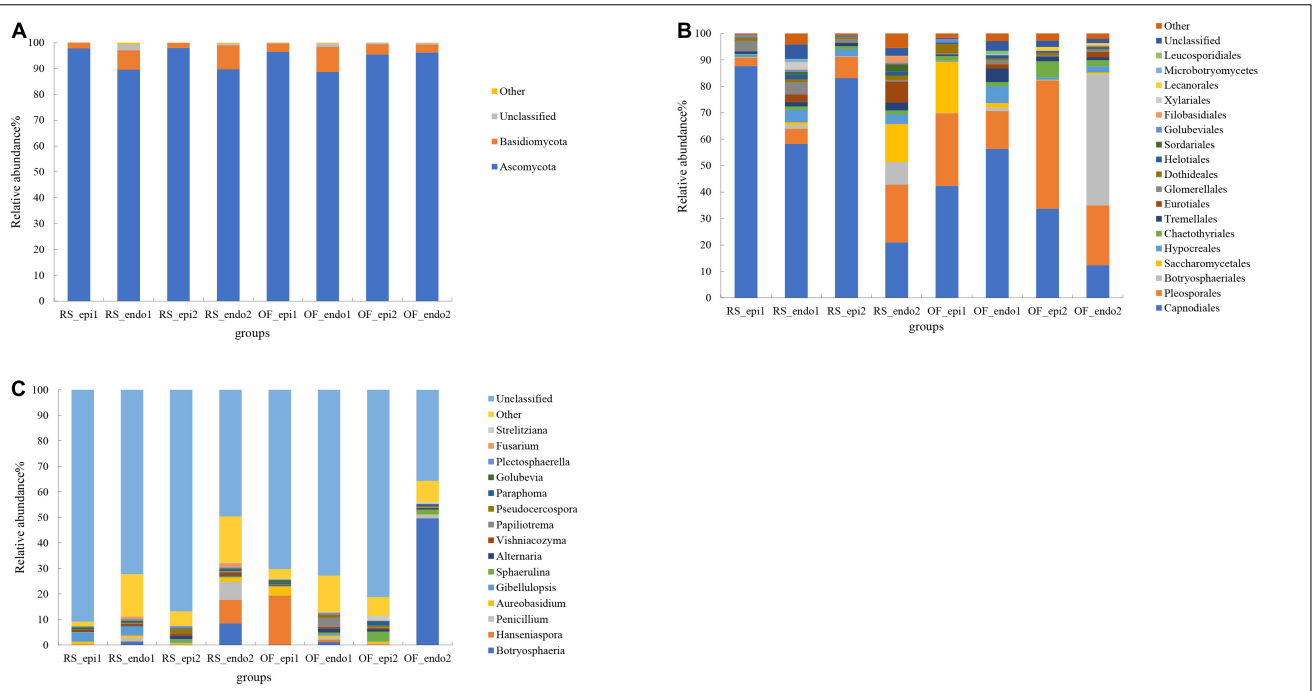

FIGURE 2 | Relative abundance of fungal taxa at the level of phylum **(A)**, order **(B)**, and genus **(C)**. The fungal taxa with a relative abundance <1% were grouped together and are designated as "Other." Samples labeled "RS" and "OF" designate rain-shelter (RS) and open-field (OF) samples, respectively. The terms "epi" and "endo" designate epiphytic and endophytic sample groups, respectively, and the designations "1" and "2" indicate "Hongyang" and "Cuiyu" cultivars, respectively. The samples were taken in September 2019.

α Diversity Analysis of Bacterial and Fungal Communities

The Shannon index of the bacterial community in RS_epi2 samples was significantly higher ($p < 0.05$) than it was in other groups (**Table 2**), while the Shannon index of OF_epi1 and OF_epi1 were the lowest. No significant differences in diversity were observed between OF_endo1, RS_endo1, and OF_endo2 samples. The Chao1 index of the bacterial community in epiphytic samples was significantly higher ($p < 0.05$) than it was in endophytic groups.

The Chao1 index of the fungal community was highest in the OF_epi2 sample group, which contained the greatest number of species, followed by RS_epi2 and OF_epi1 (**Table 3**). The Chao1 index in epi2 sample groups, regardless of cultivation system, was higher than it was in epi1 samples. The highest Shannon index was observed in RS_endo2 and OF_endo1 sample groups, followed by RS_endo1 and OF_epi2, with RS_epi1 having the lowest Shannon index.

TABLE 2 | α diversity indices (Chao1 and Shannon) of the epiphytic and endophytic bacterial community of "Hongyang" and "Cuiyu" kiwifruit grown under rain-shelter and open-field cultivation systems.

Groups	Chao1	Shannon
RS_epi1	1146.77 ± 94.50^{a}	5.25 ± 0.06^{c}
RS_endo1	292.22 ± 47.50^{bc}	5.75 ± 0.05^{b}
RS_epi2	1158.70 ± 56.42^{a}	6.15 ± 0.03^{a}
RS_endo2	379.76 ± 46.33^{b}	4.67 ± 0.31^{d}
OF_epi1	1161.76 ± 29.43^{a}	4.42 ± 0.07^{d}
OF_endo1	267.74 ± 35.10^{c}	5.67 ± 0.05^{b}
OF_epi2	1147.30 ± 20.62^{a}	4.64 ± 0.10^{d}
OF_endo2	302.03 ± 27.50^{bc}	5.68 ± 0.06^{b}

Significant differences ($p < 0.05$) between sample groups are indicated by different letters. Samples labeled "RS" and "OF" designate rain-shelter (RS) and open-field (OF) samples, respectively. The terms "epi" and "endo" designate epiphytic and endophytic sample groups, respectively, and the designations "1" and "2" indicate "Hongyang" and "Cuiyu" cultivars, respectively.

β Diversity Analysis of Bacterial and Fungal Communities

The PCoA of the bacterial community (**Figure 3A**) exhibited three distinct clusters of samples. PCoA 1 accounts for 16.84% of the variation with the bacterial communities of the 24 sample groups placed in three clusters. One cluster is primarily composed of endophytic samples, while the other two clusters are mainly composed of epiphytic samples, with samples from the same cultivation system clustering near each other. PCoA 2 explains 12.72% of the variation. In PCoA 2 the epiphytic samples of the bacterial communities representing RS samples are located higher than the OF epiphytic samples. At the same time, the placement of RS_epi2 and RS_epi1 communities is closer, indicating that their species structure is more similar. RS_endo2 and RS_endo1 communities are at the same height in the vertical coordinates. Results of the PCoA analysis are also supported by an UPGMA clustering tree (**Figure 4**).

TABLE 3 | α diversity indices (Chao1 and Shannon) of the epiphytic and endophytic fungal community of "Hongyang" and "Cuiyu" kiwifruit grown under rain-shelter and open-field cultivation systems.

Groups	Chao1	Shannon
RS_epi1	671.02 ± 60.93^{c}	2.81 ± 0.02^{e}
RS_endo1	249.63 ± 46.61^{ef}	4.89 ± 0.06^{ab}
RS_epi2	907.15 ± 61.91^{b}	3.82 ± 0.04^{c}
RS_endo2	183.08 ± 15.06^{f}	5.08 ± 0.23^{a}
OF_epi1	845.89 ± 55.66^{b}	3.69 ± 0.04^{cd}
OF_endo1	343.90 ± 8.50^{d}	5.03 ± 0.37^{a}
OF_epi2	1026.04 ± 2.05^{a}	4.60 ± 0.04^{b}
OF_endo2	274.21 ± 38.23^{de}	3.46 ± 0.12^{d}

Significant differences ($p < 0.05$) between sample groups are indicated by different letters. Samples labeled "RS" and "OF" designate rain-shelter (RS) and open-field (OF) samples, respectively. The terms "epi" and "endo" designate epiphytic and endophytic sample groups, respectively, and the designations "1" and "2" indicate "Hongyang" and "Cuiyu" cultivars, respectively.

In the PCoA plot of the fungal community (**Figure 3B**), PCoA 1 explains 18.65% of the variation and the distance between epiphytic and endophytic communities is large and the distance between the fungal communities in the two different cultivations systems (RS and OF) is much closer. PCoA 2 explains 10.90% of the variation and the distance between the epiphytic OF samples is greater than the distance between the epiphytic RS samples. Among the endophytic samples, the distance between the fungal communities in "Cuiyu" (endo2) and "Hongyang" (endo1) was great. The results of the PCoA analysis were also supported by an UPGMA clustering tree (**Figure 5**).

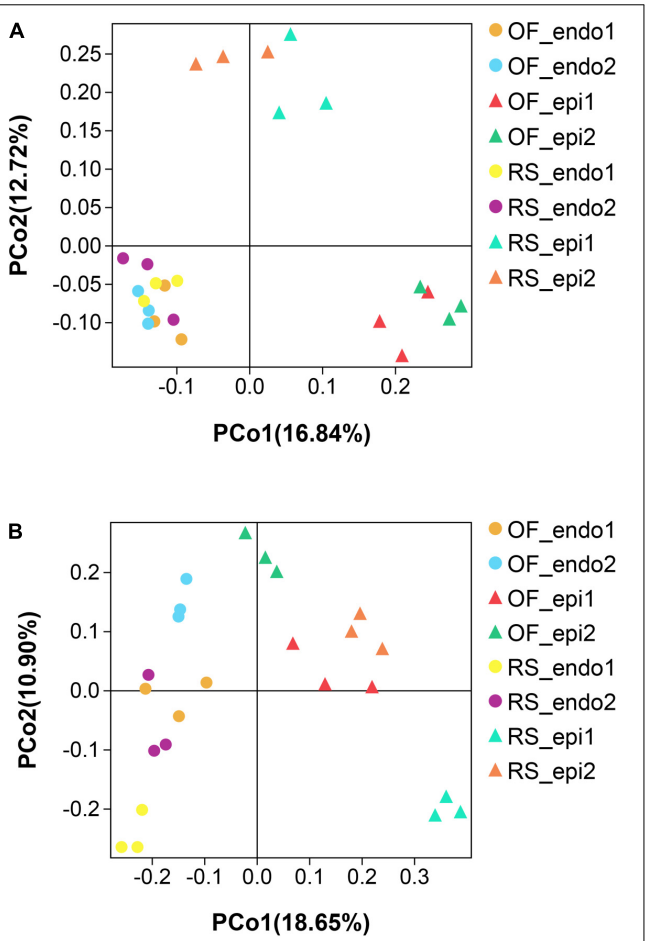

FIGURE 3 | Principal Coordinate Analysis (PCoA) analysis of bacterial **(A)** and fungal **(B)** communities in the different kiwifruit sample groups based on unweighted_unifrac distance. Samples labeled "RS" and "OF" designate rain-shelter (RS) and open-field (OF) samples, respectively. The terms "epi" and "endo" designate epiphytic and endophytic sample groups, respectively, and the designations "1" and "2" indicate "Hongyang" and "Cuiyu" cultivars, respectively. In the figure, to facilitate the distinction, we use circles to represent endophytes and upward triangles to represent epiphytes. The samples were taken in September 2019.

DISCUSSION

Pre- and post-harvest diseases of fruits resulting from microbial pathogens result in significant economic losses. Similar to reports in other fruit crops (Meng et al., 2012; Claire et al., 2018), cultivation of kiwifruit under a RS system effectively reduced the level of plant disease, relative to OF cultivation. While air pollutants are spread by wind, they are often deposited on plants and the soil surface by rainfall, which may directly or indirectly increase the incidence of both foliar and soilborne diseases (Dimabuyu et al., 2016). Compared with the OF cultivation, The humidity level and soil organic matter content are often higher in RS systems than OF systems, which can provide a more stable growth environment for plant growth (Lim et al., 2016).

The data in **Table 1** indicate that disease incidence was significantly reduced ($p < 0.05$) when kiwifruit was grown under a RS. The level of disease incidence, however, differed between the two varieties of kiwifruit. The level of disease incidence was higher in "Hongyang" kiwifruit than it was in "Cuiyu." "Hongyang" kiwifruit has been reported to be more susceptible to canker and *Penicillium* than other kiwifruit varieties (Luo et al., 2019; Zhao Z. et al., 2019). The plant host and its resident microbiota interact with each other. In the present study, we characterized the epiphytic and endophytic community composition in the two different cultivars grown under two different cultivation systems (OF and RS) to determine if there was an association between the composition of the microbial community and the observed levels of disease incidence.

The phyla, Proteobacteria, Actinobacteria, Bacteroidetes, and Firmicutes have been reported to be widely distributed on the fruit surface of plant species, and contain a variety of taxa with different ecological roles, functioning as antagonists, symbionts (especially endophytes), and saprophytes (Insuk et al., 2020; Lee et al., 2020; Mamphogoro et al., 2020). Actinobacteria have been reported to have a higher abundance in the endophytic community of kiwifruit cultivars that are more resistant to bacterial canker (Cho et al., 2018). Insuk et al. (2020) assessed the *in vitro* and *in vivo* growth- promoting activity of 13 strains of Actinomycetes isolated from bryophytes. They found that all of the tested isolates produced IAA and also sequestered iron, which promoted the growth of bryophytes. In the

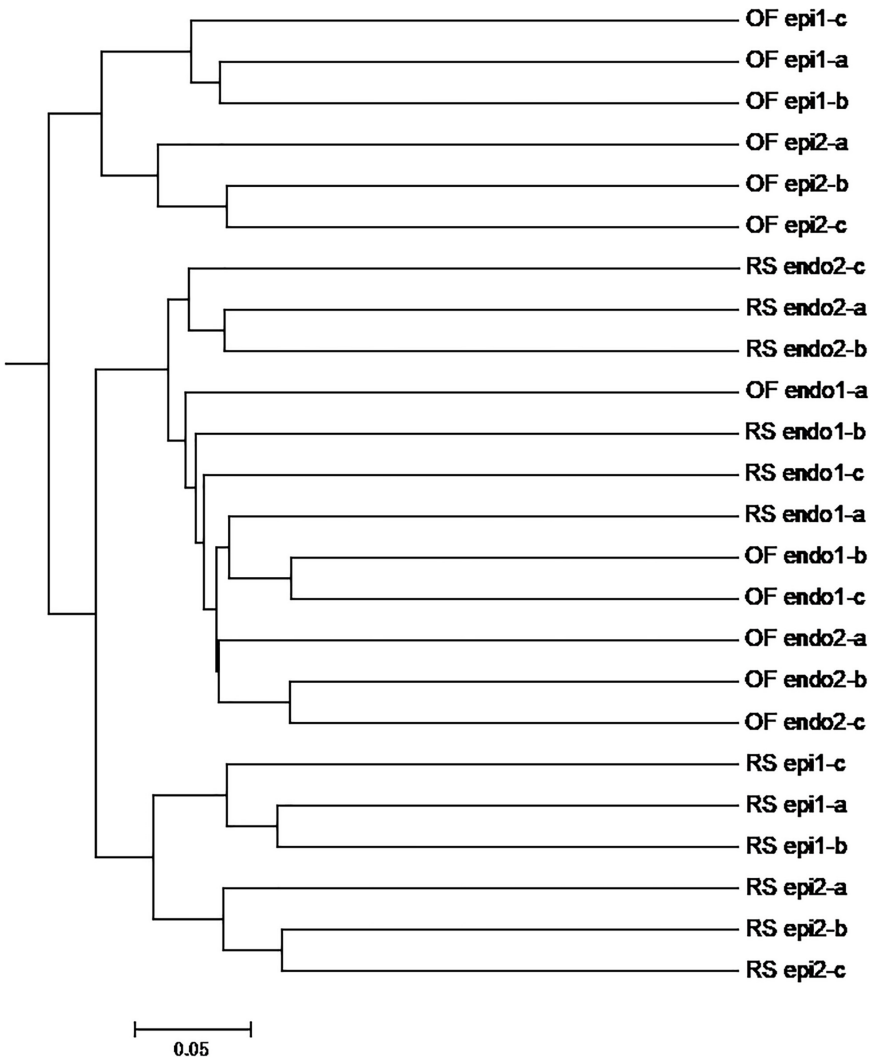

FIGURE 4 | UPGMA analysis of OTUs of bacteria community in different kiwifruit samples based on unweighted_unifrac distance. Note: In the samples, the prefix "RS" and "OF" mean rain-shelter cultivation and open-field cultivation, respectively; "epi" and "endo" represent epiphytic and endophytic, respectively; "1" and "2" indicate "Hongyang" and "Cuiyu" cultivars, respectively.

present study, Actinobacteria, exhibited a higher abundance in RS samples than in OF samples, within the same cultivar (**Figure 1A**). The genera *Pseudomonas*, *Sphingomonas,* and *Methylobacterium* have also been reported to be antagonists of fungal pathogens, and to reduce the biomass of *Fusarium oxysporum* and other fungal pathogens by inhibiting their growth, thus, ameliorating disease symptoms (Mamphogoro et al., 2020). The proportion of *Sphingomonas* observed in our study was higher in RS samples than in OF samples and the proportion of *Methylobacterium* was higher in "Cuiyu" epiphytic samples than it was in epiphytic samples of "Hongyang" (**Figure 1C**). Some strains of *Sphingomonas* have been reported to induce resistance to *Fusarium graminearum* in host plants (Innerebner et al., 2011; Cho et al., 2018). Moreover, the number of colonies of *P. syringae* obtained from tomato leaves and the population of *Xanthomonas campestris* in leaves of *Arabidopsis* were significantly reduced, relative to a control, when plants were inoculated with *Sphingomonas* (Purahong et al., 2018). Notably, healthy kiwifruits were found to contain a greater diversity and abundance of bacterial taxa belonging to *Methylobacterium*, *Sphingomonas,* and *Nocardioides* than diseased fruit (Wu et al., 2019). Some species of *Pseudomonas* synthesize antibacterial metabolites, such as 2,4-diacetyl phloroglucinol and hydrogen cyanide. These two compounds have been reported to be the main active compounds responsible for the biocontrol activity of *Pseudomonas* in different agricultural ecosystems (López et al., 2020). Therefore, it is plausible to suggest that these beneficial bacteria may play a role in reducing the level of disease incidence observed in kiwifruit grown under a RS system.

Surveys have indicated that Ascomycota is the most abundant fungal phylum in soils throughout the world (Yousef et al., 2018). Different species of Ascomycota have been used to improve the

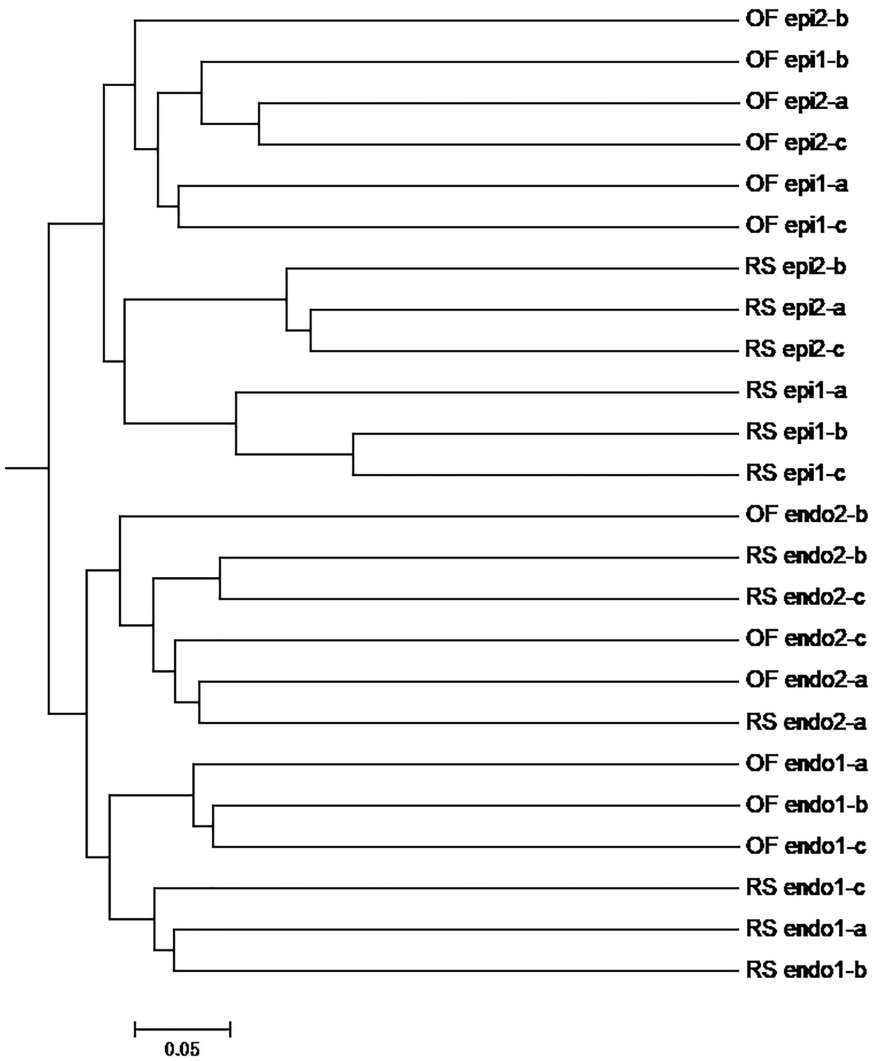

FIGURE 5 | UPGMA analysis of OTUs of fungal community in different kiwifruit samples based on unweighted_unifrac distance. Note: In the samples, the prefix "RS" and "OF" mean rain-shelter cultivation and open-field cultivation, respectively; "epi" and "endo" represent epiphytic and endophytic, respectively; "1" and "2" indicate "Hongyang" and "Cuiyu" cultivars, respectively.

quality of food crops and several species exhibit a strong tolerance to heavy metals (Lin et al., 2019). The growth rate of species of Ascomycota in soils is linked to soil nitrogen availability, and Ascomycetes play a major role as decomposers in soils (Liu et al., 2020). The order Capnodiales, within the Ascomycota, is common on the surface of leaves, and the abundance of this taxa is dependent on the level of soil organic matter (Detheridge et al., 2020). The relative abundance of Ascomycota and Capnodiales in our study was higher in RS samples than it was in OF samples (**Figures 2A,B**), suggesting that the soil environment under the RS may have had a higher content of organic matter, making it more suitable environment for Capnodiales and for plant growth. The higher organic matter content in the RS system can be attributed to its relatively closed environment, such as occurs in a greenhouse, where soil microorganisms may be the main source of epiphytic fruit fungi (Dong et al., 2021). Species in the order Hypocreales have been reported to exhibit an inhibitory effect on mycelial growth, hyphal formation, and ascospore germination, of the fungal pathogen, *Sclerotinia sclerotiorum*, on soybean plants (Peitl et al., 2020). Therefore, members of this order are ideal candidates for use as biological control agents. Our results indicated that the abundance of Hypocreales was lower in "Hongyang" samples than in "Cuiyu" samples (**Figure 2B**), indicating that there were a greater number of beneficial fungi present in "Cuiyu" than in "Hongyang" fruit, which was also reflected in the lower disease incidence observed in RS samples of "Cuiyu."

Soft rot is responsible for severe economic losses in many fruits. The order Botryosphaeriales contains several species causing soft rot (Li et al., 2017). The relative abundance of Botryosphaeriales within the same cultivation system (RS vs. OF), and within the same cultivar, was significantly lower ($p < 0.05$)

in RS samples than it was in OF samples (**Figure 2B**). The relative abundance of *Botryosphaeria* as endophyte was relatively high compared to its abundance as an epiphyte (**Figure 2C**), suggesting that it may represent a latent pathogen in kiwifruit. In this regard, *B. dothidea* has been shown to colonize healthy tissues of woody plants as an endophyte where it remains latent until specific environmental cues trigger the onset of infection and disease, although the specific cues and infection mechanism of *B. dothidea* remain to be elucidated (Kim et al., 1999). The genus Hanseniaspora, displayed in **Figure 2C**, has been used as a biocontrol agent. For example, Ruiz-Moyano et al. (2020) reported that *H. uvarum* strain793, can be used to decrease the incidence of gray mold (*B. cinerea*) in strawberries and cherries. Lutz et al. (2020) combined *Vishniacozyma victoria* NPCC 1263 with $CaCl_2$, and found that the combination effectively inhibited *Penicillium expansum* and *B. cinerea* on pear fruit, and that *V. victoria* readily colonized the fruit surface. Kusstatscher et al. (2019) reported that microbial diversity was significantly lower ($p < 0.05$) in rotten beets (*Beta vulgaris*), relative to non-infected beets. In that study, *Plectosphaerella* and *Vishniacozyma* were the dominant genera present on healthy sugar beets. Notably, in our study, the proportion of these two genera was higher in RS samples than in OF samples.

All fruits and vegetables possess a rich, post-harvest microbiota that is specific to the host species and includes both beneficial and pathogenic microorganisms. Microbial diversity and microbial networks have been shown to be linked to the health of fruits and vegetables, with diseased products exhibiting a significant microbial imbalance (Kusstatscher et al., 2020). Purahong et al. (2018) compared differences in the bacterial community of healthy and infected tissues of two different kiwifruit varieties. They found that the population evenness and biodiversity of "Hongyang" (flowers and leaves) and "Hayward" (leaves only) infected with *P. syringae* pv. actinidiae was significantly lower ($p < 0.05$) than they were in healthy fruit and that infected tissues possessed only a relatively low number of genera, with *Pseudomonas* being the most dominant. Williams and Marco (2014) found that the number of bacterial species on lab-grown lettuce was much lower than the number of species on field-grown lettuce. The potential sources of bacteria in the field include seeds, irrigation water, soil, human contact, dust, and air. That study may help to explain the differences observed in the Shannon index for epiphytic bacteria between RS and OF samples of kiwifruit (**Table 2**). The Shannon index of epiphytic RS samples was significantly higher ($p < 0.05$) than it was for epiphytic OF samples of kiwifruit within the same cultivar (**Table 3**). Zhang et al. (2020) reported that RS cultivation significantly increased the Shannon index of the rhizosphere bacterial community in pear and suggested that pear quality could be improved by regulating the diversity of the soil microbial community.

We characterized differences in the composition and structure of the bacterial and fungal communities in different sample groups of kiwifruits at the level of phylum, order, and genus. Our results indicated that the distribution of Enterobacteriales and Betaproteobacteriales varied in endophytic and epiphytic bacterial communities, and that the abundance of *Methylobacterium* and *Stenotrophomonas* was much lower in endophytic bacterial samples than it was in epiphytic bacterial samples. These latter results may explain the observed distance between epiphytic and endophytic bacterial communities in the PCoA plot (**Figure 3A**). Differences between endophytic bacterial samples, however, are not as obvious as they are for epiphytic samples. Cui et al. (2020) reported that the use of reclaimed irrigation water on pepper (*Capsicum annuum*) plants had no effect on the endophytic bacterial community structure in roots and fruits, indicating that the endophytic bacterial community has a certain level of resiliency. In the current study, we found that Proteobacteria in OF_epi2 samples was significantly higher ($p < 0.05$) than it was in other groups, which again may help to explain why this group was more distant from other groups in the PCoA plot. The relative abundance of Actinobacteria, Bacteroidetes, Enterobacteriales, and Acetobacterales in RS sample groups was higher than in OF sample groups. *Sphingomonas*, *Pseudomonas,* and *Sphingobacterium* have been reported to have a positive impact on plant health and have been used as plant-growth-promoting bacteria (Innerebner et al., 2011; Cho et al., 2018). In our results, their relative abundance in RS samples was higher than it was in OF samples. Different cultivation systems appear to be able to alter the microbial community of fruits. Notably, the Shannon index of the RS_epi2 sample group was significantly higher ($p < 0.05$) than it was in other groups. Disease incidence was also the lowest in RS samples. Interestingly, microbial diversity was also reported to be higher in disease-resistant cultivars than susceptible cultivars. Zhang et al. (2020) reported that the Shannon and Chao1 indices of the bacterial community in kiwifruit grown in RS systems were significantly higher ($p < 0.05$) than kiwifruit grown in OF systems. In that study, the abundance of Proteobacteria was significantly lower ($p < 0.05$) in RS samples than it was in OF samples. Similar to our results, the level of total nitrogen and total potassium were also significantly higher ($p < 0.05$) in RS soils than in OF soils.

In the fungal community, Botryosphaeriales, *Penicillium,* and Hypocreales accounted for a greater percentage of the endophytic community than they did in the epiphytic community in all samples. Differences in the relative abundance of these fungal genera had a distinct impact on the differences in fungal community composition observed between epiphytic and endophytic samples. The proportion of Ascomycota, including Capnodiales, *Vishniacozyma*, and *Plectosphaerella,* was higher in RS samples than in OF samples Within the same cultivar of kiwifruit. Basidiomycota and Saccharomycetales, however, accounted for a higher proportion of the taxa in OF samples. The proportion of Pleosporales in OF_epi2 was close to 50%, which may explain the separation of these samples from other epiphytic samples in the PCoA plot (**Figure 3B**). Wassermann et al. (2019) compared microbial community abundance in healthy and rotten apples and found that the diversity of bacteria and fungi in rotten apples was significantly lower ($p < 0.05$). The characteristics of a "healthy" apple microbial community were high diversity and evenness of bacterial and fungal taxa, while the microbial community in diseased apples exhibited a biological "imbalance" characterized by a loss of diversity, with pathogenic taxa becoming the dominant fungi. A greater abundance of

bacterial genera, such as *Sphingomonas*, *Pseudomonas*, and *Methylobacterium* were found in healthy apples, as well as the fungal genera, *Vishniacozyma*, *Cladosporium*, and *Acremonium*. These findings suggest that regulating the composition of the fruit microbiota may represent a promising strategy for preventing post-harvest decay.

The comprehensive analysis of species composition, α diversity, and β diversity conducted in the present study, revealed differences in the number and abundance of species in the microbial community of kiwifruit between the fungal disease-resistant cultivar, "Cuiyu," and the susceptible cultivar, "Hongyang." Some distance in the clustering of the bacterial and fungal communities of RS and OF samples was also observed, indicating that RS cultivation can improve species richness. We found that Actinobacteria, Bacteroidetes, Enterobacteriales, Acetobacterales, *Sphingomonas*, *Pseudomonas,* and *Sphingobacterium* accounted for a large proportion of the bacterial community of "Cuiyu" kiwifruit cultivated under a RS, and that the fungal taxa, Capnodiales, Hypocreales, *Vishniacozyma,* and *Plectosphaerella* exhibited a high relative abundance. Similar patterns in community composition, genera, and relative abundance have been reported to exist in healthy plant tissues (Wu et al., 2019). Therefore, we suggest that the differences observed in the microbial community of kiwifruit between cultivars and between cultivation systems may contribute to the lower incidence of natural disease in kiwifruit observed under RS conditions and within the Cuiyu cultivar. Yu et al. (2020) applied a combination of three species of *Bacillus* on blueberries and found that the inoculated plants had a 14.56% increase in yield, relative to the untreated control, and that application of the bacterial consortium improved the quality of blueberry fruits. Beneficial bacteria can also increase the level of available nitrogen and organic matter in soils and are an important component of sustainable agricultural systems. The present study provides evidence that regulating the composition of the microbial community through cultivar selection and cultivation system can increase the abundance of beneficial bacterial taxa, resulting in reduced levels of disease (Daranas et al., 2018; Wang et al., 2019). Future research should focus on identifying the most effective species and strains of bacteria and/or fungi for fostering a beneficial microbial community, and more research should be conducted on the interactions that occur between members of the microbial community that may be responsible for the enhanced and synergistic impact of the microbial community on plant health and productivity (Tontou et al., 2016; Kusstatscher et al., 2020).

CONCLUSION

A 2-year study indicated that RS cultivation reduces the level of disease incidence in kiwifruit. Further analysis of the microbial community of kiwifruit demonstrated that RS cultivation can affect the composition of the microbial community of kiwifruit. RS samples exhibited a greater abundance of beneficial microbial taxa, as well as a higher epiphytic microbial diversity, relative to samples obtained from OF plants. The composition and relative abundance of the fruit microbial community may potentially be used to evaluate the health status of fruits before and after harvest. A future goal is to effectively utilize a beneficial microbial community in conjunction with the use of biocontrol agents in support of ecological approaches for the production of kiwifruit.

DATA AVAILABILITY STATEMENT

The data sets generated for this study can be found at NCBI Accession No. PRJNA669580.

AUTHOR CONTRIBUTIONS

QY, HZ, and JiaL: conceptualization. QW, QY, and HZ: project administration. JianL, JinL, and QL: resources. QZ, ZW, and JY: data curation. YS and HZ: writing—original draft. JiaL, MJ, ZW, QY, and HZ: writing—review and editing. All authors contributed to the article and approved the submitted version.

FUNDING

This work was supported by National Natural Science Foundation of China (31972133), Open Project Program of Guangxi Key Laboratory for Polysaccharide Materials and Modifications (GXPSMM20-4), and Specific Research Project of Guangxi for Research Bases and Talents (AD18281066).

REFERENCES

Abarenkov, K., Nilsson, R. H., Larsson, K.-H., Alexander, I. J., Eberhardt, U., Erland, S., et al. (2010). The UNITE database for molecular identification of fungi–recent updates and future perspectives. *N. Phytol.* 186, 281–285. doi: 10.1111/j.1469-8137.2009.03160.x

Busby, P. E., Soman, C., Wagner, M. R., Friesen, M. L., Kremer, J., Bennett, A., et al. (2017). Research priorities for harnessing plant microbiomes in sustainable agriculture. *PLoS Biol.* 15:e2001793. doi: 10.1371/journal.pbio.2001793

Caporaso, J. G., Kuczynski, J., Stombaugh, J., Bittinger, K., Bushman, F. D., Costello, E. K., et al. (2010). QIIME allows analysis of high-throughput community sequencing data. *Nat. Methods* 7, 335–336. doi: 10.1038/nmeth.f.303

Cheng, L., Nie, X., Jiang, C., and Li, S. (2019). The combined use of the antagonistic yeast *Hanseniaspora uvarum* with β-aminobutyric acid for the management of postharvest diseases of kiwifruit. *Biol. Control* 137:104019. doi: 10.1016/j.biocontrol.2019.104019

Cho, G., Kim, M. J., Kwon, Y., and Kwak, Y. S. (2018). Comparison of endophytic microbial community in kiwifruit plant cultivars. *Plant Pathol. J.* 34, 341–346. doi: 10.5423/PPJ.NT.12.2017.0284

Claire, D., Watters, N., Gendron, L., Boily, C., Pépin, S., and Caron, J. (2018). High productivity of soilless strawberry cultivation under rain shelters. *Sci. Hortic-Amsterdam* 232, 127–138. doi: 10.1016/j.scienta.2017.12.056

Cui, B., Hu, C., Fan, X., Cui, E., Li, Z., Ma, H., et al. (2020). Changes of endophytic bacterial community and pathogens in pepper (*Capsicum annuum* L.). as affected by reclaimed water irrigation. *Appl. Soil Ecol.* 156:103627. doi: 10.1016/j.apsoil.2020.103627

Daranas, N., Badosa, E., Frances, J., Montesinos, E., and Bonaterra, A. (2018). Enhancing water stress tolerance improves fitness in biological control strains of *Lactobacillus plantarum* in plant environments. *Plos One* 13. doi: 10.1371/journal.pone.0190931

Dees, M. W., Lysøe, E., Nordskog, B., and Brurberg, M. B. (2015). Bacterial communities associated with surfaces of leafy greens, shift in composition and decrease in richness over time. *Appl. Environ. Microb.* 81, 1530–1539. doi: 10.1128/AEM.03470-14

Detheridge, A. P., Cherrett, S., Clasen, L. A., Medcalf, K., Pike, S., Griffith, G. W., et al. (2020). Depauperate soil fungal populations from the St. Helena endemic *Commidendrum robustum* are dominated by Capnodiales. *Fungal Ecol.* 45:100911. doi: 10.1016/j.funeco.2020.100911

Dimabuyu, H. B., Gonzaga, Z. C., Lusanta, D. C., Mangmang, J. S., Capuno, O. B., and Rogers, G. S. (2016). Reducing disease incidence and increasing productivity of ampalaya (Momordica charantiaL.). through pruning and protected cultivation. *Acta Horticulturae* 1128, 177–182. doi: 10.17660/ActaHortic.2016.1128.26

Dong, C., Wang, L., Li, Q., and Shang, Q. (2021). Epiphytic and endophytic fungal communities of tomato plants. *Hortic. Plant J.* 7, 38–48. doi: 10.1016/j.hpj.2020.09.002

Edgar, R. C. (2013). UPARSE, highly accurate OTU sequences from microbial amplicon reads. *Nat. Methods* 10:996. doi: 10.1038/nmeth.2604

Enya, J., Shinohara, H., Yoshida, S., Tsukiboshi, T., Negishi, H., Suyama, K., et al. (2007). Culturable leaf-associated bacteria on tomato plants and their potential as biological control agents. *Microb. Ecol.* 53, 524–536. doi: 10.1007/s00248-006-9085-1

Fujikawa, T., Hatomi, H., and Sawada, H. (2020). Draft genome sequences of 10 strains of *Pseudomonas syringae* pv. *actinidiae* Biovar 1, a major kiwifruit bacterial canker pathogen in Japan. *Microbiol. Resour Ann.* 9, e759–20. doi: 10.1128/MRA.00759-20

Innerebner, G., Knief, C., and Vorholt, J. A. (2011). Protection of Arabidopsis thaliana against leaf-pathogenic *Pseudomonas* syringae by Sphingomonas strains in a controlled model system. *Appl. Environ. Microb.* 77, 3202–3210. doi: 10.1128/AEM.00133-11

Insuk, C., Kuncharoen, N., Cheeptham, N., Tanasupawat, S., and Pathom-Aree, W. (2020). Bryophytes harbor cultivable Actinobacteria with plant growth promoting potential. *Front. Microbiol.* 11:563047. doi: 10.3389/fmicb.2020.563047

Ippolito, A., and Nigro, F. (2000). Impact of preharvest application of biological control agents on postharvest diseases of fresh fruits and vegetables. *Crop Prot.* 19, 715–723. doi: 10.1016/S0261-2194(00)00095-8

Kim, K. W., Park, E. W., and Ahn, K. K. (1999). Pre-penetration behavior of *Botryosphaeria dothidea* on apple fruits. *Plant Pathology J.* 15, 223–227.

Kim, M. J., Chae, D. H., Cho, G., Kim, D. R., and Kwak, Y. S. (2019). Characterization of antibacterial strains against kiwifruit bacterial canker pathogen. *Plant Pathology J.* 35, 473–485. doi: 10.5423/PPJ.OA.05.2019.0154

Kim, Y. C., Leveau, J., Gardener, B. B. M., Pierson, E. A., Pierson, L. S., and Ryu, C. M. (2011). The multifactorial basis for plant health promotion by plant-associated bacteria. *Appl. Environ. Microb.* 77, 1548–1555. doi: 10.1128/AEM.01867-10

Kusstatscher, P., Cernava, T., Abdelfattah, A., Gokul, J., Korsten, L., and Berg, G. (2020). Microbiome approaches provide the key to biologically control postharvest pathogens and storability of fruits and vegetables. *FEMS Microbiol. Ecol.* 96:fiaa119. doi: 10.1093/femsec/fiaa119

Kusstatscher, P., Zachow, C., Harms, K., Maier, J., Eigner, H., Berg, G., et al. (2019). Microbiome-driven identification of microbial indicators for postharvest diseases of sugar beets. *Microbiome* 7:112. doi: 10.1186/s40168-019-0728-0

Lee, S. M., Kong, H. G., Song, G. C., and Ryu, C. M. (2020). Disruption of Firmicutes and Actinobacteria abundance in tomato rhizosphere causes the incidence of bacterial wilt disease. *ISME J.* 15, 330–347. doi: 10.1038/s41396-020-00785-x

Li, L., Pan, H., Chen, M., Zhang, S., and Zhong, C. (2017). Isolation and identification of pathogenic fungi causing postharvest fruit rot of kiwifruit (*Actinidia chinensis*). in China. *J. Phytopathol.* 165, 782–790. doi: 10.1111/jph.12618

Lim, K.-H., Gu, M., Kim, B.-S., Kim, W.-S., Cho, D.-H., Son, J.-H., et al. (2016). Tree growth and fruit production of various organic Asian pear (*Pyrus pyrifoliaNakai*). cultivars grown under a rain-shelter system. *J. Hortic. Sci. Biotech.* 90, 655–663. doi: 10.1080/14620316.2015.11668728

Lin, Y., Ye, Y., Hu, Y., and Shi, H. (2019). The variation in microbial community structure under different heavy metal contamination levels in paddy soils. *Ecotox. Environ. Safe.* 180, 557–564. doi: 10.1016/j.ecoenv.2019.05.057

Liu, Z., Guo, Q., Feng, Z., Liu, Z. D., Li, H., Sun, Y., et al. (2020). Long-term organic fertilization improves the productivity of kiwifruit (*Actinidia chinensis* Planch.). through increasing rhizosphere microbial diversity and network complexity. *Appl. Soil Ecol.* 147, 103426. doi: 10.1016/j.apsoil.2019.103426

López, S. M. Y., Pastorino, G. N., Fernández-González, A. J., Franco, M. E. E., Fernández-López, M., and Balatti, P. A. (2020). The endosphere bacteriome of diseased and healthy tomato plants. *Arch. Microbiol.* 202, 2629–2642. doi: 10.1007/s00203-020-01987-9

Luo, A., Bai, J., Li, R., Liu, Z., Fang, Y., Wang, D., et al. (2019). Difference of resistance to postharvest blue mold between Hongyang and Qihong kiwifruits. *Food Chem.* 285, 389–396. doi: 10.1016/j.foodchem.2019.01.112

Lutz, M. C., Lopes, C. A., Sosa, M. C., and Sangorrín, M. P. (2020). Semi-commercial testing of regional yeasts selected from North Patagonia Argentina for the biocontrol of pear postharvest decays. *Biol. Control* 150:104246. doi: 10.1016/j.biocontrol.2020.104246

Madbouly, A. K., Abo Elyousr, K. A. M., and Ismail, I. M. (2020). Biocontrol of *Monilinia fructigena*, causal agent of brown rot of apple fruit, by using endophytic yeasts. *Biol. Control* 144:104239. doi: 10.1016/j.biocontrol.2020.104239

Mamphogoro, T. P., Maboko, M. M., Babalola, O. O., and Aiyegoro, O. A. (2020). Bacterial communities associated with the surface of fresh sweet pepper (*Capsicum annuum*). and their potential as biocontrol. *Sci. Rep.* 10:8560. doi: 10.1038/s41598-020-65587-9

Meng, J. F., Ning, P. F., Xu, T. F., and Zhang, Z. W. (2012). Effect of rain-shelter cultivation of *Vitis vinifera* cv. Cabernet Gernischet on the phenolic profile of berry skins and the incidence of grape diseases. *Molecules* 18, 381–397. doi: 10.3390/molecules18010381

Peitl, D. C., Sumida, C. H., Gonçalves, R. M., Pascholati, S. F., and Balbi-Peña, M. I. (2020). Antagonism of saprobe fungi from semiarid areas of the Northeast of Brazil against *Sclerotinia sclerotiorum* and biocontrol of soybean white mold. *Semin. Cienc. Agrar.* 41, 2597–2612. doi: 10.5433/1679-0359.2020v41n6p2597

Pruesse, E., Quast, C., Knittel, K., Fuchs, B. M., Ludwig, W., Peplies, J., et al. (2007). SILVA: a comprehensive online resource for quality checked and aligned ribosomal RNA sequence data compatible with ARB. *Nucleic. Acids Res.* 35, 7188–7196. doi: 10.1093/nar/gkm864

Purahong, W., Orru, L., Donati, I., Perpetuini, G., Cellini, A., Lamontanara, A., et al. (2018). Plant microbiome and its link to plant health, host species, organs and *Pseudomonas syringae* pv. *actinidiae* infection shaping bacterial phyllosphere communities of kiwifruit plants. *Front. Plant Sci.* 9:1563. doi: 10.3389/fpls.2018.01563

Reyon, D., Tsai, S. Q., Khayter, C., Foden, J. A., Sander, J. D., and Joung, J. K. (2012). FLASH assembly of TALENs for high-throughput genome editing. *Nat. Biotechnol.* 30, 460–465. doi: 10.1038/nbt.2170

Richardson, D. P., Ansell, J., and Drummond, L. N. (2018). The nutritional and health attributes of kiwifruit, a review. *Eur. J. Nutr.* 57, 2659–2676. doi: 10.1007/s00394-018-1627-z

Rognes, T., Flouri, T., Nichols, B., Quince, C., and Mahe, F. (2016). VSEARCH, a versatile open-source tool for metagenomics. *PeerJ.* 4:e2584. doi: 10.7717/peerj.2584

Ruiz-Moyano, S., Hernandez, A., Galvan, A. I., Cordoba, M. G., Casquete, R., Serradilla, M. J., et al. (2020). Selection and application of antifungal VOCs-producing yeasts as biocontrol agents of grey mold in fruits. *Food Microbiol.* 92:103556. doi: 10.1016/j.fm.2020.103556

Sartori, M., Nesci, A., Garcia, J., Passone, M. A., Montemarani, A., and Etcheverry, M. (2017). Efficacy of epiphytic bacteria to prevent northern leaf blight caused by *Exserohilum turcicum* in maize. *Rev. Argent. Microbiol.* 49, 75–82. doi: 10.1016/j.ram.2016.09.008

Spadaro, D., and Droby, S. (2016). Development of biocontrol products for postharvest diseases of fruit, the importance of elucidating the mechanisms of action of yeast antagonists. *Trends Food Sci. Tech.* 47, 39–49. doi: 10.1016/j.tifs.2015.11.003

Tian, T., Qiao, G., Deng, B., Wen, Z., Hong, Y., and Wen, X. (2019). The effects of rain shelter coverings on the vegetative growth and fruit characteristics

of Chinese cherry (*Prunus pseudocerasus* Lindl). *Sci. Hortic-Amsterdam* 254, 228–235. doi: 10.1016/j.scienta.2019.04.030

Tontou, R., Giovanardi, D., Ferrari, M., and Stefani, E. (2016). Isolation of bacterial endophytes from *Actinidia chinensis* and preliminary studies on their possible use as antagonists against *Pseudomonas syringae* pv. *actinidiae*. *J. Berry Res.* 6, 395–406. doi: 10.3233/JBR-160118

Turner, T. R., James, E. K., and Poole, P. S. (2013). The plant microbiome. *Genome Biol.* 14, 209–215. doi: 10.1186/gb-2013-14-6-209

Volksch, B., and May, R. (2001). Biological control of *Pseudomonas syringae* pv. glycinea by epiphytic bacteria under field conditions. *Microbiol. Ecol.* 41, 132–139. doi: 10.1007/s002480000078

Vorholt, J. A. (2012). Microbial life in the phyllosphere. *Nat. Rev. Microbiol.* 10, 828–840. doi: 10.1038/nrmicro2910

Wang, Z., Li, Y., Zhuang, L., Yu, Y., Liu, J., Zhang, L., et al. (2019). A rhizosphere-derived consortium of *Bacillus subtilis* and *Trichoderma harzianum* suppresses common scab of potato and increases yield. *Comput. Struct. Biotechnol. J.* 17, 645–653. doi: 10.1016/j.csbj.2019.05.003

Wassermann, B., Kusstatscher, P., and Berg, G. (2019). Microbiome response to hot water treatment and potential synergy with biological control on stored apples. *Front. Microbiol.* 10:2502. doi: 10.3389/fmicb.2019.02502

Williams, T. R., and Marco, M. L. (2014). Phyllosphere microbiota composition and microbial community transplantation on lettuce plants grown indoors. *MBio* 5, e01564–14. doi: 10.1128/mBio.01564-14

Wu, W., Lei, J., Hussain, M., Cao, S., Dui, B., and Wang, R. (2019). Structure and function of the fruit microbiome in healthy and diseased kiwifruit. *Pak. J. Agr. Sci.* 56, 577–585.

Yousef, M., Alba-Ramirez, C., Jurado, I. G., Mateu, J., Diaz, S. R., Valverde-Garcia, P., et al. (2018). *Metarhizium brunneum* (Ascomycota; Hypocreales). treatments targeting olive fly in the soil for sustainable crop production. *Front. Plant Sci.* 9:1. doi: 10.3389/fpls.2018.00001

Yu, Y. Y., Xu, J. D., Huang, T. X., Zhong, J., Yu, H., Qiu, J. P., et al. (2020). Combination of beneficial bacteria improves blueberry production and soil quality. *Food Sci. Nutr.* 8, 5776–5784. doi: 10.1002/fsn3.1772

Yue, J., Liu, J., Ban, R., Tang, W., Deng, L., Fei, Z., et al. (2015). Kiwifruit Information Resource (KIR)., a comparative platform for kiwifruit genomics. *Database* 2015:bav113. doi: 10.1093/database/bav113

Zhang, Q., Pang, X., Chen, X., Ye, J., Lin, S., and Jia, X. (2020). Rain-shelter cultivation influence rhizosphere bacterial community structure in pear and its relationship with fruit quality of pear and soil chemical properties. *Sci. Hortic-Amsterdam* 269:109419. doi: 10.1016/j.scienta.2020.109419

Zhao, L., Yang, W., Zhang, Y., Wu, Z., Wang, Q. C., and Wu, Y. (2019). Occurrence and molecular variability of kiwifruit viruses in *Actinidia deliciosa* 'Xuxiang' in the Shaanxi Province of China. *Plant Dis.* 103, 1309–1318. doi: 10.1094/PDIS-09-18-1570-RE

Zhao, Z., Chen, J., Gao, X., Zhang, D., Zhang, J., Wen, J., et al. (2019). Comparative genomics reveal pathogenicity-related loci in *Pseudomonas syringae* pv. actinidiae biovar 3. *Mol. Plant Pathol.* 20, 923–942. doi: 10.1111/mpp.12803

Conflict of Interest: The authors declare that the research was conducted in the absence of any commercial or financial relationships that could be construed as a potential conflict of interest.

Publisher's Note: All claims expressed in this article are solely those of the authors and do not necessarily represent those of their affiliated organizations, or those of the publisher, the editors and the reviewers. Any product that may be evaluated in this article, or claim that may be made by its manufacturer, is not guaranteed or endorsed by the publisher.

frontiers in Microbiology

ORIGINAL RESEARCH
published: 18 October 2021
doi: 10.3389/fmicb.2021.666982

Soil Ventilation Benefited Strawberry Growth *via* Microbial Communities and Nutrient Cycling Under High-Density Planting

Yan Zhang[1,2,3†], Yujing Hu[1,2,3†], Zijing You[1,2,3†], Zhenglin Li[1,2,3†], Miao Kong[1,2,3], Mingzheng Han[1,2,3], Zhimin Liu[1,2,3], Jie Zhang[1,2,3] and Yuncong Yao[1,2,3*]*

[1] Beijing Advanced Innovation Center for Tree Breeding by Molecular Design, Beijing University of Agriculture, Beijing, China, [2] College of Plant Science and Technology, Beijing University of Agriculture, Beijing, China, [3] Beijing Key Laboratory for Agricultural Application and New Technique, Beijing, China

OPEN ACCESS

Edited by:
Yong Wang,
Guizhou University, China

Reviewed by:
Zhiqin Zhou,
Southwest University, China
Yongzhong Feng,
Northwest A&F University, China

***Correspondence:**
Yuncong Yao
yaoyc_20@126.com
Jie Zhang
anyzj034@126.com

[†]These authors have contributed equally to this work

Specialty section:
This article was submitted to Microbe and Virus Interactions with Plants, a section of the journal Frontiers in Microbiology

Received: *11 February 2021*
Accepted: *22 September 2021*
Published: *18 October 2021*

Citation:
Zhang Y, Hu Y, You Z, Li Z, Kong M, Han M, Liu Z, Zhang J and Yao Y (2021) Soil Ventilation Benefited Strawberry Growth via Microbial Communities and Nutrient Cycling Under High-Density Planting. Front. Microbiol. 12:666982. doi: 10.3389/fmicb.2021.666982

In order to increase O_2 concentration in the rhizosphere and reduce the continuous cropping obstacles under high-density cultivation, ventilation is often used to increase soil aeration. Yet, the effect of ventilation on soil microbial communities and nutrient cycling and, further, the extent to which they influence strawberry growth under greenhouse conditions are still poorly understood. Thus, four treatments—no ventilation + low planting density (LD), ventilation + LD, no ventilation + high planting density (HD), and ventilation + HD—of strawberry "Red cheeks" (*Fragaria* × *ananassa* Duch. cv. "Benihopp") were studied in a greenhouse for 3 years. The ventilation pipe (diameter = 10 cm) was buried in the soil at a depth of 15 cm from the surface and fresh air was sent to the root zone through the pipe by a blower. Ten pipes (one pipeline in a row) were attached to a blower. Soil samples were collected using a stainless-steel corer (five-point intra-row sampling) for the nutrient and microbial analyses. The composition and structure of the soil bacterial and fungal communities were analyzed by high-throughput sequencing of the 16S and 18S rRNA genes, and functional profiles were predicted using PICRUSt and FUNGuild, respectively. The results showed that soil ventilation increased the net photosynthetic rate (Pn), transpiration rate (Tr), and water use efficiency (WUE) of strawberry plants across two growth stages [vegetative growth stage (VGS) and fruit development stage (FDS)]. Soil ventilation increased its available nutrient contents, but the available nutrient contents were reduced under the high planting density compared with low planting density. Both the O_2 concentration and O_2:CO_2 ratio were increased by ventilation; these were positively correlated with the relative abundance of Bacilli, Gamma-proteobacteria, *Blastocatella*, as well as Chytridiomycota and Pezizomycetes. Conversely, ventilation decreased soil CO_2 concentration and the abundance of Beta-proteobacteria and Gemmatimonadetes. The greater planting density increased the relative abundance of Acidobacteria (oligotrophic group). Ventilation altered soil temperature and pH along with carbon and nitrogen

functional profiles in the VGS (more nitrogen components) and FDS (more carbon components), which benefited strawberry plant growth under high planting density. The practice of soil ventilation provides a strategy to alleviate hypoxia stress and continuous cropping obstacles for improving crop production in greenhouse settings.

Keywords: microbial communities, strawberry growth, soil O_2 and CO_2, planting density, nutrient cycling, multifunctional index

INTRODUCTION

Over the past century, intensive tillage (such as high-density planting) has often been used in greenhouses to increase the crop yield of per unit land area (Maboko and Du Plooy, 2013). However, long-term use of intensive tillage has major negative impacts on the ecosystem and leads to significant soil degradation, including soil compaction, soil organic carbon (SOC) loss, and essential soil function reduction, which can restrict plant growth and crop yield (Puerta et al., 2018; Stefan et al., 2021).

It is well-known that mesophytic plant roots require soil oxygen (O_2) in order to respire, grow, develop, and function normally (Li et al., 2016a,b; Ben-Noah and Friedman, 2018). Most of O_2 supply is obtained directly through diffusion gas exchange from the atmosphere to the rhizosphere soil; meanwhile, the root and microbial respiration is constrained by O_2 in the root zone (Ityel et al., 2014; Ben-Noah and Friedman, 2018). Under high-density planting condition, reduced O_2 and elevated carbon dioxide (CO_2) concentrations negatively affect plant growth and productivity partly (Kitaya et al., 1984; Li et al., 2020). Furthermore, the soil respiration and microbial biomass decreased in most cases of high CO_2 treatments (Santruckova and Simek, 1997).

Increased O_2 concentration of root zone can improve bell pepper biomass and fruit yield (Ityel et al., 2014). Meanwhile soil aeration has been reported to accelerate the growth and increase the crop yield by improving O_2 concentration, such as muskmelon and tomato (Bhattarai et al., 2006; Li et al., 2016, 2020). Thus, aerated irrigation has been widely used in agricultural systems, e.g., orchards, greenhouse, field, and pot experiments (Bhattarai et al., 2004; Friedman and Naftaliev, 2012; Hou et al., 2016; Du et al., 2019). Aerated irrigation promoted the growth of new leaves, fine roots, and new branches of grape, and accelerated air exchange in rhizosphere soil (Zhao et al., 2019). It also has been reported that ventilation (every 3 days) improved leaf functions and increased the net photosynthetic rate (Pn) of young peach trees (Xiao et al., 2015). Thus, soil aeration is considered the third most important factor affecting soil fertility after water and nutrient availability (Glinski and Stepniewski, 1985; Ben-Noah et al., 2021), and its status is an important aspect of soil quality and soil ecology (Niu et al., 2012). Soil aeration elevates the concentration of O_2 and relieves the high concentrations of CO_2 formed during respiration under anaerobic soil conditions (Ben-Noah and Friedman, 2018). Tillage is the only commonly used agricultural practice for improving soil aeration, despite its adverse effect on soil structure (Stępniewski and Stępniewska, 2009).

In addition, long-term continuous cropping usually leads to increased soil-borne disease and decreased soil nutrient content of strawberry, which may be caused by the decreased beneficial microorganisms and accumulated fungal pathogen (*Fusarium oxysporum*) in the greenhouse (Huang et al., 2018; Li and Liu, 2019). Intermittent aeration can promote functional bacteria growth in N removal process of wetlands (Liu et al., 2019). Meanwhile, aeration irrigation significantly increased the abundance of aerobic bacteria and promoted the increase of *Pseudomonas* and *Aspergillus* related to phosphate solubilization, that of *Bacillus* related to potassium solubilization, and that of *Fusarium* related to organic matter (OM) decomposition (Zhao et al., 2019).

To alleviate the negative effects of high planting density and continuous cropping, we aimed to improve soil aeration of strawberry through *in situ* ventilation using a blower. Strawberry (*Fragaria ananassa* Duch.) is classified as a plant with high oxygen demand root (Iwasaki, 2008) and is more susceptible to root hypoxic stress. However, few studies are reported that apply root zone aeration as a technique to improve strawberry production (Iwasaki, 2008). Furthermore, the mechanism by which soil aeration may facilitate strawberry growth is largely unknown, especially how it affects soil microbial community composition, and functional structure or alter nutrient concentrations under a high-density planting.

Here, we speculated that *in situ* ventilation is able to influence the soil microbial community, soil nutrient cycling, and their interaction, to benefit the growth of strawberry at high-density planting. To analyze the effect mechanism of soil ventilation on strawberry plant growth, we evaluated the response of soil microorganisms and nutrient content to cultivation management (soil ventilation and planting density treatments) at the strawberry vegetative growth stage (VGS) and fruit development stage (FDS) in greenhouses. The objectives of this study were (i) to evaluate the impact of intermittent soil ventilation on the abundance, diversity, and function of the microbial community under rational high planting density (HD) vs. low planting density (LD) conditions; (ii) to evaluate the impact of intermittent soil ventilation on the soil C and N cycling at the VGS and FDS; and (iii) to evaluate the impact of intermittent soil ventilation on strawberry plant growth.

MATERIALS AND METHODS

Study Site and Plant Materials

The field experiment was conducted in plastic greenhouses in Changping (40°19′ N, 116°16′ E), China, a city located northwest

of Beijing. The site lies at an elevation of 57 m above sea level (asl), in a region that has a warm continental monsoonal climate, whose mean temperature ranges from −4 to 26°C, with a mean annual precipitation about 556.4 mm. The soil type here is a typical light sandy loam, with a SOC content of 2.10%, and available N, P, and K concentrations of 143.95, 15.68, and 225.75 mg kg^{-1}, respectively. Strawberries were first cultivated at the study site in 2008; hence, by 2016, strawberries have been growing in the area continuously for nearly 10 years. Seedlings of the strawberry "Red cheeks" (*Fragaria* × *ananassa* Duch. *cv.* "Benihopp") similar in size (i.e., with approximately five compound leaves per plant) were selected and planted in the experimental greenhouses on the ridges in square-shaped rows. The rows were covered with black plastic film. The planting cycle lasts approximately 10 months, from August to May of the next year, amounting to a single growing season with corresponding growth stages for VGS (September to December) and FDS (January to May).

Experimental Design

Four treatments were set up in the greenhouse: no ventilation + LD, ventilation + LD, no ventilation + HD, and ventilation + HD. The randomized block design was repeated three times, with a total of 12 cultivation plots. The greenhouse was 65.0 m long and 8.0 m wide with an east–west orientation, while each cultivation plot was 5.5 m long and 1.0 m wide with a total planting area of 5.5 m^2, and crop rows were aligned north–south. The ventilation pipe (diameter = 10 cm, made of nylon fabric and supported with spiral iron wire ring) was buried in the soil at a depth of 15 cm from the surface and fresh air was sent to the root zone through the pipe by a blower (output: 0.75 kw, flow rate: 50 L min^{-1}, SCL k05-MS MOR; FBZ, Ferrara, Italy). Ten pipes (one pipeline per row) were attached to a blower, and most air in the pipe can pass through the nylon cloth to the soil (**Supplementary Figures 1–3**). The ventilation was applied every 2 h and each time lasted for 1 h in 09:00–17:00 during the growing season. The ventilation treatment was administered for 3 years from 2013 to 2016. There are two densities: low planting density (LD, with two plants per row and a plant × row spacing of 10.0 cm × 25.0 cm) vs. high planting density (HD, with four plants per row and a plant × row spacing of 10.0 cm × 12.5 cm) (see **Supplementary Figure 1** for details). Every year, seedlings were planted at the end of August and harvested in May of the following year.

Photosynthetic Characteristics and Leaf Nutrient Content of Strawberry

Leaf photosynthetic activity of strawberry plants was measured using a portable photosynthesis system (LI-6400; LI-COR Biosciences, Lincoln, NE, United States) between 09:00 a.m. and 11:00 a.m. during VGS (November 10, 2015) and FDS (April 10, 2016). Net photosynthetic rate (Pn) and transpiration rate (Tr) were measured and water use efficiency (WUE) was calculated as WUE = Pn/Tr (Ribeiro et al., 2009). Three fully expanded leaves were selected from each plant per plot for the measurements, and average values were calculated for each plant. During the measurements, the photosynthetic photon flux density was 1,200 μmol m^{-2} s^{-1}; the CO_2 concentration in the leaf chamber was 380 ± 5 μmol mol^{-1}; and the leaf temperature was 25°C. The leaf area (LA) was measured with a leaf area meter (LI-3000A; LI-COR Biosciences) (Nardini et al., 2014). Leaf N was determined by the Kjeldahl method and leaf P and K were determined by inductively coupled plasma-optical emission spectrometry (ICP-OES) (iCAP 6000; Thermo Fisher Scientific, Waltham, MA, United States) (Rivelli et al., 2012) for 15 leaves per plant that had been oven-dried at 70°C for 24 h.

Soil Sampling and Processing

Soil samples were collected on two occasions (November 10, 2015 and April 10, 2016). After removing the litter layer, five replicate samples (top 0–20 cm depth) were collected in an "S" shape on the ridge, using a standard soil auger (4.5 cm inner diameter) and then homogenized to obtain a composite sample for each plot. The samples were immediately transported to the laboratory, sieved (<2 mm), and divided into two subsamples. One was immediately stored at −80°C for soil microbial and enzymatic activity analyses; the other portion was air-dried and stored at room temperature until chemically analyzed.

Soil Physicochemical Parameters

The O_2 and CO_2 concentrations in the treated soils were measured with a gas detector (GasAlertMicro 5 IR; BW Technologies Honeywell, Calgary, AB, Canada). Soil temperature was measured with an electronic temperature and humidity recorders (RTR53A; T&D Corporation, Matsumoto, Japan). The pH was measured with a compound electrode (PE 10, Sartorius, Göttingen, Germany) at a soil-to-water ratio of 1:2.5. The SOC content was determined by the Walkley–Black method (Nelson and Sommers, 1996), albeit with some slight modifications. Total nitrogen (TN) content was determined with the Kjeldahl method (Bremner, 1996), and soil available nitrogen (AN) was determined by applying the alkaline hydrolysis diffusion method (Lu, 2000). Total and available phosphorus (TP and AP, respectively), and total and available potassium (TK and AK, respectively) concentrations were measured by ICP-OES (Rivelli et al., 2012). Soil invertase (INV), catalase (CAT), and urease (URE) activity were determined as described by Jin et al. (2009), with some slight modifications applied. To estimate the INV activity, the 3,5-dinitrosalicylic acid method was implemented, using a sucrose substrate, after which 5 g of air-dried soil was incubated at 37°C for 24 h. Catalase activity was measured using the back titration of residual H_2O_2 added to soil (2 g) with 0.1 M $KMnO_4$. URE activity was determined after incubating the soil (5 g) for 24 h at 37°C with a 10% urea solution as the substrate.

Soil DNA Extraction and Amplification

From each sample, total genomic DNA was extracted from 0.25 g of soil using the TIANamp Soil DNA Kit (Tiangen Biotech, Beijing, China) according to the manufacturer's protocol. The quality and quantity of DNA were evaluated based on the A260/280 ratio, measured on a spectrophotometer (NanoDrop 2000; Thermo Fisher Scientific) and by electrophoresis (1% agarose gel). The V3–V4 hypervariable regions of the bacterial 16S rRNA gene was amplified

using the barcoded primers 341F (5′-CCTACGGGNGGC WGCAG-3′) and 785R (GACTACHVGGGTATCTAATCC) (Klindworth et al., 2013), and the fungal 18S rRNA gene sequences were PCR-amplified using the barcoded primers EF4 (5′-GGAAGGGRTGTATTTATTAG-3′) and NS2 (5′-GGCTGCTGGCACCAGACTTGC-3′) (Smit et al., 1999; Rashad et al., 2012). The purified Polymerase Chain Reaction (PCR) amplicons were then sequenced on the MiSeq platform (300-bp paired-end reads) (Illumina, San Diego, CA, United States) by Ori-Gene Technology (Beijing, China).

Soil Microorganisms Sequence Data Analysis

High-quality paired-end reads of the 16S and 18S sequences were merged using the FLASH software (Magoč and Salzberg, 2011) and Mothur[1] was used to filter the sequences and remove the barcodes. Operational taxonomic units (OTUs) were obtained using the UPARSE pipeline based on the merged sequences (Edgar, 2013); those with ≥97% similarity were assigned to the same OTU. To obtain taxonomic information, representative 16S and 18S sequences of each OTU were generated and aligned to the SILVA and UNITE databases, respectively, using the Ribosomal Database Project (RDP) classifier (Pruesse et al., 2007).[2] The raw sequences were submitted to NCBI Sequence Read Archive under the identification PRJNA721522.

Alpha-diversity indices, including the number of species observed (Sobs) and the Chao and Shannon indices, were calculated with Mothur v. 1.34.4 (Schloss et al., 2009). The functional groups related to soil C and N cycles of the bacteria were obtained using the Functional Annotation of Prokaryotic Taxa (FAPROTAX) database,[3] which could map prokaryotic clades to metabolic and ecologically relevant functions based on the literature of cultured strains, by transforming the OUT tables into putative functional profiles (Louca et al., 2016; Xu et al., 2021). Based on the OTUs of fungi, a trophic classification of pathotrophs, saprotrophs, and symbiotrophs was performed using FUNGuild,[4] as previously described (Nguyen et al., 2016).

Statistical Analysis

The soil multifunctionality index (SMF) comprises nine soil nutrition indicators and the respective activity of the three enzymes mentioned in the earlier section *Soil Physicochemical Parameters* (Delgado-Baquerizo et al., 2016; Bastida et al., 2017). To obtain the SMF for each plot, individual functions underwent a *Z*-score transformation, and standardized rates of soil functions were then averaged.

The variables were subjected to a three-way analysis of variance (ANOVA). The three factors included in this experimental design were as follows: (i) Ventilation, which had two levels: ventilation and no ventilation; (ii) Density, which had two levels: HD and LD; and (iii) Stage: VGS and FDS. Three-way ANOVA of the abundance of bacterial and fungal populations is provided in the Supporting Information (**Supplementary Tables 3, 4**, respectively). All data were subjected to one-way ANOVA followed by *post hoc* analyses with Tukey's Honestly Significant Difference (HSD) test. Differences between the means were considered statistically significant at $p < 0.05$. Different lowercase letters represent significant differences between eight treatments.

Microbial community structure was analyzed by a principal component analysis (PCA) based on relative abundances of the dominant populations at the phylum, class, family, and genus levels. Permutational multivariate (PERM) ANOVA with 9,999 permutations was used to evaluate the influence of factor analysis upon microbial community structure. Redundancy analysis (RDA) was performed to elucidate the relationships between the environmental variables (O_2, CO_2, O_2:CO_2, temperature, and pH) and the soil chemical factors. Spearman correlation coefficients between soil, plant, and microbial (bacterial and fungal) variables and O_2 (CO_2, O_2:CO_2, or SMF) were also calculated. Figures were generated using R software v.3.5.3.[5]

RESULTS

Photosynthetic Characteristics and Leaf Nutrient Contents of Strawberry

Compared with no ventilation, soil ventilation increased the Pn, Tr, and WUE of strawberry plants in its two growth stages. Pn and WUE were slightly higher in the FDS than VGS, with no significant difference between LD and HD. Soil ventilation increased LA in both VGS and FDS stages. The leaf N concentration was increased in the VGS yet decreased in the FDS, whereas the leaf P and K concentration were both increased by ventilation in both growth stages (**Table 1**).

Soil Physicochemical Properties

Soil ventilation significantly increased the soil O_2 concentration and O_2:CO_2 ratio, while reducing the soil CO_2 concentration. It also increased soil temperature in the FDS, but had no significant effect on soil pH in either growth stage. Planting density significantly influenced the soil O_2:CO_2 ratio, in that it was reduced when a greater planting density of strawberry was used. Significant differences in soil properties (soil O_2, CO_2 concentrations, O_2:CO_2 ratio, temperature, and pH) were evident between the two growth stages (**Figures 1A–E** and **Supplementary Table 1**).

Soil ventilation and plant density influenced the levels of most soil nutrients in the two growth stages of strawberry, as seen in **Figure 1** and **Supplementary Table 2**. Soil ventilation increased the SOC content, and this effect was significant in the FDS. It also increased soil organic nitrogen (SON), TN, TP, TK, AP, and AK contents, all of which were diminished by a higher planting density. Soil TN content was higher in the VGS than FDS, while soil TP and TK contents showed the opposite trend (**Figures 1G–J**).

Soil ventilation enhanced the activities of three soil enzymes (URE, INV, and CAT). The INV activity was increased with a greater planting density. URE activity was slightly higher while

[1]https://mothur.org

[2]https://rdp.cme.msu.edu/

[3]www.zoology.ubc.ca/louca/FAPROTAX

[4]https://github.com/UMNFuN/FUNGuild

[5]https://www.r-project.org/

TABLE 1 | Photosynthetic characteristics, leaf area, and nutrient content of strawberry.

Stage	Treatment	Pn (μmol m^{-2} s^{-1})	Tr (mmol m^{-2} s^{-1})	WUE (μmol mmol^{-1})	LA (cm^2)	LN (g kg^{-1})	LP (mg kg^{-1})	LK (mg kg^{-1})
VGS	NVLD	16.72 ± 0.92d	3.77 ± 0.08e	4.44 ± 0.31ab	43.14 ± 3.00c	33.67 ± 1.14cd	287.48 ± 25.99d	962.54 ± 45.53abc
	VLD	19.94 ± 0.90bcd	4.31 ± 0.09cde	4.63 ± 0.24a	44.21 ± 2.34bc	45.68 ± 1.26a	334.15 ± 15.94cd	970.76 ± 38.46abc
	NVHD	17.94 ± 0.28cd	4.13 ± 0.27de	4.36 ± 0.34ab	44.56 ± 0.71bc	40.12 ± 1.53b	318.07 ± 21.00cd	873.35 ± 38.03c
	VHD	20.47 ± 1.03bc	4.49 ± 0.12bcde	4.56 ± 0.23ab	45.10 ± 3.45bc	47.60 ± 1.70a	320.87 ± 15.51cd	925.62 ± 14.27bc
FDS	NVLD	17.84 ± 1.80cd	5.03 ± 0.23abcd	3.55 ± 0.32b	48.39 ± 3.00bc	31.40 ± 0.60de	419.91 ± 18.21ab	918.43 ± 16.30bc
	VLD	22.43 ± 0.95ab	5.20 ± 0.63abc	4.35 ± 0.38ab	49.31 ± 2.34bc	29.58 ± 0.72e	454.03 ± 27.61a	1018.94 ± 56.89ab
	NVHD	19.78 ± 0.26bcd	5.38 ± 0.24ab	3.68 ± 0.13ab	52.01 ± 0.71b	36.25 ± 0.74c	369.16 ± 10.53bc	938.57 ± 15.23bc
	VHD	25.40 ± 2.21a	5.77 ± 0.44a	4.44 ± 0.69ab	60.94 ± 3.45a	31.59 ± 0.93de	373.61 ± 22.49bc	1066.24 ± 62.37a

Significant level	*F*	*P*	*F*	*P*	*F*	*P*	*F*	*P*	*F*	*P*	*F*	*P*	*F*	*P*
V	64.50	0.000	7.74	0.014	10.75	0.005	23.59	0.000	48.85	0.000	7.00	0.018	19.49	0.000
D	11.21	0.004	7.90	0.012	0.01	0.904	4.24	0.056	66.93	0.000	11.71	0.003	1.05	0.322
S	27.25	0.000	80.77	0.000	11.03	0.004	449.67	0.000	422.44	0.000	114.55	0.000	10.31	0.005
V × D	0.03	0.866	0.01	0.950	0.00	0.966	0.76	0.396	15.70	0.001	4.89	0.042	1.19	0.292
V × S	5.02	0.040	0.43	0.523	3.81	0.069	6.83	0.019	194.69	0.000	0.11	0.748	6.58	0.021
D × S	2.54	0.130	0.52	0.484	0.41	0.533	4.99	0.040	0.67	0.426	19.91	0.000	9.52	0.007
V × D × S	0.75	0.400	0.63	0.447	0.01	0.915	2.33	0.146	0.83	0.377	0.18	0.675	0.07	0.799

Values are shown as mean ± SD (n = 3). Different letters in the same column indicate significant differences between means ($p < 0.05$) (Tukey's test). D, planting density; FDS, fruit development stage; LA, leaf area; LK, leaf potassium; LN, leaf nitrogen; LP, leaf phosphorus; NVHD, (no ventilation + high planting density); NVLD, (no ventilation + low planting density); Pn, net photosynthesis; S, growth stage; Tr, transpiration rate; V, in situ ventilation; VGS, vegetative growth stage; VHD, (ventilation + high planting density); VLD, (ventilation + low planting density); WUE, water use efficiency.

INV activity was lower in the VGS than FDS (**Figures 1O–Q**). Soil ventilation increased the SMF, and it was higher in the FDS than VGS (**Figure 1R** and **Supplementary Table 2**).

The PCA revealed significant differences between the two growth stages of strawberry plants. The soil N cycle dominated in the VGS whereas the soil C cycle (including the P and K cycles) was dominated in the FDS (**Figure 2A**). The RDA showed that soil O_2 concentration was positively correlated with those soil nutrient variables related to N cycling; soil temperature and pH were redundant among the soil nutrient variables that are related to C cycling (**Figure 2B**).

Diversity, Composition, and Structure of Soil Bacterial Community

The Sobs, Chao, and Shannon indices for the total bacterial community, estimated in terms of its OTUs and relative abundances, were not significantly affected by ventilation according to the PERMANOVA results (**Supplementary Table 3**). However, the bacterial diversity (Shannon index) and richness were higher at HD than LD in the VGS, but there was no significant difference at the FDS (**Figure 3**).

The soil bacterial community was dominated by the following phyla: Proteobacteria (34%), Planctomycetes (12%), Acidobacteria (9%), Bacteroidetes (8%), and Actinobacteria (5%). Ventilation markedly reduced the relative abundance of Proteobacteria, Gemmatimonadetes, and Chloroflexi, and increased that of Firmicutes. Compared with LD, a greater planting density (HD) increased the relative abundance of Acidobacteria but decreased that of Bacteroidetes in the VGS. The significant differences were found between the two growth stages of strawberry. For example, the relative abundances of Proteobacteria, Acidobacteria, and Chlamydiae were all lower while those of Planctomycetes, Actinobacteria, Chloroflexi, and Firmicutes were higher in the VGS than FDS (**Figure 4A**). The dominant phyla were significantly influenced by the interaction term of ventilation × density.

The relative abundances of the top 16 dominant classes of bacteria were influenced by ventilation and planting density at the two growth stages. Ventilation altered the relative abundances of seven classes, with increases in Phycisphaerae and Bacilli and decreases in Alphaproteobacteria, Betaproteobacteria, Deltaproteobacteria, and Gemmatimonadetes. Planting density markedly influenced the relative abundances of 11 classes: in this respect, Acidobacteria and Verrucomicrobiae were higher whereas Flavobacteriia and Sphingobacteriia were lower at the HD than LD in the VGS (**Figure 4B**). Ventilation significantly increased the relative abundance of Phycisphaeraceae in the VGS and Bacillaceae in the FDS, though it reduced that of Gemmatimonadaceae in the FDS (**Figure 4C** and **Supplementary Table 4C**). The relative abundance of *Bacillus* was increased by soil ventilation whereas that of *Pseudomonas* and *Flavobacterium* was reduced by higher planting density at the VGS (**Figure 4D**).

The PERMANOVA revealed significant effects of ventilation, density, and growth stage, as well as their interactions, on microbial community structure at different taxonomic levels (**Supplementary Table 5**). Ventilation, mainly affected the structure of the total bacterial community at family and genus levels, while planting density did so at the class and genus levels. Significant differences between the two growth stages arose mainly at the genus level (**Figures 4E–H** and **Supplementary Table 5**).

Diversity, Composition, and Structure of Soil Fungal Community

The Sobs, Chao, and Shannon indices of the total fungal community were also not significantly affected by ventilation (**Supplementary Table 3**). The fungal diversity (Shannon index) was influenced by planting density and growth stage

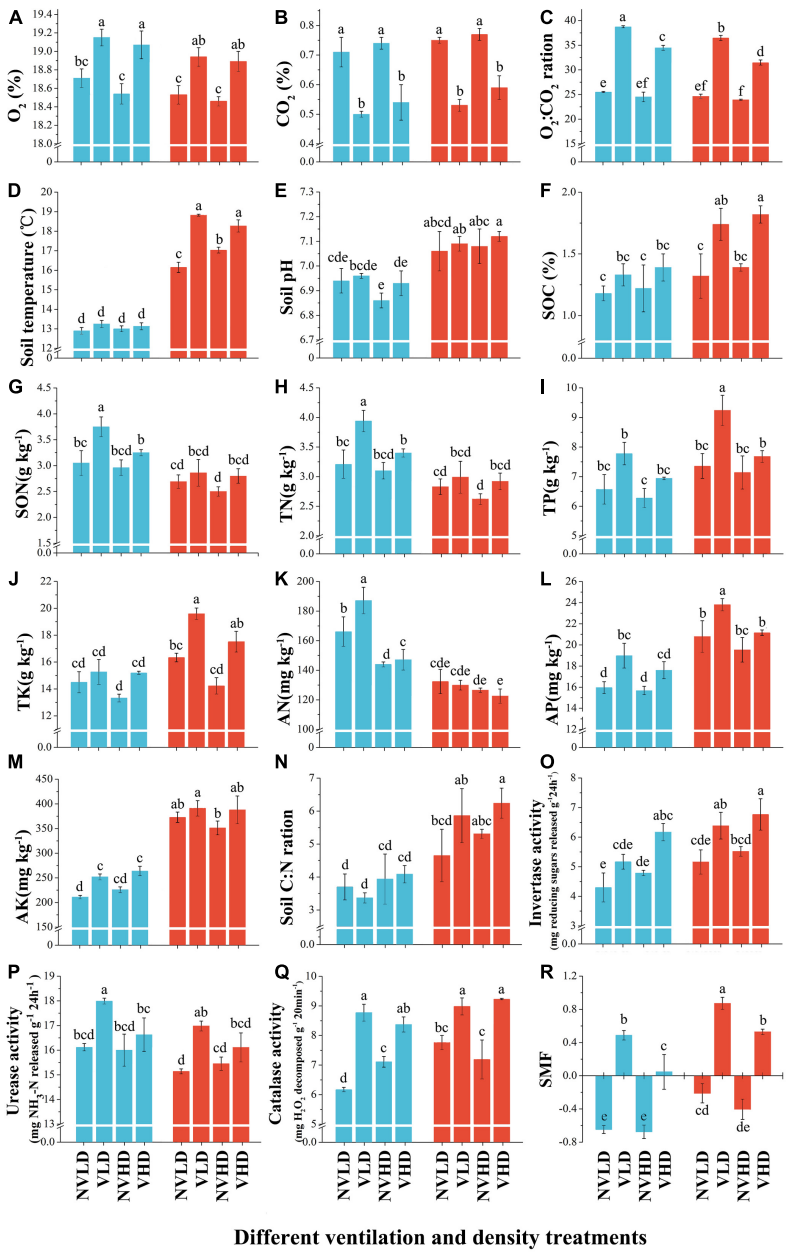

FIGURE 1 | Soil physicochemical index, nutrient index, enzyme activities, and soil multifunctional index (SMF) at two growth stages (vegetative growth stage and fruit development stage) of strawberry under different soil ventilation and planting density treatments. **(A)** O_2 concentration, %; **(B)** CO_2 concentration, %; **(C)** O_2:CO_2 ratio; **(D)** soil temperature, °C; **(E)** soil pH; **(F)** SOC (soil organic carbon), %; **(G)** SON (soil organic nitrogen), g kg^{-1}; **(H)** TN (soil total nitrogen), g kg^{-1}; **(I)** TP (soil total phosphorus), g kg^{-1}; **(J)** TK (soil total potassium), g kg^{-1}; **(K)** AN (soil available nitrogen), g kg^{-1}; **(L)** AP (soil available phosphorus), g kg^{-1}; **(M)** AK (soil available potassium), g kg^{-1}; **(N)** soil C/N ratio (soil organic carbon-to-total nitrogen ratio); **(O)** invertase activity, mg reducing sugars released g^{-1} 24 h^{-1}; **(P)** urease (URE) activity, mg NH_3-N released g^{-1} 24 h^{-1}; **(Q)** catalase activity, mg H_2O_2 decomposed g^{-1} 20 min^{-1}; **(R)** SMF (soil multifunctionality index), mg H_2O_2 decomposed g^{-1} 20 min^{-1}. The vegetative growth stage (VGS) and fruit development stage (FDS) are shown in sky blue and red, respectively. Results are shown as mean ± SD. Error bars represent standard deviation (SD) (n = 3). Different letters indicate significant differences between the means of each index ($p < 0.05$, Tukey's test).

of strawberry plants and interactions among the three factors, being lower in the FDS than VGS (**Figure 5** and **Supplementary Table 3**).

The fungal community was dominated by Zygomycota (9%), Chytridiomycota (6%), Basidiomycota (6%), and Ascomycota (3%) in all four treatment groups (**Figure 6A**). Ventilation reduced the relative abundance of Basidiomycota and increased that of Chytridiomycota. The relative abundance of Basidiomycota was higher, whereas that of Ascomycota and Zygomycota were both lower at the HD than LD. Furthermore,

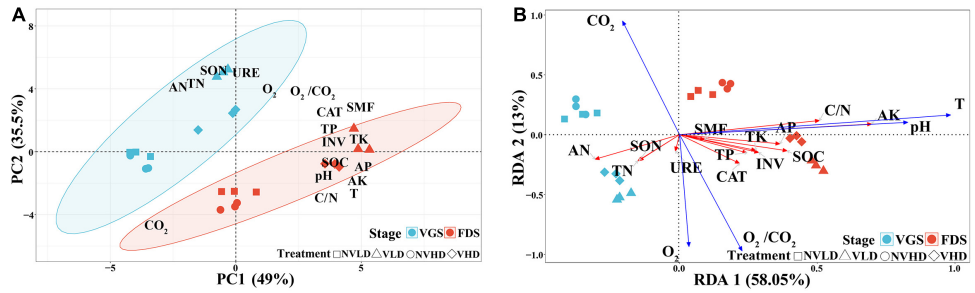

FIGURE 2 | Principal component analysis (PCA) based on soil chemical and physicochemical parameters as variables and redundancy analysis (RDA) of the soil chemical parameters data as explained by environmental variables (O_2, CO_2, O_2/CO_2, T, and pH) at two growth stages (vegetative growth stage and fruit development stage) of strawberry under different soil ventilation and planting density treatments. **(A)** PCA; **(B)** RDA. The vegetative growth stage (VGS) and fruit development stage (FDS) are shown in sky blue and red, respectively.

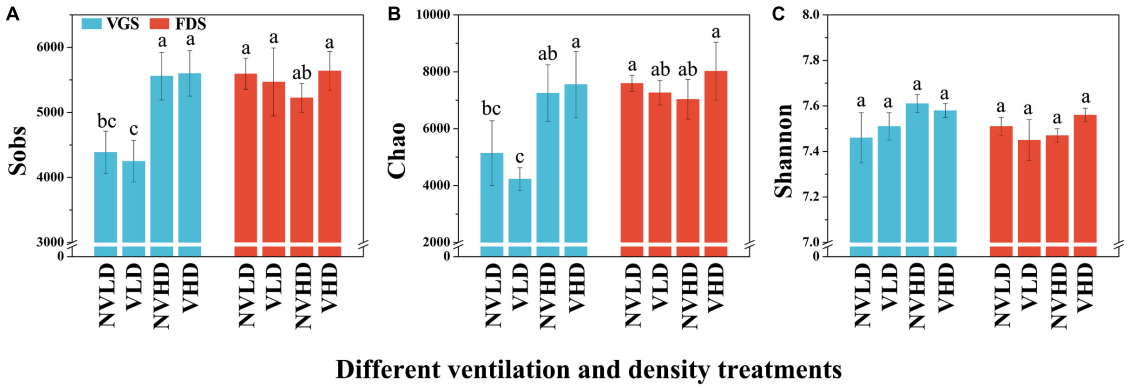

FIGURE 3 | Sobs **(A)**, Chao **(B)**, and Shannon **(C)** indices of the bacterial community in the studied soils. The vegetative growth stage (VGS) and fruit development stage (FDS) are shown in sky blue and red, respectively. Sobs is the observed operational taxonomic units (OTUs); Chao was used to evaluate community richness based on OTUs; the Shannon index was used to assess community diversity, considering the contributions of rare taxa. Results are shown as mean ± SD. Error bars represent standard deviation (SD) (n = 3). Different letters indicate significant differences between the means of each index ($p < 0.05$, Tukey's test).

the interactions of the three factors influenced the relative abundance of the fungal community to different degrees at the phylum level (**Figure 6A** and **Supplementary Table 6**).

The relative abundances of three dominant classes of fungi were altered by the treatments. For instance, soil ventilation reduced the relative abundance of Agaricomycetes and increased that of Pezizomycetes. The relative abundance of Eurotiomycetes and Pezizomycetes was higher, while that of Agaricomycetes was lower in the VGS than in the FDS (**Figure 6B**). *Aspergillus*, *Lobulomyces*, and *Triparticalcar* were the three dominant genera in soil. The relative abundance of *Aspergillus* was affected by density and growth stage and their interactions; that of *Lobulomyces* was increased by ventilation in the FDS (**Figure 6D**).

Functional Diversity of Microbial Community

Functional Groups Related to the Soil C Cycle

Among the 14 functional groups related to the C cycle in the bacterial community identified by FAPROTAX analysis, chemoheterotrophy and aerobic chemoheterotrophy assemblages were dominant. Ventilation reduced the enrichment of predatory or exoparasitic and methylotrophy groups. However, enrichment of the chemoheterotrophy, aerobic chemoheterotrophy, intracellular parasites, photoautotrophy, cyanobacteria, oxygenic photoautotrophy, and aromatic compound degradation functional groups all decreased with an increased planting density. Growth stage influenced the assemblage of 13 observed functional groups, including chemoheterotrophy, chitinolysis, and aromatic compound degradation, all of which were higher in the VGS than FDS, and *vice versa* for the photoautotrophy, cyanobacteria, and methylotrophy trends (**Figure 7A**).

Functional Groups Related to the Soil N Cycle

Functional groups related to the N cycle in the bacterial community indicated that the dominant assemblages of bacterial groups were associated with nitrate reduction, ureolysis, aerobic nitrite oxidation, nitrate respiration, N respiration, nitrification, N fixation, and nitrite respiration in the studied soils. Ventilation inhibited the assemblage of the ureolysis group yet promoted that of the nitrite respiration group. When compared with LD, HD reduced the assemblage of ureolysis and N fixation groups, but it increased that of the nitrification, nitrate respiration, and nitrite respiration groups. Growth stage influenced the assemblage of

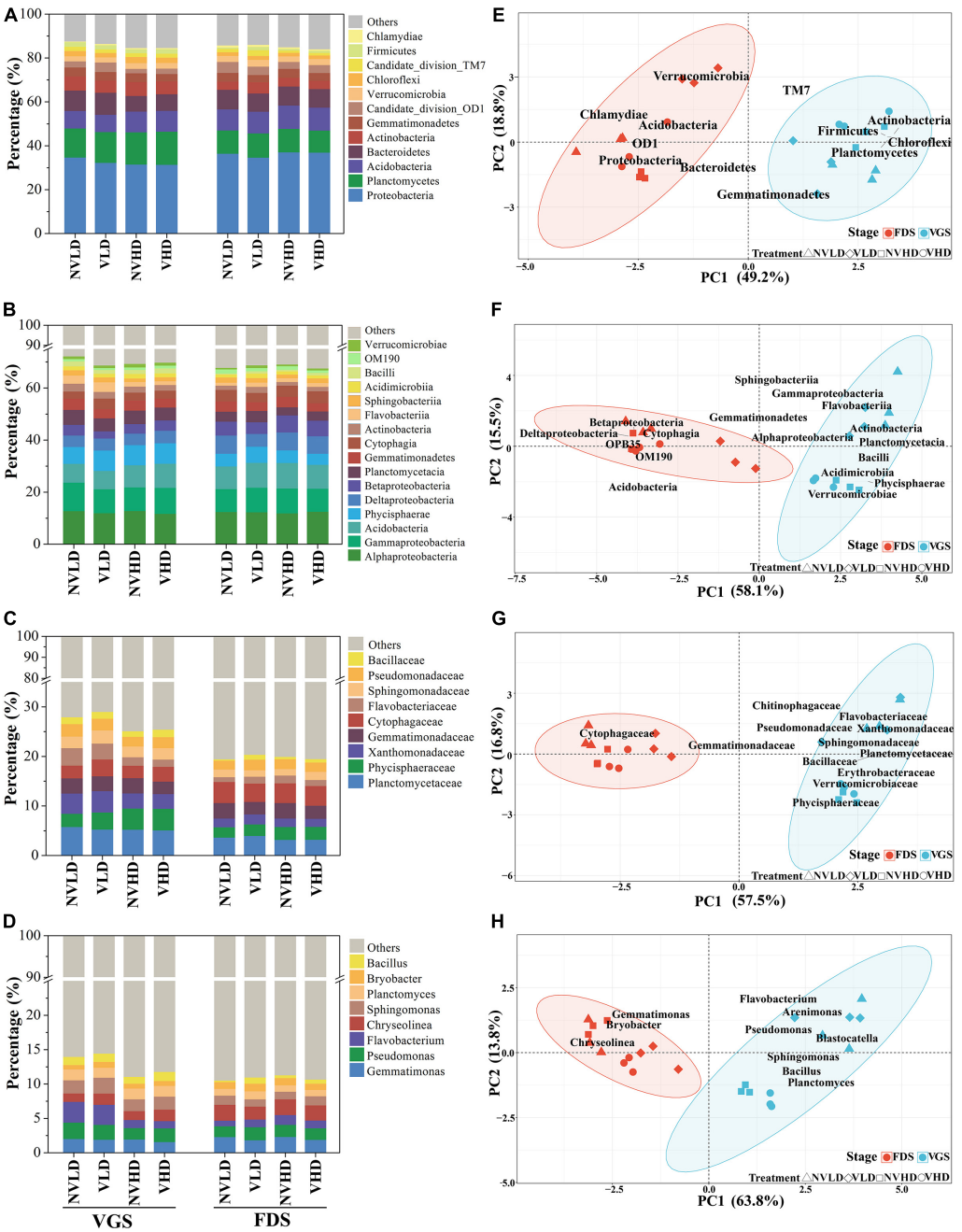

FIGURE 4 | Total bacterial community composition as determined by 16S rRNA gene sequencing. **(A–D)** Community composition at the phylum **(A)**, class **(B)**, family **(C)**, and genus **(D)** levels. **(E–H)** Community structure at the phylum **(E)**, class **(F)**, family **(G)**, and genus **(H)** levels. Only dominant populations (as long as one of the treatments has a relative abundance > 1%) are represented. The vegetative growth stage (VGS) and fruit development stage (FDS) are shown in sky blue and red, respectively.

eight functional groups related to N cycle (**Figure 7B** and **Supplementary Table 3**).

Functional Diversity of Fungal Community

Functional groups identified by FUNGuild analysis in the fungal community showed that the dominant assemblages in soil were litter saprotroph, soil saprotroph, and plant pathogen. Ventilation significantly reduced the assemblages of fungal parasite groups and enhanced that of soil saprotrophs, which were increased by the HD (**Figure 7C**).

The PCA of the relative abundances of bacterial and fungal functional groups revealed that they sorted according to the growth stage (S) of strawberry along PC1 (**Figures 7D–F** and **Supplementary Table 8**).

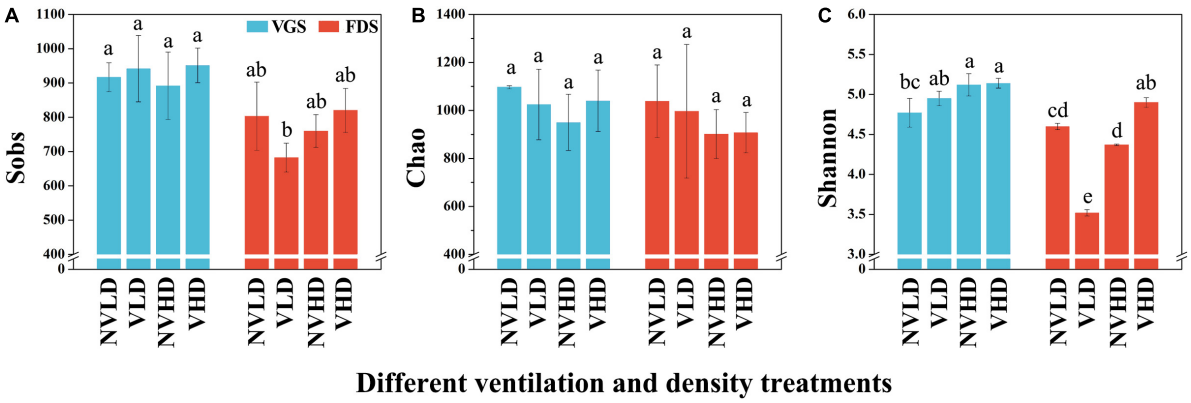

FIGURE 5 | Sobs **(A)**, Chao **(B)**, and Shannon **(C)** indices of the fungal community in the studied soils. The vegetative growth stage (VGS) and fruit development stage (FDS) are shown in sky blue and red, respectively. Sobs is the observed operational taxonomic units (OTUs); Chao was used to evaluate community richness based on OTUs; the Shannon index was used to assess community diversity, considering the contributions of rare taxa. Results are shown as mean ± SD. Error bars represent standard deviation (SD) (n = 3). Different letters indicate significant differences between the means of each index ($p < 0.05$, Tukey's test).

Correlations Between Soil Ventilation and Measured Variables

Soil O_2 concentration was positively correlated with soil N components. Importantly, it was positively correlated with the relative abundances of Firmicutes (Bacilli, Bacillaceae, and *Bacillus*); Pseudomonadaceae (*Pseudomonas*); *Arenimonas*, Blastocatella, Sphingomonadaceae, *Sphingomonas*, Chytridiomycota (Triparticalcar), and Pezizomycetes, but negatively correlated with those Betaproteobacteria and Gemmatimonadetes (Gemmatimonadetes, Gemmatimonadaceae, and Gemmatimonas). Soil O_2 concentration was positively correlated with litter and soil saprotrophs in the fungal community, but not correlated with the C and N functional groups of the bacterial community. Additionally, soil O_2 concentration was negatively correlated with the Tr of strawberry (**Figure 8A**).

For soil CO_2 concentration, the pattern of its correlations with the above indices was the opposite of that found for soil O_2 concentration. More specifically, soil CO_2 concentration was negatively correlated with the SOC content and TP and TK concentrations (**Figure 8B**). Soil temperature and pH were negatively correlated with soil CO_2 concentration. SMF was positively correlated with O_2 concentration and with the relative abundances of Verrucomicrobia and *Bryobacter*, yet negatively correlated with those of Chloroflexi and Gemmatimonadetes, as well as with the functional group capable of ureolysis. Additionally, the SMF was positively correlated with the leaf P concentration of strawberry plants (**Figure 8D**).

DISCUSSION

Soil Ventilation Effects on the Profile of Soil Microbial Community

In this study, *in situ* ventilation increased the concentration of soil O_2 and decreased that of soil CO_2 (**Figure 1**). O_2 concentration and supply rates in the root zone plays a critical role in root respiration, root elongation, nutrient absorption and transpiration, and plant growth (Zhao et al., 2019). In this process, soil bacterial and fungal communities also play vital roles in the turnover of SOC and C cycling (Zhao et al., 2018). In the present work, OM decomposition driven by the soil microbial community was activated by ventilation. It has been reported that soil microbial communities regulate many ecosystem processes and contribute to nutrient cycling through the decomposition of OM (Bender et al., 2016; Hartman et al., 2018). Moreover, the positive (soil O_2) and negative (soil CO_2) correlation with soil N components suggest that soil O_2 and CO_2 have antagonistic effects on N mineralization through soil enzyme activities. This may be consistent with the fact that rhizosphere ventilation can improve the potted tomato root zone environment, increase the soil enzyme activity, and promote the nutrient uptake (Niu et al., 2012).

In this study, ventilation increases relative abundance of Firmicutes phyla and its Bacilli (class, family, and genus) and decreases that of Gemmatimonadetes (**Figure 4**). It has been reported that aeration irrigation significantly increased the abundance of aerobic bacteria, such as *Nitrospira* and *Cytophagia* (Zhao et al., 2019). Furthermore, the abundance of *Bacillus* was positively correlated with soil O_2 concentrations (**Figure 8A**). Bacteria of the genera *Pseudomonas* and *Bacillus* can promote plant growth and protect plants from pathogens. A high relative abundance of aerobic *Bacillus* promotes plant growth and inhibits the growth of pathogenic bacteria *via* the decomposition of labile OM in soil (Razanamalala et al., 2018; Molina-Santiago et al., 2019). Conversely, Gemmatimonadetes abundance was negatively correlated with soil O_2 concentration (**Figure 8A**). This result is consistent with the finding that the relative abundance of Gemmatimonadetes decreased in the presence of wheat residues (Bernard et al., 2007) and that Gemmatimonadetes was more active in soils without leaf litter than in the litter treatments (Pfeiffer et al., 2013). Thus, members of the Gemmatimonadetes phylum may be adapted to a lifestyle

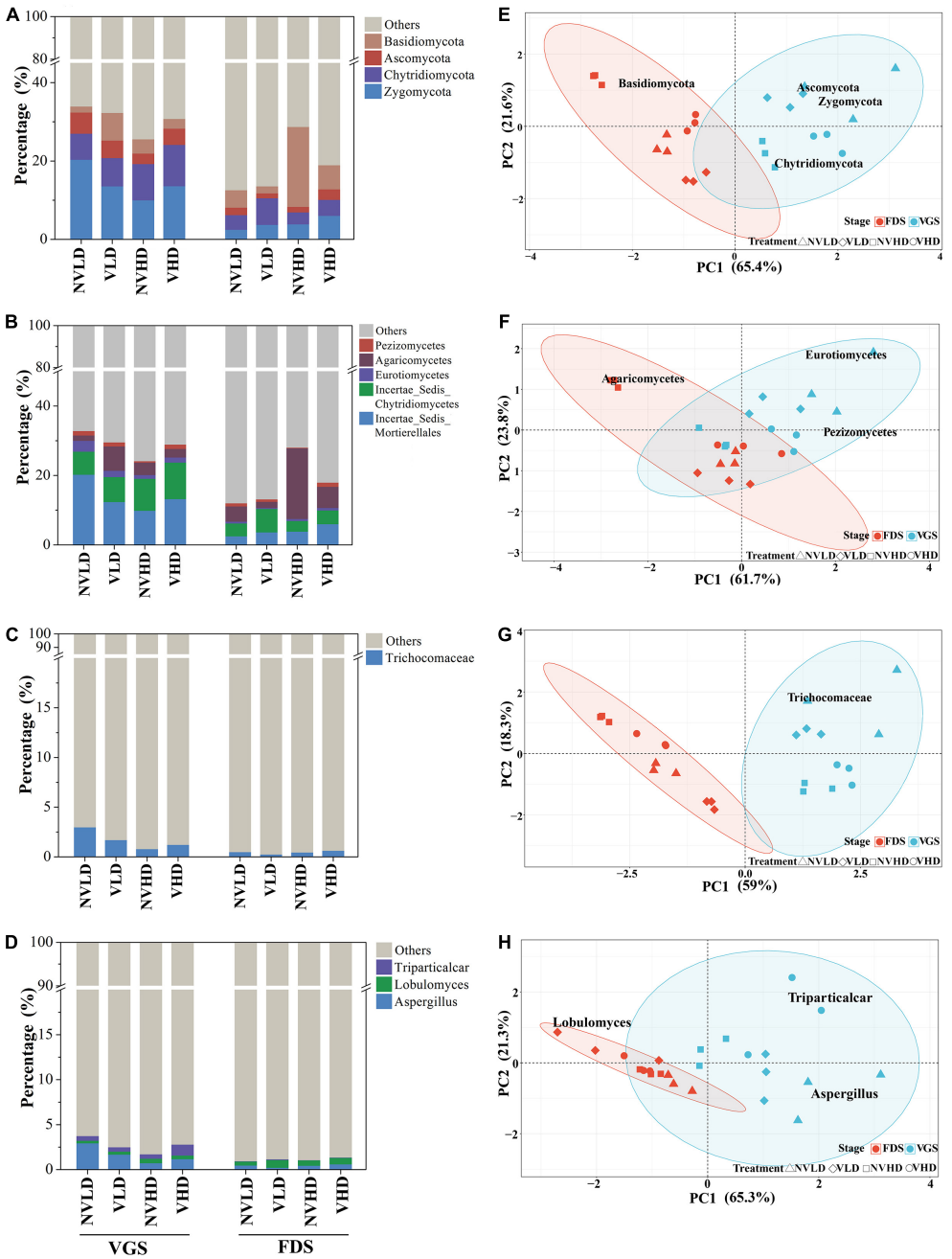

FIGURE 6 | Total fungal community composition as determined by 18S rRNA gene sequencing. **(A–D)** Community composition at the phylum **(A)**, class **(B)**, family **(C)**, and genus **(D)** levels. **(E–H)** Community structure at the phylum **(E)**, class **(F)**, family **(G)**, and genus **(H)** levels. Only dominant populations (as long as one of the treatments has a relative abundance > 1%) are represented. The vegetative growth stage (VGS) and fruit development stage (FDS) are shown in sky blue and red, respectively.

associated with OM sources that are challenging to mineralize along O_2 gradients (Whitman et al., 2016).

Ventilation did not alter the fungal alpha-diversity in soil (**Supplementary Table 3**), but enhanced Chytridiomycota and reduced Basidiomycota at the phylum level, reduced Pezizomycetes and Agaricomycetes at the class level, and increased *Triparticalcar* at the genus level (**Figure 6**). The OM decomposition rate was positively correlated with the relative abundance of Chytridiomycota, perhaps because of the association between the availability of labile C and the soil O_2 concentration, which is related to the recruitment of Chytridiomycota (Procter et al., 2014). The relative abundance of Basidiomycota decreased with soil O_2 concentration, suggesting that wood decay and plant litter decomposition were slowed

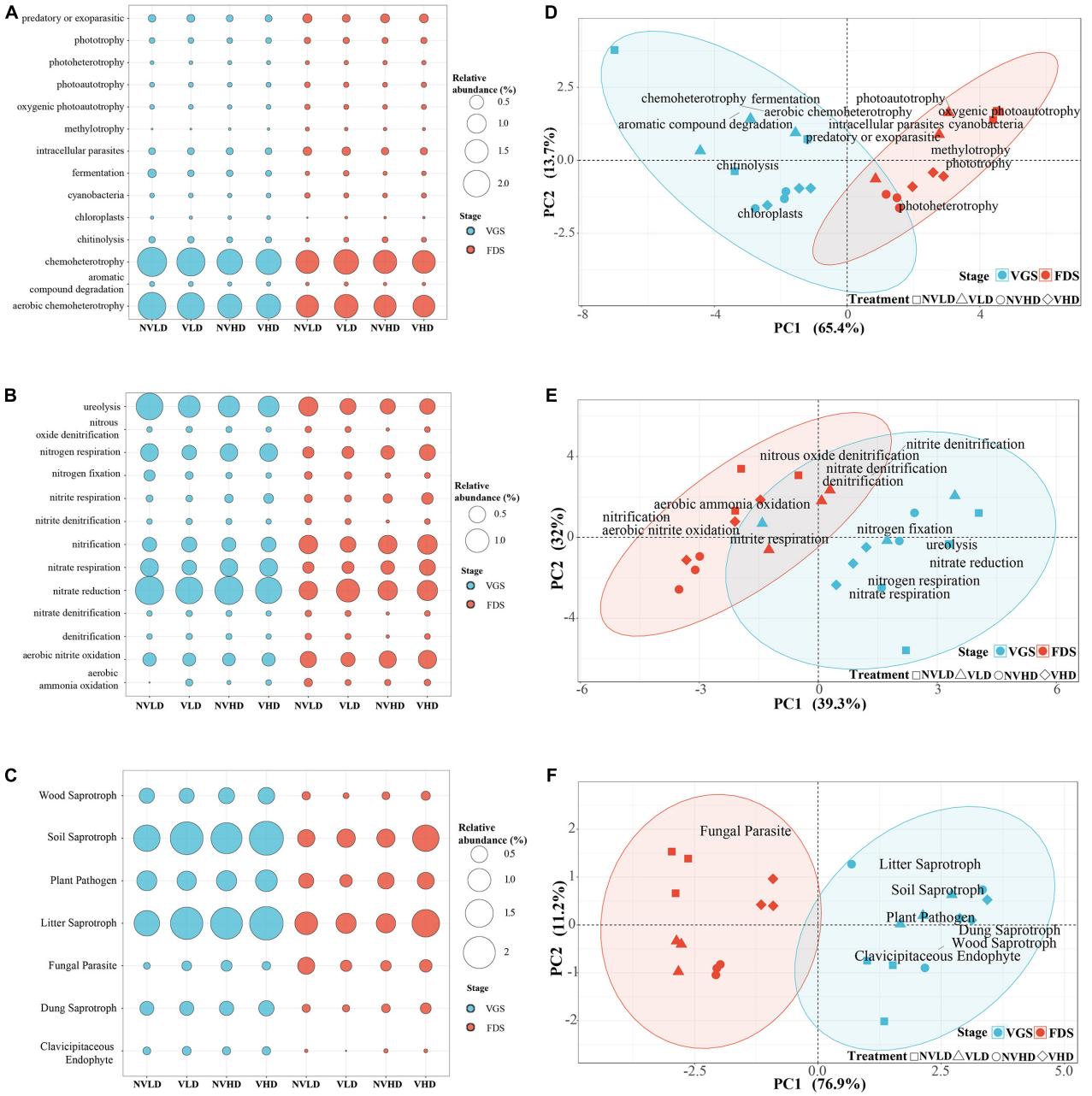

FIGURE 7 | Composition and structure of the functional groups in microbial communities. **(A–C)** Composition of the bacterial community related to the C cycle **(A)** and N cycle **(B)** and of the fungal community **(C)**. **(D–F)** Functional structure of the bacterial community related to the C cycle **(D)** and N cycle **(E)** and of the fungal community **(F)**. The vegetative growth stage (VGS) and fruit development stage (FDS) are shown in sky blue and red, respectively.

in the ventilated soil. Ventilation increased abundances of litter and soil saprotrophs groups, which were positively correlated with soil O_2 concentrations (**Figure 8**), which may promote the decomposition of soil labile OM and inhibit the occurrence of plant pathogens, resulting in accelerated N mineralization rates (Razanamalala et al., 2018). It also has been demonstrated that although some fungi are sensitive, the community remains stable upon changes in soil O_2 or CO_2 (Kaisermann et al., 2014; Zhang et al., 2016; Zi et al., 2018). Thus, aerobic bacteria and functional fungi of soil play major roles in accelerating N mineralization under ventilated conditions.

Planting Density Effects on Soil Oligotrophic and Copiotrophic Groups

The crop cultivation model can influence soil microbial attributes (Hartmann et al., 2015; García-Delgado et al., 2019; Xiao et al., 2019). For example, intra- and inter-specific plant competition,

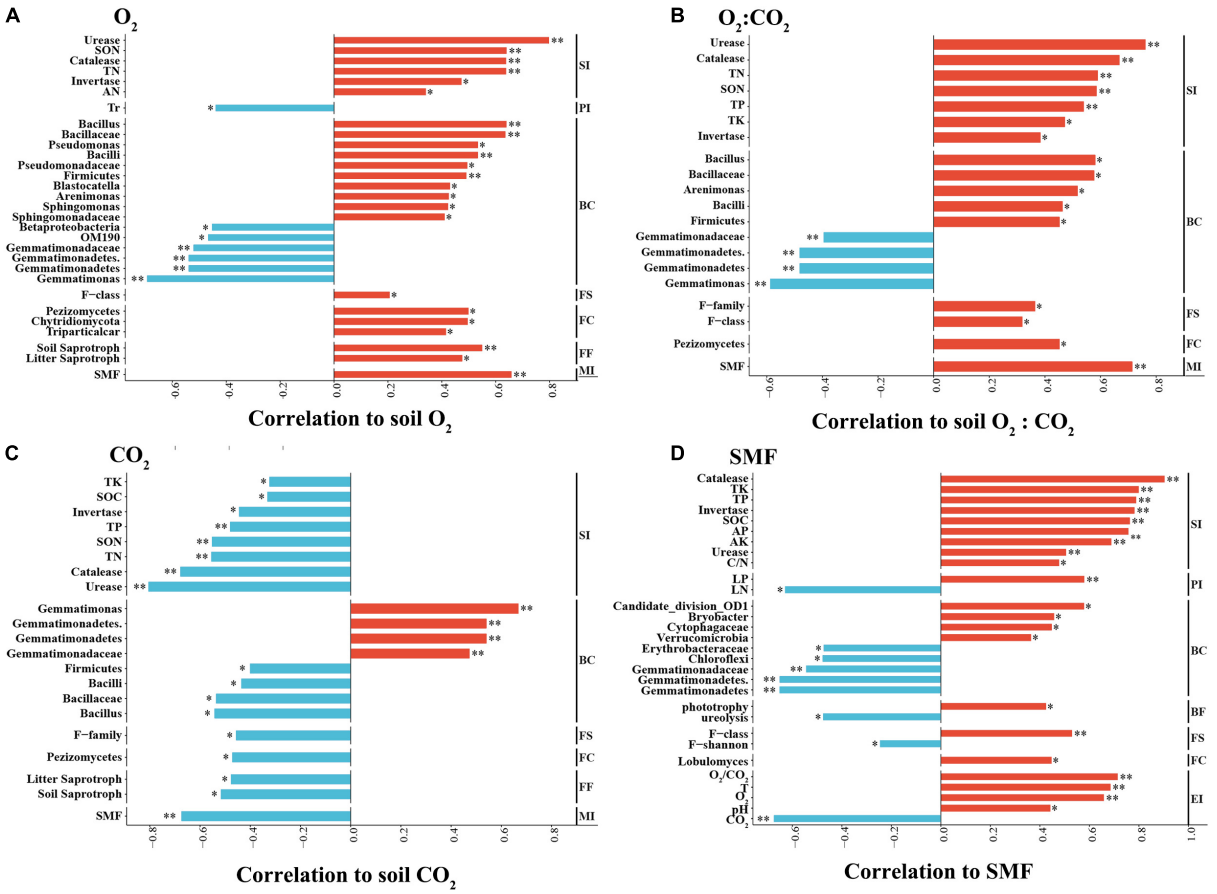

FIGURE 8 | Spearman correlation coefficients between soil environmental factors and soil physicochemical parameters and microbial community. **(A)** Soil O_2 concentration; **(B)** soil CO_2 concentration; **(C)** soil O_2:CO_2 ratio; **(D)** SMF (soil multifunctionality index). The abundance of total bacterial and fungal populations was analyzed by their 16S and 18S rRNA gene sequencing, respectively. BC, bacterial composition; BF, bacterial function; BS, bacterial structure; FC, fungal composition; FF, fungal function; FS, fungal structure; MI, multifunctional index; PI, plant index; SI, soil index; EI, environmental index. The negative and positive correlations are shown in sky blue and red, respectively. $^{*}p < 0.05$; $^{**}p < 0.01$.

especially at a high planting density, as well as the identity of the plant species themselves, can influence the rhizosphere bacterial community (Cavalieri et al., 2020). In our study, the planting density affected soil CO_2 concentration, and the TN and AN concentration and URE activity were all higher at LD when compared to HD in the VGS (**Figure 1**). Planting density has been shown to alter soil nutrient supply in the forest: increased N mineralization was beneficial to plant morphogenesis and increased the N content of leaves, while C mineralization enhanced plant C assimilation and water utilization and increased the leaf P content (Bastida et al., 2017). Consistent with those results for soil nutrients, compared with HD, we also found that the relative abundances of oligotrophic groups (Acidobacteria and Chloroflexi) were lower while those of copiotrophic groups (Bacteroidetes, Actinobacteria, and Gammaproteobacteria) were higher at LD. Similar results were reported recently, in that Proteobacteria was more abundant under a high-intensity thinning treatment, whereas Acidobacteria was more abundant under low-intensity thinning and control treatments (Dang et al., 2018). The changes to copiotrophic and oligotrophic groups according to planting density suggests that the soil microbial community composition depends on soil nutrient levels, further indicating a cooperative effect among microbial communities in adapting to the external environment. This is because N inputs significantly increased the relative abundance of the predicted copiotrophic groups (Proteobacteria and Firmicutes) but reduced those of predicted oligotrophic groups (Acidobacteria, Nitrospirae, and Chloroflexi) (Ling et al., 2017). By contrast, HD reduced the enrichment of soil functional groups related to C (cyanobacteria, photoautotrophy) and N (ureolysis, N fixation) cycling. These functional groups may be sensitive to high C input in aerated soil, resulting in decreased C and N contents in aerated HD soil, because of soil resource competition during plant growth (Dang et al., 2018; Muñoz-Rojas et al., 2018). Soil, litter, and dung saprotrophs were enriched at HD, and this probably accelerated the C and N cycling dynamics. It is likely that LD slowed the degradation of organic substances due to low C input and reduced competition for nutrients between plants and microbes (Dang et al., 2018; Mommer et al., 2018).

Growth Stage Effects Soil Nutrient Composition *via* Soil Temperature and pH

Soil temperature and pH were both higher in FDS than in VGS during the strawberry growth stage (**Figure 1**). They are important environmental factors influencing soil microflora (Cheng et al., 2017; Lammel et al., 2018; Walker et al., 2018). These caused significant differences in the soil C and N compositions and enzyme activities in the ventilation soil. Usually, soil temperature and pH also co-vary with some confounding factors, such as land use and management practices (e.g., tillage, fertilizer application), plant cover, and climatic conditions. We found that soil temperature and pH play important roles in shaping the soil nutrient composition to meet the stage requirements for plant growth and development in ventilated soil. A more comprehensive analysis of the direct (e.g., Actinobacteria) and indirect effects of pH can clarify the mechanisms that shape soil microbial communities (Lammel et al., 2018). In this study, the soil N cycle was dominant in the VGS whereas the soil C cycle (accompanied by P and K cycles) was dominant in the FDS (**Figure 2A**), with corresponding trends found for the functional groups related to soil C and N cycles. Temperature-induced differences in gross N flux are related to total C availability and the soil microbiome profile (Cookson et al., 2007). Rhizospheric microbial community profiles of a variety of plants (e.g., pea, wheat, sugar beet, and alfalfa) are altered according to the plant developmental gradient (Mougel et al., 2006; Houlden et al., 2008); for example, the root microbiota of rice varies over time during the life cycle of rice plants in the field (Zhang et al., 2018). This potential selection of microbes in the rhizosphere through plant aging may be associated with the ability of beneficial microbes to adapt to intrinsic requirements through plant growth and development by promoting systemic tolerance to abiotic stress, increasing plant's innate immunity (Zamioudis and Pieterse, 2012), and enhancing mineral nutrition (van der Heijden et al., 2008).

CONCLUSION

Our study shows that soil ventilation altered the microbial community profile and drove differences in C and N contents between VGS (more N components) and FDS (more C components), which enhanced strawberry growth under high-density planting environment. The soil aerobic bacteria (e.g., *Bacillus*) and functional fungi (e.g., litter and soil saprotrophs groups) play a major role in accelerating N mineralization under ventilation treatments. The copiotrophic and oligotrophic groups seem to cooperate to benefit strawberry growth mediated by planting density. However, further and more investigation of copiotrophic and oligotrophic bacterial groups are asked to test this hypothesis. More N components should be supplied in the VGS while both C and N components should be applied in the FDS to meet the requirements for normal strawberry plant and fruit development. Soil ventilation can be used as a tillage practice for improving soil quality, keeping soil health and maximize crop production in greenhouse ecosystems with high-density planting (hypoxia stress) or long-term continuous cropping. In order to reveal the underlying mechanism, the effect of ventilation on soil aggregate and functional genes of soil microbial community participating in N mineralization require further study. Meanwhile, it is crucial to consider the soil aeration and their effect on the whole soil microbiome when planning optimal agricultural management practices in greenhouse.

DATA AVAILABILITY STATEMENT

The microbiota sequencing data presented in the study are deposited in the National Center for Biotechnology Information (NCBI) repository, accession number PRJNA721522.

AUTHOR CONTRIBUTIONS

YY and JZ designed the study. YZ, YH, ZY, and ZLL performed the greenhouse and laboratory experiments. ZLL, MH, and ZML performed the data analysis. YZ, JZ, and YY wrote the first draft of the manuscript. All the authors contributed to the writing of this manuscript and approved the final version.

FUNDING

This study was supported by grants from the National Key Project of the Research and Development Plan (2016YFD0201116), the Beijing Key Project of the Science and Technology Plan (Z181100002418003/004), the National Natural Science Foundation of China (31171922 and 31301736), the Beijing Natural Science Fund-Municipal Education Commission (KZ201910020022), the Construction of Beijing Science and Technology Innovation and Service Capacity in Top Subjects (CEFF-PXM2019_014207_000032), the Beijing Key Laboratory of New Technique in Agricultural Application (NYYYXJS201704), and the China Postdoctoral Science Foundation (2019M650283).

ACKNOWLEDGMENTS

We thank the Beijing Collaborative Innovation Center for Eco-Environmental Improvement of Forestry and Fruit Trees; the Key Laboratory of Pomology, Beijing Nursery Engineering Research Center for Fruit Crops; the Key Laboratory of Agricultural Applications at the Beijing University of Agriculture; and the technicians at the Changping District Forestry Administration in Beijing.

SUPPLEMENTARY MATERIAL

The Supplementary Material for this article can be found online at: https://www.frontiersin.org/articles/10.3389/fmicb.2021.666982/full#supplementary-material

REFERENCES

Bastida, F., Torres, I. F., Andrés-Abellán, M., Baldrian, P., López-Mondéjar, R., Větrovský, T., et al. (2017). Differential sensitivity of total and active soil microbial communities to drought and forest management. *Glob. Chang. Biol.* 23, 4185–4203. doi: 10.1111/gcb.13790

Bender, S. F., Wagg, C., and van der Heijden, M. G. A. (2016). An underground revolution: biodiversity and soil ecological engineering for agricultural sustainability. *Trends Ecol. Evol.* 31, 440–452. doi: 10.1016/j.tree.2016.02.016

Ben-Noah, I., and Friedman, S. P. (2018). Review and evaluation of root respiration and of natural and agricultural processes of soil aeration. *Vad. Zone J.* 17, 1–47. doi: 10.2136/vzj2017.06.0119

Ben-Noah, I., Nitsan, I., Cohen, B., Kaplan, G., and Friedman, S. P. (2021). Soil aeration using air injection in a citrus orchard with shallow groundwater. *Agric. Water Manag.* 245:106664. doi: 10.1016/j.agwat.2020.106664

Bernard, L., Mougel, C., Maron, P., Nowak, V., Lévêque, J., Henault, C., et al. (2007). Dynamics and identification of soil microbial populations actively assimilating carbon from ^{13}C-labelled wheat residue as estimated by DNA-and RNA-SIP techniques. *Environ. Microbiol.* 9, 752–764. doi: 10.1111/j.1462-2920.2006.01197.x

Bhattarai, S. P., Huber, S., and Midmore, D. J. (2004). Aerated subsurface irrigation water gives growth and yield benefits to zucchini, vegetable soybean and cotton in heavy clay soils. *Ann. Appl. Biol.* 144, 285–298. doi: 10.1111/j.1744-7348.2004.tb00344.x

Bhattarai, S. P., Pendergast, L., and Midmore, D. J. (2006). Root aeration improves yield and water use efficiency of tomato in heavy clay and saline soils. *Sci. Hortic.* 108, 278–288. doi: 10.1016/j.scienta.2006.02.011

Bremner, J. M. (1996). "Nitrogen total," in *Methods of Soil Analysis Part 3: Chemical Methods, SSSA Book Series 5*, ed. D. L. Sparks (Madison, WI: Soil Science Society of America), 1085–1122.

Cavalieri, A., Bak, F., Garcia-Lemos, A. M., Weiner, J., Nicolaisen, M. H., Nybroe, O., et al. (2020). Effects of intra- and interspecific plant density on rhizosphere bacterial communities. *Front. Microbiol.* 11:1045. doi: 10.3389/fmicb.2020.01045

Cheng, L., Zhang, N., Yuan, M., Xiao, J., Qin, Y., Deng, Y., et al. (2017). Warming enhances old organic carbon decomposition through altering functional microbial communities. *ISME J.* 11, 1825–1835. doi: 10.1038/ismej.2017.48

Cookson, W. R., Osman, M., Marschner, P., Abaye, D. A., Clark, I., Murphy, D. V., et al. (2007). Controls on soil nitrogen cycling and microbial community composition across land use and incubation temperature. *Soil Biol. Biochem.* 39, 744–756. doi: 10.1016/j.soilbio.2006.09.022

Dang, P., Gao, Y., Liu, J., Yu, S., and Zhao, Z. (2018). Effects of thinning intensity on understory vegetation and soil microbial communities of a mature Chinese pine plantation in the Loess Plateau. *Sci. Total Environ.* 630, 171–180. doi: 10.1016/j.scitotenv.2018.02.197

Delgado-Baquerizo, M., Maestre, F. T., Reich, P. B., Jeffries, T. C., Gaitan, J. J., Encinar, D., et al. (2016). Microbial diversity drives multifunctionality in terrestrial ecosystems. *Nat. Commun.* 7:10541. doi: 10.1038/ncomms10541

Du, Y., Gu, X., Wang, J., and Niu, W. (2019). Yield and gas exchange of greenhouse tomato at different nitrogen levels under aerated irrigation. *Sci. Total Environ.* 668, 1156–1164. doi: 10.1016/j.scitotenv.2019.03.098

Edgar, R. C. (2013). UPARSE: highly accurate OTU sequences from microbial amplicon reads. *Nat. Methods* 10, 996–998. doi: 10.1038/NMETH.2604

Friedman, S. P., and Naftaliev, B. (2012). A survey of the aeration status of drip-irrigated orchards. *Agric. Water Manag.* 115, 132–147. doi: 10.1016/j.agwat.2012.08.015

García-Delgado, C., Barba-Vicente, V., Marín-Benito, J. M., Mariano Igual, J., Sánchez-Martín, M. J., Rodríguez-Cruz, S., et al. (2019). Influence of different agricultural management practices on soil microbial community over dissipation time of two herbicides. *Sci.Total Environ.* 646, 1478–1488. doi: 10.1016/j.scitotenv.2018.07.395

Glinski, J., and Stepniewski, W. (1985). *Soil Aeration and Its Role for Plants*. Boca Raton, FL: CRC Press.

Hartman, K., van der Heijden, M. G. A., Wittwer, R. A., Banerjee, S., Walser, J., Schlaeppi, K., et al. (2018). Cropping practices manipulate abundance patterns of root and soil microbiome members paving the way to smart farming. *Microbiome* 6:14. doi: 10.1186/s40168-017-0389-9

Hartmann, M., Frey, B., Mayer, J., Mäder, P., and Widmer, F. (2015). Distinct soil microbial diversity under long-term organic and conventional farming. *ISME J.* 9, 1177–1194. doi: 10.1038/ismej.2014.210

Hou, H. J., Chen, H., Cai, H. J., Yang, F., Li, D., and Wang, F. T. (2016). CO_2 and N_2O emissions from Lou soils of greenhouse tomato fields under aerated irrigation. *Atmos. Environ.* 132, 69–76. doi: 10.1016/j.atmosenv.2016.02.027

Houlden, A., Timms-Wilson, T. M., Day, M. J., and Bailey, M. J. (2008). Influence of plant developmental stage on microbial community structure and activity in the rhizosphere of three field crops. *FEMS Microbiol. Ecol.* 65, 193–201. doi: 10.1111/j.1574-6941.2008.00535.x

Huang, Y., Xiao, X., Huang, H., Jing, J., Zhao, H., Long, X.-E., et al. (2018). Contrasting beneficial and pathogenic microbial communities across consecutive cropping fields of greenhouse strawberry. *Appl. Microbiol. Biot.* 102, 5717–5729. doi: 10.1007/s00253-018-9013-6

Ityel, E., Ben-Gal, A., Silberbush, M., and Lazarovitch, N. (2014). Increased root zone oxygen by a capillary barrier is beneficial to bell pepper irrigated with brackish water in an arid region. *Agric. Water Manag.* 131, 108–114. doi: 10.1016/j.agwat.2013.09.018

Iwasaki, Y. (2008). Root zone aeration improves growth and yields of coir-cultured strawberry (*Fragaria ananassa* Duch.) during summer. *Acta Hortic.* 319, 251–254. doi: 10.17660/ActaHortic.2008.779.30

Jin, K., Sleutel, S., Buchan, D., De Neve, S., Cai, D. X., Gabriels, D., et al. (2009). Changes of soil enzyme activities under different tillage practices in the Chinese Loess Plateau. *Soil Till. Res.* 104, 115–120. doi: 10.1016/j.still.2009.02.004

Kaisermann, A., Maron, P. A., Beaumelle, L., and Lata, J. C. (2014). Fungal communities are more sensitive indicators to non-extreme soil moisture variations than bacterial communities. *Appl. Soil Ecol.* 86, 158–164. doi: 10.1016/j.apsoil.2014.10.009

Kitaya, Y., Yabuki, K., and Kiyata, M. (1984). Studies on the control of gaseous environment in the rhizosphere. Effect of carbon dioxide in the rhizosphere on growth of cucumber. *J. Agric. Met.* 40, 119–124. doi: 10.2480/agrmet.40.119

Klindworth, A., Pruesse, E., Schweer, T., Peplies, J., Quast, C., Horn, M., et al. (2013). Evaluation of general 16S ribosomal RNA gene PCR primers for classical and next-generation sequencing-based diversity studies. *Nucleic Acids Res.* 41:e1. doi: 10.1093/nar/gks808

Lammel, D. R., Barth, G., Ovaskainen, O., Cruz, L. M., Zanatta, J. A., Ryo, M., et al. (2018). Direct and indirect effects of a pH gradient bring insights into the mechanisms driving prokaryotic community structures. *Microbiome* 6:106. doi: 10.1186/s40168-018-0482-8

Li, W., and Liu, Q. (2019). Changes in fungal community and diversity in strawberry rhizosphere soil after 12 years in the greenhouse. *J. Integr. Agric.* 18, 677–687. doi: 10.1016/S2095-3119(18)62003-9

Li, Y., Niu, W., Cao, X., Zhang, M., Wang, J., Zhang, Z., et al. (2020). Growth response of greenhouse-produced muskmelon and tomato to sub-surface drip irrigation and soil aeration management factors. *BMC Plant Biol.* 20:141. doi: 10.1186/s12870-020-02346-y

Li, Y., Niu, W., Dyck, M., Wang, J., and Zou, X. (2016a). Yields and nutritional of greenhouse tomato in response to different soil aeration volume at two depths of subsurface drip irrigation. *Sci. Rep-UK* 6:39307. doi: 10.1038/srep39307

Li, Y., Niu, W., Xu, J., Wang, J., Zhang, M., Wang, V., et al. (2016b). Root morphology of greenhouse produced muskmelon under sub-surface drip irrigation with supplemental soil aeration. *Sci. Hortic.* 201, 287–294. doi: 10.1016/j.scienta.2016.02.018

Ling, N., Chen, D., Guo, H., Wei, J., Bai, Y., Wei, J., et al. (2017). Differential responses of soil bacterial communities to long-term N and P inputs in a semi-arid steppe. *Geoderma* 292, 25–33. doi: 10.1016/j.geoderma.2017.01.013

Liu, F., Fan, J., Du, J., Shi, X., Zhang, J., Shen, Y., et al. (2019). Intensified nitrogen transformation in intermittently aerated constructed wetlands: removal pathways and microbial response mechanism. *Sci. Total Environ.* 650, 2880–2887. doi: 10.1016/j.scitotenv.2018.10.037

Louca, S., Parfrey, L. W., and Doebeli, M. (2016). Decoupling function and taxonomy in the global ocean microbiome. *Science* 353, 1272–1277. doi: 10.1126/science.aaf4507

Lu, R. K. (2000). *Methods of Soil And Agro-Chemical Analysis*. Beijing: China Agricultural Science and Technology Press.

Maboko, M. M., and Du Plooy, C. P. (2013). High-density planting of tomato cultivar's with early decapitation of growing point increased yield in a closed hydroponic system. *Acta Agric. Scand. Sect. B Soil Plant Sci.* 63, 676–682. doi: 10.1080/09064710.2013.851276

Magoč, T., and Salzberg, S. L. (2011). FLASH: fast length adjustment of short reads to improve genome assemblies. *Bioinformatics* 27, 2957–2963. doi: 10.1093/bioinformatics/btr507

Molina-Santiago, C., Pearson, J. R., Navarro, Y., Berlanga-Clavero, M. V., Caraballo-Rodriguez, A. M., Petras, D., et al. (2019). The extracellular matrix protects *Bacillus subtilis* colonies from *Pseudomonas* invasion and modulates plant co-colonization. *Nat. Commun.* 1011:1919. doi: 10.1038/s41467-019-09944-x

Mommer, L., Cotton, T. E. A., Raaijmakers, J. M., Termorshuizen, A. J., Ruijven, J., Hendriks, M., et al. (2018). Lost in diversity: the interactions between soil-borne fungi, biodiversity and plant productivity. *New Phytol.* 218, 542–553. doi: 10.1111/nph.15036

Mougel, C., Offre, P., Ranjard, L., Corberand, T., Gamalero, E., Robin, C., et al. (2006). Dynamic of the genetic structure of bacterial and fungal communities at different developmental stages of *Medicago truncatula* Gaertn. cv. Jemalong Line J5. *New Phytol.* 170, 165–175. doi: 10.2307/3694642

Muñoz-Rojas, M., Román, J. R., Roncero-Ramos, B., Erickson, T. E., Merritt, D. J., Aguila-Carricondo, P., et al. (2018). Cyanobacteria inoculation enhances carbon sequestration in soil substrates used in dryland restoration. *Sci. Total Environ.* 636, 1149–1154. doi: 10.1016/j.scitotenv.2018.04.265

Nardini, A., Õunapuu-Pikas, E., and Savi, T. (2014). When smaller is better: leaf hydraulic conductance and drought vulnerability correlate to leaf size and venation density across four Coffea arabica genotypes. *Funct. Plant Biol.* 41, 972–982. doi: 10.1071/FP13302

Nelson, D. W., and Sommers, L. E. (1996). "Total carbon, organic carbon, and organic matter," in *Methods of Soil Analysis, Part 3. Chemical methods*, ed. D. L. Sparks (Madison: American Society of Agronomy Inc.), 961–1010.

Nguyen, N. H., Song, Z., Bates, S. T., Branco, S., Tedersoo, L., Menke, J., et al. (2016). FUNGuild: an open annotation tool for parsing fungal community datasets by ecological guild. *Fungal Ecol.* 20, 241–248. doi: 10.1016/j.funeco.2015.06.006

Niu, W. Q., Jia, Z. X., Xuan, Z., and Shao, H. B. (2012). Effects of soil rhizosphere aeration on the root growth and water absorption of tomato. *Clean–Soil Air Water* 40, 1364–1371. doi: 10.1002/clen.201100417

Pfeiffer, B., Fender, A., Lasota, S., Hertel, D., Jungkunst, H. F., and Daniel, R. (2013). Leaf litter is the main driver for changes in bacterial community structures in the rhizosphere of ash and beech. *Appl. Soil Ecol.* 72, 150–160. doi: 10.1016/j.apsoil.2013.06.008

Procter, A. C., Ellis, J. C., Fay, P. A., Polley, H. W., and Jackson, R. B. (2014). Fungal community responses to past and future atmospheric CO_2 differ by soil type. *Appl. Environ. Microb.* 80, 7364–7377. doi: 10.1128/AEM.02083-14

Pruesse, E., Quast, C., Knittel, K., Fuchs, B. M., Ludwig, W., Peplies, J., et al. (2007). SILVA: a comprehensive online resource for quality checked and aligned ribosomal RNA sequence data compatible with ARB. *Nucleic Acids Res.* 35, 7188–7196. doi: 10.1093/nar/gkm864

Puerta, V. L., Oereira, E. I. P., Wittwer, R., Heijden, M., and Six, J. (2018). Improvement of soil structure through organic crop management, conservation tillage and grass-clover ley. *Soil Till. Res.* 180, 1–9. doi: 10.1016/j.still.2018.02.007

Rashad, Y. M., Abdel-Fattah, G., and Hafez, E. E. (2012). Diversity among some Egyptian isolates of *Rhizoctonia solani* based on anastomosis grouping, molecular identification and virulence on common bean. *Afr. J. Microbiol. Res.* 6, 6661–6667. doi: 10.5897/AJMR12.1096

Razanamalala, K., Razafimbelo, T., Maron, P., Ranjard, L., Chemidlin, N., Lelièvre, M., et al. (2018). Soil microbial diversity drives the priming effect along climate gradients: a case study in Madagascar. *ISME J.* 12, 451–462. doi: 10.1038/ismej.2017.178

Ribeiro, R. V., Machado, E. C., Santos, M. G., and Oliveira, R. F. (2009). Photosynthesis and water relations of well-watered orange plants as affected by winter and summer conditions. *Photosynthetica* 47, 215–222. doi: 10.1007/s11099-009-0035-2

Rivelli, A. R., De Maria, S., Puschenreiter, M., and Gherbin, P. (2012). Accumulation of cadmium, zinc, and copper by *Helianthus Annuus* L.: impact on plant growth and uptake of nutritional elements. *Int. J. Phytoremediat.* 14, 320–334. doi: 10.1080/15226514.2011.620649

Santruckova, H., and Simek, M. (1997). Effect of soil CO_2 concentration on microbial biomass. *Biol. Fertil. Soils* 25, 269–273. doi: 10.1007/s003740050313

Schloss, P. D., Westcott, S. L., Ryabin, T., Hall, J. R., Hartmann, M., Hollister, E. B., et al. (2009). Introducing mothur: open-source, platform-independent, community-supported software for describing and comparing microbial communities. *Appl. Environ. Microb.* 75, 7537–7541. doi: 10.1128/AEM.01541-09

Smit, E., Leeflang, P., Glandorf, B., van Elsas, J. D., and Wernars, K. (1999). Analysis of fungal diversity in the wheat rhizosphere by sequencing of cloned PCR-amplified genes encoding 18S rRNA and temperature gradient gel electrophoresis. *Appl. Environ. Microb.* 65, 2614–2621. doi: 10.1128/AEM.65.6.2614-2621.1999

Stefan, L., Hartmann, M., Engbersen, N., Six, J., and Schöb, C. (2021). Positive effects of crop diversity on productivity driven by changes in soil microbial composition. *Front. Microbiol.* 12:660749. doi: 10.3389/fmicb.2021.660749

Stępniewski, W., and Stępniewska, Z. (2009). Selected oxygen-dependent process—response to soil management and tillage. *Soil Till. Res.* 102, 193–200. doi: 10.1016/j.still.2008.07.006

van der Heijden, M. G. A., Bardgett, R. D., and van Straalen, N. M. (2008). The unseen majority: soil microbes as drivers of plant diversity and productivity in terrestrial ecosystems. *Ecol. Lett.* 11, 296–310. doi: 10.1111/j.1461-0248.2007.01139.x

Walker, T. W. N., Kaiser, C., Strasser, F., Herbold, C. W., Leblans, N. I. W., Woebken, D., et al. (2018). Microbial temperature sensitivity and biomass change explain soil carbon loss with warming. *Nat. Clim. Chang.* 8, 885–889. doi: 10.1038/s41558-018-0259-x

Whitman, T., Pepe-Ranney, C., Enders, A., Koechli, C., Campbell, A., Buckley, D. H., et al. (2016). Dynamics of microbial community composition and soil organic carbon mineralization in soil following addition of pyrogenic and fresh organic matter. *ISME J.* 10, 2918–2930. doi: 10.1038/ismej.2016.68

Xiao, D., Tan, Y., Liu, X., Yang, R., Zhang, W., He, X., et al. (2019). Effects of different legume species and densities on arbuscular mycorrhizal fungal communities in a karst grassland ecosystem. *Sci. Total Environ.* 678, 551–558. doi: 10.1016/j.scitotenv.2019.04.293

Xiao, Y., Peng, F., Dang, Z., Jiang, X., Zhang, J., Zhang, Y., et al. (2015). Influence of rhizosphere ventilation on soil nutrient status, root architecture and the growth of young peach trees. *Soil Sci. Plant Nutr.* 61, 775–787. doi: 10.1080/00380768.2015.1045404

Xu, Z., Ma, Y., Zhang, L., Han, Y., Yuan, J., Li, G., et al. (2021). Relating bacterial dynamics and functions to gaseous emissions during composting of kitchen and garden wastes. *Sci. Total Environ.* 767:144210. doi: 10.1016/j.scitotenv.2020.144210

Zamioudis, C., and Pieterse, C. M. J. (2012). Modulation of host immunity by beneficial microbes. *Mol. Plant Microb. Int.* 25, 139–150. doi: 10.1094/mpmi-06-11-0179

Zhang, J., Zhang, N., Liu, Y., Zhang, X., Hu, B., Qin, Y., et al. (2018). Root microbiota shift in rice correlates with resident time in the field and developmental stage. *Sci. China Life Sci.* 61, 613–621. doi: 10.1007/s11427-018-9284-4

Zhang, K., Shi, Y., Jing, X., He, J., Sun, R., Yang, Y., et al. (2016). Effects of short-term warming and altered precipitation on soil microbial communities in alpine grassland of the Tibetan Plateau. *Front. Microbiol.* 7:1032. doi: 10.3389/fmicb.2016.01032

Zhao, F., Sun, J., Yu, S., Liu, H., and Yu, K. (2019). Aeration irrigation can improve growth of table grape cv. Red Globe (*Vitis vinifera* L.) in greenhouse. *Hortscience* 54, 732–737. doi: 10.21273/HORTSCI13732-18

Zhao, F. Z., Ren, C. J., Zhang, L., Han, X. H., Yang, G. H., and Wang, J. (2018). Changes in soil microbial community are linked to soil carbon fractions after afforestation. *Eur. J. Soil Sci.* 69, 370–379. doi: 10.1111/ejss.12525

Zi, H. B., Hu, L., Wang, C. T., Wang, G. X., Wu, P. F., Lerdau, M., et al. (2018). Responses of soil bacterial community and enzyme activity to experimental

warming of an alpine meadow. *Eur. J. Soil Sci.* 69, 429–438. doi: 10.1111/ejss.12547

Conflict of Interest: The authors declare that the research was conducted in the absence of any commercial or financial relationships that could be construed as a potential conflict of interest.

Publisher's Note: All claims expressed in this article are solely those of the authors and do not necessarily represent those of their affiliated organizations, or those of the publisher, the editors and the reviewers. Any product that may be evaluated in this article, or claim that may be made by its manufacturer, is not guaranteed or endorsed by the publisher.

frontiers in Microbiology

ORIGINAL RESEARCH
published: 29 October 2021
doi: 10.3389/fmicb.2021.745144

Polymerase Chain Reaction-Assisted Evaluation of the Efficacy of Seed-Treatment Prevention of *Sporisorium reilianum* Infection in Sorghum Seedlings

Zhi Zhang[1], Juan Fan[2], Mucai Feng[3], Hongbo Qiu[1] and Anlong Hu[2]**

[1] College of Agriculture, Maize Institute, Guizhou University, Guiyang, China, [2] College of Agriculture, Crop Protection Institute, Guizhou University, Guiyang, China, [3] Agricultural Technology Extension Center, Weifang, China

OPEN ACCESS

Edited by:
Jia Liu,
Chongqing University of Arts and Sciences, China

Reviewed by:
Xiaobao Ying,
University of Maryland, College Park, United States
Weilin Sun,
Purdue University, United States

***Correspondence:**
Hongbo Qiu
qhb001122@163.com
Anlong Hu
alhu@gzu.edu.cn

Specialty section:
This article was submitted to Microbe and Virus Interactions with Plants, a section of the journal Frontiers in Microbiology

Received: *21 July 2021*
Accepted: *30 September 2021*
Published: *29 October 2021*

Citation:
Zhang Z, Fan J, Feng M, Qiu H and Hu A (2021) Polymerase Chain Reaction-Assisted Evaluation of the Efficacy of Seed-Treatment Prevention of Sporisorium reilianum Infection in Sorghum Seedlings. Front. Microbiol. 12:745144. doi: 10.3389/fmicb.2021.745144

Head smut, caused by *Sporisorium reilianum* [(Kuhn) Langdon and Fullerton], is a major disease of sorghum. Seed treatment is considered to be the most effective way to control the disease; however, the pathogen can infect at the seedling stage and the infected plant will not display symptoms until the reproductive stage is reached. The evaluation of the efficacy of seed treatments is time consuming and is dependent upon visible symptoms. Polymerase chain reaction (PCR) methods have the ability to identify pathogens and diagnose their presence at an early stage of infection. In this study, the *S. reilianum*-specific primer SR3 was used for PCR detection pathogen. We optimized temperature, humidity, and spore quantity test conditions and were able to achieve >88% infection incidence in sorghum seedlings. Sorghum seeds were soaked in various concentrations of tebuconazole and planted for 7 days in soil containing 0.2% teliospores. The efficacy of tebuconazole against *S. reilianum* was evaluated by PCR and recorded as disease incidence. Results indicated that the reduction in disease incidence after exposure to 0.15, 0.30, 0.45, 0.60, and 0.75 μg/mL tebuconazole was 6.24, 37.48, 67.74, 81.24, and 93.74%, respectively. Significant differences between the concentrations of tebuconazole were observed. The PCR assay represents a valuable tool for evaluating the efficacy of fungicide seed treatments for the control of *S. reilianum* in sorghum under laboratory conditions.

Keywords: sorghum, head smut, seed treatment, PCR, fungicide

INTRODUCTION

Sorghum [*Sorghum bicolor* (L.) Moench] is the fifth most important cereal crop produced globally (Mengistu et al., 2019). It is a source of animal feed and fodder, used in traditional and processed foods and beverages, and in the production of biofuel. Head smut of sorghum, caused by *Sporisorium reilianum* (Kuhn) Langdon and Fullerton [syn. *Sphacelotheca reiliana* (Kühn) G.P. Clinton and Sorosporium reilianum (Kühn) McAlpine], is an economically important disease of sorghum worldwide (Zhang et al., 2011). The pathogen can infect both maize and sorghum. Although the fungus is a biotroph, infection of a plant results in a complete loss of any harvestable

seed (Poloni and Schirawski, 2016). Teliospores overwinter in the soil and crop debris and provide primary inoculum for the next cycle of infection. Teliospores are released can remain viable for at least 3 years. Teliospores can also adhere to seed surfaces and during seed storage remain viable for much longer periods. The presence of the pathogen is very difficult to eradicate from the soil once it has become established in a cultivated field (Little et al., 2011).

Current disease management strategies include the use of host resistance and integrated pest management (IPM). Integrated pest management strategies that emphasize reduced pathogen pressure, providing optimal plant growth conditions, and the utilization of disease resistance (or tolerance) represent the future trend in disease control (Anitha et al., 2020). The use of crop protection products is the most common approach used to control *S. reilianum* as most commercially available hybrids lack a high level of resistance. In this regard, seed treatments can be used to reduce the subsequent infection of young seedlings and represent an important component of IPM systems. A variety of seed treatments have been developed to reduce pathogen and insect damage, promote uniform stand development, and increase seedling vigor. Fludioxonil, tebuconazole, sedaxane, triadimenol, and azoxystrobin are chemical fungicides that are commonly used as seed treatments (Lamichhane, 2020).

Sporisorium reilianum infects sorghum at the seedling stage, when they are only 1.5–2 cm long (Matheussen et al., 1991). After infection, the pathogen continues to proliferate in sorghum tissues without inducing any symptoms in vegetative tissues. The disease manifests itself when the host plant becomes reproductive, and symptoms then become readily visible. In the majority of cases, however, control measures at this stage are not effective. Therefore, developing a convenient, rapid, and accurate detection method for sorghum head smut infection is crucial. Chlorotic flecking along the midrib of maize leaves has been reported as a primary symptom of *S. reilianum* infection (Matyac and Kommedahl, 1985a). *Sporisorium reilianum* hyphae has also been observed in the epidermal tissues of maize coleoptiles stained with cotton blue (Shen et al., 2006). These assessment approaches, however, have not proven to be consistent.

Polymerase chain reaction (PCR)-based methods can be very effective in confirming the presence of a pathogen and detect infections before symptoms appear (Martinelli et al., 2015). In this regard, PCR-based assays for the detection development of head smut of maize caused by *S. reilianum* are readily available, sensitive, and reliable (Xu et al., 1999; Shen et al., 2006; Ren et al., 2008; Fessehaie and Munkvold, 2010).

As noted, the use of seed treatments with fungicides are a primary method for controlling *S. reilianum*. Since the disease does not show symptoms until the reproductive stage of plant growth, however, conventional methods of evaluating the efficacy of seed treatments using field trials is time-consuming and labor-intensive. Therefore, to improve the ability to evaluate the efficacy of fungicidal seed treatments, Anderson et al. developed a real-time PCR-based seedling assay for *S. reilianum* in maize. In that study, they compared five commercially available formulations of fungicides used as seed treatments for their ability to reduce seedling disease incidence using a PCR analysis of root and mesocotyl tissues (Anderson et al., 2015).

The studies of Anderson et al. (2015) focused on the detection of *S. reilianum* in maize at the seedling stage using PCR technology to determine the efficacy of seed treatments. The extension of their approach to the detection of *S. reilianum* in sorghum, however, has not been investigated as of now. In fact, due to the slow growth of mycelia on culture media and the low germination rate of teliospores (Shetty and Safeeulla, 1979; Qian, 1990), few lab studies have been conducted on the efficacy of fungicides against *S. reilianum*. Currently, tebuconazole, applied as a seed treatment, is a major strategy used to protect sorghum seedlings from *S. reilianum* (Yang et al., 2014). In the present study, a PCR assay was used to detect the presence of *S. reilianum* in sorghum seedlings and determine the efficacy of a sorghum seed treatment with tebuconazole in preventing the establishment of *S. reilianum* in sorghum seedlings.

MATERIALS AND METHODS

Sorghum Seeds and *Sporisorium reilianum* Culture

Seeds of the glutinous sorghum variety Qiangao 8 were obtained from the Guizhou Subcenter of Chinese Wheat Improvement. The seeds were washed with tap water to remove any fungicidal residues from the surface of the seeds and then dried at room temperature. The dried seeds were then surface sterilized with 1% sodium hypochlorite in 10% ethanol for 10 min, rinsed with sterile distilled water three times, and immersed in sterile distilled water for 4 h. This was followed by a hot water treatment in sterile distilled water at 60°C for 5 min to kill any endophytic fungi inside the seeds. Lastly, the seeds were rinsed with sterile distilled water, air-dried, and stored at 4°C until use (Huang and Backhouse, 2005).

Teliospores of *S. reilianum* were collected in August 2020 from naturally infected, smutted panicles of sorghum plants growing in Qianxi county, Bijie City, Guizhou Province, China (**Figure 1**). Smut galls were broken up and sieved through a 40-mesh sieve to remove plant material and other debris. Teliospores were collected and then air-dried in paper sacks.

Subsequently, 10 mg of teliospores were placed in a 1.5 mL centrifuge tube and mixed well with 1 mL sterile water, followed by centrifugation at 4000 rpm for 2 min at 4°C (ST16R, Thermo Fisher SCIENTIFIC, Braunschweig, Germany) and the supernatant was removed along with any floating debris. The precipitated teliospores were treated with 2% chloramine T for 15 min, followed by centrifugation as described, after which the supernatant was again removed. The teliospores were then washed three times with distilled water with centrifugation between each wash. A small portion of the teliospores was then plated on YEPS medium (2% peptone, 2% sucrose, 1% yeast extract, and 2% agar powder) amended with 30 mg penicillin and 200 mg streptomycin per liter, and the plates were cultured at 28°C under a 12 h light/dark cycle (Martinez et al., 2001). The viability of teliospores was evaluated after 3 d of incubation by monitoring the number of germinated spores out of at least

FIGURE 1 | Characteristic symptoms of sorghum head smut caused by *S. reilianum* in naturally infected, smutted panicles of sorghum plants growing in Qianxi county, Guizhou Province, China.

100 spores in each of four plates. Germination was visually determined using a compound microscope and teliospores were counted as germinated when the length of the germ-tube was longer than one half of the spore diameter. The viability test was repeated three times and the percentage of teliospore germination was calculated based on the collective observations.

Evaluation of Polymerase Chain Reaction Primers for *Sporisorium reilianum* Amplification

Two sets of primers were compared to select a set of appropriate PCR primers which provided the best PCR amplification results using *S. reilianum* genomic DNA as a substrate. The sequences of the primer pair, YGSP1/GSP2, designed by Ren et al. (2008), are YGSP1 (5′-TCGCCG ACGGATGATAATCG-3′) and GSP2 (5′-GAGTCACCCGCCCAAAGTTA-3). The sequences of the SR3 primer pair, designed by Xu et al. (1999), are SR3-F (5′-GCAGCCTCAGCATTACT C3′) and SR3-R (5′-ATACACCTGTGACGGCTG-3). Genomic DNA was extracted from *S. reilianum* mycelia, cultured as previously described, using an Ezup column fungal genomic DNA extraction kit (Sangon Biotech Co., Ltd., Shanghai, China), and used as a template for PCR amplification with the designated primers. The primers were synthesized by Biotech Co. Ltd. (Shanghai, China). The reaction system and procedure are listed in **Table 1**. PCR amplification was conducted in a Bio-Rad C1000 Touch^{TM} Thermal Cycler (Bio-Rad, Hemel Hempstead, United Kingdom). The amplified products were assessed on a 1% agarose gel using a PowerPac electrophoresis (Bio-rad Laboratories, Inc., United States) unit.

The minimal concentration of fungal DNA needed for amplification using the designed primer pairs was also assessed. The concentration of DNA in the extracted DNA solution was quantified using an ultra-low volume spectrophotometer. In brief, 1 μL of the extracted DNA solution was diluted with 9 μL sterile water, followed by six serial dilutions of 1 in 10. The diluted DNA solutions were then used as a template for PCR amplification with the designated primer pairs. The amplified products were visualized by 1% gel electrophoresis.

Seed Treatments

Five concentrations (0.15, 0.30, 0.45, 0.60, and 0.75 μg/mL) of tebuconazole were prepared based on a preliminary assay. The level of inhibition determined in the preliminary test at the lowest concentration of tebuconazole was about 10%, while the inhibition level at the highest concentration was about 90%. A stock solution was prepared by dissolving the fungicide in acetone, along with Tween80 as an emulsifier, and then adding water. A total of 50 seeds were soaked in 10 mL of the prepared fungicide solutions for 12 h and then removed and air dried in preparation for subsequent use. Three replicate lots of seed were treated at each fungicide concentration and a solution containing acetone and Tween80, but no fungicide, was used as a control.

TABLE 1 | Reaction systems and PCR protocols using YGSP and SR3 primer pairs for the detection of *S. reilianum* in sorghum seedlings.

Reaction system	Reaction program		
Primer F 0.5 μL, Primer R 0.5 μL, 2xTaq PCR Master Mix 10 μL, ddH2O 8 μL	94°C		3 min
	94°C	↑	30 s
	50°C	↑	30 s
	72°C	↑ 35 cycl	50 s
	72°C		5 min

Laboratory Assays of Disease Incidence

The soil used for planting the sorghum was a light sandy clay collected from the teaching farm of Guizhou University and had a pH of 5.7 (H_2O). The soil was autoclaved for sterilization and then sifted for use.

The main factors affecting *S. reilianum* infection are soil moisture and temperature (Baier and Kruger, 1962; Matyac and Kommedahl, 1985b). Therefore, the incubation conditions were optimized by adjusting the soil moisture, temperature, and spore quantity present in the soil. The optimized protocol for obtaining the highest level of disease incidence was as follows: Soil was mixed with 0.2% (by weight) teliospores and then added to a plug-designed planting tray. Sterilized sorghum seeds were then planted at 2 seeds per well. The seeds were placed 2 cm deep in the pathogen-contaminated soil. The plug trays were then placed in an incubator and cultured at 10°C, 60% humidity, and 20% soil moisture. The trays were then transferred to a greenhouse set at 25°C and a 12 h light/dark cycle. Seedlings were collected after seven days when they were 2–3 cm in length. A total of 18 similar-sized seedlings were collected from each replicate tray and used for the extraction of genomic DNA.

Extraction of Genomic DNA From the Sorghum Seedlings

Eighteen seedlings were used within each replicate for DNA extraction. Genomic DNA was extracted from individual seedlings using a DNA extraction kit (Sangon Biotech Co., Ltd., Shanghai, China). Seedling were cleaned of visible soil by rinsing under running tap water and then surface disinfected by submersion in 10% NaOCl solution with agitation for 2 min. Plants were rinsed twice in sterile water for 30 s each time (Anderson et al., 2015). Seedling were placed in a sterilized mortar, ground into a powder with a pestle in liquid nitrogen, and then immediately transferred into a 1.5 mL Eppendorf tube. Next, 800 μL of CTAB extraction buffer solution (preheated in a water bath to 65°C) was added to each of the tubes containing the ground seedling tissues and the mixture was then thoroughly mixed several times on a vortexer (5 min/time) for a total of 20 min. The seedlings were subsequently centrifuged for 2 min (12000 rpm, 4°C). The supernatant was then removed and mixed with an equal volume of phenol: chloroform (1:1, 400 μL each) and the mixture was then centrifuged for 10 min. The resulting supernatant was then mixed with an equal volume of chloroform, followed by centrifugation for 2 min. This process was repeated several times until no protein layer was visible. Genomic DNA was precipitated from supernatant by addition of 2 volumes of ice-cold absolute ethanol and storage at −20°C for 1 h, followed by centrifugation for 2 min. The resulting supernatant was discarded, and the precipitated samples of genomic DNA were washed with 70% ethanol, precipitated twice, dried at room temperature, and finally dissolved in 50 μL of DEPC treated water for subsequent use.

PCR Detection

The genomic DNA obtained from sorghum seedlings was used as a template for PCR amplification using the SR3 primers. The reaction system and procedure are provided in **Table 1**. The PCR products were detected using 1% agarose gel electrophoresis. The incidence of infection of seedlings by the smut pathogen *S. reilianum* was determined by the analysis of bands present on the agarose gels.

Evaluation of Fungicide Efficacy by Inhibition of Teliospore Germination

Inhibition of spore germination is a common method to determine the efficacy of fungicides. Therefore, the EC_{50} and EC_{95} of tebuconazole were determined by measuring teliospore germination after exposure to the prepared solutions of tebuconazole.

The teliospores were fumigated for 45 min with a mixture of 10 mL/m^3 40% formaldehyde and 5 g/m^3 potassium permanganate (Liu et al., 2007). Spore suspensions were prepared with sterile water and adjusted to about 100 spores per field of microscope. A tebuconazole acetone solution was added to sterilized and slightly cooled YEPS medium (pH = 7.0) and fully mixed. Medium amended with an equal amount of acetone was used as a control. Three replicates were used for each concentration of fungicide. Five concentrations of fungicide (0.02, 0.04, 0.08, 0.16, and 0.32 μg/mL) were used based on a preliminary assay. The level of inhibition determined in the preliminary test at the lowest concentration of tebuconazole was about 10%, while the inhibition level at the highest concentration was about 90%. A 0.1 mL drop of spore suspension was evenly distributed on the surface of each YEPS plate (9 cm), and the plates were then placed in an incubator at 28°C (Jiang et al., 2004). The rate of spore germination was determined after 48 h of culture by counting 100 spores in three different fields of view (300 spores per plate). A spore was considered germinated when the length of the germ-tube was longer than one half of the spore diameter.

Data Analysis

The level of infection and teliospore germination were calculated using the following equation:

$$\text{Inhibition rate} = \frac{CK - T}{CK} \times 100\%$$

T and CK infection in the seedling assay were determined by a positive PCR amplification in the treated and control seedlings. T and CK in the teliospore germination assay were determined by observations of spore germination in the treated and control teliospores.

The EC_{50} and EC_{95} values were calculated by regressing the percentage inhibition (probability value transformed) against the logarithm value of the fungicide concentration (log transformed). Regression analysis was performed using Microsoft Excel 2007 software (Li et al., 2015).

Analysis of Variance

Analysis of Variance between treatments was analyzed using the DPS® (Data Processing System, version7.05; Hangzhou RuiFeng Information Technology Co. Ltd., Hangzhou, China) software.

RESULTS

Sporisorium reilianum Colony Morphology

Many small colonies of *S. reilianum* were present on the YEPS medium after incubation for 10 days (**Figure 2A**). A single colony was selected and cultured on YEPS medium to make observations of colony morphology (**Figure 2B**). All the morphological observations of colony appearance were consistent with the description of *S. reilianum* in the *Manual of Fungal Identification* (Wei, 1979). The percentage of teliospore germination was 67.5%.

PCR-Amplification of *Sporisorium reilianum* Genomic DNA With Select Primers

The expected band size by SR3 primer was 680 bp. The PCR products amplified by SR3 yielded four clear, distinct bands on an agarose gel (**Figure 3**). In contrast, only one product was generated by the PCR-amplification using YGSP primers, evidenced as a single band with low definition on an agarose gel. As a result, the SR3 primers were selected for assessment of the presence of *S. reilianum*, based on the clarity of the bands that were produced by PCR-amplification of *S. reilianum* genomic DNA.

Limit of Detection of *Sporisorium reilianum* Genomic DNA by PCR

The concentration of the extracted, genomic DNA of *S. reilianum* was 107 ng/μL, which was diluted in 10-fold dilution series to obtain concentrations of 10.7 ng/μL, 1.07 ng/μL, 1.07×10^{-1} ng/μL, 1.07×10^{-2} ng/μL, 1.07×10^{-3} ng/μL, and 1.07×10^{-4} ng/μL. The various concentrations *S. reilianum* genomic DNA were then used as a template for PCR-amplification with the SR3 primers. As shown in **Figure 4**, the designated target band was amplified and visible on an agarose gel at concentrations of 10.7 ng/μL, 1.07 ng/μL, and 1.07×10^{-1} ng/μL of *S. reilianum* genomic DNA. The band size was approximately 680 bp. The amplification using the 10.7 ng/μL concentration of genomic DNA produced the strongest (brightest) band, while concentrations of 1.07×10^{-2} ng/μL, 1.07×10^{-3} ng/μL, and 1.07×10^{-4} ng/μL did not produce any visible PCR products. Therefore, a

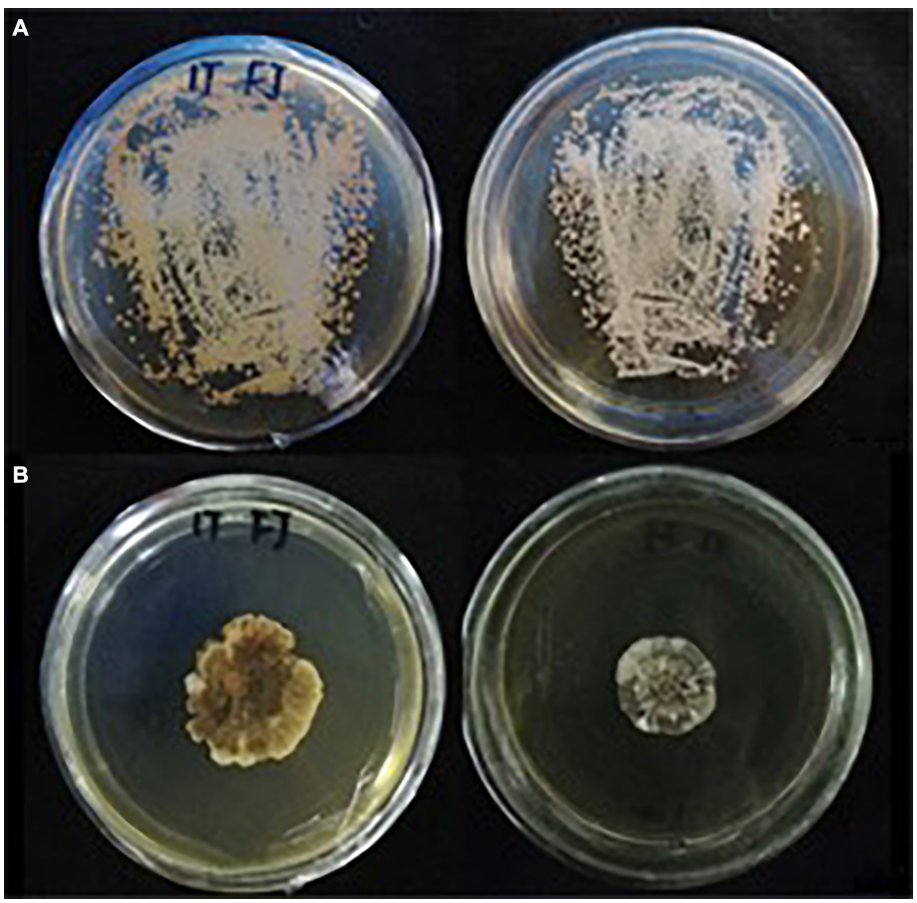

FIGURE 2 | Morphology of *S. reilianum* colonies growing on YEPS medium at 28°C with a 12 h light/dark cycle. **(A)** a small amount of teliospore suspension was distributed on YEPS medium and cultured for 10 d; **(B)** single colony cultured on YEPS medium for 30 d.

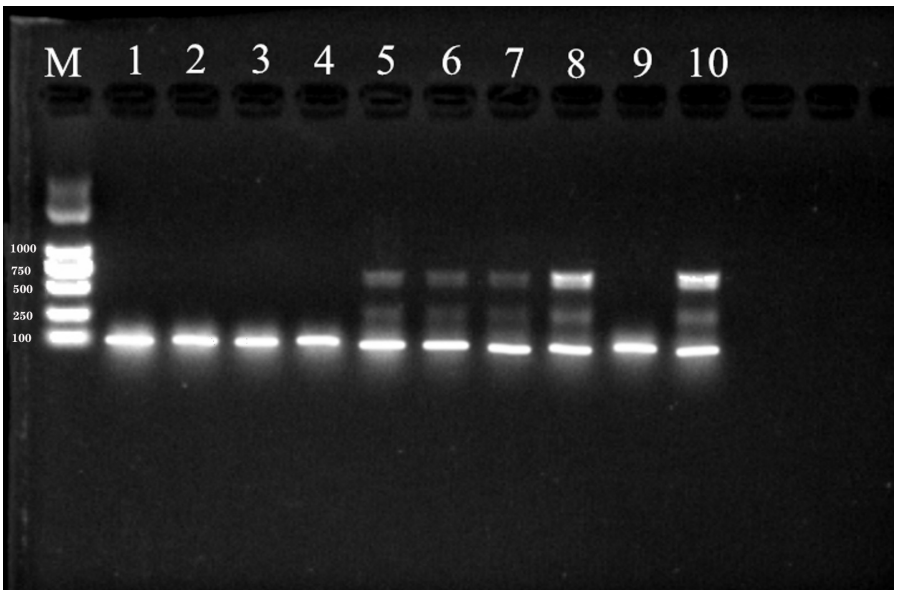

FIGURE 3 | PCR products amplified from genomic DNA of *S. reilianum* using YGSP (lane 1–5) and SR3 (lane 6–10) primer pairs, subsequently separated on a 1% agarose gel. Lane M is DNA ladder DL2000.

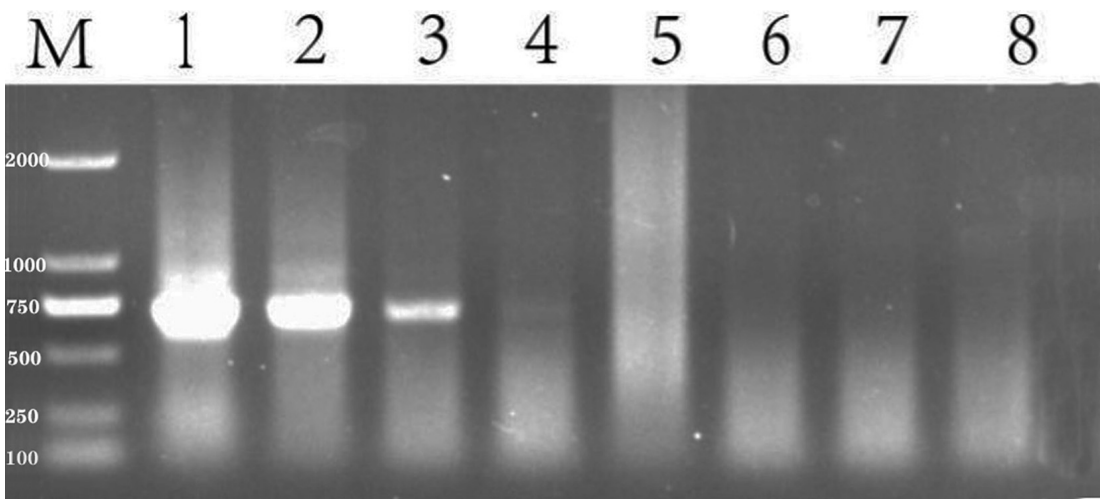

FIGURE 4 | Sensitivity of detection of *S. reilianum* using the SR3 primer pair. PCR products amplified from a 10-fold dilution series of *S. reilianum* genomic DNA and visualized on a 1% agarose gel. Lane 1:107 ng/μL, Lane 2: 10.7 ng/μL, Lane 3: 1.07 ng/μL, Lane 4: 1.07×10^{-1} ng/μL, Lane 5: 1.07×10^{-2} ng/μL, Lane 6:1.07×10^{-3} ng/μL, Lane 7:1.07×10^{-4} ng/μL. Lane M: DNA ladder DL2000.

concentration of 1.07 ng/μL genomic DNA was considered to be the limit for the detection of *S. reilianum*.

Efficacy of Seed Treatments Against *Sporisorium reilianum* Infection Determined by PCR

The incidence of pathogen infection of sorghum seedlings was assessed after seven days of seedling growth. Incidence was determined to be positive if *S. reilianum* was detected by PCR, while negative PCR results were considered to be a non-infected seedling (**Figure 5**). Treatment efficacy was determined by the number of negative vs. positive PCR results. The fewer positive PCRs observed, the better the efficacy of the fungicidal treatment.

The incidence of infection in seeds treated with 0.15, 0.30, 0.45, 0.60, and 0.75 μg/mL tebuconazole was 83.33%, 55.56%, 27.78%, 16.67%, respectively, while the incidence of infection in the untreated control was 88.88% (**Figure 6**). Conversely, the infection inhibition rate was 6.24%, 37.48%, 67.74%, 81.24, and 93.74%, respectively.

A linear regression of the level of inhibition vs. the logarithmic concentration of tebuconazole, yielded the equation

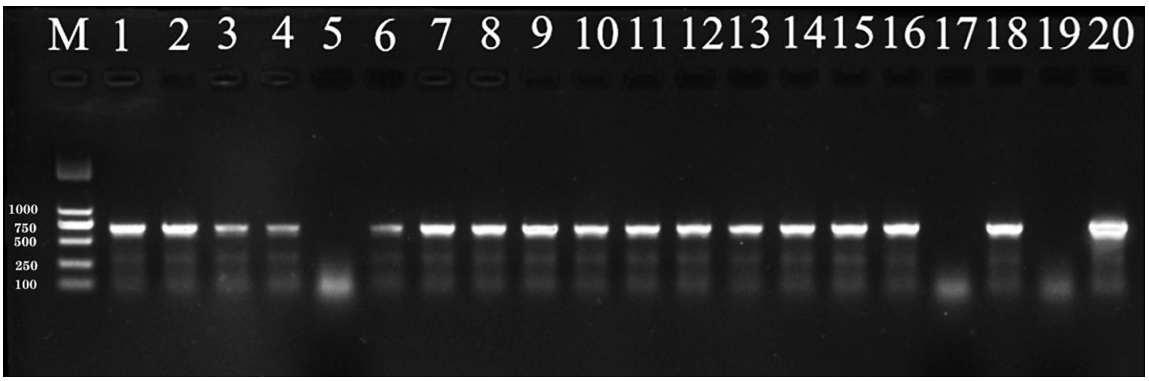

FIGURE 5 | PCR products amplified from DNA extracted from sorghum seedings and visualized by 1% agarose gel electrophoresis. Sorghum seeds were planted in soil containing 0.2% (by weight) teliospores of *S. reilianum*. After 3 days of incubation at 10°C, 20% soil moisture, and 60% relative humidity, the planted seed trays were transferred to a greenhouse (25°C and a 12-h light/dark cycle) for 4 days after which the seedlings were collected for DNA extraction. Lane M: DNA ladder DL2000. Lane 1–18: sorghum seedings. 19: negative control (Seedlings from pathogen-free soil); 20: positive control (DNA from *S. reilianum* mycelia).

y = 6.9494+4.2741x (r = 0.9953). Based on this equation, the EC_{50} value was calculated to be 0.35 μg/mL tebuconazole (95% confidence limit: 0.33–0.37 μg/mL), and the EC_{95} was 0.85 μg/mL (95% confidence limit: 0.78–0.92 μg/mL).

Efficacy of Tebuconazole Against *Sporisorium reilianum* Determined by Inhibition of Spore Germination

The percentage of teliospore germination after 48 h of incubation on media amended with 0.02, 0.04, 0.08, 0.16, and 0.32 μg/mL tebuconazole was 73.58%, 52.44%, 26.83%, 13.00%, and 4.06%, respectively. The germination on media without tebuconazole was 82.00%. Conversely, the teliospore germination inhibition rate was 10.27%, 47.56%, 67.28%, 84.14, and 95.04%, respectively (**Figure 7**).

Linear regression of the level of inhibition vs. the logarithmic concentration of tebuconazole yielded the equation y = 7.8689+2.2968x (r = 0.9837). Based on this equation, the EC_{50} value was calculated to be 0.056 μg/mL (95% confidence limit: 0.046–0. 070 μg/mL) and the EC_{95} was 0.293 μg/mL (95% confidence limit: 0.210–0.410 μg/mL).

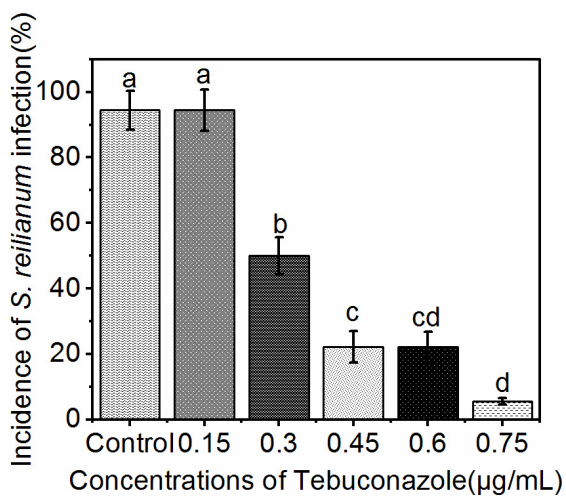

FIGURE 6 | Incidence of *S. reilianum* infection in sorghum seedlings determined by positive PCR reactions. Sorghum seeds were treated with five different concentrations of tebuconazole (x-axis), then planted in soil containing 0.2% (by weight) teliospores of *S. reilianum* and grown 7 days. Each bar represents the mean ± se (n = 3) level of disease incidence (y-axis). Different lowercase letters indicate a significant difference between the different concentration of tebuconazole ($p < 0.05$).

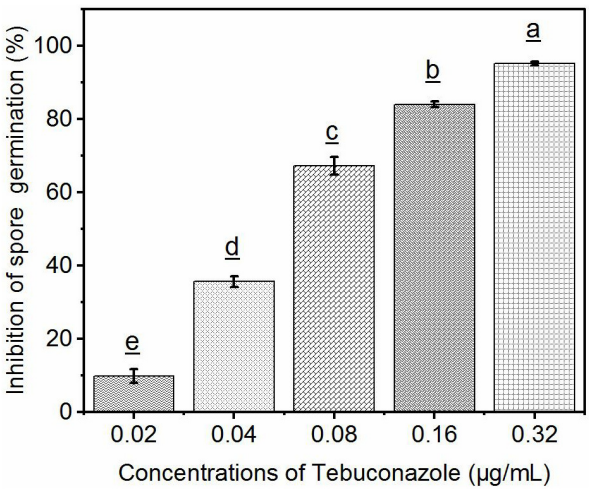

FIGURE 7 | Efficacy of tebuconazole against *S. reilianum* determined by inhibition of spore germination. Spore suspension was evenly distributed on the surface of YEPS plate containing different concentrations of fungicides, after 48 h of culture at 28°C, the rate of spore germination was determined by counting 100 spores in three different fields of view (300 spores per plate). A spore was considered germinated when the length of the germ-tube was longer than one half of the spore diameter. Each bar represents the mean ± se (n = 3). Different lowercase letters indicate a significant difference between the different concentration of tebuconazole ($p < 0.05$).

DISCUSSION

The efficacy of fungicides can be tested under either laboratory or field conditions. Inhibition of spore germination and mycelial growth are typically the parameters measured under laboratory conditions while a disease index is calculated to determine fungicidal efficacy in the field.

Tebuconazole is one of the most commonly used fungicides in agriculture and efficacy under laboratory conditions has been extensively examined. For example, the EC_{50} and EC_{90} values, based on the inhibition of mycelial growth, for *Alternaria mali* are 0.034 and 0.587 μg/mL, and 0.019 and 0.394 μg/mL for *Physalospora. piricola*, respectively (Jian-lu et al., 2007). The mean EC_{50} of tebuconazole, based on the inhibition of mycelial growth of 10 *Fusarium graminearum* isolates, was reported to be 0.19 mg/L (Avozani et al., 2014). The EC_{50} and EC_{90} values for 43% tebuconazole suspension concentrates against *Phomopsis asparagi* is 7.4241 and 47.1322 mg/L, respectively (Jia et al., 2009). EC_{50} and EC_{95} of tebuconazole for sensitive strains of *Sclerotinia homoeocarpa* is 0.078 and 1.943 μg/mL, respectively (Couch, 2003).

In our study, a PCR method was used to determine infection incidence of *S. reilianum* in sorghum seedlings. Based on our dose–response data, we performed a linear regression and determined an EC_{50} (0.35 μg/mL) and an EC_{95} (0.85 μg/mL) value for tebuconazole using the derived regression equation. The EC_{50} value for tebuconazole determined by PCR was higher than most it was in reports of several other pathogens that determined efficacy based on the inhibition of mycelial growth and/or teliospore germination. Our present results suggest that inhibition of spore germination or mycelial growth alone may not completely reflect efficacy. Spores in the soil that are not in direct contact with the seed may still germinate and their mycelia may infect the germinated seedling, even though mycelial growth may be inhibited. Thus, in actuality a higher concentration is needed to prevent infection than may be indicated in a petri dish assay. EC_{50} (0.056 μg/mL) and EC_{95} (0.293 μg/mL) value determined by inhibition of spore germination were all lower than these determined by PCR method. This result was consistent with our conclusion above. Therefore, we assume that our calculations are reliable under the conditions used in our study.

An important objective in our study was to improve the level of infection achieved in untreated, control seedlings. Methods for artificial inoculation using *S. reilianum* have been previously reported (Xiaowei Zhou et al., 2017). Four methods were used to render different maize varieties highly susceptible to infection by *S. reilianum*. The methods included injection of coleoptiles, mixing teliospores in the soil, root irrigation with water containing teliospores, and soaking seeds in water containing teliospores. Their results revealed that injection of corn coleoptiles provided the highest levels of infection. Since the purpose of our study was to evaluate the efficacy of tebuconazole as a seed treatment, the method of mixing the soil with teliospores was utilized, as it also more closely reflects field conditions.

The optimal temperature for infection of sorghum by *S. reilianum* has been reported to be 21∼28°C, with a low to medium level of soil moisture (Wu et al., 1981). It has reported that *S. reilianum* infection was the highest when soil moisture content was 15.5%. In the present study, a 0.2% concentration of teliospores in soil and a 20% of soil moisture level provided a high rate of infection. Notably, a previous study indicated that a suitable soil temperature for *S. reilianum* infection was 20∼30°C, with 35°C as the highest temperature and 10°C as the lowest temperature (Zhang, 1980; Wang et al., 2002). The approach used in the present study to achieve a high rate of infection was as follows. Seedlings were first placed at the minimum temperature of 10°C for 3 days and then transferred to 25°C. The objective of placing the seedlings at 10°C for the first three days was to stress the plants and make them susceptible to pathogen infection. The rate of infection achieved in our study was 88.88%, which is consistent with the results reported by Craig and Frederiksen (1992) and Jiang et al. (2014).

Modern approaches for detecting fungal plant pathogens utilize high-throughput molecular strategies. These include qualitative polymerase chain reaction (qPCR), real-time, quantitative PCR (RT-qPCR), nested PCR, loop-mediated isothermal amplification (LAMP), rolling circle amplification (RCA), and nucleic acid sequence-based amplification (NASBA) (Hariharan and Prasannath, 2021). Thus, PCR has become an essential diagnostic tool.

Real-time, quantitative PCR (RT-qPCR) has become increasingly used in plant pathogen diagnostics (Mirmajlessi et al., 2015). An advantage of RT-qPCR over qPCR is that the former is quantitative and can provide an estimate of the level of infection (i.e., how much pathogen is present) (McCartney et al., 2003). In our study, however, qPCR was selected as a diagnostic tool since we were simply trying to determine infection incidence, so a quantitative assessment was not required, and because qPCR is easier to conduct than RT-qPCR, the latter of which also requires greater expertise. In summary, due to the slow growth of mycelia and the low germination rate of teliospores of *S. reilianum,* as well as the time-consuming nature of field observations and evaluations, PCR-based evaluation of sorghum seedlings provides an excellent approach for evaluating the efficacy of fungicide-based seed treatments in preventing *S. reilianum* infection of sorghum seedlings.

DATA AVAILABILITY STATEMENT

The original contributions presented in the study are included in the article/supplementary material, further inquiries can be directed to the corresponding authors.

AUTHOR CONTRIBUTIONS

HQ and AH contributed to conception and design of the study. ZZ performed the experiments, analysis, and wrote first draft of

the manuscript. JF and MF validated the methodology, analysis, and provided supervision. All authors contributed to manuscript revision and read and approved the submitted version.

FUNDING

This research was supported by the National Natural Science Foundation of China (32060488 and 31760531) and the Guizhou Province Science and Technology Cooperation Plan [LH (2015)7671].

ACKNOWLEDGMENTS

Many thanks to Guozhong Luo of Fujian Agriculture and Forestry University and Xiangbo Luo of Hubei University for their technical guidance in this study.

REFERENCES

Anderson, S., Simmons, H., and Munkvold, G. (2015). Real-time PCR assay for detection of *Sphacelotheca reiliana* infection in maize (*Zea mays*) seedlings and evaluation of seed treatment efficacy. *Plant Dis.* 99, 1847–1852. doi: 10.1094/PDIS-07-14-0776-RE

Anitha, K., Das, I., Holajjer, P., Sivaraj, N., Reddy, C. R., and Balijepalli, S. B. (2020). "Sorghum diseases: diagnosis and management," in *Sorghum in the 21st Century: Food–Fodder–Feed–Fuel for a Rapidly Changing World*, eds A. K. Are, B. V. Bhat, C. R. Reddy, H. S. Talwar, T. J. Dalton, and V. A. Tonapi (Singapore: Springer), 565–619. doi: 10.1007/978-981-15-8249-3_23

Avozani, A., Reis, E. M., and Tonin, R. B. (2014). In vitro sensitivity reduction of *Fusarium graminearum* to DMI and QoI fungicides. *Summa Phytopathol.* 40, 358–364. doi: 10.1590/0100-5405/1970

Baier, W., and Kruger, W. (1962). Sphacelotheca reiliana on maize. II. Field studies on the effect of soil conditions. *South Afr. J. Agric. Sci.* 5, 183–190.

Couch, H. B. (2003). Strategies for preventing and managing fungicide resistance. *Golf Course Manag.* 71, 111–115.

Craig, J., and Frederiksen, R. (1992). Comparison of sorghum seedling reactions to *Sporisorium reilianum* in relation to sorghum head smut resistance classes. *Plant Dis.* 76, 314–318. doi: 10.1094/PD-76-0314

Fessehaie, A., and Munkvold, G. (2010). "Real-time PCR to measure head smut infection in maize seedlings," in *Phytopathology*, ed. N. Wang Vol. 100, (Saint Paul, MN: American Phytopathological Society), S36–S36.

Hariharan, G., and Prasannath, K. (2021). Recent advances in molecular diagnostics of fungal plant pathogens: a mini review. *Front. Cell. Infect. Microbiol.* 10:829. doi: 10.3389/fcimb.2020.600234

Huang, L. D., and Backhouse, D. (2005). Induction of defense responses in roots and mesocotyls of sorghum seedlings by inoculation with fusarium thapsinum and *f. proliferatum*, wounding and light. *J. Phytopathol.* 153, 522–529. doi: 10.1111/j.1439-0434.2005.01013.x

Jia, H., Zhao, J., Li, S., and Chen, D. (2009). Toxicity and efficacy of six fungicides against *Phomopsis asparagi* (Sacc.) Bubak. *Agrochemicals* 12:3.

Jiang, X. Y., Yi, M. Q., Wang, K. Y., and Tian, W. X. (2004). Inhibition and toxicity of four fungicides on *Sphacelotheca reiliana*. *Chinese J. Pestic. Sci.* 8, 375–376. doi: 10.16820/j.cnki.1006-0413.2009.12.021

Jiang, Y., Xu, X., Hu, L., Xu, J., and Zhang, M. (2014). Effect of head smut pathogen on activities of protective enzymes in sorghum. *J. Shenyang Agric. Univ.* 45, 617–620.

Jian-lu, Q., Xiao-jun, L., Yong, Z., and Kun, F. (2007). Evaluation of fungitoxicity of tebuconazole against *Alternaria mali* and *Physalospora piricola* on apple in laboratory and in field. *Chinese J. Pestic. Sci.* 9, 149–152.

Lamichhane, J. R. (2020). Parsimonious use of pesticide-treated seeds: an integrated pest management framework. *Trends Plant Sci.* 25, 1070–1073. doi: 10.1016/j.tplants.2020.08.002

Li, J. L., Liu, X. Y., Xie, J. T., Di, Y. L., and Zhu, F. X. (2015). A comparison of different estimation methods for fungicide EC50 and EC95 values. *J. Phytopathol.* 163, 239–244. doi: 10.1111/jph.12312

Little, C. R., Perumal, R., Tesso, T. T., Prom, L. K., Odvody, G. N., and Magill, C. W. (2011). Sorghum pathology and biotechnology-A fungal disease perspective: part I. Grain mold, head smut, and ergot. *Eur. J. Plant Sci. Biotechnol.* 6, 10–30.

Liu, H. L., Wang, X. F., Liu, H., Shen, G. S., and Xie, L. H. (2007). Study on germination conditions of teliospore of maize head smut. *China Plant Protect.* 27, 5–8.

Martinelli, F., Scalenghe, R., Davino, S., Panno, S., Scuderi, G., Ruisi, P., et al. (2015). Advanced methods of plant disease detection. A review. *Agron. Sustain. Dev.* 35, 1–25. doi: 10.1007/s13593-014-0246-1

Martinez, C., Buée, M., Jauneau, A., Bécard, G., Dargent, R., and Roux, C. (2001). Effects of a fraction from maize root exudates on haploid strains of *Sporisorium reilianum* f. sp. zeae. *Plant Soil* 236, 145–153. doi: 10.1023/A:1012776919384

Matheussen, A.-M., Morgan, P. W., and Frederiksen, R. A. (1991). Implication of gibberellins in head smut (*Sporisorium reilianum*) of *Sorghum bicolor*. *Plant Physiol.* 96, 537–544. doi: 10.1104/pp.96.2.537

Matyac, C. A., and Kommedahl, T. (1985a). Factors affecting the development of head smut caused by *Sphacelotheca reiliana* on corn. *Phytopathology* 75, 577–581. doi: 10.1094/Phyto-75-577

Matyac, C. A., and Kommedahl, T. (1985b). Occurrence of chlorotic spots on corn seedlings infected with *Sphacelotheca reiliana* and their use in evaluation of head smut resistance. *Plant Dis.* 69, 251–254. doi: 10.1094/PD-69-251

McCartney, H. A., Foster, S. J., Fraaije, B. A., and Ward, E. (2003). Molecular diagnostics for fungal plant pathogens. *Pest Manag. Sci.* 59, 129–142. doi: 10.1002/ps.575

Mengistu, G., Shimelis, H., Laing, M., and Lule, D. (2019). Assessment of sorghum genetic resources of Ethiopia for anthracnose (*Colletotrichum sublineolum* Henn.) resistance and agronomic traits.". *J. Phytopathol.* 167, 667–678. doi: 10.1111/jph.12861

Mirmajlessi, S. M., Loit, E., Maend, M., and Mansouripour, S. M. (2015). Real-time PCR applied to study on plant pathogens: potential applications in diagnosis-a review. *Plant Protect. Sci.* 51, 177–190. doi: 10.17221/104/2014-PPS

Poloni, A., and Schirawski, J. (2016). Host specificity in *Sporisorium reilianum* is determined by distinct mechanisms in maize and sorghum. *Mol. Plant Pathol.* 17, 741–754. doi: 10.1111/mpp.12326

Qian, J. J. Z. (1990). Studies on the germination of the telispore of maize head smut pathogen. *J. Plant Protect.* 27, 5–8.

Ren, L., Li, L., and Bai, R. (2008). PCR detection of *Sporisorium reilianum*. *J. Maize Sci.* 16, 138–139.

Shen, N. X., Yan, N., and Wang, F. (2006). The research of *Sporisorium reiliana's* infection efficiency and spreading in maize based on PCR assays. *Sci. Agric. Sin.* 39:6.

Shetty, H. S., and Safeeulla, K. (1979). Stimulation of teliospore germination in smut fungi. *Proc. Indian Acad. Sci. B Part 2 Plant Sci.* 88, 479–486. doi: 10.1007/BF03046138

Wang, Z. H., Wang, Y. J., Wang, L., Yi, J., Li, X., and Shi, H. (2002). Research advance on head Smut disease in maize. *J. Maize Sci.* 4, 61–64.

Wei, J. C.(1979). *Manual of Fungal Identification*. Shanghai: Science and Technology Press.

Wu, X., Pang, Z., and Hu, J. (1981). Study on the environmental factors affecting infection and cultural meadures of controlling corn head smut [*Sphacellotheca reiliana* (KUHN) CLINT.]. *J. Plant Protect.* 8, 41–46.

Xiaowei Zhou, L. X., Wang, N., Jiang, Z., Li, L., and Zhang, Y. (2017). Screening of efficient inoculation methods of head smut and common

smut of corn. *J. Northeast Agric. Sci.* 42, 28–30. doi: 10.16423/j.cnki.1003-8701

Xu, M., Melchinger, A., and Lübberstedt, T. (1999). Species-specific detection of the maize pathogens *Sporisorium reiliana* and *Ustilago maydis* by dot blot hybridization and PCR-based assays. *Plant Dis.* 83, 390–395. doi: 10.1094/PDIS.1999.83.4.390

Yang, D., Wang, N., Yan, X., Shi, J., Zhang, M., Wang, Z., et al. (2014). Microencapsulation of seed-coating tebuconazole and its effects on physiology and biochemistry of maize seedlings. *Colloids Surf. B* 114, 241–246. doi: 10.1016/j.colsurfb.2013.10.014

Zhang, F., Ping, J., Du, Z., Cheng, Q., and Huang, Y. (2011). Identification of a new race of *Sporisorium reilianum* and characterization of the reaction of sorghum lines to four races of the head smut pathogen. *J. Phytopathol.* 159, 342–346. doi: 10.1111/j.1439-0434.2010.01770.x

Zhang, Z. (1980). Studies on the infection of head smut fungus from corn. *J. Northwest Sci. Tech. Univ. Agric. For. (Nat. Sci. Edn.)* 4, 67–78.

Conflict of Interest: The authors declare that the research was conducted in the absence of any commercial or financial relationships that could be construed as a potential conflict of interest.

Publisher's Note: All claims expressed in this article are solely those of the authors and do not necessarily represent those of their affiliated organizations, or those of the publisher, the editors and the reviewers. Any product that may be evaluated in this article, or claim that may be made by its manufacturer, is not guaranteed or endorsed by the publisher.

Advantages of publishing in Frontiers

OPEN ACCESS
Articles are free to read for greatest visibility and readership

FAST PUBLICATION
Around 90 days from submission to decision

HIGH QUALITY PEER-REVIEW
Rigorous, collaborative, and constructive peer-review

TRANSPARENT PEER-REVIEW
Editors and reviewers acknowledged by name on published articles

Frontiers
Avenue du Tribunal-Fédéral 34
1005 Lausanne | Switzerland

Visit us: www.frontiersin.org
Contact us: frontiersin.org/about/contact

REPRODUCIBILITY OF RESEARCH
Support open data and methods to enhance research reproducibility

DIGITAL PUBLISHING
Articles designed for optimal readership across devices

FOLLOW US
@frontiersin

IMPACT METRICS
Advanced article metrics track visibility across digital media

EXTENSIVE PROMOTION
Marketing and promotion of impactful research

LOOP RESEARCH NETWORK
Our network increases your article's readership